is space time?
a blog

Predrag Cvitanović and Matthew N. Gudorf

November 6, 2022

Contents

CONTENTS

Chapter 1

Space-time, sliced & sectioned

The Day Dynamics Died
January 24, 2016 at 6 AM PST, Santa Barbara, CA
— Predrag Cvitanović

Abstract

Motivated by space-time translational invariance 'spatiotemporally chaotic' or 'turbulent' flows are recast as a $D+1$ dimensional spatiotemporal theory which treats space and time equally. In this formulation time evolution is replaced by a repertoire of spatiotemporal patterns taking the form of $D + 1$ invariant tori. Infinite space-time is then explained by the shadowing of these tori. This is formalized by the development of a $D + 1$ dimensional symbolic dynamics whose alphabet is comprised of space-time tori of minimal size. Enumerating these spatiotemporal building blocks enables the construction of all admissible spatiotemporal patterns. These ideas are investigated in the context of the Kuramoto-Sivashinsky equation using new open source spatiotemporal computational codes. These codes offer easy access to new spatiotemporal techniques, persistent homology, convolutional neural networks and more.

Spatiotemporal tiling of the Kuramoto-Sivashinsky system
Abstract Nov 19, 2020
   Using (1) spacetime translational invariance, and (2) exponentially unstable dynamics, 'spatiotemporally chaotic' or 'turbulent' flows are reformulated as a (D+1)-dimensional spatiotemporal theory which treats space and time on equal footing. In this theory there is no evolution in time: time evolution is replaced by the enumeration of the repertoire of the spatiotemporal solutions (translationally invariant (D+1)-dimensional invariant tori, or 'periodic orbits') of system's equations, very much as the statistical mechanics' weighted partition function of Ising model is constructed as a sum formed by enumerating all its lattice states.

Our hypothesis is that the entirety of the spacetime solutions can be constructed by gluing together tiles from a finite collection of 'fundamental tiles' that shadow larger solutions. We demonstrate that (1) these fundamental tiles can be extracted from generic, large spacetime domain solutions, and (2) that they in turn can be used as the 'building blocks' of turbulence. Left for the future work is (3) our conjecture that these results should enable us to construct a (D+1)-dimensional symbolic dynamics with an alphabet (whose 'letters' are these fundamental tiles) enables one to systematically enumerate and label all 'turbulent' solutions.

These ideas are investigated in the context of the 1+1 dimensional spacetime of the Kuramoto-Sivashinsky equation in one spatial dimension, using my open source Python package 'OrbitHunter'.

1.1   Introduction

Recent experimental and theoretical advances [33] support a dynamical vision of turbulence: For any finite spatial resolution, a turbulent flow follows approximately for a finite time a pattern belonging to a finite alphabet of admissible patterns. The long term dynamics is a walk through the space of these unstable patterns. The question is how to characterize and classify such patterns? [1] Chaotic nonlinear systems constitute one of the few classical physics problems yet to be solved. The behaviors exhibited are so peculiar that it has permeated into popular culture via the butterfly effect. This behavior poses a serious challenge which has effects everything from weather prediction to air travel. In the recent past computational successes were made by studying turbulent flows on minimal cells: small domains that could support turbulence and remain computationally tractable. These successes came in form of time invariant solutions alkso known as "exact coherent structures" (ECS) [55, 57]. These solutions are important because it is their unstable and stable manifolds that dictate the dynamics [7]. Not only have conventional methods not worked on large domains, we argue that they never could have worked. The motivation behind minimal cells was to develop an intuition for turbulence which would be used to obtain results on progressively large domains.

In light of all of these difficulties we believe that new bold ideas are required to resume forward progress. We retreat from the conventional wisdom to start anew with a truly spatiotemporal theory, one that treats infinite space-time as the shadowing of a finite number of fundamental patterns which we denote as "tiles".

[2] The primary claim that we make is that in hindsight, describing turbulence via an exponentially unstable dynamical equation never could have worked. Conventional methods treat spatial dimensions as finite and fixed and time as inherently infinite. Our spatiotemporal formulation of chaos treats all continuous dimensions with translational invariance democratically as $(1 + D)$ differ-

---

[1]Matt 2020-01-20: [Background]
[2]Matt 2020-01-20: [Revolution] WHY?

ent 'times'. The proposal is inspired by the Gutkin and Osipov [31] modelling of chain of N coupled particle by temporal evolution of a lattice of N coupled cat maps.

The alternative that we propose to describe infinite space-time chaos via the shadowing of fundamental patterns which we refer to as "tiles". These tiles are the minimal "building blocks" of turbulence; they are realized as invariant 2-tori which are global solutions with compact support. Finding the tiles of turbulence is fundamentally easier than finding invariant 2-tori on larger domains due to the exponential growth in complexity of solutions. In other words there are fewer important solutions on smaller domains. This in turn implies that there can only be a small number of fundamental tiles. This is what makes the problem tractable: if we can collect the complete set of tiles then we have the ability to construct every invariant 2-torus according to our theory.

The lack of exponentially unstable dynamics has powerful and immediate effects. Because there is no time integration, the problem of finding invariant 2-tori is now a variational one. The benefit of this is that there is no need to start an initial guess on the attractor; the optimization process handles this entirely. This allows us to find arbitrarily sized invariant 2-toribut in fact there is no need to. Our hypothesis is that we need only to find the building blocks which shadow larger invariant 2-tori and infinite space-time.

The spatiotemporal formulation allows a much easier categorization of what is "fundamental" by virtue of the frequency that patterns admit in the collection of invariant 2-tori. By identifying the most frequent patterns, we shall clip these patterns out of the invariant 2-tori they shadow and use them as initial conditions to search for our tiles.

The notion of "building blocks of turbulence" is one of the reasons for studying fluid flows in the first place. There is evidence that certain physical processes are fundamental, but they have yet to be used in a constructive manner. The spatiotemporal description is able to actually put these ideas in practice. The spatiotemporal completely avoids this by constructing larger invariant 2-tori from the combination of smaller invariant 2-tori. The reason why the search for the fundamental tiles is classified as "easy" is because in the small domain size limit there just aren't that many invariant 2-tori; the dynamics is relatively simple.

The first key difference is that the governing equation dictates the spatiotemporal domain size in an unsupervised fashion. The results here are not The only reason why L was treated as fixed is due to the inherent instability it includes when treated as a varying quantity. This small detail, allowing the domain size L to vary, is not as trivial as it seems. This difficulty is especially evident in the Kuramoto-Sivashinsky equation, whose spatial derivative terms are of higher order than the first order time derivative, but also there is a spatial derivative present in the nonlinear component.

Specifically, we propose to study the evolution of Kuramoto-Sivashinsky on the 2-dimensional infinite spatiotemporaldomain and develop a 2-dimensional symbolic dynamics for it: the columns coding admissible time itineraries, and rows coding the admissible spatial profiles. Our spatiotemporal method is the

clear winner in both a computational and theoretical sense. By converting to a tile based shadowing description we have essentially removed the confounding notion of an infinite number of infinitely complex invariant 2-tori from the discussion. Now we must put these ideas into practice. The testing grounds for these ideas will be the spatiotemporal Kuramoto-Sivashinsky equation

$$u_t + u_{xx} + u_{xxxx} + uu_x = 0 \quad \text{where} \quad x \in [0, L], t \in [0, T] \qquad (1.1)$$

where $u = u(x,t)$ represents a spatiotemporal velocity field. This equation has been used to model many different processes such as the laminar flame front velocity of Bunsen burners. While (18.1) is much simpler than the spatiotemporal Navier-Stokes equation, we would argue that the main benefit is the simplicity of visualizing its two-dimensional space-time. This visualization makes the arguments more understandable and compelling in addition to making the tiles easier to identify. The translational invariance and periodicity of (18.1) make spatiotemporal Fourier modes a natural choice. The inherently infinitely dimensional equations are approximated by a Galerkin truncation of these spatiotemporal Fourier modes. The Kuramoto-Sivashinsky equation (18.1) in terms of the Fourier coefficients $\hat{u}$ is a system of differential algebraic equations $\hat{u}$

$$F(\hat{u}, L, T) \quad \equiv \quad (\omega - k^2 + k^4)\hat{u} + \frac{k}{2}\mathcal{F}(\mathcal{F}^{-1}(\hat{u})^2) \, . \qquad (1.2)$$

The nonlinear term is computed in a *pseudospectral* fashion: a method which computes the nonlinear term as a product in physical space as opposed to a convolution in spectral space. The definitions of each term is as follows; $\mathcal{F}$ and $\mathcal{F}^{-1}$ represent the forward and backwards spatiotemporal Fourier transform operators. Likewise, ω and k contain the appropriate temporal and spatial frequencies to produce the corresponding derivatives. Any and all indices are withheld to avoid unnecessary confusion at this stage. The spatiotemporal system of differential algebraic equations (18.2) is of the form $F(\hat{u}, L, T) = 0$. This type of optimization problem is ubiquitous in engineering and optimization literature. Therefore solving (18.2) is a matter of adapting known numerical methods to its idiosyncrasies. Once we have the ability to solve (18.2) we need to first create a collection of invariant 2-tori. The only requirement that the collection must satisfy is that it must capture all fundamental patterns by adequately sampling the set of invariant 2-tori. In other words an exhaustive search is not our aim; not only that, but also the collection need not sample all spatiotemporal domain sizes. We hypothesize that there is some upper bound on the spatiotemporal size of fundamental tiles due to spatiotemporal correlation lengths. Once the collection is deemed sufficient we proceed to visual inspection. In this manner we determine the most frequent patterns and single them out as tile candidates. This is done by literally clipping them out of the invariant 2-tori that they shadow. Each clipping is then treated as an initial guess for a fundamental tile which is itself a invariant 2-torus. Therefore, these represent initial conditions for the optimization method. It is not a guarantee that every clipping converges to a invariant 2-torus; therefore the number

of attempts to find a tile should continue until it does in fact converge. The number of convergence attempts is typically proportional to how confident we are that the pattern being scrutinized is in fact a tile. Once a collection of tiles is collected, we can construct new and reproduce known invariant 2-tori. This is completed with a method we refer to as "gluing". It is as straightforward as one might infer: tiles are combined in a spatiotemporal array to form initial conditions used to find larger invariant 2-tori. Methods of gluing temporal sequences of invariant 2-tori exist but never has the ability to glue invariant 2-tori spatiotemporally existed before. With the implementation of the gluing method can begin to probe the 2-dimensional spatiotemporal symbolic dynamics previously mentioned. A fully determined symbolic dynamics is sufficient to describe infinite space-time completely. We already have the two edges of this symbol plane - the $L = 22$ minimal cell [10, 44] is sufficiently small that we can think of it as a low-dimensional ("few-body" in Gutkin and Klaus Richter [17–20] condensed matter parlance) dynamical system, the left-most column in the Gutkin and Osipov [31] $2D$ symbolic dynamics spatiotemporal table (not a 1-dimensional symbol sequence block), a column whose temporal symbolic dynamics we will know, sooner or later. Michelson [46] has described the bottom row. The remainder of the theory will be developed from the bottom up, starting with small spatiotemporal blocks.

The plans for our spatiotemporal formulation have been laid bare. The main concept is that the infinities of turbulence can be described by spatiotemporal symbolic dynamics whose letters are fundamental spatiotemporal patterns. Consequentially, we have created numerical methods which not only perform better than conventional methods but also present incredible newfound capabilities. These newfound capabilities include but are not limited to finding small invariant 2-tori which shadow larger invariant 2-tori but also constructing larger invariant 2-tori from smaller ones. These new and robust methods alone present a way forward for turbulence research, hence their is merit in a spatiotemporal formulation even though the theory has not been fully fleshed out. To test our spatiotemporal ideas we require three separate numerical methods: the first should be able to find invariant 2-tori of arbitrary domain size. The second needs to be able to clip or extract tiles from these invariant 2-tori. Lastly, we need a method of gluing these tiles together. All three of these techniques require the ability to solve the optimization problem $F(\hat{u}, T, L) = 0$ on an arbitrarily sized doubly periodic domain.

[3] As previously discussed, this work does not use approximate recurrences or time integration to generate initial conditions. Instead we simply initialize a lattice of Fourier modes by first deciding on the dimensions of the lattice and then assigning random values to the modes. Specifically, random values in this case are drawn from the standard normal distribution and then normalized such that the physical field $u(x, t)$ has the assigned maximum value. Manipulations of the Fourier spectrum can also be made but we have no specific recommendation for how to do so as it can be rather unintuitive.

---

[3]Matt 2020-02-18: How?

The first method substitutes an equivalent optimization problem instead of directly solving $F = 0$. The optimization problem is formed by the construction of a scalar cost function

$$\mathcal{I}(\hat{u}, T, L) = \frac{1}{2} ||F(\hat{u}, T, L)||_2^2 \,. \tag{1.3}$$

taking a derivative with respect to a fictitious time τ

$$
\begin{aligned}
\frac{\partial \mathcal{I}}{\partial \tau} &= \nabla \Big(\frac{1}{2} ||F(\hat{u}, T, L)||_2^2 \Big) \partial_\tau [\hat{u}, T, L] \\
&= \left(\Big[\frac{\partial F}{\partial \hat{u}}, \frac{\partial F}{\partial T}, \frac{\partial F}{\partial L} \Big]^\top F(\hat{u}, T, L) \right) \cdot \partial_\tau [\hat{u}, T, L] \\
&\equiv \left(J^\top F \right) \cdot \partial_\tau [\hat{u}, T, L] \quad .
\end{aligned}
\tag{1.4}
$$

This equation (18.4) by itself does not provide us with a descent direction because $\partial_\tau [\hat{u}, T, L]$ remains unspecified. The simplest choice is the negative gradient of the cost function; this choice corresponds to the gradient descent algorithm.

$$\partial_\tau [\hat{u}, T, L] = - \left(J^\top F \right) , \tag{1.5}$$

such that

$$\frac{\partial \mathcal{I}}{\partial \tau} = - \left|\left| \left(J^\top F \right) \right|\right|_2^2 \le 0 \,. \tag{1.6}$$

In order to "descend" we use Euler's method to integrate in the descent direction. Note that this integration is with respect to fictitious time and represents making successive variational corrections; it is not dynamically unstable time integration. We elect to use a combination of step limit and absolute tolerance to determine when the descent terminates. If the cost function doesn't cross the threshold by the step limit then the descent is terminated. The descent algorithm can be viewed as a method of converging approximate solutions close enough to a final invariant 2-torus such that the least-squares algorithm can converge them, akin to [21].

The second method is application of a least-squares solver to the root finding problem $F = 0$. The Newton system is derived here for context.

$$F(\hat{u} + \delta\hat{u}, T + \delta T, L + \delta L) \approx F(\hat{u}, T, L) + J \cdot [\delta\hat{u}, \delta T, \delta L] + \dots \,. \tag{1.7}$$

substitution of zero for the LHS (the root) yields

$$J \cdot [\delta\hat{u}, \delta T, \delta L] = -F(\hat{u}, T, L) \,. \tag{1.8}$$

where

$$J \equiv \Big[\frac{\partial F}{\partial \hat{u}}, \frac{\partial F}{\partial T}, \frac{\partial F}{\partial L} \Big] \,. \tag{1.9}$$

Technically this equation is solved iteratively, each time producing its own least-squares solution which guides the field to invariant 2-torus. The equations are augmented to include variations in T, L and as such the linear system is actually rectangular. We chose to solve the equations in a least-squares

manner as we are not focused on finding a unique solution; any member of a invariant 2-tori group orbit will do. The price of this indefiniteness is that we might collect invariant 2-tori which belong to the same group orbit. To improve the convergence rate of the algorithm we also include backtracking: the length of the Newton step is reduced until either a minimum length is reached (failure) or the cost function decreases. As a caveat, our specific least-squares implementation is memory limited. That is, we can only apply it to some maximum dimension as it requires the explicit construction of a large, dense matrix. Currently it suits our purposes such that we do not include any other numerical methods in this discussion. The primary numerical methods that we apply have been described. Now we can move onto describing exactly how we used these method to further our spatiotemporal theory.

As previously mentioned, we must first find a collection of invariant 2-tori which we believe adequately samples the space of invariant 2-tori, up to some maximum size. We automated the search over a range of periods and domain sizes. Periods were chosen from the range $T \in [20, 180]$. Meanwhile, the spatial range was $L \in [22, 88]$. The discretization size depended on the spatiotemporal domain size; more modes are needed to resolve larger solutions. The number of lattice points in each dimension were typically chosen to be powers of two in order because of their interaction with discrete Fourier transforms. A strict rule for lattice size was never developed so we offer is the approximate guidelines

$$M = 2^{\text{int}(log_2(L)+1)} \tag{1.10}$$

for space and

$$N = 2^{\text{int}(log_2(T))}. \tag{1.11}$$

for time. The tolerance of the cost function for the gradient descent was typically set at 10^{-4} and the step limit was set as a function of the size of the lattice. For the least-squares with backtracking the tolerance for termination was originally 10^{-14} and the step limit was 500. The large step limit was because of the allowance of back-tracking, which reduces the step length. The final tolerance can likely be relaxed as there is minimal change in solutions over many orders of magnitude of the cost function; an indication that a different norm should be used. As a reminder, our claim is that the tiles are invariant 2-tori which shadow larger invariant 2-tori. Therefore we should be able to converge subdomains which have been numerically clipped out of larger invariant 2-tori. After visual inspection, we believed the number of fundamental tiles to be small. Therefore, a precise and unsupervised algorithm for clipping was not developed. Instead the only criteria we abided by is that the clipping must include the tile being sought after; of course, clippings that were closer to being doubly periodic were sought after. For the original invariant 2-torus with dimensions $x \in [0, L_0]$ and $t \in [0, T_0]$ defined on a lattice, the clipping can be described as follows. Find the approximate domain on which the shadowing occurs and then literally extract the subregion of the parent lattice, setting the new spatiotemporal dimensions according to the smaller lattice. In other words, the same grid spacing was maintained throughout this procedure. This

process in combination with our numerical methods was sufficient for finding tiles. It is one thing to claim that certain spatiotemporal invariant 2-tori are the building blocks of turbulence for the Kuramoto-Sivashinsky equation. It is another thing entirely to put our money where our mouth is by actually using them in this manner. We would like to remind the audience that the ability to construct and find solutions in this manner has not been witnessed in the literature. With this in mind our choices should be treated as preliminary ones; it is entirely possible and likely that many improvements could be made. Much like the clipping process used to find tiles combining solutions in space-time, the overarching idea of gluing is straightforward and intuitive. Specifically, the tiles represent the Brillouin zone, fundamental domain, unit cell of a lattice, etc. of each fundamental invariant 2-torus. The general case is that we have a general $s_n \times s_m$ sized mosaic of tiles. The admissibility of the gluing is determined by the (currently unknown) symbolic dynamics. Gluing is only well defined if the lattices being combined have the same number of grid points along the gluing boundary. This creates a problem, however, as different tiles will have different spatiotemporal dimensions T, L because they are fundamentally different solutions. This actually helps provide a precise meaning to the term "gluing". Gluing is a method of creating initial conditions which approximates a non-uniform rectangular lattice (combination of tiles) as uniform. This of course introduces local error which depends on the grid size; therefore there should not be an extreme discrepancy between the invariant 2-tori or tiles being glued. With this in mind, we simply rediscretize and concatenate the new lattices. The dimensions of the new lattice are determined by the sum or average of the original dimensions. For example, if gluing two tiles together in time, the new period would be $T = T_1 + T_2$ but the new spatial period is $L = \frac{L_1 + L_2}{2}$. In this case the number of spatial grid *points* and temporal grid *spacing* should be the same. There are many more complicated alternatives, limited only by the imagination.

1.2 Kuramoto-Sivashinsky equation

The Kuramoto-Sivashinsky equation [42, 51], which arises in the description of stability of flame fronts, reaction-diffusion systems and many other physical settings [40, 49], is one of the simplest nonlinear PDEs that exhibits spatiotemporally chaotic behavior. In one space dimension it is defined on the doubly infinite spacetime plane

$$u_t + u\,u_x + u_{xx} + u_{xxxx} = 0\,, \quad (x,t) \in \mathbb{R}^2\,, \tag{1.12}$$

where t is the time, x is the spatial coordinate, subscripts $(\cdot)_x$ and $(\cdot)_t$ denote partial derivatives with respect to x and t, and the field $u = u(x,t)$ can be thought of as the 'flame front velocity' at the spacetime point (x,t). Occasionally the form of (18.1) will include a coefficient ν on the "hyper-viscosity" term, i.e., νu_{xxxx}. We have exchanged this control parameter for non-dimensional

length via the relation

$$L = \frac{L}{2\pi\sqrt{\nu}} \,, \tag{1.13}$$

and setting $\nu = 1$. This seems to be the more natural choice as solutions have on the order of L number of wavelengths at any given time; this allows for quick interpretation and verification of figures of scalar fields later on. We do note that this may be a frustrating choice as there is much literature in which $L = 22$ is the spatial domain size being reported on [5, 10, 14, 15, 25]. This translates to $L_{22} \approx 3.50$ for reference. An alternative choice would be to set the scale in terms of the most unstable wavelength $\tilde{L}^* = \frac{L}{2\pi\sqrt{2}}$

There is much interest in Kuramoto-Sivashinsky equation because (18.1) is a 1-dimensional PDE analogue of the 3-dimensional Navier-Stokes PDEs

$$\frac{\partial \mathbf{v}}{\partial t} + (\mathbf{v} \cdot \nabla)\mathbf{v} - \frac{1}{R}\nabla^2\mathbf{v} + (\cdots) = 0 \,, \qquad (\mathbf{x}, t) \in \mathbb{R}^4 \,, \tag{1.14}$$

where $(\cdots)$ stands for various forcing terms. Holmes, Lumley and Berkooz [34] offer a delightful discussion of why Kuramoto-Sivashinsky system deserves study as a staging ground for studying turbulence in full-fledged Navier-Stokes boundary shear flows. First, high quality simulations of Navier-Stokes [26, 58] are much harder than Kuramoto-Sivashinsky simulations [38]. Second, and the real reason why in this paper we introduce the reader to the spatiotemporal theory of turbulence using Kuramoto-Sivashinsky as an example, is that it is very hard to visualize 3-dimensional velocity field at every 3-dimensional spatial pointand at every instant in time. In contrast, spatiotemporal visualization of Kuramoto-Sivashinsky as color-coded magnitude of 1-dimensional velocity field u over the spacetime (x, t), as in figure 1.1, is immediate.

It suffices to inspect a single generic spatiotemporal solution of Kuramoto-Sivashinsky equation such as figure 1.1, to be almost always able to recognize any other solution u as a solution of Kuramoto-Sivashinsky equation. Indeed, the goal of this paper is to explain *why*, by deriving the alphabet of admissible patterns from the Kuramoto-Sivashinsky equation, and assigning a unique spatiotemporal "word" to any solution that can be seen embedded into the chaotic (turbulent) attractor (inertial manifold). It is intuitive by inspection that there is a typical spatial "mean wavelength" (sect. 1.5) and a typical time scale, that the patterns are exponentially decorrelated beyond several space and time scale units (sect. 1.5 and sect. 1.6), and that all statistical averages, such as energies and dissipation rates, should be extensive (see sect. 1.6.4).

1.3 Exact solutions of Kuramoto-Sivashinsky

1.3.1 Equilibria and relative equilibria

Equilibria (or the steady solutions) are the fixed profile time-invariant solutions,

$$u(x, t) = u_q(x) \,. \tag{1.15}$$
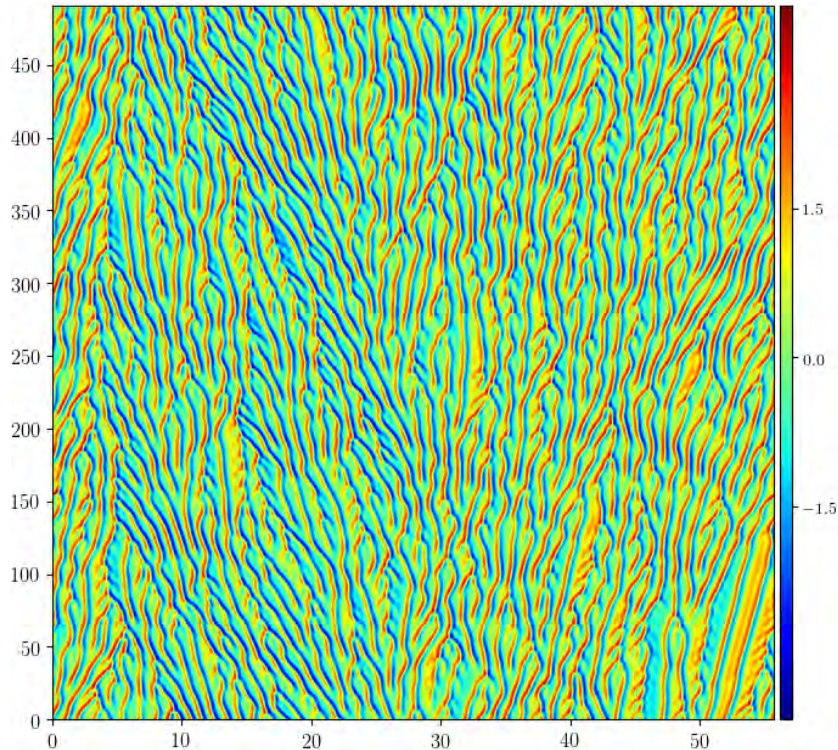
Figure 1.1: A spacetime heat map of a typical "steady state turbulence" Kuramoto-Sivashinsky solution $u(x,t)$, integrated forward in time on a periodic domain of size $L \approx 79.57$ (after the initial transient has died out). The most unstable wavelength $2\pi\sqrt{2}$ of the u=0 equilibrium (see sect. 1.5) is an estimate the mean spatial wavelength of the turbulent Kuramoto-Sivashinsky flow, so there are approximately 55 wiggles across the spatial domain at any instant in time. The color bar indicates the heat map scheme for $u(x,t)$, used also for the subsequent figures of this type.

Due to the spatial translational symmetry, the Kuramoto-Sivashinsky system also allows for relative equilibria (traveling waves, rotating waves), characterized by a fixed profile $u_q(x)$ moving with constant speed c, i.e.

$$u(x,t) = u_q(x - ct).$$ (1.16)

Here suffix $_q$ labels a particular invariant solution. Because of the reflection symmetry (12.45), the relative equilibria come in counter-traveling pairs $u_q(x - ct)$, $-u_q(-x + ct)$.

The relative equilibrium condition for the Kuramoto-Sivashinsky PDE (18.1) is the ODE

$$\tfrac{1}{2}(u^2)_x - c\,u_x + u_{xx} + u_{xxxx} = 0$$ (1.17)

which can be analyzed as a dynamical system in its own right. Integrating once we get

$$\tfrac{1}{2}u^2 - cu + u_x + u_{xxx} = E.$$ (1.18)

[4] This equation can be interpreted as a 3-dimensional dynamical system with spatial coordinate x playing the role of 'time,' and the integration constant E can be interpreted as 'energy,' see sect. 1.6.4.

For $E > 0$ there is rich E-dependent dynamics, with fractal sets of bounded solutions investigated in depth by Michelson [46].

From (1.24) we see that the origin $u(x,t) = 0$ has Fourier modes as the linear stability eigenvectors. The $|k| < \tilde{L}$ long wavelength perturbations of the flat-front equilibrium are linearly unstable, while all $|k| > \tilde{L}$ short wavelength perturbations are strongly contractive. The high k eigenvalues, corresponding to rapid variations of the flame front, decay so fast that the corresponding eigendirections are physically irrelevant. The most unstable mode, nearest to $|k| = \tilde{L}/\sqrt{2}$, sets the scale of the mean wavelength $\sqrt{2}$ of the Kuramoto-Sivashinsky 'turbulent' dynamics, see figure 1.1.
[5]

1.3.2 Relative periodic orbits, symmetries and periodic orbits

Kuramoto-Sivashinsky equation (18.1) is time translationally invariant, and space translationally invariant under the 1-d Lie group of O(2) rotations: if $u(x,t)$ is a solution, then $u(x + d, t)$ and $-u(-x, t)$ are equivalent solutions for any $-L/2 < d \leq L/2$. As a result of invariance under $\tau_{d/L}$, Kuramoto-Sivashinsky equation can have relative periodic orbit solutions with a profile $u_p(x)$, period T_p, and a nonzero shift d_p

$$\tau_{d_p/L} u(x, T_p) = u(x + d_p, T_p) = u(x, 0) = u_p(x).$$ (1.19)

---

[4]Predrag 2019-09-21: Is this an interesting form?

$$\tfrac{1}{2}(u - c/2)^2 + u_x + u_{xxx} = E + c^2/8.$$

[5]Matt 2019-05-13: Spatiotemporal symmetries are discussed in sect. 12.3.2, I think it is worthy to elaborate on the different classes of solutions but I don't think pre-periodic orbits should be referred to as relative periodic orbit solutions with reflection

Relative periodic orbits (1.19) are periodic in $v_p = d_p/T_p$ co-rotating frame, but in the stationary frame their trajectories are quasiperiodic. Due to the reflection symmetry (12.45) of Kuramoto-Sivashinsky equation, every relative periodic orbit $u_p(x)$ with shift d_p has a symmetric partner $-u_p(-x)$ with shift $-d_p$.

Due to invariance under reflections, Kuramoto-Sivashinsky equation can also have relative periodic orbits *with reflection*, which are characterized by a profile $u_p(x)$ and period T_p

$$\sigma u(x + d, T_p) = -u(-x - d, T_p) = u(x + d, 0) = u_p(x), \qquad (1.20)$$

giving the family of equivalent solutions parameterized by d (as the choice of the reflection point is arbitrary, the shift can take any value in $-L/2 < d \le L/2$).

As d is continuous in the interval $[-L/2, L/2]$, the likelihood of a relative periodic orbit with $d_p = 0$ shift is zero, unless an exact periodicity is enforced by a discrete symmetry, such as the dihedral symmetries discussed above. If the shift d_p of a relative periodic orbit with period T_p is such that d_p/L is a rational number, then the orbit is periodic with period nT_p. The likelihood to find such periodic orbits is also zero.

However, due to the Kuramoto-Sivashinsky equation invariance under the dihedral D_n and cyclic C_n subgroups, the following types of periodic orbits are possible:

(a) The periodic orbit lies within a subspace pointwise invariant under the action of D_n or C_n. For instance, for D_1 this is the $\mathbb{U}^+$ antisymmetric subspace, $-u_p(-x) = u_p(x)$, and $u(x, T_p) = u(x, 0) = u_p(x)$. The periodic orbits found in refs. [8, 44] are all in $\mathbb{U}^+$, as the dynamics is restricted to antisymmetric subspace. For $L = 3.5014087480216975$ the dynamics in $\mathbb{U}^+$ is dominated by attracting (within the subspace) heteroclinic connections and thus we have no periodic orbits of this type, or in any other of the D_n–invariant subspaces.

(b) The periodic orbit satisfies

$$u(x, t + T_p) = gu(x, t), \qquad (1.21)$$

for some group element $g \in O(2)$ such that $g^m = e$ for some integer m so that the orbit repeats after time mT_p (see ref. [28] for a general discussion of conditions on the symmetry of periodic orbits). If an orbit is of reflection type (1.20), $\sigma\tau_{d/L}u(x, T_p) = -u(-x - d, T_p) = u(x, 0)$, then it is pre-periodic to a periodic orbit with period $2T_p$. Indeed, since $(\sigma\tau_{d/L})^2 = \sigma^2 = 1$, and the KS solutions are time translation invariant, it follows from (1.20) that

$$u(x, 2T_p) = \sigma\tau_{d/L}u(x, T_p) = (\sigma\tau_{d/L})^2 u(x, 0) = u(x, 0) .$$

Thus any shift acquired during time 0 to T_p is compensated by the opposite shift during evolution from T_p to $2T_p$. Pre-periodic orbits are a hallmark of any dynamical system with a discrete symmetry, where they have a natural interpretation as periodic orbits in the fundamental domain [9, 11].

For any given relative periodic orbit a convenient visualization is offered by the *mean velocity frame*, i.e., a reference frame that rotates with velocity $v_p =$

d_p/T_p. In the mean velocity frame a relative periodic orbit becomes a periodic orbit. However, each relative periodic orbit has its own mean velocity frame and thus sets of relative periodic orbits are difficult to visualize simultaneously.

1.4   Pre-periodic orbits

As discussed in Sect. 1.3.2, a relative periodic orbit will be periodic, i.e., $d_p = 0$, if it either **(a)** lives within the $\mathbb{U}^+$ antisymmetric subspace, $-u(-x, 0) = u(x, 0)$, or **(b)** returns to its reflection or its discrete rotation after a period: $u(x, t+T_p) = gu(x, t)$, $g^m = e$, and is thus periodic with period mT_p.

1.5   Spatially periodic Kuramoto-Sivashinsky

It is not possible to integrate numerically the Kuramoto-Sivashinsky equation on the spatiotemporally doubly infinite domain (18.1). Instead, the standard practice is to confine the system to a spatially L-periodic domain, specify a smooth spatially periodic initial condition $u(x, t) = u(x + L, t)$, and integrate

$$u_t + u_{xx} + u_{xxxx} + u_x u = 0\,, \quad x \in [0, L) \tag{1.22}$$

forward in time on the spatiotemporal cylinder of figure 1.2 (a). Though stable periodic solutions do exist [23], for a generic, sufficiently large spatial domains, all numerical Kuramoto-Sivashinsky solutions exhibit "steady state turbulence" illustrated by figure 1.1.

Smooth, spatially periodic velocity field u is naturally represented in the Fourier space,

$$u(x, t) = \sum_{m=-\infty}^{+\infty} a_m(t)\, e^{i2\pi mx/L}\,, \tag{1.23}$$

with the 1D PDE (1.22) replaced by an infinite set of ODEs for the complex Fourier coefficients $a_m(t)$:

$$\dot{a}_m = (q_m^2 - q_m^4)\, a_m - i\frac{q_m}{2} \sum_{k=-\infty}^{+\infty} a_k a_{m-k} \tag{1.24}$$

where $q_m = 2\pi m/L$. Since $u(x, t)$ is real, $a_m = a_{-mm}^*$, and we can replace the sum by a $m > 0$ sum.

Consider the Kuramoto-Sivashinsky equation (18.1) on a spatiotemporal cylinder $(x, t) \in ([0, L), \mathbb{R})$, defined on a a spatial strip of width L, with spatially periodic boundary condition $u(x, t) = u(x + L, t)$, see figure 1.2 (a). Discretize spatially the Kuramoto-Sivashinsky system by Fourier expanding the
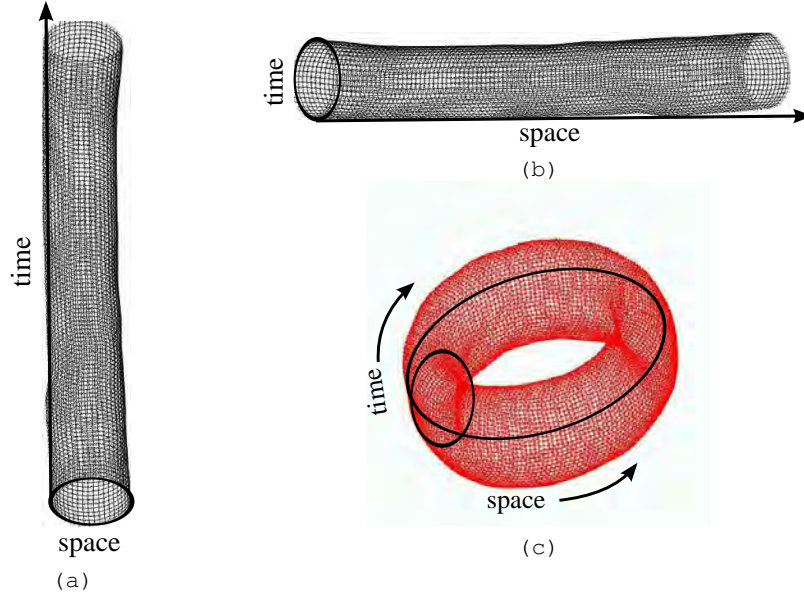
Figure 1.2: (a) The 1D Kuramoto-Sivashinsky equation is usually integrated on a spatiotemporal cylinder of an arbitrary fixed L periodic spatial extent, with time $t \in \{-\infty, \infty\}$; for an example, see figure 1.1. (b) It is also possible to integrate the equation on a spatiotemporal cylinder of an arbitrary fixed T periodic temporal extent, with position ranging over $x \in \{-\infty, \infty\}$, see sect. 1.6. (c) Here we shall seek spatiotemporally invariant 2-torus solutions $u(x, t)$ over a 2-torus of dynamically determined size (L, T) , see sect. 1.6.1.

field $u(x_n, t) = u_n(t)$ over N points of a periodic spatial 1D lattice $x_n = nL/N$,

$$\hat{u}_k(t) = \frac{1}{N} \sum_0^{N-1} u_n(t) e^{-iq_k x_n} = \frac{1}{N} \sum_0^{N-1} u_n(t) e^{-i2\pi kn/N} , \quad q_k = \frac{2\pi k}{L}$$

$$u_n(t) = \sum_{k=0}^{N-1} \hat{u}_k(t) e^{iq_k x_n} = \sum_{k=0}^{N-1} \hat{u}_k(t) e^{i2\pi kn/N} , \tag{1.25}$$

and expressing (18.1) in terms of discrete spatial Fourier modes as N ordinary differential equations (ODEs) in time

$$\frac{d}{dt} \hat{u}_k(t) = (q_k^2 - q_k^4) \, \hat{u}_k(t) - \frac{iq_k}{2} \sum_{k'=0}^{N-1} \hat{u}_{k'}(t) \hat{u}_{k-k'}(t) . \tag{1.26}$$

In the Fourier representation the relative equilibria time dependence is

$$a_k(t) e^{-itcq_k} = a_k(0) . \tag{1.27}$$

Differentiating with respect to time, we obtain the Fourier space version of the relative equilibrium condition (1.17),

$$v_k(a) - iq_k c a_k = 0,\qquad(1.28)$$

which we solve for (time independent) a_k and c.

Temporal stability

To calculate the temporal stability of a spatial equilibrium $\hat{u}_q$ [6] we need to evaluate the stability matrix (the matrix of temporal velocity gradients)

$$A_{ij}(\hat{u}_q) = \left.\frac{\partial \dot{\hat{u}}_i}{\partial \hat{u}_j}\right|_{\hat{u}=\hat{u}_q}.\qquad(1.29)$$

For Kuramoto-Sivashinsky we can compute $A(\hat{u}_q)$ efficiently using the linearity of the Fourier transform, see ref. [10]. Consider the four matrices $\frac{\partial \dot{b}_k}{\partial b_j}, \frac{\partial \dot{b}_k}{\partial c_j}, \frac{\partial \dot{c}_k}{\partial b_j}, \frac{\partial \dot{c}_k}{\partial c_j}$, where the real and imaginary parts of $\hat{u}_k$ are $\hat{u}_k = b_k + ic_k$. For illustration, consider the $b_k = 0$ invariant antisymmetric subspace $\mathbb{U}^+$,

$$\dot{c}_k = v_k(c) = (q_k^2 - q_k^4)\, a_k - \frac{q_k}{2}\sum_{m=-\infty}^{\infty} c_m c_{k-m},\qquad q_k = k/2\pi L.\qquad(1.30)$$

The temporal stability matrix (1.29) restricted to the invariant antisymmetric subspace $\mathbb{U}^+$ follows from (1.30):

$$A_{kj}(c) = \frac{\partial v_k(a)}{\partial c_j} = (q_k^2 - q_k^4)\delta_{kj} + q_k(c_{k-j} - c_{k+j}).\qquad(1.31)$$

For the full state space, consult sect. 6.2 *Calculating stability of equilibria* of Siminos thesis [50].

Kuramoto-Sivashinsky $u = 0$ temporal equilibrium

The Kuramoto-Sivashinsky flat flame front $u(x,t) = 0$ is always a temporal equilibrium of (18.1), whose temporal stability matrix (1.30) is diagonal, with real temporal stability exponents $\lambda^{(k)} = q_k^2 - q_k^4$, the eigenvectors are spatial Fourier modes, and consequently the temporal Jacobian matrix is diagonal as well, $J_{kj}^t = \delta_{kj}\Lambda_k(t),\ \Lambda_k(t) = e^{(q_k^2 - q_k^4)\,t}$.

1.6 Temporally periodic Kuramoto-Sivashinsky

Consider next the case of temporally periodic velocity field

$$u(x,t) = u(x, t+T)\qquad(1.32)$$

---

[6]Predrag 2019-05-16: dropped (or a temporally periodic orbit).

on temporal domain of fixed period T, and any x, i.e., cylinder $(x, t) \in \mathbb{R} \times [0, T)$, see figure 1.2 (b). In order to express Kuramoto-Sivashinsky as a set of first-order PDEs, define four fields

$$(u_0, u_1, u_2, u_3) \equiv (u, u_x, u_{xx}, u_{xxx}) . \tag{1.33}$$

Using the values of the four fields for all $t \in [0, T)$ at a fixed space point x_0, as initial values, one may attempt to determine $u(t, x)$ for any x on a time-periodic strip $t \in [0, T)$ by solving the Kuramoto-Sivashinsky (18.1) rewritten as a set of equations first order in spatial derivatives [7]

$$\frac{\partial}{\partial x} u_0 = u_1 , \quad \frac{\partial}{\partial x} u_1 = u_2 , \quad \frac{\partial}{\partial x} u_2 = u_3 , \tag{1.34}$$
$$\frac{\partial}{\partial x} u_3 = -\frac{\partial}{\partial t} u_0 - u_2 - u_0 u_1 .$$

Given the time-periodic boundary condition (1.32), it is natural to expand the Kuramoto-Sivashinsky field $u(x, t_n) = u_n(x)$ as a temporal Fourier $u(x, t_n) = u_n(x)$ over M points of a periodic temporal lattice $t_n = nT/M$, $n = 0, 1, \cdots, M-1$:

$$u_i(x, t) = \sum_{n=0}^{M-1} \hat{u}_{i,n}(x) \, e^{i\omega_n t_n} , \quad \text{where } \omega_n = 2\pi n/T . \tag{1.35}$$

Rewriting (1.34) in terms of temporal Fourier modes, we obtain $4M$ ordinary differential equations,

$$\frac{\partial}{\partial x} \hat{u}_{0,n} = \hat{u}_{1,n}$$
$$\frac{\partial}{\partial x} \hat{u}_{1,n} = \hat{u}_{2,n}$$
$$\frac{\partial}{\partial x} \hat{u}_{2,n} = \hat{u}_{3,n} \tag{1.36}$$
$$\frac{\partial}{\partial x} \hat{u}_{3,n} = -i\omega_n \hat{u}_{0,n} - \hat{u}_{2,n} - \sum_{n'=0}^{M-1} \hat{u}_{0,n-n'} \hat{u}_{1,n'} .$$

[8]

Integrating Kuramoto-Sivashinsky on a $T = 0$ line

[2016-02-06 Predrag summarize the Michelson [46] case on the spatial $L \rightarrow \pm\infty$ domain. Review the reflection-invariant subspace discussed in Lan's thesis [43] and his thesis-work article [16, 44]. Then set up the full O(2) equivariant case, and describe the O(2)-symmetry reduced case, following refs. [5, 6].]

---

[7]Predrag 2016-07-23: The equations seem correct to me. The notation of refs. [43, 44] is different, but Burak's $u^{(j)}$ fields are easier to keep track of. **2019-05-18 PC** experimenting with u_j format.

[8]Predrag 2016-09-12, 2016-09-23: Checked, except for the range of n'.
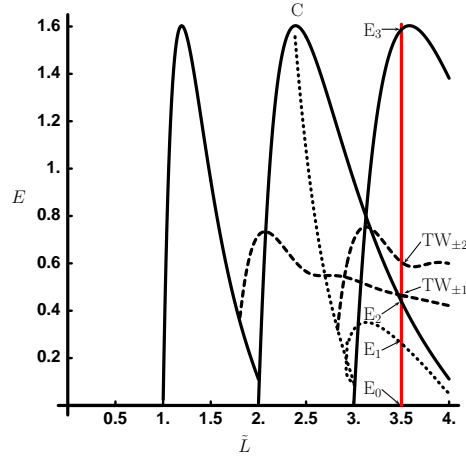
Figure 1.3: The energy (1.38) of the equilibria and relative equilibria that exist up to $L = 22$, $\tilde{L} = 3.5014\ldots$, plotted as a function of the system size $\tilde{L} = L/2\pi$ (additional equilibria, not present at $L = 22$ are given by Greene and Kim [29]). Solid curves denote n-cell solutions E_2 and E_3, dotted curves the GLMRT equilibrium E_1, and dashed curves the relative equilibria $TW_{\pm 1}$ and $TW_{\pm 2}$. The parameter α of refs. [29, 40] is related to the system size by $\tilde{L} = \sqrt{\alpha/4}$. (From Cvitanović, Davidchack and Siminos [10])

If u is a temporal equilibrium, $u = u(x + vt, 0)$ whose spatial profile does not change in time, with a vanishing $u_t = 0$ (for an equilibrium) or a constant traveling wave velocity $u_t = v$ (for a relative equilibrium), one can integrate (18.1)

$$u_t - v = 0 = -\left(u^2/2 - u_x - u_{xxx}\right)_x \qquad (1.37)$$

once over space, and the highest order derivative in (1.34) becomes the third order [16, 43, 44, 46]. We shall refer to this case as the $T = 0$ temporal strip, as specifying $u = u(x_0, 0)$ at $t = 0$ instant suffices to initialize the spatial evolution, which in this case is given by a set of three ODEs and an integration constant, which can be interpreted as the energy density E,

$$E = \tfrac{1}{2}u^2 - cu + u_x + u_{xxx}\,. \qquad (1.38)$$

Computationally, it is more robust to compute E by averaging over L, as in (1.51).

Eqs. (1.34), however, remain a set of four PDEs for any $T > 0$ temporal strip.

Spatial stability of $u = 0$ equilibrium

To calculate the spatial stability of a spatial equilibrium, we need to evaluate the stability matrix of the system in the complex representation (1.36) in terms

of the 16 sub-blocks

$$A_{ij}^{IJ}(\hat{u}) = \frac{\partial \hat{u}_i^{'(I)}}{\partial \hat{u}_j^{(J)}}, \qquad \hat{u}' = \hat{u}_x \,. \tag{1.39}$$

The trivial equilibrium of (1.36) is given by $\hat{u}_j^{(I)} = 0$. In terms of $[M \times M]$ temporal Fourier modes blocks its spatial stability matrix is

$$A^{IJ}(0) = \begin{bmatrix} 0 & 1 & 0 & 0 \\ 0 & 0 & 1 & 0 \\ 0 & 0 & 0 & 1 \\ \text{Diag}\{-i\omega_k\} & 0 & -1 & 0 \end{bmatrix} \tag{1.40}$$

1.6.1 Kuramoto-Sivashinsky on a torus

Here we propose to describe all solutions $u(x,t)$ of Kuramoto-Sivashinsky equation (18.1) as the closure of the union of the set of all prime (non-repeating) invariant 2-tori

$$\begin{aligned} u(x,t) &= u(x,t+T) = u(x+L,t) \\ &= u(x+L,t+T), \quad (x,t) \in ([0,L),[0,T)) \,. \end{aligned} \tag{1.41}$$

Consider a torus (L,T) with spatiotemporally doubly-periodic $u(x,t) = u(x+L,t+T)$, $(x,t) \in ([0,L),[0,T))$, see figure 1.2 (c), and combine the discrete spatial Fourier modes expansion (1.25) with the discrete temporal Fourier modes expansion (1.35). Discretize $u(x_n,t_m) = u_{nm}$ over N points of a periodic spatial lattice $x_n = nL/N$, and M points of a periodic temporal lattice $t_m = mT/M$,

$$\begin{aligned} \hat{u}_{kj} &= \frac{1}{NM} \sum_{n=0}^{N-1} \sum_{m=0}^{M-1} u_{mn}\, e^{-i(q_k x_m + \omega_j t_n)}, \quad q_k = \frac{2\pi k}{L}, \; \omega_j = \frac{2\pi j}{T} \\ u_{mn} &= \sum_{k=0}^{M-1} \sum_{j=0}^{N-1} \hat{u}_{kj}\, e^{i(q_k x_m + \omega_j t_n)}, \end{aligned} \tag{1.42}$$

In its Fourier discretization, Kuramoto-Sivashinsky PDE (1.26) is a set of MN algebraic equations for the spatiotemporal Fourier coefficients $\hat{u}$,

$$\left[i\omega_j - (q_k^2 - q_k^4)\right] \hat{u}_{kj} + i\frac{q_k}{2} \sum_{k'=0}^{M-1} \sum_{j'=0}^{M-1} \hat{u}_{k'j'} \hat{u}_{k-k',j-j'} = 0 \,. \tag{1.43}$$

In other words, we have reduced the problem of either temporal or spatial evolution on a spatiotemporally periodic domain to the fixed point problem of determining an invariant 2-torus, a fixed point in the NM-dimensional state space.

[9] First, however, we must eliminate the temporal translation marginal eigenmode by a Poincaré section, and the spatial translation marginal eigenmode by a slice. Generically, they both can fixed by the first Fourier mode Poincaré section / slice. The Newton method then requires inversion of $1-J$, i.e., $\det(1-J)$, where J is the 2-torus Jacobian matrix. [10]

We can generalize the notion of average 'energy' density (1.51) and apply it to any invariant 2-torus p by also averaging over time

$$E_p = \frac{1}{LT} \oint dx \oint dt \frac{u^2}{2} \,, \tag{1.44}$$

The Fourier space average spatial energy density (1.52) generalized to any spatiotemporal solution (1.42) is then:

$$E = \sum_{k=0}^{N-1} \sum_{n=0}^{M-1} \tfrac{1}{2} |\hat{u}_{kn}|^2 \,. \tag{1.45}$$

1.6.2 Spatiotemporal $u = 0$ equilibrium

[11] Consider the $\hat{u}_{kn} = 0$ equilibrium of (1.43). Its linearization is [12]

$$\begin{aligned}
i\omega_n &= q_k^2 - q_k^4 \\
i\frac{2\pi n}{T} &= \left(\frac{2\pi k}{L}\right)^2 - \left(\frac{2\pi k}{L}\right)^4 \,.
\end{aligned} \tag{1.46}$$

The two special cases are the spatial strip of sect. 1.5, which yields the $2N$ real temporal stability exponents $\lambda_k = i\omega(k)$ for a fixed spatial strip of width L, and the temporal strip of sect. 1.6, which yields the $4 + 8(M - 1)$ complex spatial stability exponents $iq^{\pm,\pm}(n)$ for a fixed temporal strip of period T, as the four solutions of the quartic equation (1.43) for each $i\omega_n$, $n = 0, \pm 1, \pm 2, \pm M/2$:

$$(iq_k)^4 + (iq_k)^2 + i\omega_n = 0 \quad \Rightarrow \quad iq^{\pm,\pm}(n) = \pm\sqrt{(-1 \pm \sqrt{1 - 4i\omega_n})/2} \tag{1.47}$$

[13] Each solution appears twice, corresponding to $(\omega_n, -\omega_n)$, except for

$$q^{\pm,\pm}(0) = \mp i\sqrt{(-1 \pm 1)/2} = (0, 0, -1, 1)\,. \tag{1.48}$$

There are two root magnitudes for each $n \neq 0$, independent of the sign of n:

$$|2q^{\pm,\pm}(n)|^2 = 1 + \sqrt{1 + 16\omega_n^2} \pm \sqrt{1 + 4i\omega_n} \pm \sqrt{1 - 4i\omega_n}\,. \tag{1.49}$$

[9]Matt 2019-05-13: Elimination of space and time translations effectively reduces the codimension of each solution by two, this is undesirable when numerically solving the (**??**) in a least-squares sense

[10]Predrag 2018-04-08: see also sect. 1.6.3.

[11]Predrag 2019-03-16: Incorporate here the spatial evolution stability analysis of blog posts starting with **2016-09-02 Matt Stability of u=0 equilibria**.

[12]Matt 2016-09-12 : Added the factor of i that was missing in (1.43) 2016-09-23 restored signs to match (1.26) and (1.43)

[13]Matt 2016-09-20: I think I should have been looking for iq_k not q_k? If so, it matches the stability exponents of (1.40)

1.6.3 Spatiotemporal stability

Let $u_q(x,t)$ be a doubly-periodic solution of (1.43) on the $(x,t) \in [0,L) \times [0,T)$ torus, a point in the LT-dimensional state space. Add an arbitrary small perturbation field $\delta u(x,t)$, also doubly periodic. Linearize (1.43). The linearized operator acting on $\delta u(x,t)$ must annihilate it, i.e., (WRONG AS IT STANDS)

$$(J(u_q) - \Lambda_j \mathbf{1})\delta u = 0$$

where the Jacobian matrix is the linearization over the whole 2-torus

$$J(\hat{u}_q)_{kn} = \left[i\omega_n - (q_k^2 - q_k^4) \right] \delta_{kn} + iq_k \sum_{k'=0}^{N-1} \sum_{m'=0}^{M-1} \hat{u}_{k'm'} \delta_{k-k',m-m'} . \qquad (1.50)$$

In $d = 1$ case (pure temporal evolution) $\det(J(u_q) - \mathbf{1})$ is the usual period T cycle weight, this time obtained not by integration in time but by evaluating the determinant of the Toeplitz matrix over the whole cycle in one go (this might be familiar to some from the path-integral derivation of Gutzwiller formula cycle weight. With (1.50), $\det(J(u_q) - \mathbf{1})$ is the pattern weight in $d = 2$, and this generates to defining the invariant weight for any d-torus.

1.6.4 Energy transfer rates

In physical settings where the observation times are much longer than the dynamical 'turnover' and Lyapunov times (statistical mechanics, quantum physics, turbulence) periodic orbit theory [9] provides highly accurate predictions of measurable long-time averages such as the dissipation and the turbulent drag [27]. Physical predictions have to be independent of a particular choice of ODE representation of the PDE under consideration and, most importantly, invariant under all symmetries of the dynamics. In this section we discuss a set of such physical observables for the 1-d Kuramoto-Sivashinsky invariant under reflections and translations. They offer a representation of dynamics in which the symmetries are explicitly quotiented out.

⇓PRIVATE

The time-dependent L^2 norm of u,

$$E(t) = \frac{1}{L} \oint dx \, \frac{u^2}{2} , \qquad (1.51)$$

has a physical interpretation [29] as the average energy density. The energy density is intrinsic to the flow, invariant under translations and reflections, and independent of the particular ODE basis set chosen to represent the PDE. In the Fourier space the energy density (1.51) is a diagonalized quadratic norm,

$$E(t) = \sum_{k=-\infty}^{\infty} E_k(t), \qquad E_k(t) = \tfrac{1}{2}|\hat{u}_k(t)|^2 . \qquad (1.52)$$

⇑PRIVATE

The space average of a function $a = a(x,t) = a(u(x,t))$ on the interval L,

$$\langle a \rangle = \frac{1}{L} \oint dx \, a(x,t) \,, \tag{1.53}$$

is in general time dependent. Its mean value is given by the time average

$$\bar{a} = \lim_{t \to \infty} \frac{1}{t} \int_0^t d\tau \, \langle a \rangle = \lim_{t \to \infty} \frac{1}{t} \int_0^t \frac{1}{L} \oint d\tau \, dx \, a(x,\tau) \,. \tag{1.54}$$

The mean value of $a = a(u_q) \equiv a_q$ evaluated on q equilibrium or relative equilibrium $u(x,t) = u_q(x - ct)$ is

$$\bar{a}_q = \langle a \rangle_q = a_q \,. \tag{1.55}$$

Evaluation of the infinite time average (1.54) on a function of a periodic orbit or relative periodic orbit $u_p(x,t) = u_p(x, t + T_p)$ requires only a single T_p traversal,

$$\bar{a}_p = \frac{1}{T_p} \int_0^{T_p} d\tau \, \langle a \rangle \,. \tag{1.56}$$

Equation (18.1) can be written as

$$u_t = -V_x \,, \qquad V(x,t) = \tfrac{1}{2}u^2 + u_x + u_{xxx} \,. \tag{1.57}$$

If u is 'flame-front velocity' then E, defined in (1.18), can be interpreted as the mean energy density. So, even though Kuramoto-Sivashinsky is a phenomenological small-amplitude equation, the time-dependent L^2 norm of u,

$$E = \frac{1}{L} \oint dx \, V(x,t) = \frac{1}{L} \oint dx \, \frac{u^2}{2} \,, \tag{1.58}$$

has a physical interpretation [29] as the average 'energy' density of the flame front. This analogy to the mean kinetic energy density for the Navier-Stokes motivates what follows.

The energy (1.58) is intrinsic to the flow, independent of the particular ODE basis set chosen to represent the PDE. However, as the Fourier amplitudes are eigenvectors of the translation operator, in the Fourier space the energy is a diagonalized quadratic norm,

$$E = \sum_{k=-\infty}^{\infty} E_k \,, \qquad E_k = \tfrac{1}{2}|a_k|^2 \,, \tag{1.59}$$

and explicitly invariant term by term under translations (12.46) and reflections (12.45).

Take time derivative of the energy density (1.58), substitute (18.1) and integrate by parts. Total derivatives vanish by the spatial periodicity on the L domain:

$$\begin{aligned}
\dot{E} &= \langle u_t \, u \rangle = -\langle (u^2/2 + u_x + u_{xxx})_x \, u \rangle \\
&= \langle u_x \, u^2/2 + u_x{}^2 + u_x \, u_{xxx} \rangle \,. \tag{1.60}
\end{aligned}$$

The first term in (1.60) vanishes by integration by parts, $3\langle u_x u^2 \rangle = \langle (u^3)_x \rangle = 0$, and integrating the third term by parts yet again one gets [29] that the energy variation

$$\dot{E} = P - D, \qquad P = \langle u_x{}^2 \rangle, \quad D = \langle u_{xx}{}^2 \rangle \tag{1.61}$$

balances the power P pumped in by anti-diffusion u_{xx} against the energy dissipation rate D by hyper-viscosity u_{xxxx} in the Kuramoto-Sivashinsky equation (18.1).

The time averaged energy density $\overline{E}$ computed on a typical orbit goes to a constant, so the expectation values (1.62) of drive and dissipation exactly balance each out:

$$\overline{\dot{E}} = \lim_{t \to \infty} \frac{1}{t} \int_0^t d\tau \, \dot{E} = \overline{P} - \overline{D} = 0. \tag{1.62}$$

In particular, the equilibria and relative equilibria fall onto the diagonal in reffigf:drivedrag, [14] and so do time averages computed on periodic orbits and relative periodic orbits:

$$\overline{E}_p = \frac{1}{T_p} \int_0^{T_p} d\tau \, E(\tau), \qquad \overline{P}_p = \frac{1}{T_p} \int_0^{T_p} d\tau \, P(\tau) = \overline{D}_p. \tag{1.63}$$

In the Fourier basis (1.59) the conservation of energy on average takes form

$$0 = \sum_{k=-\infty}^{\infty} (q_k^2 - q_k^4) \, \overline{E}_k, \qquad E_k(t) = \tfrac{1}{2} |a_k(t)|^2. \tag{1.64}$$

The large k convergence of this series is insensitive to the system size L; $\overline{E_k}$ have to decrease much faster than q_k^{-4}. Deviation of E_k from this bound for small k determines the active modes. For equilibria the L-independent bound on E is given by Michaelson [46]. The best current bound [3, 24] on the long-time limit of E as a function of the system size L scales as $E \propto L^2$.

1.7 Spatiotemporal symbolic dynamics

The square lattice discretization u_z of a spacetime field $u(x, \tau)$ is obtained by specifying its values $u_{mn} = u(x_m, t_n)$ on lattice points $z = (m, n) \in \mathbb{Z}^2$. Examples are diffusive coupled map lattices [36, 37] and Gutkin *et al.* spatiotemporal cat [12, 30, 31]. In this paper the first index will refer to configuration space, and the second to time. In the Fourier representation $\hat{u}_{kj}$, the first index will refer to the spatial Fourier mode, and the second to the frequency.

There are two lattices at play here: (i) the spacetime discretization (1.42), and (ii) the symbolic dynamics discretization. What follows refers to as yet unattained latter.

Lattices. Consider a 2-dimensional square lattice infinite in extent, with each site labeled by 2 integers $z = (m, n) \in \mathbb{Z}^2$. Assign to each site z a letter

---

[14]Predrag 2019-12-06: Reference 'f:drivedrag' undefined

s_z from a finite alphabet $\mathcal{A}$. A particular fixed set of letters s_z corresponds to a particular lattice state $\mathsf{M} = \{s_z\}$. In other words, a 2-dimensional lattice requires a d-dimensional code $\mathsf{M} = \{m_{n_1 n_2}\}$ for a complete specification of the corresponding state U. The *full shift* is the set of all 2-dimensional symbol blocks that can be formed from the letters of the alphabet $\mathcal{A}$

$$\hat{\Sigma} = \{\{s_z\} : s_z \in \mathcal{A} \quad \text{for all} \quad z \in \mathbb{Z}^2\}. \tag{1.65}$$

Multidimensional shifts. For an autonomous dynamical system, the evolution law f is of the same form for all times. If f is also of the same form at every lattice site, the group of lattice translations, acting along the spatial lattice direction by shift σ, is a spatial symmetry that commutes with the temporal evolution. A temporal mapping f that satisfies $f \circ \sigma j = \sigma \circ f$ along the spatial lattice direction is said to be *shift invariant*, with the associated symmetry of dynamics given by the d-dimensional group of discrete spatiotemporal translations.

Blocks. Let $\mathcal{R}_z \subset \mathbb{Z}^2$ be a finite $[\ell_1 \times \ell_2]$ rectangular lattice region, $\ell_k \geq 1$, whose lower left corner is the $z = (n_1 n_2)$ lattice site

$$\mathcal{R} = \mathcal{R}_n^{[\ell_1 \times \ell_2]} = \{(n_1 + j_1, \cdots n_2 + j_2) \mid 0 \leq j_k \leq \ell_k - 1\}. \tag{1.66}$$

The associated finite block of symbols $s_z \in \mathcal{A}$ restricted to $\mathcal{R}$, $\mathsf{M}_\mathcal{R} = \{s_z | z \in \mathcal{R}\} \subset \mathsf{M}$ is called the block $\mathsf{M}_\mathcal{R}$ of area $n_\mathcal{R} = \ell_1 \ell_2$. For example, a $\mathcal{R} = [3 \times 2]$ block is of form

$$\mathsf{M} = \begin{bmatrix} s_{12} s_{22} s_{32} \\ s_{11} s_{21} s_{31} \end{bmatrix} \tag{1.67}$$

and volume (in this case, an area) equals $3 \times 2 = 6$. In our convention, the first index is 'space', increasing from left to right, and the second index is 'time', increasing from bottom up.

Cylinder sets. While a particular admissible infinite symbol array $\mathsf{M} = \{s_z\}$ defines a point U (a unique lattice state) in the state space, the *cylinder set* $\mathcal{M}_\mathcal{R}$, corresponding to the totality of state space points U that share the same given finite block $\mathsf{M}_\mathcal{R}$ symbolic representation over the region $\mathcal{R}$. For example, in $d = 1$ case

$$\mathcal{M}_\mathcal{R} = \{\cdots a_{-2} a_{-1} . s_1 s_2 \cdots s_\ell a_{\ell+1} a_{\ell+2} \cdots\}, \tag{1.68}$$

with the symbols outside of the block unspecified.

Invariant 2-tori. A state space point is *spatiotemporally periodic* if it belongs to a invariant 2-torus, i.e., its symbolic representation is a block over region $\mathcal{R}$ defined by (16.61),

$$\mathsf{M}_p = \mathsf{M}_\mathcal{R}, \qquad \mathcal{R} = \mathcal{R}_0^{[L \times T]}, \tag{1.69}$$

that tiles the lattice state M periodically, with period L in the spatial lattice direction, and period T in the time lattice direction.

Subshifts. Let $\hat{\Sigma}$ be the full lattice shift (16.60), i.e., the set of all possible lattice state M labelings by the alphabet $\mathcal{A}$, and $\hat{\Sigma}(\mathsf{M}_\mathcal{R})$ is the set of such blocks over a region $\mathcal{R}$. The principal task in developing the symbolic dynamics of a

dynamical system is to determine Σ, the set of all *admissible* itineraries/lattice states, i.e., all states that can be realized by the given system.

Pruning, grammars, recoding. If certain states are inadmissible, the alphabet must be supplemented by a *grammar*, a set of pruning rules. Suppose that the grammar can be stated as a finite number of pruning rules, each forbidding a block of finite size,

$$\mathcal{G} = \{b_1, b_2, \cdots b_k\} \,, \tag{1.70}$$

where a *pruned block* b is an array of symbols defined over a finite $\mathcal{R}$ lattice region of size $[L_1 \times L_2]$. In this case we can construct a finite Markov partition by replacing finite size blocks of the original partition by letters of a new alphabet. In the case of a 1-dimensional, the temporal lattice, if the longest forbidden block is of length $L + 1$, we say that the symbolic dynamics is Markov, a shift of finite type with L-step memory.

Let $\mathsf{U} = \{u_z \in \mathbb{T}^1, \ z \in \mathbb{Z}^2\}$ be a spatiotemporally infinite solution of Kuramoto-Sivashinsky equation (1.42), and let $\mathsf{M} = \{s_z \in \mathcal{A}, \ z \in \mathbb{Z}^2\}$ be its symbolic representation. By the presumed connection between U and M, the corresponding symbolic dynamics block M is unique and admissible, i.e., M defines the unique spatiotemporal state U and vice-versa.

Assume now that only partial information is available, and we know only a finite block of symbols $\mathsf{M}_\mathcal{R} \subset \mathsf{M}$, over a finite lattice region $\mathcal{R} \subset \mathbb{Z}^2$. What information about the local spatiotemporal pattern $\mathsf{U}_\mathcal{R} = \{x_z \in \mathbb{T}^1, z \in \mathcal{R}\}$ does this give us? To be specific, let $\mathcal{R}$ be a rectangular $[\ell_1 \times \ell_2]$ region (see (16.61) for the definition), and let $\mathsf{M}_\mathcal{R}$ be the $[\ell_1 \times \ell_2]$ block of M symbols.

This formalism is necessary for us to interpret results but it cannot inform us of the grammar (rules which dictate admissible combinations) of the symbolic dynamics. To uncover the grammar of the symbolic dynamics we can combine tile solutions numerically and find which combinations are inadmissible. The manner with which we combine such tiles is described in sect. 1.9. This can proceed in an automated manner, taking all possible spatiotemporal combinations of tiles. This portion has not been completed just yet and there are some key details that must be worked out before we can proceed. The main problem is in regards to false negatives. Because the gluing procedure of sect. **??** is a numerical effort, utmost care must be taken in combining solutions. If the tiles are not combined properly, the combination of tiles may be falsely deemed an inadmissible combination which would give us the incorrect grammar or set of pruning rules. We will provide a number of examples of what can go wrong but the list is far from exhaustive. The first example of how a false negative may occur is that if the wrong members of the continuous families are combined then the combination may not converge even though the corresponding symbolic block is admissible. Another example is that when the tiles are being combined there must be some numerical procedure for how to smooth discontinuities where the boundaries of the tiles are conjoined. This typically isn't a huge issue but it definitely has a larger effect on smaller combinations. One must also take into consideration the initial conditions for the extent of the spatiotemporal domain $[T \times L]$. For this we approximate the spa-

tiotemporal domain as simply being the arithmetic average of the dimensions but this may be too crude as it does not take into account how the coupling between tiles affects the domain size. Our last example is a debate between whether to glue progressively larger symbolic blocks together (i.e., the "tiles" are replaced by larger and larger numerically converged invariant 2-tori). Alternatively, we can start each attempt by gluing the indivisible elements, the tiles. These two methods both take combinations of numerically converged invariant 2-tori. The difference lies in the size of the continuous families of solutions. Anecdotal evidence seems to suggest that the tiles exist on a smaller interval of spatial domain sizes $L \pm \epsilon$ when compared to larger invariant 2-tori.

The goal of the previous discussion is to enumerate and describe the "best" method to produce the grammar of the spatiotemporal symbolic dynamics. Once the details are in place, the combinations would be tested in an automated fashion which would hopefully produce a consistent set of pruning rules which could be used to define the inadmissible symbolic blocks of the spatiotemporal symbolic dynamics.

1.8 Examples

Example 1.1. ***Equivariance under infinitesimal transformations.*** *A flow $\dot{x} = v(x)$ is G-equivariant, if symmetry transformations commute with time evolution*

$$v(x) = g^{-1} v(g\,x)\,, \qquad \text{for all } g \in G\,. \tag{1.71}$$

For an infinitesimal transformation the G-equivariance condition becomes

$$v(x) = (1 - \phi \cdot \mathbf{T})\,v(x + \phi \cdot \mathbf{T}x) + \cdots = v(x) - \phi \cdot \mathbf{T}v(x) + \frac{dv}{dx}\,\phi \cdot \mathbf{T}x + \cdots\,.$$

The $v(x)$ cancel, and ϕ_a are arbitrary. Denote the group flow tangent field at x by $t_a(x)_i = (\mathbf{T}_a)_{ij}x_j$. Thus the infinitesimal, Lie algebra G-equivariance condition is

$$t_a(v) - A(x)\,t_a(x) = 0\,, \tag{1.72}$$

where $A = \partial v/\partial x$ is the stability matrix. A learned remark: The directional derivative along direction ξ is $\lim_{t\to 0}(f(x + t\xi) - f(x))/t$. The left-hand side of (1.72) is the Lie derivative of the dynamical flow field v along the direction of the infinitesimal group-rotation induced flow $t_a(x) = \mathbf{T}_a x$,

$$\mathcal{L}_{t_a} v = \left(\mathbf{T}_a - \frac{\partial}{\partial y}(\mathbf{T}_a x) \right) v(y) \bigg|_{y=x}\,. \tag{1.73}$$

The equivariance condition (1.72) states that the two flows, one induced by the dynamical vector field v, and the other by the group tangent field t, commute if their Lie derivatives (or the 'Lie brackets ' or 'Poisson brackets') vanish.

Example 1.2. ***Stability of spatiotemporal patterns.*** *How does one determine the eigenvalues of the finite time local deformation J^t for a general nonlinear smooth flow? The Jacobian matrix is computed by integrating the equations of variations*

$$x(t) = f^t(x_0)\,, \quad \delta x(x_0, t) = J^t(x_0)\,\delta x(x_0, 0)\,. \tag{1.74}$$

The equations are linear, so we should be able to integrate them–but in order to make sense of the answer, we derive this integral step by step.

Consider the case of a general, non-stationary trajectory $x(t)$. The exponential of a constant matrix can be defined either by its Taylor series expansion or in terms of the Euler limit:

$$e^{tA} = \sum_{k=0}^{\infty} \frac{t^k}{k!} A^k = \lim_{m \to \infty} \left(1 + \frac{t}{m} A\right)^m. \tag{1.75}$$

Taylor expanding is fine if A is a constant matrix. However, only the second, tax-accountant's discrete step definition of an exponential is appropriate for the task at hand. For dynamical systems, the local rate of neighborhood distortion $A(x)$ depends on where we are along the trajectory. The linearized neighborhood is deformed along the flow, and the m discrete time-step approximation to J^t is therefore given by a generalization of the Euler product (1.75):

$$
\begin{aligned}
J^t(x_0) &= \lim_{m \to \infty} \prod_{n=m}^{1} (1 + \delta t A(x_n)) = \lim_{m \to \infty} \prod_{n=m}^{1} e^{\delta t \, A(x_n)} \tag{1.76} \\
&= \lim_{m \to \infty} e^{\delta t \, A(x_m)} e^{\delta t \, A(x_{m-1})} \cdots e^{\delta t \, A(x_2)} e^{\delta t \, A(x_1)},
\end{aligned}
$$

where $\delta t = (t - t_0)/m$, and $x_n = x(t_0 + n\delta t)$. Indexing of the product indicates that the successive infinitesimal deformation are applied by multiplying from the left. The $m \to \infty$ limit of this procedure is the formal integral

$$J_{ij}^t(x_0) = \left[\mathbf{T} e^{\int_0^t d\tau A(x(\tau))}\right]_{ij}, \tag{1.77}$$

where $\mathbf{T}$ stands for time-ordered integration, defined *as the continuum limit of successive multiplications (1.76). This integral formula for J^t is the main conceptual result of the present chapter. This formula is the finite time companion of the differential definition (??). The definition makes evident important properties of Jacobian matrices, such as their being multiplicative along the flow,*

$$J^{t+t'}(x) = J^{t'}(x') \, J^t(x), \qquad \text{where } x' = f^t(x_0), \tag{1.78}$$

which is an immediate consequence of the time-ordered product structure of (1.76).

Example 1.3. *Floquet multipliers of a spatiotemporal torus are invariant.* *The 1-dimensional map Floquet multiplier is a product of derivatives over all points around the cycle, and is therefore independent of which periodic point is chosen as the initial one. In higher dimensions the form of the Floquet matrix $J_p(x_0)$ does depend on the choice of coordinates and the initial point $x_0 \in \mathcal{M}_p$. Nevertheless, as we shall now show, the cycle Floquet multipliers are intrinsic property of a cycle in any dimension. Consider the ith eigenvalue, eigenvector pair $(\Lambda_j, \mathbf{e}^{(j)})$ computed from J_p evaluated at a periodic point x,* [15]

$$J_p(x) \, \mathbf{e}^{(j)}(x) = \Lambda_j \, \mathbf{e}^{(j)}(x), \quad x \in \mathcal{M}_p. \tag{1.79}$$

Consider another point on the cycle at time t later, $x' = f^t(x)$ whose Floquet matrix is $J_p(x')$. By the semigroup property (1.78), $J^{T+t} = J^{t+T}$, and the Jacobian matrix at x' can be written either as

$$J^{T+t}(x) = J^T(x') \, J^t(x) = J_p(x') \, J^t(x),$$

---

[15]Predrag : fix scale in figure **??**, refer to it

or $J^t(x)\,J_p(x)$. Multiplying (1.79) by $J^t(x)$, we find that the Floquet matrix evaluated at x' has the same Floquet multiplier,

$$J_p(x')\,\mathbf{e}^{(j)}(x') = \Lambda_j\,\mathbf{e}^{(j)}(x')\,,\quad \mathbf{e}^{(j)}(x') = J^t(x)\,\mathbf{e}^{(j)}(x)\,, \qquad (1.80)$$

but with the eigenvector $\mathbf{e}^{(j)}$ transported along the flow $x \to x'$ to $\mathbf{e}^{(j)}(x') = J^t(x)\,\mathbf{e}^{(j)}(x)$. Hence, in the spirit of the Floquet theory one can define time-periodic eigenvectors (in a co-moving 'Lagrangian frame')

$$\mathbf{e}^{(j)}(t) = e^{-\lambda^{(j)}t}\,J^t(x)\,\mathbf{e}^{(j)}(0)\,, \qquad \mathbf{e}^{(j)}(t) = \mathbf{e}^{(j)}(x(t))\,,\ \ x(t) \in \mathcal{M}_p\,. \qquad (1.81)$$

J_p evaluated anywhere along the cycle has the same set of Floquet multipliers $\{\Lambda_1, \Lambda_2, \cdots, 1, \cdots, \Lambda_{d-1}\}$. As quantities such as $\mathrm{tr}\,J_p(x)$, $\det J_p(x)$ depend only on the eigenvalues of $J_p(x)$ and not on the starting point x, in expressions such as $\det\big(\mathbf{1} - J_p^r(x)\big)$ we may omit reference to x,

$$\det\big(\mathbf{1} - J_p^r\big) = \det\big(\mathbf{1} - J_p^r(x)\big) \quad \textit{for any } x \in \mathcal{M}_p\,. \qquad (1.82)$$

We postpone the proof that the cycle Floquet multipliers are smooth conjugacy invariants of the flow; time-forward map (1.80) is the special case of this general property of smooth manifolds and their tangent spaces.

1.9 Tiling spatiotemporal solutions

1.9.1 Tiling state space

The crux of our hypothesis is the ability to enumerate fundamental spatiotemporal invariant 2-tori that will comprise a symbolic dynamical alphabet. The defining quality of these building block solutions, or "tiles", is that they are invariant 2-torus solutions with minimal spatiotemporal extent that represent fundamental patterns seem frequently in large spatiotemporal simulations. The size of these tiles are on the order temporal and spatial scales of the Kuramoto-Sivashinsky equation. Their importance is two fold, Firstly, from the theory of cycle expansions for dynamical systems [1] it is known that the shortest cycles are the most important of all cycles. Secondly, even though the complexity of solutions grows exponentially in each continuous direction this is not due to emergence of unique spatiotemporal patterns but rather combinations of spatiotemporal tiles. In other words, these tiles serve as the "building blocks" for all invariant 2-tori.

Analyzing fundamental geometrical shapes and how they combine is not a new idea. The importance of time invariant sets and exact coherent structure has been known for quite some time in dynamical systems. What is new is to treat continuous time as merely another dimension which parameterizes our special patterns, the tiles. That is to say, there is nothing special about time and it should be treated on the same footing as space. The identification and utilization of special patterns appears in other disciplines such as the study of topological defects in nematic liquid crystals [22] and cosmology [52], as well

as the study of motifs in complex networks [45, 47]. The patterns are important for different reasons in the different fields of study, but all are relevant and connected for our study. In the case of liquid crystals the difference of defects from "regular" patterns is that they carry an energy cost. Cosmologically, topological defects are suspected as possible sources for the structures seen in the universe today [2]. Motifs in complex networks are important because they represent subgraphs which appear much more frequently than one would expect in randomized networks, and certain patterns seem to be specific to different categories of networks (biological, technological, etc.) [47]. There are many different perspectives with which we can view the Kuramoto-Sivashinsky equation. Perhaps we should view the infinite spacetime problem as structure imposed on an infinite isotropic field by virtue of linear instability of the equations. Or we could view it from a liquid crystal point of view and say that the patterns present themselves in the manner that they do because of energetically favorable configurations. Using network motifs we could generalize these ideas to other equations and claim that it is the equations which determine the motifs and statistics thereof. There are many fascinating concepts at play in our formulation but sadly our time is not infinite so we shall try to focus on the rules that determine which combinations of tiles are admissible. These concepts provide strong foundation for our theory; all three examples strongly reinforce the fact that in many systems there are special patterns whose importance stands far above the rest.

In order to progress this theory we first need to actually find a collection of tile solutions. The first method to find tiles is simply to search for them directly, for instance by applying the methods formed in sect. **??** to initial conditions defined on small spatiotemporal domains. There is no harm in doing this, but we apply a more supervised technique which is much more effective.

1.9.2 Tile extraction

To find tiles in a smarter and more guided manner, we use scalar fields directly clipped from converged invariant 2-torias our initial conditions. First we identify a pattern which appears frequently in the library of converged invariant 2-toriand is nearly doubly-periodic. After a pattern has been specified we choose a invariant 2-torus which contains this pattern and proceed to numerically clip if from the invariant 2-torus. Specifically, If the invariant 2-torus has spatiotemporal dimensions $[L, T]$ and is given numerically by a rectangular discretization $[M, N]$ with M points in space and N points in time, then candidate tile is a discretization subdomain $[\tilde{M}, \tilde{N}]$, $\tilde{M} \leq M$, $\tilde{N} \leq N$, with a spatiotemporal invariant 2-torus whose initial periodicities are guessed to be $[\tilde{L}, \tilde{T}] = \left[\frac{\tilde{M}L}{M}, \frac{\tilde{N}L}{N} \right]$. This initial condition for the tile is clearly not going to be doubly periodic else it would have covered the original invariant 2-torus. Therefore, there are going to be discontinuities introduced at the boundaries which need to be accounted for numerically. A cheap method to do so is to truncate the spatiotemporal Fourier spectrum before passing the initial con-

dition to our numerical methods described in sect. **??**,sect. **??**. If the numerical optimization routine is successful then we add the converged invariant 2-torus to the collection of known tiles. Because tiles are few in number, one can and should visually inspect the converged tile to ensure that it indeed a realization of the desired pattern, as it is possible to converge to larger invariant 2-toriwhich are not themselves tiles (this usually happens as a result of the domain size changing over the course of the optimization process).

Extracting tiles

By following this schematic we were able to converge a number of initial conditions, some of which are spatiotemporal tiles. This process is summarized in the Figures 18.2, 18.1, 18.3, 18.4, 18.5, 17.12, 17.13 and 17.14 which show (a) the initial invariant 2-torus, (b) initial guess extracted as a subdomain, and (c) the final, converged tile (invariant 2-torus).

Sequential subdomain extraction

While typically robust enough to find tiles in "one step",i.e.with a single initial condition, we can also employ our numerical methods iteratively to find tiles by sequentially converging to progressively smaller subdomains. We demonstrate this process in its entirety in figure 18.6; the result is the same as figure 18.5 but it is still a good example. The advantage of this method is that by converging progressively smaller invariant 2-tori we increase our chances of converging to a spatiotemporal tile. Numerically, this is because the invariant 2-tori adjust themselves to account for the change in spatiotemporal domain size and so each succeeding subdomain becomes a more "accurate" initial condition. Note that this procedure is only applicable if there is a sequence of subdomains which are approximately doubly periodic; choosing an arbitrary subdomain would likely fail. A disadvantage of this method is, of course, that the repeated computations require more time and, in our implementation, the selection of each subdomain is done manually.

Ternary tile alphabet

As one would expect from "fundamental" solutions, the patterns represented by our tiles can be described very succinctly. Typically, each of the tiles contains no more than two wavelengths as can be seen by the red-blue (crest-trough) pairs in the corresponding scalar fields. Because of this we will refer to them by shorthand names that capture their general behavior and makes a connection to pattern names which, as we shall see, are relatively common in the study of fluid flows [35, 48, 54]. In the spirit of topological defects [22, 41, 45] we shall give the tiles new names so that they can be easily identified and referred to. The first pattern is the single wavelength equilibrium solution which we shall refer to as the "streak" ((a) from figure 1.10. The streak tile is the smallest tile solution, as it has no temporal dimension because its an equilibrium solution

Figure 1.4: (a) $[L_a, T_a] = [3.50 \cdots, 94.59 \cdots]$ fundamental domain of an already computed invariant 2-torus with spatial translation symmetry. (b) The clipped-out $[L_b, T_b] = [2, 17]$ subdomain used the initial guess for the fundamental domain of a shift-reflect symmetric tile. (c) The converged $[L_c, 2T_c] = [2.07 \cdots, 18.46 \cdots]$ invariant 2-torus with spatial translation symmetry.

Figure 1.5: (a) $[L_a, T_a] = [3.50 \cdots, 94.59 \cdots]$ fundamental domain of an already computed invariant 2-torus with spatial translation symmetry. (b) The clipped-out $[L_b, T_b] = [2.2, 20]$ subdomain used the initial guess for the fundamental domain of a shift-reflect symmetric tile. (c) The converged $[L_c, 2T_c] = [2.07 \cdots, 15.46 \cdots]$ invariant 2-torus with spatial translation symmetry.
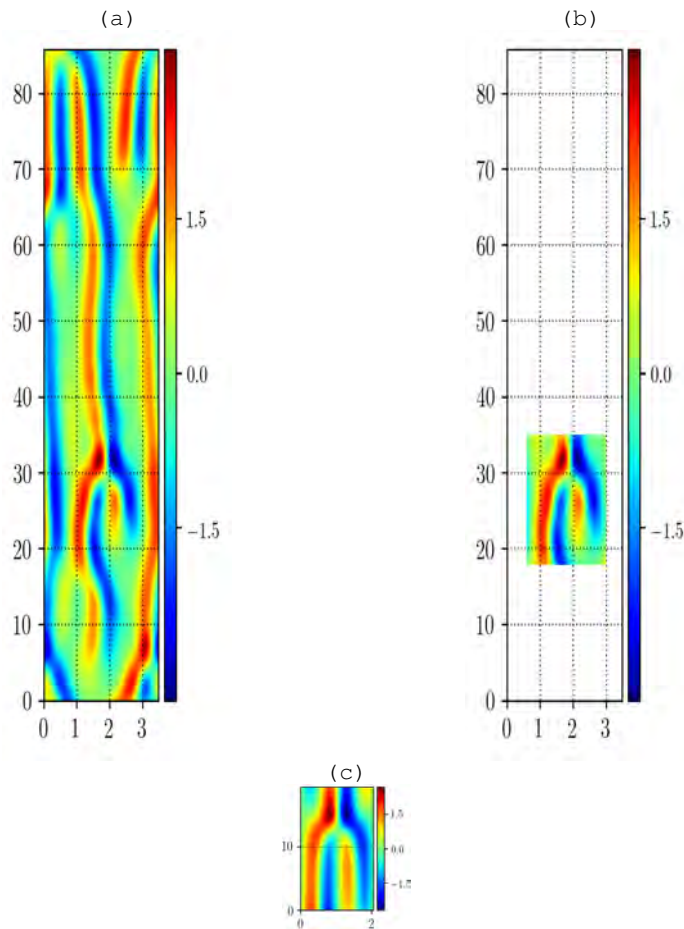
Figure 1.6: (a) $[L_a, T_a] = [3.50 \cdots, 85.73 \cdots]$ fundamental domain of an already computed invariant 2-torus with spatiotemporal shift-reflection symmetry. (b) The clipped-out $[L_b, T_b] = [2.6, 17]$ subdomain used the initial guess for the fundamental domain of a shift-reflect symmetric tile. (c) The converged $[L_c, T_c] = [2.06 \cdots, 19.92 \cdots]$ invariant 2-torus with spatial translation symmetry.
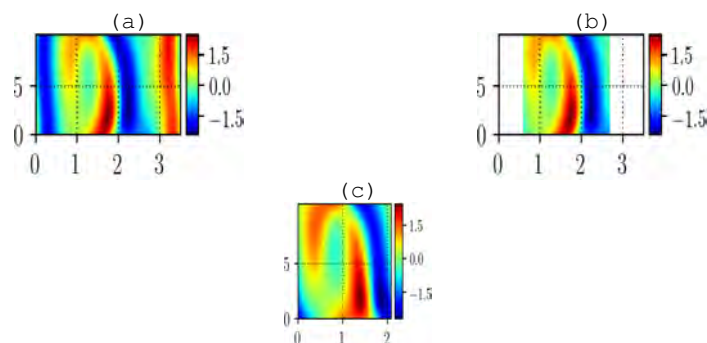
Figure 1.7: (a) $[L_a, T_a] = [3.50\cdots, 10.25\cdots]$ fundamental domain of an already computed invariant 2-torus with spatiotemporal shift-reflection symmetry. (b) The clipped-out $[L_b, T_b] = [2.1, 10.5]$ subdomain used the initial guess for the fundamental domain of a shift-reflect symmetric tile. (c) The converged $[L_c, T_c] = [2.08\cdots, 9.22\cdots]$ invariant 2-torus with spatial translation symmetry.

but it also has the smallest spatial extent, $\frac{L}{2\pi} \approx 1.02$. As seen by its near integer value, this spatial extent happens to be in line with the important spatial scale of the Kuramoto-Sivashinsky equationThe streak tile was found directly as an equilibrium solution without any extraction efforts. Although it has no temporal extent, we shall still refer to this as a invariant 2-torus because the shadowing events *do* have temporal variations. There seems to be no single time scale for these shadowing events, but rather the time scale is determined by the local interactions with its neighbors. In this way the streak almost plays role as a space filler and perhaps we should view spatiotemporal state space as defects inserted into an infinite equilibrium solution.

Next we have a tile whose behavior is best summarized as a two-to-one wavelength merger. Two wavelengths propagate in time while adjacent spatially; eventually turning inwards and colliding such that only the "outer" pair of remain and form a single wavelength. We shall refer to this pattern as a "merger". This pattern is strikingly similar to what is know as "edge dislocations" [41] but we prefer to refer to it as a "merger" because in our system this pattern does not arise as the result of physical strain. This tile, ((b) figure 1.10), is a invariant 2-torus with dimensions $L \approx 2.07$, $T \approx 18.5$ and continuous spatial translation symmetry parameter value approximately equal to a quarter of the domain size $\sigma \approx 0.2529L$. This tile might be the most important out of all as we shall see

The last tile consists of a pair of wavy streaks. This is exactly how it sounds; a streak pattern which waves back and forth in the spatial direction before returning to its original position. Not only is it a invariant 2-torus but it is a invariant 2-torus that lies in the reflection invariant subspace sect. 12.3.2, which allows us to think of the tile in one of two ways. We could consider a single
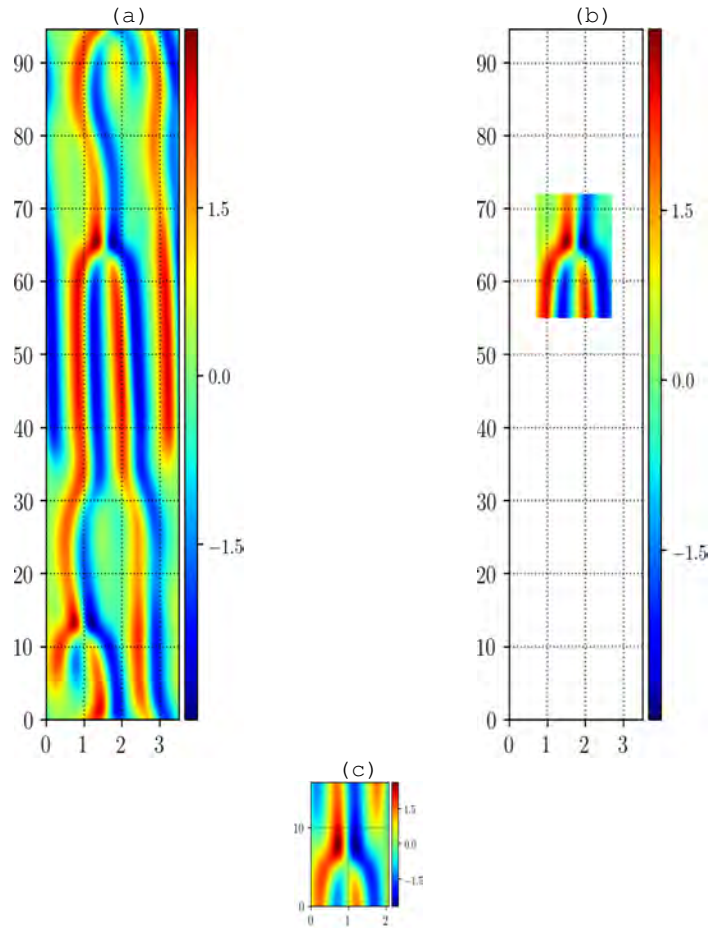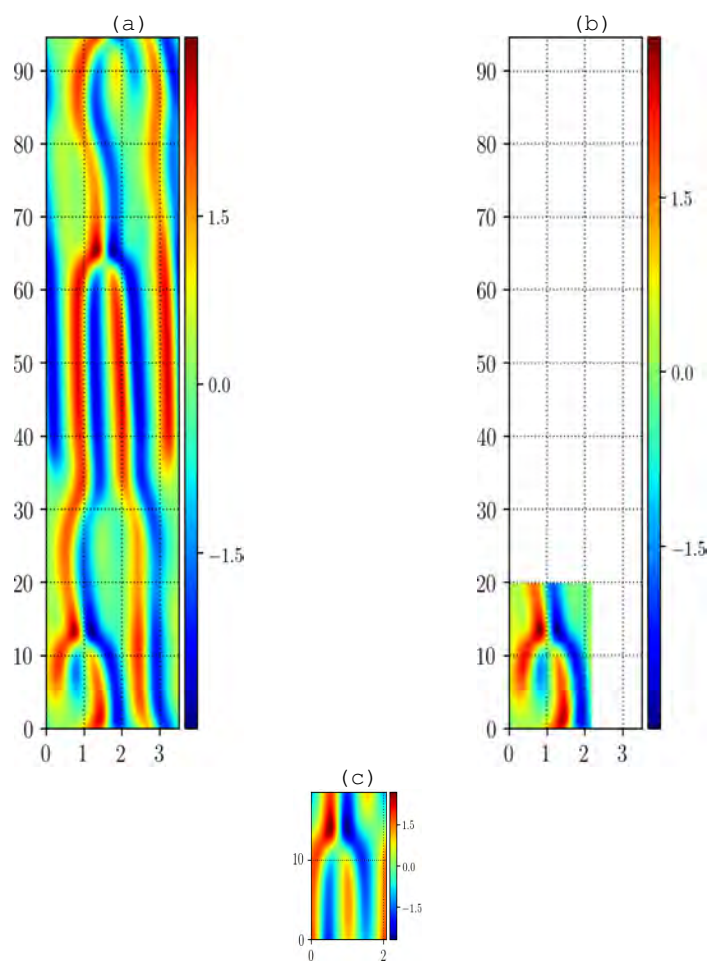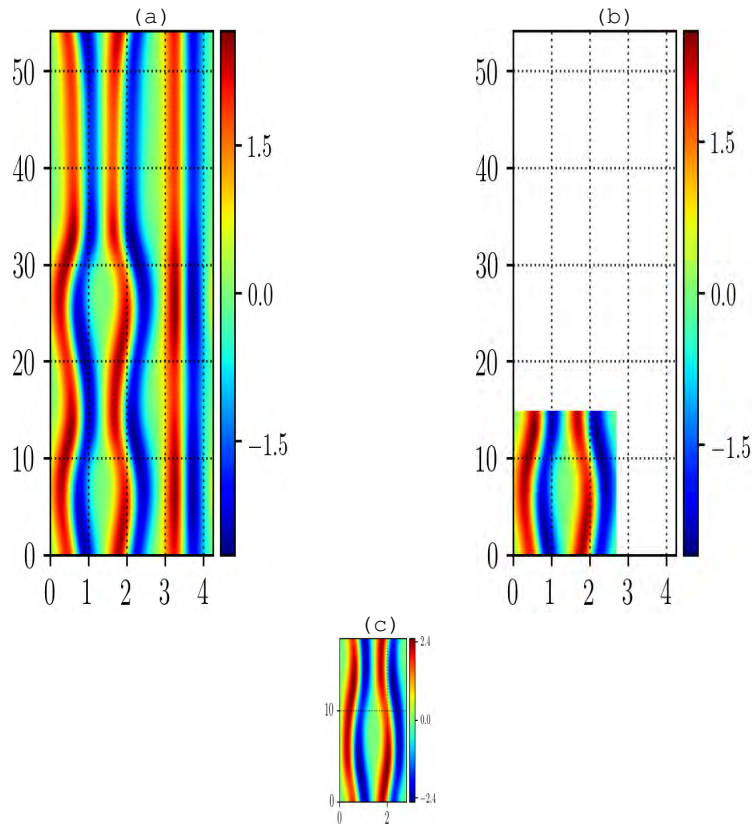
Figure 1.8: (a) $[L_a, T_a] = [4.25 \cdots, 54.13 \cdots]$ fundamental domain of an already computed invariant 2-torus with spatiotemporal shift-reflection symmetry. (b) The clipped-out $[L_b, T_b] = [2.7, 15]$ subdomain used the initial guess for the fundamental domain of a shift-reflect symmetric tile. (c) The converged $[L_c, T_c] = [2.90 \cdots, 17.95 \cdots]$ full reflection symmetric invariant 2-torus.
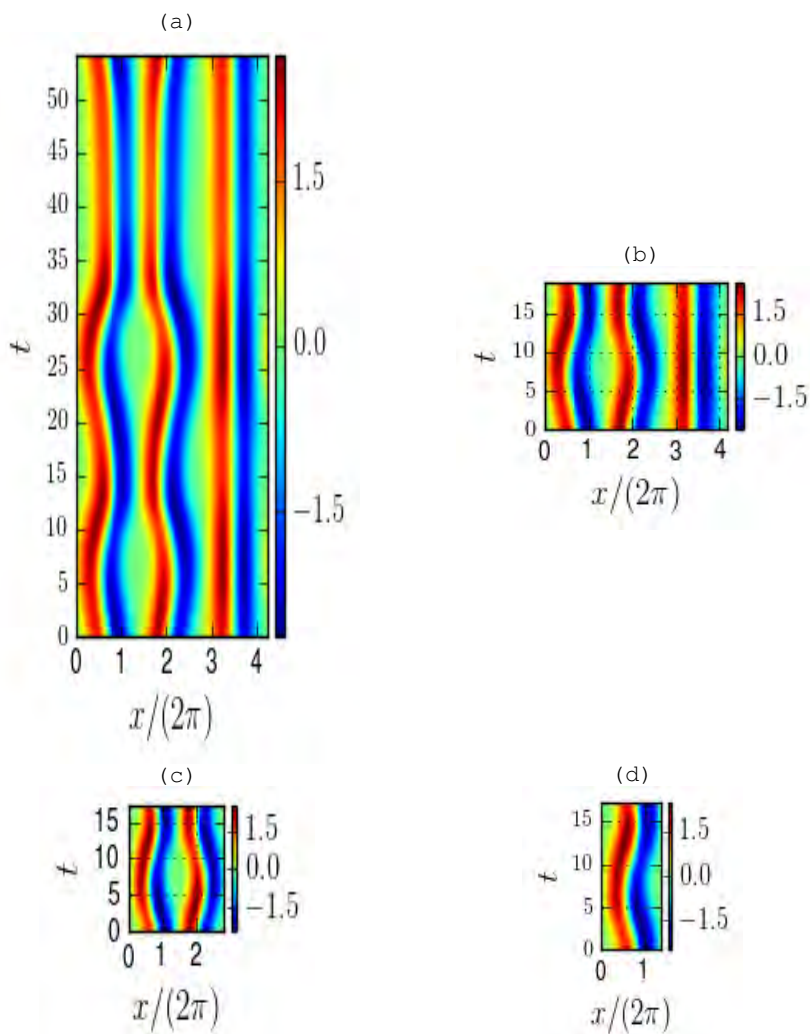
Figure 1.9: Sequential subdomain extraction to find tiles. (a) A periodic orbit from the collection of new solutions $[L_a, T_a] = [4.25\cdots, 54.12\cdots]$. By taking progressively smaller subdomains (b)-(d) and numerically converging them to invariant 2-tori at each step, we are able to find the smallest subdomain of (a) which can be converges to a invariant 2-torus, namely (d). (b)$[L_b, T_b] = [4.16\cdots, 18.93\cdots]$ (c)$[L_c, T_c] = [2.79\cdots, 17.14\cdots]$ (d)$[L_d, T_d] = [1.39\cdots, 17.14\cdots]$
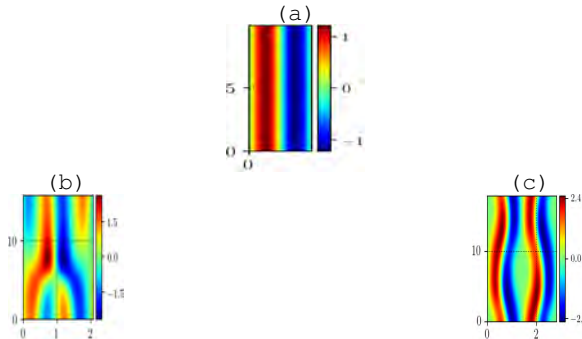
Figure 1.10: (a) The "streak tile". Converged equilibrium $L_s = 1.02 \cdots$ demonstrating the fundamental streak pattern. There is no temporal variation or scale but the solution $u(x)$ is plotted as a spatiotemporal function simply to be consistent with other spatiotemporal figures. (b) The "merger" tile. Converged invariant 2-torus depicting two-to-one wavelength merging. This tile is a relative periodic invariant 2-torus $[L_m, T_m] = [2.07\cdots, 15.86\cdots]$ with spatial shift parameter $\tau_x \approx 1.06$. This represents a spatial shift approximately equal to a quarter of the domain. (c) The "gap" tile. Converged invariant 2-torus depicting "wavy streak" behavior. $[L_d, T_d] = [2.80\cdots, 17.14\cdots]$ (plotted in the full state space for reasons described in sect. 1.9).

wavelength to be the tile; there are a number of reasons why we avoid this. Firstly, sometimes it isn't clear how to distinguish a single wavy streak from a regular streak deformed by coupling to its neighbors. Numerically, these patterns are so similar that it is possible to converge to the same solution using either type of streaks; one would merely increase the cost functional value as its more "out of place" that the other. It might be hard to distinguish between a single wavy streak and a regular streak, but when you have a pair of wavy streaks it is quite clear, as they are symmetry partners which are adjacent to one another. Secondly, it seems that the pair of wavy streaks is shadowed more often, indicating that it is in fact the representation that we should use. We will refer to the tile comprised of two wavy streaks as the "gap" tile, because when two wavy streaks repel each other, it creates a region of spacetime where the magnitude of the scalar field is small,i.e., a "gap" in the scalar field. This can be seen in plot (c) of figure 18.6. The gap tile shown in figure 1.10 has dimensions $L \approx 2.81, T \approx 17.95$.

The merger tile captures a key spatiotemporal process in a minimal amount of information. Let us transgress back into a dynamical systems context to elaborate. Performing linear stability analysis on the Kuramoto-Sivashinsky equation shows that there is a range of modes which are linearly unstable [10]. In addition to this, there exists a mode which is the most unstable such that the number of wavelengths fluctuates around the most unstable wavenumber as a function of time. The number of wavelengths is calculated by taking the

average of the number of local minima and maxima (which exceed a certain tolerance value in magnitude to avoid extraneous counting). The fluctuation of this of quantity indicates that there are wavelengths being both "annihilated" and "created" in time. The merger tile encapsulates both of these processes. Previously, we described the merger tile as being a two to one wavelength merger; this is the "annihilation" process in action. There's slightly more to the story, however, as very shortly after the wavelength merger a new wavelength is born in the vacant space. This can be seen in the depiction of the converged merger tile (c) from figure 18.1. These three tiles provide us with an entirely new perspective of how to view the Kuramoto-Sivashinsky equation, which is that the spatiotemporal behavior of solutions seems to be described by the interaction of crest-trough pairs. Specifically, the streak tile describes how wavelengths remain constant in time, the gap tile describes how wavelengths repel each other and the merger tile captures how wavelengths attract and combine. Technically, on a small spatiotemporal domain the gap tile can be interpreted as both attracting and repelling because the domain is periodic. Therefore, an alternative description of the gap tile is that it represents wavelength attraction without the wavelength merger. This emergent behavior seems to be unique to the spatiotemporal formulation or is at least not obvious by inspection of the Kuramoto-Sivashinsky equation (18.1) alone.

The largest concern regarding this formulation is whether or not our alphabet is missing a tile. This would likely be devastating as we know from the work on cycle expansions that short cycles has the greatest importance [8]. The only evidence we have to indicate that we have found all tiles is that we simply have not found any more unique tiles despite a thorough search. Most trials converge to known tiles (up to symmetry operations). This can be seen in the comparison between converged invariant 2-tori in figure 1.11.

There are also examples which do not converge to tiles but to combinations of tiles. Examples include figure 17.12, figure 17.13, figure 17.14. These attempts all started with what appears to be two patterns conjoined in time. One might ask why we chose these as tile candidates given they have more than one constituent pattern; our reason is that they were frequently shadowed and we did not know *a priori* what tiles existed, hence their consideration as tile candidates. Their respective converged invariant 2-tori all appear to be two (symmetry related) copies of the merger tile conjoined temporally, indicating that the initial conditions were indeed two separate patterns conjoined in time. As just mentioned, in the converged invariant 2-tori the two conjoined patterns are much more similar that in the initial conditions. The explanation for this process can be explained by the discovery that tiles do not exist as stand alone solutions; rather, they exist in continuous families (related by smooth deformations) parameterized by spatiotemporal domain size parameters L and T.

[16] [17]

---

[16]Predrag 2019-09-20: Length units (ticks on x-axis) in figure 17.14 (vs. the numbers stated in the caption) seem screwy, they should be in units of $\tilde{L} = L/2\pi$, or (but I do not think that would be good) in "mean wavelength" units $2\pi\sqrt{2}$, see figure 1.1. Or are you plotting lengths in L units?

[17]Predrag 2019-05-16: Perhaps replace spatial period everywhere with $\tilde{L} = L/2\pi$, define $\tilde{L}$
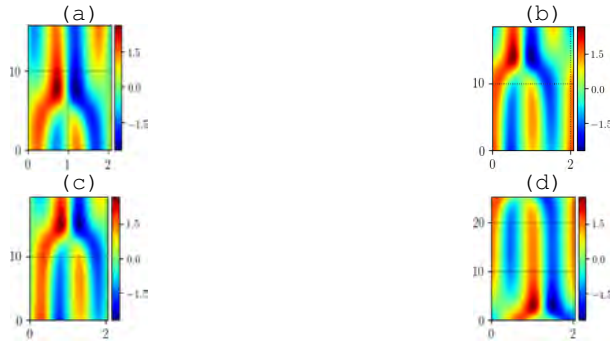
Figure 1.11: (a) Invariant 2-torus from figure 18.1(c), $[L_a, 2T_a] = [2.07\cdots, 18.46\cdots]$ invariant 2-torus with spatial translation symmetry. (b) Invariant 2-torus from figure 18.2(c), $[L_c, 2T_c] = [2.07\cdots, 15.46\cdots]$ invariant 2-torus with spatial translation symmetry. (c) Invariant 2-torus from figure 18.3(c), $[L_c, T_c] = [2.06\cdots, 19.92\cdots]$ invariant 2-torus with spatial translation symmetry. (d)Invariant 2-torus resulting from performing pseudo-arclength continuation on figure 18.4(c). Final invariant 2-torus has $[L_c, T_c] = [2.06\cdots, 23.21\cdots]$ and spatial translation symmetry.

1.9.3 Continuous families of tiles

The streak, gap, and merger tiles will be used to construct known and new solutions. This of course supports our claim that invariant 2-tori and tiles are shadowing partners. Tiles are never exhibited exactly in invariant 2-tori, however, because of spatiotemporal coupling. Another way of phrasing this is that the shadowed tiles deform in order to fit on a spatiotemporal domain and obey the Kuramoto-Sivashinsky equation simultaneously. This deformation makes it hard to quantify the shadowing process as we lack a good metric. This coupling also creates difficulties and raises questions when combining tiles to form initial conditions as we shall see in sect. **??**. Through some investigation it seems that these "deformations" are in fact various instances of continuous families. This can be shown to by applying pseudo-arclength continuation of the tiles with respect to the parameters T, L. One such related pair of tiles that appear different but are in fact representations of the same pattern are the converged invariant 2-tori from figure 18.1 and figure 18.4. Their comparison by numerical continuation is shown in figure 1.11, along with other similar patterns. In summary, the comparison of figure 1.11 demonstrates that the tiles appear identical up to translational symmetries; we could fix the phases of the spatiotemporal Fourier coefficients to demonstrate their equality but we would rather stress that the same tile can be represented in numerous ways. Not only is there a continuous family parameterized by the spatiotemporal area, but also for each spatiotemporal area there is a group orbit (states reachable

---

with a numbered equation early on. Than have to do it for the time $T/2\pi$ as well...?
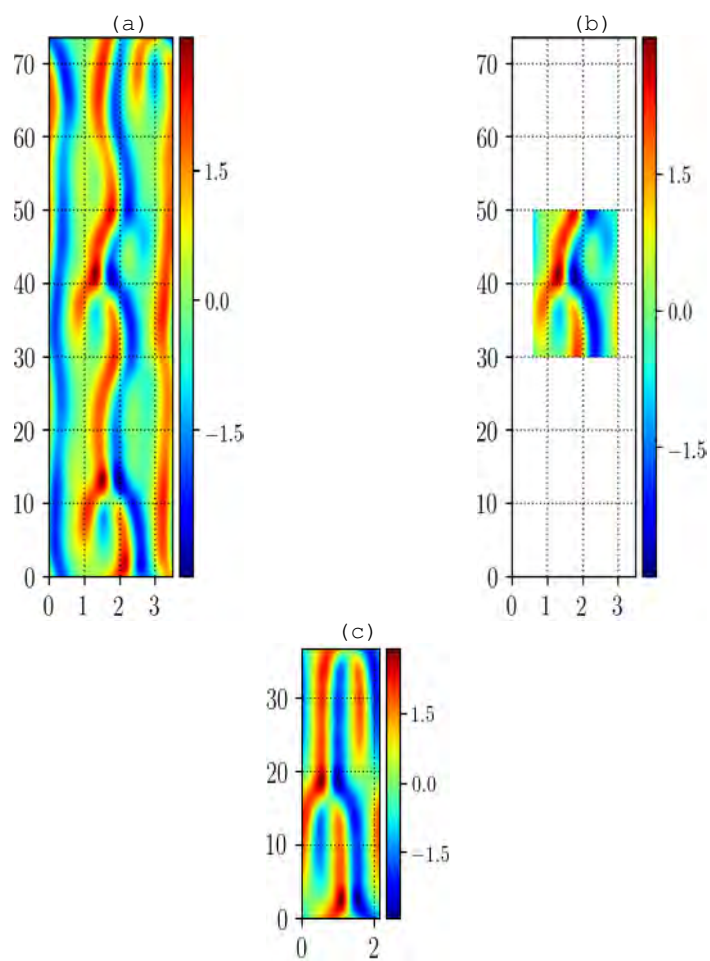
Figure 1.12: (a) $[L_a, T_a] = [3.49 \cdots, 73.52 \cdots]$ fundamental domain of an already computed invariant 2-torus with spatiotemporal shift-reflection symmetry. (b) The clipped-out $[L_b, T_b] = [2.4, 20]$ subdomain used the initial guess for the fundamental domain of a shift-reflect symmetric tile. (c) The converged $[L_c, T_c] = [2.09 \cdots, 52.00 \cdots]$ full shift-reflect symmetric invariant 2-torus.
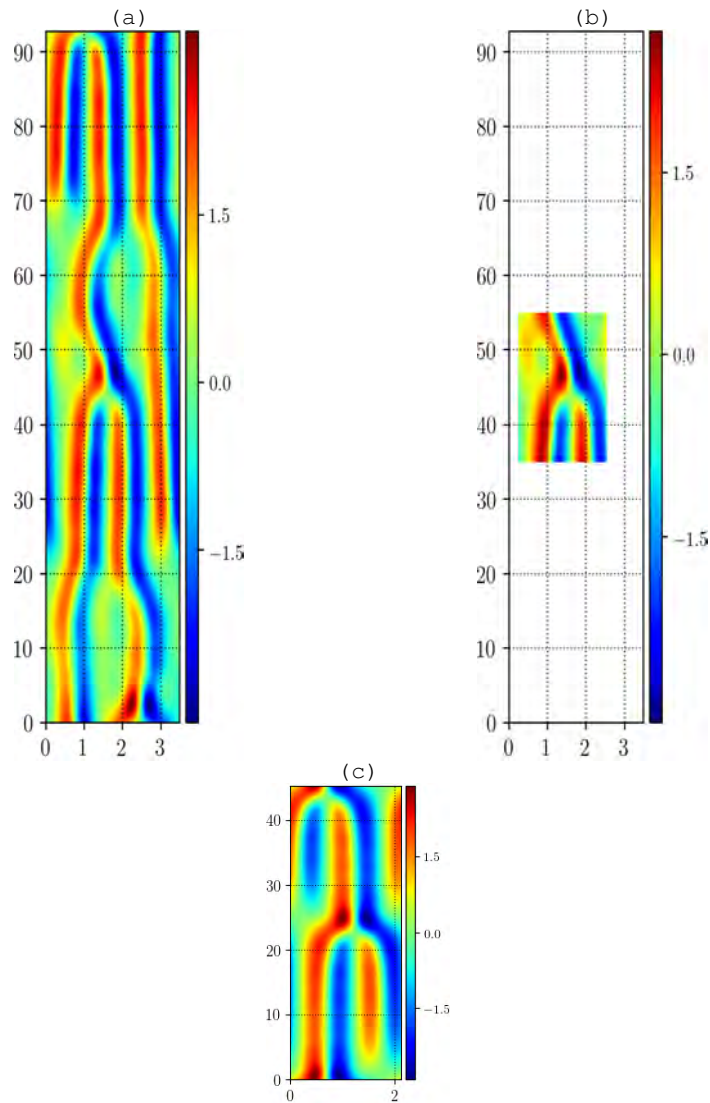
Figure 1.13: (a) $[L_g, T_g] = [3.49\cdots, 92.77\cdots]$ fundamental domain of an already computed invariant 2-torus with spatiotemporal shift-reflection symmetry. (b) The clipped-out $[L_g, T_g] = [2.3, 20]$ subdomain used the initial guess for the fundamental domain of a shift-reflect symmetric tile. (c) The converged $[L_g, T_g] = [2.12\cdots, 45.25\cdots]$ full shift-reflect symmetric invariant 2-torus.
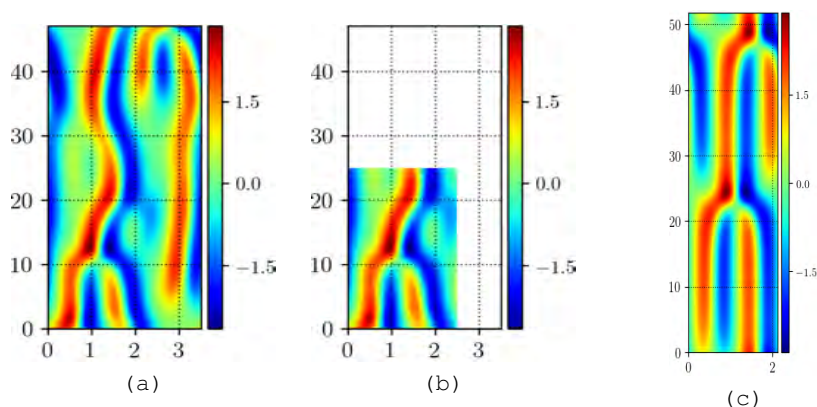
Figure 1.14: (a) $[L_0, T_0] = [3.49 \cdots, 47.77 \cdots]$ fundamental domain of an already computed invariant 2-torus with spatiotemporal shift-reflection symmetry. (b) The clipped-out $[L_g, T_g] = [2.06, 25]$ subdomain used the initial guess for the fundamental domain of a shift-reflect symmetric tile. (c) The converged $[L_p, 2T_p] = [2.12 \cdots, 51.73 \cdots]$ full shift-reflect symmetric invariant 2-torus.

by symmetry operations) resulting from continuous and discrete symmetries. The comparison of figure 18.1 and figure 18.4 we have demonstrated allows us to reinterpret the results from figure 17.12, figure 17.13, figure 17.14. This new interpretation is that the initial conditions shadow the same tile *family* twice; not the same exact tile twice. Upon hindsight this actually makes a lot of sense as no shadowing events are ever identical. Perhaps this should have been obvious from the start because larger invariant 2-tori also exist in continuous families, but the reverse idea might be more enlightening. For instance, it might be more correct to say that invariant 2-tori exist in continuous families *because* the tiles exist in continuous families, not the other way around. This interpretation seems to have more impact but it is not without bias as it supports our tiling methods, however, showing that invariant 2-tori can be constructed from specific tile combinations provides some good evidence. To account for continuous families of tiles we must adjust our description of our spatiotemporal symbolic dynamics. The two-dimensional symbolic blocks (one dimension for each continuous symmetry) now consist of "lattice sites" which are not of the conventional discrete type but rather each site will represent a invariant 2-torus solution defined on a malleable spatiotemporal domain parameterized by T, L, σ. This is perhaps what we should have expected to begin with, as the deformability aligns itself with the principle of shadowing. The shadowing of spatiotemporal invariant 2-tori can be described by regions of spacetime that are "close" to the invariant 2-torus in some norm. The explanation for why these shadowing events appear as one family member over another is quantitatively hard to describe but qualitatively the invariant 2-torus must be coupled to its spatiotemporal neighbors in order to locally solve the Kuramoto-Sivashinsky equation, so whichever family member fits on the domain with
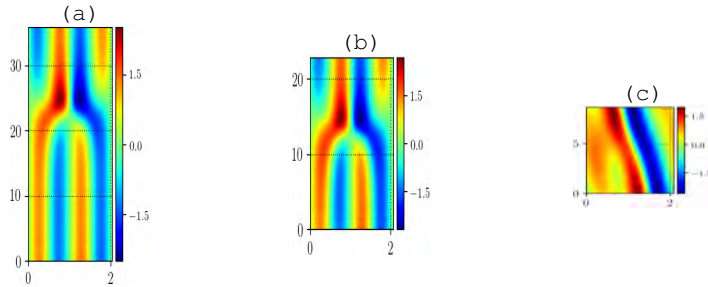
Figure 1.15: Demonstration of the continuous merger tile family via numerical continuation. The family exists approximately on the range of domain sizes $\frac{L}{2\pi} \in [\approx 2, \approx 2.13]$. Invariant 2-torus solutions reached by numerical continuation of the merger tile solution with spatiotemporal dimensions, (a) $[L_a, T_a] = [2.03 \cdots, 35.73 \cdots]$, (b) $[L_b, T_b] = [2.06 \cdots, 22.80 \cdots]$, (b) $[L_c, T_c] = [2.08 \cdots, 8.61 \cdots]$

its neighbors is the one that is realized. The numerical continuation performed in figure 1.15 demonstrates at the very least that the merger tile can exist on multiple spatiotemporal domain sizes. It does not exist on all domain sizes, however; the displayed examples are close to the "boundaries" of the continuous family (with respect to L). When the solutions (a) and (c) are numerically to smaller (larger) L they approach a homoclinic connection and relative equilibrium solutions, respectively. We expect that the discovery of continuous families actually helps us immensely. The benefit is that it provides a much needed flexibility towards finding admissible patterns. In summary, an optimistic interpretation is that we have a ternary alphabet for our symbolic dynamics parameterized by parameters such as L and T. This dramatic reduction in the number of available patterns (seemingly innumerable down to three, give or take an infinite number of continuous deformations) seems too good to be true. As we shall see, however, this trinary alphabet is indeed sufficient to reproduce known solutions and produce new solutions which provides empirical evidence that shows we are on the right track. In fact, with some manual labor, we were able to produce an initial condition that converged to the known solution. This is demonstrated in figure 18.11. The explicit construction of the initial condition used in figure 18.11 is given by figure 18.12.

Invariant 2-tori from tiles

We have displayed that it is possible to find small spatiotemporal invariant 2-tori that are embedded in larger invariant 2-tori. Now we will demonstrate the opposite, finding larger invariant 2-tori by combining smaller invariant 2-tori, is also possible in a method we call "tiling". Not only will this provide us with yet another method to find invariant 2-tori but also it will allow us to investigate the symbolic dynamics of our spatiotemporal system. Specifically, we
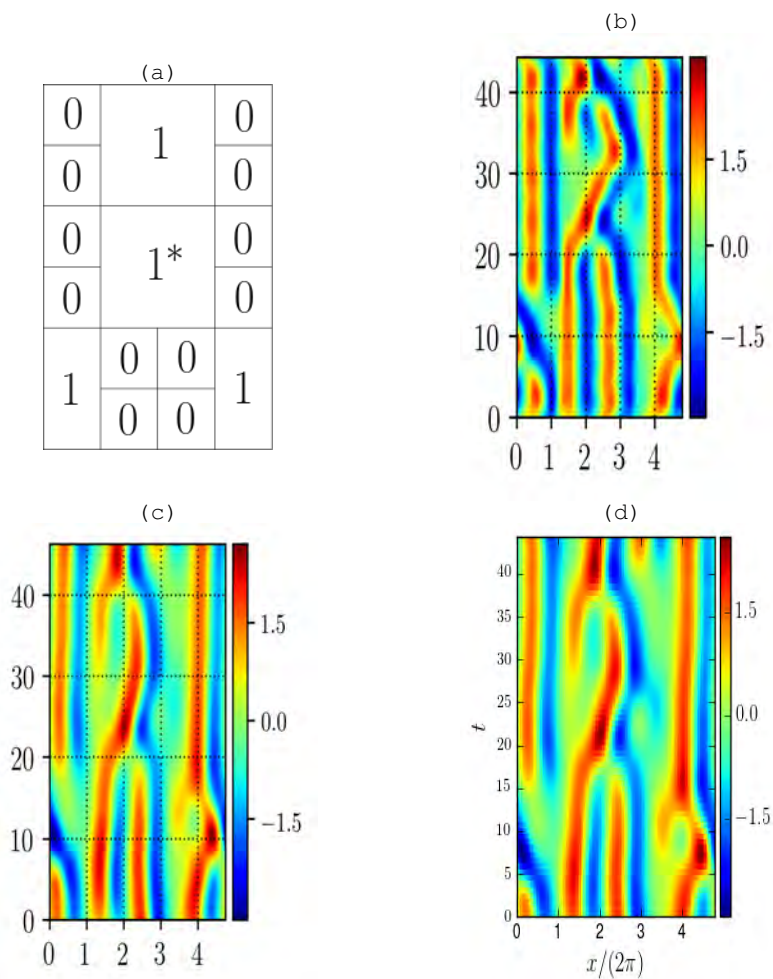
Figure 1.16: (a) Spatiotemporal symbolic block representation created using group orbits of three tile families, (b) initial condition produced by combining tiles according to (a); dimensions initialized at $[L_b, T_b] = [4.79\cdots, 88.62\cdots]$, (c) converged invariant 2-torus when using (b) as an initial condition, (d) targeted invariant 2-torus which (c) was trying to match.

Figure 1.17: Demonstration of how to construct an initial condition corresponding to a specific spatiotemporal symbolic block. (a),(b) and (c) together are the set of tiles used for all other plots in this figure. (d) is a subdomain comprised of two copies of (a) and one copy of (b). (e) is a subdomain comprised of two copies of (a) and one copy of the reflection of (b). (f) is a subdomain comprised of two copies of (a) and a single copy of (c). The last row of figures demonstrate how to combine (d),(e), and (f). (g) is the combination of (d) and (e). (h) is the combination of (d),(e) and (f) (equivalently, (g) and (f)). Lastly (i) is the smoothed version of (h) which will serve as the initial condition.

will investigate the grammar [1, 4] or set of rules that dictates which symbolic sequences are admissible or, in other words, which tilings will be physically realized as invariant 2-tori. In general, symbolic dynamics may be arbitrarily complex even in systems as simple as the logistic map [1]. In spite of this, we will attempt to reverse engineer the grammar by using brute force, no less. This brute force method consists of finding all admissible tilings. With the inadmissible tiling combinations we hope to construct a consistent grammar, or at least find an approximate grammar that can be used as rough guideline. First, however, a method to create initial conditions from combining tiles was required. The crudest way to do so is to numerically combine them without any preprocessing; this introduces numerical discontinuities at every conjunction of tiles. We expend slightly more effort handling these discontinuities by numerically padding the tiles with a boundary of grid points, all initialized with a field value of zero. This creates buffer regions between tiles or "zero padding", which aims to smooth the field and bring it closer to being periodic. In addition to this zero padding, we also truncate the spatiotemporal Fourier coefficients for further smoothing. One downside to this two step method is that it creates initial conditions with localized spatiotemporal features; this is unnatural for the Kuramoto-Sivashinsky equation because of its linearly unstable modes. An alternative would be to approximately solve the boundary value problem induced by the zero padding, using a Chebyshev polynomial collocation method, for instance. Because of the non periodic boundary conditions in this augmented problem, it may very well be more difficult that our original problem, hence why we avoid such calculations.

There are many subtleties and details to consider for the automated tiling method. For instance, the discretization of each tile needs to be modified so that tiles are combined with the correct aspect ratios. In the case of the streak tile this is not very straightforward because it does not have an intrinsic timescale (other than zero if you would like). Currently, we make the simple but crude choice which is to say that the period is not affected by combination with streak tiles. We leave any error introduced by this assumption to our numerical optimization procedure. Because we are only creating initial conditions which are not themselves solutions we are able to be less than perfect. There are of course many other numerical details but also theoretical details which would improve this process. Some details that we have not implemented nor investigated are how the energetics of the tiles or their local Galilean velocities affect the tiling procedure. We stated in sect. 12.3.2 that the Galilean invariance (12.31) is used to set the mean velocity of the overall front to zero. For an arbitrary subregion of width $L_1 < L$, the mean velocity is generically $\langle u \rangle(t) \neq 0$. Actually, we know that as function of L the velocity front executes a random walk, [18] and hence the range of the color bar in a figure such as figure 1.1 has to grow proportionally to $\sqrt{L}$. The variance grows only in the spatial direction, in the time direction $E(t) \to E$. That implies that in gluing letters u_j of alphabet

---

[18]Predrag 2019-12-06: make sure that this is explained in the text elsewhere, then link here to the variance equation "with variance $E(t) = \frac{1}{2}\langle u^2 \rangle(t) \propto L$ by the extensivity of Kuramoto-Sivashinsky,"

figure 1.10 into larger patterns, one also has to vary $\langle u_j \rangle(t)$ averaged over the tile of width L_j, in order to glue optimally. In other words, we have to use the Galilean symmetry group orbit of the letter u_j, and slice that group orbit at $\langle u_j \rangle(t_0) = 0$ for purposes of plotting its representative in figure 1.10. The tiles figure 1.10 were all converged with under the zero mean velocity condition; locally, subdomains of the tiling has local Galilean velocities so long as the subdomain is not a tile (or a tile plus zero padding, as zeroes do not contribute to the integral (12.31)). In summary there are many different properties that we have not taken into account and so any results can really only be validated numerically.

We move on to the results and utility of our tiling method. We begin with a simple tiling example which iteratively adds the streak tile in the spatial direction to the merger tile. The symbolic blocks (1.83),(1.84),(1.85) represent these tilings (in theory). In all tiling examples that follow, the invariant 2-tori are converged in the full state space; that is, they have only the trivial subgroup as their isotropy subgroups.

$$\mathsf{M} = \left[\begin{array}{c} 01 \end{array} \right] \tag{1.83}$$

$$\mathsf{M} = \left[\begin{array}{c} 001 \end{array} \right] \tag{1.84}$$

$$\mathsf{M} = \left[\begin{array}{c} 0001 \end{array} \right] \tag{1.85}$$

As we can see in the collection of figure 18.13, figure 18.15, figure 1.20. From the spatiotemporal dimensions of the tiles in figure 1.10 we can see that simple addition would predict that figure 18.13 should have spatial domain size approximately equal to $L_{01} \approx L_s + L_m = 3.09$. The true value comes out to $L_{01} = 3.13\cdots$. Likewise, each new streak addition should approximately modify the spatial domain size in the same way, which is exactly what occurs, as $L_{001} = 4.12\cdots$ and $L_{0001} = 5.16\cdots$. Note that in each step both L and T change by a different amount such that the resulting invariant 2-torus satisfies (18.1). This is expected as we are allowing both dimensions to change, we are solving the equations in a least-squares manner, and of course the equations are nonlinear.

We have established that it is at least possible to find solutions by our tiling method but we need some way to confirm our results. First, the converged invariant 2-torus resulting from a symbolic sequence should be invariant under symmetry transformations of the symbols themselves. We provide an example of this in (1.86) and (1.87). The two symbolic blocks in question are spatial rotations of one another but they numerically converge to invariant 2-tori which are only approximately related by the same rotation, as seen in figure 1.21 and figure 1.22. The reason why the two converged solutions do not differ only by spatial rotation, as one might expect, is because the solutions are being found in a least-squares manner and the initial spatiotemporal Fourier coefficients differ by a phase factor. This phase difference is sufficient enough to affect

Figure 1.18: (a) Initial spatiotemporal field for the one-by-two symbolic block given by (1.83) (b) Invariant 2-torus resultant from numerically converging (a), $[L_b, T_b] = [3.13 \cdots , 20.84 \cdots]$

Figure 1.19: (a) Initial spatiotemporal field for the one-by-three symbolic block given by (1.84) (b) Invariant 2-torus resultant from numerically converging (a), $[L_b, T_b] = [4.12 \cdots , 23.15 \cdots]$.

Figure 1.20: (a) Initial spatiotemporal field for the one-by-four symbolic block given by (1.85) (b) Invariant 2-torus resultant from numerically converging (a), $[L_b, T_b] = [5.16 \cdots , 23.77 \cdots]$.

Figure 1.21: (a) Initial spatiotemporal field for the one-by-three given by (1.86) (b) Invariant 2-torus resultant from numerically converging (a), $[L_b, T_b] = [6.36\cdots, 24.98\cdots]$.

the numerical results. In this manner, the numerical methods and symmetry actions are only approximately "conjugate"; in other words, the order technically matters. Specifically, the discrepancy of the solutions can mainly be explained by their differing domain sizes. These spatiotemporal domain sizes are $[L_b, T_b] = [6.36\cdots, 24.98\cdots]$ and $[L_b, T_b] = [6.07\cdots, 16.58\cdots]$ for (1.86) and (1.87) respectively. We expect that numerical continuation in spatiotemporal domain size would be able to connect these solutions such that the results would be the same field up to a symmetry operation. This belief comes from performing exactly this computation for tiles in figure 1.11. This idea should of course be applicable to all symmetry related symbolic blocks but it is technically possible that for a large tiling the phase factor can change which invariant 2-torus the initial condition converges to. This has not been confirmed not denied but we offer this possibility as a caution for others.

$$M = \begin{bmatrix} 0\,1\,2 \end{bmatrix} \tag{1.86}$$

$$M = \begin{bmatrix} 2\,0\,1 \end{bmatrix} \tag{1.87}$$

Both examples so far have only considered spatial tiling. The general case, tiling spatiotemporal patterns, is a much more appropriate demonstration of tiling. To demonstrate this extension, we create two initial conditions corresponding to the two-by-two symbolic blocks (1.88) and (1.89), as well as a simple three-by-three symbolic block example (1.90).

$$M = \begin{bmatrix} 0\,1 \\ 1\,0 \end{bmatrix} \tag{1.88}$$

$$M = \begin{bmatrix} 0\,2 \\ 1\,0 \end{bmatrix} \tag{1.89}$$

Figure 1.22: (a) Initial spatiotemporal field for the one-by-three symbolic block given by (1.87) (b) Invariant 2-torus resultant from numerically converging (a), $[L_b, T_b] = [6.07 \cdots, 16.58 \cdots]$.

$$\mathsf{M} = \begin{bmatrix} 0\,0\,0 \\ 0\,0\,0 \\ 0\,0\,2 \end{bmatrix} \tag{1.90}$$

All three of these initial conditions converge numerically, as indicated in the corresponding figures figure 1.23, figure 1.24, figure 1.25. Figure 1.23 converges to a invariant 2-torus closest to what one might expect as the second half of the orbit (in time) seems to be very close to a reflection of the first half, a property restricted to shift-reflection invariance. This makes sense due to the antisymmetric (approximately in the merger tile's case) nature of the tiles themselves. Meanwhile, it is hard to distinguish whether figure 1.25 is a quality result or not. By construction of the initial condition there are three wavelengths represented by the first two "rows" of the symbolic block, but four wavelengths in the last row. The converged invariant 2-torus, however, seems to converge to a solution that has three well defined (amplitude) wavelengths at any given time. This result appeals to our knowledge of the physical scales of the Kuramoto-Sivashinsky equation as the initial domain size is closer to three multiples of the most unstable wavelength than four.

In light of these results, recall that our original goal was to explain the spatiotemporal symbolic dynamics by enumerating all admissible tilings; so far, the results have been good numerically but poor in regards to the symbolic dynamics. Most of the tilings converge numerically but it is not evident that they always converge to the targeted symbolic block. We have only been able to tell by manually inspection of the features of each converged block. The features in the converged invariant 2-torus should of course match the symbolic block, at least up to continuous deformations. If invariant 2-tori shadow too many or too few invariant 2-tori, then that initial condition has likely converged to a different symbolic block. This possibility is unsettling in terms of the development of our symbolic dynamics. Errant convergence only serves to misinform us regarding the grammar of the symbolic dynamics. How can we determine if a converged invariant 2-torus is indeed a representation of a specific symbolic sequence or not? For validation of our results we seek a numerical method that
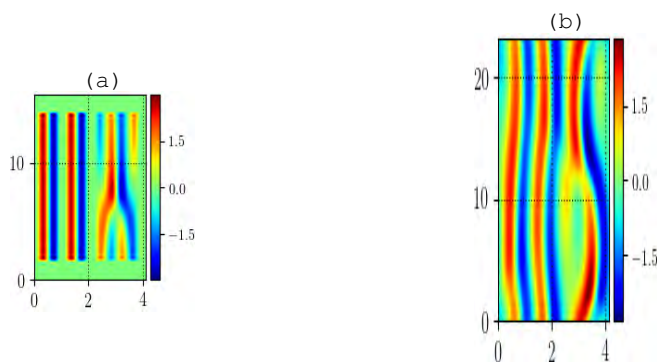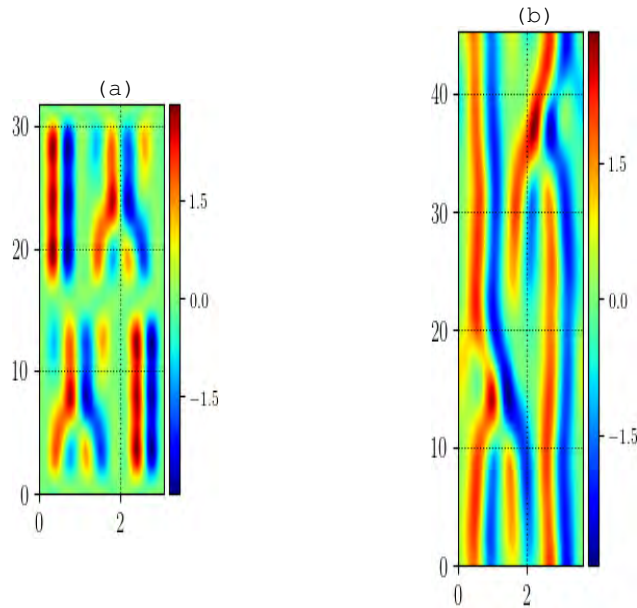
Figure 1.23: (a) Initial spatiotemporal field for the two-by-two symbolic block given by (1.88) (b) Invariant 2-torus resultant from numerically converging (a), $[L_b, T_b] = [3.64 \cdots, 45.26 \cdots]$.

can detect tiles embedded in large invariant 2-tori. This method also needs to account for continuous families of tile deformations; therefore, it seems natural to search for a method which searches for specific features.

We can postulate some methods but we have not created a method that can automatically validate converged symbolic invariant 2-tori. For instance, we can use an image processing technique, "feature detection". Image "features" are very loosely defined and they can be as general as corners or edges; of course we need to tune this to detect signatures of different tiles instead. The primary property of these features is that they can be detected even after different transformations of the image such as affine transformations. This of course is good as the signatures of our tiles manifest differently for each continuous tile deformation. First, we begin by representing the invariant 2-torus as a grey scale images. Once a gray scale image is produced, we utilize numerical methods from the Python package `scikit-image` for the feature detection. The results are quite striking in regards to how tiles are represented by specific shapes even after such a large amount of data reduction. In this representation streaks still manifest as streaks. Creations of streaks, however, is represented by an upwards facing pitchfork. Annihilation of streaks (merger tile) is represented by downward facing pitchforks (in this case there it is possible to see "imperfect pitchforks" like from bifurcation theory). There is a thick wishbone type shape which represents a gap and a ring like structure on the left side on the domain
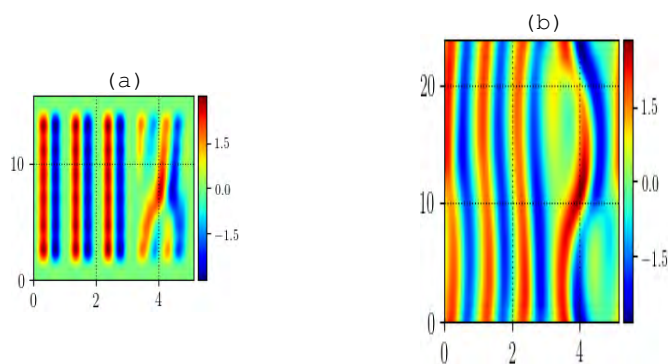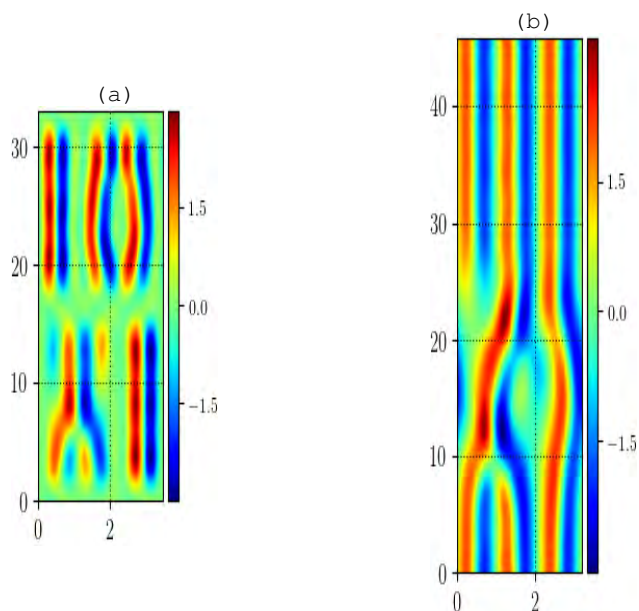
Figure 1.24: (a) Initial spatiotemporal field for the two-by-two symbolic block given by (1.89) (b) Invariant 2-torus resultant from numerically converging (a), $[L_b, T_b] = [3.19 \cdots , 45.81 \cdots]$.
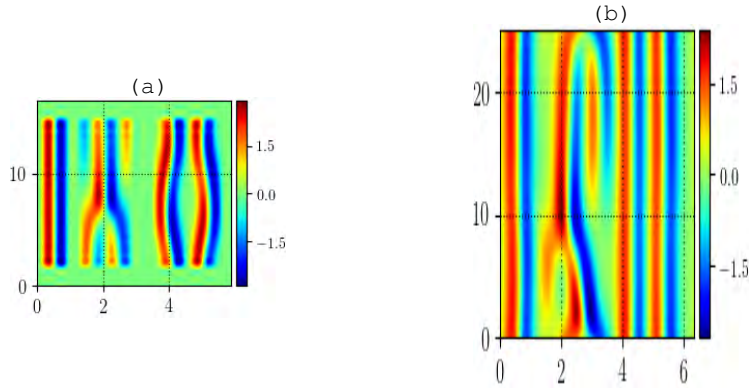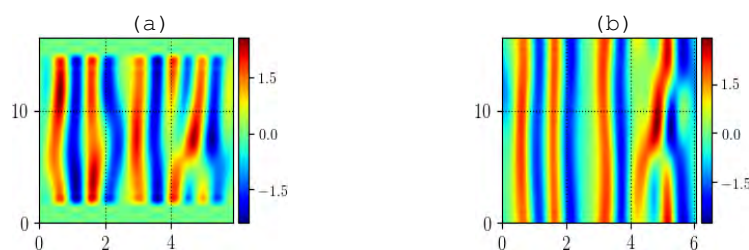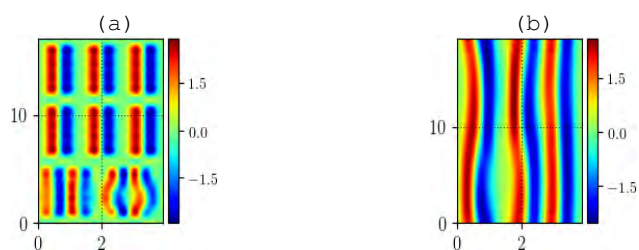

Figure 1.25: (a) Initial spatiotemporal field for the three-by-three symbolic block given by (1.90). (b) Invariant 2-torus resultant from numerically converging (a), $[L_b, T_b] = [3.89 \cdots , 19.22 \cdots]$.

| (a) | (b) | (c) |
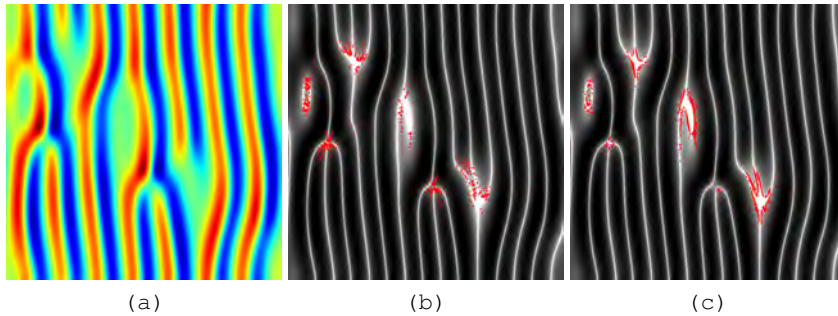
Figure 1.26: (a) Invariant 2-torus converged in full state space purported to be symbolic block 1012 (spatial sequence) (b),(c) are two separate attempts at "feature detection" using the "ORB" numerical routine that is part of `scikit-image`

which appears to represent either a hook (member of the merger tile family). Using these shapes as indicators we believe that figure 1.26(a) is *not* a representation of the symbolic sequence 1012 as previously believed; determined by inspecting the spatiotemporal ordering of these features. The features that are detected seems to be heavily dependent on the parameter values input into the numerical method. The ideal case for us is to only detect non-streak features. This is desirable because if we find locations of all gap and merger tiles, the remainder of the invariant 2-torus should be covered by streaks if the alphabet is trinary. The problem with this is that the feature detection picks up creation of streaks which isn't useful. Tuning the different parameters of the `ORB` feature detection scheme from `scikit-image` package produces a set of data points which cluster around the desired features. by analyzing the pixel intensities of the image. We apply this to two different examples; the converged invariant 2-torus from a tiling and a ergodic trajectory segment with large spatiotemporal extent. The first example is to attempt to validate the symbolic representation we claim, the second it to see how this scheme holds up when the features are small relative to the image.

While the accuracy of our symbolic dynamics is still suspect, it is worth repeating that we have formulated multiple techniques for finding invariant 2-tori. These include finding large invariant 2-tori by combining small invariant 2-tori, finding small invariant 2-tori embedded in large invariant 2-tori, and numerical continuation of invariant 2-tori. These methods work in tandem with one another; giving us the ability to search for nearly any sized invariant 2-torus using previously acquired data. The flexibility and agility gained from the combination of these methods is substantial and it allows for a targeted search for invariant 2-tori. This flexibility can help us overcome some problems which are currently present in numerical studies of fluid flow. Once such example is the wide variety of parameter values and geometries (boundary conditions) studied in the world of fluid dynamics which makes comparison

between periodic orbits in different flows difficult. If connections between geometries can be made then obviously direct comparisons between periodic orbits could be made by also the specific effect of geometry could be more easily targeted.

In any fluid dynamics research one of the most critical pieces of information is the value of the Reynolds number. Its importance cannot be understated as this single parameter dictates entire regimes of fluid behavior; unfortunately its value varies wildly depending on the geometry and phenomena being studied. For instance, in computational studies of plane Couette flow, $Re = 400$ is a common value [32, 53, 56]. For experimentalists, the Reynolds number is on the order of thousands in small scale experiments [13] to tens, even hundreds, of thousands in large scale experiments [39]. Continuation of solutions from one Reynolds number to another is already performed in dynamical systems calculations [7] but much like the initial value problem it can be very sensitive to perturbations; we appeal again to spatiotemporal techniques. The difference becomes apparent when attempting to perform numerical continuation of the spatial domain size. In the numerical studies of plane Couette flow [32, 53, 56] there have been differing choices as to the size of the computational domain. In this case the qualitative effect isn't drastic because all three domain sizes are comparatively small. However, quantitative comparisons and reproduction of results becomes difficult. One could technically include spatial domain size as a variable in the dynamical system formulation but we posit that the ill conditioning of changing the domain size in combination with the exponential instability of the dynamics will make this a fruitless endeavor. As we have seen shown it is not only possible for us to numerically continue invariant 2-tori with respect to domain size but keep domain size as a variable; we have seen neither of these techniques in the literature.

A possible objection to these methods is that there is no real point in varying the domain size as if there was a desire to study a specific domain size, then one would do just that. The problem is that as domain size increases it becomes harder and harder to simply find periodic orbits. Therefore, the more we can leverage already known data the less we waste computational time. One of the more compelling arguments is by far in favor of numerical continuation in spatial domain size is the ability to match changes in experimental setups for whatever reason; perhaps more precise measurements of the geometry were made, or perhaps there was a systematic reason why the setup needs to be changed. Essentially, numerical continuation and the ability to change the domain size allows for the tuning of numerical data to match experimental data. The limits of continuation in spatial domain size are unknown but we do know it depends on the specific invariant 2-torus being continued. This method likely won't be able to doubling the spatial domain size, but for smaller changes it seems useful.

In addition to tiling; combining spatiotemporal tiles to find larger invariant 2-tori, we can also glue larger invariant 2-tori together to find yet larger invariant 2-tori. Although quite similar, we make the distinction between the two methods because tiling has a symbolic dynamic motivation while gluing does

not.

1.9.4 "Rubbery" tiles in far-from equilibrium dynamics

As we have shown in sect. 1.9.3 for (1+1)-dimensional spacetime, our tiles form continuous families of solutions which are not related by exact geometrical symmetries, but rather by deformations, with continuously varying physical properties, such as their dissipation rates.

It is a situation familiar from Hamiltonian dynamics, where the unstable compact solutions are isolated on a fixed energy shell, but form continuous families as functions of the energy parameter. The fixed energy shell is protected by energy conservation at all times.

In steady-state far-from-equilibrium systems solutions also form continuous families (see figure 10 of ref. [**HGC08**]), but only on average. There is no instantaneous 'energy shell' - the driving power-in and the dissipation rate are equal only in the infinity-time average sense (the mean power-in and mean dissipation rates for each unstable solution lie on the diagonal in figure 8 of ref. [**HGC08**]).

Which solution one is to pick from a continuous family depends on what averages one wants to balance. For example, for a plane Couette flow restricted to a 'minimal cell' [27], every solution can be continuously deformed by the width or the length of the cell (see figure 11 of ref. [**HGC08**]). However, imposing zero mean pressure gradient, or zero mean velocity leads to different solutions (see sect. 3 of ref. [27]).

For the Kuramoto-Sivashinsky system at hand, we impose the constant mean dissipation rate (computed as along-time average over any ergodic trajectory) to be satisfied by every compact unstable solution, resulting in a single (or no) solution contribution for each continuous family. All cycle averaging formula are evaluated on these isolated compact solutions, there are no rubbery continuous families of rubbery deformations of tiles to worry about.

References

[1]   R. Artuso, E. Aurell, and P. Cvitanović, "Recycling of strange sets: I. Cycle expansions", Nonlinearity **3**, 325–359 (1990).

[2]   R. H. Brandenberger, "Topological defects and structure formation", Int. J. Mod. Phys. A. **9**, 2117–2189 (1994).

[3]   J. C. Bronski and T. N. Gambill, "Uncertainty estimates and L_2 bounds for the Kuramoto-Sivashinsky equation", Nonlinearity **19**, 2023–2039 (2006).

[4]   N. B. Budanur, D. Borrero-Echeverry, and P. Cvitanović, "Periodic orbit analysis of a system with continuous symmetry - A tutorial", Chaos **25**, 073112 (2015).

[5] N. B. Budanur and P. Cvitanović, "Unstable manifolds of relative periodic orbits in the symmetry-reduced state space of the Kuramoto-Sivashinsky system", J. Stat. Phys. **167**, 636–655 (2015).

[6] N. B. Budanur, P. Cvitanović, R. L. Davidchack, and E. Siminos, "Reduction of the SO(2) symmetry for spatially extended dynamical systems", Phys. Rev. Lett. **114**, 084102 (2015).

[7] N. B. Budanur, K. Y. Short, M. Farazmand, A. P. Willis, and P. Cvitanović, "Relative periodic orbits form the backbone of turbulent pipe flow", J. Fluid Mech. **833**, 274–301 (2017).

[8] F. Christiansen, P. Cvitanović, and V. Putkaradze, "Spatiotemporal chaos in terms of unstable recurrent patterns", Nonlinearity **10**, 55–70 (1997).

[9] P. Cvitanović, R. Artuso, R. Mainieri, G. Tanner, and G. Vattay, *Chaos: Classical and Quantum* (Niels Bohr Inst., Copenhagen, 2022).

[10] P. Cvitanović, R. L. Davidchack, and E. Siminos, "On the state space geometry of the Kuramoto-Sivashinsky flow in a periodic domain", SIAM J. Appl. Dyn. Syst. **9**, 1–33 (2010).

[11] P. Cvitanović and B. Eckhardt, "Symmetry decomposition of chaotic dynamics", Nonlinearity **6**, 277–311 (1993).

[12] P. Cvitanović and H. Liang, Spatiotemporal cat: A chaotic field theory, In preparation, 2022.

[13] D. B. DeGraaff and J. K. Eaton, "Reynolds-number scaling of the flat-plate turbulent boundary layer", J. Fluid. Mech **422**, 319–346 (2000).

[14] X. Ding, H. Chaté, P. Cvitanović, E. Siminos, and K. A. Takeuchi, "Estimating the dimension of the inertial manifold from unstable periodic orbits", Phys. Rev. Lett. **117**, 024101 (2016).

[15] X. Ding and P. Cvitanović, "Periodic eigendecomposition and its application in Kuramoto-Sivashinsky system", SIAM J. Appl. Dyn. Syst. **15**, 1434–1454 (2016).

[16] C. Dong and Y. Lan, "Organization of spatially periodic solutions of the steady Kuramoto-Sivashinsky equation", Commun. Nonlinear Sci. Numer. Simul. **19**, 2140–2153 (2014).

[17] T. Engl, J. Dujardin, A. Argüelles, P. Schlagheck, K. Richter, and J. D. Urbina, "Coherent backscattering in Fock space: A signature of quantum many-body interference in interacting bosonic systems", Phys. Rev. Lett. **112**, 140403 (2014).

[18] T. Engl, P. Plöss, J. D. Urbina, and K. Richter, "The semiclassical propagator in fermionic Fock space", Theor. Chem. Acc. **133**, 1563 (2014).

[19] T. Engl, J. D. Urbina, Q. Hummel, and K. Richter, "Complex scattering as canonical transformation: A semiclassical approach in Fock space", Ann. Phys. **527**, 737–747 (2015).

[20] T. Engl, J. D. Urbina, and K. Richter, "The semiclassical propagator in Fock space: dynamical echo and many-body interference", Philos. Trans. Royal Soc. A **374**, 20150159 (2016).

[21] M. Farazmand, "An adjoint-based approach for finding invariant solutions of Navier-Stokes equations", J. Fluid M. **795**, 278–312 (2016).

[22] A. Fernández-Nieves, V. Vitelli, A. S. Utada, D. R. Link, M. Márquez, D. R. Nelson, and D. A. Weitz, "Novel defect structure in nematic liquid crystal shells", Phys. Rev. Lett. **99**, 157801 (2007).

[23] U. Frisch, Z. S. She, and O. Thual, "Viscoelastic behavior of cellular solutions to the Kuramoto-Sivashinsky model", J. Fluid Mech. **168**, 221–240 (1986).

[24] L. Giacomelli and F. Otto, "New bounds for the Kuramoto-Sivashinsky equation", Commun. Pure Appl. Math. **58**, 297–318 (2005).

[25] D. Giannakis, A. Ourmazd, J. Slawinska, and Z. Zhao, "Spatiotemporal pattern extraction by spectral analysis of vector-valued observables", J. Nonlin. Sci., 1–61 (2019).

[26] J. F. Gibson, Channelflow: A spectral Navier-Stokes simulator in C++, tech. rep., `Channelflow.org` (U. New Hampshire, 2019).

[27] J. F. Gibson, J. Halcrow, and P. Cvitanović, "Visualizing the geometry of state-space in plane Couette flow", J. Fluid Mech. **611**, 107–130 (2008).

[28] M. Golubitsky and I. Stewart, *The Symmetry Perspective* (Birkhäuser, Boston, 2002).

[29] J. M. Greene and J.-S. Kim, "The steady states of the Kuramoto-Sivashinsky equation", Physica D **33**, 99–120 (1988).

[30] B. Gutkin, L. Han, R. Jafari, A. K. Saremi, and P. Cvitanović, "Linear encoding of the spatiotemporal cat map", Nonlinearity **34**, 2800–2836 (2021).

[31] B. Gutkin and V. Osipov, "Classical foundations of many-particle quantum chaos", Nonlinearity **29**, 325–356 (2016).

[32] J. Hamilton, J. Kim, and F. Waleffe, "Regeneration mechanisms of near-wall turbulence structures", J. Fluid Mech. **287**, 317–348 (1995).

[33] B. Hof, C. W. H. van Doorne, J. Westerweel, F. T. M. Nieuwstadt, H. Faisst, B. Eckhardt, H. Wedin, R. R. Kerswell, and F. Waleffe, "Experimental observation of nonlinear traveling waves in turbulent pipe flow", Science **305**, 1594–1598 (2004).

[34] P. Holmes, J. L. Lumley, and G. Berkooz, *Turbulence, Coherent Structures, Dynamical Systems and Symmetry* (Cambridge Univ. Press, Cambridge, 1996).

[35] J. Jimenez and M. P. Simens, "Low-dimensional dynamics of a turbulent wall flow", J. Fluid. Mech **435**, 81–91 (2001).

[36] K. Kaneko, "Transition from torus to chaos accompanied by frequency lockings with symmetry breaking: In connection with the coupled-logistic map", Prog. Theor. Phys. **69**, 1427–1442 (1983).

[37] K. Kaneko, "Period-doubling of kink-antikink patterns, quasiperiodicity in antiferro-like structures and spatial intermittency in coupled logistic lattice: Towards a prelude of a "field theory of chaos"", Prog. Theor. Phys. **72**, 480–486 (1984).

[38] A.-K. Kassam and L. N. Trefethen, "Fourth-order time-stepping for stiff PDEs", SIAM J. Sci. Comput. **26**, 1214–1233 (2005).

[39] J. M. Kendall, "Wind tunnel experiments relating to supersonic and hypersonic boundary-layer transition", AIAA **13**, 290–299 (1975).

[40] I. G. Kevrekidis, B. Nicolaenko, and J. C. Scovel, "Back in the saddle again: a computer assisted study of the Kuramoto-Sivashinsky equation", SIAM J. Appl. Math. **50**, 760–790 (1990).

[41] M. Kleman, "Defects in liquid crystals", Rep. Prog. Phys. **52**, 555–654 (1989).

[42] Y. Kuramoto and T. Tsuzuki, "Persistent propagation of concentration waves in dissipative media far from thermal equilibrium", Progr. Theor. Phys. **55**, 356–369 (1976).

[43] Y. Lan, *Dynamical Systems Approach to $1 - d$ Spatiotemporal Chaos – A Cyclist's View*, PhD thesis (School of Physics, Georgia Inst. of Technology, Atlanta, 2004).

[44] Y. Lan and P. Cvitanović, "Unstable recurrent patterns in Kuramoto-Sivashinsky dynamics", Phys. Rev. E **78**, 026208 (2008).

[45] N. D. Mermin, "The topological theory of defects in ordered media", Rev. Mod. Phys. **51**, 591–648 (1979).

[46] D. Michelson, "Steady solutions of the Kuramoto-Sivashinsky equation", Physica D **19**, 89–111 (1986).

[47] R. Milo, S. Shen-Orr, S. Itzkovitz, N. Kashtan, D. Chklovskii, and U. Alon, "Network motifs: simple building blocks of complex networks", Science **298**, 824–827 (2002).

[48] J. Moehlis, H. Faisst, and B. Eckhardt, "Periodic orbits and chaotic sets in a low-dimensional model for shear flows", SIAM J. Appl. Dyn. Syst. **4**, 352–376 (2005).

[49] E. L. Rempel, A. C. Chian, and R. A. Miranda, "Chaotic saddles at the onset of intermittent spatiotemporal chaos", Phys. Rev. E **76**, 056217 (2007).

[50] E. Siminos, *Recurrent Spatio-temporal Structures in Presence of Continuous Symmetries*, PhD thesis (School of Physics, Georgia Inst. of Technology, Atlanta, 2009).

[51] G. I. Sivashinsky, "Nonlinear analysis of hydrodynamical instability in laminar flames - I. Derivation of basic equations", Acta Astronaut. **4**, 1177–1206 (1977).

[52] A. Vilenkin and E. P. S. Shellard, *Cosmic Strings and other Topological Defects* (Cambridge Univ. Press, Cambridge UK, 2000).

[53] D. Viswanath, "Recurrent motions within plane Couette turbulence", J. Fluid Mech. **580**, 339–358 (2007).

[54] F. Waleffe, "On a Self-Sustaining Process in shear flows", Phys. Fluids **9**, 883–900 (1997).

[55] F. Waleffe, "Exact coherent structures in channel flow", J. Fluid Mech. **435**, 93–102 (2001).

[56] F. Waleffe, "Homotopy of exact coherent structures in plane shear flows", Phys. Fluids **15**, 1517–1543 (2003).

[57] H. Wedin and R. R. Kerswell, "Exact coherent structures in pipe flow", J. Fluid Mech. **508**, 333–371 (2004).

[58] A. P. Willis, "The Openpipeflow Navier-Stokes solver", SoftwareX **6**, 124–127 (2017).
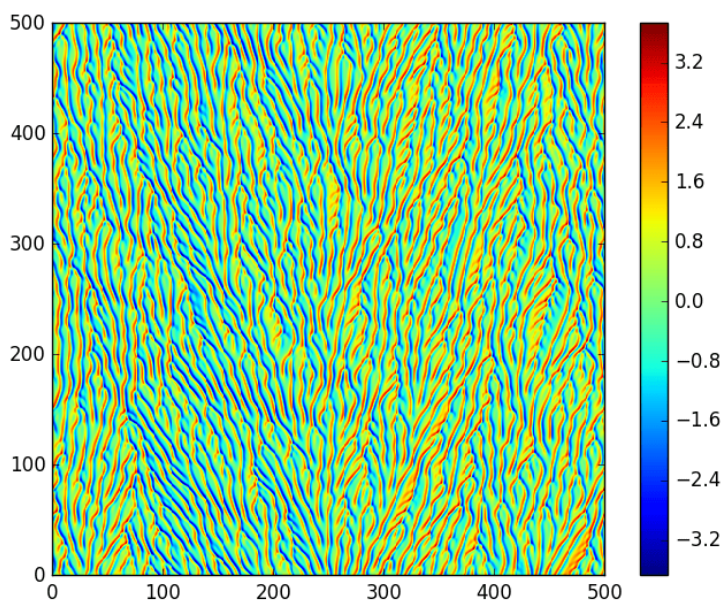
(a)
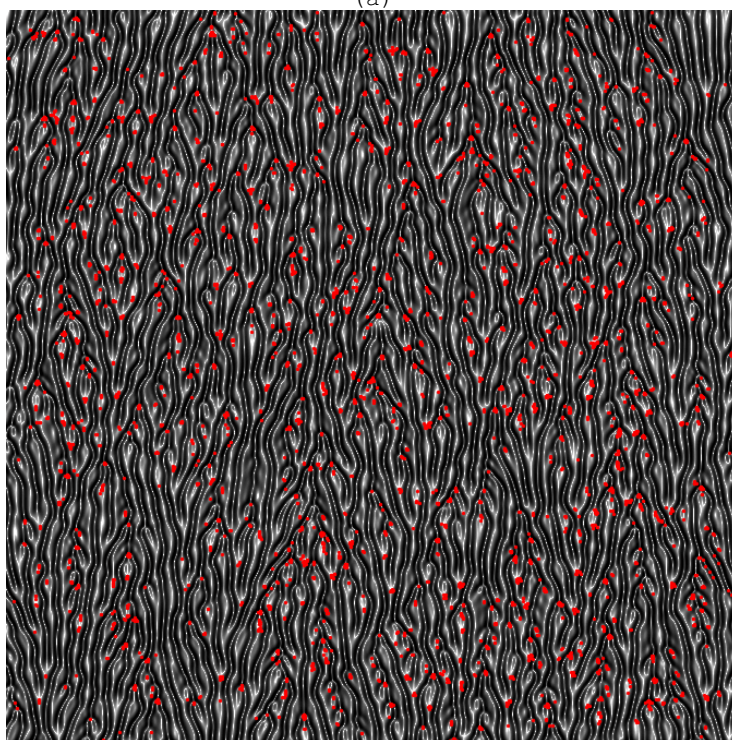
(b)

Figure 1.27: (a)Segment of ergodic trajectory produced by time integration at defined on $[L, T] = [79.57 \cdots, 500 \cdots]$ (b The result of passing a modified gray scale image of (a) to the "ORB" feature detection numerical routine that is part of `scikit-image`

Chapter 2

Space-time numerical methods

2.1 Variational methods

Chapter 3

Variational methods

In this section we cast the problem of searching for invariant 2-tori as a variational optimization problem. In variational formulations of the spatiotemporal problem there is no dynamics, and no numerical integrations of the equations of motion. Instead, one looks for *global* solutions whose tangent space satisfies the given set of ODEs or PDEs *locally* and everywhere over a given spacetime domain $\mathcal{R}$, with given b.c.'s. For example, consider the function

$$G = u_t + u\,u_x + u_{xx} + u_{xxxx} \tag{3.1}$$

of the Kuramoto-Sivashinsky field u and its spacetime derivatives. The Kuramoto-Sivashinsky equation (18.1) is satisfied only for those spacetime field configurations $u(x,t)$ for which the spatial and temporal tangent fields (local field derivatives) balance each other so that $G(u) = 0$.

The standard, simplest approach to numerical determination of a field u that solve $G(u) = 0$ over region $\mathcal{R}$ (see, for example, refs. [7, 23]) is to assume that one has a guess field configuration u_g that is everywhere close to the desired solution u, compute $G(u_g)$, and then minimize the error $G(u_g) - G(u)$ over $\mathcal{R}$ as a least squares sum.

That requires having a norm XXXXXXXX

The functional that is the center of our discussion is the L_2 norm of (3.1), known as the *cost functional*

$$F[u] = \frac{1}{2} \int_0^T \int_0^L \mathrm{d}x\,\mathrm{d}t\,||G(u(x,t))||^2 \tag{3.2}$$

In order to perform numerical compute quantities relevant to this problem, we need to discretize the scalar field $u(x,t)$. This discretizes the expression for the cost functional such that

$$F(u(x,t)) = \frac{1}{2} \sum_{n=0}^{N-1} \sum_{m=0}^{M-1} ||G(u(x_m, t_n))||^2 \tag{3.3}$$

where $t_n = \frac{nT}{N}$ and $x_m = \frac{mL}{M}$. For convenience, we will exchange index notation in favor of vector notation

$$F = \frac{1}{2}||\mathbf{G}||^2 . \tag{3.4}$$

whose critical points correspond to invariant 2-tori. Intrinsic to the definition (3.4) is the choice of norm. We have not avoided the crutch of choosing an arbitrary norm, or so it seems. In the dynamical system context, the norm is used as a metric of distance between points in state space. As previously discussed there is an underlying geometry which is not being taken into consideration. In our variational formulation however the norm merely becomes a measure of whether our current state is a solution or not. In other words, the use of an arbitrary norm in the variational problem does not seem to share the same pitfalls as in the dynamical systems context. Note that we are not saying that our choice of norm is absent of all negative consequences however as it may not be the best indicator of whether we are numerically close to a solution or not. Therefore the norm here, while still not motivated by any underlying geometry, manages to avoid the previously described pitfall.

The cost functional is a mathematical construction that assists the numerical optimization required to find the solutions that we desire. The cost functional (3.4) is a specific example of a much broader class of variational problems. To avoid confusion, the analysis is different than the study of "discrete Lagrangian systems", commonly seen in the context of variational time integrators refs. [25, 26].
[1] [2]

[3] For Kuramoto-Sivashinsky they break the reflection symmetry by introducing a constant drift c, so the remaining symmetry is SO(2). They do not remark that symmetry should be reduced, perhaps because they break it by considering a 2-boundary points problem? We will have to slice the equations.

Loop L: a smooth, differentiable closed curve $\tilde{x}(\tilde{t}) \in L \subset \mathcal{M}$, parameterized by $\tilde{t} \in [0, L]$ with $\tilde{x}(\tilde{t}) = \tilde{x}(\tilde{t} + L)$, with the magnitude of the loop tangent vector fixed by the (so far arbitrary) parametrization of the loop,

$$\tilde{v}(\tilde{x}) = \frac{d\tilde{x}}{d\tilde{t}}, \quad \tilde{x} = \tilde{x}(\tilde{t}) \in L .$$

There are other spatiotemporal variational formulations that are worth describing in detail. Wang *et al.* [33] explain why in the future spatiotemporal methods will be required in order leverage parallel computing power. The algorithm they deploy is standard, except for the implicit inclusion of a "space-time parallel iterative solver" which can take many different forms depending

---

[1]Predrag 2019-09-11: Isn't here a start of a distinct, new section?

[2]Matt 2019-09-12: was a leftover chunk of text from when `variational.tex` was the introduction to the numerical methods section I believe; which it may be better to revert to now that Ibragimov style analysis has been migrated to `LieGroupAnalysis.tex`

[3]Predrag 2017-02-12: Transcription of Wang *et al.* [33] *Towards scalable parallel-in-time turbulent flow simulations*, "least squares shadowing (LSS) method" to ChaosBookese starts here.

on the numerical implementations. Therefore, instead of worrying about the algorithmic details we instead describe the general procedure for how they setup the variational problem.

Consider a dynamical system

$$\dot{x}(t) = v(x) \,. \tag{3.5}$$

Rescale the time $\frac{\partial \tilde{t}}{\partial t} = 1 + \eta(\tilde{t})$, so

$$(1 + \eta(\tilde{t})) \frac{\partial x(t(\tilde{t}))}{\partial \tilde{t}} = v(x) \,. \tag{3.6}$$

Assume that the action is given by the integral over a Lagrangian, a quadratic cost function together the equations of motion constraint,

$$S[L] = \int_0^T dt \left(\frac{1}{2} \langle x - \tilde{x} | x - \tilde{x} \rangle + \frac{1}{2} \eta^2 + \langle w | \dot{x} - v(x) \rangle \right) \,, \tag{3.7}$$

where $w(\tilde{t})$ is the Lagrange multiplier. The critical points of this Lagrangian ensures that η and $u - u_r$ is minimized and that u satisfies the equations of motion.

Varying the Lagrange function with arbitrary perturbations $\delta x, \delta \eta$ and integrating by parts yields

$$
\begin{aligned}
\delta S[L] &= \int_0^T dt \left(\langle \delta x | x - \tilde{x} \rangle + \delta \eta \, \eta + \delta \eta \langle w | \frac{\partial x}{\partial \tilde{t}} \rangle + \langle w | \frac{\partial \delta x}{\partial t} - A \delta x \rangle \right) \\
&= \int_0^T dt \, \langle \delta x | x - \tilde{x} - \frac{\partial w}{\partial t} - A^\top w \rangle \\
&\quad + \int_0^T dt \, \delta \eta \left(\eta + \langle w | \frac{\partial x}{\partial \tilde{t}} \rangle \right) + \langle \delta x | w \rangle |_0^T \,,
\end{aligned}
\tag{3.8}
$$

where A is the *stability matrix* or *velocity gradients matrix*, i.e., the linearized operator

$$A_{ij}(x) = \frac{\partial}{\partial x_j} v_i(x) \tag{3.9}$$

evaluated at $\tilde{x}$, and $A^\top$ is the adjoint of A. Setting $\delta S[L] = 0$ for arbitrary δx and $\delta \eta$ provides two independent equations

$$
\begin{aligned}
x &= \tilde{x} + \frac{\partial w}{\partial t} + A^\top w \\
\eta &= -\langle w | \frac{\partial x}{\partial \tilde{t}} \rangle \,.
\end{aligned}
\tag{3.10}
$$

Whereupon substitution of the expression for x from (3.10) into (3.5) produces a second order boundary value problem with a transformed time derivative due

to the second component of (3.10). The second order boundary value problem can be summarized by the following optimality system

$$
\begin{aligned}
u &= \tilde{x} + \frac{\partial w}{\partial t} + A^\top w \\
0 &= \frac{\partial}{\partial t}(\tilde{x} + \frac{\partial w}{\partial t} + A^\top w) - v(\tilde{x} + \frac{\partial w}{\partial t} + A^\top w) \\
\eta &= -\langle w | \frac{\partial x}{\partial \tilde{t}} \rangle \\
w|_{\tilde{t}=0} &= 0 \\
w|_{\tilde{t}=T} &= 0
\end{aligned}
\tag{3.11}
$$

where the general procedure would be to solve for w and then substitute into the equation for u. The solutions w are acquired via a "space-time parallel iterative solver" whose implementation is left to the reader as previously mentioned. The authors use Newton's method by solving the linearized system of equations that represent the linearization of the double boundary value problem in (3.11). This linearization is the consequence of assuming $u - u_r$ and η are small and simplifying. This linearization is the quintessential piece of the numerical process we derive here in the same form as Wang *et al.* [33]. The first term is handled by simple application of the time derivative, while the second term is expand as $R(\frac{\partial w}{\partial t} + \mathcal{L}^* w + u_r) \approx R(u_r) + \mathcal{L}(\frac{\partial w}{\partial t} + \mathcal{L}^* w)$ because $u - u_r = \frac{\partial w}{\partial t} + \mathcal{L}^* w$ is small. This brings us to the simplified form

$$
\frac{\partial^2 w}{\partial t^2} + (\frac{\partial}{\partial t}A^\top - A\frac{\partial}{\partial t})w + AA^\top w = -\frac{\partial}{\partial t}\tilde{x} + v(\tilde{x}).
\tag{3.12}
$$

where we have yet to utilize the assumption that η is small which will be used in the expression for the transformed time derivative. Assuming that this only implies that we discard terms quadratic in η we can group the η terms after substitution of $\frac{\partial}{\partial t} = (1 + \eta)\frac{\partial}{\partial \tilde{t}}$ into (3.12). This yields

$$
\frac{\partial^2 w}{\partial \tau^2} + (\frac{\partial}{\partial \tau}A^\top - A\frac{\partial}{\partial \tau})w + AA^\top w + [\eta\frac{\partial^2}{\partial \tau^2} + \frac{\partial}{\partial \tau}\eta\frac{\partial}{\partial \tau} - \eta\frac{\partial}{\partial \tau}A^\top - A\eta\frac{\partial}{\partial \tau}]w = -(1+\eta)\frac{\partial}{\partial \tau}\tilde{x} + v(\tilde{x}).
\tag{3.13}
$$

Now as one can see this includes a number of terms with the variable η which are not present in the final representation in ref. [33]. It's apparent that the terms are neglected because of the assumption η is small, but there is the presence of a term $\mathcal{P}w$ which can be accounted for by the term $-(1 + \eta)\frac{\partial}{\partial \tau}\tilde{x}$ on the RHS of the equation. Specifically, this can be handled by the substitution (from the optimality system (3.11)) for η.

$$
(1 + \langle w | \frac{\partial x}{\partial \tilde{t}} \rangle)\frac{\partial \tilde{x}}{\partial \tau} = (1 + \langle w | \frac{\partial}{\partial \tilde{t}} \rangle(\tilde{x} + \frac{\partial w}{\partial t} + A^\top w))\frac{\partial \tilde{x}}{\partial \tau}
\tag{3.14}
$$

and by using the assumption $u - u_r = \frac{\partial w}{\partial t} + A^\top w$ is small this can be rewritten

$$
(1 + \langle w | \frac{\partial}{\partial \tilde{t}} \rangle(\tilde{x} + \frac{\partial w}{\partial t} + A^\top w))\frac{\partial \tilde{x}}{\partial \tau} \approx (1 + \langle w | \frac{\partial \tilde{x}}{\partial \tau} \rangle)\frac{\partial \tilde{x}}{\partial \tau}
\tag{3.15}
$$

where the term with the inner product accounts for the term in ref. [33].

$$\mathcal{P}w = \langle w | \frac{\partial \tilde{x}}{\partial \tau} \rangle \frac{\partial \tilde{x}}{\partial \tau} \, . \tag{3.16}$$

We walked through this derivation to attempt to reproduce the same equations as Wang *et al.* [33] because they are general and quintessential to the spatiotemporal optimization process. As the following discussion seems to suggest is that they chose the final form that they did because of its numerical properties.

In summary, this section is a survey on the tools and algorithms that are relevant for a variational formulation. We reserve discussion regarding the optimization of the various functionals described in this section to the numerical methods sect. **??**, sect. **??**, and sect. **??**. All of the numerical discussions are centered around finding the minimizers of (3.4) by a combination of descent and iterative methods.

The spatiotemporal reformulation of a dynamical problem also requires a reformulation of its linear stability analysis.

The absence of this tool in the new variational formulation is a large handicap because it disallows one of the most intuitive and common types of analysis of time invariant solutions to chaotic nonlinear equations (more references for papers that look at linear stability).

Therefore, if possible, we want to find an alternative type of analysis which is as useful without having to change our spatiotemporal formulation. There are two avenues of pursuit towards this endeavor. The first is known as Hill's formula [4]. It discusses how the determinant of a finite matrix of the Hessian of an action functional of a discrete Lagrangian system, can be related to the eigenvalues of the monodromy matrix corresponding to a critical point of said action functional, which represents a critical point. As stated in [4], Hill proposed this formula without any proof of convergence of the determinant (his derivation utilized an infinite dimensional Hessian), but a rigorous proof was later presented by Poincaré. The application of this formula requires a discrete Lagrangian system, which means we need equations which have a Lagrangian structure. The cost functional as described by (3.4), although a scalar function of our system variables, does not have the correct Lagrangian structure that is needed, so instead we introduce the concept of *formal Lagrangians* refs. [18, 20, 22]. In this context the Lagrangian structure is imposed by construction, allowing for a valid application of Hill's formula. The interpretation of this application is slightly confusing however as the Hessian and monodromy matrix are now functions of the "original" velocity field and its partial derivatives but also a collection of adjoint variables.

3.1 Formal Lagrangian adjoint derivation

Following sect. 2 *Quasi-self-adjoint equations* of Ibragimov [18] (which does not reference refs. [16, 17]), we can write the *formal Lagrangian* of the Kuramoto-Sivashinsky equation to derive the spatiotemporal adjoint equations in terms

of the original spatiotemporal field $u(x, t)$, and then one is free to use whatever representation suits the user in discretization; the cavaet is that numerically it seems better to use a real valued representation Fourier representation for the adjoint descent. [4]

Ibragimov notation, for the Kuramoto-Sivashinsky case: the independent variable is denoted by x. The dependent variable is u, used together with its first-order partial derivative $u_{(1)}$:

$$u_{(1)} = \{u_i^\alpha\}, \quad u_i^\alpha = D_i(u^\alpha),$$

and higher-order derivatives $u_{(2)}, \ldots, u_{(4)}$, where

$$u_{(2)} = \{u_{ij}^\alpha\}, \quad u_{ij}^\alpha = D_i D_j(u^\alpha), \ldots,$$

$$u_{(s)} = \{u_{i_1 \cdots i_s}^\alpha\}, \quad u_{i_1 \cdots i_s}^\alpha = D_{i_1} \cdots D_{i_s}(u^\alpha).$$

Here D_i is the total differentiation with respect to x^i :

$$D_i = \frac{\partial}{\partial x^i} + u_i^\alpha \frac{\partial}{\partial u^\alpha} + u_{ij}^\alpha \frac{\partial}{\partial u_j^\alpha} + \cdots . \tag{3.17}$$

Using the definition for the *formal Lagrangian* $\mathcal{L}$,

$$\mathcal{L} \equiv v \left[u_t + u_{xx} + u_{xxxx} + u u_x \right], \tag{3.18}$$

and then taking the functional derivative,

$$\frac{\delta \mathcal{L}}{\delta u} = 0 . \tag{3.19}$$

The surviving terms from this functional derivative are

$$
\begin{aligned}
\frac{\partial \mathcal{L}}{\partial u} &= v u_x \\
-\partial_t \frac{\partial \mathcal{L}}{\partial u_t} &= -v_t \\
-\partial_x \frac{\partial \mathcal{L}}{\partial u_x} &= -v u_x - u v_x \\
\partial_x^2 \frac{\partial \mathcal{L}}{\partial u_{xx}} &= v_{xx} \\
\partial_x^4 \frac{\partial \mathcal{L}}{\partial u_{xxxx}} &= v_{xxxx},
\end{aligned}
\tag{3.20}
$$

where the sum of these terms equals (3.19) and hence must be zero. The resultant adjoint equation is ($\pm v u_x$ terms cancel),

$$- v_t + v_{xx} + v_{xxxx} - u v_x = 0 . \tag{3.21}$$

---

[4]Predrag 2018-05-08: Ibragimov [18] is included in Archives of ALGA **4**.
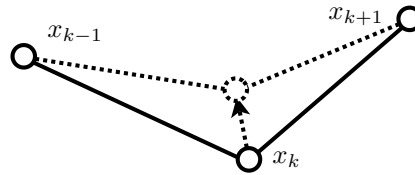
Figure 3.1: Discrete Euler-Lagrange equations are an extremum of the action.

If we take the adjoint variable to be the Kuramoto-Sivashinsky equation,

$$F \equiv v = - \left[u_t + u_{xx} + u_{xxxx} + u u_x \right] , \tag{3.22}$$

we arrive at the equation which *I claim* provides adjoint descent direction without explicit construction of the gradients matrix J,

$$- J^\dagger F = (\partial_t + \partial_x^2 + \partial_x^4)F + u\partial_x F \tag{3.23}$$

(I believe the negative sign in (3.22) is motivated so that the functional derivative is strictly decreasing or zero).

Numerical evidence is suggestive as the real valued adjoint descent is working better than before when I was trying to reverse engineer $J^\dagger F$ in a matrix-free way.

3.2 Discrete Lagrangian methods

In our Newton methods we measure the distance of the guess to the solution by Euclidian sums of squares.

In discrete Lagrangian methods the distance between a guess solution and the exact solution is measured in the symplectic area between the two.

Lagrangian: $L(q, \dot{q}) = K(\dot{q}) - V(q)$

Action: $S(q) = \int_0^T dt L(q, \dot{q})$

Hamilton's principle: $\delta S(q) = 0$

if we vary the path slightly, action is unchanged to first order.

The variational principle: path extremizes action

Discrete treatment of Lagrangian mechanics:

Approximate action integral by a quadrature rule

$$L(q_k, q_{k+1}) \approx \int_{t_k}^{t_{k+1}} L(q, \dot{q}) \, dt = \Delta t L(q_k, q_{k+1}) \, .$$

Symplecticity: If we graph trajectories in the phase plane, symplectic methods preserve areas in time. This means that a closed loop (e.g. a periodic motion, like the pendulum) won't expand or contract.

The Legendre transforms between different generating function are of form

$$H(q_k, p_{k+1}) = p_{k+1} q_{k+1} - L(q_k, q_{k+1}) \,,$$

where q_{k+1} is implicitly defined by $p_{k+1} = \partial_2 L(q_k, q_{k+1})$

Search for:

Asynchronous variational integrators (AVI). They assign different time steps at different points in space (where more/less accuracy is needed).

Example: falling object

Discrete Lagrangian:

$$L(q_k, q_{k+1}) = \Delta t \left[\frac{1}{2} m \left(\frac{q_{k+1} - q_k}{\Delta t} \right)^2 - mg \left(\frac{q_k + q_{k+1}}{2} \right)^2 \right] \,.$$

Discrete Euler-Lagrange equations

$$\frac{\partial}{\partial q_n} \left(L(q_{n-1}, q_n) + L(q_n, q_{n+1}) \right) = 0 \,. \tag{3.24}$$

lead to

$$-m \frac{q_{k+1} - q_k}{\Delta t} - \frac{1}{2} \Delta t \, mg + m \frac{q_k - q_{k-1}}{\Delta t} - \frac{1}{2} \Delta t \, mg = 0 \,.$$

hence, writing the acceleration as s discrete time Laplacian, the falling object equation is

$$\frac{1}{\Delta t^2} \Box \, x_n \;\; = \;\; -g$$
$$\Box \, x_n \;\; \equiv \;\; x_{n+1} - 2 \, x_n + x_{n-1} \,. \tag{3.25}$$

Adding forcing/dissipation

For non-conservative forces, use the discrete Lagrange d'Alembert principle by varying the *action*

$$\delta S_{n,n+k} + \sum_{i=n}^{n+k-1} \left(F^-(q_i, q_{i+k}) \, \delta q_k + F^+(q_i, q_{i+k}) \, \delta q_{k+1} \right) \,, \tag{3.26}$$

This gives the forced discrete Euler-Lagrange equations

$$\frac{\partial}{\partial q_n} L(q_{n-1}, q_n) + \frac{\partial}{\partial q_n} L(q_n, q_{n+1}) + F^-(q_i, q_{i+k}) + F^+(q_i, q_{i+k}) = 0 \,. \tag{3.27}$$

This is then illustrated by two strengths of frictional (linear in velocity) damping of a damped pendulum.

3.2.1 Literature survey

2018-03-28 PC Henry O. Jacobs course notes Crash course in discrete Lagrangian mechanics [21] are in their entirety based on Marsden and West [25] *Discrete mechanics and variational integrators*, which has some 600 citations, so ther is a large amount of literature to scan through.

Eva Kanso says that the discrete Lagrangian integration is formulated for Euler in Pavlov [28] *Structure-preserving discretization of incompressible fluids*, arXiv:0912.3989, but if it works, it should also work for Navier-Stokes by "modelling the dissipation." They write: " Euler fluids have Lagrangian and Hamiltonian descriptions, where the configuration space is defined as the volume-preserving diffeomorphisms, and Kelvin's circulation theorem is viewed as a consequence of Noether's theorem associated with the particle relabeling symmetry of fluid mechanics. However computational approaches to fluid mechanics have been largely derived from a numerical–analytic point of view, and are rarely designed with structure preservation in mind, and often suffer from spurious numerical artifacts such as energy and circulation drift. In contrast, this paper geometrically derives discrete equations of motion for fluid dynamics from first principles in a purely Eulerian form. Our approach approximates the group of volume-preserving diffeomorphisms using a finite-dimensional Lie group, and associated discrete Euler equations are derived from a variational principle with non-holonomic constraints. The resulting discrete equations of motion yield a structure-preserving time integrator with good long-term energy behavior and for which an exact discrete Kelvin's circulation theorem holds.

[...] understanding what this geometric picture of fluid flows brings compared to traditional Large Eddy Simulation or Reynolds-Averaged Navier-Stokes methods would be interesting, as our structure-preserving approach is also based on local averages (i.e., integrated values) of the velocity field.

The discretization of the Euler equations that we have obtained on the regular grid coincides with the Harlow-Welsh scheme [14], and our Eq. (28) is a Crank-Nicolson (trapezoidal) time update. Therefore, our variational scheme can be seen as an extension of this approach to arbitrary grids, offering the added bonus of providing a geometric picture. "

2018-03-29 Evangelos Good people to ask about such methods might be Cristel Chandre or Phil Morrison.

2018-03-30 PC Cristel is a regular visitor, but it is all about Dirac brackets - not sure it helps for dissipative flows. I think it is the same / similar story for Phil. But we can ask - Jeffrey Heninger is now his PhD student.

2018-03-30 PC Eva Kanso sent us Grinspun *et al.* [12] *Discrete Differential Geometry: An Applied Introduction* set of coure=se notes to read. Presumably
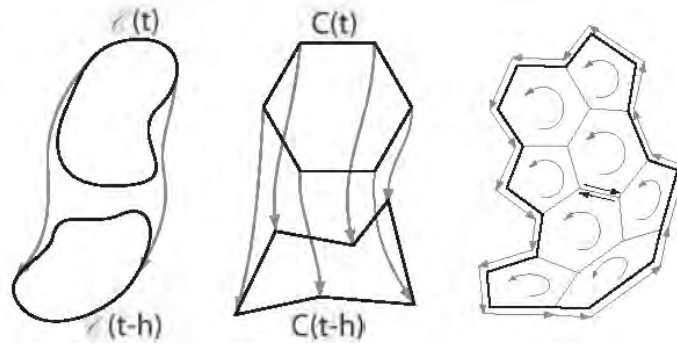
Figure 3.2: Kelvin's Theorem: (left) in the continuous setting, the circulation on any loop being advected by the flow is constant. (middle) the discrete integration scheme enforces this property on each Voronoi loop, (right) thus on any discrete loop. (Fig. 5 on page 63 ofn ref. [12])

we should read *Discrete differential forms for computational modeling*, which is a mostly mathematical discussion of "discrete differential modeling," which I intend to skip, unless really forced to learn it. *Stable, circulation-preserving, simplicial fluids* is perhaps more relevant:

" the approach also provides an accurate treatment of vorticity through a discrete preservation of Kelvin's circulation theorem."

The code, however, for all examples discussed, is spatial, and steps forward in time.

" For purposes of computation one must derive discrete (in space and time) representations of the underlying equations. The theories, which are discrete from the start, and have key geometric properties built into their discrete description can often more readily yield robust numerical simulations which are true to the underlying continuous systems: they exactly preserve invariants of the continuous systems in the discrete computational realm.

Jos Stam [1999; 2001] introduced to the graphics community the method of characteristics for fluid advection and the Helmholtz-Hodge decomposition to ensure the divergence-free nature of the fluid motion [Chorin and Marsden 1979].

Discrete exterior calculus (DEC) leads to numerically robust and efficient simulations of the Navier-Stokes equations. "

" Fluid simulation are rarely designed to conserve defining physical properties. Consider, for example, the need in many methods to continually project the numerically updated velocity field onto the set of divergence free velocity fields; or the need to continually reinject vorticity lost due to numerical dissipation as a simulation progresses. We describe a

geometry-based algorithm for fluid simulation which exactly preserves vorticity at a discrete level.

A careful setup of discrete differential quantities, designed to respect structural relationships such as vector calculus identities, leads to a numerical simulation method which respects the defining geometric structure of the fluid equations.

We construct an integration scheme which employs intrinsically divergence-free variables, and removes the need to enforce the usual divergence-free constraint through a numerically lossy projection step.

The fundamental idea of geometric integration algorithm is to ensure that Kelvin's theorem holds in the discrete setting: the circulation around any loop in the fluid remains constant as the loop is advected, see figure 3.2. "

2018-04-27 Samuel Hadden A widely used method for integrating multi-planet systems is Wisdom and Holman [36], see also discussion of it in Wisdom [35].

Tsang *et al.* [32] generalize symplectic integration to treat dissipative forces, arXiv:1506.08443

2018-04-27 Noah DeTal, Predrag Michael Kraus is a busy beaver, developing variational integrators for MHD.

Kraus and Maj [22] *Variational integrators for nonvariational partial differential equations* seems to be one of the most recent treatments with all features we talked about: variational / Lagrangian formulation, enforcement of conserved quantities / incompressibility, and applicability to viscous / dissipative systems.

It's quite interesting - it imposes the constraint of satisfying the equations of motion locally as we always do, by a Lagrangian multiplier. But then one gets quite a bit of milage out of that matter of fact statement.

Kraus works with Phil Morrison, and by extension with Jeffrey Heninger, who is currently his PhD student, see **2018-03-29 Evangelos** remark above. They presented a 2017 poster titled *First numerical results towards a 3D MHD equilibrium solver via artificial relaxation mechanisms* , but I do not see a published version yet.

They say:

Embed an arbitrary dynamical system into a larger Lagrangian system using the method of formal (or adjoint) Lagrangians, and thereby extend the application domain of variational integrators to include all dynamical systems.

To obtain a formal Lagrangian L, the equation $F[u] = 0$ is multiplied by an adjoint variable v, giving $L = v \cdot F[u]$. Variation of the resulting action functional $A = \int d^{n+1}xL$ with respect to v recovers the original equation

$F[u] = 0$. Variation of the action functional with respect to the physical variable u gives an additional equation that determines the evolution of the adjoint variable v.

The dynamics of v play a key role in relating symmetries of the formal Lagrangian to conservation laws satisfied by u. Ibragimov [16–18] developed conservation laws of arbitrary differential equations by extending the Noether theorem to formal Lagrangians for the extended system (u, v), which can be restricted to the original system provided that it is possible to express the solution of the adjoint variable v in terms of u.

About Ibragimov: see here, ALGA, and his collected works. Further articles to check out:

Ibragimov [19] *Nonlinear self-adjointness and conservation laws*: " The general concept of nonlinear self-adjointness of differential equations is introduced. It embraces the strict self-adjointness and quasi-self-adjointness. The equations possessing nonlinear self-adjointness can be written equivalently in a strictly self-adjoint form by using appropriate multipliers. All linear equations possess the property of nonlinear self-adjointness, and hence can be rewritten in a nonlinear strictly self-adjoint form. "

Ibragimov [20] *Conservation laws and non-invariant solutions of anisotropic wave equations with a source*.

The good news is the Ibragimov is a triviality, says Anco [1] *On the incompleteness of Ibragimov's conservation law theorem and its equivalence to a standard formula using symmetries and adjoint-symmetries*

Then come along Ruggieri and Speciale [29] *Conservation laws by means of a new mixed method*, and, citing but ignoring Anco's contemporaneous gripe, "merge the Ibragimov's method and the 1966 one by Anco and Bluman."

2019-04-17 Predrag Wei and Wang [34] *Symmetry analysis, conserved quantities and applications to a dissipative DGH equation* describe and utilize Ibragimov's approach:

" Sophus Lie introduced the notion of Lie group in order to study the solutions of ordinary differential equations. He showed that the order of an ordinary differential equation can be reduced if it is invariant under one-parameter Lie group of point transformations. The applications of Lie groups to differential systems were mainly established by Lie and Emmy Noether. In 1918, Noether presented the relationship between a mathematics symmetry and conservation law of a physical system. Noether's (first) theorem states that every differentiable symmetry of the action of a physical system has a corresponding conservation law. [...]

Noether's theorem can only be applied to equations with variational structure. A large number of differential equations without variational structure admit conservation laws. Thus, many authors developed some methods which do not rely on the knowledge of Lagrangian functions to ob-

tain conservation laws, such as the characteristic method [27] and the direct method [2, 3]. Ibragimov [17] proved a result which allows one to construct conservation laws for equations without variational structure. Ibragimov theorem is an extension of Noether's theorem where a formal Lagrangian is introduced in order to get rid of the variational limitation. This paper uses the viewpoint of Lie symmetry analysis to construct conservation laws by Ibragimov's theorem in this paper.

They start by presenting the notations, definition of nonlinear self-adjointness and Ibragimov's theorem on conservation laws. Next, they carry out Lie symmetry analysis, derive some symmetry reductions and invariant solutions for their system, a dissipative DGH equation. They then study the self-adjointness and conservation laws of DGH by the Ibragimov's theorem. "

2019-05-21 Predrag Mikhail Skopenkov (smart cookie; for slides, see skopenkov.ru) *Discrete field theory: symmetries and conservation laws* [31], arXiv:1709.04788, gives "a general algorithm constructing a discretization of a classical field theory from a Lagrangian, with a discrete Noether theorem relating symmetries to conservation laws and an energy conservation theorem not based on any symmetry. This gives exact conservation laws for electrodynamics, gauge theory, Klein-Gordon and Dirac theory. He constructs a conserved discrete energy-momentum tensor, approximating the continuum one at least for free fields. The theory is stated in topological terms, such as coboundary and products of cochains."

His *principles of discretization* are:

- keep approximation of continuum theory;
- keep conservation laws exact;
- drop spatial symmetries easily.

He obtains:

- discretization of several field theories in a similar fashion keeping conservation laws exact;
- a discrete Noether theorem relating symmetries to conservation laws;
- a discrete energy conservation theorem not based on a symmetry.

2019-11-05 James Hanna <hannaj@vt.edu> from Virginia Tech writes: Could you please point me to the discrete Noether business you referred to?

Arash Yavari is an interesting neighbor of yours. He has been teaching at GaTech since 2005. He studies computational mechanics, and in particular has been working to develop systematic theories of discrete mechanics for crystalline solids with defects.

Here is something else interesting:

Gay-Balmaz and Yoshimura [8] *A Lagrangian variational formulation for nonequilibrium thermodynamics. Part I: Discrete systems*, early version arXiv:1510.00792

Gay-Balmaz and Yoshimura [11] *A free energy Lagrangian variational formulation of the Navier-Stokes-Fourier system*, arXiv:1706.09010

2019-11-06 Predrag More of such, some of it impossible to read:

Scholle and F. Marner [30] *A non-conventional discontinuous Lagrangian for viscous flow*, also here looks quite interesting, and perhaps even implementable: " In an analogy with Madelung quantum mechanical fluid, a new Lagrangian is proposed for a variational formulation of the Navier–Stokes equations. "

Gay-Balmaz and Yoshimura [9] *Dirac structures in nonequilibrium thermodynamics*, arXiv:1704.03935: " In absence of irreversible processes these Dirac structures reduce to canonical Dirac structures associated to canonical symplectic forms on phase spaces. Our geometric formulation of nonequilibrium thermodynamic thus consistently extends the geometric formulation of mechanics, to which it reduces in absence of irreversible processes. "

Gay-Balmaz and Yoshimura [10] *Variational discretization of the nonequilibrium thermodynamics of simple systems*, arXiv:1601.04882: " [...] extend the variational integrators of Lagrangian mechanics to include irreversible processes. The structure preserving property of the flow of such systems is an extension of the symplectic property of the flow of the Euler–Lagrange equations. In the discrete setting, we show that the discrete flow solution of our numerical scheme verifies a discrete version of this property. "

Bourdin *et al.* [5] *Variational integrators of fractional Lagrangian systems in the framework of discrete embeddings*, arXiv:1601.04882: " [...] interested in the conservation at the discrete level of this Lagrangian structure by discrete embeddings. We then replace in this framework the variational integrators developed in [Hairer *et al.* [13], Chapter VI.6, (click here)] and Marsden and West [25].

Not directly related, but I liked Harmeet Singh and J. Hanna *Impulse and material symmetry* APS DFD talk at Virginia Tech (Jean-Luc Thiffeault would like it too, I think): " The balance of material momentum, also known as impulse or pseudomomentum, arises from material (relabeling) symmetry. We will present a brief overview of the history of this balance law of continuum mechanics, and discuss it in the context of an ideal fluid. It will be shown that Kelvin's circulation theorem, Cauchy's invariants, Weber's integral, and other related quantities follow from this balance law "

3.3   Noether's theorem

2016-11-23 Predrag A variational principle (such as the action (20.42) in case at hand) together with a continuous symmetry implies

> **Noether's theorem**: To every one-parameter, continuous group of symmetries of a Lagrangian dynamical system there corresponds a scalar, real-valued conserved quantity.

Is there is a version of it for discrete translations? What is the conserved quantity for a single cat map? What is it for the lattice? Internet says many contradictory things:

"The fact that a Lagrangian is unchanged by a discrete transformation is of no significance. There is no conserved quantity associated with the transformation."

"For infinite symmetries like lattice translations the conserved quantity is continuous, albeit a periodic one. So in such case momentum is conserved modulo vectors in the reciprocal lattice. The conservation is local just as in the case of continuous symmetries."

Read about it here.

Mansfield [24] in proceedings here and in her talk defines *total difference* and says " Just as an integral of a total divergence depends only on the boundary data, so does the sum over lattice domain of a total difference."

She states the discrete Noether's Theorem, and in her Example 1.3.7 she shows that for a discretization of a standard mechanical Lagrangian, time invariance yields "energy" as a the conserved quantity.

Hydon and Mansfield [15].

Capobianco and Toffoli [6] *Can anything from Noether's Theorem be salvaged for discrete dynamical systems?* is fun to read (but ultimately unsatisfactory):

" we take the Ising spin model with both ferromagnetic and antiferromagnetic bonds. We show that –and why– energy not only acts as a generator of the dynamics for this family of systems, but is also conserved when the dynamics is time-invariant."

The *microcanonical Ising model* is strictly deterministic and invertible: on a given step, a spin will flip (that is, reverse its orientation) if and only if doing so will leave the sum of the potential energies of the four surrounding bonds unchanged. The Ising dynamics is a second-order recurrence relation. They define "energy" as the length of the boundary between 'up' and 'down' domains. While the magnetization—number of spins up minus number of spins down—may change with time, that length, and thus the energy, remains constant. The total energy of a system may be defined as

1. A real-valued function of the system's state,

2. that is additive,

3. and is a generator of the dynamics.

In a discrete Hamiltonian dynamics, a state is no longer a "position / momentum" pair $< q, p >$ as in the continuous case, but an ordered pair of configurations $< q_0, q_1 >$.

A second-order dynamical system has an evolution rule of the form

$$x_{t+1} = g(x_t, x_{t-1}).$$

References

[1] S. Anco, "On the incompleteness of Ibragimov's conservation law theorem and its equivalence to a standard formula using symmetries and adjoint-symmetries", Symmetry **9**, 33 (2017).

[2] S. C. Anco and G. Bluman, "Direct construction method for conservation laws of partial differential equations Part I: Examples of conservation law classifications", Eur. J. Appl. Math. **13**, 545–566 (2002).

[3] S. C. Anco and G. Bluman, "Direct construction method for conservation laws of partial differential equations Part II: General treatment", Eur. J. Appl. Math. **13**, 567–585 (2002).

[4] S. V. Bolotin and D. V. Treschev, "Hill's formula", Russ. Math. Surv. **65**, 191 (2010).

[5] L. Bourdin, J. Cresson, I. Greff, and P. Inizan, Variational integrators of fractional Lagrangian systems in the framework of discrete embeddings.

[6] S. Capobianco and T. Toffoli, "Can anything from Noether's theorem be salvaged for discrete dynamical systems?", in *Unconventional Computation: 10th Intern. Conf., UC 2011, Turku, Finland*, edited by C. S. Calude, J. Kari, I. Petre, and G. Rozenberg (Springer, Berlin, Heidelberg, 2011), pp. 77–88.

[7] P. Cvitanović and Y. Lan, Turbulent fields and their recurrences, in Correlations and Fluctuations in QCD : Proceedings of 10. International Workshop on Multiparticle Production, edited by N. Antoniou (2003), pp. 313–325.

[8] F. Gay-Balmaz and H. Yoshimura, "A Lagrangian variational formulation for nonequilibrium thermodynamics. Part I: Discrete systems", J. Geom. Phys. **111**, 169–193 (2017).

[9] F. Gay-Balmaz and H. Yoshimura, "Dirac structures in nonequilibrium thermodynamics", J. Math. Phys. **59**, 012701 (2018).

[10] F. Gay-Balmaz and H. Yoshimura, "Variational discretization of the nonequilibrium thermodynamics of simple systems", Nonlinearity **31**, 1673–1705 (2018).

[11] F. Gay-Balmaz and H. Yoshimura, "A free energy Lagrangian variational formulation of the Navier-Stokes-Fourier system", Int. J. Geom. Methods Mod. Phys. **16**, 1940006 (2019).

[12] E. Grinspun, M. Desbrun, K. Polthier, P. Schröder, and A. Stern, *Discrete Differential Geometry: An Applied Introduction*, SIGGRAPH 2006 Courses (ACM, 2006).

[13] E. Hairer, C. Lubich, and G. Wanner, *Geometric Numerical Integration. Structure-Preserving Algorithms for Ordinary Differential Equations*, 2nd ed. (Springer, Berlin, 2006).

[14] F. H. Harlow and J. E. Welch, "Numerical calculation of time-dependent viscous incompressible flow of fluid with free surface", Phys. Fluids **8**, 2182–2189 (1965).

[15] P. E. Hydon and E. L. Mansfield, "Extensions of Noether's Second Theorem: from continuous to discrete systems", Proc. R. Soc. London A **467**, 3206–3221 (2011).

[16] N. H. Ibragimov, "Integrating factors, adjoint equations and Lagrangians", J. Math. Anal. Appl. **318**, 742–757 (2006).

[17] N. H. Ibragimov, "A new conservation theorem", J. Math. Anal. Appl. **333**, 311–328 (2007).

[18] N. H. Ibragimov, "Quasi-self-adjoint differential equations", Arch. ALGA **4**, 55–60 (2007).

[19] N. H. Ibragimov, "Nonlinear self-adjointness and conservation laws", J. Phys. A **44**, 432002 (2011).

[20] N. H. Ibragimov, "Conservation laws and non-invariant solutions of anisotropic wave equations with a source", Nonlinear Anal. Real World Appl. **40**, 82–94 (2018).

[21] H. O. Jacobs, Crash course in discrete Lagrangian mechanics, tech. rep. (U. Michigan, 2012).

[22] M. Kraus and O. Maj, "Variational integrators for nonvariational partial differential equations", Physica D **310**, 37–71 (2015).

[23] Y. Lan and P. Cvitanović, "Variational method for finding periodic orbits in a general flow", Phys. Rev. E **69**, 016217 (2004).

[24] E. L. Mansfield, Noether's theorem for smooth, difference and finite element schemes, in Foundations of computational mathematics, santander 2005, Vol. 331, London Math. Soc. Lect. Notes (2006), pp. 230–254.

[25] J. E. Marsden and M. West, "Discrete mechanics and variational integrators", Acta Numerica **10**, 357–514 (2001).

[26] J. Marsden, S. Pekarsky, S. Shkoller, and M. West, "Variational methods, multisymplectic geometry and continuum mechanics", J. Geom. Phys. **38**, 253–284 (2001).

[27] P. J. Olver, *Applications of Lie Groups to Differential Equations* (Springer, New York, 1998).

[28] D. Pavlov, P. Mullen, Y. Tong, E. Kanso, J. E. Marsden, and M. Desbrun, "Structure-preserving discretization of incompressible fluids", Physica D **240**, 443–458 (2011).

[29] M. Ruggieri and M. P. Speciale, "Conservation laws by means of a new mixed method", Int. J. Non Linear Mech. **95**, 327–332 (2017).

[30] M. Scholle and F. Marner, "A non-conventional discontinuous Lagrangian for viscous flow", R. Soc. Open Sci. **4**, 160447 (2017).

[31] M. Skopenkov, Discrete field theory: symmetries and conservation laws, 2017.

[32] D. Tsang, C. R. Galley, L. C. Stein, and A. Turner, "Slimplectic integrators: Variational integrators for general nonconservative systems", Astro. J **809**, L9 (2015).

[33] Q. Wang, S. A. Gomez, P. J. Blonigan, A. L. Gregory, and E. Y. Qian, "Towards scalable parallel-in-time turbulent flow simulations", Phys. Fluids **25**, 110818 (2013).

[34] L. Wei and Y. Wang, "Symmetry analysis, conserved quantities and applications to a dissipative DGH equation", J. Diff. Equ. **266**, 3189–3208 (2019).

[35] J. Wisdom, "The dynamical systems approach to numerical integration", Mon. Not. R. Astron. Soc. **474**, 3273–3279 (2017).

[36] J. Wisdom and M. Holman, "Symplectic maps for the n-body problem", Astron. J. **102**, 1528 (1991).

Chapter 4

Symmetries of space-time Kuramoto-Sivashinsky equation

In this chapter we look at the discrete subgroups of $O(2) \times SO(2)$ that arise when calculating invariant 2-torus spatiotemporal solutions, and write up the projection operators algebra needed to restrict the computations to invariant subspaces. The discussion will be restricted to solutions that lie in the flow invariant antisymmetric subspace $\mathbb{U}^+$, whose spatiotemporal subgroup is $Z_2 \times (e)$, and pre-periodic orbits whose discrete symmetry subgroup is $Z_2 \times C_2$. [1]

4.1 Symmetries of Kuramoto-Sivashinsky equation

The Kuramoto-Sivashinsky equation (18.1) is equivariant under spatial translations, spatial reflections and temporal translations and Galilean transformations. The Galilean symmetry $u(x,t)$ is a solution, then $u(x - ct, t) - c$, with c an arbitrary constant speed, is also a solution. Without loss of generality, in our calculations we shall set the mean velocity of the front to zero,

$$\langle u \rangle(t) \;=\; \int_0^L dx \, u(x,t) = 0 \,. \qquad (4.1)$$

If the system is compactified on a 2-torus, with periodic boundary conditions $u(x,t) = u(x + L, t + T)$, the symmetry group is

$$G = O(2)_x \times SO(2)_t = D_{1,x} \ltimes SO(2)_x \times SO(2)_t \,. \qquad (4.2)$$

---

[1]Predrag 2018-04-24: Summarize here the Kuramoto-Sivashinsky analogue of relevant parts of the plane Couette flow equilibria and relative equilibria classification of Gibson, Halcrow and Cvitanović [7].

The elements of the 1-parameter group of spatial shifts and reflections are $O(2)_x : \{\tau_{d/L}, \sigma\}$, and the elements of the 1-parameter group of temporal shifts are $SO(2)_t : \{\tau_{d/T}\}$. If $u(x,t)$ is a solution, then $\tau_{d/L}\, u(x,t) = u(x+d, t)$ is an equivalent solution for any shift $0 \leq d < L$, as is the reflection ('parity' or 'inversion')

$$\sigma\, u(x,t) = -u(-x,t) \,. \tag{4.3}$$

Consider a cyclic group

$$C_m = \{e, \tau, \tau^2, \cdots, \tau^{m-1}\}\,, \qquad \tau^m = e \,.$$

where τ is an $SO(2)$ rotation by $2\pi/m$. C_m is a discrete subgroup of $SO(2)$ for any $m = 2, 3, \cdots$.

A field u on the $2\pi/m$ domain is now a tile whose m copies tile the entire domain. It is periodic on the $2\pi/m$ domain, and thus has Fourier expansion with Fourier modes $\exp(2\pi i m j x)$. This means that $SO(2)$ always has an infinity of discrete subgroups $C_2, C_3, \cdots, C_m, \cdots$; for each the non-vanishing coefficients are only for Fourier modes whose wave numbers are multiples of m.

If we take discrete subgroups in $C_{2,x}$ in place of both $SO(2)$ groups then the order of the discrete group $\widetilde{G} = D_{1,x} \ltimes C_{2,x} \times C_{2,t}$ is of order 8. All spatiotemporal symmetries of discussion can be described by *isotropy subgroups*, which are symmetry subgroups which leave solutions invariant. Specifically the discrete symmetries, spatial reflection symmetry and spatiotemporal shift-reflection symmetry. These particular symmetries have isotropy subgroups $G = D_{1,x}$ and $G = C_{2,t}$ respectively. To cover the discrete spatiotemporal symmetries that are realized by invariant 2-tori we need to investigate the group $G = D_{1,x} \times C_{2,t}$, because its description includes reflection and shift-reflection symmetries. The term shift-reflection denotes solutions which are left invariant only after spatial reflection and a time translation by half a period. We have disregarded $C_{2,x}$ for the discussion of discrete symmetries. This is permitted because spatial half-cell shifts, even in combination with other group elements only permit equivariant solutions, not invariant. Solutions invariant under half-cell shifts in space would have to be doubly periodic in space. For combination with the cyclic group in time it would be a yet undiscovered invariant 2-toruswhich is invariant after a half-cell shifts in space and then time. The general $C_{M,x} \times C_{N,t}$ case is harder to describe; if $M = N$ then one example of a way to construct an invariant solution would be to construct a solution which would be invariant after N total rotations. For instance, a solution with the form

$$u(x,t) = \begin{bmatrix} 1\,2\,3 \\ 3\,1\,2 \\ 2\,3\,1 \end{bmatrix} \tag{4.4}$$

would be invariant after a cycle consisting of one space rotation and two time rotations or two space rotations and one time rotation (each by one third of the domain in the respective, positive directions). This seems incredibly unlikely as it requires the solution to be comprised of permutations of three patterns

which are all equivalent in domain size. This unlikelihood only gets worse for higher order cyclic groups We return from our tangent by getting into the meat of the discussion by analyzing the group $D_{1,x} \times C_{2,t}$. We demonstrate some standard group theoretic calculations such as looking at the character table table 12.1 and projection operators (12.35).

Table 4.1: Because the direct product group is abelian we only have one dimensional representations and as such the character table follows directly.

	e	σ_x	τ_t	$\sigma_x \tau_t$
E	1	1	1	1
Γ_1	1	1	-1	-1
Γ_2	1	-1	1	-1
Γ_3	1	-1	-1	1

The character table table 12.1, leads to the construction of four linear projection operators

$$
\begin{aligned}
P^{++} &= \frac{1}{4}(1 + \sigma_x + \tau_t + \sigma_x \tau_t) \\
P^{+-} &= \frac{1}{4}(1 + \sigma_x - \tau_t - \sigma_x \tau_t) \\
P^{-+} &= \frac{1}{4}(1 - \sigma_x + \tau_t - \sigma_x \tau_t) \\
P^{--} &= \frac{1}{4}(1 - \sigma_x - \tau_t + \sigma_x \tau_t),
\end{aligned}
\tag{4.5}
$$

where σ_x, τ_t denote spatial reflection about the $x = 0$ line and time translation by half a period, respectively. The solution space can be decomposed into the irreducible subspaces produced by these projection operators $\mathbb{U} = \mathbb{U}^{++} \oplus \mathbb{U}^{+-} \oplus \mathbb{U}^{-+} \oplus \mathbb{U}^{--}$. In the context of a real valued spatiotemporal Fourier basis each of these subspaces corresponds to a subset of coefficients in the expansion (??)

$$
\begin{aligned}
u^{-+}(x,t) &= \sum_k \sum_j \hat{a}_{kj} \cos(\omega_j t_n) \cos(q_k x_m) \\
u^{--}(x,t) &= \sum_k \sum_j \hat{b}_{kj} \sin(\omega_j t_n) \cos(q_k x_m) \\
u^{++}(x,t) &= \sum_k \sum_j \hat{c}_{kj} \sin(q_k x_m) \cos(\omega_j t_n) \\
u^{+-}(x,t) &= \sum_k \sum_j \hat{d}_{kj} \sin(q_k x_m) \sin(\omega_j t_n).
\end{aligned}
\tag{4.6}
$$

We won't use these equations just yet but they are good for classifying what each projection operator corresponds to. This classification comes naturally from the parity (odd, even) of the trigonometric functions therein. They can

later be used to derive constraints on the spatiotemporal Fourier coefficients pertaining to invariance under certain symmetry operations.

Before we continue, it will first be convenient to calculate the relationships between the projection operators (12.35) and the spatial differentiation operator. The utility comes later when we apply these projection operators to the Kuramoto-Sivashinsky equation, specifically when considering the nonlinear term.

$$
\begin{aligned}
D_x P^{++} &= \frac{1}{4} D_x (1 + \sigma_x + \tau_t + \sigma_x \tau_t) \\
&= \frac{1}{4} (1 - \sigma_x + \tau_t - \sigma_x \tau_t) D_x \\
&= P^{-+} D_x \\
D_x P^{+-} &= \frac{1}{4} D_x (1 + \sigma_x - \tau_t - \sigma_x \tau_t) \\
&= \frac{1}{4} (1 - \sigma_x - \tau_t + \sigma_x \tau_t) D_x \\
&= P^{--} D_x \\
D_x P^{-+} &= \frac{1}{4} D_x (1 - \sigma_x + \tau_t - \sigma_x \tau_t) \\
&= \frac{1}{4} (1 + \sigma_x + \tau_t + \sigma_x \tau_t) D_x \\
&= P^{++} D_x \\
D_x P^{--} &= \frac{1}{4} D_x (1 - \sigma_x - \tau_t + \sigma_x \tau_t) \\
&= \frac{1}{4} (1 + \sigma_x - \tau_t - \sigma_x \tau_t) D_x \\
&= P^{+-} D_x \,.
\end{aligned}
\tag{4.7}
$$

These identities allow us to rewrite the nonlinear terms present in each projection of the Kuramoto-Sivashinsky equation as derivatives of projection components as opposed to projections of derivatives, which we believe leads to less confusing analysis. Note that the effect can be summarized by flipping the first $\pm$, pertaining to the coefficient of the spatial reflection terms in (12.35) The surviving nonlinear terms after the application of each projection operator are as follows

$$
\begin{aligned}
P^{++}(u \partial_x u) &= u^{\pm\pm} \partial_x (u^{\pm\pm}) \\
P^{+-}(u \partial_x u) &= u^{\pm\pm} \partial_x (u^{\pm\mp}) \\
P^{-+}(u \partial_x u) &= u^{\pm\pm} \partial_x (u^{\mp\pm}) \\
P^{--}(u \partial_x u) &= u^{\pm\pm} \partial_x (u^{\mp\mp}) \,.
\end{aligned}
\tag{4.8}
$$

Using these relations (12.38) we can produce the projections of the Kuramoto-Sivashinsky equation onto the different irreducible subspaces, noting that the

projection operator commutes with the linear terms such that

$$
\begin{aligned}
P^{++}F(u) &= u_t^{++} + u_{xx}^{++} + u_{xxxx}^{++} \\
&+ (u^{++}\partial_x(u^{++}) + u^{+-}\partial_x(u^{+-}) \\
&+ u^{-+}\partial_x(u^{-+}) + u^{--}\partial_x(u^{--})) \\
P^{+-}F(u) &= u_t^{+-} + u_{xx}^{+-} + u_{xxxx}^{+-} \\
&+ (u^{++}\partial_x(u^{+-}) + u^{+-}\partial_x(u^{++}) \\
&+ u^{-+}\partial_x(u^{--}) + u^{--}\partial_x(u^{-+})) \\
P^{-+}F(u) &= u_t^{-+} + u_{xx}^{-+} + u_{xxxx}^{-+} \\
&+ (u^{++}\partial_x(u^{-+}) + u^{+-}\partial_x(u^{--}) \\
&+ u^{-+}\partial_x(u^{++}) + u^{--}\partial_x(u^{+-})) \\
P^{--}F(u) &= u_t^{--} + u_{xx}^{--} + u_{xxxx}^{--} \\
&+ (u^{++}\partial_x(u^{--}) + u^{+-}\partial_x(u^{-+}) \\
&+ u^{-+}\partial_x(u^{+-}) + u^{--}\partial_x(u^{++})) \,.
\end{aligned}
\tag{4.9}
$$

Solutions to (18.1) satisfy $F = 0$ by definition so by extension solutions must also satisfy $P^{\pm\pm}F = 0$. With this we can determine the combinations of projection operators whose equations are "self contained". This is similar to the notion of *flow invariant subspaces* but because we do not have dynamics we can't really use this term. Instead, these subspaces correspond to a constrained set of equations that solutions with particular discrete symmetries must adhere to. For example, assume that the only nonzero component u is $u = u^{++}$. Substitution of (12.39) yields

$$
\begin{aligned}
P^{++}F(u^{++}) &= u_t^{++} + u_{xx}^{++} + u_{xxxx}^{++} + u^{++}\partial_x(u^{++}) \\
P^{+-}F(u^{++}) &= 0 \\
P^{-+}F(u^{++}) &= 0 \\
P^{--}F(u^{++}) &= 0 \,,
\end{aligned}
\tag{4.10}
$$

so $\mathbb{U}^{++}$ is an invariant subspace. In fact, this subspace corresponds to equilibria solutions which live on the $T = 0$ line. The meaning of self contained in this example is that we assumed that $u = u^{++}$ and the only nonzero part of (12.40) is the $P^{++}F(u^{++})$ component. Perhaps a more elucidating example is generated by the assumption that $u = u^{--} \neq 0$. Substitution yields

$$
\begin{aligned}
P^{++}F(u^{--}) &= u^{--}\partial_x(u^{--}) \\
P^{+-}F(u^{--}) &= 0 \\
P^{-+}F(u^{--}) &= 0 \\
P^{--}F(u^{--}) &= u_t^{--} + u_{xx}^{--} + u_{xxxx}^{--}
\end{aligned}
\tag{4.11}
$$

which indicates that the equations are not self contained as components other than $P^{--}F(u^{--})$ are non-zero. Recall that each of these components is equivalently equal to zero. Because these equations represent scalar field values

defined at every x, t this implies that in order to satisfy $u^{--}\partial_x(u)^{--} = 0$ either u^{--}, its derivative $\partial_x(u)^{--}$, or both must equal to zero at every point on the spatiotemporal domain. The only nontrivial possibility is if there are (at least) two disjoint regions such that $\Omega_u = \{(x, t) : u(x, t) = 0\}$ and $\Omega_{u_x} = \{(x, t) : u_x(x, t) = 0\}$. By smoothness, if $u = 0$ then $u_x = 0$. This implies that $u_x = 0$ for all (x, t); if $u_x = 0$ everywhere and $u = 0$ for some (x, t) then it must be the case that $u = 0$ everywhere which contradicts our original assumption that $u = u^{--} \neq 0$. The rest of the symmetry invariant subspaces follow from a similar substitutions. To expedite the derivation process, note that the equation for $P^{++}F$ contains all of the symmetric terms $u^{\pm\pm}\partial_x(u^{\pm\pm})$ such that there is no possibility of an invariant subspaces which does not intersect $\mathbb{U}^{++}$. Following a process of elimination we can show that the possible symmetry invariant subspaces are $\mathbb{U}^{++}$, $\mathbb{U}^{++}\oplus\mathbb{U}^{--}$, $\mathbb{U}^{++}\oplus\mathbb{U}^{+-}$ and $\mathbb{U}^{++}\oplus\mathbb{U}^{-+}$ and of course the full space $\mathbb{U}$. There are no triplet subspaces (comprised of three components) which can be shown using the parity of the different subspaces. We can interpret these subspaces by addition of the corresponding projection operators (12.35)

$$\begin{aligned}
P_0 \equiv P^{++} &= \frac{1}{4}(1 + \sigma_x + \tau_t + \sigma_x\tau_t) \\
P_{\sigma_x} \equiv P^{++} + P^{+-} &= \frac{1}{2}(1 + \sigma_x) \\
P_{\tau_t} \equiv P^{++} + P^{-+} &= \frac{1}{2}(1 + \tau_t) \\
P_{\sigma_x\tau_t} \equiv P^{++} + P^{--} &= \frac{1}{2}(1 + \sigma_x\tau_t).
\end{aligned} \tag{4.12}$$

With these projection operators we can interpret the symmetry invariant subspaces as follows: $\mathbb{U}^{++}$ represents the fixed point ($T = 0$) subspace, $\mathbb{U}^{++}\oplus\mathbb{U}^{+-}$ the spatial reflection invariant subspace, $\mathbb{U}^{++}\oplus\mathbb{U}^{--}$ the shift-reflection invariant subspace, and lastly $\mathbb{U}^{++}\oplus\mathbb{U}^{-+}$ which contains solutions that are invariant after a half period shift in time. This subspace of "twice repeating" solutions is trivial and not useful; doubly periodic solutions can always be made to repeat twice in time by definition. The interpretation of the corresponding subspace is therefore not very intuitive.

The next question to answer is how continuous spatial translation symmetry manifests itself in this spatiotemporal context. How do these subspaces relate to the continuous spatial translation symmetry? The three subspaces $\mathbb{U}_0, \mathbb{U}_{\sigma_x}, \mathbb{U}_{\sigma_x\tau_t}$ share an interesting property in a real valued (SO(2)) representation. Specifically, the subspaces of spatiotemporal Fourier coefficients corresponding to invariance under these discrete symmetries are all orthogonal to the space of spatial translations. This can be seen by acting on the different orbits with the spatial derivative operator which is the generator of infinitesimal translations. The subgroup $H = C_{M,x}$ represents continuous spatial translation symmetry after discretization. We utilize a co-moving frame ansatz to handle this symmetry, which we will now develop. As previously mentioned, we use a real valued (SO(2)) representation for the spatiotemporal Fourier co-

efficients. This choice makes the matrix representations of the group elements slightly more complicated as they will be block diagonal as opposed to exactly diagonal. Note that because of doubly periodic boundary conditions, translations are the same as rotation. The matrix representation of the group element which spatially rotates M Fourier modes by a value θ is a block diagonal matrix with M blocks; each block being a representation of two dimensional rotations for the corresponding wavenumber k

$$\tilde{g}(\theta) \equiv \begin{bmatrix} \cos q_k \theta & -\sin q_k \theta \\ \sin q_k \theta & \cos q_k \theta \end{bmatrix}. \tag{4.13}$$

This block diagonal matrix acts on M Fourier modes; the corresponding extension to the set of spatiotemporal Fourier coefficients is simply N copies of (12.43). In other words we have N blocks of (12.43). This form lends itself to the matrix representation for the co-moving reference frame transformation. The co-moving reference frame is the reference frame which makes relative periodic orbits periodic by applying a time-dependent spatial translation to every point of the invariant 2-torus. Using (12.43) the matrix representation of the co-moving frame transformation is as follows

$$g(\frac{\sigma t_n}{T}) \equiv \begin{bmatrix} \tilde{g}(\frac{\sigma t_1}{T}) & 0 & \cdots & 0 \\ 0 & \tilde{g}(\frac{\sigma t_2}{T}) & \cdots & 0 \\ \vdots & \vdots & \ddots & \vdots \\ 0 & 0 & 0 & \tilde{g}(\frac{\sigma t_N}{T}) \end{bmatrix}. \tag{4.14}$$

Transformations of the type (12.44) will be used in our ansatz for doubly periodic solutions of the Kuramoto-Sivashinsky equation which are relatively periodic.

4.1.1 OLD: Symmetries of Kuramoto-Sivashinsky equation

G, the group of actions $g \in G$ on a state space (reflections, translations, etc.) is a symmetry of the KS flow (18.1) if $g\, u_t = F(g\, u)$. The Kuramoto-Sivashinsky equation is time translationally invariant, and space translationally invariant on a periodic domain under the 1-parameter group of O(2) : $\{\tau_{d/L}, \sigma\}$. If $u(x, t)$ is a solution, then $\tau_{d/L}\, u(x, t) = u(x+d, t)$ is an equivalent solution for any shift $-L/2 < d \leq L/2$, as is the reflection ('parity' or 'inversion')

$$\sigma\, u(x) = -u(-x). \tag{4.15}$$

The translation operator action on the Fourier coefficients (1.23), represented here by a complex valued vector $a = \{a_k \in \mathbb{C} \,|\, k = 1, 2, \ldots\}$, is given by

$$\tau_{d/L}\, a = \mathbf{g}(d)\, a, \tag{4.16}$$

where $\mathbf{g}(d) = \text{diag}(e^{iq_k\, d})$ is a complex valued diagonal matrix, which amounts to the k-th mode complex plane rotation by an angle $k\, d/\tilde{L}$. The reflection acts

on the Fourier coefficients by complex conjugation,

$$\sigma\, a = -a^*\,. \tag{4.17}$$

Reflection generates the dihedral subgroup $\mathrm{D}_1 = \{1, \sigma\}$ of $\mathrm{O}(2)$. Let $\mathbb{U}$ be the space of real-valued velocity fields periodic and square integrable on the interval $\Omega = [-L/2, L/2]$,

$$\mathbb{U} = \{u \in L^2(\Omega) \mid u(x) = u(x+L)\}\,. \tag{4.18}$$

A continuous symmetry maps each state $u \in \mathbb{U}$ to a manifold of functions with identical dynamic behavior. Relation $\sigma^2 = 1$ induces linear decomposition $u(x) = u^+(x) + u^-(x)$, $u^{\pm}(x) = P^{\pm}u(x) \in \mathbb{U}^{\pm}$, into irreducible subspaces $\mathbb{U} = \mathbb{U}^+ \oplus \mathbb{U}^-$, where

$$P^+ = (1 + \sigma)/2\,, \qquad P^- = (1 - \sigma)/2\,, \tag{4.19}$$

are the antisymmetric/symmetric projection operators. Applying P^+, P^- on the Kuramoto-Sivashinsky equation (18.1) we have [14]

$$
\begin{aligned}
u_t^+ &= -(u^+ u_x^+ + u^- u_x^-) - u_{xx}^+ - u_{xxxx}^+ \\
u_t^- &= -(u^+ u_x^- + u^- u_x^+) - u_{xx}^- - u_{xxxx}^-\,.
\end{aligned}
\tag{4.20}
$$

If $u^- = 0$, Kuramoto-Sivashinsky flow is confined to the antisymmetric $\mathbb{U}^+$ subspace,

$$u_t^+ = -u^+ u_x^+ - u_{xx}^+ - u_{xxxx}^+\,, \tag{4.21}$$

but otherwise the nonlinear terms in (12.50) mix the two subspaces.

Any rational shift $\tau_{1/m} u(x) = u(x + L/m)$ generates a discrete cyclic subgroup C_m of $\mathrm{O}(2)$, also a symmetry of Kuramoto-Sivashinsky equation. Reflection together with C_m generates another symmetry of Kuramoto-Sivashinsky equation, the dihedral subgroup D_m of $\mathrm{O}(2)$. The only non-zero Fourier components of a solution invariant under C_m are $a_{jm} \neq 0$, $j = 1, 2, \cdots$, while for a solution invariant under D_m we also have the condition $\mathrm{Re}\, a_j = 0$ for all j. D_m reduces the dimensionality of state space and aids computation of equilibria and periodic orbits within it. For example, the 1/2-cell translations

$$\tau_{1/2}\, u(x) = u(x + L/2) \tag{4.22}$$

and reflections generate $\mathrm{O}(2)$ subgroup $\mathrm{D}_2 = \{1, \sigma, \tau, \tau\sigma\}$, which reduces the state space into four irreducible subspaces (for brevity, here $\tau = \tau_{1/2}$):

$$
\begin{array}{lcccc}
 & & \tau & \sigma & \tau\sigma \\
P^{(1)} = \dfrac{1}{4}(1 + \tau + \sigma + \tau\sigma) & \quad & S & S & S \\[4pt]
P^{(2)} = \dfrac{1}{4}(1 + \tau - \sigma - \tau\sigma) & \quad & S & A & A \\[4pt]
P^{(3)} = \dfrac{1}{4}(1 - \tau + \sigma - \tau\sigma) & \quad & A & S & A \\[4pt]
P^{(4)} = \dfrac{1}{4}(1 - \tau - \sigma + \tau\sigma) & \quad & A & A & S\,.
\end{array}
\tag{4.23}
$$

$P^{(j)}$ is the projection operator onto $u^{(j)}$ irreducible subspace, and the last 3 columns refer to the symmetry (or antisymmetry) of $u^{(j)}$ functions under reflection and 1/2-cell shift. By the same argument that identified (12.51), the Kuramoto-Sivashinsky flow stays within the $\mathbb{U}^S = \mathbb{U}^{(1)} + \mathbb{U}^{(2)}$ irreducible invariant D_1 subspace of u profiles symmetric under 1/2-cell shifts.

While in general the bilinear term $(u^2)_x$ mixes the irreducible subspaces of D_n, for D_2 there are four subspaces invariant under the flow [14]:

- $\{0\}$:   the $u(x) = 0$ equilibrium

- $\mathbb{U}^+ = \mathbb{U}^{(1)} + \mathbb{U}^{(3)}$:
  the reflection D_1 irreducible space of antisymmetric $u(x)$

- $\mathbb{U}^S = \mathbb{U}^{(1)} + \mathbb{U}^{(2)}$:
  the shift D_1 irreducible space of $L/2$ shift symmetric $u(x)$

- $\mathbb{U}^{(1)}$:
  the D_2 irreducible space of $u(x)$ invariant under $x \mapsto L/2 - x,\ u \mapsto -u$.

With the continuous translational symmetry eliminated within each subspace, there are no relative equilibria and relative periodic orbits, and one can focus on the equilibria and periodic orbits only, as was done for $\mathbb{U}^+$ in refs. [3, 16, 17]. In the Fourier representation, the $u \in \mathbb{U}^+$ antisymmetry amounts to having purely imaginary coefficients, since $a_{-k} = a_k^* = -a_k$. The 1/2 cell-size shift $\tau_{1/2}$ generated 2-element discrete subgroup $\{1, \tau_{1/2}\}$ is of particular interest because in the $\mathbb{U}^+$ subspace the translational invariance of the full system reduces to invariance under discrete translation (12.52) by half a spatial period $L/2$.

Each of the above dynamically invariant subspaces is unstable under small perturbations, and generic solutions of Kuramoto-Sivashinsky equation belong to the full space. Nevertheless, since all equilibria of the KS flow studied in ref. [5] lie in the $\mathbb{U}^+$ subspace, $\mathbb{U}^+$ plays important role for the global geometry of the flow. However, linear stability of these equilibria has eigenvectors both in and outside of $\mathbb{U}^+$, and needs to be computed in the full state space.

Predrag's notes - temporary section

Symmetries of plane Couette flow are discussed in Gibson, Halcrow and Cvitanović [8] *Equilibrium and traveling-wave solutions of plane Couette flow.* Here I adopt clips from the repository `halcrow/n00bs/n00bs.tex` to the spatiotemporal Kuramoto-Sivashinsky, and will use this text as a temporary staging ground before editing Matt's *chap:disc_symm* text. Not very important, but my life is a bit easier if I harmonize the notation with ChaosBook.org.

We denote the spatial reflection through the origin by σ. The σ symmetry generates a discrete dihedral group $D_{1,x} = \{e, \sigma\}$ of order 2, where

$$\sigma\, u(x,t) = -u(-x,t)\,. \tag{4.24}$$

With periodic boundary conditions, the spatial and time translation symmetries become the $\mathrm{SO}(2)_x \times \mathrm{SO}(2)_t$ continuous two-parameter group of commuting spacetime translations

$$\tau(d_x)_x \tau(d_t)_t u(x,t) = u(x+d_x, t+d_t)\,. \tag{4.25}$$

The Kuramoto-Sivashinsky equations are thus equivariant under the group $G = \mathrm{O}(2)_x \times \mathrm{O}(2)_t = \mathrm{D}_{1,x} \ltimes \mathrm{SO}(2)_x \times \mathrm{SO}(2)_t$, where $\ltimes$ stands for a semi-direct product, x subscripts indicate spatial translations and reflections in x, and t subscripts indicate time translations in t.

The solutions of an equivariant system can satisfy all of the system's symmetries, a proper subgroup of them, or have no symmetry at all. For a given solution $\mathbf{u}$, the subgroup that contains all symmetries that fix $\mathbf{u}$ (that satisfy $s\mathbf{u} = \mathbf{u}$) is called the isotropy (or stabilizer) subgroup of $\mathbf{u}$ [9, 10, 13, 20]. For example, a typical turbulent trajectory $\mathbf{u}(\mathbf{x}, t)$ has no symmetry beyond the identity, so its isotropy group is $\{e\}$. At the other extreme is the laminar equilibrium, whose isotropy group is the full symmetry group G.

Consider $S = \{e, \tau_x, \tau_t, \tau_{xt}\}$, where

$$\begin{aligned}
\tau_x\, u(x,t) &= u(x + L/2, t) \\
\tau_t\, u(x,t) &= u(x, t + T/2) \\
\tau_{xt}\, u(x,t) &= u(x + L/2, t + T/2)\,.
\end{aligned} \tag{4.26}$$

2018-05-01 TO BE CONTINUED

 Four isotropy subgroups of order 4 are generated by picking σ_{xt} as the first generator, and σ_t, $\sigma_t \tau_x$, $\sigma_t \tau_t$, or $\sigma_t \tau_{xt}$ as the second generator (*R* for reflect-rotate):

$$\begin{aligned}
R\ &= \{e, \sigma, \sigma_t, \sigma_{xt}\} &&= \{e, \sigma_{xt}\} \times \{e, \sigma_t\} \\
R_x\ &= \{e, \sigma\tau_x, \sigma_t\tau_x, \sigma_{xt}\} &&= \{e, \sigma_{xt}\} \times \{e, \sigma\tau_x\} \\
R_t\ &= \{e, \sigma\tau_t, \sigma_t\tau_t, \sigma_{xt}\} &&= \{e, \sigma_{xt}\} \times \{e, \sigma_t\tau_t\} \\
R_{xt} &= \{e, \sigma\tau_{xt}, \sigma_t\tau_{xt}, \sigma_{xt}\} &&= \{e, \sigma_{xt}\} \times \{e, \sigma_t\tau_{xt}\} \simeq S\,.
\end{aligned} \tag{4.27}$$

These are the only isotropy groups of order 4 containing σ_{xt} and no isolated translation elements. Together with $\{e, \sigma_{xt}\}$, these 5 isotropy subgroups represent the 5 conjugacy classes in which expect to find equilibria.

The R_{xt} isotropy subgroup is particularly important, as many equilibria belong to this conjugacy class.

4.2 Fourier transform normalization factors

[2] We have time-periodic solutions, namely two repeats of pre-periodic orbits, however, in my intuition (which might be wrong) we don't necessarily need to start simulations from those. Since the dynamics is chaotic, after a finite time,

---

[2]Matt 2016-06-17: Burak Budanur wrote this.

say 20 Lyapunov times ($e^{-20} \sim O(10^{-9})$), correlations between initial condition and final point will be so low that imposing periodicity in time will not effect the outcome.

With this in mind, let's say that you solved the Kuramoto-Sivashinsky equation in spatially periodic domain, with an initial condition on the strange attractor (no transients), and obtained $u(x, t)$, for $x \in [0, L)$ and $t \in [0, T)$. You can find the spatial derivatives by inverse Fourier transformations:

$$
\begin{aligned}
u_x(x, t) &= \mathcal{F}^{-1}\left\{iq_k u_k\right\}, \quad u_{xx}(x, t) = \mathcal{F}^{-1}\left\{(iq_k)^2 u_k\right\}, \\
u_{xxx}(x, t) &= \mathcal{F}^{-1}\left\{(iq_k)^3 u_k\right\}, \quad u_{xxxx}(x, t) = \mathcal{F}^{-1}\left\{(iq_k)^4 u_k\right\}. \quad (4.28)
\end{aligned}
$$

In fact, you must compute spatial derivatives as above (not by approximating with finite-differences) because otherwise they will not be as accurate numerically. Side note: depending on the implementation you're using, Fourier transforms would need you to add a normalization factor, usually a division by N (number of modes).

Now that you have $u_x(x, t)$ and its space derivatives, you should take their value at $x = 0$ for $t \in [0, T)$ as your initial condition and input it to the space-integrator. Then you can compare the outcome with the one you already have from time-integration.

[3] In this section we go through the derivation of (1.36) and state the correct normalizations for Fourier transforms.

Let us start from the following definition of the Fourier expansion of the time-periodic function $u(t) = u(t + T)$:

$$
u(t) = \sum_{k=-\infty}^{\infty} \hat{u}_k e^{i\omega_k t}, \quad \text{where } \omega_k = 2\pi k/T. \quad (4.29)
$$

In order to find Fourier coefficients $\hat{u}_k$, we multiply the above equation from the left by $\frac{1}{T}\int_0^T dt\, e^{-i\omega_m t}$, on the RHS we get:

$$
\sum_{k=-\infty}^{\infty} \hat{u}_k \frac{1}{T}\int_0^T dt\, e^{i(\omega_k - \omega_m)t} = \sum_{k=-\infty}^{\infty} \hat{u}_k \frac{1}{T}\int_0^T dt\, e^{i2\pi(k-m)t/T}. \quad (4.30)
$$

If $k \neq m$, then the integral above is integral of a periodic function over one full period, hence 0. If $k = m$, then it is the integral of 1 from 0 to T, and we can replace the integral by $T\delta_{km}$, which picks out $\hat{u}_m$ from the sum. Hence we obtain the forward Fourier transform of $u(t)$ as

$$
\hat{u}_k = \frac{1}{T}\int_0^T dt\, u(t)e^{-i\omega_k t} \quad (4.31)
$$

We can approximate the above transformation by replacing the integral by a Riemann sum $\int_0^T dt \rightarrow \sum_{n=0}^{N-1} \Delta t$, $\Delta t = T/N$, hence we obtain the discrete

---

[3]Matt 2016-07-13: Burak Budanur wrote this section.

Fourier transform as

$$
\begin{aligned}
\hat{u}_k &= \frac{1}{N} \sum_{n=0}^{N-1} u(t_n) e^{-i\omega_k t_n} \text{ , where } t_n = nT/N \\
&= \frac{1}{N} \sum_{n=0}^{N-1} u(t_n) e^{-i2\pi nk/N} \text{ ,} \\
&= \frac{1}{N} \mathcal{F}\{u(t_n)\} \text{ ,}
\end{aligned}
\tag{4.32}
$$

where $\mathcal{F}\{.\}$ denotes the Fourier transformation in Matlab's normalization convention. Consequently, if we take $2N+1$ terms from the series (4.29), we obtain the inverse discrete Fourier transform as

$$
\begin{aligned}
u(t_n) &= \sum_{k=-N/2}^{N/2} \hat{u}_k e^{i\omega_k t_n} \text{ ,} \quad = \sum_{k=-N/2}^{N/2} \hat{u}_k e^{i2\pi kn/N} \text{ ,} \\
&= N\mathcal{F}^{-1}\{\hat{u}_k\} \text{ ,}
\end{aligned}
\tag{4.33}
$$

where $\mathcal{F}^{-1}\{.\}$ is the inverse Fourier transform in the Matlab's convention.

In Matlab it is probably is computationally preferable to carry out the convolution in the fourth equation of (1.36) in time-domain as

$$
\sum_{m=-\infty}^{\infty} \hat{u}_{\ell-m}^{(0)} \hat{u}_m^{(1)} = \mathcal{F}\left\{ \mathcal{F}^{-1}\left\{ \hat{u}^{(0)} \right\} \mathcal{F}^{-1}\left\{ \hat{u}^{(1)} \right\} \right\} \text{ ,}
\tag{4.34}
$$

where $\mathcal{F}$ and $\mathcal{F}^{-1}$ denote the Fourier transform and its inverse, respectively. One should experiment with time-domain sizes and truncation of the Fourier expansion.

One can insert the definition (4.29) into (1.34) and then multiply from left by the integral $\frac{1}{T}\int_0^T dt\, e^{-i\omega_m t}$ in order to confirm that the equation (1.36) is correct. But in order to compute the nonlinear term pseudospectrally, we take the Fourier transform of $u^{(0)}u^{(1)}$, that is

$$
\begin{aligned}
\frac{1}{T}\int_0^T dt\, e^{-i\omega_m t} u^{(0)}(t) u^{(1)}(t) &\approx \frac{1}{N} \sum_{n=0}^{N-1} u^{(0)}(t_n) u^{(1)}(t_n) e^{-i\omega_m t_n} \text{ ,} \\
&= \frac{1}{N} \mathcal{F}\{u^{(0)} u^{(1)}\} \text{ .}
\end{aligned}
\tag{4.35}
$$

4.3 Selection rules for Fourier coefficients

4.3.1 Selection rules for Kuramoto-Sivashinsky

4.3.2 Selection rules for real-valued Fourier coefficients

Although the spatiotemporal Kuramoto-Sivashinsky equation is easier to write in terms of a complex Fourier-Fourier basis, the symmetry invariant subspaces generated by symmetry constraints is easier to describe in terms of real valued Fourier coefficients. The real valued spatiotemporal Fourier expansion can be written

This is the expansion for a general spatiotemporal solution. For each discrete symmetry of the spatiotemporal Kuramoto-Sivashinsky equation there is a unique set of constraints or "selection rules" for the spatiotemporal Fourier coefficients. These selection rules constitute *symmetry invariant subspaces* of solutions of the spatiotemporal Kuramoto-Sivashinsky equation. In this section we commit to the description of the selection rules of the Fourier coefficients. For more discussion on the symmetries themselves we refer the reader to sect. 12.3.2.

The two discrete symmetries we will describe are spatial reflection symmetry and spatiotemporal shift-reflection symmetry. The shift-reflection symmetry is a special case of the broader symmetry group $D_n \times C_n$ ($n = 2$). Due to the uncommon appearance of solutions with $n > 2$ and the relatively easy generalization of the $n = 2$ shift-reflection case, we shall only consider the $n = 2$ symmetry group.

The general procedure for producing these selection rules is not very complicated. Let R represent an arbitrary symmetry operation. If a solution is invariant under R then it satisfies the *invariance condition* $Ru = u$ or equivalently $(R - 1)u = 0$. Substitution of the expansion (**??**) produces a set of constraints that can only be satisfied when a subset of real valued Fourier coefficients are individually equal to zero. To begin we start with spatial reflection symmetry, as it is almost trivial. Solutions invariant under spatial reflection only admit spatially antisymmetric basis functions. Therefore, the selection rules for spatial reflection symmetry are

$$\hat{a}_{kj}, \hat{b}_{kj} = 0 \text{ for all } k, j \,. \tag{4.36}$$

Spatiotemporal shift-reflection is the composition of two symmetry operations: spatial reflection σ_x and time translation by $\tau_{T/2}$. The action of this symmetry is as follows $\sigma_x \tau_{T/2} u(x, t) = -u(-x, t + T/2)$. When directly applied to the real valued Fourier expansion (**??**) and by virtue of trigonometric identities and the

parity of $\sin$ and $\cos$ we have

$$
\begin{aligned}
\sigma_x \tau_{T/2}\, u(x_m, t_n) = &-\sum_{k,j} \cos(q_k(-x_m))(\hat{a}_{kj}\cos(\omega_j(t_n + T/2)) + \hat{b}_{kj}\sin(\omega_j(t_n + T/2))) \\
&+ \sin(q_k(-x_m))(\hat{c}_{kj}\cos(\omega_j(t_n + T/2)) + \hat{d}_{kj}\sin(\omega_j(t_n + T/2))) \\
= &\sum_{k,j} -\cos(q_k x_m)(\hat{a}_{kj}\cos(\omega_j t_n)\cos(\pi j) + \hat{b}_{kj}\sin(\omega_j t_n)\cos(\pi j))) \\
&+ \sin(q_k x_m)(\hat{c}_{kj}\cos(\omega_j t_n)\cos(\pi j) + \hat{d}_{kj}\sin(\omega_j t_n)\cos(\pi j)) \\
= &\sum_{k,j} (-1)^{j+1}\cos(q_k x_m)(\hat{a}_{kj}\cos(\omega_j t_n) + \hat{b}_{kj}\sin(\omega_j t_n)) \\
&+ (-1)^j \sin(q_k x_m)(\hat{c}_{kj}\cos(\omega_j t_n) + \hat{d}_{kj}\sin(\omega_j t_n)),
\end{aligned}
$$

By combining this with the invariance condition $(\sigma_x \tau_{T/2} - 1)u = 0$, we find that the selection rules for spatiotemporal shift-reflection are as follows

$$
\begin{aligned}
\hat{a}_{kj}, \hat{b}_{kj} &= 0 \text{ for } j \text{ even} \\
\hat{c}_{kj}, \hat{d}_{kj} &= 0 \text{ for } j \text{ odd} .
\end{aligned} \tag{4.37}
$$

4.3.3 Selection rules for Fourier coefficients of Navier-Stokes pre-periodic orbits

This section makes the assumption that one is not in the flow invariant subspace defined by Golubitsky and Stewart [10] and Gibson, Halcrow and Cvitanović [7], and also assumes that outside of this flow invariant subspace that there are pre-periodic orbits. Then one can calculate the number of active variables much like sect:selection_KS (?) if one took real valued transforms.

The main results which I'll describe is for s_1 and s_3 "pre-periodic orbitsolutions" if they exist, which I couldn't confirm. Think of this as an algebra check on the previous work if its worthless or not interesting.

For s_1 we have $[u, v, w](x, y, z, t) = [u, v, -w](x + \frac{L_x}{2}, y, -z, t + \frac{T}{2})$. The functions u, v, w have generic expansions (i.e. there is a sum over index m that denotes unit directions $\hat{x}_m$ that I'm not including) given by the following.

$$
\begin{aligned}
\mathbf{u}(\mathbf{x}, t) = &\sum_{jkn\ell} T_\ell(y)[\cos(q_j x)\cos(q_k z)(a_{jkn\ell}\cos(w_n t) + b_{jkn\ell}\sin(w_n t)) \\
+ &\cos(q_j x)\sin(q_k z)(c_{jkn\ell}\cos(w_n t) + d_{jkn\ell}\sin(w_n t)) \\
+ &\sin(q_j x)\cos(q_k z)(e_{jkn\ell}\cos(w_n t) + f_{jkn\ell}\sin(w_n t)) \\
+ &\sin(q_j x)\sin(q_k z)(g_{jkn\ell}\cos(w_n ct) + h_{jkn\ell}\sin(w_n t))]
\end{aligned} \tag{4.38}
$$

applying symmetry operation τs_1 results in (with trigonometric identities and

parity of functions)

$$
\begin{aligned}
u(\mathbf{x}, t) \quad = \quad & \sum_{jkn\ell} T_\ell(y)[(-1)^{j+n} \cos(q_j x) \cos(q_k z)(a_{jkn\ell} \cos(w_n t) + b_{jkn\ell} \sin(w_n t)) \\
+ \quad & (-1)^{j+n+1} \cos(q_j x) \sin(q_k z)(c_{jkn\ell} \cos(w_n t) + d_{jkn\ell} \sin(w_n t)) \\
+ \quad & (-1)^{j+n} \sin(q_j x) \cos(q_k z)(e_{jkn\ell} \cos(w_n t) + f_{jkn\ell} \sin(w_n t)) \\
+ \quad & (-1)^{j+n+1} \sin(q_j x) \sin(q_k z)(g_{jkn\ell} \cos(w_n t) + h_{jkn\ell} \sin(w_n t))] \quad (4.39)
\end{aligned}
$$

which results in the selection rules that $j + n$ must be even for the terms $a_{jkn\ell}, b_{jkn\ell}, e_{jkn\ell}, f_{jkn\ell}$ and $j + n$ must be odd for $c_{jkn\ell}, d_{jkn\ell}, g_{jkn\ell}, h_{jkn\ell}$ for terms in the sums to be non-zero. These selection rules also apply to the v component of the velocity field, but they switch for the w component due to the extra -1 that results from s_1 symmetry operation.

For $j + n$ to be even, they either both half to be even, or both have to be odd, which reduces the number of terms in the summation by a factor of 4. Likewise, $j+n$ to be odd, the indices j, n need to either be odd,even or even,odd pairs; again reducing the number of terms in the summation by a factor of four. Therefore by imposing this type of symmetry and having an spatiotemporal discretization only increases the dimensionality of the problem by a factor of $N_t/4$, making it more manageable memory wise.

For solutions with invariant under τs_3 we have

$$
[u, v, w](x, y, z, t) = [-u, -v, -w](-x, -y, -z + \frac{L_z}{2}, t + \frac{T}{2}),
$$

using the parity of Chebyshev polynomials (because this transformation includes changes to y), trigonometric identities, and parity of sine and cosine functions, we get

$$
\begin{aligned}
u(\mathbf{x}, t) \quad = \quad & \sum_{jkn\ell} T_\ell(y)[(-1)^{l+k+n+1} \cos(q_j x) \cos(q_k z)(a_{jkn\ell} \cos(w_n t) + b_{jkn\ell} \sin(w_n t)) \\
+ \quad & (-1)^{l+k+n} \cos(q_j x) \sin(q_k z)(c_{jkn\ell} \cos(w_n t) + d_{jkn\ell} \sin(w_n t)) \\
+ \quad & (-1)^{l+k+n} \sin(q_j x) \cos(q_k z)(e_{jkn\ell} \cos(w_n t) + f_{jkn\ell} \sin(w_n t)) \\
+ \quad & (-1)^{l+k+n+1} \sin(q_j x) \sin(q_k z)(g_{jkn\ell} \cos(w_n t) + h_{jkn\ell} \sin(w_n t))], \quad (4.40)
\end{aligned}
$$

where the selection rules are identical for each component of the velocity field because the symmetry transformation changes the sign on all of the components. Because the result has the same requirement but over three indices I believe that this just reduces the number of variables by a factor of 8, so including a time dimension only increases the dimensionality by a factor of 8.

4.3.4 Selection Rules for C_n shift-reflection symmetries in Kolmogorov flow

I've been working towards two dimensional Kolmogorov flow code and I realized that it was imperative to figure out the symmetry invariant subspace related for shift reflection where the shift is not a half domain but rather a cyclic

shift of order n as determined by the forcing profile in the doubly periodic domain of numerical simulations.

Because the algebra get's exceedingly long I'll present the final result for the selection rules as the equivalent problem of finding the kernel of a matrix operator. The idea is to work completely with the vorticity field $\omega(x, y, t)$, which has symmetries of n-cell shift and spatial reflection, as well as rotation by π. Specifically shift reflection on a spatial domain $x \in [0, 2\pi]$ and $y \in [0, 2\pi]$, with forcing profile of n cells is given by,

$$\omega(x, y, t) \to -\omega(-x, y + \frac{\pi}{n}, t) \tag{4.41}$$

and the rotation is given by,

$$\omega(x, y, t) \to \omega(-x, -y, t). \tag{4.42}$$

By using applying the invariance condition only for shift-reflection invariant (three) tori solutions, we start with the expansion for the scalar field in terms of the real-valued Fourier basis functions.

$$
\begin{aligned}
\omega(x, y, t) &= \sum_{jkn} [\cos(q_j x) \cos(q_k y)(a_{jkn} \cos(w_n t) + b_{jkn} \sin(w_n t)) \\
&+ \cos(q_j x) \sin(q_k y)(d_{jkn} \cos(w_n t) + f_{jkn} \sin(w_n t)) \\
&+ \sin(q_j x) \cos(q_k y)(g_{jkn} \cos(w_n t) + h_{jkn} \sin(w_n t)) \\
&+ \sin(q_j x) \sin(q_k y)(m_{jkn} \cos(w_n t) + p_{jkn} \sin(w_n t))]
\end{aligned} \tag{4.43}
$$

If we assume there are preperiodic solutions under (ℓ)-cell shift reflection after a prime period T_p, the general selection rules can be written as constraint conditions

$$
\begin{aligned}
a_{jkn} &= (-1)^{n+1}[a_{jkn} \cos(\frac{q_k \pi}{\ell}) - b_{jkn} \sin(\frac{q_k \pi}{\ell})] \\
b_{jkn} &= (-1)^{n}[a_{jkn} \cos(\frac{q_k \pi}{\ell}) - b_{jkn} \sin(\frac{q_k \pi}{\ell})] \\
d_{jkn} &= (-1)^{n}[d_{jkn} \cos(\frac{q_k \pi}{\ell}) + f_{jkn} \sin(\frac{q_k \pi}{\ell})] \\
f_{jkn} &= (-1)^{n}[-d_{jkn} \cos(\frac{q_k \pi}{\ell}) + f_{jkn} \sin(\frac{q_k \pi}{\ell})] \\
g_{jkn} &= (-1)^{n+1}[g_{jkn} \cos(\frac{q_k \pi}{\ell}) + h_{jkn} \sin(\frac{q_k \pi}{\ell})] \\
h_{jkn} &= (-1)^{n}[g_{jkn} \cos(\frac{q_k \pi}{\ell}) - h_{jkn} \sin(\frac{q_k \pi}{\ell})] \\
m_{jkn} &= (-1)^{n}[m_{jkn} \cos(\frac{q_k \pi}{\ell}) + p_{jkn} \sin(\frac{q_k \pi}{\ell})] \\
p_{jkn} &= (-1)^{n}[-m_{jkn} \cos(\frac{q_k \pi}{\ell}) + p_{jkn} \sin(\frac{q_k \pi}{\ell})]
\end{aligned} \tag{4.44}
$$

By doing some algebra one realizes that the coefficients are zero unless k_y the wavenumber associated with the direction that the forcing profile varies

over is only nonzero for integer multiples of the forcing wavelength. In other words, if the forcing repeats four times, the only nonzero k_y are $k_y = 4, 8, 12, \cdots$. The way that the preperiodic (time) condition comes into play is just like how it comes into play in the Kuramoto-Sivashinsky equation equation, half of the modes are zero depending on whether the time index n is even or odd. Specifically, the modes that are zero are,

For k_y being an odd number of multiples of the forcing profile index ℓ, we have the following constraints

$$
\begin{aligned}
d_{jkn}, f_{jkn}, m_{jkn}, p_{jkn} &= 0 \text{ for } n \text{ odd} \\
a_{jkn}, b_{jkn}, g_{jkn}, h_{jkn} &= 0 \text{ for } n \text{ even}
\end{aligned}
\tag{4.45}
$$

For k_y being an even number of multiples of the forcing profile index ℓ, we have the following constraints

$$
\begin{aligned}
d_{jkn}, f_{jkn}, m_{jkn}, p_{jkn} &= 0 \text{ for } n \text{ even} \\
a_{jkn}, b_{jkn}, g_{jkn}, h_{jkn} &= 0 \text{ for } n \text{ odd}
\end{aligned}
\tag{4.46}
$$

Of course for equilibria this simplifies due to not having a third continuous dimension, and we only have four distinct sets of coefficients (combinations of $\sin$ and $\cos$ in x, y). In fact, it simplifies even more due to not having the extra factor -1^n, such that the only non-zero coefficients

$$
\begin{aligned}
a_{jk}, b_{jk} &= 0 \text{ for } k_y \text{ even multiple of forcing index} \\
d_{jk}, f_{jk} &= 0 \text{ for } k_y \text{ odd multiple of forcing index}
\end{aligned}
\tag{4.47}
$$

In summary, for equilibria with discrete shift reflection symmetry, the number of non-zero modes equals $N_x * \frac{N_y}{2*\ell}$ and for preperiodic orbits it totals $N_x * \frac{N_y}{\ell} * \frac{N_t}{2}$.

Note, this is also useful for the Kuramoto-Sivashinsky equation if one desires the selection rules for ℓ cyclic shift reflection, as there is no difference between shift reflection in two continuous spatial dimensions versus one space and one time; the analogy is perfect with y playing the role of t in the Kuramoto-Sivashinsky equation.

4.4 Tiles' GuBuCv17 clippings and notes

Move good text not used in ref. [12] to this file, for possible reuse later.

2016-11-05 Predrag A theory of turbulence that has done away with *dynamics*? We rest our case.

2019-03-19 Predrag Dropped this:

In what follows we shall state results of all calculations either in units of the 'dimensionless system size' $\tilde{L}$, or the system size $L = 2\pi\tilde{L}$.

Due to the hyperviscous damping u_{xxxx}, long time solutions of Kuramoto-Sivashinsky equation are smooth, a_k drop off fast with k, and truncations of (1.24) to $16 \leq N \leq 128$ terms yield accurate solutions for system sizes considered here (see appendix **??**).

For the case investigated here, the state space representation dimension $d \sim 10^2$ is set by requiring that the exact invariant solutions that we compute are accurate to $\sim 10^{-5}$.

4.4.1 GuBuCv17 to do's

Internal discussions of ref. [12] edits.

2019-03-17 Predrag to Matt My main problem in writing this up is that I see nothing in the blog that formulates the variational methods that you use, in a mathematically clear and presentable form. Perhaps there is some text from

`siminos/gudorf/thesisProposal/proposal.tex`

that you can use to start writing up variational justification for your numerical codes, section 3 *Variational methods*.

2019-03-17 Predrag to Matt Please write up *tile extraction* and *glueing* in the style of a SIADS article.

2019-03-17 Predrag to Matt Should any of Appendix 4.2 *Fourier transform normalization factors* be incorporated into **GuBuCv17** [12]?

2019-04-10 Matt writing To begin `variational.tex` I included two equivalent formulations of the variational problem; the first is written in a more concise manner while the second is written in a more explicit manner. The longer of the two is commented out. The more explicit description uses dummy variables (Lagrange multipliers) which replace parameters (L, T) as independent variables.

I'm including explanations of the numerical algorithms but I don't think I should present them in their style for algorithms, because we didn't invent them just applied them in a unique way. If desired I think the

easiest way of including them per SIADS style guide is to use the algorithm package they suggest: `algpseudocode` and `algorithmic` are the package names.

I feel conflicted as to whether to define the gradient matrix using a new letter or the "mathematician way". e.g. $A(x)$ or $DG(x)$. Also, I started using **z** to represent state space vectors. I'm not a fan of using z but I don't want to confuse people by using u,x, etc.

I need to get better at writing or stop being OCD over how sentences are written.

2019-04-16 Matt update In an effort to make the chapters and `GuBuCv17.tex` more modular, I've split apart some of the chapters into smaller, more manageable pieces. For example, `variational.tex` was covering too many topics to be reflected by the file name and `numerics.tex` predominately covered discrete lagrangian systems and Noether's theorem. The algorithms (matrix free adjoint descent, matrix free GMRES and Gauss-Newton) have yet to be discussed in excruciating detail. This is my fault, in hindsight I've done a poor job with recording what I do and how I do it. I'm going to get better at this.

For the time being, until it is deemed unnecessary or unintelligent, I am going to break the chapters into the files `adjointdescent.tex` and `iterativemethods.tex`. I'm going to change the discourse so that instead of requiring the current order, namely, `variational.tex->adjointdescent.tex->iterativemethods.tex` the pieces will be written as to be independent of one another.

In order to get specific, I needed to include the Kuramoto-Sivashinsky equation written in the Fourier-Fourier basis; I put this in `sFb.tex`

2019-04-17 MNG update Realized that in order to get specific with the numerical methods I need to include both an exposition on the spatiotemporal Fourier modes as well as the matrix-free computations. The latter really stresses the improvements over the finite-difference approximation of the Jacobian that requires time integration ubiquitous in plane-couette and pipe numerics. Expanding on `adjointdescent.tex` and `iterativemethods.tex`. Again, the main stratagem is to make the separate `.tex` files as independent as possible to avoid "long distance references".

2019-04-18 MNG Heavy edits to `tiles.tex` Added section on preconditioning `preconditioning.tex` Formatting edits to `matrixfree.tex` can be ignored.
Added details in `iterativemethods.tex` regarding GMRES and SciPy wrapper for LAPACK solver GELSD

2019-04-23 MNG Converting indices to abide by the conventions: physical space indices $u(x_m, t_n)$, and spatiotemporal Fourier space indices $\hat{u}_{kj}$.

2018-05-09 PC can do. Also, remember that $u(x_m, t_n)$ implies that everywhere the ordering is (L, T), and not (T, L).

Luca Dieci asked (borderline pleaded) to abide by the mathematics convention that n is the index for discrete time. I'm avoiding ℓ and τ_t due to the unnecessary confusion with domain size L and period T.

2018-05-09 PC Agreed. τ_t we usually control by macro $\backslash zeit$, so currently t_n.

2019-04-24 MNG Discussion of how I foresee paper(s) playing out in `blogMNG.tex` by considering subject matter, narratives, and paper length. Perhaps unsurprisingly I lean towards structuring a paper similar to my thesis.

I'm unsure how to approach spatiotemporal symmetries in a practical manner. Projection operators which produces symmetry invariant subspaces are nice and complements the selection rules for different symmetries nicely. Specifically it provides the reason for why the selection rules exist and motivates the use of symmetry constrained Fourier transforms. The only issue I have with this is that the results of the formal derivation are not really used beyong that. I think this is likely a case of "It-is-trivial-now-that-I-know-it' syndrome. Perhaps it would be sufficient to say that the selection rules constitute these subspaces without the formalism?

2019-04-29 MNG Rewrite of `KSsymm.tex` after double checking the derivations. Going to rewrite `sFb.tex`, I'm paying for the expedient manner in which is was written; in other words just use a single Fourier basis as opposed to a real basis and a complex basis, Matt.

2019-04-30 MNG Rewrites to describe the spatiotemporal Kuramoto-Sivashinsky equation only in terms of real valued Fourier coefficients for consistency. The index notation gets a little rough but the pseudospectral form of the equation is nice enough.

Tried to find the most concise description of how I handle relative periodic orbits using mean velocity frame (time dependent rotation transformation).

2019-05-02 MNG Is it necessary to recap all of the results in sect. 1.5 in this paper? Other than the spatial integration calculation the results described in refs. [4, 5]. I'm unsure how to connect the spatiotemporal calculations to results pertaining to the dynamical system formulation, e.g. temporal stability and energy budget.

Moved `SpatTempSymbDyb.tex` to after `tiles.tex` such that it proceeds from finding tiles to using tiles.

The bulk of each section is complete; perhaps need to add some more detail to `glue.tex` and `tiles.tex` but mostly need to work on picking, producing, and inserting figures.

Going to list suggestions for figures at the top of each section in commented text.

2019-05-02 MNG Added tile figures: Extraction and converged results in `tiles.tex`.

Modifying scripts to produce figures of general numerical convergence (initial condition to final converged invariant 2-torus), produce figures demonstrating step-by-step gluing for repeated gluing, and produce figures for the "frankenstein" plots (combining tiles to produce invariant 2-tori). Basically just producing more figures.

2019-05-11 PC moved Ibragimov to `gudorf/thesis/thesis.tex` until we find it useful.

2019-05-13 MNG • Added spatial gluing figures

• Added description of gluing procedure

2019-05-13 PC Figures are looking great, and in my talks people seem to "get" tile extraction and gluing, so they are very important. A few notes, before you produce the next versions:

- I think you should label all u color bars in multiples of 1, or or 0.5 if that is really needed, not different units in every plot.
- Once you have improved a given figure, keep the same name rather than renaming it (they are often shared between different articles, presentations and blogs)

2019-07-05 PC dropped from trawl.tex: " In both formulations there is no guarantee of convergence but it is clearly better to take less time regardless of convergence.

In our formulation, convergence can not be guaranteed either, but the resources committed to the initial guesses generation are negligible. "

$$
\begin{aligned}
q_k &= 2\pi\frac{k}{L}\,, & k &= 1, \cdots, M/2 - 1 \\
\omega_j &= 2\pi\frac{j}{T}\,, & j &= 0, \cdots, N/2 - 1 \\
x_m &= \frac{m}{M}L\,, & m &= 0, \cdots, M - 1 \\
t_n &= \frac{n}{N}T\,, & n &= 0, \cdots, N - 1\,.
\end{aligned}
\tag{4.48}
$$

2019-08-21 MNG Moved discussion of recurrence plots and multiple shooting from trawl.tex to variational.tex

It seemed more coherent to first describe the disadvantages of the IVP to motivate the variational problem. I'm going to refer to what I do as "solving a variational problem" as opposed to boundary value problem because it insinuates (at least to me) that we're solving a Dirichlet BC in $1 + 1$ dimensions problem.

General narrative of variational.tex

- Exponential instability bad
- Variational formulation good
- How to solve variational problem (general description of optimization)
- Losses from variational formulation (notion of dynamics, stability, bifurcation analysis).
- How to recoup from these losses (adjoint sensitivity, Lagrangian, Hill's formula)

It's currently a hot mess.

2019-09-20 MNG Input references to topological defects and motifs in complex networks. Renamed the "defect tile" to the "merger tile" but also made the connection that similar patterns in crystals are referred to as "edge dislocations".

Just clean up and rewriting `tiles.tex` mainly; it's almost in shape.

2018-05-09 PC Dropped: The following definitions will be devoid of symmetry considerations such that the equations represent the general case.

For $\tilde{L} < 1$ the only equilibrium of the system is the globally attracting constant solution $u(x,t) = 0$, denoted E_0 from now on. With increasing system size L the system undergoes a series of bifurcations. The resulting equilibria and relative equilibria are described in the classical papers of Kevrekidis, Nicolaenko and Scovel [14], and Greene and Kim [11], among others. The relevant bifurcations up to the system size investigated here are summarized in figure 1.3: at $\tilde{L} = 22/2\pi = 3.5014\cdots$, the equilibria are the constant solution E_0, the equilibrium E_1 called GLMRT by Greene and Kim [11, 18], the 2- and 3-cell states E_2 and E_3, and the pairs of relative equilibria $TW_{\pm 1}$, $TW_{\pm 2}$. All equilibria are in the antisymmetric subspace $\mathbb{U}^+$, while E_2 is also invariant under D_2 and E_3 under D_3.

Due to the translational invariance of Kuramoto-Sivashinsky equation, they form invariant circles in the full state space. In the $\mathbb{U}^+$ subspace considered here, they correspond to $2n$ points, each shifted by $L/2n$. For a sufficiently small L the number of equilibria is small and concentrated on the low wave-number end of the Fourier spectrum.

dropped this: G, the group of actions $g \in G$ on a state space (reflections, translations, etc.) is a spatial symmetry of a given system if $gu_t = F(g\,u)$.

An instructive example is offered by the dynamics for the $(L, T) = (22, T)$ system that ref. [5] specializes to. The size of this small system is ~ 2.5 mean wavelengths ($\tilde{L}/\sqrt{2} = 2.4758\ldots$), and the competition between states with wavenumbers 2 and 3.

The two zero Lyapunov exponents are due to the time and space translational symmetries of the Kuramoto-Sivashinsky equation.

For large system size, as the one shown in figure 1.1, it is hard to imagine a scenario under which attractive periodic states (as shown in ref. [6], they do exist) would have significantly large immediate basins of attraction.

2019-10-17 MNG : Merged symmetry discussions. `KSsymmMNG1` was deleted because seems to be an old discussion predating the spatiotemporal symmetry group discussion as it still mentions equivariance. The focus should only be on invariance under symmetry operations, as invariance gives rise to the the practical application of the symemtry discussion which is constraints on the spatiotemporal Fourier coefficients. `KSsymmMNG` was deleted because it is just an older version of `KSsymm`. `KSsymmPC` uses different notation and says things better than I do so I'll have to figure out how to merge it in.

2019-10-25 PC dropped from *variational.tex*:

Linear stability analysis has been used in bifurcation analysis of describe the existence and bifurcations of solutions as well as the geometry of state spaces corresponding to different flows refs. [7, 17, 23].

Commonly time variational integrators preserve symplectic structure

2019-09-05 MNG Dropped from *variational.tex*: multishooting optimization of cost functional because it doesn't jive with spatiotemporal methods (based on integration)

Adjoint sensitivity and Hill's formula sections when I figure them out or they seem useful:

Section on adjoint sensitivity The spatiotemporal reformulation of a dynamical problem also requires a reformulation of its linear stability analysis.

Nevertheless, we still have the notions of tangent spaces and derivatives so the natural replacement is the notion of sensitivity. In the context of finite element (finite difference) representation, instead of computing a derivative and transporting it around a periodic orbit, it instead computes the derivative of the temporal average of the quantity with respect to whichever parameter is desired [1, 19, 24]. Because there is no transport, one need not worry about the exponential instability present. Essentially sensitivity is to stability as boundary value problem is to initial value problem in this context. Because the spatiotemporal boundary problem is defined on a compact domain on which the scalar field does not diverge, dynamical observables are bounded; they do not experience numerical overflow (underflow) associated with unstable (stable) manifolds.

$$ S = \int_{\mathcal{M}} \mathcal{L}(u, v, u_x, v_x, u_t, v_t, u_x x, v_x x) dx dt \qquad (4.49) $$

such that the matrix of second variations, or Hessian, of this action functional is defined as

$$H = \nabla\nabla^\top S \tag{4.50}$$

such that the derivatives are taken with respect to the infinite dimensional scalar fields $u, v, \ldots$, such that the Hessian matrix is infinite dimensional prior to discretization of the scalar fields. The resultant discrete Lagrangian system and subsequent Hessian should be the Hessian of Hill's formula, I believe. If one is trying to derive Hamilton's action principle as a result of discretization (i.e., finite differences) as in ref. [15] then one must take care to define spatiotemporal differentiation operators in a manner consistent with an action principle. A large amount of the derivation of the discrete action principle and discrete Noether's theorem of [15] relates to using a finite element discretization in physical space. I am unsure how these ideas extend to a Fourier basis; I currently am assuming that as long as the differentiation operators, and hence the derivatives (jet bundle) is properly defined then everything should work out. When two total derivatives of the Lagrangian density are taken, one arrives at the following matrix representation of the Hessian. Keep in mind that we have ordered the variables in terms of the order of the corresponding derivatives $(u, v, u_t, v_t, u_x, v_x, u_x x, v_x x)$.

$$\begin{bmatrix}
-v_x(t,x)/3 & u_x(t,x)/3 & 0 & -1/2 & v(t,x)/3 & -2u(t,x)/3 & 0 & 0 \\
u_x(t,x)/3 & 0 & 1/2 & 0 & u/3 & 0 & 0 & 0 \\
0 & 1/2 & 0 & 0 & 0 & 0 & 0 & 0 \\
-1/2 & 0 & 0 & 0 & 0 & 0 & 0 & 0 \\
v(t,x)/3 & u(t,x)/3 & 0 & 0 & 0 & & -1 & 0 & 0 \\
-2u(t,x)/3 & 0 & 0 & 0 & -1 & 0 & 0 & 0 \\
0 & 0 & 0 & 0 & 0 & 0 & 0 & 1 \\
0 & 0 & 0 & 0 & 0 & 0 & 1 & 0
\end{bmatrix}. \tag{4.51}$$

This is an infinite dimensional matrix, but upon discretization each block will represent a diagonal matrix whose diagonal contains the scalar field values of the corresponding spacetime coordinates. For instance, $u_x/3 \equiv \frac{1}{3}u_x(x,t) \to \frac{1}{3}u_x(t_n, x_m)$. Because each of the blocks are diagonal, i.e., $1 \equiv \mathcal{I}^{N*M}$, the determinant expansion is long but not impossible to decipher. Note the presence of the adjoint variables v, v_x. There is freedom in the choice of what these variables should be, because they are non-physical.

2020-02-28 MNG Reformatted the paper into sections which follow the outline so far: `,tileoutline.tex`
`tileintro.tex`
`tilebody.tex`
`tilesummary.tex`
`tilefuture.tex`

2020-05-04 PC might reuse these somewhere:

Motivated by the presence of continuous symmetries we recast chaotic nonlinear dynamical systems via a $(D+1)$-dimensional space-time theory.

Space-time translationally recurrent solutions are invariant $(D+1)$-tori

larger tori can be constructed from the combination of smaller tori.

the entirety of space-time can be explained via the shadowing by these tori.

This sets the stage for a 2-dimensional symbolic represention of the infinite space-time Kuramoto-Sivashinsky equation wherein the fundamental patterns constitute the symbolic alphabet.

As longer periods periodic orbits are shadowed by the shorter ones, truncations of the theory to finite sets of periodic orbits should suffice to predict any observable of the 'turbulent' flow to a finite accuracy.

There is a vast literature on relative periodic orbits since their first appearance, in Poincaré study of the 3-body problem [2, 21], where the Lagrange points are the relative equilibria. They arise in dynamics of systems with continuous symmetries, such as motions of rigid bodies, gravitational N-body problems, molecules, nonlinear waves and the plane Couette fluid flow [22].

2020-05-12 PC Who's this Gunzberger02 in rf{BorSch11,Gunzberger02,BoyVan04}?

2020-05-14 MNG It's a text on numerical optimization.

2020-05-19 PC Cannot find any such Gunzberger textbook, removed the reference, sticking with the traditional Russian BorSch.

2020-02-26 MNG Let's get this done. I'm realizing how little was actually written now that I'm done with my thesis and it is kind of laughable.

2020-02-28 Flushing out `tileintro.tex`.

Note to Predrag - send this paper to

References

[1] P. J. Blonigan, "Adjoint sensitivity analysis of chaotic dynamical systems with non-intrusive least squares shadowing", J. Comput. Phys. **348**, 803–826 (2017).

[2] A. Chenciner, "Three body problem", Scholarpedia **2**, 2111 (2007).

[3] F. Christiansen, P. Cvitanović, and V. Putkaradze, "Spatiotemporal chaos in terms of unstable recurrent patterns", Nonlinearity **10**, 55–70 (1997).

[4] P. Cvitanović, R. Artuso, R. Mainieri, G. Tanner, and G. Vattay, *Chaos: Classical and Quantum* (Niels Bohr Inst., Copenhagen, 2022).

[5] P. Cvitanović, R. L. Davidchack, and E. Siminos, "On the state space geometry of the Kuramoto-Sivashinsky flow in a periodic domain", SIAM J. Appl. Dyn. Syst. **9**, 1–33 (2010).

[6] U. Frisch, Z. S. She, and O. Thual, "Viscoelastic behavior of cellular solutions to the Kuramoto-Sivashinsky model", J. Fluid Mech. **168**, 221–240 (1986).

[7] J. F. Gibson, J. Halcrow, and P. Cvitanović, "Visualizing the geometry of state-space in plane Couette flow", J. Fluid Mech. **611**, 107–130 (2008).

[8] J. F. Gibson, J. Halcrow, and P. Cvitanović, "Equilibrium and traveling-wave solutions of plane Couette flow", J. Fluid Mech. **638**, 243–266 (2009).

[9] R. Gilmore and C. Letellier, *The Symmetry of Chaos* (Oxford Univ. Press, Oxford, 2007).

[10] M. Golubitsky and I. Stewart, *The Symmetry Perspective* (Birkhäuser, Boston, 2002).

[11] J. M. Greene and J.-S. Kim, "The steady states of the Kuramoto-Sivashinsky equation", Physica D **33**, 99–120 (1988).

[12] M. N. Gudorf, N. B. Budanur, and P. Cvitanović, Spatiotemporal tiling of the Kuramoto-Sivashinsky flow, In preparation, 2022.

[13] R. Hoyle, *Pattern Formation: An Introduction to Methods* (Cambridge Univ. Press, Cambridge, 2006).

[14] I. G. Kevrekidis, B. Nicolaenko, and J. C. Scovel, "Back in the saddle again: a computer assisted study of the Kuramoto-Sivashinsky equation", SIAM J. Appl. Math. **50**, 760–790 (1990).

[15] M. Kraus and O. Maj, "Variational integrators for nonvariational partial differential equations", Physica D **310**, 37–71 (2015).

[16] Y. Lan, Dynamical Systems Approach to $1 - d$ Spatiotemporal Chaos – A Cyclist's View, PhD thesis (School of Physics, Georgia Inst. of Technology, Atlanta, 2004).

[17] Y. Lan and P. Cvitanović, "Unstable recurrent patterns in Kuramoto-Sivashinsky dynamics", Phys. Rev. E **78**, 026208 (2008).

[18] R. E. LaQuey, S. M. Mahajan, P. H. Rutherford, and W. M. Tang, "Nonlinear saturation of the trapped-ion mode", Phys. Rev. Lett. **34**, 391–394 (1974).

[19] D. Lasagna, A. Sharma, and J. Meyers, Periodic shadowing sensitivity analysis of chaotic systems, 2018.

[20] J. E. Marsden and T. S. Ratiu, *Introduction to Mechanics and Symmetry* (Springer, New York, 1999).

[21] V. Szebehely, *Theory of orbits* (Academic, New York, 1967).

[22] D. Viswanath, "Recurrent motions within plane Couette turbulence", J. Fluid Mech. **580**, 339–358 (2007).

[23] F. Waleffe, "On a Self-Sustaining Process in shear flows", Phys. Fluids **9**, 883–900 (1997).

[24] Q. Wang, "Forward and adjoint sensitivity computation of chaotic dynamical systems", J. Comput. Phys. **235**, 1–13 (2013).

Chapter 5

Chronotopic literature

2020-06-24 Predrag This chapter is now included into
siminos/spatiotemp/blogCats.tex blog.

Chapter 6

Spatiotemporal literature

The Nature of Space and Time
— Kaća Bradonjić

6.1 Spatiotemporal rocket science

2017-01-23 Predrag not sure where to put this - into pipe blog or here, but
Wang *et al.* [108] *Towards scalable parallel-in-time turbulent flow simulations*
introduces "the least squares shadowing (LSS) method" and uses Kura-
moto-Sivashinsky to illustrate the power of their method: " The initial
condition is relaxed and information is allowed to propagate both for-
ward and backward in time. [...] next-generation simulation paradigm
can likely be spacetime parallel simulations. These simulations subdivide
the four-dimensional spacetime computational domain. Each comput-
ing core handles a contiguous subdomain of the simulation spacetime.
Compared to subdivision only in the three-dimensional space, spacetime
parallel simulations can achieve significantly higher level of concurrency,
and reduce the ratio of inter-core communication to floating point opera-
tions. [...] Efficient time domain parallelism can only be achieved through
reformulating turbulent flow simulation into a well-conditioned prob-
lem. We reformulate turbulent flow simulation into a well-conditioned
problem by relaxing the initial condition. [...] Instead of trying to find the
flow solution that satisfies both the governing equation and the initial
condition, we aim to find a flow solution satisfying only the governing
equation. [...] Stability of the trajectory with a relaxed initial condition is
achieved by splitting a perturbation into stable and unstable components,
and propagating their effects forward and backward in time, respectively.
"

Blonigan and Wang [8, 9, 11] might also be of interest.

2017-01-25 Evangelos In the sense that you describe in the last paragraph,

hasn't dynamics been dead already since Poincaré and Lorenz? I mean that they showed that we have to study geometry and then time becomes irrelevant. It's more like "Dynamics is dead, long live dynamics!"

Wang *et al.* [108] is very interesting indeed. I find it very similar to your variational method for finding periodic orbits [34, 68]. In G. Sanchez-Arriaga *et al.* [95] we have developed (without much thinking) a boundary value solver discretized with finite differences both in time and in space in order to detect periodic orbits. It resulted in a sparse linear algebra system that was parallelizable, but we didn't study how performance scales. There should be a straightforward extension of Wang *et al.* [108] for periodic orbits.

The main two challenges that I see with methods such as the above refs. [34, 68, 95, 108] is 1) finding a suitable initial guess and 2) increased memory requirements. The first one is there already when we search for periodic orbits and I suspect that it will be worse for turbulence simulations. The second one might not be as serious in next generation HPC platforms.

2017-03-09 Predrag Andrej Junginger, Jörg Main, Günter Wunner and Rigoberto Hernandez, *Variational principle for the determination of unstable periodic orbits and instanton trajectories at saddle points*, arXiv:1703.02472 (Prof. Uzer knows the authors well) write: " The complexity of arbitrary dynamical systems and chemical reactions, in particular, can often be resolved if only the appropriate periodic orbit - in the form of a limit cycle, dividing surface, instanton trajectories or some other related structure - can be uncovered. Determining such a periodic orbit, no matter how beguilingly simple it appears, is often very challenging. We present a method for the direct construction of unstable periodic orbits and instanton trajectories at saddle points by means of Lagrangian descriptors. Such structures result from the minimization of a scalar-valued phase space function without need for any additional constraints or knowledge. We illustrate the approach for two-degree of freedom systems at a rank-1 saddle point of the underlying potential energy surface by constructing both periodic orbits at energies above the saddle point as well as instanton trajectories below the saddle point energy.

2014-11-15,2017-01-26 Burak Fazendeiro, Boghosian, Coveney and Lätt [43] *Unstable periodic orbits in weak turbulence* seem to have applied the variational periodic orbit finding method to fluid flow by parallelizing the whole thing.

2017-05-05 Predrag Boghosian *et al.* [13] *New variational principles for locating periodic orbits of differential equations* is the most detailed discussion (see also refs. [12, 43]):

They reformulate the space–time algorithm of Lan and Cvitanović [68] in a clear-headed way, and use using the methods of gradient descent or conjugate gradients to solve the variational equations.

They apply it to the lattice-Boltzmann method for the solution of the Navier–Stokes equations, with a fully parallel implementation using the Message Passing Interface. The method has first been tested on the Lorenz equations [12]. They apply this to weak homogeneous turbulence driven by an Arnold–Beltrami–Childress force field in three spatial dimensions. Because the algorithm requires storage of the space–time lattice, even the smallest orbits require resources on the order of tens of thousands of computing cores. Using this approach, two UPOs have been identified and some of their properties have been analysed.

In ref. [44] they discuss "Ginzburg–Landau-type minimization." (Probably not worth pursuing, they do not return to it)
"

2017-08-16 Matt : Discussed David Lasagna's paper [70] on time averages and their sensitivity to parameters. PC brought up the fact that derivatives of averages tend to be fractal in nature due to horseshoes?

2017-08-16 Ashley, 2019-02-21 Predrag Davide Lasagna [70] *Sensitivity analysis of turbulence using unstable periodic orbits: a demonstration on the Kuramoto-Sivashinsky equation*.
Ashley Periodic orbits are finite, so can compute sensitivity avoiding the time integral.

Sets up a Lagrangian depending on parameters, takes variational derivative

ends up with the adjoint equation

(8b) is not a condition, it is fact.

Lasagna, Sharma and Meyers [72] *Periodic shadowing sensitivity analysis of chaotic systems*, arXiv:1806.02077 is a continuation of Wang [106, 107]. The find Wang [106] Shadowing Lemma a major advance. They credit Lasagna [70] for "deriving periodic boundary conditions in time for the sensitivity equations." The contribution of ref. [72] is a shadowing-based algorithm, based on the idea of enforcing periodic boundary condition in time to the sensitivity equations, leading to the time periodic shadowing. Providing such boundary conditions directly not only results in a method that is potentially simpler, but it sufficient to obtain bounded (periodic) solutions almost always, resulting in accurate gradients.

The adjoint periodic shadowing method we employ a classical Lagrangian approach [15, 18] starts by constructing the finite-time Lagrangian function (16).

"Sum-of-squares" papers (seem unrelated to the spatiotemporal effort):

Huang, Chernyshenko, Goulart, Lasagna, Tutty and Fuentes [53] *Sum-of-squares of polynomials approach to nonlinear stability of fluid flows: an example of application*

Lasagna, Huang, Tutty and Chernyshenko [71] *Sum-of-squares approach to feedback control of laminar wake flows*

Huang, Jin, Lasagna, Chernyshenko and Tutty [54] *Expensive control of long-time averages using sum of squares and its application to a laminar wake flow*

The "adjoint periodic shadowing methods" papers are rather tedious read (lots of variational equations!):

Cacuci [18] *Sensitivity theory for nonlinear systems. I. Nonlinear functional analysis approach* is cited by many authors up to 2019, with suggestive paper titles, like

Luchini and Bottaro [78] *Adjoint equations in stability analysis*

Cacuci [19] *Second-order adjoint sensitivity analysis methodology (2nd-ASAM) for computing exactly and efficiently first- and second-order sensitivities in large-scale linear systems: I. Computational methodology*

Cacuci [20] *Second-order sensitivities of a general functional of the forward and adjoint fluxes in a multiplying nuclear system with source*:
2nd-order (Hessian) sensitivity information accelerates the convergence of optimization algorithms.
In atmospheric sciences "second-order adjoint models" were used to compute products between the Hessian of the cost functional and a vector (representing a perturbation in sensitivity analysis, a search direction in optimization, an eigenvector, etc.) to perform sensitivity analysis of the cost function with respect to distributed observations.

2017-02-05 Tobias Schneider <tobias.schneider@epfl.ch> There were several talks about these topics at pasc16.org. In a session I organised Diego Donzis gave an exciting talk about fluid dynamics simulations in the future. Donzis and Aditya [37] *Asynchronous finite-difference schemes for partial differential equations* is one of the papers but there is a lot of unpublished stuff.

Check MS14 at pasc16.org/program for Donzis abstract: " Turbulence is the most common state of fluid motion in nature and engineering and is critical in environmental, astrophysical and engineering flows. However, the complexity of the governing equations leads to wide ranges of temporal and spatial scales and render the problem almost intractable analytically. Thus, simulations, in particular direct numerical simulations (DNS) which resolve the entire range of scales from the exact governing equations, have become an indispensable tool to advance the field. While very accurate spectral methods have been used extensively up to petascale levels, they typically require collective communications and synchronizations, two well-known potential bottlenecks at exascale. We present our recent work on novel asynchronous numerical schemes that virtually remove computational obstacles at a mathematical level and present a path towards exascale DNS of turbulent flows. We will highlight implications,

challenges and opportunities in terms of numerical issues, parallel performance, and implementation issues on future exascale systems. ″

2019-03-19 Tobias update I haven't seen any further developments beyond what Diego Dozis was talking about but I am also not following the field too closely. These developments are moreover aimed at something less exciting than treating space and time on an equal footing. The idea is: How to relax the requirement that all CPUs in a large computer have to work in a perfectly synchronised way. This leads to numerical time-marching schemes for which the individual CPU cores can work asynchronously. It's a big question that arises with modern computers with literally thousands of CPU cores. Essentially the idea is that you split the spatial domain and time-integrate this domain independently of the others. When one needs info on the neighbouring domains (typically at the boundaries) one does not insist that the data for all subdomains is given at exactly the same time step. Of course that leads to small errors but those integration errors can be controlled. It's really just about time-marching schemes that pose fewer synchronisation constraints and are thus better suited for huge computers where inter-CPU communication is expensive.

I think numerical schemes that truly appreciate that space and time are to be treated together will be on us and our community.

I have a few ideas that I would love to discuss. We are working on constructing a variational code for Navier-Stokes (matrix-free). We will start with a Kuramoto-Sivashinsky demonstration (by the early fall?) and then move to 3D Navier-Stokes.

My plan is to develop *variational adjoint methods* [97].

Machine learning will be used for constructing initial guesses.

Matrix-free adjoints [40].

Setup for 3D Navier-Stokes: combine parallelized Channelflow 2.0 with a robust, variational tool for computing periodic orbits of 3D flows.

Historically, guesses are extracted from approximate recurrences observed in long turbulent simulations [2]. This is inefficient, useful only for the short, least unstable orbits.

2017-09-04 Predrag Junginger *et al.* [59] *Variational principle for the determination of unstable periodic orbits and instanton trajectories at saddle points* seem specific to Hamiltonian dynamics. They write:

The complexity of arbitrary dynamical system (chemical reaction, in particular) can often be resolved if only the appropriate periodic orbit - in the form of a limit cycle, dividing surface, instanton trajectories, or some other related structure - can be uncovered. We present a method for the direct construction of unstable periodic orbits and instanton trajectories at saddle points by means of Lagrangian descriptors. Such structures result from the minimization of a scalar-valued phase-space function without the need for any additional constraints. We illustrate the approach

2CB

for two-degree of freedom systems at a rank-1 saddle point of the underlying potential-energy surface by constructing both periodic orbits at energies above the saddle point as well as instanton trajectories below the saddle-point energy.

Check also Jiménez Madrid and Mancho [57] *Distinguished trajectories in time dependent vector fields*: Fixed points and periodic orbits are keystones for describing solutions of autonomous and time periodic dynamical systems, as the stable and unstable manifolds of these hyperbolic objects form the basis of the geometrical template organizing the description of the dynamical system. They give a new definition of "distinguished trajectory" that encompasses the concepts of fixed point and periodic orbit and which when applied to finite time and aperiodic dynamical systems identifies special trajectories that play an organizing role in the geometry of the flow. The definition is valid for identifying distinguished trajectories with hyperbolic and nonhyperbolic types of stability. The definition is implemented numerically and the procedure consists of determining a path of limit coordinates. In the context of highly aperiodic realistic flows the definition characterizes distinguished trajectories in finite time intervals, and states that outside these intervals trajectories are no longer distinguished.

2017-11-03 Predrag Jianke Yang [112] *A numerical method for computing time-periodic solutions in dissipative wave systems* is another paper that finds Kuramoto-Sivashinsky and complex Ginzburg-Landau relative periodic orbits using spatiotemporal methods.

It looks quite interesting, but it will requires bit of work to understand the paper. Yang's Matlab codes are available online, so one can download his Kuramoto-Sivashinsky code and give it a go on some of our solutions.

2019-02-06 Predrag Catching up on the more recent work of Patrick Blonigan (who happens to be recent Farazmand coauthor :) and Qiqi Wang.

Wang [106] *Forward and adjoint sensitivity computation of chaotic dynamical systems* has 44 citations. It uses Lyapunov eigenvector decomposition for sensitivity analysis, but that has high computational cost when the dynamical system has many positive Lyapunov exponents.

Blonigan and Wang [6] *Multigrid-in-time for sensitivity analysis of chaotic dynamical systems*:

Wang [107] *Convergence of the least squares shadowing method for computing derivative of ergodic averages*

Their papers say that LSS was introduced in Wang, Hu and Blonigan [109] *Least Squares Shadowing sensitivity analysis of chaotic limit cycle oscillations*. The paper has 42 citations.

LSS computational cost is $O(mn^3)$ where m is the number of time steps, and n is the number of dynamical degrees of freedom.

When the dynamical system is high dimensional, e.g., a discretized partial differential equation, iterative solution methods should be used instead of direct matrix solvers. Because the system is well-conditioned and only twice as large as an initial value problem, an iterative solution can potentially cost only a small multiple of an initial value solution.

What I do not get is the cost function - it is usual squares, but with respect to a "pre-specified reference trajectory."

Sensitivity analysis [74] computes the derivative of outputs to inputs (derivative with respect a control parameter) of a simulation. Conventional methods, including the tangent and the adjoint method, fail when the dynamical system is chaotic and the outputs are long time averaged quantities.

ensemble adjoint method [74]

Chater *et al.* [23] *Least squares shadowing method for sensitivity analysis of differential equations*

Chater, Ni and Wang [24] *Simplified Least Squares Shadowing sensitivity analysis for chaotic ODEs and PDEs*

Blonigan and Wang [10] *Multiple shooting shadowing for sensitivity analysis of chaotic dynamical systems* present a variation of the method suitable for high-dimensional systems, using multiple-shooting strategies.

Craske [28] *Adjoint sensitivity analysis of chaotic systems using cumulant truncation*

Blonigan [7] *Adjoint sensitivity analysis of chaotic dynamical systems with non-intrusive least squares shadowing* introduces a "non-intrusive least-squares shadowing (NILSS)" algorithm.

Ni and Wang [88] *Sensitivity analysis on chaotic dynamical systems by Non-Intrusive Least Squares Shadowing (NILSS)*

Ni [87] *Hyperbolicity, shadowing directions and sensitivity analysis of a turbulent three-dimensional flow* uses the NILSS algorithm.

Kim and H. Choi [64] *Space-time characteristics of a compliant wall in a turbulent channel flow*

2019-03-19 Predrag to Matt One of our problems is that we do not know what our spatiotemporal variational method is called by other people who have presumably already crossed this bridge before us.

In *CCIS 2019 Conference of Computational Interdisciplinary Sciences* Darrell Pepper gave a pleasant engineering talk to non-specialist audience on his "meshfree approach." He has have been at this for a while, but is still active. His students use the method in fluid dynamics problems. He tells many jokes, like older professors from Las Vegas tend to. Sometime. His claims to fame are many, but in particular he computed the direction of the radioactive plumes for both 3-Mile Island and Chernobyl.

Most recently, Pepper has been working on how to equip Las Vegas firemen with real time info which way the plumes are going, see Pepper and Gonzalez [91] *A localized meshless technique for generating 3-D wind fields*. For us Sect. 4. *The Meshless Method* is helpful, as a succint summary. The point there is that they replace a square mesh by support on a set of irregularly placed points (for example, Las Vegas firehouses). Few bullet points from his talk

1. boundary element methods reduce the problem by one dimension (boundary instead of the bulk)

2. Local Petrov-Galerkin good for steep gradients, i.e., shocks

3. Mashless methods work for Navier-Stokes, heat transfer, etc. They work with primitive equations (velocity fields) rather than with vorticities, as boundary conditions are difficult in the vorticity formulations.

4. Multiquadrics are good as they have explicit expressions for derivatives

5. Global mashless equation (linearized?) is a large matrix equation. It can suffer poor conditioning, and is efficient only for square domains.

6. Local mashless methods loop through all points one by one. They are not ill conditioned.

7. They are engineers, they are happy if solutions are good to a few %.

8. FreeFEM finite element code is free and can be downloaded

9. In atmospheric simulations: minimize variance between the observed and the computed.

10. My feeling: meshless methods are good for inhomogenous discretizations, funky boundary conditions. In our case, spectral methods (Fourier represenatations) probably work better.

The rest is my reading. The meshless method was introduced by Fasshauer [41] from whom I gleaned this:

They are interested in the numerical solution of a generic nonlinear (elliptic) PDE as a boundary value problem on some domain. Instead of discrete meshes, they work with the globally supported radial basis function (RBFs). Not clear to me how well these bases can be used on periodic domains. Globally supported multiquadric radial basis functions can be used for Newton iteration numerical solution of nonlinear partial differential equations. The use of coarse meshes during the initial iterations along with a multiquadric parameter which is adjusted with the meshsize increases the efficiency and stability of the algorithm.

Fasshauer [41] "test problem" is a nonlinear elliptic (i.e., a single $2D$ Laplacina) PDE on a unit square, different from but not totally irrelevent

for our Kuramoto-Sivashinsky application: he computes what we would call solution $u(t, x)$ over a quadratic domain, compatible with the given PDE. His solutions are of much simpler shape than most of Matt's solutions, so Matt seems to be solving a harder problem.

If of interest, try to check out the Fasshauer book [42] with MATAB codes. Maybe we also have to learn about "Nash iteration" and the Kansa [60, 61] or "multiquadric method" for solving problems in 2D and 3D arbitrary domains. Engineers like it for applying it to inhomogeneous and irregular complex geometries. Closer to home, it has been used for computing solutions to Burger's equation [46, 96].

6.1.1 Adjoint sensitivity analysis

Sensitivity analysis, according to Julia:

The local sensitivity of a solution of an ODE or a PDE model is given by the derivative of the ith independent field of the solution with respect to the jth parameter, $\partial u_i / \partial p_j$. There are three types of sensitivity analysis. Local forward sensitivity analysis gives the gradient of the solution along the time evolution with respect to a parameter. Local adjoint sensitivity analysis gives the gradient of some functional of the solution, such as a cost function. Global sensitivity analysis methods computes the sensitivity over a domain without calculating derivatives.

Adjoint sensitivity analysis is used to find the gradient of the solution $x(t, p)$ with respect to some functional of the solution. This adjoint requires the definition of a scalar observable $a(x)$ where x is a solution to the differential equation. Adjoint sensitivity analysis finds the gradient of the integrated observable

$$A^t(x_0, p) = \int_0^t d\tau a(x(\tau, p)),\qquad(6.1)$$

I also like this introduction by Marc Schwalbach. Unfortunately he lost steam after one post :) For a weatherman's angle, see Errico [39] *What is an adjoint model?*.

Traditional adjoint sensitivity methods face fundamental limitations when applied on turbulence, which are addressed by development of robust methods for adjoint analysis [109].

Over the past two decades it has been established that the numerically exact invariant solutions of the Navier-Stokes equations ("recurrent flows") serve as the "building blocks" that shape turbulent dynamics.

This dynamical framework will be used to solve (and design) turbulent drag reduction and optimisation problems in turbulence, in particular design of compliant surfaces for drag reduction in plane channel flow.

Lasagna and Sharma are developing so called adjoint-based variational methods for sensitivity analysis. With sensitivity information, they can design optimal drag-reducing surfaces by using gradient-based optimisation methods.

The existing periodic orbit theory, so far successfully applied only to low-dimensional dynamical systems, posits that the description of the chaotic / turbulent state space is given by ensembles of hierarchically organised unstable period solutions of increasing length. In contrast, Lasagna's working hypothesis is that a few periodic orbits of long periods, embedded in state-space regions most frequented by turbulence and thus capturing the full range of dynamical events, suffice. Which strategy works best in practice remains an open question, and the approach proposed here should certainly be explored.

They plan to develop new space-time parallel numerical methods to find periodic orbits with long period and then develop adjoint solverss (formulated as a boundary value problem with periodic boundary condition) to obtain gradient information.

The approach is based on the idea that adjoint analysis of such structures can provide accurate sensitivities of time averaged quantities with respect to the design surface parameters.

The proposed adjoint approach offers the ability to obtain gradient information with respect to a large number of parameters (the spatial distribution of material properties)

For small perturbations, the sensitivity of a system is given by the gradient with respect to a parameter. Lasagna and Sharma have shown that this gradient can be obtained by adopting adjoint techniques to periodic orbits.

A variation of any of the system's parameters (the viscosity in case of Kuramoto-Sivashinsky) produces a computable state-space distortion of periodic trajectories. They illustrate this by varying viscosity ν from $(2\pi/39)^2$ to $(2\pi/38.5)^2$ for their shortest periodic orbit.

They compute a few thousand periodic orbits of period $\simeq 1000\nu$. The question is: what is the right orbit to use?

[1] They plan to consider only one periodic orbit, having a sufficiently long period such as to span all possible dynamical events encountered by long chaotic trajectories, i.e. shadowing many shorter, more elementary recurrent structures. This is a different direction, where long-period orbits capture statistics of turbulence. The approach is based on empirical evidence that, at least for low dimensional systems, the variability across periodic orbits of similar period T, e.g. the standard deviation of distribution follows the central limit theorem and decreases as $1/\sqrt{T}$.

They view turbulent flows as stationary equilibria of a four-dimensional PDE, the Navier-Stokes equations in three spatial directions plus time, with periodic conditions in time justified by the invariance under time translation of statistically developed flows. With sufficiently long temporal domains (akin to spatial domains larger than a minimal flow unit), they expect that averages and their gradients will converge with the size of the temporal domain.

Their goals are to a) demonstrate that these periodic orbits exists in Navier-Stokes problems b) develop an understanding of their significance in describ-

---

[1]Predrag 2019-03-19: It is Japanese heresy all over again (see comments at the end of this section)

ing turbulent structure and evolution, b) formalise a framework for control and optimisation of turbulence.

Time-parallel methods for long orbits They plan to develop new computational methods, suitable for arbitrarily long orbits.

The system arising in the Newton search iterations is the adjoint of this. The global-in-time nature of the adjoint problem on periodic orbits enables mixed space/time domain decomposition methods, to distribute computation across independent nodes of a distributed memory system.

They use multiple-shooting techniques, exploiting time as an additional direction for distributed memory parallelism. The approach consists in partitioning the temporal interval into independent sub-domains and than seeking the terminal adjoint solution at the shooting points, imposing that the solution is globally periodic and continuous at the shooting points. [2]

Matrix-vector products for the construction of the Krylov basis vectors in the GMRES solver can now exploit the block-banded structure of this problem, by distributing the sub-matrix/sub-vector products to different computational nodes in a time-parallel fashion, and using independent adjoint timesteppers to calculate actions, with minimal communication required. Mixing spatial/temporal parallelism, via processor grouping routines is a natural extension.

Even if the proposed approach based is likely not applicable to high-Reynolds number flows, the work holds the potential to accelerate future development of adjoint methods suitable for chaotic systems [72].

Task A.1 – This will be based on in-house codes under development at Southampton and freely available software (e.g. J Gibson's channelflow). The influence of the compliant wall will be modelled by linearised kinematic boundary conditions, using standard modelling procedures [64, 79].

Space-time parallel algorithms for long periodic orbits.

A dedicated c++ parallel Krylov subspace library being developed at Southampton github.com/gasagna/ParK. The Newton-Krylov-hookstep [105] approach will be used. They will initially rely on temporal parallelism and subsequently extend the library to spatial parallelism.

Space-time parallel adjoint solver. We will then couple the adjoint time steppers developed in B.1 with the available parallel Krylov solver to solve the adjoint boundary value problem.

The intersection of recurrent flow analysis with adjoint techniques for optimisation is largely unexplored. So far, recurrent flows have been primarily used as a proxy to understand dynamics, i.e. as an analysis tool. Their program is complementary to our efforts, because they aim to employ these ideas for control and design.

On **Japanese Heresy**, from `dasbuch/book/chapter/recycle.tex`:

---

[2]Predrag 2019-03-19: Just to drive Predrag more bewildered, they plot time horizontally, space vertically :)

2011-11-15 Predrag Then there is in literature an 'Alternative Periodic Orbit Theory' so bold that one can only call it The Heresy: the conjecture is that if one looks carefully enough, there exists a *single* periodic orbit that captures all dynamical averages of a turbulent flow. This is so wrong that one is at loss what to say: there is NO such single periodic orbit. Instead, there is the well established theory that says how periodic orbits are to be used, and how many are needed to capture the hyperbolic parts of the non–wandering set to a desired accuracy. It is as elegant and systematic as Statistical Mechanics and Quantum Field Theory. Read Chaos-Book.org. But who reads books nowadays?

Of course, if one picks at random a very long periodic orbit, one will get estimates as good as from an ergodic trajectory of comparable length, but then why make life hard by insisting on exact recurrence? When one starts out, The Heresy is one of the paths to enlightenment: Berry diplomatically writes "he found one orbit" in a pean to Gutzwiller [4]. Indeed, in Gutzwiller first paper (1969) on anisotropic Kepler system, the *one* periodic orbit obtained by adiabatic deformation of a Kepler ellipse yielded 10% accuracy, which was great, as in those days it was generally believed that semiclassics should be bad for the ground state. Two years later Gutzwiller invented periodic orbit theory as a tool for physicists, applied it to the full anisotropic Kepler problem, and since then there is no turning back. Similarly, Kawahara [62] computed the first Navier-Stokes periodic orbit solution embedded in turbulence, and observed that it gave rather accurate estimates of observables such as the dissipation rate.

From `siminos/blog/UPO.tex`:

2012-05-13 Predrag [...] until the first unstable periodic solutions of Navier-Stokes were computed by Kawahara and Kida [62] in 2001, determining such solutions seemed utterly out of reach. Their plane Couette flow 'upper' periodic orbit appears embedded in the turbulent sea, and captures statistics so well that it lead to the 'Heresy', a belief of the innocent that there exists a *single* periodic orbit (!) that captures turbulent statistics; we do not cite these papers, as that was a vain hope of those too busy to read ChaosBook.org.

2011-11-15 Predrag From `pipes/blog/Alabama.tex`:
Can you try this? Compute the averages for $(D(t), I(t))$ for one period of $\overline{rpo}_{36.92}$ and for your S-subspace turbulent trajectory. That should yield two point on the diagonal. Kawahara was lucky there - they were unreasonably close, the root of the Japanese Heresy. If they are not close, $\overline{rpo}_{36.92}$ does not go through the most concentrated regions of natural measure.

From ref. [33]: " Similarly close prediction of mean dissipation rate in the plane Couette flow from a single-period periodic orbit computed by Kawahara and Kida [62] has lead to optimistic hopes that 'turbulence' is

different from low-dimensional chaos, insofar that the determination of one special periodic orbit could yield all long-time averages. Regrettably, not true – as always, here too one needs a hierarchy of periodic orbits of increasing length to obtain accurate predictions [32]. "

2007-11-28 Predrag: Japanese heresy We do not want to refer to wrong papers, but here it is, for the internal record, so we do not forget not to cite it:

Mitsuhiro Kawasaki and Shin-ichi Sasa [63], "Statistics of unstable periodic orbits of a chaotic dynamical system with a large number of degrees of freedom."

2012-08-12 Predrag Goldobin [47] *Limit distribution of averages over unstable periodic orbits forming chaotic attractor*, arXiv:1208.1691, is much weirder still: it is motivated by the Japanese Heresy and cites only the Maryland non-theory paper as the source on the periodic orbit theory. Remind him to cite ChaosBook.

From `siminos/lyapunov/Henon.tex`:

2011-10-06 Kazz There should be many periodic orbits flowing like the chaotic trajectory. They therefore have long periods and are non-hyperbolic (almost, always). But, in my view, it would be interesting to decompose properties of the chaotic trajectory into those of only a few number of periodic orbits, whose period is rather short and thus each of which covers only a local region of the attractor. For the Hénon map, we are still lacking such a minimal periodic orbit, which accounts for the remaining non-hyperbolic points of the chaotic trajectory.

2011-10-06 Predrag Wow! This comment makes no sense, but it does smack of the famous Japanese Heresy. There is NO such thing - instead of this there is perfectly well developed theory that says how you use periodic orbits and how many do you need to capture the hyperbolic parts of the non–wandering set.

6.2 Spatiotemporal literature - a blog

2018-07-17 Matt Notes on Literature review in thesis proposal I tried to motivate the need to go spatiotemporal by the wall that's been hit in pipe and channelflow while still celebrating the amount of work that codes like `channelflow` and `openpipeflow` have been able to accomplish. It probably comes off as arrogant and I need to rewrite it but I'm trying to get the point across that: There are lots of people stepping back and trying to find other paths to solving the issues of high-dimensional systems because the direct approach is providing diminishing returns.

Don't mind all of the names and bibtex references, it was just brainstorming that I didn't remove.

2018-07-21 Predrag "Lots of people stepping back and trying to find other paths?" Only our Wednesday Hangout crowd has computed Navier–Stokes exact coherent structures in small computational domains, and I'm not aware of anyone thinking of "other paths" to computing exact coherent structures in spatially infinite domains other than you and me. Looking forward to reading the literature review of these many paths that I'm unaware of.

2018-07-23 Matt I meant more along the ideas of what people are to do after the small computational domain calculations are exhausted, not that others are attempting to explain infinite spatiotemporal domains. For instance, some of the "other paths" are looking for edge states, families of self-similar solutions, investigating localized solutions, reduced-order models using Koopman modes, Nigel Goldenfeld's predator-prey ideas. My statement was merely attempting to describe the many branches of turbulence research. They are unrelated to my project so I'll use the excuse that this was just an expedient comment in my blog and not a deep philosophical statement.

2016-11-10 Predrag Sobolev norms we have pondered a lot (sprinkled through various blogs) but for now stick to the L2 (AKA Euclidean) norm.

Papers to read, possibly to test your variational code on the soultions reported there:

Rempel *et al.* [93] *Analysis of chaotic saddles in high-dimensional dynamical systems: the Kuramoto-Sivashinsky equation.* Only in the antisymmetric subspace $\mathbb{U}^+$, periodic on 2π and vary hyper-viscosity ν. Might be good - do not know. For some reason neither Siminos nor Budanur nor Xiong seem to have looked at this paper, nor the subsequent ones.

Saiki *et al.* [94] *Reconstruction of chaotic saddles by classification of unstable periodic orbits: Kuramoto-Sivashinsky equation*: they work only in the anti-symmetric subspace $\mathbb{U}^+$, see their Eq. (3), but are periodic on 2π and vary hyper-viscosity ν, so you'll have to convert. Looks like cut and paste of their earlier ref. [93]. They use the PIM triple method [90, 92]. BTW, calling a periodic orbit UPO is like saying "I am riding unstable bicycle" every time you get on a bike (all bicycles are unstable): 'Note that our notation "a-UPO" may sound awkward when expanded as "attractor-unstable periodic orbit."' In all fairness, stupider things are known, like "nonchaotic orbit" instead of periodic orbit, check the next cubicle :)

What is obvious from looking at a paper like this one is that spacetime invariant 2-tori persist in continuous families, as one change the domain size L, so that must mean an additional marginal direction eigenvector for the torus-finding variational routine...

Croft's papers [27, 29–31] probably use pseudoinverse - Levenberg-Marquardt described in an appendix of ref. [33] is might be an example.

2016-12-20 Matt Read through half of Moser [86]. It is indeed hard to read but I'm hoping that in conjunction with de la Llave's *Introduction to KAM Theory* I will get something out of it.

Read through about a quarter more of Trefethen [102] as well as went to the physical library to skim some texts that another student recommended for me. They were math texts on par with Moser [86] about functional analysis. Read some more of numerical linear algebra, Trefethen [102], starting to enjoy it as I think it is written quite well.

2017-05-05 Matt Read Boghosian *et al.* [13].

2017-05-08 Matt I was reading a number of papers [17, 26, 83, 85] having to do with ill-conditioned linear systems and how to circumvent issues with GMRES.

2017-06-06 Matt Read some Guckenheimerref. [50]

2017-09-05 Matt Read Junginger *et al.* [59] *ez, "Variational principle for the determination of unstable periodic orbits and instanton trajectories at saddle points*, I think it could possibly introduce some important topics.

2017-04-14 Matt I've been reading a bunch of papers [101] on preconditioning methods; and specifically for GMRES algorithm.

2018-01-23 Matt Browsed through arXiv to try to survey the recent literature in fluid dynamics and chaotic dynamics fields just to try and branch out a little bit so that my world view isn't a single leaf of the forest. Trying not to spend too much time with them, just skimming and reading abstracts until my curiosity is peaked.

Also rereading the cats' blog, and subsequent papers in depth so that I can attempt to be of some use to Han Liang. I find Predrag's write-up about the relative action definitions that appeared in ref. [75] to be much more understandable than the actual paper, and am hoping to understand the spatiotemporal cat map definition version of the relative action soon.

Recently checked out a book on spectral methods in fluid dynamics from the Gatech library, it's a secondary read for sure but I find it useful in formalizing the ideas I have learned through coding.

2018-02-12 Matt Been reading the same texts as well as refs. [14, 76, 81].

2018-02-16 Matt Read Mackay and Meiss [80]. Even though its three pages I didn't really understand the corollary where they prove that multipliers corresponding to the stability of the second variation of the action (because the first variation is by definition to be zero) are reciprocal reals, past the point that they know that there is a matrix that can be written in a certain way under certain circumstances

2018-02-16 Matt Reading Lopez [76] 2015. It seems that what we're doing is very close to being identical except the fact that I am allowing the spatial domain size to vary. In the appendices she also notes that the best (among numerous different behaviors) convergence behavior was when she used GMRES as well as a preconditioning matrix that is the inverse of the linear portion of the Jacobian matrix. (The matrix of variations of the corresponding linear portion of the nonlinear algebraic equations), so with that I would argue that what is being done on my front is *only* different in the fact that I am working with the Kuramoto-Sivashinsky equation and am allowing the spatial domain size to vary, which I believe is a non-trivial addition.

2018-07-17 Matt To that effect I gave examples of the "stepping stones" between toy models and full three-dimensional turbulence. In my experience they are the Kuramoto-Sivashinsky equation and the two-dimensional Kolmogorov flow.

I intend to go over all of the spatiotemporal literature that I could find, namely refs. [16, 65, 76, 77, 98, 108], with the work by Vanessa López' having the closest resemblance to my own, which is unsurprising due to the fact that I used López [77] as a resource; however, none of these studies formulate a spatiotemporal *theory* of turbulence.

2018-07-17 Matt KnoMoor90 Knobloch and Moore [65] write:

> We have checked our results by expanding each modal amplitude in a Fourier series in time, and obtaining algebraic equations for the amplitudes of the Fourier components. We have found that this method works well for our parameter values provided all the harmonics through fourth order are retained.

Due to this statement its hard to tell if Knobloch and Moore [65] *Minimal model of binary fluid convection* accomplished something similar to me due to the fact there are still parameters being set and not determined by the equations.

2018-07-21 Predrag There is probably much to be learned from Knobloch and Moore [65], but your calculations seem much harder. They have three fields, and in eq. (11) they expand them in three real spatial Fourier modes, i.e., we are looking at a 9-dimensional dynamical system. They fix the domain $x \in [0, 1]$ and impose Dirchlet boundary conditions, their eq. (2). They have two parameters (σ, τ) that they vary, and as they mostly care about bifurcations, the few spatial Fourier modes suffice for their goals.

The only thing that seem not the usual is that they indeed Fourier expand in time and obtain algebraic equations, to study a time-modulated wave (MW), which is weakly oscillating relative periodic orbit, a Hopf bifurcation in Fig. 4.2 (a) giving rise to a a single MW branch. Hopf bifurcation

is a pure circle (one complex Fourier coefficient), and their MW is weekly distorted circle that it suffices to keeping only 4 time Fourier coefficients.

Expanding time dependence of a periodic orbit in Fourier is much older than their work, see for example Divakar Viswanath [104] *The Lindstedt-Poincaré technique as an algorithm for finding periodic orbits*, as is discussed in other blogs in the *siminos* repo. Divakar credits Lindstedt and Poincaré, but has many more recent references that use time Fourier series to compute periodic orbits, probably worth reading and citing some of those.

I owe nothing to this paper, honestly; I just thought that due to the fact that it presented a spatiotemporal idea it was worth mentioning.

2018-07-17 Matt SoiMei91 Soibelman and Meiron [98] numerical procedures are spatiotemporal minus being able to change the spatial domain; their analysis however is still in terms of continuation of solutions in Reynolds number to find bifurcations. Bifurcations imply changes of stability which implies analysis that views the problem as a time dynamical system. Therefore I think this is along the lines of Lan and Cvitanović [69] where the periodic orbit's are found spatiotemporally but the analysis is done as a time-dynamical system.

2018-07-17 Matt BrKevr96 State the premise of going to a spatiotemporal Fourier basis, but because they were investigating modulating traveling waves they claim that it would be too costly due to the time discretization required to resolve the high frequency temporal oscillations. Claims Soibelman and Meiron [98] and Knobloch and Moore [65] have done it... see above.

2018-07-17 Matt WGBGQ13 They show its possible, even with the modified Kuramoto-Sivashinsky equation that doesn't have reflection symmetry, but they're more interested in the scalability and possibility rather than analysis of the results.

2018-07-17 Matt lop05rel Similar to the exposition of ref. [98]. These numerical procedures are the closest to my code but still they do not allow system size to change, and then they play around with the parameters in López [76].

6.3 Summary: Lan thesis

The beginning of Yuheng Lan's PhD thesis [66] *Dynamical Systems Approach to* $1 - d$ *Spatiotemporal Chaos – A Cyclist's View*, is concerned with the history of, and ways how to approach turbulence from the dynamical systems, periodic orbit theory point of view.

6.3.1 Periodic orbit theory

This section offers a brief review of periodic orbit theory [32], including dynamical systems both discrete and continuous. The first topic is how to calculate physical averages: space and time averages over ergodic trajectories. For a quantity on a trajectory segment defined by

$$A^t(x_0) = \sum_{k=0}^{t} a(f^k(x_0)), \tag{6.2}$$

the time average is defined as

$$\bar{a}(t) = \lim_{t \to \infty} \frac{1}{t} A^t(x_0), \tag{6.3}$$

and a weighted space average is defined as

$$\langle a \rangle (t)_\rho = \int_{\mathcal{M}} dx\, \rho(x) a(f^t(x)) \tag{6.4}$$

The second topic discussed is how to formulate evolution operators and invariant measures. The time evolution operator defined by a continuous function $h(x)$ is defined as,

$$\mathcal{L}^t \circ h(x) = \int_{\mathcal{M}} dy\, \delta(x - f^t(y)) e^{\beta A^t} h(y) \tag{6.5}$$

The important results are the trace formula, spectral determinant and dynamical zeta function for flows, which are respectively:

$$tr\mathcal{L}^t = \sum_p T_p \sum_{r=1}^{\infty} \frac{e^{r\beta \cdot A_p}}{|\det(1 - J_p^r)|} \delta(t - rT_p) \tag{6.6}$$

$$F(s) = \det(s - \mathcal{A}) = \exp\left[-\sum_p \sum_{r=1}^{\infty} \frac{1}{r} \frac{e^{\beta \cdot A_p - sT_p}}{|\det(1 - J_p^r)|}\right] \tag{6.7}$$

$$\frac{1}{\zeta(z)} = \exp\left(-\sum_p \sum_{r=1}^{\infty} \frac{1}{r} t_p^r\right) = \prod_p (1 - t_p) \tag{6.8}$$

The definition of the dynamical zeta function is impractical so it is best rewritten as a sum of terms listed in order of decreasing contributions.

$$\frac{1}{\zeta(z)} = 1 - t_0 - t_1 - [t_{01} - t_0 t_1] - \ldots \tag{6.9}$$

$$= 1 - \sum_f t_f - \sum_n c_n \tag{6.10}$$

where t_f are "fundamental" terms and c_n are corrections.

6.3.2 Variational method

The variational method is employed via an initial guess and equation:

$$\frac{\partial^2 \tilde{x}}{\partial s \partial \tau} - \lambda A \frac{\partial \tilde{x}}{\partial \tau} - v \frac{\partial \lambda}{\partial \tau} = \lambda v - \tilde{v} \tag{6.11}$$

Wherein a true periodic orbit can be found which minimizes the functional:

$$I = \int_0^{2\pi} \left(\tilde{v} - \lambda \frac{\partial x}{\partial s} \right)^2 ds \tag{6.12}$$

If there is a parameter c, a different equation can be employed:

$$\left(A - \lambda \frac{\partial}{\partial s} \right) \frac{\partial x}{\partial \tau} + \frac{\partial v_c}{\partial c} \frac{\partial c}{\partial \tau} = - \left(v_c - \lambda \frac{\partial x}{\partial s} \right), \tag{6.13}$$

The main benefit of this method avoids using multiple Poincaré sections due the numerical stability originating from topological sources.

Search for equilibria

Steady solutions play an important role in organization of the state space, albeit in a coarse manner. The equation that governs the steady solutions (equilibria and relative equilibria) of the Kuramoto-Sivashinsky equation is: [3]

$$\frac{1}{2} u^2 + u_x + u_{xxx} = c$$

With a substitution of variables, this equation can be written as a set of first order ODE's, namely:

$$u_x = v, \quad v_x = w, \quad w_x = u^2 - v - c$$

This equation exhibits a reversal symmetry, $x \to -x, u \to -u, v \to v, w \to -w$.

$$(u + w)_x = u^2 - c$$

The last equation's behavior is dependent on the constant c, where equilibria exist if $c > 0$, namely at $c_\pm = (\pm\sqrt{c}, 0, 0)$

Thirteen periodic solutions for $L = 43.5$, $\nu = 1$, were found using the the variational method, with their importance varying. The importance was measured by determining the distance between points on a typical orbit and the equilibria. Typical orbits in the non-wandering set seem to be similar to these equilibria.

The average number of peaks of $u(x,t)$ seems to follow closely to the average number of peaks in these thirteen equilibria.

---

[3]Predrag 2016-08-08: Much of this has already been said in sect. 12.1.3. Merge the material, label relevant equations there and here refer to them only by their numbers/labels.

6.3.3 Steady solutions for a given c value

Further study was done with $c = 0.40194$. In this regime, there are four periodic orbits that lay the foundation for the symbolic dynamics developed in this paper. Specifically, these four important periodic orbits were labelled a, b, ac_-, ac_+. These were redefined as 0, 1, 2, 3, respectively, for convenience.

Four cycles of topological length 2 were found, namely: 01, 02, 03, 23. Fourteen cycles of topological length 3 were found, and 43 cycles of topological length 4 were found. It is believed that cycles with 12 and 13 are pruned from the symbolic dynamics.

The power of the symbolic dynamics and variational method lies in their combination. When used in conjunction, they can be used to find long orbits.

Study of 2D return maps on a Poincaré section was the next step in order to further devolve the state space into partitions.

6.3.4 Bifurcations

This section investigates how the fundamental cycles used to develop the symbolic dynamics bifurcate when changing the value of c. For cycles 0 and 1, there is evidence that a saddle-node bifurcation exists at $c = 0.80167$ and an inverse period-doubling bifurcation occurs at $c = 0.00078$, both of which are supported by eigenvalues of the respective Jacobians near these bifurcation points. In the limit of small c, $c \to 0^+$, perturbation techniques are used to analyze the properties of the equations governing the steady solutions.

For cycle 2, there is a very similar cycle near $c = 0.29304$. There is evidence of a saddle-node bifurcation, supported by the eigenvalues of the Jacobian of both cycles near the bifurcation point. A similar phenomenon appears at $c = 0.42031$.

A table provides evidence that there are intervals of periods for which certain cycles do not exist. When within the "bands" of the table, the cycles exist with the corresponding period and c value, which was undetermined.

6.4 Kuramoto-Sivashinsky equilibria literature survey

2017-10-02 Andy Michelson [84] searches for relative equilibria moving with velocity c^2

$$u(x, t) = -c^2 t + v(x) \tag{6.14}$$

for the Kuramoto-Sivashinsky equation and arrives at the ODE

$$\frac{d^4 v}{dx^4} + \frac{d^2 v}{dx^2} = c^2 - \frac{1}{2}\left(\frac{dv}{dx}\right)^2. \tag{6.15}$$

However, the version of the Kuramoto-Sivashinsky equation that Michelson uses differs from (10.1) in the first derivative term: ChaosBook has

takes the square first and then the derivative while Michelson reverses the operations. As a result, Michelson's initial Kuramoto-Sivashinsky equation would allow for degenerate solutions of parity symmetry with respect to x. Section 4 of Michelson [84] employs a finite difference algorithm to find the steady state solutions $y = \frac{dv}{dx}$. I have gone through the steps to obtain (4.2) and the finite difference equation. I am currently writing a script to recreate the solutions that Michelson found with certain c values.

I extended the iteration to include when the trajectory diverges from the periodic orbit.

2017-10-23 Predrag For whatever that is worth, my lecture on the equilibria of Kuramoto-Sivashinsky is here.

2016-01-12 PC Literature related to Michelson [84]:

Carmona *et al.* [21] *Noose structure and bifurcations of periodic orbits in reversible three-dimensional piecewise linear differential systems*

Barker *et al.* [3] *Stability of periodic Kuramoto-Sivashinsky waves*

Aderogba, A. A. and Chapwanya, M. and Djoko [1] *Travelling wave solution of the Kuramoto-Sivashinsky equation: A computational study*

Dumortier, Ibanez and Kokubu [38] *Cocoon bifurcation in three-dimensional reversible vector fields*

Heidel and Zhang [51] *Nonchaotic and chaotic behavior in three-dimensional quadratic systems: Five-one conservative cases*,

Nickel [89] *Travelling wave solutions to the Kuramoto–Sivashinsky equation*

Blomgren, Gasner, and Palacios [5] *Hopping behavior in the Kuramoto–Sivashinsky equation* seems to be specific to $2D$: " numerical 'hopping' cellular flame patterns are characterized by nonuniform rotations of a ring of cells, in which individual cells make abrupt changes in their angular positions while they rotate around the ring. Until now, these states have been observed only in experiments but not in truly two-dimensional computer simulations. A modal decomposition analysis of the simulated patterns, via the proper orthogonal decomposition, reveals spatiotemporal behavior in which the overall temporal dynamics is similar to that of equivalent experimental states but the spatial dynamics exhibits a few more features that are not seen in the experiments. "

Dumortier, Ibanez and Kokubu [38] *Cocoon bifurcation in three-dimensional reversible vector fields*

Rempel *et al.* [93] Analysis of chaotic saddles in high-dimensional dynamical systems: the Kuramoto-Sivashinsky equation: " study the role played by nonattracting chaotic sets called chaotic saddles in chaotic transitions of high-dimensional dynamical systems. Our methodology is applied to the Kuramoto-Sivashinsky equation. The paper describes a novel
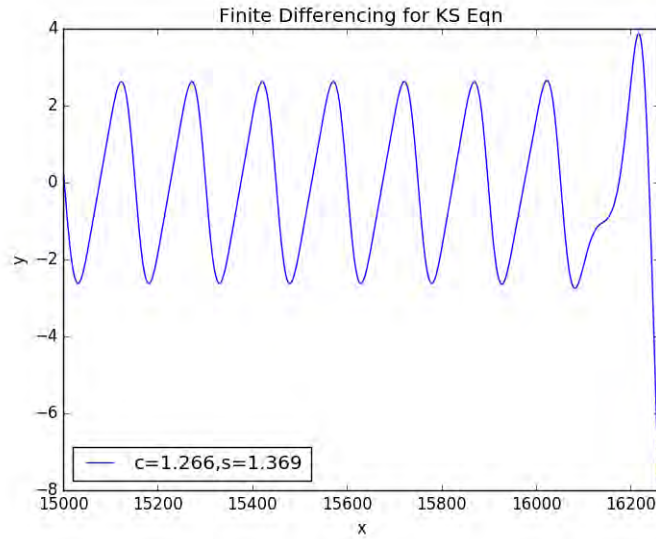
Figure 6.1: (xy) plot. The trajectory generated through a finite difference scheme outlined in Michelson [84] for $c = 1.266$ and $s = 1.369$.
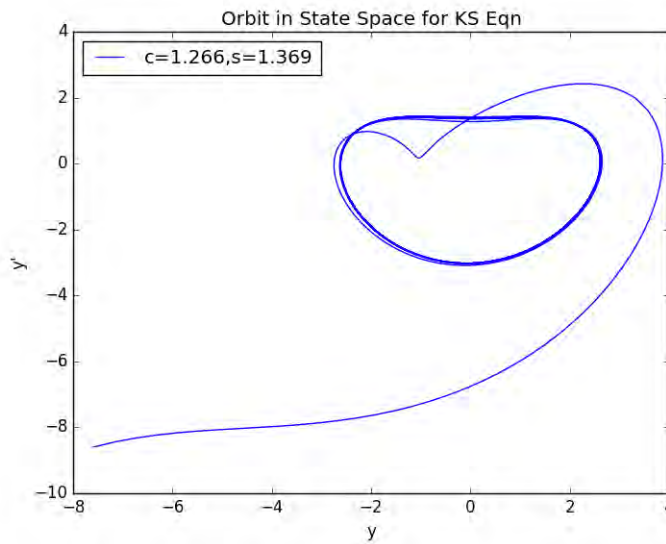
Figure 6.2: State space plot. The near-periodic orbit generated through a finite difference scheme outlined in Michelson [84] for $c = 1.266$ and $s = 1.369$.

technique that uses the stable manifold of a chaotic saddle to characterize the homoclinic tangency responsible for an interior crisis, a chaotic tran-

sition that results in the enlargement of a chaotic attractor. The numerical techniques explained here are important to improve the understanding of the connection between low-dimensional chaotic systems and spatiotemporal systems which exhibit temporal chaos and spatial coherence."

Wilczak [110] *Chaos in the Kuramoto-Sivashinsky equations – a computer-assisted proof*

Strauss and Wang [100] *Instability of traveling waves of the Kuramoto-Sivashinsky equation*

Ishimura [55] *Remarks on third-order ODEs relevant to the Kuramoto-Sivashinsky equation*

Ishimura and Nakamura [56] *Nonexistence of monotonic solutions of some third-order ode relevant to the Kuramoto-Sivashinsky equation*

Wittenberg and Holmes [111] *Scale and space localization in the Kuramoto-Sivashinsky equation*: " Using a wavelet basis, the spatiotemporally chaotic regime of the KSe is explored where a good seperation of scales is observed. In large scales, the dynamics is Gaussian. In the intermediate scales, the dynamics is reminiscent of travelling waves and heteroclinic cycles which is the typical behavior for small system size. In the small scales, the dynamics is intermittent. Through investigation of the interaction between different scales, we see the intermediate structures give the defining shape of the cell and the large scales trigger the spatiotemporal chaos. The small scales dissipate energy and modify the background in a average sense.

Yang [113] *On travelling-wave solutions of the Kuramoto-Sivashinsky equation*

Lau [73] *The cocoon bifurcations in three-dimensional systems with two fixed points*

Jones, Troy and MacGillivary [58] *Steady solutions of the Kuramoto-Sivashinsky equation for small wave speed*

Grimshaw and Hooper [49] *The non-existence of a certain class of travelling wave solutions of the Kuramoto-Sivashinsky equation*,

Troy [103] *The existence of steady solutions of the Kuramoto-Sivashinsky equation*

Hooper and Grimshaw [52] *Travelling wave solutions of the Kuramoto-Sivashinsky equation*

Stanislavova and Stefanov [99] *Asymptotic estimates and stability analysis of Kuramoto-Sivashinsky type models*

6.4.1 Dong and Lan / DoLa14

Dong and Lan [36] *Organization of spatially periodic solutions of the steady Kuramoto-Sivashinsky equation*

2017-07-17 Matt DoLa14 The goal of Dong and Lan [36] is to formulate a systematic way to locate periodic orbits with variational method developed by Lan and Cvitanović [34, 68], as well as develop symbolic dynamics to classify these periodic orbits.

2013-12-29 PC Dong and Lan [36] study equilibria of Kuramoto-Sivashinsky at $L = 43.5$. Previous system sizes were was for antisymmetric subspace, system size $\tilde{L} = 2.89109$ in ref. [25], $L = 38.5$ in ref. [69], $L = 40.95$ in Lan *et al.* [67], and full state space $L = 22$ in ref. [33]. Dong and Lan continue the discussion of Lan's thesis [66]. Only equilibria, no mention of relative equilibria.

They credit Troy [58, 103] and Greene & Kim [48] with first studies of Kuramoto-Sivashinsky equilibria.

2017-11-01 Andy DoLa14 Reading this paper's introduction and background tremendously helped me understand the Kuramoto-Sivashinsky equation more.

$$u_t = (u^2)_x - u_{xx} - \nu u_{xxxx} \tag{6.16}$$

The first derivative term is responsible for the interactions between spatial modes at different scales (assuming this means length scales L) and transfers energy from the low wavenumber modes to the higher ones. The second term pumps energy into the system and makes it unstable at large scales while the third term dissipates energy and damps at small scales.

Matt has gone over the spectral decomposition of the solution many times, but I will just repeat it here for reference: using the form

$$u(x,t) = i \sum_{k=-\infty}^{+\infty} a_k(t)e^{ikqx} \qquad \text{where } q = 2\pi/L, \tag{6.17}$$

we can obtain an infinite ladder of coupled ODEs

$$\dot{a}_k = [(kq)^2 - \nu(kq)^4]a_k - kq \sum_{m=-\infty}^{+\infty} a_m a_{k-m}. \tag{6.18}$$

Since the dissipation term $\nu(kq)^4$ dominates for large wavenumber components, these terms will not be excited enough significantly contribute to the dynamics. Thus, we can truncate the set of ODEs such that $a_k = 0$ for $|k| > N$. In most cases, we take $N = 16$. For small L, all Fourier modes are linearly stable, but the system quickly becomes increasingly turbulent once L increases by a significant amount.

From the video that Predrag recommended as well as the paper, the Ku-

ramoto-Sivashinsky equation can be written as

$$u^2 - u_x - \nu u_{xxx} = c \tag{6.19}$$

$$\implies \begin{cases} u_x = v \\ v_x = w \\ w_x = u^2 - v - c \end{cases} \tag{6.20}$$

$$\implies (u + w)_x = u^2 - c \tag{6.21}$$

We can see that $u + w$ increases without bound when $c < u^2$. When $c > u^2$ we can find attractors appear in the state space. However, something weird happens when $c = u^2$ such that the derivative on the left side of Eqn 4.10 equals 0: both an attractor and repeller appear in the state space, and it seems that trajectory enters the sink and reappears at the source (if I'm understanding Predrag's drawing in the video correctly).

I'm still working through the variational methods part of the paper to see what they actually did with the numerical simulations. So far, it seems that there exists four simple building blocks for creating allowable orbits. This numbering notation reminds me of the billiard (or pinball) orbit example that was covered in the Group Theory class.

2013-12-29 PC we still have to study Dong and Y. Lan [35] *A variational approach to connecting orbits in nonlinear dynamical systems*

" At fixed system size $L = 43.5$, important equilibria are identified and shown to organize the dynamics. The first integral of the steady KSe leads to a 3D dynamical system with an integration constant c. At a typical value of $c = 0.40194$, four simplest cycles are identified and used as basic building blocks to construct longer cycles. The symbolic dynamics based on trajectory topology are very effective in classifying all short periodic orbits. The the return map on a chosen Poincaré section shows the complexity of the dynamics and the bifurcation of building blocks provides a chart to look for possible cycles at given periods. "

The n cell state [45] is stable in finite windows for arbitrarily large system sizes.

" the antisymmetric heteroclinic orbit $\in \mathbb{U}^+$ connecting the two equilibria in (9) is the only bounded nonconstant solution when the integration constant $c \to \infty$ [82]. For c large enough, the heteroclinic orbit remains the unique bounded solution [84]. It continues to be numerically observable with c down to 0.07 [52], and was computed analytically with normal form analysis for $c \ll 1$ [22]. When c decreases from large values, new connections with more zeroes are born through saddle-node bifurcations until one periodic orbit emerges as a limit of the connecting orbit with infinite number of zeros. Bifurcation analysis with spatial Fourier modes gives interesting features of spatially periodic steady solutions in certain parameter regime [48]. "

References

[1] A. A. Aderogba, M. Chapwanya, and J. K. Djoko, "Travelling wave solution of the Kuramoto-Sivashinsky equation: a computational study", AIP Conf. Proc. **1479**, 777–780 (2012).

[2] D. Auerbach, P. Cvitanović, J.-P. Eckmann, G. Gunaratne, and I. Procaccia, "Exploring chaotic motion through periodic orbits", Phys. Rev. Lett. **58**, 2387–2389 (1987).

[3] B. Barker, M. A. Johnson, P. Noble, L. M. Rodrigues, and K. Zumbrun, "Stability of periodic Kuramoto-Sivashinsky waves", Appl. Math. Lett. **25**, 824–829 (2012).

[4] M. V. Berry, "Martin Gutzwiller and his periodic orbits", Commun. Swiss Phys. Soc. **37**, 4839–4849 (2012).

[5] P. Blomgren, S. Gasner, and A. Palacios, "Hopping behavior in the Kuramoto-Sivashinsky equation", Chaos **15**, 013706 (2005).

[6] P. Blonigan and Q. Wang, "Multigrid-in-time for sensitivity analysis of chaotic dynamical systems", Numer. Linear Algebra Appl. (2014) `10.1002/nla.1946`.

[7] P. J. Blonigan, "Adjoint sensitivity analysis of chaotic dynamical systems with non-intrusive least squares shadowing", J. Comput. Phys. **348**, 803–826 (2017).

[8] P. J. Blonigan and Q. Wang, "Least squares shadowing sensitivity analysis of a modified Kuramoto-Sivashinsky equation", Chaos Solit. Fract. **64**, 16–25 (2014).

[9] P. J. Blonigan and Q. Wang, Multiple shooting shadowing for sensitivity analysis of chaotic systems and turbulent fluid flowsflows, in 53rd AIAA Aerospace Sciences Meeting (2015).

[10] P. J. Blonigan and Q. Wang, "Multiple shooting shadowing for sensitivity analysis of chaotic dynamical systems", J. Comput. Phys. **354**, 447–475 (2018).

[11] P. Blonigan, Q. Wang, E. Nielsen, and B. Diskin, Least squares shadowing sensitivity analysis of chaotic flow around a two-dimensional airfoil, in 54th AIAA Aerospace Sciences Meeting (2016).

[12] B. M. Boghosian, A. Brown, J. Lätt, H. Tang, L. M. Fazendeiro, and P. V. Coveney, "Unstable periodic orbits in the Lorenz attractor", Philos. Trans. Royal Soc. A **369**, 2345–2353 (2011).

[13] B. M. Boghosian, L. M. Fazendeiro, J. Lätt, H. Tang, and P. V. Coveney, "New variational principles for locating periodic orbits of differential equations", Philos. Trans. Royal Soc. A **369**, 2211–2218 (2011).

[14] S. V. Bolotin and D. V. Treschev, "Hill's formula", Russ. Math. Surv. **65**, 191 (2010).

[15] A. Borzi and V. Schulz, *Computational Optimization of Systems Governed by Partial Differential Equations* (SIAM, Philadelphia, 2011).

[16] H. S. Brown and I. G. Kevrekidis, "Modulated traveling waves for the Kuramoto-Sivashinsky equation", in *Pattern formation: symmetry methods and applications*, edited by D. Benest and C. Froeschlé (AMS, Providence, RI, 1996), pp. 45–66.

[17] P. N. Brown and H. F. Walker, "GMRES on (nearly) singular systems", SIAM J. Matrix. Anal. Appl. **18**, 37–51 (1997).

[18] D. G. Cacuci, "Sensitivity theory for nonlinear systems. I. Nonlinear functional analysis approach", J. Math. Phys. **22**, 2794–2802 (1981).

[19] D. G. Cacuci, "Second-order adjoint sensitivity analysis methodology (2nd-ASAM) for computing exactly and efficiently first- and second-order sensitivities in large-scale linear systems: I. Computational methodology", J. Comput. Phys. **284**, 687–699 (2015).

[20] D. G. Cacuci, "Second-order sensitivities of a general functional of the forward and adjoint fluxes in a multiplying nuclear system with source", Nucl. Eng. Des. **344**, 83–106 (2019).

[21] V. Carmona, F. Fernández-Sánchez, E. García-Medina, and A. E. Teruel, "Noose structure and bifurcations of periodic orbits in reversible three-dimensional piecewise linear differential systems", J. Nonlin. Sci **25**, 1209–1224 (2015).

[22] H.-C. Chang, "Travelling waves on fluid interfaces: Normal form analysis of the Kuramoto-Sivashinsky equation", Phys. Fluids **29**, 3142 (1986).

[23] M. Chater, A. Ni, P. J. Blonigan, and Q. Wang, "Least squares shadowing method for sensitivity analysis of differential equations", SIAM J. Numer. Anal. **55**, 3030–3046 (2017).

[24] M. Chater, A. Ni, and Q. Wang, "Simplified Least Squares Shadowing sensitivity analysis for chaotic ODEs and PDEs", J. Comput. Phys. **329**, 126–140 (2017).

[25] F. Christiansen, P. Cvitanović, and V. Putkaradze, "Spatiotemporal chaos in terms of unstable recurrent patterns", Nonlinearity **10**, 55–70 (1997).

[26] K. T. Chu, "A direct matrix method for computing analytical Jacobians of discretized nonlinear integro-differential equations", J. Comput. Phys. **228**, 5526–5538 (2009).

[27] D. L. Crane, R. L. Davidchack, and A. N. Gorban, Minimal cover of high-dimensional chaotic attractors by embedded coherent structures, 2016.

[28] J. Craske, "Adjoint sensitivity analysis of chaotic systems using cumulant truncation", Chaos Solit. Fract. **119**, 243–254 (2019).

[29] J. J. Crofts, Efficient method for detection of periodic orbits in chaotic maps and flows, PhD thesis (Dept. of Mathematics, Univ. of Leicester, Leicester, UK, 2007).

[30] J. J. Crofts and R. L. Davidchack, "Efficient detection of periodic orbits in chaotic systems by stabilizing transformations", SIAM J. Sci. Comp. **28**, 1275–1288 (2006).

[31] J. J. Crofts and R. L. Davidchack, "On the use of stabilizing transformations for detecting unstable periodic orbits in high-dimensional flows", Chaos **19**, 033138 (2009).

[32] P. Cvitanović, R. Artuso, R. Mainieri, G. Tanner, and G. Vattay, *Chaos: Classical and Quantum* (Niels Bohr Inst., Copenhagen, 2022).

[33] P. Cvitanović, R. L. Davidchack, and E. Siminos, "On the state space geometry of the Kuramoto-Sivashinsky flow in a periodic domain", SIAM J. Appl. Dyn. Syst. **9**, 1–33 (2010).

[34] P. Cvitanović and Y. Lan, Turbulent fields and their recurrences, in Correlations and Fluctuations in QCD : Proceedings of 10. International Workshop on Multiparticle Production, edited by N. Antoniou (2003), pp. 313–325.

[35] C. Dong and Y. Lan, "A variational approach to connecting orbits in nonlinear dynamical systems", Phys. Lett. A **378**, 705–712 (2014).

[36] C. Dong and Y. Lan, "Organization of spatially periodic solutions of the steady Kuramoto-Sivashinsky equation", Commun. Nonlinear Sci. Numer. Simul. **19**, 2140–2153 (2014).

[37] D. A. Donzis and K. Aditya, "Asynchronous finite-difference schemes for partial differential equations", J. Comput. Phys. **274**, 370–392 (2014).

[38] F. Dumortier, S. Ibanez, and H. Kokubu, "Cocoon bifurcation in three-dimensional reversible vector fields", Nonlinearity **19**, 305–328 (2006).

[39] R. M. Errico, "What is an adjoint model?", Bull. Amer. Meteor. Soc. **78**, 2577–2591 (1997).

[40] M. Farazmand, "An adjoint-based approach for finding invariant solutions of Navier-Stokes equations", J. Fluid M. **795**, 278–312 (2016).

[41] G. E. Fasshauer, "Newton iteration with multiquadrics for the solution of nonlinear PDEs", Comput. Math. Appl. **43**, 423–438 (2002).

[42] G. E. Fasshauer, *Meshfree approximation methods with MATLAB* (World Scientific, Singapore, 2007).

[43] L. Fazendeiro, B. Boghosian, P. Coveney, and J. Lätt, "Unstable periodic orbits in weak turbulence", J. Comput. Sci. **1**, 13–23 (2010).

[44] L. I. Finn, B. M. Boghosian, and C. N. Kottke, "Vortex core identification in viscous hydrodynamics", Philos. Trans. Royal Soc. A **363**, 1937–1948 (2005).

[45] U. Frisch, Z. S. She, and O. Thual, "Viscoelastic behavior of cellular solutions to the Kuramoto-Sivashinsky model", J. Fluid Mech. **168**, 221–240 (1986).

[46] F. Gao and C. Chi, "Numerical solution of nonlinear Burgers' equation using high accuracy multi-quadric quasi-interpolation", Appl. Math. Comput. **229**, 414–421 (2014).

[47] D. S. Goldobin, Limit distribution of averages over unstable periodic orbits forming chaotic attractor, 2012.

[48] J. M. Greene and J.-S. Kim, "The steady states of the Kuramoto-Sivashinsky equation", Physica D **33**, 99–120 (1988).

[49] R. Grimshaw and A. P. Hooper, "The non-existence of a certain class of travelling wave solutions of the Kuramoto-Sivashinsky equation", Physica D **50**, 231–238 (1991).

[50] J. Guckenheimer and P. Holmes, *Nonlinear Oscillations, Dynamical Systems, and Bifurcations of Vector Fields* (Springer, New York, 1983).

[51] J. Heidel and F. Zhang, "Nonchaotic and chaotic behavior in three-dimensional quadratic systems: Five-one conservative cases", Int. J. Bifur. Chaos **17**, 2049–2072 (2007).

[52] A. P. Hooper and R. Grimshaw, "Travelling wave solutions of the Kuramoto-Sivashinsky equation", Wave Motion **10**, 405–420 (1988).

[53] D. Huang, S. Chernyshenko, P. Goulart, D. Lasagna, O. Tutty, and F. Fuentes, "Sum-of-squares of polynomials approach to nonlinear stability of fluid flows: an example of application", Proc. Roy. Soc. Ser A **471**, 20150622 (2015).

[54] D. Huang, B. Jin, D. Lasagna, S. Chernyshenko, and O. Tutty, "Expensive control of long-time averages using sum of squares and its application to a laminar wake flow", IEEE Trans. Control Systems Tech. **25**, 2073–2086 (2017).

[55] N. Ishimura, "Remarks on third-order ODEs relevant to the Kuramoto-Sivashinsky equation", J. Diff. Eqn. **178**, 466–477 (2002).

[56] N. Ishimura and M. Nakamura, "Nonexistence of monotonic solutions of some third-order ode relevant to the Kuramoto-Sivashinsky equation", Taiwanese J. Math. **4**, 621–625 (2000).

[57] J. A. Jiménez and A. M. Mancho, "Distinguished trajectories in time dependent vector fields", Chaos **19**, 013111 (2009).

[58] J. Jones, W. C. Troy, and A. D. MacGillivary, "Steady solutions of the Kuramoto-Sivashinsky equation for small wave speed", J. Diff. Eqn. **96**, 28–55 (1992).

[59] A. Junginger, J. Main, G. Wunner, and R. Hernandez, "Variational principle for the determination of unstable periodic orbits and instanton trajectories at saddle points", Phys. Rev. A **95**, 032130 (2017).

[60] E. J. Kansa, "Multiquadrics–A scattered data approximation scheme with applications to computational fluid-dynamics–I surface approximations and partial derivative estimates", Comput. Math. Appl. **19**, 127–145 (1990).

[61] E. J. Kansa, "Multiquadrics–A scattered data approximation scheme with applications to computational fluid-dynamics–II solutions to parabolic, hyperbolic and elliptic partial differential equations", Comput. Math. Appl. **19**, 147–161 (1990).

[62] G. Kawahara and S. Kida, "Periodic motion embedded in plane Couette turbulence: Regeneration cycle and burst", J. Fluid Mech. **449**, 291 (2001).

[63] M. Kawasaki and S. Sasa, "Statistics of unstable periodic orbits of a chaotic dynamical system with a large number of degrees of freedom", Phys. Rev. E **72**, 037202 (2005).

[64] E. Kim and H. Choi, "Space-time characteristics of a compliant wall in a turbulent channel flow", J. Fluid Mech. **756**, 30–53 (2014).

[65] E. Knobloch and D. R. Moore, "Minimal model of binary fluid convection", Phys. Rev. A **42**, 4693–4709 (1990).

[66] Y. Lan, Dynamical Systems Approach to $1 - d$ Spatiotemporal Chaos – A Cyclist's View, PhD thesis (School of Physics, Georgia Inst. of Technology, Atlanta, 2004).

[67] Y. Lan, C. Chandre, and P. Cvitanović, "Variational method for locating invariant tori", Phys. Rev. E **74**, 046206 (2006).

[68] Y. Lan and P. Cvitanović, "Variational method for finding periodic orbits in a general flow", Phys. Rev. E **69**, 016217 (2004).

[69] Y. Lan and P. Cvitanović, "Unstable recurrent patterns in Kuramoto-Sivashinsky dynamics", Phys. Rev. E **78**, 026208 (2008).

[70] D. Lasagna, "Sensitivity analysis of systems using unstable periodic orbits", SIAM J. Appl. Dyn. Syst. **17**, 547–580 (2018).

[71] D. Lasagna, D. Huang, O. R. Tutty, and S. Chernyshenko, "Sum-of-squares approach to feedback control of laminar wake flows", J. Fluid Mech. **809**, 628–663 (2016).

[72] D. Lasagna, A. Sharma, and J. Meyers, Periodic shadowing sensitivity analysis of chaotic systems, 2018.

[73] Y.-T. Lau, "The cocoon bifurcations in three-dimensional systems with two fixed points", Int. J. Bifur. Chaos **2**, 543–558 (1992).

[74] D. J. Lea, M. R. Allen, and T. W. N. Haine, "Sensitivity analysis of the climate of a chaotic system", Tellus A **52**, 523–532 (2000).

[75] J. Li and S. Tomsovic, "Exact relations between homoclinic and periodic orbit actions in chaotic systems", Phys. Rev. E **97**, 022216 (2017).

[76] V. López, Numerical continuation of invariant solutions of the complex Ginzburg–Landau equation, 2015.

[77] V. López, P. Boyland, M. T. Heath, and R. D. Moser, "Relative periodic solutions of the complex Ginzburg-Landau equation", SIAM J. Appl. Dyn. Syst. **4**, 1042–1075 (2006).

[78] P. Luchini and A. Bottaro, "Adjoint equations in stability analysis", Annu. Rev. Fluid Mech. **46**, 493–517 (2014).

[79] M. Luhar, A. S. Sharma, and B. J. McKeon, "On the design of optimal compliant walls for turbulence control", J. Turbul. **17**, 787–806 (2016).

[80] R. S. MacKay and J. D. Meiss, "Linear stability of periodic orbits in Lagrangian systems", Phys. Lett. A **98**, 92–94 (1983).

[81] J. E. Marsden and M. West, "Discrete mechanics and variational integrators", Acta Numerica **10**, 357–514 (2001).

[82] C. K. McCord, "Uniqueness of connection orbits in the equation $y^{(3)} = y^2 - 1$", J. Math. Anal. Appl. **114**, 584–592 (1986).

[83] J. Meza, A modification to the GMRES method for ill-conditioned linear systems, tech. rep. (Sandia National Laboratories, 1995).

[84] D. Michelson, "Steady solutions of the Kuramoto-Sivashinsky equation", Physica D **19**, 89–111 (1986).

[85] R. C. Mittal and A. H. Al-Kurdi, "An efficient method for constructing an ILU preconditioner for solving large sparse nonsymmetric linear systems by the GMRES method", Comput. Math. Appl. **45**, 1757–1772 (2003).

[86] J. Moser, "Minimal solutions of variational problems on a torus", Ann. Inst. H. Poincaré **3**, 229–272 (1986).

[87] A. Ni, "Hyperbolicity, shadowing directions and sensitivity analysis of a turbulent three-dimensional flow", J. Fluid Mech. **863**, 644–669 (2019).

[88] A. Ni and Q. Wang, "Sensitivity analysis on chaotic dynamical systems by Non-Intrusive Least Squares Shadowing (NILSS)", J. Comput. Phys. **347**, 56–77 (2017).

[89] J. Nickel, "Travelling wave solutions to the Kuramoto-Sivashinsky equation", Chaos Solit. Fract. **33**, 1376–1382 (2007).

[90] H. E. Nusse and J. A. Yorke, "A procedure for finding numerical trajectories on chaotic saddles", Physica D **36**, 137–156 (1989).

[91] D. Pepper and M. R. Gonzalez, "A localized meshless technique for generating 3-D wind fields", Computation **6**, 17 (2018).

[92] E. L. Rempel and A. C. Chian, "Intermittency induced by attractor-merging crisis in the Kuramoto-Sivashinsky equation", Phys. Rev. E **71**, 016203 (2005).

[93] E. L. Rempel, A. C. Chian, E. E. Macau, and R. R. Rosa, "Analysis of chaotic saddles in high-dimensional dynamical systems: the Kuramoto-Sivashinsky equation", Chaos **14**, 545–56 (2004).

[94] Y. Saiki, M. Yamada, A. C.-L. Chian, R. A. Miranda, and E. L. Rempel, "Reconstruction of chaotic saddles by classification of unstable periodic orbits: Kuramoto-Sivashinsky equation", Chaos **25**, 103123 (2015).

[95] G. Sánchez-Arriaga, E. Siminos, V. Saxena, and I. Kourakis, "Relativistic breather-type solitary waves with linear polarization in cold plasmas", Phys. Rev. E **91**, 033102 (2015).

[96] M. Sarboland and A. Aminataei, "The dual reciprocity boundary element method for two-dimensional Burgers' equations with inverse multiquadric approximation scheme", Journal of Concrete & Applicable Mathematics **12**, 102–115 (2014).

[97] T. M. Schneider, Variational adjoint methods coupled with machine learning, private communication, 2019.

[98] I. Soibelman and D. I. Meiron, "Finite-amplitude bifurcations in plane Poiseuille flow: two-dimensional Hopf bifurcation", J. Fluid Mech. **229**, 389 (1991).

[99] M. Stanislavova and A. Stefanov, "Asymptotic estimates and stability analysis of Kuramoto-Sivashinsky type models", J. Evol. Eqs. **11**, 605–635 (2011).

[100] W. Strauss and G. Wang, "Instability of traveling waves of the Kuramoto-Sivashinsky equation", Chin. Ann. Math. **23**, 267–276 (2002).

[101] T. E. Tezduyar, M. Behr, S. K. Aliabadi, S. Mittal, and S. E. Ray, "A new mixed preconditioning method for finite element computations", Comp. Meth. Appl. Mech. Eng. **99**, 27–42 (1992).

[102] L. N. Trefethen and D. Bau, *Numerical Linear Algebra* (SIAM, Philadelphia, 1997).

[103] W. C. Troy, "The existence of steady solutions of the Kuramoto-Sivashinsky equation", J. Diff. Eqn. **82**, 269–313 (1989).

[104] D. Viswanath, "The Lindstedt-Poincaré technique as an algorithm for finding periodic orbits", SIAM Rev. **43**, 478–496 (2001).

[105] D. Viswanath, "Recurrent motions within plane Couette turbulence", J. Fluid Mech. **580**, 339–358 (2007).

[106] Q. Wang, "Forward and adjoint sensitivity computation of chaotic dynamical systems", J. Comput. Phys. **235**, 1–13 (2013).

[107] Q. Wang, "Convergence of the least squares shadowing method for computing derivative of ergodic averages", SIAM J. Numer. Anal. **52**, 156–170 (2014).

[108] Q. Wang, S. A. Gomez, P. J. Blonigan, A. L. Gregory, and E. Y. Qian, "Towards scalable parallel-in-time turbulent flow simulations", Phys. Fluids **25**, 110818 (2013).

[109] Q. Wang, R. Hu, and P. J. Blonigan, "Least Squares Shadowing sensitivity analysis of chaotic limit cycle oscillations", J. Comput. Phys. **267**, 210–224 (2014).

[110] D. Wilczak, "Chaos in the Kuramoto-Sivashinsky equations – a computer-assisted proof", J. Diff. Eqn. **194**, 433–459 (2003).

[111] R. W. Wittenberg and P. Holmes, "Scale and space localization in the Kuramoto-Sivashinsky equation", Chaos **9**, 452 (1999).

[112] J. Yang, "A numerical method for computing time-periodic solutions in dissipative wave systems", Stud. Appl. Math. **134**, 420–455 (2015).

[113] T.-S. Yang, "On travelling-wave solutions of the Kuramoto-Sivashinsky equation", Physica D **110**, 25–42 (1997).

Chapter 8

Kolmogorov flow

2018-12-07 Predrag Moved *elton/blog/KFsymm.tex* Mohammad and Predrag 2D
  Kolmogorov flow discussions to here, current sect. 8.1.

2018-12-07 Matt Mhm

8.1 Notes on Kolmogorov flow

2017-07-10 Mohammad Read Smith and Wissink [23] *Asymptotic analysis of the
attractors in two-dimensional Kolmogorov flow.*

> **2015-06-24 Predrag** I was careless. Looks much simpler than D_4. The gen-
> erator g of the vertical *cyclic symmetry group* $Z_{2n} = \{e, g, g^2, \cdots, g^{2n-1}\}$ of
> order $2n$ is a *glide reflection* [20]
>
> $$ g\, \mathbf{u}(x, y) = \begin{pmatrix} -u(-x, y + \pi/n) \\ v(-x, y + \pi/n) \end{pmatrix}, \tag{8.1} $$
>
> All $2n$ irreps are 1-dimensional, with characters $\chi(g^k) = \omega^k, \omega = \exp(\pi/n)$.
> For $n = 4$ the 8 irreps Frobenius character projection operators (8.22) are
> the discrete Fourier transforms
>
> $$
> \begin{aligned}
> \mathbf{e}_1 &= \frac{c_1}{8}(1 + \omega^{-1}g + \omega^{-2}g^2 + \cdots + \omega^1 g^{2n-1})\, \mathbf{u}_{\text{EQ}} \\
> \mathbf{e}_2 &= \frac{c_2}{8}(1 + \omega^{-2}g^2 + \omega^{-4}g^4 + \cdots + \omega^2 g^{2n-2})\, \mathbf{u}_{\text{EQ}} \\
> \mathbf{e}_3 &= \frac{c_1}{8}(1 + \omega^{-3}g^3 + \omega^{-6}g^6 + \cdots)\, \mathbf{u}_{\text{EQ}} \\
> \mathbf{e}_{2n-1} &= \frac{c_2}{8}(1 + \omega g^{2n-1} + \cdots)\, \mathbf{u}_{\text{EQ}},
> \end{aligned} \tag{8.2}
> $$
>
> The invariant subgroups are the cyclic groups $\{e\}$, $Z_2 = \{e, g^4\}$ (transla-
> tions by π), $Z_4 = \{e, g^2, g^4, g^6\}$ (translations by $\pi/2$), and Z_8.

Aside: Should also understand first the relation between a fundamental domain for Z_3 (3-disk in magnetic field) and these complex eigenvectors.

However, the rotation

$$R\,\mathbf{u} = [-u(-x, -y), -v(-x, -y)] \tag{8.3}$$

does not commute with vertical Z_{2n}, [1]

$$Rg\,\mathbf{u} = R[-u(-x, y+\pi/4), v(-x, y+\pi/4)] = [u(x, -y-\pi/4), -v(x, -y-\pi/4)]$$

$$gR\,\mathbf{u} = g[-u(-x, -y), -v(-x, -y)] = [u(x, -y+\pi/4), -v(x, -y+\pi/4)]\,,$$

so the full order 16 group is more complicated than $Z_8 \times Z_2$ (for possible groups click here). Instead, we have

$$g^{-1}R\,\mathbf{u} = g[-u(-x, -y), -v(-x, -y)] = [u(x, -y-\pi/4), -v(x, -y-\pi/4)]\,,$$

so the generator algebra is of D_8:

$$R^2 = e\,, \quad g^8 = e\,, \quad Rg = g^{-1}R\,. \tag{8.4}$$

A presentation of D_n is

$$\langle g, R \mid g^n = R^2 = e, Rg = g^{-1}R \rangle \tag{8.5}$$

Dihedral group D_8.   The D_8 group

$$D_8 = \{e, g, g^2, g^3, \cdots, g^7, R, Rg^2, Rg^3, \cdots, Rg^7\}$$

has a 8 shift elements and 8 shift-reflect elements. There are 7 classes: $\{e\}$, $\{g^4\}$, $\{g^2, g^6\}$, $\{R, Rg^4\}$ and $\{Rg^2, Rg3/4\}$. There are four different one-dimensional irreducible representations, whose characters are ± 1 under reflection R and shift-reflect operation Rg. There are three 2-dimensional representations E_j. It has 3 subgroups: Z_4, D_2 and Z_2. Life can be made easier by defining the quarter-shift as $g = g$, with $R^2 = e$, $g^8 = e$, and $Rg = g^{-1}R$. The character table is given in table 8.1. [2]

2015-06-24 Mohammad Lets define

$$(\tau\mathbf{u})(x_1, x_2) = \begin{pmatrix} u_1(x_1, x_2 + \pi/2) \\ u_2(x_1, x_2 + \pi/2) \end{pmatrix}, \tag{8.6}$$

and

$$(\sigma\mathbf{u})(x_1, x_2) = \begin{pmatrix} -u_1(-x_1, x_2 + \pi/4) \\ u_2(-x_1, x_2 + \pi/4) \end{pmatrix}. \tag{8.7}$$

---

[1]Predrag 2015-06-24: please recheck

[2]Predrag 2015-06-25,2019-03-29: Table 8.1 not completed yet; needs 2 more E irreps to get the sum of $(\dim)^2$ to 16. I started with Xiong's thesis D_n, not yet cross-checked with tables on the web.

D_8	A_1	A_2	B_1	B_2	E_1	E_2	E_3
$\{e\}$	1	1	1	1	2	2	2
$\{g^2\}$	1	1	1	1	-2		
$\{g, g^{-1}\}$	1	1	-1	-1	0		
$\{R, Rg^2\}$	1	-1	1	-1	0		
$\{Rg, Rg^{-1}\}$	1	-1	-1	1	0		
$\{g^2, g^{-2}\}$	?	?	-?	-?	?		
$\{g^3, g^{-3}\}$	?	?	-?	-?	?		

Table 8.1: Character table of dihedral group D_8.

Then all elements of the glide reflection symmetry can be written as

$$D_4 = \{e, \tau^{1/4}, \tau^{1/2}, \tau^{3/4}, \sigma, \sigma\tau^{1/4}, \sigma\tau^{1/2}, \sigma\tau^{3/4}\}.$$

However,

$$\sigma\tau \neq \tau^{-1}\sigma, \quad \sigma^2 \neq e.$$

Instead we have

$$\sigma\tau = \tau\sigma, \quad \sigma^2 = \tau.$$

Do formulas (8.23) still work?

2015-07-07 Now need sum over 16 elements, otherwise the same.

2015-06-21 Predrag Reading Platt, Sirovich, and Fitzmaurice [20]:

For Kolmogorov flow they credit V. I. Arnold and L. D. Meshalkin, Usp. Mat. Nauk 15, 247 (1960), an article that I have not had a look at.

Stability was studied in the above article, as well as by Green [9]. Green studies various stable solutions, and does not cite Kolmogorov.

A stationary cellular pattern that appears beyond the first bifurcation was discussed G. I. Sivashinsky, Physica D 17, 243 (1985).

G. I. Sivashinsky and V. Yakhot, Phys. Fluids 28, 1040 (1985); V. Yakhot and G. I. Sivashinsky, Phys. Rev. A 35, 815 (1987) interpret long-wavelength instabilities as 'negative viscosity'.

One needs to also look at N. F. Bondarenko,. M. Z. Gak, and F. V. Dolzhansky, Atmos. Ocean. Phys. 15, 711 (1979).

This system has equilibrium solution

$$u(x,y) = \frac{Re}{n^2} \sin(ny), \quad v(x,y) = 0, \tag{8.8}$$

A Reynolds number *Re* for the flow may be naturally based on the maximum speed of this solution, and the forcing length scale. This equilibrium goes unstable at $Re = n\sqrt{2}$. Sufficiently high wavenumber eigenvectors are always stable. They define doubly-periodic rectangular domain

$$(x,y) \in [0, 2\pi] \times [0, 2\pi]$$

They use a spectral basis that is automatically divergence free, and compute for the $n = 4$ case. All runs are initiated as random perturbations off the ustable equilibrium (8.8). 5000 + time units were integrated before before any data were recorded. [16×16] spatial grid gave rise to under-resolved flows that were drastically different in nature, so their computations are for [32×32] (i.e., 1024 ordinary differential equations). This was found adequate for the parameter range $\Omega/\Omega_c < 12.5$.

A stable relative equilibrium bifurcates of an equilibrium up at $\Omega/\Omega_c = 2.2$, with phase velocity starting with 0.

For $1.97 < \Omega/\Omega_c < 2.2$ one is in regime where stable equilibrium with horizontal Z_2 (or D_2 or some other symmetry?) rules. This symmetry is also noted by Green [9]. Apparently all stable equilibria up to and including this one are invariant under the full 16-element discrete symmetries.

They find it remarkable that narrow stability windows in Ω/Ω_c appear interspersed between chaotic episodes. Looks sensible to me.

Of all the chaotic states they observed, fig. 14 is the only state that they dare chaotic both spatially and temporally and hence turbulent, according to common convention.

Their Kaplan-Yorke ('Lyapunov') dimension is accurate to the first digit only. By the time they get to $\Omega/\Omega_c = 12.5$ it is about 11.

Poincaré sections were computed following Keefe [14]. They realize that the Poincaré section planes should be invariant under the symmetry (both discrete and continuous). They find it a good practice to choose as a section a plane for which the flow projections maximize the energy with respect to the L2 norm.

Their *discussion of symmetries* is clear and succinct. Will have to use all of it. The generator of the vertical cyclic symmetry group of order $2n$ is a *glide reflection* (here eq. (13)). In eqs. (31), (32) they give explicit action of symmetries on the Fourier basis.

Rotation through π in is another group generator, i.e., if **u** is a Kolmogorov flow then

$$R\mathbf{u} \to [-u(-x, -y), -v(-x, -y)]$$

is one also. In all there are $4n$ discrete symmetries group elements.

The remaining symmetry group is the continuous group of translations in the x direction.

2015-06-24 Predrag Even though Sirovich [22] cites Birkhoff and MacLane [2] for *glide reflection*, I did not find it in that book. However, glide reflection is standard, described many places. Perhaps these would be good references, if a citation is needed (I have not looked at them):

H.S.M. Coxeter. Introduction to Geometry. John Wiley and Sons, Inc. 1969.
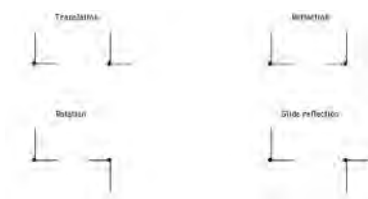
Figure 8.1: The four isometries in the plane.
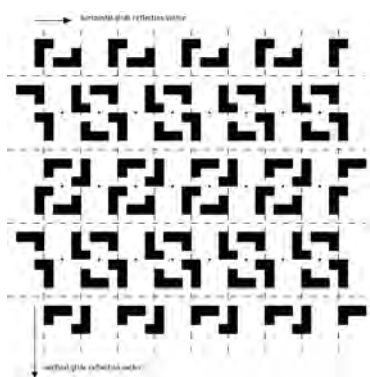
Figure 8.2: A wallpaper pattern of pgg type, invariant under glide reflections (represented by dotted lines) in two perpendicular directions.

Heinrich W. Guggenheimer. Plane Geometry and its Groups. Holden-Day. 1967.

Killingbeck [15] might be a potentially useful reference (maybe too chemical?)

There are four isometries in the plane: translation, rotation, reflection, and glide reflection, see figure 8.1. A *reflection* flips points over an invariant axis or line. A *glide reflection* combines a reflection with a translation along the direction of the mirror line.

Glide reflections commute with each other, which is not generally the case for any two given isometries. Given two congruent sets on the plane, it is in general either a rotation or a glide reflection – depending on the orientation between them – that maps one to the other. Reflections and non-trivial glide reflections are mutually exclusive.

The isometry group of a polygon may only consist of rotations and reflections. In fact only 2 types of such groups are possible, the cyclic groups Z_n and the dihedral groups D_n (Leonardo (da Vinci)'s Theorem). Translations and glide reflections may leave an infinite set invariant (and presumably a finite set defined on a periodic domain), see for example figure 8.2, taken from notes by George Baloglou.

The lattice unit is always a *generating region*, but a generating region (fundamental domains) may be smaller than the lattice units.

2015-06-21 Predrag In ref. [22], Sirovich discusses how to incorporate symmetries of flows in computation of a correlation matrix from data, for

- Plane Poiseuille (channel) flow
- Poiseuille flow in a rectangular channel
- Bénard problem (convection).
- Flow past bodies of revolution
- Flow in a circular pipe
- Plane Couette flow
- Taylor-Couette flow
- Flow past a circular cylinder

However, he does not mention Kolmogorov flow.

V. I. Arnold [1]

Chandler, Lucas & Kerswell [4, 16, 17]

R. Mitchell [19] PhD thesis (in `ChaosBook.org/library`), *Transition to turbulence and mixing in a quasi-two-dimensional Lorentz force-driven Kolmogorov flow*.

2012-11-07 Predrag In systems with continuous symmetries there are important classes of invariant solutions referred to as 'relative' or 'equivariant' [13, 21].

8.2 Symmetries and isotropy subgroups

On an infinite domain and in the absence of boundary conditions, the Navier-Stokes equations are equivariant under any $2D$ translation, $2D$ rotation, and $\mathbf{x} \to -\mathbf{x}$, $\mathbf{u} \to -\mathbf{u}$ inversion through the origin [5]. In $2D$ the inversion is the same as rotation by π. In Kolmogorov flow, the parallel side walls restrict the rotation symmetry to rotation by π about the z-axis. We denote this rotation by σ_x and the inversion through the origin by σ_{xy}. The suffixes indicate which of the homogeneous directions x, z change sign and simplify the notation for the group algebra of rotation, inversion, and translations presented in sects. 8.2.1 and 8.2.2. The σ_{xy} and σ_x symmetries generate a discrete dihedral group $D_1 \times D_1 = \{e, \sigma_x, \sigma_z, \sigma_{xy}\}$ of order 4, where

$$\begin{aligned}
\sigma_x \, [u, v](x, y) &= [-u, -v, w](-x, -y, z) \\
\sigma_y \, [u, v](x, y) &= [u, v, -w](x, y, -z) \\
\sigma_{xy} \, [u, v](x, y) &= [-u, -v](-x, -y) \, .
\end{aligned} \tag{8.9}$$

The walls also restrict the translation symmetry to $1D$ streamwise translations. With periodic boundary condition, these translations become the $SO(2)$ continuous one-parameter group of streamwise translations

$$\tau(d)[u,v](x,y) = [u,v](x+d,y)\,. \tag{8.10}$$

The equations of Kolmogorov flow are thus equivariant under the group $\Gamma = O(2) \times D_4 = D_{1,x} \ltimes SO(2) \times D_4$, where $\ltimes$ stands for a semi-direct product, and sign changes in x, and y subscripts indicate spanwise translations and sign changes in y.

The solutions of an equivariant system can satisfy all of the system's symmetries, a proper subgroup of them, or have no symmetry at all. For a given solution $\mathbf{u}$, the subgroup that contains all symmetries that fix $\mathbf{u}$ (that satisfy $s\mathbf{u} = \mathbf{u}$) is called the isotropy (or stabilizer) subgroup of $\mathbf{u}$. [7, 8, 12, 18]. For example, a typical turbulent trajectory $\mathbf{u}(\mathbf{x},t)$ has no symmetry beyond the identity, so its isotropy group is $\{e\}$. At the other extreme is the laminar equilibrium, whose isotropy group is the full Kolmogorov symmetry group Γ.

In between, the isotropy subgroup of most of the equilibria reported here is $S = \{e, s_1, s_2, s_3\}$, where

$$
\begin{aligned}
s_1\,[u,v](x,y) &= [u,v,-w](x+L_x/2, y, -z) \\
s_2\,[u,v](x,y) &= [-u,-v,w](-x+L_x/2, -y, z+L_y/2) \\
s_3\,[u,v](x,y) &= [-u,-v,-w](-x,-y,-z+L_y/2)\,.
\end{aligned}
\tag{8.11}
$$

Flow-invariant subgroups might play an important role in the turbulent dynamics. In this section we provide a partial classification of the isotropy groups of Γ, sufficient to classify all currently known invariant solutions and to guide the search for new solutions with other symmetries.

8.2.1 Flips and half-shifts

A few observations will be useful in what follows. First, we note the key role played by the rotation and reflection symmetries σ_x and σ_y (8.9) in the classification of solutions and their isotropy groups. The equivariance of Kolmogorov flow under continuous translations allows for relative equilibria solutions, i.e., solutions that are steady in a frame moving with a constant velocity in (x). In state space, relative equilibria either trace out circles or wind around tori, and these sets are both continuous-translation and time invariant. The sign changes under σ_x and σ_y, however, imply particular centers of symmetry in x and y, and thus fix the translational phase of fields that are fixed by these symmetries. Thus the presence of σ_x or σ_y in an isotropy group prohibits relative equilibria in x or z, and the presence of σ_{xy} prohibits any form of relative equilibrium. Guided by this observation, we will seek equilibria only for isotropy subgroups that contain the σ_{xy} inversion symmetry.

Second, the periodic boundary conditions impose discrete translation symmetries of $\tau(L_x, 0)$ and $\tau(0, L_y)$ on velocity fields. In addition to this full-period

translation symmetry, a solution can also be fixed under a rational translation, such as $\tau(mL_x/n, 0)$ or a continuous translation $\tau(\ell)$. If a field is fixed under continuous translation, it is constant along the given spatial variable. If it is fixed under rational translation $\tau(mL_x/n, 0)$, it is fixed under $\tau(mL_x/n, 0)$ for $m \in [1, n-1]$ as well, provided that m and n are relatively prime. For this reason the subgroups of the continuous translation SO(2) consist of the discrete cyclic groups Z_n for $n = 2, 3, 4, \ldots$ together with the trivial subgroup $\{e\}$ and the full group SO(2) itself. For rational shifts $\ell_x/L_x = m/n$ we simplify the notation a bit by rewriting (8.10) as

$$\tau_x^{m/n} = \tau(mL_x/n, 0) . \tag{8.12}$$

Since $m/n = 1/2$ will loom large in what follows, we omit exponents of $1/2$:

$$\tau_x = \tau_x^{1/2} , \ \tau_z = \tau_z^{1/2} , \ \tau_{xz} = \tau_x\tau_z . \tag{8.13}$$

If a field $\mathbf{u}$ is fixed under a rational shift $\tau(L_x/n)$, it is periodic on the smaller spatial domain $x \in [0, L_x/n]$. For this reason we can exclude from our searches all equilibrium whose isotropy subgroups contain rational translations in favor of equilibria computed on smaller domains. However, as we need to study bifurcations into states with wavelengths longer than the initial state, the linear stability computations need to be carried out in the full $[L_x, 2]$ cell. For example, if EQ is an equilibrium solution in the $\Omega_{1/3} = [L_x/3, 2]$ cell, we refer to the same solution repeated thrice in $\Omega = [L_x, 2]$ as "streamwise-tripled" or $3 \times$ EQ. Such solution is by construction fixed under the $Z_3 = \{e, \tau_x^{1/3}, \tau_x^{2/3}\}$ subgroup.

Third, some isotropy groups are conjugate to each other under symmetries of the full group Γ. Subgroup H' is conjugate to H if there is an $s \in \Gamma$ for which $H' = s^{-1}Hs$. In spatial terms, two conjugate isotropy groups are equivalent to each other under a coordinate transformation. A set of conjugate isotropy groups forms a conjugacy class. It is necessary to consider only a single representative of each conjugacy class; solutions belonging to conjugate isotropy groups can be generated by applying the symmetry operation of the conjugacy.

In the present case conjugacies under spatial translation symmetries are particularly important. Note that O(2) is not an abelian group, since reflections σ and translations τ along the same axis do not commute [11]. Instead we have $\sigma\tau = \tau^{-1}\sigma$. Rewriting this relation as $\sigma\tau^2 = \tau^{-1}\sigma\tau$, we note that

$$\sigma_x\tau_x(\ell_x, 0) \quad = \quad \tau^{-1}(\ell_x/2, 0) \, \sigma_x \, \tau(\ell_x/2, 0) . \tag{8.14}$$

The right-hand side of (8.14) is a similarity transformation that translates the origin of coordinate system. For $d_x = L_x/2$ we have

$$\tau_x^{-1/4} \, \sigma_x \, \tau_x^{1/4} = \sigma_x\tau_x , \tag{8.15}$$

and similarly for the spanwise shifts / reflections. Thus for each isotropy group containing the shift-reflect $\sigma_x\tau_x$ symmetry, there is a simpler conjugate isotropy group in which $\sigma_x\tau_x$ is replaced by σ_x (and similarly for $\sigma_y\tau_y$ and σ_y).

We choose as the representative of each conjugacy class the simplest isotropy group, in which all such reductions have been made. However, if an isotropy group contains both σ_x and $\sigma_x\tau_x$, it cannot be simplified this way, since the conjugacy simply interchanges the elements.

Fourth, for $d_x = L_x$, we have $\tau_x^{-1}\,\sigma_x\,\tau_x = \sigma_x$, so that, in the special case of half-cell shifts, σ_x and τ_x commute. For the same reason, σ_y and τ_y commute, so the order-16 isotropy subgroup

$$G = D_{1,x} \times \mathbf{Z}_2 \times D_{1,z} \times C_{2,z} \subset \Gamma \tag{8.16}$$

is abelian.

8.2.2 The 67-fold path

We now undertake a partial classification of the lattice of isotropy subgroups of Kolmogorov flow. We focus on isotropy groups involving at most half-cell shifts, with $\mathrm{SO}(2) \times \mathrm{D}_4$ translations restricted to order 4 subgroup of spanwise-streamwise translations (8.13) of half the cell length,

$$T = \mathbf{Z}_2 \times C_{2,z} = \{e, \tau_x, \tau_z, \tau_{xz}\}\,. \tag{8.17}$$

All such isotropy subgroups of Γ are contained in the subgroup G (8.16). Within G, we look for the simplest representative of each conjugacy class, as described above.

Let us first enumerate all subgroups $H \subset G$. The subgroups can be of order $|H| = \{1, 2, 4, 8, 16\}$. A subgroup is generated by multiplication of a set of generator elements, with the choice of generator elements unique up to a permutation of subgroup elements. A subgroup of order $|H| = 2$ has only one generator, since every group element is its own inverse. There are 15 non-identity elements in G to choose from, so there are 15 subgroups of order 2. Subgroups of order 4 are generated by multiplication of two group elements. There are 15 choices for the first and 14 choices for the second. However, each order-4 subgroup can be generated by $3 \cdot 2$ different choices of generators. For example, any two of $\tau_x, \tau_y, \tau_{xz}$ in any order generate the same group T. Thus there are $(15 \cdot 14)/(3 \cdot 2) = 35$ subgroups of order 4.

Subgroups of order 8 have three generators. There are 15 choices for the first generator, 14 for the second, and 12 for the third. There are 12 choices for the third generator and not 13, since if it were chosen to be the product of the first two generators, we would get a subgroup of order 4. Each order-8 subgroup can be generated by $7 \cdot 6 \cdot 4$ different choices of three generators, so there are $(15 \cdot 14 \cdot 12)/(7 \cdot 6 \cdot 4) = 15$ subgroups of order 8. In summary: there is the group G itself, of order 16, 15 subgroups of order 8, 35 of order 4, 15 of order 2, and 1 (the identity) of order 1, or 67 subgroups in all [10]. This is whole lot of isotropy subgroups to juggle; fortunately, the observations of sect. 8.2.1 show that there are only 5 *distinct conjugacy classes* in which we can expect to find equilibria.

The 15 order-2 groups fall into 8 distinct conjugacy classes, under conjugacies between $\sigma_x\tau_x$ and σ_x and $\sigma_y\tau_y$ and σ_y. These conjugacy classes are represented by the 8 isotropy groups generated individually by the 8 generators σ_x, σ_y, σ_{xy}, $\sigma_x\tau_y$, $\sigma_y\tau_x$, τ_x, τ_y, and τ_{xz}. Of these, the latter three imply periodicity on smaller domains. Of the remaining five, σ_x and $\sigma_x\tau_y$ allow relative equilibria in z, σ_y and $\sigma_y\tau_x$ allow relative equilibria in x. Only a single conjugacy class, represented by the isotropy group

$$\{e, \sigma_{xy}\}, \tag{8.18}$$

breaks both continuous translation symmetries. Thus, of all order-2 isotropy groups, we expect only this group to have equilibria.

Of the 35 subgroups of order 4, we need to identify those that contain σ_{xy} and thus support equilibria. We choose as the simplest representative of each conjugacy class the isotropy group in which σ_{xy} appears in isolation. Four isotropy subgroups of order 4 are generated by picking σ_{xy} as the first generator, and σ_z, $\sigma_z\tau_x$, $\sigma_z\tau_z$, or $\sigma_z\tau_{xz}$ as the second generator (R for reflect-rotate):

$$
\begin{aligned}
R &= \{e, \sigma_x, \sigma_y, \sigma_{xy}\} & = \{e, \sigma_{xy}\} \times \{e, \sigma_z\} \\
R_x &= \{e, \sigma_x\tau_x, \sigma_y\tau_x, \sigma_{xy}\} & = \{e, \sigma_{xy}\} \times \{e, \sigma_x\tau_x\} \\
R_y &= \{e, \sigma_x\tau_z, \sigma_y\tau_z, \sigma_{xy}\} & = \{e, \sigma_{xy}\} \times \{e, \sigma_z\tau_z\} \\
R_{xz} &= \{e, \sigma_x\tau_{xz}, \sigma_y\tau_{xz}, \sigma_{xy}\} = \{e, \sigma_{xy}\} \times \{e, \sigma_z\tau_{xz}\} \simeq S\,.
\end{aligned}
\tag{8.19}
$$

These are the only isotropy groups of order 4 containing σ_{xy} and no isolated translation elements. Together with $\{e, \sigma_{xy}\}$, these 5 isotropy subgroups represent the 5 conjugacy classes in which expect to find equilibria.

8.3 State-space visualization

Ref. [6] presents a method for visualizing low-dimensional projections of trajectories in the infinite-dimensional state space of the Navier-Stokes equations. Briefly, we construct an orthonormal basis $\{\mathbf{e}_1, \mathbf{e}_2, \cdots, \mathbf{e}_n\}$ that spans a set of physically important fluid states $\mathbf{u}_A$, $\mathbf{u}_B$, ..., such as equilibrium states and their eigenvectors, and we project the evolving fluid state $\mathbf{u}(t)$ onto this basis using the L^2 inner product (**??**). This produces a low-dimensional projection

$$a(t) = (a_1, a_2, \cdots, a_n, \cdots)(t)\,, \qquad a_n(t) = (\mathbf{u}(t), \mathbf{e}_n)\,, \tag{8.20}$$

which can be viewed in $2d$ planes $\{\mathbf{e}_m, \mathbf{e}_n\}$ or in $3d$ perspective views $\{\mathbf{e}_\ell, \mathbf{e}_m, \mathbf{e}_n\}$. The state-space portraits are *dynamically intrinsic*, since the projections are defined in terms of intrinsic solutions of the equations of motion, and *representation independent*. Such bases are effective because moderate-*Re* turbulence explores a small repertoire of unstable coherent structures, so that the trajectory $a(t)$ does not stray far from the subspace spanned by the key structures.

There is no *a priori* prescription for picking a 'good' set of basis fluid states, and construction of $\{\mathbf{e}_n\}$ set requires some experimentation. As shown in

ref. [6], the dynamics of different regions of state space can be elucidated by projections onto basis sets constructed from combinations of equilibria and their eigenvectors.

A group element $g \in G$ acts on a function $\rho(a)$ defined on state space $\mathcal{M}$ by its *operator representation*

$$U(g)\,\rho(a) = \rho(D(g)^{-1}a)\,. \tag{8.21}$$

This is the conventional, Wigner definition of the effect of transformations.

The Frobenius 'character orthogonality' theory of irreps (irreducible representations) of finite groups says that all invariant subspaces are obtained by weighted averages ('projections')

$$\rho^{(\mu)}(a) = \frac{d_\mu}{|G|}\sum_g \chi^{(\mu)}(g)\,U(g)\,\rho(a) = \frac{d_\mu}{|G|}\sum_g \chi^{(\mu)}(g)\,\rho(D(g^{-1})a) \tag{8.22}$$

The simplest example is afforded by the 1-dimensional subspace (irrep) given by the fully symmetrized average of components of the regular basis function $\rho^{reg}(a)$

$$\rho^{(A_1)}(a) = \frac{1}{|G|}\sum_g^G \rho(D(g)\,a)\,.$$

By construction, $\rho^{(A_1)}$ is invariant under all actions of the group, $U(g)\,\rho^{(A_1)}(a) = \rho^{(A_1)}(a)$. This $\rho^{(A_1)}(a)$ invariant subspace is a special case of (8.22), with all $\chi^{(A_1)}(g) = 1$. In other words, for every g this is an eigenvector of the regular representation $D^{reg}(g)$ with eigenvalue 1.

By now the group acts in many different ways, so let us recapitulate:

g	abstract group element, multiplies other elements
$D(g)$	$[d\times d]$ state space transformation matrix, multiplies $a \in \mathcal{M}$
$U(g)$	operator, acts on functions $\rho(a)$ defined over state space $\mathcal{M}$
$D^{(\mu)}(g)$	$[d_\mu\times d_\mu]$ irrep, acts on invariant subspace $\rho^{(\mu)}(\hat{a})$

Note that the state space transformation $D(g) \neq D(e)$ can leave sets of '*boundary*' points invariant (or 'invariant points'); for example, under reflection σ across a symmetry plane, the plane itself remains invariant.

Dihedral group D$_4$. The D$_4$ group

$$\mathrm{D}_4 = \{e, \tau^{1/4}, \tau^{1/2}, \tau^{3/4}, \sigma, \sigma\tau^{1/4}, \sigma\tau^{1/2}, \sigma\tau^{3/4}\}$$

has a 4 shift elements and 4 shift-reflect elementS. There are 5 classes: $\{e\}$, $\{\tau^{1/2}\}$, $\{\tau^{1/4}, \tau^{3/4}\}$, $\{\sigma, \sigma\tau^{1/2}\}$ and $\{\sigma\tau^{1/4}, \sigma\tau^{3/4}\}$. There are four different one-dimensional irreducible representations, whose characters are ± 1 under reflection σ and shift-reflect operation $\sigma\tau^{1/4}$. There is one 2-dimensional representation e. It has 3 subgroups: Z_4, D_2 and Z_2. Life can be made easier by

D_4	A_1	A_2	B_1	B_2	E
$\{e\}$	1	1	1	1	2
$\{\tau^2\}$	1	1	1	1	-2
$\{\tau, \tau^{-1}\}$	1	1	-1	-1	0
$\{\sigma, \sigma\tau^2\}$	1	-1	1	-1	0
$\{\sigma\tau, \sigma\tau^{-1}\}$	1	-1	-1	1	0

Table 8.2: Character table of dihedral group D_4.

defining the quarter-shift as $\tau = \tau^{1/4}$, with $\sigma^2 = e$, $\tau^4 = e$, and $\sigma\tau = \tau^{-1}\sigma$. The character table is given in table 8.2. [3]

In this paper we present global views of all invariant solutions in terms of the orthonormal 'translational basis' constructed in ref. [6] from the eight translated or translated/reflected copies of any state, for example $\mathbf{u}_{\mathrm{EQ}}$, projected using the Frobenius character projection operators (8.22) on the 4 one-dimensional representations: [4]

$$
\begin{aligned}
\mathbf{e}_{A_1} &= \frac{c_{A_1}}{8}(1 + \tau + \tau^2 + \tau^{-1} + \sigma + \sigma\tau + \sigma\tau^2 + \sigma\tau^{-1})\,\mathbf{u}_{\mathrm{EQ}} \\
\mathbf{e}_{A_2} &= \frac{c_{A_2}}{8}(1 + \tau + \tau^2 + \tau^{-1} - \sigma - \sigma\tau - \sigma\tau^2 - \sigma\tau^{-1})\,\mathbf{u}_{\mathrm{EQ}} \qquad (8.23) \\
\mathbf{e}_{B_1} &= \frac{c_{B_1}}{8}(1 - \tau + \tau^2 - \tau^{-1} + \sigma - \sigma\tau + \sigma\tau^2 - \sigma\tau^{-1})\,\mathbf{u}_{\mathrm{EQ}} \\
\mathbf{e}_{B_2} &= \frac{c_{B_2}}{8}(1 - \tau + \tau^2 - \tau^{-1} + \sigma + \sigma\tau - \sigma\tau^2 + \sigma\tau^{-1})\,\mathbf{u}_{\mathrm{EQ}}\,,
\end{aligned}
$$

where c_n is a normalization constant determined by $\|\mathbf{e}_n\| = 1$, and a group element is a shorthand for (8.21), action of the group on function $\mathbf{u}_{\mathrm{EQ}}$,

$$
g\,\mathbf{u}_{\mathrm{EQ}}(a) = U(g^{-1})\mathbf{u}_{\mathrm{EQ}}(a) = \mathbf{u}_{\mathrm{EQ}}(D(g)a)\,. \qquad (8.24)
$$

for example $\tau\,\mathbf{u}_{\mathrm{EQ}}(a) = \mathbf{u}_{\mathrm{EQ}}(D(\tau)a)$.

This is a low-dimensional projection intended for visualization. The dimensionality is lower than the full state space, so trajectories can appear to cross in such projections. We emphasize again that this is one of many possible projections that can be constructed from linear combinations of exact solutions, their spatial translations, and their stability eigenfunctions.

---

[3]Predrag 2015-06-21: I started with Xiong's thesis D_n, cross-checked with tables on the web. Hopefully correct. :

[4]Predrag 2015-06-20: I have not thought through yet how to use the two copies of the two-dimensional representation E, bringing the number of group-theoretically orthonormal coordinates to 8; no Gram-Schmidt orthogonalizations required. Presumably the fundamental domain is the 1/8-space, with all $\mathbf{e}_1 > 0$.
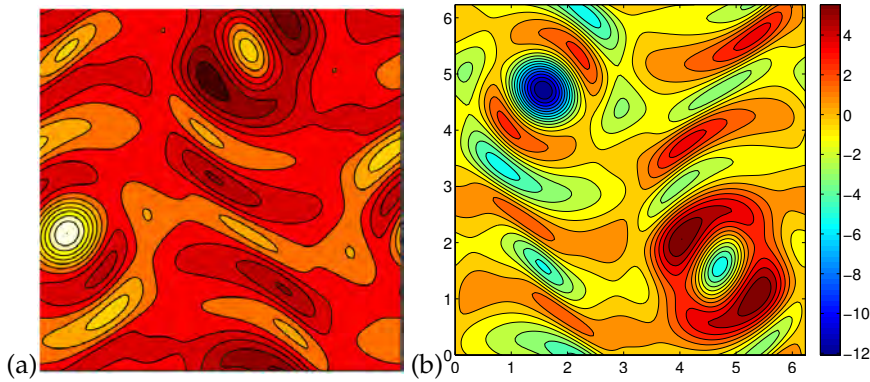
Figure 8.3: (a) Equilibrium E1 found by Chandler & Kerswell, JFM 722 (2013) (b) The same equilibrium found by adjoint equation integrated for 4×10^4 time units (takes approximately 3 minutes) plus 7 iterations of Newton-GMRES to decrease the L^2 error to 5×10^{-13}. Here, Re = 40. Note that panels (a) and (b) appear to be related by a shift-and-reflect symmetry.

8.4 Kolmogorov flow blog

2015-04-21 Mohammad The Kolmogorov flow

$$\partial_t \mathbf{u} = -\mathbf{u} \cdot \nabla \mathbf{u} - \nabla p + \frac{1}{\text{Re}} \Delta \mathbf{u} + \sin(4y)\mathbf{e}_1, \quad \nabla \cdot \mathbf{u} = 0, \qquad (8.25)$$

is solved with periodic boundary conditions in x and y on the domain $(x, y) \in [0, 2\pi] \times [0, 2\pi]$.

2015-06-20 Predrag The Kolmogorov flow domain $(x, y) \in [0, 2\pi] \times [0, 2\pi]$ in (8.25) really bugs me. The Rayleigh number controls the viscosity legth scale, as compared to the strip width. Experimentally one fixes the number n of spanwise strips, and can chose any streamwise length, so the domain should be a rectangle, such that for given n and Re if one doubles the streamwise length, on doubles the number of vortices, while keeping their shape intact. Forcing them into a square domain would squash the vortices. 3rd floor people must have thought all this through...

2015-06-19 Mohammad Define the projection operator

$$\mathcal{P}\mathbf{u} = \frac{1}{4n} \sum_{m=0}^{2n-1} \mathcal{S}^m \left[\mathbf{u} + \mathcal{R}\mathbf{u} \right], \qquad (8.26)$$

as the average over all discrete symmetries of the Kolmogorov flow in the slice. Let $I[\mathbf{u}]$ denote the energy input for the state $\mathbf{u}$. For Kolmogorov flow, the energy input $I[\mathbf{u}]$ is linear in $\mathbf{u}$. Due to its linearity and since the

energy input is conserved under any symmetry action, we have $I[\mathcal{P}\mathbf{u}] = I[\mathbf{u}]$. Therefore,

$$I[\mathbf{u} - \mathcal{P}\mathbf{u}] = 0,$$

that is all the contribution to the energy input comes solely from the projection $\mathcal{P}\mathbf{u}$!

2018-12-07 Predrag Blah blah.

8.4.1 Kolmogorov Flow doubly periodic formulation

The equations governing two dimensional Kolmogorov flow can be written in terms of velocity field $\mathbf{u}$(eliminated later) and vorticity ω in the following manner. For now I will just write the homogeneous equations, with forcing easily added afterwards

$$\omega_t - \hat{z} \cdot (\nabla \times (\mathbf{u} \times \omega \hat{z})) - \frac{1}{Re} \nabla^2 \omega = 0 \qquad (8.27)$$

The only difficult part of rewriting this equation in terms of $(2+1)$ spatiotemporal Fourier coefficients (assuming periodic boundary conditions) is the nonlinear term, not only due to the cross products but the necessity to express the velocity field in terms of the streamfunction, and consequently the vorticity field as $\mathbf{u} = \nabla \times (\nabla^{-2}\omega)$ which is possible due to the two dimensional approximation. The operator ∇^{-2} is the inverse of the Laplacian, which is technically singular; I asked around and the standard practice is to essentially define it in fourier space as $\frac{1}{|\mathbf{k}|^2}$, where $|\mathbf{k}|^2 = k_x^2 + k_y^2$. For numerical purposes its apparently common practice to say that the inverse of the $k_x = k_y = 0$ term equals 1. In other words, $1/0 = 1$. It's just a means of approximating the operator in spectral space.

Although [4] give nice formula that is almost entirely of Fourier coefficients, I find it more useful to completely eliminate the velocity field components $\mathbf{u} = (u, v)$ from the equation.

Therefore, the pseudospectral (homogeneous) spatiotemporal equation takes the form,

$$
\begin{aligned}
i\omega\Omega \quad &+ \quad ik_x \mathcal{F}[\mathcal{F}^{-1}(\frac{ik_y}{|\mathbf{k}|^2}\Omega) * \mathcal{F}^{-1}(\Omega)] \\
&- \quad ik_y \mathcal{F}[\mathcal{F}^{-1}(\frac{ik_x}{|\mathbf{k}|^2}\Omega) * \mathcal{F}^{-1}(\Omega)] \\
&- \quad \frac{|\mathbf{k}|^2}{Re}\Omega = G(\Omega, T, L_x, L_y) = 0 \qquad (8.28)
\end{aligned}
$$

Likewise, if allowed to write differentiation operators via D_t, D_x, D_y, etc, then the jacobian takes on the form in pseudospectral representation,

158

$$
\begin{aligned}
J \;=\;& D_t + D_x \mathcal{F}[diag(D_y \nabla^{-2}\omega)\mathcal{F}^{-1} + diag(\omega)D_y \nabla^{-2}\mathcal{F}^{-1}] \\
-\;& D_y \mathcal{F}[diag(D_x \nabla^{-2}\omega)\mathcal{F}^{-1} + diag(\omega)D_x \nabla^{-2}\mathcal{F}^{-1}] \\
-\;& \frac{\nabla^2}{Re}
\end{aligned}
\tag{8.29}
$$

By taking the complex conjugate and multiplying by the Feynman equation (16.101), the expression for the adjoint descent direction, $-J^\dagger G$.

$$
\begin{aligned}
-J^\dagger G \;=\;& [D_t + \mathcal{F}diag(D_y \nabla^{-2}\omega)\mathcal{F}^{-1}D_x \\
-\;& \mathcal{F}\nabla^{-2}D_y diag(\omega)\mathcal{F}^{-1}D_x \\
-\;& \mathcal{F}diag(D_x \nabla^{-2}\omega)\mathcal{F}^{-1}D_y \\
+\;& \mathcal{F}\nabla^{-2}D_x diag(\omega)\mathcal{F}^{-1}D_y \\
-\;& \frac{\nabla^2}{Re}] \cdot G
\end{aligned}
\tag{8.30}
$$

8.4.2 Kolmogorov Flow non periodic boundary conditions

Mike Schatz and I had a conversation today via Hangouts because he wanted to follow up on our presentation and discuss how this could possibly be relevant to his group. The main goal we discussed was to pursue a spatiotemporal numerical formulation for a experimentally comparable setting, namely Kolmogorov flow without doubly periodic boundary conditions and incorporating Rayleigh friction. I explained that the key difference would be to change to a Chebyshev polynomial basis due to the boundary conditions but work with the vorticity field as is common practice.

For starters, I'll describe the basic formulation for equilibria in a Chebyshev-Chebyshev basis. The key details is that to have accurate or viable numerics the spatial grid would have to be defined not on an equidistant, rectangular grid but rather defined at (this is a specific choice, but a common one) what are known as the Chebyshev-Gauss Lobatto quadrature nodes. In other words, any initial condition would either have to be either initialized in spectral space (very very preferable), or initialized on the discretized grid defined by the set of points in physical space,

$$
(x_m, y_n) = (\cos(\frac{\pi m}{M}), \cos(\frac{\pi n}{N})).
\tag{8.31}
$$

It is this discretization that allows us to use a (Chebyshev) polynomial basis in a collocation method, as an equally spaced grid would induce error from the Runge phenomenon (like the Gibbs phenomenon for Fourier

modes but for polynomial bases). One benefit (I believe?) is that the discretization has a higher resolution near the walls. Another benefit of this specific choice of quadrature nodes is that by definition they are the points at which the derivative of the Chebyshev polynomials are zero, i.e.$T'(x_m) = 0$. Other choices, such as the Chebyshev-Gauss nodes would instead provide the condition $T(x_m) = 0$.

With a two-dimensional spatial grid defined on the Chebyshev-Gauss-Lobatto nodes, we can use a discrete cosine transform to determine the spectral coefficients of the Chebyshev polynomial basis [3].

For a scalar vorticity field, $\omega(x_m, y_n)$, the corresponding Chebyshev modes are calculated with the following formula

$$\Omega_{jk} = \frac{2}{M * N} \frac{1}{\bar{c}_j \bar{c}_k} \sum_{n,m} \frac{\omega_{nm}}{\bar{c}_n \bar{c}_m} \cos(\frac{\pi m j}{M}) \cos(\frac{\pi n k}{N}) \qquad (8.32)$$

and the corresponding inverse transformation given by

$$\omega_{nm} \Omega_{jk} = \sum_{j,k} \Omega_{jk} \cos(\frac{\pi m j}{M}) \cos(\frac{\pi n k}{N}) \,. \qquad (8.33)$$

In this context there are no continuous translation symmetries, nor does the shit-reflect exist. The only remaining symmetry is in fact the rotational symmetry, defined by action on the vorticity field $R \cdot \omega(x, y) \to \omega(-x, -y)$.

Via the invariance condition,

$$\omega - R \cdot \omega = 0 \,, \qquad (8.34)$$

one can derive selection rules for the Chebyshev modes with spatial rotation symmetry. The rotation action is equivalent to the coordinate transformation $x \to -x, y \to y$. Via the Chebyshev-Gauss-Lobatto relation,

$$
\begin{aligned}
x_m &= \cos(\pi m/M) \\
-x_m &= -\cos(\pi m/M) \\
-x_m &= \cos(\pi)\cos(\pi m/M) \\
-x_m &= \cos(\pi m/M + \pi) \\
\cos^{-1}(x_m) &= \pi m/M + \pi
\end{aligned}
$$

$$(8.35)$$

which after substitution into the invariance condition (in terms of Chebyshev modes),

$$\sum_{j,k} \Omega_{jk} \cos(\frac{\pi m j}{M}) \cos(\frac{\pi n k}{N}) = \sum_{j,k} \Omega_{jk} \cos(\frac{\pi m j}{M} + j\pi) \cos(\frac{\pi n k}{N} + k\pi),$$

(8.36)

in turn implies the following,

$$\Omega_{jk} = (-1)^{j+k} \Omega_{jk} \text{for all} j, k.$$

(8.37)

Therefore the subset of modes $(\Omega_{jk} : j + k = \text{odd})$ are forced to be zero by discrete symmetry.

These selection rules hold only for solutions in the rotationally invariant subspace, naturally.

References

[1] V. I. Arnol'd, "Kolmogorov's hydrodynamic attractors", in *Vladimir I. Arnold - Collected Works*, Vol. 2, edited by A. Givental, B. Khesin, A. Varchenko, V. Vassiliev, and O. Viro (Springer, Berlin, 1991), pp. 429–432.

[2] G. Birkhoff and S. MacLane, *A Survey of Modern Algebra* (C. R. C. Press, 1963).

[3] C. Canuto, M. Y. Hussaini, A. Quateroni, and T. A. Zhang, *Spectral Methods: Fundamentals in Single Domains* (Springer, New York, 2006).

[4] G. J. Chandler and R. R. Kerswell, "Invariant recurrent solutions embedded in a turbulent two-dimensional Kolmogorov flow", J. Fluid Mech. **722**, 554–595 (2013).

[5] U. Frisch, *Turbulence* (Cambridge Univ. Press, Cambridge, 1996).

[6] J. F. Gibson, J. Halcrow, and P. Cvitanović, "Visualizing the geometry of state-space in plane Couette flow", J. Fluid Mech. **611**, 107–130 (2008).

[7] R. Gilmore and C. Letellier, *The Symmetry of Chaos* (Oxford Univ. Press, Oxford, 2007).

[8] M. Golubitsky and I. Stewart, *The Symmetry Perspective* (Birkhäuser, Boston, 2002).

[9] J. S. A. Green, "Two-dimensional turbulence near the viscous limit", J. Fluid M. **62**, 273–287 (1974).

[10] J. Halcrow, Geometry of Turbulence: An exploration of the State-space of Plane Couette Flow, PhD thesis (School of Physics, Georgia Inst. of Technology, Atlanta, 2008).

[11] W. G. Harter, *Principles of symmetry, dynamics, and spectroscopy* (Wiley, New York, 1993).

[12] R. Hoyle, *Pattern Formation: An Introduction to Methods* (Cambridge Univ. Press, Cambridge, 2006).

[13] C. Huygens, *L'Horloge à Pendule* (Swets & Zeitlinger, Amsterdam, 1673).

[14] L. R. Keefe, "Dynamics of perturbed wavetrain solutions to the Ginzburg-Landau equation", Stud. Appl. Math. **73**, 91–153 (1985).

[15] J. Killingbeck, "Group theory and topology in solid state physics", Rep. Prog. Phys. **33**, 533 (1970).

[16] D. Lucas and R. R. Kerswell, "Spatiotemporal dynamics in 2D Kolmogorov flow over large domains", J. Fluid Mech. **750**, 518–554 (2014).

[17] D. Lucas and R. R. Kerswell, "Recurrent flow analysis in spatiotemporally chaotic 2-dimensional Kolmogorov flow", Phys. Fluids **27**, 518–554 (2015).

[18] J. E. Marsden and T. S. Ratiu, *Introduction to Mechanics and Symmetry* (Springer, New York, 1999).

[19] R. Mitchell Jr., Transition to turbulence and mixing in a quasi-two-dimensional Lorentz force-driven Kolmogorov flow, PhD thesis (School of Physics, Georgia Inst. of Technology, Atlanta, 2013).

[20] N. Platt, L. Sirovich, and N. Fitzmaurice, "An investigation of chaotic Kolmogorov flows", Phys. Fluids A **3**, 681–696 (1991).

[21] H. Poincaré, "Sur les solutions périodiques et le principe de moindre action", C. R. Acad. Sci. Paris **123**, 915–918 (1896).

[22] L. Sirovich, "Turbulence and the dynamics of coherent structures. Part II: Symmetries and transformations", Q. Appl. Math. **45**, 573–582 (1987).

[23] W. R. Smith and J. G. Wissink, Asymptotic analysis of the attractors in two-dimensional kolmogorov flow, Eur. J. Appl. Math., to appear, 2017.

Chapter 11

Persistent homology

2018-07-05 Burak A possible method to systematically classifying the patterns could be the persistent homology. Matt, If you could generate a large spatiotemporal plot along and a corresponding peak-detected version, then I can take them to Herbert Edelsbrunner and ask for his advice on how to go about extracting a finite library of patterns.

2018-09-11 Matt [Persistent homology] Spent the morning searching through literature on persistent homology in conjunction with pattern detection, partial differential equations. I have about ten papers that I need to add them to the bib but I need to skim them to pick out the good ones first.

Set-up a meeting for tomorrow at 3:00 pm. with Brett Tregoning from the Schatz' group to discuss their ref. [1] *Analysis of Kolmogorov Flow and Rayleigh-Bénard Convection using Persistent Homology* and to get a general introduction on the subject.

2018-09-12 Matt Happy Birthday to me. Now back to work.

Konstantin Mischaikow Seminar on Persistent Homology Youtube The audio cuts in and out so be warned its annoying to listen to.

Talked to Brett Tregoning Went through the idea of persistent homology. He recommends (as do I) watching the videos to get an idea on persistent diagrams in the supplementary materials at [1]

PHAT I can't believe that I have to say this again but I spent an incredibly frustrating amount of time trying to install a different package to be able to run persistent homology code in Python, as opposed to writing my own code.
Little did I know that the developers have not updated the description of their package on their webpage since circa 2013, but it's a fools errand to attempt to install it on a Windows machine. It's

---

[1]Predrag 2018-09-25: "at" what? Ref. [1]?

almost comical because their installation instructions literally include only one command line, `pip install phat`. Only after five hours did I realize that they did not update the dependencies required for the Windows version, but perhaps I should have known what it meant for the "Python Bindings" to only work on linux and MacOS.

Maybe I'm stupid for not exclusively working in Linux land but the documentation for packages written without an installer is really terrible.

Going to attempt to install a different package named Perseus next, or just only run phat from Light terminal.

2018-09-14 Matt Persistent Homology Testing implementations on Linux running Ubuntu to see what persistent homology code will be easiest to implement. Out of Rachel Levanger's (tda-persistent-homology) package, Perseus (perseus) and the barebones PHAT package (PHAT) (the framework that Rachel Levanger's code is built upon.

I think the easiest is going to be Rachel Levanger's code because its setup to take a folder of greyscale images and create the corresponding persistence diagrams. Therefore it should be somewhat easy to reproduce figures for families of solutions and pass them to these Python functions. The downside for me is that my main machines are Windows based and this is only active on Linux, so I will have to see if there are any permission issues in regards to the installation process; I think I should be fine but I had to find work arounds for channelflow 2.0.

The other two might are not nearly as expedient but if something comes out of Rachel Levanger's codes then it might be worthwhile to learn the PHAT framework and write my own codes.

09-18-2018 Matt Persistent Homology Went through testing of Rachel Levanger's Python module. While I can get the persistent homology code to run it seems that in the documentation that periodic boundary conditions haven't been implemented yet; although this seemingly contradicts the data that I saw for two dimensional Kolmogorov flow in the supplemental materials for the ref. [1].

The whole idea is that it is supposed to be picking out topological information, specifically, for a scalar field $u(x,t)$ and its image under a homeomorphism $g \circ u(x,t)$ should have the same "Persistence Diagrams" but figure 11.1 shows otherwise. Attempting this with relative periodic invariant 2-torus solutions in the mean-velocity frame and full state space leads to two different persistence diagrams, thereby somehow encoding the quantitative difference of the doubly periodic nature in the mean velocity frame.

I am going to attempt to establish contact with the author of the code
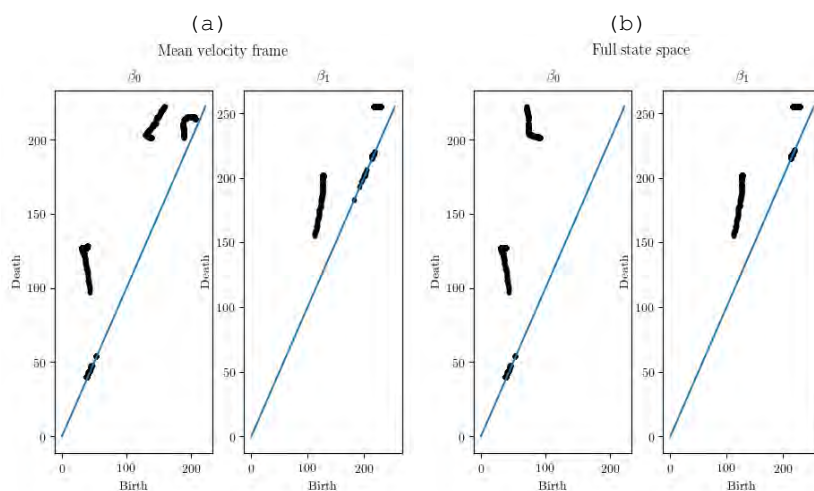
Figure 11.1: (a) Persistence diagrams for hook family in mean velocity frame (doubly-periodic representation) (b) Persistence diagrams for hook family of solutions in full state-space. Evidence that code doesn't support periodic boundary conditions or else these two plots would be the same.

to see if there is any way to adapt my images to be able to utilize the code properly.

Explanation of persistence diagrams The general concept regard persistence diagrams is fairly straightforward; its only the details of the algorithmic implementation when it gets tricky.

If we imagine a two dimensional scalar field $u(x, t)$ as a topographical height map, and then we imagine scanning through the landscape with a constant valued plane $f(\theta)$ (which is easiest to visualize as the "sea-level") that defines sublevel sets $\{u(x, t) : u(x, t) \leq f(\theta)\}$, then we can count the number of topologically distinct components, labeled by the nth *Betti number*, β_n. The first three Betti numbers can be described by the following: β_0 counts the number of connected components, β_1 counts the number of one-dimensional holes, and β_2 counts number of voids or "cavities" (not applicable with two dimensional scalar fields). In this case, these components are defined with respect to the sub-level sets or "sea-level". Connected regions above sea-level define [2]

To get an intuition for these quantities it is probably easiest to watch the supplementary videos (click here) for Schatz group's persistent homology paper [1].

What one sees in figure 11.1 are the compilation of persistence diagrams for the family of solutions of the Kuramoto-Sivashinsky equa-

---

[2]Predrag 2018-09-25: "define" what?

tion associated with the "hook" or "defect" pattern, in the (a) mean velocity frame and in the (b) full state space. Because these are continuous families of solutions, there should be continuity in the space of persistence diagrams.

The troubling evidence shown in figure 11.1 is that the data displayed is supposed to be invariant under homeomorphisms. I believe that this Python package is not taking the periodic boundary conditions into account and therefore cannot be fully utilized at this point.

Confirmed by Rachel Levanger, does not support periodic boundary conditions

2018-09-24 Matt Persistent Homology Schatz' group forgot to bring it up in their weekly meeting but they believe that Miroslav Kramár perhaps produced a persistent homology calculation with the doubly periodic 2-D Kolmogorov flow numerical data (as opposed to experimental data).

Michael Schatz made a comment about a small difference between persistent homology of two dimensional scalar fields with and without periodic boundary conditions. Coding-wise there are distinctions because one needs to make sure to not overcount the connected sub-level sets or else the persistence diagram will not be mathematically consistent between different images, i.e., the technique is useless if not written specifically to take periodic boundary conditions into consideration. I believe the point he was trying to make is that because we are working with a topological torus there is the emergence of a single birth-death event on the β_2 (Betti number equals two) diagram, which counts the number of "cavities" (think of isovorticity surfaces) of the torus. I believe for him that this is just a trivial piece of information due to the topology of tori; there is an "inside" to the two dimensional surface, therefore a β_2 birth-death event occurs.

I reached out to Dr. Kramár, asked him that he share his algorithms with me.

He replied and pointed me towards a library named GUDHI (it's almost like its saying "Hi Gudorf!" so maybe its a sign) that uses cubical complexes (fancy words to say that it tracks the level sets where scalar field $u(x,t) < \theta$) on a lattice to produce the persistence diagrams. I'm hoping to get this up and running soon.

2018-09-25 Matt All of the documentation is laid out so much better than some other libraries that I've recently dealt with and it seems that its a relatively widely used library, see (GUDHI code website).

While the only thing I need to do is "make install" and then test with "make test," the input file needs to be of a very specific format and the

output seems to be of a very specific format so it looks like I will be writing some python scripts to be able to use the library. First, I need to use the same algorithm (either custom or built-in) that takes a greyscale bitmap image and converts it to numbers $n \in [0, 255]$ to represent the invariant 2-torus in the correct way.

The input file must list the following, the first line lists the dimension $d = 2$ of the array to be input. Next the negative of the number of rows and columns **negative for periodic boundary conditions** $-N$ and $-M$ are listed on successive lines.

Lastly the bitmap data of the scalar field (in my case a matrix) is flattened into a vector, starting at the bottom left of the field.

So, for example, the following "data"

$$U = \begin{bmatrix} 7 & 8 & 9 \\ 4 & 5 & 6 \\ 1 & 2 & 3 \end{bmatrix} \tag{11.1}$$

would be represented by a text file written exactly as such,

2 (number of dimensions)
-3 (number of rows, periodic boundary conditions imply negative)
-3 (number of rows, periodic boundary conditions imply negative)
1
2
3
4
5
6
7
8
9

The output is a text file containing the lists of births and deaths of different Betti number components. I do not believe that this has plotting functionality so I'll take the output and run it through a python script that processes the data and plots the persistence diagrams of the invariant 2-torus. I kind of wished that [3] [4]

2018-09-25 Matt Including a figure of the persistence diagrams for the continuous family of solutions produced by numerical continuation of the hook tile in domain size. The heat map represents the energy of the solution; one can see that the coloring is not a nice continuous gradient therefore the family is not parameterized by energy, nor is it parameterized by T or L.

---

[3]Predrag 2018-09-26: 'wished that" what?
[4]Predrag 2018-09-26: Is figure 11.2 really tracking the hook family figure 16.25 (d-f)?
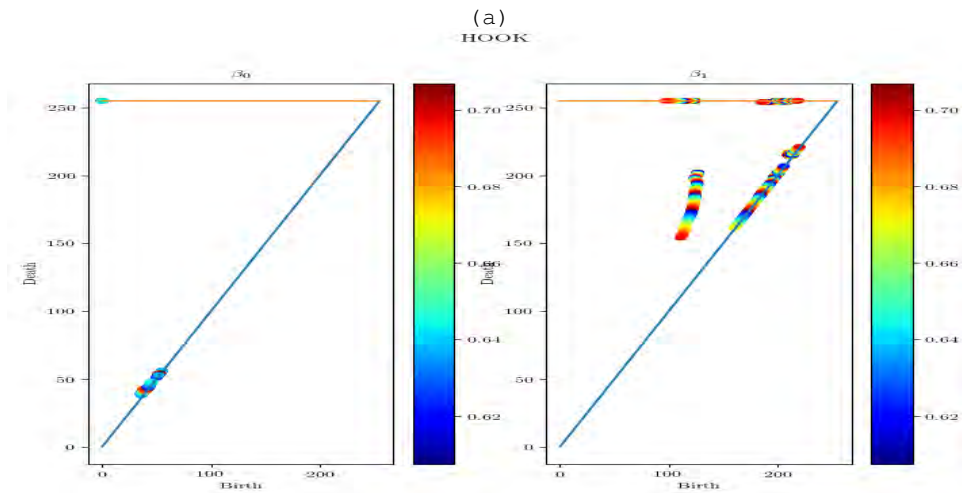
Figure 11.2: Persistence diagrams of the hook family of solutions figure 16.25 (d-f) for zeroth and first Betti numbers. The heat map represents energy; the same qualitative coloring is producing if you track the period of solutions or the spatial domain size. In other words the continuity of the persistence diagrams cannot be described by system parameters.

While I got the code running on light (it runs really quickly) I'm still learning the details, specifically about the use of *cubical complexes*, which I believe is just a way of approximating the infinitely dimensional scalar field after it has been discretized, i.e., think of the scalar field as a height map of rectangular prisms analogous to Riemann integration.

The horizontal lines of figure 11.2 represent "infinity," i.e., there are features that are born at a finite "time" (threshold value for level sets of cubes arranged in grid) and persist as the threshold passes the maximum of the function.

The Betti number zero point at infinity makes sense and can be explained. For mathematical consistency whenever two simply connected regions are merged the younger one dies; therefore the global minimum lives from the beginning until the end.

The Betti number one points along the infinity boundary make absolutely no sense to me and have convinced me that I'm missing a small detail in the calculation thats giving me errant data. What these points imply is that there are holes that persist past the maximum of the function, but at that point everything would be beneath the "sea level" leaving only one Betti number zero region (as previously described). Yet despite this I get lots of points at infinite for Betti number one persistence diagrams.

I believe that the code that produces correctly formatted text files is correct. What I believe I needed to do (and therefore implemented this)

is to first map the values of the scalar field $u(x, t)$ to the 8 bit integers $(z \in (0, 1, 2, \cdots, 255))$ as these numbers are sufficient (and necessary in certain formats) to represent a grayscale image.

The transformation that I apply is to add the absolute value of the minimum value of the scalar field across the scalar field such that the global minimum has a value of zero. Then, the scalar field is rescaled by dividing the values of the field by the sum of the old minimum plus old maximum, which after the first transformation is the new global maximum value. This leaves us with a scalar field valued between zero and one; multiplying by 255 and then casting the field from floats to integers leaves us with the correctly valued field.

The lexicographical ordering that is mentioned in my previous post is relatively straightforward, we just need a vector whose elements are ordered such that they represent the values of the field going from left to right $x = 0 \to L$ starting at the bottom $t = 0$ and ending at the top $t = T_p$. This is easily accomplished by rearranging the array with built in functions in Python (numpy, scipy).

I thought that perhaps the errors were occurring because I had to manually make the field periodic as opposed to the normal representation where the leftmost values $x = 0$ do not equal the right most values $x = L$ but the connect is assumed; this is generally how discrete Fourier transforms format the data. I tested this and the results made even less sense, so I'm going to attempt to see if I can get Brett Tregoning or Michael Schatz to join us next week (this week is likely too short notice).

2018-09-26 Predrag I do not think anyone of us can make sense of figure 11.2 without seeing the corresponding black-white diagram of the hook family figure 16.25 (d-f), in the spirit of video 1 (click here) from Schatz group's persistent homology paper [1].

Chose one constituent member of the family of solution to produce such an animation, located in `figs` titled `animated_PDhook0` which can be viewed via google chrome.

2018-09-27 Matt [Numerical Continuation] Still working on the visualization for persistent homology calculations, data management. The plan for tomorrow is likely to numerical continue some solutions and then try to compute persistence diagrams of the entire family and see if any useful information comes out.

2018-09-27 Matt [Persistent Homology] Spent a lot of time playing with persistent homology tools today.I went through a variety of tests to gain intuition on persistence diagrams and ensure I understand what they mean, and they are correct. I'm much more confident than I was before today about what is actually going on with persistence diagrams, especially the difference between components with different Betti numbers. I searched for good examples of what the different numbers actually mean but I
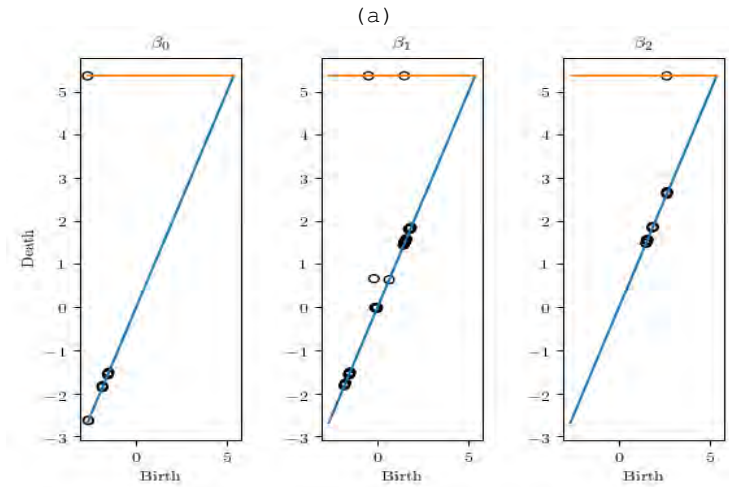
Figure 11.3: Persistence diagrams of the hook family of solutions for zeroth, first, and second Betti numbers $\beta_0, \beta_1, \beta_2$. The persistent homology calculation was performed by concatenating the family of solutions to form a scalar field in three dimensions.

found only the basic description of zero being simply connected regions, one meaning "one-dimensional holes", and two being cavities.

I didn't really have an intuition for what constitutes a one dimensional hole, but now I understand it is just a hole that you can draw a one dimensional curve around, much like how a cavity is a hole that is enclosed by a two dimensional surface. This explains the two points at infinity for tori, which are equivalent to the direct product of two circles. Its these two circles that give rise to the two infinitely persistent holes. The other, transient, holes on the persistence diagram correspond to the torus not being completely filled in during the thresholding process. An easy way to explain this is to think of the thresholding process applied to the scalar field as coloring in the surface of the torus. Now imagine this coloring process continues until almost all of the torus is filled in except a small patch of the surface. This small patch would lead to a point on the β_1 persistence diagram because you can draw a curve around it, and the point at which the point dies is when this patch gets filled in.

These comments might seem obvious after the fact but I feel like there aren't many people that attempt to explain it in an easy manner so I am going to do it for myself. Many of the tests were sanity checks like, can I input the scalar field information as real numbers?(yes). Does the data have to be periodic or is periodicity assumed(has to be periodic)? Why are there births on the β_1 diagram when it appears as though nothing is happening? (It turns out that merely sharing a vertex is sufficient to be

connected in the "cubical complex" scheme).

I agree that figure 11.2 is terrible to look at, especially because the color coding isn't labeled. After today's training I thought of something that might be a good idea. figure 11.2 is a superposition of an entire family of solutions' persistence diagrams which is hard to analyze. Normally the scalar fields that are being used to produce persistence diagrams are temporal snapshots and so the natural means of visualizing this is a movie of persistence diagrams. I don't know why this hasn't been done for the time series case, but instead of attempting to parameterize the "family" of persistence diagrams, or make a movie, why not just compute the persistent homology of the entire set of snapshots at once; in other words my idea is to think of families of solutions as a scalar field in three dimensions;two of which have periodic boundary conditions.

This thought is what produced figure 11.3, which is the persistence diagram computed for the entire family of numerically continued hook solutions at different domain sizes at once. I am unsure as to whether the different spatiotemporal domain sizes matters in this case, as I know (due to Konstantin Mischaikow) that persistence diagrams are invariant under homeomorphism, so if the rescaling transformation is a homeomorphism (which I think is the case?) then it would not matter if the "total" transformation comprised on individual two dimensional homeomorphisms is itself a homeomorphism. One other problem is that in order to visualize the thresholding in this case (The type of movie that makes the diagrams easy to understand as Predrag and I both believe) it needs to be drawn in three dimensions which isn't easy and likely not as enlightening. I believe this is an idea worth thinking through but I am unsure if it is worth pursuing unless some interesting information comes out of the consequent persistence diagrams.

[Numerical Continuation and other codes] Still working on the initial condition generation for glueing together solutions and symbolic dynamics, as well as numerical continuation, visualization for persistent homology calculations, data management. The plan for tomorrow is likely to numerical continue some solutions and then try to compute persistence diagrams of the entire family and see if any useful information comes out.

[Persistent homology calculations] The main takeaway seems to be numerical continuation of relatively large solutions does not change the main features that much and so solutions (subdomains, really) could possibly be identified by their persistence diagrams.

Although I put a decent amount of work into the three-dimensional family versions of this code I think the single two-dimensional snap shot captures all of the important information. The three dimensional representation just shows that familes of solutions are continuous deformations of

one another, which we really already knew.
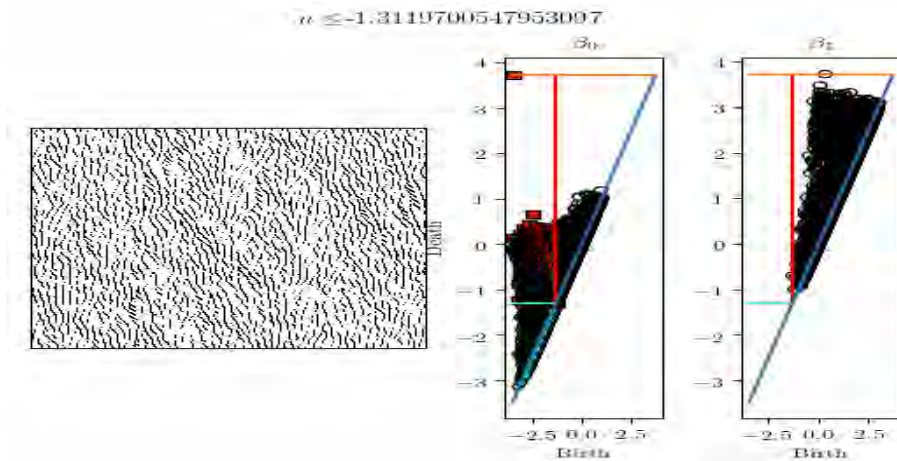
Figure 11.4: Persistence diagram for a large spatiotemporal trajectory (not periodic in time) disaplying a particular thresholding value for the scalar field immediately before and β_1 events are born occur (right figure).

2018-10-05 Matt Trying to make up for lost time by working overtime during the week and completely crashing on weekends. I'm hoping I can keep it up

> **Persistent Homology** I'm only including one figure I produced from a persistent homology calculation on segments of an ergodic trajectory, $t \in [0, 20]$,$t \in [0, 40]$, etc. as the temporal extent of the time series was increased the Betti number zero events seemingly get squashed into the bottom of the persistence diagram and vice versa for the Betti number one events. In other words I guess as one samples more and more of the attractor the persistence diagram asymptotically approaches some regularized distribution. This could just be a red herring because as one takes in more data the more regularized it will be. It's essentially the bottom third of the range of values that the scalar field can take on is dominated by spots. Around the two thirds point (as measured from the bottom of $[-u_{min}, u_{max}]$) all of the black spots become connected, which I find kind of surprising, due to the fact that it just seems to be at some arbitrary value that long time series approach asymptotically. Likewise, for the one-dimensional holes, Betti number one events, none exist until a certain threshold point. It could be meaningly less but perhaps after accounting for noise one could derive a relation between persistence diagrams and solution, or characterize the attractor as an asymptotic state in persistence diagram space. Something to pon-

der.

2018-10-10 Matt Persistent homology of large ergodic segments In this post I will report on the recent results from applying the theory of persistent homology to solutions of the Kuramoto-Sivashinsky equation.

Persistent homology calculations with small spatiotemporal solutions has not yet provided anything fruitful, at least in my interpretation. Because the solutions are defined on small domains there is no room for very complex features and therefore the persistence diagrams have very few features.

I had the idea that perhaps the persistent homology of a long ergodic segment might prove enlightening, as this is the opposite of the small spatiotemporal area limit. I was unsure if the results were trivial so I reported them to Predrag after the weekly plumbers meeting. Both of us found the results interesting but couldn't really explain them.

(Side Note: I'm only going to provide the static persistence diagrams for the ergodic trajectories because the spatiotemporal solution is too large to make any sense out of the black and white spatiotemporal field being animated.)

An interesting observation is that there seems to be two transitions. The first is where all thresholded regions become connected, the second is a minimum value for loops to be born. This is slightly surprising to me. It makes sense that there would be a maximum value after which everything is connected, but I would have expected it to be much closer to the global maximum of the solution. More surprising is that no β_1 events exist before a certain threshold; this is strange to me. It says that there is nowhere on the solution where thresholded region make a "loop" until a certain minimum value. Perhaps this is not supposed to be surprising, as the general behavior in time is of pairs of streaks, where successive minima are generally separated by maxima spatially.

Something that I found really interesting is that there appears to be a symmetry relation between the Betti number zero and Betti number one diagrams. By reflecting the Betti zero β_0 events across the line $y = -x$ (technically $Death = -Birth$ using correct axis labels) maps the Betti zero events to the approximate region of the persistence diagram that Betti one events populate. I don't know what this "approximate symmetry" means, but if I had to bet I believe the most likely explanation is that it is a manifestation of reflection equivariance of the Kuramoto-Sivashinsky equation and nothing more. Also, this is technically ignoring the infinite persistence points, I think this is valid as these point are special and need to be considered separately.

The observations (without proof) that I believe are important are
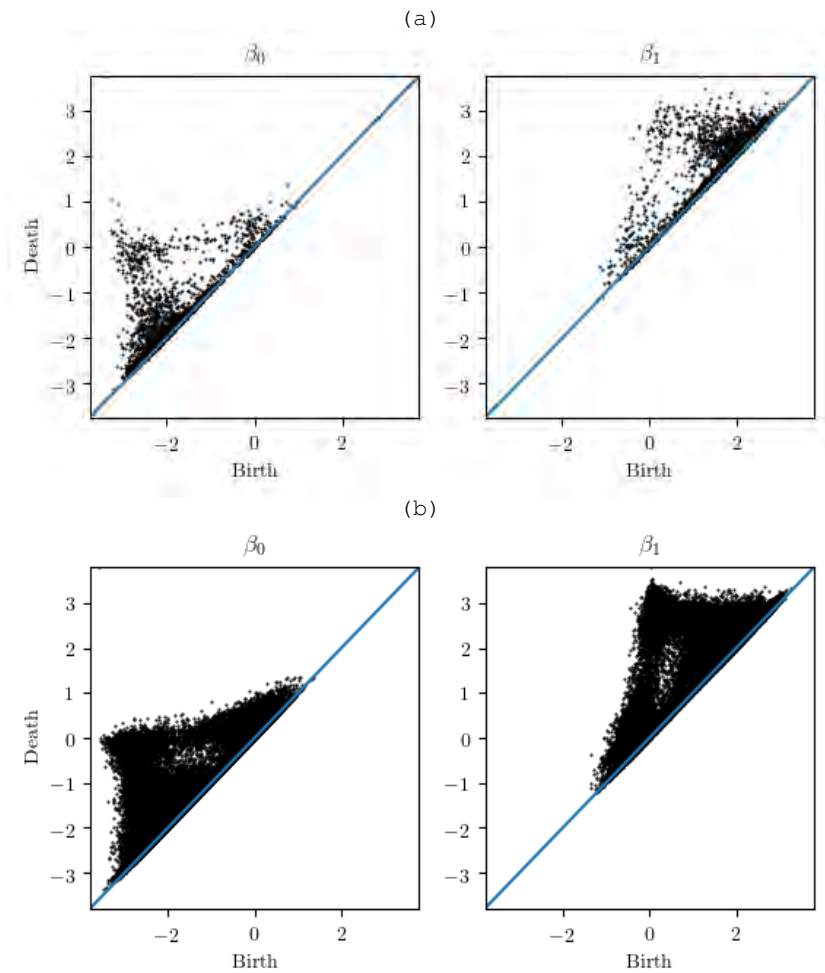
Figure 11.5: (a) Persistence diagram of ergodic segment with temporal extent $T = 200$. (b) Persistence diagram of ergodic segment with temporal extent $T = 4800$, (includes (a) as the first 200 time units)
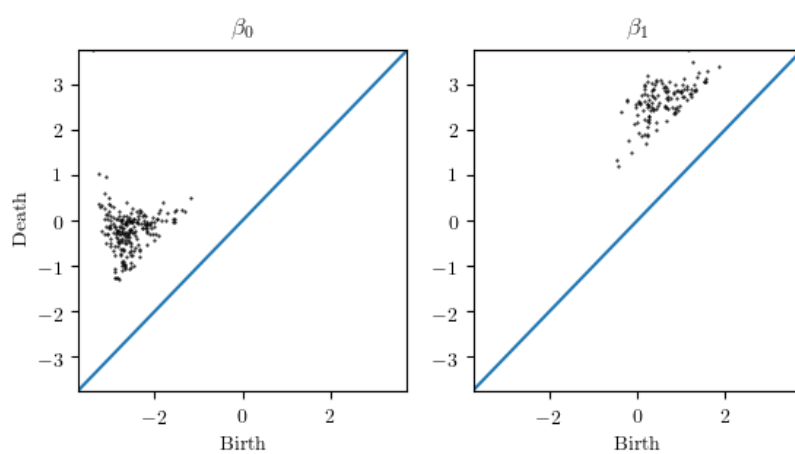
(a)
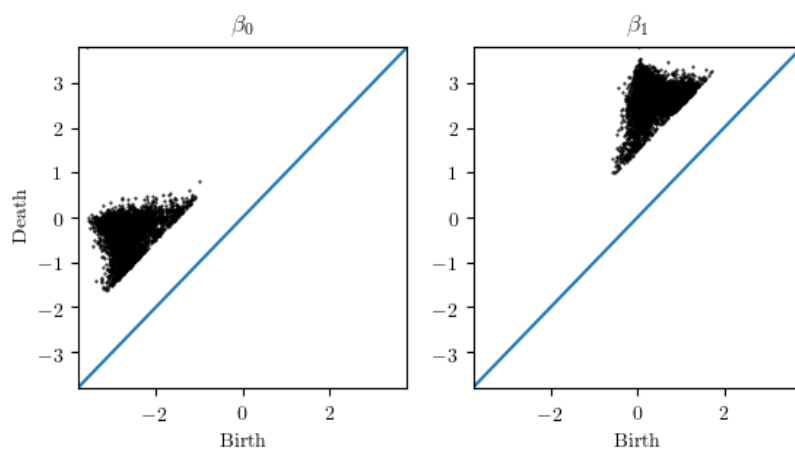
(b)

Figure 11.6: (a) Filtered persistence diagram (lifetime ≤ 1.5 eliminated arbitrarily) of ergodic segment with temporal extent $T = 200$ (b) Filtered persistence diagram of ergodic segment with temporal extent $T = 4800$ (includes (a) as the first 200 time units)

(a)

(b)
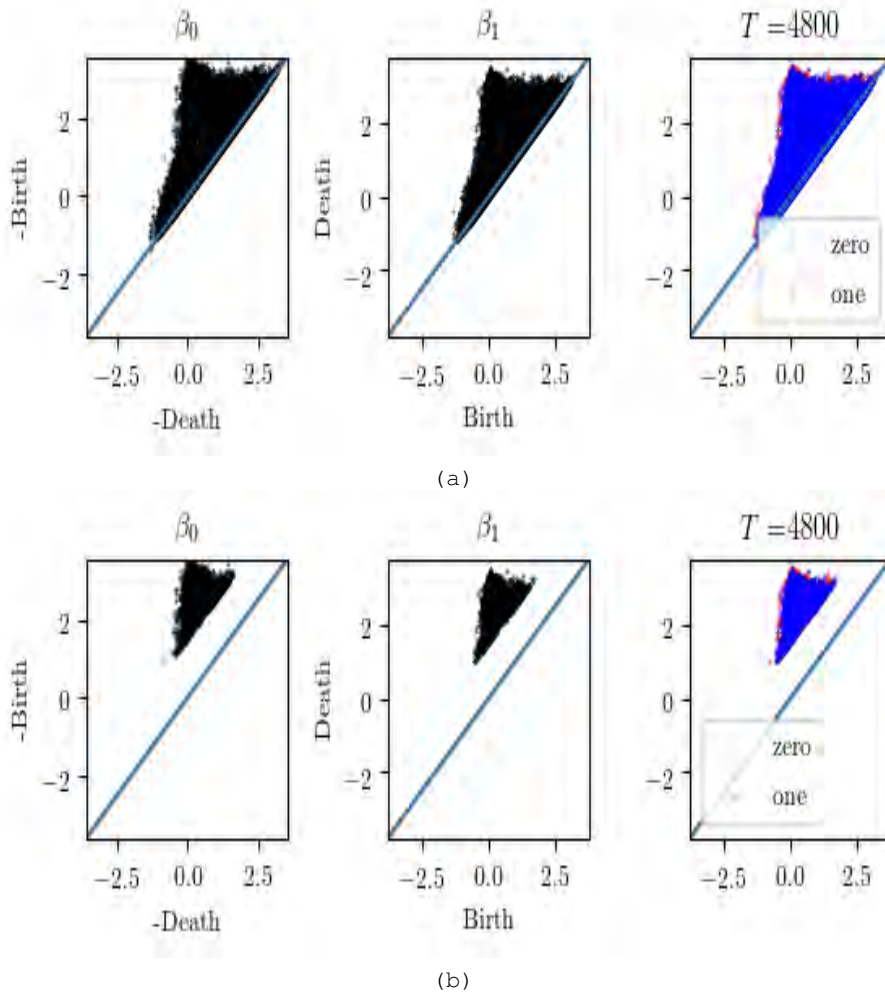
Figure 11.7: Demonstrations of apparent reflection symmetry that relates reflections of the β_0 (simply connected regions persistence diagram) to the β_1 (one-dimensional holes) persistence diagram. (a) Persistence diagrams showing (left) reflected β_0, (middle) β_1 and (right) colored comparison. (b) Filtered persistence diagrams showing (left) Reflected β_0, (middle) β_1 and (right) colored comparison. Both (a) and (b) were computed for ergodic segment with temporal extent $T = 4800$.

- As $T \to \infty$ the region on the persistence diagrams where events exist becomes smaller. A mathy way of saying this is something along the lines of for a sequence of increasing T_k, the induced sequences of "areas" (as measured by, the convex hull of the set of points for instance) A_k of the persistence diagrams follow the approximate rule $A_k + 1 \subseteq A_k$ and as $k \to \infty$, $A_k \to \bar{A}$, where $\bar{A}$ appears to be some statistically steady state. It could be that there is more going on under the multiple layers of data but the general idea that there is some asymptotic behavior I think is well merited. This convergence of the occupied regions in the persistence diagrams is demonstrated by computing multiple persistence diagrams for ergodic trajectory segments of varying temporal extents. In figure 11.5 (a) is the persistence diagram computed for the first $T = 200$ time units of the ergodic segment and (b) is the first $T = 4800$ units. This asymptotic behavior perhaps implies that some statistical information can be retrieved from persistence diagrams in the large T limit.

- The persistence diagrams looked like they had reflection symmetry over the line $y = -x$, and so I produced figures demonstrating this approximately. This is demonstrated for the unfiltered data and filtered data in of figure 11.7 (a) and (b) , respectively. The two regions overlap but it isn't an exact mapping as I had hoped. I'm still thinking through this but as I previously stated I believe that it is reflection equivariance shining through the data. I think I might test this by seeing what pops out when I perform the persistent homology computation on a trajectory in the antisymmetric subspace.

- If events with lifetimes (death minus birth) less than a certain threshold are removed(i.e. require a minimum distance away from diagonal) the picture becomes more clear, especially the symmetry claim. This lifetime threshold was a guess to attempt to eliminate the least persistence information (near-diagonal events). The filtering for two different time segments can be seen in figure 11.6.

2018-10-24 Matt [Plumbers] We discussed the interesting information that seems to arise from performing persistent homology calculations on large spatiotemporal domains (pieces of ergodic trajectory). While currently in its early stages, we believe that the asymptotic behavior captures statistical information about the inertial manifolds; I'm going to produce a comparison between the large ergodic trajectory and all invariant 2-tori in the libraries I've formed to see if any interesting comparisons can be made.

2018-10-29 Predrag Curious - is it possible that there is only one reference on the whole field of persistent homology, the Kramár, Levanger, Tithof, Suri, Paul, Schatz and Mischaikow [1] paper? Or is that the only paper

you have looked at?

The only other paper we have in `siminos.bib` is Krishan, Kurtuldu, Schatz, Gameiro, Mischaikow and Madruga [2] *Homology and symmetry breaking in Rayleigh-Bénard convection: Experiments and simulations.*

2019-04-05 Predrag Just to keep track of the activities in the field - Jean-Philippe Lessard (McGill University), Jason D. Mireles James (Florida Atlantic University) and Jan Bouwe van den Berg (Vrije Universiteit Amsterdam) gave an April 1, 2019 tutorial on *A Computer-Assisted Constructive Approach to Nonlinear Dynamical Systems.*

This was followed by a workshop *Rigorous Computational Dynamics in Infinite Dimensions*, a tutorial *A Topological-Combinatorial Framework for Dynamics*, and a workshop *Data Driven Dynamics: Algebraic Topology, Combinatorics and Analysis.*

Snippets:

"Some early successful applications of these methods for infinite dimensional problems have been: [...] proving spatio-temporal behaviour in the Kuramoto-Sivashinsky PDE; [...] and proving spontaneous periodic orbits in the Navier-Stokes flow. "

"Connecting orbits in ill-posed PDEs. Ill-posed PDEs (with no suitable initial value problem) that come with a variational structure allow for the construction of a Floer homology. Connecting orbits are essential ingredients of this construction. If we can rigorously compute such connecting orbits, they yield specific *local* information, which when combined with generic global analytic arguments, will lead to powerful forcing results."

"explores the computational challenges of rigorously identifying and extracting fundamental dynamical features such as equilibria, periodic orbits, connecting orbits and invariant manifolds in infinite-dimensional dynamical systems."

Mike Schatz is representing us this meeting:

1. Dimension reduction. Data sets often have extremely high extrinsic dimension, but the information content is much lower dimensional. As an example, using Navier-Stokes as a model makes an infinite dimensional problem. Numerical simulations and experimentally collected data can easily involve million dimensional approximations. However, for many problems of interest the dimension of the attractor is on the order of 100 or less.

2. State space reconstruction from data. Typically only a subset of the relevant variables are observed. Therefore to capture the full dynamics requires some form of reconstruction of a model of state space.

3. Information extraction. Typically the information of interest involves identification of dynamic structures or the possibility of prediction

of dynamic behavior. Given that the input data is noisy and that steps 1 and 2 involve processing the data, one needs robust techniques for extracting information.

References

[1] M. Kramár, R. Levanger, J. Tithof, B. Suri, M. Paul, M. Schatz, and K. Mischaikow, "Analysis of Kolmogorov flow and Rayleigh-Bénard convection using Persistent Homology", Physica D **334**, 82–98 (2016).

[2] K. Krishan, H. Kurtuldu, M. F. Schatz, M. Gameiro, K. Mischaikow, and S. Madruga, "Homology and symmetry breaking in Rayleigh-Bénard convection: Experiments and simulations", Phys. Fluids **19**, 117105 (2007).

Chapter 12

Space-time investigation of Kuramoto-Sivashinsky system

Matthew N. Gudorf <matthew.gudorf@gatech.edu>

12.1 Turbulence? An overview

Fluid flows are well described by the Navier-Stokes equation. Instead of beginning research with a partial differential equation with three spatial dimensions, it is wiser to begin with simpler partial differential equation, e.g. "Navier-Stokes" in one spatial dimension, in order to gain some intuition about the larger picture.

12.1.1 Kuramoto-Sivashinsky system

One of the simplest partial differential equations that exhibits spatiotemporal chaotic behavior is the Kuramoto-Sivashinsky [henceforth KS] system [9, 13], which is used to model a number of different phenomena, such as unstable flame fronts. The equation for the velocity of such a flame front $u(x, t)$ on a periodic domain, $u(x, t) = u(x + L, t)$.

$$u_t + \frac{1}{2}(u^2)_x + u_{xx} + \nu u_{xxxx} = 0 \quad x \in [0, L] \tag{12.1}$$

The terms each contribute differently to the dynamics: u_{xx} contributes to instability, u_{xxxx} provides damping, and u_x^2 transfers energy between large and small scales (e.g. between Fourier modes with small and large wavenumbers).

The equations can be made dimensionless by scaling out the 'viscosity' ν with transformations $x \to x\nu^{1/2}, t \to t\nu, u \to u\nu^{-1/2}$. Hence the Kuramoto-Sivashinsky equation takes the non-dimensionalized form:

$$u_t + \frac{1}{2}(u^2)_x + u_{xx} + u_{xxxx} = 0 \quad x \in [0, L\nu^{-1/2}] = [0, 2\pi\tilde{L}] \tag{12.2}$$

In these dimensionless units, periods of periodic solutions are also rescaled following the relation: $T_p = \frac{T_p^*}{\nu}$.

Possible avenues of study of the equation and its behavior include varying L while keeping $\nu = 1$, or varying ν while keeping $L = 1$ or 2π.

The Kuramoto-Sivashinsky equation have a number of different symmetries, namely: spatial translational invariance, temporal translation invariance, reflection invariance, and Galilean invariance. In order to exploit the periodicity of the equations, we recast the field in its Fourier representation

$$u(x, t) = \sum_{k=-\infty}^{\infty} \hat{u}_k e^{iq_k x} \quad \text{where } q_k = \frac{2\pi}{L} . \tag{12.3}$$

The Kuramoto-Sivashinsky equation's representation in terms of spatial Fourier modes is then:

$$\dot{\hat{u}}_k = (q_k^2 - q_k^4)\hat{u}_k - i\frac{q_k}{2} \sum_{m=-\infty}^{\infty} \hat{u}_m \hat{u}_{k-m} . \tag{12.4}$$

The hyper-viscosity term $-q_k^4$ term, damps the higher modes such that a truncation of Fourier modes still yields accurate results, however different numbers of modes can inherently change the nature of the solution in the asymptotic limit.

One can also look at the antisymmetric subspace of the full state space defined by $u(x, t) = -u(-x, t) \in \mathbb{U}^+$. The subspace $\mathbb{U}^+$ can be described with the case of purely imaginary Fourier coefficients $\hat{u}_k \to i\hat{u}_k$, such that the evolution equation becomes:

$$\dot{\hat{u}}_k = (q_k^2 - q_k^4)\hat{u}_k - \frac{q_k}{2} \sum_{m=-\infty}^{\infty} \hat{u}_m \hat{u}_{k-m} . \tag{12.5}$$

By doing so, one eliminates the continuous translational symmetry that is present in the full state space formulation.

12.1.2 Visualizations

There are plenty of ways to visualize the evolution of solutions to the Kuramoto-Sivashinsky equation, however not all visualizations are equal in terms of insight or usefulness. In our applications, pretty plots of the spatiotemporal dynamics of $u(x, t)$ are usually not the most useful for further analysis; projections of trajectories in ∞-dimensional state spaces are often more useful. Furthermore, Poincaré return maps often offer more information than the full state space pictures, specifically about the fractal structure of strange attractors.

12.1.3 Equilibria

By setting $u_t = 0$ and integrating over (12.2) once, one arrives at

$$\frac{1}{2}u^2 + u_x + u_{xxx} = c\,, \tag{12.6}$$

which we can write as 3 ODEs in x,

$$u_x = v\,, \quad v_x = w\,, \quad w_x = u^2 - v - c\,. \tag{12.7}$$

This equation exhibits a reversal symmetry, $x \to -x, u \to -u, v \to v, w \to -w$. The third equation can be rewritten as

$$(u + w)_x = u^2 - c\,. \tag{12.8}$$

For us the interesting dynamics occurs for $c > 0$. The sets of bounded solutions are complex and fractal in nature. The equilibria in this regime are given by $c_+ = (\sqrt{c}, 0, 0)$ and $c_- = (-\sqrt{c}, 0, 0)$. One can acquire the Floquet multipliers by linearizing the flow around one of the equilibria; the opposite equilibria will exhibit a reversed stability profile due to the 'time' reversal symmetry previously mentioned.

For fixed system size L, the only surviving equilibria have periodicity equal to L. The corresponding equilibrium condition is then:

$$q_k^2(1 - q_k^2)\hat{u}_k + i\frac{q_k}{2}\sum_{m=-\infty}^{\infty} \hat{u}_m\hat{u}_{k-m} = 0\,. \tag{12.9}$$

On a finite periodic domain, the spatially periodic equilibria have periods which are multiples of L. There is a bifurcation every time $\tilde{L}$ crosses and integer value, i.e. when $\tilde{L} = n$, n-cell states are generated through pitchfork bifurcations.

In the full state space they form an invariant circle due to translational invariance.

In the antisymmetric subspace $\mathbb{U}^+$ the aforementioned equilibria correspond to two points, which are half-period translations of each other:

$$u(x, t) = -2\sum_k \hat{u}_{kn}\sin(knx) \quad \text{where,} \quad \hat{u}_{kn} \in \mathbb{R}$$

The spatially periodic solutions is finite, due to the finite allowance of zeros of analytic functions on a finite-dimensional compact manifold.

12.1.4 Time-stability analysis: why flame fronts flutter?

The time-evolution stability matrix evaluated at an equilibrium x_q is constant, therefore the Jacobian follows by exponentiation:

$$\mathsf{J}^t(x_q) = e^{At} \quad \text{where,} \quad A = A(x_q)\,.$$

For small $\tilde{L} < 1$, $u(x, t) = 0$ is a globally attractive stable equilibrium. As $\tilde{L}$ increases, there is a sequence of bifurcations that affects the dynamics in an unstable and 'turbulent' manner.

Long wavelength perturbations are linearly unstable, while short wavelength perturbations are strongly contractive. For example, an equilibrium solution can be very unstable in 5 eigen-directions, but with strong contraction in higher, stable eigen-directions. In particular, the equilibrium $u(x, t) = 0$ has Fourier modes as linear stability eigenvectors. The Fourier modes who satisfy $|k| < \tilde{L}$ are unstable. The most unstable mode has k closest to $\frac{\tilde{L}}{\sqrt{2}}$.

Truncation of higher Fourier modes can by justified through the following analysis: If the initial $\hat{u}_k$ are small then the bilinear term $\hat{u}_m \hat{u}_{k-m}$ can be neglected. Then the equations become decoupled linear equations whose solutions are exponentials. There are then a finite number of modes growing with time. These unstable modes excite the higher modes through the bilinear term. However, higher modes are highly damped. Therefore the intermediate wavelengths play an important role in maintaining a dynamic, on-average equilibrium, but truncation can be employed so long as all important modes are kept. A consequence of this is that an infinite-dimensional problem has become finite dimensional.

There is no chance of reversing the evolution because of the high (in principle infinite) number of highly-contracting modes. The time reversal turns these into highly unstable modes.

Equilibria are important because they play two different roles:

- More unstable directions implies less time spent by an orbit in its neighborhood.

- Orbits spend large fractions of time in neighborhoods of equilibria with only a few unstable directions.

Intrinsic parameterization

The best coordinate system to use are generated by the stable/unstable manifolds. It would be best to find a coordinate transformation to new, curvilinear coordinates where the dynamics take place but it's not known if this can be done, let alone if it can be done globally.

12.1.5 Energy budget

The space average of a function $a(x, t)$ periodic on the interval L is given by

$$\langle a \rangle = \langle a \rangle(t) = \frac{1}{L} \oint a(x, t)\, dx \qquad (12.10)$$

Total derivatives vanish via spatial periodicity, and integration by parts yields

$$\langle f_x \rangle = 0, \quad \langle f_x g \rangle = -\langle f g_x \rangle$$

The mean value of time dependent $\langle a \rangle (t)$ is given by

$$\bar{a} = \lim_{t \to \infty} \frac{1}{t} \int_0^t d\tau \ \langle a \rangle \tag{12.11}$$

The average value of a function on a periodic orbit only requires the integration over one period. For an equilibrium the time average is equal to the space average, which is in turn equal to the value of the function evaluated at the equilibrium.

For the Kuramoto-Sivashinsky equation the local velocity square, $u^2/2$, can be interpreted as the kinetic energy density when used in the spatial average equation.

Because the Fourier modes are eigenvectors of the translation operator, the energy is a diagonalized quadratic norm in Fourier space.

$$E = \sum_{k=1}^{\infty} E_k, \quad E_k = \frac{1}{2}|a_k|^2 \tag{12.12}$$

By applying a time derivative, a substitution of variables and integration by parts, one arrives at

$$\dot{E} = P - D, \quad P = \langle u_x^2 \rangle, \quad D = \langle u_{xx}^2 \rangle \tag{12.13}$$

As the time averaged energy density on a generic orbit is expected to go to a constant, on average the power-in P and the dissipation rate D balance each other.

In the Fourier basis the conservation of energy can be written

$$\sum_{k=-\infty}^{\infty} (q_k^2 - q_k^4)\overline{E}_k \tag{12.14}$$

Therefore $\overline{E}_k$ have to decrease faster than q_k^{-4}. [1]

12.1.6   Numerical methods

There are three main methods by which one can attempt to integrate a PDE:

- Discretize the configuration space by means of a grid of N points and approximate the derivatives u_x, u_{xx}, and u_{xxxx} with a finite difference scheme of appropriate order.

- Integrate the equations for a finite number of (truncated) Fourier modes, paying attention to the stability of the integrator and stiffness of the equations.

- Pseudo-spectral integration of the equations: at each step calculate the nonlinear term in configuration space and then bring the result back to Fourier space.

[1]Predrag 2016-08-15: I disagree (asymptotic bound says nothing about small k), so I have removed this: "The active Fourier modes can be determined by whether they deviate from this bound."

12.2   Summer 2016 Report

In this report I will describe my efforts towards implementing MATLAB code that allows for spatial integration of the Kuramoto-Sivashinsky equation. The big caveat is that I have still not been able to accomplish this, at least as of the time of the current version of this report.

Kuramoto-Sivashinsky equation

The one spatial dimension Kuramoto-Sivashinsky equation is given by

$$u_t + uu_x + u_{xx} + \nu u_{xxxx} = 0\,, \tag{12.15}$$

The terms of this equation all play different roles: u_{xx} is an "anti-diffusion" term, that pumps energy into the system and feeds instabilities on large length scales, u_{xxxx} which provides damping on small length scales, and the non-linear, inertial term uu_x which transfers energy between large and small scales. The "hyper-viscosity" ν plays through the dimensionless parameter $\tilde{L} = L/(2\pi\sqrt{\nu})$ a role analogous to the role that the Reynolds number Re plays in the Navier-Stokes equation.

When the Kuramoto-Sivashinsky equation is taken with spatially periodic boundary conditions $u(x+L,t) = u(x,t)$, $u(x,t)$ can be interpreted as the vertical velocity field of a "ring of fire", produced by a Bunsen burner, for example. A number of studies [4–6, 12, 14] explore the steady solutions of this system, i.e., where $u_t = 0$. These solutions are important when viewed from a topological perspective, as the equilibria play a role in the organization of the state space.

12.2.1   Time integration

In order to get into spatial integration of a time-strip, one must first generate the time strip. Because of the spatial periodicity of $u(x,t)$, the time evolution of solutions is best done in Fourier space. The Kuramoto-Sivashinsky equation in Fourier space takes the form,

$$\dot{\hat{u}}_k = (q_k^2 - q_k^4)\hat{u}_k - i\frac{q_k}{2}\sum_{m=-\infty}^{\infty}\hat{u}_m\hat{u}_{k-m} \tag{12.16}$$

The term with $-q_k^4$ serves to damp higher Fourier modes, which allows accurate and stable results even when truncating the infinite number of Fourier modes, a notion that makes numerical implementation feasible. Also, because $u(x,t)$ is a physical and hence, a real quantity, there also exists the relation between Fourier coefficients $u_{-k} = u_k^*$. Therefore for a truncation that keeps N Fourier modes, we can rewrite the Fourier space equation as,

$$\dot{\hat{u}}_k = (q_k^2 - q_k^4)\hat{u}_k - i\frac{q_k}{2}\sum_{m=0}^{N/2-1}\hat{u}_m\hat{u}_{k-m} \tag{12.17}$$

To integrate this equation numerically, we first start with spatially discretizing the Kuramoto-Sivashinsky system by Fourier expanding the field $u(x_n, t) = u_n(t)$ over N points of a periodic spatial lattice $x_n = nL/N$,

$$
\begin{aligned}
\hat{u}_k(t) &= \frac{1}{N} \sum_{0}^{N-1} u_n(t) e^{-iq_k x_n} = \frac{1}{N} \sum_{0}^{N-1} u_n(t) e^{-i2\pi kn/N}, \quad q_k = \frac{2\pi k}{L} \\
u_n(t) &= \sum_{k=-N/2+1}^{N/2} \hat{u}_k(t) e^{iq_k x_n} = \sum_{k=-N/2+1}^{N/2} \hat{u}_k(t) e^{i2\pi kn/N},
\end{aligned}
\tag{12.18}
$$

where k ranges from $-N/2 + 1$ to $N/2$ due to how MATLAB's Fast Fourier Transform (FFT) handles an even number of configuration space points. In order to have a completely symmetric spectrum, one would need to have an odd number of configuration space points, which depending on the number and size of prime factors, would increase the computation time.

Following in the footsteps of others, MATLAB code `kursiv.m` originating from Kassam and Trefethen [7], is adapted in order to provide accurate time-evolution data of $u_n(t)$. The scheme used in this implementation is a combination of two different methods, Exponential Time Differencing (ETD) and Fourth Order Runge-Kutta (RK4) to form a new schema aptly abbreviated ETDRK4. All of this is applied in `ksint.m` which was written by Xiong and Ruslan. This generates the time evolution data for spatial Fourier modes with $k = \pm 1, \pm 2, \ldots, \pm 15$. The amplitudes for the $k = 0$ and $k = -N/2$ (N even), are taken to be zero.

In order to get the correct fields u, u_x, u_{xx}, and u_{xxx}, one must reorder the values produced by `ksint.m`, this is because the real and imaginary components of $\hat{u}_k$ are stored separately in the array returned by the function. In order to comply with MATLAB's Inverse Fast Fourier Transform (IFFT), the correct way to order the coefficients, $\hat{u}_k$, based on mode number k is,

k:	0	1	...	N/2	-N/2+1	-N/2+2	...	-1

The velocity field $u(x,t)$ is retrieved via application of MATLAB's Inverse Fast Fourier Transform (IFFT) on each column of time-evolution data, which correspond to different times. The first three spatial derivatives of the velocity field are retrieved through the spectral method known as spectral differentiation via the equations [2]

$$
\begin{aligned}
u_x(x,t) &= \mathcal{F}^{-1}\left\{ iq_k \hat{u}_k \right\}, \quad u_{xx}(x,t) = \mathcal{F}^{-1}\left\{ (iq_k)^2 \hat{u}_k \right\}, \\
u_{xxx}(x,t) &= \mathcal{F}^{-1}\left\{ (iq_k)^3 \hat{u}_k \right\},
\end{aligned}
\tag{12.19}
$$

A as we shall see in sect. 12.2.2, the values of the spatial derivatives on a time strip are required for spatial integration.

The initial conditions for the time evolution of $\overline{ppo}_{10.2}$ were provided by Xiong Ding's `ks22h02t100E.mat`.

---

[2] Predrag 2016-08-15: Shouldn't u_k be $\hat{u}_k$ in (12.19)?

12.2.2 Spatial integration

Fourier expansions

In order to begin spatial integration, we will expand the time periodic data generated from time integration into its discretized temporal Fourier modes. First we will start with the expansion of a time periodic function $u(t) = u(t+T)$, in terms of its temporal Fourier modes.

$$u(t) = \sum_{k=-\infty}^{\infty} \hat{u}_k e^{i\omega_k t}, \quad \text{where } \omega_k = 2\pi k/T. \tag{12.20}$$

The Fourier coefficients $\hat{u}_k$ can be retrieved by inverting (12.20),

$$\hat{u}_k = \frac{1}{T} \int_0^T dt \, u(t) e^{-i\omega_k t} \tag{12.21}$$

The discrete version of these relations can be obtained with the approximation $\int_0^T dt \to \sum_{n=0}^{N-1} \Delta t$, $\Delta t = T/N$, namely for the discrete Fourier transform,

$$
\begin{aligned}
\hat{u}_k &= \frac{1}{N} \sum_{n=0}^{N-1} u(t_n) e^{-i\omega_k t_n}, \text{where } t_n = nT/N \\
&= \frac{1}{N} \sum_{n=0}^{N-1} u(t_n) e^{-i2\pi nk/N}, \\
&= \frac{1}{N} \mathcal{F}\{u(t_n)\},
\end{aligned}
\tag{12.22}
$$

and likewise for the inverse discrete Fourier transform,

$$
\begin{aligned}
u(t_n) &= \sum_{k=-N/2+1}^{N/2} \hat{u}_k e^{i\omega_k t_n} \\
&= \sum_{k=-N/2+1}^{N/2} \hat{u}_k e^{i2\pi kn/N}
\end{aligned}
\tag{12.23}
$$

The next step is to derive the form that Kuramoto-Sivashinsky equation takes in terms of spatial Fourier modes. First we define,

$$u^{(0)} \equiv u, \quad u^{(1)} \equiv u_x, \quad u^{(2)} \equiv u_{xx}, \quad u^{(3)} \equiv u_{xxx} \tag{12.24}$$

which allows us to write the Kuramoto-Sivashinsky equation as a system of equations,

$$
\begin{aligned}
u_x^{(0)} &= u^{(1)} \\
u_x^{(1)} &= u^{(2)} \\
u_x^{(2)} &= u^{(3)} \\
u_x^{(3)} &= -u_t^{(0)} - u^{(2)} - u^{(0)}u^{(1)}.
\end{aligned}
\tag{12.25}
$$

Now we write the equivalent expression in its Fourier representation, taking into consideration a truncated number of Fourier modes N.

$$
\begin{aligned}
\frac{\partial}{\partial x}\hat{u}_k^{(3)} &= -i\omega_k \hat{u}_k^{(0)} - \hat{u}_k^{(2)} - \sum_{m=0}^{N/2-1} \hat{u}_m^{(0)}\hat{u}_{k-m}^{(1)} \\
\frac{\partial}{\partial x}\hat{u}_k^{(2)} &= \hat{u}_k^{(3)}, \\
\frac{\partial}{\partial x}\hat{u}_k^{(1)} &= \hat{u}_k^{(2)}, \\
\frac{\partial}{\partial x}\hat{u}_k^{(0)} &= \hat{u}_k^{(1)},
\end{aligned}
\tag{12.26}
$$

The rationale behind the truncation in this context is currently not as solid as opposed to the time-integration of a (spatial Fourier mode discretization). There is no longer a term in our equations that damps the higher modes. There isn't any term that provides energy either, but the damping was a good control of numerical accuracy. Burak has proposed to introduce an artificial diffusion term of form $\epsilon u_{tt}^{(3)}$ into the fourth equation in (12.25). In the Fourier space this would take the form $-ew_k^2 \hat{u}_k^{(3)}$, where e is known as an *artificial diffusion constant*. In our numerics, implementing this with $e = 10^{-4}$ produced no significant effect. According to Burak, a value $e = 10^{-4}$ is still a very large value for the artificial diffusion constant. Therefore, I did not include this term in most of my computations.

Handling nonlinearity

The nonlinear term can be handled in a couple of different ways. The first is to directly calculate the convolution sum; this is undesired as it is slow and more importantly does not treat floating-point truncation errors well. The second method is to calculate it via pseudo-spectral method,

$$
\sum_{m=0}^{N/2-1} \hat{u}_m^{(0)}\hat{u}_{k-m}^{(1)} = \frac{1}{N}\mathcal{F}\left\{u^{(0)}u^{(1)}\right\}.
\tag{12.27}
$$

The third option is to calculate it in a fully spectral manner via the circular convolution function included in MATLAB, `cconv`. It's hard to tell which is the best from looking at the values produced because they are all similar up to numerical accuracy, but I would believe the pseudo-spectral method is the best because of how the circular convolution function works, the lack of speed of the convolution sum.

Aliasing errors and dealiasing

An additional procedure can be applied to the pseudo-spectral method in order to combat what is known as *aliasing*. Aliasing is byproduct of discretization, wherein the amplitude of higher frequency (or similarly high wavenumber)

modes can affect the amplitudes of lower modes. The happens when higher modes are misrepresented as lower modes. For $k = -N/2 + 1, \ldots, N/2$ and $j \in \mathcal{Z}$,

$$
\begin{aligned}
e^{\frac{i2\pi(k+jN)}{N}} &= e^{\frac{i2\pi k}{N}} * e^{i2\pi j} \\
&= e^{i2\pi k}.
\end{aligned}
\tag{12.28}
$$

In order to account for this, one must apply a dealiasing formula to the computation of the pseudo-spectral term. One way of accomplishing this is to zero-pad the corresponding Fourier mode data before computing the IFFT which results in $u^{(0)}$ and $u^{(1)}$. For example, the number of Fourier mode coefficients is increased from N to $2N$ by including N zero-valued coefficients. The IFFT is then applied which produces $u^{(0)}$ and $u^{(1)}$ arrays each of length $2N$. Element wise multiplication is used with these new arrays of length $2N$ to produce an array equal to the product $u^{(0)}u^{(1)}$. The product is then brought back to Fourier space via FFT. The final step is taking the new Fourier mode data, an array of $2N$ Fourier Coefficients, and extracting the coefficients belonging to modes $k = -N/2 + 1, \ldots, N/2$.

Numerical integration

The actual implementation concerning the integration of these equations was to use the MATLAB's stiff-ODE integrator `ode15s`. This integrator has higher accuracy than some of its counterparts, such as `ode23s` and `ode23tb`. The integrator is designed to be used with its own variable step size algorithms in order to deal with the stiffness of equations, however, linearly space steps can be used if so desired. The error tolerances can also be controlled using `ode15s` while using a variable step size.

so that the relative tolerance is much more useful when dealing with small numbers. If the relative tolerance is set to be too low, accumulated round off errors will dominate the inaccuracy, while if it is set too high the local discretization errors will dominate.

The integrator requires a separate MATLAB file, `velocityfunction.m` whose input is $\hat{u}_k^{(i)}$, for $i = 0, 1, 2, 3$ according to (12.24) and whose output is $\frac{\partial}{\partial x}\hat{u}_k^{(i)}$ i.e. it is the implementation of (12.26).

Once the integrator has finished running, my current MATLAB code `timeperiodic.m` converts the spatial evolution of the Fourier coefficients $\hat{u}_k^{(i)}$ $i = 0, 1, 2, 3$ into the four (discretized) spatial fields $(u, u_x, u_{xx}, u_{xxx})$ via the use of MATLAB's IFFT.

Spatial integration results

In its current form, my code is only able to give somewhat sensible results for short spatial integrations $x = [0, L]$, $L = \approx 1$, where the period of the desired spatially periodic solution is known to be $L = 22$.
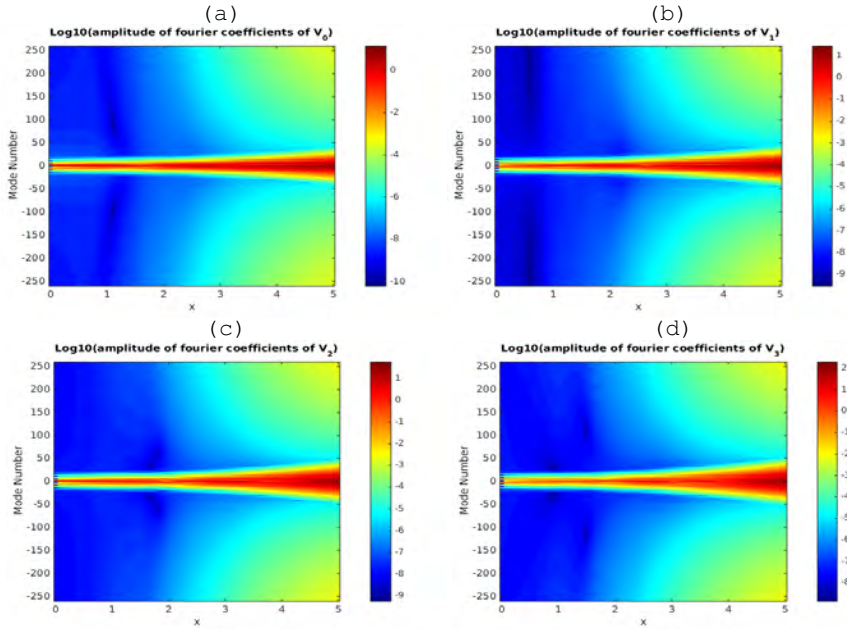
Figure 12.1: Spatial integration $x = [0, 5]$ of temporal Fourier mode amplitudes plotted on a $\log_{10}$ scale. (a) $\hat{u}_k^{(0)}$, (b) $\hat{u}_k^{(1)}$, (c) $\hat{u}_k^{(2)}$, and (d) $\hat{u}_k^{(3)}$.

This can be seen by looking at the Fourier coefficient amplitudes over the course of spatial integration, see figure 12.1. The spectrum seems to flatten, i.e. the amplitudes of the higher modes grow dramatically as the spatial extent of the integration is increased.

Considering these limitations I work around the fact that there is a limited spatial extent on which my integrator seems to work. The way that I decided to deploy my code was the take increase the number of configuration space points to 64 in order to increase the resolution and then integrate the 64 corresponding time-periodic strips over $x = [0, 22/64] = [0, 0.34375]$. I then combine the results such that the resulting figure attempts to represent spatial integration for $x = [0, 22]$. This technique is not able to exploit the variable step size of the integrator, as the strips would be of varying sizes and hence the compilation would not be a very meaningful visualization.

The figure 12.2 is a comparison between the spatial integration of (12.26) using the compilation method I employed in `timeperiodic.m` and the time integration of (12.17) using the ETDRK4 numerical scheme implementation of MATLAB file `ksint.m`. The behavior of these figures seem to exhibit similar patterns up to a what appears to be a reflection in the time direction, implying that there is some unaccounted symmetry. This can be seen by what I call the "tails" of the pattern in the middle being pointed in opposite directions for time
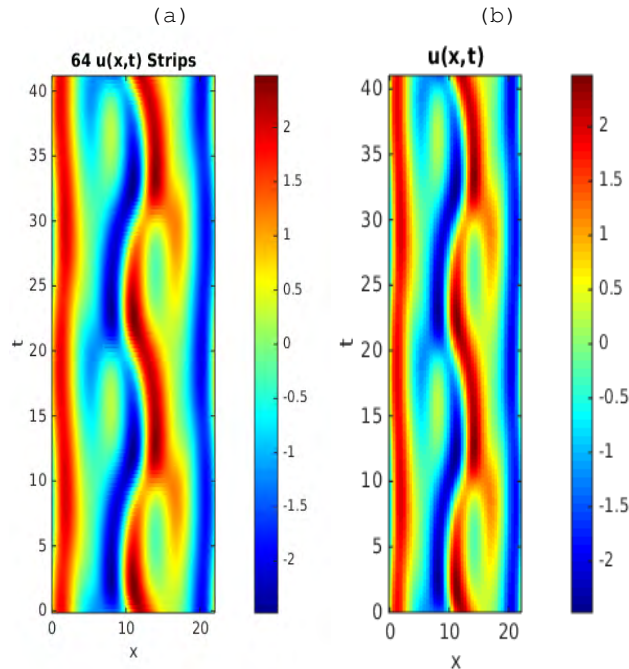
Figure 12.2: Comparison of (a)compilation of 64 spatial integration strips integrated over $x = [0, 0.34375]$ and (b) time integration of $\overline{ppo}_{10.2}$ integrated over time $T = [0, 4\,T_{\overline{ppo}_{10.2}}$, for system size $L = 22$

and space integration. [3]

Future work and comments

The hope for my code is to be capable of spatial integration of infinite extent. My results are disappointing to me to say the least, having been thrown for loops by what should have been insignificant details, but I hope to use what I've learned in terms of coding in the future.

Some possible means of improving the equations is to look for better ways to dealias the pseudo-spectral term or to use the same method but require it to be more rigorous (e.g. more zero-padding).

Second would be to write an integration scheme that could produce more accurate results. My first thought is to apply the ETDRK4 schema to spatial integration, however, I'm not sure if this would work with a system of equations rather than a single PDE.

Another possible, yet dubious and not warranted, course of action is to find a different way to apply damping in the equations, as the steady growth of the

---

[3]Predrag 2016-08-15: in your **2016-08-11 Matt** blog entry you seem to say that you have now corrected this, and replaced figures by the correct ones?

Fourier amplitudes is the main cause of all of my problems.

12.3 Spatiotemporal solutions of Kuramoto-Sivashinsky

To find doubly-periodic spatiotemporal solutions to the Kuramoto-Sivashinsky equationwhile allowing the domain size, period, and any extra parameters (e.g. shift due to SO(2) rotations) to change, we use a Fourier-Fourier basis due to the expected exponential convergence behavior of the (spatiotemporal) Fourier coefficients to zero if a sufficient number of discretization points is used as the spatiotemporal functions are smooth in space and time.

12.3.1 Kuramoto-Sivashinsky in spacetime

The Kuramoto-Sivashinsky equation is a dissipative partial differential equation in one spatial dimension. In a dimensionless form, it can be written as,

$$u_t(x,t) = -u_{xxxx,t} - u_{xx,t} - uu_{x,t} \tag{12.29}$$

The explorations into the geometry of its state space [2], the dimension of a possible inertial manifold [3], and many other studies have been done on it as it proves itself an interesting case study of chaotic dynamical systems in continuous variables. The steady solutions were studied by Michelson [12] as well as Dong and Lan [4] in attempts to categorize the geometry and symbolic dynamics of solutions on the $T = 0$ line. Generally, most studies have been spatiotemporal, with the time being a continuous parameter that induces a dissipative semi-flow $t \geq 0$. In this case study, we pose the problem of finding spatiotemporal invariant solutions by assuming doubly periodic initial conditions, transforming to a Fourier-Fourier basis, and then solving the truncated set of nonlinear algebraic equations

$$(-i\omega_j + (-q_k^2 + q_k^4))\hat{a}_{kj} + \frac{iq_k}{2} \sum_{k',j'=-\inf,-\inf}^{\inf,\inf} \hat{a}_{kj} a_{k-k',j-j'} = 0 \tag{12.30}$$

The numerical details of the solving this equation are explained in sect. **??**, where we elect to use a real valued equivalent form of (12.30). Before the numerical procedure of solving these equations is tractable, we need to inquire into the nature of the symmetries of the Kuramoto-Sivashinsky equationand how they affect the spatiotemporal spectrum of Fourier coefficients first.

12.3.2 Spatiotemporal symmetries of the Kuramoto-Sivashinsky equation

The Kuramoto-Sivashinsky equation (18.1) is equivariant under spatial translations, spatial reflections and temporal translations and Galilean transforma-

tions. The Galilean symmetry $u(x, t)$ is a solution, then $u(x - ct, t) - c$, with c an arbitrary constant speed, is also a solution. Without loss of generality, in our calculations we shall set the mean velocity of the front to zero,

$$\langle u \rangle(t) = \int_0^L dx\, u(x, t) = 0 \,. \tag{12.31}$$

If the system is compactified on a 2-torus, with periodic boundary conditions $u(x, t) = u(x + L, t + T)$, the symmetry group is

$$G = \mathrm{O}(2)_x \times \mathrm{SO}(2)_t = \mathrm{D}_{1,x} \ltimes \mathrm{SO}(2)_x \times \mathrm{SO}(2)_t \,. \tag{12.32}$$

The elements of the 1-parameter group of spatial shifts and reflections are $\mathrm{O}(2)_x : \{\tau_{d/L}, \sigma\}$, and the elements of the 1-parameter group of temporal shifts are $\mathrm{SO}(2)_t : \{\tau_{d/T}\}$. If $u(x, t)$ is a solution, then $\tau_{d/L}\, u(x, t) = u(x + d, t)$ is an equivalent solution for any shift $0 \leq d < L$, as is the reflection ('parity' or 'inversion')

$$\sigma\, u(x, t) = -u(-x, t) \,. \tag{12.33}$$

Consider a cyclic group

$$\mathrm{C}_m = \{e, \tau, \tau^2, \cdots, \tau^{m-1}\}, \qquad \tau^m = e \,.$$

where τ is an $\mathrm{SO}(2)$ rotation by $2\pi/m$. C_m is a discrete subgroup of $\mathrm{SO}(2)$ for any $m = 2, 3, \cdots$.

A field u on the $2\pi/m$ domain is now a tile whose m copies tile the entire domain. It is periodic on the $2\pi/m$ domain, and thus has Fourier expansion with Fourier modes $\exp(2\pi i m j x)$. This means that $\mathrm{SO}(2)$ always has an infinity of discrete subgroups $\mathrm{C}_2, \mathrm{C}_3, \cdots, \mathrm{C}_m, \cdots$; for each the non-vanishing coefficients are only for Fourier modes whose wave numbers are multiples of m.

If we take discrete subgroups in $\mathrm{C}_{2,x}$ in place of both $\mathrm{SO}(2)$ groups then the order of the discrete group $\tilde{G} = \mathrm{D}_{1,x} \ltimes \mathrm{C}_{2,x} \times \mathrm{C}_{2,t}$ is of order 8. All spatiotemporal symmetries of discussion can be described by *isotropy subgroups*, which are symmetry subgroups which leave solutions invariant. Specifically the discrete symmetries, spatial reflection symmetry and spatiotemporal shift-reflection symmetry. These particular symmetries have isotropy subgroups $G = \mathrm{D}_{1,x}$ and $G = \mathrm{C}_{2,t}$ respectively. To cover the discrete spatiotemporal symmetries that are realized by invariant 2-tori we need to investigate the group $G = \mathrm{D}_{1,x} \times \mathrm{C}_{2,t}$, because its description includes reflection and shift-reflection symmetries. The term shift-reflection denotes solutions which are left invariant only after spatial reflection and a time translation by half a period. We have disregarded $\mathrm{C}_{2,x}$ for the discussion of discrete symmetries. This is permitted because spatial half-cell shifts, even in combination with other group elements only permit equivariant solutions, not invariant. Solutions invariant under half-cell shifts in space would have to be doubly periodic in space. For combination with the cyclic group in time it would be a yet undiscovered invariant 2-toruswhich is invariant after a half-cell shifts in space and then time. The general $\mathrm{C}_{M,x} \times \mathrm{C}_{N,t}$ case is harder to describe; if $M = N$ then one example

of a way to construct an invariant solution would be to construct a solution which would be invariant after N total rotations. For instance, a solution with the form

$$u(x,t) = \begin{bmatrix} 1\,2\,3 \\ 3\,1\,2 \\ 2\,3\,1 \end{bmatrix} \tag{12.34}$$

would be invariant after a cycle consisting of one space rotation and two time rotations or two space rotations and one time rotation (each by one third of the domain in the respective, positive directions). This seems incredibly unlikely as it requires the solution to be comprised of permutations of three patterns which are all equivalent in domain size. This unlikelihood only gets worse for higher order cyclic groups We return from our tangent by getting into the meat of the discussion by analyzing the group $D_{1,x} \times C_{2,t}$. We demonstrate some standard group theoretic calculations such as looking at the character table table 12.1 and projection operators (12.35).

Table 12.1: Because the direct product group is abelian we only have one dimensional representations and as such the character table follows directly.

	e	σ_x	τ_t	$\sigma_x \tau_t$
E	1	1	1	1
Γ_1	1	1	-1	-1
Γ_2	1	-1	1	-1
Γ_3	1	-1	-1	1

The character table table 12.1, leads to the construction of four linear projection operators

$$
\begin{aligned}
P^{++} &= \frac{1}{4}(1 + \sigma_x + \tau_t + \sigma_x \tau_t) \\
P^{+-} &= \frac{1}{4}(1 + \sigma_x - \tau_t - \sigma_x \tau_t) \\
P^{-+} &= \frac{1}{4}(1 - \sigma_x + \tau_t - \sigma_x \tau_t) \\
P^{--} &= \frac{1}{4}(1 - \sigma_x - \tau_t + \sigma_x \tau_t),
\end{aligned}
\tag{12.35}
$$

where σ_x, τ_t denote spatial reflection about the $x = 0$ line and time translation by half a period, respectively. The solution space can be decomposed into the irreducible subspaces produced by these projection operators $\mathbb{U} = \mathbb{U}^{++} \oplus \mathbb{U}^{+-} \oplus \mathbb{U}^{-+} \oplus \mathbb{U}^{--}$. In the context of a real valued spatiotemporal Fourier basis each of these subspaces corresponds to a subset of coefficients

in the expansion (**??**)

$$
\begin{aligned}
u^{-+}(x,t) &= \sum_k \sum_j \hat{a}_{kj} \cos(\omega_j t_n) \cos(q_k x_m) \\
u^{--}(x,t) &= \sum_k \sum_j \hat{b}_{kj} \sin(\omega_j t_n) \cos(q_k x_m) \\
u^{++}(x,t) &= \sum_k \sum_j \hat{c}_{kj} \sin(q_k x_m) \cos(\omega_j t_n) \\
u^{+-}(x,t) &= \sum_k \sum_j \hat{d}_{kj} \sin(q_k x_m) \sin(\omega_j t_n) .
\end{aligned}
\tag{12.36}
$$

We won't use these equations just yet but they are good for classifying what each projection operator corresponds to. This classification comes naturally from the parity (odd, even) of the trigonometric functions therein. They can later be used to derive constraints on the spatiotemporal Fourier coefficients pertaining to invariance under certain symmetry operations.

Before we continue, it will first be convenient to calculate the relationships between the projection operators (12.35) and the spatial differentiation operator. The utility comes later when we apply these projection operators to the Kuramoto-Sivashinsky equation, specifically when considering the nonlinear term.

$$
\begin{aligned}
D_x P^{++} &= \frac{1}{4} D_x (1 + \sigma_x + \tau_t + \sigma_x \tau_t) \\
&= \frac{1}{4} (1 - \sigma_x + \tau_t - \sigma_x \tau_t) D_x \\
&= P^{-+} D_x \\
D_x P^{+-} &= \frac{1}{4} D_x (1 + \sigma_x - \tau_t - \sigma_x \tau_t) \\
&= \frac{1}{4} (1 - \sigma_x - \tau_t + \sigma_x \tau_t) D_x \\
&= P^{--} D_x \\
D_x P^{-+} &= \frac{1}{4} D_x (1 - \sigma_x + \tau_t - \sigma_x \tau_t) \\
&= \frac{1}{4} (1 + \sigma_x + \tau_t + \sigma_x \tau_t) D_x \\
&= P^{++} D_x \\
D_x P^{--} &= \frac{1}{4} D_x (1 - \sigma_x - \tau_t + \sigma_x \tau_t) \\
&= \frac{1}{4} (1 + \sigma_x - \tau_t - \sigma_x \tau_t) D_x \\
&= P^{+-} D_x .
\end{aligned}
\tag{12.37}
$$

These identities allow us to rewrite the nonlinear terms present in each projection of the Kuramoto-Sivashinsky equation as derivatives of projection components as opposed to projections of derivatives, which we believe leads to less

confusing analysis. Note that the effect can be summarized by flipping the first $\pm$, pertaining to the coefficient of the spatial reflection terms in (12.35) The surviving nonlinear terms after the application of each projection operator are as follows

$$
\begin{aligned}
P^{++}(u\partial_x u) &= u^{\pm\pm}\partial_x(u^{\pm\pm}) \\
P^{+-}(u\partial_x u) &= u^{\pm\pm}\partial_x(u^{\pm\mp}) \\
P^{-+}(u\partial_x u) &= u^{\pm\pm}\partial_x(u^{\mp\pm}) \\
P^{--}(u\partial_x u) &= u^{\pm\pm}\partial_x(u^{\mp\mp}) \,.
\end{aligned}
\tag{12.38}
$$

Using these relations (12.38) we can produce the projections of the Kuramoto-Sivashinsky equation onto the different irreducible subspaces, noting that the projection operator commutes with the linear terms such that

$$
\begin{aligned}
P^{++}F(u) &= u_t^{++} + u_{xx}^{++} + u_{xxxx}^{++} \\
&+ (u^{++}\partial_x(u^{++}) + u^{+-}\partial_x(u^{+-}) \\
&+ u^{-+}\partial_x(u^{-+}) + u^{--}\partial_x(u^{--})) \\
P^{+-}F(u) &= u_t^{+-} + u_{xx}^{+-} + u_{xxxx}^{+-} \\
&+ (u^{++}\partial_x(u^{+-}) + u^{+-}\partial_x(u^{++}) \\
&+ u^{-+}\partial_x(u^{--}) + u^{--}\partial_x(u^{-+})) \\
P^{-+}F(u) &= u_t^{-+} + u_{xx}^{-+} + u_{xxxx}^{-+} \\
&+ (u^{++}\partial_x(u^{-+}) + u^{+-}\partial_x(u^{--}) \\
&+ u^{-+}\partial_x(u^{++}) + u^{--}\partial_x(u^{+-})) \\
P^{--}F(u) &= u_t^{--} + u_{xx}^{--} + u_{xxxx}^{--} \\
&+ (u^{++}\partial_x(u^{--}) + u^{+-}\partial_x(u^{-+}) \\
&+ u^{-+}\partial_x(u^{+-}) + u^{--}\partial_x(u^{++})) \,.
\end{aligned}
\tag{12.39}
$$

Solutions to (18.1) satisfy $F = 0$ by definition so by extension solutions must also satisfy $P^{\pm\pm}F = 0$. With this we can determine the combinations of projection operators whose equations are "self contained". This is similar to the notion of *flow invariant subspaces* but because we do not have dynamics we can't really use this term. Instead, these subspaces correspond to a constrained set of equations that solutions with particular discrete symmetries must adhere to. For example, assume that the only nonzero component u is $u = u^{++}$. Substitution of (12.39) yields

$$
\begin{aligned}
P^{++}F(u^{++}) &= u_t^{++} + u_{xx}^{++} + u_{xxxx}^{++} + u^{++}\partial_x(u^{++}) \\
P^{+-}F(u^{++}) &= 0 \\
P^{-+}F(u^{++}) &= 0 \\
P^{--}F(u^{++}) &= 0 \,,
\end{aligned}
\tag{12.40}
$$

so $\mathbb{U}^{++}$ is an invariant subspace. In fact, this subspace corresponds to equilibria solutions which live on the $T = 0$ line. The meaning of self contained in

this example is that we assumed that $u = u^{++}$ and the only nonzero part of (12.40) is the $P^{++}F(u^{++})$ component. Perhaps a more elucidating example is generated by the assumption that $u = u^{--} \neq 0$. Substitution yields

$$
\begin{aligned}
P^{++}F(u^{--}) &= u^{--}\partial_x(u^{--}) \\
P^{+-}F(u^{--}) &= 0 \\
P^{-+}F(u^{--}) &= 0 \\
P^{--}F(u^{--}) &= u_t^{--} + u_{xx}^{--} + u_{xxxx}^{--}
\end{aligned}
\tag{12.41}
$$

which indicates that the equations are not self contained as components other than $P^{--}F(u^{--})$ are non-zero. Recall that each of these components is equivalently equal to zero. Because these equations represent scalar field values defined at every x, t this implies that in order to satisfy $u^{--}\partial_x(u)^{--} = 0$ either u^{--}, its derivative $\partial_x(u)^{--}$, or both must equal to zero at every point on the spatiotemporal domain. The only nontrivial possibility is if there are (at least) two disjoint regions such that $\Omega_u = \{(x,t) : u(x,t) = 0\}$ and $\Omega_{u_x} = \{(x,t) : u_x(x,t) = 0\}$. By smoothness, if $u = 0$ then $u_x = 0$. This implies that $u_x = 0$ for all (x,t); if $u_x = 0$ everywhere and $u = 0$ for some (x,t) then it must be the case that $u = 0$ everywhere which contradicts our original assumption that $u = u^{--} \neq 0$. The rest of the symmetry invariant subspaces follow from a similar substitutions. To expedite the derivation process, note that the equation for $P^{++}F$ contains all of the symmetric terms $u^{\pm\pm}\partial_x(u^{\pm\pm})$ such that there is no possibility of an invariant subspaces which does not intersect $\mathbb{U}^{++}$. Following a process of elimination we can show that the possible symmetry invariant subspaces are $\mathbb{U}^{++}$, $\mathbb{U}^{++} \oplus \mathbb{U}^{--}$, $\mathbb{U}^{++} \oplus \mathbb{U}^{+-}$ and $\mathbb{U}^{++} \oplus \mathbb{U}^{-+}$ and of course the full space $\mathbb{U}$. There are no triplet subspaces (comprised of three components) which can be shown using the parity of the different subspaces. We can interpret these subspaces by addition of the corresponding projection operators (12.35)

$$
\begin{aligned}
P_0 \equiv P^{++} &= \frac{1}{4}(1 + \sigma_x + \tau_t + \sigma_x\tau_t) \\
P_{\sigma_x} \equiv P^{++} + P^{+-} &= \frac{1}{2}(1 + \sigma_x) \\
P_{\tau_t} \equiv P^{++} + P^{-+} &= \frac{1}{2}(1 + \tau_t) \\
P_{\sigma_x\tau_t} \equiv P^{++} + P^{--} &= \frac{1}{2}(1 + \sigma_x\tau_t).
\end{aligned}
\tag{12.42}
$$

With these projection operators we can interpret the symmetry invariant subspaces as follows: $\mathbb{U}^{++}$ represents the fixed point ($T = 0$) subspace, $\mathbb{U}^{++} \oplus \mathbb{U}^{+-}$ the spatial reflection invariant subspace, $\mathbb{U}^{++} \oplus \mathbb{U}^{--}$ the shift-reflection invariant subspace, and lastly $\mathbb{U}^{++} \oplus \mathbb{U}^{-+}$ which contains solutions that are invariant after a half period shift in time. This subspace of "twice repeating" solutions is trivial and not useful; doubly periodic solutions can always be made to repeat twice in time by definition. The interpretation of the corresponding subspace is therefore not very intuitive.

The next question to answer is how continuous spatial translation symmetry manifests itself in this spatiotemporal context. How do these subspaces relate to the continuous spatial translation symmetry? The three subspaces $\mathbb{U}_0, \mathbb{U}_{\sigma_x}, \mathbb{U}_{\sigma_x \tau_t}$ share an interesting property in a real valued (SO(2)) representation. Specifically, the subspaces of spatiotemporal Fourier coefficients corresponding to invariance under these discrete symmetries are all orthogonal to the space of spatial translations. This can be seen by acting on the different orbits with the spatial derivative operator which is the generator of infinitesimal translations. The subgroup $H = \mathrm{C}_{M,x}$ represents continuous spatial translation symmetry after discretization. We utilize a co-moving frame ansatz to handle this symmetry, which we will now develop. As previously mentioned, we use a real valued (SO(2)) representation for the spatiotemporal Fourier coefficients. This choice makes the matrix representations of the group elements slightly more complicated as they will be block diagonal as opposed to exactly diagonal. Note that because of doubly periodic boundary conditions, translations are the same as rotation. The matrix representation of the group element which spatially rotates M Fourier modes by a value θ is a block diagonal matrix with M blocks; each block being a representation of two dimensional rotations for the corresponding wavenumber k

$$\tilde{g}(\theta) \equiv \begin{bmatrix} \cos q_k \theta & -\sin q_k \theta \\ \sin q_k \theta & \cos q_k \theta \end{bmatrix} . \tag{12.43}$$

This block diagonal matrix acts on M Fourier modes; the corresponding extension to the set of spatiotemporal Fourier coefficients is simply N copies of (12.43). In other words we have N blocks of (12.43). This form lends itself to the matrix representation for the co-moving reference frame transformation. The co-moving reference frame is the reference frame which makes relative periodic orbits periodic by applying a time-dependent spatial translation to every point of the invariant 2-torus. Using (12.43) the matrix representation of the co-moving frame transformation is as follows

$$g\left(\frac{\sigma t_n}{T}\right) \equiv \begin{bmatrix} \tilde{g}(\frac{\sigma t_1}{T}) & 0 & \cdots & 0 \\ 0 & \tilde{g}(\frac{\sigma t_2}{T}) & \cdots & 0 \\ \vdots & \vdots & \ddots & \vdots \\ 0 & 0 & 0 & \tilde{g}(\frac{\sigma t_N}{T}) \end{bmatrix} . \tag{12.44}$$

Transformations of the type (12.44) will be used in our ansatz for doubly periodic solutions of the Kuramoto-Sivashinsky equation which are relatively periodic.

12.3.3   OLD: Symmetries of Kuramoto-Sivashinsky equation

G, the group of actions $g \in G$ on a state space (reflections, translations, etc.) is a symmetry of the KS flow (18.1) if $g\, u_t = F(g\, u)$. The Kuramoto-Sivashinsky equation is time translationally invariant, and space translationally invariant

on a periodic domain under the 1-parameter group of O(2) : $\{\tau_{d/L}, \sigma\}$. If $u(x,t)$ is a solution, then $\tau_{d/L}\, u(x,t) = u(x+d,t)$ is an equivalent solution for any shift $-L/2 < d \leq L/2$, as is the reflection ('parity' or 'inversion')

$$\sigma\, u(x) = -u(-x)\,. \tag{12.45}$$

The translation operator action on the Fourier coefficients (1.23), represented here by a complex valued vector $a = \{a_k \in \mathbb{C}\,|\,k = 1, 2, \ldots\}$, is given by

$$\tau_{d/L}\, a = \mathbf{g}(d)\, a\,, \tag{12.46}$$

where $\mathbf{g}(d) = \mathrm{diag}(e^{iq_k\, d})$ is a complex valued diagonal matrix, which amounts to the k-th mode complex plane rotation by an angle $k\, d/\tilde{L}$. The reflection acts on the Fourier coefficients by complex conjugation,

$$\sigma\, a = -a^*\,. \tag{12.47}$$

Reflection generates the dihedral subgroup $D_1 = \{1, \sigma\}$ of O(2). Let $\mathbb{U}$ be the space of real-valued velocity fields periodic and square integrable on the interval $\Omega = [-L/2, L/2]$,

$$\mathbb{U} = \{u \in L^2(\Omega)\,|\,u(x) = u(x+L)\}\,. \tag{12.48}$$

A continuous symmetry maps each state $u \in \mathbb{U}$ to a manifold of functions with identical dynamic behavior. Relation $\sigma^2 = 1$ induces linear decomposition $u(x) = u^+(x) + u^-(x)$, $u^\pm(x) = P^\pm u(x) \in \mathbb{U}^\pm$, into irreducible subspaces $\mathbb{U} = \mathbb{U}^+ \oplus \mathbb{U}^-$, where

$$P^+ = (1+\sigma)/2\,, \qquad P^- = (1-\sigma)/2\,, \tag{12.49}$$

are the antisymmetric/symmetric projection operators. Applying P^+, P^- on the Kuramoto-Sivashinsky equation (18.1) we have [8]

$$
\begin{aligned}
u_t^+ &= -(u^+ u_x^+ + u^- u_x^-) - u_{xx}^+ - u_{xxxx}^+ \\
u_t^- &= -(u^+ u_x^- + u^- u_x^+) - u_{xx}^- - u_{xxxx}^-\,.
\end{aligned}
\tag{12.50}
$$

If $u^- = 0$, Kuramoto-Sivashinsky flow is confined to the antisymmetric $\mathbb{U}^+$ subspace,

$$u_t^+ = -u^+ u_x^+ - u_{xx}^+ - u_{xxxx}^+\,, \tag{12.51}$$

but otherwise the nonlinear terms in (12.50) mix the two subspaces.

Any rational shift $\tau_{1/m} u(x) = u(x + L/m)$ generates a discrete cyclic subgroup C_m of O(2), also a symmetry of Kuramoto-Sivashinsky equation. Reflection together with C_m generates another symmetry of Kuramoto-Sivashinsky equation, the dihedral subgroup D_m of O(2). The only non-zero Fourier components of a solution invariant under C_m are $a_{jm} \neq 0$, $j = 1, 2, \cdots$, while for a solution invariant under D_m we also have the condition $\mathrm{Re}\, a_j = 0$ for all j. D_m

reduces the dimensionality of state space and aids computation of equilibria and periodic orbits within it. For example, the 1/2-cell translations

$$\tau_{1/2}\, u(x) = u(x + L/2) \tag{12.52}$$

and reflections generate O(2) subgroup $D_2 = \{1, \sigma, \tau, \tau\sigma\}$, which reduces the state space into four irreducible subspaces (for brevity, here $\tau = \tau_{1/2}$):

$$
\begin{array}{cccc}
 & \tau & \sigma & \tau\sigma \\
P^{(1)} = \dfrac{1}{4}(1 + \tau + \sigma + \tau\sigma) & S & S & S \\[4pt]
P^{(2)} = \dfrac{1}{4}(1 + \tau - \sigma - \tau\sigma) & S & A & A \\[4pt]
P^{(3)} = \dfrac{1}{4}(1 - \tau + \sigma - \tau\sigma) & A & S & A \\[4pt]
P^{(4)} = \dfrac{1}{4}(1 - \tau - \sigma + \tau\sigma) & A & A & S\,.
\end{array}
\tag{12.53}
$$

$P^{(j)}$ is the projection operator onto $u^{(j)}$ irreducible subspace, and the last 3 columns refer to the symmetry (or antisymmetry) of $u^{(j)}$ functions under reflection and 1/2-cell shift. By the same argument that identified (12.51), the Kuramoto-Sivashinsky flow stays within the $\mathbb{U}^S = \mathbb{U}^{(1)} + \mathbb{U}^{(2)}$ irreducible invariant D_1 subspace of u profiles symmetric under 1/2-cell shifts.

While in general the bilinear term $(u^2)_x$ mixes the irreducible subspaces of D_n, for D_2 there are four subspaces invariant under the flow [8]:

- $\{0\}$:   the $u(x) = 0$ equilibrium

- $\mathbb{U}^+ = \mathbb{U}^{(1)} + \mathbb{U}^{(3)}$:
  the reflection D_1 irreducible space of antisymmetric $u(x)$

- $\mathbb{U}^S = \mathbb{U}^{(1)} + \mathbb{U}^{(2)}$:
  the shift D_1 irreducible space of $L/2$ shift symmetric $u(x)$

- $\mathbb{U}^{(1)}$:
  the D_2 irreducible space of $u(x)$ invariant under $x \mapsto L/2 - x$, $u \mapsto -u$.

With the continuous translational symmetry eliminated within each subspace, there are no relative equilibria and relative periodic orbits, and one can focus on the equilibria and periodic orbits only, as was done for $\mathbb{U}^+$ in refs. [1, 10, 11]. In the Fourier representation, the $u \in \mathbb{U}^+$ antisymmetry amounts to having purely imaginary coefficients, since $a_{-k} = a_k^* = -a_k$. The 1/2 cell-size shift $\tau_{1/2}$ generated 2-element discrete subgroup $\{1, \tau_{1/2}\}$ is of particular interest because in the $\mathbb{U}^+$ subspace the translational invariance of the full system reduces to invariance under discrete translation (12.52) by half a spatial period $L/2$.

Each of the above dynamically invariant subspaces is unstable under small perturbations, and generic solutions of Kuramoto-Sivashinsky equation belong

to the full space. Nevertheless, since all equilibria of the KS flow studied in ref. [2] lie in the $\mathbb{U}^+$ subspace, $\mathbb{U}^+$ plays important role for the global geometry of the flow. However, linear stability of these equilibria has eigenvectors both in and outside of $\mathbb{U}^+$, and needs to be computed in the full state space.

References

[1] F. Christiansen, P. Cvitanović, and V. Putkaradze, "Spatiotemporal chaos in terms of unstable recurrent patterns", Nonlinearity **10**, 55–70 (1997).

[2] P. Cvitanović, R. L. Davidchack, and E. Siminos, "On the state space geometry of the Kuramoto-Sivashinsky flow in a periodic domain", SIAM J. Appl. Dyn. Syst. **9**, 1–33 (2010).

[3] X. Ding, H. Chaté, P. Cvitanović, E. Siminos, and K. A. Takeuchi, "Estimating the dimension of the inertial manifold from unstable periodic orbits", Phys. Rev. Lett. **117**, 024101 (2016).

[4] C. Dong and Y. Lan, "Organization of spatially periodic solutions of the steady Kuramoto-Sivashinsky equation", Commun. Nonlinear Sci. Numer. Simul. **19**, 2140–2153 (2014).

[5] J. M. Greene and J.-S. Kim, "The steady states of the Kuramoto-Sivashinsky equation", Physica D **33**, 99–120 (1988).

[6] J. Jones, W. C. Troy, and A. D. MacGillivary, "Steady solutions of the Kuramoto-Sivashinsky equation for small wave speed", J. Diff. Eqn. **96**, 28–55 (1992).

[7] A.-K. Kassam and L. N. Trefethen, "Fourth-order time-stepping for stiff PDEs", SIAM J. Sci. Comput. **26**, 1214–1233 (2005).

[8] I. G. Kevrekidis, B. Nicolaenko, and J. C. Scovel, "Back in the saddle again: a computer assisted study of the Kuramoto-Sivashinsky equation", SIAM J. Appl. Math. **50**, 760–790 (1990).

[9] Y. Kuramoto and T. Tsuzuki, "Persistent propagation of concentration waves in dissipative media far from thermal equilibrium", Progr. Theor. Phys. **55**, 356–369 (1976).

[10] Y. Lan, Dynamical Systems Approach to $1 - d$ Spatiotemporal Chaos – A Cyclist's View, PhD thesis (School of Physics, Georgia Inst. of Technology, Atlanta, 2004).

[11] Y. Lan and P. Cvitanović, "Unstable recurrent patterns in Kuramoto-Sivashinsky dynamics", Phys. Rev. E **78**, 026208 (2008).

[12] D. Michelson, "Steady solutions of the Kuramoto-Sivashinsky equation", Physica D **19**, 89–111 (1986).

[13] G. I. Sivashinsky, "Nonlinear analysis of hydrodynamical instability in laminar flames - I. Derivation of basic equations", Acta Astronaut. **4**, 1177–1206 (1977).

[14]   W. C. Troy, "The existence of steady solutions of the Kuramoto-Sivashinsky equation", J. Diff. Eqn. **82**, 269–313 (1989).

Chapter 13

Matt's 2016 blog

Matthew N. Gudorf <matthew.gudorf@gatech.edu>
The latest entry at the bottom for this blog

13.1 Summer 2016 project description

2016-05-22 Predrag [x] 2016-05-22 went through plane Couette tutorial

[x] numerically reproduce Kuramoto-Sivashinsky evolution forward in time for several finite L periodic domains (use Xiong Ding codes)

[ ] read ChaosBook.org chapter Turbulence?, very critically! It aims to explain the relation between L and the hyperviscosity ν, and it should be the fastest introduction to Kuramoto-Sivashinsky equation, for our purposes, so blog about what is unclear and what is missing.

[ ] summarize Kuramoto-Sivashinsky in sect. 1.5 Course 2, week 16 might also be helpful.

[ ] derive Michelson [34] ODEs and reproduce numerically some equilibria and relative equilibria for the $T = 0$, spatially infinite domain

[ ] Reading part of the project: The best papers on $T = 0$ seem to be

[ ] Michelson [34]

[ ] Lan and Cvitanović [30], summarize it here in sect. 1.6

[ ] Lan [27] thesis, summarize it here in sect. 1.6

[ ] understand Dong and Lan [12] *Organization of spatially periodic solutions of the steady Kuramoto–Sivashinsky equation* in detail, summarize it here in sect. 6.4.1.

check off the boxes once you have read the above sources and entered material learned from them either here, or in separate sections (one for each source, as, for example, sect. 6.4.1)

[ ] summarize $T = 0$ in sect. 1.6

[ ] write a code that solves Kuramoto-Sivashinsky evolution forward in space for finite T periodic, spatially infinite domain (see sect. 1.6; ask Burak for help)

[ ] discuss the patterns that you see

[ ] describe at length the $T \neq 0$ results in sect. 1.6

Matt, check off the boxes, with the date, as you complete them. That, written up in your blog (this *blogMNG16.tex* file), is good enough for the completion of the Summer 2016 term project.

2016-05-22 Predrag If, in addition, you

[ ] reproduce some periodic orbits and Poincaré sections for $L = 22$ periodic domain (use Xiong Ding codes)

[ ] write up a literature survey, sect. 6.4

[ ] compute any (by definition, new) periodic orbits and/or relative periodic orbits for a fixed finite T time-periodic spatial strip

[ ] reduce the O(2) symmetry of the equilibrium equations (my impression is that no one in the literature has done that)

[ ] there should be also solutions that belong to invariant subspaces, much group-theoretical analysis not done yet (that would mean that there are all kinds of important relative equilibria that the literature has missed)

That is most likely worth a publication.

13.2 Matt's blog

2016-05-26 Matt Here is an example of text edit by me, and here one of a footnote by me[1].

2016-05-22 Matt my SVN repo is *svn://zero.physics.gatech.edu/siminos* userID is `mgudorf3`, the password is rather aspirational

2016-05-22 Matt Discussion with Predrag, Kuramoto-Sivashinsky equilibria and relative equilibria project Summer 2016:

- blog the project progress here
- blog whatever I'm reading and learning about dynamical systems here

2016-05-23 Matt I've been working on reading the ChaosBook, so far chapts. 1 and 2.

Considering doing the online Course 1.

---

[1]Matt 2016-05-26: test footnote

2016-05-22 Matt   • Installed Anaconda, Latex, Visual Studio to multiple machines.

• Studied Movies of Plane Couette Tutorial

2016-05-23 Matt   • Read Chapters 1,2 of Chaosbook

• Read Nagata [37] *Three-dimensional finite-amplitude solutions in plane Couette flow: bifurcation from infinity.* Describes the calculation of the Nagata lower/upper branches pair of equilibrium solutions to plane Couette flow. [2]

2016-05-24 Matt   • Video lectures for Chaosbook chap 1-2

• Read Chapter 3

• Gathered papers and resources for Computational Fluid Dynamics and Kuramoto-Sivashinsky system

2016-05-25 Matt   • Video Lectures for Chaosbook Chapter 3

• Began Working through Chaos Book HW1.

2016-05-26 Matt   • Finished Chaosbook: Homework 1 (server error couldn't submit)

• Read Chapters 4, 5 Chaosbook

• Read Dong and Lan [12], summarize it here in sect. 6.4.1

• Watched video lectures for Python learning via 1

• Began reading Newman [38] *Computational Physics* (a python book) [3]

2016-05-26 Skype screen-sharing session Predrag Showed how to use *SVN-tortoise* (svn up, commit, log, diff), *WinEdt* (master file, locate errors) and *JabRef*.

2016-05-26 Matt Still figuring out if I'm referring to articles properly.

2016-05-27 Xiong For 1d Kuramoto-Sivashinsky system, you can start with Kassam and Trefethen [24] *Fourth-Order Time-Stepping for Stiff PDEs*. This has a sample code to integrate Kuramoto-Sivashinsky. You probably also need to understand the pseudo-spectral method - a good introduction is (you can look at my copy): Trefethen [52] *Spectral Methods in MATLAB*.

Cvitanović, Davidchack and Siminos [8] *On the state space geometry of the Kuramoto-Sivashinsky flow in a periodic domain* discusses Kuramoto-Sivashinsky dynamics. You may have a look at it and try to find the 2 relative equilibria by yourself.

---

[2]Predrag 2016-06-29: A very technical paper, not (yet) relevant to your project. Do not worry if you do not understand parts of it

[3]Predrag 2016-06-29: ask Xiong for what he likes as an introduction to python

2016-05-31 Burak I agree with Xiong in that Matt should learn the essentials of the pseudo-spectral methods as he will need to write his own integrator at some point.

Kassam–Trefethen time-stepping scheme is elegant, also the paper [24] is a good read, but it is not crucial since a generic ode integrator does the job once the velocity function is correctly defined.

For a fast start, Matt can run my (fortran + python and matlab), Xiong's (cpp + matlab), and Ruslan's (matlab) codes in the siminos repository, and pick one that suits his taste.

My matlab codes

siminos/ksConnected/ksETDRK4.m (integrator, 73 lines)

and

siminos/ksConnected/vel.m (velocity function, 26 lines)

might be easier to read because I calculate linear and nonlinear terms in separate lines and calculation of nonlinear term is really all Matt needs to understand.

As always, I'm available for skype/hangout whenever Matt might have a question.

2016-05-31 Predrag Please try to keep Matt's workload within realistic bounds. Matt will have to first write forward ODEs integration code for the time-periodic, ∞-space Kuramoto-Sivashinsky. Finding equilibria, relative equilibria, and periodic orbits is another level, with a Newton code. Let's postpone that (see the project outline in the beginning of this chapter, edit as you see fit).

2016-05-30 Matt .

Review Took notes on ChaosBook.org Chapters 2-5 and Dong and Lan [12] Watched video lectures for chapters 4-6. Edit: For week two of ChaosBook.org

Learning Read chapter 6, began reading chapter 14 of ChaosBook.org, began video lectures for chapter 14. I'm trying to get to chapter 30 but I'm not sure if this is skipping too much but the book recommends only 2-5, 14, 15 to get to Chapter 30.

Reading Read and took notes (per Xiong's recommendation) on Kassam and Trefethen [24]; planning on doing the same with Cvitanović, Davidchack and Siminos [8] tomorrow.

2016-05-31 Matt .

Tangent Went off on a tangent on materials way beyond the scope of my project (and most likely unrelated) before I brought myself back to Earth. Ranged from C^*-Algebras to KK-Theory to Bézier Curves. (I.E. Brownian Motion through Wikipedia)

Reading Began thorough reading of Cvitanović, Davidchack and Siminos [8]

Review Went over Kassam and Trefethen [24] notes

2016-06-01 Predrag C^*-Algebras? Strongly unrecommended.

2016-06-02 Matt Matlab Downloaded and installed Matlab, spent time learning syntax and tried for some time to implement Matlab codes for Kuramoto-Sivashinsky that Burak mentioned in **Burak 2016-05-31**, with an addition of a surface plot similar to Figure 6 of Kassam and Trefethen [24]. Produced a nonsensical plot; I believe it's because I don't know what to use for x_0.

Learning Reviewed some materials and completed ChaosBook.org/course1 homework 2.

Reading Took some more notes on Cvitanović, Davidchack and Siminos [8]

2016-06-03 Matt Matlab Reproduced Figure 6 of Kassam and Trefethen [24]. Took a long time to debug a simple mistake but it was a good learning experience.

Reading Finished thorough notes on Cvitanović, Davidchack and Siminos [8]

Comments Am I writing these posts too often and/or should I reserve this space for more important messages? I don't want to make it a personal diary but I find it helpful for organizing what I've done so far.

2016-06-04 Predrag That's great - more detail, rather than less, especially if you run into something that you feel you do not understand well enough - there Burak, Xiong and I can be of help.

Looks like you are moving right along - if your code produces something that is qualitatively like Fig. 2.1 of Cvitanović, Davidchack and Siminos [8], then you are ready to start coding equations of sect. 1.6. However, there is still much theory to read before you feel confident about the results, see the project outline above, chapter 13.

2016-06-06 Matt Learning Watched ChaosBook.org/course1 video lectures for weeks 3, 4. Read and took notes on ChaosBook.org chapters 7, 10, 11.

Went over notes on Cvitanović, Davidchack and Siminos [8] and met with Predrag to talk about the bases with which visualizations are produced. What I learned was it's better to get into the action by going to points of interest (e.g. equilibria) and then look at their unstable manifolds directly by projecting onto the respective

eigenvectors. For $2 - D$ unstable manifolds this includes also using a third eigenvector corresponding to the least contracting eigenvalue/Floquet exponent, or eigenvector with sufficient symmetry properties and contracting eigenvalue.

KS Played with the ETDRK4 code for Kuramoto-Sivashinsky a bit more; varying parameters, size of spatial domain, number of modes/spatial resolution, timestep. Was able to reproduce for different spatially periodic domains.

I want to get a better idea of what I'm looking at. I believe I grasped a better idea of what transient behavior looks like, because after a certain time, there were no more distinguishable patterns no matter how many modes I included, but the patterns after this critical time change depending on the number of modes.

2016-06-06 Burak I found this wikibook a very practical introduction to the spectral methods for the solution of PDEs. It starts with fundamentals and simple examples and goes all the way to the parallel integration of Navier-Stokes equations in a 3D box. Lectures also have accompanying Matlab/Python codes with them, and the advanced parts have Fortran/MPI examples.

2016-06-07 Predrag :

1. The goal right now is to develop some intuition about spatiotemporal turbulence, but not (as yet) write Newton codes for finding equilibria, relative equilibria, and periodic orbits.

2. The goal of the project is to start simulating Kuramoto-Sivashinsky on a finite time-periodic, infinite configuration space domain. (you would be the first to do it, Burak and I believe). That would be a successful summer project.

3. The ultimate goal of the large research project is to take both time and configuration space coordinates to infinity, and incorporate into this PDE (for the first time for any PDE) Gutkin and Osipov [21] $2D$ discrete time, discrete space symbolic dynamics ideas.

4. *The dream* is to then port this to the infinite-length exact turbulent Navier-Stokes pipe flow.

2016-06-09 Matt **Review** Reviewed Chapters 7, 10, 11 of ChaosBook.org

Meeting Met and discussed projects with Rana and Adrien. Decided to meet up and discuss Ch. 14 of ChaosBook.org together on Monday.

Reading Read and took notes on ref. [34].

Exercises Completed Assignments 3 and 4 for ChaosBook.org/course1

Additional Stumbled across some ways one could possibly improve Newton-Raphson method such that it isn't as reliant on initial value. A quote from: Abbasbandy *et al.* [1]:

"When the initial value x_0 is not good, comparing with the results given by other methods, much fewer iterations are needed by HAM; even if a bad initial approximation is chosen, which leads to divergent results by other method, we can still find the root efficiently"

Similar applications are discussed by Wu and Chueng [57]

2016-06-10 Matt Spent a lot of time messing around with matlab code on progressively larger spatial domains to see if anything similar to Michelson [34] popped up. For instance, when $L = 256\pi$ what appears to be a discontinuity in $u(x, t)$ develops at $x \approx 200$ and then at $x \approx 200$ and $x \approx 600$, a distance $L/2$ away, turbulent patterns emerge. I was trying to see if this had anything to do with the discussion about bifurcations in Michelson [34] but I don't think I know enough about bifurcations.

2016-06-13 Predrag Instead of reading Michelson, it is probably easier to read the later references I gave above (Lan, our papers, ChaosBook). There is no chance now that you can see anything Michelson-related by integrating PDEs in time - it applies only to $t = 0$. However, it should be important for study of the time-periodic PDE.

There can be no discontinuity in Kuramoto-Sivashinsky evolution - hyperviscosity term in the equation prohibits that. Presumably you are using too few Fourier modes. Roughly speaking, if you double the domain lengh L, you should double the number of Fourier modes in order to attain the same accuracy...

2016-06-13 Matt I don't know what I'm seeing then, as I made sure to be overzealous with the number of modes. For $L = 256\pi$ I used 20000 modes; it wasn't really a discontinuity but just a region of sharp change in u. I probably overlooked something else.

Learning Read and took notes on chapters 12, 13, 14 ChaosBook.org
Watched video lectures for weeks 5, 6 ChaosBook.org

2016-06-17 Predrag When in doubt whether a calculation returns a sensible answer, include your plot / figure here, in the blog. Then Xiong, Burak and I can have a look at it...

2016-06-13 Matt Read ChaosBook.org Chapter 15
Had a spatiotemp meeting

2016-06-13 Matt Began my attempt to code space integration of Kuramoto-Sivashinsky but quickly got confused; The section sect. 1.6 presumes that we know $u(x, t)$ and its derivatives for $t \in [0, T)$; Does this imply that we know the initial conditions/analytic form of these functions, and then evolve them at time at fixed x to initiate the grid of time values, and then commence the space integration?

2016-06-17 Predrag By construction, any temporal Fourier modes initial condition is time-periodic with the fixed time period T. We have no very good idea what the attractor looks like, so you can start with a first few Fourier modes of order 1, rest 0. Or perhaps you can pick T to be the shortest (relative) periodic orbit T_p for $L = 22$, take the time sequence at some fixed x as the initial condition (Xiong will tell you where it is in this repository). We do not know what's a good starting guess. My hope is that for $T < T_p$, the time domain is too small to accommodate spatiotemporal turbulence, and the attractor converges to a Michelson-type $T = 0$ spatially chaotic strange set (no interesting time dynamics).

2016-06-13 Matt KSspaceint Spent most of the day trying to code spatial integration. I have the part that takes in data for the velocity function $u(x, t)$ and its derivatives down. Trying to apply fourth order Runge-Kutta on the rest; It likes to blow up to infinity, when I put in even dumber initial conditions it still likes to blow up. I believe this is due to one of three things:

1. Runge-Kutta is insufficient in it's accuracy.
2. Not handling the non-linear term correctly.
3. Not handling time derivative term correctly.

Will attempt to reach Burak soon.

Spatiotemp Meeting: I came in late due to real life but the gist of what I gathered was the procedure on how to get inequalities to generate lines in order to describe the certain fixed symbols in a sequence. When a symbol is fixed, the area bounded by these lines describes the frequencies of that symbol. Longer chains of symbols generate more lines, and more conditions/rules on which pieces of area are of interest. The general formulae involve Chebyshev polynomials. Adrien and Rana are going to look for $[2 \times 2]$ squares next I believe.

Sidenote I'm getting some sort of error with siminos.bib that won't allow me to compile the blog. I would try to fix it myself but I'm unsure what the error message means.

2016-06-21 Predrag "some sort of error" does not cut it as an explanation to the IT squad. If it is a comma that Xiong forgot, I fixed it now. You can fix such errors yourself, the error message tells you what line of the *.bib file to fix. But, if you have not edited *siminos.bib* and are getting such errors, try going to *siminos/bibtex/*, remove all *siminos.bib** files, svn up. Should fix it.

2016-06-17 Burak The numerical instability was something that I was expecting. While the points you mentioned can definitely cause it (especially make sure that you treat all terms correctly), there is an obvious difficulty with (1.34), that is the absence of the diffusion term. Let us have a

look at the original Kuramoto-Sivashinsky equation in the Fourier space

$$\dot{\hat{u}}_k = (q_k^2 - q_k^4)\hat{u}_k - \frac{iq_k}{2}\mathcal{F}\{u^2\}_k \quad \text{where, } q_k = 2\pi k/L\,, \hat{u}_k = \mathcal{F}\{u\}_k\,. \quad (13.1)$$

Now pay attention to the coefficient of the linear term:

$$q_k^2 - q_k^4 = \frac{(2\pi)^2 k^2}{L^2} - \frac{(2\pi)^4 k^4}{L^4} \quad (13.2)$$

If we set (13.2) to 0, we find $k = L/2\pi$; for k smaller than this value, (13.2) is positive and negative if $k > L/2\pi$. For large enough k, this term falls down as k^4, dominating everything and strongly damping the high Fourier modes. This is the main justification of using a finite Fourier mode truncation for the numerical study of Kuramoto-Sivashinsky equation. In many PDEs with diffusion (second order space derivatives), this damping goes like k^2, however, in Kuramoto-Sivashinsky equation (18.1) , the second-order space derivative has negative sign, thus it supplies energy to the low wave numbers (negative diffusion), while the energy is dissipated like k^4 (hyper diffusion) at higher ones. Another consequence of this fact is time-irreversibility: In principle, we have a deterministic PDE at hand, present (an initial condition) describes future perfectly well, so we may expect to recover the initial condition if we know the final one. However, this is may not be the simple task of backwards-integrating (13.1) in time. The reason is once we reverse the arrow of time, the negative diffusion vs. hyper diffusion story becomes the opposite and we supply energy to the system at higher and higher Fourier modes which are all unstable, hence no finite-truncation can be justifiable.

With this in mind, let us look back at (1.34) and (1.36). You can see that there is no (hyper)diffusion term that damps Fourier modes corresponding to high frequencies. There is no obvious production term (energy supply) either, but still control of numerical accuracy in this case is not as obvious as it was for the spectral discretization in space. The similar situation appears for advection equations in fluid mechanics and one way to deal with that is adding an "artificial diffusion" term, such as $\epsilon u_{tt}^{(3)}$ to the RHS of the first equation in (1.34), which would show up as $-\epsilon\omega_k^2\hat{u}_k^{(3)}$ in Fourier space. Once you do that, of course, there is a new parameter to experiment with. You should make sure that ϵ is small enough so that it's effect for long time scales (low frequencies) are negligible and it effects only very-high frequency modes, that corresponds to the time scales you don't really care.

Once you make sure all your terms are correct, please try adding an artificial diffusion term to the equation and see if it stabilizes the numerics. We can then check if it gives a numerically correct result by comparing it to time-integrated results. Also please commit your code.

Another potential problem we might have is so-called "aliasing", that is generation of artificial sub-harmonics from the finite-truncation of the

nonlinear term (you can learn about it from any pseudospectral methods for PDEs book, see for instance ref. [5]). This may or may not cause numerical instability issues but certainly has an effect on the accuracy. But hopefully is secondary at this level.

This, by the way, was my main concern about insisting on having an initial condition from a time-integrated simulation, because in time-evolution, we know that high Fourier modes damp and the flow is driven towards an energy-balanced (on average) chaotic attractor. We don't have such a guarantee in space-integration, and that's why I was thinking we should start with a point on the attractor.

2016-06-21 Predrag email to Lan Yueheng <lanyh@bupt.edu.cn>, Skype yueheng_lan :

Matt, a graduate student here, is reading your Kuramoto-Sivashinsky papers (with me and Dong) and your thesis, parts on the Michelson strange attractor that describes $T = 0$ equilibria for infinite spatial domain. Burak and I have not decided to whether to first look at it in the reflection antisymmetric invariant subspace $\mathbb{U}^+$ (as we did - probably preferable, as there are no relative equilibria, no relative periodic orbits and no continuous symmetry to quotient), or study the full O(2)-equivariant problem.

I'm going away for a few weeks, a real vacation - do you mind helping Matt by Skype (matthew.gudorf) or whatever is convenient? It's a lot of material to master, and he has no background in nonlinear dynamics.

2016-06-21 Matt :

KSSpaceInt After shedding much sweat and many tears I think I made a little bit of headway into the integration process. There are still many problems but I can at least generate a plot for very limited sizes of spatial integration i.e. $L = 2$ with step size .01. I'm going to include my matlab files, that include many comments on what I'm attempting to do. the main Matlab file is `timeperiodic.m` so if you have the other two files around and plug in the initial conditions indicated at the top you'll be able to see what I see; I'm not sure how to include figures directly into the blog.

2016-06-23 Matt :

Meeting with Burak and Predrag Talked about the progress so far, explained my Matlab code `timeperiodic.m` for the spatial integration of Kuramoto-Sivashinsy a fixed finite T time-periodic spatial strip.

My strategy, in order to initialize the x integration of (1.34), was to time-integrate $L = 22$ Kuramoto-Sivashinsky for $t \in \{0, 1000\}$, store this as a large matrix, decide by eyeballing that transients have died out by $t = t_{in} = 400$, take $t \in \{t_{in}, t_{in} + T\}$ column of values of $u(x_0, t)$, where $x_0 = 250$, arbitrarily picked, and $T = ??$, all in my

own units. Fourier transform $u(x_0, t)$ to $\tilde{u}(x_0, k)$, assuming periodicity in T, construct from it $\tilde{u}_x(x_0, k)$, $\tilde{u}_{xx}(x_0, k)$ and $\tilde{u}_{xxx}(x_0, k)$, then Fourier transform these back to discretized time-vector

$$(u(x_0, t), u_x(x_0, t), u_{xx}(x_0, t), u_{xxx}(x_0, t)) \tag{13.3}$$

$t \in \{0, T\}$ time-periodic strip. These 4 spatiotemporal fields are then integrated forward in x using (1.34) and my own Runge-Kutta routine (no FFTs).

Burak was cool with all of this. Still, the time Fourier modes seem to explode. Some of the talking points:

1. Use real time and space units instead of the number of discretization steps.

2. Improve the notation for the variables.

3. For a space integrator, use a built-in Matlab integrator such as "ODE45" as opposed to my manually coded fourth-order Runge-Kutta.

4. My ergodic segment $u(x_0, t)$ is discontinuous (a Heaviside function discontinuity) at $T \to 0$ point, and so are $u_x(x_0, t)$, $u_{xx}(x_0, t)$ and $u_{xxx}(x_0, t)$. That means that Fourier spectrum will be essentially flat to arbitrarily high frequencies, and useless as an initial condition. Burak's diffusion regulator might mitigate some of that, but in any case, regularized initial condition will be off the strange attractor.

5. Perhaps pick t_{in} by requiring that it corresponds to a close recurrence in time direction, $u(x_0, t_{in}) \approx u(x_0, t_{in} + T)$, as a possible initial condition on a time-strip? Probably continuity in $u(x_0, t)$ alone does not help, as $u_t(x_0, T)$ and higher derivatives in t are still discontinuous, Fourier transform does not like that either.

6. Use a cubic spline through a range of points spanning across the point of discontinuity $u(x_0, T)$. This, however, would necessarily lift us off of the attractor, which was the whole point of waiting that time-transients die, etc.

7. Taking into account all of the above problems of picking good initial $t = 0$ time-vector (13.3), we gave up on initialization by a time-segment of an ergodic trajectory, and decided to use Xiong periodic orbit data for one of the shortest T_p relative periodic orbits or pre-periodic orbits on the $L = 22$ spatial strip as an initial condition.

8. Will have to time-reintegrate Xiong periodic orbit using $\Delta t = T_p/2^M$ time-step to set up time-discretization needed for a spatial direction pseudo-spectral FFT integrator.

9. How do we know that the integrator in space is working? It presumably has to reproduce the initial $u(x_0, t)$ and its derivatives at $u(x_0 + L, t)$ and its repeats $u(x_0 + mL, t)$. If this is correct, it

should also give us some sense of the stability of the $u(x_0 + x, t)$ orbit in the x-evolution.

10. Boris says that in a secret document he has shown that for a spatiotemporaly periodic solution (a torus that tiles the spacetime)

$$\det (1 - J) = \det (1 - K), \qquad (13.4)$$

where the Jacobian matrix K is computed for the linearization of the evolution in the x, spatial direction. That would be an additional check on the integrator.

11. Will have to think what does it mean to start with an relative periodic orbit? The tiling is by parallelepiped rather than by rectangles. Can cheat by starting with a periodic orbit obtained by a repeat of an pre-periodic orbit. That's considered good enough for government work.

Exercise Derive (13.4). You get Lenin Medal for that.

Discussion with Xiong Xiong showed me where the codes for his time integration are and how to retrieve the data for periodic orbits from a file. I'll need to install a linux virtual machine image to run the time integration code.

2016-06-24 Matt : **KSSpaceInt** Worked all day to try and get `ksint.m` to run. With some help from my brother (who is also a code guru) I created a virtual image that runs 64 bit Ubuntu as well as a shared folder between my current Windows operating system and my Ubuntu virtual image.

I believe that I need Ubuntu to run `MEXksint.mexa64` which is called in previously mentioned MATLAB function, but there seems to be a problem with some missing libraries which I was unable to locate; due to how they are imported it looks like they are some custom made files and not MATLAB libraries. I e-mailed Xiong about this and hope to clarify this issue so that I will have some results come Monday.

2016-06-24 Predrag It would be easier (and faster in the long run) to do this on the CNS linux cluster. Your userID is *gudorf*, I emailed you the password separately.

You can use the linux box in the second bay to the left in the grad students office W503 (if Kinsey is not there), or linux terminal in the computer cubicle W508E (Xiong has the key), or Boris Gutkin's linux box (he is never there before 4-5 pm :) in W501B. Login as *gudorf*. Then *ssh -X gudorf@hard.physics.gatech.edu*; that puts you into Xiong's linux box which has all the packages you need already installed.

If you start generating lots of data, store it locally, somewhere in

/usr/local/home/gudorf/

(a)   (b)
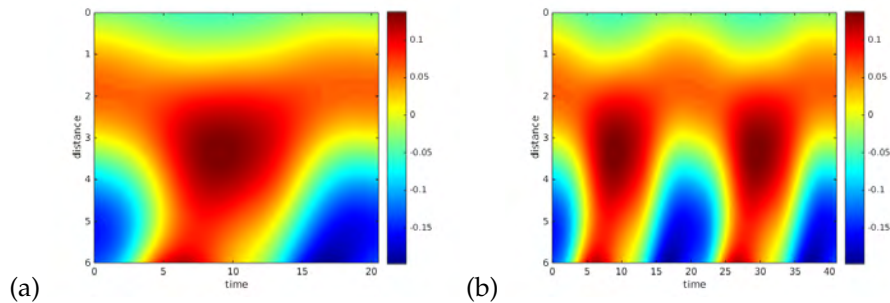
Figure 13.1: Spatiotemporal plots of $u(11, t)$; for the spatial integration of (1.36) for time periodic-domains (a) $T = 2\,T_{\overline{ppo}_{10.2}} = 20.5058$ and (b) $T = 4\,T_{\overline{ppo}_{10.2}} = 41.0116$, from $x = 0$ to $x = 6$ (starting at the top). The initial $u(11, t)$ are given by the $\overline{ppo}_{10.2}$ time profile at $x = 11$. This is a reproduction (PC what is "reproduction?") of Xiong's code `ksint.m` along with application of fast Fourier transforms and their inverses.

> You can get there by *cd localHard*. That is needed because your home directory is backed up every night, and if there are Mr. Rump-self-perception size files in it, it will break the backup for everyone.
>
> If not using a CNS linux box, VPN to get past the firewall. Then
> *ssh -X gudorf@zero.physics.gatech.edu*
> From there,
> *ssh -X gudorf@hard.physics.gatech.edu*
> This *-X* enables you to open the *hard.physics.gatech.edu* Matlab etc. on your own laptop, provided ... (simpler you talk to Xiong about it).

2016-06-24 Matt KSspaceint Revamped my code over the weekend and debugged today with help of Xiong. Solutions still blow up past $L = 12$ and are not very descriptive past $L \approx 8$. In figure 13.1 I show $u(x, t)$ resulting from my curreent spatial integration of $u^{(\ell)}(x_0, t)$ for the periodic domains $T = 2\,T_{\overline{ppo}_{10.2}} = 20.5058$ and $T = 4\,T_{\overline{ppo}_{10.2}} = 41.0116 = 2 * T_a$ and $x_0 = 11$ (by random choice of spatial grid coordinate $x_i = 16$, $1 \leq x_i \leq 32$). Fourier modes are my next objective, which will be easier.

Concerns   1. I don't know what the order of magnitude is considered large for the artificial diffusion constant e so I went with $e = 0.1$, will talk to Burak to get a better idea.

    2. Even with using `ode45.m` in MATLAB, the solutions still diverge at $L \approx 12$. Past $L \approx 6$ the plots of $u(11, t)$ became very undescriptive as the magnitude begins to diverge. Will try implementing `ode15s.m` which deals with stiff differential equations better than (`ode45.m` unless there is a better suggestion.

2016-06-24 Matt Meeting with Burak Burak and I discussed the current prob-
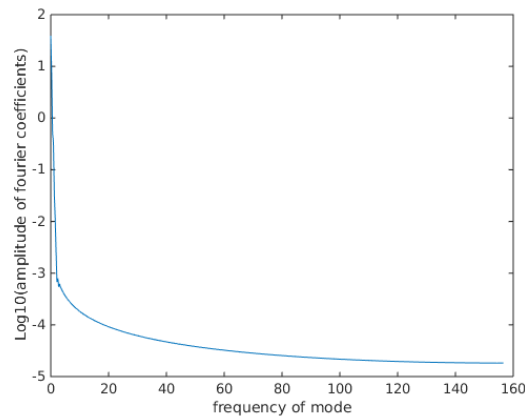
Figure 13.2: Initial amplitudes of Fourier coefficients of temporal Fourier modes (512 positive frequency modes) for two periods of the shortest pre-periodic orbit $\overline{ppo}_{10.2}$, plotted on a logarithmic (base 10) scale.

lems I am having and also questions I had regarding Kuramoto-Sivashinsky spatial integration. The main pieces of advice were as follows:

- Should verify that the truncation of Fourier modes is reasonable, i.e. the amplitudes decrease towards zero. Recommended that I plot the logarithm of the Fourier mode amplitudes to look at their initial values.

- An implicit integration method might need to be deployed because explicit methods can be unstable. Burak suggested to look at both the "Implicit Midpoint Method" and "Fixed Point Iteration Method". [4]

- Also mentioned Symplectic Integrators because they are energy-preserving. Noted that I should probably start with the artificial diffusion term should be zero when I begin these implicit methods, although that will probably be inaccurate when integrating over large spatial domains.

Initial Fourier mode amplitudes The following is the initial Fourier mode amplitudes plotted against their frequencies on a logarithmic scale. The zero-frequency mode dominates and I'm not sure if that is problematic or not.

KSspaceint More attempts at trying to get my spatial integration code to

---

[4]Burak 2016-06-25: Implicit midpoint method is a symplectic integrator, which is appropriate for Hamiltonian dynamics. When you implement it, you get an algebraic equation for the next step in integration, one way of solving for the next step is "Fixed point iteration". There might be better methods.

work so that the temporal Fourier amplitudes do not diverge/blow up.

Switching from `ode45` to `ode15s` had little to no effect. Attempting to correct for aliasing by zero-padding when calculating the nonlinear term via pseudo spectral method. That is, when calculating:

$$\sum_{m=-\infty}^{\infty} \hat{u}_{k-m}^{(0)} \hat{u}_m^{(1)} = \mathcal{F}\left\{ \mathcal{F}^{-1}\left\{ \hat{u}^{(0)} \right\} \mathcal{F}^{-1}\left\{ \hat{u}^{(1)} \right\} \right\}, \qquad (13.5)$$

The "zero-padding" process can be described as the following: Firstly we add extra elements, which are equal to zero, to each array representing $u^{(0)}$ and $u^{(1)}$ (the length of each array is determined by the temporal resolution, let's call it N). Typically, the number of zeros we add is equal to (or greater than) the original number of elements in each array. After "padding" with zeros, each array now contains $2N$ elements. The inverse FFT's are then applied is the equation above, as well as the convolution. The next step is to apply the FFT to the convolution, leaving us with an array that still has $2N$ number of elements. The final step is to prune N elements away so that the final result has N elements. This is done to eliminate artificial sub-harmonics produced by finite truncation of Fourier modes.

Sadly, this did not seem to help the lack of damping and divergence was still present.

2016-07-02 Burak Zero-frequency mode is the average value of the initial signal. I don't see a problem with it having a large value. Please give us more detail about what is on figure 13.2, does the initial condition correspond to two periods of the shortest pre-periodic orbit $\overline{ppo}_{10.2}$? How many Fourier modes are there? Does it go below 5 orders of magnitude drop-off if you include more modes?

2016-07-04 Matt KSspaceint Spent the day trying to figure out the best way to compute the convoluted sum on the left hand side of following equation:

$$\sum_{m=-\infty}^{\infty} \hat{u}_{k-m}^{(0)} \hat{u}_m^{(1)} = \mathcal{F}\left\{ \mathcal{F}^{-1}\left\{ \hat{u}^{(0)} \right\} \mathcal{F}^{-1}\left\{ \hat{u}^{(1)} \right\} \right\}, \qquad (13.6)$$

and keep my code consistent. Wrote this in `convolutionsum.m`. Sort of worried about how trying to evaluate an infinite sum with a truncated number of modes.

In order to keep the code consistent I also edited `timeperiodic.m` by reordering the Fourier mode from negative frequencies to positive frequencies. Hopefully this will solve once and for all the problem of whether my Fourier modes are normalized correctly. I keep finding conflicting notation, no doubt due to the difference in conventions between engineers and everyone else.

Misc. Edited the caption for the figure 13.2, will try adding more Fourier modes to see how the amplitudes behave.

2016-07-05 Predrag I am a bit worried about figure 13.2, where the modes flatten out to about $10^{-4.7}$. That presumably means that the initial condition -should have been on the domain $T = 2\,T_{\overline{ppo}_{10.2}} = 20.5058$- is not smoothly periodic, but it someplace has either a δ-function singularity, or - more likely, a Heaviside θ-function step? A good initial time-periodic $u(x_0, t)$ should fall off at least exponentially, with Fourier modes leveling off only at the machine precision. And I doubt one needs 512 modes (I assume that means 256 complex Fourier modes?). I would have guessed that 64 would have been plenty...

Consult with Xiong about the quality of your initial $u(x_0, t)$ "periodic" profile? You have to be much more explicit about what you and Xiong did to $\overline{ppo}_{10.2}$ to obtain your initial $u(x_0, \cdot)$ for Burak and me to ponder what went wrong. While you are at it, perhaps do not pick arbitrary $x_0 = 11$ initial $u(x_0, \cdot)$. When you look at the time evolution of $\overline{ppo}_{10.2}$ on the $L = 22$ domain, pick initial x_0 such that $u(x_0, t)$ looks as smooth as possible (not sure that what I recommend here really matters).

2016-07-05 Predrag Your $T = 2\,T_{\overline{ppo}_{10.2}} = 20.5058$ in figure 13.1 (a) initial should be strictly periodic, I agree. But there is no need to yet again double the size of the periodic domain, as in figure 13.1 (b). That is asking for more trouble than needed right now.

The good news is that your evolution of the two domains is consistent.

2016-07-05 Predrag Why from $x = 0$ to $x = 6$, when the initial $u(x_0, t)$ are given by the $\overline{ppo}_{10.2}$ time profile at $x_0 = 11$?

You sure that it is $u(x_0, t)$ "starting at the top?". Judging by the color scale on the right, the initial $u(0, \cdot)$ is essentially flat, and it is still rather small by $u(6, \cdot)$: I do not remember u to be so small in magnitude, but my memory can be wrong. You can crosscheck with plots in Cvitanović, Davidchack and Siminos [8] whether your u magnitudes are what they typically see.

2016-07-05 Xiong Matthew had a question about FFT used in my code.

> Hey Xiong,
> I know we discussed the matlab file ksint.m in detail, and it is working well, but I have a question that you might be able to help me with.
> The inverse fast Fourier transform implemented by MAT-LAB divides the result by N where N is the number of modes. I am applying this inverse transformation to values returned by ksint.m, and I'm unsure how the normalization should be treated in order to recover the correct values for u(x,t).

> I have a suspicion that I need to multiply the results by N in order to cancel out the division by N from IFFT, this is because otherwise the initial values seem too small, on the order of hundredths.
>
> If you have any idea I would be very thankful!
>
> -Matt

The truth is that the normalization convention of discrete Fourier transform I am using is different from the standard one. The reason is that I need to keep my code consistent with the code and data provided in folder `siminos/matlab/ruslan`, which is also the convention used in ref. [8]. I almost forget this difference after identifying it 3 years ago. Please search `2013-08-01` in `siminos/lyapunov/blog.pdf` to see the details.

PS Compile it first. `cd sinimos/lyapunov && pdflatex blog.tex`.
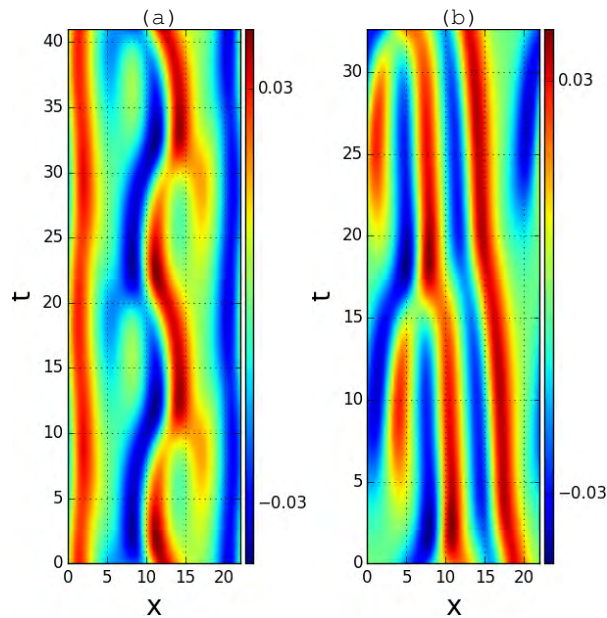
Figure 13.3: (a) Preperiodic orbit $\overline{pp}_{10.25}$ and (b) relative periodic orbit $\overline{rp}_{16.31}$ for total evolution time $4\,T_{pp}$ and $2\,T_{rp}$, respectively. The spatial shift for $\overline{rp}_{16.31}$ after one prime period $\simeq -2.863$. From Ding and Cvitanović [11].

2016-07-05 Predrag The first test is to see whether your *time* integration reproduces figure 13.3 over the $t \in [0, 2\,T_{\overline{ppo}_{10.2}}]$ time interval, starting with Xiong's data set for $\overline{ppo}_{10.2}$. If that is working, a vertical line for some $x_0 \in [0, 22]$ is used for initial $u(x_0, \cdot)$ for *space* integration. If the integrator is working, the updated version of figure 13.1 (a) should coincide with

figure 13.3 (a) over the $x \in [0, 22]$ space interval. That would be enough to declare victory for this summer project.

2016-07-05 Predrag Figure 13.3 from Cvitanović, Davidchack and Siminos [8] gives you some indication of what are typical sizes of (u, u_x, u_{xx}) for the $L = 22$ spatial domain.

2016-07-06 Matt BurakTalks Burak believes that the easiest way for me to pick up a spurious divergence is there is someplace, (most likely calculating the nonlinear term via pseudospectral method) where the normalizations of fft and ifft are incorrect.

In order to verify this, he suggested calculating the nonlinear term via both methods in (13.6), i.e. a convolution sum and the other via the pseudo spectral method. The following is how I formulated `convolutionsum.m` for future reference.

Step Zero: Original ordering of Fourier modes ($N = 2^p$), mode numbers range from $-N/2$ to $N/2 - 1$ in increments of 1, based on `fft` function in MATLAB

Mode-numbered ordering of $\hat{u}^{(0)}$:	-N/2	-N/2+1	...	-1	0	1	...	N/2-1	N/2-1
Mode-Numbered Ordering of $\hat{u}^{(1)}$:	-N/2	-N/2+1	...	-1	0	1	...	N/2-1	N/2-1

Step One: Cyclically permute $\hat{u}^{(0)}$ by $k - 1$, reverse the ordering of $\hat{u}^{(1)}$, (Note: extra shift by 1 to get into the right position due to reversing $\hat{u}^{(1)}$)

Mode-numbered o of $\hat{u}^{(0)}$:	N/2+k+1	...	k-2	k-1	k	k+1	...	N/2+k-1	N/2+k
Mode-numbered ordering of $\hat{u}^{(1)}$:	N/2-1	...	2	1	0	-1	...	-N/2+1	-N/2

Final Step: Element-wise multiplication and summation of allowed combinations

Depending on whether we shift to the right($k < 0$) or left($k \geq 0$), the admissible combinations to the convolution sum are either the last $N - k$ elements (for $k < 0$) or the first $N - k$ elements(for $k \geq 0$). The admissability is a condition that arises from truncating the infinite sum to a sum from $-N/2$ to $N/2 - 1$

Although Burak predicted that I would need to multiply by a factor of $1/N$ in order to get my pseudo-spectral calculation to agree with the convolution sum calculation, I found the terrifying result that they matched when I multiplied the pseudo-spectral calculation by N, which would cause my equations to be even more unpredictable and has me questioning all of the different FFT's and IFFT's normalizations in my code.

XiongTalks Asked Xiong about how the spatial Fourier mode data produced by `ksint.m` is normalized and the correct procedure to acquire the correct amplitudes for $u(x_0, t)$ and its derivatives. He pointed me in the direction of `siminos/lyapunov/blog.pdf` which even though he claims is normalized unconventionally, I believe it fits

with the MATLAB convention of including $1/N$ with the inverse FFT. This is a problem because this is what lead to the small values of $u(x_0, t)$ in the first place, more reasonable values (relative to the scale of figures in ref. [8]).

KSspaceint Still trying to find what I'm missing when it comes to whether the reason for numerical instability in my code is due to Fourier transform normalizations, the integration method I'm using, etc. Compared initial and final values produced by time integration of `ksint.m` of spatial Fourier modes, and the corresponding values of $u(x_0, 0)$ and $u(x_0, 20.5058)$ and found $u(x_0, 0) - u(x_0, 20.5058) \approx 10^{-9}$ for $x_0 = 1.375$ (point 2 out of 32 on spatial grid). I found this value of x_0 to yield somewhat smoother results than $x_0 = 11$, that's the reason for the change.

2016-07-08 Predrag When you write "20.5058" you mean not 20.5058, but $T = 2\,T_{\overline{ppo}_{10.2}}$ to all 11 digits (or however many Xiong gives you) of precision, not a 6-digit number, right?

2016-07-07 Matt Still trying to figure out why the temporal Fourier modes do not drop off exponentially, as I believe this is one of the factors for the numerical instability I am faced with. Like I mentioned in my previous post, the order of the difference between the initial value $u(x_0, 0)$ and $u(x_0, 20.5058)$ for $x_0 = 1.375$ is $\approx 10^{-9}$, just to make sure this small discrepancy wasn't the problem, I forced the initial value and final value to be identical but this yielded no fruitful results.

I have been scouring documentation and testing new editions of my code `timeperiodic.m`. I tried to see if varying the amount of steps and amounts of temporal modes affected the amplitudes in a beneficial way but they did not.

2016-07-07 Matt From Xiong's blog in *siminos/lyapunov/blog.pdf* eq. (7.97) (label xfft2): he seems to show that when converting from a convolution sum of continuous Fourier modes, as in (13.6), to a discrete Fourier transform representation, there is an additional factor of $1/N$ (N = number of modes) that I hadn't accounted for. The importance behind this is that I believe this factor cancels the multiplication of the pseudospectral term by N that Burak and I had discussed, which incidentally was creating bad results.

Edited 2016-07-08

Another development: I was not defining the frequencies for temporal Fourier modes correctly. For continuous Fourier transforms, i.e. $\omega_k = 2\pi k/T$, but for the discrete transforms $w_k = 2\pi k/N_t$, where N_t is the number of data points input into the FFT.

This did not fix the code completely, but when I had, by accident, input $w_k = 2\pi k/T N_t$, I got somewhat stable (able to integrate from $x = 0$

to $x \approx 40$) results; will include a figure later. I believe I am close to meaningful results.

2016-07-08 Xiong Discrete FFT in matlab is

$$a_k = \sum_0^{N-1} u(x_n)e^{-iq_k x_n}\,, \quad u(x_n) = \frac{1}{N} \sum_{k=0}^{N-1} a_k e^{iq_k x_n}$$

But we are using

$$a_k = \frac{1}{N} \sum_0^{N-1} u(x_n)e^{-iq_k x_n}\,, \quad u(x_n) = \sum_{k=0}^{N-1} a_k e^{iq_k x_n}$$

So the normalization is different. ksint.m uses the C++ implementation of `siminos/matlab/ruslan/ksfmetd2.m`. In this file, you can find the nonlinear term coefficient is $g = 0.5i\,k\,N$, not $0.5i\,k$. This is how Ruslan took care of the normalization difference. If you follow this rule, your code should be fine. Embarrassingly, I forgot this difference when producing figure 13.3, and Predrag did not catch error in time, so the wrong scale is in the published Ding and Cvitanović [11]. The scale in figure 13.3 is about 0.03. Multiplying it with 64 (I use 64 modes in ref. [11]), you should get the scale in figure 16.18.

2016-07-09 Predrag to Xiong: Wow, that's painful - is it too late to fix figure 13.3 in Ding and Cvitanović [11]? The paper is not on line yet. And can you fix this in all current codes that you are using for Kuramoto-Sivashinsky Poincaré section calculations, so this error does not seep into the coming Kuramoto-Sivashinsky symbolic dynamics paper?

2016-07-09 Matt Results from ref. [11] reproduced in figure 13.4 (a). Vertical line from this data is used as initial condition for space-integration. Still can't get numerically stable results after more testing and editing.

According to Wikipedia *Discrete-time Fourier transform*, the correct formulation for the frequencies is

$$\omega_k = \frac{2\pi k}{NT} \tag{13.7}$$

(N is the number of modes). [5]

2016-07-09 Predrag Your code is an integrator. A suggestion, for testing purposes:

Why don't you test it as a *time integrator* (instead of Kassam and Trefethen [24] code - your code should be good enough for short times integrations), start with Xiong's $u(x,0)_{\overline{ppo}_{10.2}}$, integrate Kuramoto-Sivashinsky to $u(x,2T)_{\overline{ppo}_{10.2}}$, see how well you reproduce figure 13.4 (a). When that works, return back to testing it as an integrator in *space*.

---

[5]Matt : Edited the 2016-07-09 post to abide by this.

(a)   (b)
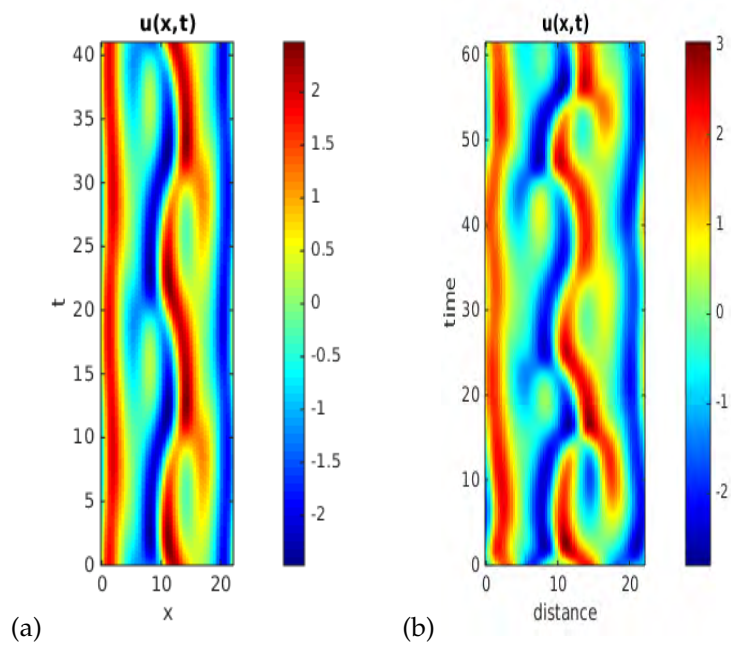
Figure 13.4: Pre-periodic orbit $\overline{ppo}_{10.2}$ of $L = 22$ system integrated over (a) $t \in [0, 4\, T_{\overline{ppo}_{10.2}}]$ in order to compare to figure 13.3. Produced by Kassam and Trefethen [24] `ksint.m`, but now correctly scaled, following Xiong. (b) $t = [0, 6\, T_{\overline{ppo}_{10.2}}]$. Produced by MATLAB function `ode23s`.

2016-07-11 Matt Realized after more testing that the stiffness of equations (1.34) was not being addressed by the integrator I was implementing. I used MATLAB integrator `ode23s` to test time integration and produced figure 13.4 (b). As anyone can see this does not reproduce results from ref. [11]. Even with that in mind, I attempted to apply `ode23s` to spatial integration and was left waiting for code to compile that never completed. I now beginning to believe that in order to get quick and accurate results from integration of these stiff PDE's that I will have to adapt a different scheme for my code, possibly the code from Kassam and Trefethen [24] in order to properly integrate. This would involve using Chebyshev Differentiation Matrices as mentioned in Kassam and Trefethen [24] or a similar method to represent the linear terms because I don't believe the linear part of the equation can be represented by a diagonal matrix.

2016-07-12 Predrag At least visually, the two integrators in figure 13.4 agree pretty well. Have you maybe committed the wrong figure 13.4 (b)? If not, why don't you show us the plot of the spatial integrator, if not for $L = 22$, at least for $x \in \{0, 1\}$ with very small space-step integration, so we can see that you are starting with $u(0, t)$ that agrees with figure 13.3.

At this time, it is more important to get qualitatively right space integration. We can worry about improving the integrator later. Perhaps it is not the problem of a numerical integrator. Our starting (1.36) might be wrong in some deep and profound way...

2016-07-12 Xiong to Matt `ode23s` has options to set the accuracy of each integration step, and you can print out the integration statics. This implicit integrator has order 2, so you should not expect your result to be very accurate. Other choice maybe `ode15s`.

You observed that `ode23s` halted forever for spatial integration. It means that it is reducing the time step to an extremely small value so as to match the local error tolerance. Probably, you can increase this tolerance to get a qualitative picture. As you know, implicit scheme like `ode23s` are always stable.

2016-07-05 Predrag I order to match up with our temporal evolution of Kuramoto-Sivashinsky plots, in $u(x, t)$ spacetime heat maps plots always plot the spatial x coordinate along the x-axis, increasing from the left to the right, and the temporal t coordinate along the y axis, increasing from $t = 0$ upwards. Label axes x and t, not using words. Try to use the same units, i.e., if one plot is time-periodic on $T = 7$ and the other on $T = 14$, the strip representing the second plot should be twice as wide.

Makes it easier to eyeball different plots...

2016-07-08 Predrag In preparing the initial condition for the space integration, when you write "20.5058" you mean not the 6-digit number 20.5058, but

$T = 2\,T_{\overline{ppo}_{10.2}}$ to all 11 digits (or however many Xiong gives you) of precision, right?

2016-07-13 Matt Comments I am indeed using $T = 2\,T_{\overline{ppo}_{10.2}}$.

On the comments about the graphical conventions, I will adhere to this from now on; I think it will be easier to scale in LaTeX, rather than scaling the MATLAB output as I have been doing.

Found another resource [MATLAB forum](#) that uses $\omega_k = \frac{2\pi k}{N}$ for the frequencies. Using this in latest formulation.

MattToXiong I think I have experienced what you have mentioned in the past, in regards to error tolerances; when my code was incorrect it was reducing the step size to $\Delta x \approx 10^{-14}$. I will definitely look into the error tolerances tomorrow.

QuestionForBurak I think I might have misinterpreted what Burak wrote down some time ago, in reference to his statement:

$\epsilon u_{tt}^{(3)}$ to the RHS of the first equation in (1.34), which would show up as $-\epsilon \omega_k^2 \hat{u}_k$ in Fourier space.

Does this mean that I should have a term that looks like $-\epsilon \omega_k^2 \hat{u}_k^{(3)}$? or $-\epsilon \omega_k^2 \hat{u}_k^{(0)}$? (Note: The only difference is the superscripts) I have been using $-\epsilon \omega_k^2 \hat{u}_k^{(3)}$ and now I am full of doubts.

2016-07-13 Burak to Matt: Your original interpretation was right, I corrected my previous post.

2016-07-13 Matt I have included plots figure 13.5, 13.6, 13.7, and 13.8 of spatial integration of (1.36) using my code `timeperiodic.m` and `velocityfunction` (which I really should rename).

I varied the definitions of ω_k because I still find conflicting sources. I believe figure 13.8 is evidence showing that indeed $\omega_k = \frac{2\pi k}{N\,T}$ is the correct formulation because I could not produce similar results for integration over $x = [0, 44]$ with the alternative definition: $\omega_k = \frac{2\pi k}{N}$.

The specific value of $e = 0.1$ was initially random. After some testing, it seemed to have no effect for $\omega_k = \frac{2\pi k}{N\,T}$ plots. Its effect on the $\omega_k = \frac{2\pi k}{N}$ plots was such that for $e \leq 0.05$ the values of $u(x, t)$ would diverge faster. For values $e \geq 0.1$ there were diminishing returns, as the results for $e = 1$, $e = 10$ and $e = 100$ were almost identical.

2016-7-14 Matt Spent today with more testing and investigation into why the values of $u(x, t)$ seem to increase as the integration range is increased. In figure 13.8 I show that after some initial length x the derivatives appear periodic. I am hesitant to say there is "transient" behavior because this happens in a finite spatial interval, not time, but the fact remains that the spatial derivatives $u_x(x, t)$, $u_{xx}(x, t)$ and $u_{xxx}(x, t)$ seem to be well-behaved while $u(x, t)$ itself is not.

$$\omega_k = \frac{2\pi k}{NT} \quad e = 0.1 \qquad \omega_k = \frac{2\pi k}{N} \quad e = 0 \qquad \omega_k = \frac{2\pi k}{N} \quad e = 0.1$$
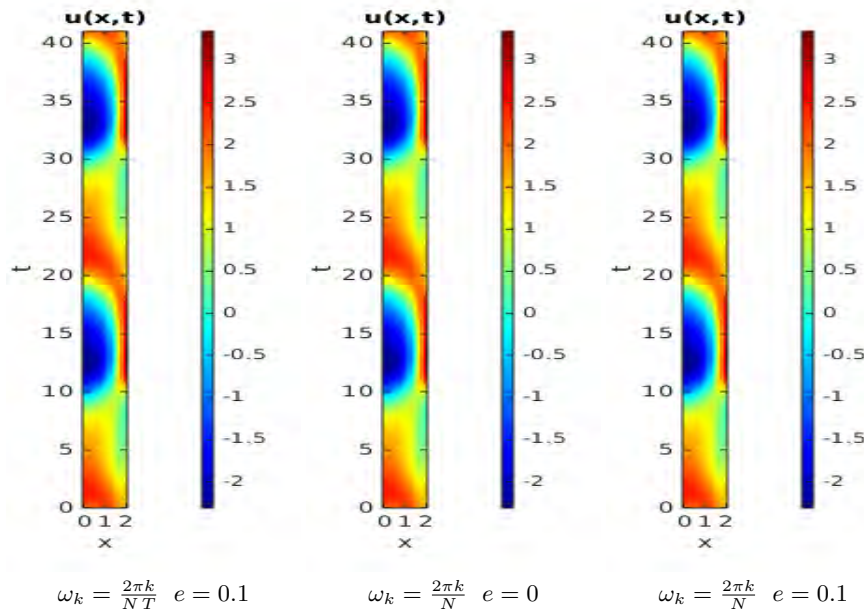
Figure 13.5: Spatial integration of initial temporal strip of $u_{\overline{ppo}_{10.2}}$, ($T = 4\,T_{\overline{ppo}_{10.2}}$) for $x = [0, 2]$ with varying the conflicting definitions for the frequencies ω_k and varying the artificial diffusion constant e. I believe that the reason why there is no difference between the first and second panel is because both were poorly formulated due to the misstep I had with the frequencies mentioned in my post of 2016-07-21. I also changed the $-i\omega_k \hat{u}_k^{(0)}$ to both $i\omega_k \hat{u}_k^{(0)}$ and $\omega_k \hat{u}_k^{(0)}$, with no effect on the spatial integrations displayed here. In retrospect, the plots displayed here are quite meaningless.

I believe this is due to the first equation of (1.36) being dominated by the term $\hat{u}_k^{(2)}$.

2016-07-22 Predrag According to (4.29) the correct definition for a continuous time Fourier transform is is $\omega_k = 2\pi k/T$. You say that figure 13.8 shows that $\omega_k = \frac{2\pi k}{NT}$ is the correct definition. Maybe you can add some further text to the discretization approximation (4.32) and show that the continuous time Fourier transform (4.29) indeed leads to (13.7).

Matt 2016-07-25 Because ω_k is coming from term $-u_t^{(0)}$ when written in terms of continuous time Fourier modes, I believe the correct definition to use is the expression $\omega_k = \frac{2\pi k}{T}$. It is then that the terms $\hat{u}_k$ are replaced by their discretized versions, namely
$\hat{u}_k = \frac{1}{N} \sum_{n=0}^{N-1} u(t_n) e^{-i2\pi nk/N} = \frac{1}{N} \mathcal{F}\{u(t_n)\}$ Unless there is something I didn't understand from what Burak has told me (and written in sect. 4.2), I believe I have done this correctly.

$$\omega_k = \frac{2\pi k}{N\,T} \quad e = 0.1 \qquad\qquad \omega_k = \frac{2\pi k}{N} \quad e = 0 \qquad\qquad \omega_k = \frac{2\pi k}{N} \quad e = 0.1$$

Figure 13.6: Spatial integration of initial temporal strip of $u_{\overline{ppo}_{10.2}}$, ($T = 4\,T_{\overline{ppo}_{10.2}}$) for $x = [0, 16]$ with varying the conflicting definitions for the frequencies ω_k and varying the artificial diffusion constant e

2016-07-13 Burak In sect. 4.2 I go through the derivation of (1.36) in order to clarify all possible normalization related issues in Fourier transforms. Please go through sect. 4.2, make sure each step is correct, both on paper and in your code.

2016-07-18 Matt Went through calculations as Burak requested. I was in agreement with the results but would like to hear whether there is a reason for the pseudospectral term to be written as $\frac{1}{N}\mathcal{F}\{u^{(0)}u^{(1)}\}$ versus an expression that is completely in terms of Fourier modes. There might be a subtlety I'm not picking up on, but my derivations implied that it could be written instead as a convolution between $\hat{u}_k^{(0)}$ and $\hat{u}_k^{(1)}$. The reason why I would want to keep everything in terms of Fourier modes is because I feel like it would make the integrator more efficiently.
Predrag 2016-07-23 I think the general strategy of pseudospectral codes is to evaluate nonlinear terms in the configuration space, then do integration stepping in the Fourier representation.
Xiong 2016-07-24 Using $\frac{1}{N}\mathcal{F}\{u^{(0)}u^{(1)}\}$ instead an expansion in Fourier modes because of their different computational complexity: $O(N \log N)$ versus $O(N^2)$.

Thanks a lot for the help Burak! I really do appreciate it.

$$\omega_k = \frac{2\pi k}{NT} \quad e = 0.1 \qquad\qquad \omega_k = \frac{2\pi k}{N} \quad e = 0 \qquad\qquad \omega_k = \frac{2\pi k}{N} \quad e = 0.1$$

Figure 13.7: Spatial integration of initial temporal strip of $u_{\overline{ppo}_{10.2}}$, ($T = 4\,T_{\overline{ppo}_{10.2}}$) for $x = [0, 22]$ with varying the conflicting definitions for the frequencies ω_k and varying the artificial diffusion constant e.

2016-07-19 Matt I finished applying changes to my code that Burak helped me with.

After more testing and still having diverging results, but having seemingly good results for small spatial integration $x \in [0, \approx 1]$ I decided that the best test for my code in its current state was to glue a bunch of spatial integration results together and see if they agreed with the time-integrated results. Specifically, there were a total of 64 strips integrated over intervals $[x_n, x_{n+1}]$ with $x_n = 22\frac{n}{64}$, $n = 0, ..., 63$. The main integrator used was `ode15s` from MATLAB, with step sizes of $\Delta x = 0.01375$ (each strip had 25 steps for the spatial integration).

The results look better than I expected because my code hasn't been able to produce results from a single time periodic strip, integrated over $x = [0, 22]$. Although I made a small mistake when producing this figure, it should not be the cause of why it seems to be evolving backwards in time when compared to the time evolution of $\overline{ppo}_{10.2}$ seen in figure 13.3 from Ding and Cvitanović [11].

Although it turned out better than expected, I'm unsure if these results are meaningful in the long run because of the small spatial extent of each spatially integrated strip, they may not be large enough to truly demonstrate spatial evolution; but I am still hopeful about the result.

$$\omega_k = \frac{2\pi k}{NT} \quad e = 0.1$$
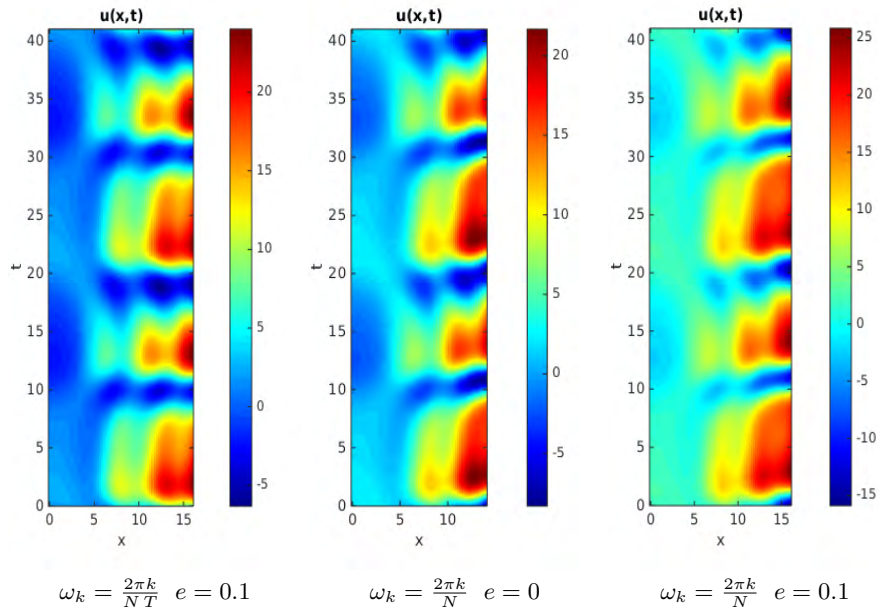
Figure 13.8: Spatial integration of initial temporal strip of $u_{\overline{ppo}_{10.2}}$, $(T = 4\,T_{\overline{ppo}_{10.2}})$ for $x = [0, 44]$.

2016-07-20 Burak Figure 13.10 looks nice and I think it is a meaningful test. Although I can see a discontinuity around $x = L/2$, that is probably a minor error. I wonder if you can reproduce this figure with $\epsilon = 0$; 10^{-4} is still very high. Moreover, if your spatial integration works for $\Delta x \approx 1$, then why don't you use 22 different strips rather than 64 so that we can see more clearly if something went wrong.

I had a quick look at your code to check one thing: When you are taking initial time strip data from time-integration, I think you are taking an interval $t = [0, 4T]$, including $t = 4T$, if this is the case, you should change it to $t = [0, 4T)$ excluding the final point in time, see definitions of Fourier transforms above. I'm not sure how much change this would cause but this might be the reason why figure 13.2 does not drop off as it should, because including final point messes up the smoothness.

2016-07-20 Matt MattToBurak Fixed the the time interval to be $t = [0, 4\,T_{\overline{ppo}_{10.2}})$ as opposed to $t = [0, 4\,T_{\overline{ppo}_{10.2}}]$, and set $e = 0$. Both had no effect on the solutions. I believe that I just messed up the indices on the loop I am running, which fixed the discontinuity that was apparent in figure 13.10, and no longer in the respective figure, (d), in figure 13.11. The intricacies are hard to notice but I attempted to keep them scaled the same as figure 13.10. The qualitative behavior for 8 strips is wildly different from the others. Although hard to see,

$$\omega_k = \frac{2\pi k}{NT} \quad e = 0.1 \qquad \omega_k = \frac{2\pi k}{NT} \quad e = 0.1 \qquad \omega_k = \frac{2\pi k}{NT} \quad e = 0.1$$
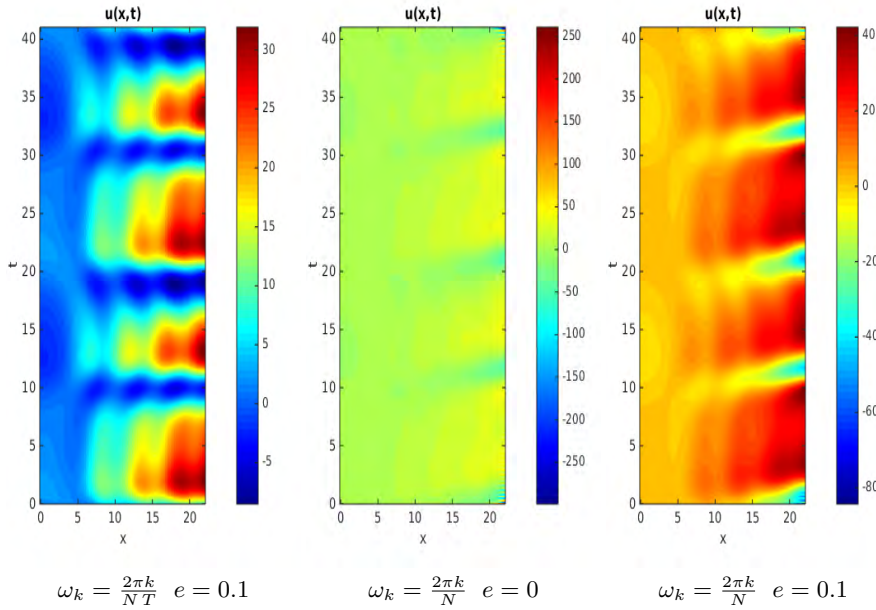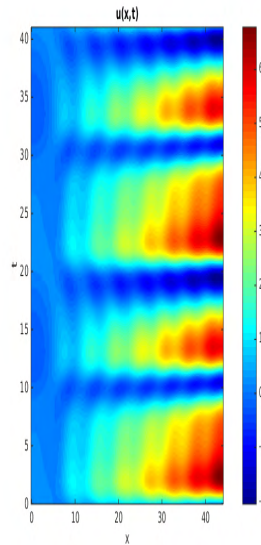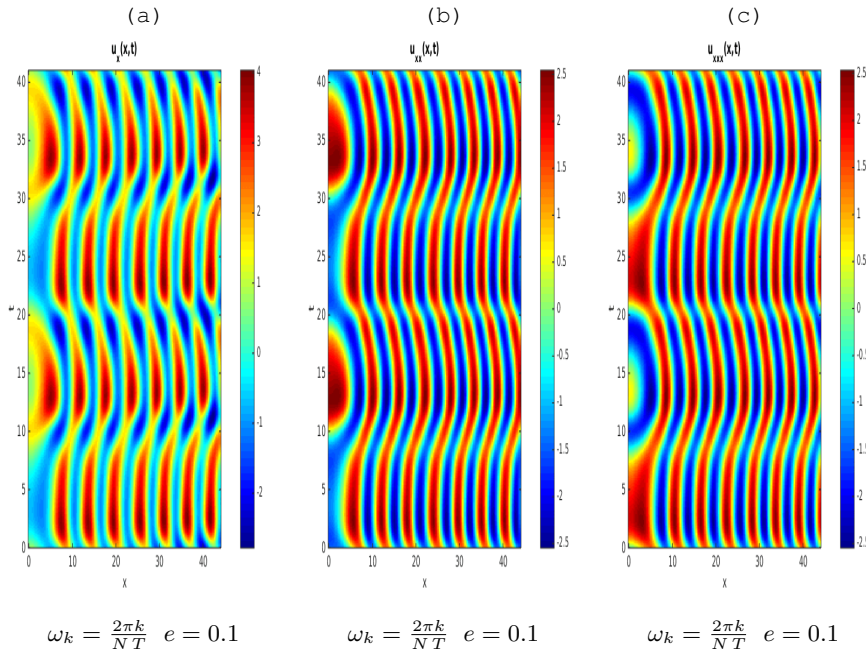
Figure 13.9: Spatial integration of initial temporal strip derivatives of $u_{\overline{ppo}_{10.2}}$, ($T = 4\,T_{\overline{ppo}_{10.2}}$) for $x = [0, 44]$. (a) $u_x(x, t)$, (b) $u_{xx}(x, t)$, and (c) $u_{xxx}(x, t)$. In retrospect, the plots here are not correct, due to the confusion I was having with frequencies. In the spirit of the experimenter's notebook, we keep here the record of all results, good and bad.

there are a number of discontinuities for 16 strips, and the behavior for 32 and 64 seem identical.

Predrag 2016-07-22 I interpret figure 13.11 (a) as indication that the spatial integration is not working, the remaining plots as indication that the spatial transient is longer than $L/16$ or so... Do you agree?

Matt I agree. It seems the best my code can do in its current form is spatial integration to about $x \approx 1$ if there are to be no discontinuities.

Based on Predrag's recommendation I changed the time interval from $t = [0, 4\,T_{\overline{ppo}_{10.2}})$ to $t = [0, 2\,T_{\overline{ppo}_{10.2}})$ as it might help the solutions be more stable.

KSspaceint Attempted again to find the cause of the divergence by playing with equations (1.36) by introducing scaling factors on the different terms and proceeding with spatial integration. So far the only definitive result is that making the nonlinear term larger makes the equations blow up faster, which is not very surprising. I also changed the $-i\omega_k \hat{u}_k^{(0)}$ to be both $i\omega_k \hat{u}_k^{(0)}$ and $\omega_k \hat{u}_k^{(0)}$ with no effect on the spatial integrations for figure 13.11. My main motivation was

64 u(x,t) Strips

$$\omega_k = \frac{2\pi k}{T} \quad e = 0.0001$$
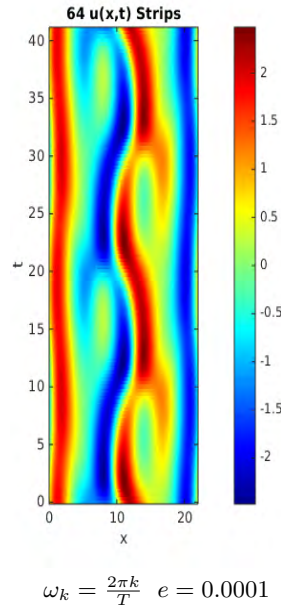
Figure 13.10: Spatial integration results for 64 time periodic strips $T = 4\,T_{\overline{ppo}_{10.2}}$ from the time evolution of $\overline{ppo}_{10.2}$ compiled into one image. The time periodic strips were generated by Xiong's MATLAB code `ksint.m`. The initial time periodic strips were integrated over spatial intervals $[x_n, x_{n+1}]$ with $x_n = 22\frac{n}{64}$, $n = 0, ..., 63$.

> to try simple things which could possibly have an effect. I thought the main problem was the nonlinear term, but if I recall correctly I removed it from the equation in an albeit ridiculous procedure, and I still had the divergence problem. I'll verify this tomorrow because I'm having trouble recalling if that's actually what I did, but I wanted to write it down to remind myself.

2016-07-21 Matt :

> **PowerSpectrumFigures** The first set of figures in figure 13.12 are the power spectra for initial time-periodic conditions for $t = [0, 2\,T_{\overline{ppo}_{10.2}}]$ and $t = [0, 2\,T_{\overline{ppo}_{10.2}})$ in order to compare whether there are any differences. Because the interesting details are hard to see, I've also included figure 13.13 which are merely magnified versions of figure 13.12. There seems to be no difference between the two, when taking my poor windowing into consideration.
>
> Some key things to note about the plots in figure 13.14 is that this is the power spectrum on a logarithmic scale, $\log_{10} |\hat{u}_k^{(0)}|^2$, as opposed to the amplitude spectrum in figure 13.2. The other key difference
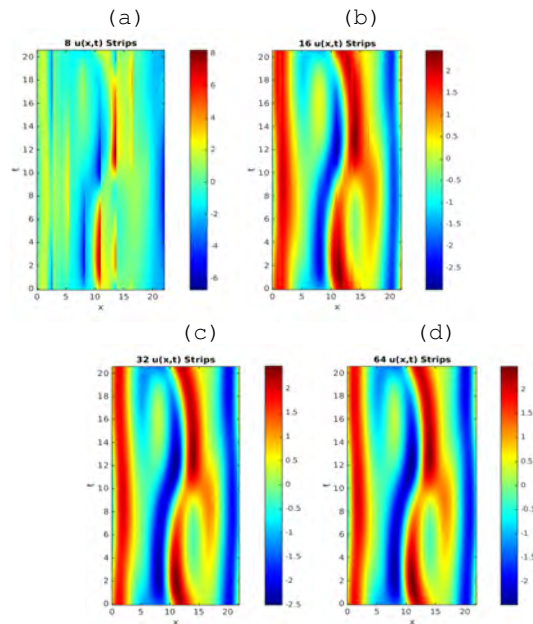
Figure 13.11: Spatial integration $x = [0, 22]$ with zero artificial diffusion ($e = 0$). Initial conditions are time periodic strips $t = [0, 2\,T_{\overline{ppo}_{10.2}})$ provided by `ksint.m`. The number of integration strips, (i.e., the number of time-periodic initial conditions from `ksint.m` used for spatial integration) are: (a) 8, (b) 16, (c) 32, and (d) 64.

is that I am using the normalization convention $\hat{u}_k = \frac{1}{N}\mathcal{F}\{u(t_n)\}$. Previously I was dividing by N on application of the inverse FFT.

When the number of modes is smaller than the number of time steps, the amplitudes are much larger in magnitude. When the number of modes is taken to be greater than the number of time steps, the amplitudes resemble the Fourier transform of a rectangular window function. The optimal (smallest amplitudes) number of modes seems to be equal to the number of time steps.

FourierSpaceInt Also included in this blog post are plots of the spatially integrated Fourier mode *amplitudes* $|\hat{u}_k^{(0)}|$, plotted on a $\log_{10}$ scale, in an attempt to see why the equations are still unstable. I thought that this might be useful in identifying any peculiar behavior, but all of the plots in figure 13.14 are very similar to each other. $\hat{u}_k^{(3)}$ seems to blow up first which drags the rest $\hat{u}_k^{(0)}$, $\hat{u}_k^{(1)}$, $\hat{u}_k^{(2)}$, with it. This interpretation is based on the scales included in the figures.

2016-07-23 Predrag I do not understand the difference between (a) and (b) in figure 13.12 and figure 13.13. Presumably they are time-power spectra
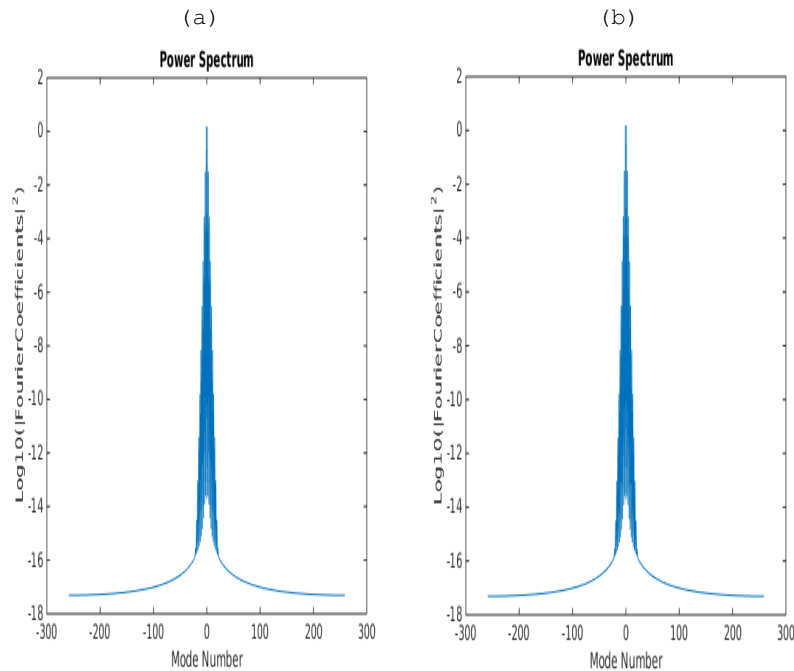
Figure 13.12: Double-sided power spectrum: $\log_{10}|\hat{u}_k^{(0)}|^2$ for initial time-periodic strips (a) $t = [0, 2\,T_{\overline{ppo}_{10.2}}]$ and (b) $t = [0, 2\,T_{\overline{ppo}_{10.2}})$ where the number of modes is $N = 520$

for time-periodic $u(x_0, t)$ at different fixed x_0?

Matt The difference in (a) and (b) is the figure 13.12 and figure 13.13 was based on Burak's recommendation to check and see whether having $t = [0, 4T]$ vs. $t = [0, 4T)$, (the latter being correct) had an impact on the amplitude spectrum / power spectrum. I was using MATLAB's absolute value feature $abs()$ so I'm certain they are being calculated the correct way.

Why are they oscillating wildly? Are you really looking at complex amplitudes when you write $|\hat{u}_k^{(0)}|^2$, or are you squaring the imaginary and real part separately? It looks like your even modes mean something, and all odd modes are vanishing. That is probably not good, as do not see off hand why $\hat{u}_0$ should be vanishing, for example.

Matt 2016-07-25 I'm still confused as to this oscillation as well.

Matt 2016-07-26 The rapid oscillation of figure 13.12 seems to only occur for the Fourier Coefficients of temporal FFT of $1st$, and $16th$ configuration space points when a resolution of 32 points is used. The other sets of Fourier Coefficients seem to be better behaved, i.e. much less oscillatory but not completely monotonic.
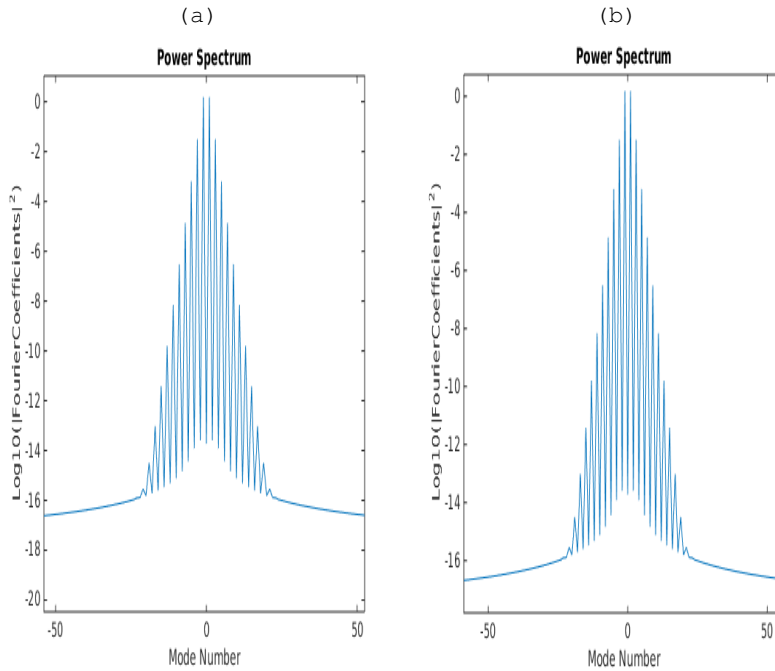
Figure 13.13: Double-sided power spectrum: $\log_{10} |\hat{u}_k^{(0)}|^2$ for initial time-periodic strips (a) $t \in [0, 2\, T_{\overline{ppo}_{10.2}}]$ and (b) $t \in [0, 2\, T_{\overline{ppo}_{10.2}}]$). This is the same as figure 13.12 except zoomed in to show ≈ 100 modes. Note: The windowing is slightly off between the two as I did this by hand.

> Then again, it might be a peculiarity of the orbit being pre-periodic orbit, though I do not see how symmetry under a spatial reflection transfers into vanishing temporal Fourier modes...
>
> No matter, figure 13.12 tells you that $N = 520$ is vastly too many modes, something like $N = 20$ should suffice.
>
> **Matt 2016-07-25** I took N to be different from the number of configuration space points was mainly for testing to see if the amplitudes behaved as expected, i.e., decaying exponentially.

2016-07-23 Predrag So the problem with your integrand is elsewhere, perhaps in the normalization of the nonlinear-linear term?
Matt I'm still trying to figure out the problem, but I don't believe it has to do with the normalization of the nonlinear term. The evidence for this is that I can compute the nonlinear term using multiple methods: MATLAB's built-in convolution function, a convolution sum, and manual fully-spectral calculation and they all yielded the same results.

2016-07-23 Predrag Above, on 2016-7-14, you write that $u(x, t)$ is not well-
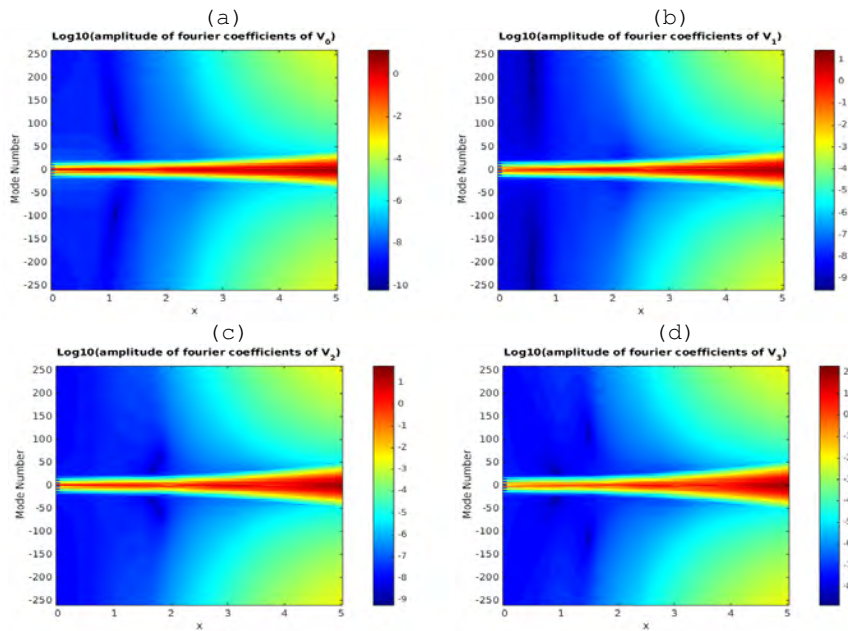
Figure 13.14: Spatial integration $x = [0, 5]$ of temporal Fourier mode amplitudes plotted on a $\log_{10}$ scale. Each vertical strip is a fast Fourier transform of a time periodic strip $t = [0, 2\,T_{\overline{ppo}_{10.2}})$ provided by `ksint.m`. (a) $\hat{u}_k^{(0)}$, (b) $\hat{u}_k^{(1)}$, (c) $\hat{u}_k^{(2)}$, and (d) $\hat{u}_k^{(3)}$.

behaved "due to the first equation of (1.36) being dominated by the term $\hat{u}_k^{(2)}$." I do not see that.

2016-07-23 Predrag $u_x(x, t)$, (b) $u_{xx}(x, t)$, and (c) $u_{xxx}(x, t)$ of figure 13.9 seem to go to a spatial limit cycle of fixed spatial frequency, except $u(x, t)$ is drifting off in amplitude. Cannot be right...

2016-07-23 Predrag I do not see why would you use N different from $T/\Delta t$, where Δt is your (Xiong's?) time discretization? It is a discrete Fourier transform of a discrete periodic lattice, so the number of Fourier modes should strictly equal the number of configuration space points, right? As in sect. 4.2, and confirming your observation: "The optimal (smallest amplitudes) number of modes seems to be equal to the number of time steps."

Matt 2016-07-25 If the configuration space has 520 discretized time points, would it not be correct to take $N = 520$? I don't believe fewer time steps suffice for Xiong's integrator. When I tried in the past to take 128 steps, for example, it would produce poor results (not periodic in time).

Predrag 2016-07-26 That is true of the integration - the orbit is unstable. However, once you have the point on the orbit, which is quite smooth, a

smaller number of Fourier modes might do the job to the machine accuracy (as you see in your power plots). Try using every second point, ie $N = 260$, see what it's power spectrum looks like.

BTW, you should redo Xiong's integrations by using $N = 2^m$, to be able to exploit FFT. Best to discuss this with Xiong.

2016-07-23 Predrag To me the plots in figure 13.14 all blow up at the same time, not $\hat{u}_k^{(3)}$ blowing up first. More worrisome is that high frequencies all grow, meaning the spectrum is flattening out, so there is some singularity (a step?) growing in $u(\cdot, x)$ with increasing x. That should not happen, the correct $u(\cdot, x)$ is smooth for all x.

2016-07-23 Predrag I am stumped, I cannot think of a good test of your spatial integrator. You could try to reproduce equilibria of refs. [12, 27, 30, 34] - that would only have the zeroth Fourier mode in your integration of $\hat{u}_0^{(i)}(x)$, i.e., you would test your PDE integrator on time-independent initial condition.

I do not see anything wrong with the spatial evolution (1.34), except I'm puzzled that I do not remember ever having read that one can trade in a temporal evolution for spatial evolution on a spatiotemporally periodic domain (a 2-torus).

I suspect there are still errors in the way (1.34) has been coded...

2016-07-25 Matt : Still trying to figure out any fixes I can apply to my code. Began outlining/drafting for report due next week.

2016-07-26 Matt ErrorHunting Started looking at parts of the code that I may have been taking for granted. I thought most of the problems were arising from normalization issues, error tolerances, frequencies, spectral methods, and the actual integrator, `ode15s`, so that's where most of my time has been spent. Having still not achieved spatial integration for $x \in [0, 22]$, I've been picking through everything for a while now to see if there's something I might have been taking for granted or overlooked.

Previously, I had checked the results from the time integrator by reproducing figure 13.3 in figure 13.4. Also, as an secondary check of periodicity, I plotted orbits in $u(x, t)$, $u_x(x, t)$, $u_{xx}(x, t)$ coordinates, and other combinations such as $u_x(x, t)$, $u_{xx}(x, t)$, $u_{xxx}(x, t)$ just to see if the time-integrated data formed a closed orbit, which they appeared to.

This being said, it seems I was unaware that checking the periodicity of derivatives calculated by spectral differentiation in (4.28) was insufficient. The derivatives don't seem to demonstrate the actual rates of change of $u(x, t)$, which might be why the spatial integration could be blowing up. As one can see in figure 13.15. (Apologies
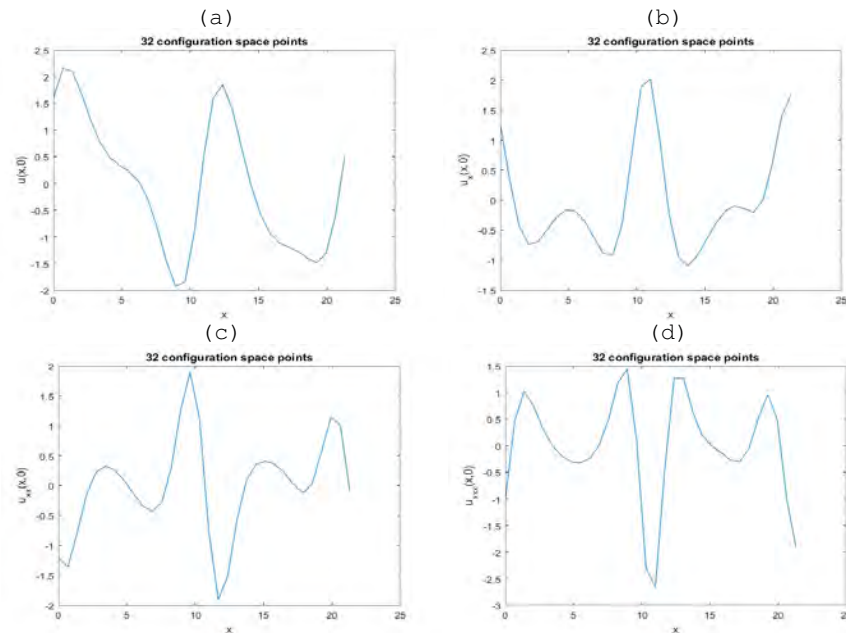
Figure 13.15: Results from Spectral Differentiation method (4.28) and comparison to $u(x,t)$. (a) $u(x,t)$, (b) $u_x(x,t)$, (c) $u_{xx}(x,t)$, and (d) $u_{xxx}(x,t)$.

> for the custom paint job on the figures, I realized that the titles were incorrect after leaving the office.)
>
> I found in fftderiv that one needs to treat the even and odd numbers of derivatives differently in terms of the form the wave numbers need to take, c.f. **Algorithm 1 Algorithm 2**. When applying this to my code it didn't change the results from the spectral differentiation.
>
> Burak pointed out I was making a mistake. Updated the figures in response.

> **RegardingPCpost** (I will also put these comments in the appropriate place in regards to the correspondence of the previous couple days.) The rapid oscillation of figure 13.12 seems to only occur for the FFT corresponding to the $1st$, and $16th$ configuration space points when a resolution of 32 points is used.

2016-08-08 Matt Was Ill for the majority of last week so I didn't accomplish much outside of my report, hence the lack of blog posts.

> **Dealiasing** Instead of the so called "3/2 rule" delaliasing method (where the nonlinear term is computed on a larger grid created by zero-padding arrays), I applied the so-called "2/3 rule" where the values of the highest $1/3$ of Fourier coefficients are set to zero when calcu-

lating the nonlinear term of (1.36). Got the idea from arXiv. This did not seem to help in any way after testing.

Equilibrium test Tested spatial integration for initial condition that was constant in time (i.e. only nonzero Fourier coefficient was the $0th$ mode. I wasn't completely sure what to do for the initial conditions of the spatial derivatives so I assumed they fell under the same condition. I tested with multiple sets initial values for the derivatives (the zeroth modes $\hat{u}_0^i \quad i = 1, 2, 3$). When all of the derivatives were set to zero, there was no change in $u(x, t)$ (done as a sanity check). When the initial conditions for the spatial derivatives were taken from the time integration the values of $u(x, t)$ (constant in time but not space) oscillate between negative and positive values before escaping to $-\infty$. The amplitude of the Fourier coefficient $\hat{u}_0^0$ was the only nonconstant value.

FutureWork I'm unsure where I should proceed from here. I am still searching for further improvements to my code but I am really running out of ideas, other than scrapping the integration routine I am running and *trying* to apply the ETDRK4 schema from ref. [24]; which I'm not sure can even be applied.

MeetingRocklin Made plans to talk to Prof. Rocklin this Wednesday.

2016-08-10 Matt MeetingWithZeb I met with Professor Rocklin as was planned. We discussed topological transformable materials and their implications and properties. The primary topic of this discussion was *floppy modes*. Which are soft deformations of the system with small energy costs. This is done in order to create materials whose mechanical properties can change by means of such a transformation. We touched on other topics as well such as elasticity theory and amorphous materials. Papers read/skimmed: arXiv:1512.06839v1 [cond-mat.soft], arXiv:1510.04970v1 [cond.mat.mes-hall], arXiv:1403.0936v1 [cond-mat.soft].

KSspaceint I've been looking for more ways to change my code/find methods that are of use in spatial integration, looking for different ideas across the internet and in ref. [52].

Tested whether or not the higher modes are corrupting the lower modes by doing different tests; namely forcing higher modes to be equal to zero. This had no effect on the evolution of the lower modes who are so dominant the behavior of $u(x, t)$ was also unchanged.

Did more testing on the $2/3 - rule$ dealiasing scheme. This showed marginal improvements over no aliasing, but it is better than the $3/2 - rule$ because it's cheaper computationally.

2016-08-11 Matt KSspaceint Looked at the spatial evolution of $u(x, t)$ in a new way today in hope to get some new idea on how to make some progress. I made the integrator plot $u(x, t) = N\mathcal{F}^{-1}\left(\hat{u}_k^0\right)$ at every

step and watched it like an animation. What I observed was that $u(x,t)$ is seemingly unchanged until some critical point where the field seems to destabilize, at which point the field inverts itself, and then at (usually one or two) a few points diverges towards infinity. I investigated this further by introducing some parameters into equation (1.36). The most notable result from this experimentation was that the equations became more stable after making the contribution of $\hat{u}_k^2$ larger in comparison to the other terms in,

$$\frac{\partial}{\partial x}\hat{u}_\ell^{(3)} = -i\omega_\ell\hat{u}_\ell^{(0)} - \hat{u}_\ell^{(2)} - \sum_{\ell'=-\infty}^{\infty} \hat{u}_{\ell-\ell'}^{(0)}\hat{u}_{\ell'}^{(1)},$$

which I was not expecting due to how the terms behave in time integration.

Windowing Looked into applying a windowing function in order to deal with spectral leakage and any discontinuities present; had little effect on the integration process but completely corrupted $u(x,t)$. At least I learned something I suppose.

ErrorCorrection I realized through my animation method described above that the integrator was mishandling the initial conditions which caused a couple of figures to display backwards time-behavior over spatial integration, e.g. figure 13.10. I have uploaded new figures which should be correct.

2016-08-15 Predrag I do not quite understand "until some critical point" (you mean a value of the integration coordinate x?) and "at (usually one or two) a few points diverges towards infinity" (you mean values of time t?) while looking at $u(x,t) = N\mathcal{F}^{-1}\left(\hat{u}_k^0\right)$, but that might be a hint that there is something seriously wrong with the concept of integration of these equations along the spatial coordinate. But why then can one integrate it for the $T = 0$, i.e., equilibria?

I have not yet put together sect. 1.5 and sect. 1.6, and recast the problem of finding a periodically repeating spatio-domain as a fixed point condition, like Boris likes to do (allegedly - I have not seen the formulas for the fixed point Jacobian matrix yet), but:

There are two ways of solving differential equations. One is as integrate-forward problem, with given initial conditions - that is what we are trying to do now.

The other is as a variational problem, where one makes a guess loop [9, 29] (for a periodic orbit) or a guess torus [28] (for an invariant torus, such as we search for here), and then defines an error function that measures the integral squared of the local deviation of the tangent space to the guess from the tangent space as defined by the equations of motion at the point. That is guaranteed to converge by Newton descent, for a decent

enough initial guess (and our guess is the numerically exact solution). The stability is $1 - J$, and Boris says that its determinant does not care whether one integrates time or space. Still not obvious to me, but feels right.

What I am saying is that I still worry that your code has an error, such that locally the tangent fields are not as given by the (instantaneous) equations of motion. If there is any error in that, the integration must go awry. Concretely, if tangents to surface your integrator sweeps out by integrating the initial time-periodic state do not agree with the tangents to the exact solution (the instantaneos equations of motion), the code has an error. That is a *local* test, it requires no integration.

2016-08-16 Matt Testing Did more code testing yesterday and today, but no progress to report.

Report Small additions and edits to `reportMNG.tex`.

Reading Began parsing through the literature on (variational) Newton descent, specifically refs. [9, 29] and for invariant tori ref. [28].

MattToPC The derivatives at this stage are be calculated by spectral differentiation method, if I'm understanding you correctly you're saying if my tangent fields are wrong then the integration cannot proceed correctly, which I agree with. Do we know of a way to check this outside of something like finite difference methods?
Predrag 2016-08-19 Wish I knew. Whatever goes into the integration subroutine as the equations to integrate must (instantaneously, or in one integration step) satisfy (12.2) and (12.25).

2016-08-18 Burak to Matt:

If I'm not mistaken, you have been trying to use Matlab's built-in integrators most of the time. My suggestion for you is to look for implicit integrators used for Hamiltonian systems, which are symmetric under time-reversal. We have an analogous situation here since we have space-reversal symmetry. You can start with the implicit midpoint method.

2016-08-18 Predrag I would not use much time on improving integrators at this stage (the flow is not Hamiltonian, but there is lots of literature on time-reversal invariant dynamical systems - ref. [3, 25, 26] are a few examples). We either have a bug in the code, or there is something seriously amiss about the whole idea. First we need to go step by step through the code, then someone re-derives the equations and writes an independent code from the scratch. If two independent codes produce the same trajectories, then we need to rethink the whole idea.

2016-08-18 Matt :

MNGtoPC Would it be worthwhile to write up a step-by-step summary, i.e. a walk-through, of my code and perhaps add it to my report?
Predrag 2016-08-19 Hope not - seems like too much work...
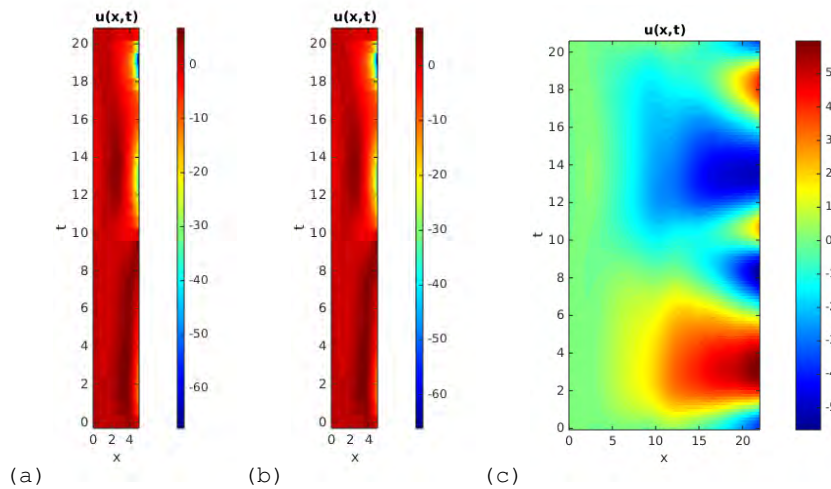
Figure 13.16: Spatial integration $x \in [0,5]$ comparison of integrators (a) `ode15s` and (b) implicit midpoint method. Initial condition was a time strip of $\overline{ppo}_{10.2}$. (c) Spatial integration $x \in [0,22]$ using values for $u_{xxxx}(x,t)$ acquired from spectral differentiation as opposed to evaluation of the Kuramoto-Sivashinsky equation. The implicit midpoint method was employed as the integrator as I found it easier to control the step size.

ImplicitMidpointMethod According to figure 13.16 (a) and (b) my implementation of the implicit midpoint method generates the same results as ode15s, albeit at a slower pace. The figure includes spatial integration data for $x \in [0,5]$ using the same initial condition as usual, a time strip of $\overline{ppo}_{10.2}$.

AnotherTest I decided to test my integrator with one more (final?) method. Instead of evaluating the Fourier coefficients $\hat{u}_k^{(3)}$ corresponding to $u_{xxxx}(x,t)$, during the integration process using the Kuramoto-Sivashinsky equation, I generated them by means of spectral differentiation using the initial condition.

I acknowledge that I am bypassing the entire point of my project but I just figured I might as well test this case as I thought it might demonstrate whether the accuracy of the derivatives I have been using all along has been adequate. Sadly, not even this test will reproduce the $\overline{ppo}_{10.2}$ orbit, as can be seen in figure 13.16 (c). I believe that this indeed shows that the inaccuracy is playing a larger role than I might have initially anticipated, as even the values for the derivatives taken directly from the time integration were inadequate in reproducing the orbit. I used a spatial discretization of 1024 configuration space points in order to help smooth out the derivatives for spatial integration, i.e. $x_n = n\,22/1024$, $n = 0, 1, \ldots, 1024$.

2016-08-19 Predrag Figure 13.16 (a) and (b) are sure going off the charts: $u(x, t) \to -65$. Flummoxed.

2016-08-20 Matt : There are two different programs one can apply to regarding working at UC Santa Barbara.

> **Graduate Fellowship Program** According to Graduate Fellowship Program the process of the applying to the graduate fellowship program is as follows: the *advisor* is required to fill out a nomination form consisting of the personal information of the student and a short letter of recommendation for the program and acknowledge the **minimum five month** stay at UC Santa Barbara. (The student can also stay up to 6 months). They support up to four graduate students at a time, either in Summer (July-December) or Spring (January-June).
>
> The student is reimbursed up to 2100 dollars a month for housing and food; there is also a rather ambiguous statement about round-trip travel "some assistance can also be provided".
>
> The deadline for nominations for the January-June stay is September 1st, while the deadline for the July-December stay is February 1st.
>
> **KITP Affiliate Program** I couldn't find a page describing this program other than the actual form itself Affiliate Program Form; wherein it requires the advisor's information/stay information, information about the student or postdoc, and the proposed stay for the student or postdoc. This is supposed to be a minimum of three weeks. If there is a plan for the student/postdoc to stay greater than or equal to six weeks financial support can be requested.
>
> The main requirement is that the advisor has already received an invitation; I could not find deadline information pertaining to this form; any questions are supposed to be sent to the director of the program via Contact Director. I sent a message via this link requesting the deadline information.

2016-08-20 Matt : With help of Lan and Cvitanović [29] I rederived,

$$\frac{\partial^2 \tilde{x}}{\partial s \partial \tau} - \lambda A \frac{\partial \tilde{x}}{\partial \tau} - v \frac{\partial \lambda}{\partial \tau} = \lambda v - \tilde{v}$$

in order to get a better understanding of all of the working pieces and where the terms originate from.

From what I understand, a guess loop (which is required to be a relatively good guess to a periodic orbit) is parameterized/discretized with variables s_n (which has to be done carefully to avoid clumping, which would destroy the numerical smoothness). The periodic orbit is discretized with variable t_n. Each point on this guess loop, L, has two important vector quantities associated with it, namely, the loop tangent $\tilde{v}$ and the flow

velocity v. A cost functional is minimized such that after a process of continuous deformations parameterized by fictitious time variable τ the two vectors converge in the limit of the loop L approaches the periodic orbit. The magnitudes of these two vectors are matched with a scaling coefficient $\lambda = \frac{\Delta t_n}{\Delta s_n}$.

If I am understanding this correctly, in the scope of my problem, if a time periodic orbit is taken to be the initial guess loop, then the flow velocities take over the role of loop tangents, and the flow velocities role is replaced with the corresponding spatial derivatives.

While I haven't begun the actual implementation of this I'm sure there are some subtleties that I am missing out on, I especially have my doubts about whether the form of variational equation should look the same as the role of time is being replaced by a spatial variable, although perhaps I'm supposed to merely view them as means by which the loop is parameterized.

The part that troubles me is that as far as I see this will not enable spatial integration of infinite extent because the end result would be a spatially periodic loop if functioning properly, but for my purposes this is better than getting no results i.e., where my project currently stands with direct spatial integration in Fourier space.

2016-08-22 Predrag The periodic orbit examples [9, 29] illustrate the Newton descent idea. The power of the method is that arbitrarily long, arbitrarily unstable long cycles can be found (see the long Kuramoto-Sivashinsky orbit in Fig. 6 (d) of ref. [30]; also $T = 0$ spatial periodic orbits of Sect. III could not have been found without the Newton descent). In our project we are interested in determining a doubly-periodic time- and space- translation invariant torus from a guess torus. An example, admittedly a pretty mild one, is worked out in ref. [28].

2016-08-22 Matt :

MeetingWithPC Discussed the variational Newton descent in the case of spacetime torus. Briefly mentioned the motivation in regards to its benefits of stability versus integration procedures. The main idea is that there are two tangent spaces defined at each spacetime point. My goal is to formulate fictitious time integration that minimizes a cost-functional between these two tangent spaces.

This process will be implemented by minimizing the angle of separation between the tangent hyperplanes defined by the two tangent spaces. In order to have computational progression and not stall out, I must decide on a method of symmetry reduction in order to break both continuous symmetries present in the problem at hand: time and translational symmetries. By doing so I will force the system to evolve in a "tranverse" direction, i.e. the direction of interest.

Variational Newton Method for spacetime torus We begin with an initial condition that takes the form of a spacetime torus. In my case, this will specifically be the short periodic orbit $\overline{ppo}_{10.2}$ of the $L = 22$ Kuramoto-Sivashinsky system. The state space points $\mathbf{x}$ will be parameterized by [6] $\mathbf{s} = (s_1, s_2, ..., s_m) \in [0, 2\pi]^m$ such that

$$\mathbf{x}(\mathbf{s} + 2\pi\mathbf{k}) = \mathbf{x}(\mathbf{s}) \quad \text{for all} \quad \mathbf{k} \in \mathcal{Z}^m.$$

The torus we are searching for will be an invariant set of the mapping

$$\mathbf{f}(\mathbf{x}(s)) = \mathbf{x}(\mathbf{s} + \omega(\mathbf{s}))$$

where ω is the parametrization dependent shift. With this initial condition, a fictitious time parameter τ is to be defined such that it parameterizes a continuous transformation between the initial guess torus and the torus invariant under the mapping (homotopy?).

The fictitious time evolution will be defined by the minimization of a cost functional [7]

$$\mathbf{F}(\mathbf{s}, \tau)^2 = (\mathbf{x}(\mathbf{s} + \omega(\mathbf{s}, \tau), \tau) - \mathbf{f}(\mathbf{x}(\mathbf{s}, \tau)))^2 \qquad (13.8)$$

2016-08-23 Matt : Still trying to understand the variational Newton descent;

What I originally thought was that given the initial condition, the time integrated solution $\overline{ppo}_{10.2}$ (thanks for the ghostbusting) defined on an $N \times M$ grid. N is determined by the spatial resolution/discretization and M is determined by the number of time steps in the integration process. For computational speed, N and M should be taken to be powers of 2 to exploit the speed of MATLAB's FFT algorithm.

For simplicity it's probably best to have $N = M$, but for the sake of unambiguous subscripts I will keep it as M for the time being. [8] By doing so, the parameterization / discretization of the initial condition becomes, [9]

$$\mathbf{s} = (s_1, s_2) = (x_n, t_m)$$

where $x_n = \frac{nL}{N}$ and $t_m = \frac{mT}{M}$ for $n = 0, \dots, N-1$ and $m = 0, \dots, M-1$.

With this discretization, I believe the tangent space defined over the discretization and in terms of space and time Fourier modes becomes:

$$\mathbf{v}(\mathbf{s}, \tau) = \begin{bmatrix} i \sum_k q_k a_k(\tau) e^{iq_k x_n} \\ i \sum_j w_k b_k(\tau) e^{iw_k t_m} \end{bmatrix} \text{ where, } \quad q_k = \frac{2\pi k}{L}, w_j = \frac{2\pi j}{T} \qquad (13.9)$$

---

[6] Predrag 2016-08-22: that presupposes a very special parametrization, where all s_i sit on unit circles. For example, the curvilinear length $ds = (\sum_i (dx_i)^2)^{1/2}$ is not normalized like that.

[7] Predrag 2016-08-22: Have not wrapped my head around (13.8) yet

[8] Predrag 2016-08-24: please keep N and M distinct. Ideally, use the same letters that Cats use in the spatiotemporal cats project

[9] Predrag 2016-08-24: please use a different letter for space length s_1

with $k = -N/2 + 1, \ldots, N/2$ and $j = -M/2 + 1, \ldots, M/2$.

There are a number of things I am getting very confused with. At first I thought I was going to be performing fictitious time evolution such that a cost functional involving the tangent space of the evolving torus and the tangent space of an invariant torus would be minimized. In other words, I thought I would use the definition for the tangent space in (13.9) and evolve the torus until

$$\mathbf{v}(\mathbf{s}, \tau) = \begin{bmatrix} \sum_k \dot{a}_k(\tau) e^{iq_k x_n} \\ i \sum_j w_j b_j(\tau) e^{iw_j t_m} \end{bmatrix} \tag{13.10}$$

where $\dot{a}_k$ is calculated from the representation of Kuramoto-Sivashinsky equation used for the time integration of the spatial Fourier modes (13.1). This is what I thought at first, but by doing so I will be neglecting (1.36) in this process, although I don't see how to incorporate (1.36) as this would introduce four independent variables for the temporal Fourier modes, making my 2-torus into a 5-torus?

2016-08-24 Predrag It does not matter how many dimensions it is embedded in, and how many first-order equations you have, the torus is 2-dimensional, one dimension for each continuous symmetry. It's tangent space is a 2-dimensional plane embedded in your $N \times M$ dimensions. You compute it by doing infinitesimal shifts in time and space, i.e., by taking derivatives... I think.

2016-08-24 Matt Also by keeping the second component constant I believe I'm ignoring parts of the dynamics. [10]

One of the other reasons why I believe I don't understand what's going on is because in Lan's paper [28], his formulation of the cost functional (13.8) includes the difference between the mapping **f** and the state space representation of the torus **x**. I'm quite confused how to formulate the mapping in this circumstance, unless this is exactly the point, meaning that it's numerically determined by the fictitious time evolution of the Jacobian matrix.

In short, I still have a lot of work to do in order to understand this method.

2016-08-24 Matt : Spent the day reading Schilder *et al.* [48] and rereading ref. [9], Lan and Cvitanović [29], as well as ref. [28] in hopes of better understanding this method.

In regards to some of the statements in my blog post yesterday; for a torus to be invariant after the application of **f**, which is the criterion that we're using to guide the fictitious time evolution according to ref. [28], the only intepretation my brain can think of is that **f** represents the tangent space

---

[10]Matt 2016-08-24: I believe this is okay as the Fourier coefficients depend on the fictitious time τ so it's not holding anything constant in actuality.

of the torus that results from this fictitious time evolution. If so I feel like maybe I was a little hasty in my judgment of the equation I came up with for the mapping **f**, namely (13.10).

For a little more investigation of (13.8), I believe the reason behind the ω in the term $\mathbf{x}(\mathbf{s}, \omega(\mathbf{s}, \tau), \tau)$ is that the orbit reached by fictitious time evolution *could* be a relative periodic orbit as opposed to a pre-periodic orbit. In this case the application of the **f** would not leave the orbit unchanged after one period until the corresponding shift is taken into account? That is of course if my interpretation of **f** is indeed the flow field. The only other idea I've been able to think of is some sort of circle map that permutes items around the discretization.

This is why I still don't understand why **x** is in (13.8) as opposed to **v**.

On how one can handle this quantity, ω, it may or may not be fixed a priori, and one can use the following rules: for a fixed shift equal to ω one must require

$$0 = \frac{\partial \omega}{\partial \tau} \tag{13.11}$$

while for searching for an torus of a "given topology", one must employ what Lan refers to as the *phase condition*

$$0 = \oint ds\, \mathbf{v} \cdot \frac{\partial x}{\partial \tau} \tag{13.12}$$

where **v** is a $[d \times 2]$ dimensional tensor, where d is the dimension of the statespace. **x** incorporates both the spatial and temporal Fourier modes so it is $[2 \times d]$ in size.

2016-08-24 Predrag Sorry, I have to go to bed now, and might not be able to help in days ahead. For specific questions, ask

Yueheng Lan
Home: yueheng_lan@yahoo.com
Work lanyh@bupt.edu.cn
Mobile +86861013520900575
School of Science, Beijing University of Posts and Telecommunications
Skype yueheng_lan

2016-08-29 Matt CodeFromLan Received some code from Lan, trying to interpret it at the moment; I have no experience in Fortran so at best I'm trying to get a sense of what he has done so that I can start to produce my own code.

Readings Still trying to figure out the best way to implement variational Newton descent code. Read Fox [16] *A brief life and death of a torus, computation of quasiperiodic solutions to the kuramoto-sivashinsky equation* and skimmed through a number of papers, with the most time spent on Rasmussen and Dieci [42], and Ge and Leung [19].

2016-08-30 Predrag Thanks for checking the literature! Remember, our torus is much easier than what most literature tries to find - it suffices to find the relative periodic orbit in the time direction, with period *L*, the torus is then swept out by a rigid rotation by *L* in the spatial direction. Finding invariant tori not due to symmetries (like refs. [28, 39, 40] and the above Fox manuscript [16]) is very interesting, but do not work too hard on that right now - our spatiotemporal domain is "trivial" in the spatial direction.

Here, for completeness are some more torus papers: [6, 14, 15, 17, 18, 22, 31, 32, 46–48, 50, 54]. Just to glance at, not necessarily read in any depth.

2015-09-15 Predrag (reposted here from `elton/blog/AdamBlog.tex`)

Reading about robustness of invariant tori. Farazmand likes to refer to Fenichel [13] (to read it, click here). My understanding is that if a stability exponent is purely imaginary, it can destroy a torus at an rational resonance; but if it has a real part (hyperbolic case), there is no way for the Floquet exponent to approach the purely imaginary winding number of the torus, there can be no resonance, and the torus remains smooth and robust for an open interval of the system parameter values.

Figueras and Haro [14] write: "it has been known for a long time that persistence of invariant manifolds is closely related to the concept of normal hyperbolicity [13, 44]. We consider the analogous concept, tailored for skew products over rotations. Roughly speaking, an invariant torus is fiberwise hyperbolic if the linearized dynamics on the normal bundle is exponentially dichotomous, that is, the normal bundle splits into stable and unstable bundles on which the dynamics is uniformly contracting and expanding, respectively. Notice that the tangent dynamics is dominated by the normal dynamics, since the former presents zero Lyapunov exponents. This implies that fiberwise hyperbolic invariant tori are robust and are as smooth as the system [28]. "

Figueras' thesis might be an easier read: click here.

2016-08-31 Matt Bib Skimming Dieci, Lorenz and Russell [10], but I get lost in the mathematical formalism.

KSspaceInt Tried some new ideas but they didn't accomplish anything and weren't very well founded anyway.

TalkWithBoris Had a preliminary meeting with Boris talking about some of the spatial integration results. He said he would think on whether the divergent results are fundamental to the equations and if there is some method to keep the spatial integration bounded without changing the nature of the equations. We scheduled a meeting at 3 pm Thursday September 1st.

Reason behind my confusion: I think the reason why I've been so confused for the past week or so is due to Lan [28] and Fox [16], i.e. I was mixing up two different methods.

I'm going to include what I had already typed up for completeness, but I want to reiterate that I was mistaken on what I needed to do.

- Fox [16] evolution process for a 2-torus involves the use of Poincaré sections to reduce it to a mapping of a 1-torus. The section is taken, due to its simplicity, is normally a hyperplane of codimension 1. This also reduces one of the two continuous symmetries inherent in the problem, i.e., invariance under time translations.

- The remaining SO(2) continuous symmetry can be handled by an additional condition, for instance the "phase condition" in (13.12), which ensures that the "average motion of points in the loop equals zero" [28].

- The initial condition is then taken to be a loop on the Poincaré section; How one decides on the points taken is still unknown to me. I thought they might be generated by just evolving the system in time or space via the equations (1.36) and (13.1) but I'm not sure.

- Together with the initial condition and the Newton descent equation,

$$\frac{\partial x}{\partial \tau}(s+\omega,\tau) + \frac{\partial x}{\partial s}(s+\omega,\tau)\frac{\partial \omega}{\partial \tau}(\tau) - J(x(s,\tau))\frac{\partial x}{\partial \tau}(s,\tau) = f(x(s,\tau)) - x(s+\omega,\tau),$$
(13.13)

one performs fictitious time integration until the maximum of the cost functional (13.8), evaluated over the loop points is less than a certain cut-off threshold.

- The previous part takes a nontrivial inversion of the Jacobian matrix due to it being so large. This was done with a combination of LU decomposition and using the LU-Decomposition to approximate the inverse

Work In Progress/Comments

- Trying to understand why the Jacobian matrix in ref. [28] only has one index, as it is supposed to represent a matrix. Also puzzling to me is how it can be represented as a single Fourier series.

- I'm working on trying to figure out if the Poincaré section formulation will really work for me.

- In a discussion with PC I was told to work with the tangent space in a manner that would involve two different systems of autonomous ODEs. Namely, the spatial evolution equations of (1.36) and the time evolution equations (13.1). I'm unsure if it was meant to just use one of these systems for evolution and then look at the tangent spaces or to use both in some combined

> manner. I imagine I would use one as the spatial and temporal Fourier modes both depend on $u(x,t)$ but I'm not sure if this would just reproduce previous results or would take things a step further.
>
> - Fox [16] mentions that the the function **f** in (13.8) is actually the Poincaré return map, so I'm trying to figure out how one can the deduce the derivatives needed in order to compute the Jacobian matrix.

2016-09-01 Matt : The following is a description of the meeting with Boris and Predrag.

Boris said he hadn't yet looked at my blog for results, but his main concern is whether the problems I have are fundamental or numerical, as are seemingly everyone's feelings about my project.

One of Boris' main suggestions were to check the spatial integration for the zeroth mode, and see what the results are.

Another suggestion was to examine the stability of the $u(x,t) = 0$.

There was much discussion on (13.4) and whether or not there is actually a constant term present that was not previously accounted for. For the specific cat map example it seems that this constant is not present, which is why it had previously eluded Boris. (I think?)

The idea was brought up that somehow the spatial direction reflection symmetry (analogue of time reversal for time direction) was affecting the spatial integration in a manner that has so far been unaccounted for. Also was the idea that somehow the stability in the time-direction would cause instability in the spatial direction; leading to the idea of perhaps taking a smaller temporal domain as the initial condition, much like how one would take a smaller spatial domain in the time-integration process in order to provide stability. Noted in this discussion were the $T = 0$ domain from Lan*et al.* [12, 30] solutions, and the sequence of bifurcations that occur (in time direction) as domain size L is increased.

2016-09-02 Matt Spatial integration of the zeroth Fourier mode Adapted the code for spatial integration of the zeroth temporal Fourier mode. Because this is a purely real quantity, one can plot the amplitude versus spatial variable x, as can be seen in figure 13.17. The integration blows up ($\hat{u}_0^{(0)} \to -\infty$) at $x \approx 12.292453$, so in order to capture what happens before this divergence the plot represents the value of the zeroth Fourier coefficient for $x \in [0, 11]$.

2016-09-02 Predrag To me your initial version of the spatial stability matrix (13.14) looked too diagonal - it is all off-diagonal, I tried to rewrite it in (1.40) (also, more logically, in the increasing order of $\hat{u}^{(J)}$). (has been fixed since I wrote the above comment). However, Boris has a quick way to the eigenvalues in terms of a quartic equation, he'll show you how. Basically,
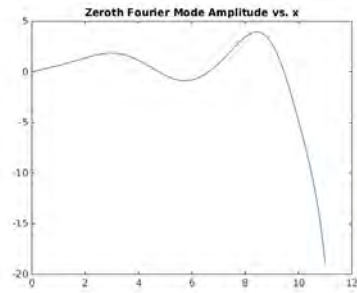
Figure 13.17: Value of the zeroth Fourier coefficient versus the spatial variable x for spatial integration $x \in [0, 11]$. The initial time-periodic loop was retrieved from time integration of Kuramoto-Sivashinsky equation using `ksint.m` over $T = [0, 2\,T_{\overline{ppo}_{10.2}}]$ using 1024 steps.

in spatial evolution we seem to have a repeller, not a strange attractor, and all spatial evolution will take off to infinity, unless we ensure it is staying on the repelling set. We kind of know that already from the $T = 0$ spatial evolution.

2016-09-02 Matt Stability of u=0 equilibria By rearranging the system of ODEs of (1.36), the velocity gradients matrix A evaluated with $u = 0$ takes the form,

$$A(\mathbf{0}) = \begin{bmatrix} 0 & 1 & 0 & 0 \\ 0 & 0 & 1 & 0 \\ 0 & 0 & 0 & 1 \\ Diag\{-i\omega_k\} & 0 & -1 & 0 \end{bmatrix} \tag{13.14}$$

[11] where each entry is of size $N \times N$ where N is the number of temporal Fourier modes kept in the truncation. (i.e. $1 = I_N$) and $\omega_k = \frac{2\pi k}{T}$ for $k = -N/2 + 1, \ldots, N/2$.

The eigenvalues (stability exponents $\lambda^{(j)} = \mu^{(j)} + i\omega^{(j)}$) of this stability matrix for a system of 32 Fourier modes (i.e. the size of $\mathbf{A} = [128 \times 128]$) can be categorized in the following manner:

- 60 stability exponents with positive real parts, $\mu^{(j)} > 0$, with the largest being the complex conjugate pair $\lambda^{(\pm)} \approx 1.1985 \pm i0.6154$

- 60 stability exponents with negative real parts, $\mu^{(j)} < 0$,

- 2 stability exponents equal to zero (up to machine precision).

- 2 purely imaginary stability exponents, $\lambda^{(j)} = 0 \pm i$

---

[11]Matt 2016-09-05: Sleep deprivation : I had originally written this in the wrong order because it looked pretty
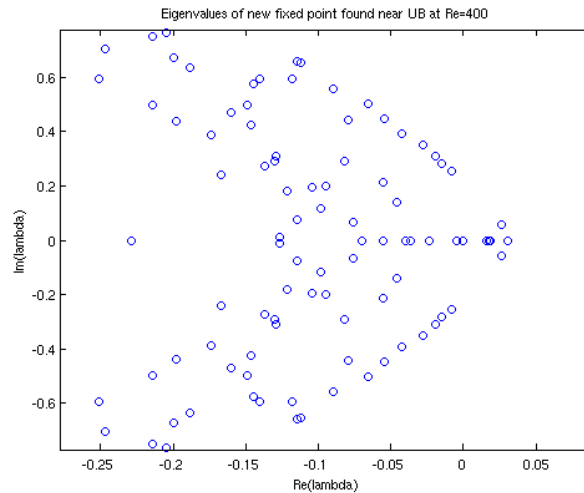
Figure 13.18: Stability eigenvalues spectrum for one of the plane Couette flow equilibria studied by Halcrow, Gibson and Cvitanović (unpublished). Just an example of the spectrum, not the one we are studying here.

2016-09-08 Predrag This numerical spectrum looks like what Boris would expect from his quick way to get the eigenvalues in terms of a quartic equation, I guess you two have not talked about it yet. You do not mention it, but the negative exponents are the reflections of the positive ones, you might want to arrange j range in such a way that $\mu^{(-j)} = -\mu^{(j)}$. You should get exact analytic formula for this spectrum as a solution of a quartic equation.

The easiest way to survey the spectrum is to plot it the (μ, ω) plane; as an example I take a random stability exponents plot from my plane Couette flow work with Gibson and Halcrow, figure 13.18. That flow is dissipative (no "time"-reversal invariance), so you expect a few expanding (positive) exponents, few marginal due to symmetries, and infinity of negative ones. In the case at hand, spectrum is symmetric under $\mu^{(-j)} = -\mu^{(j)}$, so it will suffice to plot the $\mu^{(j)} \geq 0$ half-plane.

By the way, do not plot multipliers Λ_j for equilibrium solutions in the complex plane like Marcotte and Grigoriev do. That is nonsensical for equilibria; to get a multiplier, you have to pick a (totally arbitrary and unnatural) T in the formula $|\Lambda_j| = \exp(T\mu^{(j)})$.

2016-09-02 Matt Predrag stopped in to see how I was doing and asked me to also determine the eigenvalues of the stability matrix for the zero-mode only system i.e. the eigenvalues of the $[4 \times 4]$ stability matrix, in order to verify whether the spatial integration results of figure 13.17 are valid. My question, is where the stability matrix should be evaluated, presumably

near the point of divergence? i.e. ($x \approx 12.292453$)?

2016-09-08 Predrag $u(x, t) = 0$ is an equilibrium both in the temporal and spatial direction. So I would first look at stability eigenvalues (stability exponents) of the spatial stability matrix on the $T = 0$ temporal "strip", along the x axis. That is, first the zero with temporal strip, than a small T temporal strip. Not sure about this...

2016-09-02 Predrag I guess I do not know what figure 13.17 means. I meant that if you start with $T = 0$ spatially periodic profile (but not changing in the time direction) its evolution is given by 4 ODEs, uncoupled to evolution for any other initial time. So you need it to initialize the four $u^{(I)}(0, t)$ with precise values corresponding to one of our equilibrium or relative equilibrium points, the same four numbers for *every* t. For that you need to use one of our equilibrium or relative equilibrium solutions, not the relative periodic orbit $\overline{ppo}_{10.2}$. After Fourier transform one still has 4 precise numbers $\hat{u}_0^{(I)}$, and the rest of Fourier components vanishes.

2016-09-06 Matt KsSpaceInt Performed spatial integration on a time-strip from one of the equilibrium solutions of Kuramoto-Sivashinsky equation , received from Xiong's data file `ksReqx32.h5`. I believe that this corresponds to E_1 of ref. [8], due to the label in the data file. I can't seem to locate my flash drive that had the plot on it, but the general procedure was familiar. I took a time-strip of values (now constant) and attempted spatial integration.

The resulting behavior was a monotonic decrease of the zeroth mode Fourier amplitude to negative infinity, seen in figure 13.19 differing from the result of figure 13.17, where I integrated the zeroth Fourier mode data retrieved from a time strip of $\overline{ppo}_{10.2}$; I think this is worth mentioning because it seems that by using an equilibrium as the initial condition for spatial integration behaves much worse, however this could be idiosyncratic property of the particular time strip used.

2016-09-10 Predrag To me figure 13.19 and figure 13.17 look comparable. Can you replot figure 13.19 as $\log |u(x, 0)|$? I expect that would give you a straight line, whose slope is the leading spatial stability exponent.

2016-09-06 Matt TalkWithPC Discussed the apparent truth that we are dealing with a strange repeller. As I grasp it, this is not necessarily confirmation that my code is performing its duties, there could still be some numerical issues, but the repeller guarantees that these are the death of any attempt to reproduce $\overline{ppo}_{10.2}$. The best way to handle this problem seems to be the variational Newton descent. I currently have Fortran95 code sent to me by Lan that produces invariant tori, but I'm new to Fortran and don't quite understand it. **PC** mentioned I should talk to Lan and ask him about code that produces periodic
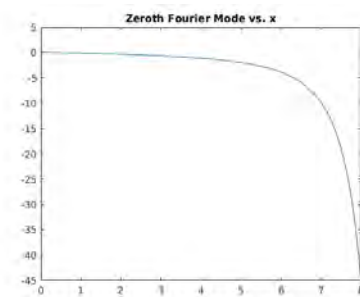
Figure 13.19: Plot of the amplitude of the zeroth temporal Fourier mode coefficient versus x for $x \in [0, 8]$. The initial condition is a time strip of (identical) values taken from the first equilibrium E_1, in the notation of ref. [8].

orbits as opposed to tori for the time being, and to learn Fortran via by my own merits (and perhaps Xiong's).

NewtonDescent Sent an e-mail to Lan asking for direction towards the codes for finding periodic orbits using Newton method.

2016-09-07 Matt Fortran Spent most of the day so far learning how to code in Fortran, trying to walk through some of Lan's codes. I feel like I learned quite a bit; I also ended up finding his Fourier transform code online, as it was taken from *Numerical Recipes*.

I wonder if it would be worthwhile to re-do my spatial integration code in a different language and see if the results are identical. I feel like this wouldn't be too taxing with enough help from *Numerical Recipes* [41].
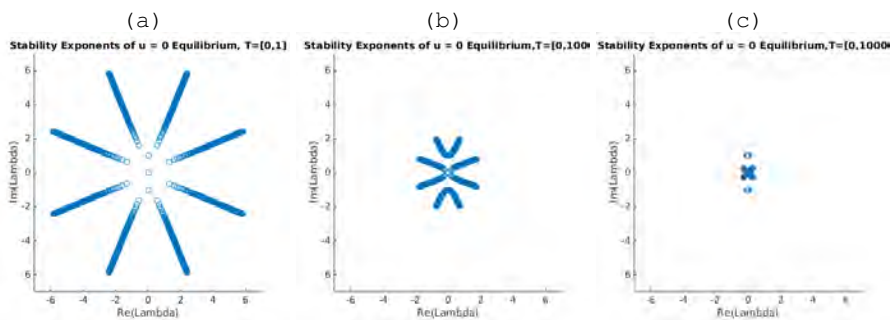
Figure 13.20: $(\mu^{(j)}, \omega^{(j)})$ complex plane plots of the stability exponents $\lambda^{(j)} = \mu^{(j)} + i\omega^{(j)}$ for the stability matrix from (13.14), 512 Fourier modes were kept in each instance, meaning the stability matrix is of size 2048×2048. The temporal extent for each plot is (a) $T = [0, 1]$, (b) $T = [0, 10]$, and (c) $T = [0, 10000]$

2016-09-09 Matt :

Yesterday I was learning Python, gave up on Fortran due to suggestions. I think I should be able to program a variational Newton descent code with a little bit more Python practice.

Stability exponents I'm including three separate plots figure 13.20 of the stability exponents $\lambda^{(j)}$ for the $u(x,t) = 0$. Equilibrium of a temporal strip of differing T, but with the number of modes constant. The only effect that the differing temporal extents have on (13.14) is on $w_k = 2\pi k/T$. In all three figures I've kept 512 temporal Fourier modes, meaning that the stability matrix is of size: 2048×2048.

The temporal extents of each, $T = [0,1]$, $T = [0,100]$, $T = [0,10000]$, were chosen because they elucidate different patterns when plotted on the complex plane; however, I'm not sure if this is meaningful because, again, the different temporal extents only affects the frequencies w_k. Also, 10000 seemed absurdly large but I was curious to what happened at an extreme range.

2016-09-10 Predrag Mhmmm - not sure what to make of $\omega^{(j)}$ in the (μ, ω) plane plots of figure 13.20. Anyway, Boris says assume that eigenvector of the $u(x,t) = 0$ equilibrium is of form $\sin(\omega t)\exp(kx)$ (missing some 2π's and T's), stick it into the Kuramoto-Sivashinsky equation, you get a quartic equation for $\lambda^{(j)}$. The eigenvalues plotted in figure 13.20, their symmetries and their multiplicities presumably follow.

2016-09-12 Predrag to Matt: Does (1.43) explain your figure 13.20? Happy birthday!

2016-09-12 Matt There was a missing factor of $-i$ in the ω_ℓ term in (1.43). It comes from to the time derivative of the Fourier expression for $\hat{u}_{k,\ell}$. I corrected (1.43). I wasn't getting equivalent scatter plots for the solutions to the (initial, erroneous) quartic equation (1.43) and the stability exponents of (13.14), which lead me to find the error.
[12]

2016-09-12 Matt : Thank you for the birthday wishes. It's actually really timely because I have quite good news today.

EqvaStbExp Even with the corrected (1.43), the spectra of figure 13.21 only agree up to an exchange of the real and imaginary parts. I haven't quite figured out why this is, but during my experimentations I found that modifying (13.14) in certain ways produces exciting results.

ModifiedFksX If I introduce a sign change to the identity matrices on the super-diagonal of (13.14), the two formulas for eigenvalues agree. [13]

---

[12]Matt 2016-09-22: Copied the wrong plot to flash drive, will update MNGquareq8 tomorrow
[13]Predrag 2016-09-13: you do not mean "approximately agree," you mean "exactly," i.e., to the numerical accuracy of whatever program you are using to compute the eigenvalues, right?

Figure 13.21: Plots of (a) the spatial stability exponents of (13.14), (b) solutions to the (corrected) quartic equation (1.43). 8 temporal Fourier modes.

Likewise if I changed the sign of the diffusion term in the bottom row of (13.14), the spectra agree.

The really interesting part comes when you apply both of these transformations; it leaves the stability exponent spectrum invariant, leaving me to believe I had stumbled upon some sort of symmetry. The corresponding modified equations (13.15) after such a transformation are as follows (only sign changes),

$$
\begin{aligned}
\frac{\partial}{\partial x}\hat{u}_\ell^{(0)} &= -\hat{u}_\ell^{(1)} \\
\frac{\partial}{\partial x}\hat{u}_\ell^{(1)} &= -\hat{u}_\ell^{(2)} \\
\frac{\partial}{\partial x}\hat{u}_\ell^{(2)} &= -\hat{u}_\ell^{(3)} \\
\frac{\partial}{\partial x}\hat{u}_\ell^{(3)} &= i\omega_\ell\hat{u}_\ell^{(0)} + \hat{u}_\ell^{(2)}\sum_{\ell'=-\infty}^{\infty} \hat{u}_{\ell-\ell'}^{(0)}\hat{u}_{\ell'}^{(1)}.
\end{aligned}
\tag{13.15}
$$

I applied this transformation to my spatial integration equations, and *voila*! They worked, for at least up to $L = 22$, when using a time strip of E_1 as an initial condition. Figure 13.22 are plots of both the time and spatial integration of E_1 from ref. [8]. The spatial integration uses (13.15), the temporal integration uses (1.26).

It should be noted that after the application of a FFT, the Fourier coefficients except the zeroth mode were set to zero (i.e. equivalent to taking a truncation of a single temporal Fourier mode). Failure to do so lead to numerical catastrophe.

It seems that the symmetries are playing a much larger role than I
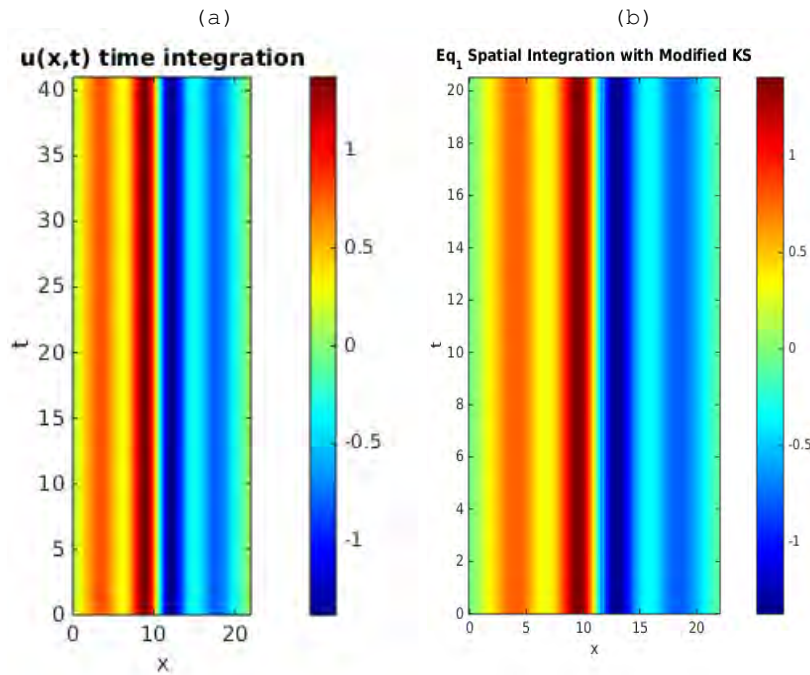
Figure 13.22: Integration of E_1 from ref. [8], periodic on domain $L = 22$, (a) in time, using (1.26), and (b) in space, using (13.15). The initial condition for the spatial integration was the time strip $u(x, t)$, $x = L/2$, $t = [0, T]$, where T happened to be $2\overline{ppo}_{10.2}$, for no particular reason. Also, in order to produce the spatial integration plot, a spatial shift equal to $\frac{68L}{128}$ was employed.

might have believed. I also haven't gotten to the bottom to which of the spectra is the correct representation.

Now of course with every bit of good news comes bad news. I was unable to extend the spatial integration of $\overline{ppo}_{10.2}$ for $x = [0, 22]$. The behavior of the spatial integration of $\overline{ppo}_{10.2}$ did change as can be seen in figure 13.24, however, I believe we still do not have the whole picture.

The initial Fourier transform included 1024 modes, of which all but 32 were truncated. The reason for this is that in order to ensure accuracy in the production of the initial condition via *time* integration, one must take an adequate number of steps. However, there are residual effects due to the non-zero values of the higher modes, therefore another truncation was applied.

All in all, having a pretty good birthday.

2016-09-13 Predrag Nice birthday present to yourself. Congrats. Some of these minus signs come from the Fourier transform conventions, i.e., whether
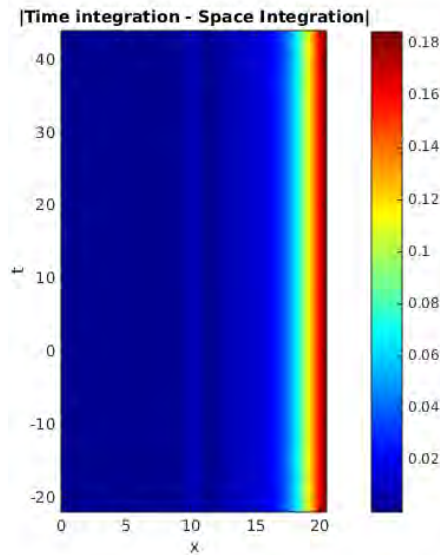
Figure 13.23: Absolute error between time integrated and spatially integrated solutions of Eq_1.

you use $\exp(-iq_k x_n)$ or $\exp(+iq_k x_n)$. Please make sure that conventions we use in chapter 1 and in this blog agree with ref. [8], fix everything accordingly. $\hat{u}_\ell$ are complex Fourier modes, so morally, there perhaps should be a factor $-i$ for every single $\partial/\partial x$ derivative in the definitions of $\hat{u}_\ell^{(J)}$ in (12.26) (not sure that this suggestion makes sense). Fix all formulas accordingly (if Burak or I do not like your redefinitons, we can always revert them, be fearless).

2016-09-13 Predrag Please recheck (1.47). If correct, it agrees with figure 13.21 (b), so there is a problem with the figure 13.21 (a) calculation. They must agree.

2016-09-14 Matt Coding and Misc Rescaled figure 13.22 and figure 13.20 Still working on calculations regarding the stability exponents. Worked out code to reorder stability exponents of (13.14) in ascending order with respect to the real part, likewise with solutions to (1.43) to make sure they are within machine precision of each other, which they are (as long as I swap the real and imaginary parts, which is still an issue with (13.14) that I'm working on).

Fourier Conventions The conventions agree with ref. [8] as far as I can tell, leading me to be somewhat confused. I'll try to be more explicit tomorrow when I get a chance to complete sorting things out.
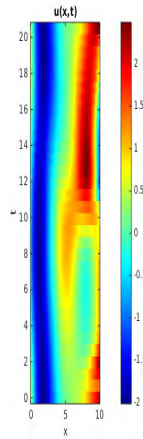
Figure 13.24: Spatial integration using a time-strip solution of $\overline{ppo}_{10.2}$ as an initial condition, located at $x = L/2$. The extent of the integration is $x = [0, 10]$.

2016-09-15 Matt KsSpaceInt There are three different ways to get my spatial integration code to produce the result (b) figure 13.22, which are

1. Use (13.15) instead of (1.36)
2. Take the complex conjugate of initial conditions produced by `ksint.m`
3. Use $-iq_k$ instead of iq_k in the spectral differentiation for producing initial conditions.

For spatial integration of a time strip of $\overline{ppo}_{10.2}$, the equations (13.15) do not seem to be very helpful, meaning my choices are narrowed down to items 2, 3 on the previous list.

I trust Xiong's description of how to reorder the spatial Fourier mode coefficients, but what I'm left with doesn't work either; from the description of the FFT page the spectral differentiation should be iq_k by all accounts.

Quartic equation and stability exponents Realized I made a mistake, it should be a positive factor of i not $-i$ in (1.47) and the like. Even with this correction I still cannot finger the problem behind all of this, it's like there is a missing factor of i that is somehow eluding me, as this would switch the real and imaginary parts (and because all complex stability exponents are coming in complex conjugate pairs, this would fix everything, one need not worry about the sign of the complex part).

2016-09-19 Matt :

ErrorHunting I found a possible reason behind poor spatial integration
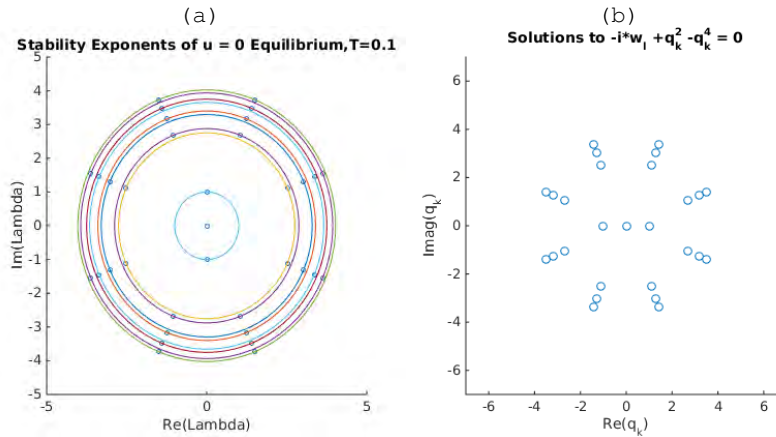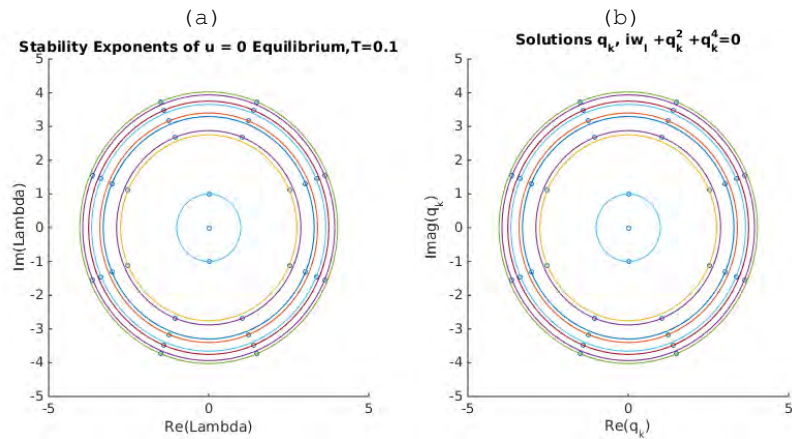
Figure 13.25: Plots of (a) the spatial stability exponents of (13.14), (b) solutions to the (again corrected?) quartic equation (1.43). 8 temporal Fourier modes.

results; While looking at `ksfmetd2.m`, Ruslan's code for Kuramoto-Sivashinsky time-integration, on which `ksint.m` is supposedly based, I noticed when he stores each step of the solver into an array, he separates the Fourier coefficients into their real and imaginary parts, and I believe he means to transpose this array but in fact performs a conjugate transpose on accident. The notation in MATLAB is an apostrophe for a conjugate transpose, and and a period followed by an apostrophe for a transpose, so it's an easy mistake to make. I can't think of any reason to conjugate the time-integrated values of the Fourier coefficients; hence, why I believe this is a mistake.

That being said, I don't know if this somehow carried over into `ksint.m`, but if this is the case, then there is no need for one to use the modified equations (13.15), or to use the different (and conflicting) definition for spectral differentiation, (i.e. the definition would then follow the conventions of (12.19).)

KSspaceInt In figure 13.26, I have plotted what I believe to be the correct version of the time integration of Kuramoto-Sivashinsky, as I really don't see why Ruslan would conjugate the time-stepped Fourier coefficients unless there is something I missed in his code. Along with this is a spatial integration of a time strip (Located at $x_0 = L/2 = 11$ that is a compilation of two separate integrations, $x \in [0, 11]$ and $x \in [-11, 0]$ relative to the location of the initial condition, $x_0 = 11$. Note, there is a small discontinuity where the two separate integrations meet, which is due to even more numerical issues. To produce the plots, I took a truncation of 32 Fourier modes and required that $1/3$ of the spectrum was completely damped i.e. equal to zero. I also
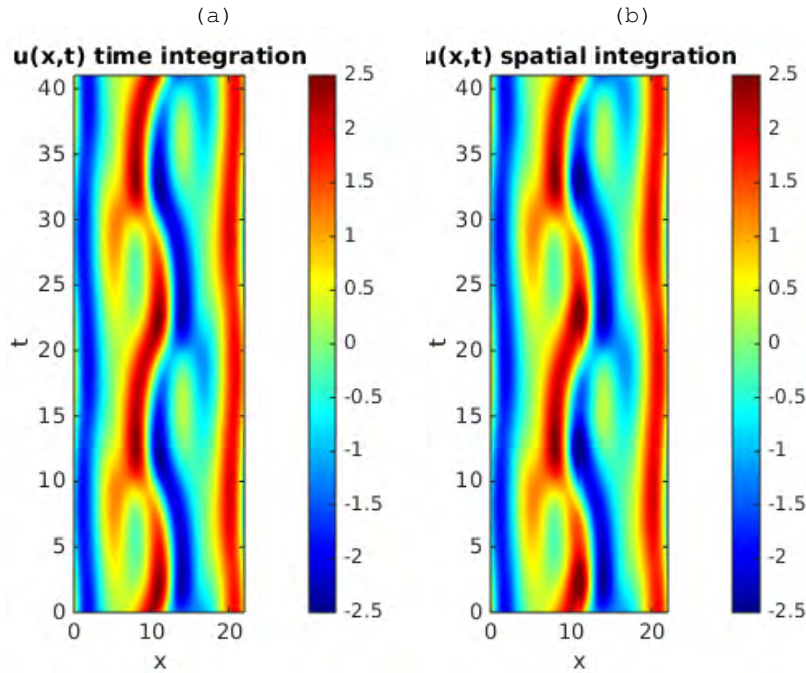
Figure 13.26: Integration of $\overline{ppo}_{10.2}$, (a) in time using (1.26), (b) in space using (1.36). The initial condition for the spatial integration was the time strip $u(x,t)$, $x = L/2$, $t = [0, 2\overline{ppo}_{10.2})$. The spatial integration was carried out in two separate pieces, $x \in [0, 11]$ and $x \in [-11, 0]$ and then were conjoined to produce (b). There is a discontinuity at $L/2$ due to numerical instability that has still not been resolved. (I believe (a) here is correct, it differs from (a) in figure 13.3 by conjugation of spatial Fourier coefficients).

> used the MATLAB circular convolution function `cconv` to compute the nonlinear term as it yielded less of a discontinuity.

VariationalNewtonDescent Began coding in Python.

FksSpatTemp Is it correct to solve for iq_k and not q_k in example (1.43)? I tried to provide corrections because I believe that is the case but my eyes are starting to give so I might have missed something.

PPOstbExp [14] Wrote MATLAB code that can compute the eigenvalues of the spatial stability matrix at a given x instant. An example of is plotted in figure 13.27. These are meaningful only for temporal equilibria. They are not the *spatial stability exponents* of a spatially evolving state, initialized at some x_0. To compute spatial stability exponents, i.e., the mean rates of expansion/contractions and rota-

---

[14]Predrag 2016-09-20: please recheck, correct all other relevant text and figure captions accordingly, then remove `PCedit`.

tions of infinitesimal trajectory deviations along the distinct eigendirections of the *spatial* Jacobian matrix, I would need to integrate the spatial Jacobian matrix from x_0 to x, compute its eigenvalues (the stability multipliers), take their logs, divide by $x - x_0$ and make sure that their phase has not slipped by 2π.

Talking about phase slips: I have to ask Xiong why he claims that the "unwrapped phase" cannot be computed?

$$A(\hat{u})^{IJ}_{jk} = \begin{bmatrix} 0 & \delta_{jk} & 0 & 0 \\ 0 & 0 & \delta_{jk} & 0 \\ 0 & 0 & 0 & \delta_{jk} \\ -i\omega_k\,\delta_{jk} - \hat{u}^{(1)}_{k-j} & -\hat{u}^{(0)}_{k-j} & -\delta_{jk} & 0 \end{bmatrix} \quad (13.16)$$
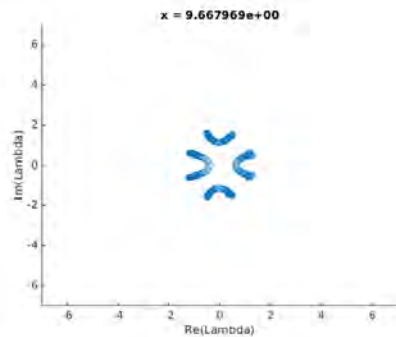
Figure 13.27: Eigenvalues of the spatial stability matrix (13.16) for time-strip initial condition $x_0 = 0$ (?) from $\overline{ppo}_{10.2}$, evaluated at $x = 9.6680\cdots$. 32 temporal Fourier modes. These numbers have no dynamical meaning, I show here just that I can plot them, with correctly scaled axes.

2016-09-08, 2016-09-20 Predrag I guess number $\neq$ log(number) cannot be taught. Λ_j is a stability *multiplier*. Its logarithm(magnitude) divided by time is the real part of the *stability exponent*, denoted everyplace here by $\mu^{(j)}$. That's why I use these clumsy macros - cannot confuse the number for its logarithm if one uses the macros.

2016-09-13, 2016-09-20 Predrag Please plot all complex plane plots (such as figure 13.21) with fixed, same scale on both axes. You always want $r\exp(\theta)$ to trace out a circle, not an ellipse. Figure 13.27 is good, but probably need only $[-2, 2]$ range, or less. Label axes (μ, ω), not by words.

2016-09-20 Matt : In reference to (13.16), I was in the process of thinking about whether it was meaningful or not, tending towards not... sometimes I make dumb mistakes and interpretations of things at 2 a.m. apologies

2016-09-20 Predrag Please plot all complex plane plots (such as) with fixed, same scale on both axes. You always want $r \exp(\theta)$ to trace out a circle, not an ellipse. Figure 13.27 is good, but probably need only $[-2, 2]$ range, or less. Note that the eight $\ell = 0$ Fourier modes,

- 2 stability exponents equal to zero
- 2 purely imaginary stability exponents, $\lambda^{(j)} = \pm i$, each with multiplicity 2,

in the center of plots of figure 13.25 have vanished in figure 13.21. Except for the $\lambda^{(j)} = \pm i$ cases? Cannot tell from the microscopic plot. Explain why? Usually marginal eigenvalues indicate that the solution has continuous symmetries. $u(x,t) = 0$ presumably has all the symmetries Kuramoto-Sivashinsky equation can have, but an arbitrary state $u(9.6680\cdots, t)$ presumably has no symmetries. Also, I cannot tell from the ellipses of figure 13.25 whether the remaining eigenvalues come in octets, on circles of given radios, and phases rational fractions of 2π. That would also need to be explained. The spatiotemporal evolution might be Hamiltonian, not only time-reversal invariant (that is less restrictive than the Hamiltonian symplectic volumes conservation).

2016-09-20 Matt :

PlumbersLocal0430 See pipes blog.

KsSpaceInt Worked towards improving the accuracy of spatial integration to no avail. Also worked towards producing a figure representing the error between the spatial integration and time integration results in regards to Eq_1.

DiffReview I plan to look over PC's diffs so that I can stop repeating the same mistakes over and over again. I'll try to be better with this in the days ahead.

2016-09-22 Predrag The $\ell = 0$ roots of figure 13.25 (b) do not agree with my (1.48), can you recheck both? To me figure 13.21 (b) seems correct. Maybe also draw a few circles of radia (1.49), so we can see that all $\ell \neq 0$ roots are the correct distance from the origin, with 4 roots on each circle?

2016-09-22 Predrag Having stability eigenvalues paired with opposite real parts $\mu^{(k)} = -\mu^{(k+1)}$ is very standard, both for the time-reversal invariant and the Hamiltonian ODEs and PDEs. Everything discussed in sect. 6.4 is of that type, so they all are integrating hyperbolically unstable systems, both forward and backward in time. How do they do it?

2016-09-22 Matt Errors Updated figure 13.22 to reflect what I believe is the correct time-integration. Also included in figure 13.23 is the absolute value of the difference between spatial integration and time integration results of figure 13.22. The accuracy of integration the ODEs of
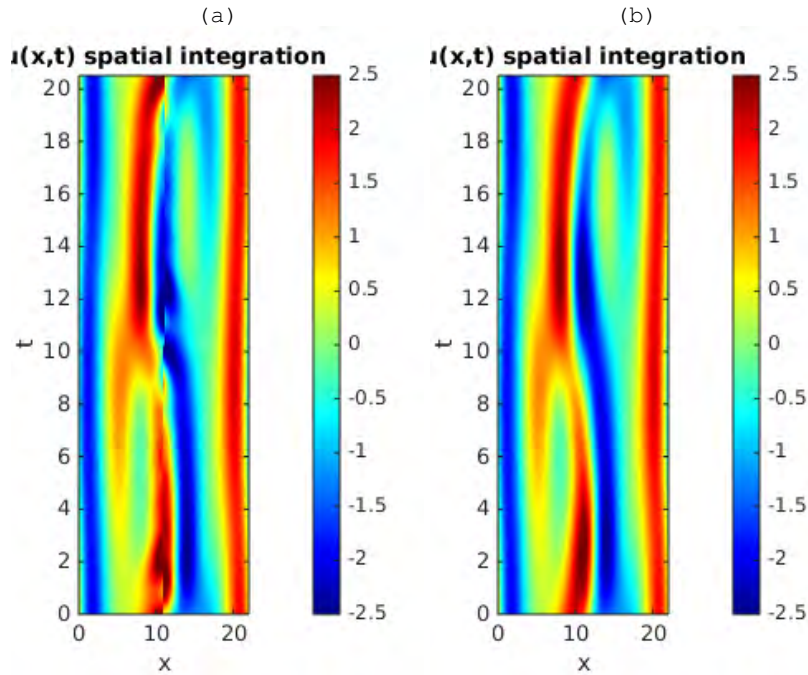
Figure 13.28: Time-strip initial condition $T = [0, 2\, T_{\overline{ppo}_{10.2}})$, located at $x = L/2 = 11$ integrated in two parts over $x = [0, 11]$ and $x = [-11, 0]$. The number of undamped Fourier modes of each plot are (a) 21 and (b) 7.

(1.36), even with the more stringent MATLAB integrator `ode113`, is not reliable past spatial extent $x \approx 18$. The reason for the relatively high error at the beginning of the integration is due to the

Spatial Integration Accuracy I was worried about the how a time strip of $\overline{ppo}_{10.2}$ with $T = [0, 2\, T_{\overline{ppo}_{10.2}})$ was less accurate than a strip of temporal extent $T = [0, 4\, T_{\overline{ppo}_{10.2}})$ so I did some more investigation. For plot (b) from figure 13.26, one third of the Fourier spectrum was damped to avoid aliasing errors (Damped in this context means the Fourier coefficients were set to 0 at every integration step). After some testing, I found that the error can be minimized further by keeping *fewer* modes active, i.e. setting more modes to zero. This discrepancy can be seen in figure 13.28, where the number of active Fourier modes are (a) 21, and (b) 7. These specific values for the number of modes were determined by (a)Damping one-third of the spectrum as previously mentioned, and (b) keeping all modes with frequency $|\omega_k| \leq 0.9192\ldots = 6\pi/T_{\overline{ppo}_{10.2}}$ active. The specific bound on the frequencies was determined by numerical testing the error, and looking for when it was minimized.
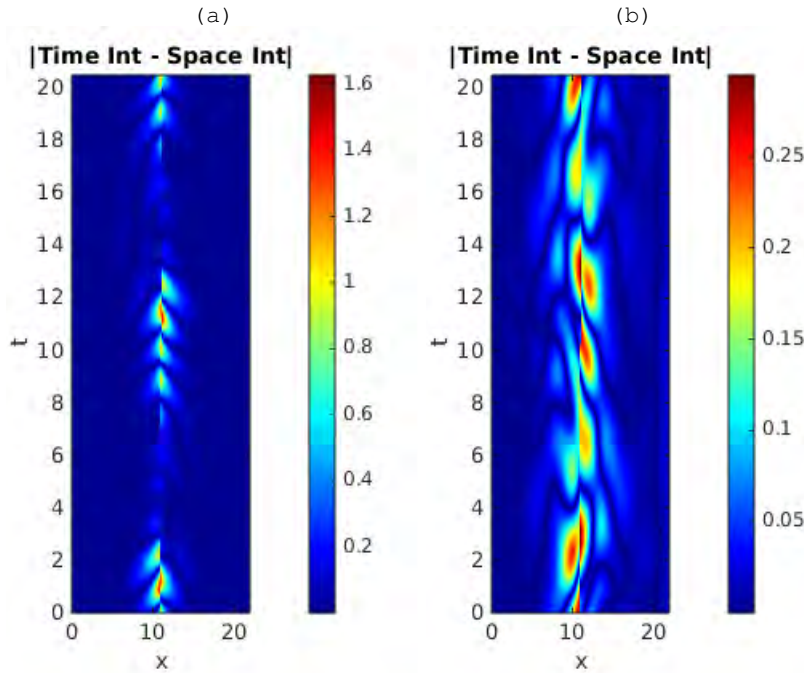
Figure 13.29: Absolute error between time-integrated solutions of $\overline{ppo}_{10.2}$ and spatially integrated solutions. A Time-periodic initial condition $T = [0, 2\,T_{\overline{ppo}_{10.2}})$ was taken from the time integrated solution. This initial time-strip was integrated spatially in two parts, $x = [0, 11]$ and $x = [-11, 0]$. The number of active Fourier modes in each plot are (a) 21, and (b) 7.

This bound also held for the strip $T = [0, 4\,T_{\overline{ppo}_{10.2}})$. This is be-cause if $|\omega_k| \leq 0.9192\ldots < 1$, then the following inequality holds, $|i\omega_k \hat{u}_k^{(0)}| < |\hat{u}_k^{(0)}|$. While there is still a numerical error when damp-ing this thoroughly,the major patterns of the time-integrated solu-tion persist in the spatially integrated solution produced in figure 13.28, so I thought this was worth noting.

StabilityExponents I went through the derivations of the equations mul-tiple times but it only yielded the same results of (1.47) and (1.49). The only way that I know of getting (a) and (b) from figure 13.21 to match is to require $q_k \to iq_k$, i.e. q_k is purely imaginary. There are ways to change the stability matrix to get the two to match but I feel that this is ill-founded as the equations of (1.36) have recently been providing reasonable yet inaccurate results in regards to reproduc-ing $\overline{ppo}_{10.2}$. I've, however, fixed a couple of negative signs that were remnants of changing the equations multiple times.

I've updated figure 13.21 and figure 13.25 by adding in circles that

demonstrate that the $\lambda^{(j)}$ lie in quartets on circles of radii $|\lambda^{(j)}|$, as given by (1.49).

The discrepancy between 4 marginal $\lambda^{(j)}$ and 8 marginal values was due to me copying the convention for ω_k from the FFT frequencies, a mistake on my part. It included the 0 frequency twice. The current figure 13.21, figure 13.25 should reflect the frequency spectra $\omega_\ell = \frac{2\pi\ell}{T}$, with ℓ symmetric about 0, i.e. $\ell = -N/2, \ldots, 0, \ldots, N/2$.

2016-09-29 Matt KSspaceInt Tried to use finite differences as a way to compute the time derivative term as a potential alternative to $i\omega_\ell \hat{u}_\ell^{(0)}$, in hopes that it might enable keeping more modes but the results were poor on my first attempt; I thought it still might be worth tweaking because of the frequency bound condition that determines the best results with integration in Fourier space. Just to recall, this was keeping $|\omega_\ell| < 1$ modes.

MeetingWithDeLaLlave E-mailed Professor de la Llave from the Mathematics Department to have a meeting, no response as of posting.

VariationalMethod More coding... slower than I hoped due to the transition from Matlab to Python.

DDays2017 Began the application process for poster presentation.

2016-10-03 Matt : The day was spent working on variational method code.

2016-10-04 Matt NewtonMethod Continued working on coding while rewriting some of the previous code I had written. Trying to be extra careful and take nothing for granted due to my previous frustrations.

CatsAndSpacetime Meeting with Boris, Predrag, Rana, Adrien and Li Han. The cats were playing with yarn (for Adrien neither the old Matlab code, nor the new Mathematica implementation works so far, and Li Han Skyped infrom an M-theory modular domain) so most of the discussion was regarding Aizenman's analysis of the 2D Ising model using the Ihara zeta function (see chapter **??**). Predrag mentioned that he had formulated a planar field theory and never found physical problems to apply it to. Also, he feels that the zeta function approach a much better way to look at the problem due to the difficulties of interpreting Onsager's previous solution. There were some subtleties involving the admissability of certain graphs, their symbolic dynamics, and the pruning rules therein.

Also mentioned was the Smale school and de la Llave's work (see sect. 19 posts starting with **2016-09-28**), in which they treat multiple 'times' simultaneously. Our work, with space and time being treated on the same footing, is an example of that perspective. Predrag, however, has found tracking down and understanding that literature very difficult. So far he finds Politi *et al.*'s 'chromotopic'

papers (which we are reading and bloggin about in chapter **??** and subsequent sections) closest in the spirit to our work.

Bunimovich and Sinai [4] (see sect. **??**) was briefly discussed. It appears that nobody before Gutkin and Osipov [21] has studied the strong coupling ($\epsilon = 1$ case).

2016-10-06 Matt Getting closer to finishing Newton descent for loops code. Still needs work on the "approximate iterative inversion" as denoted by Lan in ref. [27], but as of right now most of the meat has been written.

2016-10-10 Matt : Still debugging Newton method code. I got it running but there are still errors somewhere as it's not performing well. Asked Chris for advice on if I was handling the Differentiation matrix for the finite difference scheme that approximates tangent to the loop properly; after some changes the performance worsened. So as it stands I am still in the debugging/rewriting phase.

2016-10-11 Matt : Uploading the working copies of previous MATLAB codes for spatial integration of finite extent and Python codes for Newton method, which is still giving me trouble. Still trying to get all the pieces working together properly. After some preliminary results I feel like the biggest problem currently is with approximation of the loop tangent. The initial error seems to be too large considering the initial loop I am using as a check is $\overline{ppo}_{10.2}$. However, I have found and fixed a couple parts of the code `MNGvnd.py`, or more specifically the functions that it uses which are located in `MNGvndfunctions.py`.

2016-10-13 Matt :Still no exciting results. Xiong told me to switch to Python 2.7 as opposed to the current build I was using due to the fact that the majority of the Physics community uses this. I had to track down some of the differences which took some time, spent some time discussing with some of my colleagues in our hopes that sharing with others would lead to not missing the bigger picture and we would be able to help each other. It seems I was able to help them more than they could help me.

Currently still rewriting parts of the code trying to get used to Pythons conventions...there are many silly things that are happening for unknown reasons; such as taking the difference of two arrays is somehow changing their shape.

Trying to also keep up with the Cat map postings made by PC in hopes I can contribute next time the feline circus makes it into town.

2016-10-19 Matt :

Readings Still trying to find an adequate answer to PC's question "How do they do it?" in reference to reversible systems. I haven't found an adequate answer yet in sect. 6.4 but I am still trying to cover it. The only peculiarity that I've found so far are that apparently was

in ref. [2] they "split" the full Kuramoto-Sivashinsky equation into two parts; I think might have been related to something specific in ref. [20] but I haven't looked at ref. [20] yet.

Python Trying to be more careful with every step to make sure I'm not overlooking anything. I think I took the fact that MATLAB is more of a tool and less of a language like Python for granted. Specifically I've found and corrected mistakes in the calling of functions and broken broke them down into individual steps; there are other changes regarding the handling of arrays but that was just a careless error.

To improve the efficiency I also am in the process of changing the code to take advantage of the real valued $u(x, t)$, i.e. taking half of the Fourier spectrum.

I've been doing the computation in Fourier space as when I worked through Lan's prescription I didn't find any assumptions that would preclude this but I had a moment of doubt today. Hopefully some of the changes I've been making will help in this regard.

MATLAB I should have noted that while I've been mainly trying to learn Python and create Newton descent code I've also been going back to MATLAB every so often when I have an idea that I feel might help the numerical accuracy. I suppose it's a case of the first child being the favorite.

2016-10-20 Matt Cats Adrien presented his verification efforts of some of his results. It looked quite a bit like the partner orbits of Boris' presentation, but I couldn't confirm as Adrien was pressed for time and had to get back to grading.

Rana also presented results regarding entropy and relative frequencies. To be more specific I believe it was Measure-Theoretic Entropy (according to wikipedia's definition seemingly matching was Boris had written down). There was much discussion about this entropy between PC and BG, as well as log-log plots. There was then a discussion about relative frequencies, which Boris claimed to look parabolic; I rather felt like they were more trapezoidal, but I don't think the geometries of the histogram were important. Boris felt that the way that Rana had ordered the trajectories was good and maybe insightful? She plotted the frequencies in a sort of modulo arithmetic way, using the symbolic dynamics as the base for the number system. Also discussed was how inadmissable trajectories or pruning rules could be accounted for by redefining the symbolic dynamics. PC made reference to Smale horseshoes and how longer trajectories typically have smaller "gaps" due to pruning rules but there were be more of them.

Python Still just chugging along. PC stressed that I should test a much simpler system, (e.g. Rössler) to get it working correctly to start; I

believe this is useful advice, but I need to be careful as most of the functions are written to be directly related to the spatial Kuramoto-Sivashinsky system, perhaps this is a bad choice.

2016-10-22 Matt MeetingWithDeLaLlave I discussed my work with Professor de la Llave and a Mathematics post-doc Livia yesterday. I ran them through the numerical schema and general procedure used to produce spatial integrations such as figure 13.28. Professor de la Llave expressed the difficulties with such an integration and really stressed that it would be quite difficult, but he had some suggestions as to possible ways to eliminate some of the instability. He didn't want to get into the proofs or the procedure but he suggested some resources namely refs. [33, 35, 55] which I've been trying to read through. His general comment was that I might be able to eliminate certain unstable directions (which he believes I might have been crudely doing via the damping of high frequency Fourier Coefficients in the spatial integration process)

Python Still wrestling with snakes. Professor de la Llave voiced his concerns with the variational method but he also says that this has been discussed with PC in the past and there have been agreements to disagree.

2016-10-24 Matt MathColloquium Went to a colloquium titled 'Estimations on Diffusion Constants for Chaotic Billiards' presented by Prof. Hong-Kun Zhang of the University of Massachusetts Mathematics Department; The topics discussed were Billiard maps, Motivations from Fluid and Statistical Mechanics, Diffusion of Lorentz gas, Superdiffusion of Billiards. To get a flavor, in an "infinite horizon" Lorentz gas, there exist channels where no deflections occur which leads to superdiffusive properties. In the example given the Green-Kubo Formula fails and the Central Limit Theorem doesn't apply so Professor Zhang and her Ph.D. student used Borel σ-algebras /(Stochastic) Filtrations / Martingale Approximation to somehow get a superdiffusion constant (I think?). The main question raised by Professors de la Llave and Bonetto was if this had an analogous PDE description but Professor Zhang said that it hadn't been thought through.

Python I was being stubborn and trying to get the spatial variational method code to work. All I can really say at this point is that I will continue to try hard. I currently had been working on trying to reconfigure the problem such that I could perform the fictitious time integration with only positive frequency ω_ℓ modes and exploit the real valued field to decrease the dimension of the problem, but realized this is more trouble than it's worth for the time being. I have also been working out an equivalent expression for a calculation that is completely entirely in configuration space; I realized that

I had only undertaken the Fourier space expression out of habit although it would most likely guarantee smoother results than finite difference schemes in configuration space. To further remedy my situation I spent the last part of my day writing code to enable me to perform the variational method on the Rössler system before I waste any more time.

Reading Read more of ref. [35] and ref. [33], while interesting I feel like I should probably shelve these for the time being.

2016-10-25 Matt : Variational Newton code for the Rössler system has been adapted from the code for spatial Kuramoto-Sivashinsky equation that I have been working on previously. It behaves mostly how it should however it stalls out once the loop gets close to the periodic orbit. The final result remains smooth and visually looks similar to the shortest periodic orbit of Rössler flow but the period and numerical values are off; such that trying to verify the trajectory via numerical integration proves that it is indeed not periodic.

I made what I believe to be corrections/improvements to the iterative refinement of the corrections but it still only allowed for the final error to be near 10^-2, nowhere near the required machine precision to be reputable. The period of the loop is within 10^-1, again not near close enough.

Possible reasons for this are is that the initial condition I am using is not refined enough to produce desired results or there are more errors lurking. Once I am confident that it is working properly I will move on to the antisymmetric subspace $\mathbb{U}^+$ results that Lan has produced for Kuramoto-Sivashinsky equation.

2016-10-27 Matt : Spent the past two days gutting my variational method code and rewriting most of it from scratch using what I've learned from debugging. It seems to be working for the Rössler system under certain conditions. The main condition is that the quantity being constrained in order to break the translational invariance needs to be fairly close to its true value or else the fictitious time integration stalls very quickly. The order of error for this value also depends on how close the rest of the initial guess loop is. To be concrete, if x_0 is the constrained coordinate then $\delta x_0 < 10^{-4}$ seems to be a reasonable bound even if the rest of the loop is relatively far away from the periodic orbit. My initial thoughts were that so long as the periodic orbit didn't miss the Poincaré section completely then we were in business but seems to be much more delicate than that.

I plan to apply what I've learned to Kuramoto-Sivashinsky equation tomorrow, if I can't get anywhere then I will pursue the antisymmetric subspace $\mathbb{U}^+$. My biggest worry at the moment is whether the finite differences make sense in the scope of complex valued variables; I feel like I might have to separate the real and imaginary parts or apply the differentiation matrix in configuration space and then bring the results back

to Fourier space, similar to how I computed the nonlinear term using a pseudospectral method in the code I have written for numerical integration of (1.36).

2016-10-31 Matt :

NewtonDescent After waffling back and forth on which is the best way to proceed I've written what I believe to be a correct version to my code; I haven't been able to get it to run yet however as the discretization I chose for accuracy seems to eat up too much memory at the time being, I'll try again when I get home to my desktop but I might have to trim down the loop from 128 spatially discretized points to 64 or even 32; however I feel like this might not be sufficient. I found a few mistakes in my rewriting of the code for Kuramoto-Sivashinsky since I completing my Rössler code. Another problem was that the damping of the higher frequency temporal modes that I thought would help the computations by making the matrix of (13.18) sparse. This was actually making the matrix singular, which was the source of some of the numerical problems I had been having.

My main concern at the moment is that in previous tests the negative, positive frequency pairs of Fourier coefficients are not maintained as complex conjugates of one another; this is what maintains the inverse Fourier transform as real valued. I'll hopefully be able to fix this, but I might have to revert to taking the real fast Fourier transform (RFFT) which only keeps the positive frequency components thus eliminating the balancing act that I have been trying to get to. I tried this before but it introduced further complications in my head and in the coding procedure for the stability matrices. It should not be hard to do, but I kept making mistakes and was unsure about my equations such that I decided to revert back to the full FFT for my purposes. Perhaps there is a way to encode this condition into the constraint that is being used to break the translational invariance, $\hat{r}$ in (13.18), but I have not figured out if that is possible either.

The main equation being employed in this process is that of fictitious time flow from Lan's thesis [27]

$$\frac{\partial^2 \tilde{x}}{\partial s \partial \tau} - \lambda A \frac{\partial \tilde{x}}{\partial \tau} - v \frac{\partial \lambda}{\partial \tau} = \lambda v - \tilde{v} \tag{13.17}$$

rewritten as the matrix equation

$$\begin{bmatrix} \hat{A} & -\hat{v} \\ \hat{r} & 0 \end{bmatrix} \begin{bmatrix} \delta \tilde{x} \\ \delta \lambda \end{bmatrix} = \delta \tau \begin{bmatrix} \lambda v - \tilde{v} \\ 0 \end{bmatrix} . \tag{13.18}$$

The key definitions of this equation for a spatially discretized system $\tilde{x}$ of N points in d dimensions, with the parameterization variable s_n such that $\tilde{x}_n = \tilde{x}(s_n)$:

- Finite $[Nd \times Nd]$ difference matrix,

$$\hat{D} = \frac{1}{12h} \begin{bmatrix} 0 & 8 & -1 & 0 & \ldots & 1 & -8 \\ -8 & 0 & 8 & -1 & 0 & \ldots & 1 \\ 1 & -8 & 0 & 8 & -1 & 0 & \ldots \\ \vdots & \vdots & \vdots & \vdots & \vdots & \vdots & \vdots \end{bmatrix} \quad \text{where,} \quad h = \frac{L}{N}$$

- $[Nd \times Nd]$ matrix composed of finite difference matrix and stability matrices,

$$\hat{A} = \hat{D} - Diag(A(x(s_1)), A(x(s_2)), ..., A(x(s_n)))$$

- Discretized loop langent

$$\tilde{\mathbf{v}} = \frac{\partial \tilde{\mathbf{x}}}{\partial s} = (\hat{D}\tilde{\mathbf{x}})$$

- $[Nd \times 1]$ velocity field v vector given by (1.36)
- Constraint to break translational invariance, a $[1 \times Nd]$ vector $\hat{r}$,
- λ is a mean "tangential speed" that converts the parameterization variable into the length (the parameter is time if using (13.1) for the velocity and loop is parameterized by time) of the periodic orbit.

$$\lambda \Delta s_n = \Delta x_n \qquad (13.19)$$

2016-11-01 Matt :

PlumberMeeting See pipes blog.

SpacetimeCats Meeting regarding the cats paper and my current work. Professor de la LLave joined in while I was attempting to discuss what I had done so far. There was much discussion about the parameterization I had been using and whether it was better to use a curvilinear parameterization rather than time.

NewtonDescent Wrote functions for the Newton descent for the time equation (13.1). The only differences between the code I had currently written for the spatial Newton descent and this are the definitions of the velocity field and therefore, the definition of the stability matrix. The only other additions that would have to be taken into account depend on how the initial conditions are produced and or formatted.

FiniteDifferenceSchema The coefficients of the five-point stencil method were called into question as to where they arise from. The general idea is that for an equidistant grid of points one can define Lagrange interpolating polynomials and then derive a recursion relation for the correct weighting of the grid points which depends on the order of accuracy and the order of the derivative being approximated.

PseudoInverse After the suggestion from de la Llave, I investigated the pseudoinverse formulation for the matrix equation (13.18). There are many different ways to define a pseudoinverse but the most common seems to be the Moore-Penrose pseudoinverse, see mathworld.wolfram.com pseudoinverse. The most important property in my opinion is that for the non-square matrix equation,

$$\mathbf{B}\mathbf{x} = \mathbf{y}$$

the application of the pseudoinverse $\mathbf{B}^+$ (Wolfram notation) leads to the shortest length least squares solution

$$\mathbf{x} = \mathbf{B}^+\mathbf{y}$$

If I understood professor de la Llave, the corresponding formula for variational Newton descent using this formulation would be,

$$\begin{bmatrix} \hat{A} & -\hat{v} \end{bmatrix} \begin{bmatrix} \delta\tilde{x} \\ \delta\lambda \end{bmatrix} = \delta\tau \begin{bmatrix} \lambda v - \tilde{v} \end{bmatrix}, \tag{13.20}$$

which neglects the constraint that was previously used to break the translational invariance in order to get fictitious time flow that is transverse to the direction of the velocity field, but still enforces transversality, by selecting the shortest least squares solution.

After application of this to the Rössler system, I noticed that the code runs slower due to the calculation of the pseudoinverse matrix. However, there were fewer fictitious time steps required to reach the desired error threshold of the cost functional. As long as the pseudoinverse isn't required to be calculated too frequently, the method might be preferable to the Newton with a constraint. In addition, it avoids the somewhat arbitrary definition of a constraint.

2016-11-06 Matt VariationalNewtonMethod Taking hints from Lan's thesis [27] I've been trying to improve the code handling the fictitious time evolution to improve the efficiency. The main idea that Lan provides is repeatedly using the same matrix as an approximate to the true matrix, in order to avoid recomputing it at every step. What I believe he means by this is to reuse the matrix,

$$\mathbf{M} = \begin{bmatrix} \hat{A} & -\hat{v} \\ \hat{r} & 0 \end{bmatrix}$$

or equivalently the non-square matrix,

$$\mathbf{M} = \begin{bmatrix} \hat{A} & -\hat{v} \end{bmatrix}$$

for multiple fictitious time τ steps, as an approximation. This is available to us because as long as the cost functional is being minimized, the fictitious time evolution is proceeding in the "correct" direction.

Currently in my code, once the matrix M, or equivalently, $M_n = M(\tau_n)$ is defined, it is used in the calculation of corrections to the loop, $\delta\tilde{x}(\tau_k)$ for as many steps $k = n, n+1, \ldots, m$ as possible until the cost functional increases; at this point I apply an iterative improvement scheme, which is an iterative method used to improve the numerical accuracy of solutions, defined by the process,

$$
\begin{aligned}
\mathbf{r}_m &= \mathbf{b} - \mathbf{M}\mathbf{x}_m \\
\mathbf{M}\mathbf{d}_m &= \mathbf{r}_m \\
\mathbf{x}_{m+1} &= \mathbf{x}_m + \mathbf{d}_m
\end{aligned}
\tag{13.21}
$$

The general idea is that by solving the same linear equation using the remainder, $\mathbf{r}_m$ of the original equation, one can find corrections $\mathbf{d}_m$ to the original solution $\mathbf{x}_m$.

I feel that this process is not so useful in practice, as the approximate inversion of the matrix $\mathbf{M}$ is seemingly accurate enough to always provide a close solution to matrix equations such as (13.20).

If this iterative method to improve the accuracy cannot enable further fictitious time evolution, then the matrix $\mathbf{M}_n$ is recomputed at the current location of the loop in state space.

Variational method for antisymmetric subspace $\mathbb{U}^+$ of KS Still trying to find a systematic way of producing initial conditions for the use of variational Newton descent. The main equation governing the fictitious time evolution is again (13.18) or the non-square matrix variant, (13.20). The only differing components from that of the Rössler system, or spatial Kuramoto-Sivashinsky is the definition of the velocity field v and therefore the definition of the stability matrices A.

For a spatially periodic initial conditions, the (truncated) evolution equations in time for the spatial Fourier coefficients a_k are,

$$
\dot{a}_k = (q_k^2 - q_k^4)a_k - q_k/2 \sum_{m=-N/2}^{N/2-1} a_{((k-m))} a_m
\tag{13.22}
$$

where the parentheses for the index in the sum indicates a modulo N operation due to the truncation. Didn't use this fact in practice, much easier and faster to compute via FFT. Therefore the stability matrix is defined by the sum of a diagonal matrix and circulant matrix multiplied by a factor of q_i, or in terms of the elements of the stability matrix,

$$
A_{ij} = \frac{\partial \dot{a}_i}{\partial a_j} = (q_i^2 - q_i^4)\delta_{ij} - q_i(a_{(i-j)} - a_{(i+j)})
\tag{13.23}
$$

Apparently forgot to finish writing this. Forever:)

Figure 13.30: $u(x, t)$ for $L = 22$ spatial size (a) before and (b) after, application of the variational Newton descent code to the first equilibrium plus periodic deformations proportional to $\delta a_k(t) = \cos(2\pi kt/T)$. The value of the cost functional F^2 is decreased from ≈ 40 to ≈ 8. The time period of the final result is $T \approx 39$. (Poor formatting: time is vertical axis, space is the horizontal axis, will fix that another time...)

2016-11-07 Matt Preliminary results for antisymmetric subspace $\mathbb{U}^+$ I finally got the variational Newton descent to run for the antisymmetric subspace $\mathbb{U}^+$ equations (13.22) and (13.22). The error is still not being minimized to an acceptable level but there are many things going on that could be the culprit. Namely, as it was preliminary testing I was using 32 spatial Fourier modes and 32 time discretized points; I believe that the testing will be further improved by sacrificing Fourier modes and increasing the number of discretized points; however, this might not necessarily be the case as the initial conditions themselves may be flawed.

In their current construction I first took the spacetime data corresponding to the first equilibrium and $\overline{ppo}_{10.2}$ integrated in time for $2\,T_{\overline{ppo}_{10.2}}$ (for arbitrary reason for the equilibrium) and reduced them to the antisymmetric subspace $\mathbb{U}^+$ by taking the imaginary parts of the spatial Fourier spectra. Then I (perhaps unwisely for a first test) added periodic deformations to the spectra of the form (using the convention of (13.22) where $a_k(t)$ denotes the kth spatial Fourier coefficient)

$$\tilde{a}_k(t) = a_k(t) + a_k(0)\cos(2\pi kt/T) \qquad (13.24)$$

Applying the variational Newton descent with these initial conditions produced figure 13.30 and figure 13.31. It should be noted that varying the initial fictitious time step $\delta\tau$ alters the final result of the descent but I haven't figured out if this is a major flaw as of yet.

Improvements and Ideas • Start with unaltered equilibrium and $\overline{ppo}_{10.2}$ with varying sizes of time domains.
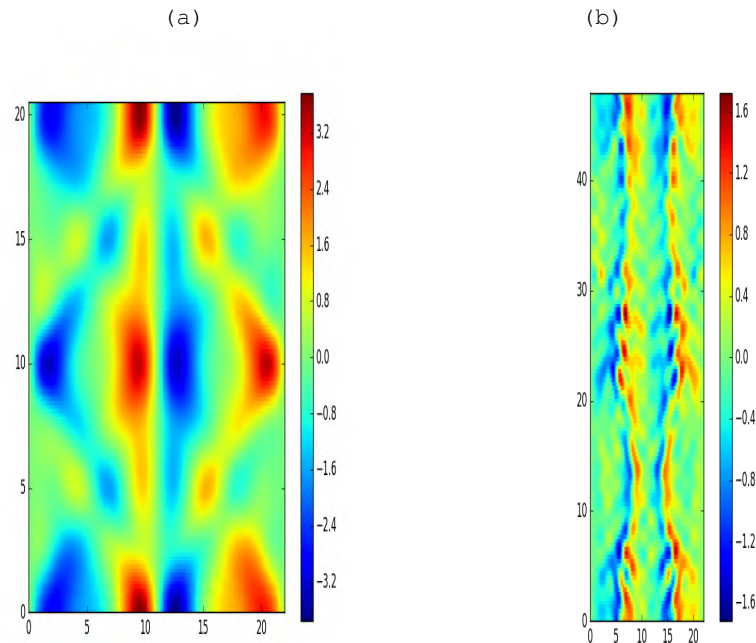
Figure 13.31: $u(x, t)$ $L = 22$ domain size (a) before and (b) after the application of the variational Newton descent code to $\overline{ppo}_{10.2}$ plus periodic deformations proportional to $\delta a_k(t) = \cos(2\pi kt/T)$. The cost functional F^2 is reduced from ≈ 350 to ≈ 4.5. The time period of the final result is $T \approx 47$. (Time is vertical axis, space is the horizontal axis.)

- Use completely different and hopefully smarter initial conditions
- Increase the size of the temporal discretization.
- Decrease the number of spatial Fourier modes.
- Incremental improvements to efficiency and accuracy

2016-11-08 Matt : Went to the PDE seminar hosted by the Mathematics department. It was titled "Global existence for quasilinear wave equations close to Schwarzschild" presented by Mihai Tohaneunu from the University of Kentucky. He only had time to really sketch the proof but it involved using harmonic coordinates, Klainerman vector field method, Klainerman-Sobolev type bounds to prove the stability of exact solutions with a metric that is semilinear in nature.

2016-11-08 Matt : Variational Newton method code still not performing to expectations. Varying the number of discretized points seemingly had no effect on how well the initial conditions converged, just made the code

run slower as the matrices involved are larger. I believe this is merely a property of the initial conditions and not of the code itself, however, I am still making changes to the code such as reordering the main time-stepping loop and double checking the velocity and stability matrix functions. I've been trying to find mention of the initial values for the cost functional so that I can compare to how close my initial guess loops are to a specific periodic orbit but the only mention so far has been in the unpublished ref. [16], in which the initial value of the cost functional is of order $F^2(0) = 10^-4$. In comparison my initial conditions $F^2(0) \approx 10^2$ meaning that my guess loops are far from any periodic orbit and hence will likely fall. They do however contract quite well, as the cost functional appears to be decaying exponentially in τ however they tend to get stuck.

I've been thinking that if the variational Newton descent shakes the orbit until the method stalls why not hit it with a hammer? My idea is to first find the component of $\lambda v - \tilde{v}$ that is contributing the most to the cost functional and introduce some sort of perturbation that would increase the cost functional before (hopefully) being minimized again. I'd be curious to hear what others think about this as I haven't really done anything rigorously so it might be a fool's errand but I just dislike how in this method it seems like (at least from my interpretation of ref. [16]) that you need to be relatively close to any periodic orbit to get it to work correctly.

2016-11-10 Matt :

> **General comments** I'm trying to understand what I myself was thinking about when I wrote my last blog post. I wasn't really making sense as the variational method is supposed to be smooth deformations parameterized by tau. Also, I don't know how the parameterization in the loop would be affected...at least I didn't put any real time or effort into it. f Briefly chatted with PC after class. We discussed how there might be continuous families of solutions that would imply the need to derive a non trivial way to deal with the symmetries, which might be handled by rescaling in a undisclosed manner. These symmetries would allow for sliding around any periodic orbits found due to the marginal directions not accounted for. Asked about one of the more general ideas behind using a pseudoinverse matrix as opposed to a Poincaré section constraint. PC recommended looking up some of the literature from neural networks and to work through simple type problems to really get a feel for the method.
>
> Also mentioned that I should have been working with a different sized system in order to match Lan's results, and that I should make sure to check out the Levenberg-Marquardt methods mentioned in ref. [8].
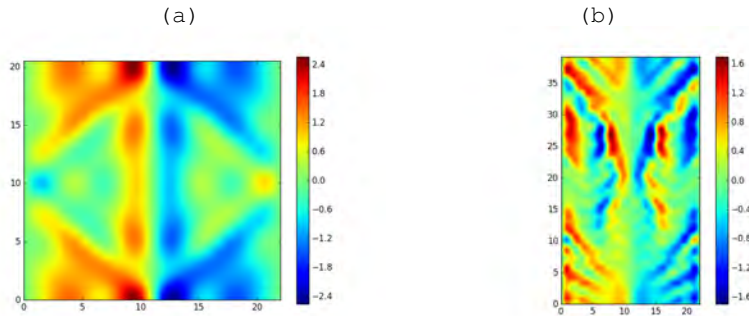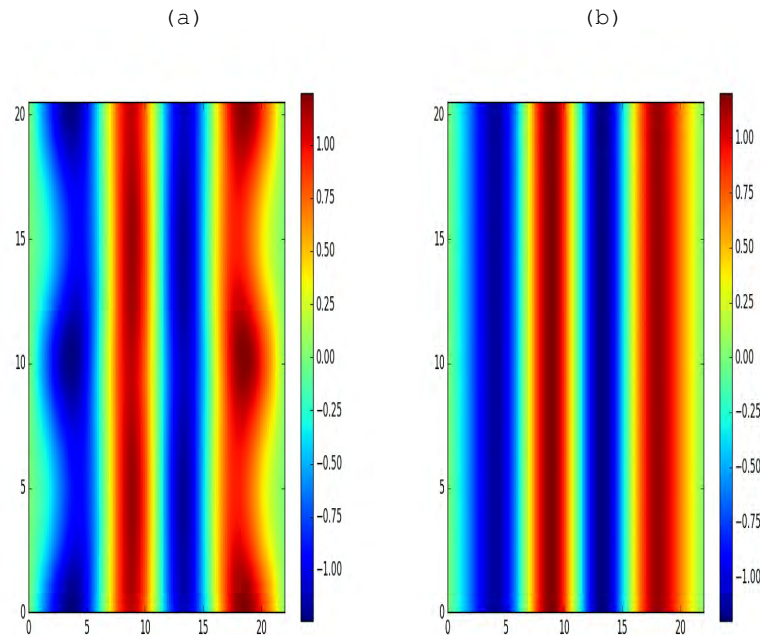
Figure 13.32: $u(x, t)$ $L = 22$ spatial size (a) before and (b) after application of the variational Newton descent code to the imaginary part of $\overline{ppo}_{10.2}$ over a full state space period. The time "period" (b) is $T \approx 0$, but has been blown up for viewing pleasure. (Poor formatting, time is vertical axis, space is the horizontal axis will fix.... still haven't wrapped head around Python formatting)

Newton method I realized and fixed an error in regards to the variational Newton method code for the antisymmetric subspace $\mathbb{U}^+$ of Kuramoto-Sivashinsky. The problem was that in the calculation of the nonlinear term the Nyquist frequency mode was allowed to have a nonzero value through my calculation of the nonlinear term in the definition of the velocity, (13.22), which is a big problem as both the zeroth mode and $k = -N/2$ mode need to be real, and hence zero in the antisymmetric subspace $\mathbb{U}^+$. This fix resulted in a fast, but somewhat strange calculation; one of the initial conditions I had previously prepared that has very little variation in time, (a) figure 13.32 seemingly fell into an equilibrium, which cause the loop parameterization to behave poorly; The "period" seemingly oscillated around zero as if the loop was fluctuating around a $T = 0$ equilibrium. I don't even know if what I'm saying makes sense as this occurrence is quite strange to me. My bug fixing might have opened doors for other creatures to get in I suppose but I'm not sure as of right now. It should be noted that I made these changes before changing the

system size to correspond to previous work.

Reading Forgot to include that I also skimmed some relatively random papers about symmetries and bifurcations near families of solutions and Sobolev spaces (in regards to the latter it caught my eye because it has to do with solutions to PDEs suppository and might be a better definition for a norm instead of the current L2 norm being used? I haven't read enough to know the differences but I was trying to expose myself).

2009-09-13 Predrag Previous computational domains for Kuramoto-Sivashinsky (clip & paste from *siminos/lyapunov/KS.tex*)

[...] We have stability of a periodic orbit from ref. [7], for Kuramoto-Sivashinsky on the periodic b.c., antisymmetric subspace $\mathbb{U}^+$, system size $\tilde{L} = 5.8$ close to the onset of chaos, 16 real Fourier modes. As (perhaps?) discussed in ref. [30], one has to be careful about defining the effective system size $\tilde{L}$ for the antisymmetric subspace $\mathbb{U}^+$, so these computations are done on $L = 36.31$ (or $L = 18.155$ if one considers the fundamental $[0, L/2]$ domain only). Going from $(L, \nu) = (2\pi, 0.029924)$ of ref. [7] to $(L, \nu) = (L, 1)$ convention used here requires that the time be rescaled as $t \to \nu t$, and the Lyapunov exponents as $\lambda_i \to \lambda_i / \nu = \lambda_i / 0.029924$, which would mean that then we computed only the first pair of isolated eigenvalues. The reason is that for periodic orbits we are computing *Floquet multipliers* which underflow numerically very quickly, so we cannot compute many *Floquet exponents*. The covariant vector methods are apparently much smarter.

In ref. [30] computations are done at $L = 38.5$, but we listed only 4 eigenvalues per periodic orbit, and considering hopeless organizational skills on the Lan astral plane, I doubt that the full spectra can be rescued from Lan's calculations.

2016-11-11 Predrag I do not know whether Helleman and Bountis [23] *Periodic solutions of arbitrary period, variational methods* is any good, but you might want to have a glance at it, not at least for the earlier literature on the variational methods that Lan and I had most likely missed. The Poincaré quotes are surely inspirational!

2016-11-15 Matt Plumbers Meeting See pipes blog.

Reading Finished reading through refs. [23, 43], I had access to both refs. [43, 45] as of yesterday and although I can't believe I'm this unlucky it seems the accessibility to refs. [43, 45] has changed in the past day. I have a copy of ref. [43] but not ref. [45].

KITP conference Trying to get lodging and other details figured out. Began writing abstract for application for poster presentation (Due December 9th). Hopefully will have better variational method results

by the time the conference comes around, would welcome recommendations on what to include, but I have a general idea in my head of what I can include; namely time-integration equations and previous results (with proper citations for Xiong's initial conditions) in comparison to spatial Kuramoto-Sivashinsky equation and integration procedures and results. Motivation for variational Newton descent, the respective equations and results.

Random Had to spend a chunk of time catching up on TA duties; I usually grade papers over the weekend but was unable to this week due to sickness.

2016-11-18 Matt :

Newton method I've been working on getting better initial conditions to use for the Newton descent method for antisymmetric subspace $\mathbb{U}^+$ of Kuramoto-Sivashinsky, as everything so far either stalls out, goes to the equilibrium as in figure 13.32.

Currently I was either just taking something familiar, such as $\overline{ppo}_{10.2}$ and taking only the imaginary components of the Fourier coefficients and ran my code to see what happens by shooting in the dark, I found this adequate for debugging purposes but not for practical application.

Next I chose just Fourier coefficients that are periodic in time and smooth, such as $\hat{u}_k = A_k \cos(kt)$.

The way to do this is to use a Poincaré section but I've had problems implementing this due to the fact that the time integration that I'm accustom to is written in MATLAB and I'm trying to work in Python currently. That being said, I've been writing code that adapts the time-integration of `ksint.m` to Python so that I can do exactly this. For antisymmetric subspace $\mathbb{U}^+$ of Kuramoto-Sivashinsky I can integrate in time and then once I've found a close recurrence I will be able to use Fourier smoothing (e.g. discarding higher Fourier modes) and then try to learn Lan's black magic of "manually deforming" the loop to be smooth as to avoid discontinuities in the time direction [27].

There is a storm in the distance however, as this general procedure is ruined for the spatial problem. As we know from the chronotopic literature (see chapter 5), that iteration in space typically does not converge to the same attractor as iteration in time, and generally corresponds to a strange repeller. Therefore I cannot hope to form an initial guess loop from using a Poincaré section in the spatial direction, as typically all of my Fourier coefficients go off to infinity before a recurrence is found.

My idea to remedy this is to actually use *time* integration to form a initial guess loop for applying Newton descent in *space*. If I integrate

a spatially periodic initial condition in time, by virtue of the spatial periodicity there is a close recurrence in the spatial direction (close and not exact only due to discretization I believe). If I've thought about this the right way. It's the smartest way I can think of to generate an initial condition for the spatial Newton descent (1.36) given that my spatial integration code is ill-behaved. If my *spatial* code was working and there is no lapse in my rationale then it might actually have been a way to produce smooth initial guess loops for the *time* direction Newton descent code. [15]

Reading In between coding sessions I've been trying to not lose sight of the bigger picture which in my head is periodic orbit theory. I've been trying to spend any downtime/breaks from Python by rereading the Bible (Chaosbook)

misc A lot of time spent on random errands that come with being an adult and preparing for trip to UCSB. Also students had a hard time with their homework this week so I've had to put more work into shepherding.

Prof. Grigoriev was able to remedy the issue with the computer I'm working with on; Updating graphics drivers did not accomplish this so he installed a new version of Linux Mint (v17.3), which resolved my issues. I made sure to notify Burak as to disrupt his calculations as little as possible.

2016-11-21 Matt : Spent all day and night trying to convert time integration code to Python to no avail. I'm convinced there is a specific reason why Kassam and Trefethen [24] use MATLAB. I have checked it in so many different ways yet it just numerically fails around $T \approx 300$. It makes no sense to me as I can easily manipulate the code while working in MATLAB....implying that I have an understanding of what it's doing. The only resources I found were that perhaps the matrix exponentiation that takes place could possibly be less accurate; checking everything manually yields quantities that are within machine precision to the corresponding MATLAB quantitites.

This puts a wrench in my plans of writing Python code to develop a procedural way to generate initial conditions for Newton descent using a Poincaré section and elbow grease; I will try to do this using MATLAB and ask around for solutions towards why I'm so bad at Python. I'm honestly at a loss for words.That being said there ain't no rest for the wicked so I'll try to implement this in MATLAB and see where it leads.

2016-11-22 Matt :

---

[15]Matt 2016-11-18: I kept thinking about the process of using time integration to produce loops for spatial Newton descent. The newest thought concerns the fact that time and spatial directions do not usually converge to the same attractor. Maybe this implies that my idea of using *time* integration with spatially periodic boundary conditions to produce an initial guess loop for *spatial* Newton descent could be the *worst* way of doing so...still haven't thought it through enough.

Rooftop Plunge Talked with Professor Molei Tao of the Mathematics department. We discussed methods other than the Newton descent on how to find repelling (hyperbolic) periodic orbits. He suggested that I apply a method which parameterizes an interval of points which crosses a separatrix such that a point on this discrete interval is guided to the orbit by means of using the dynamical system redefined with a fictitious time, and iterative reparameterization that is applied repeatedly as points defined on this interval are swept along the unstable directions.

Specifically if the original dynamical system is given by,

$$\dot{\mathcal{X}} = f(\mathcal{X})$$

Then an interval of points $\Phi(\tau, \alpha)$ parameterized by α which undergo fictitious dynamics in a new variable τ obeys,

$$\Phi_\tau(\tau, \alpha) = f(\Phi(\tau, \alpha)), \tag{13.25}$$

with endpoints of the interval at any fictitious time are given by $\alpha = 0, 1$. Over the course of this fictitious time evolution the interval will begin to shoot apart due to the unstable manifold of the hyperbolic periodic orbit. As I understood it, after evolution of finite fictitious time τ_0 a new interval I_n is interpolated between two points that have yet to be completely swept away by the unstable manifold in order to begin the procedure again. I must maintain the original parameterization when defining these subintervals, e.g. if the original interval $I_0 = [0, 1]$ then each subsequent interval is decided by $I_n = [\alpha_n^-, \alpha_n^+]$ where $\alpha_n^\pm$ are the corresponding values of the parameterization of points previously interior to the proceeding interval that will define the endpoints of the newest interval iteration.

Additionally, a forcing term may be included in order to balance the expansion due to the unstable manifold. (Committed from memory, but I believe it to be correct).

$$\Phi_\tau(\tau, \alpha) = f(\Phi(\tau, \alpha)) + \Lambda_\alpha \Phi(\tau, \alpha) \tag{13.26}$$

Professor Tao also showed me a different way of defining the cost-functional currently being used. In his notation of ref. [51], an action functional of the form

$$S[\mathcal{X}] = \frac{1}{2} \int_0^T ||\dot{\mathcal{X}} - f(\mathcal{X})||_{L_2}^2 dt \tag{13.27}$$

can be rewritten if we expand out the norm,

$$S[\mathcal{X}] = \frac{1}{2} \int_0^T ||\dot{\mathcal{X}}||^2 + ||f\mathcal{X}||^2 - 2 < \mathcal{X}, f(\mathcal{X}) > dt \tag{13.28}$$

and finally upon usage of the Cauchy-Schwarz Inequality, we see,

$$S[\mathcal{X}] \geq \hat{S}[\mathcal{X}] = \int_0^T ||\dot{\mathcal{X}}|| \cdot ||f(\mathcal{X})|| - 2 < \mathcal{X}, f(\mathcal{X}) > dt \qquad (13.29)$$

The benefit of rewriting this is that one can see that the equality holds when $\mathcal{X} = f(\mathcal{X})$ which can be guaranteed by rescaling time.

The main idea of this new equation is that it is maximizing how parallel the two vectors are by virtue of the inner product. By rescaling the time the entire functional can be minimized. There was a subtle point about how the two minimizers are not generally the same but the time rescaling procedure guaranteeing the equality makes it so that solving both problems are equivalent.

literature Began poking through the literature cited in ref. [51] to get more feel for variational methods.

Newton Descent Abandoned Python in the hunt for initial conditions for the time being. Began adapting time integration code from ref. [24] to develop a Poincaré section to find a close recurrence in order to begin manually deforming integrated results into a relatively closed loop. I attempted today to produce such an orbit but I need to first rearrange the time integration code for reflect time integration of the antisymmetric subspace $\mathbb{U}^+$. I believe that otherwise I have a good idea of how to create the Poincaré section and an idea of how to smooth out the loop manually by using an interpolation and introducing some sort of weighting function such as a sine curve that will forcibly make the higher modes periodic in time.

2016-11-25 Matt :

Mostly done with matlab code to produce initial conditions for variational method using Poincaré section and Fourier smoothing to produce initial guess loops that are smooth and generally better than what I had previously been producing.

The code takes an arbitrary initial condition and integrates it for a long enough time such that any transient behavior dies out. Then finds an initial and first return points of intersection with a Poincaré section described by the hyperplane $a_1 = 0$.

After words this loop is processed by Fourier smoothing of the individual coefficients in order to make them periodic. I couldn't get a rewritten version of the ETDRK4 code to work for the antisymmetric subspace $\mathbb{U}^+$ for long times yet so I worked around this by taking the imaginary part of an antisymmetric initial condition. I seem to have be having similar problems to what I encountered when trying to adapt the code to a python implementation, it breaks down right when the transients are filtered out. Naturally there shouldn't be any issues as the code only requires
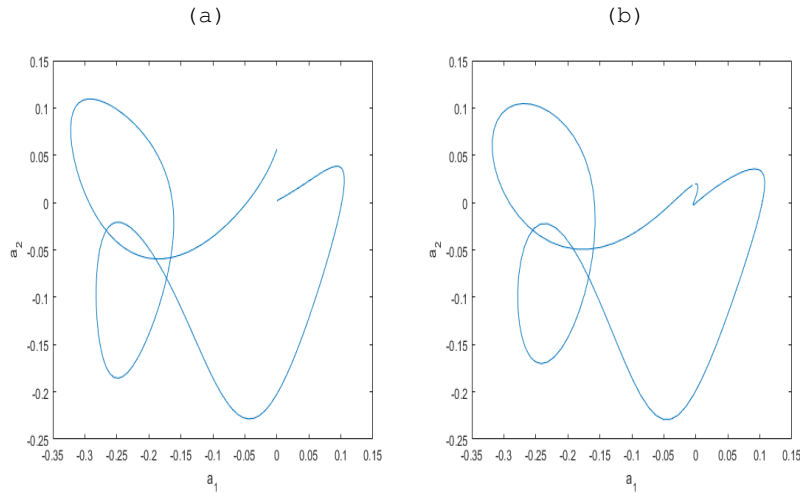
Figure 13.33: An initial guess loop projected onto the (a_1, a_2) Fourier coefficient coordinate axes, (a) before and (b) after application of Fourier smoothing.)

a change of the definition of the nonlinear term and taking the imaginary part of the initial condition, but even so, I've been able to produce some loops with my jerry-rigged code namely figure 13.33

2016-11-29 Matt :

Staying up all night to code changed very little in regards to my status sadly. I reworked the Poincaré section MATLAB code and I feel more confident in it as I get trajectories that look like figure 1 (a) in ref. [30].

Plugging these new initial conditions into my Newton descent code changed nothing however, so I reworked this as well to only evolve the Fourier coefficients corresponding to positive frequencies, thereby reducing the dimensionality of the problem. I had to rewrite the stability matrix and velocity function to exploit this. In the current version the contributions from the nonlinear term are calculated explicitly via the sum also used by Rempel et al. [43],

$$\frac{-q_k}{2} \sum_{m=-N}^{m=N} a_m a_{k-m} = \frac{-q_k}{2} \left(\sum_{m=k-N}^{m=-1} a_{-m} a_{k-m} - \sum_{m=1}^{m=k-1} a_m a_{k-m} + \sum_{m=k+1}^{m=N} a_m a_{m-k} \right),$$

where the positive frequency modes are denoted by $k = 1, \ldots, N$, and

$q_k = \frac{2\pi k}{L}$. The corresponding equation of evolution is therefore

$$\dot{a}_k = (q_k^2 - q_k^4)a_k + \frac{q_k}{2}\left(\sum_{m=k-N}^{m=-1} a_{-m}a_{k-m} - \sum_{m=1}^{m=k-1} a_m a_{k-m} + \sum_{m=k+1}^{m=N} a_m a_{m-k}\right)$$

(13.30)

(Before approximately halving the spectrum there were $2N + 1$ modes in the notation of ref. [43]. I'm following their notation because having N/2 everywhere just serves to clutter the equation.) It's possible that I made a mistake in implementing the stability matrix in this form, the corresponding equation that I derived was, I need to double check tomorrow.

$$A_{ij} = (q_i^2 - q_i^4)\delta_{ij} + \frac{-q_k}{2}(a_{i+j} + 2a_{j-i} - a_{i-j}),$$

(13.31)

where $i, j = 1, \ldots, N$ and terms like $a_{i-j} = 0$ for $i < j$. Implementing these changes sped my code up considerably but I still was unable to achieve good results. I believe this might have been due to using too few discritized time points. I increased the number of points but was unable to get the code to run in a timely manner, and due to the amount of memory it was using I decided to leave it for tomorrow after double checking.

Also still unable to determine why the ETDRK4 code works perfectly in MATLAB but fails after finite time in Python. The problem is that the intermediate modes seem to diverge which I thought was a sign that I had possible defined the nonlinear term incorrectly but as far as I can tell it yields results identical to MATLAB results early in the integration process. I don't know much about the discrepancies between the precision of the built-in MATLAB functions vs. numpy. I read that there might be a problem with matrix exponentiation that's required due to differing definitions of the Padé approximants but I haven't been able to confirm.

All in all, walking the sad road of a wandering gunslinger in the Wild West (In honor of HBO's WestWorld).

2016-11-30 Matt : Past two days have been spent making changes to Newton descent and testing those changes. For any changes that I make that translate generically to any system I try to test them with Rössler first before applying them to antisymmetric subspace $\mathbb{U}^+$ of Kuramoto-Sivashinsky. The other changes that are unique to antisymmetric Kuramoto-Sivashinsky must of course be tested in that realm. The changes are looking promising, as I can find longer periodic orbits in the Rössler system now, however the period seems to be slightly off (Integrating the solution after application of Newton descent yields a solution that is periodic but overlaps). This is my number one suspect for why the Newton descent code continues to stall at the moment; however, for the Rössler system although it is much slower for longer periodic orbits, it still converges very quickly once $F^2 < 1$.
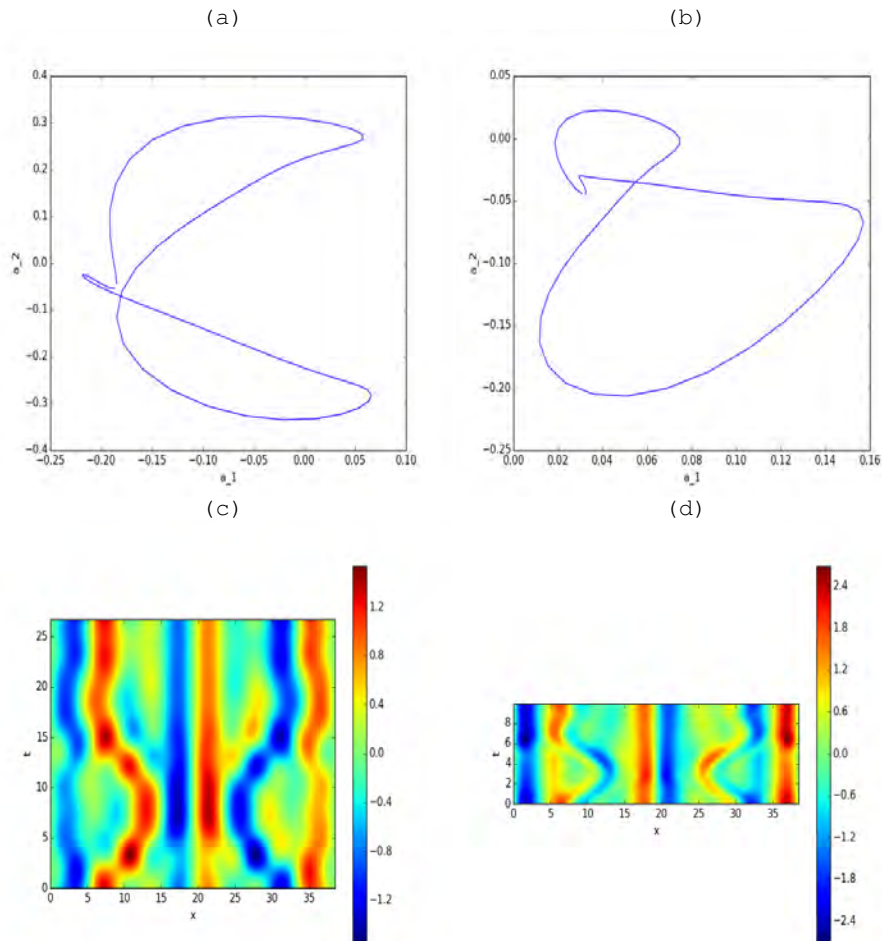
Figure 13.34: Preliminary results of 2016-11-29 version of Newton descent code. (a) Tailored initial guess loop for system size $L = 38.5$ with approximate period of $T \approx [0, 26)$ defined with 16 Fourier modes with 64 discretized time points, (b) Resulting loop after application of Newton descent code. The approximate values for the cost functional are (a) $F^2_{initial} \approx 200$ and (b) $F^2_{final} \approx 10$. The (a) initial and (b) final spacetime plots of the values of $u(x, t)$ have also been included for comparison.

After applying these changes to antisymmetric subspace $\mathbb{U}^+$ of Kuramoto-Sivashinsky I produced results in figure **??** that look much more like [30] fig 1(a) (ergodic trajectory belonging to antisymmetric subspace) and less like figure **??**, figure **??**, figure **??**. I believe these results, although comparable in their final values of cost functional $F^2 \approx 10$, are much more demonstrative and close to actual periodic solutions belonging to the antisymmetric subspace $\mathbb{U}^+$ of Kuramoto-Sivashinsky. I'm using the similarity as a gauge of how good the results are but I understand that once I find periodic orbits I will use the quantitative approach of verification which compares spectra of periodic orbits.

Applied Professor Tao's definition of cost functional (13.29) with very poor results (initial values of $F^2 \approx 10^6$). I don't think I handled the time rescaling that is required correctly but I didn't get much time working through it yet.

2016-12-05 Matt Sanity check I went back through the calculations for keeping only the positive Fourier modes for antisymmetric subspace $\mathbb{U}^+$ of Kuramoto-Sivashinsky, as I felt like that was the only place I could have made a mistake at this point; I did indeed discover a mistake in the definition for the stability matrix equation, and will lay the derivation here as proof I am accomplishing something; albeit minor. I also rederived the equation for the velocities for the positive Fourier modes but this was less interesting as it was just rewriting sums (13.30). Therefore beginning with (13.30),

$$\dot{a}_k = (q_k^2 - q_k^4)a_k + q_k \left(\sum_{m=k-N}^{m=-1} a_{-m}a_{k-m} - \sum_{m=1}^{m=k-1} a_m a_{k-m} + \sum_{m=k+1}^{m=N} a_m a_{m-k} \right)$$

$$\frac{\partial \dot{a}_k}{\partial a_j} = (q_k^2 - q_k^4)\delta_{kj}$$
$$+ q_k \left(\sum_{m=k-N+1}^{0} a_{-m}\delta_{(k-j)m} + a_{k-m}\delta_{-mj} \right)$$
$$- q_k \left(\sum_{m=0}^{k} a_{k-m}\delta_{mj} + a_m \delta_{(k-j)m} \right)$$
$$+ q_k \left(\sum_{m=k}^{N-1} a_{m-k}\delta_{mj} + a_m \delta_{m(k+j)} \right)$$

whereby using the bounds for the sums over m in conjunction with the Kronecker delta functions leads to inequalities for j which determine the contributions from each sum depending on the value of j. Specifically there are three separate triangular matrices that can

be calculated according to these recipes for A_{kj},

$$
\begin{array}{|c|c|}
\hline
0 \leq j \leq k & -2a_{k-j} \\
0 \leq j \leq N-1-k & 2a_{k+j} \\
k \leq j \leq N-1 & 2a_{j-k} \\
\hline
\end{array}, \tag{13.32}
$$

where all indices excluding the summation indices m range from $0, \ldots, N-1$ in order to adhere to how Python indexes arrays.

I have triple checked this and spent the majority of the day testing and debugging this, and yet it seems to completely destroy all of the progress I have made; it destroys the smoothness of the initial guess loop immediately and therefore ruins the entire fictitious integration process. This makes no sense to me as the motivation for such endeavors were Rempel's use of only the positive Fourier spectrum [43] and some of Lan's old codes that I have looked at in order to get some divine inspiration from the astral plane.

This is disheartening as I thought I finally figured out my problems but I suppose its back to the drawing board.

2016-11-07 Matt :

variational methods for dummies Spent too much time figuring out why explicitly calculating the sums seem to be so different than the previous ways of calculating the velocity and stability matrix elements. I spent some time tracking down what I believed was an indexing error either in the derivation or how I have written the code, I made some mistake when rewriting the equation to correspond to Python's indexing situation but I believe I know how to fix the issues.

After testing I believe that the number of discretized point I have been using is much too small in order to induce smooth fictitious time dynamics (PC: believe what?) and noting that the number of discretized points used in in ref. [30] are larger than what I have been using. I have been trying to improve the efficiency of the code that I already have, as previous efforts with discretizations larger than $N = 128$ when using the first $d = 16$ positive Fourier modes tends to run very very slowly due to the generation of pseudoinverses of matrices of such large size, $Nd \times Nd + 1$. Lan used $N = 512$ for in certain examples. I believe that the number of discretized point I have been using is much too small in order to induce smooth fictitious time dynamics.

KITP Almost done writing the abstract that I need to submit for poster presentation. I'm definitely interested in feedback.

Navier Stokes Sent out a line of communication to Professor Gibson about codes and Krylov subspace methods that he mentioned in the email correspondence with PC. Tried to pick up a few texts but the end

of the year ramp up and my own stupidity has left me desiring for more hours in the day.

2016-12-13 Matt :

coding The coding struggles continue. I don't know how Lan was able to accurately sum the nonlinear term as whenever I do it explicitly I get inaccurate results when compared to the FFT method of doing so. I've only seen sources claiming that these sums are inaccurate and so I am throwing out these sums which is disappointing because I am so utterly frustrated at this problem and I thought it would be my savior. proof?

I am trying a new way of calculating the stability matrices that I will write up once I've confirmed that I haven't gone insane/made errors in how I wrote it down. Also found and removed a few small errors that my eyes had somehow missed. This fixed the problem I was having with the periods of the periodic orbits of the Rössler system.

To speed up the code I starting using a different implementation of the pseudoinverse that comes from the same Python library. This implementation uses the matrix's singular value decomposition as opposed to a least squares solver and seems to speed up the process by quite a bit; not enough however to really make an impace into the exceedingly long times that come with finely discretized initial guess loops (16 spatial modes, 512 time points).

I'm letting the code run overnight with these new definitions so I might have a happy surprise in the morning.

reading Read a few chapters of Numerical Linear Algebra by Trefethen and Bau [53]. If I had more time I would've also try to brush up on my coupled-map

2016-12-15 Matt :

Code I'm making some strides in rewriting the code such that it is more efficient by trying to use less memory; so now I get my bad results even faster. I found out now that the smooth loops that I had been generating for initial conditions only looked nice because the specific Fourier coefficient projections I was using (normally (a_1, a_2)) were not exhibiting the Gibbs Phenomena nearly as much as the higher Fourier modes are. i.e. I didn't consider how smoothing the Fourier spectrum can actually take the initial guess loop quite far away from the integrated results using the hyperplane Poincaré section and therefore is probably the main reason why improvements to my code seemingly have no effect. I need to treat these discontinuities in the higher ($k > 1$) Fourier modes more carefully. The main

idea that popped into my head is to use a cubic spline before initiating the Fourier smoothing (discarding the higher Fourier mode data). I've been trying to look for better methods or information as splines have their own related Gibbs phenomenon [58] when uniform discretizations are used and I am trying to avoid rewriting the code the generates my initial conditions to be defined on anything but uniform meshes; Chebyshev point interpolation might be an option as I know that a good MATLAB package called `chebfun` written by the One (Trefethen) exists for these purposes, but I haven't looked into it yet. Also added ref. [56] in case it proves useful. Didn't get around to implementing this as my day was cut in half with exam grading.

Calculations Currently I am using only the positive part of the Fourier spectrum but doing the calculations for the velocities/stability matrices with the full spectrum as I cannot get the summation formulae for the convolution sum (nonlinear) term to behave as well as Lan did. I must say that this sideways motion of waffling between methods is disappointing but as I get more and more used to the method I believe the more natural concepts are rising to the top.

The new equation for the elements of the stability matrix that I arrived at, [16]

$$\frac{\partial \dot{\hat{u}}_k}{\partial \hat{u}_j} = (q_k^2 - q_k^4)\delta_{kj} - 2q_k N \mathcal{F}\{\mathcal{F}^{-1}(\delta_{\ell j}) \times \mathcal{F}^{-1}(\hat{u}_{\tilde{\ell}})\}_k \,, \qquad (13.33)$$

where $q_k = 2\pi k/L \,, \hat{u}_k = \mathcal{F}\{u\}_k \,.$

The factor of N (power of 2, size of spatial discretization) is to follow the convention that the normalization of $1/N$ is applied upon the forward transformation (but in Python and MATLAB it is applied upon inverse FFT, therefore we need two factors of N to cancel the built-in normalizations). The multiplication of the inverse FFTs is carried out element-wise hence the explicit multiplication symbol. Although the result looks completely obvious I wanted to make sure that I didn't mess anything up such that I don't spend any more time trying to define quantities I should have known so this is what I arrived at after writing the nonlinear term explicitly in terms of the

---

[16]Predrag 2017-01-10: What's $\ell, \tilde{\ell}$ in (13.33)?

discrete Fourier transform summations. I.e.,

$$
N \frac{\partial}{\partial \hat{u}_j} \sum_{n=0}^{N-1} \left(\sum_{\ell, \tilde{\ell}=-N/2}^{N/2-1} \hat{u}_\ell \, \hat{u}_{\tilde{\ell}} e^{i(q_l + q_{\tilde{\ell}}) x_n} \right)_n e^{-i q_k x_n}
$$

$$
= \sum_{n=0}^{N-1} \left(\sum_{\ell=-N/2}^{N/2-1} \delta_{\ell j} e^{i q_l x_n} \sum_{\tilde{\ell}=-N/2}^{N/2-1} \hat{u}_{\tilde{\ell}} e^{i q_{\tilde{\ell}} x_n} \right.
$$

$$
\left. + \sum_{\tilde{\ell}=-N/2}^{N/2-1} \delta_{\tilde{\ell} j} e^{i q_l x_n} \sum_{\ell=-N/2}^{N/2-1} \hat{u}_\ell e^{i q_\ell x_n} \right)_n e^{-i q_k x_n}
$$

$$
= 4N \mathcal{F} \{ \mathcal{F}^{-1}(\delta_{\ell j}) \times \mathcal{F}^{-1}(\hat{u}_{\tilde{\ell}}) \}_k \tag{13.34}
$$

2016-12-17 Matt :

  Coding Still getting the "falling into equilibrium" problem with changes
  to initial condition generation, i.e. the loop is deformed to a very
  small (in terms of temporal length) loop around the trivial equilib-
  rium $u = 0$. Somehow this is the only local minimum that my code
  sees and I haven't been able to figure out why.

  misc Downloaded and played with the `chebfun` package produced by
  Trefethen and others but with the other changes I made I haven't
  implemented anything involving this. Also got my new laptop up
  to task for programming/subversion needs.

  KITPabstract Read through the changes PC made to abstract. I like them
  especially the rephrasing for the motivation for variational method,
  every way I wrote it made it seem tacked on and not a central con-
  cept. (PC - thanks! every little bit of praise helps:)

2016-12-17 Predrag Can you offer to Boris (by email - he's showing up on Sat-
  urday, but I do not know for how long) to help him install whatever on
  his laptop, teach him how to use subversion? It seems that he can edit
  our article only if he is logged onto the linux machine in his office, which
  really slows down everything...

2016-12-17 Predrag This might be a red herring, but Moser was very good (he
  is the M in KAM-theory), and maybe there is something useful for you
  in Moser [36] *Minimal solutions of variational problems on a torus*. Do not be
  discouraged if it is hard to read - we might have to ask Prof. de la Llave
  to translate it for us.

2016-12-20 Matt :

  Coding Wrote MATLAB code using `chebfun` to trigonometrically inter-
  polate time-integrated Fourier coefficient data as well as convolute
  this interpolated data with a Gaussian mollifier to manually deform

initial loop guesses into continuous curves. In conjunction with the Fourier smoothing and paying attention to how the mollified data behaves at the boundaries it works quite well.

Almost there. I can taste it. Initial Loops now have initial values for the cost functional $\mathcal{F}^2 \approx 1 - 10$ if I'm lucky. The only place I believe that there could possibly be an error still is in the code for the stability matrices, however, it could just be that the initial guess loops as well. (Mostly tested with older initial conditions so far, according to [27] 3/10 initial conditions failed, considering I don't know how he explicitly produced these my rates might just be much higher).

Played around with implementing the Poincaré section constraint on the more unstable modes but to not effect, went back to pseudoinverses in the end.

Misc Wrote a nearly exhaustive (I believe at least) tutorial for Boris on how one uses subversion. I made sure to not leave any breathing room for mistakes. I can be sure of this as I just recently had to go through the entire procedure for my new laptop as of a couple days ago.

Misc2 Submitted poster presentation abstract and began working on formatting/gathering plots that I intend to use. So far I have the time-integrated and spatially integrated versions of $\overline{ppo}_{10.2}$, and the variational Newton descent applied to the Rössler system. I'm really hoping I'll have something for Kuramoto-Sivashinsky antisymmetric subspace $\mathbb{U}^+$ by the time I need to print. I am hopeful.

2016-12-20 Matt :

Newton descent 99 percent of the way there, I believe. Very close to reproducing center periodic orbit $\overline{01}$ from ref. [30] (without looking at stability multipliers/exponents, basing this off of the period, as well as figure 5 (b) of ref. [30] as crude guideline.) Currently I have figure 13.35, which is close but there is a discrepancy as the period is $T \approx 25.6768$ which differs from the value $T = 23.6356$ from [30]. I'm thinking this might be due to the difference in the implemented methods as he calculated everything explicitly using sums.

2017-01-10 Predrag It's probably as good as you can expect it - we do not know what was the dependence of Lan's computation on various truncations. Tthe answer could be reproducible in a given setup to many digits, but systematic errors due to the truncations might be much larger. The leading Channelflow stability eigenvalue (let's say) might be reproducible to machine precision, but when you change the discretization, the answer changes in 6th digit.

poster The journey continues, happy with antisymmetric results for now and will try to get spatial results on the poster if I'm lucky. I think I
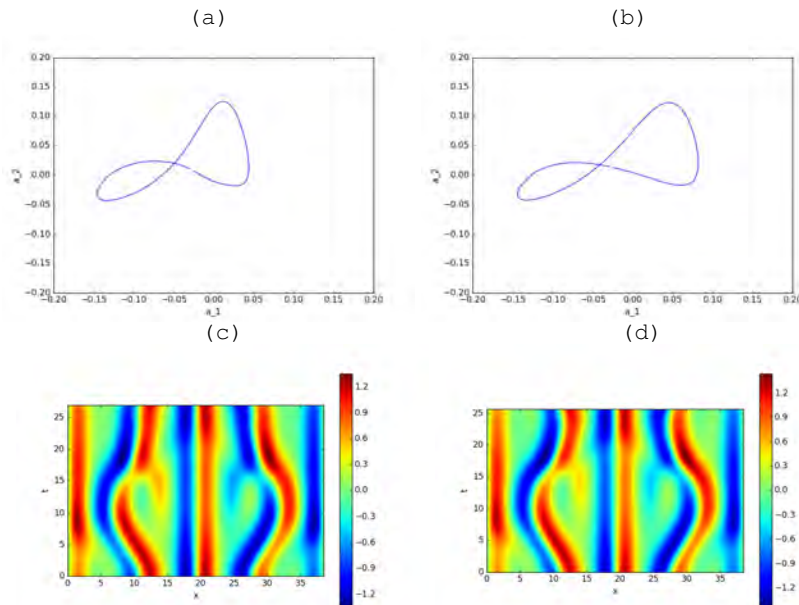
Figure 13.35: (a) Initial condition for variational Newton descent using $N = 15$ positive spatial frequency Fourier modes discretized over 128 points in time. (b) Final loop after application of Newton descent. (c) Initial and (d) final spatiotemporal plots of $u(x,t)$. The initial value and final cutoff value for the cost functional were $\mathcal{F}^2 = 0.61460192$ and $\mathcal{F}^2 = 10^{-10}$.

should be able to if I exploit ref. [49] properly and learned from my mistakes. Setting the bar high as per usual.

2016-12-21 Matt Code I managed to get an alternate version of the Newton method code working using previous mistakes as a guide. I now have two versions, one that uses FFTs to calculate the velocities and stability matrices and one that uses explicit sums like Lan's. The results agree to within a certain precision, based on their periods. Also included are the run times as a means of showing which version is favorable, which of course is the FFT version as it requires fewer operations. In all calculations I made it such that the cutoff value for the cost functional was to machine precision.

	T	T comp.
FFT + pseudoinverse	25.6768522498	42 seconds
FFT + inverse	25.6768522713	36 seconds
Explicit sums + pseudoinverse	25.678522628	185 seconds
Explicit sums + inverse	25.6768522555	151 seconds

What I believe this means is that there are small differences in imple-

mentation of the loop that controls fictitious time evolution between Lan's codes and mine that are causing the discrepancies. I've tried redefining this in multiple ways but other than the obvious change between pseudoinverses or inverses they all have been failures.

Poster I have most of the information that I believe should be on the poster but its too much text.

spatial code Worked a little in making changes that helped me with antisymmetric subspace $\mathbb{U}^+$ work, but mainly spent the day trying to verify my results and figure out why they are different than Lan's.

2016-12-22 Matt :

Code After more testing I found one of the discrepancies between Lan's code and my own; the number of Fourier modes used in computation. I don't know why I didn't think of it earlier as it seems obvious now that including more modes changes the periodic orbit in a numerical sense. By using $N = 16$ positive frequency modes my code now yields the period to be $T = 25.6355$ vs. Lan's $T = 25.6356$. I wish he had included more digits as it's hard to distinguish if this is actually still a discrepancy or if it's just a rounding issue. Regardless, I'm one step further.
2017-01-10 Predrag Lan's numbers might be given to more digits in the svn repository `y-lan` (alert me if your svn ID/password does not let you check it out). Possibly you can find them by some linux magic, like
`>cat FileName | grep 25.63`
Also, you can fish through y-lan directories on zero.physics.gatech, but those are not tidy (to put it mildly:).

The only other difference that I know of between our codes is his matrix inversion process. He does this using LU decomposition for the banded diagonal matrix and the Woodbury formula for the cyclic border terms [27].

Poster Almost done with draft. Having a hard time condensing important information while sounding coherent.

2016-12-24 Matt : Mainly worked on getting poster to a presentable state. Multiple critics deemed there to be far too much text so I gutted the poster and tried to focus on the visual elements and equations more. pdf uploaded to repository under `/gudorf/presentations/KITPposter`.

2016-12-24 Predrag Slowly re-reading the blog for the past few months - I really like how clearly Matt records step-by-step progress in the project.

A comment about calculations in the Kuramoto-Sivashinsky invariant antisymmetric subspace $\mathbb{U}^+$. Your (13.22) unfamiliar at the first glance (I have not rechecked it, as it is derived and discussed in ChaosBook.org),

but the Fourier coefficients should all be real, and the calculation is carried out only on $1/2$ of the L-domain, with the correct antisymmetric subspace $\mathbb{U}^+$ boundary conditions: *they are not periodic*. Morally, when comparing the antisymmetric subspace $\mathbb{U}^+$ to the full state space dynamics, on should say that its domain size is $L/2$. That is why there is so little going on in this invariant subspace when $L = 22$; have to go much higher in L to get chaotic dynamics. No matter what are initial guesses, you only can find some equilibria in the invariant subspace for $L = 22$, so your "solutions" are very unlikely to be solutions. You can see this clearly in figure 13.30 - the left half is just the right half reflected and multiplied by -1. So the cost function (if you define it on spatial mesh) is computed only on the $[0, L/2]$ domain. The b.c.'s are automatically enforced by the form of the Fourier expansion, with coefficients beyond $N/2$ set equal to zero, not moded as you do in defining $a_{((k-m))}$. You might be right, I had not used aliasing in my calculations, but maybe should have.

Taking the spacetime data corresponding to the first equilibrium and $\overline{ppo}_{10.2}$ integrated in time for $2\,T_{\overline{ppo}_{10.2}}$ reducing them to the antisymmetric subspace $\mathbb{U}^+$ by taking the imaginary parts of their spatial Fourier spectra will land you a mile from any solution in the invariant subspace. Not sure why you added the deformation (13.24). At lest I think it does satisfy the b.c.'s. Anyway, you could have used a first few Fourier modes for Feynman's trousers belt, and it would have been as good initial guess.

The structure of the "solution" in figure 13.30 is unfamiliar to me, but the scales of the features seem not too small (small rapidly varying shapes would indicate that something is very wrong). The value of the cost functional F^2 decreasing from ≈ 40 to ≈ 8 in figure 13.30 probably means that the descent has gotten hung up in a false "minimum," and it is not converging to a true spatiotemporal solution. Figure 13.31 looks more suspect (lots of unfamiliar small-size structures). Figure 13.32, however, looks totally credible - is is one of the equilibria that we list in our papers? As explained above, for $L = 22$ I agree with you: I expect everything to either stall or go to a known equilibrium, as in figure 13.32.

2016-12-27 Predrag : Is the poster source file too big to commit? More fun if one can tinker with it.

References

[1] S. Abbasbandy, Y. Tan, and S. J. Liao, "Newton-homotopy analysis method for nonlinear equations", Appl. Math. Comput. **188**, 1794–1800 (2007).

[2] A. A. Aderogba, M. Chapwanya, and J. K. Djoko, "Travelling wave solution of the Kuramoto-Sivashinsky equation: a computational study", AIP Conf. Proc. **1479**, 777–780 (2012).

[3] H. Bosetti, H. A. Posch, C. Dellago, and W. G. Hoover, "Time-reversal symmetry and covariant Lyapunov vectors for simple particle models in and out of thermal equilibrium", Phys. Rev. E **82**, 1–10 (2010).

[4] L. A. Bunimovich and Y. G. Sinai, "Spacetime chaos in coupled map lattices", Nonlinearity **1**, 491 (1988).

[5] C. Canuto, M. Y. Hussaini, A. Quateroni, and T. A. Zhang, *Spectral Methods in Fluid Dynamics* (Springer, New York, 1988).

[6] C. Q. Cheng and Y. S. Sun, "Existence of invariant tori in three-dimensional measure-preserving mappings", Celest. Mech. Dynam. Astronom. **47**, 275–292 (1990).

[7] F. Christiansen, P. Cvitanović, and V. Putkaradze, "Spatiotemporal chaos in terms of unstable recurrent patterns", Nonlinearity **10**, 55–70 (1997).

[8] P. Cvitanović, R. L. Davidchack, and E. Siminos, "On the state space geometry of the Kuramoto-Sivashinsky flow in a periodic domain", SIAM J. Appl. Dyn. Syst. **9**, 1–33 (2010).

[9] P. Cvitanović and Y. Lan, Turbulent fields and their recurrences, in Correlations and Fluctuations in QCD : Proceedings of 10. International Workshop on Multiparticle Production, edited by N. Antoniou (2003), pp. 313–325.

[10] L. Dieci, J. Lorenz, and R. D. Russell, "Numerical calculation of invariant tori", SIAM J. Sci. Stat. Comput. **12**, 607–647 (1991).

[11] X. Ding and P. Cvitanović, "Periodic eigendecomposition and its application in Kuramoto-Sivashinsky system", SIAM J. Appl. Dyn. Syst. **15**, 1434–1454 (2016).

[12] C. Dong and Y. Lan, "Organization of spatially periodic solutions of the steady Kuramoto-Sivashinsky equation", Commun. Nonlinear Sci. Numer. Simul. **19**, 2140–2153 (2014).

[13] N. Fenichel, "Persistence and smoothness of invariant manifolds for flows", Indiana Univ. Math. J. **21**, 193–226 (1971).

[14] J.-L. Figueras and À. Haro, "Reliable computation of robust response tori on the verge of breakdown", SIAM J. Appl. Dyn. Syst. **11**, 597–628 (2012).

[15] A. M. Fox, Destruction of Invariant Tori in Volume-Preserving Maps, PhD thesis (Applied Math, U. Colorado, Boulder, 2013).

[16] A. M. Fox, A brief life and death of a torus: Computation of quasiperiodic solutions to the Kuramoto-Sivashinsky equation, in preparation, 2015.

[17] A. M. Fox and J. D. Meiss, "Critical invariant circles in asymmetric and multiharmonic generalized standard maps", Commun. Nonlinear Sci. Numer. Simul. **19**, 1004–1026 (2014).

[18] A. M. Fox and J. D. Meiss, "Computing the conjugacy of invariant tori for volume-preserving maps", SIAM J. Appl. Dyn. Sys. **15**, 557–579 (2016).

[19] T. Ge and A. Y. T. Leung, "Construction of invariant torus using Toeplitz Jacobian matrices/fast Fourier transform approach", Nonlinear Dyn. **15**, 283–305 (1998).

[20] R. Grimshaw and A. P. Hooper, "The non-existence of a certain class of travelling wave solutions of the Kuramoto-Sivashinsky equation", Physica D **50**, 231–238 (1991).

[21] B. Gutkin and V. Osipov, "Classical foundations of many-particle quantum chaos", Nonlinearity **29**, 325–356 (2016).

[22] J. H. Hannay and M. V. Berry, "Quantization of linear maps on a torus – Fresnel diffraction by a periodic grating", Physica D **1**, 267–290 (1980).

[23] R. H. G. Helleman and T. Bountis, "Periodic solutions of arbitrary period, variational methods", in *Stochastic Behavior in Classical and Quantum Hamiltonian Systems*, edited by G. Casati and J. Ford (Springer, Berlin, 1979), pp. 353–375.

[24] A.-K. Kassam and L. N. Trefethen, "Fourth-order time-stepping for stiff PDEs", SIAM J. Sci. Comput. **26**, 1214–1233 (2005).

[25] J. S. W. Lamb and J. A. G. Roberts, "Time reversal symmetry in dynamical systems: A survey", Physica D **112**, 1–39 (1998).

[26] J. S. W. Lamb and C. Wulff, "Reversible relative periodic orbits", J. Diff. Eqn. **178**, 60–100 (2002).

[27] Y. Lan, Dynamical Systems Approach to $1 - d$ Spatiotemporal Chaos – A Cyclist's View, PhD thesis (School of Physics, Georgia Inst. of Technology, Atlanta, 2004).

[28] Y. Lan, C. Chandre, and P. Cvitanović, "Variational method for locating invariant tori", Phys. Rev. E **74**, 046206 (2006).

[29] Y. Lan and P. Cvitanović, "Variational method for finding periodic orbits in a general flow", Phys. Rev. E **69**, 016217 (2004).

[30] Y. Lan and P. Cvitanović, "Unstable recurrent patterns in Kuramoto-Sivashinsky dynamics", Phys. Rev. E **78**, 026208 (2008).

[31] S. Lange, M. Richter, F. Onken, A. Bäcker, and R. Ketzmerick, "Global structure of regular tori in a generic 4D symplectic map", Chaos **24** (2014) `10.1063/1.4882163`.

[32] C. Leis, "Hopf-bifurcation in systems with spherical symmetry. I: Invariant tori", Doc. Math. **2**, 61–113 (1997).

[33] R. de la Llave, "A smooth center manifold theorem which applies to some ill-posed partial differential equations with unbounded nonlinearities", J. Dynam. Differential Equations **21**, 371–415 (2009).

[34] D. Michelson, "Steady solutions of the Kuramoto-Sivashinsky equation", Physica D **19**, 89–111 (1986).

[35] A. Mielke, *Hamiltonian and Lagrangian flows on center manifolds* (Springer, New York, 1991).

[36] J. Moser, "Minimal solutions of variational problems on a torus", Ann. Inst. H. Poincaré **3**, 229–272 (1986).

[37] M. Nagata, "Three-dimensional finite-amplitude solutions in plane Couette flow: bifurcation from infinity", J. Fluid Mech. **217**, 519–527 (1990).

[38] M. E. J. Newman, *Computational Physics* (Createspace Independent Pub, 2012).

[39] R. Paškauskas, C. Chandre, and T. Uzer, "Dynamical bottlenecks to intramolecular energy flow", Phys. Rev. Lett. **100**, 083001 (2008).

[40] R. Paškauskas, C. Chandre, and T. Uzer, "Bottlenecks to vibrational energy flow in OCS: Structures and mechanisms", J. Chem. Phys. **130**, 164105 (2009).

[41] W. H. Press, B. P. Flannery, S. A. Teukolsky, and W. T. Vetterling, *Numerical Recipes in Fortran 77*, 2nd ed. (Cambridge Univ. Press, Cambridge, 1996).

[42] B. Rasmussen and L. Dieci, "A geometrical method for the approximation of invariant tori", J. Comput. Appl. Math., 388–412 (2008).

[43] E. L. Rempel, A. C. Chian, E. E. Macau, and R. R. Rosa, "Analysis of chaotic saddles in high-dimensional dynamical systems: the Kuramoto-Sivashinsky equation", Chaos **14**, 545–56 (2004).

[44] R. J. Sacker, "A new approach to the perturbation theory of invariant surfaces", Commun. Pure Appl. Math. **18**, 717–732 (1965).

[45] Y. Saiki, M. Yamada, A. C.-L. Chian, R. A. Miranda, and E. L. Rempel, "Reconstruction of chaotic saddles by classification of unstable periodic orbits: Kuramoto-Sivashinsky equation", Chaos **25**, 103123 (2015).

[46] J. Sánchez and M. Net, "A parallel algorithm for the computation of invariant tori in large-scale dissipative systems", Physica D **252**, 22–33 (2013).

[47] J. Sánchez, M. Net, and C. Simó, "Computation of invariant tori by Newton–Krylov methods in large-scale dissipative systems", Physica D **239**, 123–133 (2010).

[48] F. Schilder, H. M. Osinga, and W. Vogt, "Continuation of quasi-periodic invariant tori", SIAM J. Appl. Dyn. Syst. **4**, 459–488 (2005).

[49] E. Siminos, Recurrent Spatio-temporal Structures in Presence of Continuous Symmetries, PhD thesis (School of Physics, Georgia Inst. of Technology, Atlanta, 2009).

[50] P. Takáč, "Invariant 2-tori in the time-dependent Ginzburg-Landau equation", Nonlinearity **5**, 289–321 (1992).

[51] M. Tao, "Hyperbolic periodic orbits in nongradient systems and small-noise-induced metastable transitions", Phys. D **363**, 1–17 (2018).

[52] L. N. Trefethen, *Spectral Methods in MATLAB* (SIAM, Philadelphia, 2000).

[53] L. N. Trefethen and D. Bau, *Numerical Linear Algebra* (SIAM, Philadelphia, 1997).

[54] T. Tsankov and R. Gilmore, "Strange attractors are classified by bounding tori", Phys. Rev. Lett. **91**, 134104 (2003).

[55] A. Weinstein, "Periodic nonlinear waves on a half-line", Commun. Math. Phys. **99**, 385–388 (1985).

[56] R. K. Wright, "Local spline approximation of discontinuous functions and location of discontinuities, given low-order Fourier coefficient information", J. Comput. Appl. Math. **164-165**, 783–795 (2004).

[57] Y. Wu and K. F. Chueng, "Two-parameter homotopy method for nonlinear equations", Numerical Algorithms **53**, 555–572 (2010).

[58] Z. Zhang and C. Martin, "Convergence and Gibbs' phenomena in cubic spline interpolation of discontinuous functions", J. Comput. Appl. Math. **87**, 359–371 (1997).

Chapter 14

Matt's KITP blog

2017-01-03 Matt Happy New Year!

KITP chats Chatted with Ismail Hameduddin about his project in laymen's terms about defining non-zero mean velocity near the walls in pipe flow and how he and his adviser's model predicts this. Chatted with Burak about puffs in pipe flow, I believe he's going to run his presentation by me as practice for himself and education for me.

Burak is also convinced beyond a reasonable doubt that the key to spatial integration is symplectic integration, even though we have discussed at length with Predrag that the formulation of the Kuramoto-Sivashinsky equation is *not* of the symplectic form (i.e., does not have the coordinate/momentum type structure). That being said he wants me to look into this more.

KITP poster Made arrangements for the poster to be printed on campus after some minor edits.

Numerical Linear Algebra Read through more of Trefethen and Bau [13] in preparation of meeting with PC and JG. Arnoldi iteration, GMRES, Krylov subspaces were main topics covered. Trying to work through some of the problems to gain a better intuition rather than just reading.

Newton descent antisymmetric subspace $\mathbb{U}^+$ In response to PC's comments of December 24th. All of the figures *prior* to figure 13.35 were either ill-conditioned initial conditions that did not converge to periodic orbits (figure 13.34) or completely numerically wrong codewise (figure 13.30, figure 13.31, figure 13.32). I was trying to show any progress I was making in terms of quantitative pieces as opposed to me merely claiming "I'm making progress". I suppose I should have gone back for the record and stated "avoid looking at this" or "this is complete nonsense" to prevent confusion, as there is no way anyone could know otherwise. Equations such as (13.24)

328

should be avoided like the plague.

Predrag 2017-01-03 No need to revisit any of that, it's just the log of your work as it progresses. It's my fault for having fallen so far behind in reading your blog. Sorry...

Figure 13.35 (b) and (d) is the periodic orbit $\overline{01}$ as defined in ref. [11] (the Newton descent applied in figure 13.35 is with $L = 38.5$).

Spatial Newton descent Made small contributions to the code, but needs a quite a bit more work. Still working through how to properly handle real and imaginary parts separately in an efficient manner.

2017-01-04 Matt :

Waleffe is trying to answer the question of "which solutions are fundamental in shear flows". In investigation he looked at optimum transport solutions on a reduced length scale (relative to solutions of Boussinesq equation) and looked at the scaling of solutions in regards to Nusselt and Rayleigh numbers.

Main take-away: claims that 2-D sheet scaling being close to 3-D data scaling implies that the dynamics can be described by sheets alone(?)

Wesfreid gave an experimenter's look into Bénard – von Kármán instabilities and use of vortex generators as actuators for flow control as well as Couette-Poiseuille puffs/spots.

Main take-aways: Vortex generators can be used to reduce total drag in expense of local regions of higher drag. In Couette-Poiseuille spots the Couette flow was generally antiparallel to the Poiseuille flow.

John Gibson introduced me to Channelflow and we discussed some of the methods that it uses, specifically Arnoldi iteration. Discussed the general layout of Channelflow in terms of library and scripts but ran out of time to do anything specific. I'm trying to get it up and running (see Misc.) so that I can give the c++ a whirl.

Reading Reviewed some material from Trefethen & Bau [13], began picking out some Navier-Stokes papers to read [5, 9]. Gibson *et al.* refer to Aubry *et al.* [1].

Spatial Newton descent In between all of the informal meetings and cookie breaks I maybe some more small edits to this code, but minimal progress from yesterday.

Misc Installing a virtual machine image of Linux mint in hopes that I would be able to get Channelflow up and running so I can toy around with it... I'm convinced that I should just reinstall Linux mint to be the main operating system of my computer immediately, I know I would have to do this eventually anyway as performance is

otherwise split between the machine image and the Windows operating system. I'm going to try and do this early tomorrow in hopes that I can look at channel flow before talking to John again.

2017-1-5 Matt :

Ati Sharma tries to answer the question of why Koopman modes look like resolvent modes... a question I ask myself daily (just kidding... I'm hoping the tutorial to be quite extensive). Previewed Koopman operators and their use in rewriting nonlinearities into a different form such that one can expand about the mean flow solution. Use of Singular Value Decomposition (SVD) acts as a filter iff there is separation of the singular values σ_i. The main connection that popped into my head was how Arnoldi iteration picks out dominant eigenvalues... I looked into DMD and wikipedia mentioned both Arnoldi iteration and SVD methods so maybe the similarity is not entirely in my head.

Dennice Gayme investigates "restricted nonlinear methods" (RNL). The main question posed was "does momentum redistribution lead to structure?". I.e. does a streamwise description of plane Couette flow with unstructured noise, lead to similar structure present in plane Couette flow. Dennice claims it does, although this was undertaken with relatively low Reynolds number. I believe it was Prof. Caulfield who suggested (and Prof. Gayme agreed completely) that the next step is to undertake some sort of linear stability analysis in order to see if this is somehow related to the transition of streaks/rolls to self-sustained turbulence.

Reading Tried to familiarize myself with dynamic mode decomposition methods in preparation for the Koopman mode tutorial tomorrow. Borrowed Pope [12] from Ismail Hameduddin in order to prepare for the second talk tomorrow per recommendation of Burak.

Channelflow Going through a C++ tutorial recommended by Ismail to help with the transition towards Channelflow. Still trying to set it up properly such that I can run some example files before starting any of my own endeavors.

Misc. • Discussed the Lagrangian formulation of Kuramoto-Sivashinsky equation with Burak and Predrag.
  • Briefly discussed machine learning to find inertial manifolds with Genta Kawahara.

2017-1-7 Matt :

Koopman à la Mezić (video).

Koopman à la Clarence Rowley (video).

Mean flow tutorial à la Laurette Tuckerman (video).

readings More Pope [12] and Channelflow documentation

spatial Newton descent Did a little bit more work towards completion
of code; specifically deriving matrix elements for stability matrices;
I want to rederive everything a second time before I upload it here
as small mistakes held me back in antisymmetric $\mathbb{U}^+$ of Kuramo-
to-Sivashinsky. I believe I will be reducing the number of modes
in numerical implementation as I have to keep track of 8 times the
number of coefficients (factor of two from real and imaginary parts
of Fourier coefficients, factor of four from system of four equations
for each mode number). The only tasks I have left are making sure
the velocity function, stability matrix elements, and differentiation
matrix used to approximate the loop tangent are defined correctly.
I guess there is one additional factor which is producing the initial
conditions for searches

Weekend Plans • Review literature posted to transturb wiki wikispace

- Familiarize myself with Channelflow by going through tutorial,
  finish c++ review c++ resource
- Finish spatial Newton code hopefully

2017-01-09 Matt :

Channelflow Still learning how to manipulate things in c++ and linux.
I'm still getting errors when trying to compile the simple example
files, and it's obvious from the output that the libraries paths aren't
defined correctly but I've tried a number of different ways to change
this and they don't work. I'll be asking my office mates in hopes that
they will be kind enough to elucidate the matter. Trying to keep the
chin held high.

reading Read some of the literature from transturb, I am trying to focus
on the video feeds however as I find that these are better avenues
for review.

spatial Newton descent I suppose I was quite hopeful in trying to get
this done over the weekend.

2017-1-09 Matt :

R. Kerswell Talk (video).

G. Kawahara Talk (video).

R. Grigoriev Talk (video).

C. Cossu Talk (video). Near wall streak structures known since the six-
ties. Self-sustaining process is main source of turbulent kinetic en-
ergy at low to moderate Re. Increasing Re contributes to an emerg-
ing energy peak in terms of streamwise wavelength and wall dis-
tance. This emerging peak has to do with structures scaling with

outer units, and is believed by some to be dominant at very large Re.

Looking at linearized equation with turbulent mean flow and include eddy-viscosity associated with turbulent mean flow and look at the most amplified perturbation as a function of the spanwise scale. There are two peaks, one that does not change with Re and the second peak which does scale with Re.

Showed that linear instability can be a source of energy, but asks if large scale structures can self sustain in the absence of small scales.

The opposite case, showing small-scale structures can self-sustain, was done by using minimal flow units to remove any large active scales.

To do this with large scales there were two ideas, use a very coarse discretization, or filter the small scales and take into account dissipation such that there is no unphysical energy production peak at the scale of the grid.

Using a local spatial filter, (spatial average around each point). This yields and additional term which is the divergence of the Reynolds stress. Reynolds stress modeled with eddy viscosity and Smagorinsky.

To damp more small scales, increase the Smagorinsky constant. Although this produces unphysical solutions, want to see if large-scale structures survive, which they do.

For intermediate sized structures, take a smaller sized box than that which was used for large scaled structures, and then kill out the small scale structures using the method that was used for large scale structures.

The takeaway is that structures of all scales can self-sustain, contradicting the hypothesis of multiple hairpin vortices being advected by the mean flow contribute to large scale structures. These larger structures extract energy from the mean flow via lift-up.

Using Newton's Method to find invariant solutions, then do continuation in the Smagorinsky constant, to find upper branch solutions. The filtered steady solutions are connected to the branch of Navier-stokes solutions found by many others.

M. Avila Talk (video).

A. Duran Talk (video).

S. Tobias Talk (video). *The generalised quasilinear approximation: Application to jets, HMRI, and rotating Couette flows*. Quasilinear really means to keep only certain interaction terms. Divide the quantity of desired investigation and split it into a mean term, and fluctuation term about that mean.

The quasilinear approximation is to discard interaction terms which are contribute to fluctuations and are based on only fluctuation terms.

I.e. mean and fluctuation interaction that effects the mean is kept, fluctuation interactions that affect the mean are kept, but fluctuation-fluctuation interactions that affect the fluctuations are discarded.

Effectiveness of this approximation in fluids is ofter measured by Kubo number, but you need to do the full calculation in order to find this number; it is not something one can know a priori.

In the Generalised quasilinear approximation (GQL) the terms are separated into short-scale and large-scale interactions.

GQL consists of keeping interactions of large scale mean-mean interactions (large scale determined by low wavenumber, for example), large scale mean and small scale fluctuation interactions, and small scale fluctuation-fluctuation interactions.

GQL with a wavenumber cutoff keeping only three spatial Fourier modes outperforms the regular QL approach, as QL overemphasizes the role of waves. (Rossby wave can only reinforce Rossby wave). GQL allows for scattering into different wave numbers.

2017-1-10 Matt :

Channelflow Practicing using Channelflow. Trying to learn all of the command line switches and codes through practice, went through the tutorial.

T. Mullin Talk *The sensitivity of transition in a pipe* (video).
Poiseuille flow, add perturbations. Measured the probability of transition to turbulence versus the normalized amplitude of perturbation. A way to introduce these perturbations is to introduce a jet with a small hole. At $Re \approx 3,000$ the transition probability is still sharp (sigmoid like curve), but with $Re \approx 2000$, you get a small hump that proceeds the main transition. Two different amplitudes of disturbance leads to two different behaviors even though the centerline velocities behave in the same manner showing similar patterns to Marc Avila's slug profiles.

Velocity defect and variance seem to settle in same place for puffs. For the amplitudes between these two large transition probability areas (the region where you have small probability to transition) the correlation does not not follow this behavior.

S. Rubenstein Talk *Colliding vortex rings; Rapid breakup of coherent structures* (video). How do coherent structures break up, how large scales give energy to small scales. Basing off of Lim and Nickels (1992). Small Reynolds number vortex ring collision produced a tiara of (which looked self-similar) rings. Inviscid process of vortex reconnection described by vortex filaments and sheets to explain energy cascade.

Rodolfo introduced the numerical side of the vortex ring collisions. Navier-Stokes fluids look like Biot-Savart equations vortex collision.

Fatter cores in the numerics is able to reproduce the vortex reconnection.

R. Poole Talk *Low-drag turbulent states in Newtonian and non-Newtonian fluids* (video).
Drag reduction is something that you can measure in non-Newtonian fluids in any geometry In non-Newtonian fluids you have to talk about different viscosities, extensional, biaxial, etc. Separation of dynamics into active and hibernating turbulence, where hibernating is defined by Virk limit (away from Blasius) characterized with low Reynolds shear stresses. Stereoscopic PIV (2D3C) results show hibernating turbulence is not laminar flow, and mainly consists of a spanwise motion of counter rotating vortices.

E. Wesfreid Talk *New experiments on the subcritical transition to turbulence in Couette-Poiseuille flow* (video) Two types of Couette-Poiseuille flow, depending on direction of pressure gradient. Can measure the velocity profile to verify it is behaving correctly. Centrifugal instability in plane-Couette flow is the Taylor instability while in plane Couette-Poiseuille flow is the Taylor-Dean instability.

Introduce pertubation with hole in stationary wall in Couette-Poiseuille flow. Streamwise perturbations of spot due to transient forcing of temporal extent "1". Can produce large scale structures with inhomogeneous friction. Self-sustaining iff the amplitude of the perturbation is sufficiently large.

M. Schatz *Forecasting turbulence using the geometry of invariant solutions: Experiments, theory, and numerics* (video). Talking about shadowing invariant solutions in state space. Are there specific experiments that can elucidate the unstable/stable manifolds of these invariant solutions? Kolmogorov flow. Spatially sinusoidal forcing. Can't really do 2-d flows experimentally so do quasi 2-d flows instead. Separation of variables to introduce vertical velocity profile, results in modified Navier-Stokes equation with a parameter β on the advection term, and a linear friction (Rayleigh friction) term. Inertial term (prefactor) introduced to delve into bifurcations of solutions in more detail. Doubly periodic, singly-periodic + no slip, NPS boundary conditions.

Modulated flow; rotation symmetry. Imperfect bif. from laminar. Non-periodic simulation (NPS). recurrence diagram.

Using norm of flow fields to find times of slow "state space speed" to initiate Newton-Krylov searches for periodic orbits.

C. Beaume *Transitional shear flows: Computing exact coherent states in two dimensions* (video). Using asymptotic reductions as reduced order modeling of nonlinear flows. Introduction to plane Couette flow. Introduction to Waleffe flow. Free-slip boundary conditions, sinusoidal forcing. coexistance of laminar (attractive) and turbulent so-

lutions. Constrain to the separatrix between laminar basin of attraction and these unstable manifolds of invariant solutions. Typically the fixed points that organize the dynamics are upper branch solutions.

Lower branch solution Wang, Gibson, Waleffe (2007). Fourier decomposition for steady-state ECS, shows the coefficients of decomposition scale with Re number.

Wants to solve for fluctuations (fast time scale) while keeping averaged quantities (slow-time scale) fixed. This yields an eigenvalue equation for the fluctuations.

Using his specific algorithm, he wants to bring the "leading" eigenvalue (discarding eigenvalues with larger real parts but also imaginary parts) to zero, as the marginality is an indicator of a steady state.

Uses L. Tuckerman algorithm for preconditioning, semi-implicit Euler scheme to solve for linear term explicitly and nonlinear term implicitly. Results in resolvent $(I - \omega L)^{-1}$.

Do not need same preconditioner for mean, fluctuation equations. mean equation preconditioner $P = I - L$ fluctuation equation preconditioner $P = (I - Re^{-1}L)$

Messy Bifurcation curves for modulated solutions, strange behaviors. They make Rich Kerswell nervous. Increasing resolution smoothes them, has to do with low-dimensional representation.

B. Budanur *Unstable manifolds of recurrent flows in pipe flow* (video). Unstable manifolds shape the separatrix of the chaotic attractor. Unstable manifolds for Poiseuille flow/pressure driven flow Continuous symmetries lead to relative invariant solutions. Reducing the symmetry by removing the parameterization of translation, leads to something much nicer topologically. Introducing time evolution as mapping f. Listing symmetries. In group notation, flow mapping f commutes with group element operation (group action). Each solution has infinitely many symmetry copies on its group orbit. Symmetry reduction is a coordinate transformation such that group orbit is mapped to one orbit.

Intro to SO(2) reduction via first Fourier mode slice. Not geometry dependent, can define coordinates as you see fit. Can use these projections to project neighbors onto slice. Therefore one can project the tangent space onto the slice. which allows for numerical integration that is completely contained in the symmetry reduced space if you are careful.

Example, unstable manifolds of traveling waves. Create a small ball (circle for 2d unstable manifold) and integrate to map out unstable manifold. Use a PIM triple/bisection to increase resolution and capture more of the unstable manifold.

Using a recurrence based norm, can use small values of the norm to begin Newton searches for invariant solutions. Then one can play the game of mapping this invariant solution's unstable manifold

Going over using higher energy solution as energy control that drives system towards laminarisation. "too much turbulence kills turbulence".

Talking about localized relative periodic orbits, M. Avila's paper.

Can reduce dynamics/Floquet vectors of map of first Fourier mode slice with Poincaré section.

Calculating unstable manifolds of traveling waves and relative periodic orbits and generalizing so long as symmetries are of the SO(2) class.

Puff formation in this subspace seems to be forming along heteroclinic connection between LB and UB solutions.

E. Knobloch Comments Bifurcations from a group orbit. Derived 25 years ago. Projections lose structure about the global structure of the manifolds. Lose information of the vector field that is orthogonal to the group orbit.

P. Cvitanović *Turbulence: How fat is it?* (video). Strange attractor stuffed into a finite-dimensional body bag. Computation of covariant Lyapunov vectors, covariant vectors are non-normal. Algorithmic approach to compute these. Physical dynamics is hyperbolically separated from the infinity of transient modes.

Kuramoto-Sivashinsky equation spectrum of eigenvalues (Lyapunov spectrum). The values of the Lyapunov exponents. Sharp shoulder where you fall off the cliff.

Doubling the spatial length doubles the number of "physical" dimension. Increasing modes in same length just increases the number of "transient" modes.

Transient and "entangled" = "physical" perturbations. Entanglements is between stable and unstable manifolds, where stable can win for a short time until unstable takes back over. Inertial manifold locally spanned by entangled covariant vectors.

Dimension of the inertial manifold. Distribution of angles between eigenvectors. Need to take stable eigenvectors into account due to nonlinearities. Kaplan-Yorke wrong by factor of two. Transient eigenvectors cannot have angle of zero and in fact are likely to be orthogonal to one another.

With these linearizations we are still embedded in higher dimensions so where the blip are we.

Cartography. Cover the inertial manifold with a set of flat charts/tiles. The tiles determine when you need to switch your maps.

Computing Floquet vectors of periodic orbits to machine precision.

From periodic Schur decomposition, 8 modes are entangled, the rest are transient.

Believed that this is only necessary to do for one periodic orbit, as this computation done for 500 periodic orbits all provided the same number of entangled modes.

The more honest answer to Laurette. Take the first n eigenvectors, defines linear space, find complement to that space, find the angle between those two spaces.

When you do not have enough eigenvectors to span the neighborhood of periodic orbit then the angles of ergodic trajectories will not be small as you will be "poking" out.

inertial manifold spanned locally by entangled covariant vectors, tangent to unstable/stable manifolds. The rest is transient.

2017-1-11 Matt :

coding Small amount of work put into spatial Newton descent code but most of the evening was used chatting with people over dinner at KITP residence.

K. Julien Talk *Quasigeostrophic investigations of non-hydrostatic, stably-stratified and rapidly rotating flows* (video). Motivations are strong system rotation and stable density stratification characterize many geophysical flows. Rossby and Froude numbers much less than unity. Large spatial size leads to normal mode analysis, eddy dynamics on different scale than gravity waves and coriolis terms(Related to Froude and Rossby number respectively). Classical QG equations. Scale of the forcing leads to either inverse energy cascade or direct enstrophy cascade.

With Froude order unity get columnal waves. Try to get reduced equations as these things are hard to resolve due to aspect ratio.

This leads to non-dimensional Boussinesq Equations, which in turn with assumptions about scale lead to non-hydrostatic quasi-geostrophic equations. Results simulation results in large scale barotropic modes. To explain the layering of the solutions to some of the simulations.

N. Constantinou Talk *Understanding self-organization in turbulent flows by studying the statistical state dynamics* (video). Long streaky structures in boundary layer turbulence of the Earth. Claims. "Underlying dynamics of structure formation lies in the interaction of turbulent eddies with mean flows" "Often structure formation only has analytic expressions in statistical state dynamics" "Because of the first claim, a second-order closure of SSD is often adequate"

Introduction to SSD.

1. Split into mean + eddy terms
2. Form hierarchy of same-time statistical moments/cumulants

3. Find how each of the moments/cumulants evolve

4. Throw away everything above second order (S3T)

"By studying the dynamics of the statistics, new phenomena arise that are not present or obscured in single flow realizations."

How does a state with no mean flow become unstable? Perturbations produce Reynolds stresses that reinforces the perturbation. Applies to 2d as well as 3d.

Find eigenvalues and eigenfunctions and then plug into dynamics.

K. Deguchi *The high-Reynolds number limit of self-sustained magnetohydrodynamic dynamos* (video). MHD dynamo introduction, exchange kinetic and magnetic energy. Applying nonlinear analysis of subcritical shear flows to MHD dynamos. Zero net flux implies purely driven by shear. Asymptotic expansion in inverse Reynolds number. Stretching coordinate and matching.

Self-consistent asymptotic analysis Many different ways to handle the order the leading powers of asymptotic expansion.

Vortex-wave interaction, self-sustaining process theories for the driving mechanism of streamwise vortices. Explanation of these processes.

Using MHD equations with Hall term. Derive a wave equation, produce Alfven wave.

Stress jump in roll component, Resonant Absorption Theory.

Lots of really long equations, with the effect of system rotation and linear instability following as analysis.

J. Klewicki Talk *Invariant representation of mean inertia provides a theoretical basis for the log law in turbulent boundary layers* (video). High Reynolds number boundary layers. Logarithmic mean velocity profile. Von Kàrmàn constant.

Open question for logarithmic dependence in boundary layers not well understood.

Rationalizing the log law. Prandtl derivation (distance from the wall scaling hypothesis).

Looking for invariant formulation (coordinate independent) version of equation that we can solve to get log law.

Rescaling equations when viscous, pressure gradient, turbulent inertial forces are all of same order leads to invariant representation in this layer.

Taken equations of motion, used similarity for closure, rescaled them in a way such that you get a nonlinear equation that you can integrate to get a log-law.

Apply similar transformation for boundary layers after finding that one of the terms is constant.

2017-1-12 Matt :

> **spatial Newton descent** Worked on code a slight bit more in between talks.
>
> **B. Mckeon Talk** *Self-similarity in the resolvent model: Linear response and nonlinear interactions* (video). Summary of resolvent analysis, expansions around mean such that nonlinearity all contained in one term. Resolvent operator transports, singular values. Randomized scheme because resolvent operator is very low rank in regime of turbulence, i.e. only few singular values from decomposition are required. Low rank related to critical layers.
>
> Discussion about the shapes of these resolvent modes, regions of different behaviors based on wave speed. Wave speed localizes reponse of resolvent operator. Low wave speed implies that all resolvent modes are "attached" to the wall, then an intermediate region, then a region of wave speed values such that all modes are "detached".
>
> Dynamics dictated by when wave speed is equal to local turbulent mean, that is to say these are the values that result in physical behaviors.
>
> In the inner regions the singular values "do all of the hard work".
>
> Required that U-c should be scalable in y for geometric self-similarity, shows after scaling that. Self similarity related to attached eddy ideas of Townsend et al. Shows similar results for broadband forcing.
>
> Nonlinear interacting hierarchies, interaction of triatically consistent modes allows for excitation of another set?
>
> Everything seems predicated on knowing the mean, or giving a good guess for the mean based on experiment rather than a priori knowledge.
>
> **M. Jovanović** *Color of Turbulence* (video). Spatiotemporal spectrum of stochastic forcing. Using linear navier-stokes equations with stochastic input, linearized around the turbulent mean.
>
> "Can I choose stochastic input based on spectrum such that linear dynamics produce correct statistical information"
>
> Proposed approach: view second-order statistics as data for an inverse problem. His contribution is a principled way of turbulence model as an inverse problem.
>
> A good way of getting insight is to look at how quantities are scaled into observable quantities that we care about.
>
> Stochastic forcing that is white in time and y, harmonic in x, z.
>
> Linear equations can capture coherent structures.
>
> Using Lyapunov equation propagates white correlation of sources into colored statistics of coordinates, using spatial covariance matrix. $AX + XA* = -BWB$. If W positive definite, then X positive

semi-definite, but converse not true. Colored in time $AX + XA* = -(BH + HB*)$

Convex optimization problem.

White-noise too restrictive, cannot reproduce dns with whit in time forcing. Suprising: quality of completion of incomplete data, retrieving matrix structure. Without keeping physics in the mix, you would get complete garbage.

A. Sharma Talk *Resolvent Modes and invariant solutions* (video) Using resolvent modes to find new invariant solutions of Navier-Stokes. Linearization about the mean (w=0) mode. leads to equation relating second order terms to u. Nonlinear terms are exciting the mean,invert (explanation of resolvent operator equation) $(wI - L)^{-1}$. Resolvent is well approximated via projection, use SVD to give a basis.

To fix the coefficients properly is a quadratic optimisation problem of an algebraic equation. Hopefully resolvent mode analysis is representative of the effect of invariant solutions on state space and the low dimensionality of said solutions.

Showing actual solutions to pipe flow and their projections onto small number of modes and comparison.

using mean flow of solutions, "at that point in state space"....this isn't right is it?

Projection of upper branch solution looks like lower branch counterpart. If you put upper branch projection and search for solution, looks like equilibria.

Using a project-and-search algorithm (project onto resolvent modes, then use Newton-Krylov). Dissipation continuations graphs.

Clancy Rowley (video). *Data-driven methods for identifying nonlinear models of fluid flows* Dynamic Mode Decomposition, Koopman Operator, data approximating Koopman.

Eigenfunctions of the Koopman operator determine coordinates in which a system evolves linearly.

If U has enough eigenfunctions so that we can reconstruct the state x from the values of the eigenfunctions then there is a coordinate change in which the dynamics is linear.

Data-driven inner product. Subspace S spanned by a set of observables Projection Theorem Approximate Koopman operator by projection onto the subspace S.

Numerical method that is obtained is the same as DMD, but will be able to say more about correspondence about Koopman operator and DMD.

The data driven inner product converges to normal L2 norm in limit of large numbers. Create subspace spanned by n observables, define projection operator.

Theorem(Data-Driven Projetion) Let A = X+X then for any $v \in \mathcal{C}^n$ then PU F(v)= F(Av), that is A is the matrix representation of the projection of Koopman.

Turns out this matrix, A, is identical to matrix computed in EDMD. (Extended Dynamic Mode Decomposition).

What if there is an eigenfunction that is in subspace S, then this method is able to find it.

If subspace is invariant under U. If v is eigenfunction of A, then ϕ is an eigenfunction of u, with $\phi = F(v)$.

Hard to actually check if S is invariant under U.

Choice of observables to determine the basis is nontrivial.

Using this model with POD modes and comparison to Galerkin truncation of Fourier modes. Works much better than Galerkin when white noise introduced.

M. Green Talk *Tracking coherent structures in massive-separated and turbulent flows* (video). pFTLE and nFTLE: finite time Lyapunov exponents. (positive and negative time). This is a field that is used to differentiate between dynamically distinct regions. Negative time FTLE is where fluid is attracted in forward time.

What can we do with this information about these ridges? Non-parallel intersections interesting. Saddle-like behavior of these intersections.

Intersection starts on cylinder and seems to track vortices. Extracting physics from the distances of vortex core and cylinder, etc.

Can tie vortex shedding to the dynamics of the saddle point.

Can you track similar coherent structures in 3D turbulence? Subsequent vortex generation can be tracked by additional saddle generation.

Tracking material transport that will be involved in secondary hairpin generation, drawn up from the wall.

nFTLE, pFTLE surfaces calculated in channel flow. Projected onto 2-d plane, used PIV program to calculate average velocity of saddle points correlations Comparison to velocity profiles, slower than mean in bulk, faster than mean near walls. Similar to perturbation profile of ...

Can we use these saddle tracking methods to follow coherent structures in 3d? not so simple because they actually live on 2d surfaces. Large amounts of velocity data needed but it's really hard to mess up the general direction of unstable/stable manifolds of these structures.

Y. Hwang Talk *Self-sustaining attached eddies in wall-bounded turbulence* (video). Attached Eddy Hypothesis, Townsend. Viscous layer, buffer layer, Log region (scales with wall), wake region. Linear spanwise length

scale growth is intimately related to the log region scaling. Isolating motions at given spanwise length scale growth, filter out larger scaling, damping out smaller structures. Smagorinsky scale damping.

Showing self-sustaining process of attached eddies with correlation functions.

"real" part of the talk. Pressure fluctuation generated by nonlinear feeding processes of vortices. Showing length scale of streamwise vortices is the same as the length scale of pressure off of the wall.

Both rapid and slow pressure is generated in streamwise wavy structures. Rapid pressure is mediating the lift-up effects which controls the generation of streaks from streamwise vortices.

Slow pressure generation is dominated by streamwise vortical structure.

Skin-friction generation. Not generated by singular structure at a given length scale. Everyone is important at high Reynolds number.

Three methods for skin-friction, identifying size of structures responsible. Using Fukugata-Iwamoto-Kasagi identity. Only include structures up to given length scale, artificial damping of large structures.

FIK say that large scale structures contribute the most to skin-friction. Getting rid of largest structures doesn't reduce drag that much, it's actually disposing of log-region scale structures that will reduce drag the most.

Supressing the lift-up reduces drag.

Upper branch is more related to large scale structures.

E. Knobloch *A nonlinear model of noise-sustained structure in subcritical systems* (video). Lots of interesting things happen when you diverge from periodic boundary conditions. Changes convective instability to absolute instability. Convective instability is things that grow and are then advected with the flow, other stability is things that grow in place and fill the domain.

Complex-Ginzburg Landau. For range of bif. parameter things are convectively unstable, and outside this region structures are absolutely unstable.

Study the model problem that has the same dichotomy. Bifurcation diagram with different amplitudes of disturbances.

Scale the equations in limit of large advection, use Liénard transformation to change the problem to a BVP. Spatial van der Pol oscillator.

The coincidence of the two manifolds results in an "orbit flip bifurcation".

Talking about the front location, originally "found" using phase diagrams, then looking at inlet perturbations eta and seeing how the location of the front changes.

"the observed sensitivity finds a natural explanation in the presence of canard segments on solutions of the spatial BVP for the steady states of the model. These results are obtained by recasting the mode as a slow-fast system in space and focusing on its steady states subject to

Even very small changes to inlet boundary conditions have a huge effect.

S. Zammert *Coherent structures in boundary layers in the quasilinear approximation* (video). Exact solutions with smaller scales or multiple scales. Rescale coherent structure with factor λ and plug back into Navier stokes and find that this is related to scale factor λ at $Reynolds/\lambda^2$. With this scaling, coherent structures of multiple scales can coexist, creating a hierarchy of scaled solutions.

Lower branch solutions only. Wall normal localization gets lost. Method also works for localized solutions. Apply rescaling procedure to axes of wall-normal localization leads to results that are completely self-similar.

Linear stability analysis, stablity eigenvalues, have same self-similar spectrum, therefore can use larger structures at lower reynolds numbers to do analysis at higher reynolds numbers.

Quasilinear approximation, split into spanwise and no-spanwise variation. Define projection operators s.t. you get either of these. Nonlinear term split into parts, some discarded others kept. $(u2 \cdot \nabla)u1 + p1(u2 \cdot \nabla)u2$ discard part that effects mean flow.

Much simpler dynamics in quasilinear approximation, attracting state in this approx is always steady. Qualitatively the profiles of the nonlinear, quasilinear cases are similar. Profiles scale in the same way that solutions did.

How turbulent mean profiles are related to exact coherent solutions. Bifurcations of quasilinear states, what's going on?

The amplitudes of modes vs. reynolds number, decrease quite rapidly at low re, but dip then plateau at higher Re. Whenever a new mode becomes active, bifurcations of quasilinear.

Look at how new modes contribute to profile. Modes do not interact, turn off certain modes as way of initializing initial condition for ECS search. Low mode numbers lead to linear profiles in the bulk and high contribute to boundary layer.

Continuation to nonlinear system. Homotopy introduced such that the parameter equal to one are ECS in quasilinear, 0 equal to ECS in nonlinear.

In order to synthesize turbulence, you need constant energy scaling.

2017-1-13 Matt :

L. Tuckerman Talk *Transition to turbulence in Waleffe and Kolmogorovian flows* (video). Taking quasi-turbulent (no kolmogorov scaling) and quasi-laminar flow to larger scale domain.

Using coupled map lattice to analyze structures on this large domain.

Are results from coupled map lattice continuous? Turbulence fraction graphs have same slope on log-log plot as directed percolation.

Shows how large domains are necessary to pick up on structures.

Waleffe Flow Reproduces interior of Plane-Couette well by having sinusoidal body force and free-slip boundary conditions.

Truncated Waleffe flow results in system of seven PDEs.

Simulations find that transition is continuous, shares same critical exponent.

Directed Percolation is the basis of these exponents, although never truly realized in physical systems.

Can be classified by three independent exponents, turbulent fraction, laminar gaps in time, laminar gaps in space.

(turbulent and laminar taking the role which is normally discussed as excited and unexcited in directed percolation).

Streamwise spatial gaps do not agree.

B. Hof Talk *Transition to turbulence in channel flow* (video). Stripes present in channel flow.

Edge-tracking of tilted domain (tilted so that stripes are perpendicular to domain boundaries). Using Newton method to converge the solution.

Lower branch bifurcates into RPO solution which becomes the new edge state, followed to upper branch. Following shows more bifuracations and then a boundary crisis, this scenario gives rise to transient striped patterns.

Might be able to find in experiment as it is a stable RPO, but would need a localized version without periodic boundary conditions.

There is an angular dependence of the bifurcation diagram (angle of tilted domain). 45 degrees seems optimal.

Transient stripes and puffs to sustained. Time scales are very long and very important because turbulent fraction continues to climb as system is evolved.

Memoryless process of pipe flow puffs lead to measuring characteristic life time. Growing more than decay is being used as a indirect method of characterizing the critical Reynolds number at which sustained turbulence occurs ($Re_c \approx 2040$).

$Re = 2020$ the turbulent fraction goes the zero after a large number of advective time units, while at $Re = 2060$ there appears to be a statistical steady state w.r.t. turbulent fraction.

Using a directed percolation analogy, discrete model based on life-time and splitting statistics, but cannot get critical exponents because interactions are not taken into consideration in model. When interactions are taken into account, the percolation exponent comes out.

B. Eckhardt Talk *Dynamical systems analysis of transition in boundary layer flows* (video). Looking at spatiotemporal development of flow downstream from a thin plate.

Five main spatial behaviors of flow, arranged in a streamwise fashion:

- free-stream turbulence
- streak growth
- breakdown into turbulent spots or nucleation.
- spatio-temporal intermittency (spots spreading and merging)
- turbulent boundary layer

Localized edge-state that produces secondary structures. It's difficult to access asymptotic dynamics because there is spatial development.

This is complicated, so instead apply suction such that the developing boundary layer is translationally invariant. Then can look at asymptotic suction boundary layer. It is linearly stable up to $Re_c = 54370$, but goes turbulent with bypass transition at much smaller $Re = 270$.

In short-wide domains, edge states evolved in time go through a process that results in spatial translation; can relate to self-sustaining mechanism.

Can development multiple edge states the move left, right, oscillate, and move erratically when tuning parameters.

Can compare edge states and nucleation events. When starting with an initial random perturbation field, there is a transient period where perturbations decay, leading to streak growth. Before the streaks transition into turbulence via nucleation events, look at the streak structure. These spatiotemporal structures are similar in width, strength, and sinuous instability wavelength to the edge states found previously.

Looking at random initial conditions in a state space view. The energies of velocity components of initial conditions come close to those of edge states and then are either ejected towards turbulent behavior, or cross the edge states and decay.

Measuring "intermittency factor" which seems identical to Tuckerman's "turbulent fraction" from directed percolation.

The nucleation model in conjunction wth the probabilistic cellular automaton gives a good description of bypass transition.

2016-1-14 Matt : Looking at Lan's directory, I was able to find what I believe is the period of $\overline{01}$ orbit to six decimal digits, $T_{\overline{01}} = (25.6356)82$ which conflicts with my value of $T_p = 25.635484$

Spent some time learning c++. H

2017-1-16 Matt :

G. Falkovich Talk *Interaction between mean flow and turbulence* (video).
Isotropic homogeneous turbulence is basically nonsense because it discards interactions.

Has a localized edge, so it leaves a wake, edge has asymptotic behavior. Drag coefficient goes to constant as Re goes to infinity. Friction factor for pipe flows scales like 1/Log(Re) as Re goes to infinity.

Cannot describe turbulence generated by a flow, so instead try to describe a flow generated by turbulence. How to predict a glow generated by an inverse cascade in two dimensions.

How? Set the small scale forcing, change the geometry to change the flow.

Guiding principle to guess is to guess that it occupies the lowest available wavenumber.

In a box with symmetry, expect dipole or large central vortex with four small counter rotating vortices at the corners. If discarding symmetry expect flow along long direction.

Two-dimensional turbulence, including forcing and friction. Condition for a strong mean flow estimated by kolmogorov factor. $\epsilon^{-1/3} L^{2/3} \alpha <<$ 1. Epsilon is total net force.

This friction is not viscous friction, for example its set by the layer of lubricant à la Schatz.

Two-dimensional vortex sustained by small-scale forcing. J Laurie et al PRL 2014. Radial forcing generalization Frishman and Falkovich, unpublished. Next step is describing correlation functions of turbulence, long calculation, resulting in expression for pressure as a function of radius.

Prediction that first harmonic is independent of radius. Graphs of mean flow and momentum flux quantities vs. r showing valid region of theory.

Numerical modeling in a box with no-slip boundary Clear symmetry breaking, vortices have direction. Takes many turnover times to see behavior.

Inverse cascade on a sphere, non-rotating. Same procedure as before, argument for neglecting large velocity, pressure correlation terms, leading to a new closed equation on the momentum flux.

Can we have a plane flow out of a two-dimensional turbulence with forcing and friction? Aspect not equal to one, argument of lowest wavenumber makes jets, not vortices.

Inverse cascade on a torus. Starting with aspect ratio one, have vortices, changing the aspect ratio produces jets, but vortices remain.

Long time means restore translational invariance that is broken on small time scales.

Lowering friction increases the number of vortices. Radius of curvature going to zero is very interesting limiting case.

Inverse cascade and vortices in compressible 2d turbulence. Compression creates shock waves which dissipate energy on small scales. Use of shallow water equations for the density fluctuations, density equated to height. Viscosity is an irrelevant perturbation in regards to large vortices and or inverse cascade.

D. Lecoanet: Introduction to Dedalus (video). Pseudo-spectral, open-source, python code. Enter equations as strings. Hard to install, otherwise easy to use.

Great for equations that do not have specific optimized implementations (e.g. asymptotic equations) and data analysis.

Can solve reduced model equations to verify their accuracy.

Example problems: Burgers equation, Kelvin-Helmholtz instability.

Initial value problem, need equations, domain, timestepping scheme.

Goes into Solver variable, which gives a state and integrator, and fields.

Implicit, explicit time stepped. Implicit on LHS of equality, explicit on RHS of equality. i.e. linear terms on LHS and nonlinear on RHS.

Restricted to Fourier and Chebyshev bases, only allowed one Chebyshev basis at the moment.

Can have non-constant coefficients for Chebyshev but not Fourier bases.

Channelflow Got the basics of c++ down, going through Channelflow scripts and documentation to understand what each of them do in detail.

reading Reading and rereading ref. [7] to understand the process employed for Kuramoto-Sivashinsky equation. Filling in gaps with ref. [13] as I see fit.

misc Rewatched S. Tobias' talk as review and transcribed notes for it.

2017-1-17 Matt :

B. Marston Talk *El niño as a topological insulator: A surprised connection between geophysical fluid dynamics and quantum physics* (video). Kelvin waves play key role. Intro to integer quantum hall effect and topological insulators.

Immunity to macroscopic messiness is due to topological robustness. Leftward, Rightward bulk movement prevents back scattering

due to inhomogeneities. This leads to quantum spin hall effect and topological insulators. Special curves of dispersion relations are the states that propagates along the edges of the physical object (surface states). Spin-orbit interactions stratifies the spin states are produce the quantum spin Hall effect.

Dispersion relation of shallow water waves on a spherical surface, coriolis force switches direction at equator. Wave that propagates along equator is trapped. Gravity waves, Yanai waves, Kelvin waves, Rossby waves.

Two layer model, behaves very differently with and without rotation. Need enough rotation for time-scale separation.

Numerical spectrum from shallow-water simulations. shallow means wavelength of waves in relation to depth.

Topologically protected systems, i.e coupled gyros, acoustic modes. Key factors of topologically insulation is gaps in dispersion relation other than these edge modes. Can interpret equatorial divide as the edge modes. Need to break time-reversal symmetry in part of the system.

Shallow water equations on Lieb lattice. Leads to dispersion diagram that has bulk states, and edge states (linearly dispersing modes), which equal Kelvin, Yanai waves.

Linearized equations of motion, leads to Chern number and Bulk-Edge correspondence. Parameterize eigenstates of frequency space equations (linearized), kx, ky, f parameterized by trigonometric functions. Multiply by phase factor to repair the ill-defined azimuthal coordinate at the north-pole and south-pole.

Chern number comes from quantum analog, magnetic field being applied to a sphere.

Plots verifying protection from obstacles, (analogous to inhomogeneities in quantum systems).

Claims that Kelvin waves at ocean basin boundaries, Magneto-Rossby waves, Fluids with mean flows are all topologically protected. This is related to the lack of back scattering, but maybe this is related to E. knobloch's talk? only persists in convective instability regime? Or is this back-scattering completely unrelated to upstream growth.

Protection from interactions/nonlinearities, Fractional Quantum Hall effect arises from strong interactions.

Marie Farge and Kal Schneider Talk *Energy dissipation caused by boundary layer instability at vanishing viscosity* d'Alembert's paradox, dissipative properties of vortices in wall bounded 2d flow, differences in navier-stokes, euler, prandtl solutions.

Finite-time singularities are a candidate for explaining the dissapation rate at high reynolds number.

Kato's theorem, navier-stokes solutions converge toward Euler solution iff the viscosity vanishes.

Volume-penalization (pseudo-spectral). Brickman term added to Navier-Stokes equation that produces vorticity at the wall, and boundary layers are detached from the wall. What happens at the wall that makes boundary layers detach?

Vortex dipole produces many small scall vortices from lifting the boundary layer off of the wall. Looking locally at the combined vortex structure, the dissipation of the attached vorticity layer goes to zero, but the detached vortex has constant dissipation. Detached vortex scales like $1/Re$ term, while attached vorticity layer scales like $1/Re^{1/2}$.

Wall assumed solid, but there is a porosity ($1/\eta$ where, $\eta = permeability$) that induces the volume penalization term.

Comparison between Navier-Stokes and Euler, Prandtl solutions. Replacing no-slip with this volume-penalization term. Replacing spectral method (due to its order) with compact finite differences. The big plus is that it is applicable at higher Re numbers because you can take larger permeability values.

Reformulate Prandtl equations to be in terms of vorticity. Only have viscous term in y-direction, but not in wall-normal direction. Coupling between Prandtl and Euler is the pressure gradient. Scaling argument saying that you can discard wall-normal terms, but keep wall-normal derivatives. Non-uniform grid that depends on time, before and after the boundary layer detachment.

Prandtl solution finite time singularity well known, expected due to Kato's theorem that navier stokes converges to euler.

Production of dissipative structures is the key feature of boundary layer detachment.

In DNS the Prandtl boundary layer is used to justify the coarseness of numerical grids, trying to show that one needs to be careful and this thickness may not be the correct guiding factor. Results suggest that new aymptotic description of flow beyond the breakdown of the Prandtl regime is possible.

Prandtl is great for when the boundary layer remains attached "keep it alive".

$1/Re$ number scaling is wall-number scaling.

Reynolds number original definition is ratio of norm of nonlinear term, to the norm of the linear term.

2017-1-19 Matt :

T. Schneider *Computing Clouds: Why turbulent coherent structures are crucial for predicting climate change* (video).

Shows that equilibrium climate sensitivity is a great tool for predicting various quantities related to climate change. (carbon dioxide concentration, amount of total reflectance).

Equilibrium climate sensitivity (ECS) vs. Low-cloud reflectance variations (normalized w.r.t. seasonal fluctuations in temperature).

Most atmospheric water is vapor not in clouds. Clouds form where small residual of water condenses in coherent turbulent updrafts.

Difficulty in these limited area simulations is that they have typically have not respected the energy flux balances previously, such that you get an exponential growth in atmospheric water vapor.

PyCLES code. Anelastic Navier-Stokes, discontinuity capturing (WENO) advection schemes.

Every climate model has three subscale schemes. Deep convection, shallow convection, boundary layer turbulence. Parametric and structual discontinuities for processes with common limits.

Reduce number of free parameters by using adiabatically conserved variables. Let Coherent structures interact with the isotropic part (mean flow)? But do not allow coherent structures to interact with each other.

New EDMF scheme, have draft equations and grid-mean equations.

Koopman Coalition There is a connection between Koopman and using periodic orbits to compute manifolds. How can we go beyond doing simulations and looking at good modes?

Hyperbolic objects as opposed to attracting sets? Can we use this for transient.

How to tame the continuous spectrum, in order to not just do point spectrum, need Colm's input and need functional space to be "correct" somehow.

Transition to turbulence: highway through the edge of chaos is charted by Koopman modes Plane-couette flow: potential to be turbulent, what is the minimal energy state and its structure that allows you to transition to turbulence. Shortest distance to the edge manifold (energy norm). Follow edge state's stable manifold and then get ejected to turbulence by unstable manifold.

Can do Koopman analysis around plateau of energy of perturbations, specifically around the GMRES residual minimum. The point is to do the Koopman analysis around the edge state.

The structure at this instant can almost completely be described by three modes.

Least-squares fitting of the amplitudes of modes that best reproduce the structure of original structure.

The three modes that best describe the state are labeled "growth, neutral and decaying". The neutral mode mataches the GMRES solution of the edge state, the growing mode matches relatively well

the evolution in time of DNS. The decaying mode matches simulation backwards in time.

Minimal seeding accomplished by adjoint looping, look to Rich Kerswell papers for info. Can accomplish the same with edge tracking.

Pick up a lot of continuous spectrum in different time segments because you're in the basin of attraction of something else.

Can use pullbacks to linearize anywhere on basin of attraction. How do you expand about the edge state as it isn't an attractor.

For saddles, define Koopman eigenfunctions about the saddle, can continue it as a strip about the manifold via the dynamics. This foliation produces a distribution. Can define bouncing between invariant solutions via the Koopman analysis.

Exponentials give rigorous expansion when dealing with autonomous system. Koopman is non-normal in dissipative flows.

M. Farge Talk Introduction by L. Tuckerman: L' économie 101, inelasticity of journal prices.

Journals aren't evil, well, some are. dessim.in

misc Almost done reviewing the more advanced concepts in c++ that I'm not so familiar with.

2017-1-20 Matt :

I. Marusić Talk *Modeling high Reynolds number wall turbulence using the attached eddy hypothesis* (video). Using data and recent discoveries to test Townsend's attached eddy hypothesis.

Description of different regions of wall bounded flow, viscous region close to wall and log-region and beyond where attached eddy models are defined (viscous not leading order).

Demonstrating that log region dominates at high Re. Quotes from Townsend 1976. Perry and Chong (1982) claim that hierarchy or structures lead to equations and log dependence of mean flow.

Inviscid structures can be predicted by inviscid equations, of course expect them to be invariant. Continuous hierarchy of scales. Geometric progression of scales. Telephone poles and dead cats attached to horizon. Flip, shear, and squint and it looks like boundary layer.

"Are attached eddies real or just a statistical construct?" Interpretation of eddies is energy contributing structures, organized motion that contributes to kinetic energy. Contributions to vorticity from attached eddies only give the mean, which is a very small contribution.

Thinks that instead of looking at energy and enstrophy should look at instantaneous changes in velocity fields. Thinks of logarithmic layer as stair case that jitters around a line. Organized velocity fields that have vorticity associated with them but do not contribute to the enstrophy.

Count the number of realizations of momentum zones, average over Reynolds number. The number of momentum zones follows logarithmic growth.

Take hierarchical approach, keep dividing by scale factor and rescale velocities of demarcated structure, randomly scatter them about and look at mean velocity field. Get logarithmic scaling of the number of momentum zones that agree with DNS, claim that the requirement is that the objects are self-similar.

Looking at spatial statistics, central limit theorem, poisson statistics, definitions of moments and cumulants.

Any statistic with a wall-normal part, no logarithm. No wall-normal part means logarithm. Correlation statistics asymptotically approach Gaussian distribution in limit of high Re, much like Poisson statistics.

Problems arise from treating everything as point processes that have no spatial exclusion with hierarchical structures of different scales.

J. Jimenez *Can we see coherent structures in wall-bounded turbulence?* (video).
Can we relate turbulence structures to coherent structures that people have found? Structures to javier are autonomous identities that determine their futures.

Even if most of the flow may be structureless, it's important to identify key structures because they are useful. (Seeing a storm cloud, even an isolated one, means you should bring an umbrella).

Javier's requirements:

- Strength (Stronger than background)
- Observable
- Relevant
- Either: Energy production or sink, or energy repository.

Using joint pdf (pdf in two variables) can find important structures by quadrant analysis. How does one look for these things? Need to look at where things are of comparable scale. You do not want to mix energy and vorticity. How do you separate energy and dissipation or vorticity.

Energy produced by eddies has to be coupled by the shear. Corrsin parameter. There is a characteristic time, nonlinear eddy turnover time, and shear deformation time. Corrsin parameter is the ratio of turnover time to shear deformation time. Shear dominated, means "linear" energy input. Corrsin parameter of order unity is "the playground" and of very small means shear independence, nonlinear, no energy input.

Near wall, reynolds stresses small so has to be carried by shear. By looking at phase velocity of velocity field, minimizing a wave equation relation you can get phase velocity of individual Fourier components which corresponds to different distances from the wall.

Stratification of spectra of different components of phase velocity are similar when subsets of scales are viewed. Can plot the scaled derivatives with respect to distance to the wall to decompose into structural regions, from regions of large and small scale structures to transient areas.

Small scale structures have to do intimately with the near-wall viscous region, large scales are linked to the bulk phase velocity, log layer is the transient regions.

Looking down (spanwise streamwise representation) can get the energy contained in a small subsection that represents the energy contained in the viscous spectral subregion, and then plotting vs. the wall normal coordinate leads to a maximum velocity intensity of 11.

Doing the same with the large-scale region, agrees quite well with highest POD mode of the velocity. i.e. the phase velocity.

Linear transient growth analysis of the flow yields the same result. Doing the same with logarithmic layer gives good agreement with the mean profile and the advection velocity, as well as the phase velocity profile as a function of wall normal coordinate.

Things are similiar in the log layer but outside of this the large structures are not self-similar when you get to the scale of the channel.

Structures bursting. Measured by quick changes in energy production and dissipation, has nothing to to with the wall.

A theory for tilting things, Linearised Orr-Sommerfeld equation (inviscid Orr). As the tilting angle changes continuously, get build up of the wall-normal component of the velocity.

Video demonstrating the connection between tilting and growth of wall normal velocity component.

2017-01-23 Matt :

G. Chini Talk *An asymptotic theory for coupled uniform momentum zones and vortical fissures in turbulent wall flows* (video). What is the role of invariant solutions in the limit of very large Re_τ Lower branch states seem to be important for transitional turbulence. Might be able to explain near-wall coherence by these invariant solutions because they only see a moderate effective Re_τ.

Far from the wall, quasi-coherent motions with streamwise length scales approximately 5-15h are observed at high Re_τ. Are these associated with ECS?

Hwang and Cossu say yes, with their Smagorinsky constant continuation, others who claim that large scales come by via small scale hairpin vortex trains advected by the flow.

Reference to instantaneous velocity profiles of Marusić, decomposition into uniform momentum zones and vortical fissures.

Can invariant solutions explain these instantaneous velocity profiles near the wall?

Implications of mean momentum balance analysis. Long-time averaged x-momentum equation has mean viscous term, turbulent inertia term (gradient of Reynolds stress), and pressure gradient term.

The claim is that the momentum zone jumps correspond to regions of vorticity, or vortical fissures.

Want to construct invariant solutions that somehow explain these momentum zones and velocity profiles.

Tracking the lower branch solution to high Reynolds number, and it also converges to solution of Vortex-Wave Interaction equations. Looking at Fourier analysis and scalings of different Fourier modes.

When looking at the streamwise averaged streamwise momentum equation using VWI scalings you get an effective Reynolds number felt by mean flow is order unity.

Asymptotic analyses of do not show sharp gradients of the rolls and streaks.

Reynolds number continuation of upper branch states leads to converges to lower branch scaling.

Wants an invariant solution whose mean flow looks like instantaneous profiles. They get more and more unstable directions but also get more isolated. Reference to Clancy Rowley's previous work into scaling with symmetries involved, but cannot do this with mean values.

Do local analysis of vortical fissures, with periodic boundary conditions. Does Navier-Stokes admit a solution like this? Decompose into mean and fluctuation term. Two different time scales. Why not two spatial scales? There could be but for here there is not.

Mean-flows are isolated points in state space that mean nothing in terms of the dynamics. Streamwise fluctuations are not of order u_τ, thinks that this implies that there should be discontinuities in the mean flow.

Dennice: There's a physical reason why it's ok to do this, looking at streamwise vortices, so it seems that it might be ok to average in the streamwise direction to produce a mean because these vortices are only z and y dependent??

Assume that the scaling of the average is s.t. the mean scales with inverse Reynolds, but not as strongly as $1/Re$. Employ two-timing, Parse Navier-Stokes into mean and fluctuation equations.

Reduced PDE equations for the mean, fluctuations. Fluctuation equation is quasilinear. This implies they admit separable and single mode (traveling wave) solutions in x. No direct coupling between fundamental mode and higher harmonics. Gradients of mean valued things are small, because of the assumption that they are smooth.

Linear stability analysis of Orr-Sommerfeld to help deduce scaling arguments for fluctuation terms. Can do this because this is a steady state solution? It's a local, steady state solution?

Reynolds stress not driving the mean-flow seen via the streamwise Fourier transformed quantities, of rescaled velocity components.

Can restore three dimensional incompressibility because of how the critical layer scales velocities. Insist spanwise fluctuations drive mean flow?

Get critical layer variants of mean equations and fluctuation equations.

Turbulence à la D. Barkley A nice recap of the key concepts and ideas; didn't type down much because eating took priority. Key concepts: Turbulence and scaling laws, dynamical systems approach, manifolds of invariant solutions, self-sustaining processes, transitional turbulence, edge states, puffs, splitting of puffs and growth and decay rates, directed percolation picture.

Reading Started through Blonigan, Wang *et al.* papers [2–4, 14]. Interesting, I find ref. [14] similar to variational Newton descent. I'm not really sure how the spatial evolution is included, and if you look at their converged solutions they are seemingly on the same spatial domain size as the initial condition; I might just be missing something that I need to reread. The ability to parallelize is of course a large distinction, and the continuation through their advection velocity parameter is distinct as well.

2017-1-24 Matt :

T. Schneider *From turbulence transition to shell buckling* (video). Look at when prebuckled state loses linear stability, to see when buckling occurs. Extreme sensitivity to inhomogeneity, imperfections.

See this via thin shell structures. Studied in reality via axially loaded cylinders and sphere under uniform pressure.

Classical approach of understanding, bifurcation diagram of shortening versus load parameter. Linear instability of the imperfect system, given imperfections can predict buckling load. Of course, typically imperfections are not known a priori.

Instead of looking at linear instability of the imperfect system, look at the nonlinear finite amplitude instability of the perfect system.

Characterize basin of attraction as a function of load, get unstable equilibria edge states in some norm, etc.

Geometric nonlinearity in elastic systems. Displacement fields in terms of Lagrangian(fixed in material) coordinates. get change in distance between material points, Green-Lagrange strain tensor, typically nonlinear function of displacement field, usually linearized.

Relation for cauchy stress tensor for isotropic Hookean material, relation to original coordinates?

Donnell-Mushtari-Vlassov theory, for deformations of thin elastic shell. Find in-plane stress of mid-plane to get the nonlinear term that matters, which is the one who only depends on normal direction of midplane.

Leads to DMV equations. Nonlinear and nonlocal equations like Navier-Stokes. Want to construct nonlinear equilibria on the basin boundary of the unbuckled state.

Use edge-tracking. the edge state equilibrium is localized dimple on the surface. Do continuation in axial load parameter. Leads to shrink of depth of dimple, at zero the eigenmodes are not localized. Dimple pattern grows and wraps around shell.

Azimuthal symmetry, impose reflection invariance, could have also imposed translational invariance.

Very high number of modes that become unstable at the same parameter value. Increasing axial length induces snaking along axial direction.

Finite amplitude perturbations of a shell in fluids. Taking a perfect solution and use perturbations that are known, much like in elastic materials.

Finding edge state with claim that the force should increase, and then return to zero as you reach the edge-state equilibrium.

S. Bagheri Talk *Flow of non-smooth surfaces* (video). Outline:

- Find favorable fluid-structure interaction mechanisms
- Effective boundary conditions induces by non-smooth surfaces
- Fabrication of surfaces and experiments

Fiber in cylinder wake breaks symmetry, induces lift and reduces drag. Filament in oscillating flow, symmetry breaking in intermediate pulsation range.

Look at collection of filaments. Need to do coarse grained effective representation, such that the average interactions are the same.

Take effective boundary conditions generated by poroelastic surface or reduce to porous surface. Leads to two second order tensor relations for boundary conditions on the velocity components taking the place of no-slip.

Streamwise velocity profiles shifted up or down based on the roughness in the form of slip-lengths.

Wall tangential velocity condition If structures are small, only contributions to flow are linear shear in the viscous layer. If the structures extended into the buffer layer, this would not be the case.

Related to drag reduction via a skin friction coefficient equation, looks like dispersion relation?

Wall normal velocity condition Permeability of interior related to boundary conditions on the interface, not completely intuitive.

In this porous version of the equations, need to solve continuity equation inside the coating to account for permeability.

How does one generate the two different tensors, **M** and **K**.

DNS of two dimensional model, with porous media. Look at streamwise velocity close to the interface to identify the slip. FreeFEM plus to do DNS.

Use coarse grained representation to derive the same quantities. Take unit cell, with multiscale expansion of microscale equations. Solving leading order equations in unit cell, slip-length comes out. Get similar slip-length as DNS.

Coupling porous wall boundary conditions to turbulent channel flow, seeing how it affects near-wall structures.

Experimentally, use UV lithography on polymers to induce roughness.

Inclined water table experiments. PIV measurements and comparison to smooth wall setup leads to a smaller velocity near the wall and higher velocity away from the wall (log-layer).

There is a decision that needs to be made of where to decide where the "wall" is. Currently being taken to be the top of the filaments.

Would like to use filaments as actuators and sensors once studied.

Channelflow Began writing some code and chipping away at the checklist I wrote for myself. Currently trying to figure out how I'm going to numerically obtain small-time Jacobian matrices in a reasonable amount of time. I've been looking through the Channelflow documentation as to use the resources at hand to the fullest extent. The main problem is that the top-level machinery is all relatively easy but getting into the guts is somewhat daunting considering the sheer number of amounts of parts. One step at a time is the name of the game. Thinking of fine-grained additions I can make to the checklist previously written, again, hopefully the organization will help in this effort.

2017-1-25 Matt :

M. Kiewat Brown Bag talk Looking to some how get more yield out of currently unused data created by their simulations. Using Large eddy simulation and some other methods for DNS.

Pressure induced drag accounts for most of the drag, but still look at vortex induced drag.

DMD used but due to intense memory requirements. Discussion from much of Clancy's talk, streaming DMD missed out.

A. Willis Brown bag talk Have relative equilibria , have dynamics so therefore have trajectory. Compose group orbit with shifts. Interested in association of group orbit members?

Begin with template point on the group orbit via symmetry reduced point. Looking at minimal distance between subsequent time snapsnots of template? Slice condition $< \bar{a} - a' | t' > = 0$, locally $||g(\theta)\bar{a}|| = constant$ s.t. $< \bar{a} | t' > = 0$. this leads to slice condition $< \bar{a} | t' > = 0$. Temporal evolution equivalent to shifting in space for traveling wave, so can relate.

dynamics within slice using defintions of $\bar{a}$ and symmetry invariant velocity, $\dot{\bar{a}} = v(\bar{a}) - \dot{\theta}\bar{t}$, slice condition $< \bar{a} | \bar{t}' > = 0$ get condition for $\dot{\theta} = < v(\bar{a}) | \bar{t}' > / < \bar{t} | \bar{t}' >$

Complicated group orbit, get lifting out of the slice which makes the denominator equal to zero, which is a problem.

Method of connections (not slicing) put $\bar{t}' = \bar{t} = t$ Projecting out motion along the group orbit. Dynamics from a_0 to a_1, project. dynamics back to a_0, means different tangent vector so projection leads to a phase change such that you aren't brought back to original point, phase change is known as geometric phase.

Principle component analysis. Reducing shift and reflect symmetry. Two clouds which are related to shift and reflect. Zooming in on one of the clouds and using Poincaré sections. Get ergodic clouds on Poincaré section, zooming in around dense areas get connection between period doubling by looking at manifold.

Excitable Media Discussion (video). R. Grigoriev beginning. Spiral wave chaos: tiling, local symmetries, and asymptotic freedom. Phase singularity at spiral core.

Model of cardiac dynamics, reaction-diffusion system. Karma model. Forget about diffusion initially by ignoring spatial properties connections between cells.

Looking at nullclines and equilibria. Apply dynamical systems views to the problem, have varieties of solutions, look for periodic/relative equilibria on chaotic attractor. Use recurrence plot to initiate search for invariant solutions (exact coherence structures). Double periodicity includes symmetry operations (translation, finite rotation). Use minima as initial guesses for Newton-Krylov solver. Notes on symmetry and symmetry breaking, two dimensional planar model is better model of atria as opposed to ventricles.

Some intial conditions converge to small residuals but not non-zero residuals. Why? THere is structure that does not disappear after certain time.

Complex Ginzburg-Landau equation discussion. Split into amplitude and phase (its complex so easily done). The amplitude has very long time dynamics that slows down over time. Real part is

fast dynamics. In amplitude diagram there are boundaries where the interiors each support one spiral.

Use enclosed area of trajectories instead of amplitude, Can find the elapsed time from crossing a Poincare section instead of phase.

Complex Ginzburg-Landau equation is general form for any system that goes through oscillatory instability, i.e. hopf bifurcation with zero wavenumber.

Can describe tile boundaries analytically. Can describe dynamics by imposing Neumann boundary conditions at the edges of tiles. Boundaries meander after time evolution.

Meandering of spiral cores is possible but not necessary. Meandering, stable, alternans type cores depending on parameter. in Complex Ginzburg-Landau equation the cores all have the same frequency and you would have periodic orbit.

Break-up, drift, and collapse. Looking at the Floquet multipliers of spiral wave. Multipliers are mostly inside the unit circle in the complex plane but there are a few multipliers that corresponds to absolute instability. Pair of multipliers near the boundary of the unit circle correspond to convective instability.

Anternans instability, action potential with multiple length scales. Refractory (relaxation period where it can not be excited). Breaking up of a plane wave into spiral waves.

Looking at Stroboscopic map (time measured in periods). Get core drifting, tile deformation. In order to understand this, can show that periods are exponentially decaying functions of linear scale. Matching phase at tile boundaries, moving boundaries depending on spiral frequencies. Small tiles become larger, large tile become smaller. Unless tiles are all the same size, cannot have periodic solutions.

Imposing boundaries break global symmetry, right eigenfunctions (goldstone modes), adjoint eigenfunctions are exponentially localized. Symmetry is perfect on the interior but gets fuzzy near the boundary.

Midway conclusion: do not expect to find periodic solutions. On a small enough domain there is an amount of spatiotemporal coherence. You will never find solutions on large domains because of the lack of coherent.

Dwight's work of applying oscillating field with near resonant frequency that makes them synchronize.

Channelflow Looking through the programs to see what I can incorporate from what John has already written. I'm going to see if he has time tomorrow to talk through things.

2017-01-26 Matt :

M. Graham Talk (video). Model turbulent drag reduction in polymer solutions. Polymers reduce drag. Maxiumum drag reduction asymptote. Asymptotic curve between poiseuille limit and Prandtl-von Karman limit. Log-law for polymers, Virk law.

Long linear polymers work best, when dissolved in water they turn into a long brownian motion like path. Relaxation time, time it takes to approximately diffuse its own length. Weissenberg number, which describes: Polymer chains tumble in shear flows such that they have little effect on viscosity. In extensional flows, polymer chains stretch, "Lagrangian chaotic velocity fields are extensional". Hyperbolic flows = extensional?

Intermittent dynamics for Newtonian and moderate Weissenberg number, active and hibernating turbulence. Area averaged velocity profile switches between quiescent periods near Virk limit and von Karman limit.

Polymer stretching generates torque which works to undo streamwise vortices. Estimate on polymer stress using Lyapunov exponents. Believes that active turbulence is amount of time that the polymer stress remains below a critical threshold.

There is a family of solutions that have the property that within a certain parameter range, the upper branch solution is near von Karman and the lower branch is near Virk.

Could do Newton searches for viscoelastic solutions but hasn't been done yet, edge-tracking viscoelastic has been done.

At this Re the hypothesis is that polymer effect is to increase the Weissenberg number, which brings the states closer to the edge state in some sense.

Looking at spatial variation of drag, Detector functions vs. clustering methods, k-means clustering or Otsu's method. Once you have the regions you can do conditional averaging to get mean profiles. Mean profiles of these low drag regions, low-speed streaks are similar to lower branch coherent states.

Y. Duguet *Turbulent bifurcations in intermittent shear flows: From puffs to stripes* (video). Shear flows with linearly stable laminar base flows implies a possibility of sustained laminar turbulent coexistence. Exposition of D. Barkley's work on expanding slugs.

Exposition of laminar, intermittent and turbulent regions of Re scales for a variety of geometries.

In 2D plane Couette solutions, look at 2D spectrum, there appears to be a gap in the spectrum so they used two Gaussian filters to look at large length scale and small length scales separately.

Investigation of overhang regions (preference towards one of two channel flows at edges of puffs). By mass conservation, there is a constraint includes streamwise velocity deviation and spanwise ve-

locity deviation w.r.t spanwise. Therefore because there is stream-
wise velocity variation, there must be spanwise velocity variation.
Interfaces must have oblique growth.

Why do spots organize into stripes, they also conserve mass.

Homotopy with a new parameter which is the aspect ratio of span-
wise to wall normal length scale, in this case things die out near the
walls so it doensn't really help show puffs to stripes.

New homotopy, based on annular pipe flow. New homotopy pa-
rameter which is the radius ratio in pipeflow. Relevant length unit
is the cylinder gap, the difference between radii. The dynamical pa-
rameter is frictional Reynolds number. Even though the asymptotic
limit is not Hagen-Poiseuille flow, want to show that the same phe-
nomenology exists.

Showing results of simulations at various values of new homotopy
parameter. Changing from helical (oblique on unwrapped cylinder)
structures to spatially localized puffs.

Same mass budgeting as before but now in cylindrical coordinates.
Looking at spectra of each direction. Graphs of length scales as func-
tions of the homotopy parameter. Get regions of different behaviors
of confinement. The regions are strong confinement at both walls,
confinement only at inner wall, and no confinement.

Statistics, generate PDFs after filtering. PDFs of azimuthal velocities
and angles. Bifurcation diagrams of statistical modes (maximum of
PDF).

Goldenfeld hypothesized that it is crucial to think about zonal flows
in a pipe, but Yohann thinks that they are of no statistical importance
due to the lack of peaks in his PDFs.

P. Cvitanović Math Colloquium

periodic eigendecomposition Plan to meet to with J. Gibson tomorrow,
undisclosed time based on his schedule.

Misc. Listened to C. Rowley, S. Bagheri, P. Cvitanović talk about Koop-
man, singular eigenfunctions of Koopman operator.

2017-1-29 Matt *Physics of puffs and slugs*

(video). Main mechanism that extracts energy from mean flow is
nonlinear interactions with velocity profile. $-\overline{uv} < u >$. Produc-
tion exceeds dissipation at interfacial upstream edge, slightly down-
stream dissipation exceeds production, and later there is a region in
equilibrium.

In comoving frame, the interfacial edge moves upstream (source of
confusion). Turning down Reynolds number serves to eliminate
the region of energy equilibrium. Describing the puffs as flame
fronts, making the analogy that the "flame" is moving upstream,

but because it is also being advected by the flow it leads to confusion. Fluid parcels are constantly flowing through the interfacial upstream edge, and are being "entrained" by the structure of the puff. Likewise for the downstream front, fluid is constantly leaving the downstream interface and relaminarizing. Can get entrainment at both edges.

D. Barkley, Avila Movies of various slugs, much discussion on the upstream and downstream edges and why you should treat them the same. Dwight claims that this is because of the entrainment that occurs at both ends. Roman Grigoriev bringing up the transport of momentum at the interfaces.

Investigations using Lagrangian frame moving with a patch of isoenstropy surface.

J. Gibson Discussed periodic eigendecomposition with John, first question that was brought up was whether periodic Schur decomposition is required, as opposed to performing Arnoldi iteration of periodic orbits to get Floquet vectors.

Most of the discussion was both of us trying to reconcile our opinions and how we both are thinking of the problem in the context of ref. [6].

2017-1-31 Matt P. Hall *Canonical exact coherent structures: The emergence of distributed states and the Law of the Wall* (video).

Looking at structures as Re goes to infinity gives insight on finite Re solutions.

Looking at two non-localized states for arbitrary shear flows, they are the foundation for producing families of solutions. Type 1: (Self sustained processes) Vortex-wave interactions. Type 2: Freestream coherent structures. Relevant to transition induced by free-stream turbulence.

VWI reduction applied to asymptotics. $3D$ time dependent navier stokes transformed to 2d steady navier stokes, convection diffusion, eigenvalue problem.

Logarithmic jump in pressure when you cross the critical layer, unless the critical layer is flat.

Three time scales for VWI. 1. slow roll-streak diffusion timescale t 2. fast inviscid wave timescale $Re * t$ 3. birth death timescale for vwi states $Re^{1/2} * t$

Drag vs. alpha bifurcation diagram. Looking at VWI solutions and their Reynolds stresses, which for lower branch solutions concentrate in critical region. For upper branch solutions they begin in the critical layer but after continuation they begin to become exotic, but this can be explained by asymptotics.

Looking at bifurcations of upper and lower branch solutions show why upperbranch is so much more unstable than lower branch. Instabilities on three different time scales.

Rescaling by taking streamwise and spanwise wavenumbers

Generate new solution by introducing spatial periodicity, by stacking solutions on top of each other. where interactions depend on the spatial period.

Get a time periodic solution from this stacking procedure due to single mode waves?

Defining the infinite array computational problem.

Starting with spatially periodic solution in Couette flow, generalizes to arbitrary shear flow, but only in flows that have a logarithmic profile.

Locally looks like Couette flow locally, but phase speeds slowly changes similar to WKB, eikonal equation.

R. Monaco *Convection: from small plumes to large coherent structures* (video).
Taylor-Couette and Rayleigh-Benard. Transition turbulence of Taylor-Couette flow. Conflicting evidence of Taylor-Couette flows, showing large scale structures can persist conflicting with previous experiments.

Azimuthal and time averaging. Aspect ratios are different but can explain apparently.

Streamwise velocity behavior in large variety of flows follows Virk log-law.

Adding riblets doesn't really change structure in bulk.

Turning off rotation, rolls persist for relatively large times. Changing behavior of rotation, corotating, outer rotating, etc.

Rayleigh benard flow, boundary conditions changing the nature of solutions dramatically.

mixed temperature boundary conditions seemingly have no effect, by means of different geometries of adiabatic and conducting regions at boundaries.

Spatial KS Had the idea to involve Galilean invariance in spatial integration, i.e. somehow formulate $0 = \int u(x,t)dx$ into a local constraint that can be used to constrain the integration to the repeller. Burak thinks is is definitely something worth pursuing.

Shadowing Lemma Read some papers, had short discussion with PC, I agree it isn't too informative and takes too much time to get anything worthwhile out.

Variational methods Discussion about the general practice, Why didn't we use Fourier instead of finite differences, using fourier would be diagonal, instead of having cyclic border terms. How to deal with continuous families of tori still needs to be explained. Roman gave me contact of another GT student working on such methods.

Num Lin Alg Review of QR, arnoldi iteration, GMRES. Will begin using arnoldi iteration on periodic orbits from J. Gibson's repository and then comparing angles tomorrow.

2017-02-01 Matt Inertial Manifold Used Channelflow's arnoldi iteration on two periodic orbits of plane couette, I am a little confused as to how the eigenfunctions are represented as output so I wasn't able to produce any pairwise angles or norms yet. I spent too much time digging through the code with little benefit; although I hate bugging John with these types of questions it's probably best to just ask.

Lagrangian Formulation of KS Poked through literature on Lagrangian formulations of partial differential equations tt seems that it is relatively common to formulate these things for KdV equation but not really any other equations.

KS spatial integration Looked around for a way to follow up on the idea of using Galilean invariance as a constraint condition for spatial integration, haven't found or come up with any local condition that could be applied as of yet.

Avila meeting Shared current projects and work with Marc Avila whom was curious since he saw my poster. Discussed spatial integration, variational methods, invariant spatiotemporal tori and the benefits of variational methods versus shooting methods.

He was interested in using spatial integration to reconstruct boundary layer information from PIV data. He also suggested using a test case of applying the spatiotemporal variational method that we are trying to deploy to a case where a stable torus exists and then see if one could track tori and the breakdown of tori.

Li Xi viscoelastic flow, Weissenberg number better than Deborah number because it's more physical. Comparison of relaxation time vs. deformation time (shear rate).

If time scale of polymer contraction is slow relative to flow, then can introduce new nonlinearity that consists of how the polymer reacts to the "new" dynamically evolved flow.

In general Re and weissenberg number Wi are changed via changing the flow rate, which simultaneously changes both.

In channel flow, there tends to be a proportionality of Wi and the transition to turbulence. "above" this transition, only get drag reduction above a critical Wi number.

Velocity of FENE p models is the same as experimental data, but otherwise results are qualitative. depiction of parameter space.

Description of "phase transition" between LDR and HDR regime. In LDR the velocity profile in the buffer layer increases in magnitude, until the HDR regime where the slope of the velocity profile in the log layer increases, so there are obviously two different processes

occuring. He thinks that vortices burst/break up less such that the flow is more coherent.

Wants to identify the time-scale that identifies the transition.

Ismail Hameduddin Continuation of viscoelastic talks. Mathematics of viscoelastic modeling. Get a linear equation for the elements of the conformation tensor under some assumptions.

2017-02-02 Matt :

J. Gibson *Julia: the future of scientific computing* (video). Combines best properties of Python, Matlab, LISP, and C. Demonstration of Julia through notebooks via jupyter. c

N. Goldenfeld *Statistical mechanics of the phase transition to turbulence: zonal flows, ecological collapse and extreme value statistics* (video). Statistical approach to turbulence. Going from finite number of particles in a box, use statistical mechanics to explain equilibrium behavior. Claim is that the same is true for an infinite number of particles in a box (fluid)

Comparison of puff splitting decay mean time plot to predator-prey model as a function of prey birth rate. Does extinction equal turbulence?

There is a possibility that turbulence is a long lived transient, changed after Hof's experiment that measured the survival probability of puffs.

Believes that superexponential scaling is the correct interpretation. Relating metastable puffs to directed percolation. Four fundamental processes.

Phase transition characterized by universal exponents, as functions of parameter p, the probability of continuing.

Directed percolation done spatiotemporally, using correlation length as a means of generating scales in the problem. Do statistics on these simulations.

Reasoning behind super exponential scaling and extreme statistics. Mean follows central limit theorem, maximum follows three types of distributions. Probability the largest fluctuation exceeds Re threshold then decay superexponentially. Looking at statistics

The reason you expect super exponential decay, is the means by which decay is measured.

Once correlation length gets to the order of the spatial extent, the statistics switch from superexponential to power law.

Logic of modeling phase transitions

- Magnets
- Electronic structure
- Ising Model

- Landau Theory
- Renormalization group universality class
- Turbulence
- Kinetic Theory
- Navier Stokes equation
- ?
- ?

Identification of collective modes at the laminar-turbulent transition, similar to Landau theory only look at important structures near the transition.

Zonal Flows. Computing instantaneous reynolds stress is anisotropic, which flows into the walls, which drives the zonal flow. Zonal flow inhibits reynolds stress (makes it more isotropic). Zonal flow isn't driven by the mean flow because there is orthogonal to mean flow.

Comparison of zonal mode-turbulence and predator-prey models. Predator prey models driven stochastically. Lotka-Volterra. Oscillatory effects from satiation model. Fluctuations and oscillations produced by demographic stochasticity.

Predator-prey path integrals and quantum field theory. Try to write down a Landau theory for this.

Allowed field theoretical processes look like the same four fundamental processes of directed percolation.

Demonstrated turbulence to directed percolation via predator prey and field theory.

Superexponential vs. critical scaling.

Crutchfield and Kaneko

B. Eckhardt Secret *The transition to turbulence in shear flows: a dynamical systems perspective*

No video because it was held in South hall. Sort of recap of previous presentation. How fat is turbulence? Apparently as fat as an elephant. Nikuradse in 1930s shows the frictional factor dependence on Re.

Intermittent case is defined by linear stability of laminar profile. Expect smooth transition when you have subcritical bifurcation. Coherent structures and state space. Create a new basin of attraction via homoclinic bifurcation. Transition from attracting closed state to fractal open set.

Crises for attracting set of one coherent structure isn't really enough to explain statespace. Conglomerate of crises is sufficiently stable such that it is possible to never return to laminar.

Arnoldi Producing eigenfunctions and Floquet exponents and multipliers for a range of periodic orbits from John's repository, pinned

down John for a quick talk on whether I'm getting reasonable values for exponents, etc. I was also confused on how the eigenfunctions were being represent, he somewhat cleared it up and directed me towards matlab scripts to use to reproduce fields as to begin taking norms and computing angles. Looking through matlab scripts.

Readings The first part of Farrell et al. on generalized stability theory. Horseshoes and blenders via

KAM Even though I'm not employed by Rafael de la Llave I found myself sidetracked by KAM theory to gain some insight into what is generally done with tori.

2017-02-03 Matt **Jörg Schumacher** *Boundary layer dynamics and large-scale structure in turbulent convection* Announcement of Euromech colloquium.

Intro to thermal convection. What are dynamics at bottom and sidewall boundary layer. Going from laminar boundary layers to turbulent boundary layers, can see that bulk is turbulent via Kolmogorov spectrum.

Always work with Boussinesq approximation, boundary layers for low and high Pr, changes thickness of thermal boundary layer.

Numerical simulations for liquid mercury required to be parallelizable.

Skin friction field at bottom is complex even in the laminar boundary layer regime. Seems like avoiding calling it turbulent. Looks turbulent to me.

One can remove the precession of "impact" and "ejection" zones (convection cells component on bottom plate) by proposed coordinate transformation.

Pure fluid turbulent cascade is extended with Prandtl number. Trying to understand velocity profile in boundary layers, no answers for now?

Large-scale order in convection. Large aspect ratios.

Time averaging at a higher Reynolds number makes results look like lower Re.

Koopman analysis projected back into state space, grouped around these modes.

Don't lose structure from lower Prandtl numbers under continuation.

P. Arratia Talk Flow of polymeric solutions. High shear serves to unwrap polymers. Reduced navier stokes equations, introduce new nonlinearity with terms that describe the polymers interaction with the fluid. FENE-p models.

Flows that stretch polymers really well, high velocity gradients. Role of curvature, curved streamlines lead to "hoop stresses". Taylor Couette flow is linearly unstable even at zero Re.

Schematic for transition in viscoelastic similar to Newtonian fluids.

Is there a nonlinear instability to laminar viscoelastic flow at low Re? Discussion of global instability, once you have finite perturbations, no longer talking about linear stability.

Experimental setup, cylinders, subcritical instability demonstrated by graphs of velocity fluctuations vs Wi for different numbers of cylinders. Saturation implies subcritical instability, hysteresis in Wi continuation seems to confirm this.

Little bit of discussion of velocity profile in the middle of the channel, as there was confusion on how one of the graphs was being produced.

2017-02-06 Matt Channelflow Learning how to write bash shell scripts to automate the process of using Channelflow commands to compute generate time discretization of periodic orbits, arnoldi iterations for eigenfunctions, and pairwise angles of eigenfunctions.

Spatial integration Spent more time trying to figure out if I can use galilean invariance as an integration constraint.

Spatiotemporal parallelization debriefing Debriefing of ref. [14] with Ashley Willis taking the lead. Discussion over coffee he said that he would work through some calculations and then let me compare it to variational Newton descent.

What would Koopman do Listened to Igor Mezić discuss Koopmanism and answer questions from Mohammad Farazmand, R. Grigoriev, M. Schatz.

2016-2-7 Matt C. Caulfield *Telling the time, using the clockwork of turbulence to answer open questions in fluid dynamics* What is shortest distance between edge manifold in energy norm, therefore could find the smallest perturbation to transition to turbulence.

Linear optimal perturbation is not sufficient as it is streamwise invariant? Therefore use a localized nonlinear perturbation.

Using variational methods that maximizes energy, makes sure that navier-stokes is imposed for all space and time, imcompressibility, initial energy c of perturbation.

Finding adjoint equations via integration by parts, can use Newton solver to solve adjoint equation. It's like a backwards in time Newton-solver which doesn't blow up due to using the adjoint variable.

Identify transition by the energy gain and optimal time.

Localization of initial condition has nothing to do with edge state it's only to exploit the Orr mechanism. Edge state is a streamwise structure due to the box size?

Use DNS results as initial condition for GMRES algorithm. Use Koopman/DMD modes applied to snapshots. Looking at spectrum,

relatively well peaked. Three Koopman modes is enough to capture the DNS results near the energy plateau region of time, otherwise known as the edge-state.

Discussion about whether this is linear or nonlinear.

Using adjoint somehow requires converge on arbitrarily long time, so adjoint methods.

Stratified flows. Get spontaneous layers that aren't taylor vortices, i.e. structures that don't scale with the gap width.

Most linearly unstable mode connection to nonlinear interactions. Recurrent structures in stratified flows.

Rama Govindarajan Talk *Droplet Dynamics in model vortices* Heavy particles converge to regions of high strain and leave regions of high vorticity, bubbles would do the opposite.

Behavior dependent on spatial position of particles relative to the vortex. Polar coordinate equations that arise are parameter free, they would normally take into account time dependence of length scale which is associated with both the particles and the vortex core. The particles do not interact, do not affect the flow.

Dynamical simulations show that vortices appear to behave as solid objects that experience the Magnus effect. Can create vorticity through baroclinic torque.

Buoyancy definitely affects the size of structures that appear in 2-D DNS simulations.

Looking towards clouds, general description of a self-sustaining process, equations that now involve the vapor pressures and saturation and Stokes number.

Solving Turbulence Debrief Relation between fictitious time and time, seems to become blended Discussions of variational Newton descent and how it's really crude. Discussions about parallelization, no longer doing time integrations, Parameterizing the space of curves in "fictitious time" isn't obvious in this method.

How second order equation is sufficient for parallelization. Looking at secord order equation that Ashley has written down, the RHS looks like the current formulation of the variational Newton descent.

John seems to be implying that instead of the normal variational Newton descent matrix equation that arises from the fictitious time PDE, one can use Krylov methods, PC doesn't see how to incorporate small steps into this.

Is cost function always the $L2$ norm? The issue has to do with the area where localization is valid, higher norms reduces this size. Mathematicians like to use a $1 + \epsilon$ norm, which bypasses the kinky structure of the one norm.

Cost functional version of multishooting Ashley wants me to attempt to implement the minimization of the cost functional (**??**) which leads to the variational equations (under the assumption that there is no symmetry operation $g(\phi)$, which is the simplest case to take), (**??**).

The general procedure indicated by Ashley is that you shoot the reference points i.e. the set of $x_i i = 0...M - 1$ to retrieve $y_i = f^t(x_i)$ and then set the second of these variation equations equal to zero to get $w_i(T_i)$. You use an adjoint equation for w to pull back $w_i(T_i)$ to $w_i(0)$, and then use the variations in T_i and x_i to update your reference state in order to proceed until the cost functional described by (**??**) is minimized to desired cut off.

I'm going to apply this to antisymmetric subspace $\mathbb{U}^+$ of Kuramoto-Sivashinsky equation and then work with Ashley to hopefully parallelize it.

I wrote a crude version by repurposing function definitions from variational Newton descent, as well as the numerical time-stepping algorithm from ref. [10].

The main part that is left is to derive the adjoint equation and decide on how to evaluate it, and then include that in the crude version I have currently.

2017-02-08 Matt M. Gudorf Brown Bag Talked about spatial integration and variational methods. B. Eckhardt brought up similarities to Burgers equation and was concerned with how Kuramoto-Sivashinsky equation deals with shocks.

J. Jimenez was concerned about how well-posed the spatial integration problem is and what we hope to get out of it Shortly after the talk in the cafe next door, B. Eckhardt brought up ideas very similar described $T = 0$ steady state equation from ref. [8] about how the solutions to the steady state equation (equilibria in time) form a very coarse way to partition the time dynamics. He also mentioned that the talk was good, he cited Divakar Viswanath and his approach of thinking about the problem and adapting methods, and how this was crucially important for results in Plane-Couette

J. Gibson thinks that the variational Newton descent is bad method due to its number of steps and formulation as essentially a gradient descent method. He thinks an alternative description with

He also brought up that although there are continuous symmetries in the Plane-Couette problem, Newton-Krylov methods are well suited to picking out solutions without "sliding" around due to the continuous symmetries.

Other suggestions were to use Krylov methods in combination with variational Newton descent.

R. Grigoriev Excitability talk, review of spirals using Karma model. Square boundary (no periodic boundary conditions) , three marginal eigen-

values on square domain. Discussion of relative equilibria on square domain. As long as spiral is in center of domain it doesn't drift but when offset it begins to drift.

Rotation and translation of square domains, don't overlap, so take smaller circular domain in the interior of the intersection of rotated square domains has some property? Sort of confused here, Roman said people taking circular domains were lazy, but ends up having to do that in some respect. Once spirals are far from the walls, or far from each other, exponential decay of response functions tell you that they spiral-wall or spiral-spiral pairs do not really interact anymore. The converse statement is that small domain sizes will strongly impact the spiral core.

Spiral chaos and excitable systems can be decomposed into slow dynamics of tiles and fast dynamics of spirals.

Implications for fluid turbulence, need to look at adjoint and the role of pressure on localized solutions. The adjoint in detail means the adjoint eigenfunctions about the linearization of localized solutions.

Dwight Barkley explains that perturbations along the adjoint of a certain eigenvector is what leads to perturbations along the eigenvector desired. This is due to the fact that the adjoint is orthogonal to the complement of the desired eigenvector.

Variational multishooting I rederived the equations (**??**) and (**??**) in order to solidify the thought process. Ashley was kind enough to produce the equation for the adjoint (**??**) which I also went through.

A. Willis Coffee discussion Discussed variational methods with Ashley, and in detail discussed how I implemented the variational Newton descent. I personally feel there is much room for optimization, and that automation of generating initial conditions would be a much sought after device for many people interested in exact coherent solutions. One of his methods that differed from mine was using the angle between successive descent directions as a means to control the step size.

2017-02-09 Matt M. Farazmand Talk *Extreme events in turbulent flows: A variational approach* Trying to explain intermittent bursts in energy dissipation by explaining it away by saying there is an ECS that is visited albeit rarely. The solution wasn't find by Newton-Krylov methods, so needed another method. Chose to work with Adjoint method.

Lots of discussion on gradient methods, John really would like to see comparisions with these variational methods with modified Newton.

Looking at nonlinear energy transfers through by using a graph with Fourier modes as the vertices.

Needs a new variational method,

- Classical case of these types of bursts is a symmetry breaking bifurcation. (Near-equilibrium systems)
- Multi-scale methods, requires separation of slow and fast degrees of freedom
- Theory of large deviations (multi-equilibrium driven by stochastic force)
- Optimally time-dependent modes (Using Lyapunov exponents, predictive, not physics)

Looking for initial states that trigger extreme growth of observable. The idea is that the solutions are in some submanifold of state space, and try to find states that shoot you away from the submanifold. Look for states that maximize a time delayed supremum of observable.

Modified Newton's Method Talked with John and Ashley about the method that John always likes to bring up when the topic of the variational Newton descent is brought up. The only way to know which is the best is to do testing it seems.

Tower room Discussions about the program and where do we go from here. Javier Jimenez thinks it is time to formulate interactions between different scales, i.e. multiscale theory. Shell models, examples, and the history of turbulence were discussed.

References

[1] N. Aubry, P. Holmes, J. L. Lumley, and E. Stone, "The dynamics of coherent structures in the wall region of a turbulent boundary layer", J. Fluid Mech. **192**, 115 (1988).

[2] P. Blonigan and Q. Wang, "Multigrid-in-time for sensitivity analysis of chaotic dynamical systems", Numer. Linear Algebra Appl. (2014) `10 . 1002/nla.1946`.

[3] P. J. Blonigan and Q. Wang, Multiple shooting shadowing for sensitivity analysis of chaotic systems and turbulent fluid flowsflows, in 53rd AIAA Aerospace Sciences Meeting (2015).

[4] P. Blonigan, Q. Wang, E. Nielsen, and B. Diskin, Least squares shadowing sensitivity analysis of chaotic flow around a two-dimensional airfoil, in 54th AIAA Aerospace Sciences Meeting (2016).

[5] P. Cvitanović and J. F. Gibson, "Geometry of turbulence in wall-bounded shear flows: Periodic orbits", Phys. Scr. T **142**, 014007 (2010).

[6] X. Ding, H. Chaté, P. Cvitanović, E. Siminos, and K. A. Takeuchi, "Estimating the dimension of the inertial manifold from unstable periodic orbits", Phys. Rev. Lett. **117**, 024101 (2016).

[7] X. Ding and P. Cvitanović, "Periodic eigendecomposition and its application in Kuramoto-Sivashinsky system", SIAM J. Appl. Dyn. Syst. **15**, 1434–1454 (2016).

[8] C. Dong and Y. Lan, "Organization of spatially periodic solutions of the steady Kuramoto-Sivashinsky equation", Commun. Nonlinear Sci. Numer. Simul. **19**, 2140–2153 (2014).

[9] J. F. Gibson, J. Halcrow, and P. Cvitanović, "Visualizing the geometry of state-space in plane Couette flow", J. Fluid Mech. **611**, 107–130 (2008).

[10] A.-K. Kassam and L. N. Trefethen, "Fourth-order time-stepping for stiff PDEs", SIAM J. Sci. Comput. **26**, 1214–1233 (2005).

[11] Y. Lan and P. Cvitanović, "Unstable recurrent patterns in Kuramoto-Sivashinsky dynamics", Phys. Rev. E **78**, 026208 (2008).

[12] S. B. Pope, *Turbulent flows* (Cambridge Univ. Press, Cambridge, 2000).

[13] L. N. Trefethen and D. Bau, *Numerical Linear Algebra* (SIAM, Philadelphia, 1997).

[14] Q. Wang, S. A. Gomez, P. J. Blonigan, A. L. Gregory, and E. Y. Qian, "Towards scalable parallel-in-time turbulent flow simulations", Phys. Fluids **25**, 110818 (2013).

Chapter 15

Matt's 2017 blog

2017-02-13 Matt Inertial manifold dimension Installed Channelflow to terminal in Howey, wrote and currently running scripts to automatically compute Floquet vectors generated via Arnoldi iteration at 256 points around the shortest periodic orbit of the HKW (Hamilton, Kim, Waleffe) minimal flow unit. Split into four tasks and hopefully my crude script writing hasn't overlooked anything. Will probably run for a couple of days.

> More details: Using 100 arnoldi iterations to produce all unstable and marginal eigenvectors, in addition to 50 stable eigenvectors. I'm hoping 100 iterations is enough for convergence, seems to be from preliminary tests in Cali.

Fritz John PDE book On order from library, should arrive tomorrow.

Variational multishooting Still trying to implement adjoint equation.

2017-02-15 Matt :

Variational multishooting I have implemented all of the pieces, but it seems to share some of the bad behavior that I encountered when implementing the variational Newton descent, the problem is that I do not know how to compensate for this unlike the other time, as there isn't much wiggle room other than increasing the discretization or the number of integrations steps in the shooting process. I think the problem is due to the ability of allowing the shooting times to vary independently of one another. Either way, it seems to run much slower than what I already have so I think I will shelve this idea for now, as it is much more important to use what I am comfortable with to produce tori than discuss and investigate the differences between numerical methods. (The other investigation would be modified Newton with trust region that John Gibson talked to Ashley Willis and I about). I personally think conjoining Krylov

subspace methods with the variational Newton descent is the way to go.

Fritz PDE Read the first chapter (of four total) of the partial differential equations book. It went over the method of characteristics for first order equations. It seems to pick up in the next chapter so I'm excited to see where this leads.

Guckenheimer and Holmes Picked up this book via suggestion of Burak

2017-02-16 Matt Pairwise angles Spent most of the day trying to figure how to correctly write bash scripts in linux, and how to apply them to Channelflow. Uploading first results from pairwise angle calculations of Floquet vectors for Channelflow. Rereading about how to move onto principal angles between linear subspaces as was done in ref. [11]

2017-02-21 Matt Spatial Newton descent Debugging and changing spatial Newton descent code. I think I've pinned down the main problem to be an error in trying to use Fourier transforms rather than explicit sums in my definition for the stability matrix elements, or initial condition generation. I'm currently using the shortest periodic orbit in time as an initial guess; Therefore, I would expect the value of the cost functional to be small relative to something that isn't already doubly-periodic in time and space. While the value of the cost functional is relatively small, it still may be too large for an initial guess.

That being said I can at least list what I believe to be the most likely cause of errors.

- Error in definition of stability matrix elements; this can be seen from the inability of the fictitious time evolution to lower the value of the cost functional.
- Poor initial conditions, in a specific sense. I think a periodic orbit is a good start, but the number of Fourier modes kept or discretization in space might be impeding progress; One problem is memory requirements due to having a system of equations for spatial derivatives as opposed to a single ODE prevents large discretizations.

Fritz PDE It's taking a while to digest; There are a lot of geometrical notions about solutions to PDEs that I have never really considered before. Apparently cones are much more abundant that I would have previously believed.

2017-02-21 Matt spatial Newton descent Put a lot of time into debugging spatial Newton descent code. Due to size of the system it takes much longer to run than antisymmetric subspace $\mathbb{U}^+$ calculations making it more time consuming to check to see if its running properly. Currently I am able to take initial conditions with initial value of cost

functional $\mathcal{F}^2 \approx 150$ to a final value of $\mathcal{F}^2 \approx 10^{-5}$. This leads me to believe I have caught most of the small errors and only have a little bit more work into finding what I am overlooking before it will be fully operational (if I may be so bold as to sound like an engineer).

One of the main problems I have been having is that the fictitious time evolution is much more temperamental; increasing step sizes seems to be much more "unstable" in the sense that even when close to (spatially) periodic solutions it is still possible to overshoot and therefore ruin the run. In order to combat this I am going to make a run on Light with much smaller step sizes than I would normally use, and let it run overnight.

Fourier differentiation for later use I also have been playing around with using Fourier series (spectral differentiation) as a means to calculate the approximate tangent space. As one would expect, it is much faster than multiplying a large matrix (finite differencing scheme) with a large vector (Approximately 100 times faster), but there I am somewhat confused on how to include this into the matrix equation (13.18) that is the meat of the computation process, without completely rewriting my code.

The reason for this is such: Spectral differentiation with respect to a parameterization variable, s, can be rewritten as multiplication by a diagonal matrix with elements is, but this requires the vector that is representing the entire loop to be ordered in a very specific way. If the loop was ordered in this specific way it would reduce to multiplication of a large diagonal matrix which would be repeating the (small) diagonal matrices with elements is. If one wants to do it this way I believe the easiest way, in order to avoid reordering the stability matrix elements, would be to formulate it this way mathematically: The matrix $D_{\mathcal{F}}$, which produces the approximate tangent space after multiplication with the "loop vector" $\mathbf{x}$, could be represented in such a way,

$$D_{\mathcal{F}} = \mathbf{P}^{-1}\mathbf{F}^{-1}\mathbf{Diag}(is)\mathbf{FP} \quad \text{where,}$$

$\mathbf{F}$ = Block diagonal matrix composed of Fourier transform matrices (i.e. to Fourier transform each of the Fourier coefficient series with respect to parameterization variable), $\mathbf{P}$ = Permutation matrix to reorder in specific way to enable easy Fourier transforms.

This is probably too convoluted as it is somewhat hard to explain, but keeping a record for future possible implementations.

2017-02-22 Matt Checklist Modifying and relocating checklist from before to correctly denote what is currently being accomplished for finding principal angles of subspaces for channel flow.

[**x**] 1-24-2017 Generate time discretized periodic orbit using Channelflow.

[x] 2-2-2017 Use Arnoldi iteration to find eigenfunctions of periodic orbits

[x] 2-13-2017Produce eigenfunctions around periodic orbit in an *automatic* rather than manual fashion

[x] 2-16-2017Compute $L2$ pairwise norms of eigenfunctions as first measure of angles.

[ ] Compute principal angles between subspaces of eigenfunctions.

Principal angles Here is a description that I am trying to implement in c++ in order to work with Channelflow, this corresponds to the last step in the checklist, but has multiple steps itself.

Procedure taken from ref. [1]:

[ ] For the nth subspace, form two matrices A, B such that $Range(A) = spane_1, ..., e_n, Range(B) = spane_{n+1}, ..., e_N$, $e_k = k^{th} eigenvector$

[ ] Use Eigen c++ package to perform Householder triangularization to produce QR decompositions of A and B.

[ ] Form matrix $M = Q_A \dagger Q_B$ and apply c++ JacobiSVD on it to get principal values σ_k

[ ] σ_k from previous step $= \cos \theta_k$ where θ is the principal angle between the kth subspace of A,B. (only care about the first principal angles, not orthogonal complements).

spatial Newton descent Bad results from overnight trial; stalls out around cost functional value $\mathcal{F}^2 \approx 10^{-8}$. Final configuration space velocity field is a highly oscillating very non-physical type solution that looks like the result of aliasing; I believe I need to incorporate more Fourier modes as a first step to fix the issue, or the number of discretization points, although doing so leads me to run out of memory

After talking to PC today he pointed out that this is likely due to forgetting to slice the orbit; Need to do this with first Fourier mode slice.

Reading Read a little bit more of Fritz, linear subspace angles [1], symmetry reduction [5]

Xiong's comments Xiong really thinks that in order to get anything meaningful I need to find Floquet vectors along all possible periodic orbits, as well as orbits that shadow these orbits.

updates Updated codes to svn, updated pairwise angle figure from feb 16th.

arnoldi iteration Getting more Floquet vectors from periodic orbits from Channelflow database; there seems to be a problem this time around. Background of the problem: before arnoldi iteration proceeds, the arnoldi program of Channelflow computes the $L2$ norm of $\sigma f^T(u) - u$ and warns if it is greater than 10^-8; for the first point on the orbit

this time around this error is 10^{-10} but for other points it's $\approx 10^{-1}$. Need to figure out what is causing this discrepancy. The first thing that this points to is that the DNS of the periodic orbit is unstable and I need to go back and decrease the step size, but the step size was already smaller than the default when I generated the data in the first place.

Xiong to Matt 2017-02-23 With only a few periodic orbits, I think it may be easier to check the local Floquet exponents first. They are defined as

$$\lambda_j(x) = \boldsymbol{e}_j(x)^\top D(x)\,\boldsymbol{e}_j(x) = \lim_{\tau\to 0}\frac{1}{\tau}\ln\|J^\tau(x)\boldsymbol{e}_j(x)\|\,. \tag{15.1}$$

D is the strain tensor $D = (A + A^\top)/2$ with A the stability matrix. It may be hard to obtain the transpose of A, but we can evolve the Floquet vectors $\boldsymbol{e}_j(x)$ (of the full cycle) by the Jacobian matrix for a short time to get the instantaneous expansion/contraction rates. figure **??** shows the local Floquet exponents for $\overline{rpo}_{16.31}$ in Kuramoto-Sivashinsky equation. There is a clearly separation between the leading 8 modes and the rest. Maybe you can observe similar phenomenon in the channel flow. That will give an estimate of the dimension.

2017-02-23 Predrag "Local Floquet exponents" are back? This is like calling function $f(x)$ "local integral"

$$\lim_{x''\to x}\frac{1}{x''-x}\int_x^{x''}dx'\,f(x')\,.$$

$A(x)$ is d-dimensional generalization of $dv(x)/dx$, and that is an object that is not invariant under general nonlinear coordinate transformations. The value of such derivative could be anything - the only meaningful quantity is the spectrum of the Floquet matrix, which is invariant. There is no reason to give any particular significance to

$$\boldsymbol{e}_j(x)^\top D(x)\,\boldsymbol{e}_j(x) = \boldsymbol{e}_j(x)^\top A(x)\,\boldsymbol{e}_j(x)$$

and one does not need to evaluate $A^\top$, as the transpose of a scalar is itself,

$$(\boldsymbol{e}_j{}^\top A\,\boldsymbol{e}_j)^\top = \boldsymbol{e}_j{}^\top A^\top\,\boldsymbol{e}_j\,.$$

We put up with this nonsense in ref. [11] only in order to finally get the paper submitted - it is not my job to teach adult collaborators nonlinear dynamics, if they are unwilling to learn. Grad students - that's different. Oscillations in (15.1) happen to be mild, but we have no argument that they should be mild. That's fortuitous.

Xiong to Predrag 2017-02-23 Yes, you are right. We do not need $A^\top$ get the instantaneous expansion/contraction rate. But it is required in the definition because $\boldsymbol{e}_j{}^\top A^\top\,\boldsymbol{e}_j$ is a complex number for complex vectors. I

do not think that such an instantaneous rate is nonsense. The idea is backed by the domination of Oseledec splitting. Experiments with complex Ginzburg-Landau equation with covariant vectors also use this idea. For now, if we do not have enough orbits to study the principle angles statistically, why not try to have a look at local Floquet exponents? Maybe it gives us some intuition.

2017-02-23 Matt :

J. Demmel talk *Communication-Avoiding Algorithms for Linear Algebra and Beyond* (Link with Slides) (Additional Info)

Motivation is that algorithms have two costs, flops and moving data. Counting costs, flops measured in time per flop, "words moved" measured in bandwidth, messages (described as groups of "words") measured by latency.

Minimize communications to save energy.

Redesign algorithms to avoid communication, between all memory hierarchy levels. Obtain lower bounds if possible.

Some Numbers: 12 times faster matrix multiplication (on 64 thousand cores) (doesn't scale too well, larger matrices achieve only something like 2.7 times) 3 times faster tensor contractions

Outline of Communication-Avoiding (CA) algorithms.

Survey of CA Linear Algebra Direct Linear algebra, lower bounds on communication on $Ax = b$, $Ax = \lambda x$, least squares, svd. being added to LAPACK, PLASMA, MAGMA.

Lower bound on Bandwidth cost for all n^3 like (three nested loops) linear algebra. Let M = fast memory size per processor Lower bound Words_moved(per processor) = $\mathcal{O}($ flops(per proc) / $M^{1/2})$

"When can you obtain this lower bound in sparse case?" (not considering things like diagonal matrix multiplication which is highly optimized)

Lower bound on the Latency cost
words_moved(per processor) = flops(per processor)/ $M^{3/2}$

Naive intro to linear algebra, matrix multiplication with three loops.

Split matrices into $b \times b$ How big should b, be? Need b sized blocks to fit into fast memory, lower bound of $flops/M^1/2$

Parallel matrix multiplication, Break matrix into small submatrices.

Summary of dense parallel algorithms attaining communication lower bounds. obtain lower bounds with lower bounds of messages and words. (with b constant).

Algorithms have been optimized to follow, but there is an additional step of optimization with regards to the memory size M. "Can we always hit the lower bound no matter how much memory there is?" yes.

12 times factor of speeding up is due to a 95 percent reduction in communication time Algorithm was sold to company that was later acquired by intel.

Same thing with Tall-skinny QR. Break into blocks, do local QR decomposition. break into smaller and smaller blocks via repeated QR. (MPI reduce).

"how does this affect the stability?" QR: only use multiplication by orthogonal matrices, still works. When abandoning partial pivoting had to prove stability (which was proved in an unreferenced paper).

Where do $M^{1/2}$ come from in the lower bounds: generalization of lower bounds General case of matrix multiplication, as many indices as you want. only really need the indices.

Access locations indexed by group homomorphisms, maps list of indices to specific matrix element?

Ongoing: Implement and improve algorithms to generate lower bounds, optimal algorithms. Extend speedups by using extra memory ($n + 1/2$) dimension algorithms

Krylov subspace methods (Arnoldi, Lanczos, CG, GMRES) Assume matrix well-partitioned. Serial implementation: (k sparse matrix multiples. moves slow to fast memory) New case: read from slow memory to fast memory **once** parallel implementation on p processors: price we pay is some redundant computation (flops are cheap). Challenges: Poor partition, preconditioning, num. stability.

Instead of using monomial basis, use a "Newton basis" for CA-GMRES to achieve same convergence properties of GMRES.

2017-02-24 Matt :

S. Berman Math Colloquium *A classical Hamiltonian model for HHG* High Harmonic Generation, send in intense laser pulse into gas, focused in directions transverse to propagation.

Measured the transmitted light, the spectrum typically is composed of three distinct behaviors for intensity as a function of frequency, monotonic decrease, plateau, and then convergence to zero. Interested in plateau region in a classical sense.

Introducing an electric field description for the incident light. Radiation from incident light interacting with gas. Main goal is to try to describe plateau region classically.

The basis for the classical model is to assume there are N single electron atoms indexed by position. Assume ions do not interact with each other, and therefore there is only potential due to the interactions between atoms and their electrons. Therefore, the different ions will interact indirectly through the electric and magnetic fields.

Have a set of ODEs that come from Lorentz force law and Maxwell's equations. Has a Hamiltonian structure, want to try and preserve this structure.

Defines a Hamiltonian and the derived Poisson Bracket. Need a finite discrete implementation that captures all of the Physics.

Reduction of the Hamiltonian by defining a periodic box such that one can Fourier transform in all three spatial coordinates. Find expressions for Functional derivatives that were present in Poisson Bracket, i.e. trying to get expressions for dynamical equations in Fourier space.

Make linear transformations that eliminate trivial time dependence, changes the Hamiltonian to look like harmonic oscillator, and modifies the poisson bracket but still satisfies Jacobi identity.

This transformed system still isn't tractable due to its size. Doesn't take into consideration ionization, but theory predicts comoving electric fields so that you only care about electric field in a small box.

2017-02-27 Matt :

spatial Newton descent Further changes to spatial code, yielding equilibria in time. Previously when I was working with antisymmetric subspace $\mathbb{U}^+$ in time, this typically indicated that there was some mistake with a numerical factor somewhere, but here I am not so sure as it is still a periodic orbit in space. Although, if I had to wager, it would be a mistake that I'm looking over somewhere.

Another main challenge is how to implement a slice condition to deal with translational invariance. Typically this is dealt with when the spatial Fourier series is being used, and therefore it is easier to represent a hypersurface that eliminates this marginal direction; in the spatial Newton descent code (this is what I call using (1.36) with variational Newton descent) I am trying to eliminate the translational freedom but it's not as straightforward as the first Fourier mode slice; as the first Fourier mode slice in this case would eliminate time translations. I've been looking towards some of the papers about invariant tori and their "phase conditions" as a possible means of escape.

Floquet vectors I've been having a problem with computing the Floquet vectors associated with relative periodic orbits.

I produce a discretized periodic orbit by using Channelflow's DNS, while restricting solutions to remain in their symmetry subspace as dictated by the symmetries listed in the data base at (Channelflow). Then at each of these discretized points along the periodic orbit, I begin arnoldi iteration. One of the first checks of the arnoldi iteration verifies whether $\sigma f^T(u) - u \approx 0$, as this is what dictates a relative periodic solution. Now, the problem is that for the first point of the discretization (i.e. the initial condition taken from the database, u_0), $\sigma f^T(u_0) - u_0 \approx 10^{-8}$, but for any other point of the discretization, the error is more like 10^{-1}, which is unacceptable as it means

we've somehow been set off course. At first I thought this doesn't seem unreasonable as we are dealing with unstable solutions, but if the relative periodic orbit is so unstable, then why does the initial condition yield a reasonable result after time integration?

The only thing left is the fact that the discretized points of the periodic orbit are being generated by me, meaning that there is room for human error; I must be not properly using the symmetries in when generating the time discretization of the relative periodic orbits. This is the only thing I can think of as everything works well when there are no symmetry group elements other than the identity. That being said, until I figure out what is going on I will be producing Floquet vectors of periodic orbits that have this trivial symmetry group.

2017-03-01 Predrag I think of slices and Poincaré on the same footing, in the spirit of spacetime democracy. That's why I reformulated the invariant invariant 2-torus as an algebraic fixed point condition, for a set of MN algebraic equations for the spatiotemporal Fourier coefficients (1.43).

I believe that the Jacobian matrix that linearizes (1.43) has *three* marginal directions.

Two are for the exact continuous spatial and temporal symmetries. I have left to you and our other collaborators is to decide how to section (in time direction) and slice (in the spatial direction) these equations. I believe if you use a version of Newton method that uses a pseudeinverse (Appendix of ref. [9], Gibson's person-to-person advice to you), you do not have to impose the section/slice constraints. If you do, try first to use first Fourier mode slice (rotate both time and space modes, separately, to set the $\cos(\phi_x) = 0$, $\cos(\phi_t) = 0$ for both Fourier series, thus decreasing the dimensionality to $(M-1)(N-1)$-dimensional symmetry-reduced state space, and hope that we are safely away from the slice border. We also have to quotient the spatial reflection symmetry, but let's wait with that one...

Then there is one marginal direction (I believe) for the continuous family of physically different solutions (what we usually call "adiabatic continuation" while varying a continuous parameter, let's say the domain size L in the old-fashioned fixed spatial domain calculations). For $T = 0$ spatial equilibria case, this is the "energy" E, the integration constant in the integral of (1.37), see Sect. 2.2 of ref. [9] and Sect. 5.3 of Lan's thesis [22]. I have not thought through what that is for $T > 0$, but I cannot see how it can be ignored - there will be finite curves in the LT plane where such continuous families exist between their birth and their destruction. In the spacetime they will look like a rubber-sheet deformations of a given geometrical pattern.

If we are lucky, a version of Newton method that uses a pseudeinverse might be able to find one solution in a family, which then we can continue

into the whole family. In any case, you have the 60 000 periodic orbits to play with at $L = 22$ value. And then sit and think about what does this'all mean :)

2017-03-02 Matt :

Floquet Vectors Was able to find the error of why I couldn't get good results for relative periodic orbits of Channelflow. It turns out that instead of taking the symmetry information from the Channelflow website I should have been using the Channelflow command "find-symmetries" to produce the generators of the symmetry group for particular solutions. John's input from our correspondence definitely helped out; that being said, I am now be able to produce Floquet vectors for all of the periodic orbits in the Channelflow repository. Although after noting the convergence properties I have doubled the number of Arnoldi iterations as a precaution.

Xiong's Thesis Finished proofreading Xiong's thesis. My main focus in corrections was to improve some grammatical errors and offer suggestions on how to reword things. If I was a revolutionary I probably would have gone through and rewritten entire paragraphs, as I still find the sections on periodic eigendecomposition to be relatively convoluted; my main focus was that if its good enough to be published than I probably should just leave it be. Regardless, he seemed very pleased with the comments that I left, and said that they were very helpful.

spatial Newton descent I realized that I should not have to worry about implementing a slicing condition in the spatial version of variational Newton descent; All that was required in the time case was to reduce the symmetry associated with the marginal direction parallel to velocity, i.e. a Poincaré section. I didn't worry about the spatial translational invariance and it was able to converge to a solution just fine in the time case.

In this line of thought, because space and time have their roles reversed, I should only have to take into consideration the translational invariance in the spatial direction and not the SO(2) symmetry in the (now periodic) time direction.

I also changed the definition of the stability matrix elements that arise due to the nonlinearity in hopes this will fix my problems; All in all, things are working *much* better than they were even when compared to yesterday, although the convergence properties are still not where they need to be in order to say I "found" an new solution yet (For an initial condition whose initial cost functional value is $\mathcal{F}_0^2 \approx 5$ my code is able to reduce it to $\mathcal{F}_\tau^2 \approx 10^{-1}$). I'm currently testing my code with discretized versions of $\overline{ppo}_{10.2}$, but I am going to try to see what happens to an more general initial condition next.

There also might be a smarter way of choosing a constraint that enables better convergence, as opposed to the "first coordinate" hyperplane (i.e. the first Fourier mode in most systems). I'm currently playing around with using a hyperplane condition on the "more dynamical" variables which is a hasty and crude name not to be taken seriously. What I mean by this is that in (1.36) the spatial derivatives of the Fourier coefficients of $u^{(3)}$, which represents the third derivative, are much more complex than the other derivatives, so perhaps using a hyperplane condition on one of these coordinates would be better; this hasn't seemed to be the case yet.

2017-03-06 Matt :

Variational Newton Descent (General) Realized I made a small mistake when thinking about using Fourier transforms along the parameterization direction in order to approximate the loop tangent space (15.1).

I thought that I would have to somehow permute the elements (15.1) of the "Loop Vector" (vector that encodes the parameterization of initial condition for periodic orbit search). The reasoning behind this was in order to use differentiate with respect to a parameterization variable s, I would need the elements to be in sequential order with respect in parameterization variable s, in order to multiply by vector $i\vec{m}$, where m is the conjugate variable (in a Fourier transform sense) to s. This is **not** the case, as I can merely exploit the Kronecker outer product to produce a diagonal matrix such that along the diagonal there are M duplicates of each element of $\vec{m}$

I should have realized this sooner but I'm still not convinced this will enable faster calculations.

We are essentially diagonalizing a sparse matrix for $\mathcal{O}(M\,(nlog(n)))$ flops from taking M Fourier transforms of length n = power of 2. This is all well and good, but I think that there might be complications from the stability matrices; I need to go through the calculation, but the naive way to write the stability matrices in their new representation is: $\tilde{\mathbf{A}} = \mathbf{FAF}^*$, where F is a unitary matrix representing the discrete Fourier transform. [1]

When you include the amount of flops needed to produce the product of these matrices, I don't think the benefits outweigh the costs *unless* a much smaller discretization can be used due to the convergence of Fourier coefficients (i.e. a truncation in the parameterization variable).

Next is the representation of the fictitious time evolution as a system of linear equations, similar to (13.20), which is restated here for comparison to the new system of equations.

---

[1]Matt : Note that Kronecker product again makes matrices sparse, such that previously full DFT matrix is now sparse

The old linear system is given by,

$$\begin{bmatrix} M & -v \end{bmatrix} \begin{bmatrix} \delta\tilde{x} \\ \delta\lambda \end{bmatrix} = \delta\tau \begin{bmatrix} \lambda v - \tilde{v} \end{bmatrix}, \tag{15.2}$$

where $M = D - \lambda Diag(A_n)$ with D being the finite difference matrix, and A_n a block diagonal matrix containing stability matrices.

Now, the equations the same form, with new variables described by over-bars

$$\begin{bmatrix} \bar{M} & -\bar{v} \end{bmatrix} \begin{bmatrix} \delta\tilde{\bar{x}} \\ \delta\bar{\lambda} \end{bmatrix} = \delta\tau \begin{bmatrix} \lambda\hat{\bar{v}} - \tilde{\bar{v}} \end{bmatrix}, \tag{15.3}$$

where $\bar{M} = \mathbf{F}Diag(i\vec{m})\mathbf{F}^* \otimes \mathbf{I}_d - \lambda Diag(A_n)$ and $\bar{v} = \mathcal{F}(v)$, $\tilde{\bar{v}} = (Diag(i\vec{m}) * \tilde{\bar{x}}$. [2]

Spatial Newton Descent Rewrote the main body of the fictitious time evolution loop to hopefully deal with memory management a bit better, but still getting memory issues. Waiting on latest Arnoldi iteration to finish before using terminal to do calculations.

Waffling between implementation of least squares solver for pseudoinverse variational Newton descent.

GMRES seems to be locked by memory. Also tried to implement QR decomposition as in TrefethenT̊refethen97 but trying to stick to pseudoinverse and least squares solvers as they typically work better; also keeping track of large matrices is a downside.

The best results, (i.e. better than square matrix problem, but still not good enough) was with SciPy's LSQR algorithm, which, in the paper that it is based on ref. [29], describes it as a "conjugate-gradient-like" algorithm, with better stability. I haven't gotten into the nitty gritty as of yet.

Floquet vectors Spent some time checking results to make sure I'm doing everything correctly before proceeding. Began writing c++ code that will calculate principal angles between subspaces; I think I might be able to get away with writing this in Python and I might try to do so as I think it would take less time than writing in c++.

Still just running arnoldi iterations on light to produce data for future use.

Physics Colloquium: Vadim Roytershteyn *Turbulence and Magnetic Resonance in Space and Astrophysical Plasmas* Large range of scales by astrophysical nature.

Variety of models and approximations used to tackle range of scales.

Hope to answer: How dynamics of small scales affect the large scales.

---

[2]Matt : I changed this such that the only difference between my current code and this formulation is the calculation of approximate tangent space via Fourier methods.

Magnetic reconnection; rapid change in magnetic field topology. Movie that demonstrates reconnection of field lines; important process because plasma transport is essentially determined by these field lines, with transport in the transverse direction being quite slow.

The amount of plasma transported to Earth from solar wind is dependent on two boundary layers of the Earth's magnetic field.

Mesoscale simulation; Hybrid particle in cell calculation, this is a Monte-Carlo Technique. These are easily parallelizable, and are therefore well-suited for large scale computing.

Quasi-Parallel vs Quasi perpendicular Shock; interaction between shock waves and turbulence.

How do results generalize to three dimensions?

Large-scale Reconnection: Sweet-Parker Model. Has a peculiar scaling law that can be explained by transition to turbulence, or the fact that at a certain point you reach the kinetic scale of the plasma.

Flux conservation is hard because there is separation of magnetic field lines due to turbulence.

Plasma Turbulence: Three scales, f^{-1} range, inertial range, sub-ion range.

Incredible simulation of a Kelvin-Helmholtz instability.

2017-03-09 Predrag Roytershteyn was so kind to find out who I was, and send me a copy of Riley [34] *On the probability of occurrence of extreme space weather events*. The historically important is the Carrington extreme space weather event of 1859. With all the caveats, his estimate of the probability of another Carrington event occurring within the next decade is $\sim 12\%$, which worries me much more in the short term than the climate change, a slowly rolling chronic accumulation of relatively localized disasters, with more time for adaptation. And in 2012 we seem to have had a close call.

2017-03-07 Matt :

Plumbers' hangout See pipes blog.

March Meeting practice talks Was invited by Sabetta Matsumoto to participate in listening to talks and providing feedback in exchange for free food.

I thought it would be good to experience short 10 minute talks to see the general practices.

S. Markande *A chiral minimal surface from space group symmetries.*

Principal curvatures, gaussian curvature, mean curvature; minimal surfaces. appearance in nature.

Use discrete symmetry groups to represent minimal surfaces as a prime patch. Three commuting symmetries due to lattice.

Weierstrass-Ennepper representation and Gauss Map.

Keep succinct paraphrase on the slides. Describe his role better and accomplishments better.

Jon Michel System viewed as connections and nodes, key property is connectivity. In d dimensions, 2 d is necessary to be stiff.

Spending too much time on "Our system slide". Hard to see what you're talking about, be more demonstrative with multiple slides.

Perry Ellis Nematics on a Torus Defining defects by (Conley Index of nematics?). Poincaré Hopf Theorem.

Tracking defects with inherent topological charge, similar to spiral cores of Grigoriev et al.

No flux of defects across boundary? Locally everywhere zero as you increase the velocity, which is a measure of the activity.

Michael Tennenbaum *Reconfigurable mechanical properties of fire ant aggregations* Collections of fire ants are active in terms of stress and rheology as opposed to a simple liquid. Research on how to model the activity of these ants as well as measure physical quantities associated with the aggregation.

Variational multishooting After talking to Ashley, who told me to start the multishooting effort with only a few number of points rather than the large discretization used as if it was a Newton descent, I looked back into the variational multishooting technique that he described back in Santa Barbara. I took four point on the original orbit, while my code is minimizing the cost functional (**??**) I am yet again getting the "equilibrium descent" for an antisymmetric initial condition $\in \mathbb{U}^+$ that converges with my variational Newton descent code. This resulting equilibrium "solution" is a typical result when something is ill-defined. I would speculate that the manner in which I am handling the adjoint equations is the culprit, as I tried to modify the ETDRK4 of ref. [19] to be the numerical integration routine to integrate the equations.

Kuramoto-Sivashinsky on a torus While waiting for Arnoldi iteration to finish so that I could begin testing the spatial variational Newton descent without fear of memory problems I was trying to think about the best way to use (1.43), which I will restate here:

$$\left[i\omega_\ell - (q_k^2 - q_k^4) \right] \hat{u}_{k,\ell} + i \frac{q_k}{2} \sum_{k'=0}^{N-1} \sum_{m'=0}^{M-1} \hat{u}_{k',m'} \hat{u}_{k-k',m-m'} = 0 \,. \quad (15.4)$$

PC elaborated that in order to find the fixed point associated with this, "The Newton method then requires inversion of $1 - J$, i.e., $\det (1 - J)$, where J is the 2-torus Jacobian matrix, yet to be elucidated."

I was hoping to work towards this goal today, by rewriting (1.43) in manner that fits the form $f(x) - x = 0$.

First, $\hat{u}_{k,\ell}$ represents matrix elements, so it makes sense to rewrite the equation as a matrix equation. Define matrices $\mathbf{Q_1} \equiv Diag(-q_k^2 + q_k^4)$, $\mathbf{W} \equiv Diag(i\omega_\ell)$, $\mathbf{Q_2} \equiv Diag(\frac{iq_k}{2})$, and let the two dimensional FFT be represented by matrix multiplication $\mathbf{U} = \mathbf{F}_M \mathbf{u} \mathbf{F}_N$, where the matrix elements $U_{k,\ell} = \hat{u}_{k,\ell}$.

With these definitions the equation can be rewritten as:

$$\mathbf{Q_1 U W} + \mathbf{Q_2 F_M}(\mathbf{u} \otimes \mathbf{u})\mathbf{F_N} = 0 \tag{15.5}$$

where the nonlinear term is calculated in configuration space as to avoid the two dimensional convolution.

Because $\mathbf{Q_1}$ and $\mathbf{W}$ are diagonal, their inverses are easily found, and the equation (15.5) can be rewritten

$$\mathbf{Q_1}^{-1}\mathbf{Q_2 F_M}(\mathbf{u} \otimes \mathbf{u})\mathbf{F_N W}^{-1} + \mathbf{U} = 0 \tag{15.6}$$

Now we can redefine $\mathbf{U} \to -\mathbf{U}$, and remember to convert back after finding the fixed point.

Define

$$f_{k,\ell}(\hat{u}_{k,\ell}) \equiv \mathbf{Q_1}^{-1}\mathbf{Q_2 F_M}(\mathbf{u} \otimes \mathbf{u})\mathbf{F_N W}^{-1} \tag{15.7}$$

and therefore we have an equation of the form: $f_{k,\ell}(\hat{u}_{k,\ell}) - \hat{u}_{k,\ell} = 0$, where the Jacobian matrix is given by the fourth rank tensor that arises from taking partial derivatives with respect to $\hat{u}_{k,\ell}$ More to be derived in the future, hoping to make headway into finding tori; I can't tell if this equation is going to be useful or if I should really be working towards deriving and learning variational Newton descent equations for finding tori similar to Lan, Chandre and Cvitanović [23].

2017-03-08 Matt :

Xiong's Last Stand Attended Xiong's thesis defense. I thought it went well overall;

spatial Newton descent Fixed memory issue by making it such that the "Newton descent matrix" i.e. the matrix in (15.3) is not evaluated before each least squares evaluation; rather, we keep this matrix constant as an approximation and then when the cost functional can no longer decrease, i.e. we have left the local neighborhood of the stability matrices that define the matrix, we redefine the matrix and then restart the search; this is similar to what is implemented in other variational Newton descent code; forgot this fact when I rewrote the spatial Newton descent code to use LSQR to solve the least squares problem as opposed to using matrix inversion.

Application of the spatial Newton descent code to ergodic trajectories that have been deformed to be periodic in time were resulting in

the "falling into equilibrium" problem, this was due to a bug where the wrong temporal system sizes were being used.

Application of spatial Newton descent on $\overline{ppo}_{10.2}$ results in a reduced cost functional but seems rather obstinate in regards to convergence. Luckily, the approximate loop seems to fluctuate around spatial extent $L = 22$. I think this is a good indication as it means the spatial Newton descent is capturing the spatial geometry of $\overline{ppo}_{10.2}$. That is to say, even while reducing the cost functional the solution doesn't want to betray itself, as it originates from the spatial system size $L = 22$.

I implemented (15.3) and am currently testing whether or not this makes a difference. Fourier methods are only slightly different than finite difference methods when calculating the approximate tangent spaces (usually determined by the initial value of cost functional) but it might help the convergence capabilities, currently running a test on an ergodic trajectory from $L = 88$ initial domain size.

I think part of the problem is due to how I am solving the least squares problem at this point. I want to avoid actually taking a pseudoinverse, as this can take an enormous time and end up being a futile effort.

I've been toying around with some ideas of maybe somehow converting the currently underdetermined system into an overdetermined one by looking to maybe constrain the least changing coordinates, as this is an indication that they are close to being converged to the orbit. Regardless, I am looking towards more ways and hopefully better ways of solving the least squares equations.

initial condition production rewrote some parts of the matlab code I am using to generate the initial conditions, in order to get a more exact period in time.

2017-03-10 Matt : Spent all of my time today trying to figure out ways to get spatial Newton descent to work properly. but alas all that I tried whether it be the error tolerances, step sizes (variable or constant), initial condition discretizations, least squares solvers, pseudoinverse or regular inverse methods, hypersurface constraints, matrix preconditioners, etc, did not help the converge properties.

By examining the corrections being applied to deform the loop, specifically the maximum correction applied in each step it seems most of the steps are modifying the "period" i.e. the spatial extent of the initial condition the most. There might be some way to discourage this with an additional condition on the rescaling factor λ that matches the magnitudes of the approximate tangent space to the actual tangent space.

The majority of modifications being put into changing this rescaling factor seem to be the cause of the critical slow down of the algorithms, which

might be indication of the presence of a continuous symmetry that needs to be dealt with that isn't currently being dealt with.

The one thing that I've learned is that there must be some crucial fact that I have overlooked that I took for granted in searching for periodic orbits in time.

2017-03-13 Matt :

Floquet vectors and principal angles Finished code that will allow for computation of principal angles between linear subspaces of Floquet vectors. Should have plots soon, specifically the angles between subspaces of Floquet vectors at 64 points along the orbit titled p19p06 on the channelflow database. Need to figure out a way to make it presentable as opposed to just a bunch of lines on a figure. I think I need more evidence before any claims are made, but from this particular periodic orbit, the angles between subspaces decreases until $n = 13$, afterwards it increases. I do not see the distinction of being bounded away from zero only for $n > n_c$ as of yet. More investigation required.

spatial Newton descent Still haven't been able to get this to work, after some thought over the weekend I have been trying to implement a major change to the code. The general idea is this, the first three equations of (1.36) will by definition match the approximate loop tangents as they are generated via spectral differentiation, which is now how I am computing the approximate loop tangents. I have been trying to work out how this can be exploited as to greatly reduce the dimensionality of the system. I.e. instead of keeping track of the real and imaginary components of the Fourier coefficients of u, u_x, u_{xx}, u_{xxx}, I should be able to only keep track of u, and then match the last equation of (1.36) to the fourth derivative of u computed by spectral differentiation. The main problem with this formulation is that I haven't been able to rewrite figure out the best way to rewrite the stability matrix elements, other than they should only depend on the real and imaginary components of the temporal Fourier modes of u.

If I am successful in this endeavor, I should be able to reduce the dimensionality by a factor of four, i.e. reducing the size of matrices involved by a factor of sixteen, which should also eliminate "redundant degrees of freedom" as I have denoted them in my head, as the derivatives u_x, u_{xx}, u_{xxx} are (obviously) coupled to u; so by reducing the dimensionality and making it such that only corrections are made to u, we inherently are correcting the derivative fields as well.

Arnoldi Iteration Still just chugging along, using about 32 points per orbit for calculations of Floquet vectors. I haven't decided on a standard as of yet but this will allow for relatively speedy calculations as opposed to higher discretizations.

2017-03-14 Matt :

Floquet vectors More principal angle calculations and arnoldi iterations. Still producing data;

Spatial Newton descent Went through my overhaul ideas with Xiong, before implementing anything. He said he needed some time to think about what I was trying to do. I found some matrix element equations that might be useful in the near future; the problem is that I am confused on how to compute (local) stability matrix elements if I use spectral differentiation (global) to produce spatial derivative fields in (1.36). I need more time to work through it but if it's as I think it might be it could drastically simplify calculations.

After discussing this with Xiong he seemed to imply it might be better to just work on solving the fixed point condition for invariant tori; which I have been doing.

tori While running other codes, I've been writing code that will solve the fixed point, i.e. algebraic nonlinear equation that determines invariant tori. Xiong lead me to look at López *et al.* [25], which I took the time today to read. I feel like it covers a lot of useful ideas and concepts that I will be able to directly apply to my own problem. They use a numerical least squares solver `lmder` to find fixed points, but I think it might be good to invest time into implementing Newton-Krylov hookstep since J. Gibson holds it in such high esteem. The general idea is to use a nonlinear solver to solve (15.5) augmented with a number of conditions for shifts and periods such that the system is not underdetermined.

2017-03-18 Matt :

KS tori More work on torus fixed point codes; uploaded current version to svn. Took time today to redefine functions to be in terms of new class variables.

I was sort of confused on how to use the Matrix-vector product approximation to the Jacobian matrix in order to use the Newton-Krylov method in conjunction with SciPy's implementation of GMRES. I want to use their version as opposed to creating my own version as is optimal considering it is optimized outstanding code, and will leave less room for error on my behalf; but there's the problem that it only works if you provide A and b in order to solver $Ax = b$.

I'm currently working on something that I believe should work, which is to split the Jacobian matrix into nonlinear and linear contributions; The normal equation that arises is $J\delta u = -F(u)$. Due to the fact that I am looking for fixed points this reduces to figuring out the kernel of the linear map defined by the Jacobian matrix.

There might be much more specifics in for this endeavor, but what I am planning on doing is abusing the fixed point condition, splitting

the Jacobian matrix into an explicitly defined linear contribution, and an approximately defined (via matrix-vector product approximation: $J_{NL}\delta u = F(u + \delta u) - F(u)/\epsilon$, where epsilon is a small (but not too small, as stated in López *et al.* [25]), it should probably be around $\sqrt{\epsilon}_{machine}$ and $\mathcal{O}(\epsilon) \approx \mathcal{O}\delta u$.

Then I would have a system of the form (L stands for linear, NL stands for nonlinear) $J_L\delta u \approx -J_N L\delta u$, where I would be able to plug this system into SciPy's GMRES function with $J_L = A, -J_N L\delta u = b$ and solve for x.

I haven't come across any reason why this shouldn't work, the things I know I still have to include are the generators of symmetry operations σ, which should be present in the Matrix-vector approximant equation, and in the definitions of the mapping F.

On these comments, the main references I have been studying are refs. [4, 6, 21, 25]. [3]

Floquet Vectors Still producing more sets of Floquet vectors and running principal angle codes on them.

K. Krishan Talk Listening to Mike Schatz' former student, Kapil Krishan, talk about the differences between industry and academia, his experiences at Proctor and Gamble, what he thinks could be done better (communication of research between private sector and scientific communities mainly), networking, CV building and many other real world necessities for success.

2017-03-23 Matt :

Floquet Vectors Still doing arnoldi iterations; 200 iterations per point on every orbit is too time consuming so I reduced the number of arnoldi iterations back to 100.

Tori hunting Rewrote lots of `MNGkstorifunc.py` as I've decided to abandon computing any Jacobian matrix explicitly as the Matrix-vector approximation seems to be quite ubiquitous, and employed with Newton-Krylov methods it is also known as Inexact Newton-Krylov as well as Jacobian matrix-free Newton Krylov. This was somewhat hard of a decision to make as it meant I wasted some time deriving explicit forms for the matrix elements of the Jacobian matrices, but such is life.

Therefore, I began writing my own Newton-Krylov (i.e. Arnoldi iteration, GMRES) code as opposed to using the SciPy package implementation. The idea is that even though I previously claimed that I wanted to avoid this as their GMRES implementation is optimized, it will probably benefit me to avoid explicitly defining any Jacobian matrix.

---

[3]Predrag 2019-05-08: what is bibitem *KK04jfnk*? Different from *KK04*?

I was hung up on how to actually compute these "matrix-vector approximations" in my context, after some exploring ref. [2, 15, 36]. I think I've figured them out but I plan on talking to J. F. Gibson to confirm. The other things I am trying to reconcile between the different notations is how López *et al.* [25] handles symmetries of solutions as it's slightly different than when one has a forward time mapping, I believe. These things and working in the class objects I've defined in python turned out to be somewhat trickier than I had first intended but I hope to get things up and running by the weekend.

As a first test of this code I'll be using time integrations of rpo's from the svn repository, as they are well converged solutions that have all of the information attached.

Also a note on symmetry, the way that J. Gibson (channelflow) handles the spatial and temporal translation symmetry is to constrain the Newton steps to only progress in directions transverse to the spatial and temporal equivariance directions; the idea is to use additional equations of the currently underdetermined system of equations (because we are keeping track of "extra" variables: time and spatial periods, spatial phase shifts from relative periodic orbit).

The additional equations that are tacked onto the Matrix-vector product approximation of the Jacobian matrix are the inner products $(du, \frac{du}{dx})$, $(du, \frac{du}{dL})$, $(du, \frac{du}{dT})$ in this case. I am slightly worried that the galilean invariance will also make this more complicated; The reduction of the galilean invariance in usually handled by setting the zeroth spatial Fourier coefficient equal to zero, but in this two dimensional spectrum of Fourier coefficients this corresponds to a whole row of coefficients in the matrix of coefficients equal to zero. In other words if the time series of these zeroth modes is always zero, then the time Fourier transform of this information will also be identically zero.

Also, I still need to implement the Viswanath [40] hookstep algorithm.

2017-03-28 Matt :somehow this didnt save before I submitted it and I accidentally closed out so the description of the talk I went to and the web meeting might be a little rough. need to commit more often.

plumbers meeting Burak showed the two dimensional unstable manifold and displayed the size in comparision to an original neighborhood in order to show the size of the domain in which the linearization is valid.

Ashley showed a traveling wave solution in pipeflow that was acquired via his feedback-mechanism (variable Reynolds number).

I described what I am doing with the torus search Newton-Krylov code and Floquet vectors.

Predrag commented on how Xiong did statistics of Floquet vectors using 400 periodic orbits, and how he used orbits that shadow periodic orbits and showed how the displacement vector (in state space) lays in the subspace spanned by a finite number of Floquet vectors of the shadowed orbit.

PDE seminar: Xukai Yan *-1 homogeneous solutions of stationary incompressible Navier-Stokes equation with singular rays* I went to the PDE seminar hoping to learn more about continuous families of solutions, and see how Mathematicians deal with Navier-Stokes. The work that was done was for incompressible navier stokes solutions that are axisymmetric and swirless ($u_\phi = 0$ in spherical coordinates). Description and proof that even when there is a singularity at the south pole, there exist families of solutions with different properties (bounded, finite, etc.) in certain parameter ranges. I think I should do some secret mathematics training in order to get more out of these talks because at the end of the day it's interesting but extremely hard to take anything away from these talks for me.

ks tori Spent the remainder of the day working on my Newton-Krylov code to find tori of Kuramoto-Sivashinsky . I believe everything is ready for testing after preparation of an initial condition. I have a number of ideas of what could go wrong due to the fact that I still get confused over this specific formulation of GMRES.

The way I have it formulated right now is order to find roots $F(u, T, L) = 0$, I begin with the general formulation of Newton's method for fixed points which (due to $F(x^*)$ equaling zero, with x^* being the fixed point of this mapping, including variations to period and spatial length of the system and any parameters that control other continuous symmetries.). takes the form $J(x_N)\delta x_N = -F(x_N)$. Just to specify if the dimension of the state space (i.e. the number of two dimensional Fourier coefficients) is $2MN$, where the factor of two is due to splitting the coefficients into real and imaginary parts, then the vector x^* is $2MN + 3$ (I think), due to freedom to change the period, length and spatial phase. This is different than dealing with a symmetry reduced equations (which I feel like I should know is what I have to do, but evidence in channelflow makes it seem like it is not necessary to find solutions).

To begin the hunt with Newton-Krylov Methods we need to produce a test vector for the power iteration that will produce the Krylov subspace. This is taken to be the vector whose norm is the residual to be minimized, i.e. $r_0 = -\mathbf{b} - \mathbf{A}\delta x^{(0)}$ where b is a vector containing $F(x)$ with a finite number of zeros concatenated at the end to make b a $2MN + 3$ dimensional vector. Likewise, constraints formed by inner products are appended to the vector $J\delta x$ (a 2MN dimensional vector) in order to make the corrections unique, and not solutions to an underdetermined system. These conditions constrain the correc-

tions to be orthogonal to directions of equivariance.

This "residual vector" is sent to Arnoldi iteration in order to produce the regular Hessenberg and Orthonormal matrices of this iterative procedure. In between Arnoldi iterations, we check the new value of the residual, i.e. $||b - A\delta x^{(k)}||$. If this meets a specific tolerance, it is then passed to the least squares problem that defines GMRES [39], find y that minimizes $||H_n y - ||b||e_1||$, this solution to the least squares problem y is then converted to Newton correction via multiplication of orthonormal matrix $x = Q_n y$. If this Newton correction does not minimize the residual sufficiently, GMRES is restarted. Until either a maximum iteration number is met, or the relative differences between residuals stalls out.

GMRES specific problems to take into consideration, breakdown of the arnoldi iteration, if the test vector lies in the Krylov subspace, then there will be a subdiagonal element of the Hessenberg matrix equal to zero (due to linear dependence and orthogonalization with respect to the Krylov subspace). If this occurs then GMRES is restarted with another random test vector. Numerically, this should be a condition on the value of the norm of the vector being iterated upon.

In order to evaluate the matrix vector product $J\delta x$, the matrix-vector approximation previously discussed is used, where we use $J\delta x \approx F(x + \delta x) - F(x)/\epsilon$, where $\epsilon = ||\delta x||$.

Floquet vectors Still doing arnoldi iterations in order to do statistics of Floquet vectors

2017-03-29 Matt :

PDE talk Yue Liu *Asymptotic analysis on the modeling of the shallow-water waves with the Coriolis effect* Rotation-Camassa-Holm equation Rotation-Green-Naghdi equation Rigorous justification wave-breaking phenomena Solitary wves Camassa-Holm in two dimensions.

Wants to focus on cammassa-holm and quadratic nonlinearities. Comparison with euler equation to justify mathematical model Do we still get wave breaking phenomena

Key defining features of Camassa-Holm, higher order nonlinearities that quadratic, (cubic and quartic terms). These are the terms that deal with rotation, so it makes sense to have a constant (wave speed) term such that if the rotation defined by another constant is zero, these terms disappear. I.e. in the limit of no coriolis force we retrieve the Korteger de-vries equation.

Another way of saying this is that there is a parameter range in which the model returns to KdV, sometimes need to investigate the transition between two regimes.

Camassa-HOlm models the existence of permanent and breaking waves. Breaking waves similar to burgers equation, the wave form

is bounded but the spatial derivative blows up in finite time. Solitary waves are peaked solitons "peakons".

Derivation of RCH equations from euler equation + coriolis force. Use asymptotic expansions to find relationship between constant and part of the velocity field, doing so allows for substitution and will lead to CH equation after derivation.

H1 energy norm, $\int u^2 + \beta ux^2 u$

In order to justify this equation or model first do a comparison to KdV.

In the KdV regime: Throwing away highing order terms, comparisons between Ch equation and RKdV equation via the sobolev norm between solutions that start with the same initial velocity field data, remains bounded a constant to second order for a finite time.

In the CH regime, do similar comparision between green-naghdi and camassa-holm equations.

torus code Mostly debugging the code that I've been writing. There is a big problem with the class objects that I wrote most of the code to revolve around, I'm fixing it I think as we speak but they are behaving as I thought they would so it doesn't look like I will be able to do much testing today.

2017-03-30 Matt :

torus code I think I've fixed the problems I was getting yesterday from passing of class objects around from function to function, it had to do with using a variable named after the class instance itself, which made the code really screwy. Currently I'm just ironing out the small errors but the thing that seems the most problematic is the Matrix-vector approximation for the Jacobian matrix.

Currently it is returning a vector whose norm is way too large to be correct. I haven't been able to figure out why yet.

2017-04-02 Matt :

Floquet vectors Another batch of arnoldi iterations started.

torus code Finding bugs in GMRES code and elsewhere. Matrix vector products were too large because I forgot square root when defining a norm method for my class objects.

I'm trying to work out the kinks and get some results by Tuesday so I can show and get comments from the plumbers during the web meeting. There's yet another bug in the GMRES portion of the code that I haven't found yet, but I suspect it has something to do with the matrix-vector approximation. I wasn't able to figure it out today but will hopefully get it done tomorrow.

pdes Went to the library to try and read a little on PDEs in a formal mathematical way. Fritz is too esoteric for my taste, so I've started reading Lawrence Evan's intro book on suggestion.

2017-04-03 Matt :

torus code Still just trying to get this code to work. Doesn't look like I'll have results to show at the meeting today. Hate to share a lack of progress but I still haven't figured out what's wrong with my GMRES code.

I generated some new initial conditions and after much debugging I found that it is indeed the matrix vector approximation of the action of the Jacobian matrix that is messing things up. Numerically, this amounts to $J\delta x_j \approx F(u + \epsilon\delta x_j) - F(u)/\epsilon$ producing a vector whose norm monotonically increases regardless of the orthonormalization process of arnoldi iteration. I haven't been able to find any issues in how I've coded the arnoldi iteration after debugging so I'm convinced that it is how the mapping function has been coded, but I haven't had much luck in finding errors there either.

Still hoping to get it running soon, maybe I'll get lucky and find the mistake in time for the meeting.

2017-04-06 Matt :

torus code Still do not have results but put a lot of work into the past two days into rewriting and debugging. Added more pieces of code to act as contigencies in case GMRES fails, but currently there is a type of stalling that I am attributing to the factor that my matrix-vector approximations are still baffling me.

With what I have all reason to believe is a reasonable initial condition, a 64 by 64 discretization of the first pre-periodic orbit of Kuramoto-Sivashinsky the initial value of the norm of the value of the mapping $||F(u, T, L)||_2 \approx 10^-3$. I take this to be a good initial condition as the other values of norms I have seen have had much higher initial values of this norm. The problem arises when I approximate $J\delta x$. With almost any randomly generated δx, the norm of the vector $||J\delta x||_2 \approx F(u+\delta u, T+\delta T, L+\delta L) - F(u, T, L)/\epsilon$ with $||\delta x||_2 = \epsilon$. yields a value that is dramatically larger than $||F(u, T, L)||_2$, and as such it does not allow for a convergent Newton-Krylov search. The fact that the norm of the mapping of the spatiotemporal field is small, leads me to believe that the code involving the mapping is correct, but if this is the case then the matrix-vector approximation should be well written as well, as all it involves is this mapping function. It's this circular logic with a hole in it that has been frustrating me to no end.

Something I can try is to use a second order approximation as opposed to a first order. This would replace the approximate with

$$||J\delta x||_2 \approx F(u + \delta u, T + \delta T, L + \delta L) - F(u - \delta u, T - \delta T, L - \delta L)/\epsilon$$

I thought it might be the form of the randomly generated perturbations that was possibly making things go awry, as I believe it's logically justified to restrict perturbations such that the perturbed field would yield a real field if transformed back into configuration space. I wasn't doing this before, but it seemed to help my woes to a small extent, at least in terms of GMRES convergence; but again, in the scheme of things it is a negligible benefit as the residual of the matrix-vector approximate far outstrips any change I have made.

I reworked the GMRES code and validated that the arnoldi iteration portions were working properly by testing the orthonormality of the Krylov subspace matrices (matrix whose columns are Krylov subspace basis vectors) and rewrote the portion when it comes to updating residuals and verifying that the GMRES is actually reducing the residuals.

Also added more update messages and warning messages in order to help the debugging process.

Floquet vectors Another set of arnoldi iterations started. There are a couple of orbits from the database that are not periodic after DNS. I've been trying to figure them out as to why what I am doing works for other orbits but not these. Running a Newton-Krylov search to perhaps converge the orbits to a higher precision. In hopes that will help. Not really worried about it right now as I still have a number of other orbits to run before I deplete the database.

2017-04-10 Matt :

torus code Tried a number of new ideas (well...new to me) in order to get convergence of my Newton-Krylov code.

The second order finite difference approximation didn't really help the values I was getting from approximating the Jacobian matrix so instead I tried to look for why the approximation seems so poor; I hadn't looked at the contributions from the nonlinear and linear parts separately (I actually thought I did this a while ago but I think I had poor initial conditions before). It turns out that the stiff components of the spatiotemporal mapping (i.e. high wavenumber modes due to the fourth power of q_k) are what are contributing to the (what I consider too large) magnitude of the approximation the most.

I tried playing around with the perturbation magnitudes again, since it is mostly the high wavenumber modes contributing to the magnitude of the approximate matrix-vector product I played around with having the perturbations to these modes be smaller in magnitude than the rest, (i.e. some subset of the perturbations of the matrix of spatiotemporal Fourier coefficients is smaller in magnitude than the lower (wavenumber, frequency number) modes). This didn't have

enough of an effect so I instead started trying to think of a way to justify a $2/3$ rule dealiasing (i.e. damping by setting equal to zero) of these contributions. This is usually done during time-stepping, and is justified via an energy input argument. There is usually a contribution to the energy of a solution due to aliasing and as such the higher modes are damped in any calculations in order to maintain energy-balance.

Also, the GMRES procedure is stalling out, so I have been looking towards ways to fix this. It seems that this is a relatively well studied problem and the answer is to introduce preconditioning matrices into the GMRES scheme. This is done in a number of ways and I have to find the best one for my problem, but I am also trying to find one that fits into my code already. I think I will implement FGMRES, where the F stands for "Flexible" [35]. It is called this because it encourages the preconditioner to change at every outer-loop (Newton) step, while remaining the "same" for the inner-loop (arnoldi or GM-RES) steps. (same in quotes because at every iteration the rule to generate the preconditioner stays the same, but the matrix technically changes in size).

Yet another condition that I have been investigating is the effect of changes to the period and spatial size in expressions such as $F(u + \delta u, T + \delta T, L + \delta L)$. I'm trying to wrap my head around why it makes sense to take difference between two solutions where I am essentially changing the domain size while keeping the discretization the same. What I mean by this is that traditionally the (spatial) domain remains constant, and the mapping time T is changed, but I think this only makes sense when the time-dependence is implicit. What I would be attempting to do is, for instance, change the box size in a Navier-Stokes solution and then subtract it from a minimal unit cell solution, which I am pretty sure doesn't make sense, or at least not to me. This might just be due to my inability to abstractify the solution space of an equation; it could possibly make sense as the solutions would still be close in continuation parameters, time and space.

Floquet vectors More arnoldi iterations. Trying to think of a proper way to generate shadowing orbits in a procedural manner by adding a point on periodic orbit to a perturbation, maybe in the direction of a weakly unstable mode.

2017-04-14 Matt :

torus code I was being dumb with how I was creating the random perturbation vectors for my GMRES procedure. After thinking about it a little more I realized I should just create a random field of initial conditions in configuration space and then perform a spatiotemporal Fourier transform to get the correct form of field. I can't explain

how much easier this is than what I was doing before. With this the stiff parts of the linear portion of the mapping and as such I have returned the previous damping of higher modes back to undamped status.

This helps the GMRES steps converge to a reasonable amount but with all coding there is still something else wrong as the Newton step that would be generated from GMRES still does not reduce the residual, meaning that even though I'm solving the linear system, there is something wrong in the piece of my code that produces corrections.

I've also been reading a bunch of papers [6, 14, 18, 27, 32, 35, 38] on preconditioning methods; and specifically for GMRES algorithm. It seems to be a heuristic science much like taking Poincaré sections so I might have to try a number of different preconditioners before I get one that works, or use a combination of multiple different ones with different properties.

evans pde Some more reading for my formal pde education.

Floquet vectors Still producing arnoldi iterations, figure out the problem with the few solutions I couldn't get to converge so all I need is time to run iterations to produce sets of Floquet vectors now.

2017-04-14 Matt :

torus code Talked to xiong to get some new ideas; He thinks that what I was trying to do with the initial perturbation is somewhat of a misleading idea as it is reasonable to take the zero vector to be the initial perturbation and begin arnoldi iteration with the vector $-F(u) = b$, such that the Krylov subspace being generated through GMRES is $K_n = <b, Ab, A^2b, ... >$.

Also I think I should be only using GMRES on half of the spectrum and such that there are fewer variables in memory, and this way the structure of the Fourier coefficients remains representative of a real valued velocity field when inverse Fourier transforms are applied. I didn't do this until now because I didn't think it would be necessary as I didn't see any mention of it in John's code but I think I should have known better as this is what I have done in the variational codes at least.

While they aren't the most original ideas this gives me some new things to try over the weekend, if they don't work I'll return to the preconditioner ideas.

Floquet vectors Another round of arnoldi iterations.

physics forum Listen to Chris Crowley talk about his work on localized solutions in Taylor-Couette flow

misc Helped Kimberly with channelflow for a bit.

2017-04-17 Matt :

> **Floquet** Still performing arnoldi iterations.
>
> **torus code** Was hoping to push through the changes and have them work in order to have some results by the time the invariant solutions meeting happens in a couple hours but they don't seem to be affecting the resulting Newton corrections that much. I rewrote large chunks of the code in order to only perform arnoldi iteration on half of the spatiotemporal Fourier coefficients, those independent from the other (negative) half of the spectrum. I thought this would enable good Newton corrections due the fact that the full spectrum could be reproduced by some matrix operations, and now I would have a determined system rather than keeping track of a number of redundant variables.
>
> Going to move on to preconditioners next, and I added (I believe up to the standards of a decent human being modifying the bib file) two more papers, ref. [17, 33] in this effort.

2017-04-19 Matt : Not too much on the docket today, just trying some new methods and rewriting torus code. One of the things I tried to get the Newton steps in my Newton-Krylov to reduce the residual adequately. One of the things I implemented was to break up the mapping into linear and nonlinear parts, and in the calculation of matrix-vector products, compute the linear Jacobian matrix explicitly while keeping the nonlinear matrix-vector product as an approximation via finite differences. This is due the the fact that the matrix-vector product approximation for both was producing vectors that were very large in magnitude. I haven't seen this method mixed in this way and as such it might be beneficial to compute the nonlinear Jacobian matrix as well, but this seemed like something I can try to get more accurate results for $J\delta x$.

Still trying to implement preconditioners for the GMRES problem as well, but haven't been successful in that regard, and even with the explicit formulation for the linear Jacobian matrix the GMRES still stalls, and produces Newton steps that reduce the residual very little, on a relative basis.

2017-04-26 Matt :

> **torus code** Realized I haven't posted in a while which I regret but I haven't had much to say as not much progress has been made since I posted last anyway.
>
> I'm attempting to rewrite and use a new combination of techniques to solve for invariant tori. This is predicated on the fact that the linear portion of the spatiotemporal mapping seems to be causing the problems with my GMRES code.
>
> I haven't been able to determine for a fact if varying both the temporal and spatial lengths of solutions at the same time is the correct

way of going about things but I'm going to try this new combination in hopes that it helps my issues.

The basis of my thought is this, iterative methods work best when eigenvalues of the matrix in the linear equation one is trying to solve are gathered; This is why preconditioners work so well in conjunction, with say, GMRES. The best preconditioners resemble the inverse of the matrix in question and are easily computed.

With this in mind, it is the convenience of matrix vector products, i.e. never forming the Jacobian matrix explicitly in this case that are the basis of my computations. The problem I have is that without forming the Jacobian matrix explicitly I am confused on how to get the information required to construct a preconditioner; although I have seen mention that even the matrix-vector products with the preconditioning matrix and the vector in question may be approximated.

I am hoping to bridge the gap between these two with a hybrid method that uses the convenience of matrix-vector products, the easily formed Jacobian matrix corresponding to the linear portion of the spatiotemporal mapping, and preconditioning.

Because I believe it is the linear portion of the mapping that is dominating the spectrum of the full (without treating linear, nonlinear portions of the mapping as separate entities), I am going to attempt computing the nonlinear portion of $J\delta x$ with a finite difference approximation, while computing the linear portion explicitly. I will then use a preconditioner that is solely based on the linear portion of the mapping in order to hopefully have a clustered spectrum of eigenvalues, which will in turn hopefully enable my GMRES code's functionality to improve.

I am hopeful that this will work and I will cite these things better after I get the 20 plus GMRES papers I've been looking at sorted out. They're all similar so it's hard to disseminate the knowledge when writing blog posts.

Floquet vectors Three more periodic orbits to compute Floquet vectors for; trying to keep the number of sample points per time constant so the longer orbits get more points. I'm not sure if this is necessary but it seems a valid precaution; unfortunately more points means more time to complete.

2017-04-27 Matt :

torus code Rewrote functions in Newton-Krylov code to run with right-preconditioning $JM(M^{-1}\delta x) = -F(x)$ with a Jacobi (approximate inverse of Jacobian matrix based on diagonal elements) as a preconditioner, using the hybrid finite-difference and explicit linear Jacobian matrix method I am trying and mentioned in yesterday's blog

post. Still have more testing to do and the Jacobi preconditioner is usually not the best preconditioner from what I have seen. Another common precondition uses the incomplete LU factorization which I think I will try if it doesn't work. Still have a couple more things to do before I can test properly but given the prior difficulties I don't see things magically working out.

Sadly most of my time rewriting everything is because I tried to be fancy when I should have kept everything as arrays. I'm basically converting it back to simpleton code because it just makes changing things way too involved when it should be a few lines.

reading Read some fluid dynamics texts [31] in between coding sprees.

2017-05-01 Matt : More work on torus code; After implementing my idea of defining the nonlinear Jacobian matrix via finite-differences and the linear Jacobian matrix explicitly didn't work too well, I moved on to trying to see if doing everything explicitly with use of SciPy's implementation of GMRES does the trick.

I didn't attempt this before because I was trying to explicit define Jacobian matrices due to the memory usage but now considering I couldn't get the finite-difference approximation to work (or maybe it's better to say that I don't think it's suited for this problem) I decided to try doing everything explicitly, or at least without using finite-differences

Xiong recommended using a Jacobi preconditioner (taking the inverse of the diagonal elements of the Jacobian matrix) but I haven't had good results with this yet. I implemented an ILU (incomplete LU factorization) preconditioner which approximates the inverse of the entire Jacobian matrix, as opposed to only the diagonal elements. This worked better, with Newton steps that actually reduced the residual and didn't send the period or length to zero and or negative values. The only problem is that after a few steps it would then fail to decrease the residual. I have a feeling this is an indication I am on the right track but there are still some bugs to work out.

2017-05-03 Predrag :

Matt 2017-04-10 "the effect of changes to the period and spatial size in expressions such as $F(u + \delta u, T + \delta T, L + \delta L)$: [...] why does it make sense to take difference between two solutions where I am essentially changing the domain size while keeping the discretization the same?"

Predrag I do not think of it as subtracting domains of different sizes: as far as the discretization is concerned, it is always the same (N, M) discrete lattice, only the values of the field $u(x, t)$ on the lattice sites are changing as you vary parameters (L, T).

Look at the Fourier-discretized torus (1.43). The discretizations (N, M) are the numbers of spatial, temporal Fourier modes kept in the calculation. Clearly you can keep (N, M) constant while you vary (L, T) to

$(L', T') = (L + \delta L, T + \delta T)$. Spatiotemporal domain size (L, T) enters only through the parametrization $q_k = 2\pi k/L$, $\omega_\ell = 2\pi \ell/T$.

You can think of the way it was traditionally done in continuing solutions. First we fixed the spatial domain to a constant L, varied T to $T + \delta T$ in order to find a spatiotemporally periodic solution $u^{(1)}(x, t)$. Then we increased the spatial domain size L to $L + \delta L$, and used $u^{(1)}(x, t)$ (the same N Fourier modes) as a starting guess, varied T to $T + \delta T$ and determines the spatiotemporally periodic solution $u^{(2)}(x, t)$, parametrized by $(L + \delta L, T + \delta T)$.

But this traditional continuation is like having a function $F(x_1, x_2, x_3)$ which happens to have zeros lying on a curve in 3-space, fixing (x_2, x_3), using 1D Newton to determine x_1, then changing x_2 to $x_2 + \delta x_2$, using 1D Newton to determine the new x_1, etc.. Clearly not smart, you want to use the 3D Newton instead. As solutions are not isolated –they lie on a curve– you need some extra condition to parametrize them along the curve. Could be L or T, but we should probably think of something smarter, like the energy of the solution.

2017-05-03 Matt :

R.I. Sujith Talk *Synchronization transition in a thermoacoustic system* A talk given organized by the aerodynamic engineering department.

Known for his work on non-normal systems. Sound makes flame fluctuate, fluctuation causes oscillations when tend to break things into pieces.

This talk looks at the onset of thermoacoustic instability. Combustion noise is a stable operation, instability has a sharp frequency.

There is also an intermittent state, it is not a transient phenomena.

Spatiotemporally, there are no large scale structures present in the "stable operation". In the "unstable operation" there is a large scale structure.

Look at acoustic energy production, and phases between pressure and heat "instantaneous hilbert phase between pressure and heat produces oscillations".

Intermittency can be described by intermittent synchronization of the phases of heat release and pressure.

Use recurrence plot to describe probability to return to set in state space.

Desynchronized (generic turbulence) have low prob, phase synch has intermediate prob, general synch are essentially periodic orbits. (Invariant solutions return to themselves. amazing)

Modeling combustion oscillator using a kicked rotor model. There is a progression of the type of turbulence one sees: chaos, intermittent phase synchronization, phase synchronization, general synchronization (phase and amplitude).

using a spatiotemporal kicked rotor with kicks that are localized in time and space, along with a galerkin truncation to develop ODEs for the model.

phenomenological model shows the transition from desynchonized chaos to generalized synchronization.

spatiotemporal dynamics!

They have a large spatial grid, with a lot of different snapshots. Looking at the instantaneous phase of the snap shots. In different stages of synchronization, different structures are present, in desynchronized chaos there are no large scale structures.

"Chimera state" where there is a coexistence of synchrony and asynchrony is found in the network of coupled identical osciallators.

Sounds like the close pass to a periodic orbit to me.

characterization of global synchrony through the kuramoto order parameter. Close to zero implies desynch. close to unity implies synch.

on the importance of being nonlinear.

"using a term like nonlinear science is like describing the study of zoology is the study of non-elephant animals".

acoustics can also cause coherence much like hydrodynamics.

torus code Working on a test case where I do not allow for any changes to period and length to see if just trying to solve for Fourier coefficients on a spatiotemporal spectral grid enables convergence of GMRES algorithms.

If this doesn't work I think I will attempt an even simpler problem, i.e. the two modes problem as per Burak's recommendation; much like how I started with the Rössler system for the variational method.

two mode Eliminating variations in period and spatial size didn't enable GMRES code to work. Thinking about how to Lower the difficulty by going to two-modes system without variations to parameters. Taking initial parameter values from Chaosbook sect. 12.4.2.

I'm sort of confused as to how to generalize the results to a fixed point of a spatiotemporal mapping but I'm thinking maybe I should just test my GMRES algorithm to find periodic orbits first. I could also do this with Kuramoto-Sivashinsky so I'm thinking maybe I should just do that.

2017-05-04 Matt :

De Le Llave Talk Talking about tori whose dynamics given by rotation. Need a condition number to describe whether you have a bad parameterization/embedding. Can tell whether or not what you are

calculating is "garbage" using condition number. Example of rotating henon map (henon map with cubic term and trigonometric coupling) and standard map.

"Lyapunov multipliers constant but the angles (I wish I knew which ones) are changing." Seemed somewhat relevant to the crossing of Floquet vectors in inertial manifold calculations.

Molei Tao *Hyperbolic periodic orbits in nongradient systems and small-noise-induced metastable transition* By adding a small amount of noise to a deterministic system anything is possible. The concrete example of this would be having three fixed points on a line. In a deterministic system, one cannot go from the left-most fixed point to right-most fixed point due to the middle fixed point. When there is noise, however, one can transition from "van't Hoff-Arrhenius law": transition rate $\alpha \exp{-2\Delta V/\epsilon}$.

Rare event dynamics, running the dynamics would be an exponential cost, instead use Freidlin-Wentzell large deviation theory.

Minimum Energy Path (MEP) coincides with maximal likelihood path (MLP) in a gradient system, therefore can find these transitions by using "string method".

MLPs need not go through saddle points, as they may or may not exist, but by introducing a fictional rotation, a periodic orbit whose stable manifold is the rotated seperatrix, and whose unstable directions separate the attracting fixed points.

Deal with unstable periodic orbits by reparameterizing the equations such that the points on the line of discretized points remains uniformly spaced. *This is a way to deal with ill-conditioned problems.*

Angel Jorba *Computational of power expansions of Poincaré maps* Talking about automatic differentiation Given an example, make a variable substitution,

General idea is we have a program where you input data and outputs a certain result. Replace operations with corresponding power series operations to produce the power series of the result with respect to initial data.

I.e. by having a program that does "something" it is relatively easy to get derivatives to any order.

MPFR is a package for extended levels of precision.

Taylor method need not reduce step size to increase accuracy. Modify Taylor's method to work on jets (polynomials from automatic differentiation) as opposed to numbers.

Marc Jorba-Cusco *Computation of invariant manifolds related to hyperbolic fixed points of Poincaré maps* (Battery died)

torus code After listening to Rafael De Le Llave's talk I am going to write some code to check the condition number associated with the

spatiotemporal Kuramoto-Sivashinsky system. I thought condition numbers had to do with the accuracy of numerical integration only and had overlooked this. I imagine from all of my previous work that it will turn out that the problem is ill-conditioned, but I think it is worthwhile to calculate this for future reference and in order to describe whatever special and or custom method I will eventually come up with.

2017-05-05 Matt :

torus code A quick computation of the condition number of the explicitly defined Jacobian matrix using singular value decomposition reveals that it's in the tens of millions, which I believe proves that I am dealing with a highly ill-conditioned system of equations.

By disabling changes to the period and length of the system this is lowered by an order of magnitude, however, I believe this still implies that the system is highly ill-conditioned even when trying to find fixed points of the spatiotemporal mapping on a fixed spatiotemporal domain.

Xiong suggested that perhaps I can use the singular values to produce a preconditioner that might help, I'm looking into this as well as some other papers [26]

readings Looking for better was to deal with ill conditioned systems within the realm of GMRES as noted above.

2017-05-08 Matt :

angel jorba conversation and torus code Angel Jorba explicitly stiffness and extrapolation in terms of linear finite difference operators, and then recommended using LAPACK solver routines as opposed to GMRES to see if that's where some errors lie.

He also recommended an interesting way to "get out of a hole" which is to tack on extra terms to the equation being studied such that is permits a (imposed) known simple solution. Usually this method does not require anything fancy and it can be used to figure out if anything funny is going on, i.e. a symmetry that is unaccounted for.

Still trying to find a simple test case for the spatiotemporal problem. As a sanity check I had the solve routine implemented by SciPy (which I believe uses LAPACK, will look into wrappers in the near future), solve the linear system. As expected it finds the $u_{kl} = 0$ solution within machine precision in exactly one Newton step; that being said it seems it might be better to avoid GMRES for the time being.

I still think the problem lies in the accuracy of the calculation of the nonlinear contributions to the jacobian and think that I might need to talk to Angel again about automatic differentiation before

he leaves on Friday (I believe). The problem with this is from what I've seen it's a relatively large time commitment, and if there are easier errors to fix in the code then this method might not produce better results.

2017-05-11 Matt : Spent the entire day going about coding a new way; I felt like I might have slipped into some of my old habits of jumping in too quickly so I felt I should write down derivations and pseudo-code before even touching my python code in order to make sure everything makes sense.

Today's dealings mainly involved working through the "direct matrix method" in ref. [8]. The reasons why I opted to rewrite my code in this way are: I feel like it is less prone to errors than index notation, it agrees with how I think about things, as it very much resembles (15.5), something that I worked through myself.

The basis of the method is to rewrite everything into either component-wise products (also known as, entrywise product, hadamard product, schur product) or matrix multiplications. In this form, the spatiotemporal mapping is given explicitly by the following equation. Note that $\star$ implies component wise products (saves computing time versus matrix-vector products with diagonal matrices and a vector) and $\dot{()}$ implies matrix multiplication. $\hat{u}$ from here on is going to be a vector $\in \mathcal{R}^{MN}$ where M is number of discretized points in time and N is the number of discretized points in space. In practice, due to the symmetries of the problem, (galilean invariance, real valued velocity field implies a symmetry in the spatiotemporal Fourier coefficients), $\hat{u} \in \mathcal{R}^{mn}$ where $m = M - 1$ and $n = N/2 - 1$. (I could have likewise chosen $m = M/2 - 1$ and $n = N - 1$ if so desired.) In this formulation, the Fourier coefficients kept $(\tilde{u}_{k\ell})$ pertain to values of indices $k = 1, 2, \ldots, N/2 - 1$ and $\ell = 0, 1, \ldots M/2 - 1, -M/2 + 1, \ldots, -1$ (Nyquist frequency removed, $l = M/2$).

As will be seen, this makes the formulation of the matrices corresponding to Fourier transforms, also known as "DFT matrices", rectangular; but I made sure the matrix multiplications are well defined if defined correctly. One might argue that making this change is undesirable due to the number of operations of matrix multiplication, but I feel like it will be competitive once I do the calculations on how many operations are gained or lost.

For the time being I formulating this method to fix T and L; this *should* be an easy addition afterwards.

$$(Q_1 \star \hat{u}) + (W \dot{\hat{u}}) + Q_2 \dot{F}((F^{-1}\dot{\hat{u}}) \star (F^{-1}\dot{\hat{u}})) \qquad (15.8)$$

2017-05-12 Matt : With the definition of the spatiotemporal mapping in place, it is convenient to now describe the "direct-matrix calculus" operations as defined in ref. [8]

For arbitrary matrices A, functions of $\hat{u}$, $F(\hat{u}), G(\hat{u})$, the rules for differentiation are as follows, (note asterisks indicate component wise multiplication and dots indicate matrix multiplication.)

$$\frac{\partial}{\partial \hat{u}} (A \cdot \hat{u}) = A \tag{15.9}$$

$$\frac{\partial}{\partial \hat{u}} (F(\hat{u}) * G(\hat{u})) = diag(G(\hat{u})) * \frac{\partial F(\hat{u})}{\partial \hat{u}} + diag(F(\hat{u})) * \frac{\partial G(\hat{u})}{\partial \hat{u}} \tag{15.10}$$

$$\frac{\partial}{\partial \hat{u}} = A \cdot \frac{\partial F(\hat{u})}{\partial \hat{u}} \tag{15.11}$$

With the use of these identities, I find the the form of the Jacobian matrix as,

$$J = W + Q_1 + Q_2 2 \cdot F \cdot diag(F^{-1} * \hat{u}) \cdot F^{-1} \tag{15.12}$$

In order to exploit the matrix vector notation, I construct matrices that would apply element-wise multiplication of powers of q_k and ω_ℓ to the spectral grid at fixed k and ranging ℓ (or vice-versa) and then exploit Kronecker products to form a matrix that applies this multiplication over all indices.

For a quick example, a diagonal matrix whose diagonal elements equal $-q_k^2 + q_k^4$ is made, and then a right-hand Kronecker product is taken such that the final matrix is of size $(mn)^2$ (note: small letters represent reduced dimensionality due to symmetry of Fourier coefficients). I.e. it is a matrix whose diagonal contains m copies of the elements of the vector of length n whose elements equal $-q_k^2 + q_k^4$.

Because we also want to split into real and imaginary parts, this is actually done twice, such that the final matrix diagonal is two copies of the diagonal of the matrix of size $(mn)^2$. In this manner, we can correctly apply the operation of multiplication by $-q_k^2 + q_k^4$ to a vector whose elements equal a_{kl}, b_{kl} where $a_{kl}, b_{kl} = Real[\hat{u}_{kl}], Imag[\hat{u}_{kl}]$. Note, due to the how python arranges indices upon reshaping of arrays, the second index ℓ is the "inner" index, what I mean by this is that all values of ℓ are cycled through, at which time the "outer" index k is cycled once. Also, the vector is formatted such that all real parts of the coefficients are cycled through before reaching the imaginary parts of the coefficients.

The definitions of the matrices are as follows,

$$\begin{bmatrix} W = 0 & -\omega_\ell \\ \omega_\ell & 0 \end{bmatrix} \tag{15.13}$$

$$\begin{bmatrix} Q_1 = -q_k^2 + q_k^4 & 0 \\ 0 & -q_k^2 + q_k^4 \end{bmatrix} \tag{15.14}$$

$$\begin{bmatrix} Q_2 = 0 & -q_k/2 \\ q_k/2 & 0 \end{bmatrix} \tag{15.15}$$

The matrices governing the forward and backward inverse transforms are confusing and I don't think will be well elucidated when written in equation form, therefore, I will try to explain them. With the forward two dimensional discrete Fourier transform defined as $F = F_T \cdot F_X$.

F_X is a matrix of shape $2\,M\,n \times M\,N$, which is produced by taking the real-valued FFT of the identity $\mathcal{I}_N$, and deleting the first and last rows (this is due to symmetries in the Fourier coefficients), after some reordering of the rows (due to discrepancies of scipy convention and how I would like to order my state space vectors), a right-hand Kronecker product is taken with the identity $\mathcal{I}_M$.

F_T is a matrix of shape $2*m*n \times 2*M*n$ which is produced by taking the regular(complex) FFT on the identity $\mathcal{I}_M$, at which point the row corresponding to $\ell = M/2$ is removed. Because the state space vector is split into real and imaginary parts at this point (due to the real valued fft applied by F_X, we must split the real and imaginary components of the current matrix into blocks, such that this matrix is also real valued.

The inverse to these matrices are computed in a similar manner, only with columns removed instead of rows, and inverse fft's being applied.

Therefore once finished, I should be able to define these matrices only once per Newton-Krylov search (or linear solver whichever I settle on) when I am not allowing for variations to either the period or system size.

That being said, this is almost the entire code so I still haven't completed it. The trickiest part is the matrices representing Fourier transforms. Note: I am only deleting rows and columns that would correspond to zero-valued Fourier coefficients, so I should not be losing any information in the process. That being said, there is a small error somewhere that I haven't been able to find that is preventing the operation of $F^{-1} \cdot F$ from equalling the identity.

2017-05-12 Matt :

Floquet vectors Only one more iteration to go, then analysis will be able to be performed.

torus code Some encouraging results after implementing the changes described over the past two days. My code is performing the best it has so far, although with results up to interpretation as of now.

After applying Newton's method to spatiotemporal mapping described by the matrix vector equation (15.8) on a fixed domain size

and period (only a temporary measure to provide an intermediate step between the full problem and where I was), with a discretization (fishnet stocking) of 16-by-64 $x \times t$ points of $\overline{ppo}_{10.2}$, the mapping was minimized to within machine precision. BUT!

The only problem is that the resulting solution is essentially the $u = 0$ equilibrium within machine precision. My thought is that it is at least minimizing a fully nonlinear mapping as opposed to all of my other efforts, and usually when applied to periodic orbit hunting the period is allowed to vary. So it might just be that fixing both space and time is so unnatural that the only direction left for the Newton corrections is towards the equilibrium.

The reason the discretization of 16-by-64 $x \times t$ points was chosen is due to the condition number of the initial Jacobian matrix $J(u_0)$ (index denotes Newton step).

The condition number of the initial Jacobian matrix for my 64-by-64 $x \times t$ points was a whopping $\approx 1.4 * 10^8$, while in the 16-by-64 case it was a more manageable $\approx 6.7 * 10^3$.

I think this is very encouraging considering how much I have been struggling. I also really like this method as I do not have to really think about indices one-by-one. The only downside is that I must calculate Jacobian matrices explicitly, but with a discretization of approximately this size, the code runs and finishes in less than a second (literally 0.84 seconds using the time feature in python.)

The problems I had with implementing the matrices governing the Fourier transforms was resultant of applying the Kronecker products in the wrong order, leading to nonsensical transforms. (The reason I was so confused is that I was consistent in my error, $F\dot{F}^{-1}$ was equalling the identity, so I thought the error must have been elsewhere.

Now I need to add on the parameter (period and spatial domain size) dependence to the Jacobian matrix with the equivariance conditions as the additional constraints for Newton steps. I think I am just going to write this part from scratch as well as it seems coming from a different angle is helping quite a bit.

2017-05-16 Matt :

torus code Added code to enables varying period and spatial dimension of the spatiotemporal Newton's method code. It converges to within machine precision, however, there is a slight problem that I've been trying to hunt down. For the initial condition that I described in the prior posts, my spatiotemporal fishnet stocking (or two dimensional spectral grid), the period ends up being stretched by a large factor, the spatial size shrinks, and the spatiotemporal Fourier coefficients shrink to the equilibrium solution $u = 0$.

In the past with my variational code this usually implied bad constraint equations, or a small numerical error somewhere in the code. (i.e. a factor of two as was the case for the variational code.) I spent the remainder of the day hunting for errors but haven't found any so far. To be honest, I am again encouraged just by the fact that the full problem is at least converging to something, even if it is a horrible numerical result.

I'm looking into other constraints that I could possibly implement to hope to settle this once and for all. It might just be that these constraints work better for GMRES versus linear solvers based on LAPACK, I'm not sure right now.

2017-05-16 Matt :

Floquet vectors It turns out I was mistaken, there is one more arnoldi iteration to perform. Analysis will begin once it finishes.

Torus Code In order to avoid headaches with constraints, I chose the easy road which was to use a least squares (pseudoinverse) solver as opposed to the solver I was using.

This dramatically changed the behavior of corrections to the period and spatial size of the system, but sadly, the initial condition I used still went to the trivial equilibrium. I am going to try to improve the initial condition I am using as the initial residual is relatively large, so it could just be a mistake in the initial condition generation. Going to test on other equilibria and see what comes out from the black box.

As a test I think it is prudent to rewriting my variational codes using these new methods and compare them with the old codes.

Cristel Chandre Talk *Driving the formation of the RbCs dimer using a laser pulse* An in-depth explanation of a formulation of a model of how dimers are formed in a composite Rubidium, Cesium mixture. Hamiltonian system, Poincaré section, Numerical modeling, lasers, interaction potential.

2017-05-17 Matt : Spent the entire day rewriting old codes to follow the new conventions that I find useful. Specifically spent the entire day on variational Newton descent code that will in theory find periodic orbits of (1.36), the system of spatial equations of Kuramoto-Sivashinsky.

Still need to try new initial conditions for both torus code and this new formulation of the spatial Newton descent code; Almost done rewriting the spatial Newton descent code. Amazing to me that experience can change the time scale of a project that took weeks and or months on the first go-around into a project that takes days, of course, there is now guarantee that it will work but one has to be optimistic.

The key idea is that because the initial conditions for the spatial system, u, u_x, u_{xx}, u_{xxx} were all being generated through spectral differentiation,

it made matching the tangent spaces redundant in three variables, as the approximate tangent spaces were being generated with spectral differentiation as well. Therefore, the idea is to turn only the last equation in (1.36) into a "direct-matrix" [8] equation similar to the spatiotemporal mapping, and match it to the velocity field's fourth derivative.

By proceeding in this manner, the equation for the fourth derivative, (which I will refer to from here on as *the* tangent space) takes the following "direct-matrix" [8] form. Note, that I am attempting to devise an equation that is only dependent on the Fourier coefficient of the velocity field and not any of the spatial derivatives. This is acceptable because the spatial derivatives are derived from the original velocity field anyway. What appears now in the equations are linear operators that produce the derivatives accordingly. Therefore, $\hat{u}$ will refer to $\hat{u}^0$ in accordance with notation previously used. Finally, the velocity equation (fourth spatial derivative) now appears as follows,

$$v = -W\dot{\hat{u}} - Q_2\dot{\hat{u}} - \dot{F}((F^{-1}\dot{\hat{u}}) \star ((F^{-1}\dot{Q}1\hat{u})), \qquad (15.16)$$

Using the direct-matrix differentiation rules noted above (15.9), the stability matrix takes on the following form,

$$A = -W - Q_2 - \dot{F}(diag(F^{-1}\dot{Q}1\hat{u})\dot{F}^{-1} + diag(F^{-1}\dot{\hat{u}})\dot{F}^{-1}\dot{Q}1) \quad (15.17)$$

For a quick description of the operators, W is the operator that produces the time derivative of a given field $\hat{u}$, Q_2 produces the second spatial derivative, F performs a forward FFT of a time-series, Q_1 produces the first spatial derivative. In this notation, the approximate tangent space would be the fourth spatial derivative as produced by spectral differentiation, i.e. $\tilde{v} = Q_4\dot{\hat{u}}$. Everything else from the variational Newton descent is left untouched.

I'm hoping that this will enable convergence of the spatial system of equations to find periodic orbits in space, the main motivation for performing these changes were firstly, the code wasn't working probably due to some inaccuracies or errors, secondly, by keeping everything defined in terms of only the original velocity field $u(x,t)$ I dramatically reduce the memory requirements and degrees of freedom of the system.

2017-05-22 Matt : Spent the day debugging the spatial Newton descent code, found a negative sign error in the expression for matrices governing Fourier transforms, converted from taking real(cosine and sine) fft's in one variable (time) to complex fft's as I was having some trouble reproducing the time derivative term otherwise. Took a while to figure out what was

Figure 15.1: (a) Initial condition of the 16-by-16 space-by-time discretization of $\overline{ppo}_{10.2}$ ($L = 22$) for spatial variational Newton descent of the Kuramoto-Sivashinsky equation (b) Resulting spatiotemporal periodic orbit (perhaps badly converged temporal equilibrium), with final spatial extent of $L = 19.9324743429$

wrong until I looked at matrix-product results piece by piece and compared to expected results in MATLAB. Rewrote how matrices (derivative operators) are formulated in terms of the Fourier transform operators. Also found a peculiarity when it came to the accuracy of matrix multiplcation depending on the order in which the matrices were multiplied...haven't figured that one out yet but nonetheless I corrected it.

I believe I got it working finally, however, the results so far aren't as interesting as I had dreamed. I finished this at the end of the day so I didn't get to test it too much, but so far there are two resulting possibilities. First, with a time periodic initial condition, i.e. one of the periodic orbits in time of Kuramoto-Sivashinsky, when allowing for spatial domain changes and changes to the temporal Fourier coefficients, the solution (only tested one so far) converged to one of the temporal equilibria of the Kuramoto-Sivashinsky system. This I believe is an indication that my code is indeed working, even though this was usually a sign of numerical issues when searching for periodic orbits in time using the variational methods, (i.e. the only way to reduce the cost functional $\mathcal{F}^2 = \lambda v - \tilde{v}$ is to send v and $\tilde{v}$ to 0. The reason I believe this is still valid is because the spatial derivatives of the equilibrium state found are nonzero; i.e. one of the "spatial periodic orbits" I have found is indeed the temporal equilibrium of the system.

When using a coarse discretization of 16-by-16 space-by-time points the

spatial domain size that the solution settled to was $L = 19.9324743429$, with the value of cost functional being within machine precision of 0.

When the spatial discretization was doubled, i.e. a 32-by-16 space-by-time grid, the resulting domain size was 23.7360639824.

Likewise, when using a 16-by-32 space-by-time discretization, the resulting domain size was $L = 19.9398768032$, which indicates that the domain size of the converged solution is highly dependent on the (spatial)discretization being using.

The second possibility is a convergence to a zero domain size solution, which in my variational method for time usually indicated an equilibrium of the system. I.e. the two possibilities were either an equilibrium in time (but still a periodic orbit in space), or a spatial equilibrium.

2017-05-24 Matt :

spatial variational After more investigation it turns out that the spatial variational code is indeed not working yet. Tried to put resulting orbits into time integrator in order to reproduce the result and got an unmatching solution. figure 15.2 is my newest "results". It uses a $\overline{rpo}_{16.31}$ of the Kuramoto-Sivashinsky equation as the initial condition. I think I was deceived by how nice it looks I suppose...couldn't find any errors today that could enable reproduction via time integration.

As an additional test I put the solutions into Burak's symmetry reduced time integrator to verify whether the "solution" in figure 15.2 was a relative periodic orbit but alas there was no luck; there is some other error that I haven't been able to identify as of yet.

Found another negative sign error, updating figure 15.1.

torus code Applied changes based on implementation from spatial variational method to my torus finding code but it seems I jumped the gun as I cannot reproduce any orbits found by spatial Newton descent via time integration.

2016-05-27 Matt :

updated figures updated figure 15.2, figure 15.1, and uploaded figure 15.3 to display current results.

spatial variational Found some errors, corrected some bugs, and made some changes that I believe improve my codes. Included a constraint to the variational equations that constrains the sum of the zeroth temporal modes to be 0. This was done after noticing that the sum of the zeroth temporal modes over the spatial extent of the loop were within machine precision of 0; I don't really know what it is a manifestation of just yet but I wouldn't be surprised if this is how the galilean invariance presents itself in the spatial system.
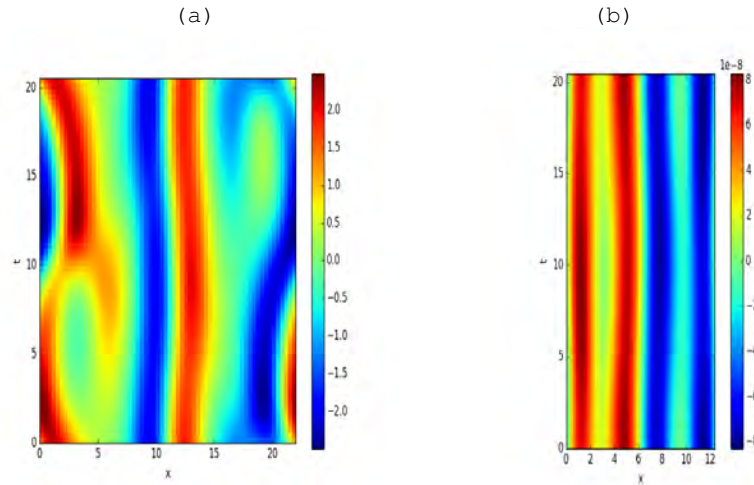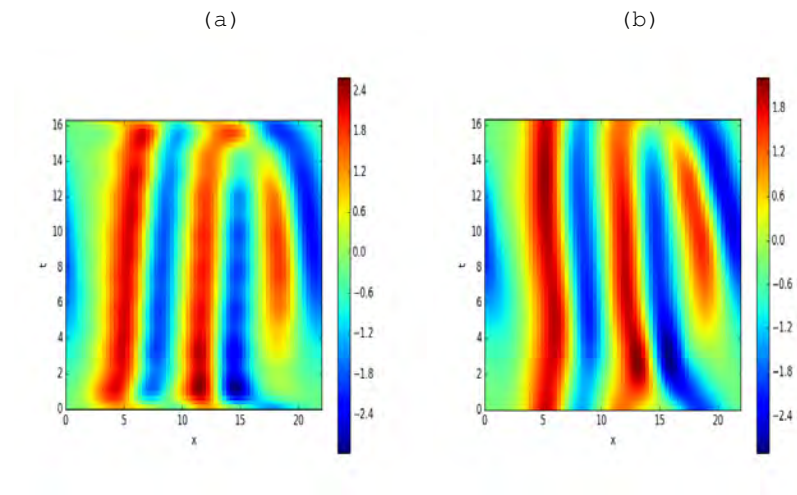
Figure 15.2: (a) Initial condition of the 16-by-16 space-by-time discretization of $\overline{rpo}_{16.31}$ ($L = 22$) for spatial variational Newton descent of the Kuramoto-Siva-shinsky equation (b)Resulting "spatial periodic orbit" (temporal equilibrium), with final spatial extent of $L = 21.9394614064$

Still haven't been able to reproduce results from figure 15.2, figure 15.1,figure 15.3 via time integration but I also haven't been able to figure out how to use Burak's symmetry reduced integrator appropriately despite my best efforts.

Floquet vectors Arnoldi iterations are complete, starting analysis after checking principal angle codes and automating it. Preliminary calculations from a single orbit are giving me weird results, in fact, the exact opposite of what I would expect.

2017-05-30 Matt : Found some bugs and errors in the spatiotemporal fixed point code. With spatiotemporal initial conditions generated by time integrating $\overline{ppo}_{10.2}$, $\overline{ppo}_{14.3}$ with initial residuals of ≈ 0.0013 and ≈ 0.000226 respectively, the residual is reduced to $\approx 10^{-9}$. Including figures. Still trying to figure out how to set up the mapping for relative periodic solutions, i.e. how to include a parameter that controls the drift associated with the group orbit.

Still can't figure out why the spatial variational converges to within machine precision but cannot reproduce results via time-integration.

2017-06-06 Matt :

vnd time part two As a means of cross-checking results I wrote variational Newton descent code for time, debugged, and got it working.
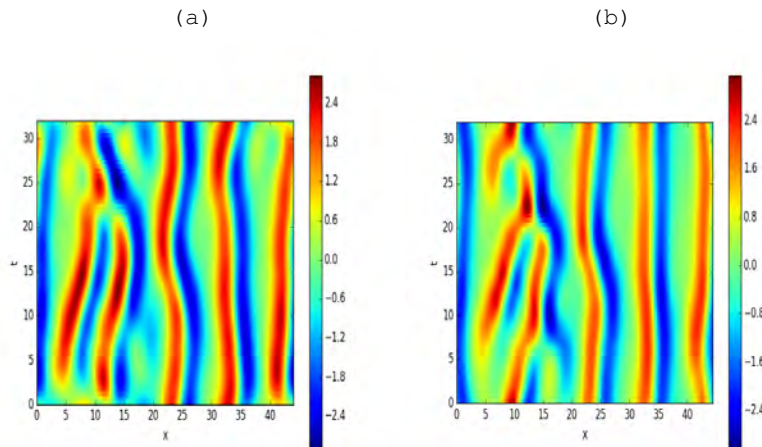
Figure 15.3: (a) Initial condition of the 32-by-16 space-by-time discretization of a piece of an ergodic trajectory that has been deformed to be periodic in time. $L = 44$. (b) Resulting spatiotemporal periodic orbit, with final spatial extent of $L = 44.3937151766$.

It follows the "direct-matrix" approach that I have been finding useful. The velocity equation takes the form

$$v = Q_1 \cdot \hat{u} - Q_2 \cdot F \cdot ((F^{-1}\hat{u}) \star (F^{-1}\hat{u})) \qquad (15.18)$$

and the stability matrix is therefore

$$A = Q_1 - 2 * Q_2 * \cdot F \cdot diag(F^{-1}\hat{u}) \cdot F^{-1} \qquad (15.19)$$

I am hoping to use this as a launchpad for other tests for the spatiotemporal fixed point code.

principal angles of Floquet subspaces Finished automating code that produces angles between linear subspaces of Floquet vectors. It is running as I type this and I am hoping that it will be finished by tomorrow morning.

misc figure 15.5 is a comparison between resulting orbits from both space and time variational Newton descent. The general structure of the resulting orbit is preserved even though the periods are quite different. At first I believed that these were supporting evidence that something is going right but now I am confused. The spatial domain resulting from the *spatial* Newton descent is largely unchanged, meaning that the orbit that results should be a unique solution with a unique period; but the *time* variational Newton descent changes the period somewhat drastically, and because the spatial domain size
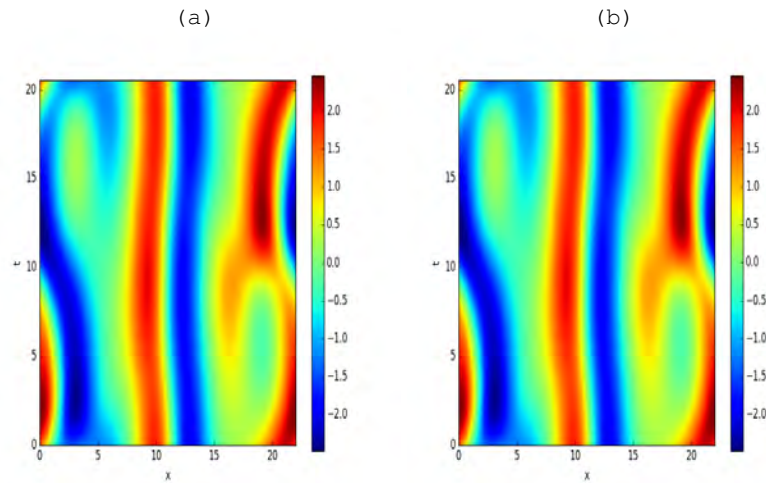
Figure 15.4: (a) Initial condition of the 32-by-32 space-by-time discretization of $\overline{ppo}_{10.2}$: $(L_0, T_0) = (L_0, 2T_{p_0}) = (22, 20.5057459345)$. (b) Resulting spatiotemporal fixed point $(L_p, 2T_p) = (22.0000104401, 20.5057499188)$

is fixed this might mean that I am finding the same solution but this is contradictory because the periods are so different. Also good evidence that there is something wrong is that the *time* Newton descent is taking a relative periodic orbit initial condition and seemingly changing it into a periodic orbit? I don't know what to think of it but I am glad that I rewrote the time Newton descent code as it'll be a good stepping stone into whether or not I need to rewrite the equations in a symmetry reduced form in order to find relative periodic orbits or not. I think that's where I'm headed at least.

2017-06-08 Matt :

torus code and symmetry reduction After more debugging and anecdotal evidence from preliminary results of the spatiotemporal fixed point code I've decided that I should implement a symmetry reduced form of the fixed point finder because it seems to only work for pre-periodic orbits and I think this if anything a good practice to implement symmetry reduction.

I debated with myself over how I should implement this; the main two methods that waffled between were 1. introducing a parameter that governs the symmetry operation of the SO(2) symmetry that would be allowed to change and or be corrected as the Newton's method implementation runs its course, or, 2. formulate a "direct-matrix" [8] for the symmetry reduced equations as to treat relative periodic orbit as an invariant 1-torus. I elected for option two, as I am sort of confused as to
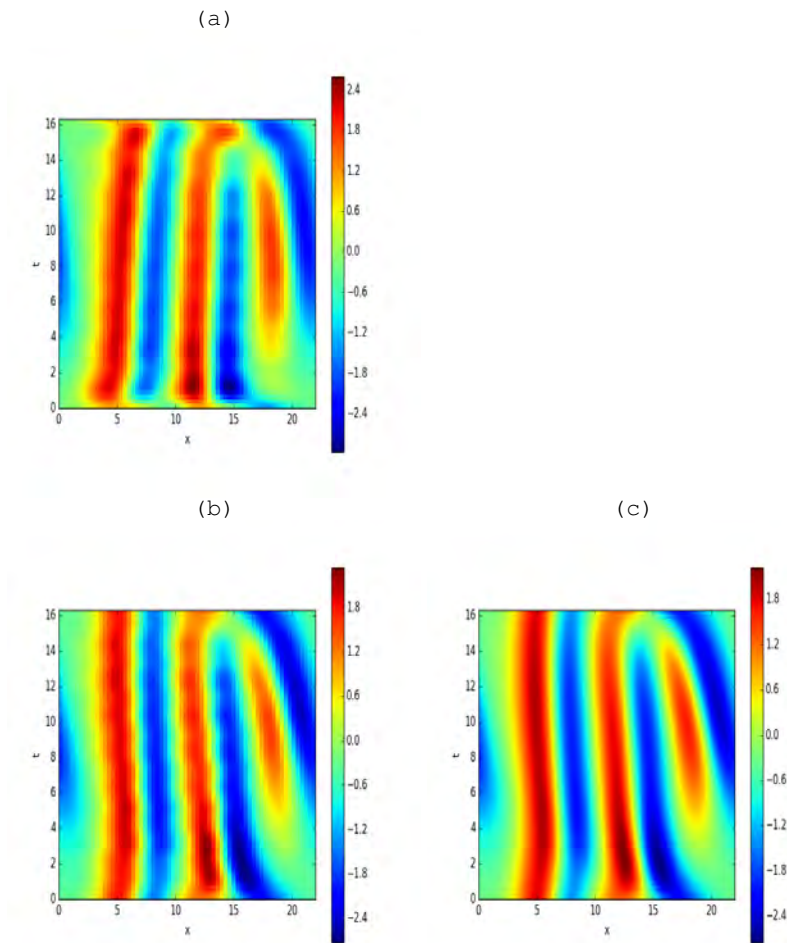
Figure 15.5: (a) Initial condition of the 16-by-16 space-by-time discretization of $\overline{rpo}_{16.31}$. $L_0 = 22$. (b) Resulting periodic orbit after variational Newton descent in time $L = 22, T = 15.7444884386$, (c) resulting periodic orbit after variational Newton descent in space.

how I would implement the parameter from option one in a spatiotemporal setting as opposed to a setting where the action of time is still in the setting of a one-parameter flow.

That being said, and taking much from Chaosbook and ref. [5], this is how I am trying to implement a symmetry reduced version of my current spatiotemporal code.

Firstly, we must generate symmetry reduced spatiotemporal initial conditions, this, plainly, is done by using a symmetry reduced time integrator such as Burak's `ksETDRK4red.m` to generate a spatiotemporal discretization that will be used for the hunt.

Next, I rewrite the direct-matrix equations in a symmetry reduced form. I find it easiest to first look at the symmetry reduced velocity equations for Kuramoto-Sivashinsky equation and then figure out what is necessary to take the leap into turning them into a spatiotemporal mapping such as (1.43).

Taking equations (8),(9) from ref. [5], the symmetry reduced flow takes the form

$$\hat{v}(\hat{a}) \;=\; v(\hat{a}) - \dot{\theta}(\hat{a})t(\hat{a})\,, \quad \dot{\theta}(\hat{a}) = \frac{\langle v(\hat{a})|t'(\hat{a})\rangle}{\langle t(\hat{a})|t'(\hat{a})\rangle}t(\hat{a})\,, \qquad (15.20)$$

Now, in order to put this symmetry reduced flow into a spatiotemporal setting, where the entire orbit is then treated as a vector in the domain the spatiotemporal mapping, we must make note that for the $N - by - M$ discretizations that we are going to use in the fixed point finder we need to expand these formulae to account for the fact that we need M copies of the template vector $t(\hat{a})$ for every point in time; likewise in order to evaluate the group tangent of at for the $2NM$ dimensional vector (2 because of Fourier) we need to take a Kronecker product between the identity and the SO(2) generator in order to have a $[2NM \times by - 2NM]$ matrix that will produce the correct group tangent after multiplication with the spatiotemporal vector.

Now once we have all of these things in place we can produce an equation similar to (15.5) for the symmetry reduced flow. Substituting v from (15.18), (the transparency) the symmetry reduced flow can be written as

$$\hat{v}(\hat{a}) = \frac{\partial a}{\partial \tau} = f(a), \qquad (15.21)$$

where τ is the in-slice time.

Then applying an operator F_t that takes the temporal Fourier transform around the orbit, and rewriting the time-derivative by exploiting the Fourier transform we are left with

$$W_\tau * \hat{u} - F_\tau \cdot f(\hat{a}) = 0 \qquad (15.22)$$

Now, for the record, I write the equation in its complete direct-matrix, symmetry reduced form.

$$
\begin{aligned}
0 \;=\;& W_\tau * \hat{u} - F_t(Q_1 \cdot \hat{u} - Q_2 \cdot F \cdot ((F^{-1}\hat{u}) \star (F^{-1}\hat{u})) \\
& - \frac{\langle Q_1 \cdot \hat{u} - Q_2 \cdot F \cdot ((F^{-1}\hat{u}) \star (F^{-1}\hat{u}))|t'(\hat{a})\rangle}{\langle t(\hat{a})|t'(\hat{a})\rangle} t(\hat{a})) \quad (15.23)
\end{aligned}
$$

where $\hat{u}$ is now the vector quantity that completely describes the spatiotemporal symmetry reduced orbit in question.

Note: the definitions of the operators before taking Kronecker products are from (15.13), (15.14), (15.15).

2017-06-08 Matt :

symmetry reduction implementation Spent the second half of my adventure writing components to reduce spatial translational symmetry in the codes I wrote earlier this week for Newton descent in time for the full-state space. I should be able to plug this right into the spatiotemporal fixed point code once I get it working and I feel that this is a good test-bed. This essentially covers what I wrote earlier this morning.

I can't seem to figure out why currently but the resulting symmetry reduced velocity isn't of the proper form i.e. it has a component out of the first Fourier mode slice still. I wasn't able to pin down the error but I'm hopeful I'll figure it out by tomorrow.

floquet small error in automation procedure means I have to run angle producing code again. graphs of angle distributions for each subspace by tomorrow most likely.

2017-06-09 Matt : Finished producing preliminary angle data and figures and codes that allow for plotting.

Went over preliminary data from angle figures with Predrag.

1. Taking a cue from the Lorenz system (see the series of ChaosBook examples on Lorenz):
the Lorenz invariant subspace –the z axis– has a very simple dynamics, with the single equilibrium the attracting equilibrium at the origin. However, if its stability is computed in the full 3D state space (as it always must be), the invariant subspace turns out to be unstable, with a strongly repelling full state space Floquet eigenvector that makes the subspace isolated from the full state space; you can exit it with any small generic perturbation, but there is no probability of coming back - indeed, all the ergodic density is concentrated on Lorenz ears, one never approaches the z axis.
Conclusion: the Lorenz chaotic dynamics, is far away from, and nothing like the invariant subspace dynamics.

2. Taking a cue from the Kuramoto-Sivashinsky system:
   The dimension of the Kuramoto-Sivashinsky (antisymmetric) invariant subspace $\mathbb{U}^+$ (imaginary parts of Fourier modes only) is half of the dimension of the full state space. To approach it, one would need half of the coordinates to tend to zero. That is possible if the invariant subspace had all eigenvectors that point out of it stable, but that is not the situation for chaotic dynamics cases studied. To approach the invariant subspace, 30 out of 60 (let's say) coordinates would have to be zero or close to it - very unlikely...

3. The invariant subspace $\mathbb{U}^+$ is the subspace of antisymmetric functions; functions that repeat themselves twice over domain L (up to a reflection). In other words, the size of the domain is $L/2$. As we expect the number of physical degrees of freedom to scale linearly with L, the physical dimension of the subspace is half of the full state space; it is much less chaotic than the full state space.
   Conclusion: the Kuramoto-Sivashinsky chaotic dynamics, is far away from, and nothing like the invariant subspace dynamics. So why in so many problems (Kuramoto-Sivashinsky, complex Ginzburg-Landau, Navier-Stokes ...) people study dynamics in invariant subspaces. For convenience only; they are easier (almost no one knows how to reduced continuous symmetries), they have periodic orbits rather than relative periodic orbits embedded in the ergodic sea, etc. That's what we are doing with Gibson's periodic orbits data set; unphysical, but available.

4. other periodic orbits on the attractor in the full state space. I.e. Make sure that Floquet vectors themselves are in the invariant subspace, otherwise will not really get good information as once one leaves an invariant subspace there is no

5. Only want Floquet vectors that lie in invariant subspace, as taking cues from Lorenz system, the invariant system is isolated from other periodic orbits on the attractor in the full state space. I.e. Make sure that Floquet vectors themselves are in the invariant subspace, otherwise will not really get good information as once one leaves an invariant subspace there is no

6. Making sure to use only prime period due to stability and that information isn't being repeated. Might have to redo arnoldi iterations such that perturbations are contained within the same invariant subspace as the solution. If not, I should definitely check if Floquet vectors of solutions of the invariant subspace lie in the invariant subspace to get good angle infromation. I can test this by whether or not the Floquet vector is invariant after application of discrete symmetry operation.

7. For Floquet multipliers that come in a complex conjugate pairs I need to treat the plane spanned by the two vectors as a single ge-

ometrical object when computing the principal angles arising from subspaces.

8. To harken back to invariant subspaces, inertial manifold described by invariant solutions on the attractor and not necessarily solutions that lie in invariant subspaces due to isolation, i.e. the solutions are "far-away" when taken in the context of the dynamics. I.e. need orbits that are part of the attractor; it is believed that solutions in channelflow database indeed are taken from the attractor due to finding initial conditions for Newton-Krylov search from ergodic trajectory and recurrence plots.

9. Need to go over an document how the statistics were produced. how the angles were produced.

10. Whether one must constrain perturbations to invariant subspace in order to guarantee the Floquet vectors all remain in the invariant subspace. (small number of orbits that I would need to redo arnoldi iteration for in this case.

2017-06-13 Matt :

symmetry reducing Still rewriting code to be able to find relative periodic orbits in hope that it will improve the spatiotemporal fixed point code. I thought it wasn't working because there were problems with how I implemented the combination of template point of the slice and symmetry reduced velocity equations but I forgot I needed to also change the stability matrix definition to pertain to symmetry reduced velocity equations.

floquet vectors Trying to figure out the best implementation for what I discussed with PC on Friday. I think I'll have to import the values of the Floquet multipliers via the text file generated by arnoldi iteration, and for each nth subspace calculation, check if the imaginary part of the Floquet multiplier is zero or not, and then either calculate the angle of the nth subspace or skip to $n + 1$ as to include the plane spanned by the two Floquet vectors instead of splitting them into two different complementary subspaces.

2017-06-13 Matt :

starting over arnoldi iterations J. Gibson, PC and I realized that in my calculation neither the orbits nor the Floquet vectors were constrained to the flow-invariant subspace. The periodic orbits stay (up to small numerical errors) in the subspace, but one should not include the Floquet vectors that point into the full state space; the dynamics within the invariant subspace has little to do with the dynamics on the full state space chaotic attractor, an object that is distant from the invariant subspace (see the **2017-06-09** discussion above) and therefore the principal angles for these Floquet vectors describe neither

the subspace inertial manifold nor the full state space inertial manifold.

In other words the procedure that I need to enact as soon as possible includes

1. Get *additional* periodic solutions of the Hamilton, Kim, Waleffe cell from J.Gibson mentioned in hangouts meeting.
2. Make sure that the solutions are highly accurate by running them through Newton-Krylov code.
3. Confirm with J. Gibson that I am handling the symmetry operations correctly as to not do this again.
4. Integrate in time while constrained to invariant subspace.
5. Arnoldi iterations with constraint on the velocity field and the perturbations to invariant subspace to get Floquet vectors that also lie in invariant subspace.
6. Check to see if Floquet vectors are invariant under symmetry operation (checks and balances).
7. Principal angle calculation with geometric properties (no splitting between complex conjugate pairs) taken into consideration
8. Check to see if trajectories shadowing periodic orbits lie in the span of the Floquet vectors
9. Produce plots of principal angles between complementary subspaces of Floquet vectors.

Most of these things are automated already, but the arnoldi iterations and Newton-Krylov codes will take time to run. I think I should elect for smaller discretizations by not saving as many time-integrated points, as it would take less time, but have some thoughts and comments about the discretizations.

I might want to take into consideration the varying importance of different orbits. The premise for this idea is that shorter orbits have a more pronounced effect on the dynamics. In this vein, weighing the shorter periodic orbits higher, through a larger discretization, might be more beneficial in elucidating the geometric structure of the inertial manifold.

On the other hand, if the goal is to capture the geometrical information without redundant information, a smaller discretization might be favorable. I am using the L_2 distance between the initial condition and the successive points of the orbit's discretization to give me an idea of how close the points are in the invariant subspace and perhaps use this as the crudest of measure to avoid repetition. Currently running the Newton-Krylov convergence in an automated fashion on the previous orbits that I had. Just to make sure that the information we are getting is as accurate as possible, considering I have to redo the entire process anyway.

symmetry reducing Made some changes for the variational Newton descent routine to take keyword arguments such that one can choose between the symmetry reduced routine for trying to find relative periodic orbits and the full state space routine for pre-periodic orbits.

Added definition of symmetry reduced stability matrix following equation 13.24 from Chaosbook, edited some other changes to quantities involved in symmetry reduction to fit with taking real valued FFTs. Preliminary tests still show bad results. Need to do more debugging and testing tomorrow.

2017-06-15 Matt :

floquet After finding some errors in filenames and symmetry files I have the solutions from John's database rerun in the Newton-Krylov solver.

Also produced the discretizations through DNS for the orbits. I am opting to have 32 points per orbit. This is a compromise to have fewer points per orbit but as the periods differ by up to a factor of 6 I feel that this still weighs the shorter periodic orbits more as there are more sample points per unit of DNS time. Again, the main motivation is time, if I could compute in infinitesimal time I would like to have more points per orbit; secondly, it's a compromise between treating different periodic orbits the same or differently.

By using a smaller number of arnoldi iterations and number of points on each orbit it will dramatically speed up the process (not to mention not making mistakes).

Arnoldi iterations are currently running such that the floquet vectors are constrained to the same invariant subspace as the solutions that they are being produced by; I'm not sure if I should run four different calculations for the possible antisymmetry and symmetry pairs or if I need to just include all of the symmetry generators for all possibilities in one run.

In more detail, the complete symmetry group of solutions that I am working with is described by the ascii representation of symmetry group elements

$$
\begin{aligned}
e &= 1,\, 1,\, 1,\, 1,\, 0,\, 0 \\
s_{xyz}t_z &= 1,\, -1,\, -1,\, -1,\, 0,\, 0.5, \\
s_z t_x &= 1,\, 1,\, 1,\, -1,\, 0.5,\, 0 \\
s_{yz}t_{xz} &= 1,\, -1,\, -1,\, 1,\, 0.5,\, 0.5
\end{aligned}
\tag{15.24}
$$

where, the symbols follow the following order, and have the respec-

tive effects on solutions

$$(c, s_x, s_y, s_z, a_x, a_z)[u, v, w](x, y, z)$$
$$\rightarrow$$
$$c[s_x u, s_y v, s_z w](s_x x + a_x L_x, s_y y, s_z z + a_z L_z)$$

J. Gibson seems to agree that I have the symmetry files in order for constraining the periodic orbits to this symmetry subspace described above. Now all I am wondering if it is only this symmetry subspace that is of interest to constrain Floquet vectors to, or if the "antisymmetry" combinations denoted by a value of $c = -1$ for combinations of two of the symmetry group elements (i.e. given the above set, the "antisymmetries" would be given by maintaining the same symmetry group but including negative signs on the following pairs, leaving the other elements unchanged.
$(-s_z t_x, -s_{yz} t_{xz}), (-s_{xyz} t_z, -s_{yz} t_{xz}), (-s_{xyz} t_z, -s_z t_x)$ needs to also be taken into consideration.

symmetry reduction Still can't get the routine to work for finding relative periodic orbits of the time system. The initial residual is a little high than what I would expect so I think I need to go over the definition of symmetry reduced velocity again. A rework might be in order for all of the symmetry reduction parts but only time will tell based on work put in tomorrow, now that I believe I have all of the arnoldi iterations running for my other project I think (as long as I got the symmetry groups for the floquet vectors correct then I can focus solely on this again).

2017-06-16 Matt :

floquet I was worried about some preliminary results from arnoldi iterations so I stopped them and try to think about the problem a little bit more. It seems that by constraining the floquet vectors to the same invariant subspace as the solution I was losing out on information and needed to also calculate the floquet vectors that lie in the "antisymmetry" subspaces as well. These subspaces are categorized by a negative sign assigned to one of the generators.

What tipped me off was that during the current iterations there is a lack of the three marginal floquet vectors, and from as far as I can tell by restricting to the same invariant subspace as the solution, the arnoldi iteration only includes one of the three.

By writing out the multiplication table of the group I am attempting to solve this problem by changing the list of generators from

$$\begin{aligned} s_{xyz} t_z &= 1, -1, -1, -1, 0, 0.5, \\ s_z t_x &= 1, 1, 1, -1, 0.5, 0 \end{aligned} \tag{15.25}$$

to the following:

$$
\begin{aligned}
s_{xyz}t_z &= 1,\ -1,\ -1,\ -1,\ 0,\ 0.5, \\
s_z t_x &= 1,\ 1,\ 1,\ -1,\ 0.5,\ 0 \\
-1 * s_{yz}t_{xz} &= -1,\ -1,\ -1,\ 1,\ 0.5,\ 0.5
\end{aligned}
\tag{15.26}
$$

where as before, the lists of numbers follow the notation $c, s_x, s_y, s_z, t_x, t_z$ where s stands for shift-reflect and t stands for shift-rotate in the appropriate variable as denoted by the subscript.

This seems to be incorrect however, as all of the floquet vectors belonging to this space are stable.

floquet after PC meeting After talking to PC about the concerns noted above it it appears that I was computing the iterations correctly, and that all my worries were for nought. This is good in a way as the communication between us gave us a better mutual understanding of what I am actually computing; however, it also means that I wasted half of my day chasing ghosts. I think it was for the best as it gave me a better understanding of the problem and will prevent confusion in the future however.

symmetry reduced variational method Finding some better numerical results with the alternate definitions for (15.20) which are, (x_i implying real part of ith Fourier mode, y_i is the imaginary part, where $i = 1, ..., N/2 - 1$

$$
\frac{\partial \hat{a}}{\partial \tau} = \hat{x}_1 v(\hat{a}) - \dot{y}_1(\hat{a}) t(\hat{a}), \quad \frac{\partial \theta(\hat{a})}{\partial \tau} = \dot{y}_1(\hat{a}), \tag{15.27}
$$

Currently trying to figure out the correct way of reconciling this new definition with direct matrix implementation.

I believe that the stability matrix with take the following form,

$$
\hat{A} = diag(x_1) \cdot A - diag(\dot{y}_1(\hat{a})) \cdot T \tag{15.28}
$$

2017-06-19 Matt :

floquet vectors Based on the current progress, I estimate that the arnoldi iterations will be done by next weekend.

I am currently writing some new portions of code that will take in the files storing the floquet multipliers as to make sure that vectors corresponding to complex conjugate multipliers are not separated into different subspaces during angle calculations.

I am currently only going to take 32 points per orbit to see if I can get a rough idea for the angles. If need be I can always procure more points on orbits and do the arnoldi iterations for the additional points.

symmetry reduction variational method Finished implementing the newer version of symmetry reduction variational method (15.27). Still having issues as initial condition for the value of the cost-functional, which is the best indication I have that I am still somehow messing up the symmetry reduced equations; the only other contributor could be the approximate loop tangent, which I realized today should also be symmetry reduced, i.e. it doesn't make sense to compare the in-slice velocity to an approximations of element in the full state space tangent bundle.

I know it isn't any of the definitions that I would be using for pre-periodic orbits because, for example, an initial loop defined on 32 points in space and 128 points in time for $\overline{ppo}_{10.2}$ starts with an initial value of the cost functional of $F^2 \approx 10^{-10}$ which is far better than anything that I have ever had before, and of course as a sign of it's working it reduces the residual to within machine precision with the correct period.

When I try this type of discretization with $\overline{rpo}_{16.3}$ I have no luck, and I get the "converging to equilibrium" problem that usually indicates I have contradictory definitions or something else the matter. So there must be something else that I am either forgetting or not paying correct attention to.

I did find a bug, however, where in the computation of the cost functional, sometimes the wrong definition of velocity would be used; this helped reduce the initial cost functional value for relative periodic orbits to order ≈ 10. I think it might be time to talk to Burak and see if he agrees with the definitions I'm using as I am running out of ideas.

2017-06-20 Matt :

symmetry reduced variational Including a checklist of possible faults of my symmetry reduced variational method code, ranked in terms of likeliness. I've already checked these definitions a number of times but until I can verify with one-hundred percent certainty that they are correct I will leave them here unmarked. In other words they are possibly the outstanding issues.

1. function definition of symmetry reduced velocity equation
2. function definition of symmetry reduced stability matrix
3. Whether approximate tangent field operator needs to be symmetry reduced. (I believe so).
4. Generation of symmetry reduced Newton descent matrix (based on velocity and stability matrix being reduced)
5. Slice template vector
6. Infinitesimal generator of rotations T
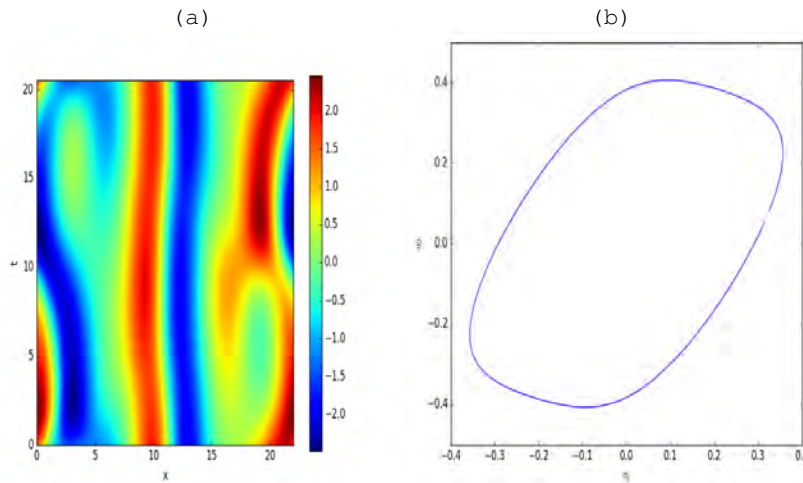
Figure 15.6: (a) 32-by-128 space-by-time discretization of $\overline{ppo}_{10.2}$ resulting from temporal variational method. (b) Fourier-mode projection of (a) on the first two real parts of spatial Fourier coefficients a_1, a_2.

Next are the things I know have no problem as they work perfectly with pre-periodic orbits.

1. Operators that produce spatial, temporal derivatives.
2. Operators that perform forwards and backwards Fourier transforms
3. full state space velocity
4. full state space stability matrices
5. fictitious time stepping routine
6. Operator that produces full state space approximation to tangent field.

meeting with burak Planning on talking to Burak tomorrow if I can't get the symmetry reduced variational code to work by tomorrow.

additional figs Included the figures of results from full state space variational method to find $\overline{ppo}_{10.2}$ for completeness. These include a two-dimensional Fourier mode projection and the full spatiotemporal velocity field.

Microextensive chaos of a spatially extended system Wanted to read ref. [37] as it was referenced in ref. [42] but ran out of time.

2017-06-23 Matt : After being frustrated for a while I finally realized the dumb mistake I have been making when it comes to symmetry reduction. I have been trying to compute the symmetry reduced velocity at every point of the discretized symmetry reduced relative periodic orbits all at once.

This was the wrong choice because the equations rely on inner products of vectors specific to each point along the discretization (namely the full state space velocity and the group tangents at the slice template point and each time discretization point).

I don't know why I didn't realize this before (I guess I'm learning?) but something clicked when I noticed that the wrong elements were being set to zero in my previous formulation, in other words the in-slice symmetry reduced velocity wasn't tangent to the slice. I tested out the formulae I have been using for a single point along the discretization in time and everything resolved.

In more detail, previously I was using a template point that was the same dimension as the entire discretized orbit, i.e. for an $N - by - M$ space-by-time discretization of an relative periodic orbit I was using M copies of the same template vector expecting it to work but this is fundamentally flawed because when I use the equations (15.20) all this does is mix all of the information of the orbit together in a jumbled fashion that makes absolutely no sense.

It probably doesn't need to be said, as I have been doing this for about a week but again I reiterate that I am working on a way of reconciling the formulae with the direct-matrix implementation that I have been using.

If I can't figure out a way then there is the back-up plan of performing operations one at a time (as opposed to using linear operators that act on the entire discretized orbit at once) by computing the symmetry reduced velocity of each state space point and each symmetry reduced stability matrix one by one and then compiling them respectively into the vector, matrix that I need: A vector containing the in-slice velocities at every point along the orbit and a block diagonal matrix whose blocks are comprised of in-slice stability matrices evaluated as the respective point along the orbit.

Before rewriting this portion I am still going through the list of other possible defects. So far I can verify that the group tangent of the template point and the generator of infinitesimal rotations is valid. I am getting wrong results for the full state space velocity as compared to Burak's MATLAB codes which I can't explain at the moment, considering those definitions worked fine for pre-periodic orbits.

All in all tomorrow will hopefully be a good day for my research.

2017-06-27 Matt : Found a negative sign compatibility error in Burak's symmetry reduction code that I was using to produce initial conditions. I believe this goes back to other MATLAB codes for Kuramoto-Sivashinsky that contained conjugation where it wasn't correct, similar to compatibility issues I had with my spatial integration code.

Wrote code that computes the symmetry reduced velocities each temporal discretization point at a time and likewise for the symmetry reduced

stability matrices.

These two combinations dramatically reduced the initial values for cost functionals in the variational Newton code, however I am still getting problems with convergence likely due to a small error somewhere, or some problems with how I am trying to circumvent the issues.

This workaround also rises concerns for how I am going to implement the symmetry reduction in the spatiotemporal fixed point codes, as I try to treat the solution to the spatiotemporal fixed point equation as one object, as I believe it should be. That being said I am still trying to find a way to work with entire orbits instead of this way because it doesn't feel too intuitive. I am working through another way which I will write up once I am confident in its accuracy.

2017-06-27 Matt :

inertial manifold Arnoldi iterations are taking longer than I had remembered. Will probably been done by next weekend.

symmetry reduced variational methods After I posted yesterday I almost immediately figured out the issue with the current formulation and why it won't work. It's a matter of the ordering of the variables; the way I have the code currently written the variables are ordered in a spatiotemporal vector that cycles through the time first and then space. I.e. if k and ℓ were indices that take values from $0, \cdots, N-1$ and $0, \cdots, M-1$ respectively representing the the space and time discretization, for every unit change to k, the index ℓ would have cycled through M values.

Now, this isn't important it's just a clerical part of coding but the problem I am now facing is that this specific ordering is going to make it much harder to finish the symmetry reduction variational code. I've tried to work things out in a number of ways but they are require some very unintuitive measures that I feel would be best to avoid. So, for now, I am going to rewrite everything such that the ordering of the state space vector cycles through spatial indices first, in other words switching to a different standard.

With this in mind, I believe I have a way to rewrite (15.20) such that it will serve my purposes of symmetry reduction. Like I've said before the problem I had from a lack of practice was that I was trying to symmetry reduce the entire orbit at once not taking into consideration that the group tangent direction (amongst other things) is a time-dependent quantity.

Here is how I believe I can fix things once I change the ordering of the spatiotemporal vector i.e. the orbit in vector form. It basically relies on computing M copies of (15.20) while keeping all of the in-

formation at different times separate. Starting with,

$$\hat{v}(\hat{a}) \quad = \quad v(\hat{a}) - \dot{\theta}(\hat{a})t(\hat{a}) \,, \quad \dot{\theta}(\hat{a}) = \frac{\langle v(\hat{a})|t'(\hat{a})\rangle}{\langle t(\hat{a})|t'(\hat{a})\rangle} t(\hat{a}) \,,$$

Let v now be matrix whose rows (instead of columns as to reshape the matrix into a vector properly) are the full state space velocity evaluated along the time discretization of a symmetry reduced relative periodic orbit. Likewise, define $\hat{a}$ as a matrix whose rows are the current (in fictitious time) representation of the symmetry reduced state space points that comprise the relative periodic orbit. Then, we can change the inner product notation to a matrix-vector product notation by virtue of the group tangent template vector being constant. For example, the velocity will now be concatenated in a matrix in the following manner.

$$v(\hat{a}) \rightarrow \mathbf{V} \equiv [v(\hat{a}(\tau_0))|v(\hat{a}(\tau_1))|\cdots|v(\hat{a}(\tau_{M-1}))] \qquad (15.29)$$

following this notation the equation for evaluating the symmetry reduced velocity at every point along our discretization will be

$$\hat{\mathbf{V}}^T(\hat{a}) \quad = \quad \mathbf{V}^T(\hat{a}) - \dot{\theta}(\hat{a})\mathbf{t}^T(\hat{a}) \,, \quad \dot{\theta}(\hat{a}) = (\mathbf{V}^T(\hat{a}) \cdot t'(\hat{a}) * /\mathbf{t}^T(\hat{a}) \cdot t'(\hat{a}))\mathbf{t}^T(\hat{a}) \,,$$

Now the onto the stability matrix; as opposed to the symmetry reduced velocity where I can just concatenate vectors into matrix and perform element-wise operations and matrix-vector products, with the stability matrices I needed to rewrite definitions of all of the matrices involved in the direct-matrix derivation which I am still in the process of. Some of them are easy, where the effect of the reordering merely results in the opposite order kronecker product.

Hoping to be testing by tomorrow to settle this once and for all. Submitting the different version of the functions implemented today in different file for versioning purposes. Will delete once finished.

chats Going to chat with Ravi on Thursday at some undisclosed time and place, probably the office on the fifth floor.

2017-06-29 Matt :

symmetry reduction Wrote code to produce more general initial conditions for symmetry reduced variational methods. Alright. I have mostly figured out the issues. I guess I was confused on how to use the in-slice time symmetry reduced velocity in conjunction with the direct-matrix formulation before. I was attempting to use equations (15.20) in place of something similar to (15.27) and this was a tragic mistake that took me a week to figure out.

The following are what I believe to be the correct implementation of symmetry reduction for the variational method when applied to a relative periodic orbit that has been generated with a symmetry reduced integrator. In other words, when the initial condition is a spatiotemporal discretization embedded in the slice

With this new formulation the initial value of the cost functional is $F^2 \approx 10^{-8}$ for a symmetry reduced reproduction of $\overline{rpo}_{16.3}$. This is comparable with an excellent initial condition with all of the correct formulae in previous works.

The new equation I am using for calculation of the symmetry reduced velocities (w.r.t. in-slice time) in the direct-matrix formulation is,

$$\hat{v} = (diag(x_1(t)) \otimes I_{N-2}) \cdot v - (diag(\dot{y}_1(t)) \otimes I_{N-2}) \cdot (I_M \otimes T) \cdot \hat{u} \quad (15.30)$$

This is relatively simple to explain when using (15.27) as a reference. $diag(a_1(t))$ is a diagonal matrix that when multiplied with the full state space velocity vector produces a vector whose entries are equal to $x_1(t_i) * v(t_i)$ where x_1 is the real component of the first Fourier mode. likewise for $diag(\dot{y}_1(t))$ except $\dot{y}_1$ is the velocity of the imaginary component of the first Fourier mode. the $\otimes$ symbol here denotes a Kronecker product (outer product) whose purpose is to copy the values x_1 and y_1 as to create a diagonal matrix whose dimension equals the dimension of the velocity vector v. i.e. I need an outer product with a $N-2$ identity matrix to ensure that I have $N-2$ copies of x_1 and y_1 so that each of the $N-2$ Fourier modes gets multiplied by the correct factor.

To simplify the notation and make it more apparent how to derive the stability matrix in direct-matrix notation, I rewrite $X_1 = diag(x_1(t)) \otimes I_{N-2}$ and $Y_1 = diag(\dot{y}_1(t)) \otimes I_{N-2}$.

The equation for the stability matrix for the entire orbit is therefore.

$$\frac{\partial \hat{v}}{\partial \hat{u}} = \hat{A} = X_1 \cdot A - Y_1 \cdot T \quad (15.31)$$

There is still a small error lurking because despite of the small initial value for the cost functional I still have not achieved convergence within machine precision.

I believe it might be that I have treated X_1 and Y_1 as constant matrices as opposed to functions of $\hat{u}$. This is the only place that I find room for errors so far.

chats Chatted with Ravi about his method of finding heteroclinic connections. Specifically, we talked about the method of using cotangent inverse as a mapping such that the curve is reparameterized on a finite interval of real numbers so that Chebyshev functions can be deployed. Also went over the current issues that he is facing

namely the oscillations that occur around equilibrium (which apparently upon a certain choice can be made to occur in the middle of the connection). Also went over the adjoint method that he learned from that Chebyshev functions

arnoldi iterations Arnoldi iterations are still going strong.

2017-07-03 Matt : Small progress on symmetry reduced variational methods front. With some small changes to how I implemented . and playing around with different discretizations of $\overline{rpo}_{16.3}$ I was able to get a final result whose value of the cost functional is $F^2 \approx 10^{-12}$. This is four orders of magnitude of improvement from the initial value of $F^2 \approx 10^{-8}$ but it's still not good enough.

The new formulations of (15.30) and (15.31) are written in the following ways, to more explicitly represent the dependence of the matrices X and Y on the underlying quantities, namely the orbit vector (vector representing the time discretizations of the spatial Fourier series) and the full state space velocity vector.

$$\hat{v} = (X \cdot \hat{u}) * v - (\dot{Y} \cdot v) * (I_M \otimes T) \cdot \hat{u} \tag{15.32}$$

with this (more) correct direct-matrix velocity equation we can then derive the corresponding stability matrix, using the rules of calculus described in ref. [8]

$$\frac{\partial \hat{v}}{\partial \hat{u}} = \hat{A} = diag(v) \cdot X + diag(X \cdot \hat{u}) \cdot A - diag(T \cdot \hat{u}) \cdot (Y \cdot A) - diag(Y \cdot v) \cdot T \tag{15.33}$$

The new formulation helped me find an error in how I was deriving the stability matrix as there was dependence on both the orbit vector $\hat{u}$ and velocity vector v in the matrices X_1 and Y_1 in (15.31) that I was not accounting for.

As I previously mentioned this did help a little bit but it did not completely solve the problem as I still do not have convergence although I have a really good initial condition (as evidenced by the initial condition's cost functional value).

I don't see any more room for errors in the stability matrix definitions, so I think it might be something more idiosyncratic of relative periodic orbits, namely, how the time discretization using in-slice time might be more unevenly distributed as opposed to the full state space dynamical time.

2017-07-06 Matt : After trying numerous small modifications to the variational method's system of equations from ref. [22] including implementing factors involving the coordinate involved in defining the in-slice time and

other quantities involving the slice tangents I didn't get any improvements over what I already had. I still think the problem has to do with the slice time so I went over the derivation of the equations and I believe I found a correction that can be made.

The derivation of the system of equations used to find the fictitious time corrections to the initial guess loop involves substitution of the partial derivative of the rescaling factor with respect to fictitious time. The way that this is done is via the definition

$$\lambda_n = \frac{\Delta t_n}{\Delta s_n} , \tag{15.34}$$

where, s is the parameterization variable, here defined with a subscript n to indicate that the parameterization need not be uniform around the initial guess loop (although this is what I work worth as it makes things much easier to program). t in this instance stands for the real dynamical time of the orbit.

If we substitute the definition for the in-slice time, this equation takes the form

$$\lambda_n = \frac{\Delta \hat{(t)}_n (x_1)_n}{\Delta s_n} \tag{15.35}$$

Going through the almost identical derivation for the system of equations there is one place where I believe they differ. Normally, there is the substitution

$$\delta t_n = \frac{\partial \lambda_n}{\partial \tau} \Delta s_n \delta \tau \tag{15.36}$$

Normally this is easily generalized in order to produce a uniform rescaling of the period around the orbit, but if the coordinate x_1 is involved I believe that this should take the form

$$\delta t_n = (\frac{\partial \lambda_n}{\partial \tau}(x_1)_n + \frac{\partial (x_1)_n}{\partial \tau} \lambda_n) \Delta s_n \delta \tau \tag{15.37}$$

As the in-slice time rescaling is coordinate dependent, this formula seems to beg for a description of the general equation that has a coordinate dependent rescaling. This is kind of what I have been stuck on as this is quite different from what I am used to.

For a orbit that is described by M points in time we would need λ_i where $i = 0, ..., M - 1$.

I'm currently working on implementing this into my current code but it's gotten the best of me so far.

2017-7-10 Matt : The way I am attempting to solve the problem I am having with in-slice time is as such, for M discretized points representing an in-slice time description of a relative periodic orbit I am introducing M different time rescaling quantities λ_m. In this way the original variational method equation changes from

$$\left[D - \lambda diag(A_0, ..., A_{M-1}), \quad -v \right] \left[\begin{array}{c} \delta\tilde{x} \\ \delta\lambda \end{array} \right] = \delta\tau \left[\begin{array}{c} \lambda v - \tilde{v} \end{array} \right], \qquad (15.38)$$

to

$$\left[D - diag(\lambda_0 * A_0, ..., \lambda_{M-1} * A_{M-1}), \quad -diag(v_0, ..., v_{M-1}) \right] \left[\begin{array}{c} \delta\tilde{x} \\ \delta\lambda_m \end{array} \right]$$
$$= \delta\tau \left[\begin{array}{c} diag(\lambda_m)v - \tilde{v} \end{array} \right], \qquad (15.39)$$

In this way the correction mentioned in (15.37) is not being resolved but I want to try to see if more flexibility in the rescaling of in-slice time with respect to fictitious time evolution is sufficient before getting into an equation I derived; it's also a simpler step whose changes could be carried over to the full in-slice time description I probably will need.

2017-07-12 Matt : Making the single change of a non-uniform parameterization rescaling did not help the variational Newton descent for relative periodic orbits so I moved onto the modified formulation (15.37) in hopes this would solve my problem.

It was a little tricky to figure out the best way to implement but I got it running with unfortunately no better performance than the original symmetry reduced variational Newton descent that I had about a week ago. It could be my derivation of the modified descent equations is off but I am testing some other avenues currently. Namely, with a non-uniform parameterization with in-slice time I am testing a non-uniform finite difference scheme to approximate the loop tangent as opposed to a Fourier description. I feel the non-uniformity of the discretization is probably something to be avoided but I am testing this as a last stand.

With a 32×128 space-by-time discretization of $\overline{rpo}_{16.3}$ the initial cost functional value is still $F^2 \approx 10^{-8}$ so it has some legs to move in the right direction, i.e. I am not losing too much accuracy by switching the numerical method approximating the loop tangent. After some testing this did not help the convergence either and took much longer.

I'm going to recheck the derivation I went through and see if there's anything I can change while also taking some of the improvements I have learned and put them to work on the spatiotemporal fixed point codes.

2017-07-20 Matt : Wrote some new code for symmetry reduced spatiotemporal fixed point finding; currently it seems a little strange to me because I only know how to quotient the spatial translation symmetry in spatial Fourier space as opposed to spatiotemporal (double) Fourier space.

The way that this I am attempting this, are with the equations, in direct-matrix notation:

Using the definition of the reduced velocity in time, (15.32), restated here for reference,

$$\hat{v} = (X \cdot \hat{u}) * v - (\dot{Y} \cdot v) * (I_M \otimes T) \cdot \hat{u}, \tag{15.40}$$

We then find the equivalent spatiotemporal system by Fourier transforming in time by means of application of F_t linear operator denoting the transform and moving everything to one side. Here, the $\hat{u}$ stands for a description of the initial solution that is only Fourier in space.

$$W \cdot F_t \cdot \hat{u} - F_t \cdot ((X \cdot \hat{u}) * v - (\dot{Y} \cdot v) * (I_M \otimes T) \cdot \hat{u}) = 0 \tag{15.41}$$

The stability matrix resulting from this symmetry reduced mapping is therefore,

where $\hat{A}$ is in reference to the equation previously defined (15.33).

$$J = W \cdot F_t - F_t \cdot \hat{A} \tag{15.42}$$

Even though the changes to the system of equations aren't too complex, the previous incarnation of the code used pretty different set of orderings and other small nuisances that have made it a debugging nightmare due to my confusion between other variants of my codes, I realize now that I shouldn't have prepared different initial conditions for every code I write and should have made everything complementary so that all initial conditions of Kuramoto-Sivashinsky equation could be used in any variant of the the variational codes (albeit still being split between symmetry reduced versions or not) as well as the Newton's method codes.

The part that troubled me for a while was how to implement symmetry reduction of the spatial translation symmetry in a spatiotemporal way as opposed to what I have now. I haven't been able to come up with anything good yet but it just seems like a little bit of a hack job to reduce the symmetry before taking things to the spatiotemporal stage. Because I am trying to find fixed points after symmetry reduction I imagined that this case should be exactly be like symmetry reduction of a relative equilibria but I haven't found a good way of treating the equations yet.

2017-07-24 Matt : Almost finished with symmetry reduced spatiotemporal fixed point code, all that remains is redefining the partial derivatives of the spatiotemporal mapping with respect to time and domain size parameters in order to get corrections to the spatial domain size and period.

Made some changes that make the problem seem more natural, namely, I included some terms such that everything is in terms of linear operators acting on vectors of spatiotemporal Fourier coefficients as opposed to a

weird mixture I had before. The upside is that everything is defined spatiotemporally, but it might look a little odd at first glance because there are certain terms which only have one type of Fourier transform operator being applied.

I also elected to change the temporal Fourier transform to a RFFT based description as opposed to a FFT based description (FFT produces both sides of the spectrum, negative and positive Fourier modes based on index where RFFT just produces half of the spectrum). I avoided this earlier because it was easier at first but now that I have some experience this RFFT based description is definitely desired as it minimizes the number of variables in the system. (It is possible, of course to take a FFT and then keep half of the terms but this would be hard to implement given my direct-matrix implementation). The problem isn't completely symmetric in terms of space and time however, as the Galilean invariance eliminates the need to keep track of the terms corresponding to zeroth and Nyquist ($N/2$) modes of the spatial spectrum; The easiest way to describe this is that the discretization in spatiotemporal Fourier space is $N-2byM$ where N is the spatial discretization and M is the temporal discretization.

With this description the new equation for the spatiotemporal mapping takes a similar form to what I was implementing the last time I posted, with a few changes.

The mapping now takes the form,

$$W \cdot \hat{u} - F_t \cdot ((X \cdot F_t^{-1} \hat{u}) * v - (\dot{Y} \cdot v) * (I_M \otimes T) \cdot F_t^{-1} \cdot \hat{u}) = 0 \quad (15.43)$$

where, $\hat{u}$ denotes a vector of spatiotemporal Fourier coefficients.

The symmetry reduced stability matrix needed for Newton's method then takes the form

$$
\begin{aligned}
M \quad = \quad & W - F_t[diag(X \cdot F_t^{-1} \cdot \hat{u}) \cdot A - diag(v) \cdot (X \cdot F_t^{-1}) \\
& + diag(Y \cdot v) \cdot (T \cdot F_t^{-1}) + diag(T \cdot F_t^{-1} \cdot \hat{u}) \cdot (Y \cdot A)] (15.44)
\end{aligned}
$$

This is in addition to the partial derivatives with respect to in-slice time and domain size that have yet to be elucidated.

Once this is finished I will be fully capable of finding spatiotemporal fixed points corresponding to pre-periodic orbits and relative periodic orbits whence I will hope to be able to make a dent in the real project.

2017-7-31 Matt : Put lots of work into the symmetry reduced spatiotemporal fixed point code trying to make up for my lack of productivity when I was back home.

Finished implementing the partial derivatives of the new equation (15.43) but had to figure out how to rewrite them because of differing definitions than previous versions, namely, the ordering of the Fourier coefficients.

Rewrote definitions for the operators pertaining to differentiation in time, space, the spatiotemporal mapping, Jacobian matrix, symmetry reduced Jacobian matrix. In other words, most of the code, to correspond to the differing Fourier transforms.

I still haven't figured out another way to do the symmetry reduction in a spatiotemporal manner, if it is even possible, so I am left with debugging what I have worked on so far; Still having issues so I have some more slogging through the trenches before getting symmetry reduced spatiotemporal fixed point to work.

I have been thinking for a while when this works how I will begin to apply it to glue different orbits together, but finding relative periodic orbits in a symmetry reduced space and pre-periodic orbits in full state space can't really be stuck together in my mind so I think the correct way would be to find the relative periodic orbits in reduced state space, reproduce them in full state space through numerical integration and then try to glue them together. This wouldn't warrant a further attempt to find another spatiotemporal fixed point however because the relative periodic orbit in full state space through one prime period would not be periodic in time, but it would be periodic in space. There a couple of thoughts I have had about this, one being that perhaps maybe when looking at the problem spatiotemporally this means that rpo's must be maintained within the interior of a spatiotemporal domain in order to ensure the tiling is a fixed point, this might point towards pruning rules of the underlying spatiotemporal dynamics but it is kind of a cheap trick and isn't really what I had imagined, which was just to treat pre-periodic orbits and relative periodic orbits on the same footing in a symmetry reduced space; even though it isn't meaningful (or possible?) to bring a pre-periodic orbit to a slice, but I was hoping to be able to get a point where the different types of periodic orbits would be building blocks treated as equal in a spatiotemporal setting.

In this vein, although I know the main goal is to work towards a spatiotemporal symbolic dynamics, I was thinking about perhaps looking at time and space separately and trying to reconcile the two. These are more of dreams than reality and my thoughts on this aren't really clear even to me at this point, but perhaps it would be beneficial to look at different combinations of allowed orbits in time and space separately before looking at a full spatiotemporal setting.

In the spatial system, with periodic boundary conditions in time, i.e. a slightly different problem than Dong and Lan [12], I am curious as to whether it would be easier to develop symbolic dynamics there, as I believe all spatial "periodic orbits" are either temporal equilibria, pre-periodic orbits in time or relative periodic orbits in time, due to the spatial boundary conditions imposed when looking at the time system. My main idea is that because the existence of these different types of "orbits" in the spatial system depend on the spatial size of the system, which is

ostensibly the parameter controlling the onset of turbulence, perhaps it would be easier to designate symbolic dynamics because there is somewhat clear hierarchy as to when the corresponding objects appear; equilibria appear first, then pre-periodic orbits and relative periodic orbits.

These ideas might come off as rambling at this point because I have nothing to back it up, but I felt it was worth expounding upon.

2017-08-01 Matt :

plumbers meeting When I came in Burak was talking about symmetry reduction of multiple commuting continuous symmetries corresponding to pipe flow, showing the derived equations.

After this description, he shows a local coordinate plot of perturbations around a solution and shows that some laminarize and some go turbulent, suggesting an edge-state type idea.

He then presented a new traveling wave solution that had some interesting properties, including a large number of unstable modes; Perturbations in the $\pm$ direction of the $11th$ eigenmode and showed that they either laminarized or went turbulent.

John had a question quite relevant to my endeavors into principal angles, which was "how did you determine the accuracy of the eigenvalues" to which Burak expounded that he increased the resolution until the eigenvalues converged.

Uses an initial condition that was originally at $Re = 10^4$ and use it for a simulation at $Re = 3 * 10^3$. The higher Reynolds number turbulence cannot be sustained and proceeds to laminarize. Scaling the turbulence down by multiplying by a small coefficient

New trajectory and new traveling wave comparison, using L_2 distance between new and old traveling wave and new traveling wave.

State space projection of trajectories with high energy that laminarize (putting high reynolds number solution into low reynolds number simulation).

Showing solution that is spanwise localized while turbulence is not, i.e. implying it is far away from turbulence.

In full-state space people only found the one traveling wave solution, however by working in the symmetry reduced state space he found another traveling wave solution that can be found by following the unstable manifold of the other traveling wave solution.

PC recommends a paper on rigorous bounds on observables in chaotic in turbulent flows by D. Goluskin, Tobasco, Doering, showing for instance in the Lorenz system that the energy for points with a certain bound on the z coordinate is saturated by the equilibria, and then when z increases then the energy is saturated by the shortest periodic orbit.

John discusses his results with different computing languages, showing off Julia and its speed.

Ravi implemented M. Farazmand's adjoint method for the Lorenz system. He was only getting convergence to the trivial solution of 0 but then made some changes that converged to a periodic orbit. Set up adjoint equation, used stiff integrator (implicit), did not work with explicit integrator. Used the "momentum method" and explicit integration and got it to work. It seems to have good convergence properties but needs to use some time of forcing factor to keep it away from the trivial solution. Is trying it on $2 - D$ Navier stokes, might run into a problem when state space dimension gets too high.

debugging Going through a checklist of possible errors in symmetry reduced spatiotemporal fixed point code. Might have to reformulate if everything checks out.

2017-08-08 Matt :

reading Read new Jimenez paper in anticipation for discussion today.

sym reduced Still debugging, I have found a number of bugs, but I'm disappointed at how long it is taking me to find small mistakes, I've been inclined to define everything in two different ways based on the ordering of the spatiotemporal Fourier coefficients and comparing almost every matrix vector product by means of plotting the resulting spatiotemporal field in order to iron out everything. It's been a very time consuming procedure considering I rewrote the code for the symmetry reduction purposes and so far it has found me a negative sign error and a pair of switched variables.

I was having some weird issues when using two real-valued fft's (half-spectrum), so I have also reverted to using a half-spectrum fft in space, and a full-spetrum fft in time. I tried rewriting this portion of the code in probably five different ways but I reverted it due to the weird issues, which were the spatiotemporal Fourier coefficients had the property that for $\hat{u}_k l$, $Re[\hat{u}_k l] = 0$ for $l = even$, $Im[\hat{u}_k l] = 0$ for $l = odd$. I don't know why this is but I've reverted back to the previous definitions, modified for different ordering.

Now that I have gotten rid of all of the nagging little bugs in all of my definitions, I'm hoping to have the symmetry reduced fixed point code done by the end of the day, if there are no numerical issues with applying a least-squares Newton to the problem.

2017-08-09 Matt : Mostly done with the core of symmetry reduced spatiotemporal fixed point code. There are some issues with the in-slice parameterization being maintained which I believe can be chalked up to using a least squares solver.

The residual by using a least-squares solver on a 32 by 32 space-by-time parameterization of $\overline{rpo}_{16.3}$ can currently be reduced to 10^{-9}. Most of

this reduction is obtained with the first few Newton steps, where after the fourth step or so the residual is reduced to 10^{-8}. Even after the application of a total of 50 Newton steps the residual only reduces minimally (to the level previous stated). The slice condition of the phase of the first Fourier mode to be zero is not being maintained, and I believe this is why the residual does not fall to within machine precision. In my experience for variables that are constrained to zero (i.e. the first Fourier mode phase) it is best to leave them out of the calculation of the least-squares solver, like what is done for the zeroth spatial mode terms (which equal zero due to Galilean invariance), such that no erroneous changes can be made, i.e. if they aren't a part of the calculation due to their values equaling zero, they really should not be carried along by the numerical method, it should be implied that they are always zero, and not kept track of.

2017-08-15 Matt :

spatiotemp code Been spending a lot of time trying to improve the convergence of the spatiotemporal symmetry reduced code, as the Newton iterations don't make the large improvements one would expect. Still only reaching a threshold of 10^{-9}.

First attempt at new constraints The first attempt to improve the algorithm was simply to include constraints that make sure the Newton steps are orthogonal to the directions of time and spatial equivariance by requiring the corresponding inner products to be zero. This was done by including two additional rows to the previously overdetermined system that correspond to $\frac{\partial \hat{u}}{\partial x}$ and $\frac{\partial \hat{u}}{\partial t}$ such that the following relations hold $< \frac{\partial \hat{u}}{\partial x}, \delta \hat{u} >= 0$, $< \frac{\partial \hat{u}}{\partial t}, \delta \hat{u} >= 0$ I believe this is what was meant by Burak and PC in last week's meeting when they mentioned the hyperplane formed by time and spatial equivariance. This offered no improvement over the least-squares solver solving the under-determined system (i.e. the system without constraints).

Second attempt at new constraints The second constraint that I tried was to hold certain spatiotemporal Fourier coefficients fixed, by fixing their real and imaginary components separately to yield two constraints. This also offered no improvements to the convergence, but I need to see if whether this is due to the particular choice of Fourier coefficient still.

More efficient code I finally got the rewrite working (to the same numerical accuracy) as its predecessor. This version uses only the real-valued FFTs (i.e. the positive halves of the spectrum for time and space, which halves the number of variables in the system as opposed to the full spectrum FFTs. While this did not improve the accuracy much if at all, it did decrease the amount of time required for computation.

Another attempt at improving convergence Another tactic that I tried to employ was to remove the symmetry reduced variables (the spatiotemporal spectrum corresponding to the symmetry reduced first spatial modes) from the computation of Newton step corrections using the least squares solver. Because the slice condition is to hold these components to be equal to zero, I removed the corresponding rows and columns from the spatiotemporal Jacobian matrix to see whether the least-squares solver was using them as extra degrees of freedom used to minimize the residual of the mapping, F^2.

What I noticed is that by removing them from the system, the residual *increases*, in other words the convergence to a spatiotemporal fixed point is worse. While it is hard for me to currently quantify, the extra degrees of freedom seem to give extra leeway to the least-squares solver, which includes "corrections" to the symmetry reduced variables of order 10^{-7} even though the computation of the mapping has zero magnitude as it should. In other words, through computation of the spatiotemporal fixed point using Newton's method in conjunction with a least-squares solver, a non-zero phase is picked up that, although relatively small, breaks the slice constraint.

Lorenz system gmres As I never got my Newton-Krylov hookstep code to work previously, I am now attempting it again now that I have most of the definitions of the spatiotemporal mapping correct. To begin, instead of starting with a GMRES implementation of the spatiotemporal code I have begun an implementation for the Lorenz system.

2017-08-16 Matt :

symmetry reduced spatiotemp code Made some small changes that went a long way, found a small error in the equivariance constraint related to spatial translation. (Even though the spatial translation symmetry has been dealt with a slice, my code requires these constraints to ensure that the Newton steps don't bring the spatiotemporal fixed point out of the slice.)

Also changed from a least-squares solver to a linear-system solver for when the constraints are in-place. This is one of the things I tend to forget to do when I put constraints in place, if I am solving a square linear system I need to do it exactly.

With these changes, the in-slice spatiotemporal representation of $\overline{rpo}_{16.3}$ in conjunction with the constraints to be orthogonal to the directions of time and space equivariance brought the Newton residual to within machine precision in two steps, when using an 32-by-32 space-by-time discretization (spatiotemporal Fourier modes) of the relative periodic orbit.

numerical experiment I am curious to see how robust my spatiotemporal code is so I am going to perform a numerical experiment that

compares three different codes I have written.

I will first pass the same initial condition, pre-periodic orbit or relative periodic orbit, through the spatial and temporal variational Newton descent separately. I will then take the results from both of these efforts and pass them through the spatiotemporal Newton code. My goal is to hopefully show that while the initial conditions will have distinct changes when trying to fit them to a spatial or temporal periodic orbit, they will both converge to the same spatiotemporal fixed point.

I appreciate any comments that deem this a irrelevant or worthwhile effort.

First I think there might be some small errors in the spatial variational Newton descent that I have to clean up but I don't think this should take too much time now that I have been through the ringer.

2017-08-21 Matt : Ran into a problem when I began the search for new periodic orbits of Kuramoto-Sivashinsky . While the symmetry reduced spatiotemporal code runs fine its full x portions don't work at all with the changes that were made.

Fixed these problems mostly but still have poor results, this is mindboggling considering this is a much easier portion of code to figure out than the symmetry reduced variant.

It works alright (final Newton residual $\approx 10^{-10}$) if I elect to use a least squares solver while removing the constraints that prevent Newton steps from moving in directions of time, and space equivariance so I thought that's where the problem must lie.

After looking at the initial condition I was using there was a very strange and currently unexplained phenomenon with the spatiotemporal Fourier coefficients, where the half corresponding to real components of the spatial spectrum, are only nonzero for even modes in time and the half corresponding to imaginary components of the spatial spectrum are only nonzero for odd modes in time, in other words half of the spatiotemporal spectrum of Fourier coefficients is zero.

I am using the same definitions for the linear operators that perform the Fourier transforms for both the symmetry reduced code and the full state space code and the symmetry reduced initial condition looks how one would expect, for $\hat{u}_{k,l}$ as you increase the value of the index in either space or time, for a periodic function the value of the corresponding coefficient decreases, i.e. higher modes contribute less.

This is due to the preperiodic nature of the solution, in other words I don't think I am handling the reflection symmetry properly in my Newton calculations. This is probably the reason why it didn't converge to within machine precision in the former calculations.

I think the most obvious choice here is to test whether rewriting the coe to not carry along any extraneous variables is the easiest choice. The later would be to find a way to reconcile my method with only using the prime period and then merely applying the reflection symmetry if one wants the entire orbit. The problem with this is that the method relies heavily on spectral methods and it only works when the solution is truly periodic, i.e. not a prime period.

Lan handled this in the variational method by using a finite difference scheme [22] that applied symmetry operations to the boundary terms, I'll attempt to check this out to see if there is something I can take from it.

The relative periodic orbit portion of the code is great, on the other hand. I thought there were some issues because the second shortest relative periodic orbit didn't converge, but this was merely a matter of discretization. The 32-by-32 space-by-time discretization would not work but a 32-by-128 discretization will converge to within machine precision. This makes sense due to the fact the orbit is nearly four times as long when parameterized using in-slice time.

The increasing nee for larger discretizations is really telling me I need to develop a method that can handle huge dimensionality i.e. John's Newton-Krylov hookstep for the problem.

I have a lot more work to do it seems!

2017-08-22 Matt : While rolling in bed I realized that there should be two different ways I can possibly handle the reflection symmetry issue,

The first would be to not have the spatiotemporal system be Fourier-Fourier in spacetime but keep the time direction in physical space. This would enable me to modify the spatiotemporal fixed point equation for pre-periodic orbits to be reduced to solving for the corresponding spatiotemporal fixed point using only prime periods if I used the finite difference scheme in conjunction with the reflection symmetry operator to evaluate the time derivative.

The modified equation would be,

$$D \cdot u + Q_1 \cdot u + Q_2 \cdot FFT_x \cdot (IFFT_x \cdot u)^2 = 0, \qquad (15.45)$$

Where the only difference is that the spatiotemporal vector would now represent $u_k(t_m)$ instead of $\hat{u}_{k,l}$.

The second option would be to remove the extraneous (zero valued) variables from the system of equations, which would require a bit of effort as I would have to modify all of the operators I am using in direct-matrix notation.

The easier of the two by-far is the finite difference method in time so that is what I am going to run through today.

2017-08-22 Matt : The finite difference scheme with the reflection symmetry operation isn't working too well for me so I am going to move on to the second method which uses spatiotemporal Fourier coefficients and then discards the variables that are zero.

I guess it makes sense that half of the spatiotemporal variables are discarded because only half of them are truly unique due to the prime period being the irreducible representation of the full orbit, and the prime period is exactly half of the full orbit. A curious manifestation of the reflection symmetry that I didn't realize.

When its finished I will be able to find spatiotemporal fixed points associated with pre-periodic orbits and relative periodic orbits but not periodic orbits in the antisymmetric subspace $\mathbb{U}^+$.

2017-08-24 Matt spatiotemp More work into pre-periodic orbit code. I figured out the best way to formulate the FFTs such that only the nonzero spatiotemporal Fourier coefficients are kept. This corresponds to keeping the odd numbered temporal modes of the real components of the spatial spectrum and even numbered temporal modes for the imaginary components of the spatial spectrum.

The way I am handling this is to formulate a matrix that performs two FFTs at the same time for the two different types of time series. The normal real-valued FFT matrix is staggered with zeros such that the real components of the spatial spectrum only are multiplied by the columns corresponding to odd modes and likewise for the imaginary spatial components. In order to ensure that the real and imaginary components aren't mixing it is important to enlarge the matrix by staggering the non-zero elements with zeros.

The matrix has been confusing to put together to say the least but the benefit of this method is that I will have a spatiotemporal vector that only consists of non-zero elements *and* is ordered in such a way that I believe only minor changes will been required in the other operators that produce the spatial, temporal derivatives. Also the added benefit is the reduced dimensionality in solving the linear system as only half of the spatiotemporal variables are "active".

The forward transform is working but I am having some difficulty finding an error in the inverse transform.

hoping for new invariant solutions After some testing and getting bad results of trying to find new solutions I believe I will have to switch to Newton-Krylov hookstep method as the dimensionality required for the longer (in-slice time) relative periodic orbits are hard to evaluate given memory restrictions.

By taking a recurrence from ergodic trajectories using a crude Poincaré section formulation, and then using convolution with a Gaussian mollifier yields bad spatiotemporal results. Due to the discrepancy between the few steps of convergence it takes for known orbits and

the complete lack of convergence for the few new orbits tried it seems to indicate that either the initial Newton residual for convergence has to be smaller than what I am starting with. 10^{-3} seems to be the maximum for the initial residual value.

In short, it could be the size of the discretizations limiting convergence, generating initial conditions in a bad way, or just Newton's method failing.

clean up and commentation Cleaned up and annotated some of the codes that Andy will need to help the spatiotemp process.

2017-08-28 Matt Spatiotemporal pre-periodic orbit code finished I believe.

The pre-periodic orbit specific formulation of most of the differentiation operators and Fourier transform operators are finished. They are hard to explain due to their very specific natures but I will try my best.

The current formulation for the spatiotemporal mapping for pre-periodic orbits is

$$W \cdot \hat{u} + Q_1 \cdot \hat{u} + F \cdot ((F^{-1} \cdot \hat{u}) * (F_x^{-1} \cdot Q_2 \cdot F_t^{-1} \cdot \hat{u})) = 0 \qquad (15.46)$$

The spatiotemporal Fourier transform operators are produced by taking the non-commutative products $F = F_t \cdot F_x$ and $F^{-1} = F_x^{-1} \cdot F_t^{-1}$. Note, they are only non-commutative due to the very specific way in which non-zero spatiotemporal Fourier coefficients are produced in order to have a numerically advantageous linear system to solve later down the line. One could, if so desired, flip the order but the matrices would have to change accordingly.

In their current formulation, F_x is the operator the enacts the spatial Fourier transform on the configuration space spatiotemporal velocity field defined on a M-by-N discretization. The output of the transformation is a vector consisting of the real and imaginary components of the spatial Fourier spectrum for positive half of the spectrum, i.e. $\tilde{u}_k$ for $k = 1, 2, 3, \ldots N/2 - 1$, as this is all the information required to reproduce the original spatiotemporal velocity field. The $k = 0$ mode is dropped due to Galilean invariance and the $k = N/2$ mode is dropped from requiring it to be zero because we begin with a real-valued field.

The operator that performs a forwards Fourier transform in time, F_t is an unusual operator that will not work outside of the context of pre-periodic orbits . It produces the nonzero portion of the spatiotemporal Fourier spectrum which consists of the odd modes in time for the real components of the spatial spectrum and the even modes in time for the imaginary component of the spatial spectrum. Another way of describing this is to say it really is performing two different Fourier transforms in time at once, one which keeps the odd numbered time modes $\hat{u}_{k,\ell}$, where, $\ell = odd$ and one which produces the even numbered time

modes $\hat{u}_{k,\ell}$, where, $\ell = even$. The benefit of such a transformation is that we can solve for only the variables that are relevant to the spatiotemporal fixed point system of equations, and the dimensionality of the problem is halved.

Due to the very specific structure of the spatiotemporal Fourier coefficients kept after the spatiotemporal Fourier transformation, all of the other operators needed to change as well.

The one tricky part of the new formulation is that the nonlinear term needs to be evaluated in a specific manner given these new definitions. It's a subtle difference, described by evaluating the nonlinear term with either $-\frac{1}{2}(u^2)_x$ or $-uu_x$. Although they represent the same quantity, the order in which the operations are applied when using my specific selection of spatiotemporal Fourier coefficients (i.e. choice of Fourier transform operators) will drastically change to result.

The quantity $-uu_x$ will produce the correct values while $-\frac{1}{2}(u^2)_x$ will produce a vector of zeros. This has to do with the underlying spectrum and the computation of the nonlinear term pseudospectrally, something that is hard for me to quantify without sounding convoluted but here is my best attempt. The reflection symmetry will make it such that the real component of the spatial spectrum always goes through one period, while the imaginary part of the spatial spectrum goes through two. If you are using a very specific formulation of the Fourier transform (like I am) and you attempt to square the function before applying the spectral differentiation operator, you will get a null vector because the product lies in the same subspace, but the square alone does not.

Now that the core code is written it should be noted that there are still many improvements that can be made to the actual numerical scheme solving the equations. I am using the Python equivalent of LAPACK's linear solver which is ok to work with with small discretizations.

Also to be noted, normally for Newton-Krylov methods, the action of the Jacobian matrix on elements of the tangent space in a dynamical system is approximated by finite-differences of integrated equations. I might be able to just employ Python's (SciPy's technically) GMRES implementation because I am explicitly forming the stability matrix of the spatiotemporal fixed points. (There is no mapping forward in "time" so I am trying to avoid using the term 'Jacobian matrix'. I believe this is consistent with other notation but I will probably be told otherwise).

2017-08-29 Matt :

spatiotemp Talked to P.C. briefly about finding new solutions and the best way to go about it. Predrag mentioned that he was worried about the coordinate dependent in-slice time parameterization so I will work towards the normal dimensionless time parameterization. There might be a need to redefine the slice condition for the spatial

coordinate as this change will introduce sharp changes in the velocity field with respect to time if the orbit comes near the singular slice boundary.

Another topic I haven't really pursued is that there is some quantification of the spatiotemporal area as entropy that I need to read up on.

For trying to find new solutions the couple of ideas shared were using the fact that we have been working on the same sized domain $L = 22$ forever so it might work to take advantage of how the number of orbits grows in time and space by looking at the limits of skinny rectangular orbits. The ideal is to grow the domain "diagonally" i.e. finding orbits that have a large spatiotemporal area but there are unique challenges, such as attracting orbits that might prove to be pitfalls.

janitorial duties Began the process of translating matlab codes still in use to python. I've been meaning to do this for a while so I can focus on working in one coding environment but it's always fallen to the bottom of the list.

This way I can annotate the codes Andy will use while rewriting and cleaning them up.

2017-09-01 Matt :

spatiotemp code Still writing code to find spatiotemporal fixed points of relative periodic orbits that are parameterized in time with the dynamical time instead of rescaled in-slice time. It's taking some time given the current formulation of my codes because the equations that primary equations that govern the in-slice velocity and stability matrices are hard to reconcile with the direct-matrix formulation using a vector that tracks the spatiotemporal Fourier coefficients.

I ran into this problem a little before and ended up switching to the in-slice time formulation because it was easier to implement; the key problem is that the inner products in the equations cannot mix time-dependent quantities, such as the velocity and group tangents. This can be alleviated by converting the $M * N$ dimensional spatiotemporal velocity vector into a $M - by - N$ matrix such that the matrix-vector product of this "velocity matrix" and group tangent template which defines the first Fourier mode slice $V \cdot t'$ equals a vector whose elements each represent an inner product. It isn't the prettiest method but it gets the job done.

The main challenge is the stability matrix equation, as the spatiotemporal direct-matrix formulation the spatiotemporal stability matrix is calculated as a single large object. In this alternate formulation, in order to calculate the symmetry reduced stability matrices everything needs to be calculated separately, what I mean by this is

that the coordinate (time) dependant terms cannot be mixed and are at odds with the spatiotemporal descriptors in place currently. I will have to either figure out a new way to produce the terms all at once or figure out a way to put separate matrices together. The first outlook seems more enticing merely because the secondary method would constitute a new set of function definitions that would most likely take some time to test and implement.

other spatiotemp Uploaded the beginnings of the python translations of the initial condition generation codes in order to enable andy and myself to work completely in Python. The idea is to have a script that depending on the user's choice will integrate in time, either in a symmetry reduced subspace or not, with a random or user provided initial condition, integrate out the transient parts, set up a Poincaré section and find a close recurrence mainly by itself, prepare the initial condition by removing higher frequency Fourier mode components and saving the file so that it may be used to test the spatiotemporal code. It's taking a while because what plan for is an amalgamation of approximately five different codes in one. The main goal is to put ease-of-use at the forefront to the user by changing function arguments rather than changing the code manually.

2017-09-05 Matt : Mainly worked on the initial condition preparation code that I will explain to Andy how to use on Wednesday at a secret meeting.

Implemented most of the function definitions needed in Python, just need to do a little clean up work and annotate for Andy's future use.

Put a little work into the dynamical time spatiotemp code, still haven't figured out how to reconcile the equation for the stability matrices.

2017-09-07 Matt invariant solns Went through Elena's progress with minimal seeds, and Burak's work with Akshunna.

The general idea insofar as I know is that the minimal seed is a perturbation that places you on the stable manifold of edge state to either attempt to send to turbulence or laminar solutions. The minimal seed that Burak shared was a perturbation localized in the spatial directions of the problem (and I suppose time as well,even though its produces a global solution later on); in the given example there were two examples, one which laminarized the solution and one that sent things to turbulence.

I didn't ask anything out loud because I tend to dwell on my thoughts rather than share but I was curious as to why the perturbation with minimal energy should be localized, but this was answered in part by Elena's attempts to filter the higher frequency components, and Predrag's comments that one would like something to be global.

In regards to Burak's work with Akshunna, alas the melatonin is fogging my memory, but I remember it had to do with homoclinic

orbits that go off from some type of invariant solution, transition to turbulence, and return.

Andy Meeting Ran through the current implementation of the initial condition generation code and the main points and ways to play around with it with Andy

spatiotemp initial condition code Finished most of the code, but in order to become functional I need to figure out one last piece which involves converting a real-valued integrator to complex-valued. I believe there are built in functions and methods to do so. Note: that I use this only to find the first intersection with the Poincaré section exactly, i.e. I use it to find the time between the last step of the ET-DRK4 integrator and the Poincaré section. So the other 99.9 percent of the integration is enacted by the ETDRK4 integrator.

2017-09-07 Matt : Still fixing all of the errors in the initial condition production code, as not all cases are producing reliable results.

I had to rewrite the "fine" time integration procedure because I am finding that using a built-in SciPy integrator requires too many redefinitions of Kuramoto-Sivashinsky equation quantities and I felt that it detracted from the simplicity and transparency of the code, so currently I rewrote it so that once one gets near a close-recurrence to the Poincaré section it uses a recursive function call with different keyword arguments to find the final value of time needed to land on the section.

There are still some bugs that I need to get through, namely i need to verify that the poincare search is doing it's job and I think I need to include a function that enforces the reflection symmetry of the problem because otherwise I am going to pick up initial conditions that are unfit for the spatiotemporal code.

2017-09-12 Matt :

symmetry reduced spatiotemp code Still ironing out bugs in the code meant to find spatiotemporal fixed points corresponding to solutions of relative periodic orbits parameterized with respect to dynamical time as opposed to in-slice time. I realized today I was drastically over complicating the operations needed to be done; The current formulation is definitely on the right track as the resulting equations for the direct-matrix expressions for the symmetry reduced spatiotemporal mapping and symmetry reduced stability matrices are essentially matrix formulations of equation (13.24), which is the symmetry reduced stability matrix.

There are still a few bugs however, but I will probably have them ironed out shortly.

The definitions that I am using for the following equations are as such, Y denotes a matrix that picks out the first imaginary spatial

mode component, such that a matrix-vector product $Y \cdot v$ is equivalent to the inner product $< v|t_p >$ where t_p is the group tangent template vector, and v is the velocity. Note that the construction of Y is completely dependent on the fact that the inner product only has one non-zero term (namely, the imaginary component of the first mode) due to the specific nature of the group tangent template t_p.

Likewise, X is a matrix that will pick out the first real component, such that the expression $X \cdot F_t^{-1} \cdot \hat{u}$ is equivalent to the inner product $< t|t_p >$. Again, this is predicated on the group tangent template having such a specific form. The general idea is that the group tangent row vectors $< t|$ are coordinate dependent, so in order to calculate them, we need to be in a Fourier-Time representation, and not Fourier-Fourier.

With these definitions in mind, the dynamical time representation of the symmetry reduced equations takes the form

$$\hat{v} = v - \frac{Y \cdot v}{X \cdot F_t^{-1}\hat{u}} \cdot * (T \cdot F_t^{-1} \cdot \hat{u}) \tag{15.47}$$

One can see that substitution of the spatiotemporal terms with their "equivalent" inner product notations makes this equation equal to equations (13.7) and (13.8). I put "equivalent" in quotes because the inner products in the equations just listed are coordinate dependent quantities, while this notation calculates everything at once.

The spatiotemporal mapping (applying Fourier transform of time of the symmetry reduced flow field) the takes the form,

$$W \cdot \hat{u} - F_t \cdot (v - \frac{Y \cdot v}{X \cdot F_t^{-1}\hat{u}} \cdot * (T \cdot F_t^{-1} \cdot \hat{u})) = 0 \tag{15.48}$$

The symmetry reduced stability matrix then takes the form,

$$\hat{A} = A - diag(\frac{Y \cdot v}{X \cdot F_t^{-1} \cdot \hat{u}}) \cdot T \cdot F_t^{-1} - diag(T \cdot F_t^{-1} \cdot \hat{u}) \cdot \frac{diag(X \cdot F_t^{-1} \cdot \hat{u}) \cdot (Y \cdot A) - diag(Y \cdot v) \cdot X}{(X \cdot F_t^{-1} \cdot \hat{u})^2} \tag{15.49}$$

Again with the substitutions $X \cdot F_t^{-1} \cdot \hat{u} \equiv < t|t_p >$ and $Y \cdot v \equiv < v|t_p >$ the equation is reminiscent of the corresponding equation in equation (13.24).

The full spatiotemporal stability matrix then takes the form,

$$\frac{\partial G}{\partial \hat{u}} = W + F_t \cdot \hat{A} \tag{15.50}$$

So far the mapping is correct in the sense that the initial Newton residual of the mapping is relatively small, 10^{-5}, so I believe the bug to be how I am implementing the division in the terms in the stability matrix.

initial condition generation code After more debugging I realize I was
just expecting the initial condition generation code to know whether
something was a pre-periodic orbit without programming it that
way, made corrections to the recurrence plot formulation to be com-
puted with $||\sigma u(t + \tau) - u(t)||$ and for the best guess to be plucked
from that array of values. This, in conjuction with modifying the
Poincaré condition, will hopefully only allow pre-periodic orbits to
be found if that is what is desired. The modification of the Poincaré
condition is that the Poincaré section is now determined by the re-
flection of the initial starting point, meaning that the procedure should
now pick out the prime period of any pre-periodic orbit. The entire
periodic orbit will then be produced by applying the reflection sym-
metry on the prime period, glueing them together, and smoothing
out any high Fourier mode components that exist.

Need to be more thorough with my changes however as I am still
picking up on orbits that seem to be relative periodic orbits.

reading In order to spread my horizon of thought outside of what is just
easiest to program I've put myself on a reading schedule of some of
the texts I find easier to read and useful, approximately 30 minutes
per text per day. I've found it helps motivate my brain to wake up
and start to engage in the right way.

2017-09-13 Matt Mark Paul *Building a Physical Understanding of High Dimen-
sional Dynamics using a Lyapunov Analysis* Beginning with linear al-
gebra foundation and the Oseledecs multiplicative ergodic theorem.

"There exists in the long time limit, the operator M whose eigenval-
ues are the Lyapunov exponents, and eigenvectors are the Lyapunov
vectors"

Backwards Lyapunov vector = using information from the past, i.e.
evolving Lyapunov vectors forward in time. Using future vectors
and bringing them back, i.e. lose information by bringing either of
these sets forward or backward in time.

This is the motivation of Covariant Lyapunov vectors, invariant set
of vectors that are non-normal that represent growth in different
perturbation directions. Ginelli, Wolfe et al. Tellus 2007, Pazo et
al.

Leads to the degree of hyperbolicity, dimensions (fractal, physical,
inertial manifold), Physics and spurious modes, Spatiotemporal dy-
namics.

Lorenz equation example.

Coupled map lattices using diffusively coupled tent-maps, work of
Takeuchi et al. Angle between Lyapunov vectors gives the decom-
position between physical and spurious modes, principal angle cal-
culations.

They use the pairwise angles between Lyapunov vectors instead of principal angles between subspaces.

"Shoulder" seems to be dependent on the diffusivity constant, but not the case in Rayleigh-Bénard?

How to visualize a Lyapunov vector? In rayleigh-benard the temperature field is a good indication of the dynamics, so look at the perturbation temperature field sliced through the mid-plane. Look at the difference between the whole vector, versus the temperature component of the leading Lyapunov vector.

Rayleigh-Benard, local defects imply large magnitude of leading Lyapunov vector.

When they calculated the principal angle they chose to use the angle between stable and unstable manifold, not the approximate physical, spurious modes.

The more local the more likely you are to land in the span of the physical modes? Ironic because the higher wave numbers are dissipated faster than the lower wavenumbers. How are global, coherent structures reconcile with the fact that the leading Lyapunov vectors seem to be the most local?

Ah, They only appear to be local because they are taking the mid-plane slice, in the most dynamically relevant direction, z, they are probably global.

2017-09-15 Matt : The day was mainly preoccupied with listening to the presentation of data assimilation by Elizabeth Cherry, giving another crash course to Andy and then listening to Andy and Predrag's conversation.

The remainder of time was split between writing additions to the initial condition code that will be used by Andy and investigating implementation of Mohammad's adjoint method [16] in its application to the spatiotemporal version of the Kuramoto-Sivashinsky equation. I investigated this before but comments by Lenard van Veen have inspired this approach yet anew.

His method was worked out in ref. [16] for equilibrium and relative equilibrium solutions in more Navier-Stokes type flows, and used to find new equilibria in $2 - D$ Kolmogorov flow. I am investigating because if one looks at the problem spatiotemporally then perhaps larger invariant structures can be found. I.e. if the problem can find fixed points of an equation, then perhaps in the spatiotemporal formulation where periodic orbits are represented by fixed points of the nonlinear mapping, they can be found with the same method.

Another motivation is because these adjoint methods seem ubiquitous whether it be in Physics or Engineering so I figure that learning them is probably a good idea.

My main problem is that I only ever see the adjoint formulation for PDEs which are first order in time; I only have a nonlinear mapping so I am

trying to figure out if I can find the adjoint of the mapping directly or perhaps if I can do something neat like figure out the adjoint equations for in time, and then treat them on a spatiotemporal level in order to get an adjoint mapping, much like how the mapping was formulated from the Kuramoto-Sivashinsky equation .

I don't know if what I am postulating is idiotic but we'll see after I talk to Mohammad

2017-09-15 Matt Uploading some changes to the initial condition preparation code. Generic starting point is now based on random initial condition, shaped to be periodic in space as the old formulation was a little hard to work around if trying to do a long search. This way there's no worry about the starting point, as long as transients are integrated out.

Changed the Poincaré constraint for pre-periodic orbits so that it finds the prime period, and added code to produce the full orbit by applying reflection symmetry to the prime period and gluing the two together.

09-18-2017 Matt : Talked to Mohammad about the adjoint method; I confirmed some of my beliefs on it but in regards to practically implementing it I think I was slightly off or misunderstood Mohammad. What I recall him saying was "if you system is already discretized then the form should take ...." after which he referenced the equation

$$G(u) = -[\nabla F(u)]^\top F(u) \tag{15.51}$$

in his 2016 paper [16], while wishing to minimize the cost functional $||F(u)||^2$ that the way to implement it was to integrate (in fictitious time) in the direction provided by $G(u)$ in (**??**), using a (adaptive) Runge-Kutta scheme or something similar for best results.

I tried implementing this for the spatiotemporal version of Kuramoto-Sivashinsky equation but it doesn't work for my implementation when $F(u)$ is defined by the spatiotemporal mapping $F_{k,\ell}(\hat{u}_{k,\ell})$.

Predrag stepped in and said I should start with a much easier system and so after trying and failing to get the adjoint method to work for Kuramoto-Sivashinsky equation I started a version that employs adjoints to minimize a cost functional for the Rössler system; Namely I tried employing it to find equilibria by taking $||F(x)||^2 \equiv ||v(x)||^2$; due to the fact that $v(x^\star) = 0$ for an equilibrium point. The form that the adjoint should take on is then $G(u) = -[\nabla v(x)]^\top v(x)$, or so I thought. I couldn't get this to work either so I must have drastically misunderstood Mohammad's explanation.

I went through a derivation of the adjoint operator $\mathcal{L}^\dagger(u; u'')$ and what I have matched the result produced by Mohammad as a practice on how to generally produce adjoints, so I'm slowly learning something. Still trying to figure everything out.

The motivation behind implementing the adjoint method is that Newton's method radius of convergence seems to be obstructively small for the spatiotemporal system. The other issue is that it doesn't make sense to me to use close recurrences and time integration to produce initial conditions for the spatiotemporal system; We are trying to work without dynamics, so why let dynamics dictate the initial condition?

Hopefully implementing the adjoint in conjunction with Newton's method once the residual of the spatiotemporal system is sufficiently minimized will allow for production of initial conditions spatiotemporally, since the adjoint methods do well until they slow down near the local minima it seems.

2017-09-20 Matt adjoint code Got the Rössler code working to find equilibria; I can already see in this simple system why a hybrid Newton-adjoint code is worthwhile, as even for this system as the residual of one of the fixed points is reduced to within machine precision while the other only goes to 10^{-8} in the same amount of fictitious time;

Some more optimization into the actual values of the fictitious time steps can and needs to be investigated by me but I think the general idea is down pat.

Now I move on to attempting to implement these newly learned ideas in conjunction with fourth-order Runge-Kutta for Kuramoto-Sivashinsky equation , and then producing a hybrid method that allows good convergence.

The procedure I will be following can be outlined as follows: Firstly for the system that we want to solve for the roots, namely $F(\hat{u}) = 0$, instead of solving for the Newton corrections directly via a linearized equation $\nabla F(\hat{u})\delta\hat{u}_n = -F(\hat{u}_n)$ we want to step in fictitious time in the "adjoint direction" given by $G(\hat{u}) = -[\nabla F(\hat{u})]^{\top} F(\hat{u})$. (My early formulation requires explicit construction of the matrix $\nabla F(\hat{u})$ but this is the easiest extension of the spatiotemporal code that I currently have so it is what I will begin with). Once the direction is known, we can use a fictitious time-stepping algorithm such as Runge-Kutta fourth order to produce the system of equations

$$
\begin{aligned}
k_1 &= G(\hat{u}_N) \\
k_2 &= G(\hat{u}_N + (h/2) * k_1) \\
k_3 &= G(\hat{u}_N + (h/2) * k_2) \\
k_4 &= G(\hat{u}_N + h * k_3) \\
u_{n+1} &= u_n + (h/6) * (k_1 + 2 * k_2 + 2 * k_3 + k_4)
\end{aligned}
$$

As we are looking for an efficient scheme, most likely to be implemented in a hybrid method, with the adjoint portion just getting us to within the radius of convergence of a Newton or Newton-Krylov Method, $G(\hat{u}_N)$ will be reused for multiple fictitious time steps as

the approximate updates aren't important in the grand scheme of eventual convergence with Newton. The form that this condition is likely to take is that we step in the direction given by $G(\hat{u}_N)$ until we can no longer reduce the residual. If the residual is small enough we then pass the approximate solution to Newton or Newton-Krylov. If it isn't small enough, we redefine $G(\hat{u}_{N+1})$ and then continue.

I am attempting to use notation here such that the lower-case letters define each step in the fictitious time-stepping procedure, while the upper-case letters indicate a redefinition of the underlying adjoint quantities.

additional investigations Lots of reading about adjoint methods, Zahr, Persson and Wilkening [44] being an interesting example, although they seem to be more interested in steady solutions (stable limit cycles). It seems that the main use of adjoint methods is to produce gradients with respect to parameters in a similar effort to how matrix vector products are used to approximate derivatives.

As an exercise I derived the adjoint operator for the Kuramoto-Sivashinsky equation , $\mathcal{L}^{\dagger}(u; u'')$ which dramatically increased my understanding of the what that expression even means, at least in the small context I am applying it. An example of what I mean by this is that I now understand that "the adjoint direction" in this context is specific to the quantity one wishes to minimize but "the adjoint equation" is a general expression that is based on the underlying PDE or operator. This also helped me understand in more detail about why Mohammad derives the analytic expression for "the adjoint direction" corresponding to multiple cases in his paper [16].

2017-09-25 Matt Decided it would be best to implement a spatiotemporal version of Mohammad's adjoint method for Rössler before moving back to Kuramoto-Sivashinsky equation . I'm trying to allow for the computation to take the same form as it will for Kuramoto-Sivashinsky , which means taking the Fourier transform with respect to time of the velocity equations and thereby devising a mapping whose zeros correspond to periodic orbits of the system.

After application of the Fourier transform, the equations take the form,

$$
\begin{aligned}
0 &= iw_k x_k + y_k + z_k \\
0 &= -x_k + iw_k y_k - ay_k \\
0 &= -b_0 + cz_k + (x \cdot z)_k
\end{aligned}
$$

Where the nonlinear term is computed via the standard pseudospectral method for computing convolution sums that we are used to by now.

2017-09-26 Matt From the plumbers meeting:

Burak wanted to know Predrag's opinion on the figure that Burak and his intern Akshunna produced. He believes it satisfies shows there is a Smale horseshoe due to the homoclinic connection and therefore the three solutions they have are really a subset of infinite solutions that necessarily exist.

John thinks I should look at the condition number of the Hessenberg matrix and that my woes may just be completely numerical. The condition number being too large is an indication that the matrix is becoming rank deficient and as such is the source of a loss of orthogonality of the Floquet vectors with respect to each other.

Went to Edgar Knobloch's talk on geostrophic turbulence. Thought it was quite amazing with how far he can get with just asymptotic analysis; Was curious to find out whether he thought the reason behind lack of inverse cascade but didn't get a chance to ask before class.

All in all just chugging along with codes and readings, starting with the papers recommended by Edgar Knobloch.

2017-09-27 Matt Today was spent either at talks, David Krejčiřík's talk on the spectral geometry of quantum waveguides and Yannis Kevrikedis' talk on a smart way to go from micro-scale to macro-scale without a equation.

The first looks at the effect of twisting and bending of tubes and how that effects the spectrum of the Laplacian, namely whether there are any discrete eigenvalues in addition to the essential (continuous) part of the spectrum. Before moving onto the quasi-cylindrical domains (can define a sequence of identically sized balls (open sets) through the entire non-compact domain), he first showed results for quasi-conical (can define an arbitrarily sized ball somewhere in the domain) and quasi-bounded domains (neither quasi-conical nor quasi-cylindrical).

The quasi-cylindrical surfaces (codimension one) that were investigated were constant (non-circular) cross section surfaces, and the transformations that were investigated were twisting and bending. The formulation relied on using the Fermi coordinate parameterization. The results were that bending can produce bound states (discrete part of spectrum) while twisting did not but rather a Hardy inequality arises.

Dirichlet boundary conditions were always used but there was an interesting comment that if you had a bent non-compact quasi-cylindrical surface, where half had Neumann boundary conditions and the other half had Dirichlet boundary conditions then bound states would only exist for the Dirichlet half.

Kevrikedis' Talk was about how when one only has microscale laws of nature (equations) there is a way to extract out useful macroscale information, granted that one either is told the important observable or has some sort of intuition. The microscale simulations are run with certain initial conditions, and then a euler step is taken in the direction of the

gradient of the macroscale observable. In this way, the very long time microscale simulations can be reduced to bursts of simulation the explore locally, while large steps in some observable are taken to explore globally. The process uses machine learning and a number of other techniques not really elucidated but the general idea is when the macroscale equation is not known, this is a way to avoid microscale computation time.

Kirchgässner I'm really trying to understand ref. [20] in depth but my lack of training in mathematical formalism is failing me. So far what I see is that for elliptic equations the best place to look for solutions that are bounded on an infinite domain is to look near the center manifold (which I believe is equivalent to the manifold spanned by marginal directions) of the trivial equilibrium. This sort of makes sense as there is no exponential blow-up in state space along this manifold but the specifics are still not clear to me, other than the fact that the "center manifold reduction" seems to play a key role. Again, the specifics are not clear to me but the general idea is to derive a new differential equation (ODE in his case) that is a reduction of the original equation and is applicable when the norm of the solution is small. In other words, there is a specific equation for solutions that are small in some norm.

coding Still working on the spatiotemporal implementation of Mohammad's adjoint descent to the Rössler system.

2017-10-02 Matt Rossler adjoint Still working out the kinks of the spatiotemporal adjoint implementation for Rössler system.

Wasted a lot of time trying to work around the built-in ode integrator that SciPy has to offer as they are more efficient in integrating equations and choosing the different integration methods alotted to it, but there's just too many open bugs with them (a surprising amount if you stray away from real-valued ode's where the only parameters are of the scalar type).

So after wasting this chunk of time I decided to go back to my original plan which was to use Runge-Kutta 4th order to integrate in the adjoint direction. After messing about with this I realized that my idea of sparingly updating the operators involved; i.e. step in a constant direction until the residual of the cost functional (which is in this case the square of the semi-norm of the spatiotemporal mapping F) no longer decreases is a bad idea as the integrator returns garbage; I think I was conflating this method with my experience with the Newton descent. Because I am using a fourth order integrator that relies on function evaluations, one can't be so cheap with the computations being put into it.

spatiotemporal initial conditions Implemented a spatiotemporal way of producing initial conditions for the Rössler system that utilizes random number generation and products of the Fourier spectrum with

Gaussian distributions. With this I can produce (non-physical) initial conditions whose spatial complexity varies with the standard deviation of the gaussian distribution. The general idea is that because we have time periodicity for the spatiotemporal fixed points, as long as the Fourier (power) spectrum (in time) exhibits a geometric convergence to zero it should converge towards a spatiotemporal fixed point when utilizing the adjoint methods employed.

The next leap is to go from completely non-physical to reshaping the initial condition according to the spatiotemporal mapping. In my experience the mapping is highly unstable, and any application needs to be treated with care. The general idea I have is to first produce a non-physical initial condition and then apply the mapping and rescale so that the initial condition is deformed into something slightly more relevant to the system of equations we wish to solve. This might not work out well as there is no intuitive manner in which to rescale the Fourier spectrum other than repeated application of the Gaussian smoothings.

Newton-Krylov hookstep I've also begun a Newton-Krylov hookstep algorithm for understanding and comparison purposes, but there isn't anything to the code as of yet.

2017-10-04 Matt : Finished up testing of Mohammad's adjoint method with lackluster sub-par results. Spent way too long optimizing the method and trying to improve its speed. While the adjoint method when applied to the spatiotemporal fixed point problem of the Rössler equations does decrease the residual of the cost functional with the semi-norm of the mapping defined by taking the discrete Fourier transform of the Rössler equation in time, the decrease in the residual in minimal. This is my claim after double and triple checking everything and comparing to straight-up Newton.

I think there is a use for it as a very crude preconditioner for Newton, or better yet Newton-Krylov hookstep.

When producing an initial condition based on close recurrences and using a Poincaré section, all but one coordinate are likely to not be periodic; By taking a Fourier transform in time and setting the high frequency (some cut off in mode number) the initial condition is smoothed out, but at the price of making the parameterized (now-smooth) loop non-representative of the equations. By applying this adjoint method in conjunction with a crude tolerance, it can be used to deform the initial condition into something more likely to converge with Newton.

Added quite a bit of functionality to the Rössler code but I'm just going to develop my own Newton-Krylov hookstep code for Rössler now, unless there is some drastic change in my opinion about the adjoint method.

2017-10-08 Predrag I do not understand "Krylov" in "Newton-Krylov hookstep" as applied to Rössler: If you are in 3 dimensions, what can Krylov

(a)

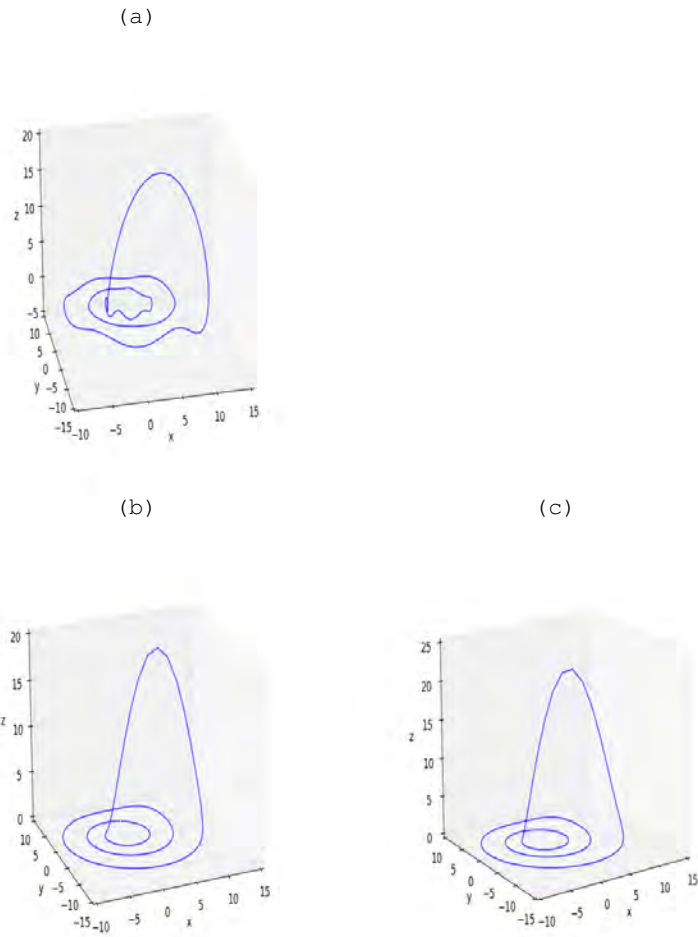

(b)   (c)

Figure 15.7:   (a) Initial condition for hybrid adjoint-Newton descent initial residual of the spatiotemporal mapping $F_0^2 = 4.14084684359$. (b) Output of the spatiotemporal adjoint method $F_{adj}^2 = 0.0992808956991$, (c) resulting spatiotemporal fixed point after applying Newton's method , $F^2 \approx 10^{-15}$.

do? Is the idea that you are using numerical derivatives instead of using the exact

The idea was to get the algorithms worked out for Rössler as even though there are only 3-dimensions, the spatiotemporal system of equations one must solve to find Newton updates will have dimensionality $3M$ where M is the number of time discretized points, therefore for a long periodic orbit even in a small dimension system the dimensionality of the spatiotemporal system can be as large as in Kuramoto-Sivashinsky equation if searching for very long orbits in Rössler, i.e. upwards of twenty Poincaré section returns.

2017-10-06 Matt : Some thoughts about numerical difficulties I have been facing. Predrag indicated that perhaps I should look towards collocation methods as a numerical remedy for my situation. I don't mean to be picky but I have been confused about this statement as Fourier (spectral) methods are collocation methods. The goal is to find coefficients s.t. the solution can be written as an expansion in some basis, (i.e. a Galerkin method is a collocation method with imaginary exponentials as the basis, Chebyshev Collocation is the same but with Chebyshev polynomials as the basis.)

I think I have realized the difficulty with application of collocation methods with finding spatiotemporal fixed points. The main problem in using spectral methods for this problem is that not only are we trying to find the coefficients that minimize some residual such that the discretized solution exactly satisfies the underlying equations, but when changing the domain size L and period T the basis functions (Imaginary exponentials etc.) are ALSO changing. One might be able to get around this by creating a numerical procedure that fixes the domain sizes, finds the best coefficients for that domain size, then allow the domain size to change but this really isn't in the spirit of finding a spatiotemporal solution, we would not like to constrain anything to change.

Therefore, I believe what perhaps Predrag is referring to is a method of relaxation, where all derivatives are rewritten as finite differences between grid points.

I am going to see if adjoint method works better in Rössler with using finite differences to approximate the time derivatives now

2017-10-06 Matt Reading my last post and realizing that I was conflating two different things; the way the what I was talking about i.e. trying to match coefficients of a collocation method whilst changing the basis functions as well is essentially is represented numerically by changing the values of a solution while also changing the domain size. I realized that this is independent of the type of methods being used because numerically the affect of changing the domain size is necessarily present in both types of methods. In other words I didn't think through it enough earlier.
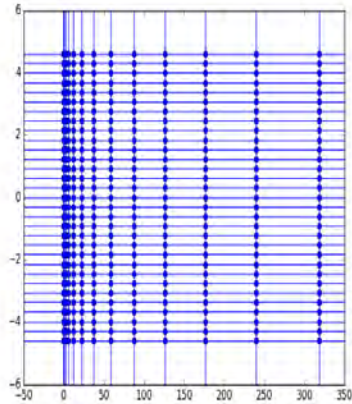
Figure 15.8: Spectrum of spatiotemporal multipliers associated with the linearization about the trivial solution to the spatiotemporal mapping F. Plot is in the complex plane. Vertical lines indicate the position of the values $-q_k^2 + q_k^4$, horizontal lines indicate the position of $\pm w_\ell$, dots indicate multipliers corresponding to this linearization.

> Finite difference code adjoint code stalls just like Fourier code. I let an idea get to my head too quickly.
>
> Ravi was kind enough to share a draft of his thesis which includes ways to speed up and improve adjoint descent, which I am currently reading through.

2017-10-10 Matt : The equations that I will describe are the spatiotemporal mapping described by discretizing the Kuramoto-Sivashinsky equation in space and time, and then taking a spacetime Fourier transform that transforms the equations into a set of nonlinear algebraic equations dependent on the spatiotemporal Fourier coefficients.

The next part of my formulation is to represent the indexed equations as matrix-vector products where the vector is a $M * N$ dimensional vector (before taking care of continuous and discrete symmetries). of spatiotemporal Fourier coefficients ordered in a a specific manner to be further elaborated on.

The matrices will be matrix representations of differential operators (time, space derivatives applied to the spatiotemporal field of coefficients) or spatiotemporal discrete Fourier transforms.

If I may be so bold as to begin with the equations written in terms of the Galerkin truncation in space and time of spatiotemporal Fourier coefficients;

I will denote the components of the mapping F which is dependent on all of the spatiotemporal Fourier coefficients $\hat{u}_{k,l}$ as such:

$$F(\hat{u})_{k,\ell} = (i\omega_\ell - q_k^2 + q_k^4)\hat{u}_{k,l} + iq_k/2 \sum_{\prime k, \prime \ell} \hat{u}_{k-\prime k, \ell-\prime \ell}\hat{u}_{k,\ell} \qquad (15.52)$$

Personally, I find it much easier in avoiding to mistakes to represent this mapping as matrix representations acting upon a spatiotemporal vector, AND I have elected to represent the spatiotemporal Fourier coefficients by their real valued representations. The reason behind the real-valued representations is that there are some underlying conjugacy conditions due to symmetries in the spectrum such that the number of independent variables is far fewer than the total number of complex spatiotemporal Fourier coefficients, and I find it easier to deal with these conditions in a real-valued representation. If one doesn't handle these conjugacy conditions then the linear system of equations we desire to solve later will be singular and yield nonsense. In the words of Viswanath, "Determining the exact dimension of the vector x can be a little tricky because one needs to eliminate Fourier coefficients that are conjugates of certain others and so on" [41], I elect for simplicity which will hopefully be agreed upon after reading this.

Due to the ordering of the Fourier coefficients previously *not* elucidated upon, the structure of the spatiotemporal vector will cycle through all values of spatial index k before changing the temporal index ℓ. In a visual example this corresponds to

$$[\hat{u}_{k,l}]^\top = [\hat{u}_{k,0}, \hat{u}_{k,1}, \ldots, \hat{u}_{k,M/2}]^\top \qquad (15.53)$$

This notation can be somewhat confusing, especially more so when discrete symmetries are taken into account, but hopefully I can clarify in this manner: When I take a spatial Fourier transform with real-valued notation, then only half of the spectrum $k > 0$ is independent information. This is because the configuration space field is real valued, the spatial Fourier coefficients take follow the conjugacy rule $u_k(t) = u_{-k}^*(t)$.

In order to have a real valued representation these must be split between real and imaginary components, i.e. $u_k(t) = a_k(t) + ib_k(t)$.

Now, $a_k(t)$ and $b_k(t)$ again constitute real valued series in time, so one follows the same procedure but in time (different ordering).

By doing so we can formulate differential operators to act on vectors with such an ordering, in an absence of knowledge about naming conventions,

I will denote W as the differential operator that, using spectral differentiation, produces the time derivative of our spatiotemporal field; equivalent to multiplication of the respective spatiotemporal Fourier coefficients by $i\omega_\ell$.

Q_1 will denote the differential operator that produces the second and fourth spatial derivatives, equivalent to multiplication by $-q_k^2 + q_k^4$

Q_2 will denote the differential operator that produces the first spatial derivative divided by two, equivalent to multiplication by $iq_k/2$.

$\mathcal{F}$ and $\mathcal{F}^{-1}$ will denote the matrix representations of forward, and backward spatiotemporal Fourier transforms.

As to the explicit structures of these matrix representations, look further down. With these definitions the nonlinear algebraic equation takes the following form.

$$F(\hat{u}) = (W+Q_1)\hat{u}+Q_2\mathcal{F}((\mathcal{F}^{-1}\hat{u})*(\mathcal{F}^{-1}\hat{u}))\text{where} * \equiv \text{entrywise multiplication}$$
$$(15.54)$$

For starters let us survey what linearizing about the trivial equilibrium $\hat{u}k, \ell = 0$ yields.

$$\frac{\partial F(\hat{u})}{\partial \hat{u}}|_{\hat{u}=0} = W + Q_1 \equiv L \qquad (15.55)$$

The structure of $L = W + Q_1$ is copies of $-q_k^2 + q_k^4$ along the diagonal, and $-w_k$ on a superdiagonal and w_k on a subdiagonal.

The structure of L is such that the multipliers take the form $\Lambda_{k,l} = (-q_k^2 + q_k^4) \pm iw_\ell$, in addition to two marginal modes which should are due to temporal and spatial translations. These two modes are dealt with by imposing two constraints.

In this regard. If we apply a perturbation to the trivial equilibrium, $\delta\hat{u} = \delta\hat{u}_{k=4,\ell=0}$ whose L^2 norm is reasonably small, then the spatiotemporal mapping yields $F(\delta\hat{u}) = (-q_4^2 + q_4^4)\delta\hat{u}_{k=4,\ell=0}$

This is relatively interesting as the spectrum of figure 15.8, if I am interpreting it correctly, seems to indicate that somehow time is related to rotation while space is related to stretching.

A similar spectrum can be obtained for spatiotemporal fixed points corresponding to pre-periodic orbits, except with some modulation in space due to the nonlinear contribution. for relative periodic orbits most of the structure is seemingly lost. I don't have any results from antisymmetric orbits $\in \mathbb{U}^+$ but I will try to provide an example of each tomorrow.

2017-10-11 Matt Proofreading Ravi's Thesis. Learning about his accelerated adjoint methods, Tried a bunch of silly things that I thought would help the method converge but upon thinking about them I found myself wanting.

Plumbers meeting with more discussion about Burak and Akshunna's homoclinic orbits, accidentally muting people, Sadly I can't remember the rest right now.

Talked with P.C. about the notion of spatiotemporal stability, Fuzzy Windows, Cat Maps, Invariants that everyone must be able to reproduce.

2017-10-11 Matt Dynamical sampling talk Talk was hard to understand for someone without Mathematical training. I didn't really understand what was going on for the most part because of the precise language he used.

What I got out of it is that in the context of viewing a Krylov subspace (he never referred to it as such but that's what it was) as a "system" in some sense you can show that certain properties of the operator are required in order to show the Krylov subspace has properties such as being "complete" or being a "frame" or its "Bessel-ness".

The most interesting part was him using spectral decomposition of the operator to show that the Krylov subspace is a "system" only if the eigenvalues are bounded away from zero and near one. This is the general condition for when arnoldi iteration (more specifically GMRES) will be a useful numerical method. Kind of interesting to see such different language applied to something I have seen so often. The problem is I don't understand what "system" means, I think it might be a linearly dependent basis?

Cynthia Reichhardt *Jamming and Clogging of Passive and Active Particles in Disordered Media* Looking at the effect of density on clogging and jamming. Clogging is dependent on some sort of geometry, Jamming isn't. Jamming is a phase transition described by a diverging length scale, i.e. in a solid in order to move one particle you would have to move them all.

Mentioning of some professor named Barringer whose experiments set the precedent for the scaling ratios of binary mixtures of disks.

Assumption that motion of disks is overdamped is related to an assumption of friction, but otherwise it is neglected.

Push a disk through 2-d nonhomogenous array of disks, look at how large its neighborhood of interactions are. As density increase the neighborhood becomes global.

Now look at density of immobile disks. (previous example was one fixed disk limit). Number of immobile disks decreases the jamming density. Corresponds to diverging length scale, once length scales are equal they should cause jamming, but it turns out there is a critical density of immobile disks that will cause jamming regardless of free moving disk density.

Takes a very long time to organize into a clogged state. I.e. an attractive fixed point with very long transient times.

Clogged state described by anisotropy of the arrangement of free-moving disks and the transient time it takes. Also there is a void that is typically normal to the direction of the motion.

Clogging states have a memory because the anisotropic voids created by one direction of forcing will become pathways for movement if the direction of the forcing is changed due to the lack of disks in that region.

To conclude, Jamming is a critical phase transition while clogging is a non-equilibrium phase transtion.

Now moving on to active matter. Active in the regard that propulsion is an internal mechanism. Specifically looked at run and rumble dynamics of bacteria such as ecoli.

Clustering of steric active particles, are velocities identical?

2017-10-13 Matt :

While it's not lost on me that I spend too much time learning numerical methods and not enough Physics, this is what I have to do to get anywhere it seems.

ravi thesis Finished proofreading Ravi's thesis and learning the material within.

Adjoint improvements Implemented changes to adjoint code that include the following combinations

- Ravi's iterative method
- Ravi's "rotation" method. (It's preconditioning)
- Momentum term from Nesterov
- (still crude) adaptive time stepping for RK4

I'm still tinkering with different combinations and definitions for all of these that maximize speed. The improvements are relatively different from Ravi's at this point, in about the same computation time as before I only manage to get an order of magnitude improvement over my previous methods when applied to the Rössler system. In the scope of the larger problem which is spatiotemporal Kuramoto-Sivashinsky equation this might do fine because most of the work should be done by Newton, we only need to get within a region where Newton will converge.

The general idea behind Ravi's "rotation" method is that there are some Fourier modes that are slowly changing in fictious time, so we want to maximize the change of these modes in any numerical algorithm we implement. His explanation of the method he decides to use and the justification falls in line with most justifications I have read for using preconditioning in any iterative or descent method, which is, namely, that it varies from problem to problem and unless the structure of the matrix from the linear system has a specific structure, then the choice of preconditioner falls to intuition and other dark arts.

Yurii Nesterov is a Russian Mathematician who has made great strides in convex optimization and some of his papers have thousands of citations due to their impact on numerical algorithms corresponding to improvements in speed [28]. The classical text on the subject however seems to be Boyd and Vandenberghe 's *Convex Optimization* [3]. If anyone is interested there are also video lectures on Convex Optimization done by Stanford with Stephen Boyd as the lecturer, He's a very enthusiastic and insightful lecturer so it's good to put on in the background while doing menial tasks. video lectures. Also the book is available for free on his personal website book.

spatiotemp Spent some time trying to think of a way to exploit symmetries in the spectrum of spatiotemporal (Floquet in this case?) multipliers. I haven't come up with anything as of yet.

Julia Began reading the documentation of Julia as a means to increase the speed of Python code.

2017-10-17 Matt : Implemented the accelerated adjoint method for Kuramoto-Sivashinsky. The initial performance on test cases was very good but for general initial conditions generated by close recurrence the performance still needs to be improved.

The general description of the adjoint method is that we are stepping in fictitious time determined by $-J(\hat{u})^\top F(\hat{u})$ as this ensures that the cost functional will monotonically decrease to 0. The description of the improvements can be summed up by the following.

The linear component of the spatiotemporal mapping, and thus the contribution to the Jacobian matrix is dominated by the contribution by the Laplacian and Laplacian squared terms of the Kuramoto-Sivashinsky equation. The way it presents itself in the contribution to the Jacobian matrix of the mapping is to have a dominant diagonal. This is one of the instances where use of a diagonal (Jacobi) preconditioner is motivated.

This is implemented by introducing the preconditioning matrix M such that the new adjoint direction is given by $\partial_\tau \hat{u} = -MJ^\top(\hat{u})F(\hat{u})$

This has its benefits for this system but there may be an even smarter choice hiding out somewhere.

The other advancement is described in (its a secret Russian paper that only few may read apparently) [28] that proves that by including a 'momentum' term in the iterative process, then the descent process can be sped up by including a contribution from the previous fictitious time direction. The algorithm that this manifests in is given by

$$
\begin{aligned}
\mu_0 &= 1 \\
\mu_k &= \frac{1 + \sqrt{1 + 4 * \mu_k^2}}{2} \\
\delta \hat{u}_{k+1} &= \delta \hat{u}_k + \frac{\mu_k - 1}{\mu_k + 1} \delta \hat{u}_{k-1}
\end{aligned}
\tag{15.56}
$$

If the residual increases then the momentum is restarted at $\mu = 1$ and the iterative procedure begins again.

Just to reiterate, I have implemented these methods for spatiotemporal Kuramoto-Sivashinsky equation and it can take a (relatively) arbitrary initial condition and descend it to reduced the residual.

Now specifically, I haven't found an initial condition that the full hybrid process in conjunction with Newton works yet. So the next steps are to implement Newton-Krylov hookstep methods (finally getting to it after everything else) and clean up the initial condition generation code (which I started today).

If both of these changes does nothing then the last resort will be to pass close recurrence initial conditions to a Newton-descent in time in order to give one of the tangent spaces the correct shape before starting the spatiotemporal hybrid descent.

The other option is to let the adjoint descent run for arbitrarily long times, but I'm not convinced this is helpful. We shall see.

2017-10-21 Matt :

spatiotemp Almost finished with the Newton-Krylov hookstep method, reading Dennis and Schnable [10] for the best way to calculate the trust region among other things.

The first implementation worked with Givens rotations such that the Hessenberg matrix produced via arnoldi iteration was transformed into an upper triangular matrix, thereby making the nonlinear optimization part of GMRES easy to solve, or so the resources say.

I have opted to just use a least squares solver on this part, and a blackbox nonlinear solver to calculate the optimal hookstep direction, as they tend to be easier to code.

Mohammad Conversation Mohammad posed the idea at the last plumbers meeting that I should just derive the spatiotemporal adjoint equations and then use these to compute the adjoint direction instead of explicitly forming the Jacobian matrix and computing $G(\hat{u}) = -1 \left[\nabla F(\hat{u}) \right]^\top F(\hat{u})$. We shared ideas back and forth, all of my ideas ended up in required that we had already discretized the equations, which is what we were trying to avoid; He mentioned that when he made the statement he thought it

shouldn't be too hard but in our conversation it was non-trivial and more complicated then he had anticipated. To this end, no real progress was made on my end after thinking about this for a while.

adjoint misc Tried playing around with some other numerical procedures that I thought would help the adjoint, but I was either not careful enough when implementing them or there is something else at play. For instance, I tried implementing dealiasing the nonlinear computation to make them more accurate but this really wasn't well received by my spatiotemporal adjoint descent code.

2017-10-24 Matt

numerics Almost done with the hybrid methods, will be posting statistics hopefully before tomorrow's meeting.

The spatiotemporal fixed point code now has the ability to run the following numerical methods in searches.

- Hybrid Preconditioned Adjoint-Momentum-Descent Newton-Krylov hookstep (Main method)
- Newton-Krylov hookstep
- Damped Newton (For really good initial conditions)
- Undamped Newton (For really good initial conditions)
- Preconditioned Adjoint Descent
- Raw Adjoint Descent
- Momentum accelerated Adjoint Descent.

Standalone Adjoint Descent code, (Preconditioned, accelerated) should be used if the numerical residual isn't too important and one just wants a fuzzy window/smoothing out an close recurrence guess.

Standalone Newton Method Type procedures should only be used if the initial condition is exceedingly close to a spatiotemporal fixed point (at least in the case of damped, raw Newton, still need to test the hookstep).

A little work needs to be done on the following before I can proclaim *Ta da!*.

- Automated Initial condition generator is still a little rough around the edges.
- The focus on numerical methods has lead me astray from the time parameterization for relative periodic orbit fixed points
- The trust-region calculation and general comments in the hookstep code need to be improved.
- Numerical statistics need to be introduced to determine the efficacy of the various methods versus each other.

- Another constraint needs to be implemented for pre-periodic orbit fixed points, the current code utilizes constraints on the Newton steps such that they are orthogonal to time,space equivariance, however in the pre-periodic orbit case the direction of spatial equivariance is an impossibility due to the peculiar form of the Fourier transforms used that exploit the discrete symmetry. (I just realized this today, it turns out that by keeping the terms I did I believe I might have 'accidentally' quotiented the SO(2) symmetry, when I thought I was getting rid of the reflection symmetry. Still looking into maybe this is close to quotienting O(2). Currently as a work around I am using something ill-advised (constraining the steps to be orthogonal to the $2nd$ and $4th$ spatial derivatives with no motivation to do so except it improved performance.

- Preconditioning for the arnoldi iteration portion of the hookstep code should probably be implemented, as it helps a lot for the adjoint descent.

In regards to the comments about quotienting O(2) for pre-periodic orbits. I've been thinking a lot about it today and trying to utilize some of the teachings of my adviser (Gasp) to try to think about symmetries spatiotemporally. I'm trying to reconcile the fact that the reflection symmetry present in pre-periodic orbit fixed points can be inverted by translating by the period of the fundamental domain. (i.e. $Ru(x,t) = u(x, t + T_p)$)

2017-10-26 Matt automated initial condition generation Still debugging the relative periodic orbit part of this code, might include the ability to pass the initial condition to a Newton descent in time just to smooth out and or correct the tangent space before sending it to spatiotemporal problem (My last resort if I can't get it to work for spatiotemporal initial conditions produced by close recurrence).

janitorial duties The spatiotemporal fixed point code has grown to an extent that it is becoming far too unwieldy and some of the functions defined by me were done without a thought as to what to call them.

Most of my time today was spent splitting the file with all of the function declarations into a number of pieces, and keeping the numerical methods separate. This isn't exactly progress but I'm hoping it will speed things up in the future. As it was previously written, for each numerical method I needed a separate function depending on the symmetry (isotropy subgroup, stabiliser, etc) of the initial condition. Now that most of the numerical methods are working I am trying to rewriting them to be independent of the symmetry of the solution other than a keyword argument ((switch,flag) for those who use command prompt to run scripts.) The reason it was written this way is because I had to formulate it in terms of test-cases and so usually I choose a certain subgroup to work in at first.

hookstep Reading Dennis and Schnable [10] to improve the trust-region calculations for hookstep, it all seems sort of heuristic to me but I'm sure there are rigorous proofs elsewhere that I wouldn't understand. Confusing as well. The general idea is that because of the specific form of an equation to calculate the optimal hookstep, Newton's method in the free parameter is suboptimal, so they introduce lower and upper bounds on the trust region and a modified linesearch and also a quadratic model to test the accuracy of the hookstep. Seems to be needed as John did it as well.

failed attempt I thought perhaps that perhaps applying the adjoint descent on a fixed spatiotemporal area would help poor initial conditions converge, but the adjoint descent really doesn't seem to agree with a fixed 'window'. The idea is that before approaching the full spatiotemporal problem, we should really correct the tangent space first.

other spatiotemp implementations Still improving functionality of the code and some small numerical procedures. During the rewrite I wrote pieces of code to apply least squares to the Newton method procedures to avoid constraints that seem to vary in there efficacy.

Here's a short list of things I am trying to get done:

- Dealiasing using 3/2 rule, via prolongation and contraction matrices (spatiotemporal zero-padding)
- Constraint-type keyword arguments
- Preconditioned GMRES
- Statistics on the numerical procedure (i.e. Residual of Cost Functional versus computation time, iterations, function calls, etc.
- Statistics and or plots of spectra and eigenvectors of spatiotemporal Jacobian matrix
- Trying to think of spatiotemporal invariants to perhaps use as axes in plots

2017-10-30 Matt spatiotemp code Finished the reorganization, added some functionality by means of being able to plot residual versus iteration number for different methods. Included preconditioning matrices for relative periodic orbit and antisymmetric orbits $\in \mathbb{U}^+$.

spatiotemp initial conditions Still debugging this. Narrowed down the problems to taking too large of steps in the integrator and something ill defined in the Poincaré section piece of code.

Schatz and Grigoriev Group By request of Ravi, I presented some results of the adjoint method and discussed how it was implemented for my spatiotemporal problem. Most of the questions came from Roman G., Mike Schatz, Kimberly S. Roman was concerned about the marginal directions and whether or not solutions exist.

(a)

(b)   (c)
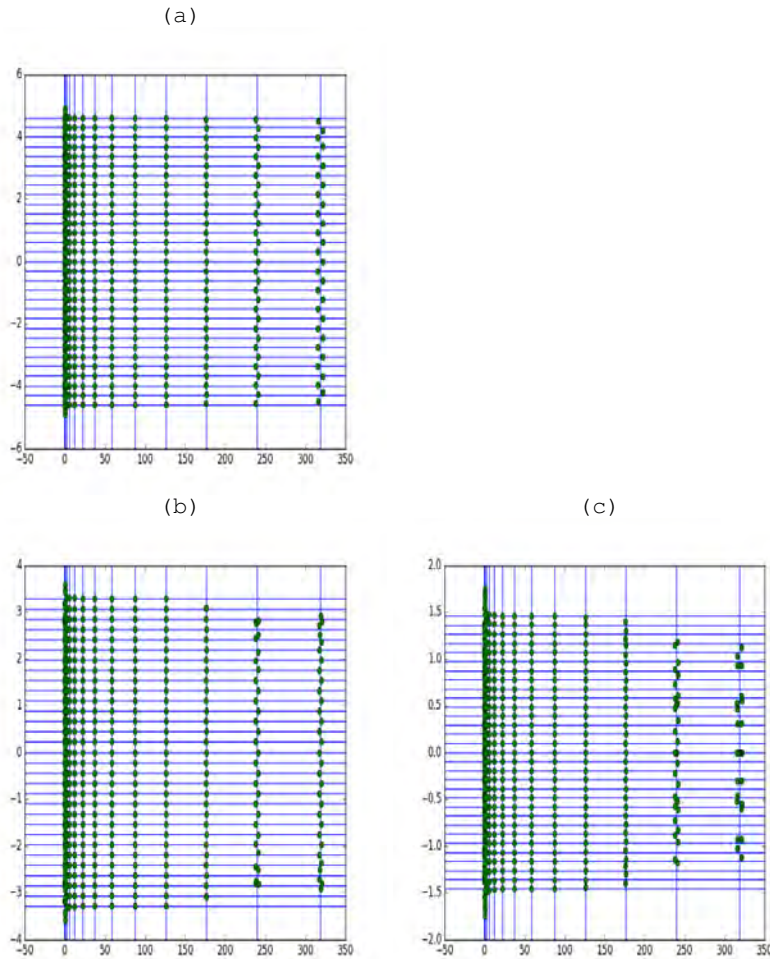
Figure 15.9: (a) Spatiotemporal multiplier spectrum for $\overline{ppo}_{10.2}$, (b) Spatiotemporal multiplier spectrum for $\overline{ppo}_{14.3}$, (c) Spatiotemporal multiplier spectrum for $\overline{ppo}_{32.3}$. Intersections between horizontal and vertical lines indicate where the multipliers would be for the $u(x,t) = 0$. In other words, changes from this grid indicate differences between the linearized spatiotemporal spectrum and the full spatiotemporal spectrum. All three solutions converged to within machine precision when defined on a 32-by-32 spacetime grid; Fourier calculations done with 15×31 spatiotemporal Fourier coefficients.

2017-10-31 Matt spatiotemp Fixed some bugs related to keyword arguments. All numerical methods are now independent of the particular type (isotropy subgroup) of solutions other than keyword argument "symmetry". Included default values for tolerances, dimension of Krylov subspaces, adjoint fictitious time, and etc. so that other users don't have to think worry about specifics if they just want black box numerical algorithms to work with.

Still working on improving the hookstep algorithm, as well as initial condition generation code, the initial conditions specifically need to be pretty precise or else the spatiotemporal convergence will not work. The hookstep improvements are just confusing as all hell to me.

The general procedure is to use a modified Newton search for the optimal hookstep; Using John's code as a guide I've realized there are quite a few more additions than I orginally thought that need to be made before I can say it's "done".

initial conditions Still trying to figure out the bug regarding Poincaré sections, will hopefully find by the end of the day. For pre-periodic orbit I am constructing Poincaré sections based on the reflected partner of the initial point returned by close recurrence. I.e. for an initial condition $u(x, 0)$ I am attempting to produce initial conditions that shadow pre-periodic orbits by constructing a hyperplane whose template point is the reflection operation (performed in Fourier space) $Ru(x, 0)$. and then defining tangent and normal vectors to the plane based on the first Fourier mode.

misc Realized that my damped Newton is actually equivalent to backtracking line-search type Newton due to the fact that I keep reducing the step size until I find a correction that reduces the residual, instead of just using a reduced step-size Newton.

2017-10-31 Matt Trying to see if there are any way to use the initial spatiotemporal spectra that would determine if a solution will converge or not. For instance, for the tenth shortest pre-periodic orbit I needed to use a 32-by-64 space by time discretization to get it to converge. I.e. I had to increase it by a factor of two.

It should be noted that this factor of two is what I chose not because it was the smallest increase but rather its the convention I'm used to due to the fact it improves the performance of FFTs. Now, because I was more focused on accuracy rather than performance, I have implemented these so-called direct-matrix methods. I.e. I am explicitly forming everything in terms of matrices and vectors, so I believe that as long as I retain even numbers my code will run, meaning that I do not have to sacrifice much performance to improve the discretization, because I only have to perform the FFTs (forwards and backwards, space and time) once.

I'm going to be testing this in the future, something along the lines of: If convergence fails, increase the time discretization by two, four, etc. For the spatial discretization there doesn't seem to be such an issue due the fourth spatial derivative, but when I get to large domains I will likely have to make some adjustments there as well.

Still improving hooksteps, can't really get this optimization using Lagrange constraints via ref. [10] to work.

2017-11-02 Matt : Reading about trace formulas and zeta functions makes me think I should rewrite my equations such that everything is a fixed point with period one. Right now I guess you could say that everything is represented by fixed points of period two, because $F(\hat{u}) = 0$, not $F(\hat{u}) = \hat{u}$.

In this case then the general formulae I have been using would only need to be tweaked in a relatively small manner. In order to formulate a function that follows $G(\hat{u}) = \hat{u}$, we need to do some rearrangement in the spatiotemporal equations I have been utilizing. (Also, I'm going to switch up the conventions I have been using for almost a year now to something more recognizable by the reader).

In what follows D_i are differential operators with respect to the index, and F are spatiotemporal Fourier transform operators.

$$(D_t - D_{xx} + D_{xxxx})\hat{u} + D_x F((F^{-1}\hat{u})^2) = 0 \qquad (15.57)$$

Noting that the operator that equates to the difference of the second and fourth spatial differentiation operators is diagonal, and not singular by construction, we can easily take the inverse of the operator (because it's diagonal), and we arrive at the equation

$$G(\hat{u}) = (D_{xx} - D_{xxxx})^{-1}(D_t\hat{u} + D_x F((F^{-1}\hat{u})^2)) = \hat{u} \qquad (15.58)$$

This might be the "proper" way of doing things, even numerically, because this essentially scales out the large spatial components due to the fourth order term.

I'm still learning (slowly) the methodology and intuition behind trace formulas and zeta functions but this might be the proper way of viewing things because then all doubly periodic orbits are in fact spatiotemporal fixed points as opposed to period two orbits. (in other words instead of a string of symbols $\bar{N}\bar{0}\bar{0}\ldots$ in the fictitious dynamics introduced by applying the mapping function, I am instead identifying the orbit by just $\bar{N}$, where N is a label given to spatiotemporal fixed points.)

2017-11-07 Matt In reference to the post of **2017-03-14**, on page 787 in chapter 19 *Space-time, blogged* I would argue that what I have done is quite similar to López *et al.* [25].

By using the spacetime Fourier-Fourier basis representation of the spatiotemporal field with Galerkin truncations in space and time

$$a_m(t) = \sum_{n \in \mathbb{Z}} \hat{a}_{kj} e^{i\omega_j t}, \tag{15.59}$$

The nonlinear algebraic equations in this basis are (1.43). I will restate the equations here for completeness and comparison to López *et al.* [25]. In the spacetime Fourier-Fourier basis, the Kuramoto-Sivashinsky equation takes the form,

$$\left[i\omega_j - (q_k^2 - q_k^4) \right] \hat{a}_{kj} + \frac{iq_k}{2} \sum_{k'} \sum_{j'} \hat{a}_{kj} a_{k-k',j-j'} = 0. \tag{15.60}$$

while in López *et al.* [25], with the ansatz for relative periodic orbit solutions (19.24) the complex Ginzburg-Landau take the form

$$i \left(\frac{2\pi n}{T} - \frac{\varphi}{T} - m\frac{S}{T} \right) \hat{a}_{kj} = R\hat{a}_{kj} - m^2(1 + i\nu)\hat{a}_{kj} \tag{15.61}$$

$$-(1 + i\mu) \sum_{m'} \sum_{n'} a_{k_1, j_1} a_{k_2, j_2} a_{k_3, j_3}^*,$$

where $m_1 + m_2 - m_3 = m'$ and $n_1 + n_2 - n_3 = n'$.

The differences between our methods arise when setting up the equation as a root solving procedure. In López *et al.* [25] the numerics is handled by solving for the roots of the function $F(\hat{a}_{kj}, \varphi, S, T) = 0$ where F is the function described by (15.61) if one moved all of the terms to one side of the equation.

In my current procedure, I solve (1.43), or for comparison, $F(\hat{a}_{kj}, T, L) = 0$, where T, L are in the factors ω_j, q_k respectively.

I do not explicitly include variables that control the spatial translations of the system and, up until now, have elected to search for relative periodic orbit solutions pertaining to (1.43) by finding them in the first Fourier mode slice. Part of the reason of this was I didn't understand the reasoning behind parameterizing the spatial translations by t by means of the factor in the ansatz $e^{-iq_k \frac{S}{T} t}$. I thought the shift factor had to be explicitly calculated by the coordinates, and not assumed through this type of time dependence.

My comments of **2017-11-02** on page 475 were mainly predicated by the fact that once we find these roots, I don't think we can apply the same type of reasoning as Politi and Torcini [30] as they aren't truly fixed points of a fictitious dynamical system, like so, $F(\hat{a}_{kj}, T, L) = \hat{a}_{kj}, T, L$. But rather, like I have already described, they are the roots of a system of nonlinear algebraic equations, $F(\hat{a}_{kj}, T, L) = 0$.

If I am so inclined to change how I search for relative periodic orbits in the same manner as López *et al.* [25] I believe all I would have to actually

implement is this $\mathrm{e}^{-\mathrm{i} q_k \frac{S}{T} t}$ factor in my ansatz, such that the new equations for solutions with SO(2) symmetry would be,

$$\left[\mathrm{i}\omega_j - m\frac{S}{T} - (q_k^2 - q_k^4) \right] \hat{a}_{kj} + \frac{\mathrm{i} q_k}{2} \sum_{n'} \sum_{m'} \hat{a}_{kj} a_{k-k', j-j'} = 0 . \qquad (15.62)$$

such that the spatiotemporal solutions would now be roots of the nonlinear system of equations, $F(\hat{a}_{kj}, S, T, L) = 0$

2017-11-08 Matt plumbers Second part of plumbers meeting was about discussing why averaging over a line in the infinite spatiotemporal case is fundamentally different than looking at a finite rectangle or strip. The latter imposes both length and time scales likely different than how nature would impose them and hence any statistics gained would be necessarily different.

conversation with Andy Discussed variational methods, Jianke Yang's code, and applications to Graduate school at length with Andy.

Jianke Yang Read through the code and ran it, the hybrid Newton and conjugate gradient descent can reach a tolerance value of 10^{-10} pretty easily, taking only seconds to run; but when the tolerance is made more strict then after experimentation with it, it doesn't converge even after running for hours; I might be missing something numerically but I guess I'm trying to test his algorithm against the same standards I'm holding my algorithms.

2017-11-13 Matt Jianke Yang spatiotemp I'll try to outline Jianke Yang's paper [43]

He begins with an exposition about the previous work specifically Lan and Cvitanović [24] and López *et al.* [25], which are two of the main papers I work around so there's likely something I can take from this paper.

Jianke Yang has the following to say about working with an infinite tower of ODEs versus PDEs.

> In this article, we develop a new numerical method for computing time-periodic solutions in dissipative wave equations. This work is motivated by several reason. First, our view is that the best way to compute such solutions in PDEs is to do so in the PDE framework, rather than converting PDEs to large systems of ODEs or algebraic equations. The advantage of the PDE framework is that the structure of the PDE is retained, and important quantities such as the linearization operator of the PDE can be calculated analytically. Second, almost all numerical methods for time-periodic solutions in PDEs involve solving lare systems of linear equations. Since conjugate-gradiate methods are widely recognized as probably the fastest numerical method for solving linear algebraic and operator equations,

we are motivated to incorporate conjugate- gradient methods into our algorithm.

He says that he prefers to work in the "PDE framework" but he uses spectral code to compute all derivatives (due to the accuracy of spectral methods versus finite differences). I don't buy the comment about working in the "PDE framework". He is making it sound like he doesn't use the ODEs in Fourier space but this is exactly what he is doing when he uses them to compute spatial and temporal derivatives. In other words the basis for his claim for working in the "PDE framework" is that he solves the resultant linear system (via a combination of Newton and conjugate-gradient) in physical space versus Fourier space.

If I had to rephrase these comments I would say that he finds it advantageous to compute all terms pseudospectrally; the derivatives are computed in spectral space but the linear system of equations that arise are solved in physical space. His claim that "no truncation to ODEs or algebraic equations is necessary" is *nonsense*. That's exactly what is necessary in order to compute the derivatives spectrally.

Another difference between his code and my own is to use "quasi Rayleigh quotients" to determine free parameters. (e.g. the period of the solution).

For example, to determine the period of periodic solutions of the Kuramoto-Sivashinsky equation he rescales time $\tau = \omega t$ such that $0 \leq \tau \leq 2\pi$, such that the PDE can be rewritten as,

$$\omega u_\tau = F(x, \partial_x, u) \text{where}, \tau = \omega t$$

and then rewrite ω in terms of the solution itself via the so called quasi Rayleigh quotient,

$$\omega = \frac{< u_\tau, F >}{< u_\tau, u_\tau >}$$

such that the original equation now takes the form,

$$\frac{< u_\tau, F >}{< u_\tau, u_\tau >} u_\tau - F(x, \partial_x, u) = 0 \tag{15.63}$$

Due to the inner products (defined as the spatiotemporal L_2 inner product) the equation to solve now takes an integro differential form, but he says that this price is worth paying for.

He then derives analytic equations for the linearization of (15.63), which is going to be the linear system that is going to be solved to yield the Newton corrections.

In order to apply his Newton conjugate gradient method, he needs to transform the system such that it becomes self-adjoint, but I feel that any

exposition into this likely would not be helpful for discussion as its all numerics at this point. He does however mention the practicality of pre-conditioning the linear system, which is something that I have been debating.

Further derivations

Due to the fact that J. Yang is writing the spatiotemporal equations as a root finding procedure, a linear expansion will be required to set up the system of equations that need to be solved in order to step in the correction direction (If one thinks about it in the scope of Newton's method, we need to be able to linearize about the root such that we derive a linear system of equations whose solution is the Newton correction).

Due to the presence of this time-rescaling factor ω and its explicit definition in terms of the so called quasi Rayleigh quotient, in order to linearize the equation (15.63) about a root, we need to derive the expression for the linearization of $\omega(u) = \frac{<u_\tau, F>}{<u_\tau, u_\tau>}$.

In other words, we need an expression for $\omega(u + \delta u)$. To get a useful form of this equation, we first use the fact that we know the linearization for the function F.

$$
\begin{aligned}
\omega(u + \delta u) &\approx \frac{< (u + \delta u)_\tau, F(x, \partial_x, u + \delta u) >}{< (u + \delta u)_\tau, (u + \delta u)_\tau >} \\
\omega(u + \delta u) &\approx \frac{< (u + \delta u)_\tau, F(x, \partial_x, u) + F_1 \delta u >}{< (u + \delta u)_\tau, (u + \delta u)_\tau >},
\end{aligned}
\tag{15.64}
$$

where F_1 is what Yang calls the "linearization operator" but others would recognize it as the Jacobian matrix.

We can simplify this expression by substituting the equality given by (15.63),

$$
\omega(u + \delta u) \approx \frac{< (u + \delta u)_\tau, \omega u_\tau + F_1 \delta u >}{< (u + \delta u)_\tau, (u + \delta u)_\tau >}
\tag{15.65}
$$

And then just for add and subtract $\omega \delta u_\tau$ in order to separate into two terms,

$$
\omega(u + \delta u) \approx \frac{< (u + \delta u)_\tau, \omega(u + \delta u)_\tau + (F_1 - \omega \partial_\tau) \delta u >}{< (u + \delta u)_\tau, (u + \delta u)_\tau >}
\tag{15.66}
$$

After keeping only first order terms in δu we get,

$$
\omega(u + \delta u) \approx \omega - \frac{< u_\tau, (\omega \partial_\tau - F_1) \delta u >}{< u_\tau, u + \delta u)_\tau >}
\tag{15.67}
$$

The whole point of this exercise was to describe the linearization of the equation whose roots will result in doubly periodic solutions, namely (15.63).

To derive the expression for the Jacobian matrix of (15.63) we will use the decomposition elucidated in (15.67). This can be explained by the following equations,

$$
\begin{aligned}
L_0(u) &= \frac{<u_\tau, F>}{<u_\tau, u_\tau>} u_\tau - F(x, \partial_x, u) \\
L_1 &\equiv \frac{\partial L_0}{\partial u} = (\omega \partial_\tau - \frac{\partial F}{\partial u}) + \frac{\partial \omega}{\partial u} u_\tau \\
L_1 &= (\omega \partial_\tau - F_1) - \frac{<u_\tau, (\omega \partial_\tau - F_1)>}{<u_\tau, u_\tau>} u_\tau \\
P &\equiv (\omega \partial_\tau - F_1) \Rightarrow \\
L_1 \delta u &= P \delta u - \frac{<u_\tau, P \delta u>}{<u_\tau, u_\tau>} u_\tau
\end{aligned}
\tag{15.68}
$$

With this definition we can then solve by iterative methods the system of equations given by,

$$
L_1 \delta u = -L_0,
\tag{15.69}
$$

such that when when $L_0 = 0$ we have found the solution.

This is the general derivation for one extra parameter (in this case ω, which is a taking the place of period), the general derivation for a two parameter case (which is necessary to allow period and domain size to vary) is the next undertaking.

2017-11-13 Matt initial condition generation In order to reduce the number of garbage initial conditions, we first pass through a close-recurrence problem that sifts through en ergodic trajectory for a possible place that we can set up a Poincaré constraint. This is done by time-integration followed up by computing $||u(x, t_0) - \sigma u(x, t_0 + \tau)||$ where σ is the relevant symmetry operation for the type of orbit we are searching for.

The current Poincaré procedure can be defined by the following:

For an example point defined by its spatial Fourier coefficient representation $u(x_n, 0) = \sum_k (a_k + \mathrm{i}b_k)e^{iq_k x_n}$,

For pre-periodic orbit solutions, I define a Poincaré section whose template point is the reflection of the real component of the first Fourier mode. Namely,

$\hat{u}_{template} = [0 - a_1 00 \cdots - a_1]^\top$

Note: $a_1 = a_{-1}$ by conjugacy symmetry of Fourier coefficients of real valued function.

Then the Poincaré section constraint is defined by this template point, as well as the transverse component of the velocity evaluated at the spatial reflection of our starting point, or written as an equation,

$$U(\hat{u}) = < \hat{u}_{template} - \hat{u}|\hat{n} > \text{ where,} \quad \hat{n} = \frac{v(R\hat{u}) - < v(R\hat{u})|\hat{t} > \hat{t}}{||v(R\hat{u}) - < v(R\hat{u})|\hat{t} > \hat{t}||}$$
(15.70)

In order to ensure that the transversality condition is always to find $U(\hat{u}) = 0$ between the two points $U(\hat{u}_{n-1}) < 0, U(\hat{u}_n) > 0$, we include the orientation of the velocity in the definition of $\hat{n}$.

2017-11-14 Matt Spatiotemp reformulation continued Working my way towards an implementation of the reposed spatiotemporal problem that involves inverting a differential operator (the sum of second and fourth spatial derivative operators) defined by equation (15.58), restated here for completeness.

$$\begin{aligned} G(\hat{u}, T, L) &\equiv& D_X^{-1}(D_t\hat{u} + D_x F(F^{-1}\hat{u})^2) - \hat{u} = 0 \\ D_X &\equiv& D_{xx} - D_{xxxx} \end{aligned}$$
(15.71)

Such that the reposed problem is truly a fixed point problem, $G(x) - x = 0$, instead of the similar root finding problem $F(x) = 0$. I believe that this can be motivated theoretically in terms the desire to have some spatiotemporal notion of stability of these solutions as well as cycle expansions.

When treated as the true fixed point problem, the action of $G(x)$ on doubly periodic solutions is an involution, meaning that points get mapped to themselves. Although this last statement is obvious, I am stating it because it demonstrates the (what I consider to be) unnatural behavior of the alternative problem, where, no matter where you are in this spatiotemporal state space, every doubly periodic solution gets mapped to zero under the action of F. I believe this to be unnatural because if you're looking at the linearization of this spatiotemporal function F you are looking at the linear neighborhood at a point in spatiotemporal state space that is necessarily far away from the original doubly periodic solution. Also, the other part I find unnatural about this is that because every doubly periodic solution is being mapped to zero, all of the solutions are in a sense being identified to one another no matter where they really exist. There is probably a smarter and or more precise way of rephrasing that last sentence but its the best I could come up with.

The other perspective on why being mapped to zero seems unnatural is in terms of the symbolic dynamics, intuitively each doubly periodic solution (tile, rectangle, etc.) should be able to be identified

by a symbol; In the root-solving formulation it is impossible to formulate a fictitious discrete time with the spatiotemporal mapping because the itinerary would look something like $\bar{N}\bar{0}0\bar{0}\ldots$.

On the other hand, this is also well motivated in a numerical sense because the reformulation inverts an operator who is comprised of numbers ranging from order unity to numbers orders of magnitude larger. This is poor for iterative methods unless one introduces a preconditioning, because these large diagonal elements will a large range of eigenvalues. The reason this is poor, for say, Newton-Krylov method is that for an example when there is one dominant eigenvalue, the power iteration that produces the Krylov subspace, $\mathcal{K}_n = b, Ab, A^2b, \ldots$ will tend to converge to the most dominant eigenvector, and hence its known that such methods work best when the eigenvalues are clustered near unity.

So effectively, by reposing the problem by inverting the diagonal operator I am effectively rescaling space as one might do by either preconditioning or by defining a Sobolev norm to use instead of the usual L_2 norm.

misc Also now that I am more comfortable with the fundamentals I am moving away from the direct matrix notation in favor of code that only uses function calls in order to evaluate the linearization of the spatiotemporal problem through finite differences rather than explicitly forming the spatiotemporal Jacobian matrix. This will take time, PC will probably argue that I have been wasting my time and or doing the wrong thing all along because this is what Newton Krylov methods really calls for but that would be wrong; a Krylov subspace need not be generated by repeatedly evaluating finite difference approximation of the Jacobian matrix, it can instead by generated by power series of the Jacobian matrix if it is formed explicitly. The main problem with form this matrix explicitly is that it can be impossible due to memory constraints but so far I haven't hit that threshold. Regardless of this disagreement it will be better to rewrite a different version of the code.

spatiotemp continueds Running current hybrid method formulation on a batch of initial conditions to see if I can get anything to converge.

known bugs The initial condition generation code still needs to be improved for pre-periodic orbit type spatiotemporal solutions as a false discontinuity is forming when I conjoin the fundamental domain and its reflection together to form spatiotemporal initial conditions.

Getting some unnatural results in the GMRES portion of the Newton-Krylov code where increasing the size of the Krylov subspace gives worse corrections, should not be possible; I think a debugging procedure using Rossler is in order; The function definitions are all written generally so it shouldn't take a lot of time.

2016-11-29 Matt :

Coding I added code that works in physical space after computing derivatives in Fourier-Fourier space, the main incentive was to try and see if Jianke Yang's claim that it's better to work in the "PDE framework" agrees with me. Sadly it doesn't seem to be the case for me. I didn't do things exactly like he did, and I guess what I in fact implemented could be described by saying "everything is the same except the linear system of equations that I need to solve are in terms of the physical velocity field u and not its spatiotemporal Fourier components."

During this process I find it rather confusing and intriguing that the code I have written that compute hooksteps minimizing the quadratic residual $|Adx-b|^2$ with the constraint $|dx|^2 \leq \delta^2$ where delta is some trust region *seems to only work in physical space for me*. The main culprit is that when trying to minimize the quadratic form $|Adx - b|^2$ we rewrite this to exploit the fact that GMRES calculations have already been performed; Namely using the arnoldi iteration recursion relation between the matrices

$$AQ_n = Q_{n+1}H_n \text{ where}$$

Q_k refers to a matrix whose columns span the kth Krylov subspace, to rewrite the quadratic residual as,

$$|H_n s - b|^2 \text{ where},$$

$dx = Q_n s$. Performing a singular value decomposition on H_n allows us to simplify the problem such that linear system becomes diagonal. i.e. with $H_n = UDV^\top$, and performing some algebra, we are left with
$$|D\hat{s} - \hat{b}|^2$$

In the above equation $\hat{s} = V^\top s$ and $\hat{b} = U^\top Q_{n+1}^\top b$, with $\hat{s}$ being constrained to be within a trust region described by delta. $|\hat{s}|^2 \leq \delta^2$. The main way that this problem is tackled by Dennis and Schnable [10] is to assume the dependence on a new parameter μ such that

$$\hat{s}_i = \frac{\hat{b}_i}{d_i + \mu},$$

and then use a modified Newton method to find zeros of the function
$$\Phi(\mu) = |\hat{s}(\mu)|^2 - \delta^2.$$

The reason why they use a modified Newton (one that seems to be very specific to the problem) is that due to the form of the presumed

dependence on μ the regular Newton is found to be suboptimal in the sense that it always undershoots when making correction. The form of the modified Newton to optimize this μ is the following

$$\Delta\mu = \frac{|\hat{s}(\mu)|\Phi(\mu)}{\delta\prime\Phi(\mu)} \tag{15.72}$$

which can be seen that the modification is in the form of the prefactor $\hat{s}/\delta$

Now the main problem (with unknown reasons) is that the for the spatiotemporal problem in Fourier-Fourier space, the residual vector is much smaller in magnitude, such that $\prime\Phi(\mu)$ is near zero; and as such the process essentially contains a division by zero. This is discomforting as it makes it seem like perhaps the hookstep isn't so well suited for whatever reason. GMRES still works fine, although the dimension of the Krylov subspace for adequate reasons reaches the hundreds per Newton iteration.

GMRES with the reformulated problem does indeed work better than in the original problem it seems. As strange as it sounds, basic Newton works for the original formulation of the spatiotemporal equations but not for the reformulated equations that have bene rescaled by the laplacian like terms; for GMRES its the exact opposite.

mohammad spatiotemporal adjoint The first iteration of this doesn't seem to work too well; I'm unsure if this is due to some parameters in the integrator (i.e., do I need more spatial Fourier modes?) or a bug elsewhere.

[4]

2017-12-12 Matt hookstep Added in sophistication that John Gibson uses, but frankly I am getting much better results by just using GMRES and little the dimension of the Krylov subspace go higher.

The sophistication compares the reduction in residual of the spatiotemporal mapping between a linear model, quadratic model, and the hookstep correction. Either I am not optimizing the parameter that determines the hookstep correctly or the trust region isn't being determined well; The change I made was to have the radius of the trust region start with a value equal to the L_2 norm squared of the residual, as an arbitrary larger number makes it so the optimization process fails; which is to be expected I suppose.

---

[4]Matt 2017-12-06: The problem seems to be one of different scales, the magnitude of the typical element of $\hat{b}$ is of order 10^{-6} while the order of the typical element of D, the diagonal matrix that arises is of order 10^2; this large discrepancy ensures that the modified Newton is ill-defined as the values for $\prime\Phi$ will be very close to zero.

Lopez reformulation Trying to rewrite the relative periodic orbit code so that I can avoid using slices for two main reasons, in order to rescale the equations to better work with GMRES and to avoid the in-slice parameterization. This will instead of quotienting the SO(2) symmetry but instead keep track of it via a shift parameter. The way the López *et al.* [25] discusses this is that it reduces the two-frequency problem on a torus to a one frequency problem. The main reason is that when using slices it makes it hard to rescale the equations by the Laplacian squared term like I have done for pre-periodic orbit solutions. The reason I want to do this is because GMRES seems to work much better with the rescaled equations as it's preconditioning in a way. The general interpretation is that it's a choice of moving frame where the parameter determining the what??

2017-12-13 Matt .

initial condition generation Testing more stringent conditions to hopefully produce better initial conditions for spatiotemporal code, they're crude bounds such that during the close recurrence searching procedure there is now a maximum allowed value for the L_2 norm, and after a Poincaré intersection has been obtained there is now a trial to compute what the L_2 norm would be for the resultant spatiotemporal mapping. This is helping produce some better initial conditions which will be passed to the hybrid adjoint Newton-Krylov code I have currently. I'm also trying to be less brash by choosing a value for the initial domain size that is closer to the $L = 22$ domain size, currently I am trying to find pre-periodic orbits for a $L = 24$ domain size.

Also instead of the whole save point routine I have elected to go for random initial conditions and integrating out the transients each time as sometimes I would end up on the stable manifold of an equilibrium for a long time which would waste a lot of computing time.

relative periodic orbit reformulation Realized that reformulating the relative periodic orbit spatiotemporal code to encode the SO(2) shift with a parameter is a larger undertaking then I thought, due to all of the different dependencies of the code I have currently; The general idea is that the shift can be parameterized by time, although I still feel like this is somehow only incorporating a specific time of translation; In other words I can't shake the feeling that

The general idea is to produce an ansatz for the relation between endpoints (initial point and the endpoint i.e. point after one prime period) on a relative periodic orbit in such a fashion (described in terms of spatial Fourier modes to make the representation of the translation easier),

$$\hat{u}_k(0) = e^{ikSt/T_p}\hat{u}_k(T)\,, \tag{15.73}$$

where the spatial drift, shift, etc. is parameterized by time and a shift parameter S. The form of the rescaled spatiotemporal mapping would then take the following form.

$$
\begin{aligned}
x &= (\hat{u}, T, L, S) \\
G(x) &\equiv D_X^{-1}((D_t + D_S)\hat{u} + D_x F(F^{-1}\hat{u})^2) - \hat{u} \\
D_X &\equiv D_{xx} - D_{xxxx}
\end{aligned}
\tag{15.74}
$$

where x is a vector representing all of the varying quantities $(\hat{u}, T_p, L, S)$, and D_S is an operator representing the time derivative of the exponential prefactor in (15.73)

Then the spatiotemporal fixed points would be the zeros to this function $G(x) = 0$ otherwise referred to by me as the spatiotemporal mapping.

2017-12-13 Matt I think most of my problems might be solved by developing a little bit more patience; By producing finer time integrations in the initial condition generation procedure and allowing the hybrid adjoint descent to run for longer I am getting closer to convergence, as opposed to have things quickly be produced and quickly converge.

The implementation of the bounds and other associated quantities for hooksteps and double doglegs in refs. [7, 13] are what ??.

2017-12-14 Matt spatiotemp Finally got a machine precision convergence for an arbitrary initial condition (i.e. not one of the solutions provided by someone else). I believe if I run the adjoint hybrid method long enough and have an accurate enough initial condition then the convergence is global.

The method uses the adjoint descent and then is followed up with Newton-Krylov hookstep where if the GMRES solution does not reduce the residual significantly enough then the hookstep is calculated with the conditions provided by ref. [7]. The trust region radius is determined by if the first hookstep in each Newton iteration is successful in reducing the residual then the radius is doubled, and every time it fails it is reduced by half.

The main issue now is to try to trawl state space for the best possible initial conditions for the method.

The solution that was found was initialized by finding minima of the L_2 norm of a close recurrence procedure and then the entire spatiotemporal representation was produced by time integration. This next point is probably going to be the most contentious point I'm going to make, but in order to get a better initial condition for the full spatiotemporal problem I passed it to the variational Newton descent I had in time to correct the tangent in time first. I don't think this is being too restrictive because the residual (L_2 norm of

(a)

(b)   (c)
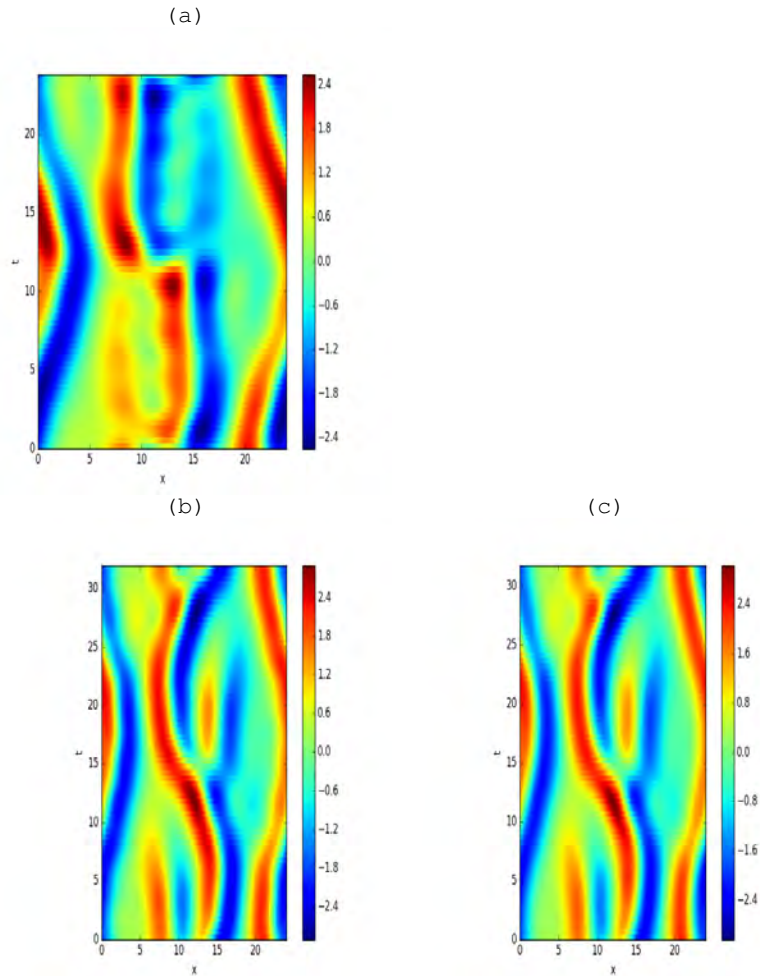
Figure 15.10:   (a) The very rough initial condition produced by close recurrence and intersection of a Poincaré hyperplane determined by a state space point's reflection $L = 24, T = 23.8125$. (b) Where the spatiotemporal initial condition ends up after variational Newton-descent in time $L = 24, T = 31.997939649161918$. (c) The final spatiotemporal fixed point after hybrid adjoint descent with the reformulation of the preperiodic spatiotemporal mapping, with final domain size and period $L = 24.0714310445, T = 31.8597201649$.

the spatiotemporal mapping) only changes by one order of magnitude in the original formulation or two orders of magnitude in the rescaled formulation (15.58). So, even though it has been converged in the time-dynamical system sense, it is still many orders of magnitude away from machine precision residual in the spatiotemporal residual sense.

For comparison, a periodic orbit that is reproduced with known coordinates and time integration would have a spatiotemporal residual would most likely start around 10^{-6} if has been produced well.

The reason I did this was merely to improve the initial conditions. I don't find it to be somehow cheating because when I pass it to the spatiotemporal problem everything is still allowed to change just in the way that it was if I had passed the original initial condition to the spatiotemporal problem. This can likely be conquered by merely producing better initial conditions, which I think can be achieved with more patience in the process.

Something else I could do is try the adjoint descent in physical space as opposed to Fourier-Fourier space.

2017-12-20 Matt : Tried to trawl state space for initial conditions for my spatiotemporal code and realized that it ran really slowly for small step sizes (large number of steps). Figured out how to speed it up by rewriting some key parts of the close recurrence calculations; realized I was sloppy when it came with the actual optimization previously. Essentially by unrolling some 'for'-loops and rewriting some key portions I was able to dramatically speed it up.

Instead of the Poincaré constraint in addition to close recurrence calculations, which are in my mind somewhat redundant because I'm trying to compute approximations I instead played around with a number of different procedures that only relied on close recurrence calculations, i.e. minimizing the L_2 norm of the difference between two state space points.

Something that I experimented with numerically was a procedure that computed a coarse time-integration and then if the L_2 norm was within a certain tolerance, it would be recomputed with an increased number of time steps. This would produce great initial conditions in a small number of cases, where the local minima in the close recurrence diagram actually corresponded to a recurrence, as it would rightly increase the accuracy of both the starting point of the orbit, the ending point, and the period. I'm sort of deciding between this and just running one close recurrence trawl with fine integration, because in the majority of cases the local minima of the L_2 norm is just happenstance and not related to a useful recurrence. One of the symptoms of this is that in certain instances the finer time-integration would actually increase the minimum of the L_2 norm. This didn't make sense to me, and could be due to the exact way I had the procedure implemented, i.e. taking the minimum from the coarse close

recurrence procedure and then using it as the starting point for the fine close recurrence procedure might be too hopeful, and it might be best to just start at the same point with the same time range.

So, essentially I sped up the routines to give at least better performance in terms of number of initial conditions, but the accuracy of such initial conditions could use a little tweaking in terms of bounds and implementation.

References

[1] Å. Björck and G. H. Golub, "Numerical methods for computing angles between linear subspaces", Math. Comput. **27**, 579–594 (1973).

[2] A. Bouras and V. Fraysse, "Inexact matrix-vector products in Krylov methods for solving linear systems: A relaxation strategy", SIAM J. Matrix Anal. Appl. **26**, 660–678 (2005).

[3] S. Boyd and L. Vandenberghe, *Convex Optimization* (Cambridge Univ. Press, Cambridge, 2004).

[4] P. N. Brown and Y. Saad, "Hybrid Krylov methods for nonlinear systems of equations", SIAM J. Sci. Statist. Comput. **11**, 450–481 (1990).

[5] N. B. Budanur, P. Cvitanović, R. L. Davidchack, and E. Siminos, "Reduction of the SO(2) symmetry for spatially extended dynamical systems", Phys. Rev. Lett. **114**, 084102 (2015).

[6] T. F. Chan and K. R. Jackson, "Nonlinearly preconditioned Krylov subspace methods for discrete Newton algorithms", SIAM J. Sci. Statist. Comput. **5**, 533–542 (1984).

[7] G. Chandler and R. Kerswell, Simple invariant solutions embedded in 2D kolmogorov turbulence, 2013.

[8] K. T. Chu, "A direct matrix method for computing analytical Jacobians of discretized nonlinear integro-differential equations", J. Comput. Phys. **228**, 5526–5538 (2009).

[9] P. Cvitanović, R. L. Davidchack, and E. Siminos, "On the state space geometry of the Kuramoto-Sivashinsky flow in a periodic domain", SIAM J. Appl. Dyn. Syst. **9**, 1–33 (2010).

[10] J. E. Dennis and R. B. Schnabel, *Numerical Methods for Unconstrained Optimization and Nonlinear Equations* (SIAM, Philadelphia, 1996).

[11] X. Ding, H. Chaté, P. Cvitanović, E. Siminos, and K. A. Takeuchi, "Estimating the dimension of the inertial manifold from unstable periodic orbits", Phys. Rev. Lett. **117**, 024101 (2016).

[12] C. Dong and Y. Lan, "Organization of spatially periodic solutions of the steady Kuramoto-Sivashinsky equation", Commun. Nonlinear Sci. Numer. Simul. **19**, 2140–2153 (2014).

[13] Y. Duguet, C. C. T. Pringle, and R. R. Kerswell, "Relative periodic orbits in transitional pipe flow", Phys. Fluids **20**, 114102 (2008).

[14] L. Elden and V. Simoncini, "Solving ill-posed linear systems with GMRES and a singular preconditioner", SIAM J. Matrix. Anal. Appl. **33**, 1369–1394 (2012).

[15] J. van den Eshof and G. L. G. Sleijpen, "Inexact Krylov subspace methods for linear systems", SIAM J. Matrix Anal. Appl. **26**, 125–153 (2004).

[16] M. Farazmand, "An adjoint-based approach for finding invariant solutions of Navier-Stokes equations", J. Fluid M. **795**, 278–312 (2016).

[17] M. van Gijzen, "A polynomial preconditioner for the GMRES algorithm", J. Comput. Appl. Math. **59**, 91–107 (1995).

[18] C. Greif, T. Rees, and D. Szyld, "GMRES with multiple preconditioners", SeMA Journal, 1–19 (2016).

[19] A.-K. Kassam and L. N. Trefethen, "Fourth-order time-stepping for stiff PDEs", SIAM J. Sci. Comput. **26**, 1214–1233 (2005).

[20] K. Kirchgässner, "Wave-solutions of reversible systems and applications", J. Diff. Equ. **45**, 113–127 (1982).

[21] D. Knoll and D. Keyes, "Jacobian-free Newton-Krylov methods: a survey of approaches and applications", J. Comput. Phys. **193**, 357–397 (2004).

[22] Y. Lan, Dynamical Systems Approach to $1 - d$ Spatiotemporal Chaos – A Cyclist's View, PhD thesis (School of Physics, Georgia Inst. of Technology, Atlanta, 2004).

[23] Y. Lan, C. Chandre, and P. Cvitanović, "Variational method for locating invariant tori", Phys. Rev. E **74**, 046206 (2006).

[24] Y. Lan and P. Cvitanović, "Variational method for finding periodic orbits in a general flow", Phys. Rev. E **69**, 016217 (2004).

[25] V. López, P. Boyland, M. T. Heath, and R. D. Moser, "Relative periodic solutions of the complex Ginzburg-Landau equation", SIAM J. Appl. Dyn. Syst. **4**, 1042–1075 (2006).

[26] J. Meza, A modification to the GMRES method for ill-conditioned linear systems, tech. rep. (Sandia National Laboratories, 1995).

[27] K. Morikun, L. Reichel, and K. Hayami, "FGMRES for linear discrete ill-posed problems", Appl. Numer. Math. **75**, 175–187 (2014).

[28] Y. Nesterov, "A method of solving a convex programming problem with convergence rate O($1/k^2$)", Sov. Math. Dokl. **27**, 372–376 (1983).

[29] C. C. Paige and M. A. Saunders, "LSQR: An algorithm for sparse linear equations and sparse least squares", ACM Trans. Math. Softw. **8**, 43–71 (1982).

[30] A. Politi and A. Torcini, "Towards a statistical mechanics of spatiotemporal chaos", Phys. Rev. Lett. **69**, 3421–3424 (1992).

[31] S. B. Pope, *Turbulent flows* (Cambridge Univ. Press, Cambridge, 2000).

[32] L. Reichel and Q. Ye, "Breakdown-free GMRES for singular systems", SIAM J. Matrix. Anal. Appl. **26**, 1001–1021 (2005).

[33] D. Reynolds, R. Samtaney, and C. Woodward, "Operator-based preconditioning of stiff hyperbolic systems", SIAM J. Sci. Comput. **32**, 150–170 (2010).

[34] P. Riley, "On the probability of occurrence of extreme space weather events", Space Weather **10**, S02012 (2012).

[35] Y. Saad, "A flexible inner-outer preconditioned GMRES algorithm", SIAM J. Sci. Comput. **14**, 461–469 (1993).

[36] G. L. G. Sleijpen, J. van den Eshof, and M. B. van Gijzen, "Restarted gmres with inexact matrix–vector products", in *Lecture Notes in Computer Science*, edited by Z. Li, L. Vulkov, and J. Waśniewski (Springer, Berlin, 2005), pp. 494–502.

[37] S. Tajima and H. S. Greenside, "Microextensive chaos of a spatially extended system", Phys. Rev. E **66**, 017205 (2002).

[38] T. E. Tezduyar, M. Behr, S. K. Aliabadi, S. Mittal, and S. E. Ray, "A new mixed preconditioning method for finite element computations", Comp. Meth. Appl. Mech. Eng. **99**, 27–42 (1992).

[39] L. N. Trefethen and D. Bau, *Numerical Linear Algebra* (SIAM, Philadelphia, 1997).

[40] D. Viswanath, "Recurrent motions within plane Couette turbulence", J. Fluid Mech. **580**, 339–358 (2007).

[41] D. Viswanath, "The critical layer in pipe flow at high Reynolds number", Philos. Trans. Royal Soc. A **367**, 561–576 (2009).

[42] M. Xu and M. R. Paul, "Covariant Lyapunov vectors of chaotic Rayleigh-Bénard convection", Phys. Rev. E **93**, 062208 (2016).

[43] J. Yang, "A numerical method for computing time-periodic solutions in dissipative wave systems", Stud. Appl. Math. **134**, 420–455 (2015).

[44] M. Zahr, P.-O. Persson, and J. Wilkening, "A fully discrete adjoint method for optimization of flow problems on deforming domains with time-periodicity constraints", J. Comp. Fluid. **139**, 130–147 (2016).

Chapter 16

Matt's 2018 blog

2018-01-08 Matt initial conditions I believe all but one issue are ironed out now, the only problem that still arises is when an orbit gets stuck near an equilibrium for the entire length of time integration of a close recurrence will the initial condition generation produce something not worthwhile.

The way that this was accomplished was by tuning the restart procedure as well as tuning time integration in the close recurrence procedure, as well as the total time being integrated, number of time steps. I have abandoned the Poincaré hyperplane in favor of this fine time integration. I also abandoned playing around with running a coarse time integration and then refining it as this produced strange results. I thought that it would merely produce a larger region around the local minimum (region of the close recurrence plot) by tuning the amount of time integrated of the second time integration as well as increasing the number of time steps but sometimes this procedure would either restart in the wrong spot or miss the local minimum returning a larger (in terms of the residual of the L_2 norm of the difference between starting and final points.) Therefore, I decided it was wrothwhile due to other speed-ups to just perform the finer close recurrence and if nothing is found then just restart.

spatiotemp code In between testing these new initial conditions I have decided to rewrite and add some different ways that the hookstep is calculated. This is due to there being a lack of safety nets for when the hookstep code previously would fail and the code would have to abort. This seems to be due to trying to optimize a hookstep for too large of a trust region. While normally you would just check the residual and then if it isn't reduced, one would reduce the trust region and continue. But, in my case this would lead to numerical overflow and the code would abort. Therefore, a safer, more constrained optimization protocol had to be adopted. Now, the pa-

rameter that computes the size of the corrections is always bounded and if it fails to lie in these bounds, a value is chosen based on the iteration.

In other words when asked to find a vector $\hat{s}$ that minimizes $||D\hat{s} - \hat{b}||_2$ subject to $\hat{s} \leq \delta$, the general solution is given by [5, 16],

$$\hat{s} = \frac{\hat{b}d_i}{d_i^2 + \mu} \text{ (no summation)}, \qquad (16.1)$$

i.e., this is the solution that minimizes $\Phi(\mu) = ||s(\mu)||^2 - \delta^2$.

Now I will elect to follow the procedure in ref. [16] that instills bounds on the parameter μ. The lower bound will be chosen by the "normal" Newton procedure instead of the one that is adapted to solve for μ for this problem.

During each iteration to update μ, we calculate lower(ℓ) and upper (u) bounds by

Initializing them at first by $\ell_0 = -\frac{\Phi(0)}{\Phi'(0)}$ and $u_0 = |\nabla F(x_c)|/\delta_c$.

Then at each step for the lower bound we increase the lower bound by taking the maximum between

$$\ell_+^N = \mu_c - \frac{\Phi(\mu_c)}{\Phi'(\mu_c)} \qquad (16.2)$$

and the current lower bound.

To update the upper bound we decrease it by taking the minimum between the current upper bound and the current value of mu,

$$u_+ = min(u_c, \mu_c) \qquad (16.3)$$

where $+$ indicates the next value of the parameters, and "c" indicates the current value (following [16] notation as to not confuse myself). The next iterate μ_+ is calculated by the 'adapted' Newton method.

$$\mu_+ = \mu_c - \frac{s(\mu_c)}{\delta_c} \frac{\Phi(\mu_c)}{\Phi'(\mu_c)} \qquad (16.4)$$

and then tested to see if it lies in our trusted region $[\ell_+, u_+]$. If it doesn't, then the next iterate μ_+ is taken to be $max((\ell_+ u_+)^{1/2}, 10^{-3}u_+)$ which Dennis and Schnable claim is most often used to calculate the initial value μ_0.

We then let the iteration run until the norm of the hookstep lies in our trust region. (I might change this to be until the residual of the function $\Phi(\mu)$ is minimized sufficiently).

After these changes, we then need to decide to do with the trust region and our current hookstep. If the hookstep does not minimize the residual sufficiently when compared to the linear model,

we need to decrease the trust region radius (which they just do by halving it but also give details on calculating a multiplier between one tenth and one half). If the residual compares favorably to the quadratic residual then we can keep this as a backup step before increasing the trust region radius by a factor of two and attempting to try again.

2018-01-10 Matt Finished the implementation of most of the changes to hook-step and initial condition generation, whether they need any changes is up to testing that is proceeding now.

Used new initial condition generation code to generate a few hundred guesses for spatial domains that take integer values in the range $L\exists[22, 43]$. Now I just need a little time to run code and see if anything converges

2018-01-12 Matt invariant 2-tori Fixed errors in the blog. Uploaded Figures, now to expand on them.

The first set of figures figure **??** is an example of using variational Newton descent in time to improve an arbitrarily poor initial condition such that it converges under application of my spatiotemporal fixed point code after the Newton Descent.

The second set of figures in figure 16.1 is an example of convergence without using any modfication beforehand via Newton Descent. The solution was converges to within machine precision by using a hybrid method. Namely, the initial condition was first run through Mohammad's adjoint descent and then once a certain number of steps had been taken (In practice this is set to a fixed number of steps but it is usually a sufficient number to reach a region where the adjoint descent only provides marginal improvement). Secondly, it was sent to an adaptive Newton method, that decreases the residual of the cost functional by decreasing the step length until this is ensured. I elected to try this method because even though I completely changed the hookstep code it still doesn't seem to be up to snuff when it comes to efficiency.

The perplexing part about the spatiotemporal fixed point in figure 16.1 is that while the initial condition represents one period of a pre-periodic orbit, the final, resulting spatiotemporal fixed point is seemingly five copies of a shorter orbit (in time). As there is little difference between (b) and (c) in figure 16.1 it seems this is due to the adjoint descent. It could just be an inaccurate initial condition, or perhaps the adjoint descent is missing the longer orbit for its shadow.

initial conditions It turns out the vast majority of initial conditions were equilibria; I instilled a lower bound that should prevent these from being generated, but it's a very heuristic process.

2018-01-16 Matt Robust modes in hydrodynamic flows Read Professor Gunaratne's paper that is the focus of his planned talk here. I was going to
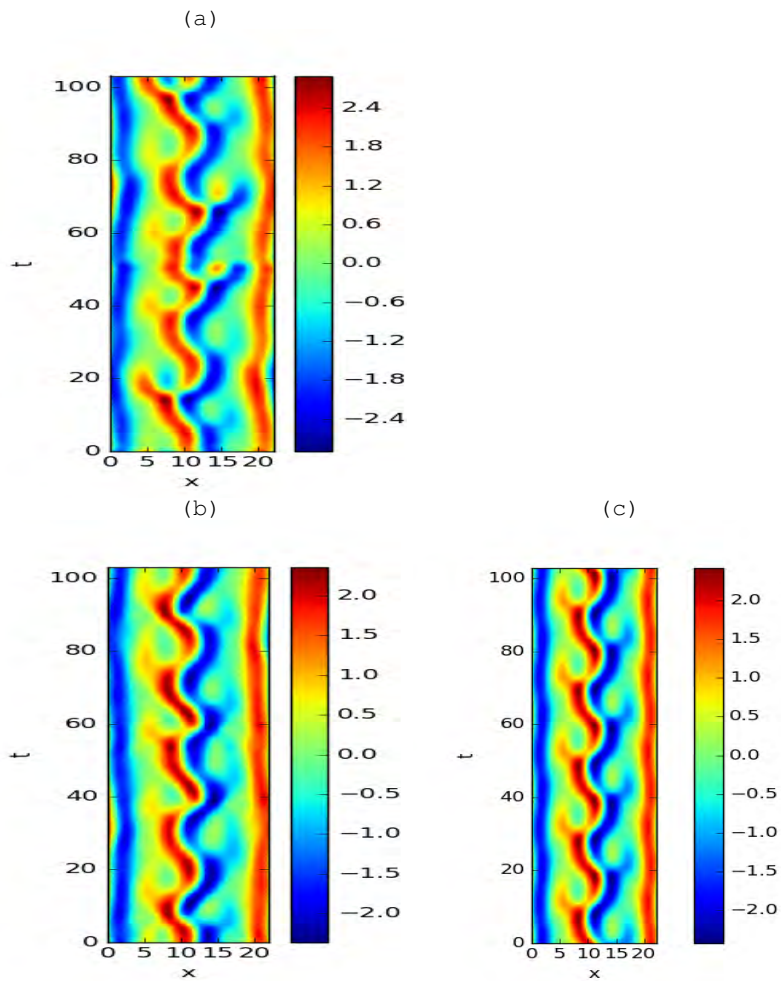
Figure 16.1: (a) Initial spatiotemporal initial condition, whose dimensions are $(L, T) = (22.0, 103.125)$. (b) Approximate spatiotemporal fixed point after adjoint descent, $(L, T) = (22.026, 103.13)$. (c) Converged spatiotemporal fixed point after hybrid method, $(L, T) = (22.232, 102.94)$.

ask whether partitioning simulations in space and comparing their spectra would also be a valid or worthwhile endeavor as currently he takes a series of snapshots of the flow in a computational cell, uses subsets to compare spectra in time. (I believe the subsets were the full series, the first half, the second half, even numbered snapshots and odd numbered snapshots). Dynamic mode decomposition is then performed on these subsets and robust modes are defined by modes that are common to all subsets.

spatiotemp Almost done with the automation procedure to find spatiotemporal fixed points associated with pre-periodic orbits. I combined the initial condition generation code and the solution converging code into one Python script. What it will do is work through different domain sizes one-by-one, produce initial conditions for the convergence code, and if the initial conditions satisfy certain requirements on the residual of the cost functional, run the convergence code on it. Currently have it setup so that long trawls of state space are performed as opposed to shorter more accurate trawls, getting some weird results so it could be the step size is too large, however.

hookstep Fixed the bugs regarding trust region being too large; in which case the optimization procedure would fail or give nonsensical results because the parameter involved would diverge towards negative infinity. In other words, it seems to work when the approximate solution first evaluted at $\mu = 0$ in (16.1) is larger than the trust region. I.e. it works when $|\hat{s}(\mu = 0)| > \delta$. Then, by the effect of increasing μ ensures that the solution's norm is being scaled back to within the trust region. If the norm of $s(\mu = 0) < \delta$ then the optimization tries to enlarge the approximate solution by making the denominator smaller via cancellation. I find no mention of the in ref. [16] but they do have a chapter on rescaling. The reason why this is so confusing to me is that I thought by using my reformulated, rescaled equations I would have already dealt with any scaling issues but it seems it isn't so easy. I'm going to test if whether the original formulation shares this property or not, meaning that it could be the case that the original equations are more useful in using the hookstep method and the rescaled equations are better for descent and regular Newton methods. I find this hard to be the case because I know a properly scaled matrix is almost required for GMRES to be useful, as it includes power iteration of matrix vector products so maybe there is still yet another problem with the hookstep code that hasn't been found as of yet.

slides Uploaded some crude slides with the basic ideas of what I'm working towards. Hopefully will be able to discuss with Professor Gunaratne.

2018-01-18 Matt tori finder Have the automated code up and running on my

terminal, still need to learn how to tweak its priority, strangely the CPU usage during the close recurrence procedure is seemingly soft limited to one core but the convergence code is jumping to all eight cores. Going to keep an eye on it for the time being.

I might elect to do a different residual criterion that just uses norms, right now it calculates a time integration series, and its reflection. Then the close recurrence criterion is based on the L_2 norm between the reflected series and the physical one; the rational being that if we pass through one prime period of a pre-periodic orbit, then the endpoint should be the reflected partner of the initial point. The problem with this is for every time t the L_2 norm of the difference with every reflected future point must be computed. A more efficient solution might be to just compute all of the L_2 norms once and then trust that if an initial point has a similar norm of a reflected endpoint, then they are symmetric under reflection. This seems hopeful, and I feel like I'm almost being academically dishonest at this point because this is yet another idea from López *et al.* [43].

rpo reformulation Reformulating the relative periodic orbit portion of the code to use a co-moving frame. This is the only option I believe if I would like to rescale the equations, as the first Fourier mode slice would be very nasty. This method also avoid rescaling time.

The general idea is akin to López *et al.* [43] where the approximate solution or initial condition is shifted into the co-moving frame to first make the initial condition truly periodic and then the inverse shift is kept track of so that the "true" solution (the one in the initial frame) can be recomputed after convergence. If I've understood everything this should allow for the following equations, note the very similar rescaling by the inverse of the diagonal operator containing the second and fourth powers of the wavenumber.

The one trade-off of this method is increasing the dimensionality of the problem by one, this is because of the extra parameter keeping track of the shift.

$$
\begin{aligned}
G(\hat{u}, T, L) &\equiv D_X^{-1}((D_t + S)\hat{u} + D_x F(F^{-1}\hat{u})^2) - \hat{u} = 0 \\
D_X &\equiv D_{xx} - D_{xxxx} \\
S &\equiv diag(\frac{-im\ell}{T})
\end{aligned}
\tag{16.5}
$$

where, the definition of the operator S comes naturally from the definition of the shift required to transform from the co-moving frame to the initial frame, $\hat{\hat{u}} = e^{\frac{-im\ell_p t}{T}}\hat{u}$. I'm cheating for the sake of simplicity in typing the equations because I'm actually using the real-valued representation where the operator is actually an off diagonal SO(2) type matrix.

2018-01-21 Matt automated code Automated code snagged over the weekend due to an error in the minimum allowed trust region length. Easy fix, restarted, It had found only the trivial equilibrium solution before this restart. On a more optimistic note, limiting the cpu usage and other related matters are much easier than I anticipated. For some reason I had it in my head I had to do this in Python which makes me laugh now because I run my scripts on the terminal through the command prompt. For reference using the 'nice' command sets priority and 'cpulimit' is pretty self explanatory.

rpo reformulation I think I have the way I need to implement the co-moving frame code down, but there are some intricacies that I need to decide on before I try to assimilate the new code into the old, like when and how I solve for the initial shift factor, whether this is done after the initial condition is generated or after its passed to convergence code. The functions that are required are well on their way. Before implementing these things spatiotemporally I'm making sure I understand the shifting procedure in Fourier $\times t$ so that I don't flounder around like I have in the past. Also going to be doing my testing with the shortest relative periodic orbit from Xiong's library.

2018-01-22 Matt Picking some of the low hanging fruit with adjoint Newton method, uploading some more figures and converged data. Still working on the co-moving frame implementation for relative periodic orbit code. Taking longer than I thought, finished the implementation for the shifting parameter now just need to redefine the spatiotemporal mapping, and some partial derivatives.

Went to an interesting talk on the dynamics and input-response analysis of worms and fruit flies. Apparently the locomotion of worms can be described by only four eigenmodes.

2018-01-23 Matt Torus Jacobian matrix In a ChaosBook course lecture, Predrag asked me to formalize the $\mathcal{T}^2$ Jacobian matrix, the Jacobian matrix of the torus that has semi-flow properties in space and time. I believe one would say this is a specific case of a Jacobian matrix for manifolds with two compact continuous directions. It must obey periodicity in space and time, as opposed to just time in the dynamical systems point of view.

coding Still writing the new relative periodic orbit code, and my treatise on why I believe it will work. Need to talk to Predrag as he believes that a comoving frame representation is just the wrong way of handling things. I agree that this is by no means quotienting any symmetries, but I figured that the main benefits (No slicing, no time rescaling,easily recovering the full state space representation of the torus) outweighed the downside of having to keep track of a shifting parameter, marginal direction. I believe Predrag would say that

I merely need to extend the idea of slicing and Poincaré sections to the spatiotemporal world view but this has always confused me, hopefully for good reason.

spatiotemporal fixed points The automated code running on my terminal has only acquired equilibria (trivial and nontrivial) so I need to make some changes. I dramatically increase the time integration lengths in order to hopefully acquire more accurate guesses, but have yet to see if this is improving things or just slowing things down. Will report tomorrow hopefully.

2018-01-30 Matt Co-moving frame write-up and motivation

Spatiotemporal Jacobian matrix on the torus

Miscellaneous Tried to define a CFL type condition for the initial condition generation code, also improved the approximate period.

Main problem is getting stuck at equilibria because time steps are too large and the time integration cannot resolve

2018-01-31 Matt plumbers Christian Hafner gave us a presentation about the elastica problem and how the basins of attraction for the convergence of Newton's method to find solutions that minimize a bending energy cost functional are fractal.

comoving frame write up large write up coming soon

2 torus Jacobian matrix write up Here are some templates from the temporal stability discussions:

example 1.1 p. 30   example 1.2 p. 30   example 1.3 p. 31

2018-02-12 Matt My writing has turned into a greater endeavor than I realized, due to the fact that when it's out of context it's hard to follow. I've added what I currently have to `siminos/spatiotemp/chapter/reportMNG.tex`, it's amazing how hard it is to write coherently in a scientific paper type style rather than a blog.

That's how I'm approaching this, as the beginning of a paper or my thesis proposal.

Also updating a bunch of codes. For more scientific writing refer to changes in `MNGReport.tex`

2018-02-12 Predrag Thanks for taking the initiative, I've been thinking along the same lines. Remember, your thesis proposal and thesis templates are in `siminos/gudorf/`, so start moving science parts of the blog rather than `siminos/spatiotemp/chapter/reportMNG.tex` (this currently has one macros to fix) there - we need this also for papers, once we are ready to write them...

2018-02-16 Matt Floquet Theory for PDEs Requested the text, Floquet Theory for Partial Differential Equations (1949) by Peter Kuchment [39] to help with spatiotemporal Jacobian matrix. On this note, I went to the math talk `A Newton-like Method for Computing Normally Hyperbolic Invariant Tori` but didn't learn much as it was de la Llave's new student's first talk. They basically discussed results from [28].

Afterwards, I questioned Prof. de la Llave and he said that what I was trying to do was basically Bloch's theorem, because Floquet Theory is a linear theory. I'm going to wait to get the book by Kuchment [39] until I make a verdict. Also he recommended the work of a poor man who was sent to a Siberian work camp and led a sad life afterwards, Serguei Kozlov, and his work on the reducibility of quasiperiodic differential operators. Sadly, I have yet to find this work in a language other than Russian. Other searches of the same topic led to multiple papers but I can't tell whether they'll be of any use. I did find one that seemed somewhat promising but I'll have to read it before I can really tell.

Introduction to Ergodic Theory The following are collections of notes from Leonid Bunimovich's talk on `Introduction to Ergodic theory`

Ergodic Theory began with Boltzmann when trying to describe the statistical behaviors of many body systems in a classical sense.

For a state space with associated σ-algebra and measure. The major questions were whether invariant measures that are consistent with dynamics exist. The definition of invariant measure was built with the notion of preimages, because even in the simplest example of a non-injective function, the image of a subset will increase in size but the pre-image of a non-injective function will remain invariant. Example given was the tent map. The length of the image of any interval will double in length, but the preimage maintains the same length, therefore length (Lebesque measure)is an invariant measure of the tent map when described with respect to preimages. Formally, this is written,

$$\mu(T^{-1}A) = \mu(A) \,,$$

where, A is a subset of the state space $\mathcal{M}$.

For a generic system there can be numerous invariant measures, so the next question that arises is what are the natures of invariant measures?

If we know an invariant measure of a system, what can we say about the time average of a system (discrete or continuous time). I.e. given an invariant measure, does

$$\lim N \to \inf \frac{1}{N} \sum_{m=0}^{N-1} f(T^m x),$$

exist? Is it finite? (T is the operation associated with mapping in discrete time, m).

What follows are known as *Ergodic Theorems*. The more important example, due to Birkhoff, proved that for $f \exists L^1$ then the aforementioned limit converges to another function denoted $\hat{f}(x)$, and the other more important result that,

$$\int_{\mathcal{M}} \hat{f}(x) d\mu = \int_{\mathcal{M}} f(x) d\mu$$

From this integral relation, between $\hat{f}$ and f it follows that the time average (the previously mentioned limit) equals the space average (integral over state space) for any measureable (invariant) function. This, stated in a slightly different context via the Poincaré Theorem on Recurrences states that for a subset, A, and invariant measure μ. If $\mu(A) > 0$ then almost all points of A return to A *infinitely* many times. This tells us explicitly that dynamics are recurrent, but tells us not about the nature of the recurrences (the times between recurrences of two distinct points in A are essentially random).

The next point I did not fully grasp when spoke about, but suppose B is a subset of points in A such that

$$B = x \exists A : \forall k > 0, T^k x \exists A \tag{16.6}$$

The follow point was that none of the preimages of B intersect B, $T^{-m}B \cap B = $, and because of the invariant measure, $\mu(B) = 0$.

The next topic, was the work of Gibbs. Define the correlation function

$$\int_{\mathcal{M}} f(T^n x) g(x) d\mu(x)$$

With invariant measure μ this converges in the infinite time limit to the product of integrals of f and g over the state space with respect to this measure. Physically, this is a statement that a non-equilibrium system converges to a equilibrium state due to the system being ergodic?

Finite Time Dynamics I was slightly late to this talk so the discussion I heard began with discussion of so-called "open systems" where you have a statespace, then cut a non-measure zero hole in it such that there is a non-zero "escape" from the system.

My favorite Bunimovich quote arose early in the discussion. "Escape rate was introduced by Physicists so even if it is a natural thing to ask about, it might not be reasonable."

He lead an introduction to the topic by introducing correlation functions between sequences (denoted "words") of a coin-tossing game, where the correlation function measured the likeness of words in such a manner. Given the word "abracadabra", the (auto)correlation of it with itself is measured by seeing if the words match, if so, we count a value of one. If not, zero. Then we shift the second word (not periodically) and then count how many times the words match. So for abracadabra the (auto)correlation would be equal to a binary sequence whose length is equal to the length of the word, with corresponding ones and zeros. (10000001001) in this case. This can easily be seen by the presence of only one letter "c" in the word, so until the shift rids us of the "c", we will not have a match. Once the "c" is gone, we match again with "abra" and the final "a".

Prof. Bunimovich then led a discussion on some of the counterintuitive results that follow from this definition of correlation function, namely that shorter words implied faster "escape" from the open system (as defined by the measure I believe)??

The second half of the talk really took me for a spin, when he started discussing the "first hitting probability" or "first passage probability". I really did not understand this but the main take away was that for finite time interval (discrete graph that was represented by a curve) before an intersection in the first hitting probability before one word ultimately wins out. Like I previously mentioned, I really didn't grasp this but I think the general idea was that there is a finite time interval where things can be predicted, but in dynamical systems we are always studying the behavior after such behavior ends?

Spatiotemporal Navier Stokes With the concept of a very small number of active spatiotemporal modes, usually due to discrete symmetries I applied this in a very rough way to test the number of active modes in one of the shortest orbits (in time) of the HKW computation cell, also known to channelflow users as "p19p02".

I first took $M = 16$ points in time (16 snapshots) of the shortest periodic orbit whose spatial discretization requires $N_x = 32 \times N_y = 49 \times N_z = 32 \times 3 = 150528 \equiv dim(\mathcal{M}_{xyz})$ physical space variables to describe. The total number of variables in the spatiotemporal discretization is then $150528 * 16 = 2408448$.

To test the number of "active modes" spatiotemporally, I used real-valued FFTs in the spanwise and streamwise direction, and the discrete cosine transform (which I think is equivalent to the Chebyshev coordinates but I could be drastically wrong) in the wall normal direction. To describe the number of active modes I counted the number of spatiotemporal coefficients, now $(Fourier \times Fourier \times Chebyshev) \times Fourier$ in three directions, had a absolute value (not the square) that was greater than 10^{-14}.

I claim that in the shortest periodic orbit 'p19p02' is $N_{active} = 564477$. In other words, approximately seventy-five percent of the spatiotemporal information is redundant/not used. Therefore, for a full spatiotemporal description using 16 points in time in this basis, the number of variables used to describe it only increases by a factor of 3.74998007015. This is a nontrivial increase in dimensionality, but much less than the expected multiple of 16.

For $M = 32$ the reduction percentage increases, but so do the number of modes corresponding to time. The multiple for $M = 32$ was 7.26536591199, which is slightly less than two times the $M = 16$ multiple. I believe that this is due to extra modes in time which themselves are non-active.

I still need to test this on a case that has non-zero shift, but in order to exploit these methods I need a truly periodic orbit not a fundamental domain, so the number of points in time would have to increase by two, and I am unclear whether it would be as beneficial or even better.

2018-02-19 Matt Reading The *Floquet Theory of Partial Differential Equations*, Kuchment [39] was a large waste of time for me. Try as I might I don't have enough formal mathematics training to understand the complexity nor the depth of such things.

Been looking for more mentions of Normal Linear stability of Tori, which in mathematics lingo is the stability pertaining to transverse directions of tori. Seems to be the right direction to go.

Added Broer, Hoo and Naudot [1] to siminos.bib, seems promising but I need to induce solitary confinement and read it 20 times to truly understand it.

code Found an error in the initial condition generation code, fixed, playing around with finite difference approximations for Jacobian matrices, which I seem to have trouble with. Spent too much time on this as I understand exactly what should happen but it seems to have a lot of difficulties when dealing with spatiotemporal equations for whatever reason.

Tried for the longest time to get it to work for the Rössler system which seems to give me more difficulty than Kuramoto-Sivashinsky for whatever reason, probably experience. My comment towards Rössler is that the variational Newton method works so well that it's the only numerical method that should ever be applied to it to find periodic orbits.

Writing Moved scientific writing to thesis proposal section, tried to get more done but it's a slow endeavor so far. Nothing is sacred in those tex files so feel free to comment.

2018-02-22 Matt Most of my day Either listened, discussed, or talked about Physics all day. Had the plumbers meeting followed up by the

talk `Particle induced viscous fingering` (which I found very accessible and overall a great talk). After lunch I had an afternoon discussion with Predrag about the spatiotemporal cat-map, the tiling used and the symbolic dynamics and the differences between Percival-Vivaldi linear code and the new linear code using Adler-Weiss coordinates. This began with a treatise on what being symplectic means in terms of the symplectic group, and its action on the normal bundle and conservation of pairwise areas, and the implications therein.

After an enjoyable mid afternoon coffee Noah DeTal began a discussion with me about working through the method of slices of the wave equation with spatially periodic boundary conditions. After some thought I came to the conclusion there was no need for such machinery really because any relative equilibrium solution could be made into an equilibrium by the appropriate Galilean coordinate transformation, and the fact that the equations are linear reinforced this idea, because we know any solution can be represented as a superposition of complex exponentials with the correct wavenumbers. My intuition might be wrong but it seems that its really the nonlinearity that makes the requirement of fancier methods to deal with symmetry. I'm no expert in PDEs but this seemed good enough to me.

Likewise, after my discussion with Noah, another one of my graduate student colleagues, Zack Jackson; Professor Wiesenfeld's student discussed his simplified model that he created and is using to describe the motion of a ring which contains so-called "smarticles" (tiny robots with a prescriptive behavior). This went on for about an hour at which point I began to describe my work to him again because, in his words, "Every time you explain what you are trying to do I feel like I understand it less." and "I don't see a clear goal in mind". This took two hours to sort out and the conversation ended with him becoming even more pessimistic due to the numerical difficulties, although I tried to end it on an upbeat note. He believes there's no way that this is going to work, but then again this isn't really his type of problem, i.e. one that's well suited with his skill set. He's great and picking out the important processes and taking averages thereby creating simple models for certain processes. The comparison between my work and many-body Quantum Mechanics was made which was slightly disheartening but I am hopeful that my research will lead to *something*, although it could be like the most recent Plumbers paper whose importance seems to me to be left to the winds of Fate.

actual work Otherwise the *actual* work was to compute the Jacobian matrix of the spatially periodic orbit resultant from one of the temporal equilibrium. It's either a numerical issue due to the dramatic digres-

sion between the orders of magnitude of Floquet Multipliers but I was unable to show prove the equality $Jv = v$, which is likely due to the lack of precision of the marginal Multiplier. This is not making me very hopeful for the spatiotemporal periodicity but there might be some issue that I didn't account for as of yet.

Readings Still chipping away at ref. [25], [4] and [1]

2018-02-25 Matt Reading Reading and really trying to understand ref. [1] as I think that there are good things there once one passes over notions such as "versal unfolding" (no prefix on versal, although they seemingly add "trans" or "uni" in front depending on very specific circumstances unknown to the reader).

It's opening my eyes because they describe a $\mathbb{T}^n$ symmetric Torus, one that is equivariant in n dimensions as being an underlying object upon which a vector field is laid onto. This isn't a revolutionary notion but it does help a bit in the abstractification. The interesting part is how they describe tori as living in a higher dimensional space $(N + 1)$ due to the varying of a parameter μ.

> The nondegeneracy condition means that the normal linear, leading part
>
> $$NX_\mu(x, y) = \omega(\mu)\frac{\partial}{\partial x} + \Omega(\mu)y\frac{\partial}{\partial y} \qquad (16.7)$$
>
> of X is transversal to the conjugacy class of NX_0 in the space of normally affine vector fields. Such a generic condition plays a role in persistence results in the following sense. At the level of affine conjugacies and affine vector fields, the transversality condition provides the persistence of the tori $(y = 0)$ by the unfolding theorem... Without the invertibility of $\Omega(0)$, this transversality property in general will be lost. As a result, the persistence of invariant tori is not guaranteed.

Piecing this together is a little tough for me, especially thinking of an entire vector field X as transversal to the conjugacy class of the normal bundle. I believe the next statement is the reason why they assume $\mu = 0$ in most examples.

> By the Inverse Function Theorem, the invertibility of Ω_0 implies that, for each μ in a neighborhood of 0, the vector field $X(\mu)$ locally has exactly one single invariant torus T_μ. Again by the Inverse Function Theorem, up to a μ-dependent translation, we have $T_\mu \cong T_n \times 0$. From now on we shall assume this simplification to have taken place.

numerical experiments While fixing inconsistencies introduced by implementing mean velocity frame code, I experimented with how
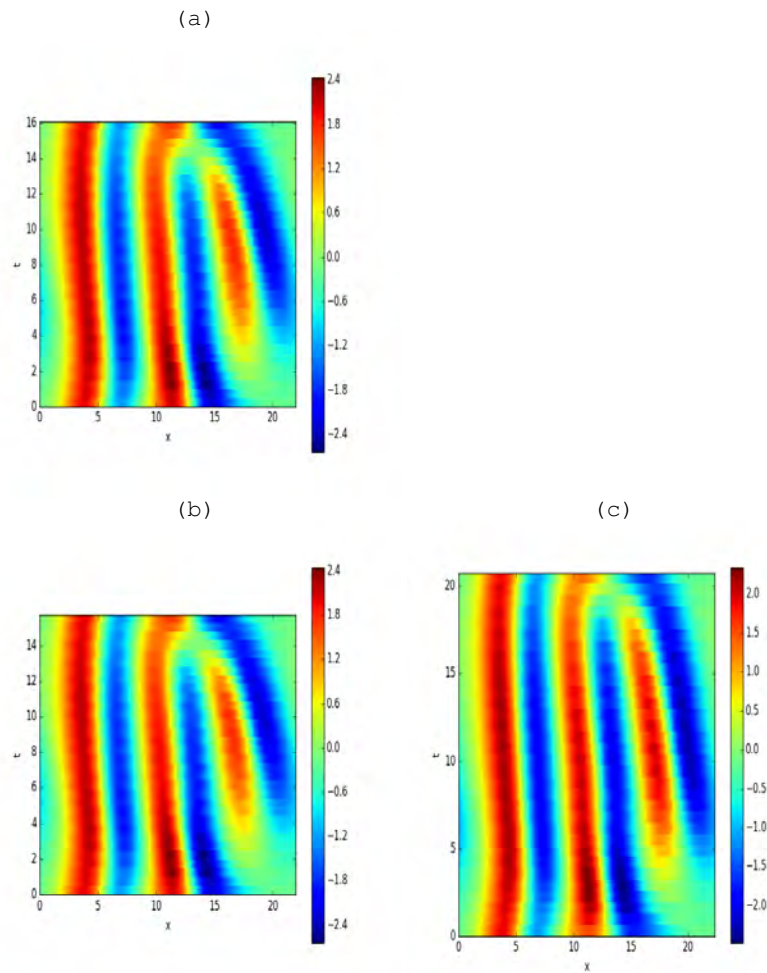
(a)

(b)   (c)

Figure 16.2: (a) Converged $\text{rpo}_{22\times16.3}$, in the mean velocity frame. (b) Identical to (a), except for $L_0 = 22 - \pi\sqrt{2}$. (c) Likewise to (b), except $L_0 = 22 + \pi\sqrt{2} - 1/8$. Exact details (numbers) in 2018-02-25 blog post.

much I could change the domain size parameter L for the test case, the shortest (time) relative periodic orbit at $L = 22$. When only varying the domain size I found that there was a wider range of convergence than I had thought.

I thought this was a result perhaps of using a least squares Newton-type method, but when I was able to create a new constraint now I have a square linear system (I tried to implement some constraint on the tranversality to shifting, but found that I have to subtract out the spatial translation direction to get this specific linear system to work). In other words, my three additional constraints that I add to make the linear system square are

$$
\begin{aligned}
< \frac{\partial u}{\partial t}, du > &= 0 \\
< \frac{\partial u}{\partial x}, du > &= 0 \\
< (\dot{\phi} - 1) \cdot \mathbb{T}, du > &= 0
\end{aligned}
\tag{16.8}
$$

The in-depth details on $\dot{\phi}$ are in `done.tex`, in my thesis proposal section, but simply put $\phi(t) \cdot \mathbb{T} \in \mathfrak{so}(2)$, such that the corresponding Lie group element $g = \exp(\phi(t) \cdot \mathbb{T})$, $\phi(t) = \frac{\sigma t}{T_p}$ transforms the relative periodic orbit into the mean velocity frame. The reason for the subtraction of one is to remove any component in the spatial translation direction, otherwise it is nearly linearly dependent with the second constraint.

New figures So, I produce a square linear system, solve it, and solutions are unique right? Not quite it seems. I am able to very (seemingly) continuously the domain size until approximately $\pm pi\sqrt{2}$ (Half of the most unstable wavelength), wherein convergence is no longer guaranteed. Therefore, the new figures depict converged solutions that start with identical quantities other than domain size. It gets even stranger, one might notice the upper bound being slightly less than half of the most unstable wavelength, this is in fact due to not being able converge at exactly half; *however* if I go to $pi\sqrt{2} + 1/64$ it *does* converge spatiotemporally. I suppose a fuzzy boundary is to be expected, but it seems counterintuitive to me at least

The exact data for figure 16.2

(a) $T_0, L_0, \sigma_0 = 16.314805095414, 22, -2.87478470726$,
$T_f, L_f, \sigma_f = 16.05715597431866, 21.976838394845288, -2.9005450692620047$.

(b) $T_0, L_0, \sigma_0 = 16.314805095414, 22 - \pi\sqrt{2}, -2.87478470726$
$T_f, L_f, \sigma_f = 17.210152777052322, 22.085913422049373, -2.9162371552096955$

(c) $T_0, L_0, \sigma_0 = 16.314805095414, 22 + \pi\sqrt{2} - 1/8, -2.87478470726$
$T_f, L_f, \sigma_f = 14.46304615768534, 21.79212000706519, -2.897881739121017$

Jupyter Finally sat down and looked into how to use jupyter code note-
books. I'm not sure it'll be that useful because of how I have seg-
mented my code but I'll probably be using it for faster calculations
from now on.

2018-02-27 Matt math talk Went to how to make a black hole in a vaccum
with gravity waves. Apparently the requirement is that all of the
papers on this topic are 600 page monoliths where mathematicians
play with bounds of objects in order to globally the metric tensor (in
terms of a finite region of spacetime) in order to prove that the result
is a trapped region, claiming that Penrose showed that a trapped
region implies a singularity. This was done by using the Einstein's
equations in Vaccuum and then implying bounds on different quan-
tities to remove all lower order terms. In six dimensions (five space
plus one time) he said he can prove that unstable naked singularities
exist, unstable in the sense that if you poke them they get shy and
cover up.

lunch talk Listened to Jim Gates and ate my fill of (free) pizza. Listened
to his story about how he became a Physicist, started a life in public
policy as well as making documentaries. When I personally asked if
he had any advice for graduate students today he really thinks that
one must be very intentional in their plans in terms of setting a goal,
then really breaking down how to achieve that goal. I think this is
generally good advice for how to live a good life.

searching for answers Spent most of the research portion of the day try-
ing to scour literature about whether collocation methods (Galerkin,
etc.) are valid in the presence of changes of domain size. Found
nothing similar. The idea I was having is that most of the time pseu-
dospectral and spectral methods are used is when they discretize
equations such that each discrete point is a fixed node on some grid
with equidistance spacing. The spatiotemporal code might behave
so poorly because although there is periodicity in time and space,
changing the period and system size L is equivalent to changing the
spacing of the rectangular spacetime grid. I couldn't find any exam-
ples where this is done other than continuation, where the domain
size, period, or likewise any other scalar parameter is treated as a
knob that remains fixed during the search for minima of the cost
function.

2018-03-06 Matt Notes on rotation number talk The following are from the notes
taken from the talk given by Evelyn Sander in her presentation.
About half of the talk was about numerics and how well things con-

verge given certain criteria. I'll try to stick to the topics as best as I can.

The following are references she mentioned at the end of the talk refs. [13–15]

The first is of letter-style, the second is longer and actually a paper that was published in Nonlinearity, and the third is a prepublished paper on arXiv.

She also cited Levnajić and Mezić but without a specific paper.

Professor Sander first introduced the notion of rotation with the mapping of a torus,

$$T_p : \theta \to \theta + \rho(mod1) \,,$$

where ρ is defined as the "rotation vector" with irrationally related components (no rigid rotation).

There is a *choice of coordinates* such that we can define,

$$F(\theta) = \theta + \rho(mod1) \,, \tag{16.9}$$

such that we can then use the trajectory of θ with respect to the map F ,which is denoted $\{\theta_n\}$, to compute the rotation vector ρ.

The next part is an example calculation of how to get ρ with a one dimensional map on a circle and a trajectory of points $\{\theta_n\}$. Let p be a point that lies in the circle's interior (not necessarily the center). Then with the trajectory of points, let $\Delta_n = \theta_n - \theta_{n-1}$. They calculate ρ using,

$$\rho = \lim N \to \inf \frac{1}{N} \sum_{n=1}^{N} \Delta_n mod1 \tag{16.10}$$

In other words, they are using averaging to calculate the irrational rotation vector. This is slow, and she admits it, that's why most of the talk was broken into two subsections, which are additional methods employed to help with convergence. The first is called the "Birkhoff weighting method", and the second is called the "Takens embedding method".

Side Note: She also wanted to be explicit about the problem being solved so there was a side note about calculating such things in higher dimensions.

Given A, a unimodular($det = \pm 1$) $d \times d$ matrix, let,

$$
\begin{aligned}
\bar{\theta} &= A\theta \\
\bar{\theta}_{n+1} &= \bar{\theta}_n + A\rho \\
d > 1 &\Rightarrow A\rho(mod1) \text{ is dense in the torus,} \tag{16.11}
\end{aligned}
$$

In such a case, she says to restrict to a submanifold M, being one or two dimensional and with the projection map from the torus to M,

$$\Phi : T \to M , \qquad (16.12)$$

to then compute ρ_Φ from $\{\Phi_n\}$.

The remainder of the talk were examples and explanations of the two methods used to speed to convergence of the averaging method to find ρ

The first of which was the Birkhoff weighted averaging. For a sequence of points of an iterative map $x_n \equiv F^n(x_0)$. Define the Birkhoff average as,,

$$B_N(f) = \frac{1}{N} \sum f(x_n) \to_{\text{large N}} \int f(x) d\mu(x) \qquad (16.13)$$

This quantity can be shown to have $\mathcal{O}(1/N)$ convergence, Prof. Sander claims this is because we're taking an inherently infinite object (non periodic trajectory) and cutting off a piece of it. To account for this she and collaborators weighted the Birkhoff sum with the following factor.

$$\omega_p(t) = \exp -[t(1-t)]^{-p} \qquad (16.14)$$

Numerical evidence suggests that the speed of convergence depends on how flat it is at the endpoints, where she showed graphs of varying smoothing procedures. Paraphrasing: Because the exponential has infinitely many derivatives equal to zero at the endpoints, we get this better behavior.

The rest of the talk is much more easily explained using figures rather than words, So I'll point them to the papers if anyone is interested.

In conclusion what I learned is that you can measure angles of quasiperiodic structures but in all of the cases where one actually sits down can averages how the angles change on a given trajectory you seemingly need to be able to pick a point inside of the quasiperiodic structure in a region where the "winding number" is equal to plus or minus one.

2018-03-07 Matt Defense of is spacetime? For today's plumbers meeting the only people who attended were Burak, Roman, Elena and I. For all intensive purposes it turned into a thesis defense for our spacetime project.

My main idea that pushed the conversation into a discussion that I feel turned into a 'thesis defense' type conversation was that for invariant 2-tori with Z_2 isotropy subgroup, I have not found a way to calculate corrections to the system size L, or in other words ways to define a constraint for the underdetermined linear system due to allowing changes

to the period and domain size T, L. The ubiquitous constraint that is imposed in almost all Newton-Krylov methods are constraints that prevent corrections (solutions) to the linear system from having components in the spatial, time translational directions. In mathematical terms, for a Newton correction, the following constraints are imposed by the first two equations in (16.8).

The problem is that the spatial translation direction is an invalid constraint for pre-periodic orbits due to the reflection symmetry.

I described the benefits of going into Fourier-Fourier space and the resulting subspaces that occur for solutions with discrete symmetries but the main point that both Burak and Roman stressed were that because these solutions constitute a one-parameter continuous families of solutions in the parameter L, that no matter the result of convergence of my code, the solution that is chosen from this family is going to be dependent on the solver. I really had to stress that I'm allowing the domain size to vary as a parameter of the calculation and the way to view it is a scaling factor that corrects the magnitude of the spatial tangent space, much like how the period will rescale the magnitude of the tangent space in time.

They still were not convinced. Burak says I should only look for periodic orbits at different domain sizes and then use pseudo arc-length continuation to get the solution at different L values. I suppose this issue will not be resolved until I introduce a constraint such that the solution that is retrieved by my code is, for instance, the particular member of the family of solutions that has minimal area, or some other constraint. This might be what *would* make my code special; it says "A'ha! you see there is a special representative of this one parameter family of solutions, and not only that but this is the one that appears in large spacetime calculations."

Burak says he is worried because I've been focused too much on numerical methods which I agree with, and am missing out on the general idea of the project. I agreed with Burak that even though the appearance of doubly periodic solutions in a large space time simulation is impossible, that likely there would be an interior region of such solutions that would be (hopefully) shadowing my tiles well; in an exponential sense much like the spatiotemporal cat map. We agreed that the manifestation of a small spacetime solution need not be a particular representative of the one parameter family of solutions, so how will any comparison be made? Again I tried to argue that there will be a subset of the interior that should satisfy shadowing exponentially well but I'm not sure if this will be the case.

- The problem arises with the domain size changing: Burak and Roman remain unconvinced that allowing the domain size to vary through the calculation is necessary or even a good idea.

- Roman claims that whichever solution I converge to is more likely a property of the solver than something special.

- Burak thinks it's much better to calculate periodic orbits in time and then use pseudo arc length continuation to get them at different sizes.

- It seems until I can find some special criterion (minimal area, energy, etc.) that picks out a representative of the continuous family of solutions, they will not be on board.

2018-03-07 Predrag Do not worry about professor's opinions, it's hard for them to digest new ideas, but that Burak does not get it is worrisome. Precocious professoritis?

The main point of going spatiotemporally infinite in both time and space is to let dynamics set both spatial and temporal scales (in our way of thinking, the spatial and temporal periods of the shortest invariant 2-tori), not impose them by hand. It works for short times, infinite space - see Michelson [44]. It is pretty and not at all mysterious. The gentlemen have not studied it, but Lan and I have, it is described in Lan's thesis [40]. We have a clean theory ("equilibria of equilibria") of why equilibria and relative equilibria have the spatial wavelengths they have, a theory that mashes well with the web of periodic orbits for Kuramoto-Sivashinsky [12].

The gentlemen just happen to be the right age to have been indoctrinated to accept that for chaotic temporal dynamics, the periods of periodic orbits are intrinsic to solutions, it would never occur anyone use a pseudo arc length continuation to find them for a given system (i.e., a system with all parameters and b.c.'s fixed). Were they born 30 years earlier, they would think deterministic chaos could not arise. Whether they can digest the idea that spatial periods are also intrinsic to the system at hand, i.e., that "space is time," I cannot predict. Not your problem.

We have conceptual and computational problems, but not on this level. Revolution will not, will not, will not be televised, but it will be on YouTube. You'll come on top:)

2018-03-07 Matt Transpose vector product. I'm indebted to Roman because even though I've scoured the literature for a matrix free representation of the product $J^\top x$, he pointed out that Ravi did this, and after some thought I realized that if I can explicitly form the Jacobian matrix, then reverse engineering what this matrix vector product might be possible. The problem lies in the fact that Ravi used finite differences to define derivatives so that the product with the transpose is much more straightforward.

In my Fourier-Fourier description this is going to be harder, but I believe that the only difficulty will be the reverse engineering of how to compute the nonlinear component, as the linear component is fairly straightforward.

In more depth, the action of the linear component for Z_2 type solutions can be represented by matrix multiplication by a tridiagonal matrix, with the main diagonal being filled with $-q_n^2 + q_n^4$, and the two off diagonals filled with terms $\pm\omega_m$ (no i because in real-valued representation). Therefore action of the transpose only affects these off diagonal terms by swapping the signs of them $\pm\omega_m \rightarrow \mp\omega_m$. This is exactly the action produced by sending $T \rightarrow -T$.

Therefore, the linear component of the matrix vector product (here lin subscript denotes 'linear'),

$$J_{lin}^{\top}(\epsilon dx) = \frac{1}{\epsilon}(F_{lin}(u+\epsilon du, -T+\epsilon dT, L+\epsilon dL) - F_{lin}(u, -T, L)),\quad (16.15)$$

where $dx = \{du, dT, dL\}$. Because the transposition only affects the component of the Jacobian matrix that is constituted by swapping the sign of the time derivative, we can make the substitution in the function call.

The nonlinear term is much less straightforward and will take a little work, if its possible at all.

The main goal is to be able to write the matrix-vector product in terms of function calls so that no matrices are explicitly formed. This would dramatically increase the speed at which my adjoint descent code runs and due to the global convergence of the method, and the speed when used in a hybrid method, this might be exactly the robustness that we need to find large doubly-periodic spacetime solutions at least.
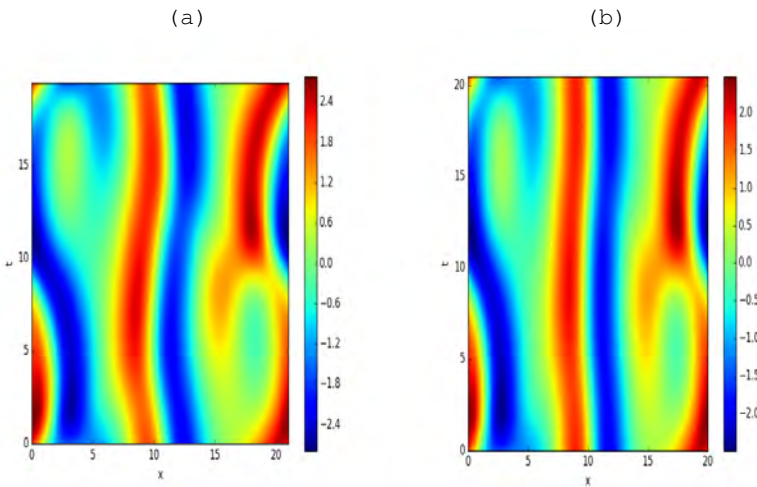
(a) (b)

Figure 16.3: (a) Spatiotemporally converged $\text{ppo}_{22\times10.2}$ given "wrong" initial domain size $L_0 = 20$. (b) Spatiotemporally converged $\text{ppo}_{22\times10.2}$.

2018-10-29 Predrag What is the difference between figure 16.3 (a) and (b)? The initial condition for (a) was identical for (b) (shortest pre-periodic

orbit from $L = 22$, *except* the initial domain size of (a) was purposefully chosen to be the ("wrong") value $L_a = 20$. This was just a test to see if the solution would still converge given relative error of domain size.

2018-03-09 Matt coding More work into relative periodic orbit matrix-vector product formulation of the spatiotemp code.

Still trying to figure out what I can use as extra constraints. For pre-periodic orbits I can still constrain to be transverse to time translations to give me corrections but because of the reflection symmetry I cannot impose tranversality to the spatial translation direction, which is what is used to complete the underdetermined linear system. Maybe I'm thinking about it the wrong way as usually these are just implemented as constraints to prevent the Newton correction from pointing in symmetry directions, and so I might be able to use the

I sort of went down a rabbit hole as to test what extra constraints are possible I tested a constraint the prevents changes in area. This was easy enough to implement, and it worked, but its the exact opposite of what I would like to accomplish. The tangent space(s) are what should be telling me the correct scales for L and T. Because of this I tried to impose a constraint such that the area is minimized but I can't currently think of a way that doesn't do this *too well*. What I mean by this is that if you say that you want to minimize $T * L$ then it will just send one of those parameters to 0, naturally.

One interesting thing that came about from the area constraint is that if you tell my code the wrong area. If for instance I changed L_0 to $L_0 - 2 = 20$ then it had to change the characteristic wavelength in time to fit in my box. Including figures for scientific curiousity.

The main idea I'm trying to flush out here is that if I cannot use tranversality constraints to complete the linear system then perhaps I need to complete the linear system by creating constraints on the parameters themselves.

pseudo arc-length constraint Investigated this method in hopes that maybe I could prove Burak wrong by including "pseudo arc-length continuation" in the actual spatiotemporal code at the same, but sadly it doesn't look like one can have cake and eat it too.

matrix free adjoint descent Calculating the nonlinear term in a matrix free way is harder than even I thought it would be. More write up on this coming soon.

pipeflow Kimberly gave me a nice introduction into pipeflow as well as personally typed notes and explanations. We did not however run anything as the PACE credentials had not come through as of our discussion, but she walked me through the structure of pipeflow and its utilities from her copy on hard. It's a lot to take in but I think with a little practice it shouldn't be too bad. If I ever decide I need

to do anything extra I will likely find ways of converting the data files to something that Python can handle just because I've become so accustom to it.

2018-03-09 Predrag Back to cranky fessors. You look at slide 12 of my APS March Meeting 2018 slides, and you can *see* spatial periodicity of about $\sqrt{2}$. I doubt that there are continuous families in the spatially infinite case - it looks like solutions come in continuous families, as we impose artificial spatial periodicity of L (the Fourier space is a subspace of the full, continuous Fourier space) and our solutions can be continued to nearby systems with slightly different L's. That does not necessarily mean the wildly unstable spatially infinite system has continued families of solutions. Though it might.

2018-03-10 Predrag Not sure why are we looking exclusively at pre-periodic orbit $\text{ppo}_{22\times10.2}$, other than that is what we had started with it (figure 13.28 and earlier). Figures 16.3 and 15.6 and the earlier such figures are equivariant under rotation by π around the appropriately chosen origin, and $u \to -u$, so one is working too hard - a fundamental domain would be easier to compute on. But I agree if the code is supposed to find a doubly-periodic orbit, it should find this one as well.

2018-03-14 Matt : Reponse to Predrag. I don't mean to look exclusively at pre-periodic orbit it just happened to be that for the longest time I only had the slicing spatiotemporal code and not the mean velocity frame code that I thought would work better. It does work better in the case where I derive explicit matrices but the additional parameter makes it slightly more complex in the matrix-free case, which is what I'm working on now: specifically matrix free Newton-Krylov hookstep (with left preconditioning) and matrix-free adjoint descent.

My main position on the fundamental domain for pre-periodic orbit is that it is unwise if you want to go to Fourier $\times$ Fourier, but is much better for using finite differences in Fourier $\times$ time. I tried to explain that using Fourier $\times$ Fourier presents us with a type of fundamental domain in `done.tex`, where only half of the spatiotemporal modes are non-zero. The analogy I tried to apply here is that we use the fundamental domain in configuration space because half of the flow field information is *redundant* due to symmetry. With using spatiotemporal Fourier modes half of the information is *unnecessary* due to symmetry. There aren't many hills that I will defend but one of them is that you want to use Fourier $\times$ Fourier without using a fundamental domain, because you get the advantage of exponential convergence of the Fourier coefficients in both (wavenumber,frequency number) indices, you get the reduced dimensionality due to the symmetry, and you get much better approximations to the derivatives due to spectral differentiation: multiplying by iq_n is much more accurate than using finite differences.
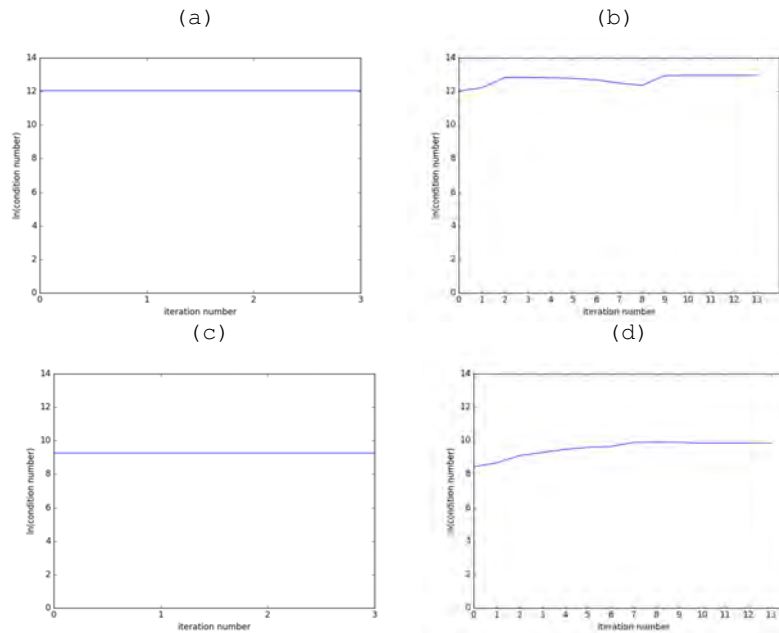
Figure 16.4: Logarithm of condition number versus iteration number for (1.43) with initial conditions (a)ppo$_{22\times10.2}$, (b) Initial condition from figure **??**(b). (c) and (d) are the same initial conditions but use (15.58).

2018-03-15 Matt : Trying to view the spatiotemporal equations in a more objective manner. Relearning some of the stuff I learned from Brown and Walker [2] on GMRES and ill-conditioned systems (output very sensitive to perturbations to input), determined by the condition number $\kappa(A) = \max(\sigma_A)/\min(\sigma_A)$.

As per usual[1] the engineers are more grounded in reality with these kinds of problems: A quote from some random lecture notes on condition numbers: "Usually, bad condition numbers, in engineering contexts, result from poor design. So, the engineering solution to bad conditioning is to *redesign*".

This is partly what I attempted to achieve by rescaling the equations in a way that I didn't realize was similar to Laurette Tuckerman's methods.

So currently this is what I'm faced with. For the matrix-free code I need constraints that do not make the approximation to the system nearly singular so what I've been doing is constructing constraints and checking the condition number of the resulting Newton-equation matrix.

This is then compared to the condition number of the underdetermined,

---

[1]Predrag 2018-03-15: Rechecked what the phrase "as per usual" means: "used for describing something annoying that often happens"
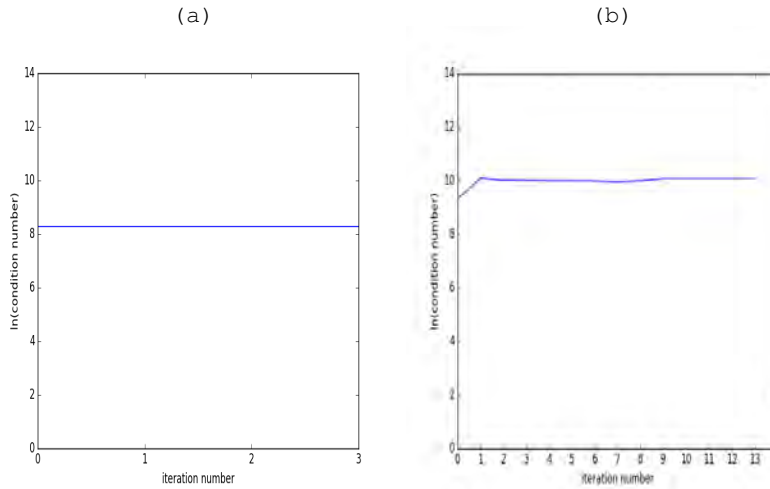
Figure 16.5: Logarithm of condition number versus Newton iteration with right preconditioning (a) $\text{ppo}_{22\times10.2}$ (b) Unnamed spatiotemporal initial condition from figure **??**

Constraint Types	κ_0
Least-Squares	172377.687831
$\frac{\partial u}{\partial t}, F$	103963203.961
$\frac{\partial u}{\partial t}$,zeroth-time	227405.009895
$\frac{\partial u}{\partial t}$,area	178091.066076

least-squares system which seemingly acts as a lower bound as far as I can tell. This is sort-of motivated by Brown and Walker [2] because they test GMRES on nearly singular systems by comparing the GMRES solution to what they would have received by using a pseudo-inverse.

Absolutely terrible constraints will make the solution singular. Bad constraints make the system nearly singular, meaning that accuracy of say, explicitly evaluating the inverse of the Newton-equation matrix would result in very inaccurate results.

Here is an example of the effect of constraints on the condition number $\kappa_{A_0} \equiv \kappa_0$ of the Newton-equation matrix.

The same computation but for (15.58) version of spatiotemporal fixed point code.

This investigation made me question whether "our condition improves" over the course of running my convergence code. figure 16.4 seems to indicate that (of course) the opposite is true! As you approach the invariant 2-torus the matrix becomes more ill-conditioned. This is mainly presented as a piece of evidence that the linear system that arises from

Constraint Types	κ_0
Least-Squares	10292.9974962
$\frac{\partial u}{\partial t}, F$	26706141.6672
$\frac{\partial u}{\partial t}$,zeroth-time	21901.7560002
$\frac{\partial u}{\partial t}$,area	10631.6286184

equations (1.43) and (15.58) are hard to solve to within machine precision. Well, no mystery there. What this really indicates to me is that without having a good preconditioner we might be lost in solving it in the more general (more complex spatiotemporal geometries) case.

Right preconditioning where the preconditioner is formed by rescaling by the linear portion of the equation (1.43), i.e., multiplying by

$$1/(q_n^2 + q_n^4 + \omega_m).$$

Comparison of figure 16.4 (c,d) and figure 16.5 (a,b) (respectively) we can see that reformulation of the equations has about the same effect as right preconditioning. I think preconditioning is going to be much easier for others to digest because technically the rescaling would make the corresponding inverse operator singular if $L = j\,\pi$, with j as any integer, but it has the advantage of being able to think of the converged solution as an actually fixed point of the reformulated equations (15.58), rather than as merely a root of (1.43).

2018-03-20 Matt spatiotemporal adjoint approximation Still trying to figure out if I can approximate the nonlinear matrix vector product $-J^\top f$, where the cost function is defined by $F = 1/2 f^\top f$. I thought this would be easy given that I have code that explicitly defines matrices so I thought it would be easy to reverse engineer what I need but it doesn't seem that easy unless I'm making some mistakes somewhere.

spatiotemp code Wrote the "reformulated" (rescaled) version of the mean velocity frame code for relative periodic orbit invariant 2-tori. As expected, it works a lot better with iterative methods such as GMRES.

I'm only able to get away with this reformulation because the diagonal terms corresponding to laplacian and laplacian squared operators dominate. For the mean velocity frame representation of $\text{rpo}_{22\times16.3}$, the condition number is reduced to around $\kappa \approx 2000$ which is about an order of magnitude better than pre-periodic orbit invariant 2-tori.

It seems that these reformulations will be necessary as the matrix free code relies on approximations to iterative methods. When the iterative methods fail for the exact problem (explicitly formed matrices) I know I'm in danger. Luckily the test cases I've run through

where, for instance, GMRES fails for the original equation but succeeds with the reformulated equations. Like I have mentioned before the reformulation is sort of a cheap trick I am using that could essentially be accomplished by preconditioning but I came up with some kooky ideas I want to try out to see if the reformulation of invariant 2-tori actually induces an iterative map or if I just think it does. Maybe I'm in fantasy land but because I am essentially rewriting (1.43), which can be drastically simplified as $F(u, T, L, \sigma) = 0$, as another equation $\tilde{F} - \hat{u} = 0$. I think the physical interpretation of the second equation is much clearer than the first, but it has its own issues as it demands for inversion of an operator that can technically become singular. The reformulated equations for the mean velocity frame invariant 2-tori can be stated as, [2]

$$G(\hat{u}) = (D_{xx} - D_{xxxx})^{-1}((D_t + S)\hat{u} + D_x F((F^{-1}\hat{u})^2)) - \hat{u} = 0, \tag{16.16}$$

where S is the derivative of the Lie algebra element, $\dot{\phi} \cdot \mathbb{T} = 2\pi n\sigma/TL$, such that $2\pi\sigma/L = \theta$ is the parameter needed to perform $SO(2)$ group action.

$$G(\hat{u}) = (D_t + S + D_{xx} - D_{xxxx})\hat{u} + D_x F((F^{-1}\hat{u})^2)) = 0, \tag{16.17}$$

where S is the derivative of the Lie algebra element, $\dot{\phi} \cdot \mathbb{T} = 2\pi n\sigma/TL$, such that $2\pi\sigma/L = \theta$ is the parameter needed to perform $SO(2)$ group action.

rabbit hole Was rereading sections about Chaosbook topics and went down the rabbit hole of Youtube lectures on modular forms, *L*-functions, asymptotics....etc. It opened my eyes on some things. I did find myself thinking about the trace formulas from today's class in ways that I might not have if I hadn't watched these lectures, and overall I said it went well other than attendance. Rasmus was afraid everyone was asleep so I tried to lead a discussion for the last thirty minutes or so about some random notions I recently learned which devolved into statistical mechanics and other topics.

grateful Rasmus I think Rasmus setup is such that as he writes, he does not see the screen with people faces, so he is talking into a grand void. You were great help to him, and stimulated a discussion about things he cares about. Rasmus writes :)

"Nå, så fik vi diskuteret sporformlen, jeg holdt mig til diskrete afbildninger, som du foreslog, og diskuterede PF og trace for Ulam-afbildningen, altså det tent map som er gennemgående eksempel.

Til sidst fik jeg engageret nogle af de andre (2!) lidt i samtalen, og så gik det meget bedre, især Matt var god til at sparke ind. Ellers var

---

[2]Matt 2018-06-28: This was not the equation I put in practice as the inversion of the Laplacian and Laplacian squared term turned out to not be useful.

det et spørgsmål om at forklare, hvordan brugen af en gen. funktion ikke "bare" er et smart trick, men at det både i det diskrete tilfælde (Z-transform) og kontinuerte (Laplace) fordrer, at man tænker på konvergensen. Det vil man jo også se, når man går lidt i dybden i forhold til hvor vi er nu. Jeg synes det er sjovt og det helt rigtige at starte arbejdet "the plumber way" uden at folk skal bruge et semester eller tre på at fare vild i Sobolev, Banach og Hilbert rum, men derfor tror jeg også man skal stoppe op en gang i mellem og sige, OK, her skal vi så lige passe på, vi har faktisk en konvergensradius, etc. Det gør du jo også i bogen, men jeg tror det er vigtigt at tage det op i diskutionerne, for der sidder en del og er lidt forvirrede...

Vi fik også talt lidt stat. mek. og termodynamik og at i stat. mek. er vores gen. funkt. af en funktionel form, der er fastlagt igennem et variationsprincip, og derfor ikke frit opfundet. Vi diskuterede også brugen af tilstandssummen, og jeg understregede dens fysiske betydning, hvilket er noget jeg ofte finder, at studerende har svært ved eller aldrig har hørt om!

Det er klart for mig, at jeg må forberede mig på en lidt anden måde til torsdag, hvor jeg går ud fra at jeg er på igen?

Jeg tror jeg skal opfordre folk fra starten til at bryde ind.

Tak for et super godt kursus, som er vildt inspirerende! For 26 år siden sad jeg til dit seminar i CATS og havde ørerne slået helt ud, og det er jo dejligt, at man kan komme tilbage efter så mange år og bare samle tråden op som om der nærmest ingen tid er gået. Det skyldes jo især det HELT ENORME arbejde der må været lagt i ChaosBook. Ganske enkelt fantastisk imponerende! "

balance I think it should be noted that I feel like my productivity has gone down over the past semester, but I've begun sleeping every day, exercising 5-6 days a week and actively participating in science outreach related volunteer work (Basically repeat volunteer of the Atlanta Science Festival). I think I'm putting this here because of the guilt that I feel when it comes to the opportunity costs of doing these activities. My mood is basically determined by how I think my research is going and its definitely been worse than it is right now, so I think I'm on the right track.

mens sana in corpore sano One cannot do twat without balance, and to me this hysterical social media era (that too will pass) seems to be a distraction that interferes with continued, calm concentration needed to solve hard problems. You are the right age to do it.

Sometimes the fastest way to get there is to go slow

2018-03-28 Matt spatiotemp I think I understand why the reformulated (rescaled) equations works so well with iterative methods even though the

pseudospectrum of eigenvalues of the Newton system is more localized. The most unstable eigenvalues correspond to the highest spatial wavenumber modes from looking at their spatiotemporal field representations. I think that the geometric convergence (i.e.small absolute value) of the spatiotemporal Fourier with high index numbers doesn't allow for the "dominant" eigenvalue to "dominate", per se. Meanwhile, the effect of the rescaling switches the roles in the pseudospectrum of the Newton system, where the small index spatiotemporal modes (who typically have the largest absolute value) get magnified, allowing the most contributing (pseudo)eigenvectors (generalized?) to dominate the iterative methods. In short, the rescaling changes the pseudospectrum so that the most dominate pseudo eigenvalues now correspond to the spatiotemporal modes with the largest magnitude.

automated spacetime convergence Now that I am comfortable with saying the the direct-matrix (forming matrices explicitly) methods will work for both Z_2 and $SO(2)$ isotropy subgroup (relative periodic orbit in its mean velocity frame) solutions I have been working on the matrix-free methods. This was done in a poor order however because I should have made the changes to the automated invariant 2-torus finder to run on light while figuring this out.

That being said, I am making some slight tweaks to the automated code such that the isotropy subgroup is not chosen a priori, but rather I just find the absolute minimum of the recurrence plot and then determine which isotropy subgroup is exhibited by this solution. In order to do this I need a more general comparison so that I don't accidentally filter out one or the other type, this is done by just looking at the absolute values of the spatial mode spectrum during the close recurrence integration, then passing the invariant 2-torus to a custom function to see if the solution has a smaller cost function residual as an relative periodic orbit or pre-periodic orbit. This is just a more general approach that I'm hoping will work in the long run. Because I am using the explicit matrix code I believe I won't be able to go further than discretizations that are much larger than $M * N = 64^2$, so I will be trawling for relatively less complex invariant 2-tori than I will hopefully achieve with the matrix free code.

matrix free code I believe the main source of error (due to the fact that I am using the same exact gmres code) for certain test cases is that the matrix-vector approximation is just too inaccurate to produce a reliable Krylov subspace to find solutions in. I'm attempting to work around this with higher order finite difference approximations for the matrix-vector approximations, but the difference upon the first iteration between the first order ($\mathcal{O}(\Delta x)^2$ error) and the higher order ($\mathcal{O}(\Delta x)^4$ error) is approximately $10^{-}10$. I need to compare the finite difference approximation to the explicit matrix computation still.

plumbers Burak and Predrag led a discussion about torus breakdown because of Burak's plots of unstable manifolds and some symmetry breaking bifurcations. I forgot my notes that I wrote down at the office but I recall refs. [21, 51] being the overarching reference along with two others I cannot recall.

Torus breakdown and Arnol'd tongues (that Arnol'd) were explained by Predrag in terms of circle maps with a weak nonlinearity, internal frequencies and external (forcing) frequencies. I never really understood what Arnol'd tongues were but the explanation of the overlapping and the width having to do with rational frequencies and resonances was enlightening.

Cilia by Eva Kanso Went to the nonlinear dynamics lecture presented by Eva Kanso of University of Southern California. I thought the physics was quite interesting and hoping that the "capturing" of particles can eventually be engineered to capture all of the crap that we humans put into the air.

EM spacetime Ref. [54] interests me and I'm hoping it might lead me to a notion of local Galilean invariance that I could use in Kuramoto-Sivashinsky equation. The dream is that it would help with spatial integration which is still in the dark recesses of my mind.
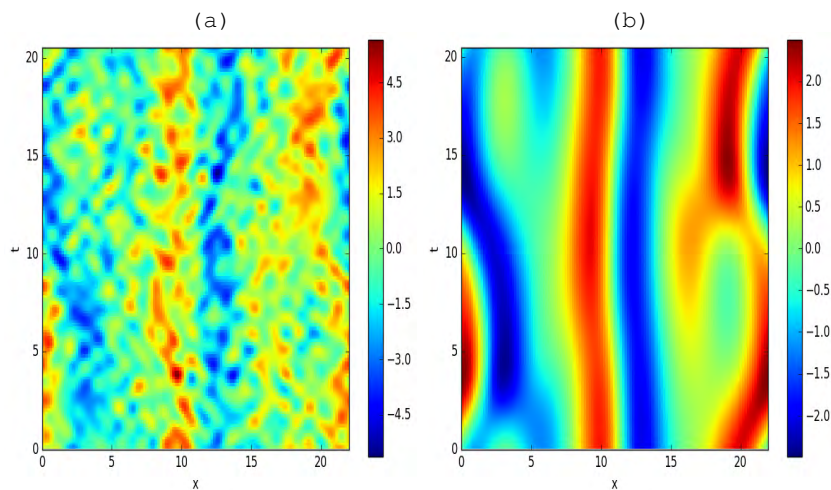
Figure 16.6: Everyone's favorite test-case invariant 2-torus is back but with a good amount of noise. (a) $ppo_{22 \times 10.2}$ with random noise added to the spatiotemporal spectrum of the same order as the solution, initial invariant 2-torus $(L_0, T_0) = (22.0, 20.5057459345)$. (b) The resulting machine-precision converged invariant 2-torus; the method used was a hybrid of adjoint descent and least-squares Newton, $(L_f, T_f) = (21.95034935834641, 20.47026321555662)$.

2018-03-30 Matt Figure 16.6 (a) is the resultant of adding random noise η to

the spatiotemporal Fourier coefficients of $\mathrm{ppo}_{22\times10.2}$, such that $|\eta|_2 = 0.5$, while the spatiotemporal Fourier coefficients of $\mathrm{ppo}_{22\times10.2}$ themselves have an approximate norm $|\hat{a}_{k_j}| \approx 0.76$. The initial condition (with noise) is then passed first the adjoint descent algorithm for discretized equations from Farazmand [20]. Using Runge-Kutta fourth order to integrate in the fictitious time direction provided by the adjoint descent equations $\partial_\tau \hat{a}_{k_j} = -J^\top F$, and taking one thousand steps of size $\Delta\tau = 0.0025$, I then pass the corrected initial condition to least-squares Newton, as it has worked better for me in the past than GMRES or Newton-Krylov-hookstep.

I almost never see a case where the adjoint descent doesn't stall out, and because the residual of the initial cost functional was so high due to the noise, the tolerance on the residual was never met, so I introduced a step number limit. I find the step number limit to be much more reliable than say, a specific amount of fictitious time, because the step sizes that reduce the residual seem to vary over a relatively large range depending on the particular solutions. (I tend to start at $\Delta\tau = 0.01$ and then divide by two until the Runge-Kutta step provides a decrease to the residual; sometimes this starting point proves to be too large and the entire scheme fails due to numerical overflow, i.e. if you take steps too large things can go very poorly instantaneously). The other additions of the adjoint descent equations were due to Ravi; although he performed the descent method in physical space and not Fourier space, there were two additional procedures that he added:

- Preconditioning
- "Momentum" factor from ref. [48]

The description of the momentum factor intuitively is that if we are able to find a sequence of fictitious time integration points that reduce the residual, then we should take larger steps. This is unwise because we are using an explicit integration algorithm and can lead to inaccurate results. Apparently one way around this is to add in a prefactor that represents "momentum" in the sense as long as we are making good steps we add the previous step weighted by this prefactor as described in (15.56). If we're going in the 'right' direction, we want to go further in that direction. Using the adaptive stepsize Runge-Kutta (RK45) never worked for me, but this seemed to work like magic. By using the correct rational function of a new parameter μ which tends to one as we make an infinite number of "correct" steps, it improves the reduction of the residual in the same amount of steps.

Most of the computational time was taken up by the adjoint descent, for figure 16.6 the adjoint descent took about 1111 seconds (≈ 18 minutes), and 4.1 seconds for the damped Least-Squares Newton.

The vast majority of the computational time (81 percent) is spent redefining the explicitly formed Jacobian transpose required to compute $-J^\top F$, otherwise known as the adjoint direction.

I think this is great news if I can get matrix-free version of adjoint descent I can at least hope to greatly improve the speed of the computation, initial error tolerance, and efficiency of finding invariant 2-tori at large (L, T).
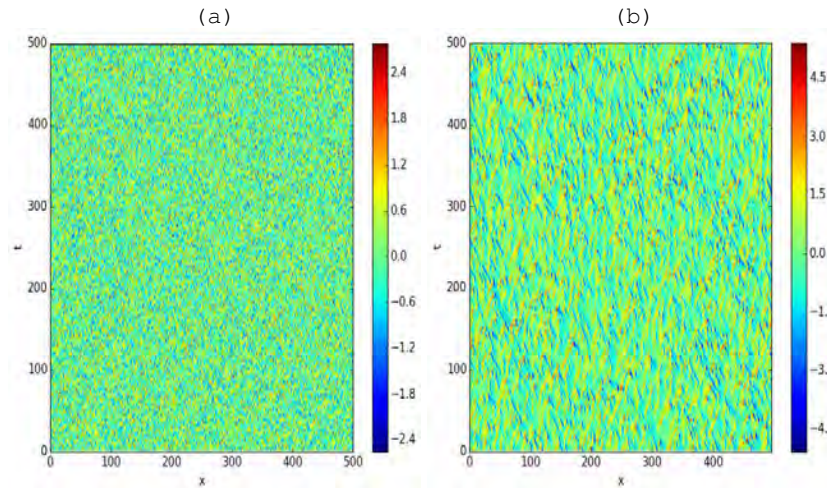

Figure 16.7: (a) Random numbers on a discretization of a spacetime area of $(L, T) = (500, 500)$. (b) As far as adjoint descent takes me the cost functional is no where near machine precision but one can see that scales are appearing. The spatiotemporal grid has a discretization of 64 points in time and 256 in space

2018-04-02 Matt spatiotemp Realized that perhaps adjoint descent would be better applied to full state space as opposed to spatiotemporal symmetry subspaces because its an integration(descent) type method. I wrote new codes that apply adjoint descent to the complex representation of the spatiotemporal Kuramoto-Sivashinsky equation, i.e. (1.43). The main benefit of doing so is that in the real-valued representation that I use for everything it isn't straight forward how to calculate the transpose of the Fourier transform and inverse transform operations, but when I use a complex representation the transformation is unitary; meaning that the conjugate transposes that arise are easily replaced using the unitarity property of the Fourier transform (with proper normalization).

Therefore, it is much faster to use adjoint descent in a complex representation than in my real-valued, symmetry dependent representations. The reason why I avoided the complex representation in the past is that there are numerous conjugacy relations between spatiotemporal modes that make the corresponding Newton system

singular if not taken care of; The trick here is that we aren't solving a linear system, but rather integrating in fictitious time direction.

If one wants to write this in terms of the adjoint operator notation that Mohammad uses; I believe the spatiotemporal adjoint operator is defined as such,

$$\frac{\partial u}{\partial \tau} = -\mathcal{L}^\dagger(u(x,t), f(x,t)) = (\partial_{xx} + \partial_{xxxx} + \partial_t)f + u\partial_x f \quad (16.18)$$

This opposes Mohammad's definition, which was the adjoint operator derived for the time dynamical system, where the "adjoint variable" was an integral over the motion.

$$\frac{\partial u}{\partial \tau} = -\mathcal{L}^\dagger(u, \int_0^T F(s)ds), \qquad (16.19)$$

He's smart so he's probably correct but I'm trying to avoid time integration in all circumstances, even initial condition generation.

Currently running tests on spatiotemporal domains initiated from random noise, large scale domains, and seeing what comes out. Random noise on a $T, L = 500, 500$ domain ran long enough starts to pick out the length scales of the Kuramoto-Sivashinsky equation, and its the matrix-free computation that allows it to run fast enough to do anything.

One problem is that when computing corrections to the period and length the system attempts to make them complex so I've just be taking the real part to make sure they remain physics constants

Figure 16.7 is an example of the limits of the method so far. Taking (pseudo) white noise on a large space-time domain and then running the adjoint descent reproduces structures that look similar to those seen within simulations of the Kuramoto-Sivashinsky equation.

I'm still hoping to use this as a way of reverse engineering the right way to implement matrix-free adjoint descent with my real representation code.

Another idea is to "mix the representations". I.e. use the complex representation with the fast, matrix-free adjoint descent code and then switch to the real representation when I get close enough to use Newton or GMRES. This would be the most efficient as opposed to rewriting all of my other codes to be in complex representations, especially because I had problems with it in the past.

Another topic I need to breach is whether I can constrain the adjoint descent to preserve the symmetry subgroup of any solutions found. If I can get the matrix-free method to work in the real representations this will automatically hold but not so in the complex

representation as I'm abusing the extra variables and unitarity of the Fourier transform so that everything is unconstrained.

2018-04-04 Matt : Everyone seemed excited at my results from figure 16.7 in the plumbers meeting; I will try to write up what I had in more depth to enable discussion. Also due to popular demand I added the ability to keep the length fixed and initiated a trial at $L = 22$, discretized over $(N, M) = (64, 64)$ (space,time) points starting from white noise. Will post results tomorrow after the run finishes. Limiting the adjoint descent to ten million steps (about eight hours computation time).

I'm worried that there is no notion of symmetry currently built into the code (although the equations are different between relative periodic orbitin the mean velocity frame, and pre-periodic orbitso it will hopefully be taken care of due to that fact) and therefore am still working towards making my real valued code matrix-free.

Spent way too long figuring out the complex variables that I need to keep, it turns out its half of the spatiotemporal spectrum, I thought I could figure out a subset of non-redundant information that would be smaller for pre-periodic orbittype solutions but that doesn't seem to be the case. The conjugacy identities only apply to the first transform (either space or time) because the first transformation is from a real valued field to a complex valued field. Regardless, the code is now running without redundant information with fixed length; I agree with Predrag this isn't the way to go about things but it is worth trying to see how versatile the code can be. The only problem with the matrix-free methods is now the second half of the hybrid algorithm, meaning getting GMRES or Newton-Krylov-hookstep to converge once the adjoint desecent, which is now fast, gets close enough to a solution.

My (discrete) symmetry woes might also be alleviated by imposing the discrete symmetry in the beginning, because then the adjoint descent will go towards the closest minimum, hopefully being a solution with Z_2 symmetry. I'm doubtful that my code is this much of an oracle, however.

So that being said, I can now initialize essentially white noise which is no where a solution to the Kuramoto-Sivashinsky equation locally and get close to the attractor without any time integration, but I need to play around with the size of the discretizations as it might be necessary to overfit if starting from a terrible (random noise) guess. I'm hoping what I've done this week helps Predrag with his talk later this week, I'm sure I can help write out something about the numerics using Farazmand [20] as a guide.

2018-04-09 Matt Finally back to the office after four days of one-armed moving apartments. The $L = 22$ run that I started last Wednesday failed due to a coding error so I'm currently running two different runs of $L = 50$ sized domain, one with the length fixed and one with nothing fixed. Both

are being put through ten million adjoint descent steps, so it'll take until tomorrow to finish.

Talked to Noah as he says that he figured out the spatiotemporal Jacobian matrix. I disagree with some of his points, namely that you can elect to choose a single point of the scalar field $u(x,t)$, and transport a scalar perturbation. The reason I don't think this is what we desire is that the spatiotemporal Jacobian matrix in this case is just a scalar because the tangent space perturbation is a scalar. After a small amount of math he arrives at a partial differential equation that the spatiotemporal Jacobian matrix must obey

$$\frac{\partial \mathcal{A}(x,t)}{\partial t} + \frac{\partial^2 \mathcal{A}(x,t)}{\partial x^2} + \frac{\partial^4 \mathcal{A}(x,t)}{\partial x^4} + u\frac{\partial \mathcal{A}(x,t)}{\partial x} + (\partial_x u)\mathcal{A}(x,t) = 0 \,, \quad (16.20)$$

which he says is then something you need to solve with appropriate boundary conditions on $\mathcal{A}(x,t)$. (I claim that $\mathcal{A}(x,t)^{0,0} = 1$ and if it truly is a scalar then $J^{T,L} = \Lambda$ is enforced I believe) so that it becomes a boundary value problem. But I think this is too simple as,

- this only produces one Floquet multiplier

- the Jacobian matrix being a scalar doesn't capture tangent space dimension

I was able to identify that if you look at equation (16.20), and rearrange it such that everything but the time derivative is on the right-hand side then it is exactly equivalent to the standard time-evolution equation for the Jacobian matrix,

$$\frac{\partial J^t}{\partial t} = AJ^t \,, \quad (16.21)$$

where $J^t \rightarrow J^{t,x}$. This can be seen by writing the stability matrix $A(u(x,t))$ in operator form,

$$A(u(x,t)) = -\partial_{xx} - \partial_{xxxx} - diag(u(x,t)_x) - diag(u(x,t))\partial_x \,. \quad (16.22)$$

This is the type of equation, one in terms of spatiotemporal operators (matrices that act on the spatiotemporal vector $u(x,t)$ through matrix multiplication), that I arrive at when calculating the explicit matrix for Newton's method, namely the matrix block defined by $\frac{\partial F}{\partial u}$, where $F \equiv$ Kuramoto-Sivashinsky equation (18.1). Some people [8, 36] [3] refer to this as the Jacobian matrix of a function F, though Viswanath [52] refers to the equation involving Jacobian matrix as a constituent as the "Newton matrix," or, more precisely, as "Newton system" as well as "Newton equations".

---

[3]Predrag 2019-05-08: what is bibitem *KK04jfnk*? Different from *KK04*?

2018-04-09 Matt Writing code that is sort of dependent on results from today's trials. I'm going to go even further in the hybrid direction which takes the best elements from all of my codes and throw them at the problem; the only issue is that the code whose results I showed last week do not specify any symmetries, but I need to specify the subgroup for my other codes.

I plan on writing code that uses matrix free adjoint descent in the complex representation, and if the trials show emergence of a symmetry subgroup I will pair this with the explicit matrix methods least squares Newton. This gives me the best chance of convergence to within machine precision from noise to invariant 2-tori I believe, but its dependent on whether the complex adjoint descent is picking out solutions with symmetries or not.

2018-04-09 Predrag Matt's (16.21), (16.22) refer to the evolution in time only, they are not the full spatiotemporal stability matrix. Noah's (16.20) is the Kuramoto-Sivashinsky (18.1) linearized $u(x,t) = u^*(x,t) + \delta u(x,t)$, about a given state space point, i.e., in our approach a given field $u^*(x,t)$ specified over a invariant 2-torus. This is what Matt and I have been discussing frequently over the last year. The matrix (generalization of the time-evolution stability matrix or the matrix of velocity gradients) of functional derivatives

$$\mathcal{A} \equiv \left. \frac{\delta F}{\delta u} \right|_{u=u^*} \tag{16.23}$$

which describes the tangent space at u^*, was initially called $J^{t,x}$ in (16.20), a notation which I changed to $\mathcal{A}(x,t)$. This is still not right, as $\mathcal{A}$ is a matrix, something like $\mathcal{A}(x',t';x,t)$, but we do it correctly in the Fourier mode expansions. One presumably integrates over the invariant 2-torus to get the Jacobian matrix J^{TL}. As the boundary conditions are doubly periodic, the perturbation $\delta u(x,t)$, and the two matrices should be expanded in terms of discrete Fourier modes (as we already do). The spectrum of J^{TL} is not one "Floquet" multiplier, J^{TL} is a variation of a function $u(x,t)$ under variation of function $\delta u(x,t)$, there are infinitely many multipliers.

2018-04-10 Matt I agree that (16.21) is the time evolution Jacobian, I suppose I was trying to claim that that (16.20) makes sense in the limit $\mathcal{A}(x,t) \rightarrow \mathcal{A}(0,t)$ as being the time evolution Jacobian only. My main issue with (16.20) is something we will have to discuss in person; Noah claims because we are starting with a scalar representative point on a two torus, then (16.20) is a scalar equation not a matrix equation, because $\mathcal{A}(x,t)$ is a scalar acting on a scalar perturbation through arithmetic multiplication. I claim that if we throw out this notion and instead view (16.20) as a matrix equation then it makes sense.

2018-04-10 Predrag I do not understand Noah. Maybe you can show him that the Fourier expansion of $u(x,t)$ is infinite-dimensional, i.e., a scalar *function* lives in an infinite-dimensional state space?
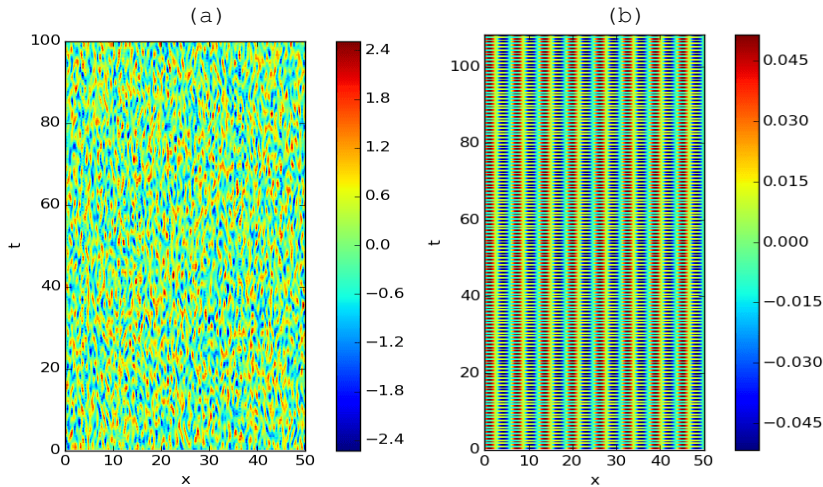
Figure 16.8: (a) Noise initialized on a spacetime domain $T = 100, L = 50$. (b) Resultant field after ten million steps of adjoint descent with fixed $L = 50$; $T \approx 108.43$.

2018-04-10 Matt Results from first run from yesterday are in. This was the adjoint descent applied to a spactiotemporal domain initialized with noise with $T = 100$, $L = 50$; keeping $L = 50$ fixed. The result is an apparent non-solution that looks like an equilibrium plus some high frequency numerical artifacts in time. I am inclined to believe these poor results are due to fixing the spatial domain size, but technically I used different codes to produce figure 16.7 and figure 16.8, so there could be a small error somewhere. Small in this instance means the adjoint descent code can still run until it hits the maximum number of steps but qualitatively wrong results. We shall see if fixing the domain size (or perhaps the initial condition was the issue).

2018-04-10 Predrag To me, figure 16.8 seems to be saying that you are computing the $u(x,t) = 0$ equilibrium, but not very accurately. It seems not to be a high frequency problem - the dominant spatial mode is $k = 8$.

2018-04-11 Matt Figure 16.9 (b) is the main result for this blog post.

Here is how I construct the initial condition (a):

I start by initializing a spatiotemporal domain with noise, and then I smooth the Fourier spatial coefficients (whose number is known only to me) by multiplying the spatial spectrum by exponentially decay (not using Gaussians but perhaps this is better) whose maximum is centered on the most unstable wavenumber $\bar{L} = 2\pi\sqrt{2} \simeq 8.886$. I'm using spatial domain sizes L which are integer multiples of $\bar{L}$ so this requires no interpolations.
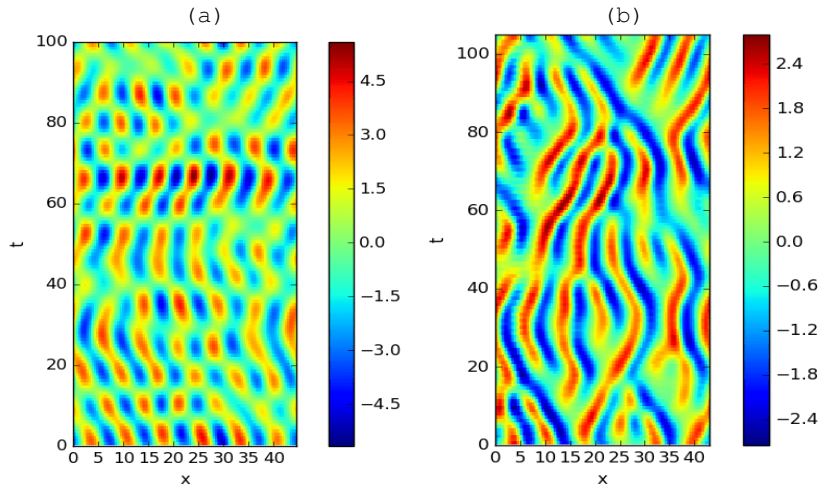
Figure 16.9:   (a) Smoothed and $\bar{L} = 2\pi\sqrt{2}$ modulated "noise" initialized on a spacetime domain $(L_0, T_0) = (5\bar{L}, 100) = (44.4, 100)$. Initial residual $F^2 = 1808$. (b) Resultant invariant 2-torus after meeting tolerance $F(\tau)^2 = 1.86 < 10^{-3}F(0)^2$. $(L_f, T_f) = (43.066, 105.08) = (L_0 - 1.363, T_0 + 5.08)$. The computation took only 7 CPU seconds on my laptop.

> I then take the temporal Fourier transform and truncate the higher (time) frequency modes (at only to me known truncation number).
>
> The key to getting solutions that are not $u(x, t) = 0$ equilibrium is to start with an initial guess whose maximum (minimum) values are greater (less) than what a non-trivial doubly periodic solution would have.
>
> The previous problem of finding equilibria is due to the fact that the adjoint descent must descend in a direction which decreases the square of the L_2 norm cost function, which in this case is the square of the Kuramo-to-Sivashinsky equation (1.43). Therefore, in order to find interesting solutions one *must* start with a spatiotemporal scalar field that has maxima (minima) that are larger (smaller) than what doubly periodic solutions would have, otherwise the only descent direction left to the method is towards doubly periodic solutions whose maxima and minima are smaller than the initial condition's; namely, the trivial equilibrium $u(x, t) = 0$. [4]
>
> For those just skimming the TL;DR version of this statement is that one should give more room for the descent methods to work by starting with initial conditions whose maxima and minima are larger than what a non-trivial spatiotemporal equilibrium would have, and one has the freedom to do so as the initial state in these cases are mere guesses that we can mold as we wish.

---

[4]Predrag 2018-04-12: That is not quite right.

The only other comment I wish to make is that with the other improvements, and heuristically guessing a discretization size that would work, the error tolerance was met in a mere seven seconds.

2018-04-11 Matt Added figure 16.10 to demonstrate that the structure of the Kuramoto-Sivashinsky equation is present in the large spatiotemporal domain results but is obscured by localized maxima and minima that distort the scale of the resultant spatiotemporal field. The computation was done on a 256-by-256 discretized spatiotemporal grid. Because of conjugacy conditions, the code uses a truncation of 126 (two less that half because of Galilean invariance) in the spatial wavenumber index and no truncation in the temporal index, resulting in $\hat{a}_{kj}$ for $n = 1, \ldots, 127$ and $-128 \leq m \leq 128$. I figured that as long as I contained the most unstable wavelength and something sufficient for time then it would be ok, but as PC says it is likely nonsense. This is one of likely many ways I can take advantage of conjugacy condition $\hat{a}_{kj} = (a_{-k,-j})^{\star}$.

2018-04-11 Predrag This is great news!

To me figure 16.9 seems initialized with $L_0 = 6\bar{L}$, even though your labels say $L_0 = 44.43$. This is close to, but not exactly the double of the historical $L = 22$ domain.

2018-04-11 Predrag I doubt figure 16.10 means anything; at least, it is worrisome, as it has large $u \approx 0$ regions that one never sees in large L, forward in time simulations. You would need at least twenty as many spatial Fourier modes as for figure 16.9 , but you do not specify the spatial and temporal Fourier mode truncations anywhere.

2018-04-11 Predrag Anyway, keep it simple, and forget insanely large spatiotemporal domains for now. Instead, start (always!) with your noisy but modulated initial guesses, with

1. (L_0, T_0) picked from sizes for which you already have exact solutions, such as figure 13.3, figure 15.5, figure 15.4, figure 13.35, figure 13.26, figure 15.3, figure **??**, figure 16.1, and some longer $(T_p, 22)$ from Xiong's library. Even though your noisy initial conditions have no symmetries, some of the solutions should converge to known periodic orbits with symmetries. If you get no known solutions, start worrying.

2. halve T_0's and see if you get anything (hopefully not, one can probably prove that the trivial equilibrium $u(x,t) = 0$ is the only solution).

3. halve L_0's and see if you get anything (hopefully not, one can probably prove that the trivial equilibrium $u(x,t) = 0$ is the only solution).

4. double T_0's and see what you get.

5. double L_0's and see what you get.
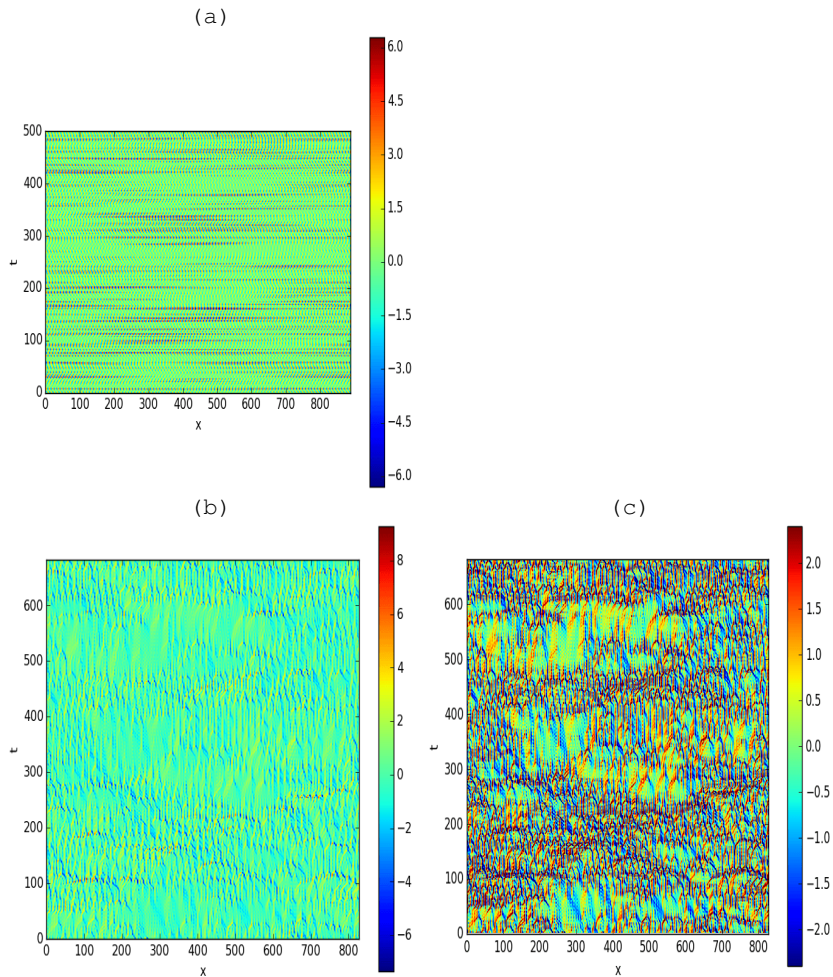
Figure 16.10: (a) Smoothed noise initialized on a spacetime domain $T = 500$, $L = 100\,\bar{L} \approx 889$, where $\bar{L} = 2\pi\sqrt{2}$. Initial residual $F^2 = 16635$ (b) Resultant spatiotemporal field after one-hundred thousand adjoint descent steps $F_f^2 = 3.66$, $T_f = 682.62$, $L_f = 828.31$. (c) The same $u(x,t)$ as in (b), except with the displayed values constrained between $-2.4 \leq u(x,t) \leq 2.4$. Computation time was approximately an hour and ten minutes.

6. play with T_0's to develop a feeling for what the time scale of the problem is.

7. If all this works, start thinking again (your current setup cannot find relative periodic orbits, etc)

2018-04-12 Matt I handle relative periodic orbits by solving the spatiotemporal equation in the mean velocity frame, as there is an added term that tracks any SO(2) shift with a parameter. I think that trying to make a sliced code matrix free would be even harder than what I am attempting for real-valued pre-periodic orbitcode. In order to fulfill these ideas in an expedient way it seems that I need do some more automation.

2018-04-11 Predrag Do not implement a sliced matrix free code, adding a spatial phase translation parameter is the right way to go.

2018-04-11 Matt The cost functional used above is

$$G \equiv \frac{1}{2}|F(u, T, L)|^2 \,, \tag{16.24}$$

where F is the Kuramoto-Sivashinsky equation (15.60) in spatiotemporal Fourier space.

2018-04-12 Matt Finished automation of initializing spatiotemporal domains whose dimensions are the periods given by either relative periodic orbits or pre-periodic orbits and domain starts at $L = 22$. The results are currently mixed and needed a few new tricks to even get to fair results.

Namely, it seems that with the tools I developed earlier this week that the adjoint descent method will drastically enlarge the spatial domain (drastic being anywhere from a factor of three to factors of thousands) or go towards solutions that look like time equilibria. I believe this is likely due to the trick I am using that takes advantage of the initial condition being a non-solution. By increasing the magnitude of the scalar field I am more likely to find "better" solutions, but when on a small domain the adjoint descent seems to be predisposed to fix the discrepancy in the tangent space by elongating the tile due to the inverse proportionality of the derivatives to T, L.

Also didn't see good results with the specific temporal wavenumber truncation I was using yesterday.

To circumvent both of these issues I made sure that the temporal scale was on the order of the spatiotemporal domain (by keeping only the first and zeroth temporal wavenumbers, $m = 0, 1, -1$) and by fixing the domain size. These changes and playing around with the normalization of the scalar field led to figure 16.11. The time period is still being stretched quite a bit (more than a factor of two) but I think fixing the tile completely is too strict of a constraint for the method to work, and it is the opposite direction I want to take the functionality of the code.
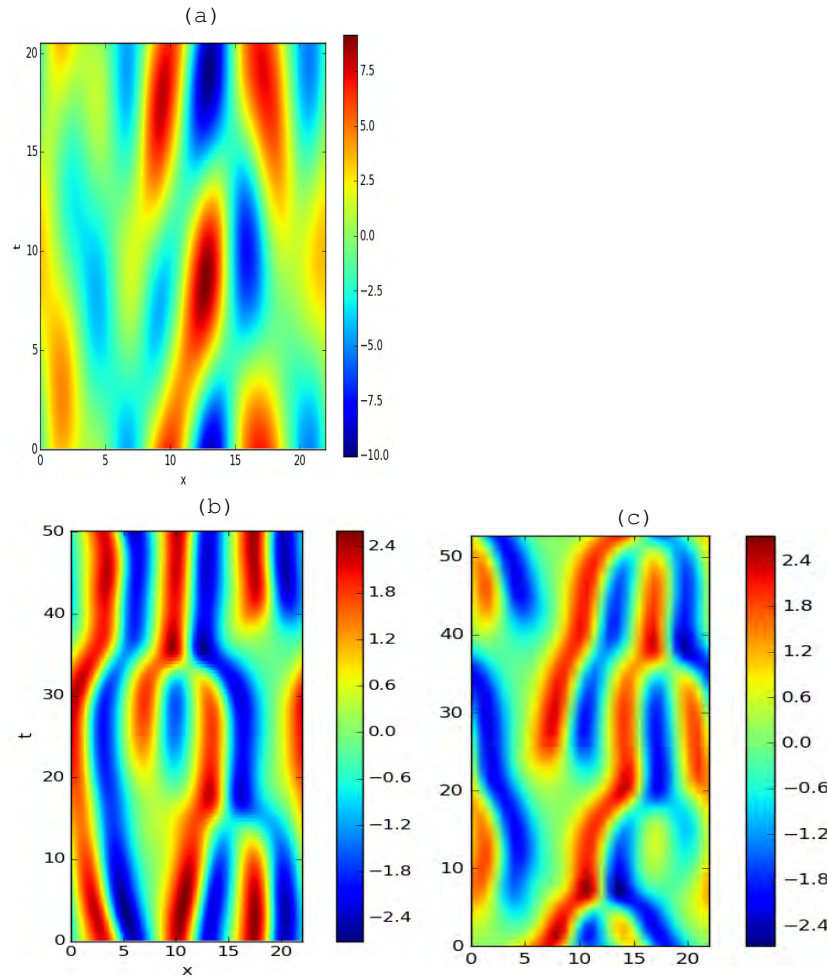
Figure 16.11:   (a) Smoothed noise initialized on a spacetime domain $T = 2\,T_{\mathrm{ppo}_{22\times10.2}}$, $L = 22$. (b) Resulting spatiotemporal field after 10^5 adjoint descent steps with $L = 22$ fixed, $T_f = 50.1981$. It bears no relation to $\mathrm{ppo}_{22\times10.2}$ of figure 16.11 (a). (c) $\mathrm{rpo}_{22\times52.6}$, the orbit whose period was closest to the result of adjoint descent (b), included purely for comparison.

2018-04-12 Predrag The code you are currently using searches only for periodic orbits. They are of two kinds: periodic (generically those exist only in the reflection antisymmetric invariant subspace $\mathbb{U}^+$, you will recognize it immediately), and even repeats of pre-periodic orbits.

If you have really found a pre-periodic orbit of period $T = 2\,T_{\overline{ppo}_{??}} = 50.1981$, that one should be in Davidchack, Siminos and Xiang tables? They are supposed to be compete for short orbits.

What happens with the example of figure 16.11 if you replace the initial guess figure 16.11 (a) (for which the resulting periodic orbit has a longer time period, but pretty much the same spatiotemporal shape) with the known, but noise-perturbed $(L, T) = (22, 2\,T_{\mathrm{ppo}_{22\times10.2}})$ pre-periodic orbit of figure 13.3 (a)? Your initial figure 16.11 (a) guess has 3 spatial wiggles, but $\mathrm{ppo}_{22\times10.2}$ has only 2, so maybe it is not surprising that it does not converge to $\mathrm{ppo}_{22\times10.2}$.

2018-04-13 Matt I'm running more stringent trials on light right now with fixed L to see what I get. I guess I wasn't thinking and assumed that I could also find relative periodic orbits but thats exactly what the explicit equation that contains SO(2) shift parameter is for. I think the error in the number of wiggles is a small mistake due to trying to pick out a wavenumber that is not represented in the discretization, i.e. if the domain isn't an integer wavenumber than without increasing the discretization in space I'm not exactly determining the scale of the most unstable wavelength because it no longer corresponds to an integer wavenumber.

I'm running more stringent (in terms of tolerance) runs on a fixed domain so if anything good pops out I'll be sure to add it.

2018-04-13 Matt Longer trials don't seem to be producing pre-periodic orbits but because of the fixed domain size the rate of convergence of the adjoint descent is slowing down much faster than usual.

I think I need to play around with switching the preconditioning on and off and figure out the correct time scale before any great achievements can be made.

And just to sound like a broken record I still need I'll need impose symmetries in the long run as its too big of a constraint to not use.

2018-04-17 Matt Can't sleep. Not good. Or is it?

While laying in bed for hours I had what I at the time thought was a good idea which begged the question "If I can add a term to (16.16) so that it knows its working with solutions with SO(2) symmetry. Why cannot do the same for solutions with Z_2 symmetry?"

The general idea is this. I know how to act the reflection symmetry onto the equations, can I not create an ansatz or modify the cost functional that mimics the way López *et al.* [43] deal with rotational symmetry?

The first idea was borne from the fact that the Kuramoto-Sivashinsky equation under reflection are still equal to zero by equivariance,

$$- u_t(-x,t) - u_{xx}(-x,t) - u_{xx}(-x,t) - u(-x,t)u_x(-x,t) = 0, \quad (16.25)$$

So is there not a way to use this to reformulate (yet again) my problem in such a way that I achieve a complex representation for solutions with Z_2 symmetry?

The reflection operator R acts on coordinate x as $Rx = -x$, and on the velocity field u (dimensionally $[x]/[t]$) as $Ru(x,t) = -u(-x,t)$. Relation $R^2 = 1$ induces [11] linear decomposition $u(x) = u^+(x) + u^-(x)$, $u^\pm(x) = P^\pm u(x) \in \mathbb{U}^\pm$, into irreducible subspaces $\mathbb{U} = \mathbb{U}^+ \oplus \mathbb{U}^-$, where

$$P^+ = (1 + R)/2 \,, \qquad P^- = (1 - R)/2 \,, \quad (16.26)$$

are the antisymmetric/symmetric projection operators. Applying P^+, P^- on the Kuramoto-Sivashinsky equation (18.1) we have [35]

$$
\begin{aligned}
u_t^+ &= -(u^+ u_x^+ + u^- u_x^-) - u_{xx}^+ - u_{xxxx}^+ \\
u_t^- &= -(u^+ u_x^- + u^- u_x^+) - u_{xx}^- - u_{xxxx}^- \,.
\end{aligned}
\quad (16.27)
$$

If $u^- = 0$, Kuramoto-Sivashinsky flow is confined to the antisymmetric $\mathbb{U}^+$ subspace,

$$u_t^+ = -u^+ u_x^+ - u_{xx}^+ - u_{xxxx}^+ \,, \quad (16.28)$$

but otherwise the nonlinear terms in (16.27) mix the two subspaces.

Let's first write (16.25) in a more suggestive form:

$$\exp i\pi(F(u(-x,t))) = R \circ F(u(-x,t)) \quad (16.29)$$

The first idea was okay, well $0 + 0 = 0$ so let's see what that yields in terms of the cost functional, let R denote the operation of reflection, then

$$\tilde{F} \equiv F + R \circ F, \quad (16.30)$$

leads to a completely wrong, just elaborating on my though process cost functional,

$$G = \frac{1}{2}\tilde{F}^\dagger \tilde{F} = \frac{1}{2}((1 + e^{i\pi})F)^\dagger((1 + e^{i\pi})F) \quad (16.31)$$

but carrying out this calculation leads to the trivial result $G = 0$ due to cancellation. Likewise, a definition

$$\tilde{F} \equiv F + R \circ F, \quad (16.32)$$

just leads to an extra factor of 4 in the original cost functional equation, but would technically alter the adjoint direction, explicitly

$$
\begin{aligned}
G &= \frac{1}{2}\tilde{F}^\dagger \tilde{F} \\
&= \frac{1}{2}((1 - e^{\mathrm{i}\pi})F)^\dagger ((1 - e^{\mathrm{i}\pi})F) \\
&= \frac{1}{2}F^\dagger (1 - e^{-\mathrm{i}\pi})(1 - e^{\mathrm{i}\pi})F \\
&= 2F^\dagger F
\end{aligned}
\tag{16.33}
$$

therefore there would be no change in the adjoint direction $-J^\dagger F$ outside of a scalar multiple.

I haven't given up hope yet however, as these formulations forgot the implicit flipping $x \to -x$ that is contained within the scalar field itself $u(-x, t)$. I think that we can exploit this.

When not using the fundamental domain, a reflection applied to a pre-periodic orbit produces an equivalent solution but not an invariant solution. This is because in terms of a spatiotemporal tile, the "top" and "bottom" (fundamental domains) get switched. Therefore in order to have an invariant representation of the solution, we need to translate in time by T_p. In other words, this is how the reflection operation acts on a pre-periodic orbitwhen viewed as a periodic orbit, and not from the fundamental domain perspective.

$$
R \circ \begin{bmatrix} -u(-x, t) \\ u(x, t) \end{bmatrix} = \begin{bmatrix} u(x, t) \\ -u(-x, t) \end{bmatrix}
\tag{16.34}
$$

As we can see, the "bottom" $0 \leq t \leq T_p$ has been switched with the "top" $T_p \leq t \leq 2T_p$, therefore in order to enforce invariance under Z_2 symmetry we also need to impose a time translation.

$$
T \circ R \circ \begin{bmatrix} -u(-x, t) \\ u(x, t) \end{bmatrix} = T \circ \begin{bmatrix} u(x, t) \\ -u(-x, t) \end{bmatrix} = \begin{bmatrix} -u(-x, t) \\ u(x, t) \end{bmatrix}
\tag{16.35}
$$

So what if we compose a function, that enforces this? Will it enable a symmetry constrained calculation much like the mean velocity frame equation? With

$$
\tilde{F} = (1 + T \circ R \circ)F,
\tag{16.36}
$$

the cost functional becomes

$$
G = \frac{1}{2}\tilde{F}^\dagger \tilde{F} = \frac{1}{2}((1 + T \circ R\circ)F)^\dagger ((1 + T \circ R\circ)F)
\tag{16.37}
$$

which I do not think can be simplified. However, this affects the adjoint descent in a non-trivial way. It requires $\tilde{F}$ be equal to zero, not only that $F = 0$.

2018-04-17 Matt response to Predrag I agree with Predrag on the following:
I understand that the antisymmetric subspace $\mathbb{U}^+$ has its own decomposition, as odd functions with respect to the spatial have only imaginary components of spatial Fourier coefficients. If I was looking for solutions in this subspace I would use the equations for the antisymmetric subspace in terms of spatiotemporal Fourier modes.

I disagree with Predrag on the following point, periodic orbits in the antisymmetric subspace $\mathbb{U}^+$ are *invariant* under reflection while pre-periodic orbit's are *equivariant*. The way to make a pre-periodic orbit*invariant* is the action defined by spatial reflection plus time translation. Periodic orbits in the antisymmetric subspace $\mathbb{U}^+$ would also fall into this category but the reverse is not true. Therefore, I believe I should be able to modify the equation (1.43) to enforce this reflection and translation property much like how I modified the equation (1.43) to incorporate a parameter that tracks the SO(2) shift.

Luca Dieci Meeting I ran Professor Dieci through my thesis proposal and the things he pointed out were to call the method I'm using Fourier collocation. He really insisted on using M for space and N for time; just because of mathematical conventions.

The parts he found lacking were lack of constraints in the adjoint descent and Gauss-Newton (the apparent official name for least-squares Newton method) method. He recommended finding solutions to the nonlinear algebraic equations $F(x) = 0$ such that $||\mathbf{x}||_2$ is minimized for instance. There are some heuristic things one must include that I pointed out because $\mathbf{x} = 0$ is a solution. I believe Molei Tao has papers on fictitious forces one can introduce such that the trivial solution is avoided so I'll look there for insight.

His main worry was whether the method works with tiling the same solution in time and space, because we're claiming they're doubly periodic therefore copies of each tile should also be valid. If they aren't he said he would start to worry (and so would I).

Appealing to his own experience he really stressed numerical continuation in the parameter L. I'm unsure if this is just an unfamiliarity with what we are trying to accomplish but he says (and I agree) this is done rather ubiquitously but I guess one has to go against the grain in some places to have a new idea.

His last question was a rather broad one, he asked what the main goal was. I told him to compute a library of invariant 2-tori to be able to be able to find them in large general invariant 2-tori in order to build predictions for infinite space and time. He seemed to me to really like and understand the idea.

The only other comment was my worry that symmetries are too important to not use, hence my post from yesterday, to which he agreed. Note: I did not show him what I wrote yesterday so do not

confuse his agreement with "symmetry is important" with "Matt is right" in this context.

Addendum: He also mentioned that because we are doing (inherently global) collocation in time and space we might be able to get away with using a coarse number of modes and then refine the guesses as we get closer to solutions

Talk with PC Had a discussion with Predrag on whether pre-periodic orbitsolutions live in an invariant subspace because if one looks at the full state space orbit corresponding to a pre-periodic orbit, then like I previously mentioned, it is equivariant under reflection but invariant under reflection and a time shift equal to the prime period.

I believe that if there is a subspace in which pre-periodic orbits live, then the antisymmetric subspace $\mathbb{U}^+$ must be contained as yet another subspace; the logic behind this is that reflection already leaves the antisymmetric orbit $\in \mathbb{U}^+$ invariant, and so time translation by half of the period leaves it invariant as well? Or would the inclusion of this translation just be an equivariant transformation? Perhaps the two spaces are something like the following:

spatiotemporal symmetries These ideas arose due to the nature of handling how to keep pre-periodic orbit type invariant 2-tori invariant under symmetry. For a generic solution of the Kuramoto-Sivashinsky equation that has not been compactified in time, the general symmetry group would be $O(2) \times \mathbb{R}$, as any time translation is valid as the equations are autonomous. Once we compactify time and assume doubly periodic solutions, then we should compactify time as well such that the general symmetry group of doubly periodic solutions is $G \equiv O(2) \times SO(2)$.

When viewed from this context we can identify the isotropy subgroups of G for each type of solution. These are not symmetry actions which the solutions are equivariant under but rather the symmetry actions that the solutions are *invariant* under.

$$G_x = \{g \in G : gx = x\} \tag{16.38}$$

With this definition, the isotropy groups of the different types of solutions have the following isotropy groups: where σ represents the

RPO	$\{e, e\}$
PPO	$\{e, e\} \cup \{\sigma, \pi\}$
ANTI	$\{e, e\} \cup \{\sigma, e\}$

reflection operation of $\mathbb{Z}_2$ and π is the proper rotation by π, or equivalently the non-identity element of C_2. Therefore, for pre-periodic orbit type solutions we **cannot** write the isotropy group as $\mathbb{Z}_2 \times C_2$ as we need an even smaller subgroup. For the antisymmetric periodic

orbits $\in \mathbb{U}^+$ the isotropy group is $Z_2 \times e$, and for relative periodic orbit 's there is only the trivial isotropy group.

This is sort of backwards in the way that we usually view symmetries of solutions, but I believe its because we usually list the symmetries that a solution is equivariant under and not invariant under. The logic behind this is that any infinitesimal transformation (spatial or time translation) will not leave the solution invariant; therefore, the only possible isotropy subgroups are discrete subgroups of $\mathrm{O}(2) \times \mathrm{SO}(2)$.

With this in mind, I believe the correct formulation for the pre-periodic orbitinvariant subspace version of the spatiotemporal function (1.43) should be the following. Let $\mathbb{I}, \mathcal{R}$ be the labels for the elements of the pre-periodic orbitisotropy subgroup. Because we can either reflection and rotations are space, and then time, they commute in this case; this is why we can just label the transformation by $\mathcal{R}$.

By defining

$$\frac{1}{2}(\mathbb{I} + \mathcal{R})\mathbf{F}(\mathbf{x}) = \mathbb{P}\mathbf{F}(\mathbf{x}) \tag{16.39}$$

The modified cost functional for pre-periodic orbits is then,

$$H = \frac{1}{2}(\mathbb{P}\mathbf{F}(\mathbf{x}))^{\dagger}(\mathbb{P}\mathbf{F}(\mathbf{x})) \tag{16.40}$$

2018-04-24 Predrag The Summit, summarized:

1) All plane Couette flow equilibria and relative equilibria classified in Gibson, Halcrow and Cvitanović [23] are (ignoring the wall normal, physically compactified y direction) are doubly-periodic solutions of 2D PDE in (x, z) = (streamwise, spanwise) infinite directions. Matt will understand the ref. [23] and then, by clip & paste from it, summarize the relevant parts of that paper in sect. 12.3.2, and illustrate the shift & reflect equilibrium solutions by their $u_j(x, 1/2, z)$ plots (to belabor the obvious: there is not *time* in the plane Couette flow equilibrium setting, and the compact y interval is there only to accommodate vortex structures and burn energy).

2) The spacetime doubly-periodic solutions of 2D Kuramoto-Sivashinsky PDE that we study are compactifications of $u(x, t)$ = (spanwise, timewise) infinite directions. The well known and understood classification of symmetries and invariant subspaces of plane Couette flow applies -as is- to the Kuramoto-Sivashinsky problem.

In particular, the much beloved shift & reflect subspace of small domain plane Couette flow is the pre-periodic subspace of small spatiotempral tile Kuramoto-Sivashinsky.

QED - Matt had a wonderful insight, and explained this way, the plumbers will follow.

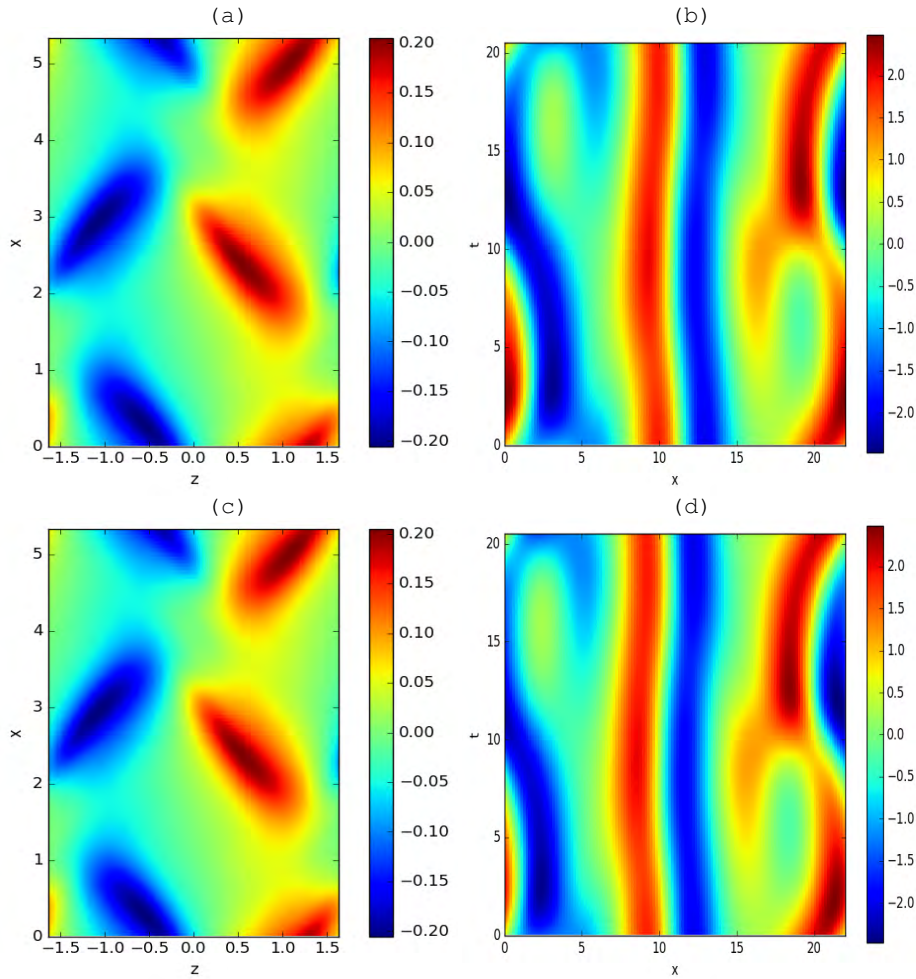Figure 16.12: (a) Plot of the z component of the vector velocity field $w(z, x)$ at the wall-normal midplane $y = 0$, $y \in [-1, 1]$ from "newbie" equilibrium of plane Couette flow. (b) The shortest preperiodic orbit Kuramoto-Sivashinsky $\text{ppo}_{22 \times 10.2}$. (c) Shift and reflected $-w(-z, x + \frac{L_x}{2})$ version of (a). (d) Shift and reflected $-u(-x, t + \frac{T}{2})$ version of (b).

2018-04-24 Matt Talks with Predrag, part one Had a discussion about the stuff
I had written up about projection operators and how I can derive in-
variant subspaces of "preperiodic solutions" for plane Couette flow
and then Predrag wondered whether I can relate the shift-reflect
symmetry of plane Couette flow to the spatiotemporal symmetry
operation for preperiodic orbits in the Kuramoto-Sivashinsky equa-
tion.

It turns out that the subgroups are identical and they provide a great
chance for an analogy between plane Couette flow and the Kura-
moto-Sivashinsky equation. In figure 16.12 we take the wall normal
midpoint $y = 0$ of the newbie equilibrium, and then plot the z com-
ponent of the velocity vector, $w(z, x)$ (the order of the variables has a
purpose). We also plot the spatiotemporal scalar field of the shortest
preperiodic orbit $u(x, t)$.

Then in (c) we the apply shift-reflect symmetry from the plane Cou-
ette, and in (d) we apply the spatial reflection and time translation
symmetry on the Kuramoto-Sivashinsky solution.

Because both solutions are invariant under these symmetries (c) and
(d) are exact copies of (a) and (b) respectively, but if we compare the
equations for the symmmetry transformation we can see the anal-
ogy take shape.

$$
\begin{aligned}
s_1 w(z, x) &= -w(-z, x + \frac{L_x}{2}) \\
\sigma \tau u(x, t) &= = -u(-x, t + \frac{T}{2})
\end{aligned}
\tag{16.41}
$$

Therefore, the two dimensional spatial cross section (z, x) of the z
component of the velocity field of plane Couette flow has the same
symmetry as the two dimensional *space-time* preperiodic orbit of the
Kuramoto-Sivashinsky equation.

The implication of this is that there is now a very precise definition
of what we mean by preperiodic orbit. It is a invariant 2-torus that
satisfies shift(in time) and reflect(in space) symmetry equivalent to
two spatial dimensional plane Couette cross-section.

Therefore not only do we believe all of the machinery available to us
from refs. [12, 23] is applicable to spatiotemporal discrete symme-
try subgroups in the Kuramoto-Sivashinsky equation, but also we
believe this fact to be a bridge to the gap between spatiotemporal
Kuramoto-Sivashinsky equation and plane Couette flow.

Talks with Predrag, part two The next topic of discussion was about how
to approximate the time scale for large invariant 2-tori, as the spatial
scale is already pretty well understood as being the most unstable
wavelength of the Kuramoto-Sivashinsky equation. We've been us-
ing an approximation of the temporal scale of about ten to twenty

dimensionless time units but we discussed and thought of a number of ways we can approximate the time scale.

- Count and average the number of maxima and minima in time strips of the scalar field originating from a large invariant 2-tori to give an average wavelength
- Count the number of maxima and minima in space, and see if and when this number changes. Numerically, this would be tracking when the spatial waveform has a "birth or death" event.
- Combine or compare the previous two methods to see if if what?
- Use the "slope" of traveling wave solutions, exponents of EQ_2 (dynamically relevant) equilibrium.
- Use Lyapunov time

2018-04-24 Matt Figured out how shift and reflect subspace for complex Fourier representation (pre-periodic orbit subspace). It's much easier than I previously thought and was doing this morning, which was taking the real-valued expression and substituting complex exponentials for sines and cosines.

First the complex spatiotemporal Fourier transform, m is the spatial index, n is the time index

$$u(x,t) = \sum_{m=-M/2,n=-N/2}^{m=N/2-1,n=N/2-1} \hat{u}_{nm} e^{i(q_m x + \omega_j t)}, \qquad (16.42)$$

which we then perform shift and reflect symmetry operation on,

$$\tau\sigma u(x,t) = \sum_{m=-M/2,n=-N/2}^{m=N/2-1,n=N/2-1} -\hat{u}_{nm} e^{i(q_m(-x)+\omega_j(t+\frac{T}{2}))}, \qquad (16.43)$$

which after some simplification can be written,

$$\sum_{m=-M/2,n=-N/2}^{m=N/2-1,n=N/2-1} (-1)^{n+1}\hat{u}_{nm} e^{i(q_m(-x)+\omega_j t)} \qquad (16.44)$$

We can't equate them just yet, but I found it most useful to make the transformation $m \to -m$ in the original sum rather than the sum after the symmetry operation, this transformation yields the following equation,

$$(-1)^{n+1}\hat{u}_{nm} = \hat{u}_{n,-m}. \qquad (16.45)$$

Now using this, in combination with the two-dimensional conjugacy relation for the two dimensional Fourier transform of a real valued field

$\hat{u}_{nm} = \hat{u}^{\dagger}_{-n,-m}$, we can figure out the invariant subspace, or at least the non redundant set of Fourier coefficients that we need to reproduce $u(x,t)$.

In order to explain this, I will do it pictorially, as the spatiotemporal Fourier transform is easiest to represent in two dimensions (i.e. a matrix).

$n \ \backslash \ m$	0	$1,\ldots,M/2-1$	$-\frac{M}{2}$	$-M/2+1,\ldots,-1$
0	0	$\hat{u}_{0m}$	0	$-\hat{u}_{0,m}$
$1,\ldots,N/2-1$	0	$\hat{u}_{nm}$	0	$(-1)^{n+1}\hat{u}_{nm}$
$\frac{-N}{2}$	0	0	0	0
$-N/2+1,\ldots,-1$	0	$(-1)^{n+1}\hat{u}^{\dagger}_{nm}$	0	$\hat{u}^{\dagger}_{nm}$

where the coefficients $\hat{u}_{nm}$ in this table only imply positive indices, $n > 0$ and $m > 0$. So in order to reconstruct the original field $u(x,t)$ we only need the spatiotemporal modes consisting of indices $n \geq 0$ and $m > 0$. The rest of the table is purely instructions on how to recreate the spatiotemporal spectrum so that the inverse Fourier transform can be applied.

2018-04-30 Matt - coding efforts Almost done implementing the new complex valued codes for the shift-reflect subspace and spatiotemporal relative periodic orbit codes, or so I thought before the previously described investigation.

For the shift-reflect complex-valued code it seems that the L_2 norm is a much better measure that it was in any of the previous codes. My favorite test case, $\text{ppo}_{22\times10.2}$ on $L = 22$ domain starts with an initial cost function residual of $\frac{1}{2}|F|^2 \approx 10^{-9}$ and is able to converge to within machine precision using adjoint descent alone in under one second. This result uses a 32-by-32 discretization in space and time which corresponds to the set of Fourier modes $n \geq 0, m > 0$; which corresponds to a set of 16-by-15 spatiotemporal modes.

There is a slight problem however because now generic smooth fields $u(x,t)$ with imposed shift-reflect symmetry, time and spatial scales, are generally terrible. There cost function residuals typically start off in upper atmosphere, i.e. the thousands. The noticeable difference between the modulated initial conditions and known preperiodic solutions is that typically there are very long nonlinear streaks in the time direction for pre-periodic orbit 's that I'll need to reliably reproduce. One attempt at this is to limit the time scale to be the entire domain i.e. start with only the $n = 0, 1$ modes on a spatiotemporal domain, but its not working too well.

2018-05-01 Matt Trying to see how robust the shift-reflect subspace is through testing.
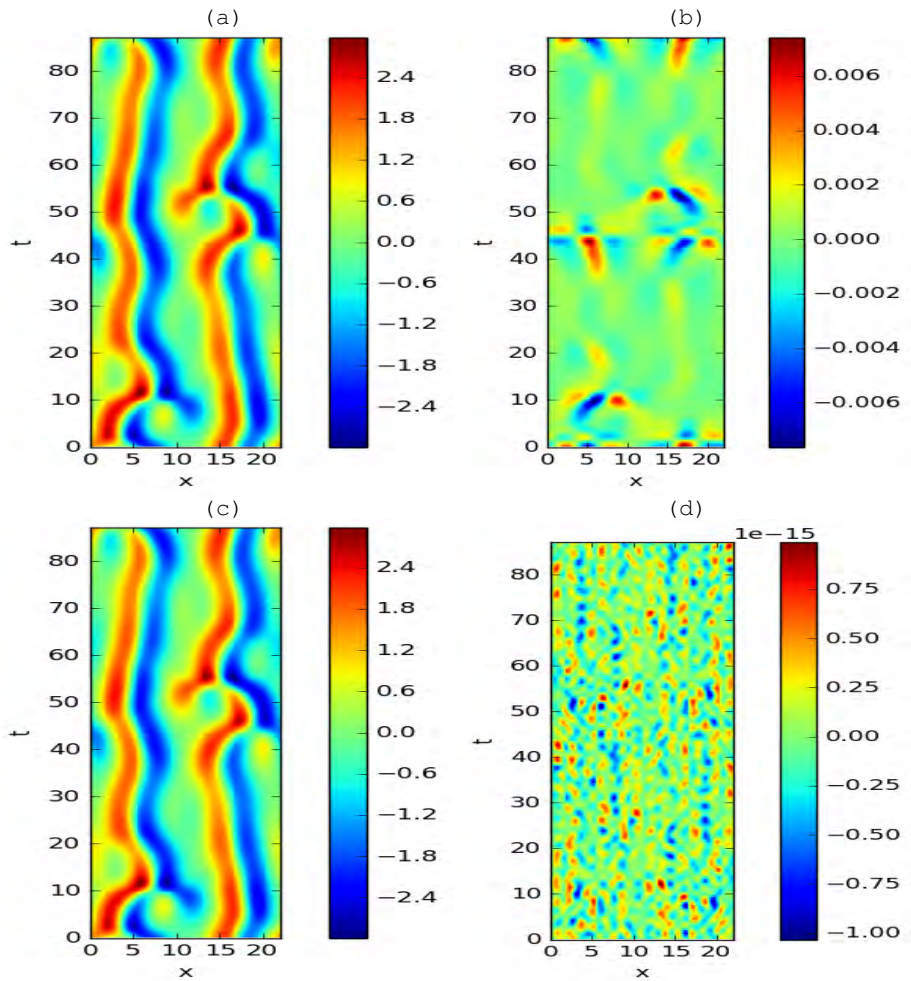
Figure 16.13: (a) Spatiotemporal $u(x,t)$ generated via time integration of $\text{ppo}_{22 \times 43.6}$. (b) The difference between (a) and its shift-reflection (c) The resulting spatiotemporal fixed point after passing (a) through direct-matrix code, $L_f = 22.0004274064$, $T_f = 87.2203435133$. (d) The difference between (c) and its shift-reflection.
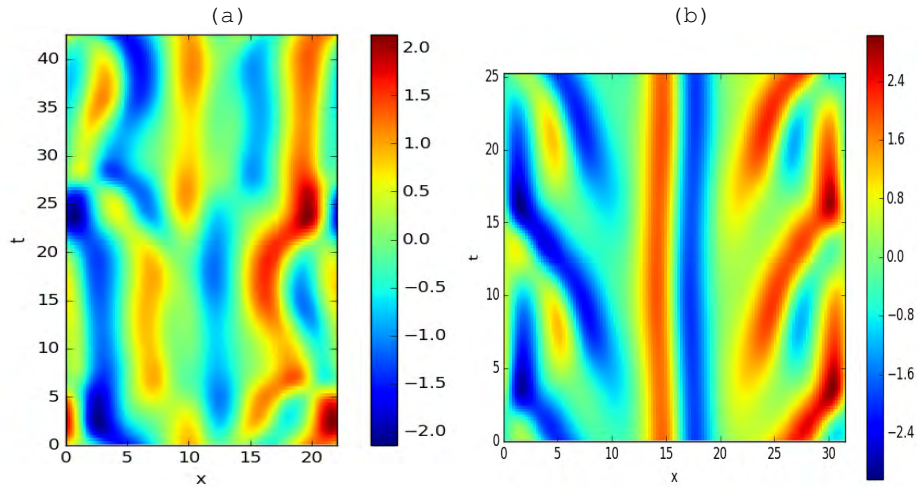
Figure 16.14: (a) Linear combination $\frac{1}{2}(\text{ppo}_{22\times10.2} + \text{ppo}_{22\times32.3})$ used as the initial guess, with starting domain size, time period $(L_0, T_0) = (22, 42.6097031254)$, where $42.6097031254 = T_{\text{ppo}_{22\times10.2}} + T_{\text{ppo}_{22\times32.3}}$. (b) Resulting invariant 2-torus with $(L_p, 2\,T_p) = (31.5056, 25.2461)$.

Linear combinations of shift-reflect subspace solutions providing better results than spatiotemporal initial conditions who start as modulated noise in the shift-reflect subspace. figure 16.14 (a) shows the linear combination of the shortest and third shortest pre-periodic orbit on the $L = 22$ domain. The resultant solution has a drastically (more than order one) different domain size and period than the original guess. I am surprised this worked, but it might show how powerful spatiotemporal invariance can be.

2018-05-01 Predrag Now figure 16.14 seems to have wandered out of the shift-reflect subspace; it is just a $r = 2$ repeat of what seems to be an inaccurate invariant 2-torus $(L_p, T_p) = (31.5056, 12.6230)$ in the antisymmetric subspace $\mathbb{U}^+$. You have to make sure you cannot float from $\mathbb{U}^s$ into $\mathbb{U}^+$ - they should be two distinct, orthonormal flow invariant subspaces. Or if you can flow from one into the other, explain in sect. **??** how that happens.

2018-05-02 Predrag Further thoughts about figure 16.14 - interrupted, might continue later:)

2018-05-02 Predrag Remarks on notation: we use curly brackets when listing group elements, as in $S = \{e, \tau_x, \tau_t, \tau_{xt}\}$. I understand why you write $\{\sigma, 1\}$, $\{1, \tau\}, \cdots$ (in order to explicitly indicate the distinction between acting in space and acting in time, but this is not how it is conventionally done, so I'll replace such by the standard subscript notation $\{\sigma, 1\} \to \sigma_x$, $\{1, \tau\} \to \tau_t, \cdots$.

2018-05-11 Matt Projection operators Played around with projection operators with the mistake of not thinking about what I was doing sadly. I need to be able catch myself more readily when going down these rabbit holes as they affect my productivity.

I was naïvely hoping that because relative periodic orbitand preperiodic orbit's appear in pairs that there would be some sort of relation between the shift-reflect subspace and relative periodic orbit's. I investigated angles between relative periodic orbit's and their projections onto the shift reflect subspace but everything lead to a garbled mess with no useful information. There seems to be no organization in the manner I had hoped in all combinations of plotting shift, period, angles between orbit and subspace, and any other dumb idea I could come up with.

Subspaces After thinking a little bit and writing it up in `discsymm.tex`, the symmetry invariant subspaces are the shift-reflect, antisymmetric $\mathbb{U}^+$ subspace, and then the "twice-repeating" in time subspace (invariant under τ_t. The quandary I have with this subspace is that I think it is completely unimportant, as a "twice-repeating" antisymmetric solution would still be in the antisymmetric subspace $\mathbb{U}^+$. Therefore, the twice repeating subspace or $\mathbb{U}^{++} \oplus \mathbb{U}^{-+}$ in the current notation is only twice repeating solutions without shift-reflect symmetry or reflection symmetry. So what are they? Projection onto the subspace leads to symmetric doubly periodic structures but there is no symmetric flow-invariant subspace so I'm confused as to why this would present itself in the derivation.

Attempt at conservation laws Tried to work through Ibragimov results to derive a "conserved vector" but after trying to work things through for far too long I realize I have no idea what I'm doing. I thought that I could make the "Formal Lagrangian" quasi-self adjoint for the shift-reflect subspace and derive a conservation law due to that but it gave me nonsense.

The general idea was to use the quasi-self adjoint criterion $v = \phi(u)$ (as opposed to $v = u$ if the equations were self-adjoint, and then figure out what $\phi(u)$ converts the adjoint equation to the original Kuramoto-Sivashinsky equation .

Substitution of $v = \phi(u)$ into (3.21) and grouping by derivatives of ϕ,denoted by primes,leads to the following equation

$$\phi'(-u_t + u_{xx} + u_{xxxx}) - u\phi'\partial_x u + \phi''(3u_{xx}^2 + 4u_x u_{xxx}) + \phi'''(6u_x^2 u_{xx}) + \phi''''u_x^4 = 0 \tag{16.46}$$

The big waste of time arises from the following desire; If I assume that a linear function ansatz, $\phi(u) = gu$ then all of the higher order derivatives vanish, resulting in

$$g(-u_t + u_{xx} + u_{xxxx}) - ug\partial_x u = 0 \tag{16.47}$$

I was trying to see if I could figure out a symmetry operation g such that the negative signs on the nonlinear term and time derivative term vanish, then the equations would be quasi self-adjoint. I wasted a lot of time without realizing the only way to flip the sign on the time derivative would be time-reversal; so this whole pursuit is worthless. Reflection would switch the sign on the nonlinear term however, so I thought maybe if $g = \sigma\tau$, i.e. shift reflection, then it would work if u was in the shift-reflect subspace but it didn't work out. Basically I was careless in the beginning and then Euler-Lagrange equation based on the "Formal Lagrangian" that is incorrect and nonsensical.

Matrix free's last hope The finite difference calculation that is used to approximate the matrix vector product is just too inaccurate to be of use for the spatiotemporal problem. Comparing the norms of the two vectors, the exact product, $|J\delta\mathbf{x}|$, and its approximation, $|\frac{F(x+\delta\mathbf{x})-F(x)}{|\delta x|}|$ they're off by almost exactly $|\delta x|$, which makes me feel like I had made some stupid mistake but changing this in the GMRES code makes it completely worthless.

I believe the best pursuit is going to be use matrix-free methods on the front end of the calculation and then pass the possible solution to least-squares Newton, explicit matrices and all unless I can find another matrix-free calculation that is more accurate than finite-difference arnoldi inside of the GMRES routine.

Just because I believe it will work I am going for the first option. Automate my code so that it produces initial conditions in the various subspaces, runs them through the adjoint descent method, and if a tolerance is reached it then solves the Newton's method equation by explicit construction of the linear system.

2018-05-14 Matt Projection Operators Trying to figure out the best way to utilize projection operators from `discsymm.tex` in trying to find invariant 2-tori in the shift-reflect subspace.

I think the problem with the shift-reflect invariant subspace code is that it finds equilibria solutions too often, which I believe is because the adjoint descent method doesn't discriminate between $\mathbb{U}^{++}$ and $\mathbb{U}^{++} \oplus \mathbb{U}^{--}$ as the zeroth temporal modes need to be included for the shift-reflect subspace calculation. So I am trying to use projection operators to either begin invariant 2-torus spatiotemporal initial conditions "closer" to shift-reflect subspace solutions and "further" from equilibria, i.e. the $\mathbb{U}^{++}$ symmetry invariant subspace.

One of the consequences of this was figure 16.15, which I'm having trouble realizing if it is entirely trivial or not because the organization when projecting onto two components squares of the $L_2 norms$ are constrained, but their distribution $0.5 < p_1 < 0.95$ seems an interesting consequence. My explanation for the discrepancy between
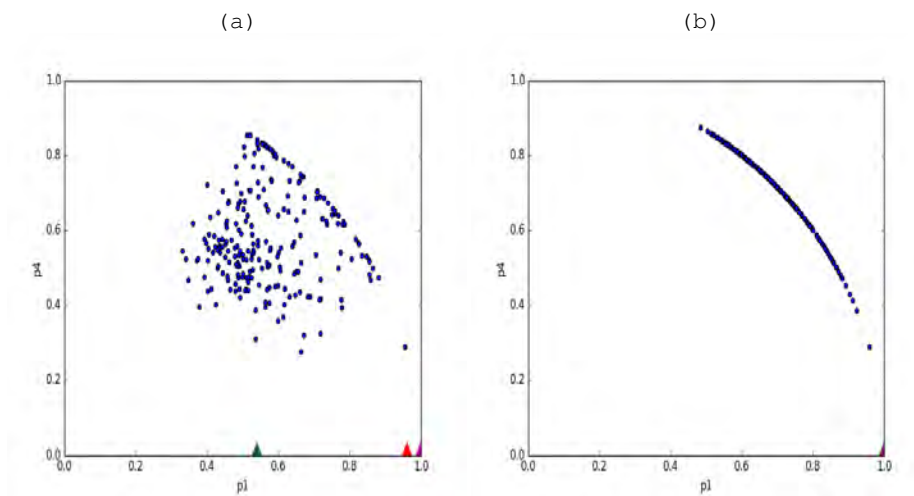
Figure 16.15: Organization of pre-periodic orbit solutions from $L = 22$ domain projected into two dimensions using projection operators that form the shift-reflect subspace. The horizontal axis is defined by $P_1 = \frac{|u^{++}|}{|u|}$, and the vertical axis is defined by $P_4 = \frac{|u^{--}|}{|u|}$. (a) Time integrated pre-periodic orbit s (blue dots) and equilibria (triangles: (red,green,magenta) for (first,second,third) equilibria) (b) Projecting all solutions onto the $\mathbb{U}^{++} \oplus \mathbb{U}^{--}$ shift reflect subspace and then plotting using the same axes.
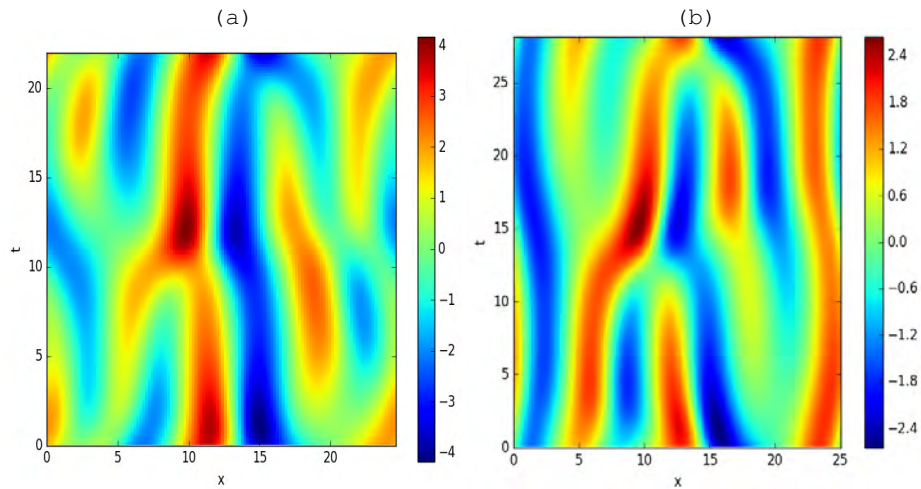
Figure 16.16: (a) Initial guess for the hybrid invariant 2-torus code: $(L_0, T_0) = (22.0, 24.5833538399)$ (b) Resulting invariant 2-torus solution: $(L_p, T_p) = (25.036, 26.584)$

(a) and (b) in figure 16.15 is picking up errors from time-integration as the shift-reflect subspace is not a flow-invariant subspace, but rather a spatiotemporal symmetry invariant subspace.

This can be applied in generating initial conditions, by ensuring that the proportionality is right before starting the matrix-free adjoint descent. I have also improved this part of the code before today as well but never took anything like this into account.

Direct Matrix Code Still going through the optimization and fat cutting so that explicit matrix methods in conjunction with matrix-free adjoint descent.

2018-05-18 Matt spatiotemp codes Nothing to report other than progressing through the tedious process of scrapping, improving, and making various codes compatible.

I'm also trying to make the code consistent with the notation of this blog and others so if anyone went through them they would understand what everything means.

Redefining almost all of the explicit matrix code improved the accuracy and reliability a lot such that I think once all of the codes are compatible I'll be in a really good spot to find lots of invariant 2-tori.

2018-05-22 Matt Still in the beginning of the automation procedure, having some coding troubles with the matrix free code for invariant 2-torus relative periodic orbit solutions. Included is a figure of something that I believe is good that came out; mostly finding equilibria and solutions close

to $u(x,t) = 0$. This is likely due to how I am starting initial conditions in a very naïve way as I tend to do whenever starting out codes instead of thinking it through I'm just testing the combination of codes by throwing anything in and seeing if something comes out. So far, the methods seem to be poor ways of trying to get solutions:

- conjoining two spatial periods of invariant 2-torus solutions seems to yield poor results.

- linear combinations of pre-periodic orbit invariant 2-torus solutions is okay in certain circumstances if the length scales are correct. Incorrect length scales tends to lead to numerical results where $L \to \infty$ for all practical purposes.

- random initial condition generation hasn't been applied yet.

Figure 16.16 is an example of what I would call a good result for the hybrid methods. Constricting a symmetry on a trivial initial condition might be too strict of a constraint and I've been wondering if perhaps I should run full-state space descent methods and then impose symmetry constraints as a secondary method. More testing to come.

I have a lot to *think* about in the days ahead. The idea of imposing symmetry as a secondary option or modifying the preconditioning of the adjoint descent are still my main pursuits as maybe I can somehow modify them or introduce a fictitious forcing that will avoid equilibria type solutions.

2018-05-23 Matt Burak still doesn't see any reason to look for invariant 2-tori with L not fixed, claims it can't work even though I showed him evidence that it does. I agree with him that I need to find the reason for why it works and why it picks out a single representative solution.

He suggested that I look at the (time) Floquet multiplier spectrum as he believes I might be finding periodic orbits at saddle-node bifurcations. I tried to test this quickly but numerical underflow prevents me from seeing such things unless I implement the algorithm from Ding and Cvitanović [18], I believe.

Much more work on automation code, just finding small inconsistencies from testing, working on converging the pre-periodic orbit invariant 2-torus solutions from Xiong's main `h5` file before moving onto randomly generated initial conditions. The main idea from this kind of testing is namely, to see if there are any errors in the automation code, but also see the number of points needed for faithful time discretizations; the pre-periodic orbit solutions are numbered based on their temporal periods in the file so I'm hoping that after some number that either the code will fail or not look accurate, because I am using a 32-by-32 space-by-time discretization for all of the initial conditions.

Qualitatively, it seems that 32 points in time, (16 real valued modes) works well up until $2\,T_{ppo} = 140$ solutions, depending on the different structures present. Convergence with this same number of modes can be achieved for periods larger than this, so I will have to take an in-depth look at the spatiotemporal spectra to see if there is anything discernable about these solutions.

It's quite possible that I merely haven't tuned the adjoint descent well enough, as I'm only allowing for two thousand adjoint descent steps where for an arbitrary initial condition I have used up to one-hundred thousand. But known pre-periodic orbit solutions should converge regardless, so I am taking it on the size of the discretization and not the methods which seem to work fine for other solutions.

I think because the spatial scale is well-defined the approach I will take is as follows for new invariant 2-tori.

For a variety of domain sizes and periods, I will slowly increase the length until I cannot find anything (as described by a number of failed trials) that converges.

As my code allows for any additive factor of two increase in the discretization size in either time or space, I'll have to describe the quantitative way to increase said discretizations in an orderly manner. At each new starting domain length, I will have a minimum number of spatially discretized points, and then gradually increase the temporal discretization as the numerics seem fit. I.e., there will be a systematic description to the growth of the discretizations instead of just multiplicative factors of two, because this grows too quickly.

I believe I fixed all of the issues in the matrix-free relative periodic orbit code so now all that is left before the computers can take over is to do testing on the initial condition generation from a modulated spatiotemporal tile, and seeing if there is any way I can weigh the cost functional to penalize moving towards the $\mathbb{U}^{++}$ symmetry invariant subspace where equilibria live.

2018-05-24 Matt I believe all of the automation and coding is done, now there is only to run it. A possible result is that it works perfectly and finds many invariant 2-tori of varying spatiotemporal symmetry subgroups. The numerical issues that remain are (1) tuning the discretizations, (2) defining the notion of spatiotemporal stability, and perhaps (3) penalizing $\mathbb{U}^{++}$ solutions.

I think more likely is that it finds some solutions, but mostly equilibria and I still need a way to think around this. I think weighing by something like $1/(u - u^{++})$ would do the trick, but Elena mentioned in the plumbers meeting that Ashley tried "something similar" (Predrag: read the pipes blog where it is described) and it didn't work.

They don't care if space is time? Barbarians! I do. Otherwise other than perhaps some small efficiency, notational changes, and antisymmetric subspace $\mathbb{U}^+$ codes the only thing left on the table are the notions of spatiotemporal stability on compactified spacetime and why the methods are picking out certain solutions.

In my mind its rather arbitrary which domain size it lands on but apparently I need a manifest reason in order to motivate it amongst the other powers that be. I am assuming this is the way it will go for the defense of my thesis proposal as well.

This is somewhat airing my grievance to Burak's comments that it is finding an arbitrary domain size (and actually he went as far as to say it shouldn't be possible without additional constraints).

As far as I'm concerned domain size and periodic boundary conditions seemed to be axiomatic. Why attempt to perform periodic orbit theory on the Kuramoto-Sivashinsky equation with $L = 22$ instead of $L = 22.030238210398$? My main point is to elucidate this grievance that I just can't seem to get through to Burak.

The conventional applications of the periodic orbit theory to Kuramoto-Sivashinsky start by *a priori* fixing the domain size. What I am suggesting is that instead we let the equations themselves dictate the periodic domain sizes which satisfy the Kuramoto-Sivashinsky spatiotemporally.

Another argument is, sure, the solutions *might* (as there might be a breakdown or some other bifurcation) be able to be continued in domain size using pseudo arc length continuation; but isn't the whole reason behind this project due to the lack of advancement in the theory of turbulence calculations and periodic orbit theory on large computational domains anyway?

2018-05-28 Matt Trying everything that I can think of to explain the reason behind why my methods work. The Gauss-Newton method, otherwise referred to as "least-squares" Newton, solves the underdetermined linear system $Ax = b$ by solving for the x of minimum norm that satisfies the equation. The translational symmetries do not need to be separately constrained because that would imply an added cost via increasing the norm of x. [5]

I am doing more analysis on whether I can constrain a physically meaningful quantity, i.e. a least energy density solution that perhaps would be more likely to be realized in the infinite spatiotemporal world-view, but this isn't obvious to me as it is coupled to other solutions nonlinearly. All in all I think I know a little more about why my code is finding the solutions it is finding, but so far I cannot tell if there is a more meaningful reason, as other calculations based on the area, energy, norm of the final

---

[5]Predrag 2018-05-28: By "the x of minimum norm" you mean Moore-Penrose pseudoinverse (13.20)?
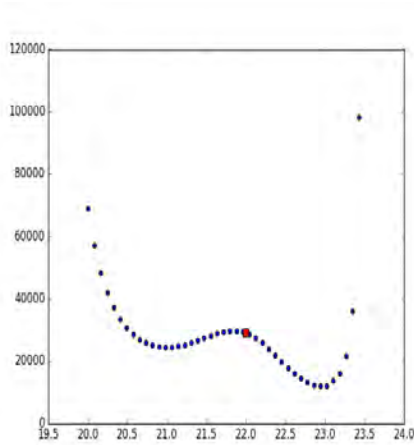
Figure 16.17: Absolute value of the leading Floquet multiplier versus domain size, calculated by numerical continuation of $ppo_{22\times10.2}$ and fixing domain size. The red square is where the numerically converged invariant 2-torus sits when converged without domain size being fixed.

state-vector, seem not to be meaningful quantities for the Gauss-Newton code.

I think my code is still worthwhile as the solutions that it finds can be used for other numerical continuation efforts if a obvious constraint (minimal area for instance) can be numerically derived. So, even if there is no motivation behind the specific solutions that I am finding, they are still great initial conditions for further efforts. They are being found without any time integration or close recurrence procedures due to the efficacy of the adjoint descent when starting with modulated noise.

2018-05-28 Predrag Re. your recent trawls: check whether E of relative equilibrium (1.38) defined in Cvitanović, Davidchack and Siminos [12] Eq. (2.17) is indeed constant when evaluated at any x in the periodic spatial domain. If the Kuramoto-Sivashinsky equilibrium solutions belong to continuous families as functions of L, I think $E = E(L)$ should vary with L. The notion of "energy density" E might be useful for periodic orbits as well, see Sect. 3 of the above paper.

For $E > 0$ equilibria and relative equilibria are organized by the equilibrium points of (1.38)

$$c_+ = (\sqrt{E}, 0, 0), \qquad c_- = (-\sqrt{E}, 0, 0), \tag{16.48}$$

as explained in ChaosBook [10], Example 30.6. *Equilibria of equilibria.*
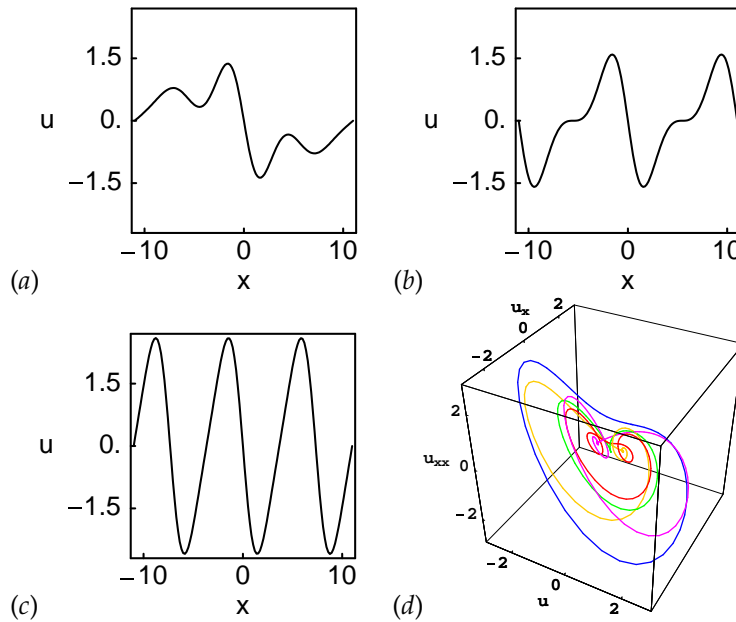
Figure 16.18: (a) E_1, (b) E_2, and (c) E_3 equilibria. The E_0 equilibrium is the $u(x) = 0$ solution. (d) (u, u_x, u_{xx}) representation of (red) E_1, (green) E_2, (blue) E_3 equilibria, (purple) TW_{+1}, and (orange) TW_{-1} relative equilibria. $L = 22$ system size. From Cvitanović, Davidchack and Siminos [12].

Now rescale u in (1.38) as $u \rightarrow u_p \sqrt{E_p}$:

$$\tfrac{1}{2} u_p^2 + \frac{1}{\sqrt{E_p}}(-cu_p + u_{p,x} + u_{p,xxx}) = 1\,, \qquad (16.49)$$

The equilibrium points of (1.38) are now

$$c_+ = (1, 0, 0)\,, \qquad c_- = (-1, 0, 0)\,, \qquad (16.50)$$

so all relative equilibria should line up nicely, like ducks in a row. You can do the same thing for any invariant 2-torus p by rescaling the Kuramo-to-Sivashinsky equation (18.1) by the invariant 2-torus p energy density (1.44).

I do not remember Lan and me doing this, but it looks like the symbolic dynamics for all equilibria and relative equilibria could be a $\pm$ for each turn around the stable manifold of $c_\pm$.

Also, I'm unsure whether my code is having a harder time finding invariant 2-torus spatiotemporal invariant solutions at larger domains or if its just a consequence of punctuating the runs more often to make more tuning and corrections.

2018-05-30 Predrag Some logical cross-checks: The Kuramoto-Sivashinsky equation is Galilean invariant: if $u(x, t)$ is a solution, then $v + u(x - vt, t)$, with v an arbitrary constant velocity, is also a solution. In our fixed L calculations we only work in the zero mean velocity frame, so let us also require that in $L \to \infty$ limit

$$\int dx \, u = 0 \,. \tag{16.51}$$

Suppose that

$$\oint dx \, u_p = C_p \neq 0 \tag{16.52}$$

for a given invariant 2-torus p. But that cannot tile the infinite space (16.51), as each repeat over a segment of length L increments the integral by C_p. Hence it is OK to demand that $\langle u \rangle = 0$ vanishes for every solution p.

Note also that $\langle u \rangle = 0$ implies that the energy density is proportional to twice the variance of u,

$$\sigma^2 = \langle (u - \langle u \rangle)^2 \rangle = \langle u^2 \rangle \,. \tag{16.53}$$

This quantity is a "random walk" in u, and expected to grow linearly with L, so the energy density (1.51) is expected to go to a limit for $L \to \infty$, justifying the rescaling of u proposed above. That also means that the range of u values for a typical relative equilibrium should (could?) grow linearly with L, and for a typical invariant 2-torus proportionally to LT.

The reason I obsess about this is that we need to have the same (covering) alphabet everywhere. So our letters should correspond to local *increments* (like the turns of the unstable spiral around the equilibrium c_-), and not be proportional to the magnitude of u.

2018-05-31 Matt Having trouble finding the magic bullet for rescaling equilibria. I believe that the correct transformation for rescaling u in (1.38) is $u \to u_p\sqrt{2E_p}$, rather than Predrag's $u \to u_p\sqrt{E_p}$.

This can be seen by looking at the equilibrium condition of (16.49). If the solution has spatial derivatives equal to zero, then (16.49) implies $\frac{1}{2}u_p^2 = 1$, which in turn implies $u_p^\pm = \pm\sqrt{2}$.

2018-05-31 Matt Therefore, I believe the correct transformation is $u \to u_p\sqrt{2E_p}$, which leads to

$$u_p^2 + \sqrt{\frac{2}{E_p}}(-cu_p + u_{p,x} + u_{p,xxx}) = 1 \,, \tag{16.54}$$

rather than Predrag's (16.49).

With my rescaling, the equilibrium points of (1.38) are now

$$c_+ = (\frac{1}{\sqrt{2}}, 0, 0) \,, \qquad c_- = (-\frac{1}{\sqrt{2}}, 0, 0) \,, \tag{16.55}$$

After further investigation and numerous checks the rescaling by the now corrected value still doesn't seem to work for equilibria solutions on arbitrary domain sizes. The issue seems to be that solutions bifurcate via crossing over $(0,0)$ in the rescaled $(u_p, u_{p,x})$ axes, almost in the act of shedding loops that do not follow the symbolic dynamics prescribed by looping around the equilibria at $(\pm 1, 0, 0)$.

2018-05-31 Matt Animation ../figs/eqva_bif.gif (run it in Chrome or in Photoshop or the like) shows the change of an equilibrium identified in the next post with increasing the domain size from $L = 12$ to $L = 32$ through numerical continuation (as opposed to hundreds of "slides"). The left frame is a plot $(u_p, u_{p,x})$, and the right frame plots $(x, u_p(x))$. The domain size is indicated in the title of each plot. Note that u_p are the *rescaled* fields, as defined by (16.49).

The domain size was numerically continued by using spatiotemporal (overkill) convergence code that fixes the domain size, unlike my other codes. The domain size was changed in step sizes of $\Delta L = 0.1$. It converged over the range of $L \in [12, 32]$, which suffices to identify several bifurcations.

2018-06-19 Predrag ../figs/eqva_bif.gif narrative
Much is known about what one expects, see figure 1.3. In the natural units $\tilde{L} = L/2\pi$ of system size length, one finds zero-energy bifurcations off the equilibrium $u(x,t) = 0$ at integer $\tilde{L} = 1, 2, 3, 4, 5, \cdots$, i.e., at
$L = 6.283, 12.566, 18.849, 25.133, 31.416, \cdots$

As E is here a very important parameter that vanishes at the birth of equilibria spun off $u(x,t) = 0$, one should *not rescale* u by (16.49) in these plots. A look at Kevrekidis, Nicolaenko and Scovel [35] Fig. 6.1 indicates that the same maxima $E = 1.6 \cdots$ for E_k, $k = 1, 2, 3$ are only apparently the same, maxima do grow larger for for larger k.

The initial $L = 12$ equilibrium is E_1. It collides with a pure harmonic at $\tilde{L} = 2.013$ (known as $L = 12.65$ in gradstud speak). We see from figure 1.3 that is the death of E_1 and its continuation as E_2. In turn, equilibrium E_2 dies someplace above $L > 25$ (details might be in the literature). Matt's continuation misses all other coexisting equilibria and relative equilibria, unless it picks up the bifurcation to equilibrium GLMRT [24] at $\tilde{L} = 2.5 \cdots$ (known as $L = 15.7 \cdots$ in gradstud speak). But I am unsure as to it actually doing that. [6]

Next, something happens at $\tilde{L} = 3.63$ (known as $L = 22.8$ in gradstud speak). Perhaps GLMRT $\to \text{TW}_{\pm 1}$. That will be easy to tell if also E is plotted as a function of L.

---

[6]Predrag 2018-06-20: According to Greene and Kim [24], GLMRT solutions (studied at length by them) are generalized LMRT solutions of LaQuey *et al.* [42], where "LMRT" are the author initials, and decoding what they would correspond to today, 45 years later, we leave as an exercise to the reader.

2018-06-05 Matt Currently running testing to determine how many spatiotemporal modes are needed for accurate representations of invariant 2-tori. Running tests where $L = 23$ with the number of spatial modes is $m = 16$ which has been shown before to be adequate at this domain size. Although I have code running I have yet to find to most convincing way of demonstrating where the temporal discretization is adequate, convergence doesn't seem to be the best means of demonstrating this because solutions can converge with a small temporal discretization but when viewed qualitatively sometimes even the converged solutions do not look like what I would expect.

This falls under the title of tuning and testing of the spatiotemporal codes; trawls still being run on light to find shift-reflect invariant 2-tori, as I wasn't sure where the error of relative periodic orbit invariant 2-tori was. Will start relative periodic orbit invariant 2-torus trawls tomorrow, also need to upload more figures from further trawls, although as the domain size increases the number of convergent solutions seems to be decreasing.

After further testing, imposing the correct spatial scale as determined by the spectrum of the Kuramoto-Sivashinsky equation $\tilde{L} = 2\pi\sqrt{2}$ leads to many equilibria solutions so imposing the incorrect spatial scale is almost more beneficial much like imposing a larger than normal magnitude of the spatiotemporal field $u(x, t)$.

2018-06-11 Matt Trawling on larger domains $L > 70$ is picking up nothing but bottom feeders currently so I've been working on improving the trivial symmetry, i.e. full state space code in hopes that relaxing symmetry requirements finds us more invariant 2-torus invariant doubly periodic solutions. Other than the relative periodic orbit invariant 2-torus solutions posted today there is only one new pre-periodic orbit invariant 2-torus solution before I left the office so I'll wait for a bigger haul before uploading.

2018-06-11 Matt Numerics: aliasing Extracted information from ref. [4] on what I thought was one of the gaps in my code which was the fact that it seemed to perform much better as a fully aliased pseudospectral calculation rather than a de-aliased calculation. I feared that this would bring criticism so as I tried to armor myself by actually *reading*. My argument is that while aliasing can be devastating for temporal evolution due to the contamination of the higher Fourier mode components by their aliases, $(k' = k + N)$ where N is the number of collocation points, the spatiotemporal problem should be fine as long as the calculation is well resolved enough. In fact, this is likely why I have solutions that "converge" on larger spatial domains than the discretizations can seem to resolve.

Aliasing commments:

> For evolution problems one must address the issue of the temporal numerical stability of the calculation. Collocation ap-

proximations must be formulated with more care than Galerkin approximations. The reason is that for evolution problems with quadratic conservation properties, the Galerkin formulation will automatically yield semi-discrete quadratic conservation laws.

Numerous comparisons have been performed for aliased and de-aliased calculations of the periodic, multidimensional Navier-stokes equations. Useful discussions may be found in [22, 34, 46, 50]. All of these authors conclude that with sufficient resolution, aliased calculations are quite acceptable.

Moser, Moin and Leonard [47] caution against aliased calculations. They present a single, poorly resolved, aliased calculation and compare it with three de-aliased calculations, one poorly resolved, one moderately resolved, and one well resolved. Their single aliased result is certainly much worse than their well resolved, de-aliased case, but their poorly resolved, de-aliased case is no better than the aliased one. Hence, their conclusion is not supported by their evidence.

In light of these comments and discussions I believe that de-aliasing is more important in the context of accurate temporal evolution, but not required in the spatiotemporal fixed point problem as long as the patterns are sufficiently resolved. One way of thinking about this is that in the discretization of the spatiotemporal Kuramoto-Sivashinsky equation we could add a term that represents the aliasing,

$$\sum_{m',n'} \sum_k \neq 0, j \neq 0 a_{m-m'+kM,n-n'+jN} a_{m+kM,n+jN} \, ,$$

as it is implicit in the fully aliased representation of the equations.

I believe the spectrum of the Kuramoto-Sivashinsky equation plays a role, and it might be wise to at least dealias the temporal convolution sum as there is less of a precedent for ignoring it; In the spatial case we can at least claim the hyperdiffusion term diminishes the amount of corruption in the spatial wave number, but this is harder to motivate for the temporal terms.

More motivation from Canuto, Hussaini, Quateroni and Zhang [4] are their fig. 7.1 and fig. 7.4, where the fully aliased but more resolved terms seem to beat out even the dealiased computations in energy conservation of the KdV equation for fig. 7.1.

Their fig. 7.4 is a reproduction of the effects of aliasing in the transition to turbulence in channel flow by Krist and Zang [38]. Only the high resolution (aliased) seems to be physically representative of the actual solution, and even the dealiased computation on a coarser discretization (while
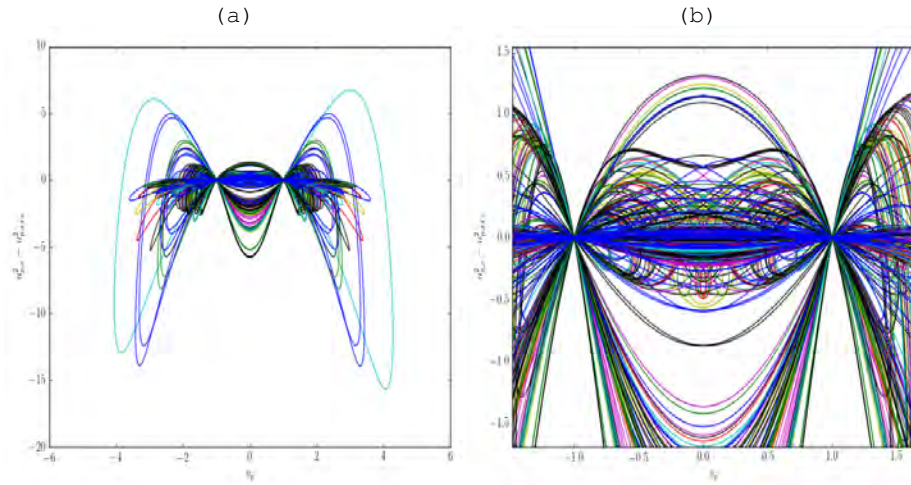
Figure 16.19: (a) Plots of u_p versus $u^2_{p,x} - u^2_{p,xxx}$ for all of the equilibria solutions in svn repository. (b) Zoomed in view showing that all spatial periodic orbits seem to intersect at $(\pm 1, 0)$ in these coordinates.

better than the equivalent aliased discretization) still does not prevent artificial oscillations. This is also a temporal evolution problem which we are not dealing with.

In light of all that I have seen, resolution is King.

2018-06-11 Matt Equilibria rescaling I've been trying to work with the rescaled equation for equilibria of the $T = 0$ system in order to best demonstrate how they are organized in space. Burak pointed out that I should be able to get a lobe if I use the Miranda and Stone [45] coordinate transformation (discussed at length in ChaosBook for the Lorenz symmetry reduction). I'm still playing around with it but here are the best results I have so far:

- Figure 16.19 is a plot of $u^2_{p,x} - u^2_{p,xxx}$ as a function of u_p. Other projections don't seem to elucidate anything and when zooming in even further than (b), all orbits come within about 10^-7 of intersecting $(\pm 1, 0)$ in terms of vertical $(u^2_{p,x} - u^2_{p,xxx})$ distance.

- Figure 16.20 finds the return map of $u^2_{p,x} - u^2_{p,xxx}$ of a family of numerically continued equilibria solutions in space by calculating when the other nonlinear coordinate transformation $v = 2u_{p,x}u_{p,xxx}$ crosses the origin, with $u^2_{p,x} - u^2_{p,xxx}$ positive, to guarantee that all section crossings are in the same direction. Color coding indicates domain size of the solution.

- Figure 16.21 The return map calculated as in figure 16.20 but with all of the equilibria solutions in the repo.
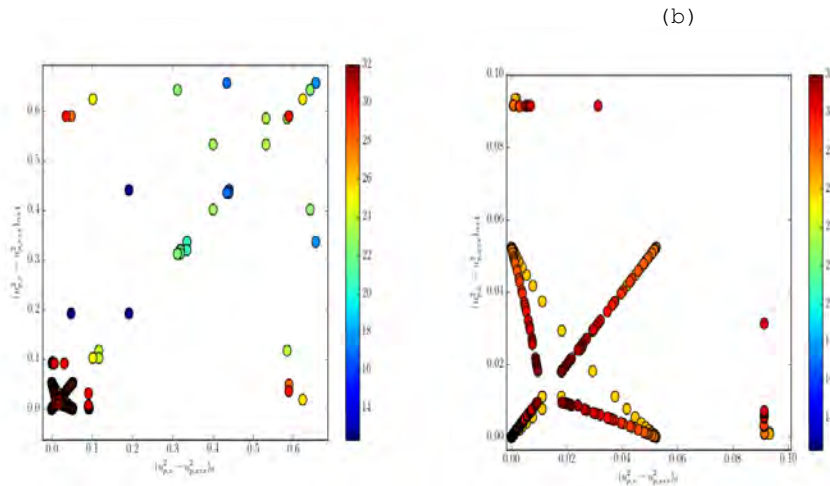
Figure 16.20: (a) Return map of $u_{p,x}^2 - u_{p,xxx}^2$ for a family of equilibria numerically continued in space. Found by looking for when the other transformed coordinate $2u_{p,x}u_{p,xxx}$ passes through zero and $u_{p,x}^2 - u_{p,xxx}^2$ is positive. (b) Window around the origin. Color scale indicates the domain size of the numerically continued equilibria
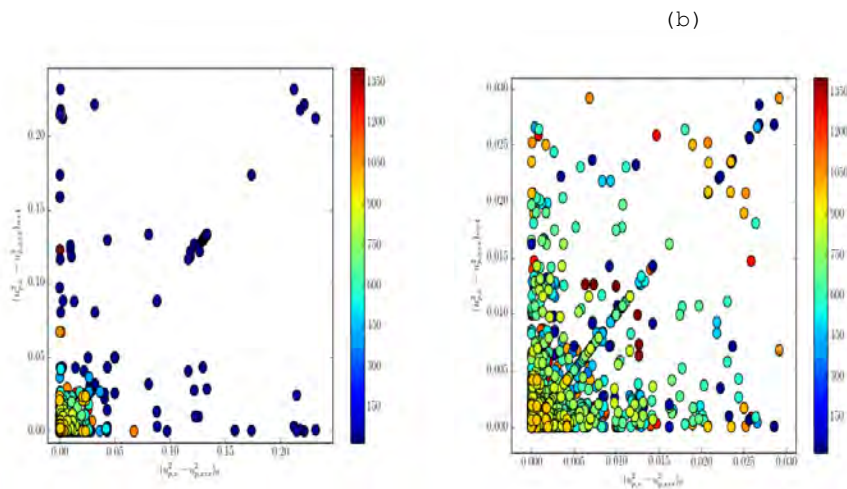
Figure 16.21: (a) Return map of $u_{p,x}^2 - u_{p,xxx}^2$ for all equilibria in svn repository. Found by looking for when the other transformed coordinate $2u_{p,x}u_{p,xxx}$ passes through zero and $u_{p,x}^2 - u_{p,xxx}^2$ is positive. (b) Window around the origin. Color scale indicates the domain size of the equilibria .
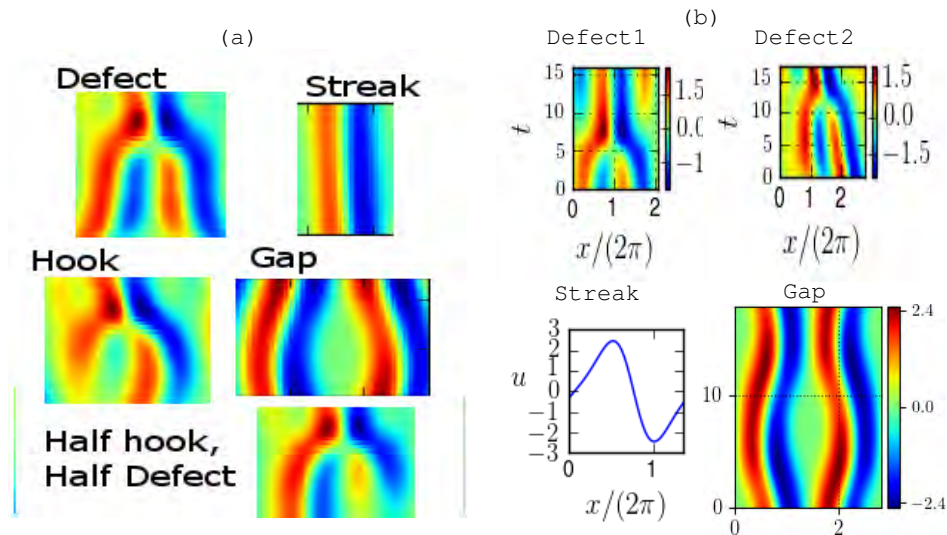
Figure 16.22: (a) A proposal for an alphabet of Kuramoto-Sivashinsky spatiotemporal patterns with catchy names. One should also quotient the spatial reflection, i.e., the fundamental domain is 1/2 of the pattern shown. (b) Corresponding representative invariant 2-tori: defect1 = $\mathrm{rpo}_{13.2\times15}$; defect2 = $\mathrm{rpo}_{17.5\times T17}$; streak = *eqva_L8.5*; gap = *po_L17.3_T15.3*.

Whether these plots will prove useful for analysis is still to be seen. Figure 16.19 might help. While its not as clear as to how to formulate the symbolic dynamics as in the Lorenz system, as there seem to be three distinct lobes as opposed to two; in the symmetry reduced projection it might change from a three-letter alphabet to a two letter alphabet; What I'm trying to say is that by using this coordinate transformation, even when plotted in a non-reflection symmetry reducing way I believe that there are three lobes, i.e., $(-1, C, 1)$, which might be useful.

2018-06-11 Matt Reading While making small coding adjustments and playing with equilibria of equilibria I've been trying to read as much on the variational integrator literature as I can; there's just a lot. Kraus and Maj [37] seems to be a good introduction but there the notation is seemingly purposefully confusing. Due to the geometrical nature there are lots of indices and substitutions and man I find it hard to get through the brush.

2018-06-25 Matt Working through using CUDA (Nvidia based GPU processing toolkit) for energy norm comparison code.

The outline of the code is as follows,

- Produce large scale ("infinite") spatiotemporal computations with a
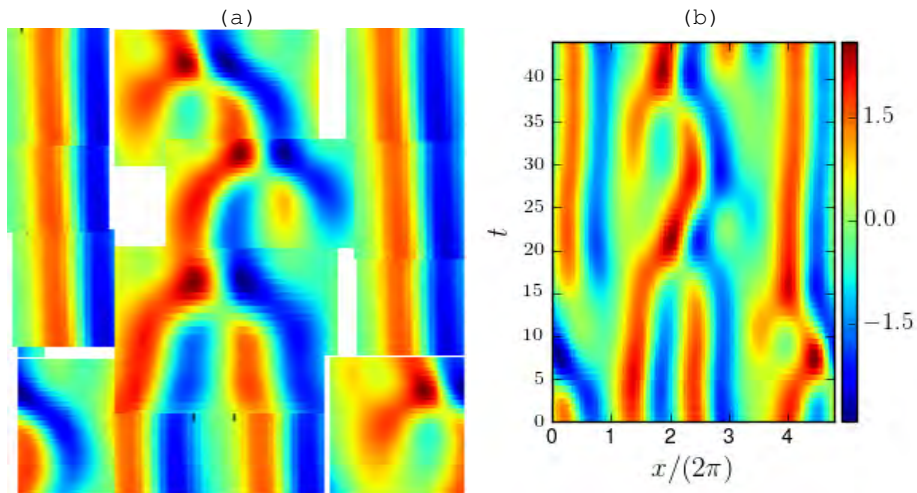
Figure 16.23: (a) A crude tiling of a (b) shift-reflect invariant invariant 2-torus $\text{ppo}_{30\times44}$. This uses only snippets from figure 16.22. Continued in the blog post of **2018-11-09**.

spatiotemporal discretization convention such that $\Delta x, \Delta t = 1$, for instance.

- Rediscretize invariant 2-tori to obey the same discretization convention.

- Either use spatiotemporal invariant 2-torus solutions or subdomains to search for regions where difference in energy norm is small.

- Do the energy norm computations in parallel so that it runs fast.

- Produce figure by cutting out where the difference in energy norm is small comparatively, label with symbol.

From staring at invariant 2-tori there are a few tiles that seem to appear frequently, see figure 16.22. Any of these patterns could also have an additional adjective "tilted" in front of them, which is the same shape with the addition of SO(2) rotation:

- Streaks (equilibria, relative equilibria)

- Defects ($2 \rightarrow 1$ wavelength mergers)

- Hooks

- Half defect/half hook (birth and death timescales for each "half" of the merger are drastically different)

- Bent streaks

- Gaps

I believe that there is a physical way of explaining the pattern formation of the defects in pre-periodic orbit invariant 2-tori. It begins when the spatial domain size becomes large enough that it can admit an additional pair of streaks (crest and trough), due to a higher spatial wavenumber becoming the most unstable. What I believe happens next is that the streaks bend giving rise to a spatiotemporal region that is for all intensive purposes "empty" of structure ($u = 0$). Because the Kuramoto-Sivashinsky equation is linearly unstable, the region becomes a site for the formation of a new defect. It begins first with the formation of a "hook" branching off from its original streak. As the magnitude of the crest and trough combination grows, it detaches from its original streak, leading the the "half-hook" or "half-defect" structure. I am categorizing this by "half" because the time-scales for birth and death of the defect are drastically different. Eventually the half defect merges with another streak, leading to the full $2 \to 1$ wavelength merger, where both halves of the defect have the same time scale. I don't know how to include rotations into this impromptu theory, but in my mind they just allow more combinations of possible streak and half-defect mergers.

2018-06-27 Predrag The love child figure 16.23 of many genders of spacetime patches is cute! Let's try to find invariant 2-tori that capture these shapes. (Continued in the blog post of **2018-11-09**.)

2018-06-27 Predrag Looking at
gudorf/python/KSTori/converged_solutions/figures/:

eqva/ Need to know energy densities - perhaps a single E.txt list would suffice.
$u(x) = 0$ solution: eqva_L26.9

eqva/figsWide $u(x) = 0$ solutions: eqva_L494.5, eqva_L594.7, eqva_L597.3, eqva_L625.7, eqva_L628.2, eqva_L666.1, eqva_L676.8, eqva_L703.8, eqva_L751.4, eqva_L813.2

reqva/ Need to know energy densities and travelling wave velocities - perhaps E.txt, c.txt lists would suffice.
$u(x) = 0$ solutions: reqva_L24.9, reqva_L32.1, reqva_L44.3,

full/ What is "full/?" A periodic orbit? If in $\mathbb{U}^+$, I would expect those should be antisymmetric under a space reflection, but I do not see the symmetry line for any of them, except for $ppo_{34.9\times23}$, full_L26.7_T54, full_L32.5_T19

I moved all $u(x) = 0$ solutions to zero/.

2018-06-29 Predrag moved from *eqva/dataWide* to *eqva/data*:
eqva_L56.4, eqva_L56.9, eqva_L77.7

2018-06-28 Matt "Full" was what I called the periodic orbits that were found with (16.17) that had a SO(2) shift that was smaller than the grid spacing,

i.e., $\sigma \leq \frac{L}{M}$, I realized after looking at the trawls that my relative periodic orbit invariant 2-torus codes did not have any guarantee they were picking out prime periods and some of the solutions look spurious.

2018-06-27 Predrag `eqva/` k wavenumber "streak" tiles:

eqva_L22.4 is 2 repeats of eqva_L11.2, find it.

eqva_L23.8 is 2 repeats of eqva_L11.9, find it.

eqva_L25.5 is 4 repeats of eqva_L6.37, find it.

eqva_L25.7 is 3 repeats of eqva_L8.6, find it.

eqva_L29.4 is 4 repeats of eqva_L7.35, find it.

eqva_L34.1 is 3 repeats of eqva_L11.4, find it.

2018-06-28 Matt All were found. As they belong to continuous families, I found them at slightly different lengths.

2018-06-27 Predrag `full/` $(L/3, T/3$ shift and translate "cat eye" or "gap" tiles:

full_L24.4_T41 seems "almost" invariant under $x \to x - L/3, t \to t + 2T/3$ and $x \to xL/3, t \to t + T/3$.

Matt, can you find a solution $\text{ppo}_{8.1\times13.7}$ with $1/3$ shifts both in space and time?

Similarly, $\text{ppo}_{25.3\times13.7}$ seems "almost" invariant under $x \to x - L/3, t \to t + T/3$ and $x \to xL/3, t \to t + 2T/3$.

Matt, can you find a solution $\text{ppo}_{8.4\times7.3}$ with $1/3$ shifts both in space and time?

In other words, both are the same solution, differing only in E. This "cat eye" appears many places, for example in $\text{ppo}_{24.4\times17}$, $\text{ppo}_{24.4\times41}$, $\text{rpo}_{26.8\times21}$, $\text{rpo}_{24.5\times55}$, $\text{rpo}_{24.9\times74}$, $\text{ppo}_{30.6\times12}$, $\text{rpo}_{31.1\times85}$, $\text{ppo}_{31.8\times40}$.

2018-06-27 Predrag $k \to k - 1$ "defect" tiles: They look like temporally heteroclinic connections, not sure it makes sense to make the spatiotemporaly periodic. Still, $\text{rpo}_{28.6\times12}$ suggests Matt might find be a $\text{rpo}_{14.3\times12}$, single "defect tile."

2018-06-27 Predrag When they go high, we go low. Try to find a set of invariant 2-tori with the smallest possible L and T.

Keep track of energy density E - some of the above are related by continuation. We have to figure out what selects a preferred solution from a continuous family with differing E.

In all of the above searches - never start by a random initial condition, always use patches of the existing solutions (perhaps smoothed out by a Fourier transform, throw away high wave numbers, Fourier transform back) as the initial conditions.

2018-06-29 Matt The fact the defects come in continuous families isn't too surprising but it makes analysis a little harder. The idea that I've been thinking through is to use invariant 2-tori to create a library of these patterns, but they emerge in all of the spatiotemporal patterns.

2018-06-29 Predrag Try to find the above **2018-06-27 Predrag** shortest time rpo_L14.3_T12 $k \to k - 1$ "defect" tile (extracted from rpo_L28.6_T12?). Then other defects might be interpreted as streaks (of varying duration) capped by the defect that might then be again followed by a streak.

2018-06-29 Matt I don't have a very robust justification for it just yet, but I believe the constituent blocks need to be cropped from minimal time and space solutions, I'm thinking this way because the smaller the spatiotemporal domain the less likely that rotations come into effect and the I believe we are more likely to get prime tilings this way. The evidence for this is by looking through my solutions it seems that if given the leeway in a larger temporal domain they tend to drift; even though we are in the shift-reflect invariant subspace I believe the key way of thinking about this is that the mean shift is equal to zero but not the instantaneous shifts. Therefore, in small temporal strips the periodic boundary conditions provide a purer realization of the subdomains.

2018-06-29 Matt I'm including animation **../figs/MNG_ppo1_energy.png**, a continuation of **2018-06-19 Predrag** ../figs/eqva_bif.gif narrative. Again, it runs in Chrome and can be edited in Photoshop.

The idea is that by numerically continuing $\text{ppo}_{22 \times 10.2}$ of the $L = 22$ domain, we track the energy of the invariant 2-torus via the diagonalized quadratic norm of the spatiotemporal Fourier coefficients and plot them together.

In the animation, the only weak spot is that the extent of time is fixed; it seems like the best solution to having multiple subplots, one of which I wanted to demonstrate "growing". I.e. the u field's spatial extent is displayed as growing as it should be; sacrificing the aspect ratio between time and length in the process, so be wary of time scales.

From the plotting, and surprising amount of numerical continuations I was able to achieve if I stepped over $L = 18.6$ (For whatever reason it couldn't converge at that exact fixed length). I believe the animation shows that at bifurcations the energy as a function of domain size remains continuous but not differentiable, as indicated by the kinks at $\tilde{L} = L/2\pi \approx 2.7, 2.9, 3.7$.

The idea of this was to show that numerical continuations of a single invariant 2-torus solution display the different types of defects based on domain size, but it seems bifurcations are at play here. The cat's eye (gap) that appears from bifurcating from the equilibrium solutions at small L occurs first, followed by a descent in energy that by eye seems to approach the antisymmetric subspace $\mathbb{U}^+$ (before and after $\tilde{L} \approx 2.9$. might

be two different solution curves but I'm not convinced). Then as we approach the pre-periodic orbit we are familiar with, the hook shape seems to form and as we get to large it transitions to the "half defect" state followed by another bifurcation I believe that leads to the full defect.

I'm trying to use this as evidence that certain shapes fundamentally exist in certain spatiotemporal areas, but it's hard to specify due to the families they come in.

2018-06-29 Predrag An attempt at **../figs/MNG_ppo1_energy.png narrative**:

The antisymmetric subspace E_1 family $\in \mathbb{U}^+$ (or $-u_{\mathrm{E}_1}$, note the tilts are a reflection of each other) in ../figs/eqva_bif.gif is followed up to $\tilde{L} \approx 2.7$, followed by a spatiotemporal bifurcation to

antisymmetric subspace $\mathbb{U}^+$ "cat eye" or "gap" at $\tilde{L} \approx 2.9$, followed by spatial-reflection symmetry breaking bifurcation to

"hook" at $\tilde{L} \approx 2.9$ (known as $\mathrm{ppo}_{22\times10.2}$ at $L = 22$), followed by bifurcation to

"defect" at $\tilde{L} \approx 3.7$.

2018-06-29 Matt : Found the equilibria solutions from **2018-06-27 Predrag**. Slight discrepancies in predicted length due to allowing it to vary as a parameter. I took the original equilibria solutions that seemed to be made of repeats and then took the fraction of the spatial domain given by 1/(number of repeats). For some of the equilibria solutions no work was needed, in this case, the residual of the cost functional after chopping up the repeated solution was already within machine precision.

For equilibria the equations that define the cost functional for the $T = 0$ Kuramoto-Sivashinsky equation in terms of (purely imaginary) spatial Fourier modes are

$$F_{eq} = (q_m^2 - q_m^4)b_m + \frac{q_m}{2} \sum_{k=0}^{M-1} b_m b_{k-m} = 0 \qquad (16.56)$$

with the the cost functional

$$S = \frac{1}{2} F_{eq}^\top F_{eq} \,. \qquad (16.57)$$

I was able to find all prime (spatial) period equilibria that Predrag predicted, but the domain sizes vary slightly as the solutions come in continuous families.

2018-06-29 Predrag `wegolow/eqva/figs/` are all the standard issue, antisymmetric space $\mathbb{U}^+$ solutions, so their actual, prime spatial period is $L/2$ (all that needs to be plotted), where L is the length Matt currently assigns them.

eqva_L6.3, eqva_L7.1, eqva_L8.5, and eqva_L11.2 are presumably the same solution, different E's.

I think this should be the E_1 family (or $-u_{E_1}$) in ../figs/eqva_bif.gif.

eqva_L11.1 and eqva_L11.9 are presumably the same solution, different E's.

If u_E is a solution, is $-u_E$ a solution? I vaguely remember that in the restriction to the antisymmetric subspace $\mathbb{U}^+$, these appear as shifts by $L/2$?

Defect1 *rpo_L13.2_T15* looks like a periodic orbit in the antisymmetric subspace $\mathbb{U}^+$, not like a relative periodic orbit. The effect after a T is a shift by $L/4$: note, no change in the wavenumber.

2018-07-04 Matt Plumbing? I'm here to tile the walls Detailing the process by which I found the tile which is currently being referred to as "gap" or "cat's eye".

I followed the following procedure;

- Look through figures of converged invariant 2-torus solutions for what could hold a minimal spatiotemporal tile.
- Note that full_L26.7_T54 in figure 16.24 (a) seems to have a subdomain $\frac{x}{2\pi} \in [0, 2.75]$, $t \in [0, 18]$ that is the "gap" or "cat's eye" pattern.
- To be safe, first truncate the temporal extent only, and converge the solution. This leads to figure 16.24 (b), where the period takes the new value $T \approx 18.9$, about a third of the initial invariant 2-torus.
- Finally, truncate the spatial extent of figure 16.24 (b) and converge, resulting in invariant 2-torus wegolow/po/po_L17.3_T15.3 of figure 16.24 (c). [7]
- We believe this invariant 2-torus to be a representative "cat's eye" pattern or "gap" sketched in figure 16.22, and seen frequently in larger invariant 2-tori.

Invariant 2-torus full_L26.7_T54, as well as the so far unnamed invariant 2-tori figure 16.24 (b) and (c) belong to the antisymmetric subspace $\mathbb{U}^+$, with reflection point $\frac{x^*}{2\pi} \approx 1.25$. The spatial $SO(2)_x$ shift of these solutions is $d_x \approx 10^{-5}$. Because the initial condition for full_L26.7_T54 was modulated noise, and no discrete symmetries was imposed during the calculation, one could not predict the final symmetry subgroup of a solution when using the relative periodic orbit invariant 2-torus spatiotemporal code.

The "full" type solutions are a subset of solutions to (16.17) where the $SO(2)$ parameter takes the value close to zero. Using a mean-velocity frame I impose in the ansatz that the $SO(2)$ shift manifests

---

[7]Predrag 2018-07-06:   po_L17.3_T15.3 is eye-balling guess, please fix, provide data file in po/data/
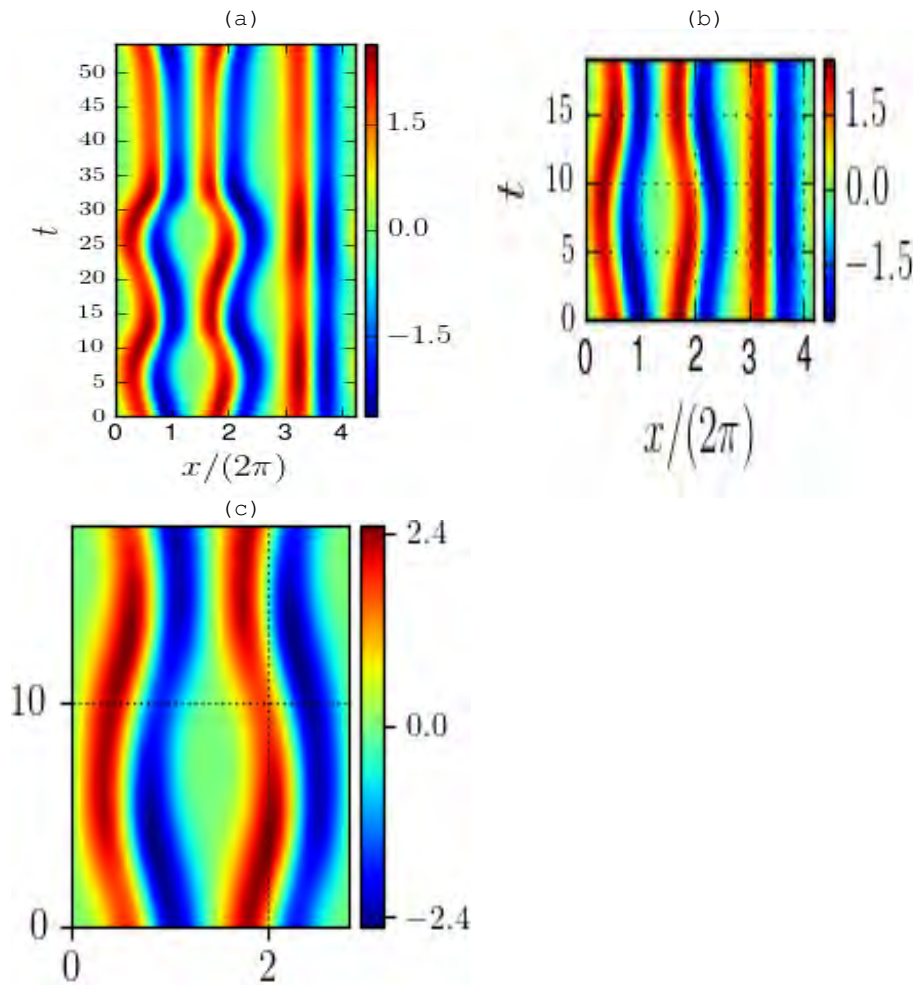
Figure 16.24: (a) Invariant 2-torus full_L26.7_T54. (b) A temporal subtile that was cut out from (a) and then converged via Gauss-Newton method. (c) The final "gap" tile, figure 16.22, that was cut out from (b) and then converged to invariant 2-torus po_L17.3_T15.3 via Gauss-Newton method.

in the equation itself, but there is nothing to prevent this shift parameter from taking a value of zero, and there is no reason to fear that either; relative equilibria some in continuous families, with corresponding intervals of spatial shifts, which can include periodic orbit $d_x = 0$ solutions.

This is similar in regards to the pre-periodic orbit invariant 2-torus spatiotemporal code. Technically, it can allow for twice repeating solutions in the antisymmetric subspace $\mathbb{U}^+$, but it is quite rare that these events happen as it requires half of the computational variables, (spatiotemporal Fourier modes) to be identically zero. An example of this is $\mathrm{ppo}_{34.9\times23}$. It is tagged as a pre-periodic orbit, only the fundamental domain is being plotted, but it turns out to be a periodic orbit with period $T \approx 23$.

This process is quite idiosyncratic by its nature, and not very easy to automate as it requires user input to tell what subdomains are good candidates for minimal tiles. Therefore I hope to have more tiles soon but its a trudge through messy waters.

Plumbers meeting Burak and Elena were present and I think now Burak is on board and excited about the direction my research is taking; not to say he was ever opposed to me, let's just be clear. He thinks that it would be beneficial to develop code that tracks the "trajectories" of local minima and maxima through time and plots them might help in terms of analysis. I agree that while looking at colored density plots of spatiotemporal fields is more confusing, I'm not sure how easy it would be to implement this type of code. I believe his idea is that the idea of looking for important structures, streaks, gaps, etc. comes down to local minima and maxima pairs, their births and deaths, and one should remove all other extraneous information. I believe he is in agreement with me that perhaps numerical continuation of minimal tiles could span a wide enough library of spatiotemporal symbols such that any solution can be constructed; where the particular realizations picked from continuous families of solutions would be determined by *a priori* choosing a spatiotemporal area to work with.

2018-07-05 Burak I really like the patterns in figure 16.22! The solid state model I mentioned in the earlier meetings is called "terrace ledge kink model" and the Wikipedia article seems to have a good introduction to the basic ideas. The analogy I had in mind was roughly the following:

- Space-time plot → 2D crystal surface

- Patterns (defect, streak, etc.) → Crystal defects (kinks, adatoms etc.)

One thing that is different is the discreteness of crystal surface as opposed to the continuous tiling in the $(1+1)-D$ spatiotemporal dynamics, where the patterns appear in different sizes. Matt nicely illustrated these things

in yesterday's meetings by pointing at frequently appearing patterns and matching them to the ones that appear along the continuation of the fundamental PPO.

I suggest the following for a systematic classification of the patterns: Take spatiotemporal plots of the Kuramoto-Sivashinsky dynamics and at each time slice t, detect local minima and maxima. Than connect these local minima and maxima along the spatiotemporal figure with, say, dashed and solid lines respectively. Roughly speaking, this is going to be drawing lines along the middle of red and blue regions of the spatiotemporal visualizations. Perhaps, some thresholding, such as assuming an $(-\epsilon, \epsilon)$ interval to be 0 since sometimes there are very pale red/blue peaks. I mentioned up to this point in yesterday's hangout.

2018-07-06 Predrag I have split periodic orbits `full/` folder into `full/` and `po/`.

`full/` belong to the continuous relative periodic orbit families. They are a subset of solutions to (16.17) for which the spatial shift happens to be close to $d_x = 0$.

`po/` solutions, antisymmetric under a space reflection across symmetry points x^* and $x^* + L_{Matt}/2$, belong to the *spatially antisymmetric subspace* $\mathbb{U}^+$, see sect. **??**. Currently Matt has found only

ppo$_{34.9 \times 23}$, full_L26.7_T54, full_L32.5_T19,

but Christiansen, Cvitanović and Putkaradze [7] ($\tilde{L} \approx 5.8$), and Lan and Cvitanović [41] ($L = 38.5, \tilde{L} = 6.12$) have hundreds of them for a few fixed system sizes L.

I have never explicitly searched for antisymmetric solutions $\in \mathbb{U}^+$ because I focused on pre-periodic orbit and relative periodic orbit solutions. I'll get on the trawling.

2018-07-06 Predrag *eqva/figs*:

The antisymmetric space $\mathbb{U}^+$ solutions prime spatial period is $L_{Matt}/2$. Center them at $x^* = 0$ or $x^* + L_{Matt}/2 = 0$, and the prime spatial period $[0, L]$ where $L = L_{Matt}/2$ is all that needs to be plotted, where L_{Matt} is the length Matt currently assigns them.
This has been fixed for equilibria. [8]

s

2018-07-06 Matt First attempts at local minima and maxima tracking algorithm. Simon Berman gave me the idea, which is to take the spatial derivative of the spatiotemporal field represented as a matrix $u_x(x_m, t_n) \equiv a_{m,n}$ and to calculate an elementwise product and subtraction $P_{m,n} = a_{m+1,n} a_{m,n}$ and $S_{m,n} = a_{m,n} - a_{m+1,n}$ to capture where the derivative changes sign,

---

[8]Predrag 2018-07-07: Today they all look centred, but plotted on fundamental domain and its copy, total width L_{Matt}.

as well as the sign of the second derivative approximated by the secant line between spatially adjacent points.

Responses to Predrag's posts:

- I haven't trawled specifically for antisymmetric invariant 2-torus solutions $\in \mathbb{U}^+$ but can do so, I was focused on pre-periodic orbit and relative periodic orbit solutions.
- equilibria figures should now reflect the prime spatial period and so will antisymmetric invariant 2-torus solutions $\in \mathbb{U}^+$.

2018-07-04 Matt Notes from Monday's Art Institute visit Called Predrag via hangouts, we discussed the two hurdles looming ahead of us in terms of the theory. He says:

0 WeGoLow, WeGoLow, WeGoLow. We keep determining the alphabet of minimal tiles, until we have a credibly complete alphabet. We do not let ourselves get disturbed by Grand Schemes of Budanurs, get batted out *again* into the far field. WeGoLow, WeGoLow, WeGoLow, as has been the goal for the last 2 years.
   Once we have an alphabet, the conceptual challenges ahead are

1 Solutions come in continuous families. Depending on the initial guess, current Matt's code picks out an arbitrary representatives from such continuous family. Is there a saddle-point condition (let's say, extremum in energy density) that picks out a single representative invariant 2-torus per family? Or will periodic orbit zeta functions involve integrals over such families?

2 To a single invariant 2-torus belongs a continuous family of tiles, one for each value of (x, t) that we take to be the origin of the tile. In other word, how will we maximize the amount of shadowing of a large invariant 2-torus by smaller invariant 2-tori

2018-07-07 Predrag There are tons of intriguing solutions in Matt's library, almost all for relatively large domains. I think new searches should focus on smaller and smaller domains, to help the intuition about the alphabet, and fusion rules - which pattern can be adjacent to which.

Some WeGoLow candidates:

rpo_L21.9_T95
(also *rpo_L22.1_T92*, *rpo_L22.1_T93*, *rpo_L22.2_T84*, *rpo_L22.3_T90*, $\mathrm{ppo}_{22.3\times96}$, *rpo_L22.5_T89*, *rpo_L22.5_T89*): start a periodic orbit search using $T = [9, 30]$ time clip, or (better) pre-periodic orbit search using $T = [9, 20]$ time clip. From that, start a pre-periodic orbit search using $L/2\pi = [0.2, 2.6]$ space clip. The result could be WeGoLow $\mathrm{ppo}_{15\times11}$ "hook" in figure 16.22. However, this solution might be rare for larger spatial periods.

rpo_L21.9_T79
(also $\mathrm{ppo}_{24.9\times58}$, *rpo_L34.8_T36*, *rpo_L36.9_T63*, *rpo_L42.6_T62*): $T = [45, 79]$

time clip suggests an interesting relative periodic orbit which is the $T = [45, 61]$ "hook" repeated.

rpo_L22.1_T81: $T = [70, 87]$ time clip is an example of $k = 3 \rightarrow k = 1$ defect.

2018-07-10 Matt After rewriting/updating the antisymmetric invariant subspace $\mathbb{U}^+$ spatiotemporal code, I was able to converge former "gap" or "cat's eye" tile *rpo_L13.2_T15* to a periodic orbit named Defect 2 *anti_L17.5_T17* in the antisymmetric invariant subspace, plotted in $[0, L/2]$ domain.

With restructuring my code into a more presentable package I've found that there are slight inconsistencies in how python interprets the "project" whether in Windows or Linux OS. It's this and bug hunting that are keeping me preoccupied sadly. Also, I went through and wrote most of the antisymmetric invariant subspace $\mathbb{U}^+$ trawling code; analogous to what I used for pre-periodic orbit and relative periodic orbit solutions. There seems to be a bug in the matrix free methods that I haven't found. I know that it lies in this specific part because the explicit matrix methods worked by producing defect2 *anti_L17.5_T17*. The matrix free code is drastically altering the domain size and needs more work before I can start trawling.

2018-07-11 Matt coding Wrote auxiliary functions to be able to more easily manipulate datasets for the sake of finding WeGoLow tiles.

Plumbers Meeting I elucidate the WeGoLow tiling ideas to Ashley and Mohammad.

2018-07-12 Matt Hook Huntin' Still hunting for more small solutions; I tried to find the 'hook' by using a number of different methods, here's the one that lead to results that converged to within machine precision but did not produce a "hook" tile. Firstly, because the hook is present in the shortest pre-periodic orbit at $L = 22$ I thought that this would give me the best chance of finding it rather than taking it from a large domain. The following list is how I attempted to find the hook solution:

1. Perform numerical continuation until the streaks in the pre-periodic orbit invariant 2-torus solution straighten out. I thought this would give me the "cleanest" version of the hook.
2. Remove streaks from pre-periodic orbit invariant 2-torus and create a subdomain that is shift-reflect invariant.
3. Run the subdomain through spatiotemporal code, assuming it lies in the shift-reflect subspace (use pre-periodic orbit invariant 2-torus code).
4. Run the subdomain through spatiotemporal code, assuming it is a periodic orbitwith near zero SO(2) shift.
5. Hope that one of these looks like a hook.

Both running the hook subdomain constrained to shift-reflect subspace and assuming it was actually a relative periodic orbit with negligible SO(2) shift converged; in fact they converged to practically the same solution. The spatial length of the two solutions are identical up to the thousandths place, the SO(2) shift is negligible in the relative periodic orbit invariant 2-torus and so by eye the figures, a pre-periodic orbit invariant 2-torus fundamental domain, looks like the first half of the relative periodic orbit invariant 2-torus.

I think there is a reason behind this; in all of the invariant 2-tori that exhibit the hook pattern, even for consecutive repeats in time, there is always a relatively straight streak partnered with the hooks in the spatial direction. I'm citing
rpo_L21.9_T95, *rpo_L22.1_T92*, *rpo_L22.1_T93*, *rpo_L22.2_T84*, *rpo_L22.3_T90*, ppo$_{22.3\times96}$, *rpo_L22.5_T89*, *rpo_L22.5_T89*
as examples. Perhaps at these relatively small domain sizes the hook isn't a prime spatiotemporal tiling but rather the hook-streak is. This doesn't feel right but its the only alternative I can think of.

Defect2 In other wegolow news, I found defect2 *rpo_L17.5_T17*, likely related to the defect1 = *rpo_L13.2_T15*, but distinct enough that I thought I would include it. It was the result of initiating the half-defect search from *rpo_L22.3_T98* subdomain $t \in [55, 70]$, $x/2\pi \in [0, 2.2]$.

2018-07-16 Predrag Of no importance, but just something to keep in mind: La-TeX gets confused if a figure file name has several dots in it, that's why I keep renaming *rpo_L17.5_T17.png* $\rightarrow$ *MNG_rpo_L17d5_T17.png*, where d stand for "dot."

Also, the Gibson not-approved phonetic abbreviation (my apologies) *eqva* stands for the *equilibria*, the plural of *eqv = equilibrium*.

2018-07-17 Matt I chose 'point' instead of 'dot' in the future invariant 2-torus labels: *rpo_L17.5_T17.png* $\rightarrow$ *MNG_rpo_L17p5_T17.png*,

2018-07-17 Matt If anyone wants to see my progress on the thesis proposal you can view (and hopefully not edit for my sake) the outline I produced via google docs:

Thesis Proposal Outline

Red text means that the initial draft is done but needs to be picked over. Black means it's still in drafting stages, and blue will mean I believe its ready to be read. I was worrying about length before but I'm just going to write my heart out and then trim if need be.

Notes on Literature review in thesis proposal are now all in sect. 6.

2018-07-18 Matt spatiotemp I believe I found the minimal hook and streak patterns (or at least members of the same families) today. This was accomplished by using the hybrid-methods that I used to trawl. Previously, I was only using Gauss-Newton to converge subdomains as it worked but the hook required adjoint descent before applying Gauss-Newton in order to converge.

Hook tile Solution hook = *rpo_L13.07_T10* was found by using a family member of the shortest pre-periodic orbit in time at $L = 22$ whose energy was a local maximum. This ended up being at $L = 20$, but this turns out to not matter. What matters in the end is that I use hybrid methods and not just Gauss-Newton to try to converge the tiles; just like how I had done for all of the invariant 2-tori beforehand. The expedient results of just using Gauss-Newton and finding "defects" and "gaps" had led me astray.

"Streak" Similar story to that of the hook; applying hybrid numerical methods allowed me to find an equilibrium solution whose spatial extent is approximately 2π, or π in the fundamental domain of the antisymmetric subspace $\mathbb{U}^{+}$.

code Rewriting energy analysis code because the script is a big mess. Separating out and writing functions that write the energies and spatial translation velocity `E.txt` and `C.txt` files for easy use.

Writing additional code that produces figures similar to the animated png `MNG_ppo1_energy.png` that shows the energy of numerical continuations of solutions.

Need to write code that utilizes hybrid-methods in numerical continuation in spatial domain size. Currently only using Gauss-Newton. I'm still unsure whether I should pursue automated could that tries to find a family member with certain properties because I can't decide on which are important. (extremum in energy, area, spatial size are a few examples).

2018-07-23 Matt continuous families Numerical continuation of the hook and gap solutions provide continuous families of solutions of which it seems the Predrag is correct that the "defect" type solution and "hook" type solution are of the same family. As a means of trying to identify some criterion by which to choose members of said families I produced plots of members of the continuous families adjacent to plots of the entire family's energy, spatiotemporal averaged energy dissipation and production. There is some slight numerical discrepancy but they should be equal in theory; It could be the quadrature rule that I am using to calculate $< u_{xx}^2 >_{LT}$ and $< u_x^2 >_{LT}$, where $< \star >_{LT}$ indicates spatiotemporal average.

I thought it might be possible to identify each family by picking out the constitutive member that had maximal or minimal dissipation and production values; but for the numerical continuation of the
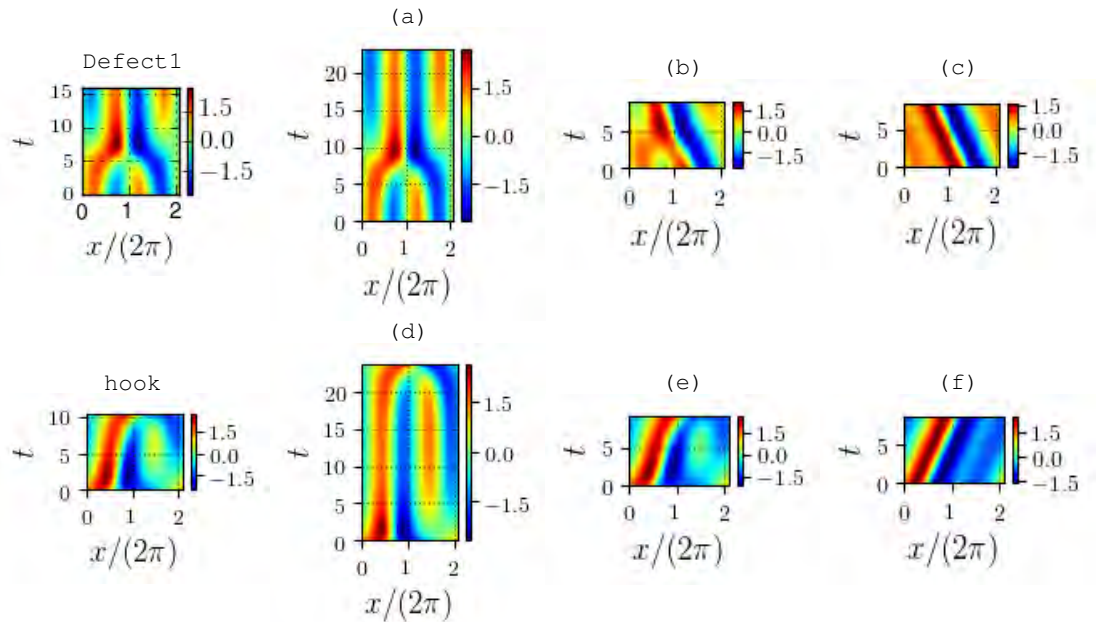
Figure 16.25:   (a) Invariant 2-torus *rpo_L12.996_T23*, (b) invariant 2-torus *rpo_L13.096_T8*, (c) relative equilibrium *reqv_L13.106_T8*. These three solutions were produced by numerical continuation in spatial domain size of invariant 2-torus defect1 = *rpo_L13.02_T15* tile (see figure 16.22). (d) Invariant 2-torus *rpo_L12.995_T23*, (e) invariant 2-torus *rpo_L13.095_T8*, (f) relative equilibrium *reqv_L13.105_T8*. These three solutions were produced by numerical continuation in spatial domain size of invariant 2-torus hook = *rpo_L13.07_T10* tile. Invariant 2-tori (a) *rpo_L12.996_T23* and (d) *rpo_L12.995_T23* are the one and the same $\mathrm{PO}_{(13.0,23)} \in \mathbb{U}^+$, differing only by relative space and time shifts. The reflection symmetry is broken by the nearby solution drifting either to the left or to the right, so (e,f) belong to the right-drifting reflection of the left-drifting branch of the solutions (a,b), i.e., they belong to the same branch of the solution after the reduction of the spatial reflection symmetry. In general, solutions can be distinguished or identified only after they are sectioned and sliced, as done in figure 16.27.

gap solution there doesn't seem to be any local maxima or minima. The benefit of this type of analysis is that while there isn't any local maxima or minima for the gap family, as I increase L to its upper limits (in terms of being able to converge the solution) the period of the solution grows extremely quickly; in my mind making it more and more of an isolated solution. The reason I hold this belief is that if we contemplate the family of gap solutions in the context of the Kuramoto-Sivashinsky equation as a dynamical system, an incredibly long period in this instance is actually prohibitive due to the fact that the antisymmetric subspace $\mathbb{U}^+$ is a flow invariant subspace. The idea I have is that the it is possible for periodic orbit's to shadow generic trajectories but as the period increases, it is essentially a statement akin to "the trajectory stays near the flow invariant subspace for longer and longer periods of time" which (although I hesitate to use this word) probabilistically doesn't seem likely.

In summary I suppose my thinking is that due to the fact that antisymmetric periodic orbit's lie in a flow invariant subspace $\mathbb{U}^+$ that trajectories can neither leave nor enter then the period is a sort of measure of how isolated these periodic orbit's must be. In this regard I think that the more relevant quantities would be a respective densities of scalar quantities than the quantities themselves (average energy, dissipation, etc.).

Performing continuation of other solutions today, will see if anything interesting pops out.

defect1 continuation The numerical continuation of defect1 = *rpo_L13.2_T15* tile, figure 16.22 (b), the first tile I entitled 'defect' seems to be a member of the family of the reflection of the "hook" family: they are the same family up to discrete symmetry. My attempt to demonstrate this is to take three representatives of each family in figure 16.25, and show that at similar spatiotemporal domains the solutions look very similar up to spatial and temporal translations.

In this respect, one can see the family progresses from "defect" to "hook" to relative equilibrium as $\tilde{L}$ increases.

My thought process on how to interpret this family goes as follows: I don't know whether to interpret the "hook" as a transition describing breakdown of the invariant 2-torus into a relative equilibrium, or maybe as "spatiotemporal heteroclinic connection" but I am unsure if such a statement makes sense in the absence of dynamics. Therefore I thought that maybe it makes sense in terms of spatiotemporal symbolic dynamics. If one was playing sudoku with spatiotemporal symbolic dynamics and there were symbols for defect and relative equilibrium, I think "hook" would be a symbol that could fit in the middle. Now, this doesn't really make sense because hook $\equiv$ defect because they are members of the same family; it just gets too complicated too quickly to extrapolate any ideas currently, much more

work required.

2018-07-23 Matt coding Mainly cleaning up analysis codes and figure refurbishing. Started on the functionality to fix the temporal domain and let spatial domain size vary.

equations for calculation of energy related quantities The equations for the spatial averages as discussed in ChaosBook tend to be more accurate being they are comparing the dissipation and energy production rates at specific points in time. Being a spatiotemporal project what I have elected to do is the following;

For the total energy in terms of spatiotemporal Fourier modes I use

$$E = \frac{1}{2}|u_{nm}|^2 \qquad (16.58)$$

For the dissipation and production I calculate both u_x and u_{xx} via spectral differentiation, and then compute the pseudospectral product in physical space, i.e. u_x^2 and u_{xx}^2. The spatiotemporal average of these quantities are the quadratic norms of the spatiotemporal Fourier modes of these pseudospectral products, such that the spatiotemporal averages can be written,

$$
\begin{aligned}
< u_x^2 >_{LT} &= \sum_{n,m} |F((F^{-1}(\mathrm{i}q_m u_{nm})^2)|^2 \\
< u_{xx}^2 >_{LT} &= \sum_{n,m} |F((F^{-1}(-q_m^2 u_{nm})^2)|^2, \qquad (16.59)
\end{aligned}
$$

where F and F^{-1} indicate the spatiotemporal Fourier transform and its inverse, respectively, and the norm is L_2.

Both the spatiotemporal average of energy production and dissipation are of order 10^{-6} or 10^{-7}. Note: if calculated at each point in time separately the accuracy increases by a few orders of magnitude as denoted by the residual of the difference $P - D$. I figured I should use the spatiotemporal average instead.

I'm hoping that figure 16.26 demonstrates pretty well that these are reflection related families of solutions. The plots for the "hook" family is sampled better; but the two constituent members' energy and SO(2) phase speed seem to be in agreement.

2018-07-24 Matt : **Ideas for continuous families of invariant 2-tori** Now that I have implemented the code to do numerical continuation while the period T of invariant 2-torus solutions is fixed I have a couple ideas of how to utilize it for analysis.

1. My first idea is to take one of the families of solutions computed via numerical continuation in L, and for each L solution, attempt
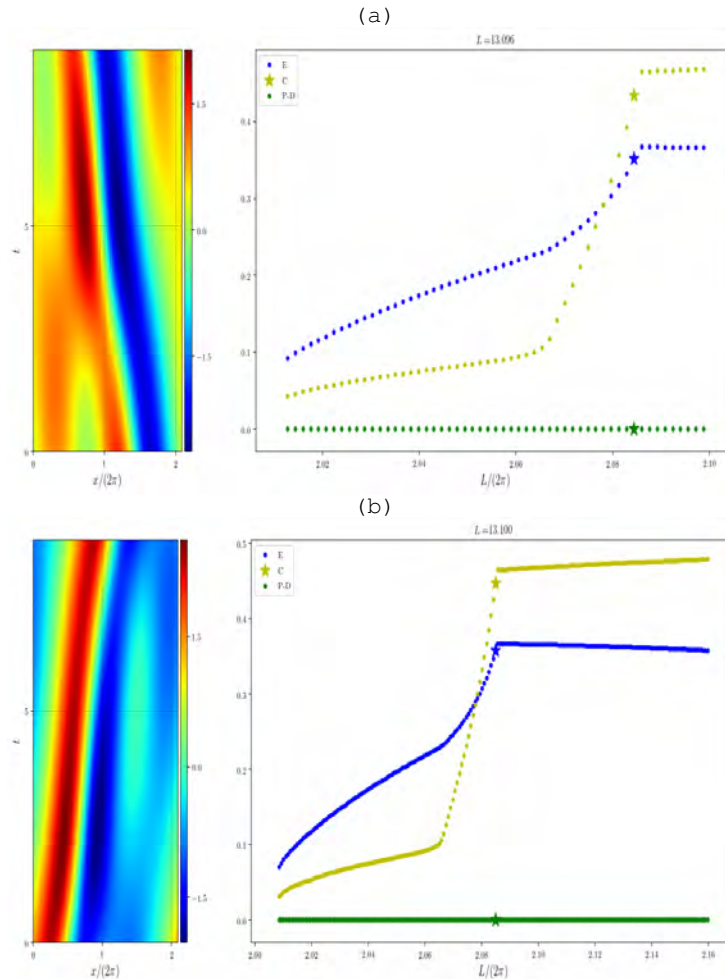
Figure 16.26:   (a) Invariant 2-torus rpo_L13p100_T8 and related spatiotemporal quantities; solution comes from numerical continuation of defect1 = *rpo_L13.2_T15* tile, figure 16.22 (b). (b) invariant 2-torus rpo_L13p096_T8 and related spatiotemporal quantities; solution comes from numerical continuation of the *rpo_L13.07_T10* "hook" tile.

to numerically continue in T. The intention is that by doing so I will be sampling the solutions in a two dimensional parameter space defined by (L, T). The idea that I have currently is to roam around (L, T) parameter space, then plot a scatter plot such that the points are color coded by spatiotemporal energy E given by (16.58).

2. The second idea is to choose an invariant 2-torus solution as a starting point and then see what happens by alternating continuations in L and T. I.e. if I numerically continue a solution by increasing L and the period T decreases as a result, I would hope that by increasing T by numerical continuation I could either arrive at the original solution or another solution via hysteresis.

Both of these ideas are essentially doing the same thing; which is, to combine the numerical continuation procedures in both continuous directions.

2018-07-27 Predrag on the eventual necessity of representing all invariant 2-tori as single points in a common section and slice: My guess is that your invariant 2-torus
rpo_L12.996_T23 in figure 16.25 (a) and invariant 2-torus
rpo_L12.995_T23 in figure 16.25 (e) are the one and the same

$$\mathrm{PO}_{(13.0, 23)} \in \mathbb{U}^+$$

($\mathbb{U}^+$ as in (16.28)), differing only by relative space and time shifts. There is probably a number of such repetitions in your tables, because solutions can be distinguished or identified only once the are sectioned and sliced.

2018-07-29 Matt : I agree, I was going to write code that slices and sections but I got caught up in producing far too much data to analyze via numerical continuations. I do not think its worth enforcing in trawling;but it might be worthwhile including in the numerical continuation in T and L code. I think what I'm going to go for is rotate the spatiotemporal Fourier modes such that the *space, time* phase of the $n = 0, m = 1$ and $n = 1, m = 1$ equal some constant

2018-07-27 Predrag spacetime indices convention I'm entering the standard lattice discretization definitions [26] here, so Matt notices them, before we move them to chapter 1. The square lattice discretization of a spacetime field $u(x, \tau)$ is obtained by specifying its values $u_{nt} = u(x_n, \tau_t)$ on lattice points $z = (n, t) \in \mathbb{Z}^2$. Examples are diffusive coupled map lattices [31, 32] and Gutkin *et al.* [26, 27]. Hence, the first index refers to configuration space, the second to time.

The thing to remember is that

the first index always refers to configuration space,
the second to time.

In the Fourier representation $\hat{u}_{k\ell}$, the first index always labels the spatial mode, the second the frequency.

There are two lattices at play here: (i) the spacetime discretization (1.42), and (ii) the symbolic dynamics discretization. What follows refers to as yet unattained latter.

Lattices. Consider a 2-dimensional square lattice infinite in extent, with each site labeled by 2 integers $z = (nm) \in \mathbb{Z}^2$. Assign to each site z a letter s_z from a finite alphabet $\mathcal{A}$. A particular fixed set of letters s_z corresponds to a particular lattice state $\mathsf{M} = \{s_z\}$. In other words, a 2-dimensional lattice requires a d-dimensional code $\mathsf{M} = \{m_{n_1 n_2}\}$ for a complete specification of the corresponding state X. The *full shift* is the set of all 2-dimensional symbol blocks that can be formed from the letters of the alphabet $\mathcal{A}$

$$\hat{\Sigma} = \{\{s_z\} : s_z \in \mathcal{A} \quad \text{for all} \quad z \in \mathbb{Z}^2\}. \tag{16.60}$$

Multidimensional shifts. For an autonomous dynamical system, the evolution law f is of the same form for all times. If f is also of the same form at every lattice site, the group of lattice translations, acting along the spatial lattice direction by shift σ, is a spatial symmetry that commutes with the temporal evolution. A temporal mapping f that satisfies $f \circ \sigma j = \sigma \circ f$ along the spatial lattice direction is said to be *shift invariant*, with the associated symmetry of dynamics given by the d-dimensional group of discrete spatiotemporal translations.

Blocks. Let $\mathcal{R}_z \subset \mathbb{Z}^2$ be a finite $[\ell_1 \times \ell_2]$ rectangular lattice region, $\ell_k \geq 1$, whose lower left corner is the $z = (n_1 n_2)$ lattice site

$$\mathcal{R} = \mathcal{R}_n^{[\ell_1 \times \ell_2]} = \{(n_1 + j_1, \cdots n_2 + j_2) \mid 0 \leq j_k \leq \ell_k - 1\}. \tag{16.61}$$

The associated finite block of symbols $s_z \in \mathcal{A}$ restricted to $\mathcal{R}$, $\mathsf{M}_{\mathcal{R}} = \{s_z \mid z \in \mathcal{R}\} \subset \mathsf{M}$ is called the block $\mathsf{M}_{\mathcal{R}}$ of area $|\mathcal{R}| = \ell_1 \ell_2$. For example, a $\mathcal{R} = [3 \times 2]$ block is of form

$$\mathsf{M} = \begin{bmatrix} s_{12} s_{22} s_{32} \\ s_{11} s_{21} s_{31} \end{bmatrix} \tag{16.62}$$

and volume (in this case, an area) equals $3 \times 2 = 6$. In our convention, the first index is 'space', increasing from left to right, and the second index is 'time', increasing from bottom up.

Cylinder sets. While a particular admissible infinite symbol array $\mathsf{M} = \{s_z\}$ defines a point X (a unique lattice state) in the state space, the *cylinder set* $\mathcal{M}_{\mathcal{R}}$, corresponding to the totality of state space points X that share the same given finite block $\mathsf{M}_{\mathcal{R}}$ symbolic representation over the region $\mathcal{R}$. For example, in $d = 1$ case

$$\mathcal{M}_{\mathcal{R}} = \{\cdots a_{-2} a_{-1} . s_1 s_2 \cdots s_\ell a_{\ell+1} a_{\ell+2} \cdots\}, \tag{16.63}$$

with the symbols outside of the block unspecified.

Invariant 2-tori. A state space point is *spatiotemporally periodic* if it belongs to an invariant 2-torus, i.e., its symbolic representation is a block over region $\mathcal{R}$ defined by (16.61),

$$\mathsf{M}_p = \mathsf{M}_\mathcal{R}\,, \qquad \mathcal{R} = \mathcal{R}_0^{[L\times T]}\,, \qquad (16.64)$$

that tiles the lattice state M periodically, with period L in the spatial lattice direction, and period T in the time lattice direction.

Subshifts. Let $\hat{\Sigma}$ be the full lattice shift (**??**), i.e., the set of all possible lattice state M labelings by the alphabet $\mathcal{A}$, and $\hat{\Sigma}(\mathsf{M}_\mathcal{R})$ is the set of such blocks over a region $\mathcal{R}$. The principal task in developing the symbolic dynamics of a dynamical system is to determine Σ, the set of all *admissible* itineraries/lattice states, i.e., all states that can be realized by the given system.

Pruning, grammars, recoding. If certain states are inadmissible, the alphabet must be supplemented by a *grammar*, a set of pruning rules. Suppose that the grammar can be stated as a finite number of pruning rules, each forbidding a block of finite size,

$$\mathcal{G} = \{b_1, b_2, \cdots b_k\}\,, \qquad (16.65)$$

where a *pruned block b* is an array of symbols defined over a finite $\mathcal{R}$ lattice region of size $[L_1 \times L_2]$. In this case we can construct a finite Markov partition by replacing finite size blocks of the original partition by letters of a new alphabet. In the case of a 1-dimensional, the temporal lattice, if the longest forbidden block is of length $L + 1$, we say that the symbolic dynamics is Markov, a shift of finite type with L-step memory.

Let $\mathsf{X} = \{x_z \in \mathbb{T}^1, z \in \mathbb{Z}^2\}$ be a spatiotemporally infinite solution of Kuramoto-Sivashinsky equation, and let $\mathsf{M} = \{s_z \in \mathcal{A}, z \in \mathbb{Z}^2\}$ be its symbolic representation. By the presumed connection between X and M, the corresponding symbolic dynamics block M is unique and admissible, i.e., M defines the unique spatiotemporal state X and vice-versa.

Assume now that only partial information is available, and we know only a finite block of symbols $\mathsf{M}_\mathcal{R} \subset \mathsf{M}$, over a finite lattice region $\mathcal{R} \subset \mathbb{Z}^2$. What information about the local spatiotemporal pattern $\mathsf{X}_\mathcal{R} = \{x_z \in \mathbb{T}^1, z \in \mathcal{R}\}$ does this give us? To be specific, let $\mathcal{R}$ be a rectangular $[\ell_1 \times \ell_2]$ region (see (16.61) for the definition), and let $\mathsf{M}_\mathcal{R}$ be the $[\ell_1 \times \ell_2]$ block of M symbols.

2018-07-30 Matt sliced and sectioned Wrote code that slices and sections invariant 2-tori. Using this, I produced figures of all relative periodic orbit invariant 2-tori in their sliced and sectioned representations,*without rescaling time* as in ref. [3].

The implementation is described as follows.
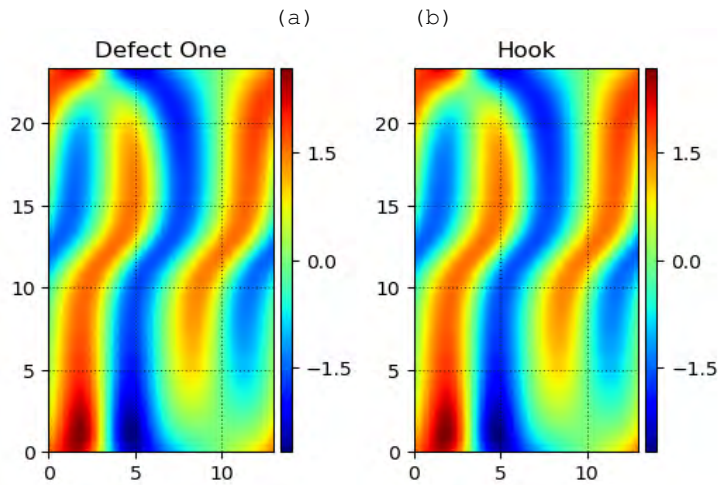
Figure 16.27: Continued from figure 16.25. Sliced and sectioned minimal invariant 2-torus solutions (not scaled relative to others in repository; horizontal axis is L); (a) Defect1 = $\mathrm{rpo}_{13.2\times15}$ tile, figure 16.22 (b), numerically continued to $(L, T) = (12.996, 23.373682)$. (b) Reflection of the hook = $\mathrm{rpo}_{13.07\times10}$ tile numerically continued to $(L, T) = (12.996, 23.373670)$.
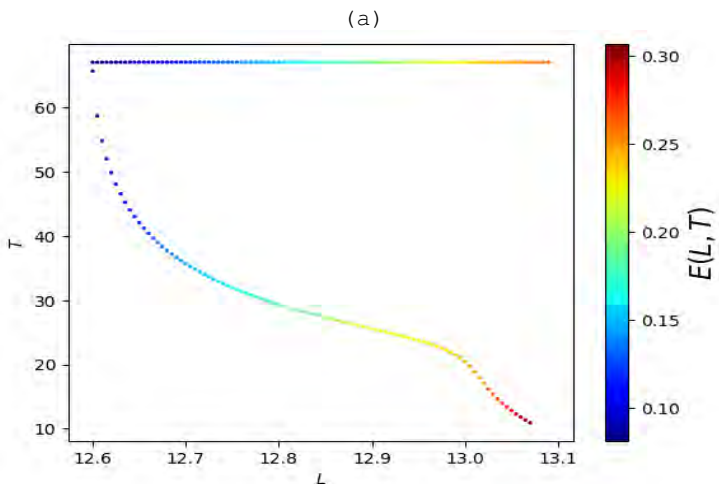
Figure 16.28: Bifurcation diagram plotted in (L, T) plane. Two branches resulting from numerical continuation in L of the hook = $\mathrm{rpo}_{13.07\times10}$ tiles family. L was decreased until the Gauss-Newton method failed; at which point, the numerical continuation began increasing L to test for hysteresis. This can be seen by the fact that the bifucation diagram has two branches.
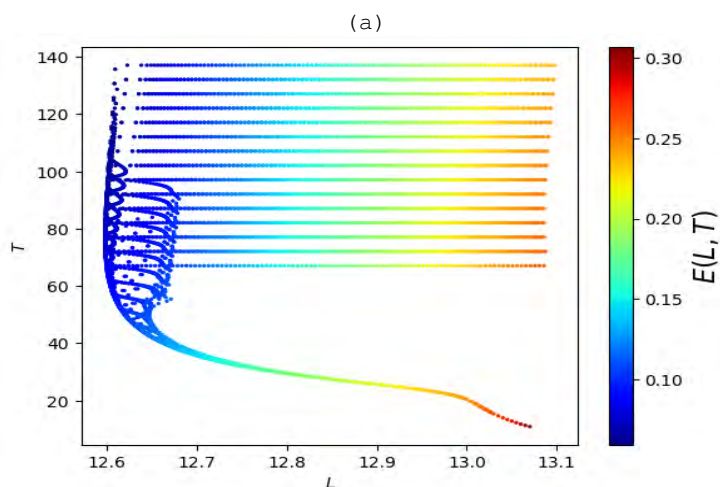
Figure 16.29: Bifurcation diagram plotted in (L, T) plane; numerical continuation of all points in figure 16.28. These points were acquired by increasing T and then decreasing T via numerical continuation of both the lower and upper spatial continuation branches. The step size that T was changed by was $\Delta T = 5$; smaller step sizes and smaller ranges seem to indicate that each branch is a one dimensional family.
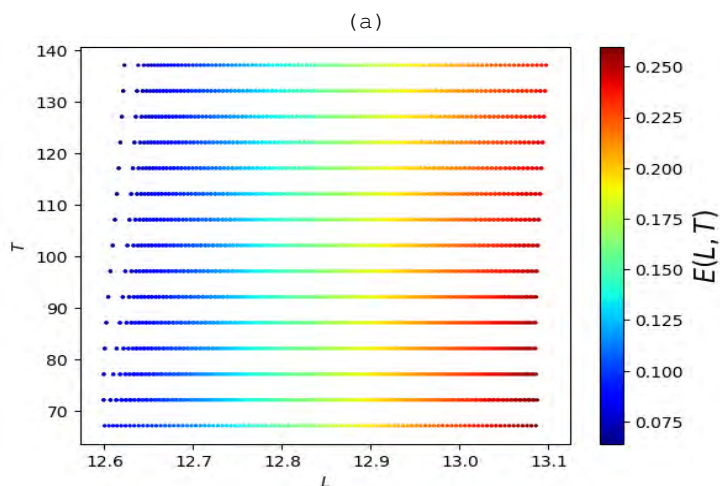
Figure 16.30: Bifurcation diagram plotted in (L, T) plane; numerical continuation of upper branch of figure 16.28. These points were acquired by increasing T and then decreasing T via numerical continuation of the upper spatial continuation branch. The step size that T was changed by was $\Delta T = 5$; smaller step sizes and smaller ranges seem to indicate that each branch is a one dimensional family.
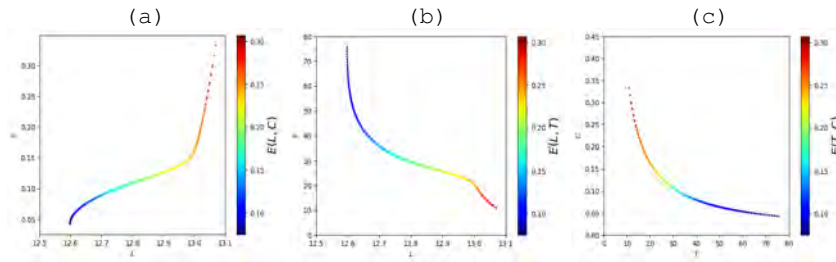
Figure 16.31: Numerical continuation of the lower spatial continuation branch of figure 16.28 by decreasing T by 10 with step sizes of $\Delta T = 1$. Plots in (a)(L, C) plane (b) (L, T) plane (c) (T, C) plane. Spatiotemporal energy is color coded.
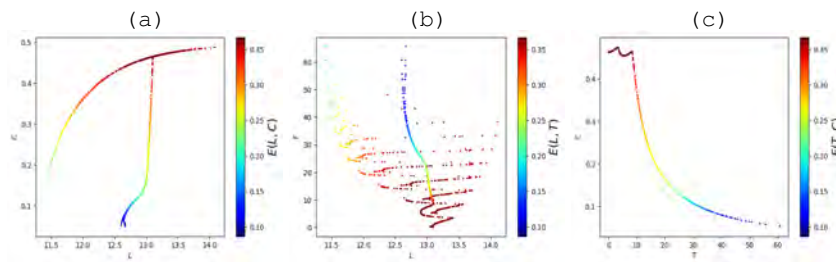
Figure 16.32: Numerical continuation of the lower spatial continuation branch of figure 16.28 by decreasing T by as much as possible (while still remaining positive) with step sizes of $\Delta T = 5$. Plots in (a) (L, C) plane, (b) (L, T) plane, and (c) (T, C) plane. Spatiotemporal energy is color coded.

1. Perform spatial Fourier transform on a invariant 2-torus
2. Put invariant 2-torus into first Fourier mode slice.
3. Perform temporal Fourier transform of the sliced solution.
4. Fix the phase of the $m = 1, n = 1$ mode such that $\mathrm{Im}\,(\hat{u}_{m,n}) = 0$.

I tried an alternate formulation where the phase of the $(m, n) = (1, 0)$ and $(m, n) = (1, 1)$ modes were fixed. The problem with this is that due to the discontinuous nature of prime periods of relative periodic orbit invariant 2-tori in state space I couldn't guarantee that the boundaries for the figures ended up in the "right place". (I.e. if the discontinuity is at the boundary it doesn't look bad but if ends up in the middle of the figure it looks terrible). It's kind of hard to explain but basically the discontinuity of relative periodic orbit's is prohibitive to merely phase fixing two spatiotemporal modes.

Therefore, the previously mentioned slicing and sectioning is what was used to confirm that "defect one" and "hook" tiles are indeed members of the same family, as can be seen by their slicing and sectioning in figure 16.27. There are slight discrepancy in the temporal extent T and SO(2) shifts. In order to get exactly the same results I believe one of these other parameters would need to be fixed in addition to fixing L.

Dissection of bifurcation diagrams for defect family First I just want to say for the record that numerical continuation by fixing T seems to behave much better than continuation in L; even though their values are dependent on one another.

Firstly, we can see that there is hysteresis in figure 16.28. The interesting behavior occurs after the numerical continuation in the spatial domain size L, when one begins numerically continuing in T. In the following discussion I will refer to the "lower" and "upper" branches; those which were obtained via numerical continuation in L only. To describe the subbranches that arise from numerically continuing the upper and lower branches I will use "downward" and "upward" to describe changes in T. For completeness I performed both orders of numerical continuation in T on the lower and upper branches; namely, increasing T then decreasing T and vice versa. The order in which I performed these numerical continuations in T seem to drastically alter the results.

I believe the main takeaways from the space-then-time numerical continuations are

1. The period T and the domain size L of the upper branch figure 16.30 seem to be minimally coupled, unlike the highly nonlinear lower branch; due to this there may be families of constant energy solutions. Burak and Simon both pointed out that this may be a homoclinic orbit and evidence (numerical continuation) suggests that this solution can be continued to very very long periods ($T \approx 772$ with a relatively small discretization).

2. The lower branch when T is decreased as much as positive while still remaining positive hits a family of traveling wave solutions, which leads to hysteresis as the invariant 2-tori transition from relative periodic orbit solutions to relative equilibria but when T is increased they remain relative equilibria . The hysteresis is best shown by the figures plotting T versus L for the upward and downward T continuations with $\Delta T = 5$, in figure 16.32.

3. The lower branch down-then-up continuation with $\Delta T = 1$ in figure 16.31 tracks a one dimensional continuous family of solutions until it hits the same family of relative equilibria as figure 16.32. I believe this is best demonstrated by the (L, C) plane plots, or (a) in both respective figures, (a) figure 16.32 (a) figure 16.31.

2018-08-04 Predrag Rummaging through day's catch in the reflection antisymmetric invariant subspace $\mathbb{U}^+$

gudorf/python/data_and_figures/converged/anti/figs/

I'm no fan of $\mathbb{U}^+$, as boundry conditions distort solutions. What look to me as distinct solutions, ordered by increasing L:

2 two-streak equilibria, both missing from *eqva/figs/*
anti_L9.199_T40 anti_L30.2_T26

(-1/4 shift) atop (1/4 shift) :
anti_L9.119_T33 = anti_L9.143_T32 = anti_L9.144_T35 = anti_L9.187_T40
= anti_L9.188_T41 = anti_L9.218_T45

cat's eye (a short wiggle)
anti_L9.180_T35 = anti_L9.182_T35 = anti_L9.190_T36 = anti_L9.215_T38
= anti_L9.219_T39 = anti_L9.296_T52 = anti_L9.841_T28 = anti_L26.1_T18

cat's eye flipped
anti_L9.249_T43

(defect + streak) atop (defect + streak)
anti_L32.9_T19 anti_L34.4_T17

cute cat's eye + streak
anti_L36.2_T29

cat's eye + streak
anti_L34.3_T20 anti_L36.7_T27

cat's eye flipped + streak
anti_L38.1_T30

defect + streak
anti_L38.4_T25

2018-08-04 Predrag The longer time period branch in figure 16.28 makes no sense to me. There cannot exist a invariant 2-torus such that $(L, T) = (L, 67. \cdots)$, with monotonically increasing energy density E for a range of L's, T constant?

This $T = 7. \cdots$ is the value at which the lower time period branch disappears?

As I have not digested the discussion that follows, I am not sure about my claim above either...

2018-08-04 Predrag OK, here is how I think about figure 16.28 to figure 16.32 passing over the meaning of taking $\Delta T = 5$ steps. Figure 16.28 and many figures in your album are examples of invariant 2-tori belonging to families of invariant 2-tori homoclinic to 2-streak (relative) equilibrium. That is discussed at length in the intermittency chapter of ChaosBook.org - these are infinite (but discrete) sequences of families spending more and more time close to the equilibrium, and for longer times to you they might look like a continuum of solutions, even if they are not.

2018-08-13 Matt : Recovering from the summer doldrums:

1. Wrote and rewrote more thesis work

2. Gutted feeblepoint presentation template and input very coarse outline.

Also I only saved the data and not the figures but the antisymmetric subspace trawling seems to have picked up on a very large number of solutions (most of which are likely repeats, reflection copies), I might have to think of a way to reduce the number of redundant copies in the repository after I produce figures, analyze, and upload them.

2018-08-17 Matt : Most of the day was spent finishing up (i.e. rewriting constantly) the first draft of thesis proposal for review.

I'm thinking that its likely unbalanced in terms of content; I feel like I should include more ideas that we plan to work on in the future rather than what has already been done but if it reads well then I won't change it.

Starting code that uses symbolic dynamics. What I hope for is code that takes as inputs:

- a symbolic block (two-dimensional array) of values
- a set of parameters (N, M, T, L), which are: number of time discretization points, number of spatial discretization points, period, domain size.
- Symmetries present in solution

The output would be a doubly periodic spatiotemporal field that has been made by glueing representative solutions together and then blending the boundaries by either truncation of higher Fourier modes, convolution with a Gaussian (Weierstrass transform) or elementwise multiplication with a Gaussian at the boundaries in physical space; will have to experiment to see what performs the best.

2018-08-20 Matt Current goals:

1. Finish presentation

2. Finish writing up a very thorough explanation of the difficulties lying in wait in the spatiotemporal symbolic dynamics.

3. Finish spatiotemporal symbolic dynamic initial condition generator.

4. Find any other important spatiotemporal tile solutions.

Beginning of Symbolic Dynamics Formulation When I began writing the Python module `symbolic_init.py` I quickly realized how daunting of a task this is. I need the ability to at least attempt any possible two dimensional symbolic block; but there's many pieces of information that are making the approach quite difficult.

Let's say for the sake of argument that I knew the exact symbolic dynamical block I wanted to look for, all of its symmetries, etc. How does one transform the symbolic dynamical block to a specific spatiotemporal field?

The "1-d" chains in space and time seem relatively easy to fabricate numerically, but there are certain instances where even they are not straightforward. Let us assume a trinary alphabet of $0, 1, 2$ for "streak","defect", and "gap" solutions respectively.

As an example, let me work through the details of the simplest example I can think of: conjoining a streak and a defect spatially. This can be represented by the symbolic block,

$$\mathsf{M} = \begin{bmatrix} 10 \end{bmatrix} \tag{16.66}$$

Because defects come in continuous families (streaks seem to be more rigid, at least in my numerical continuation attempts), a natural question arises even in this simple case; which member of the continuous family should one use to best "seed" the spatiotemporal field?

One approach to this would be to choose a member that bisects the range of domain sizes that the family exists in; another would be to specify the domain size *a priori*, but that doesn't seem natural. Other possibilities would be to attempt it for a number of different family members and see if they all converge to the same invariant 2-torus (if at all). The last is to find an immutable criterion that can be applied to *every* family of solutions which is also reasonable; as one can imagine this isn't straightforward or easy.

In this specific instance I think it is relatively straightforward conjoin the streak by setting its period to be equal to that of the defect, with the same number of discretized points in time so the two spatiotemporal fields can be concatenated numerically. The guess for the domain size would merely be additive.

For joining two different invariant 2-tori spatially, it seems that a fair position would be to either run a quick line-searching subroutine to see what period T minimizes the cost functional; or, simply take the average of the two different periods.

If these methods work then it would be straightforward to apply the analogous routines to temporal symbolic chains; domain sizes would either be put through a line-search or be averaged and the periods would be additive. The only difference is that the convergence behavior of solutions is *much* more dependent on being close to "the correct" domain size parameter (the solutions come in families but each initial condition has a specific domain size that it would be closest to in a least-squares sense).

Moving onto any symbolic block that is two dimensional difficulties arise quickly. For example, in the context of two plots of Figure 6.1 (k) and (l) in ref. [12]; a defect immediately precedes a hook. This is confusing as figure **??** seems to indicate that the defect and hook are family members. (This is not technically known as the stability or notion of spatiotemporal stability still hasn't been formulated outside of my ideas of 'sensitivity' that I posited more than a year ago).

If we assume that the defect and hook solutions *are* family members then this is what I can currently think of that might reconcile this issue. The defect and hook manifest with different periods(on domain sizes) I believe the correct way to view this is that at this specific period the solutions that can sum to the period constitute a defect and a hook. If it were continued in time I would posit that it would visit multiple defects in time (something to be tested).

Another possible test would be to find the spatiotemporal energy of all constituent pieces and the the total and see if the sum of the constituents equals the whole.

08-21-2018 Matt : Day's work:

- Started reviewing Kuramoto-Sivashinsky equation literature prior to thesis proposal

- More work on thesis proposal presentation.

- Writing up and thinking through the symbolic dynamics ideas

- Trying to read more of my backlogged literature and textbooks

- Started Stat Mech II. readings *Stochastic Problems in Physics and Astronomy* by Chandrasekhar.

- Attempted to find $k = 3 \rightarrow k = 1$ defect without luck.

- Found the one-by-two (space-by-time) symbolic block corresponding to a shift-reflection invariant invariant 2-torus composed of a defect and its reflection, figure 16.33
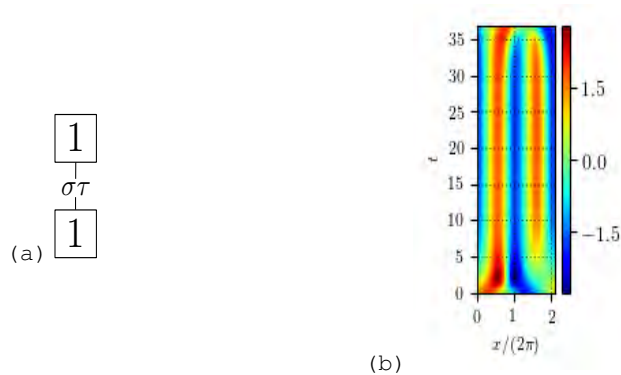
Figure 16.33: Symbolic block (a) and corresponding converged spatiotemporal solution (b). This was found by taking a member of the family of "defect" relative periodic orbits and gluing it together with its reflection copy as (hopefully) indicated by (a). Plot (b) is of shift-reflection fundamental domain (half of the invariant 2-torus in time).

Trying to garner experience with symbolic dynamical initial conditions and their numerical difficulties through simple examples. If the figure of the symbolic block is not of the correct formulation (a) in figure **??** then I can change; will need to get opinion.

2018-08-22 Predrag Matt's trial run of the thesis proposal presentation. Matt, can you complete these notes?

- Burak: Summarize in intro how people used to do this traditionally in turbulence (past 20 years). You are developing a statistical mechanics approach to spatiotemporal states in terms of building blocks.

- Burak: emphasize the bridge between small structures and large domains. Similar to homogenous turbulence in large cube.

- John: shorten introductory "what am I going to do?"

- Burak: Can do this visually - will also save time.

- Burak: can go through slides faster. When you name a symmetry, give a picture, the picture will explain it.

- Burak: in slide of invariant 2-tori, put pictures of examples.

- Burak: in Kuramoto-Sivashinsky slide need b.c.'s, explain terms by annotating the equation, make comparison to Navier-Stokes.

- Burak: relative periodic orbits; moves with mean speed

- Burak: write what symmetry a given solution has

- Burak: brag about your domains being much larger than $L = 22$

- Spatial scale $\sqrt{2}$ comes from competition of unstable diffusion and stable hyperdiffusion. John: Where does the time scale comes from? Predrag: one scale is the Lyapunov time of ≈ 0.4 for the current scale conventions. I think it has nothing to do with the actual time scale.

- John, Predrag: generate a few large spacetime domain solutions, look at magnitudes of
  (1) spatial Fourier components, averaged over time - should peak at $k_{max} = 2\pi/\sqrt{(2)}$, fall off exponentially for large wave numbers.
  (2) time Fourier components, averaged over space - does it peak anywhere? does it have a shoulder, beyond which it fall off exponentially for large frequencies?

- Predrag Xiong and predecessors work on Kuramoto-Sivashinsky inertial manifolds should serve as a guide here. Correctly scaled spectra (dimensions scales linearly with L, for example) all fall on the same curve.

- John: How are you going to do tilings? By Photoshopping?

- Matt: I'll start with my symbolic dynamics - from a given symbol array I'll generate approximate solution by corresponding tiles, the anneal it. Patterns whose boundaries are very different (in some norm) might serve to help with grammar.

- Burak: emphasize your success - your solutions are robust. Already achieved the qualitative confirmation that large solutions can split into small domains.

- John: Inability to use Newton-Krylov methods sounds wrong; in his experience cost functions are relatively smooth in all parameters. I suppose if I'm not including calculations, numerical evidence, etc., I should just not bring topics up; better to focus on other details.

- Include figures that show initial conditions and the solutions they converge to. Also show how a "random" looking initial condition can converge but a "good-looking" (looks close to Kuramoto-Sivashinsky solution) initial condition can fail.

- Ashley: Don't necessarily have to look at minimal invariant 2-tori as library of converged solutions are technically all "tiles" as well just of larger size.

- Burak: Numerical continuation of library of solutions can serve to flush out spatiotemporal invariant 2-tori.

2018-07-05 Burak Most of what I said is already in Predrag's list above. Specific additions:

- In the introduction, show very large domain simulation then mark qualitatively similar structures. Your preliminary result is that those qualitatively similar structures are in fact invariant solutions in small domains. This way, you have a story.

- The glued-up solution you presented is most likely an approximation to a homoclinic orbit. It's important to understand that because homoclinic orbits are likely to be a part of your library.

2018-09-10 Matt Skimmed ref. [55]. My general consensus: They do the proofs to prove you can cover unstable manifolds in an algorithmic way. Then once they have all of this very precise mathematical formulation, they abandon it and approximate the unstable manifold using proper orthogonal decomposition, and numerical continuation in conjunction with Monte Carlo methods. This likely doesn't help the reader as its too short to describe the paper. They work on a domain which is equivalent to $\tilde{L} \approx 2.73$ or $L \approx 17.2$ for Kuramoto-Sivashinsky equation and work with a traveling wave solution with two dimensional unstable manifold,

> We expect that the dimension of the embedded unstable manifold is approximately two since different initial conditions result in trajectories in observation space that are rotations of each other about the origin.

one on one with Burak At last week's meeting Burak described a way to "power-up" my research; He went into a description of the particular scales and the energy cascade present in Navier-Stokes flows and made different comparisons using both 3-d isotropic flows and shear flows as examples. He thinks a good use of my research would be similar to what I have done for the Kuramoto-Sivashinsky equation which is to be able to link the energy and different spatial scales of the problem by finding small invariant 2-tori embedded in large spatiotemporal simulations.

ppt thesis proposal Worked on making improvements that Burak and others mentioned for my thesis proposal presentation.

tile gluing Worked on symbolic dynamic initial condition generation and thinking through gluing codes.

I think I'll have to search for solutions using only matrix free methods which means that I will likely be employing a hybrid method comprised of adjoint descent and Newton-Krylov methods with fixed spatiotemporal area, as the method won't work otherwise. I'm unsure as to whether this will work but because solutions seemingly come in families I'm more hopeful. This will only be employed when the system size (number of independent variables) is of order 10^4 or greater, as before this threshold lienar systems can be solved directly without too much of an impact on numerics.

The general idea is to take the library of solutions that I have found and then automate the process that glues them together; i.e.the automation will contain the following subroutines:

1. Determine symmetry subgroup of the solutions.

2. Choose solutions and direction (space or time) to glue.

3. Make sure the discretizations match such that the final result is a rectangular grid.

4. Use Fourier smoothing, Gaussian mollifiers, or insertion of zeros to pad the two solutions and connect them or any combination of these procedures.

5. Determine (L, T, σ) based on averaging.

6. Use either hybrid adjoint-descent Newton or adjoint descent Newton Krylov to converge the approximate solution.

I have an inkling that liberal use of inserting streaks and traveling wave type solutions might be used to help glue solutions together as but I don't have motivation for this other than intuition currently.

Need to produce power spectrum in time and space for presentation to generate approximate time and spatial scales.

2018-09-11 Matt channelflow two I tried for five hours but I cannot get the MPI enabled version of channelflow 2.0 to work (MPI enables parallelization). I wish I could include more detail here as it took up most of my day but sadly that's just the way the cookie crumbles.

2018-09-14 Matt Spatiotemp Outlining the gluing procedure but first need to do thorough testing of recycled Newton-Krylov solvers.

2018-09-24 Matt Weekly Goals

- Finish automated gluing initial condition generator
- Finish automated symbolic dynamics initial condition generator
- Expand library of solutions by numerical continuation
- Absolutely finish presentation and thesis proposal
- Get reimbursed for DFD registration fee
- Finish Stat Mech two assignment
- Set date for thesis proposal presentation.

Powerpoint This is finally finished.

Thesis Proposal This is finally polished; just need Predrag to confirm that its OK to send out.

Glue Implemented code to glue pairs of invariant 2-tori either spatially or temporally. Larger arrangements are likely prohibitively expensive at current tolerance threshold of machine precision. The process will take either two random (if running the automated script) invariant 2-torus solutions with the same symmetry and glue them either temporally or spatially, while either maintaining the same symmetry (default option) or not. When concatenating two different invariant 2-torus solutions there are a couple key points needed to take into consideration

- The discretizations must be consistent.
- There will be a discontinuity that needs to be smoothed out for the spatiotemporal Fourier spectrum to have nice convergence properties.
- Special considerations for different symmetries.

The discretization can already be taken care of by functions written in my library. If the newly formed solution has too many points for the linear system to be solved efficiently then there are two approaches that I can consider. Rediscretize by truncating the Fourier spectrum, then process with hybrid numerical methods; or, run the large discretization through adjoint descent and then rediscretize before explicitly solving via Newton's method.

For the discontinuity I am going to elect to smooth any discontinuities by multiplying the scalar field with a Gaussian centered at the boundary. The width of the Gaussian is something to play around with but from previous experience $0.3 \leq \sigma \leq 0.5$ has worked for me in the past. The reason I would elect to use this method instead of truncating the Fourier spectrum is that the latter has a more pronounced effect on the scalar field away from the boundary than the Gaussian mollifier. In other words, I believe the multiplication with a Gaussian (local smoothing) is better than Fourier truncation (global smoothing) when merging two converged invariant 2-torus solutions, as locally away from the boundary we know that the constituent pieces satisfy the Kuramoto-Sivashinsky equation .

The symmetry considerations are relatively minor details but are important to get right; in the case of continuous symmetry I will elect to average the spatial translation when concatenating solutions.

The data of all invariant 2-tori with continuous spatial translation symmetry i.e., relative periodic orbit's, is kept in mean-velocity frame format such that the scalar field data is saved in a doubly periodic form. While its hard to motivate, and likely wrong to join two solutions in two different reference frames, I thought that perhaps I could circumvent this logical gap by cheating and just taking the average of the spatial shift, and hope that the initial condition is decent enough to converge through my numerics; the motivation isn't well founded, other than the fact that my numerical codes seem to be able to converge to solutions even when starting with "poor" initial conditions. The confusion is born out of being unsure how to spatially concatenate invariant 2-tori with continuous spatial symmetry.

I am unsure how well this will work but in the first attempt it's a simple idea to implement. For the solutions with discrete symmetry the only extra consideration is that instead of just glueing two solutions together side by side, one of the solution will have to be cut in half such that the halves can be concatenated onto both sides

of the solution. This is due to the fact that both solutions will have a symmetry axis that we need to respect if the new initial condition will have the same symmetry.

The numerics can handle everything I plan to do so all that is left is to introduce the precise smoothing functions, which will wrap up the new initial condition generation.

Families I'm going to run numerical continuation code on all invariant 2-tori in current library to test my hypothesis that as the solutions get larger in terms of spatiotemporal area they live in smaller regions in (L, T) tiles. I'm hoping that this will be analogous to the statement that specifying a invariant 2-torus with more symbols is analogous to specifying a field with more precision. This is going to produce a large amount of data so I'm going to run it on light rather than my laptop soon.

2018-09-27 Matt [Numerical Continuation and other codes] Still working on the initial condition generation for glueing together solutions and symbolic dynamics.

2018-10-01 Predrag This might be of interest: Andre Wibisono (joint work with Ashia Wilson and Michael Jordan), Georgia Tech CS, Monday, Oct 1, 2018 - 1:55pm in Skiles 005 - *"Faster convex optimization with higher-order smoothness via rescaled and accelerated gradient flows"*:

Accelerated gradient methods play a central role in optimization, achieving the optimal convergence rates in many settings. While many extensions of Nesterov's original acceleration method have been proposed, it is not yet clear what is the natural scope of the acceleration concept. In this work, we study accelerated methods from a continuous-time perspective. We show there is a Bregman Lagrangian functional that generates a large class of accelerated methods in continuous time, including (but not limited to) accelerated gradient descent, its non-Euclidean extension, and accelerated higher-order gradient methods. We show that in continuous time, these accelerated methods correspond to traveling the same curve in spacetime at different speeds. This is in contrast to the family of rescaled gradient flows, which correspond to changing the distance in space. We show how to implement both the rescaled and accelerated gradient methods as algorithms in discrete time with matching convergence rates.

In any case, Professor Molei Tao is a smart cookie, worth talking to.

2018-10-01 Matt Weekly Goals

- Finish automated gluing initial condition generator
- Finish automated symbolic dynamics initial condition generator
- Expand library of solutions by numerical continuation

- File reimbursement for DFD registration fee
- Try some new numerical methods on Kuramoto-Sivashinsky equation

Andre Wibisono Talk Universal language for describeing phenomena, Learning, economoics, Optimal Transport, Neuroscience, Statistical mechanics, statistics,biology,physics (Laws of physics as principle of least action in spacetime). Find best parameter x that minimizes some loss function. (cost function).

Convex Optimization in $\mathbb{R}^n$ in continuous and discrete time. Want to design "fast" algorithms to solve $\min f(x)$. Assuming differentiability, convexity, gets us a guarantee on convergence properties of the different methods.

Many algorithms are discretizations of dynamics in continuous time, for example gradient descent and gradient flow. Talking about convergence rates, differences between continuous and discrete time.

Gradient descent

$$x_{k+1} = x_k - \epsilon \nabla f(x_k) \tag{16.67}$$

Gradient Flow

$$\dot{X}_t = -\nabla f(X_t) \tag{16.68}$$

Nice properties for convex, nonconvex f, some conditions on bounded $\nabla^2 f$. Can say a lot about convergence.

$$x_{k+1} = x_k - \epsilon \nabla f(x_k) \tag{16.69}$$

Theorem: If f is convex and $\frac{1}{\epsilon}$ smooth then gradient descent scales like $\mathcal{O}(\frac{1}{\epsilon k})$

$$\dot{X}_t = -\nabla f(X_t) \tag{16.70}$$

Theorem: If f is convex (upper bound on Hessian) then gradient descent scales like $\mathcal{O}(1/(t))$.

i.e.these have same convergence rates if $t = \epsilon k$.

How to design (provably) fast dynamics for $\min f$. Can we get faster than gradient flow? What is the *fastest* dynamics? Not actually well defined, definition of *fast* is dependent on t parameterization; reparameterizing via speeding up time speeds up algorithm.

The sped up gradient flow $\tau = \frac{t^{p-1}}{p-1}$ (specific form dependent on convex f then gradient flow takes

$$\dot{Y}_t = -t^{p-2} \nabla f(Y_t) \tag{16.71}$$

What is sped-up gradient descent?

$$y_{k+1} = y_k - \epsilon k^{p-2} \nabla f(y_k) \tag{16.72}$$

This does not get better than $\mathcal{O}(1/k)$ Faster dynamics from optimization, Recaling gradients

$$\dot{X}_t = -\nabla f(X_t)/||\nabla f(X_t)||^{\frac{p-2}{p-1}} \tag{16.73}$$

Acceleration and speeding up time.

$$\ddot{X}_t + \frac{p+1}{t}\dot{X}_t + t^{p-2}\nabla f(X_t) = 0 \tag{16.74}$$

First, look at rescaled gradient flow

$$\dot{X}_t = -frac\nabla f(X_t)||\nabla f(X_t)||^{\frac{p-2}{p-1}} = argmin(<\nabla f, v> +1/p||v||^p) \tag{16.75}$$

Faster when the gradient is small. (This might be worth looking at).

$p = \infty$ is "normalized gradient flow".

Convergence $\mathcal{O}(frac1t^{p-1})$. Same as gradient flow when $p = 2$. Proof provided by convexity and Fenchel-Young.

He is skipping details to get to accelerated flow. How to implement as an algorithm. Proximal method, Higher-order gradient descent, rescaled gradient descent. Proximal is an implicit method (backwards discretization of rescaled gradient).

$$x_{k+1} = argminf(x) + \frac{1}{\epsilon p}||x - x_k||^p \tag{16.76}$$

$$x_{k+1} = argminf_{p-1}(x; x_k) + \frac{1}{\epsilon p}||x - x_k||^p \tag{16.77}$$

Instead of minimizing f, minimize the taylor expansion up to terms $p - 1$ order. Examples of this are, $p = 2$ leading to regular gradient descent, $p = 3$ Cubic newton.

Assumption that f is smooth of order p then convergence rate is $\mathcal{O}(\frac{1}{\epsilon k^{p-1}})$.

New stuff. If function is *strongly smooth* (all gradients up to pth order smooth), then,

$$x_{k+1} = x_k - \epsilon^{\frac{1}{p-1}}\frac{\nabla f(X_t)}{||\nabla f(X_t)||^{\frac{p-2}{p-1}}} \tag{16.78}$$

Proximal method. Higher gradient descent. Rescaled gradient descent. Lower bound given by Nemirovski, Yudin, Nesterov. Using assumption that algorithm generates $x_k \in x_0 + Lin(\nabla f(x_0), \cdots, \nabla f(x_k))$. This has order $\mathcal{O}\frac{1}{\epsilon k^2}$

Rescaled gradient and cubic-regularized require that Hessian is bounded but we can get better without this assumption with the accelerated gradient descent.

Accelerated Descents

$$
\begin{aligned}
x_{k+1} &= y_k - \epsilon \nabla f(y_k) \\
y_k &= x_k + \frac{k-1}{k+2}(x_k - x_{k-1})
\end{aligned}
\tag{16.79}
$$

gradient descent "with momentum". function value can oscillate, gradient descent is monotonic. Achieves optimal convergence rate.

Gradient descent is very intuitive, but it is not optimal. Now let's go to continuous time limit,

$$
ddx_t + 3/tdotxt + \nabla f(x_t) = 0
\tag{16.80}
$$

For accelerated gradient descent (AGD). Can show that oscillatory dynamics both in function value and trajectory. Convergence rate proofs via Lyapunov function. Question, whhy the dynamics, why the optimality. There is non constant damping. With $1/t$ damping for convex f and constant damping for strongly convex f. (strongly convex is bounded Hessian).

How would you come up with this? Use a lagrangian formulation that generates almost all of the algorithms that we know. Lagrangian, principle of least action, optimal curves satisfy Euler-Lagrange equation.

Lagrangian that he uses:

$$
L(x, v, t) = t^3(1/2||v||^2 - f(x))
\tag{16.81}
$$

Reference to Yezzi talk from last week "Accelerated optimization of PDE framework". If we speed up time in the AGD then it has $\mathcal{O}(1/t^p)$. Can we implement this? not quite he says. Reference to Bregman divergence; working on Euclidean space with metric given by the Hessian. Write the NGF as "mirror flow"

$$
\cdot \nabla h(x_t) = -\nabla f(x_t)
\tag{16.82}
$$

can be discretized as mirror descent (MD) as

$$
x_{k+1} = \arg\min_{x \in R^n} \{< \nabla f, x - x_k > + \text{Bregman divergence term}\}.
$$

Accelerated mirror descent by Nesterov (2005). Can ask, what is Lagrangian for accelerated mirror flow (AMF)?

$$
\ddot{x}_t + 3/tdotxt + (\nabla^2 h(X_t + t/2\dot{X}_t))^{-1}\nabla f(x_t) = 0
\tag{16.83}
$$

AMF is generated by the Bregman Lagrangian. Speeding up AMF with speed up time rescaling.

How to implement (polynomial rate AMF) Can be unstable. Therefore borrow Nesterov's trick and indroduce an aux sequence to stabilize the algorithm. "What actually works" Accelerated higher-order gradient descent (AHGD) has correct convergence rate.

Can also accelerate rescaled gradient descent (easier). Again due to Nesterov. AHGD is the discretized form of accelerated mirror flow.

Can convert to Bregman Hamiltonian, looks like Lyapunov function; use symplectic structure?. Madison, Paulin, Teh, O'Donoghue, Doucet 2018 (different Hamiltonian).

What's still unclear, the Lagrangian works, but still don't know if its best. Need to formulate optimal dynamics for optimization.

Takeaways from Wibisono Talk In my personal experience when looking for numerical methods that are commonly used in nonlinear optimization procedures fall into two classes: descent methods and iterative methods. I thought I was pretty exhaustive on the types of numerical optimization methods (specifically descent methods) that were out there but after this talk I realize that I came across the most common but not the most cutting edge. That being said, this talk helped provide me with some of the more recent, cutting edge algorithms in the descent method category, giving me a new list of numerical methods I add to my numerical methods suite after sufficient time. The list of different descent methods mentioned looks something like,

- proximal method
- "mirror prox" method
- higher-order gradient gescent
- rescaled gradient descent
- accelerated gradient descent
- accelerated mirror descent
- accelerated higher-order gradient descent

These are all methods I can try; in addition to these descent algorithms I can try different direct and iterative methods as well such as,

- Cubic regularized Newton
- BiCGSTAB

As opposed to the more common Newton and GMRES methods. I think The most promising of these numerical that I can try out are the so called accelerated methods, which use the acceleration techniques of the past derived by Nesterov [48] applied to newer optimization algorithms.

2018-10-05 Matt Trying to make up for lost time by working overtime during the week and completely crashing on weekends. I'm hoping I can keep it up

> **Spatiotemp Codes** Implemented a number of new numerical methods to see if any of them could compete with what I currently have. Out of the three classes of solvers, (descent methods, direct methods, iterative methods) iterative methods have work terribly for me. Therefore in order to see if its just my innate disability to be able to use these methods I am running a suite of tests using built in optimization algorithms in SciPy.
>
> On the other numerical front, I implemented two different types of Levenberg-Marquardt algorithms, the first one [19] performed much better than ref. [53], and much better than the BiCGSTAB algorithm I also implemented; but for whatever reason the Gauss-Newton with back-tracking performs better in all cases I have tried so far.
>
> I also tried more testing with the accelerated adjoint descent that I had recently forgone in favor of using a lower order integration scheme in fictitious time with preconditioning, I'm thinking I'll likely stick to that as well.
>
> The main portion of today's work was to implement the gluing algorithm that takes any two invariant 2-torus solutions with the same solution and glues them together, with a slough of options as to how one specifically wants to do this, namely, whether to concatenate in space or time, whether to pad the boundaries between the two solutions with buffer zones, and how to smooth out the glued together data. The smoothing still needs some fine tuning; I'm using circular convolution with an anisotropic Gaussian that is wider in the dimension by which two solutions were glued. Currently trying to run through some test cases. The two shortest pre-periodic orbit solutions concatenated in time after adjoint descent looks interesting but Gauss-Newton squashes it into an equilibrium. Definitely needs some more fine tuning on the smoothing front.

2018-10-10 Matt Spatiotemporal gluing I'll produce a figure that makes this entire process more obvious, as I see that it is almost assuredly completely opaque to anyone other than I.

> Had a discussion with Predrag about how no one has listened to him about how to make a figure eight orbit from two constituent periodic orbits. Instead of using L_2 norm minimizer between two orbits the smart thing to do is to find segments that follow the periodic orbits for a fraction of their periods with the segments ending / beginning on the unstable / stable manifolds of the two orbits, respectively, and then making connections with lines. This same reasoning can

be applied to my spatiotemporal situation, except now I will shave off sections of two tori so that they can be joined by a surface.

I believe the practical way of doing this is going to be to take the convex combination of the pieces of the tori that remain after chopping them up to connect them to one another. For example, if torus A and B are to be connected in time, I should take a subset of the time values of both A and B. Let these subsets be denoted by $t_A \in [T_{A_-}, T_{A_+}]$ and $t_B \in [T_{B_-}, T_{B_+}]$. The connect should now be between pairs $A(T_{A_-}), B(T_{B_+})$ and $A(T_{A_+}), B(T_{B_-})$. I propose that this is done in the following manner: (naive and simple, but more intuitive than just zero padding and smoothing).

To join the two ends of the torus we take the convex combination, for $\tau \in [0, 1]$

$$\mathbb{T}_+ = A(T_{A_-})\tau + B(T_{B_+})(1 - \tau), \qquad (16.84)$$

and likewise for the other connection,

$$\mathbb{T}_- = A(T_{A_+})(1 - \tau) + B(T_{B_-})\tau, \qquad (16.85)$$

of course while maintaining any symmetry relations (i.e.gluing fundamental domains together).

After this has been performed, one must determine the period approximate period (Could do a line search around $T_A + T_B$ to see what minimizes cost function) and decide on what kind of smoothing to perform. I believe that the convex combinations imply that we only have C^0 continuity in time, the Fourier spectrum will not converge exponentially, and as such Fourier truncation might prove to be too strong, in terms of net affect on the global spatiotemporal field. I will perform tests on Gaussian convolution versus Fourier truncation to see which seems more reasonable.

Now, I just want to state that I really do understand the unstable and stable manifold argument; but in terms of the spatiotemporal Kuramoto-Sivashinsky equation that does not contain dynamics this is the idea that I am going to (finish) implementing. As a crude (I am afraid exactly what Predrag and I both know is wrong, especially after he told me *today*) is to calculate the pairwise L_2 norms between different 1-d time or spatial strips of the solution, store the results in a matrix, and then find the minima of a weighted version of the matrix that attempts to preserve as much of the original information as possible

Let's assume that I am gluing two periodic orbits together in the time direction. After a bit of work I realize that when working in the fundamental the setup and algorithm is identical for all symmetry types. Given that we want to glue tori $\mathbb{T}_A$ and $\mathbb{T}_B$ together, we can produce a matrix that stores the $L_2 norms$ between different points

in the gluing direction, i.e.,

$$M_{i,j} = ||A(x, t_i) - B(x, T_B - t_j)|| \tag{16.86}$$

Instead of finding minima to this, I want to favor keeping as much of the fields of A and B as possible; therefore I will instead find the minima of the following weighted matrix. (Finding a minima at index pair (i, j) is equivalent to deleting the following information: $A(x, t), t \in [0, t_i]$ and $B(x, t), t \in [T_p - t_j, T_p]$ In order to favor smaller $N = i + j$, I weight the matrix M to penalize large (i, j) choices via the following.

$$\tilde{M}_{i,j} = ||A(x, t_i) - B(x, T_B - t_j)|| + i/N_A + j/N_B, \tag{16.87}$$

where N_A and N_B are the maximum values that i, j take on respectively. The first choice or calculation of (i, j) helps identify and glue one pair of boundaries together, but we still have to glue the other boundary. This can be computed by performing the same operation on the Cofactor matrix $C_{i,j}$ that is created by deleting all rows up to i and all columns up to j. In order to switch to the other boundary we also have to flip the cofactor matrix around so that the indices correspond to the correct boundary, after performing these bookkeeping operations, we find the minimum of

$$\tilde{C}_{\ell,k} = ||A(x, T_A - t_\ell) - B(x, -t_k)|| + \frac{i}{\tilde{N}_A} + \frac{j}{\tilde{N}_B}, \tag{16.88}$$

where $\tilde{N}$'s are the dimensions of the cofactor matrix. The method of penalizing large indices is another expedient, simple implementation and so I'm not claiming that it works until I test these codes, which I sadly didn't finish as I had to rewrite a number of pieces today.

This was the first idea I came up with to chop and glue tori together. I haven't finished the code yet but I hope to soon so I can do some tests.

2018-10-11 Matt Still working overtime (maybe a little too much....) in attempts to catch up on my responsibilities. Today's work mainly focused on rewriting portions of the automated gluing code and debugging it.

I found success in a variety of circumstances but there are still a large number of relations that need to be more precise before I can say my work is done. So far I have some decent results of merging the two short pre-periodic orbit 's together spatially and converging to a new solution. Other attempts have found equilibria and strangely enough there have been trials where one of the constituent solutions dominates and so the glued initial condition converges back onto a single constituent invariant 2-torus .

Figure 16.34: Plots detailing the spatial gluing of two $L = 22$ solutions described in four steps: (1) Initial invariant 2-tori. (2) Splitting initial invariant 2-tori in a symmetry preserving manner (creating new fundamental domain). (3) Initial invariant 2-torus guess resulting from the gluing procedure. (4) The numerically converged solution $(L_f, T_f) = (44.23634914249, 58.57834597407)$.
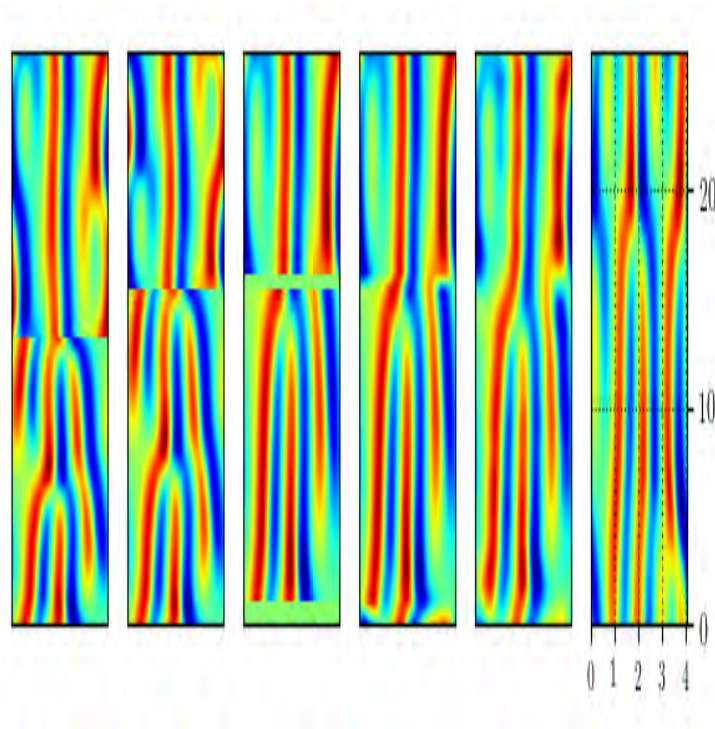
Figure 16.35: Plots detailing the temporal gluing of two $L = 22$ solutions described in four steps: (1) Initial invariant 2-tori. (2) Splitting initial invariant 2-tori in a symmetry preserving manner (creating new fundamental domain). (3) Initial invariant 2-torus guess resulting from gluing procedure. (4) The numerically converged solution $(L_f, T_f) = (44.23634914249, 58.57834597407)$.

It's all kind of strange because it is quite sensitive to certain choices such as the total discretization, the discretization of the buffers (spatiotemporal functions that are convex combinations in the "gluing direction"), whether or not the solution is Fourier smoothed,Gaussian smoothed, or just rediscretizing the solution (similar to truncation). Rediscretizing and Fourier smoothing appears to be a bad idea as it is analogous to truncating twice.

There's quite a bit of testing left; I need to make a spreadsheet to keep track of all of the variables floating around.

Regardless; due to the fact that the two shortest (period) pre-periodic orbit invariant 2-tori at $L = 22$ match almost *too well* (It's actually kind of suspicious that they match so well), I was able to glue them together with two buffer regions that used the convex combination procedure described yesterday. The two trickiest parts seem to be how much buffer to include between two solutions as it depends on how similar their boundaries are, and how much if any parts of the tori to shave off.

Figure 16.34 and figure 16.35 are the penultimate summary of today's work. It chronicles each step in the gluing process for shift-reflect invariant solutions; I recommend looking at in case there are any important comments for me. [9]

The invariant 2-tori space and time periods (a) from figure 16.34 were $(L_0, T_0) = (22.0, 20.5057459345)$ and $(L_1, T_1) = (22.0, 28.6609617454)$. Final values for this solution were $(L_f, T_f) = (42.580326368, 24.210913068)$.

Solutions were glued together by using discretizations of 128×128 for each field; the final field in the configuration space had dimensions 32×64, which corresponds to $31 * 31$ spatiotemporal Fourier modes due to symmetries. The initial guesses for the period and domain size of the solution were estimated by

$$T \approx \frac{T_1 + T_2}{2}, \tag{16.89}$$

and

$$L \approx M * (\frac{L_1}{M_1} + \frac{L_2}{M_2})/2 = M * ((\Delta x)_1 + (\Delta x)_2)/2, \tag{16.90}$$

where M is the new spatial discretization size, and M_1 and M_2 are the previous discretization sizes of the solutions respectively.

2018-10-17 Matt Glue automation I have the gluing code fully automated by it doesn't work too well as the discretizations get too large. To circumvent this, I went through testing whether I could optimize the discretization through a quantitative measure. This was attempted

---

[9] Predrag 2018-10-29: Why do you write (L_f, T_{p_f}) in figure 16.34, and not (L_f, T_f)? Why is (L_f, T_f) the same in figures 16.34 and 16.35? Looks wrong in figure 16.34.
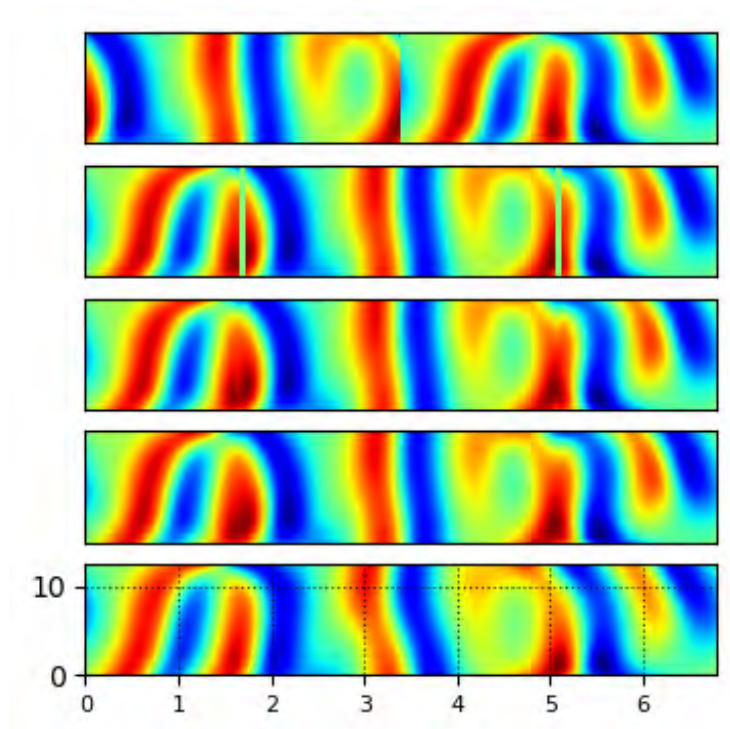
Figure 16.36: Plots detailing the spatial gluing of two $L = 22$ solutions described in four steps: (1) Initial invariant 2-tori. (2) Splitting initial invariant 2-tori in a symmetry preserving manner (creating new fundamental domain). (3) Initial invariant 2-torus guess resulting from gluing procedure. (4) The numerically converged solution $(L_f, T_{p_f}) = (44.23634914249, 58.57834597407)$
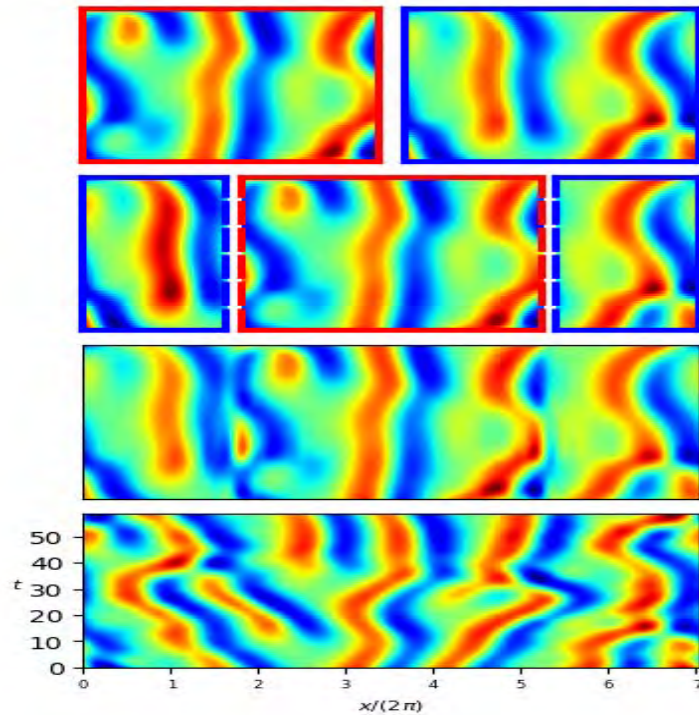
by looking at the (initial)condition number of the matrix that arises from Newton's method. This is a measure of how close the (least-squares) linear system is to being singular. From this investigation it was seen that the condition number seemed almost independent of the temporal discretization but highly dependent on the spatial discretization. I approached this from the perspectives of being both a pre-processing and post-processing step; I was hoping to be able to decrease the number of variables to speed up the numerical computations, without throwing away too much information.

In certain instances this is easy as the condition number increases as the solution starts to change dramatically; in other instances the condition number $\sigma_c \to 0$ as $M \to 0$ where M is the number of points in space. This leads to arbitrary bounds on the discretization and quickly becomes a procedure that is idiosyncratic to each solution, which is not useful. The application as a post-processing treatment is also at risk of throwing out too much information, which can take a converged solution to a non-solution. So without considering the period and domain size of each solution separately this is likely a wasted effort.

I also tested the differences between slicing solutions and chopping them; slicing is referring to concatenation of solutions by removing points from the fields and then smoothing out the boundaries. Chopping refers to splitting the fields into multiple subdomains and padding the boundaries with zeros. Both procedures use convex combinations to fill in the missing information.

Regardless; there might be a few more things to do to the gluing code before running it on light or eventually PACE.

Cheaptricks Went through the built-in minimization functions from the SciPy library to see if any would work. The method BFGS seemed promising and might be able to be used for this problem. BFGS stands for *Broyden-Fletcher-Goldfarb-Shanno*. In a couple of minutes it was able to reduce the cost function to a value of 10^{-10}; Newton on this problem gets it to within machine precision in a couple seconds so whether its useful is going to be dependent on whether it scales better than Newton with respect to system size.

Spatiotemporal Symbolic Dynamics The gluing code might work much better for surveying the spatiotemporal symbolic dynamics because the discretizations of the tiles tend to be smaller than average solutions, because they are defined on smaller spatiotemporal areas.

2018-10-18 Matt Autogluer should be ready tomorrow; the last thing I wanted to play around with was trying to optimize and or minimize the number of discretized points. I have a very rough criterion, which is just to decrease the number of points (decreasing number of spatial points only seems to be most consistent) based on the residual of the cost function.

Figure 16.37: Gluing diagram for same initial conditions as figure 16.34, except in the second to last figure the discretization of $N \times M = 32 \times 64$ points was reduced to $N \times M = 16 \times 40$; values determined by cost functional evaluations.
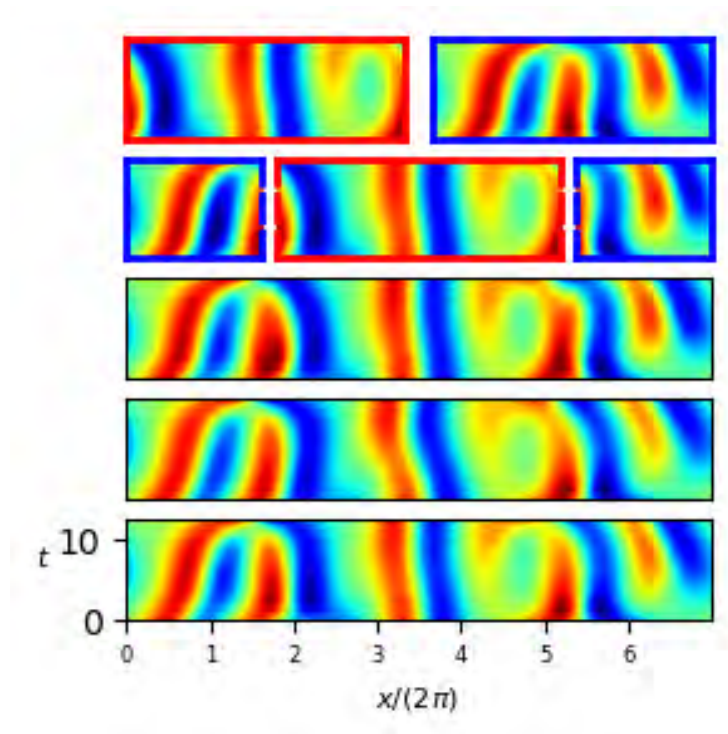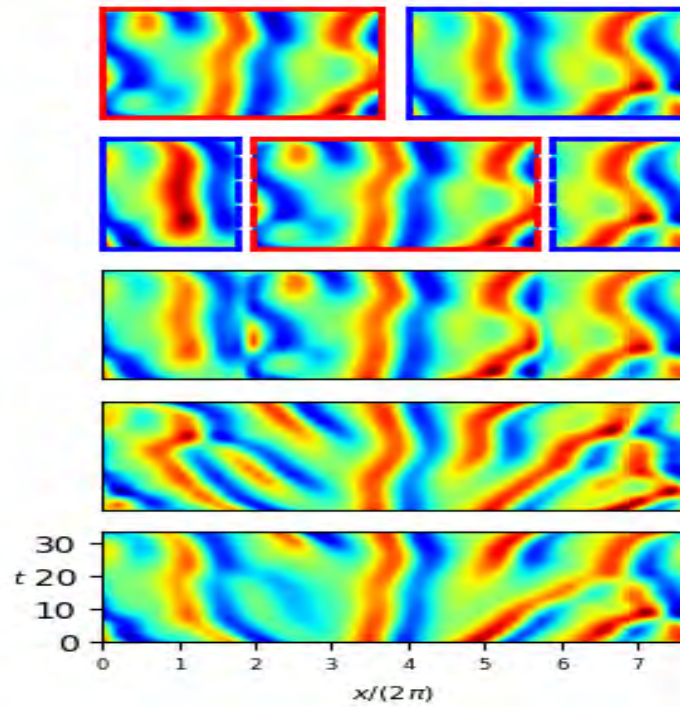
Figure 16.38: Gluing diagram for same initial conditions as figure 16.36, except in the second to last figure the discretization of $N \times M = 32 \times 64$ points was reduced to $N \times M = 32 \times 38$; values determined by cost functional evaluations.

The idea was that including extra Fourier modes only serves to contribute to the residual and there should be a minimal number that contains most of the information from the original solution, with higher order terms serving to add to the residual by the large diagonal terms of the linear component of the Kuramoto-Sivashinsky equation in spatiotemporal Fourier space. The original problem with this kind of investigation is that depending on what criterion one uses to measure this phenomenon, it can quickly take much more time than it takes to converge a solution; thereby defeating the point in the short-term, albeit if the new solution is also going to be glued then any reliable rule for decreasing the discretization is useful.

What works surprisingly well is *one of the most naïve* ideas one could think of, which is to take the new, glued initial condition, and decrease the number of points in the discretization until the value of the cost function increases. This is no where near an exact science but because we are gluing together previously converged solutions, there is some notion of being "close" to a new solution by using the residual of the cost function. Once the discretization changes start to increase the residual, a rough claim would be that we are starting to throw out required numerical information.

This investigation I believe will be of the utmost importance if we want to be able to repeatedly glue solutions together; its a very rough approximation to the minimal number of points required to resolve a invariant 2-torus. It does have its downsides; sometimes if one does not provide a lower bound it will get close to zero and then converge to equilibria solutions.

figure 16.38 and figure 16.37 detail the gluing procedure for a minimized discretization; the second to last step is the extra step. If we label the two initial conditions by 0 and 1, then this step takes the new discretization $(N_0 + N_1, M)$ $((N, M_0 + M_1))$ from temporal (spatial) gluing, and reduces it. The only cases where this has been attempted was for preperiodic orbitinvariant 2-torus solutions. The discretizations were able to be reduced to from $(N - 1) * (M - 2)/2 = 961$ to 285 for the spatial concatenation of the two shortest pre-periodic orbit invariant 2-torus solutions, and from 961 to 558 for the third and fourth shortest solutions glued torus. So although crude, it is quite effective.

Also, in order to make the gluing figures as appealing as possible I spent far too much time tinkering with the plotting features afforded to me in Python. Things get so specific its mind numbing; but after a number of wasted hours I realized my problems were born out of aspect ratios being automatically determined.

2018-10-24 Matt Abstract for March Meeting I'll get this done by the deadline.

Figure 16.39: Gluing diagram for two shortest relative periodic orbit invariant 2-tori from $L = 22$. This was the successful test case for invariant 2-tori with continuous spatial translation symmetry.

Gluing code Some woes with gluing solutions with continuous symmetry. Realized that the spatial shift parameter didn't match with the data stored for the $L = 22$ initial conditions, hence the update to the files containing relative periodic orbit data.

The method by which the two solutions are adjoined is similar to invariant 2-tori with discrete symmetries except for the minimization preprocessing that attempts to minimize the difference between the two solutions by translating them in the direction orthogonal to the gluing direction; i.e.if trying to glue two relative periodic orbit invariant 2-torus solutions in time I used spatial translations to get them to match.

Describing figure 16.39 subplots from left to right:

1. The two initial conditions (the shortest relative periodic orbit solutions from $L = 22$).
2. The first attempt at gluing the solutions in time, by padding the boundaries with zeros and then filling in the zero padding with convex combinations of the boundaries.
3. The spatiotemporal field after reducing the discretization from $N = 64$(time) and $M = 32$(space) to $\tilde{N} = 32$ and $\tilde{M} = 16$.
4. The converged spatiotemporal field resultant from adjoint descent and Gauss-Newton with backtracking (my typical numerical method)

The unjustified means by which I chose the value for the spatial translation parameter was to just use the spatial translation for the second solution. The rationale behind doing so is that I am only interested in doubly periodic solutions. This choice makes the new initial condition periodic with the tradeoff being a coordinate transformation (mean-velocity frame) that twists the first solution in a linear, but artificial manner. I want to stress that this tradeoff might be too much for future cases, but it worked well enough for the test case, and had at least *some* motivation. The spatial case is a whole other can of worms; I haven't finished this portion yet as it is hard to motivate combining solutions in two different reference frames (concatenating the solutions in their respective mean-velocity frames), other than the fact that working in the non-periodic coordinates is even worse. I have no intuition as to how to join two relative periodic orbit invariant 2-tori spatially, because they have different group tangents at every point in time.

One option might be two glue solutions whose mean-velocity frame coordinate transformations are similar or the crude method of joining the solutions together in the mean velocity frame and then averaging the spatial translation. Again these are crude methods but I haven't been able to think of better ones just yet. This is very important; however, as some fundamental "defect" tiles are relative

periodic orbitś. So unless I can resolve these issues, using gluing to survey the spatiotemporal symbolic dynamics will be impossible.

2018-10-24 Matt Plumbers Talked to the plumbers about really thorough and well performed experiment with monkeys. I believe the main take away was that the experiments were performed over a very long time period; by performing PCA or something similar they were able to find a low dimensional basis (analogous to a local basis of an inertial manifold) that "aligned" data in a way that enabled comparison and analysis of long-term experimental data as a singular set instead of many different experiments. There are of course the actual contributions to neuroscience but I didn't read enough of the paper to get that far in.

I shared my recent work with gluing solutions together; Burak made sure to mention not to miss out on the side projects that might seem trivial or easy now, it would be best to capitalize on these side-quests with relative haste; a sentiment I agree with. I unleashed my current woes of gluing solutions with continuous symmetries together and how I had a couple ideas but wanted insight. I believe Predrag indicated that this falls under the applications of slicing (quotienting the continuous symmetry). In other words, given two orbits, the lemniscate combination that arises should be calculated in slice.

I mentioned how I've been using a time-dependent group transformation as a coordinate transformation into what I and others denote the mean-velocity frame. Burak suggested that maybe in addition to matching the extent of continuous dimension perpendicular to gluing, one should also match solutions with similar shifts. For example, perhaps gluing two relative periodic orbit invariant 2-torus solutions spatially is justified when the periods of each solution and their average phase speed (or total spatial translation through a prime period) are approximately equal $T_1 \approx T_2, C_1 \approx C_2$. Burak was excited by the fact that I am able to get this to work in at least the test case scenarios, and he suggested that perhaps this would be a way of formulating the one dimensional symbolic dynamics at a particular ($L = 22$) domain size; something that has not been accomplished yet. While an exciting path to pursue there is still much work to be done.

Spatiotemp gluing Over the past few days I've made some sweeping changes in the gluing code. In order to gain intuition on all of the different changes made I assembled a battery of tests (whose size quickly got out of hand) to be applied to the gluing invariant 2-tori with continuous symmetries. The main idea that I found lacking motivation was how to decide what the new spatial translation parameter (shift over prime period) should be, given two solutions with differing spatial shifts. It turns out after some investigation that the cost functional doesn't seem very sensitive to changes in
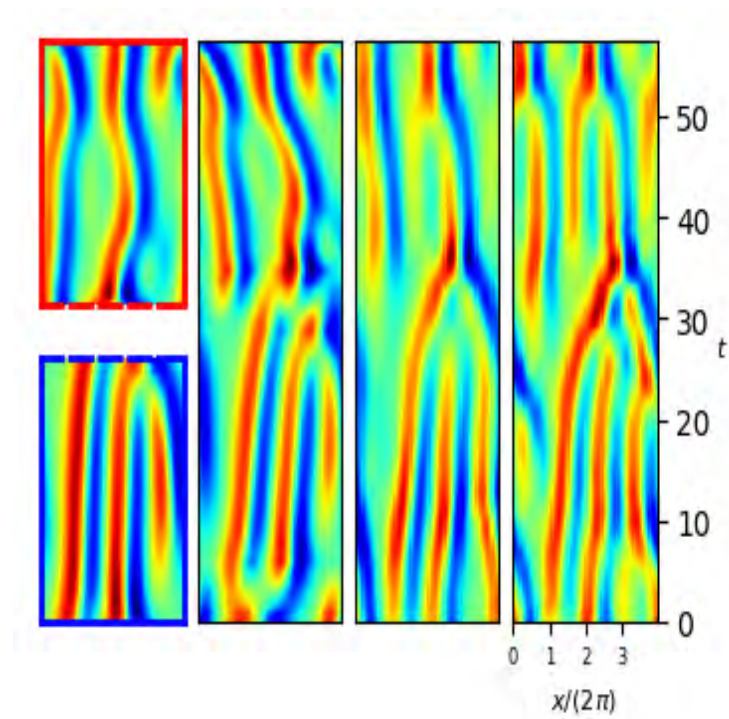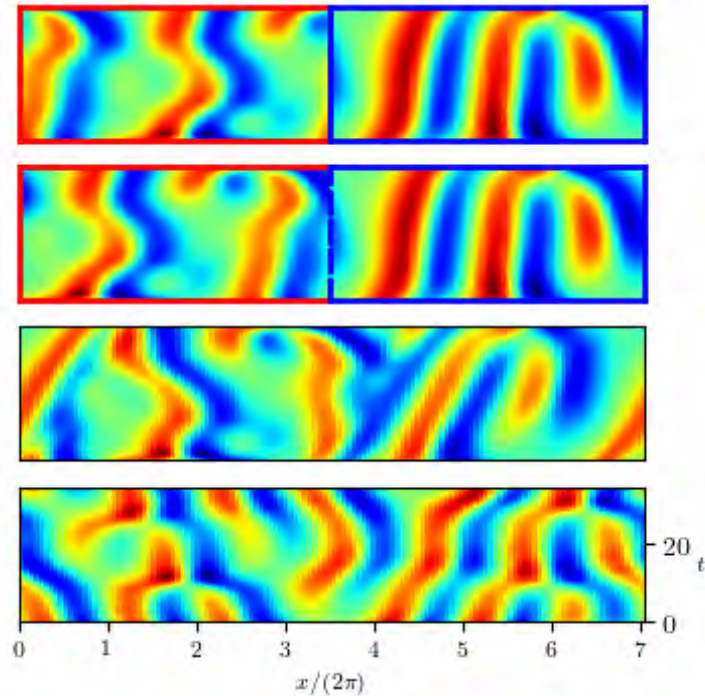
Figure 16.40: Gluing diagram for two shortest relative periodic orbit invariant 2-tori from $L = 22$. This was the successful test case for spatial gluing of invariant 2-tori with continuous spatial translation symmetry. From the top down: 1. The two initial solutions to be glued. 2. The two solutions being glued after a small attempt at minimizing the difference at the boundaries. 3. The initial condition after Fourier truncation (what I think I will call guided rediscretization, as the final discretization is guided by the cost functional). 4. The converged solution. All plots are in the physical coordinate frame, not the periodic mean-velocity frame.

(a)

(b)
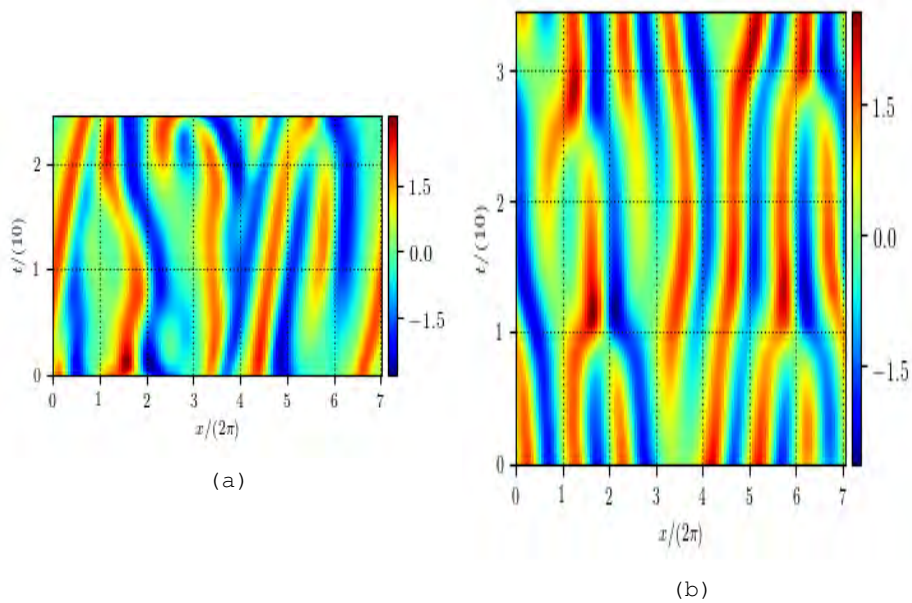
Figure 16.41: Second to last and last plots from figure 16.40 respectively, plotted here to show their approximate relative scales. (a) The initial guess after gluing and preprocessing. (b) The resulting invariant 2-torus.

this spatial shift parameter. Therefore; I believe that there is some freedom in deciding conventions, much like how I had to come up with rules for the generation of "random" initial conditions by initializing spatiotemporal Fourier modes on a grid with certain spatiotemporal extent.

I had better luck with spatially gluing invariant 2-tori with continuous symmetries after a fair bit of work today. There are still a large number of dials and knobs to play with to fine tune the procedure. In general it looks like my method of gluing solutions together, in addition to my hybrid numerical methods are strong enough to find invariant 2-torus solutions to the Kuramoto-Sivashinsky equation whether gluing solutions together spatially or temporally. An exposé on the number of parameters I am playing around with is stated below. I'm going to determine my conventions by choosing the set of parameters that make converging to a solution most likely, and therefore make the procedure the most efficient.

The main goal is use these tests to decide on conventions, then move onto attempting to merge larger (and smaller with the tiles) solutions together.

Test Battery I'm giving this part its own section just for my own book-keeping. The factors that seem to hold sway over whether solutions will converge or not (all initial conditions are manipulations of the two shortest period relative periodic orbits from $L = 22$ as test cases) are the following. Neglecting some obvious contributions to the list, such as numerical methods, choice of initial condition, etc., there are still a number of independent criteria that can be chosen, which quickly multiply and make the list of combinations large. The factors that contribute to the number of choices made are the following

- Size of the "buffer regions"
- Type of method to fill in the buffer regions.
- Which direction to glue in, space or time.
- Types of smoothing (Fourier truncations guided by cost functional)
- Algorithmic position of rediscretization, before or after adjoint descent
- The particular ordering of the solutions, using their reflection copies as well as continuous familes.
- Working in mean-velocity frame or physical coordinate frame.
- Bounds on reduction of discretization size (two relatively reasonable choices so far)

The total number of combinations is close to the thousands, meaning I have some testing and analysis ahead of me (currently in production). The largest worry currently is that there seem to be sharp cutoffs in convergence in terms of the spatiotemporal discretizations.

i.e.32×32 points might not be enough but 32×34 might be. As a general rule it seems less sensitive to the number of points in time and more sensitive to space; likely because there is a minimum number of spatial modes required to capture the inertial manifold at any given L.

I'm currently running these trials to see if anything sticks out as a clear winner; I believe rediscretizing first will win, but I need a set of more precise bounds. If the buffer regions get too large then they start introducing more error into the initial condition, or start removing too much information from original constituents, so this can probably be safely fixed at a size of 2 or 3, meaning that either there are two times this amount of zeros inserted between solutions, or this number of spatial, temporal points (entire rows of information) are used to blend solutions together.

I'm curious as to how the rediscretization before or after adjoint descent will turn out, I honestly have no idea. For the smoothing routines, I believe that which one of the four is the "best" depends on lower bounds, the solutions themselves, as well as the "gluing direction". I don't think I should worry about choosing specific members of continuous families or particular reflection copies of solutions; this can be handled automatically by seeing if the different combinations converge.

2018-10-26 Matt APS Abstract Reposting here for transparency; sadly this is all being done last minute so I won't hope for any sort of critique.

I signed up for a poster under Category: "Statistical and Nonlinear Physics" Sub-category: pattern formation and spatio-temporal chaos. (the only other option was the more general "chaos and nonlinear dynamics".

TITLE: Spatiotemporal tiling of the Kuramoto-Sivashinsky equation Abstract Body:Numerical simulations play a very important role in the study of chaotic partial differential equations due to the lack of analytic solutions. In the limit of strong chaos and or turbulence, these computations become very challenging if not completely intractable. In an attempt to circumvent these difficulties, we recast time dynamical systems as purely spatiotemporal problems in (d+1) dimensional spacetime. Specifically, the focus of this study will be on the spatiotemporal Kuramoto-Sivashinsky equation, a (1+1) dimensional system. Our main hypothesis is that spatiotemporal recurrences resultant from shadowing of invariant 2-tori are of critical import. This intuition is a spatiotemporal parody derived from the theory of cycle expansions [9]. By developing a (1+1) dimensional symbolic dynamics with invariant 2-tori as the fundamental building blocks, we hope to quantitatively characterize infinite spacetime solutions.

Gluing Testing, Testing, and more testing.

Implement a number of various means for rediscretization, reordered a bunch of processes. List of rediscretization processes, "Residual guided rediscretization": Lower N and M while $|F|^2$ is decreasing "Converged Solution guided rediscretization": Lower N to minimum value dependent on period, incrementally increase until solution converges, then do the same with M.

The first of these is the cheap, expedient procedure that should be used to produce initial conditions that have a smaller discretization that one started with; The second tries is a much more expensive procedure because it tries to find the minimal discretization for *converged* solutions; therefore, it requires a bit of computational time. From testing it seems much better to increase the discretization at all points in the calculation, and then as the very last preprocessing step, decrease the discretization. The motivation for this increased cost is because the second procedure has repeated gluings in mind; not only do we want a converged solution, but also the converged solution with minimal discretization. Because the convergence seems to be much more finicky with respect to changes in the spatial discretization when working at a fixed length $L = 22$.

A correction was made that more fairly weights solutions depending on their initial parameters; I was mistakenly creating initial conditions where solutions with drastically different periods were receiving equal number of points in the final discretization, as opposed to being weighted by how much they contribute to the final periods. In other words I wasn't incorporating the correct scales in the initial conditions.

In terms of specific testing, the main parameters that I tested were,

- Rediscretization before and after adjoint descent
- The size of the discretization of the buffers
- The method of creating the buffers
- The use of the "residual-guided" rediscretization

which lead to the following conclusions. It's always better to rediscretize before before numerical methods. A moderate buffer size is 5, a moderate number of points and likely should be proportional to the total number of points; still testing. Use of the residual guided rediscretization routine should always be used on the dimension perpendicular to the gluing dimension first. Some (seemingly) improved lower bounds on the number of points in the discretization

---
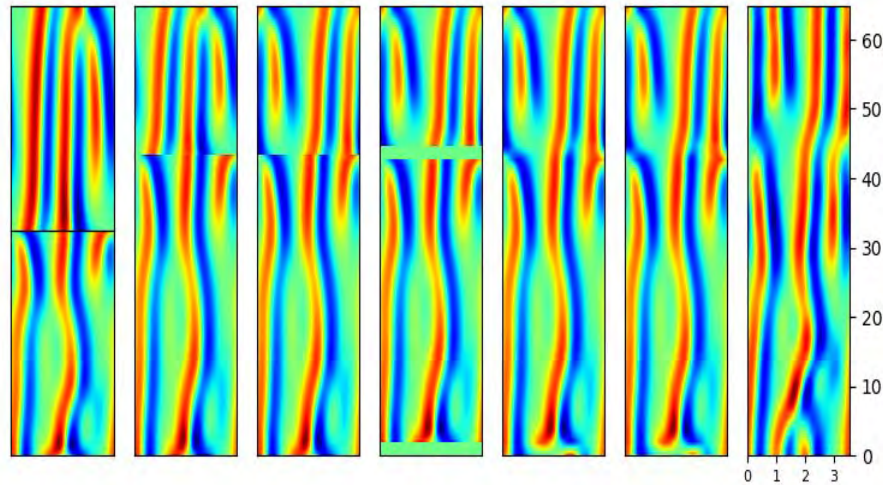
Figure 16.42: All steps and figures are annotated in long enumerated list in blog post **2018-10-31**

is something like $M = 2^{(\log_2 L + 1)}$ and $N = 2^{(\log_2 L - 1)}$. Main point: less sensitive to changing (reducing) the maximum frequency mode (less points in time).

AutoRPO I've begun code that will eventually run through all combinations (permutations excluded, even though they are technically different in the mean velocity frame) of the relative periodic orbit invariant 2-tori with $L = 22$. The hope is to illuminate the symbolic dynamics for $L = 22$, as something to run in the background. I wrote the code to be able to pick off where it left off, because there are twenty-five thousand plus combinations of relative periodic orbitś. The current efficiency (granted this is biased to the first few shortest relative periodic orbitś being combined) is $15/18 \approx 0.83$. Interestingly enough, I've found more success in spatial gluing, but the time gluing has been with fixed domain size, which can be a strict constraint.

2018-10-31 Matt RPO time gluing About to run the automated gluer on light; There are so many initial conditions to choose from I am unsure if I should just attempt to glue all invariant 2-tori that I can or if I should be more precise and target a specific subset in attempts to gain intuition into the spatiotemporal symbolic dynamics.

As I have glossed over several steps in the test case figure 16.39, here I overhaul a number of things and included some of the ideas that might lead to a more efficient (faster converging) algorithm. The improvements include:

- only combining invariant 2-tori with continuous spatial translation symmetry that go in the same direction (positive x shifts paired together, likewise for negative shifts). Allows for additive combination of spatial translation parameters.
- "buffer" size dynamically determined by the discretization as opposed to being a static number.
- Only for variable domain size L; forgetting trying to determine symbolic dynamics at $L = 22$ as its a sub-project within the bigger picture.
- Started looked at sliced and sectioned versions of figures; might include in gluing diagrams.
- Made sure everything is done and displayed in the full state space.
- Including time (or space) increments of buffer regions as omitting them underestimates the period of the glued guess invariant 2-torus.

1. Gluing the two shortest relative periodic orbit invariant 2-tori with fixed $L = 22$. Original discretizations of time-by-space 128×32. Let $u^{(1)}$ be the top invariant 2-torus, and $u^{(2)}$ the bottom invariant 2-torus.

2. (A hidden step: validate that the discretizations match so that joining two fields makes sense.)

3. The first step is rediscretizing the two initial conditions from the first figure such that they are correctly scaled relative to each other in time. I.e. if $T_1 = 1/4 * T_2$ then the initial condition corresponding to orbit 1 will appear as $1/4$ of the time domain. The second step included in this step is a dramatic increase in the size of the discretization; this is purely to make the next few steps more accurate. It is not computationally expensive because we will discard Fourier modes before computations start becomeing expensive.

4. The first step in this figure is to ensure that the solutions both have net spatial translations in the same $\pm x$ direction; if not, the top solution is reflected (not this case). The first solution is then rotated relative to the second solutions such that the impromptu cost functional $I = |u^{(1)}(x, T_1 + T_2) - u^{(2)}(x, 0)|^2 + |u^{(1)}(x, T_1) - u^{(2)}(x, T_2)|^2$ is minimized. $u^{(1)}$ indicates the solution on top, $u^{(2)}$ represents the solution on the bottom.

5. Two buffer regions, whose discretization is dynamically determined by the discretization of $u^{(1)}$ and $u^{(2)}$ in the gluing direction (in this case, the number of points in time equal $N_b = (N_1 + N_2)/8$ for both buffer regions. They are assigned with periods equal to $N_b * (\Delta t)_{\text{avg}}$. Where $(\Delta t)_{\text{avg}} = \frac{T_1/N_1 + T_2/N_2}{2}$).

6. The buffer regions filled in with convex combinations of the form $\tau u^{(1)} + (1 - \tau)u^{(2)}$ and $\tau u^{(1)} + (1 - \tau)u^{(2)}$ with the values of u being those of the respective horizontal boundaries.

7. The Fourier truncation of the previous figure. Going from some very high number of modes (I usually increase the discretization by factors of four or sixteen in each direction; arbitrarily). The figure here, however, has an additive discretization corresponding to the original initial conditions. $N = N_1 + N_2$ (time) and $M = M_1 = M_2$ (space). In this case, the resultant initial condition had 256×32 points. The domain sizes are trivially the same, and the net spatial translations and periods are additive.

8. The converged solution with the additional discretization minimization protocol. The solution being viewed has a discretization of 16×32 points, but more points are interpolated (zero padding Fourier-Fourier spectrum) so the figure looks nicer.

2018-11-02 Predrag Figure 16.7, obtained by applying the adjoint descent to a $(L, T) = (500.0, 500.0)$ large domain noisy initial condition is pleasing to the Kuramoto-Sivashinsky jaundiced eye, but deceptive. The structures look similar to those seen time-forward simulations of the Kuramoto-Sivashinsky equation, but they are not. On the $(L, T) = (500.0, 500.0)$ domain the u magnitudes in time-forward simulations peak at about 3.6, while figure 16.7 peaks at 5.2. So that's pretty bad.

What should u peak at? The overall $\langle u \rangle$ is set to 0 in order to fix the Galilean invariance of Kuramoto-Sivashinsky. For small domains, like figure 16.6, u peaks at about 2.2. However, fluctuations of $u(x, t)$ are constrained by its immediate neighborhood, and on large domains it executes a random walk, so I would expect that $\langle u^2 \rangle \approx 2D_u L$, where D_u is the spatial diffusion constant for the Kuramoto-Sivashinsky field amplitude $u(x, t)$.

The reason the fluctuations in figure 16.7 are so much larger is presumably because the numerics is crude (way too few Fourier modes?), so numerical errors add as the additional random walk.

I do not expect any diffusion along the temporal direction because (methinks) Kuramoto-Sivashinsky is a dissipative PDE, and I expect $\frac{d}{dt}\langle u^2 \rangle \approx 0$ for L fixed.

Actually, this is all explained in Cvitanović, Davidchack and Siminos [12] Sect. 3. *Energy transfer rates*, see in particular their eq. (3.6). By Ding *et al.* [17] and references therein we expect $\langle u^2 \rangle \approx 2D_u L$, while the rigorous bounds are things like $E \propto L^2$. I just did not realize that the energy density E is the consequence of the random walk in the amplitude u.

$\langle u^2 \rangle(t)$ is easy to compute for a turbulent evolution at a given L, or for any invariant 2-torus, so the diffusive guess for its magnitude is easily
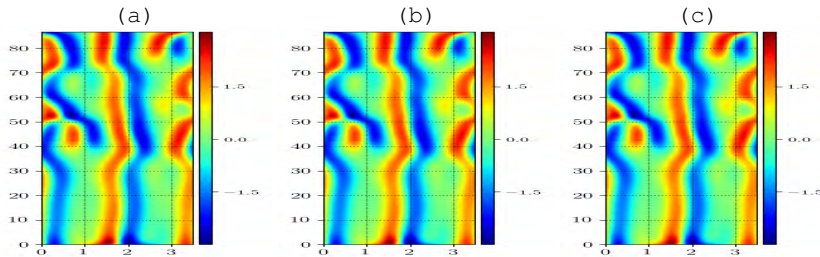
Figure 16.43:   relative periodic orbit invariant 2-torus initial condition from $L = 22$ at converged to varying tolerances of the cost function. (a) Coarse tolerance $I = 1/2||F||^2 = 10^{-3}$, (b) intermediate tolerance $I = 10^{-6}$, (c) machine precision $I = 10^{-14}$.

checked by plotting it for many different solutions with different L that should fall on a line whose slope is $2D_u$. I'm sure this must have been done in the numerical papers on Kuramoto-Sivashinsky, because that is kind of things stat mech people do instinctively.

2018-11-03 Matt Last two days have been consumed by last few touch ups with remastering data, altering gluing code, and mainly with testing the implementations of new numerical schemes BFGS and L-BFGS. BFGS stands for Broyden-Fletcher-Goldfarb-Shanno algorithm, and its relatively popular in unconstrained optimization problems but doesn't perform the best with ill conditioned problems; it requires construction of a Hessian matrix so the alternative, L-BFGS,is the preferred modification. The "L" stands for "limited memory" version. It doesn't construct any Hessian (Hessian of the cost functional, not the Kuramoto-Sivashinsky equation) but approximates it with gradients (i.e. vectors). The number of vectors that are used is a free parameter so there is some storage required but no large matrices and no solving of large linear systems (We're in the $\prime(n^2)$ range for number of operations where solving the linear system directly would be $\prime(n^3)$. I've been using ref. [49] as the reference text as I feel like it is a very well written text. Normally in these computational texts the number of variables, indices on said variables and self references to earlier discussed algorithms make it an adventure book (turn to page 5, then turn to page 63, etc.) but I feel like everything is well explained and laid out neatly enough to understand relatively quickly.

Sadly, while I got both algorithms to work their performance, in terms of cost function residual $1/2||F||^2$, mimics that of the adjoint descent algorithm previously employed. In the write up that will show up here in the near future I believe that the adjoint descent I am employing is actually a limiting case of the BFGS algorithm. Also, its interesting to note that while the algorithm requires an approximation to the inverse of a Hessian, this can be approximately well by only employing the part of the

Hessian that arises from the linear operators in the cost functional as it results in a term that is anywhere from three to twelve orders of magnitude larger than other terms. (what I mean by this is that $v^\top L^\top Lv \approx 0.99 v^\top Hv$).

The main thing I want to report is my frustration that yet again I can get something to work "half-way" but then I need to rely on Gauss-Newton to converge to within machine precision. It's interesting that in ref. [49] their tolerance criterion is not based on the cost functional but rather the magnitude of its gradient. I did some testing and I believe that this is a more lax but still strong enough condition to get invariant 2-toriThe reasons why I believe this, if we use a relatively large tolerance for the gradient of the cost functional, $|\nabla I| = |J^\top F| < 10^{-5}$, and then compare with the adjoint descent, we see that

$$I_t = -|J^\top F|^2 < -10^{10} \tag{16.91}$$

which is a statement for the stalling behind the adjoint descent, by looking for solutions $F(x) = 0$ via the construction of the cost function $I = 1/2||F||^2$, then the derivative gets negligible as we get close to the intended target.

Another argument for using a tolerance criterion based on the magnitude of the gradient of the cost function uses *converged* solutions at $L = 22$ from Xiong and Ruslan's repository, (i.e. solution where the shooting method residual is of order 10^{-9} 10^{-12}). These solutions, when a time discretization is made via time integration of the saved point "on" the orbit, have cost function typically have residuals in the $10^{-1} - 10^{-3}$ range. Therefore, what someone else would refer to as a spatiotemporal solution isn't even close to the numerical tolerance that I have been achieving. Granted, I am also allowing the spatial dimension to vary but even if I fix L the residual is the same.

A very crude argument would use the how the solution looks based on its residual. Honestly, I believe that if I created a array of figures each with a cost function residual at at different orders of magnitude, i.e.$I_k \{10^{-k}\}$, $k = 0, 1, 2, 3, ..., 15$, that no one would be able to tell the difference after about k = 5 or so. I'm going to run a test to see if I can better quantify this by derivatives rather than the objective value.

TL;DR Testing numerical algorithms, I think we're being too strict numerically, although it is more impressive, I believe if we capture the correct patterns that is sufficient. figure 16.43 is attempting to be evidence towards this.

2018-11-06 Matt List of things I need to write about when I wake tomorrow.

- BFGS and L-BFGS algorithms, motivations, etc.
- refactored automated gluing code (better bounds on discretizations, more reliable discretizations,

- attempt at minimization of spatiotemporal area; works well for initial conditions near solutions, not so much for gluers.

- Started investigating how I can best utilize PACE, talked to Simon about how to get started; need to learn how to parallelize my python scripts.

- I think I should probably look for places to optimize codes before parallelizing them and sending them to PACE, might rewrite portions and or entire implementations of some codes if it seems worthwhile.

2018-11-07 Matt I will get back to this, I've just been bouncing between so many different pursuits its hard to find time to blog

BFGS algorithm

L-BFGS algorithm

Torus gluing refactoring combinations, better residual guided discretization, better bounds, found that was well hidden by usually using powers of two in discretization, which resulted in incorrect inverse discrete Fourier transform matrices for pre-periodic orbit invariant 2-tori ; it only affected the direct matrix code for pre-periodic orbit invariant 2-tori when N was even but not a multiple of four, i.e. when $N = 4 * n + 2$. I'm surprised that this hasn't shown up until now.

kstori2C I realized that while I've been using real valued Fourier transforms that have the same number of variables as complex valued transforms, complex valued matrices would actually save a factor of four due to the matrices being ...

Torus gluing tuning

Clean up

Pace

Optimization

Tiling

2018-11-09 Matt Frankenstein, and his bride After putzing around all night I am finally content with the results from manually gluing together subdomains to try and find $\text{ppo}_{30 \times 44}$ (figure file */figs/ppo_L30_T44*) which was what I was attempting to approximate with figure 16.23. In a relatively short amount of time I was able to get a solution that was similar to $\text{ppo}_{30 \times 44}$ but I wasn't convinced. The discussion that follows is an in depth step-by-step description of how Frankenstein's bride came alive, but not before his bride.

Firstly, I decided in creating the approximate tiling to represent $\text{ppo}_{30 \times 44}$, it was more important to nail the quantitative shapes rather than
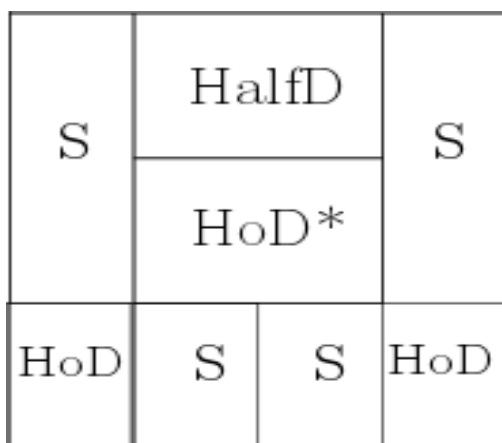
Figure 16.44: A figure representing the general blueprint for dividing the fundamental domain of $\mathrm{ppo}_{30\times44}$ into subdomains. The lettering dictates which spatiotemporal solution one should insert to generate the target invariant 2-torus. The dictionary is "S" stands for streak, "HoD" stands for hook-on-defect, and "HalfD" stands for half-defect.
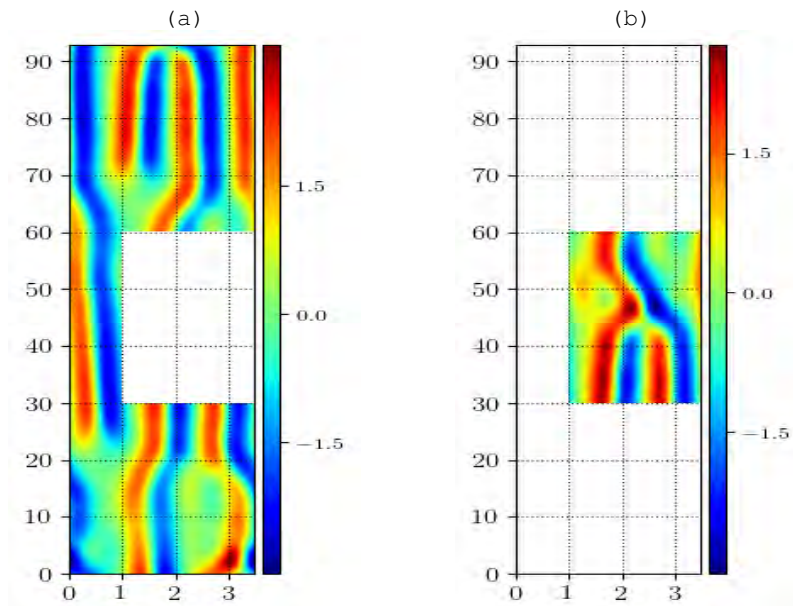
Figure 16.45: (a) $\mathrm{ppo}_{21.93\times92.77}$ with a subdomain cutout (b), which I call the "hook on top of defect" tile.

(a)

(b)

(c)
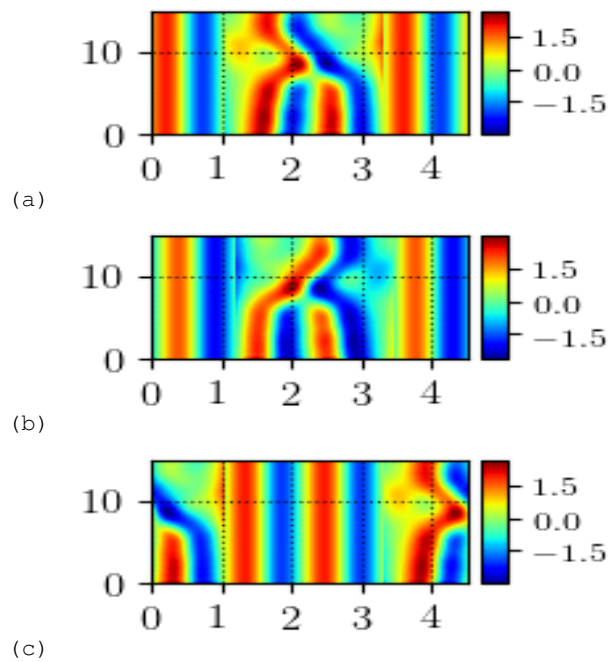
Figure 16.46: Three sub-components of the fundamental domain built from only manipulations of streaks and the "hook on top of defect" invariant 2-torus from figure 16.45. All plots consist of a pair of streaks (*eqva_L3p195* tiles) with one hook on defect solution.
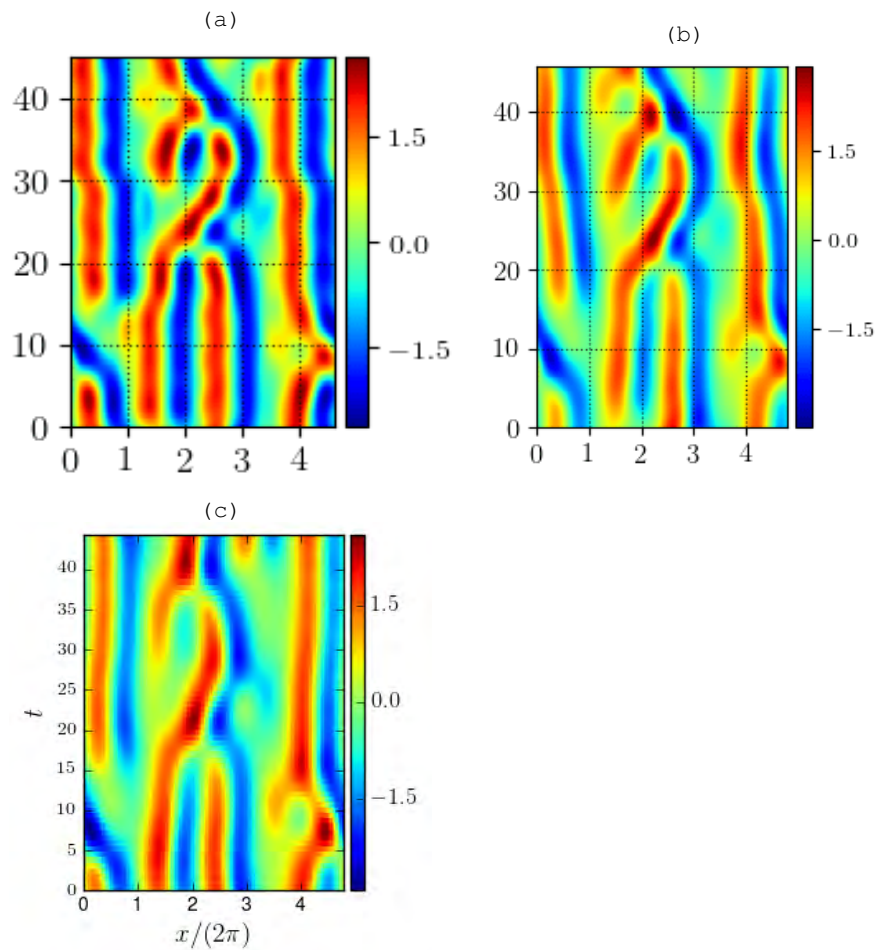
Figure 16.47: (a) Gluing together the three subdomains from figure 16.46 in the temporal direction. This is the initial condition for the fundamental domain of a invariant 2-torus with shift-reflection symmetry. (b) The convergent result of the numerics with initial condition (a). Note, this looks slightly different from the goal invariant 2-torus $\mathrm{ppo}_{30\times44}$ in (c), from figure 16.23.
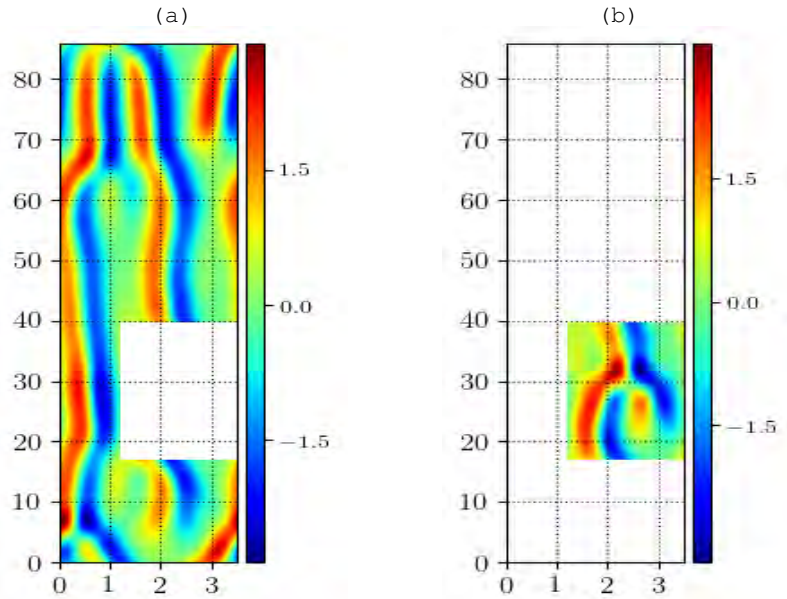
Figure 16.48:   (a) $\text{ppo}_{21.94 \times 85.73}$ with a subdomain cutout, represented in (b). This is a non-converged guess for what I title the "half-defect".

use tiles that were converged. At first, I thought I would be about to capture the spatiotemporal behavior with only two shapes, specifically *eqva_L3p195* and the hook-on-defect solution from figure 16.45. This was not sufficient to get complete agreement with $\text{ppo}_{30 \times 44}$, but it did produce a similar solution. Attempts to numerically continue this solution to $\text{ppo}_{30 \times 44}$ were unsuccessful. It took me a while guess what was wrong, which was the fact that the last spatiotemporal pattern from $\text{ppo}_{30 \times 44}$ looked different from what I called the hook-on-defect solution.

The procedure for gluing the approximate solutions together can be described as follows. First, subdivide the temporal domain into subdomains demarcated by spatiotemporal patterns with approximate periods, not including streaks as they do not have an inherent time scale as they are shadowing equilibria. With this criteria, the fundamental domain of $\text{ppo}_{30 \times 44}$ can be subdivided into three separate temporal segments, with the approximate blueprint being represented by the table of shapes in figure 16.44. The streak solutions can be used liberally to fill in the spatiotemporal area between the time varying subdomains as the streaks tend (in my experience) to not contribute much to the cost functional; in a sense they can be viewed as buffers separating the more interesting spatiotemporal dynamics.

(a)

(b)

(c)
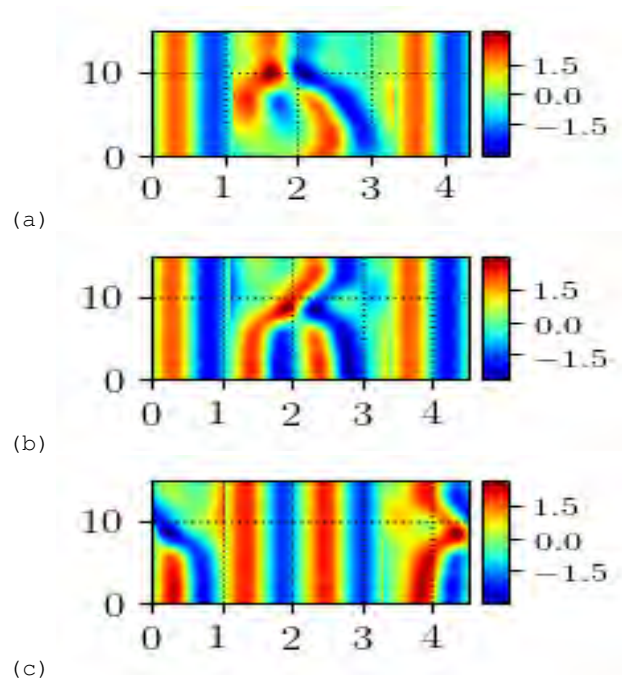
Figure 16.49: Three sub-components of the fundamental domain built from only manipulations of streaks and the "hook on top of defect" invariant 2-torus from figure 16.45. All plots consist of a pair of streaks (*eqva_L3p195* tiles), (b) and (c) contain the hook-on-defect subdomain and its reflection, respectively; while (a) contains a half-defect subdomain.
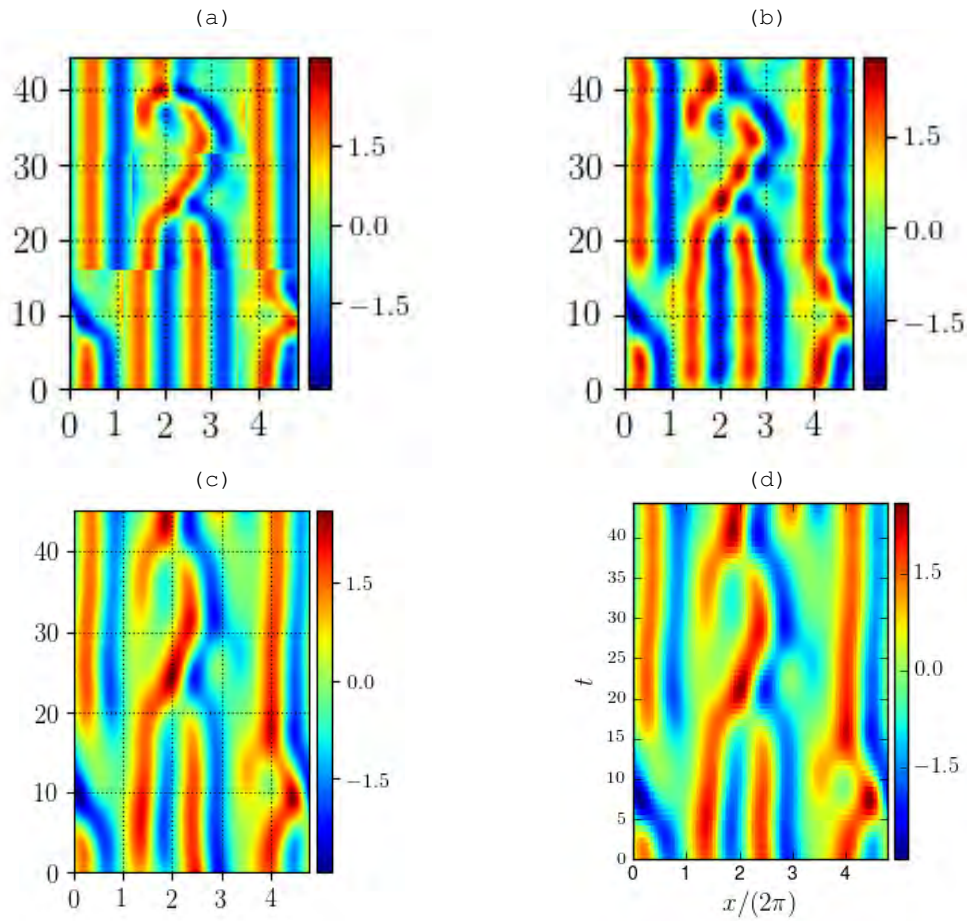
Figure 16.50: (a) Gluing together the three subdomains from figure 16.46 in the temporal direction. This is the initial condition for the fundamental domain of a invariant 2-torus with shift-reflection symmetry. (b) The convergent result of the numerics with initial condition (a). (c) figure 16.23 invariant 2-torus $\mathrm{ppo}_{30\times44}$ included for comparison to (b).

Once I produced the blueprint, I went ahead and looked for subdomains exhibited in solutions other than our goal, as that would just be a self-fulfilling prophecy. The two subdomains I elected to use (other than the streaks, which are relatively boring) were snippets from two other, similarly sized (in L) pre-periodic orbit invariant 2-tori. Namely, $\mathrm{ppo}_{21.94 \times 85.73}$ and $\mathrm{ppo}_{21.93 \times 92.77}$ for the half defect and hook-on-defect solution respectively.

Once the constituent subdomains had been produced and cutout from the collection of solutions, all that was left was to glue them. I did this in a very crude but manual manner. The lack of quality gluing was born from the fact that spatially I was gluing streaks on either side of a non-trivial spatiotemporal pattern and then applying reflections and rotations. (rotations and or translations viable because I am building up the fundamental domain only, a relevant shift reflection later guarantees it lies in the shift-reflection subspace).

An important caveat about the parameters values (L, T). I knew ahead of time what I was aiming for, but if I naïvely totaled the parameters from the subdomains one would get a drastic overestimation in time and an underestimation in space. Instead of a fundamental domain with $(L, T) \approx (30, 44)$, I would have had $(L, T) \approx (25, 65)$, which are quite far from each other, so I don't think linearly adding spatial and temporal extents is wise in the future.

There are some very numerical details I am leaving out, such as rediscretizing prior to cutting out subdomains such that the subdomains are highly resolved, ourier truncation and rediscretization to get to the initial conditions, etc. The general message is there, however. For "Frankenstein's bride" (the solution I pieced together but wasn't exactly what I was looking for) there were only two constituent spatiotemporal subdomains, with symmetry operations. One might argue that the hook-on-defect is literally a two by one, time by space, segment of symbols, which I believe is likely, but also likely hard to prove, as the small spatiotemporal solutions are typically hard to converge.

By looking at Frankenstein's bride figure 16.47 (b) and comparing with $\mathrm{ppo}_{30 \times 44}$ one can tell that there are some discrepancies in the upper middle. Only when the a third spatiotemporal pattern, the half-defect is introduced, does one get pretty good agreement with the target solution.

So, the proof of concept is quantitatively demonstrated now, I believe the hook-on-defect is a good place to look for a new tile, albeit not a fundamental tile.

I likely have more to share but I am tired and need to go to bed.

2018-11-10 Matt tiles from frankenstein Attempted to converge and find spatiotemporal tiles which exhibit similar spatiotemporal patterns. While
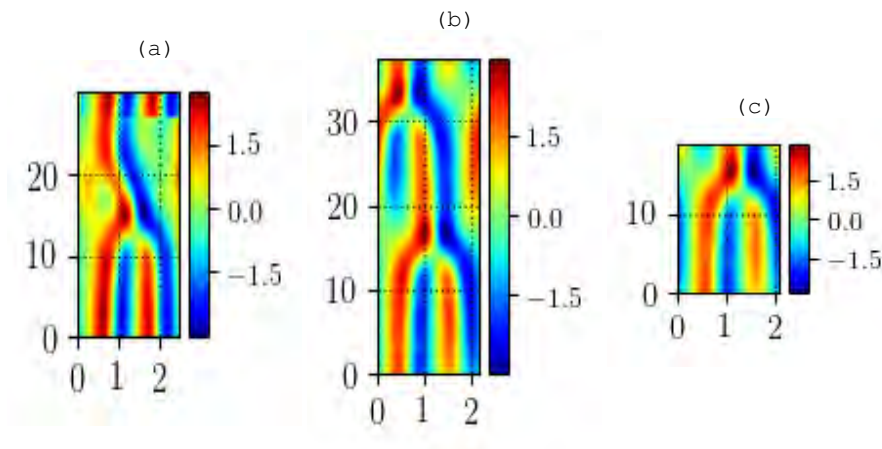
Figure 16.51: (a) An initial condition in attempt to find the "hook on defect tile" used in the tilings figure 16.47 and figure 16.50. It has been slightly modified by including the addition of two streaks at the top of the tile, in time. (b) The converged invariant 2-torus, its spatial shift after a prime period is close to zero, and it looks like it could be close to a invariant 2-torus, invariant under shift-reflection; (c) The converged $\mathrm{ppo}_{??\times??}$ fundamental domain invariant 2-torus, confirmation of (b).

certain initial conditions have converged, the resultant solutions are not similar to the initial conditions upon visual inspection.

Complex valued code refactoring Still working through the optimization of current codes, also introducing relative pathing for data instead of hardcoded directory references currently widespread.

2018-11-29 Matt Presentation for Schatz and Grigoriev journal club Interest fostered from APS DFD talk led to a desire to have me present a more technical version of the talk to their group(s) at Georgia Tech.

Verifying and testing results While progress has been made towards finding solutions, gluing solutions, and numerical continuation of solutions, I haven't been running the multitude of automated codes at all times.

Other than assuming I have trawled enough solutions, there isn't any other excuse for not running the trawling code. The continuation code hasn't been run because I don't really have a criterion for which member of the continuous families to choose. Recently, I decided to just find the instance of solutions that has the smallest period possible as we know shorter solutions contribute more in cycle expansions; i.e.there is some motivation behind the criteria.

The reason for gluing code not being run is the tuning has taken more work than I thought and the verification of ideas has shown

me that some solutions assumed to be isolated because upon visual inspection they don't look right are in fact very unstable and can't be reproduced via time integration. I'm unsure if time integration should be the verifying criterion for determining whether a solution is "valid" or not. Upon using a higher resolution discretization, sometimes these orbits will converge onto an orbit that is reproduceable via time integration, but in a couple instances attempts to glue together two invariant 2-tori results in converging to one of these original invariant 2-tori but at a different domain size. The only way that I have found to ensure that the intended solution is found is to compare numerical continuations and ensure that the final result is not equivalent to one of the initial conditions.

Some theorem by Smale I've been trying to test the theorem offered by Burak that one shouldn't be able to glue together solutions of different stability spectra. This lead to multiple different ways of integrating the Jacobians but I never developed an algorithm that was accurate enough so I'm borrowing some of Ruslan's matlab codes just for stability.

Simon recently told me that to evaluate $\dot{J} = AJ$ I should take a derivative of the actually integration scheme i.e. evaluate the matrix of velocity gradients A via the definition $A = \frac{\partial x_{n+1}}{\partial x_n}$. The idea comes from his use of a symplectic integrator and wanting to preserve the symplectic nature of the Jacobian.

I attempted this with the Exponential time differencing Runge-Kutta fourth order from ref. [33] algorithm; it's an accurate integrator used ubiquitously for the Kuramoto-Sivashinsky equation and used by Burak, Xiong, Ruslan and others. It was a quick attempt but I must have a mistake such that it didn't work.

Regardless, the main reason behind this communication is that I realized that some of my gluing results were converging to one of the two constituent invariant 2-tori just at a different domain size (numerical continuation showed that the final result and the initial condition had the same period and leading Floquet exponent to 10^{-7}. I'm unsure why they're not exactly the same but I believe it's because the two solutions are both within machine precision of the continuous family so there's a small segment of the continuous family that is unavoidable to distinguish between.

2018-12-05 Matt GMRES-hookstep After last week's plumbers union meeting I had a conversation with Michael Krygier, who works mostly on numerical Taylor-Couette. We had a chat that inspired me to get back into investigating iterative methods and I had an epiphany. My the truth was obscured because of the conventional computation in the literature, almost everyone in the field that uses Newton-Krylov or other iterative methods approximates $J^t \delta x \approx \frac{F^{t+\delta t}(x+\delta x) - F^t(x)}{|\delta x|}$.

It's due to the fact that I had seen this equation or approximation ubiquitously that I was blinded to a *far* better way of performing this computation, one that in fact *I already use in the adjoint descent!*. Namely, because the dependence on T is completely explicit in the spatiotemporal Kuramoto-Sivashinsky equation and doesn't rely on implicit forward-time mappings (i.e.time-integration), all I have to do is compute the action of the matrix $J = \frac{\partial F}{\partial x}$ on a vector δx! I can't believe I haven't realized this until today. It's literally (up to a transpose) how I've been employing the adjoint descent method for many months now, but like I said the literature blinded me I suppose.

What I mean by "compute the action of the matrix J on a vector δx" is to decompose the matrix multiplications into elementwise operations dependent on the spatiotemporal Fourier mode indices. It's actually ridiculously easy and I'm just baffled but how I didn't see it when it was right in front of my eyes. The mathematical equation that follows is,

$$J \cdot x = (\mathrm{i}\omega_j - q_m^2 + q_m^4 + \frac{\mathrm{i}q_m S}{T})x_{n,m} + \mathrm{i}q_m \mathcal{F} diag(u)\mathcal{F}^{-1}x\,. \quad (16.92)$$

Such an equation can be evaluated without the use of any matrices whatsoever (the linear term with S is for solutions with continuous symmetry. There is no error or approximation (up to machine precision) by performing the calculation in this matrix-free way (yet another boon of spatiotemporal formulation), such that the application translates nicely to iterative methods that require the matrix-vector product, such as Newton-Krylov-Hookstep.

This seems to be the last piece of the puzzle for having a complete, optimized, routine for calculating spatiotemporal invariant 2-torus solutions. I'm excited to see how far I can take it.

Ibragimov Formal Lagrangian I messed around with a calculation but just came to the same conclusion I had previously reached, namely if the adjoint variable v is chosen to be the Kuramoto-Sivashinsky equation then the variational derivative of the formal Lagrangian in the Ibragimov sense corresponds to the adjoint descent direction. This is perhaps why it works so well for me. i.e.the variational derivative obeys the equation

$$\begin{aligned}
\frac{\delta L(u, v)}{\delta u} &= -v_t + v_{xx} + v_{xxxx} - uv_x \\
\frac{\delta L(u, -F(u))}{\delta u} &= F_t - F_{xx} - F_{xxxx} + uF_x \equiv -J^\dagger F \quad (16.93)
\end{aligned}$$

Pseudospectral spatiotemporal formulation of two dimensional Kolmogorov flow
I believe I have derived most of the numerically relevant equations

except for the specific constraints due to discrete symmetries. Will write the "Feynmann equation" in pseudospectral representation, a formula for the matrix vector product Jx and a formula for the adjoint $-J^\dagger F$ tomorrow

ETDRK4 for Jacobians I tried to pursue what Simon taught me in regards to calculating Jacobians when a certain numerical integration scheme is already instantiated and known to work well. The gist of the calculation is a lot of algebra to explicitly write the equation

$$\partial_t J_n = \frac{\partial x_{n+1}}{\partial x_n} J_n \qquad (16.94)$$

where the dependence of x_{n+1} in terms of x_n depends on the underlying equations as well as the integration scheme. I haven't gotten this to work yet likely due to the number of areas for algebra errors to occur.

2018-12-06 Matt Going matrix free As a test of the new matrix-free GMRES code that utilizes the matrix free exact evaluation of the matrix vector product $J \cdot y \equiv \frac{\partial \mathbf{F}}{\partial \mathbf{x}} \cdot y$, I took an old initial condition with a larger-than-necessary discretization. As a proof of concept, I took the $N \times M$ discretization to be of the same order of magnitude of the two dimensional Kolmogorov flow calculations, namely $N = M = 128$. While technically the true number of variables is halved due to the shift-reflect symmetry of the solution, it still offered a good demonstration of why I felt this was necessary. Starting from the same initial condition, (not utilizing adjoint descent at all) GMRES and Gauss-Newton were run until machine precision convergence of the cost function. Even though it only took one Newton step to converge, the time saved by GMRES is very exciting. Specifically, the GMRES routine took 5.13613756917 seconds to converge, while Newton took 640.616473401 seconds. In other words, the matrix free iterative method is 124.727280914 times as fast as the direct matrix-forming Newton's method. I would argue that this is very significant and might allow the search for invariant 2-tori on very large domains. There is a slight cavaet, however; for numerical stability the GMRES routine does not include the spatial domain size L as a variable. Although I believe that this is not the right thing to do, I believe there is an argument to be made as to why this is acceptable. The argument I would make is this: towards the end of the adjoint descent procedure (when it stalls likely due to gradients becoming small) the order of magnitude of the changes to the domain size is of order 10^{-7}, so I believe one should heavily favor the numerical stability in favor of minimal changes to the domain size, especially because the solutions come in continuous families anyway.

On the other fronts, while I got preconditioned GMRES to work the

list of numerical schemes that don't seem to show nearly as much promise include,

- restarted GMRES
- BiCGSTAB
- BFGS
- L-BFGS

and so it isn't all good news. The main requirement for the GMRES routine to work seems to be a relatively high dimension of the Krylov subspace, compared to similar efforts in CFD. The solution that I tested required a maximum of about one hundred dimensions, compared to the 8002 computational variables, which is approximately one percent of the computational variables.

GMRES algorithm For closure, I will include the (right preconditioned) GMRES algorithm that I used to converge the example solution.

1. To solve $J\delta x = -F(x)$, for δx, follow this procedure
2. Set $q_0 = b = -F(x)$, where F is the Kuramoto-Sivashinsky equation
3. Perform arnoldi iteration to produce orthonormal matrix Q_n that spans Krylov subspace and the upper Hessenberg matrix H_n which satisfy the following relation, $JQ_n = Q_{n+1}H_n$. The shape of Q_n is $dim(\mathbf{x}) \times n$ and the shape of H_n is $(n+1) \times n$. (Described in more detail below)
4. Solve nonlinear optimization problem $||\beta e_1 - H_n y|| = 0$ for y
5. produce GMRES correction via $\delta x = P^{-1} \cdot Q_n \cdot y$

The right preconditioned arnoldi iteration (with modified Graham-Schmidt for orthogonalization) is written as follows in pseudo code.

for $j = 1, \cdots, m$

$$
\begin{aligned}
z_{j+1} &= P^{-1} \cdot q_j \\
q_{j+1} &= J \cdot z_{j+1}
\end{aligned}
\tag{16.95}
$$

for $i = 1, \cdots j$

$$
\begin{aligned}
H_{i,j} &= <w, q_i> \\
q_j &= q_j - H_{i,j} * q_i
\end{aligned}
\tag{16.96}
$$

end for

$$
\begin{aligned}
H_{i+1,i} &= ||q_j||_2 \\
q_j &= q_j/||q_j||_2
\end{aligned}
\tag{16.97}
$$

end for

BFGS algorithm The Broyden-Fletcher-Goldfarb-Shanno algorithm that I attempted to implement can be written as follows. It requires the calculation of a Hessian (of the scalar cost function)

For a quadratic model for the cost function, here designated as f,

$$m_k(p) = f_k + \nabla f_k^\top p + \frac{1}{2} p^\dagger B_k p \qquad (16.98)$$

the BFGS algorithm provides a minimization routine via the following,

Given x_0, ϵ and inverse Hessian H_0,

1. **While** $||\nabla f_k|| > \epsilon$
2. $p_k = -H_k \nabla f_k$
3. $x_{k+1} = x_k + \alpha_k p_k$ (Alpha given by Wolfe curvature conditions, will describe below)
4. $s_k = x_{k+1} - x_k$
5. $y_k = \nabla f_{k+1} - \nabla f_k$
6. $z_k = \frac{1}{y_k^{top} s_k}$
7. $H_k = (\mathbb{I} - z_k s_k y_k^\top) H_k (\mathbb{I} - z_k y_k s_k^\top) + z_k s_k s_k^\top$

The Wolfe conditions that determine the "step size" $alpha_k$ are given by the following, find $alpha_k$ such that the following hold,

$$
\begin{aligned}
f(x_k + \alpha_k p_k) &\leq& f(x_k) + c_1 \alpha_k \nabla f_k^\top p_k \\
\nabla f(x_k + \alpha_k p_k)^\top p_k &\geq& c_2 \nabla f_k^\top p_k
\end{aligned} \qquad (16.99)
$$

1. $r_+ = s_i(\alpha_i - \beta)$
2. end for
3. $p_k = -r$
4. $x_{k+1} = x_k + \alpha_k + p_k$ (alpha from wolfe conditions)
5. if $k > m$
6. Discard (s_{k-m}, y_{k-m})
7. end if
8. $s_k = x_{k+1} - x_k$
9. $y_k = \nabla f_{k+1} - \nabla f_k$
10. $p_k = -H_k \nabla f_k$
11. $x_{k+1} = x_k + \alpha_k p_k$ (Alpha given by Wolfe curvature conditions, will describe below)
12. $s_k = x_{k+1} - x_k$
13. $y_k = \nabla f_{k+1} - \nabla f_k$
14. $z_k = \frac{1}{y_k^{top} s_k}$
15. $H_k = (\mathbb{I} - z_k s_k y_k^\top) H_k (\mathbb{I} - z_k y_k s_k^\top) + z_k s_k s_k^\top$

L-BFGS algorithm The following is an adaptation of the BFGS algorithm that makes it possible to optimize the same quadratic model without holding full matrices in memory.

1. Let m be the maximum number of column vectors to hold in memory
2. **While** residual > tolerance and $k <$ maximum step number
3. $q = \nabla f_k$
4. If $k > m$,
5. for $i = k - 1, \cdots, k - m$
6. $z_i = \frac{1}{y_i^\top s_i}$
7. $a_i = z_i s_i q$
8. $q = q - a_i * y_i$
9. end for
10. $r = H_k^0 q$
11. for $k - m - 1, \cdots, k - 1$
12. $\beta = z_i y_i^\top r$
13. $r_+ = s_i(\alpha_i - \beta)$
14. end for
15. $p_k = -r$
16. $x_{k+1} = x_k + \alpha_k + p_k$ (alpha from wolfe conditions)
17. if $k > m$
18. Discard (s_{k-m}, y_{k-m})
19. end if
20. $s_k = x_{k+1} - x_k$
21. $y_k = \nabla f_{k+1} - \nabla f_k$
22. $p_k = -H_k \nabla f_k$
23. $x_{k+1} = x_k + \alpha_k p_k$ (Alpha given by Wolfe curvature conditions, will describe below)
24. $s_k = x_{k+1} - x_k$
25. $y_k = \nabla f_{k+1} - \nabla f_k$
26. $z_k = \frac{1}{y_k^{top} s_k}$
27. $H_k = (\mathbb{I} - z_k s_k y_k^\top) H_k (\mathbb{I} - z_k y_k s_k^\top) + z_k s_k s_k^\top$

BiCGSTAB algorithm Just to include this as a final algorithm,

Given $r_0 = b - Ax_0, \alpha_0 = \rho_0 = w_0 = p_0 = 1$

1. **While** residual > tolerance
2. For $i = 1, \cdots,$
3. $\rho_i = <r_0, r_i>$
4. $\beta = \frac{\rho_i}{\rho_{i-1}} \frac{\alpha_i}{w_i}$
5. $u = r_i + \beta q_i$

6. $p_i = u + beta(q_i + beta * p_i)$

7. $y = P^{-1}p_i$

8. $v = Jy$

9. $\alpha = \rho_i / < r_0, v >$

10. $q_i = u - alphav$

11. $z = P^{-1}(u + q_i)$

12. $x_{i+1} = x_i + alpha * z$

13. If x_{i+1} satifies tolerance, exit, else

14. $r_{i+1} = r_i - \alpha Jz$

Pseudospectral spatiotemporal formulation of 2-D Kolmogorov flow The equations governing two dimensional Kolmogorov flow can be written in terms of velocity field **u**(eliminated later) and vorticity ω in the following manner. For now I will just write the homogeneous equations, with forcing easily added afterwards

$$\omega_t - \hat{z} \cdot (\nabla \times (\mathbf{u} \times \omega \hat{z})) - \frac{1}{Re}\nabla^2\omega = 0 \qquad (16.100)$$

The only difficult part of rewriting this equation in terms of $(2 + 1)$ spatiotemporal Fourier coefficients (assuming periodic boundary conditions) is the nonlinear term, not only due to the cross products but the necessity to express the velocity field in terms of the streamfunction, and consequently the vorticity field as $\mathbf{u} = \nabla \times (\nabla^{-2}\omega)$ which is possible due to the two dimensional approximation. The operator ∇^{-2} is the inverse of the Laplacian, which is technically singular; I asked around and the standard practice is to essentially define it in fourier space as $\frac{1}{|\mathbf{k}|^2}$, where $|\mathbf{k}|^2 = k_x^2 + k_y^2$. For numerical purposes its apparently common practice to say that the inverse of the $k_x = k_y = 0$ term equals 1. In other words, $1/0 = 1$. It's just a means of approximating the operator in spectral space.

Although ref. [6] give nice formula that is almost entirely of Fourier coefficients, I find it more useful to completely eliminate the velocity field components $\mathbf{u} = (u, v)$ from the equation.

Therefore, the pseudospectral (homogeneous) spatiotemporal equation takes the form,

$$
\begin{aligned}
i\omega\Omega \quad &+ \quad ik_x\mathcal{F}[\mathcal{F}^{-1}(\frac{ik_y}{|\mathbf{k}|^2}\Omega) * \mathcal{F}^{-1}(\Omega)] \\
&- \quad ik_y\mathcal{F}[\mathcal{F}^{-1}(\frac{ik_x}{|\mathbf{k}|^2}\Omega) * \mathcal{F}^{-1}(\Omega)] \\
&- \quad \frac{|\mathbf{k}|^2}{Re}\Omega = G(\Omega, T, L_x, L_y) = 0 \qquad (16.101)
\end{aligned}
$$

Likewise, if allowed to write differentiation operators via D_t, D_x, D_y, etc, then the jacobian takes on the form in pseudospectral representation,

$$
\begin{aligned}
J &= D_t + D_x \mathcal{F}[diag(D_y \nabla^{-2}\omega)\mathcal{F}^{-1} + diag(\omega)D_y \nabla^{-2}\mathcal{F}^{-1}] \\
&- D_y \mathcal{F}[diag(D_x \nabla^{-2}\omega)\mathcal{F}^{-1} + diag(\omega)D_x \nabla^{-2}\mathcal{F}^{-1}] \\
&- \frac{\nabla^2}{Re}
\end{aligned}
\tag{16.102}
$$

By taking the complex conjugate and multiplying by the Feynman equation (16.101), the expression for the adjoint descent direction, $-J^\dagger G$.

$$
\begin{aligned}
-J^\dagger G &= [D_t + \mathcal{F}diag(D_y \nabla^{-2}\omega)\mathcal{F}^{-1}D_x \\
&- \mathcal{F}\nabla^{-2}D_y diag(\omega)\mathcal{F}^{-1}D_x \\
&- \mathcal{F}diag(D_x \nabla^{-2}\omega)\mathcal{F}^{-1}D_y \\
&+ \mathcal{F}\nabla^{-2}D_x diag(\omega)\mathcal{F}^{-1}D_y \\
&- \frac{\nabla^2}{Re}] \cdot G
\end{aligned}
\tag{16.103}
$$

Jacobian integration from ETDRK4 scheme The Exponential time differencing in conjunction with Runge-Kutta 4th order [33] as an integration scheme for stiff equations has used by many people to integrate the Kuramoto-Sivashinsky equation. I recall sifting through the Kuramoto-Sivashinsky literature and almost everyone used this integrator, due to its ability to handle the stiffness of the linear term and explicitly evaluate the nonlinear term.

Something that I never saw, however, was a calculation that directly follows, which is taking the derivative of the time integration scheme itself to provide a reliable integration scheme for Jacobian's. I recall in Ruslan's codes he uses some sort of interpolation to produce the Jacobian but I think maybe Burak has already done this. I can't say for certain because I haven't been through all of the codes in the repository.

Regardless, the ETDRK4 scheme evaluates the stiff, linear portion of the Kuramoto-Sivashinsky equation via what are essentially integrating factors, and then calculate the nonlinear terms accordingly.

Given v, a set of spatial Fourier coefficients, the scheme can be written relatively succinctly via the use of a number of constant operators in the problem which are created by various numerical combinations of the exponentiated linear operator of the Kuramoto-Sivashinsky equation. I'll leave the details to the reader in ref. [33], but

for any given discrete time step, we can write, (using n as a discrete time subscript)

$$
\begin{aligned}
N(v_n) &= \frac{-\mathbf{iq}}{2}\mathcal{F}((\mathcal{F}^{-1}(v_n))^2) \\
a_n &= E_2 * v_n + Q * N(v_n) \\
N(a_n) &= \frac{-\mathbf{iq}}{2}\mathcal{F}((\mathcal{F}^{-1}(a_n))^2) \\
b_n &= E_2 * v_n + Q * N(a_n) \\
N(b_n) &= \frac{-\mathbf{iq}}{2}\mathcal{F}((\mathcal{F}^{-1}(b_n))^2) \\
c_n &= E_2 * v_n + Q * (2 * N(b_n) - N(v_n)) \\
N(c_n) &= \frac{-\mathbf{iq}}{2}\mathcal{F}((\mathcal{F}^{-1}(c_n))^2) \\
v_{n+1} &= E * v_n + f_1 * N(v_n) + 2f_2 * (N(a_n) + N(b_n)) + N(c_n)
\end{aligned}
\tag{16.104}
$$

Now, we can take the derivative of the last equation for v_{n+1} with respect to v_n, to get the velocity gradient matrix, $A(v_n) \equiv \frac{\partial v_{n+1}}{\partial v_n}$
The derivatives of each of the nonlinear functions looks like the following via the chain rule

$$
\begin{aligned}
\frac{\partial N(x_n)}{\partial v_n} &= (-\mathbf{iq}\mathcal{F} \\
&\quad * \quad (diag(\mathcal{F}^{-1}(x_n))\mathcal{F}^{-1})) * \frac{\partial x_n}{\partial v_n}
\end{aligned}
\tag{16.105}
$$

Because of the nested nature of the Runge-Kutta integration scheme, a pattern quickly emerges such that it becomes smart to define the following, let the velocity gradients matrix evaluated at each variable, a_n, b_n, c_n, v_n be represented by A_v, A_a, A_b, A_c. With this and the following substitutions,

$$
\begin{aligned}
\tilde{A}_v &= (E_2 + QA_v) \\
\tilde{A}_a &= A_a(E_2 + QA_v) \\
\tilde{A}_b &= A_b(E_2 + Q\tilde{A}_a),
\end{aligned}
\tag{16.106}
$$

it becomes much easier to write an explicit expression for the desired quantity,

$$
A(x_n) = \frac{\partial v_{n+1}}{\partial v_n} = E + f_1 A_v + 2f_2[\tilde{A}_a + \tilde{A}_b] + f_3 A_c[E_2 \tilde{A}_v + 2Q\tilde{A}_b - QA_v]
\tag{16.107}
$$

I believe that this equation, in accordance with the equation

$$
\dot{J} = AJ
\tag{16.108}
$$

should yield an accurate integration scheme for finding Jacobian's and hence stability multipliers or exponents for periodic orbits.

2018-12-08 Matt Lagrangian Formalism for the Kuramoto-Sivashinsky equation

Following Ibragimov and Kolsrud [30], which uses a slightly different formulation than the "formal Lagrangian" in the other Ibragimov references such as ref. [29]. I'm unsure why the difference makes a difference as the variational derivatives reproduce the Kuramoto-Sivashinsky equation and adjoint of the Kuramoto-Sivashinsky equation properly.

Specifically, instead of the Lagrangian,

$$\mathcal{L} = v(u_t + u_{xx} + u_{xxxx} + uu_x) \tag{16.109}$$

one can derive the following Lagrangian following the prescription and examples of ref. [30],

$$\mathcal{L} = \frac{1}{2}(vu_t - uv_t) - u_x v_x + u_{xx} v_x x + \frac{u}{3}(vu_x - uv_x) \tag{16.110}$$

which provides the variational derivatives,

$$\begin{aligned}
\frac{\delta \mathcal{L}}{\delta v} &= u_t + u_{xx} + u_{xxxx} + uu_x \\
-\frac{\delta \mathcal{L}}{\delta u} &= v_t + -v_{xx} + -v_{xxxx} + uv_x
\end{aligned} \tag{16.111}$$

which equal the Kuramoto-Sivashinsky equation and its adjoint equation. Evaluation of the second variational derivative with $v = F(u)$ defines the adjoint descent direction.

While this Lagrangian is equivalent to the other in terms of its variational derivatives, something I found interesting while attempting to derive conservation laws using the Lie-Bäcklund operators corresponding to the generators of the Lie algebra.

The thing I found interesting is that with this different Lagrangian is that we can define an action given by its integrals, and upon the substitution $v = -u$, we arrive at what might be an interesting relation. Technically this need not be a spatiotemporal integral, and can be taken just to be a spatial integral, either way one arrives at the equation,

$$\int\int \mathcal{L}(u, -u) dx dt = \int\int u_x^2 - u_{xx}^2 dx dt \tag{16.112}$$

which we know from chaosbook is equivalent to the time average of the energy variation of the Kuramoto-Sivashinsky equation. I'm unsure if this is a coincidence or is a good result, hoping for better minds to help with the interpretation.

References

[1] H. W. Broer, J. Hoo, and V. Naudot, "Normal linear stability of quasi-periodic tori", J. Diff. Equ. **232**, 355–418 (2007).

[2] P. N. Brown and H. F. Walker, "GMRES on (nearly) singular systems", SIAM J. Matrix. Anal. Appl. **18**, 37–51 (1997).

[3] N. B. Budanur, P. Cvitanović, R. L. Davidchack, and E. Siminos, "Reduction of the SO(2) symmetry for spatially extended dynamical systems", Phys. Rev. Lett. **114**, 084102 (2015).

[4] C. Canuto, M. Y. Hussaini, A. Quateroni, and T. A. Zhang, *Spectral Methods in Fluid Dynamics* (Springer, New York, 1988).

[5] G. Chandler and R. Kerswell, Simple invariant solutions embedded in 2D kolmogorov turbulence, 2013.

[6] G. J. Chandler and R. R. Kerswell, "Invariant recurrent solutions embedded in a turbulent two-dimensional Kolmogorov flow", J. Fluid Mech. **722**, 554–595 (2013).

[7] F. Christiansen, P. Cvitanović, and V. Putkaradze, "Spatiotemporal chaos in terms of unstable recurrent patterns", Nonlinearity **10**, 55–70 (1997).

[8] K. T. Chu, "A direct matrix method for computing analytical Jacobians of discretized nonlinear integro-differential equations", J. Comput. Phys. **228**, 5526–5538 (2009).

[9] P. Cvitanović, "Invariant measurement of strange sets in terms of cycles", Phys. Rev. Lett. **61**, 2729–2732 (1988).

[10] P. Cvitanović, "Turbulence?", in *Chaos: Classical and Quantum*, edited by P. Cvitanović, R. Artuso, R. Mainieri, G. Tanner, and G. Vattay (Niels Bohr Inst., Copenhagen, 2022).

[11] P. Cvitanović, R. Artuso, R. Mainieri, G. Tanner, and G. Vattay, *Chaos: Classical and Quantum* (Niels Bohr Inst., Copenhagen, 2022).

[12] P. Cvitanović, R. L. Davidchack, and E. Siminos, "On the state space geometry of the Kuramoto-Sivashinsky flow in a periodic domain", SIAM J. Appl. Dyn. Syst. **9**, 1–33 (2010).

[13] S. Das, C. B. Dock, Y. Saiki, M. Salgado-Flores, E. Sander, J. Wu, and J. A. Yorke, "Measuring quasiperiodicity", Europhys. Lett. **114**, 40005 (2016).

[14] S. Das, Y. Saiki, E. Sander, and J. A. York, "Quantitative quasiperiodicity", Nonlinearity **30**, 4111 (2017).

[15] S. Das, Y. Saiki, E. Sander, and J. A. Yorke, Solving the Babylonian problem of quasiperiodic rotation rates, 2017.

[16] J. E. Dennis and R. B. Schnabel, *Numerical Methods for Unconstrained Optimization and Nonlinear Equations* (SIAM, Philadelphia, 1996).

[17] X. Ding, H. Chaté, P. Cvitanović, E. Siminos, and K. A. Takeuchi, "Estimating the dimension of the inertial manifold from unstable periodic orbits", Phys. Rev. Lett. **117**, 024101 (2016).

[18] X. Ding and P. Cvitanović, "Periodic eigendecomposition and its application in Kuramoto-Sivashinsky system", SIAM J. Appl. Dyn. Syst. **15**, 1434–1454 (2016).

[19] J. Fan and J. Zeng, "A Levenberg-Marquardt algorithm with correction for singular system of nonlinear equations", Appl. Math. Comput. **219**, 9438–9446 (2013).

[20] M. Farazmand, "An adjoint-based approach for finding invariant solutions of Navier-Stokes equations", J. Fluid M. **795**, 278–312 (2016).

[21] N. Fenichel, "Persistence and smoothness of invariant manifolds for flows", Indiana Univ. Math. J. **21**, 193–226 (1971).

[22] D. G. Fox and S. A. Orszag, "Pseudospectral approximation to two-dimensional turbulence", J. Comput. Phys. **11**, 612–619 (1973).

[23] J. F. Gibson, J. Halcrow, and P. Cvitanović, "Visualizing the geometry of state-space in plane Couette flow", J. Fluid Mech. **611**, 107–130 (2008).

[24] J. M. Greene and J.-S. Kim, "The steady states of the Kuramoto-Sivashinsky equation", Physica D **33**, 99–120 (1988).

[25] J. Guckenheimer and P. Holmes, *Nonlinear Oscillations, Dynamical Systems, and Bifurcations of Vector Fields* (Springer, New York, 1983).

[26] B. Gutkin, L. Han, R. Jafari, A. K. Saremi, and P. Cvitanović, "Linear encoding of the spatiotemporal cat map", Nonlinearity **34**, 2800–2836 (2021).

[27] B. Gutkin and V. Osipov, "Classical foundations of many-particle quantum chaos", Nonlinearity **29**, 325–356 (2016).

[28] Á. Haro, M. Canadell, A. Luque, J. M. Mondelo, and J.-L. Figueras, *The Parameterization Method for Invariant Manifolds* (Springer, New York, 2016).

[29] N. H. Ibragimov, "Conservation laws and non-invariant solutions of anisotropic wave equations with a source", Nonlinear Anal. Real World Appl. **40**, 82–94 (2018).

[30] N. H. Ibragimov and T. Kolsrud, "Lagrangian approach to evolution equations: symmetries and conservation laws", Nonlin. Dyn. **36**, 29–40 (2004).

[31] K. Kaneko, "Transition from torus to chaos accompanied by frequency lockings with symmetry breaking: In connection with the coupled-logistic map", Prog. Theor. Phys. **69**, 1427–1442 (1983).

[32] K. Kaneko, "Period-doubling of kink-antikink patterns, quasiperiodicity in antiferro-like structures and spatial intermittency in coupled logistic lattice: Towards a prelude of a "field theory of chaos"", Prog. Theor. Phys. **72**, 480–486 (1984).

[33] A.-K. Kassam and L. N. Trefethen, "Fourth-order time-stepping for stiff PDEs", SIAM J. Sci. Comput. **26**, 1214–1233 (2005).

[34] R. M. Kerr, "Higher-order derivative correlations and the alignment of small-scale structure in isotropic numerical turbulence", J. Fluid. Mech. **153**, 31–58 (1985).

[35] I. G. Kevrekidis, B. Nicolaenko, and J. C. Scovel, "Back in the saddle again: a computer assisted study of the Kuramoto-Sivashinsky equation", SIAM J. Appl. Math. **50**, 760–790 (1990).

[36] D. Knoll and D. Keyes, "Jacobian-free Newton-Krylov methods: a survey of approaches and applications", J. Comput. Phys. **193**, 357–397 (2004).

[37] M. Kraus and O. Maj, "Variational integrators for nonvariational partial differential equations", Physica D **310**, 37–71 (2015).

[38] S. Krist and T. A. Zang, Numerical simulation of channel flow transition: Resolution requirements and the structure of hairpin vortices, tech. rep. (NASA, 1987).

[39] P. A. Kuchment, *Floquet Theory for Partial Differential Equations* (Birkhäuser, Basel, 1993).

[40] Y. Lan, Dynamical Systems Approach to $1 - d$ Spatiotemporal Chaos – A Cyclist's View, PhD thesis (School of Physics, Georgia Inst. of Technology, Atlanta, 2004).

[41] Y. Lan and P. Cvitanović, "Unstable recurrent patterns in Kuramoto-Sivashinsky dynamics", Phys. Rev. E **78**, 026208 (2008).

[42] R. E. LaQuey, S. M. Mahajan, P. H. Rutherford, and W. M. Tang, "Nonlinear saturation of the trapped-ion mode", Phys. Rev. Lett. **34**, 391–394 (1974).

[43] V. López, P. Boyland, M. T. Heath, and R. D. Moser, "Relative periodic solutions of the complex Ginzburg-Landau equation", SIAM J. Appl. Dyn. Syst. **4**, 1042–1075 (2006).

[44] D. Michelson, "Steady solutions of the Kuramoto-Sivashinsky equation", Physica D **19**, 89–111 (1986).

[45] R. Miranda and E. Stone, "The proto-Lorenz system", Phys. Lett. A **178**, 105–113 (1993).

[46] F. Montigny-Rannou, "Effect of "aliasing" on spectral method solution of Navier-Stokes equations", Rech. Aerosp. **2**, 365–41 (1982).

[47] R. D. Moser, P. Moin, and L. A., "A spectral numerical method for the Navier-Stokes equations with applications to Taylor-Couette flow", J. Comput. Phys. **52**, 524–544 (1983).

[48] Y. Nesterov, "A method of solving a convex programming problem with convergence rate O$(1/k^2)$", Sov. Math. Dokl. **27**, 372–376 (1983).

[49] J. Nocedal and S. J. Wright, *Numerical Optimization*, 2nd ed. (Springer, New York, 2006).

[50] S. A. Orszag, "Computation of pseudospectral and spectral approximations", Stud. Appl. Math. **51**, 253–259 (1972).

[51] J. W. Swift and K. Wiesenfeld, "Suppression of period doubling in symmetric systems", Phys. Rev. Lett. **52**, 705–708 (1984).

[52] D. Viswanath, "The critical layer in pipe flow at high Reynolds number", Philos. Trans. Royal Soc. A **367**, 561–576 (2009).

[53] S. J. Wright and J. N. Holt, "An inexact Levenberg-Marquardt method for large sparse nonlinear least squares", J. Austral. Math. Soc. **26**, 387–403 (1984).

[54] J. Xiao, H. Qin, Y. Shi, J. Liu, and R. Zhang, "A lattice Maxwell system with discrete space-time symmetry and local energy-momentum conservation", Phys. Lett. A **383**, 808–812 (2019).

[55] A. Ziessler, M. Dellnitz, and R. Gerlach, The numerical computation of unstable manifolds for infinite dimensional dynamical systems by embedding techniques, 2018.

Chapter 17

Matt's 2019 blog

2019-01-10 Matt Paper on spatiotemporal defects Trying to put the finishing touches on the written document for my thesis proposal. While sourcing some of my written statements I stumbled across something interesting in ref. [36], displayed in the quote,

> We believe that the longer time scales for the excited modes arise from the metastability of the cellular solutions (which are stable for small L) undergoing continuous creation and annihilation events ("space-time defects") [6]

It is ref. [6] that is the earliest reference to "space-time defects" that I have found. The lion's share of the work presented is regarding wavelet-based simulation as well as statistical computations but there are certain ideas that could possibly be useful for my needs.

Both of these papers discuss spatial and temporal scales as well as reframe dynamics in terms of "metastable cellular solutions", "space-time defects" and in ref. [6] they reference the system (Kuramoto-Sivashinsky equation) being "frustrated" by the existence of multiple "metastable cellular states".

I haven't delved too deep into either paper but on the surface it seems like there is some low-hanging fruit that can be picked for spatiotemporal purposes.

2019-01-18 Matt In an attempt to restart the hunt for symbolic dynamics, some initial guess tiles that were used in the frankenstein reconstruction efforts were used to attempt to find more tiles. These by themselves did not numerically converge to spatiotemporal invariant 2-tori but by concatenation of a single streak (crest trough pair) in space is necessary and sufficient to numerically converge the solutions. I believe that this elucidates some of the spatiotemporal symbolic dynamical grammar.

Let $0, 1, 2$ represent "streaks", "defects" and "gaps" family members, respectively. If we assume that the subdomains "half-defect" and "hook-
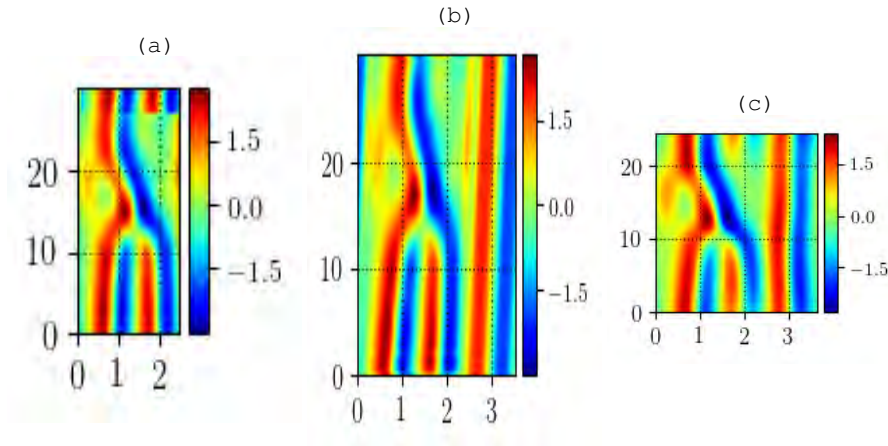
Figure 17.1: (a) Initial condition from figure **??** that converges to a solution that is believed to be a numerical continuation of (b) from figure 16.33. (b) An initial condition resulting from concatenating a streak-pair with (a), that numerically converges to (c).
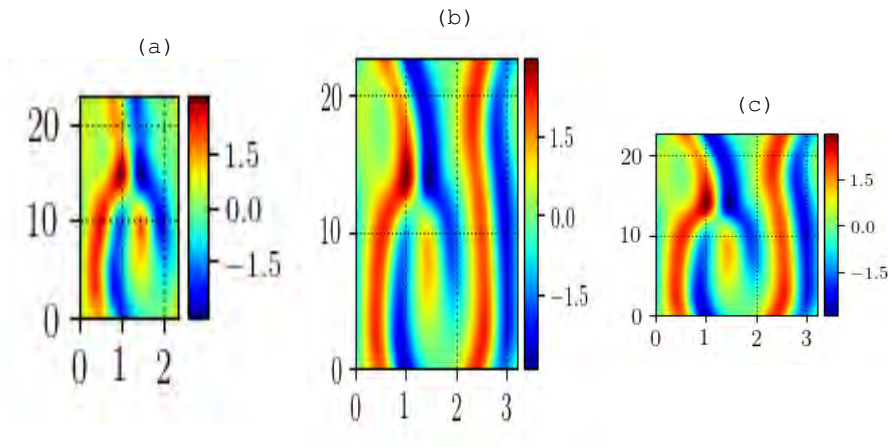
Figure 17.2: (a) Initial condition that has not been shown to numerically converge. (b) An initial condition resulting from concatenating a streak-pair with (a), that numerically converges to (c).

on-top-of-defect" correspond to a 2-by-1 time by space symbolic dynamic chain,

$$\text{hook on defect} = \begin{bmatrix} 1 \\ 1 \end{bmatrix}, \tag{17.1}$$

then this is believed to be inadmissible, but can be made to be admissible by conjoining a streak spatially, which is believe to have symbolic representation,

$$\begin{bmatrix} 1 & 0 \\ 1 & 0 \end{bmatrix}, \tag{17.2}$$

Likewise, for the half-defect symbolic tile I believe the most accurate guess would be

$$\text{hook on defect} = \begin{bmatrix} 2 \\ 1 \end{bmatrix}, \tag{17.3}$$

then this is believed to be inadmissible, but can be made to be admissible by conjoining a streak spatially, which is believe to have symbolic representation,

$$\begin{bmatrix} 2 & 0 \\ 1 & 0 \end{bmatrix}, \tag{17.4}$$

which I believe gives an inkling into the possible grammar rules; my appeal to intuition is that longer strings in time introduce instability which is balanced by introducing streaks spatially as some kind of metastability.

These are demonstrated visually in figure 17.1 and figure 17.2.

2019-02-04 Matt Application of Hill's formula using the action functional defined by the integral of the Lagrangian (density) previously derived in (16.110),

$$S[\phi] = \int \int \mathcal{L}(x, t, u, v, u_x, v_x, u_t, v_t, u_{xx}, v_{xx}) dx dt \tag{17.5}$$

yields a Hessian matrix whose determinant does not rely on the values of either the original scalar field u or the adjoint variable v. This is due to the specific matrix structure, not due to absence of u or v as matrix elements. Specifically, the matrix of second variations, or Hessian of the
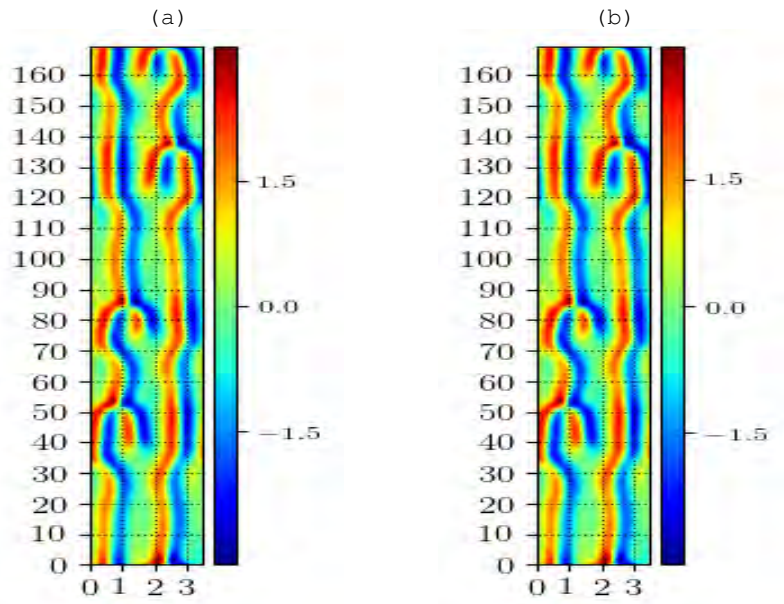
Figure 17.3: (a) $\text{ppo}_{21.94\times85.73}$ with a subdomain cutout, represented in (b). This is a non-converged guess for what I title the "half-defect".
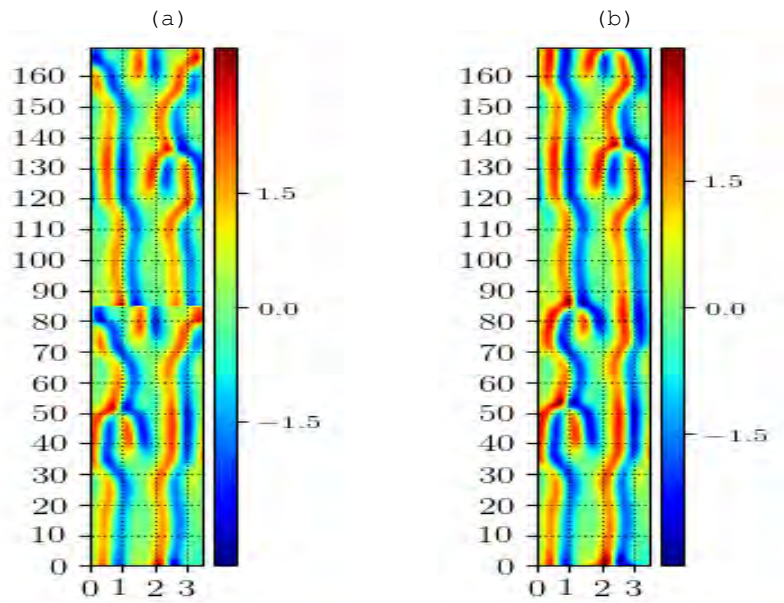
Figure 17.4: (a) $\text{ppo}_{21.94\times85.73}$ with a subdomain cutout, represented in (b). This is a non-converged guess for what I title the "half-defect".

action functional, is given by

$$
\begin{bmatrix}
2v/3 & u_x/3 & 0 & -1/2 & v/3 & 2u/3 & 0 & 0 \\
u_x/3 & 0 & 1/2 & 0 & u/3 & 0 & 0 & 0 \\
0 & 1/2 & 0 & 0 & 0 & 0 & 0 & 0 \\
-1/2 & 0 & 0 & 0 & 0 & 0 & 0 & 0 \\
v/3 & u/3 & 0 & 0 & 0 & & 0 & 0 & 0 \\
2u/3 & 0 & 0 & 0 & 0 & 0 & 0 & 0 \\
0 & 0 & 0 & 0 & 0 & 0 & 0 & 1 \\
0 & 0 & 0 & 0 & 0 & 0 & 1 & 0
\end{bmatrix} .
\tag{17.6}
$$

The determinant of this matrix is constant and equals $1/16$. The matrix elements are understood to be shorthard for the spatiotemporal integral present in the action functional definition. The constant determinant value has confused me for a some time and I have been attempting to figure out if this makes any sense. The determinant can be substituted into the expression for Hill's formula from ref. [3] to yield,

$$
\det (P - \mathbb{I}) = \sigma(-1)^m \beta/16 .
\tag{17.7}
$$

For the spatiotemporal Kuramoto-Sivashinsky equation the dimension of the configuration space manifold $m = 2$; the only comments regarding β and σ are that they are a "scaling factor" and $\sigma = \pm 1$ "takes care of orientation"; that is the extent of their explanation. I'm unsure how to interpret this unless the "scaling factor" is dependent on u, v. Also, the argument of stability of periodic solutions is predicated on the sign of the RHS, so I believe it's determined *a priori* by the fact that we know unstable solutions exist.

This result seems very artificial; I believe it is due to the artificial introduction of Lagrangian structure for problems that originally had none. This lead me to investigate as much as possible if this formulation is indeed worthless or not. Ibragimov [12] utilizes this "formal Lagrangian" to construct new conservation theorems and conserved quantities for partial differential equations using Lie theory. Other references refer to this type of construction as an "extended Lagrangian" [18]. Kraus claims that there is a better alternative to Ibragimov's quasi self-adjoint derivations in terms of simplicity. Specifically, he claims that if adjoint and or dual variables v and its collection of partial derivatives (jet prolongation) can be chosen such that the adjoint equation is satisfied when the Kuramoto-Sivashinsky equation is satisfied then the formal Lagrangian formulation is physically relevant.

> "If it is possible to select the relation (2.286) such that (2.287) is automatically respected when u solves (2.281), then a conservation law for the extended system amounts to a physical conservation law."

In other words, the stationary points of the action are where the variational derivatives of the action are equal to zero. For this Lagrangian formalism, this is equivalent to satisfying the adjoint equations and the Kuramoto-Sivashinsky equation simultaneously. This is no where near obvious as it depends on the choice of adjoint variable i.e. $v = \phi(x, t, u, u_{(1)}, ...)$. Luckily, there is no reason to not choose the Kuramoto-Sivashinsky equation itself as the adjoint variable, even though it might seem tautological on the surface. Each term in the adjoint equation is linear in v and its derivatives; therefore, choosing $v = F(\tilde{\mathbf{u}})$ guarantees the criterion that we want to guarantee. While this does not explain whether or not the use of Hill's formula makes any sense, it is an argument that any conserved quantities derived from the Lagrangian would be physically relevant. The justification from ref. [18] is that being able to express v as purely functions of the original scalar field guarantees that symmetry of the extended "formal Lagrangian" system can be reduced to symmetries of the original system. Sadly my (Lie) algebra skills need some work as I kept getting confused with what jet prolongation, the differences between Lie-Bäcklund and Lie point symmetries, and how to produce the set of generators that span the Lie algebra and extend them to include the adjoint variables. Once I derive the correct set of generators that span the Lie Algebra I should be able to derive something useful.

One proposed explanation is that technically due to doubly periodic boundary conditions, all Hessian matrix elements represent integrals, which are technically zero. This leads to a very simple expression for the characteristic polynomial of the Hessian, the eigenvalues are $\pm 1, \pm 1/2$ each with multiplicity $k = 2$.

Although it is reaching, this might be a manifestation of the action functional being $\mathcal{PT}$-symmetric, which constrains the eigenvalues to be real. It is a weaker condition than the Hessian being Hermitian although technically by being real and symmetric it is anyway. I really don't know how to explain this away so I've been attempting and failing to derive a conserved quantity that might be of future use.

2019-02-13 Matt Lie groups and algebras for Lagrangian formalism The following will hopefully serve as both a report on what I have been doing as well as a guide to refer back to.

While I haven't delved into the really mathematical formalism (pullbacks,lifts,contact) there are a few preliminaries that are absolutely essential to understand the description that follows,

1. Jet prolongation [18, 19] (sometimes referred to by the constituent pieces: jets,prolongation, jet bundles)
2. "formal" or "extended" Lagrangians [14]
3. Lie algebras and their generators (sometimes referred to as vector fields instead as the generators are differential forms that act on the relavant manifold)

4. Prolongation of Lie algebra generators
5. The difference between Lie point group operators and Lie-Bäcklund operators.
6. Extension of generators to adjoint variables
7. Conserved vectors and conservation theorems

The best single sentence I have found to describe jet bundles and prolongations comes from Wikipedia: "Jets may also be seen as the coordinate free versions of Taylor expansions".

Instead of ruining the discussion with words such as *sections, fibre bundles,holonomic sections, tangent lifts,etc.*, I'll merely define the nth jet prolongation as a mapping that takes a set of independent and dependent variables, e.g. (x, t, u), and returns all derivatives with maximum order n:

$$j^n \psi \equiv j^n(x, t, u) = (x, t, u, u_x, u_t, ..., \frac{\partial u}{\partial x^{i_1}...\partial x^{i_n}}). \qquad (17.8)$$

The concept of formal Lagrangian was previously used to derive (16.110). Introduction of new dependent variables, "adjoint variables", $(v, v_x, v_t, ...)$ can be used to impose a Lagrangian structure where there formally was none. Accordingly, a Lagrangian that depends on both the original dependent variables and their adjoints can be derived, such that the variational derivatives reproduce the Kuramoto-Sivashinsky equation and its adjoint.

The infinitesimal generators of a Lie group are vector fields which are elements of the Lie algebra. Each vector field generates a one-parameter family of symmetry transformations.

These vector fields are usually written as an expansion in terms of derivatives with respect to independent x^i and dependent variables u^α,

$$\mathbf{X} = \sum \epsilon^i \frac{\partial}{\partial x^i} + \sum \eta^\alpha \frac{\partial}{\partial u^\alpha} \qquad (17.9)$$

If the coefficients in this expansion only depend on the independent variables and the dependent variable (no dependence on derivatives), i.e.,

$$\begin{aligned} \epsilon^i &= \epsilon^i[x, t, u] \\ \eta^j &= \eta^j[x, t, u] \end{aligned} \qquad (17.10)$$

then the symmetries will be referred to as Lie *point symmetries*, otherwise they will be referred to as Lie-Bäcklund symmetries.

This expansion, while commonly presented in this form, is rather misleading as it carries an implicit assumption along with it; namely,

that it needs to be *prolonged* to the highest order of derivative of relevance in order to be correct. For example in the Kuramoto-Sivashinsky equation, this would require a prolongation of order four, due to the presence of fourth spatial derivative. The specific formula for the coefficients of these additional differentials are sometimes referred to as *prolongation formula*. It requires (total) differentiation of existing coefficients,

$$\eta_J^\alpha = D_J(\eta^\alpha + \epsilon^i u_i^\alpha) + \epsilon^i u_{(J,i)}^\alpha \qquad (17.11)$$

As previously mentioned, the specific form of the expansion is determined by the relevant PDE and assumptions. This expansion together with the invariance condition,

$$\mathbf{prX}(F(j^n\psi)) = \mathbf{0}, \qquad (17.12)$$

produces a (typically overdetermined, at least for point symmetries) system of equations that can be used to determine coefficients of the corresponding infinitesimal generators that span the symmetry Lie algebra. This step always seems to be taken for granted or not displayed, as its likely a lengthy symbolic pen-and-paper (also known as Mathematica) computation.

This isn't even the entire story for us, as the general expression for the infinitesimal generators needs to be *extended* to include the terms corresponding to the prolongation of the adjoint variables.

If the symmetry Lie algebra is known, then the spanning operators can be immediately extended to include the adjoint variables. There are formulae for determining the coefficients of extension terms depending on Lie point or Lie-Bäcklund symmetry is being considered.

In summary, symmetries or their equivalent generators are derived by the prolongation of a general expansion to the PDE of relevance. This and an invariance condition allows one to determine the coefficients of the expansion and hence the generators that span the Lie algebra.

Once the generators have been derived, they are extended to include the adjoint variables, yielding operators that can be used in conjunction with the *conservation equations*,

$$
\begin{aligned}
D_i(C^i) &= 0 \\
C^i &= \epsilon^i \mathcal{L} + W^\alpha \left[\frac{\partial \mathcal{L}}{\partial u^\alpha}\right] - D_k \frac{\partial \mathcal{L}}{\partial u_{ik}^\alpha}\right] + D_k(W^\alpha)\frac{\partial \mathcal{L}}{\partial u_{ik}^\alpha} \quad (17.13)
\end{aligned}
$$

in order to produce conserved quantities.

A very relevant and important piece of information regards symmetries and conserved quantities of the extended Lagrangian. Namely,

ref. [18] claims that if the adjoint equation is automatically satisfied when the Kuramoto-Sivashinsky equation is satisfied, i.e. if $F^*(j^4(x, t, u, v)) = 0$ when $F(j^4(x, t, u)) = 0$, then "a conservation law for the extended system amounts to a physical conservation law". Also for the conservation laws to be non-trivial, the extended equations need to be *nonlinearly self-adjoint*, which is equivalent to the previous statement regarding the adjoint being satisfied when the original equation is satisfied.

KS Lie algebra I've been trying to do the symbolic computation with Mathematica to derive the extended operators that span the Lie algebra but the process has been slow because I'm not used to Mathematica and I've found it very easy to lose my place amidst all of the indices.

Luckily, I feel more comfortable with the general procedure and ideas that constitute what I suppose amounts to a Lagrangian field theory. The entire point behind this exercise was to derive interesting and relevant conserved quantities for the spatiotemporal Kuramoto-Sivashinsky equation, i.e. to utilize the Lagrangian formalism as much as possible.

2019-02-15 Matt Notes from discussion with Lan.

- His first suggestion to get a better grasp on the spatiotemporal symbolic dynamics is to plot spatiotemporal solutions in a phase space of higher dimension but similar to that of ref. [8]. Specifically, plot partial derivatives $u_t, u_{tx}, \ldots$ as functions of space and time and see how this space is organized. This might provide a smarter way forward for determining the grammar.

- His second comment is regarding troubles on the horizon concerning the continuous families of solutions, one such worry is how to deal with boundary conditions of an infinite domain.

- Regarding the Hill's formula "result" using the formal Lagrangian, he thinks that if true it's actually a great result because the continuous families are an indication of a hidden symmetry, so if the solutions in these families all the same stability it would be nice.

- Regarding the Lagrangian itself, he believe it is a good theoretical attempt, and thinks the theory is really the lion's share of the remaining work.

- He's been thinking of this a lot and has a lot of his own ideas which we did not get into but he believes that I've done really impressive work that has gotten him really excited in regards to his ideas. It made me very happy and he even went so far as to say "This is really important" in regards to my work; not only for fluid dynamics but also for chaotic systems and PDEs in general.

Hopefully this optimism leads to good results and many publications :)

2019-02-16 Predrag We'll have to teach Lan how to use GaTech VPN - lots of hoops to start with, until it works. His GaTech ID is
```
lyueheng6 Sp....t......l?
```
His subversion ID is
```
y-lan b.T......!
```

2019-02-19 Predrag I have not really digested (17.6), but a quick remark. For for discrete time flows the Hessian of a periodic orbit is a high-dimensional finite matrix, with every point on the cycle-n varied (see Han's blog); for continuous time flows it is an infinite matrix, that's why it took Poincaré to prove that it's determinate is finite. So a single matrix (17.6) is not the Hessian, or is a Hessian only for an equilibrium solution?

2019-03-11 Matt LSS Methods I've been reading the Least Squares Shadowing method developed in [34] and mentioned in both [20, 21]. I had a former roommate explain adjoint methods and their application in an engineering context. Typically from what I have seen in adjoint methods is that engineers acknowledge that solving for the full velocity field is hard so they write the adjoint equations such that there are only a few control variables being varied instead of a very high dimensional flow field. I believe this is because engineers are predominately searching for stable equilibria by varying control parameters such as: airfoil geometry, drag coefficient, etc.
I think I need to read the Lasagna papers more thoroughly to see how the LSS method is applied to chaotic systems. I believe Wang's method only applies for finding the derivatives of observables w.r.t scalar control variables, in my case this would be the domain size, period, spatial shift (or energy, or another conserved quantity yet to be discovered).

Symbolic Dynamics Trying to get back into the swing of things by pursuing Lan's method of plotting partial derivatives in order to develop some intuition regarding the admissible spatial and temporal combinations of tiles in order to develop the symbolic dynamics.
I don't have anything worth showing really but I'm starting to believe that the spatial itineraries might be decoupled from the temporal ones; I haven't really developed an idea as to what is the best way to plot these yet, but following [8] and plotting in the u, u_x plane and taking temporal cross sections of spatiotemporal invariant 2-tori shows patterns similar to spatial equilibria ($T = 0$ system). I believe this makes sense as spatially conjoining two tiles means that each time instance must be periodic in space; therefore I believe the intuition is something like follows: To glue two tiles $0,1$ spatially, then at each instant in time the combination needs to be topologically equivalent to a spatial equilibrium 01. This is really hard to demonstrate other than rather vague attempts such as

the time dependent trajectory in (u, u_x, u_t) space needs to intersect $(u, u_x, 0)$ plane to be able to glue spatially; this always seems to be the case so I believe a first trial would be to continuously attempt to glue equilibria to an orbit and see if it can be repeated ad nauseam. This could be misguided due to unwarranted projections, but currently plotting trajectories as functions of space and time is far too obfuscating to be useful. (similar to plotting trajectories prior to quotienting continuous symmetry or plotting Fourier coefficients).

I believe this best way to proceed is to tile repetitively in space or time and then analyze the corresponding partial derivative plots.

04-04-2019 Matt comments on Pathak *et al.* [30] *Model-free prediction of large spatiotemporally chaotic systems from data: A reservoir computing approach.* Slightly confused on what they mean by the "echo state property" in their Fig. 1:

> ...all of the conditional Lyapunov exponents of the training reservoir dynamics conditioned on $\mathbf{u}(t)$ are negative so that, for large t, the reservoir state $\mathbf{r}(t)$ does not depend on initial conditions.

Is this a statement that the network is not being trained w.r.t. transient behavior but rather trained by the attractor and or inertial manifold?

My main reaction to this paper is that it once again points out how attached researchers are to the concept of time, and predictions of future behavior. They demonstrate that after a small number of Lyapunov times that their predictions become inaccurate; while the predictions extend past a few Lyapunov times I cannot help but think they would be much better off training their reservoir on invariant 2-tori so that the process isn't so much as predicting the future as it is about "facial recognition" for lack of a better term. My bias is showing, but if they themselves acknowledge that there are fundamental limits imposed by positive Lyapunov exponents I can't help but feel that it would be better to (even at different system size) develop a database of invariant 2-tori and then find the "average" much like how the "average" facial structure can be produced for different countries and ethnicities; in this sense one would develop averages for observable quantities, but, like I stated, this is spatiotemporal bias.

Least Square Shadowing Finally got around to rereading this thoroughly. I believe that we originally investigated the Least Squares Shadowing (LSS) refs. [20, 21, 34] as a means of classifying continuous families of solutions generated by dependence on system parameters T, L. From what I have gleaned from these papers the LSS method has an underlying engineering spirit I believe. It's a numerically stable means to see how observable quantities change in response

> to changing system parameters over both individual orbits and the attractor they shadow. I believe the application to the control problem in [20] regarding the Kuramoto-Sivashinsky equationis simply introducing a Lagrange multiplier and then analyzing how observable quantities are sensitive to perturbation in this multiplier.
>
> It's good work but I don't think that it can be leveraged for my own work unless it would be decided that the desirable representative from each continous family has a minimized/maximized sensitivity to changes in T, L. I don't see any basis for this reasoning however.

Partial derivative plotting and symbolic dynamics The intuition from the Kuramoto-Sivashinsky equation on the $T = 0$ line from Dong and Lan [8] doesn't seem to extend to the spatiotemporal case; in other words, there doesn't seem to be a useful projection onto partial derivatives of the velocity field (u, u_x, u_{tx}, etc..) that elicits interesting behavior.

> The way this idea was tested is as follows: For each tile, and each projection axes, the respective fields ($u(x, t)$ and its partial derivatives) were plotted for all values of x, t. If shadowing were present, then it should be present three dimensional projection is how I was thinking.
>
> This doesn't seem to be the case; therefore, unless there is some new development I'm ceasing this activity.

Slowly learning Julia I'm starting to board the Julia train lead by conductor Gibson. I enjoy how it's really tailored to scientific computing by not messing around with object oriented programming, not to mention the fact that it's very fast if programmed correctly. The problem is at this stage it seems that in order to leverage the capabilities one would have to either create wrappers for underlying C++ and Fortran codes or borrow them from other projects such as `DifferentialEquations.jl`, so I'm not sure how much independence I would have; my thoughts were to rewrite `kstori2` in Julia before writing anything new but I'm unsure if it is worthwhile at this stage. TL;DR I'm interested in pursuing this but it's low on the priority list right now.

04-09-2019 Matt :

variational methods and numerical implementations (Description of spatiotemporal problem, function defined.)

- define cost function (functional eqn.)
- adjoint equations

tile extraction :

- decide on subdomain that we believe is suitable candidate.
- retrieve the numerical subdomain, discretization and parameters

- put through same code that found the source torus
- if converge, done
- if not converge, take larger subdomain and repeat process iteratively or quit

gluing :

- two known solutions
- interpolate onto fine discretization
- aspect ratio
- if continuous symmetry, rotate
- if discrete symmetry, chop
- numerically zero pad between boundaries
- fill in with convex combinations of the boundaries of zero-padded region
- convex combination isn't differentiable; know Kuramoto-Sivashinsky equationis smooth, therefore perform filtering / smoothing / Fourier truncation
- Coarsen discretization depending on numerical method used

2019-04-22 Matt Mainly been writing daily activities in sect. 4.4 *GuBuCv17blog.tex*, see posts there for changes.

Wei and Wang (2019) article The following passage consists of outtakes from Wei and Wang [35].

Work studies dissipative Dullin-Gottwald-Holm (DGH) equation using Lie symmetry analysis à la Ibragimov [14].

The DGH equation

$$u_t - \alpha^2 u_{xxt} + k u_x + 3 u u_x + \gamma u_{xxx} = \alpha^2 (2 u_x u_{xx} + u u_{xxx}). \quad (17.14)$$

results from

> *"...using asymptotic expansions directly in the Hamiltonian for Euler's equation in the shallow water regime. It is completely integrable with a bi-Hamiltonian as well as a Lax pair..."*

The equation that is referenced far more often than the general Dullin-Gottwald-Holm equation is the special case

$$u_t - u_{xxt} + 3 u u_x - 2 u_x u_{xx} - u u_{xxx} + k(u + u_{xx})_x + \lambda(u - u_{xx}) = 0. \quad (17.15)$$

(which is quite clearly the center of the study of this paper) from [27, 28]. The title and abstract are slightly misleading as the general case is *not* the emphasis of the study.

Certain parameters values $k = \lambda = \gamma = 0$, $\alpha^2 = 1$ produces the *Camassa-Holm* equation

$$u_t - u_{txx} + 3 u u_x + u_{xxx} - 2 u_x u_x x - u u_{xxx} = 0, \quad (17.16)$$

which describes "unidirectional propagation of surface waves on a shallow layer of water that is at rest at infinity."

Wei and Wang then discuss Ibragimov's *formal Lagrangian* formalism [13, 14, 16] as well as the nonlinear self-adjointedness property [13, 14].[1]

Very briefly, the main concept at hand is that by creating a formal Lagrangian $\mathcal{L} = vE$ where E is an s-th order nonlinear equation (e.g. the DGH equation or the Kuramoto-Sivashinsky equation). An equation that is nonlinearly self-adjoint has the property that the adjoint equation

$$E^* = \frac{\delta \mathcal{L}}{\delta u} = 0 \,, \tag{17.17}$$

is satisfied by some substitution $v = \phi(x, u)$. Here, δ signifies the variational derivative (many different names, see the "Names" section of Wikipedia).

Written more explicitly, the nonlinear self-adjoint condition can be written

$$E^* \Big|_{v=\phi} = \lambda_0 E + \lambda_1 D_t E + \lambda_2 D_x E + \dots \tag{17.18}$$

where λ_i depend on u and its derivatives.

[2]The point that frustrates me to no end, maybe I'm just ignorant, is that the symmetry operators admitted by the equation are stated without derivation. By "the" symmetry operators of an equation I mean the set of operators which leave the equation invariant as well as produce the Lie algebra. The machinery developed by Ibragimov is *completely reliant on the derivation of these generators, or worse, having a priori knowledge*. For example, the following Lie point symmetry operators admitted by (17.15)

$$X_1 = \partial_t, \; X_2 = \partial_x \text{ and } X_3 = e^{\lambda t}(\partial_t + k\partial_x - \lambda u \partial_u) \,. \tag{17.19}$$

I understand the inclusion of the generators of translations, X_1 and X_2, but have *absolutely no idea* why they include X_3 without derivation as it seems very non-trivial to me. I *believe* it comes from the invariance condition

$$X_\alpha E = 0 \,, \; \text{ where } X_\alpha = \xi_\alpha^t \frac{\partial}{\partial t} + \xi_\alpha^x \frac{\partial}{\partial x} + \eta_\alpha \frac{\partial}{\partial u} \,, \tag{17.20}$$

which produces an over-determined linear system of equations wherein the coefficients $\xi_\alpha^t, \xi_\alpha^x, \eta_\alpha$ of generators X_α are determined by solving said system of equations. Moving beyond this point of con-

---

[1]Predrag 2019-04-22: Here Matt referred to *Ibragimov10*, I cannot find it.

[2]Matt If the "extended system" (the variational derivatives) satisfy $\frac{\delta \mathcal{L}}{\delta u} = \frac{\delta \mathcal{L}}{\delta v} = 0$ for some v (i.e.is nonlinearly self-adjoint) any conservation law of the extended system corresponds to a physical conservation law [18]. :

tention, they state that "...optimal system of one-dimensional sub-algebras of the Lie algebra spanned by X_1, X_2, X_3 of (17.15) given by..."

$$X_1, \ X_2, \ X_1 + aX_2, \text{ and } X_2 + bX_3 \ . \tag{17.21}$$

Again, producing the generators is the component I have had trouble with; perhaps it is because I was trying to derive the generators for Lie-Bäcklund symmetries because I did not have success with the easier case which is Lie point symmetries.

[3]The rest of the paper, although not trivial, follows the Ibragimov's blue print pretty closely. The applications and derivations include:

- Using nonlinear self-adjointedness and Ibragimov's conservation theorem [12] to derive conservation laws for (17.15)
- Using conservation laws to show solutions exhibit blow-up and the "global existence of strong solutions"
- Deriving analytic solutions from the conservation law

Details are left in the paper as the proofs and derivations are too specific to (17.15) to be of use in the spatiotemporal Kuramoto-Siva-shinsky equation.

2019-04-23 Matt Tom Day Graduate student from Peter Yunker's group presented on the manner in which yeast forms clusters. This was motivated by the evolution from single cell to multicellular organisms, want to investigate the key properties of one such evolutionary process. The general idea is that yeast cells will collect and subsequently undergo a budding process which creates branches which result in large clusters. There were two differing experimental setups which both resulted in the same mass distribution as a function of cluster diameter. The general idea was to have a tube consisting of a yeast mixture where after a set amount of time the bottom portion (clusters stratify based on mass, bottom has largest clusters) was extracted. Repeating this process iteratively is equivalent to selecting the largest. It was shown that the cells evolve by elongating (aspect ratio changes) to improve packing efficiency. The distribution of cluster sizes was only investigated for a finite period of time; nothing said about the expected limits of such a process or whether there is a critical size which clusters cannot exceed.

The two experiments both involved repeated extraction of the largest clusters, with one critical difference. For one of the setups the yeast mixture was compressed at constant force for a set amount of time prior to every extraction. In spite of this compression, the distribution of the cluster sizes were identical. A model was created that

---

[3]Matt The difference between Lie point symmetries and Lie-Bäcklund symmetries (according to Ibragimov) is whether the generators of the vector field (Lie algebra) depend on the partial derivatives of u (Lie-Bäcklund symmetry) or not (Lie point symmetry).:

related the probability for the size to change by a scalar to the "kinetics" or rate which the the clusters form. The model was based on some well known evolutionary model which had structure similar to Boltzmann distribution. There was no link between this model and experimental results sadly so it is not known whether the model is valid.

Jaemin Park *On radial symmetry of uniformly rotating stationary solutions*
TL;DR for 2D Euler equation there is a (constant) range of angular velocities where radially symmetric solutions exist. For the gSQG equation there exists a similar range but it depends on a parameter (domain size I think?).

Symmetry of relative equilibria and equilibria solutions to 2D euler. Using vorticity equations and stream function formulation. Biot-Savart law, Yudovich Theorem for uniqueness of weak solutions. Vortex patch solutions, where the vorticity field is given by linear combination of some functions.

The uniformly rotating patch with angular velocity Ω counter-clockwise satisfies

$$z_t(t, \alpha) = \Omega z(t, \alpha)^\perp \tag{17.22}$$

Boundary equation is the difference of the gradient of the stream function minue the equation for z_t dotted with some z.

Vortex patch is "uniformly rotating" if

$$\phi(x) - \frac{\Omega}{2}|x|^2 = \text{Const} \tag{17.23}$$

on each connected component of the boundaries. Call this constant function $f(x)$. If $\Omega = 0$ then ω is a stationary solution. Any radial solution is a rotating solution with any angular velocity.

Question to be answered: Among all connected patches with smooth boundary, must every rotatting patch with $\Omega \leq 0$ or $\Omega \geq 1/2$ be radially symmetric?

Kirchoff (1876) showed than an ellipse is a rotating solution where semi-axes satisfy

$$\Omega = \frac{ab}{(a+b)^2} \tag{17.24}$$

two other statements, going too fast to type. Theorem by the authors of the paper, radial symmetry is broken in the parameter range $0 \leq \Omega \leq 1/2$.

Energy functional

$$1/2 \int p(x)(p \star \mathcal{N})(x)dx - \Omega/2 \int p(x)|x|^2 dx \tag{17.25}$$

note that

$$\frac{\delta E}{\delta p} = f = \phi - \Omega/2|x|^2 \tag{17.26}$$

Perturbations for a diveregence free vector field V satisfy continuity equations "..."

Time derivative (inserting continuity equations) of the energy functional implies that

$$\frac{dE}{dt} = \int V \cdot \nabla p = 0 \tag{17.27}$$

For an integral $\mathcal{I}$ that has a long definition, can show that inequalities only hold if patch is a disk for $\Omega \leq 0$ and $\Omega \geq 1/2$ as previously stated.

Putting holes in the patches betray the constraint $\mathcal{I} = 0$; need constant values of p on boundaries. Can bound a sequence of integrals (step functions) approximating stream functions by isocontours of vorticity ω below by some integral expressions, even though the limit of this quantity is zero.

Theorem; there exist stationary nontrivial patch solutions to the 2D Euler equations even with finite energy. These solutions are "close" to nested annuli with vorticity of different sign. Proof bases on Crandall-Rabinowitz theorem.

Now consider Generalized Surface Quasi-Geostrophic equation. Shown in literature the existence of non-radial solutions in parameter range.

Difference between Euler and this is that the parameter range where simply connected patches must be radially symmetric: Euler has constant range, gSQG depends on the size of the domain. Perturbation of the energy functional under "continuous Steiner symmetrization". "Similar technique has been used to show radial symmetry of steady solutions to nonlinear aggregation-diffusion equations".

Description of continuous Steiner symmetrization. Assume non symmetric patch, split half-plane in two to split the patch in two. Define "needles" (1D cross sections); make them symmetric with respect to the half plane seperatrix.

Future work. Euler equation in unit disk. "Can we still prove the radial symmetry of stationary patches on the disks or annuli?". Kirchoff ellipse solution (rotating solution). Should be $0 \leq \Omega << 1$ such that aspect ratio is very large (or small). In other words, the future work is to investigate the parameter ranges $0 < \Omega << 1$ and $0 < 1/2 - \Omega << 1$.

"n-fold symmetric patch" exist which look like smoothed polygons which have D_n symmetry.

2019-04-24 Matt My intentions for future edits of the paper; general additions like including figures and citations are left out in favor of more explicit goals.

Others would know better than me, but my gut is telling me that if the paper is titled "Spatiotemporal tiling of the Kuramoto-Sivashinsky flow"

then incorporating Gutkin and Osipov is consistent with this message. I foresee this process unfolding in two ways: 1. The paper is aimed at the overarching topic of spatiotemporal tiling, for example, "Spatiotemporal tiling of both discrete and continuous nonlinear dynamical systems" and the computational details such as adjoint method, GMRES, etc. are left to another, more technical, paper. 2. The focus of the paper is the Kuramoto-Sivashinsky equation and the methods with which new solutions have been found and can be constructed. This would go over the specific numerical methods for finding solutions as well as gluing and tiling. I don't think spatiotemporal cats fits into this message personally.

For the second option I propose the following outline for the paper

1. Abstract
2. Intro
3. Kuramoto-Sivashinsky equation literature review
4. Spatiotemporal Kuramoto-Sivashinsky equation in Fourier basis (`sFb.tex`)
5. Spatiotemporal symmetries
6. Spatiotemporal symbolic dynamics concept
7. Descent methods
8. Iterative methods
9. Gluing methods
10. Tiling methods
11. (If possible) symbolic dynamics quantitatively explained
12. Conclusion

with the following reserved for appendices of either the paper or thesis

- Variational methods
- Matrix-free computations
- Preconditioning
- Fourier transform conventions and selection rules

with the caveat that if the Ibragimov-type study pans out, then the results would be moved to the variational methods section which would in turn be inserted between symbolic dynamics concepts and descent methods. This is the narrative that I believe has the most continuity. There is not much application of discrete Lagrangian methods similar to ref. [19]. While I believe this work is formulated as a variational problem, almost all of the key components of discrete Lagrangian methods are missing. For example, we do not formulate discrete jet bundles, discrete action principles, discrete Noether's theorem, etc. These results are inherently

different from our calculation because they work in a discretized configuration space (x, t) and define everything in terms of finite differences on these grid points.

The second option is more akin to how I believe my thesis will be structured and so I am biased to approve of this format more. Due to the already exorbitant length of `GuBuCv17.tex` I think that actually there should be three papers: A spatiotemporal cat paper, a spatiotemporal Kuramoto-Sivashinsky paper, and a "grand narrative" paper which builds on the results of the first two.

2019-05-13 Predrag I have already discussed it elsewhere, in **2019-02-26** post above, but it has to go into the paper.

In figure **??** and following figures, the most unstable wavelength $2\pi\sqrt{2}$ of the u=0 equilibrium (see sect. 1.5) is an estimate the mean spatial wavelength of the turbulent Kuramoto-Sivashinsky flow, so there are approximately 55 wiggles across the spatial domain at any instant in time. There is a very prominent leftward / rightward wave propagation speed, perhaps several. But the result is puzzling: on the left half, there are prominent leftward moving reddish lines - but there are no prominent rightward moving bluish lines. Also, both figures reveal a very persistent structure (not in our alphabet?) from $(x, t) = (9, 0)$ to $(10, 130)$ with a smaller wave velocity.

If you look at figure **??**, it has bluish regions and reddish regions, and $u \in \{-3.4, +3.4\}$. But if you look at your (over-counted) alphabet figure **??**, it has $u_j \in \{-2, +2\}$. Why is that?

You use Galilean invariance (12.31) to set the mean velocity of the overall front to zero, $\langle u \rangle(t) = \int_0^L dx \, u(x, t) = 0$. But for an arbitrary subregion of width $L_1 < L$, the mean velocity is generically $\langle u \rangle(t) \neq 0$. Actually, we know that as function of L the velocity front executes a random walk, with variance $E(t) = \frac{1}{2}\langle u^2 \rangle(t) \propto L$ by the extensivity of Kuramoto-Sivashinsky, and hence the range of the color bar in a figure such as figure **??** has to grow proportionally to $\sqrt{L}$. The variance grows only in the spatial direction, in the time direction $E(t) \to E$.

However, I think that if you plot u_x for figure **??** or figure **??**, that might have bounded variance, as $\langle u_x \rangle(t)$ is invariant under the $u(x, t) \to u(x - ct) - c$ transformation.

That implies that in gluing letters u_j of alphabet figure **??** into larger patterns, one also has to vary $\langle u_j \rangle(t)$ averaged over the tile of width L_j, in order to glue optimally. In other words, we have to use the Galilean symmetry group orbit of the letter u_j, and slice that group orbit at $\langle u_j \rangle(t_0) = 0$ for purposes of ploting its representative in figure **??**.

Perhaps the variational descent takes care of that, but it is not obvious.

2019-05-13 Matt Let me preface the discussion with saying that the colorbar units (displaying the range $[-1.5, 1.5]$) is an adopted convention for invariant 2-torus figures so that all velocity fields are displayed on the same scale. Generically, if one integrates the Kuramoto-Sivashinsky equation defined on a domain with small L (i.e. the size of tiles) then the average for the local minima and maxima over a large number of trials is ≈ 2.6. The minima and maxima for the tiles are as follows

	maxima	minima
defect #1	2.53	-2.64
defect #2	2.00	-2.37
hook	2.40	-2.67
gap	2.49	-2.47
streak	1.21	-1.21

upon further inspection the values for the solutions seem to match the time integrated simulations but the value for the streak is worrisome until one, once again, performs numerical simulations on a domain size comparable to that of the streak domain $L \approx 6.39, \frac{L}{2\pi} \approx 1$. So in summary the values of the colorbar as exaggerated by the convention to fix the limits of the colorbar. This convention was not employed for figure **??**, which is predominately the reason for the discrepancy.

As to *why* the value of local maxima(minima) increase(decrease) as a function of L, I don't have a better argument than the extensive nature of the Kuramoto-Sivashinsky equation. It is sometimes useful to modify the magnitude of u when gluing, which can probably be explained by approaching the upper bound of u from above is numerically beneficial. For instance, I would never use streaks bounded between values exhibited by figure **??**, but the solution exists with those bounds at that domain size regardless. Therefore, to take the extensive property of the Kuramoto-Sivashinsky equation into account it is fairly common to rescale the tiles from figure **??** to suit the situation and better fit together. This is not equivalent to using Galilean symmetry group orbit as the rescaled solutions still satisfy the mean velocity condition.

I agree that the mean velocity constraint is not satisfied locally ; this was the basis behind my idea of "stabilizing" spatial integration by somehow incorporating a "local" Galilean symmetry but I never figured out how to do it or even what I really meant by this.

Incorporating the degree of freedom provided by the Galilean invariance would likely make finding solutions easier (in a least squares sense) because it increases the codimension of the group orbit of solutions, identically to translations (I don't do any slicing or use Poincaré sections for this exact reason; why impose such strict constraints when there is no reason to a the moment?). I never really thought of this, as it is another case of being too comfortable with the conventions developed for time

dynamical systems. I'll try to work through this idea but it would be a pretty sizeable upheaval as most of my code eliminates the zeroth spatial modes; something that can be shelved for later.

2019-05-14 Predrag Looking at figure **??** and figure **??**: we might chose Galilean invariant elementary tiles (spatial derivatives of u), instead of Galilean equivariant u_j tiles of figure **??**.

2019-05-14 Predrag Which brings me back to figure 16.10 (b). Can you start with a figure 16.9 smoothed and $\bar{L} = 2\pi\sqrt{2}$ modulated "noise" initial guess on $(L, T) = (500, 500)$, run it through your optimizer - do you get a small error, and something that looks like (u, u_t, u_x) of figure **???** Maybe the answer is already your figure 16.7, but that looks nothing like figure **??**, so it worries me.

We need such figures anyway to illustrate your initial guesses.

2019-05-16 Matt Trying to see if I can get a nice large-domain adjoint descent optimization; its been a while since I tried. I spent some time tweaking my codes to try and get the best results but this still needs a bit of work. Not investing too much time in this, I think I just need a large chunk of computation time and something decent should pop out.

Results from large domains like figure **??** when starting with modulated noise are hard and I never really gave it much effort because of its likelihood to work and or priority not to mention the amount of time it takes. I'm attempting some trials now so hopefully I will have something that looks better than figure 16.7 in the near future.

2019-05-15 Predrag Plumbers' hangout: Predrag showed Matt's latest plots of Kuramoto-Sivashinsky velocity field u, its spatial gradient u_x and its time derivative u_t on a large $(L, T) = (500, 500)$ spacetime domain (that is ≈ 55 wiggles of u across x-axis), figure **??**. The most striking is the u_t plot - clearly visible is a dominant $\pm$ phase velocity which implies there are long range correlations, in time at least as long as the entire pattern of time period $T = 500$.
2019-05-20 Predrag figure **??** (a) is a lesson in dangers of using strange initial conditions, not checking whether transients have died out. As illustrated by figure **??** (b), there are weird 'letters', no long range correlations.

This violates our common intuition that Kuramoto-Sivashinsky decorrelates exponentially both in space and time. Burak showed us (again) the earliest simulation of turbulent body-forced 3D cube (again Predrag forgets the authors) which shows very clearly that the turbulent flow has long correlations in form of long vortex tubes. That does not help with 1D Kuramoto-Sivashinsky - no vortex tubes...

2019-05-15 Predrag Which brings me back to figure 16.10 (b). We usually plot (1.61) which balances the power P pumped in by anti-diffusion u_{xx} against
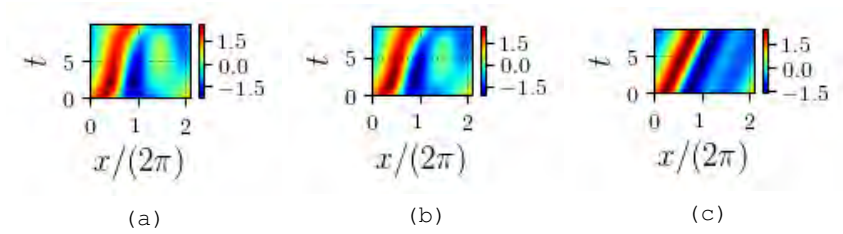
Figure 17.5: Members of the continuous family of defects (2-to-1 wavelength mergers) numerically continued and converged at spatial domain sizes (a) $L = 13.08$, (b) $L = 13.09$, (c) $L = 13.10$. Here not stated in "natural" units of $2\pi\sqrt{2}$ because of their proximity. (a) Is most reminiscent of the defect family, specifically the pattern previously often called the "hook". (b) As the "hook" gains an increasing relative equilibrium spatiotemporal shift it "tilts" more and more until it finally bifurcates into a relative equilibrium solution (c). The "hook shedding" mentioned (somewhere?) in sits precariously between (b) and (c).

the energy dissipation rate D by hyper-viscosity u_{xxxx} in the Kuramoto-Sivashinsky equation. So it might be nice to have look at plots of local power $\frac{1}{2}u_x^2$, dissipation $\frac{1}{2}u_{xx}^2$, and energy rate (the difference of the two).

All of the above were derived by thinking "in time". Might have to re-think all of these in spacetime. In particular, might plot the 4-dimensional vector field (1.34) as well.

2019-05-16 Matt Produced figure **??**, figure **??**, figure **??**, which are the power, dissipation and energy density rates respectively for the large spatiotemporal data set figure **??** (b), plotted on a logarithmic scale and thus looking like red lobsters. These look like to me like many different things, white caps in the ocean, a fan, a dispersing wave, a beat-like pattern. [4]

The energy rate seems to display two main behaviors, a highly localized maxima at 2 to 1 wavelength defects and then a much broader pattern of increased energy rate in the shape of a fan, patch, beat, wave or any other shape left to one's imagination.

2019-05-16 Matt Regarding above comments on figure **??** (a):

$u_t = -u\,u_x - u_{xx} - u_{xxxx}$ is a Galilean invariant field. There is a very prominent leftward / rightward wave propagation speed, perhaps several. But the result is puzzling: on the left half, there are prominent leftward moving reddish lines - but there are no prominent rightward moving bluish lines. Also, both figures reveal a very persistent structure (not in our alphabet?) from $(x, t) = (9, 0)$ to $(10, 130)$ with a smaller wave velocity (note, the x-axis is mislabelled).

---

[4]Predrag 2019-05-20: why all duplicate figures `MNG_P_largeL2000.png` = `MNG_P_largeL.png`, etc.?

In regards to this "missing letter", I have an explanation (as Senator War-ren says, I have a plan for that) but its a very specific case of a known "letter" so I had not mentioned before. The reason for the lack of inclusion of the coherent relative equilibria structure in the bottom right hand corner of figure **??** (a) is because it sits right at the "edge" of the defect family before it transitions into a relative equilibrium solution. This phenomenon occurs around $L \approx 1.47 \times 2\pi\sqrt{2}$.

2019-05-16 Matt Viewed as a decreasing function of L, the relative equilibrium undergoes a bifurcation (I haven't inspected any eigenvalues), likely a Hopf bifurcation, such that there is an additional (quasi) periodic behavior which is very coarsely analogous to "vortex shedding", except in this case its "hook shedding" as a function of time. The likely reason behind its presumed quasi-periodicity exhibited in figure **??** (a) is due to local spatiotemporal coupling. I surmise that the bottom right hand corner of figure **??** (a) consists (perhaps surprisingly) of members of the same defect family which pervades the entire plot.

Three 'rubber tiles' in this family which display this phenomenon are shown in figure 17.5. Note: old figs, so old units.

2019-05-16 Matt Correction: the above "missing letter" seems to have been artifact of my time-froward integrations staring with a suspiciously symmetric initial condition. Now that I've increased transient time from $T \approx 50$ to $T \approx 2,000$, all weird things, including the "missing letter," are gone.

2019-05-16 Predrag Keep the short-initial-transient $*$.png's in figures **??** (a)-**??** (b) under current file names. Give slightly different names to your asymptotic $*$.png's, transient time $T \approx 2,000$. The pre-asymptotic figures are educational for us, internally, keep them.

2019-05-19 Matt Takashi Tokieda Chain fountain (Newton's beads) demonstration. Theorem from the 19th century Once it gets going, a chain can flow in any shape in neutral equilibrium.

Looking at the net forces of a infinitesimal section of the chain. By the normal component of tension, if the flow is fast enough then the tension is independent of the radius of curvature (geometry becomes irrelevant).

This is an anomalous reaction, which appears to violate Newton's third law. A toy model for this phenomenon is a free-falling rod which lands at an angle to the ground, such that one end hits first. This contact with the ground induces a torque which "pulls" the end of the rod down faster. (Movie by Andy Ruina) of rope ladders falling, one that makes contact ends up falling faster. This is an example of tension resulting from compression. This model relies on the bending stiffness of the rods.

(Very) Basic model for the rod example using Newtonian mechanics, Half of the energy is lost to the shock dissipation.

Using this, estimate how high the newton's beads should go. Zigzag monolayer has only horizontal components, yet there is a vertical arching. Criticality (where derivative vanishes) is taken advantage of the change.

Why does the chain stand up vertically? Very singular phenomenon of minimum chain radius. Curvature induced at the location of horizontal motion. The accumulated curvatures of the curl induce buckling due to torsion.

WHITE PINE

Qiqi Wang Computation of sensitivities in chaotic systems: an overview

Overview of sensitivities in chaotic simulations.

Going to use a very real example. Using the buffets of F35 (raptor?). Shaking is due to vortex breakdown (chaos). Chaotic aerodynamics cause aircraft buffet. This also takes place with (space) launch vehicles. Length makes it so most of the body is actually in the wake of the front end. Yet another example: chaotic aerodynamics melts engine components. This mini symposium is dedicated to sensitivity analysis and optimization of chaotic dynamical systems, not merely simulation.

How is the objective function (structural damage, long time average heat transfer).

steps

1. Parameterize the autonomous equations
2. Define the objective function (average quantities, instantaneous quantities not really defined).
3. Compute the derivative of the objective function with respect to the parameters.

Why not use finite difference for sensitivity of statistics? Extremely inefficient. Argument: let X be a random variable in a uniform probability distribution on $[0, s]$. The derivative of the mean is equal to half. Sampling error (finite difference implies cancellation error?) ruins the finite difference scheme, this error is amplified by dividing by ds. Error decreases as the square root of the sample size.

Using the Lorenz equations, define the objective function as the average of the deviation of z from some mean. The "design parameter" is ρ from Lorenz. Looks like noise at low sample size.

For "small problems" you can parameterize the 2D slice

Adjoint: differentiation the output of a simulation to its inputs by tracing backwards through the calculations. The problem with this is that it doesn't work because of the instability.

Can we desensitize the adjoint method to the noise in computed statistics of chaotic simulations.

Parameter perturbation vs initial condition perturbation.

Question: Implicitly there is some flow which is very high dimensional, is this always with normally this would be an incredibly high dimensional problem, is the flow not a variable? Is the base flow always stable?

Angxiu Ni Adjoint Shadowing direction in Chaotic Systems for sensitivity analysis Classical trajectory-based sensitivity analysis fails. Small scale variations has much more profound effect on the "zoom in" slope as opposed to the "zoom out" slope. Zoom in, let $ds \to 0$ and then $T \to \infty$ Zoom out, let $T \to \infty$ then $ds \to 0$.

$$\overline{Javg} = \frac{d}{ds} \lim_{t \to \inf} \frac{1}{t} \int \partial_u J \frac{du}{ds} + \partial_s J dt \qquad (17.28)$$

Shadowing lemma: two kinds of perturbations. Perturb initial conditions, keep parameters and vice versa. If you do both, and they are coordinated, can remain close (L_2 norm of perpendicular distance (pointwise?)). Is this always continuous? bifurcations?

Changing the initial condition uses covariant Lyapunov vectors (homogeneous tangent equation). Changing the parameters results in inhomogeneous tangent equations.

$$\frac{J_a vg}{ds} \approx !/T \int_0^T [\|partial_u f v^\perp + \partial_s J + \eta (J - <J>) \qquad (17.29)$$

Interpretation of terms, in order, state space "location difference", direct dependence of J on s and the speed difference term.

This was tangent space definition, now onto the Adjoint shadowing direction now.

$$\frac{d <J>}{ds} = 1/T < v, J_u >_{L_2} \qquad (17.30)$$

$$v(t) = \frac{\delta u}{\delta s} \qquad (17.31)$$

Propagate stable parts forward, unstable part backwards. "Dual" derivation. Let

$$\bar{v}(t) = T \frac{\delta <J>}{\delta u(t)} \qquad (17.32)$$

Conditions of $\bar{v}$ imply adjoint shadowing direction, approximation of real adjoint shadowing direction.

$$\frac{dJ_\infty}{ds} \approx 1/T < \partial_s f, \bar{v} >_{L_2} \qquad (17.33)$$

Non-Intrusive Least-Squares Adjoint Shadowing Adjoint flow and tangent flow have similar structures, which allows for recycling of least squares shadowing ideas.

Violates the adjoint shadowing lemma but still works fine? Can't prove but still works well in practice. It still works as long as unstable directions are not orthogonal?

Nisha Chandramoorthy Space-split statistical sensitivity computation in chaotic systems Autonomous equations, forward time mapping, time discretized PDE or forward time mapping.

Split tangent space into stable and unstable manifolds. Unique ergodic invariant physical measure (SRB). Work with uniform hyperbolic chaotic systems. Cat map example.

PRIMROSE A

Chris Marcotte Sensitivity of spiral wave core formation and transient spiral core interactions Very behind schedule or is this dude taking all of Chris' time? Adjoint eigenfunctions and singular modes are the subject of his talk. Cardiac rhythms and arrhythmia. Using very simplified excitable models. Model allows for sustained spiral chaos. Spiral cores born in pairs die in pairs. Tangent space flow via linearization, and its adjoint

Tangent flow modes are global while adjoint modes are localized. Can quantify this localization. Adjoint modes tell us how perturbations generate transitions. Floquets modes (tangent space eigenmodes) characterize stability of solutions.

Open trajectory, when linearization fails due to distance of successive points on the trajectory. Using Golub, Kahan (probably based on Ginelli). Display of singular modes with respect to time.

Andrew Krause Pattern formation in bulk-surface reaction diffusion systems

Turing instabilities and chemical morphogenesis (how you see symmetry breaking in-vivo). Have two reaction-diffusion equations which are coupled. Mouse whiskers develop sequentially. Microsoft is genetically engineering bacteria. Develop in-vivo Turing patterns and instabilities.

Classical dispersion relation and stability analysis

Linearize autonomous system around spatially steady state and use (Lindstedt) ansatz which is base flow plus exponential growth term.

Instabilities on spheres and tori. Influence of curvature, growth, anisotropy. Laplacian is space dependent but can solve via spectral problem.

$$det(M_k) = \det(\lambda_k - \rho_k D_k - J_k) \qquad (17.34)$$

Multiregion domains Super complicated, cannot reduce problem via symmetry arguments so have to work on full problem. Cannot solve eigenvalue problem as a function of depth (y) due to coupling. Try anyway, get solutions and some expression for determinant and hence

the dispersion relation. Nontrivial coupling, relating heterogeneity to some strength parameter.

Turing instabilities in heterogeneous domains. In reaction kinetics (not the transport) is heterogeneous. Other than the initial bifurcation (one to two cells), every pattern does not occur on homogeneous background. Mouse and chicken modeling, simulations capture some behavior. Linear analysis on heterogeneous domains via WKB ansatz. WKB modes are not supported on same domains.

Raquel Gonzalez Farina Dynamics from a coupled chemical thermal microsilica partical formation model

Information of chemical reaction. Microsilica particles are spherical and growth is mediated by nucleation,condensation and aggregation (combining) Want to control the furnace to control the properties of the microsilica.

Initially well mixed chemical species One dimensional geometry, conservation equations for all chemicals,temperature and number density of particles.

Uniform concentrations, no diffusion terms. Boundary conditions on flux is related to particle number and nucleation rate, otherwise straightforward.

Derivation of dimensionless quantities and various growth and nucleation rates.

Analytical solution when $\zeta_i = 0$ (nonlinear coupling constants). Can then solve for an analytical solution of the particle density equation (method of characteristics). Divergent particle side.

Now set $\zeta_i \neq 0$. Something about equations being coupled except with respect to one degree of freedom? Asymptotic particle size.

Spatially heterogeneous chemical concentrations Diffusion comes back into the equations. Proof that there are no relative equilibria but can find solutions that have some properties of relative equilibria and self-similar solutions.

Diffusion dominant for small times and reactions dominant are large times? (obvious?, concentration approaches steady state no?)

Coupling makes it so particle size distribution pushes small particles into the "middle".

Future: more realistic flow and furnace geometry.

Robert Van Gorder Pattern Formation in reaction-diffusion systems on time-evolving domains Loss of stability of spatially homogeneous steady states for such systems can signal the onset of pattern formation.

Turing instabilities on state domains, the conditions for the onset of instability are algebraic. This is not the case for growing domains. Evolving is not the same as growing. Turing conditions for time-evolving domains. Want a linearly stable steady state in order to

get a Turing instability. This leads to complex exponential solutions, conditions on the determinant for inducing a Turing instability. This extends to arbitrary manifolds, as long as spectrum and eigenvectors can be determined.

Manifold now depends on time now. Simple case of dilation as the "equations of motion" for the manifold. Transform to co-moving coordinates. Spatial dependence when other evolution types are considered. In this case only time dependence. Steady state was perturbed spatially, but now the underlying state is dependent on time (this is a choice which makes the problem harder). Derive the linearized problem. Cannot rely on eigenvalues and eigenfunctions due to time dependence. Can prove linear instability if a differential inequality holds. Time oscillatory example was more interesting of the two, if too fast then pattern is destroyed (decoherence?).

Evolution of an area conserving rectangle, volume conserving cylinder. Slow evolution leads to spatial homogeneity as oppose to fast evolution, where it is still somewhat organized but less homogeneous.

Piyush Grover Understanding and designing emergent behavior via stability analysis of mean field games Talk is in regards to multi-agent systems (swarms of drones, traffic, etc). Features that present in nature, desirable in engineering. This has a flavor of an AI, machine learning, etc. talk.

Continuum (PDE) abstraction of collective agent dynamics.

Phase space distribution

$$\rho(x,t) = 1/N \sum \delta(x - x^k(t)) \tag{17.35}$$

Considering the $N \to \infty$ limit, this is not the most common formulation so its somewhat unique.

For flocking and swarming the model that is used is a first order model with gradient dynamics, with homogeneous population.

ODE or SDE for each agent labeled by i

$$dx_i(t) = \partial_x U(x_i)dt + 1/N \sum_j (x_j - x_i) + \sigma dw_i(t) \tag{17.36}$$

Using a potential that is quartic plus quadratic which is proportional to a strength of agent behavior parameter.

The noise induces a bifurcation, when its small then the individual motion of the agents dominate, leads to nonzero mean velocity.

Finite number of agents, introduce cost functional for each agent

$$J = \lim 1/T \int_0^T [\beta F[X_i, x_i - 1 + \frac{1}{2\sigma^2}u_i^2(t)]dt \tag{17.37}$$

Mean field approximation replaces the coupling with time dependence, which is in turn a proxy for density. Solution of the optimization and agent dynamics problem via Stochastic Hamiltonian-Jacobi-Bellman theory. HJB equation leads to (Closed loop?) Fokker-Planck which uses "consistency" equations such that the HJB is coupled to the FP equation.

Exposé on "closed loop stability analysis". Linear stability decomposes into a local and global operators, where the local is essentially the adjoint. Shows that zero mean solutions become stable when the control penalty is high and the non-zero mean solutions are never stable.

2019-05-20 Matt Gluing improvements via additional BVP After some thought I realized that the method I was using to produce the initial conditions for the gluing procedure was a terrible idea and the truncation of the Fourier modes was much better than the use of convex combinations and Fourier truncation.

The reason for this is that although the smoothing of the piecewise linear functions would result in a continuous field that would like the constituent invariant 2-tori together the tangent space would be terribly wrong. I attribute the success of the gluing in spite of this to the potency of the spatiotemporal numerical methods (adjoint descent, etc.)

I will propose an improvement (whose implementation I will reserve for after the paper is written due to the amount of work involved).

Chebyshev BVP gluing The method by which I believe that solutions should be glued, or at least the initial invariant 2-tori should be joined is to solve a supplementary problem which fills in a zero padded region by virtue of approximately solving the BVP problem induced by the connection of the boundaries of each invariant 2-torus.

Specifically, because we are more concerned with the tangent space being correct we will utilize Neumann boundary conditions for the BVP. Because of these boundary conditions the "natural" choice for the discretization of this connecting region is to either used finite difference methods or Chebyshev collocation methods. The former is rather expedient and perhaps would be better for this additional optimization problem because it will not result in an exact solution either way.

The reason we know that the intermediate area cannot have a tangent space that satisfies the Kuramoto-Sivashinsky equation everywhere locally is because we are connecting two invariant 2-torus solutions. For instance, integration of the IVP initiated at either boundary would (theoretically) result in the invariant 2-torus being repeated ad infinitum.

There is still indecision on my part as to the precise method by which the problem could be solved.

The first, a fully spatiotemporal method, would allow for use of the currently implemented (with modifications to incorporate the boundary conditions) numerical methods. The idea is to merely follow the typical procedure except the basis would be either Fourier-Chebyshev or Chebyshev-Fourier depending on the gluing direction.

The second (more straightforward in my mind) method would be to apply the variational Newton descent formalism to a Chebyshev basis with Neumann BC. This would be easily accomplished by using a Chebyshev basis and differentiation operator instead of the finite difference methods. The only difference between the spatial gluing and temporal gluing cases would then be the tangent space equations, namely, whether we are using (1.26) or (1.34) in the variational Newton descent equation.

As I'm writing this I don't think the spatiotemporal method would really be that difficult. The only difference from the current spatiotemporal method would be to incorporate Chebyshev transforms and modify the differential operators to accomodate the boundary conditions. For instance, if tackling Neumann BC in time then for an N by M time by space discretization (Fourier in space, Chebyshev in time) then the correct form of the equation would take the spectral coeff Let $u_t(A)$ and $u_t(B)$ represent the first time derivative evaluated on the "boundary" of each solution. In matrix notation we have the following ...??

2017-08-01 Matt PC recommends a paper on rigorous bounds on observables in chaotic in turbulent flows by D. Goluskin, Tobasco, Doering, showing for instance in the Lorenz system that the energy for points with a certain bound on the z coordinate is saturated by the equilibria, and then when z increases then the energy is saturated by the shortest periodic orbit.

2018-02-24 Predrag Charlie Doering writes: The absence proper instantaneous and/or long-time-averaged a priori bounds on solutions of the Kuramoto-Sivashinky equation in the large interval length (L) limit has annoyed our community for decades.

Utilizing a generalization of the background method and implementing recently developed optimization techniques, David and Giovanni (see arXiv:1802.08240) have now computed rigorous bounds —— over a large but limited range of L —— on the time averaged energy density of solutions that behave exactly as it is widely believed that they should behave, i.e., $< u^2 > \le L^0$. Moreover, their method reveals the nature of maximizing/extreme solutions: they are the largest amplitude steady solutions on the branches bifurcating from $u = 0$.

The resulting conjecture is that this precise $O(1)$ bound holds uniformly as L tends to ∞.

2019-05-20 Predrag David Goluskin *Studying Dynamics using Polynomial Optimization:* Various global properties of nonlinear ODEs and PDEs can

be inferred by constructing functions that satisfying suitable inequalities. Greater precision can be achieved by using computational methods of polynomial optimization to construct functions that satisfy the suitable inequalities. In several examples such as the estimation of average and extreme quantities on the attractors of the Lorenz equations and the Kuramoto-Sivashinsky equation, polynomial optimization produces arbitrarily sharp results.

2019-05-20 Predrag Giovanni Fantuzzi *Convex Analysis of Maximal Transient Growth Phenomena:* Various global properties of nonlinear ODEs and PDEs can be inferred by constructing functions that satisfying suitable inequalities. Greater precision can be achieved by using computational methods of polynomial optimization to construct functions that satisfy the suitable inequalities. In several examples such as the estimation of average and extreme quantities on the attractors of the Lorenz equations and the Kuramoto-Sivashinsky equation, polynomial optimization produces arbitrarily sharp results.

2019-05-21 Matt Chad Topaz A topological view of collective behavior Persistent homology using the Vietoris-Rips complex: this complex is the standard for data that is organized in a point wise fashion as opposed to Kuramoto-Sivashinsky equation invariant 2-torus data in scalar-field form.

I thought that most of the talk was relatively straight forward even with my modicum of self-taught knowledge. Every talk that I see of this flavor leaves me with the same question, how does one extract and or classify important patterns from the topological information. I understand that the topological Betti numbers pick out the topological invariants of, for instance, spatial ordering of flocks and the like. The problem I have with this research that I have is when you are trying to compare data that have similar but not identical topology. The best example that comes to mind is facial recognition. Topological data analysis would be able to tell the user that faces are connected components and perhaps that their circular structure would be picked up by Betti number 1 events, but I believe the model is far too reductive to be able to tell faces apart from one another. Perhaps this is not the point, perhaps one would merely want to be able to pick out the number of faces in the crowd as opposed to the specific people that they belong to. This is a contrived example but still a question that I struggle with slash has led me astray from Topological data analysis.

2019-05-23 Predrag Are bits of travelling waves that dominate figure **??**? related to either of the two relative equilibria TW_{+1} and TW_{+2} of figure 17.6?

2019-05-30 Matt Matt's ultimate to-do list
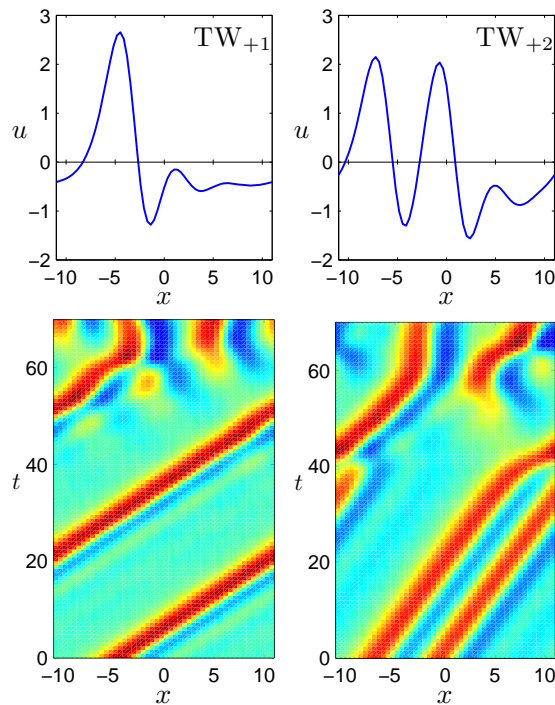
Figure 17.6: Relative equilibria: TW$_{+1}$ with velocity $c = 0.737$ and TW$_{+2}$ with velocity $c = 0.350$. The upper panels show the relative equilibria profiles. The lower panels show evolution of slightly perturbed relative equilibria and their decay into generic turbulence. Each relative equilibrium has a reflection symmetric partner related by $u(x) \to -u(-x)$ travelling with velocity $-c$. (From ref. [7]).

Short term goals This list contains the work that is currently being worked on.

- `GuBuCv17.tex` rewrites
- `GuBuCv17.tex` figures
- `GuBuCv17.tex` references fleshed out
- More thorough description of adjoint descent(garnered a lot of attention at DS19)

Intermediate term goals This list represents the work I would like to complete in the next couple months.

- Investigate more numerical methods
- Investigate convergence as function of N, M
- Find better numerical method for smoothing boundaries of gluing and tiling (Chebyshev BVP, will give experience for non-

periodic boundary conditions of higher dimensional flows)
- Investigate and improve GMRES routine

Long term Goals This list contains the work I believe I could finish before I graduate; I list Kolmogorov flow because of what I have learned will dramatic improve the efficiency with which I can code.

- Migrate to Julia
- Finish papers and thesis
- Kolmogorov with periodic boundary conditions

Unicorn tier goals • Optimize Julia
- Kolmogorov with non-periodic boundary conditions
- Navier-Stokes with periodic boundary conditions
- Plane-Coutte and Pipeflow

Matt's GuBuCv17 to-do list

- `trawl.tex` edits
- `tile.tex` edits
- Add continuous family description of tiles (The misunderstandings of the tiles and how they're used were profound and ubiquitous)

Skimmed the paper by Goluskin and Fantuzzi [10]. I need to thoroughly study the variational principles therein but it's pretty confusing for me. Perhaps PC and I could walk through? Figure 1 (b) serves as corroborating evidence for my streak tile.

The problem and or question I have is: from a dynamical systems perspective we know that the antisymmetric flow invariant subspace is isolated and not representative of the dynamics of the full (no symmetry) Kuramoto-Sivashinsky equation. I understand that the equilibria exist in this subspace so am I supposed to take this as merely energy bounds for the antisymmetric subspace? I feel like that defeats the point but I don't know how else to interpret.

07-11-2019 Matt Ideas for automatic tiling using trinary tile alphabet

Method one Concatenate the scalar fields of each tile after ensuring the discretizations accurately reflect the relative sizes of the tiles. Fourier truncate the result. The most basic of methods that doesn't really take anything into consideration other than domain sizes.

Method two The first method is to take the original tiles and rediscretize them such that the aspect ratios between tiles accurately represent the different periods T and domain sizes L that the tiles exist on.

Put the appropriately sized tiles (making sure the relative sizes are demonstrated in the discretizations) together by padding them with a boundary of zeros and then sticking the newly sized tile plus zeros together.

This takes the sizes of the tiles and the fact that they are discontinuous into account.

Method three Take the existing (slightly modified and or cleaned up) gluing code to glue the tiles together to produce one large block of tiles that is an approximate solution. This is then the initial condition that is passed to the numerical methods.

Method four The general idea is glue plus converge at every step. This glues the tiles together in a pairwise manner just like method three, but also takes into consideration that the gluing combinations are only approximations to solutions and so this goes one step further by converging after each pairwise gluing

The quick descriptions given previously describe varying levels of difficulty in regards to implementation which is not necessarily indicative of improved performance.

There are a lot of important details which are so numerous that it is actually going to take a minute to compile them all. Currently they stand at: Making the sizes of tiles relative to one another in a manner that still allows them to be combined, all the while ensuring the "best" discretization is being used. Dealing with the numerical discontinuity that arises from combining tiles in space and time. Taking into account different symmetries of tiles and the blocks they are being used to produce.

The reason why this isn't straight forward is because it is best to take the time to automate it as opposed to hard coding in a case-by-case basis. As per usual in coding, I write something only to realize that there is a better way of doing it (rinse and repeat).

2019-07-29 Matt Symbolic Tiling code Running new script `blocks.py` along with some of its new subroutines `tile.py`.

The code attempts to initialize and converge spatiotemporal solutions created via combining tiles from a trinary alphabet. The alphabet contains the "streak" equilibrium solution, "gap" antisymmetric wave-equilibrium solution, and "defect" relative periodic (approximately half-cell shift solution).

The representatives chosen from each of the three continuous families is close to being antisymmetric. This is an intrinsic property for the gap and streak tiles but for the defect tile, one could elect to take the more "hook-like" member of the continuous family. The hook like pattern is a member of the continuous family which appears before numerical continuation in domain size results in a relative equilibrium solution. The reason for this choice is to ensure that the trinary alphabet is symmetry invariant. This seemed the more natural choice instead of having two antisymmetric tiles and then a third which has a reflection symmetry partner. That is, a truly trinary alphabet instead of trinary plus one symmetry partner. This might be

hopeful but its seems more elegant when the tiles have the most in common. Numerically, it seemed the most reasonable as the other members of the defect family have non-negligible spatial shift which makes it awkward to combine with the other tiles. In other words, it is nonsensical (to me) to combine a relative periodic tile with a regularly periodic tile. One of the corresponding tiles will be non-periodic, which only depends on whether one goes to a co-moving frame or not; again this makes no sense in the context of combining tiles.

The automated version of the code is first searching for combinations under the assumption that the result has no symmetry (i.e.its isotropy subgroup is the trivial subgroup). The tiles are combined in such a manner that they are first padded with a rectangular frame of zeros numerically, such that zero padded tiles are arranged in a mosaic like fashion. This zero padding is an attempt to cut down on the Gibbs' phenomenon error associated with discontinuities.

While we know the Kuramoto-Sivashinsky equation is linearly unstable, and hence, including regions of $u(x, t) = 0$ is a relatively unintelligent idea, the adjoint descent method works with such initial conditions by "filling in" these zero regions well. In other words, we know the adjoint descent brings us closer to invariant 2-torus solutions and therefore the zero filled regions are filled in by correcting the corresponding spatiotemporal tangent space with local solutions such that the entire spatiotemporal domain approaches a invariant 2-torus solution. If this last paragraph was as convoluted as I believe it might have been the general idea is that adjoint descent brings initial conditions closer to invariant 2-tori by correcting the tangent space (making it abide by Kuramoto-Sivashinsky equation.) Therefore, implementing regions with incorrect tangent space is not an issue, so long as it does not introduce discontinuities that make the numerical procedures fail.

2019-08-01 Matt : As a preface to the following blog post: for file names of tiling combinations, zero refers to streak, one refers to defect and two refers to gap. The format of the filenames is as follows (examples that have not been found yet)

The string `012 001` would represent symbolic block, i.e.the underscoring separates the temporal portions of the blocks.

$$M = \begin{bmatrix} 012 \\ 001 \end{bmatrix} \tag{17.38}$$

All tilings (so far) have assumed that the final solution has no symmetries (its isotropy subgroup is the trivial group).

Slightly worried about tiling results. From the initial conditions formed by simply zero-padding and then concatenating tiles the solutions (which
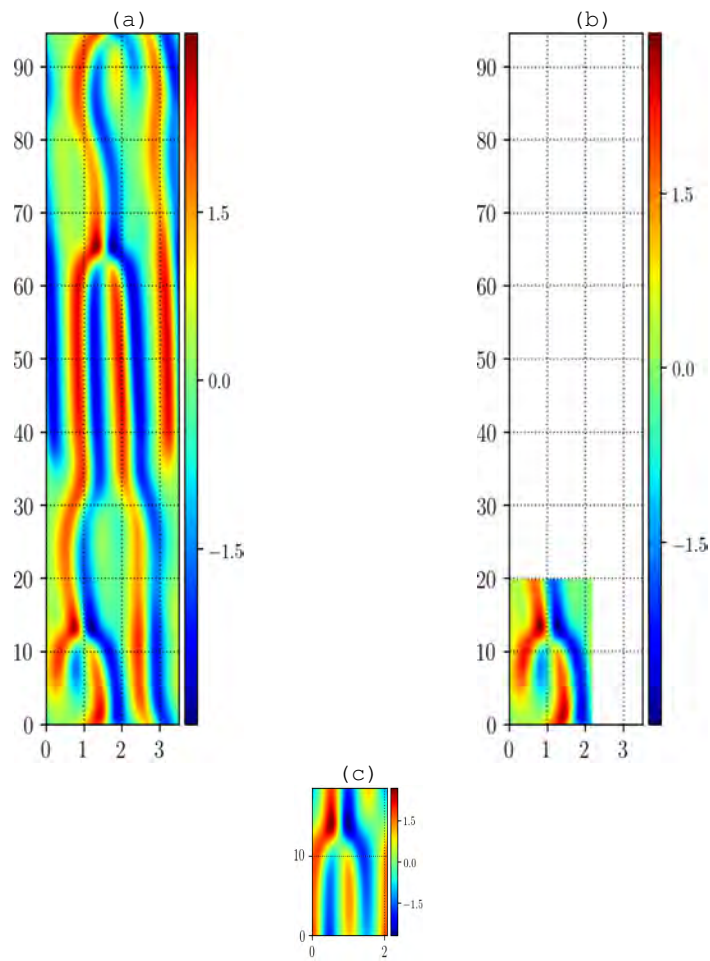
Figure 17.7: (a) Invariant 2-torus with spatial translation symmetry defined on approximate domain $x \in [0, \approx 3.5(2\pi)]$, $t \in [0, \approx 94.59]$. Truncation of significant digits is denoted by "$\approx$". (b) The extracted subdomain to serve as an initial condition for tile searching. Defined on domain size $x \in [0, 2.2(2\pi)]$, $t \in [0, 20]$.
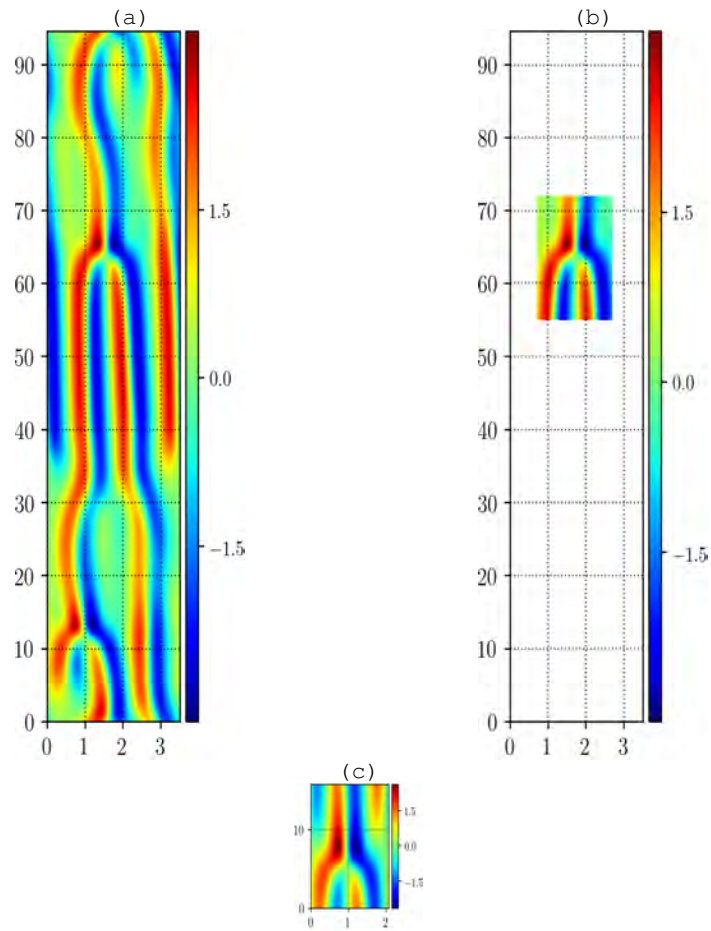
Figure 17.8:   (a) Invariant 2-torus with spatial translation symmetry defined on approximate domain $x \in [0, \approx 3.5(2\pi)]$, $t \in [0, \approx 94.59]$. Truncation of significant digits is denoted by "$\approx$" . (b) The extracted subdomain to serve as an initial condition for tile searching. Defined on domain size $x \in [0, 2(2\pi)]$, $t \in [0, 17]$.
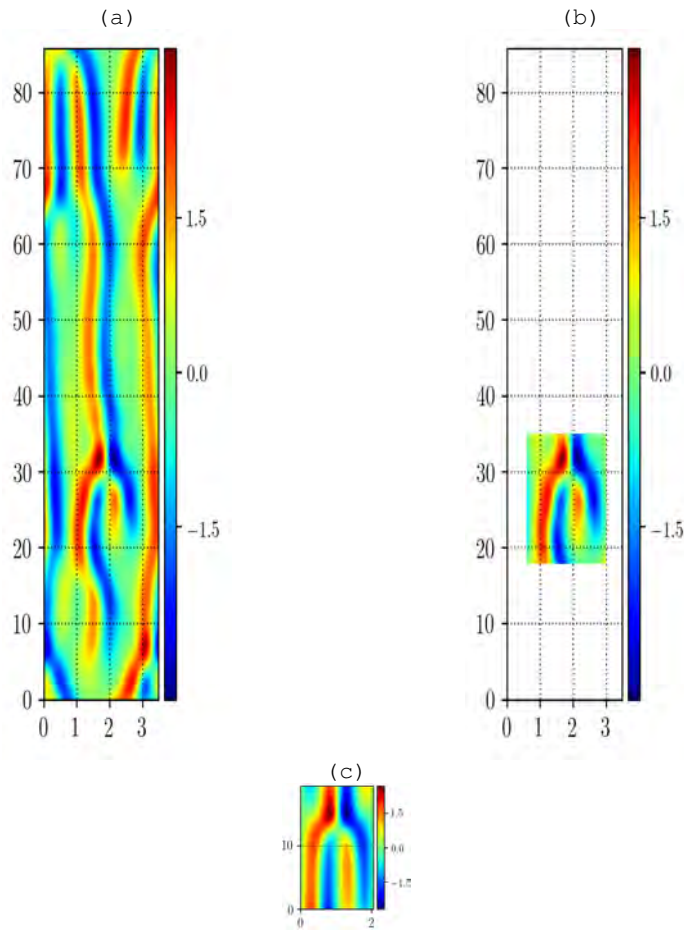
Figure 17.9: (a) Invariant 2-torus with spatial translation symmetry defined on approximate domain $x \in [0, \approx 3.5(2\pi)]$, $t \in [0, \approx 85.735]$. Truncation of significant digits is denoted by "$\approx$" . (b) The extracted subdomain to serve as an initial condition for tile searching. Defined on domain size $x \in [0, 2.6(2\pi)]$, $t \in [0, 17]$.
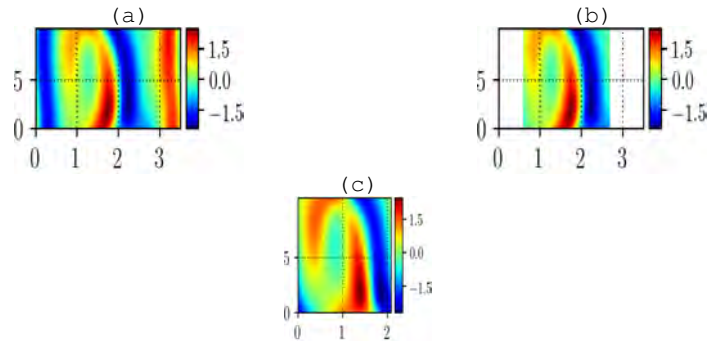
Figure 17.10: (a) Fundamental domain of Invariant 2-torus with spatiotemporal shift-reflection symmetry defined on $x \in [0, \approx 3.5(2\pi)]$, $t \in [0, \approx 10.25]$. Truncation of significant digits is denoted by "$\approx$" . (b) The extracted subdomain to serve as an initial condition for tile searching. Defined on domain size $x \in [0, 2.1(2\pi)]$, $t \in [0, 10.5]$.

have converged) look like they have too much structure as compared to where they initially begin. The result after only the first numerical method, adjoint descent, is more what I would think the tiles should converge to. As can be seen in figure 17.16. Even though my expectations are being betrayed it may just be a representation of the spatiotemporal grammar.

The streak defect spatial conjunction leads to what I believe to be a representation of a symbolic block of twice the temporal extent as what I started with. Specficically, I believe if I started with

$$\mathsf{M} = \begin{bmatrix} 01 \end{bmatrix} \tag{17.39}$$

it ends up converging (after Gauss-Newton) to the following

$$\mathsf{M} = \begin{bmatrix} 01^* \\ 01 \end{bmatrix} \tag{17.40}$$

Now obviously this is undesirable (if the targeted original symbolic block is admissible). I don't mean to sound braggadocios but perhaps this is due to the numerical methods working *too well*. Whether or not the defect tile is in its comoving frame (because its technically an relative periodic orbit with nearly a half-cell shift) does not seem to affect what solution the initial conditions converge to, up to spatial and temporal translations. I understand that it makes no sense to join something which is in a comoving frame with something that is not, but this shows that it doesn't seem to matter, numerically.

All of these facts seem to point to the fact that spatially concatenating a defect to a streak is not admissible; only the temporal concatenation (such
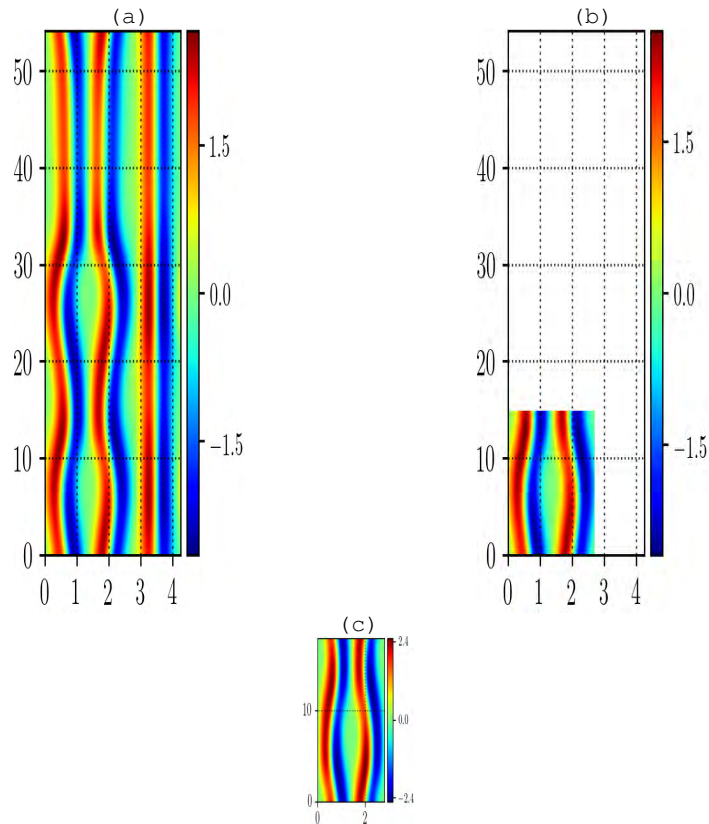
Figure 17.11: (a) Invariant 2-torus defined on $x \in [0, \approx 4.25(2\pi)]$, $t \in [0, \approx 54.12]$. Truncation of significant digits is denoted by "$\approx$". (b) The extracted subdomain to serve as an initial condition for tile searching. Defined on domain size $x \in [0, 2.7(2\pi)]$, $t \in [0, 15]$.
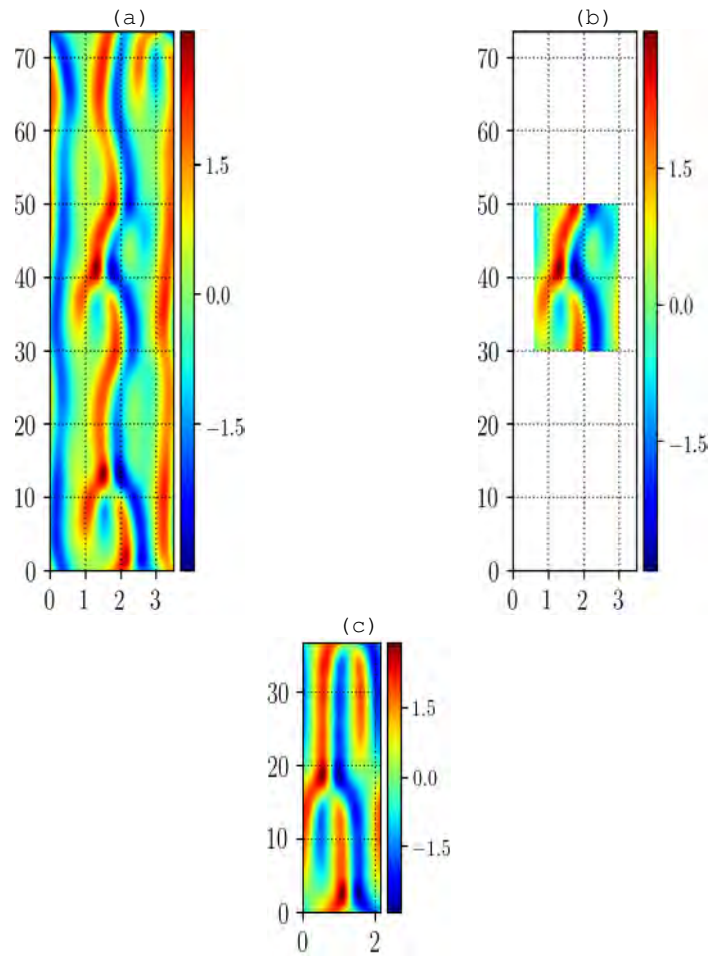
Figure 17.12: (a) Fundamental domain of invariant 2-torus with spatiotemporal shift-reflection symmetry defined on $x \in [0, \approx 21.97]$, $t \in [0, \approx 73.52]$. Truncation of significant digits is denoted by "$\approx$" . (b) The extracted subdomain to serve as an initial condition for tile searching. Defined on domain size $x \in [0, 2.4(2\pi)]$, $t \in [0, 20]$. Both figure 17.13 (c) and figure 17.14(c) demonstrate a similar pattern with similar spatiotemporal extent.
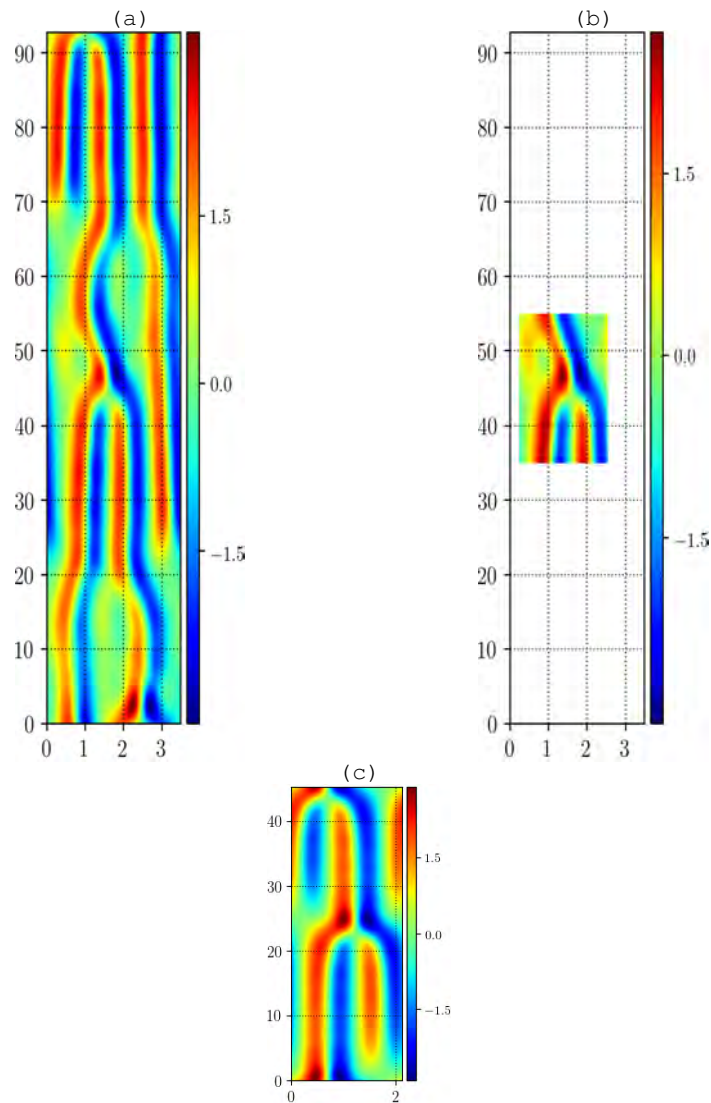
Figure 17.13: (a) Fundamental domain of Invariant 2-torus with spatiotemporal shift-reflection symmetry defined on $x \in [0, \approx 21.93]$, $t \in [0, \approx 92.77]$. Truncation of significant digits is denoted by "$\approx$" . (b) The extracted subdomain to serve as an initial condition for tile searching. Defined on domain size $x \in [0, 2.3(2\pi)]$, $t \in [0, 20]$. Both figure 17.12 (c) and figure 17.14 (c) demonstrate a similar pattern with similar spatiotemporal extent.
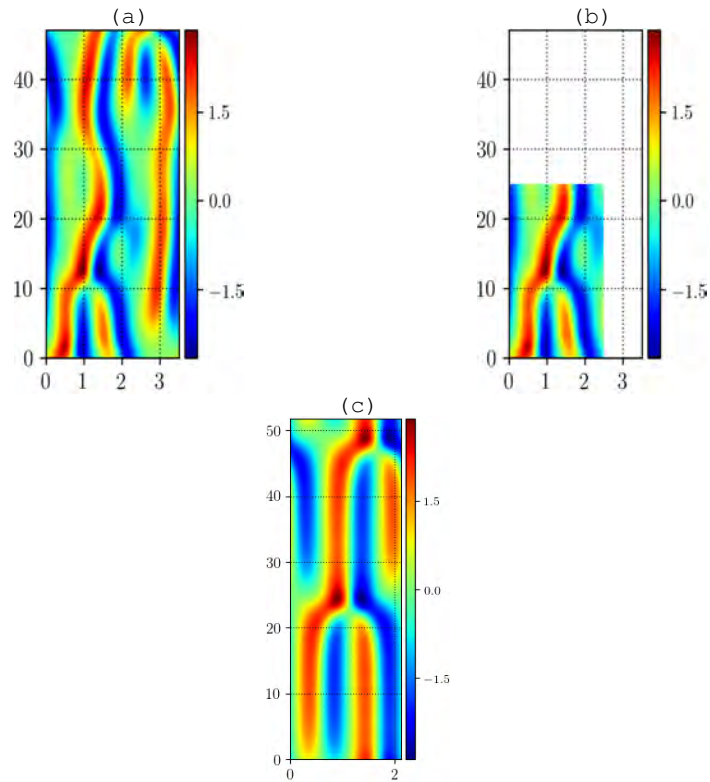
Figure 17.14: (a) Fundamental domain of Invariant 2-torus with spatiotemporal shift-reflection symmetry defined on $x \in [0, \approx 21.99]$, $t \in [0, \approx 47.77]$. Truncation of significant digits is denoted by "$\approx$". (b) The extracted subdomain to serve as an initial condition for tile searching. Defined on domain size $x \in [0, 2.5(2\pi)]$, $t \in [0, 25]$. Both figure 17.12 (c) and figure 17.13 (c) demonstrate a similar pattern with similar spatiotemporal extent.
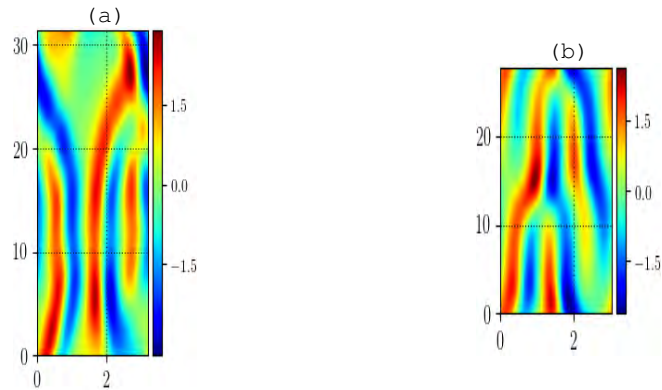
Figure 17.15: (a) Fundamental domain of Invariant 2-torus with spatiotemporal shift-reflection symmetry defined on $x \in [0, \approx 3.5(2\pi)]$, $t \in [0, \approx 10.25]$. Truncation of significant digits is denoted by "$\approx$" . (b) The extracted subdomain to serve as an initial condition for tile searching. Defined on domain size $x \in [0, 2.1(2\pi)]$, $t \in [0, 10.5]$.

that the result is a pre-periodic orbit.) seems to appear. The pre-periodic orbit in question (or rather, representatives of its continuous family) can be seen in part (c) of each figure 17.12, figure 17.13, and figure 17.14.

This is also evidenced by figure 17.18 and figure 17.17.

2019-08-05 Matt Added a number of tiling results which were found after some more tuning of the tiling methods. In order to not miss certain admissible spatiotemporal symbolic blocks, each symbolic block combination is looked for using an array of different discretizations, specifically, until a convergent solution is found (or until the available discretizations are depleted). The initial "minimum" discretization (fewest number of points) is given by $N_{\min} = \max(32, 2^{\log_2(T)+1})$, $M_{\min} = \max(32, 2^{\log_2(T)+1})$. The range of discretizations is $N = N_{\min}, ..., 2 * N_{\min}$, $M = M_{\min}, ..., 2 * M_{\min}$. These values are cycled through in a two loop recursion incrementally increasing by 4. The incremental increase (as opposed to a factor of 2 each time) is to ensure that the discretizations do not get too large; a situation which would eat up a gratuitous amount of computational time.

The solutions are always kept in a high resolution form and then the rediscretization (truncation, if you would like to think about it in spatiotemporal Fourier space) is applied at the beginning of each trial. This ensures that we are not truncating and then interpolating, merely truncating.

This helps convergence, but increases the computation time as the number of trials increases. This and other tuning efforts is the reason why I'm still working on the $1 \times M$ sized tilings. The number of runs increasing is taking a bit of time.

(a)   (c)
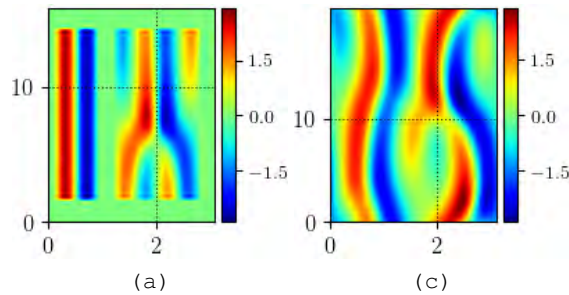
Figure 17.16: (a) Initial condition produced by taking defect and streak tiles, padded them with zeros (spatiotemporally in a window-pane like fashion), and then concatenating them. (b) The resulting spatiotemporal field after being passed through adjoint descent. (c) The fully converged solution, defined on $x \in [0, \approx 19.67], t \in [0, \approx 20.84]$.

(a)   (b)
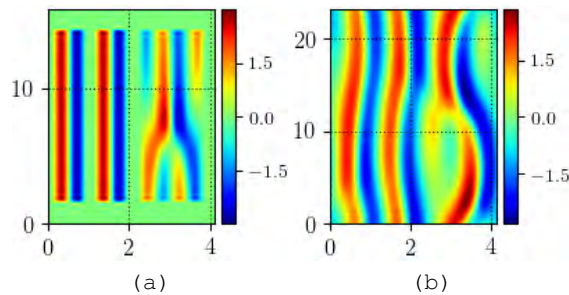
Figure 17.17: (a) Initial condition produced by taking one defect and two streak tiles, padded them with zeros (spatiotemporally in a window-pane like fashion), and then concatenating them spatially. (b) The resulting spatiotemporal field after being passed through adjoint descent. (c) The fully converged solution, defined on $x \in [0, \approx 25.90], t \in [0, \approx 23.15]$.

So far, after tuning, (a fancy way of saying trial & error) all tile combinations have been found when assuming no symmetries; again, the issue lies in whether the final, converged solutions actually pertain to the symbolic blocks in question.

Other than these tunings I've been getting back into improving the numerical side of the code; just can't seem to get enough of it.

The future work other than future tuning of the tiling; redoing the gluing method (similar but not the same to tiling), more numerical methods, working on the "average spectrum" initial conditions and "seeding" initial conditions, the latter is a process of embedding tiles (or blocks) in a large spatiotemporal domain.

I'm hoping to get to either Kolmogorov flow or Navier-Stokes doubly
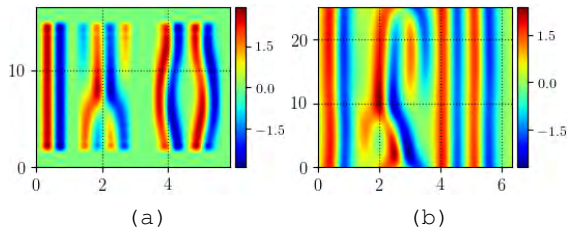
Figure 17.18: (a) Initial condition produced by taking a single defect, gap, and streak tile, padded them with zeros (spatiotemporally in a window-pane like fashion), and then concatenating them spatially. (b) The resulting spatiotemporal field after being passed through adjoint descent. (c) The fully converged solution, defined on $x \in [0, \approx 39.98]$, $t \in [0, \approx 24.97]$.

(triply) periodic flows before I leave; I could probably start one of these when tiling code is finished.

Instead of dwelling on continuous improvement/optimization of Kuramoto-Sivashinsky code I'm going to try to move onto a harder problem once the tiling code is exhausted.

I figure that my Kuramoto-Sivashinsky code can be used as a testing ground for things that I need to implement for Kolmogorov/Navier-Stokes doubly/triply periodic flows. I have most of the machinery as I've tried to make the numerical methods as modular as possible. (Literally just need to code Kolmogorov functions for the spatiotemporal function, matrix vector product, transpose matrix-vector product, FFTs).

This is, of course, as long as Predrag deems this appropriate; it seems premature because the paper isn't done yet but I want to try my hand at something new.

2019-08-06 Predrag What Predrag deems appropriate sounds like a broken record: "The paper / thesis does not write itself" "The paper / thesis does not write itself" "The paper / thesis does not write itself" "The paper / thesis does not write itself" $\cdots$ "The paper / thesis does not write itself"

If you follow what is going on with *kittens*, the other finished project, REALLY writing a readable, publishable paper, with publishable figures, correctly referenced and proofread always takes at least 3 times longer than one had planned, and in the process one discovers that there are many things one believed one understood, but did not, really.

At this point I would ration my time to 2/3rds paper / thesis writing, 1/3rd new research.

2019-08-14 Matt Added tiling figures and description to `tiles.tex` demonstrating how one can tile the spatiotemporal state space in a relatively straightforward manner, how it links with symbolic dynamics. Need to

figure out how to describe the false positives (i.e.finding solutions not corresponding to original tilings).

Splitting numerical methods descriptions to motivate a much mroe in depth discussion regarding global convergence properties, rates of convergence, etc.

2019-08-15 Matt Trying to expand the numerical methods section to look more professional by looking at global convergence and rates of convergence proofs for Gauss-Newton methods such as in [32] but haven't found anything for adjoint descent. Other, more commonly implemented iterative methods like GMRES [31] have papers on the convergence properties such as [23] but they vary in how intelligible they are, at least to me. I feel like perhaps the "adjoint descent method" from [9] is perhaps a previously derived method under a different name. Personally it seems too effective and straightforward of a derivation (in the discretized case it's just a fictitious time derivative of the cost functional construction comprised of the L_2 norm of the spatiotemporal "Feynmann equation" form of the Kuramoto-Sivashinsky equation. It seems too straightforward to have not been done before.

Starting a subsection of variational that discusses both the adjoint sensitivity analysis of [33] and [2] and Hill's formula from [3].

2019-08-19 Matt Hessian of the Kuramoto-Sivashinsky equation Lagrangian take two. in `variational.tex`

2019-08-20 Matt Expand `variational.tex` via discussions regarding Hill's formula [3], formal Lagrangians [15, 17], adjoint equations, adjoint sensitivity formulas, least squares shadowing refs. [2, 11, 21, 34, 37], calculus of variations and variational integrators refs. [19, 25].

2019-08-21 Matt `Variational.tex` started to get too convoluted. Outline stated here for writers benefit.

1. The point of transforming an IVP to a variational BVP
2. Introduction to variational notation and variational calculus?
3. cost functional and action functional
4. alternative to stability, sensitivity
5. adjoint sensitivity
6. least-squares shadowing
7. hill's formula

Read [4] to add details regarding "least-norm optimization" problems

2019-08-22 Matt Still fixing variational.tex

I want to be able to apply [12] to the paper but I haven't figured it out yet; I think perhaps if I use [35] as a guide I can do it but will focus on writing for now.

2019-08-24 Matt Found [29] through references of [1] which really inspired
me to give Lie Group analysis of Kuramoto-Sivashinsky equation and its
(formal) Lagrangian another go. Wrote a Mathematica script to help in
this regard; Everything is matching up this time I just need a little more
time to finish it up.

This and a few other resources which I will add soon gave me some clar-
ity into the steps I was missing from papers such as [17]. There was just
a few details I needed help on and [29] did the trick I think.

In other news; I found a paper regarding a certain explicit transformation
that also applies to the Kuramoto-Sivashinsky equation I believe which
is possibly a different way to handle Galilean velocity in the spirit of
Predrag's idea of matching tiles with said quantity varying. Details in
[26], the concept is that a generalized Kuramoto-Sivashinsky equation,
with addition of a forcing term, can be transformed back into the original
Kuramoto-Sivashinsky equation(by the same transformation they list for
KdV). The specific form of everything leads to the interpretation that the
forcing is due to the acceleration of the x axis. Which gives a transforma-
tion to an accelerating coordinate frame as implied by the section title of
the paper.

2019-08-26 Matt nonlinear transformation . From [26] The generalized Ku-
ramoto-Sivashinsky equation

$$u_t + u_{xx} + u_{xxxx} + uu_x = y_{tt} \tag{17.41}$$

with notable time-dependent "forcing term" can be transformed back
to the original Kuramoto-Sivashinsky equation via the set of trans-
formations

$$
\begin{aligned}
t^{'} &= t \\
x^{'} &= x - y(t) \\
u(x,t) &= u^{'}(x^{'},t^{'}) + y_{t'}(t^{'})
\end{aligned}
\tag{17.42}
$$

back to the original Kuramoto-Sivashinsky equation in primed vari-
ables.

Galilean transformations are a specific example of this transforma-
tion as can be readily seen by the substitution $y(t) = vt$, v being the
Galilean velocity.

nonlinearly self-adjointness Following Ibragimov's idea of nonlinear self
adjointness, i.e. set adjoint variable equal to some arbitrary function
of u and its derivatives and find solutions to the adjoint equation.

Unfortunately the only solution is the constant solution meaning
that both the "conservation law" from `variational.tex` is trivial

and always satisfied so that the entire process is ostensibly worthless. The only saving grace would be to look for variational symmetries (symmetries of the Lagrangian itself as opposed to equations), but [29] says that variational symmetries (of a Lagrangian) are always symmetries of the corresponding Euler-Lagrange equations, but not vice-versa. Meaning, that we already have all symmetries of the governing equations such that there are no alternative options.

It seems that the Kuramoto-Sivashinsky equation is just too simple (in terms of symmetries) to benefit from this type of analysis. Note that we did not investigate the role of parameters such as T and L as thats not really the purview of this investigation.

In other words, this investigation that took quite a bit of time for me to not only understand but implement in Mathematica bore no fruit. In fact, there isn't even a tree for said fruit.

2019-08-27 Matt Variational stuff copied from `variational.tex`

$$\mathrm{pr}v^{(4)} = \epsilon(x,t,u)\frac{\partial}{\partial x} + \tau(x,t,u)\frac{\partial}{\partial t} + \phi(x,t,u)\frac{\partial}{\partial u} + \phi^t(x,t,u^{(1)})\frac{\partial}{\partial u_t} + \phi^x(x,t,u^{(1)})\frac{\partial}{\partial u_x} + \phi^{xx}(x,t,u^{(2)})$$
$$(17.43)$$

because all other terms will annihilate when acting on the Kuramoto-Sivashinsky equation. Note that the higher the order of the coefficient the more terms it depends on due to the differentiation that takes place in (**??**)

Now that we have the general form of the vector field we can begin to derive the *infinitesimal generators* which span the Lie algebra. To accomplish this, we will derive the *determining equations* which are produced by applying (**??**) to the system of differential equations and equating to zero, that is

$$\mathrm{pr}v^{(4)}(G(u^{(\alpha)}(x,t), u_{(1)}^{(\alpha)}(x,t), \ldots, u_{(n)}^{(\alpha)}(x,t))) = 0 \qquad (17.44)$$

performing this operation yields the following equation

$$\phi^t + \phi^{xx} + \phi^{xxxx} + u\phi^x + \phi u_x = 0 \,. \qquad (17.45)$$

We finally are forced to derive the coefficients ϕ^J and to include as many details as possible we will write the exact formulas needed to derive them as well as the long form expressions that they are equal to.

$$
\begin{aligned}
\phi^t &= D_t(\phi(x,t,u) - \epsilon(x,t,u)u_x - \tau(x,t,u)u_t) + \tau(x,t,u)u_t t + \epsilon(x,t,u)u_x t \\
\phi^x &= D_x(\phi(x,t,u) - \epsilon(x,t,u)u_x - \tau(x,t,u)u_t) + \tau(x,t,u)u_t x + \epsilon(x,t,u)u_x x \\
\phi^{xx} &= D_x^2(\phi(x,t,u) - \epsilon(x,t,u)u_x - \tau(x,t,u)u_t) + \tau(x,t,u)u_{txx} + \epsilon(x,t,u)u_{xxx} \\
\phi^{xxxx} &= D_x^4(\phi(x,t,u) - \epsilon(x,t,u)u_x - \tau(x,t,u)u_t) + \tau(x,t,u)u_{txxx} + \epsilon(x,t,u)u_{xxxx}
\end{aligned}
\qquad (17.46)
$$

where D_t and D_x represent *total differentiation* operators,

$$D_i = \frac{\partial}{\partial x^i} + u_i \frac{\partial}{\partial u} + u_{ii} \frac{\partial}{\partial u_i} + \dots \tag{17.47}$$

the long form expressions from each of these are

$$\phi^t = u_t^2 \left(-\tau_u\right) - \tau_t u_t - u_t u_x \epsilon_u - \epsilon_t u_x + u_t \phi_u + \phi_t \tag{17.48}$$

$$\phi^x = -u_t \tau_u u_x - u_t \tau_x + u_x^2 \left(-\epsilon_u\right) - u_x \epsilon_x + u_x \phi_u + \phi_x \tag{17.49}$$

$$
\begin{aligned}
\phi^{\text{xx}} \;=\; & -u_t u_x^2 \tau_{\text{uu}} - 2 u_t u_x \tau_{\text{xu}} - u_t \tau_u u_{\text{xx}} \\
& -\; u_t \tau_{\text{xx}} + u_x^3 \left(-\epsilon_{\text{uu}}\right) + u_x^2 \phi_{\text{uu}} \\
& -\; 2 \tau_u u_x u_{\text{xt}} - 2 u_{\text{xt}} \tau_x - 2 u_x^2 \epsilon_{\text{xu}} \\
& +\; 2 u_x \phi_{\text{xu}} - 3 u_x u_{\text{xx}} \epsilon_u - u_x \epsilon_{\text{xx}} \\
& -\; 2 u_{\text{xx}} \epsilon_x + u_{\text{xx}} \phi_u + \phi_{\text{xx}}
\end{aligned}
\tag{17.50}
$$

$$
\begin{aligned}
\phi^{\text{xxxx}} \;=\; & -4 u_t u_x u_{\text{xxx}} \tau_{\text{uu}} - 3 u_t u_{\text{xx}}^2 \tau_{\text{uu}} - 6 u_t u_x^2 u_{\text{xx}} \tau_{\text{uuu}} - u_t u_x^4 \tau_{\text{uuuu}} \\
& -\; 12 u_t u_x u_{\text{xx}} \tau_{\text{xuu}} - 4 u_t u_x^3 \tau_{\text{xuuu}} - 6 u_t u_x^2 \tau_{\text{xxuu}} - 4 u_t u_x \tau_{\text{xxxu}} - 4 u_t u_{\text{xxx}} \tau_{\text{xu}} \\
& -\; 6 u_t u_{\text{xx}} \tau_{\text{xxu}} - u_t \tau_u u_{\text{xxxx}} - u_t \tau_{\text{xxxx}} - 12 u_x u_{\text{xt}} u_{\text{xx}} \tau_{\text{uu}} \\
& -\; 15 u_x u_{\text{xx}}^2 \epsilon_{\text{uu}} - 6 u_x^2 u_{\text{xxt}} \tau_{\text{uu}} - 10 u_x^2 u_{\text{xxx}} \epsilon_{\text{uu}} + 4 u_x u_{\text{xxx}} \phi_{\text{uu}} \\
& +\; 3 u_{\text{xx}}^2 \phi_{\text{uu}} - 4 u_x^3 u_{\text{xt}} \tau_{\text{uuu}} - 10 u_x^3 u_{\text{xx}} \epsilon_{\text{uuu}} + 6 u_x^2 u_{\text{xx}} \phi_{\text{uuu}} \\
& +\; u_x^5 \left(-\epsilon_{\text{uuuu}}\right) + u_x^4 \phi_{\text{uuuu}} - 12 u_x^2 u_{\text{xt}} \tau_{\text{xuu}} - 12 u_x u_{\text{xt}} \tau_{\text{xxu}} \\
& -\; 12 u_x u_{\text{xxt}} \tau_{\text{xu}} - 16 u_x u_{\text{xxx}} \epsilon_{\text{xu}} - 24 u_x^2 u_{\text{xx}} \epsilon_{\text{xuu}} + 12 u_x u_{\text{xx}} \phi_{\text{xuu}} \\
& -\; 4 u_x^4 \epsilon_{\text{xuuu}} + 4 u_x^3 \phi_{\text{xuuu}} - 18 u_x u_{\text{xx}} \epsilon_{\text{xxu}} - 6 u_x^3 \epsilon_{\text{xxuu}} + 6 u_x^2 \phi_{\text{xxuu}} \\
& -\; 4 \tau_u u_x u_{\text{xxxt}} - 4 u_{\text{xxxt}} \tau_x - 4 u_x^2 \epsilon_{\text{xxxu}} + 4 u_x \phi_{\text{xxxu}} - 5 u_x u_{\text{xxxx}} \epsilon_u - u_x \epsilon_{\text{xxxx}} \\
& -\; 4 u_{\text{xxxx}} \epsilon_x - 12 u_{\text{xt}} u_{\text{xx}} \tau_{\text{xu}} - 4 \tau_u u_{\text{xt}} u_{\text{xxx}} - 4 u_{\text{xt}} \tau_{\text{xxx}} \\
& -\; 12 u_{\text{xx}}^2 \epsilon_{\text{xu}} + 4 u_{\text{xxx}} \phi_{\text{xu}} - 6 \tau_u u_{\text{xx}} u_{\text{xxt}} - 6 u_{\text{xxt}} \tau_{\text{xx}} \\
& +\; 6 u_{\text{xx}} \phi_{\text{xxu}} - 10 u_{\text{xx}} u_{\text{xxx}} \epsilon_u - 6 u_{\text{xxx}} \epsilon_{\text{xx}} - 4 u_{\text{xx}} \epsilon_{\text{xxx}} \\
& +\; u_{\text{xxxx}} \phi_u + \phi_{\text{xxxx}}
\end{aligned}
\tag{17.51}
$$

upon substitution into (17.45) we can separate the terms by coefficients of monomials which gives us the determining equations as previously

mentioned

$$\phi_t + \phi_{xx} + \phi_{xxxx} = 0$$
$$-4\tau_x = 0$$
$$-6\tau_{xx} = 0$$
$$-2\tau_x - 4\tau_{xxx} = 0$$
$$-4\epsilon_x + \tau_t + \tau_{xx} + \tau_{xxxx} = 0$$
$$4\phi_{xu} - 6\epsilon_{xx} = 0$$
$$-4\tau_u = 0$$
$$4\tau_{xu} = 0$$
$$-2\epsilon_x - 4\epsilon_{xxx} + \tau_t + \tau_{xx} + \tau_{xxxx} + 6\phi_{xxu} = 0$$
$$-6\tau_u = 0$$
$$-12\tau_{xu} = 0$$
$$6\tau_{xxu} = 0$$
$$4\tau_{xu} - 10\epsilon_u = 0$$
$$-12\epsilon_{xu} + 6\tau_{xxu} + 3\phi_{uu} = 0$$
$$3\tau_{uu} = 0$$
$$3\tau_{uu} = 0 \tag{17.52}$$
$$\phi - \epsilon_t - \epsilon_{xx} - \epsilon_{xxxx} + 2\phi_{xu} + 4\phi_{xxxu} = 0$$
$$-4\tau_u = 0$$
$$-12\tau_{xu} = 0$$
$$-2\tau_u - 12\tau_{xxu} = 0$$
$$-4\epsilon_u + 2\tau_{xu} + 4\tau_{xxxu} = 0$$
$$4\phi_{uu} - 16\epsilon_{xu} = 0$$
$$4\tau_{uu} = 0$$
$$-2\epsilon_u - 18\epsilon_{xxu} + 2\tau_{xu} + 4\tau_{xxxu} + 12\phi_{xuu} = 0$$
$$-12\tau_{uu} = 0$$
$$12\tau_{xuu} = 0$$
$$4\tau_{uu} = 0$$
$$12\tau_{xuu} - 15\epsilon_{uu} = 0$$
$$-2\epsilon_{xu} - 4\epsilon_{xxxu} + \phi_{uu} + 6\phi_{xxuu} = 0$$
$$-6\tau_{uu} = 0$$
$$-12\tau_{xuu} = 0$$

$$\tau_{uu} + 6\tau_{xxuu} = 0$$
$$-10\epsilon_{uu} = 0$$
$$-24\epsilon_{xuu} + \tau_{uu} + 6\tau_{xxuu} + 6\phi_{uuu} = 0$$
$$6\tau_{uuu} = 0$$
$$6\tau_{uuu} = 0$$
$$-\epsilon_{uu} - 6\epsilon_{xxuu} + 4\phi_{xuuu} = 0$$
$$-4\tau_{uuu} = 0$$
$$4\tau_{xuuu} = 0$$
$$4\tau_{xuuu} - 10\epsilon_{uuu} = 0$$
$$\phi_{uuuu} - 4\epsilon_{xuuu} = 0$$
$$\tau_{uuuu} = 0$$
$$\tau_{uuuu} = 0$$
$$-\epsilon_{uuuu} = 0$$
$$\phi_x = 0$$
$$\tau_x = 0$$
$$\tau_x = 0$$
$$-\epsilon_x + \tau_t + \tau_{xx} + \tau_{xxxx} = 0$$
$$4\tau_{xu} = 0$$
$$6\tau_{xxu} = 0$$
$$3\tau_{uu} = 0$$
$$2\tau_{xu} + 4\tau_{xxxu} = 0$$
$$4\tau_{uu} = 0$$
$$12\tau_{xuu} = 0$$
$$\tau_{uu} + 6\tau_{xxuu} = 0$$
$$6\tau_{uuu} = 0$$
$$4\tau_{xuuu} = 0$$
$$\tau_{uuuu} = 0$$
$$\tau_x = 0$$

While initially intimidating, these equations can be solved by noticing the lower order equations such as $\tau_x = \tau_u = 0$ which means that τ can only be a function of t. Following this reasoning we find that in fact

$$
\begin{aligned}
\tau(x,t,u) &= \tau = c_1 \\
\epsilon(x,t,u) &= \epsilon(t) = c_3 t + c_1 \\
\phi(x,t,u) &= \phi = c_3
\end{aligned}
\tag{17.53}
$$

such that the Lie algebra of infinitesimal symmetries is spanned by

$$
\begin{aligned}
v_1 &= \partial_x \\
v_2 &= \partial_t \\
v_3 &= t\partial_x + \partial_u
\end{aligned}
\tag{17.54}
$$

which are the generators of space and time translations as well as Galilean transformations. This is not surprising as these symmetries are well known [5] but we need to know the prolongations of (17.54) and their extensions to the adjoint variables present in (**??**).

The prolongations of (17.54) results in

$$
\begin{aligned}
\mathrm{pr}v_1 &= y_1 = \partial_x \\
\mathrm{pr}v_2 &= y_2 = \partial_t \\
\mathrm{pr}v_3 &= y_3 = \partial_x + \partial_u - u_x \partial_{u_t} \, .
\end{aligned}
\tag{17.55}
$$

We can now derive the extended versions of (**??**) such that we can apply them to the formal Lagrangian (**??**) Once again we follow the machinery of Ibragimov to extend (17.55) to the adjoint variables. Unfortunately it seems that the symmetries were too simple to actually have extensions to the adjoint variables, but we can still go forward with the conservation law calculations regardless. Both [12] and [29] both work through the proof that there is a conserved vector (as Ibragimov calls it) such that its divergence provides a conservation law (technically infinite number of conservation laws because they are equations involving PDE solutions). The components of the conserved vector (one for each independent variable) are given by

$$
C^i = \xi^i \mathcal{L} + W^\alpha \Big[\frac{\partial \mathcal{L}}{\partial u_i^\alpha} - D_j \frac{\partial \mathcal{L}}{\partial u_{ij}^\alpha} + D_j D_k \frac{\partial \mathcal{L}}{\partial u_{ijk}^\alpha} - + D_j D_k D_l \frac{\partial \mathcal{L}}{\partial u_{ijkl}^\alpha} \Big] + D_j(W^\alpha) \Big[\frac{\partial \mathcal{L}}{\partial u_{ij}^\alpha} - D_k \frac{\partial \mathcal{L}}{\partial u_{ijk}^\alpha} + D_k D_l \frac{\partial}{\partial u}
\tag{17.56}
$$

where the equation has been extended to include all possible non-zero terms in the context of the Kuramoto-Sivashinsky equation, W^α is shorthand for $\phi^\alpha + \xi^i u_i^\alpha$. Applying this to our generators yields one unique conservation law which we shall now detail.

For the Galilean transformation generator $\mathrm{pr}v_3 = t\partial_x + \partial_u - u_x \partial_{u_t}$ the components equal

$$
\begin{aligned}
C^x &= t * \mathcal{L} + W\Big[\frac{\partial \mathcal{L}}{\partial u_x} - D_x \frac{\partial \mathcal{L}}{\partial u_{xx}} - D_x^3 \frac{\partial \mathcal{L}}{\partial u_{xxxx}} \Big] \\
&+ D_x(W)\Big[\frac{\partial \mathcal{L}}{\partial u_{xx}} + D_x^2 \frac{\partial \mathcal{L}}{\partial u_{xxxx}} \Big] \\
&+ D_x^2(W)\Big[-D_x \frac{\partial \mathcal{L}}{\partial u_{xxxx}} \Big] \\
&+ D_x^3(W)\Big[\frac{\partial \mathcal{L}}{\partial u_{xxxx}} \Big] \\
C^t &= 0 * \mathcal{L} + (1 - tu_x)\Big[\frac{\partial \mathcal{L}}{\partial u_t} \Big]
\end{aligned}
\tag{17.57}
$$

which both simplify to

$$
\begin{aligned}
C^x &= t(u_t v + u_x v_x + u_x v_{xxx} + u_{xxx} v_x + u_{xx} v_{xx}) + uv - v_x - v_{xxx} \\
C^t &= v_t - vu_x - u_x v_t t
\end{aligned}
\tag{17.58}
$$

such that the conservation law is given by the divergence

$$
\begin{aligned}
D_x(C^x) + D_t(C^t) &= 0 \\
&= v_t - vu_x - u_x v_t t + uv_x + vu_x - v_{xx} - v_{xxxx} \\
&+ t(v_x(u_t + u_{xx} + u_{xxxx}) + u_x(v_x x + v_x xxx) + 2D_x(u_{xx} v_{xx})) \\
&= t(v_x(u_t + u_{xx} + u_{xxxx}) + u_x(-v_t + v_{xx} + v_{xxxx}) + +2D_x(u_{xx} v_{xx})) \\
&= 2D_x(u_{xx} v_{xx}).
\end{aligned}
\tag{17.59}
$$

where multiple times we have substituted one of the equations from (**??**).

The conserved quantity

$$
D_x(u_{xx} v_{xx}) = 0
\tag{17.60}
$$

Or upon integration (note: there is implicit time dependence)

$$
u_{xx} vxx = y(t)
\tag{17.61}
$$

Following the analysis of Burgers' equation and the prescription of [17] we find an alternative form of the Lagrangian for the Kuramoto-Sivashinsky equation to be

There are various choices for For instance, if upon substitution $v = u$ into the adjoint equation reproduces the original equation, the equation is said to be *self-adjoint*. Introduced in [15] there are the notions of self-adjoint, quasi-self-adjoint and nonlinearly-adjoint equations.

2019-08-27 Matt I was being stubborn and had an idea regarding the variational stuff. I thought the adjoint variable $v(x,t) = u(-x,-t) = R_x R_t u(x,t)$ given by space and time reflections would solve the adjoint equation as it would flip the sign on the single derivative times but after wasting some time I realized this type of answer could never work due to the presence of $u(x,t)$ in the adjoint equations. In other words, I would retrieve something very close to the Kuramoto-Sivashinsky equation but not exactly it; therefore not being an answer.

2019-08-29 Matt Investigations into the rate of convergence of the adjoint descent method and just adjoint methods in optimization in general have lead to the revelation that the adjoint descent method, when applied to my spatiotemporal problem at least, is merely the steepest descent algorithm applied to the cost functional $\mathcal{L} = 1/2||F||^2$.

The derivation was written in `adjointdescent.tex`. This means that there should be room for numerical improvements.

2019-09-09 Matt Crunch time as the September 30th deadline is fast approaching

Focusing on expanding the writing in `trawl.tex`, `tiles.tex`, `glue.tex` (the results basically).

I wish I had more time because my codes need to be refactored yet again because they are simply getting too large and convoluted; I began the process but the shift is so large I am keeping all records of my work on github and trying to keep this as a tertiary, weekend job.

The goal is to completely revamp the project (and as a symbolic action I am going to rename the project to "torihunter".) to be much more object oriented. Currently it takes a rather intimate knowledge of the package to be able to write scripts, and it is also specific to the Kuramoto-Sivashinsky equation. By switching to object oriented programming, a general "Torus" class can be instantiated such that instead of using specific functions, general class methods can be used (basically the way to go about it is to pass functions as a class method. The general idea is that we should be able to pass *any* Jacobian and spatiotemporal function and have the numerical methods work, not just ones specific to the Kuramoto-Sivashinsky equation). The manner by which to pass spatiotemporal symmetry constraints (on the Fourier modes, I mean) is to have this built into the functions themselves.

2019-09-11 Matt Writing and running scripts which quantify the dependence on the size of the spatiotemporal discretization. Specifically I'm going to do two things. Produce plots that demonstrate the rate of convergence depending on N, M for various L, T. Also, for some given initial conditions known to converge at $\tilde{N}, \tilde{M}$, investigate the rate of convergence for $N_i, M_i < \tilde{N}, \tilde{M}$, to see if this informs us on how to minimize N, M. This information will go into `trawl.tex` as it is regarding the finding of solutions.

2019-09-12 Matt Migrated `variational.tex` Ibragimov stuff to `LieGroupAnalysis.tex` More `trawl.tex` edits, more work on `convergence_rate.py` to produce analyses on discretization sizes.

2019-09-23 Matt Got lost in the weeds trying to see if I could apply machine learning to find the "faces" of the Kuramoto-Sivashinsky equation. Specifically, "Gabor wavelets" (just a modulated Gaussian in two dimensions) [22] can be used as image processing filter and pick out "features" which can be applied to facial recognition [24].

Started to write ideas relating the spatiotemporal continuation methods to demonstrate how useful they are in the plumber's world. The basic benefits are

1. Reynolds number continuation to compare and reproduce data
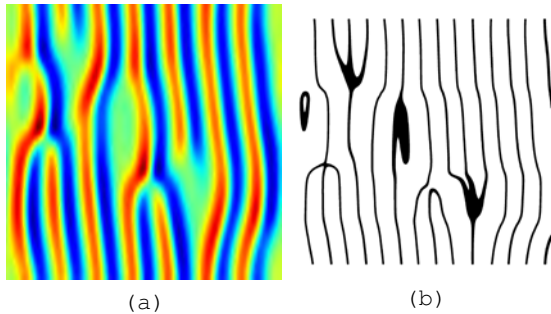
Figure 17.19: (a) Invariant 2-torus converged in full state space purported to be symbolic block 1012 (spatial sequence). (b) Local maxima peak detection of (a) using skimage package.

2. Domain size continuation to compare and reproduce data

3. Geometry continuation? (maybe? likely very very ill conditioned)

4. Able to transform data to match experiments. Idea is that one of the most common things to change in experimental setup is the size of spatial domains.

5. Being able to analyze the full spatiotemporal state space of all parameter values (as dictated by equations) instead of mistaking a tree for the forest.

2019-09-23 Matt Further investigation into image processing in the spirit of facial recognition of the "faces" of the Kuramoto-Sivashinsky equation. There are of course many many things to take into account but the main goal of this was to create a way to detect tiles embedded in shadowing orbits. Partial success so far; although features can be detected I haven't figured out a way to classify them numerically; I have a good idea for how to do so manually however.

If one takes any solution to the Kuramoto-Sivashinsky equation, invariant 2-torus or otherwise; and passes it through a image processing routine which picks out the local maxima based on image data alone (easier that making mistakes and trying to implement by hand, using skimage Python package). This produces figure 17.19 which demonstrates what picking out the local maxima would look like. The results (with these parameters, to be specific) are quite striking. Recall that we're using these methods to detect features which correspond to tiles. It appears in figure 17.19(b) that streaks are represented by, well, streaks. *New* streaks however leave a signature of an upwards facing pitchfork, while mergers are represented by downward facing pitchforks (in this case there is an example of an "imperfect pitchfork" like from bifurcation theory). There is a thick wishbone type shape which represents a gap and an annulus
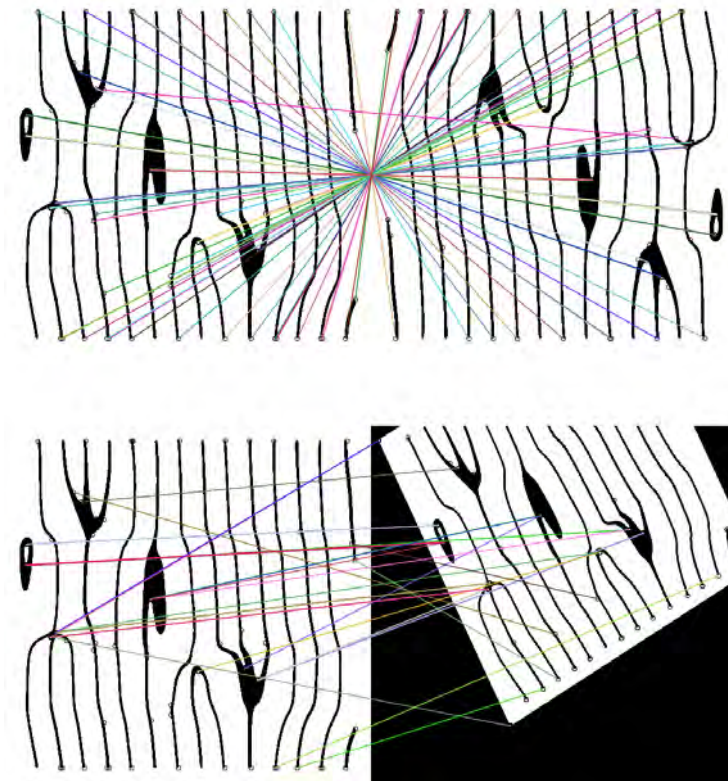
Figure 17.20: (a) Feature detection "ORB" routine applied to figure 17.19(b).

on the left side on the domain which appears to represent either a hook (member of the merger tile family) or another gap; this is hard to distinguish because of boundary effects.

The reason why these features are useful is because we can categorize all members of the tile continuous families with one distinct shape even more distinct than the color coded tiles. Using these shapes as indicators, I believe we may confidently say that this tile is not a representation of the spatial sequence 1012 as previously believed. Venturing a guess; this is a much more complicated such as

$$M = \begin{bmatrix} 0\,0\,0\,0\,0\,0\,0 \\ 2\,2\,2\,2\,0\,0\,0 \\ 0\,1\,0\,1\,0\,0\,0\,0\,0\,0\,0\,0\,0\,0 \end{bmatrix} \tag{17.62}$$

but this is a quick guess.s

Let us assume that these categorizations using new codes are valid; how do we use them? Luckily for us there is already code which can be used for feature detection; that is, it picks out features in images that are robust

(a)
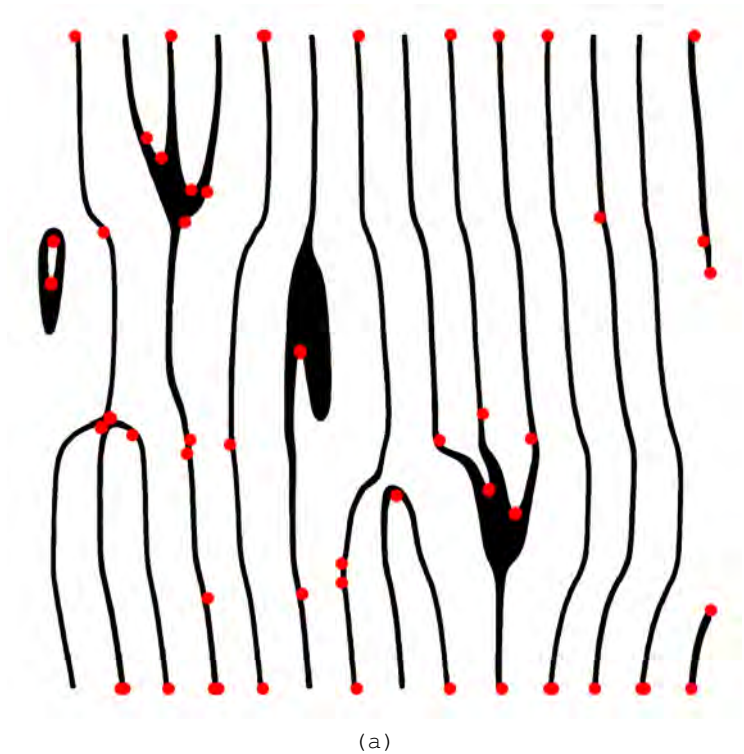
Figure 17.21: The "detected" points indicating features in the image data (without parameter tuning)s.

under affine transformations and scalings (they can be detected before and after the transformation, that is).

A beginner's level application of the feature detecting routines provides at least some "detections" around the key features described previously (upward/downward pitchfork, streaks, etc.). This can likely be tuned to reduce the number of detections of streaks; this is desireable because if we find the number (and location) of gaps and mergers, we can fill out the rest of the invariant 2-torus with streaks.

The `.png` files used in figure 17.19 are kept as large files for future use, as these methods directly use image data.

2019-10-11 Matt I tried to derive a clean result for the spatiotemporal Kuramoto-Sivashinsky equation which follows the course of action of Predrag's stability derivation but the results are inconsistent with the stability properties of the tests performed with $L = 22$ orbits with well known stability properties.

I will walk through the derivation now and hopefully someone can tell

me where I have gone wrong. I work in spatiotemporal Fourier space because not only is it most familiar but also I wanted to investigate spatial stability as well. We begin with the analog of the vector $\hat{p}$ which instead of a collection of state-space points we have a finite dimensional representation of the infinite dimensional scalar field $u(x,t)$ in spatiotemporal Fourier space. I will label the spatiotemporal modes by $\tilde{u}_{kj}$, k for space and j for time. I'm using the convention $u(x_m, t_n) \equiv u_n$ for time indices to simplify the expressions. We can use an analog of the multishooting difference function F (20.4).

$$F(\hat{u}) = \quad \hat{u} - g \circ (\hat{u} + v(\hat{u})\delta t) \tag{17.63}$$

Put very simply, this maps the field, reorders it, and then subtracts it from the original. The indices for both terms are now the same thanks to the rotation; there are implied indices which correspond to x_m and t_n The reason that I pursued a form was because I thought that I could make a block diagonal if not diagonal form. My original error was that I thought I could make use of the spectral differentiation operator $\hat{u}_t = \sum_{k,j} i w_j \hat{\tilde{u}}_{k,j} e^{i(w_j t_n + q_k x_m)}$. This is equivalent to multiplication by a diagonal matrix whose diagonal is k copies of iw_j. The problem with this is that yes; it produces the exact same velocity field $u_t = -u_{xx} - u_{xxxx} - uu_x$ but the linearization is not at all the same and as such gives us a nonsensical J which doesn't even depend on $\tilde{u}$. This was clearly wrong; substitution of $u_t = -u_{xx} - u_{xxxx} - uu_x$ yields

$$F(\hat{u}) = \quad \tilde{u}_{k,j} - \exp^{iw_j \delta t}\left(\tilde{u}_{k,j} + [(q_k^2 - q_k^4)\tilde{u}_{k,j} + \tfrac{iq_k}{2}\mathcal{F}(\mathcal{F}^{-1}\tilde{u}_{k,j})^2](\delta t)\right). \tag{17.64}$$

The nonlinear term has been written in a pseudospectral manner; $\mathcal{F}$ represents the spatiotemporal Fourier transform operation (a linear operator) For the linearization of (17.64) we have a different expressions instead of f'_k

$$\frac{\partial F}{\partial \tilde{u}} = 1 - g \circ (1 + A\delta t) \tag{17.65}$$

where

$$A = \frac{\partial v_{kj}}{\tilde{u}_{k'j'}} = (q_k^2 - q_k^4) + iq_k \mathcal{F}\mathrm{diag}(\hat{u})\mathcal{F}^{-1} \tag{17.66}$$

A quick comparison with Predrag's derivation to ensure that we aren't completely wrong; the permutation matrix σ in Predrag's derivation is a *circulant matrix*; one property of such matrices is that they are diagonalized by Fourier transforms. Therefore, the rotation, which is a matrix with the characters of C_N on the diagonal (repeated for each spatial mode) is exactly σ in a Fourier basis. The other term is slightly less easy to compare. By using a spatiotemporal Fourier basis there is no notion of having separate state space points parameterized by time; instead there is a $|p|d$ dimensional vector of spatiotemporal Fourier modes. Instead of having a block diagonal expression (20.7) I instead have a single

$[|p|d \times |p|d]$ dense matrix (almost all elements are non-zero). Now, I am fairly certain that this is the Fourier transform of (20.7). [5] am having trouble with the practical application of this expression however. Perhaps I do not understand this derivation as fully as I had thought and or how to use it. Firstly, I thought that this would lead to the block diagonal representation as it has the characters of C_N built right into the definition. The problem lies in the details of A. In Fourier space, the linear term is diagonal and the nonlinear term is dense (almost all matrix elements are non-zero); these properties are reversed in configuration space, such that regardless of basis the result won't be block diagonal. It might be that I am misunderstanding Predrag's post and that is only the case in his example and not for the Kuramoto-Sivashinsky equation.

The only place where I think I could be wrong is the attempt to apply this machinery to the spatiotemporal Fourier basis instead of the time parameterized spatial Fourier modes. The reason why I might be wrong is because I skipped over the important detail which is *exactly what am I calculating the stability of?*. This seems like a dumb question because the stability of invariant 2-tori is what we known we're trying to do; but I can't help but shake the feeling that I am looking at the stability of spatiotemporal modes with respect to time "evolution" while Predrag's equation determines the stability of spatial modes with respect to time evolution. I'm starting to think that only Predrag's way makes sense.

2019-10-11 Matt stability calculation comparision Verified that my calculation is indeed the same as Predrag's just in the spatiotemporal Fourier basis. That is, the matrix that I calculate is equal to the following,

$$
\begin{aligned}
\tilde{\mathcal{J}} &= 1 - g \circ (1 + A\delta t) \\
&= 1 - (\mathcal{F}\sigma\mathcal{F}^{-1}) \circ (\mathcal{F}J\mathcal{F}^{-1}) ,
\end{aligned}
\tag{17.67}
$$

which is simply Predrag's original expression transformed to the spatiotemporal Fourier basis. This indicates that instead of having the wrong equation, I am instead making an error in the calculation process which relates $\mathcal{J}$ and $1 - \sigma J$.

n-cycle stability relation Following the notation of chapter 20, define the one time step cycle rotation as $\mathcal{J} = (1 - \sigma f')$ such that for an n-cycle we have $\mathcal{J}_p = \mathcal{J}^n = (1 - \sigma f')^n$. We want to prove that $\text{Det}\,\mathcal{J}_p = \det(1 - J_p)$, where $J_p = (\sigma f')^n$.

Start by rewriting the binomial expansion of $(1 - \sigma f')^n$.

$$
\begin{aligned}
\mathcal{J}_p &= (1 - \sigma f')^n \\
&= \binom{\sum_{k=0}^{n}(n}{k)(-1)^{n-k}(\sigma f')^k} \\
&= \binom{(1 - J_p) + \sum_{k=1}^{n-1}(n}{k)(-1)^{n-k}(\sigma f')^k .}
\end{aligned}
\tag{17.68}
$$

---

[5]Matt I mean $\mathcal{F}A\mathcal{F}^{-1}$ when I say "Fourier transform" of a matrix: I

Note that f' is a diagonal matrix with f'_k as its entries and σ is the shift matrix (20.7) such that $(\sigma f')^k$ has no diagonal entries unless $k = 0, n$. Therefore the second term does not contribute to the trace. With this knowledge we can apply the identity $\det e^A = e^{\operatorname{tr} A}$ such that

$$\operatorname{Det} e^{\mathcal{J}_p} = e^{\operatorname{tr} \mathcal{J}_p} = e^{\operatorname{tr}(1 - J_p)} = \det e^{1 - J_p} \tag{17.69}$$

which I believe concludes our business.

References

[1]   S. C. Anco and G. Bluman, "Direct construction of conservation laws from field equations", Phys. Rev. Lett. **78**, 2869–2873 (1997).

[2]   P. J. Blonigan, "Adjoint sensitivity analysis of chaotic dynamical systems with non-intrusive least squares shadowing", J. Comput. Phys. **348**, 803–826 (2017).

[3]   S. V. Bolotin and D. V. Treschev, "Hill's formula", Russ. Math. Surv. **65**, 191 (2010).

[4]   S. Boyd and L. Vandenberghe, *Convex Optimization* (Cambridge Univ. Press, Cambridge, 2004).

[5]   N. B. Budanur, P. Cvitanović, R. L. Davidchack, and E. Siminos, "Reduction of the SO(2) symmetry for spatially extended dynamical systems", Phys. Rev. Lett. **114**, 084102 (2015).

[6]   C. C. Chow and T. Hwa, "Defect-mediated stability: an effective hydrodynamic theory of spatiotemporal chaos", Physica D. **84**, 494–512 (1995).

[7]   P. Cvitanović, R. L. Davidchack, and E. Siminos, "On the state space geometry of the Kuramoto-Sivashinsky flow in a periodic domain", SIAM J. Appl. Dyn. Syst. **9**, 1–33 (2010).

[8]   C. Dong and Y. Lan, "Organization of spatially periodic solutions of the steady Kuramoto-Sivashinsky equation", Commun. Nonlinear Sci. Numer. Simul. **19**, 2140–2153 (2014).

[9]   M. Farazmand, "An adjoint-based approach for finding invariant solutions of Navier-Stokes equations", J. Fluid M. **795**, 278–312 (2016).

[10] D. Goluskin and G. Fantuzzi, "Bounds on mean energy in the Kuramoto-Sivashinsky equation computed using semidefinite programming", Nonlinearity **32**, 1705–1730 (2019).

[11] M. Gunzburger, *Perspectives in Flow Control and Optimization* (SIAM, 2002).

[12] N. H. Ibragimov, "A new conservation theorem", J. Math. Anal. Appl. **333**, 311–328 (2007).

[13] N. H. Ibragimov, "Quasi-self-adjoint differential equations", Arch. ALGA **4**, 55–60 (2007).

[14] N. H. Ibragimov, "Nonlinear self-adjointness and conservation laws", J. Phys. A **44**, 432002 (2011).

[15] N. H. Ibragimov, "Nonlinear self-adjointness in constructing conservation laws", Arch. ALGA **7** (2011).

[16] N. H. Ibragimov, "Conservation laws and non-invariant solutions of anisotropic wave equations with a source", Nonlinear Anal. Real World Appl. **40**, 82–94 (2018).

[17] N. H. Ibragimov and T. Kolsrud, "Lagrangian approach to evolution equations: symmetries and conservation laws", Nonlin. Dyn. **36**, 29–40 (2004).

[18] M. Kraus, Variational integrators in plasma physics, PhD thesis (Technical Univ. Munich, 2013).

[19] M. Kraus and O. Maj, "Variational integrators for nonvariational partial differential equations", Physica D **310**, 37–71 (2015).

[20] D. Lasagna, "Sensitivity analysis of systems using unstable periodic orbits", SIAM J. Appl. Dyn. Syst. **17**, 547–580 (2018).

[21] D. Lasagna, A. Sharma, and J. Meyers, Periodic shadowing sensitivity analysis of chaotic systems, 2018.

[22] T. S. Lee, "Image representation using 2D Gabor wavelets", IEEE TPAMI **18**, 959–971 (1996).

[23] J. Liesen and P. Tichý, "Convergence analysis of Krylov subspace methods", GAMM-Mitteilungen **27**, 153–173 (2004).

[24] M. J. Lyons, J. Budynek, A. Plante, and S. Akamatsu, Classifying facial attributes using a 2-D Gabor wavelet representation and discriminant analysis, in Proc. 4 . IEEE Intern. Conf. on Automatic Face and Gesture Recognition (2001).

[25] J. Marsden, S. Pekarsky, S. Shkoller, and M. West, "Variational methods, multisymplectic geometry and continuum mechanics", J. Geom. Phys. **38**, 253–284 (2001).

[26] R. M. Miura, "Korteweg-de Vries equation and generalizations. I. a remarkable explicit nonlinear transformation", J. Math. Phys. **9**, 1202–1204 (1968).

[27] E. Novruzov, "Blow-up phenomena for the weakly dissipative Dullin-Gottwald-Holm equation", J. Math. Phys. **54**, 092703 (2013).

[28] E. Novruzov and A. Hagverdiyev, "On the behavior of the solution of the dissipative Camassa-Holm equation with the arbitrary dispersion coefficient", J. Diff. Equ. **257**, 4525–4541 (2014).

[29] P. J. Olver, *Applications of Lie Groups to Differential Equations* (Springer, New York, 1998).

[30] J. Pathak, B. Hunt, M. Girvan, Z. Lu, and E. Ott, "Model-free prediction of large spatiotemporally chaotic systems from data: A reservoir computing approach", Phys. Rev. Lett. **120**, 024102 (2018).

[31] Y. Saad and M. H. Schultz, "GMRES: A generalized minimal residual algorithm for solving nonsymmetric linear systems", SIAM J. Sci. Stat. Comput. **7**, 856–869 (1986).

[32] R. Schaback, "Convergence analysis of the general Gauss-Newton algorithm", Numer. Math. **46**, 281–309 (1985).

[33] Q. Wang, "Forward and adjoint sensitivity computation of chaotic dynamical systems", J. Comput. Phys. **235**, 1–13 (2013).

[34] Q. Wang, "Convergence of the least squares shadowing method for computing derivative of ergodic averages", SIAM J. Numer. Anal. **52**, 156–170 (2014).

[35] L. Wei and Y. Wang, "Symmetry analysis, conserved quantities and applications to a dissipative DGH equation", J. Diff. Equ. **266**, 3189–3208 (2019).

[36] R. W. Wittenberg and P. Holmes, "Scale and space localization in the Kuramoto-Sivashinsky equation", Chaos **9**, 452 (1999).

[37] C. Yang, L. Shengtai, L. Petzold, and R. Serban, "Adjoint sensitivity analysis for differential-algebraic equations: the adjoint DAE system and its numerical solution", SIAM J. Sci. Comp. **24**, 1076–1089 (2003).

Chapter 18

Matt's 2020-22 blog

2020-01-14 Predrag meeting notes:

    Restart of editing *tiles/current/GuBuCv17.tex*

1. Matt will have a go at editing the current *spatiotemp/chapter/abstract*
2. Matt wrote down bullet points for introduction section
   1. paragraph - great things already done, but [...]!
   2. paragraph - Revolution!
   3. to be discussed Thursday
3. *spatiotemp/chapter/intro*
   tiles/current/intro
   here just for ideas - a copy of old
   siminos/rpo_ks/current/intro.tex, remove once mined for ideas
4. For inspiration / discussion: Predrag's outline
   siminos/presentations/spatiotemp/spatiotemp.tex

2020-01-16 Predrag meeting notes:

1. Matt bullet points for introduction section
   4. paragraph - What?

   (a) Kuramoto-Sivashinsky, rather than Navier stokes

   (b) invariant 2-torus tiles (transl. inv)

   (c) gluing

   5. paragraph - How?
   6. to be discussed Tuesday

2020-1-23 Matt meeting notes:

1. Matt bullet points results section
   7. paragraph - results

   (a) The results of creating library of solutions

711

(b) The results from clipping tiles

(c) The results from gluing

8. paragraph - discussion

(a) (Don't know) How to account for rubber tiles

(b) Don't have a systematic method of gluing

(c) Haven't developed either the symbolic dynamics nor the spatiotemporal theory.

2020-01-15 Matt Introduction 2020-01-15 text moved to *spatiotemp/chapter/intro.tex*, pdflatex GuBuCv17

Revolution WHY? 2020-01-15 text moved to *spatiotemp/chapter/intro.tex*, pdflatex GuBuCv17

What is needed in the revolution?

How does the revolution take place?

[1]

2020-1-31 Matt WHY: reasons for a spatiotemporalformulation

Need new, bold ideas In light of all of these difficulties we believe that new, bold ideas are required to resume forward progress. Specifically, we have begun a completely spatiotemporal formulation of chaos which treats all continuous dimensions democratically. The

---

[1]Matt 2020-01-20: [Introduction]

The problem at hand

ECS are important

Minimal cells

Hard to visualize, use KSE

Large is too hard, new approach

Chaotic or turbulent processes categorize one of the few outstanding problems to be solved in classical physics. While deterministic, the complexity of the problem can be categorized by infrequent or lack of analytic results. It is often necessary to rely on models which capture the important quantitative properties and behavior of the underlying process. These models often take form as nonlinear partial differential equations which are hyperbolically unstable. The systems whose spatial correlations decay sufficiently fast, and the attractor dimension and number of positive Lyapunov exponents diverges with system size are said [2, 19, 26] to be extensive, 'spatio-temporally chaotic' or 'weakly turbulent.' The Lyapunov exponents or equivalently the exponential instabilities they quantify prevent prediction of future behavior outside a finite time interval. This behavior is so peculiar that it has permeated into popular culture, where it is known as the butterfly effect. This behavior poses a serious challenge which has effects everything from weather prediction to air travel. While there is no specific reason other than the difficulty for why this problem remains unsolved, the intricacies of turbulence are typically swept under the rug of "good enough" models which allow for suboptimal but sufficient engineering solutions. The lack of forward progress motivates us to approach turbulence with a new perspective, one that treats all continuous dimensions equally.

main idea is to discard the idea of a dynamical system completely; exponential instabilities mean that conventional methods never could have worked. By converting to a truly spatiotemporal formulation we have discarded dynamics and the inherent difficulties therein. This allows us to quantify and characterize infinite space-time via shadowing of fundamental spatiotemporal patterns.

Treat each dimension equally Conventional methods treat spatial dimensions as finite and fixed; meanwhile, time is treated as infinite. One interpretation is that this is natural due to the human familiarity with finite space, especially in regards to experimental setups. This assumption is actually a very unnatural one in the context of state space. The fundamental reason for this is that it disregards the translational invariance of the equations and while there are implicit physical scales, choosing a specific domain size to study is completely arbitrary. This notion must be reconsidered going forward as it is a very strict constraint on the space of solutions and on the study of turbulence in general. Finite spatial dimensions of course have practical import, but these specific constraints should only be imposed after the study of infinite space-time, as they represent special cases of the general equations. The spatiotemporal formulation handles this properly by treating all continuous dimensions as equal by respecting all translational symmetries. What are the differences and advantages of this? The first key difference is that the governing equation dictates the spatiotemporal domain size in an unsupervised fashion; the decision of what specific domain size to study is no longer present in the discussion. This is another manner in which time and space are being treated as equals; the parameters (L, T) that determine the size of the spatiotemporal domain are both allowed to vary. The values of these parameters are determined by the requirement that the equations must be satisfied locally at every lattice site. This small detail, allowing the domain size L to vary, is not as trivial as it seems. At present it has not been seen in the dynamical systems literature. The variation of the period T is common, however. The likely culprit behind this different treatment is likely a result of the equations themselves. This difficulty is especially evident in the Kuramoto-Sivashinsky equation, whose spatial derivative terms are of higher order than the first order time derivative, but also there is a spatial derivative present in the nonlinear component.

describes infinite spacetime

No instability

characterize and quantify all patterns

tiles invariant?

simply can't use conventional methods in large limit

domain size determined by equation

Spacetime computations are easier to parallelize

beats conventional methods numerically • initial conditions The conventional method to generate initial conditions involves time integration and recurrence functions, the latter simply calculates the pairwise distance between all points in a time integrated series.In the high dimensional limit, both of these components are time consuming. This is yet another component of the dynamical systems formulation that gets worse as spatial sizes increase. There are two detrimental factors that contribute towards this. The number of dimensions must increase in order to accurately resolve the domain. The other factor is that the growth of complexity of solutions can reduce the number of recurrences drastically. There isn't really a manner to deal with the increasing number of computational variables other than to wait for improvements in computing power and memory availability. As for the recurrences, the typical solution for increasingly rare events is to compute in parallel when possible. The exponential growth in complexity makes even this proposition a daunting one. The spatiotemporal completely avoids this by constructing larger invariant 2-tori from the combination of smaller invariant 2-tori. That is, we locate the fundamental tiles, which are easy to find due to their small domain size, and then build them up to create larger invariant 2-tori. The only search required is the search for the fundamental tiles. To stress this even further *one of the challenges of turbulence computations has been eliminated*. The reason why the search for the fundamental tiles is classified as "easy" is because in the small domain size limit there just aren't that many invariant 2-tori; the dynamics is relatively simple. Recurrence functions also require the introduction of a norm, typically chosen without taking the geometry of the state space into account. Points that are close in this norm can be far apart in a dynamical sense (i.e., on opposite sides of an unstable manifold). An arbitrary norm is also chosen in the spatiotemporal context but there are some subtle differences. For starters, the norm introduced in the spatiotemporal formulation is not beholden to dynamics, as there are no longer any dynamics to speak of. Additionally, the norm in the spatiotemporal case measures the distance between invariant 2-tori, not just single state space points. This is not a statement of proof but rather a suggestion that the underlying topology improves the reliability of the chosen norm. Restated in a different manner, the spatiotemporal norm takes both the magnitude and phase into account. Another numerical advantage is that the spatiotemporal formulation is able to find solutions of the

Kuramoto-Sivashinsky equation starting from modulated random noise. The specifics of "modulated random noise" are described in the numerical methods section but it can essentially be thought of as randomly assigning values to spatiotemporal Fourier modes. The ability to find solutions from this starting point is a radical improvement over the conventional capabilities. This is of course in conjunction with allowing the spatiotemporal domain to change. The reaction to these changes individually has induced skepticism and disbelief; together they comprise a completely unheard of force.

- no instability
- generalizable
- many newfound capabilities
- memory, parallelizability.

The spatiotemporal formulation also includes the improvement of a commonly practiced numerical method known as pseudo-arclength continuation. The general idea is to track a solution as a parameter is varied. In the Navier-Stokes equations this is typically the Reynolds number. The improvement is due to our common refrain: the lack of dynamical instability and the topological constraint of invariant 2-tori. There can be more confidence that if the continuation fails it is due to the solution not existing rather than not being able to converge due to dynamical instability.

2020-01-31 Matt WHAT?

KSe N-S comparison As previously stated, the testing grounds for these ideas will be the spatiotemporal Kuramoto-Sivashinsky equation

$$u_t + u_{xx} + u_{xxxx} + uu_x = 0 \quad \text{where} \quad x \in [0, L], t \in [0, T] \quad (18.1)$$

where $u = u(x,t)$ represents a spatiotemporal velocity field. This equation has been used to model many different processes such as the laminar flame front velocity of Bunsen burners. This was chosen as the testing ground for our ideas because it has a two dimensional space-time and has many similarities to the Navier-Stokes equations. It is useful to relate the terms between the two equations via the physical processes that they represent even though these processes aren't The numerical challenge is to find discretized velocity fields $u(x,t) \approx u(x_m, t_n)$ which satisfy the Kuramoto-Sivashinsky equation locally at every lattice site.

2-tori, translational invariance, Fourier The translational invariance and periodicity make spatiotemporal Fourier modes the natural representation of our equations. The inherently infinitely dimensional equations are approximated by a Galerkin truncation of the spatiotemporal Fourier modes. The velocity field $u(x_m, t_n)$ with $x_m =$

$\frac{mL}{M}$ and $t_n = \frac{nT}{N}$ can be described by a set of spatiotemporal Fourier coefficients, represented as a vector $\hat{u}$. The indices which indicate the spatiotemporal frequencies each mode represents are withheld as computational details that would only bog us down at this stage of the discussion. The Kuramoto-Sivashinsky equation (18.1) in terms of the Fourier coefficients $\hat{u}$ is a system of differential algebraic equations $\hat{u}$

$$F(\hat{u}, L, T) \equiv (\omega_j - q_k^2 + q_k^4)\hat{u} + \frac{q_k}{2}\mathcal{F}(\mathcal{F}^{-1}(\hat{u})^2). \quad (18.2)$$

The nonlinear term is computed in a *pseudospectral* fashion: a method which computes the nonlinear term as a product in physical space as opposed to a convolution in spectral space. The definitions of each term is as follows; $\mathcal{F}$ and $\mathcal{F}^{-1}$ represent the forward and backwards spatiotemporal Fourier transform operators. Spatial and temporal derivatives are calculated (most efficiently) by element-wise multiplication with the appropriate power of the appropriate frequency vector. Differentiation can be alternatively viewed as the "lattice-wise" multiplication of the Fourier modes and a lattice of frequencies (this is sometimes referred to as the Hadamard product or Schur product).

Optimization problem

find library

large to small

small to large

This attempt to overthrow the status quo includes multiple techniques and methods that have not yet been witnessed in the literature. The novelty of these methods result in newfound capabilities, which in turn allow for new analyses. The utility and important properties of these methods will be detailed later but we provide a preview here.

In this formulation we describe turbulence not as a series of temporal snapshots but rather as a collection of spatiotemporal patterns. This formulation is unconventional but appeals to our intuition; an example of spatiotemporal patterns would be weather phenomena from the benign clouds to deadly hurricanes. Although they technically represent movies, we treat space and time as equally as possible by referring to these objects as spatiotemporal *patterns*. The claim is that when the laws of motion have several commuting continuous symmetries (time-translation invariance; space-translation invariance), all continuous symmetries directions should be treated democratically, as $(1+D)$ different 'times'. The proposal is inspired by the Gutkin and Osipov [16] modelling of chain of N coupled particle by temporal evolution of a lattice of N coupled cat maps. Specifically, we propose to study the evolution of Kuramoto-Sivashinsky on the 2-dimensional infinite spatiotemporaldomain and

develop a 2-dimensional symbolic dynamics for it: the columns coding admissible time itineraries, and rows coding the admissible spatial profiles. We already have the two edges of this symbol plane - the $L = 22$ minimal cell [3, 22] is sufficiently small that we can think of it as a low-dimensional ("few-body" in Gutkin and Klaus Richter [8–11] condensed matter parlance) dynamical system, the left-most column in the Gutkin and Osipov [16] $2D$ symbolic dynamics spatiotemporal table (not a 1-dimensional symbol sequence block), a column whose temporal symbolic dynamics we will know, sooner or later. Michelson [27] has described the bottom row. The remainder of the theory will be developed from the bottom up, starting with small spatiotemporal blocks.

The first step required to construct our spatiotemporal theory is to collect a library of invariant 2-tori. There are infinitely many such solutions but our search does not need to be exhaustive, it only has to provide an adequate sampling of the solution space. The notion of "adequate" is an inexact one, broadly speaking, it consists of collecting invariant 2-tori of various size and symmetry types until all unique patterns have been accounted for. Using this library the fundamental patterns will be determined by their frequency in the library. It is possible to miss a specific pattern but this is an indication that it is not fundamental and in all likelihood does not account for any substantial porti An example of this would be an isolated invariant 2-torusin state space. It may have unique properties but it doesn't get shadowed frequently enough to influence the infinite space-time behavior. The search ranges over all types of symmetries; the shadowing events within the symmetric solutions are not symmetric themselves hence they may represent fundamental tiles. This is important especially for relative periodic orbits as they may contain tiles whose local spatial drift is non-zero.

By definition shadowing is not the exact realization of a invariant 2-torus; it is a "fuzzy window" which represents a local region of space-time that is in the proximity of the invariant 2-torus in question (in some norm). As the size of the shadowed invariant 2-torus increases, so does the accuracy of the shadowing region. that is, away from the boundary, the shadowing becomes exponentially more accurate.

Once a satisfactory library has been created, the search for tiles can begin. Visual inspection of the library of invariant 2-tori (enabled by the ease of visualization) helps develop an intuition as to which patterns represent fundamental tiles. The tiles by our definition are subdomains which shadow large invariant 2-tori. It should be intuitive, therefore, to search for these tiles by numerically "clipping" them out of the larger invariant 2-tori. This amounts to extracting sub-lattices from the larger invariant 2-torusThis process is straightforward and intuitive; at least in the context of a numerical method that can converge initial conditions that are periodic in neither space nor time. These clippings are clearly not invariant 2-tori so they need to be run through the same numerical meth-

ods that were used to converge the original invariant 2-torus from which they originated. A successful outcome is not guaranteed; this is likely a numerical property and not indicative of the importance of the tile. The number of attempts to converge a tile should be proportional to its frequency in our library. If a suspected tile repeatedly fails to converge then either it is not a tile or it is not a minimal tile but a component of one; this latter hypothesis would be evidenced by common occurrence of the suspected tile with another pattern.

The next portion of the overarching spatiotemporal method assumes that not only a large number of invariant 2-tori have been found but also a handful of tiles. The idea is to use these solutions as spatiotemporal building blocks in order to find new solutions. Going even further, the eventual goal is to create a spatiotemporal symbolic dynamics wherein the tiles are the alphabet. If this can be done then all solutions are theoretically enumerable by spatiotemporal symbol blocks. This symbolic dynamics has not been constructed as of yet but it is worth mentioning as it serves as the overarching motivation. This method of "gluing" solutions by combining them in space-time presents not only a very attractive method for describing invariant 2-tori through fundamental physical behaviors but also for constructing initial conditions to find arbitrary invariant 2-tori. This method in theory constitutes an improvement over both the dynamical systems formulation as well as our own search using "random" initial conditions. This improvement results from the ability to produce better initial conditions for our spatiotemporal searches. The proof of concept for this method was the reproduction of a known solution by gluing together tiles.

After the detailing and application of these methods we will have a collection of fundamental tile solutions. With these tiles we layout out case that infinite space-time can be described by these tiles. In addition, we set the stage for how the investigation can process in a systematic manner.

2020-1-31 Matt The formulation of the spatiotemporal theory is dependent upon three main numerical processes; finding invariant 2-tori of arbitrary domain size, cutting out tiles from these invariant 2-tori, and gluing the tiles together. The first of these procedures requires the solving of the optimization problem

There are many ways to solve this type of problem but before we can begin solving the equation we need a method of generating initial conditions. As previously discussed, this work does not use approximate recurrences; or time integration at all, to generate initial conditions. Instead we simply initialize a lattice of Fourier modes by first deciding on the dimensions of the lattice and then assigning random values to the modes. Random values in this case are drawn from a normal distribution. The Fourier spectrum is then rescaled to better represent the physical scales of the Kuramoto-Sivashinsky equationand typical field magnitude of in-

variant 2-tori. This modulation of the spectrum is determined by two factors: the smoothness of spatiotemporal solutions and the linear stability profile of the Kuramoto-Sivashinsky equation. The smoothness or differentiability combined with the bounded magnitude of the field implies that the Fourier coefficients should decrease exponentially in the in the infinite mode limit. Our heuristic approach is not identical for space and time, so we describe the process in detail. The rescaling with respect to the spatial index linear stability profile of the original dynamical equation is used as a rough guide for the magnitude of the Fourier coefficients; the easiest implementation is to just truncate the spatiotemporal modes at the boundary between linearly unstable and linearly stable modes with respect to the spatial index. For time, the strategy is the truncation of nearly all of the modes. There is a time scale associated with the problem, the Lyapunov time, but this simple strategy avoids the calculation of this time. The intuition behind this choice is that the general solution is comprised of many meandering "streaks"; shadowing of a one wavelength (in terms of physical scale) equilibrium. The truncation attempts to account for this approximately time independent behavior in the locality of these streaks.

There are many different ways to approach this problem; we focus on two different methods whose combination comprises a robust numerical method. The first method substitutes an equivalent optimization problem instead of directly solving $F = 0$. The optimization problem is formed by the construction of a scalar cost function. Because we are concerned with finding exact solutions to (18.2) we elect to simply use the L_2 norm of (18.2) (with a constant factor for convenience)

$$\mathcal{I}(\hat{u}, T, L) = \frac{1}{2}||F(\hat{u}, T, L)||_2^2. \tag{18.3}$$

There is no motivation for the specific choice of norm or cost function other than they are simple choices which satisfy our needs. The gradient of this cost function with respect to a fictitious time, τ, results in the fictitious flow

$$
\begin{aligned}
\frac{\partial \mathcal{I}}{\partial \tau} &= \nabla\Big(\frac{1}{2}||F(\hat{u}, T, L)||_2^2\Big)\partial_\tau[\hat{u}, T, L] \\
&= \left(\Big[\frac{\partial F}{\partial \hat{u}}, \frac{\partial F}{\partial T}, \frac{\partial F}{\partial L}\Big]^\top F(\hat{u}, T, L)\right) \cdot \partial_\tau[\hat{u}, T, L] \\
&\equiv \left(J^\top F\right) \cdot \partial_\tau[\hat{u}, T, L] \quad . \tag{18.4}
\end{aligned}
$$

This equation (18.4) by itself does not provide us with a descent direction because the partial derivative of the independent variables with respect to τ, $\partial_\tau[\hat{u}, T, L]$ remains undefined. Luckily, we are free to choose what it is. The only requirement is a monotonically decreasing cost function. In other words, $\partial_\tau[\hat{u}, T, L]$ needs to be chosen such that $\frac{\partial \mathcal{I}}{\partial \tau}$ is never positive.

The most obvious choice is the negative gradient of the cost function; this choice corresponds to the gradient descent algorithm. This is the most basic descent method, but it works very well when preconditioning is also included. The details regarding the preconditioning are left out for brevity; it's a rough approximation to the inverse of the linear portion of the equation. Regarding this choice of numerical method: originally, we believed that our implementation represented a more sophisticated numerical method called the *adjoint descent algorithm* [12]. Technically, the algorithm *is* the adjoint descent method, its just that with a lack of dynamics the adjoint descent method collapses onto the gradient descent method. This fact wasn't realized until much later but it worked so no harm no foul. If anything, this shows how much room there is for numerical improvements. In any case, the choice that was made for the descent direction was

$$\partial_\tau [\hat{u}, T, L] = -\left(J^\top F \right),$$ (18.5)

such that

$$\frac{\partial \mathcal{I}}{\partial \tau} = -\left\| \left(J^\top F \right) \right\|_2^2 \leq 0 .$$ (18.6)

It is clearly never positive but it can be equal to zero; this occurs at roots of F but also local extrema of F. The former is of course the desired state; the latter presents the problem of getting stuck at local minima. Getting stuck at local minima is a very common problem in the field of optimization. Instead of trying to eliminate this possibility we elect to merely account for this by termination of the computation after a threshold is met. The actual optimization process takes the form of numerical integration of the fictitious flow. Numerical integration is of course affected by the integration scheme used. Luckily, we do not care about the accuracy of the intermediate states as they are still approximations and not exact solutions. The only true requirement is that the cost function must monotonically decrease. Therefore we elected to use the simplest integration scheme: Euler's method. Because this is first order and explicit, the accuracy depends on the step size. The step size was determined by finding the first value of $\Delta x = 2^{-n}, n = 0, 1, \dots$ which reduced the cost function. To again save time, this calculation was only performed once. Finding the optimal distance to step using a line-search algorithm, for instance, drastically slows the calculation. Another possibility would be to adapt the step size not at every step, but at a finite number of checkpoints during the descent. These attempts always returned the original step size such that these efforts are no longer attempted. If, at any point, the numerical integration no longer decreases the cost function, then the step size would be further reduced. The descent process was terminated whenever the step size was reduced beyond a minimum value of 10^{-13}. It could be argued that this threshold should be changed to a larger value. Experientially it doesn't seem to affect the calculation; further reduction

of the step size almost always resulted in termination of the descent. To increase the efficacy of our descent method, we also employed the notion of preconditioning. The reason why we felt that preconditioning was warranted was due to the stiff spatial derivative terms. The descent direction is dominated by the components with high spatial frequencies but the magnitude of the corresponding Fourier coefficients are typically small. This can be counteracted by scaling the descent direction such that the lower frequency modes are favored. The exact choice of preconditioner is the inverse of the linear spatial derivative operators. This comes very cheap as these operators are diagonal and is very effective for its price. Technically, an absolute value is individually applied as to avoid division by zero. It is also very beneficial to rescale the partial derivatives with respect to the spatiotemporal domain parameters. The specific reason results from how poorly the initial conditions approximate invariant 2-tori. If nothing is done to control the magnitude of these gradients, a very common occurence is that the solutions are stretched out to incredibly large domains and either do not converge or converge only to equilibria. These large equilibria, while perhaps desirable in some circumstances, are not desired for our purposes as they are far too unstable to be witnessed in infinite space-time. The decision of when to cut off the gradient descent can be determined in a variety of ways, the most common involve either the absolute tolerance (magnitude of the cost function) or the relative tolerance (change in cost function magnitude between steps). We elect to use a combination of step limit and absolute tolerance. If the cost function doesn't cross the threshold by the step limit then the descent is terminated. Again these are some of the simplest conditions that ensure that the descent will end in a reasonable amount of time. The reason why this is acceptable is because the majority of the heavy lifting is done by the back-end algorithm, the least-squares solver with backtracking. In this context, the descent algorithm can be viewed as bringing approximate solutions close enough to invariant 2-tori such that the least-squares algorithm can converge them, akin to [12]/

The second portion of our hybrid numerical method is to apply a least-squares solver to the root finding problem $F = 0$. The first step is everyone's favorite derivation, the derivation of Newton's equations from the linearization about a root of F

$$F(\hat{u} + \delta\hat{u}, T + \delta T, L + \delta L) \approx F(\hat{u}, T, L) + J \cdot [\delta\hat{u}, \delta T, \delta L] + \ldots . \quad (18.7)$$

substitution of zero for the LHS (the root) yields

$$J \cdot [\delta\hat{u}, \delta T, \delta L] = -F(\hat{u}, T, L) . \quad (18.8)$$

where

$$J \equiv \left[\frac{\partial F}{\partial \hat{u}}, \frac{\partial F}{\partial T}, \frac{\partial F}{\partial L} \right] . \quad (18.9)$$

This equation is of the general form for a linear system $Ax = b$; it is convenient to refer the system of equations in this form. Technically, this

equation is solved a number of times, each time producing its own least-squares solution which guides the field to invariant 2-torus. We avoid this here just to keep the notation clean. It is implicit in the definition of J that this is a rectangular linear system; there are more columns in J than rows. The equations are augmented to include variations in T, L and there are no components of the Kuramoto-Sivashinsky equation associated with this. Two choices for how the handle this are: create and include additional constraints on either the Fourier coefficients or the spatiotemporal parameters, or solve the equations in a least-squares sense. We chose to solve the equations in a least-squares manner. We are not focused on finding specific solutions so we can get away with this. Another reason is that a common choice for the constraints is to fix the translational degrees of freedom, that is, ensure that the solutions to the linear system (18.8) are orthogonal to the partial derivatives $\frac{\partial \hat{u}}{\partial x}$ and $\frac{\partial \hat{u}}{\partial t}$. These constraints are suboptimal for two reasons: they specify a particular member of a group orbit beforehand reducing the likelihood to converge and the orthogonality to the direction of spatial translations is not well defined for invariant 2-tori with discrete symmetry. As briefly mentioned, we also include the notion of backtracking; that is, the least-squares step is repeatedly divided by a factor of two until either the cost function decreases or the step size becomes too small. This saves time in comparison to line searching methods which find the optimal step size which produces the largest reduction in the cost function. Now that the numerical methods have been detailed, we can move onto how we want to use them.

As mentioned multiple times the first step is to produce a library of invariant 2-toriusing the numerical methods developed above. It was not known if we would even be able to find invariant 2-tori given our formulation. It was possible that the particular numerical methods chosen wouldn't work; of course, if the methods described previously didn't work then we would not be reporting on them. To apply the numerical methods an initial condition needs to be created which requires selection of the discretization size, the initial mode values, the period and the domain size. In our searches the process was automated by searching over a range of periods and domain sizes over the following ranges. For the period the range was wider, due to the experience from the study of the equation at system size $L = 22$. Periods were chosen from the range $T \in [20, 180]$. Meanwhile, the spatial range was $L \in [22, 88]$. The discretization size depended on the spatiotemporal domain size; more modes are needed to resolve larger solutions. The number of lattice points in each dimension were typically chosen to be powers of two in order to exploit the speed of fast Fourier transforms. A strict (well motivated) rule for the size of the lattice was never developed so all that can be offered are approximate guidelines: The number of typical spatial lattice points fol-

lowed the formula

$$M = 2^{\text{int}(log_2(L)-1)} \tag{18.10}$$

and for time

$$N = 2^{\text{int}(log_2(T))} . \tag{18.11}$$

Once the initial condition is defined, it is passed to the gradient descent algorithm. The tolerance of the cost function for the gradient descent was typically set at 10^{-4} and the step limit was set as a function of the size of the lattice, the maximum number of steps being $16NM$. Once either the tolerance or step limit was reached, the approximate solution would be passed to the least-squares algorithm, where the tolerance for termination was 10^{-14} and the step limit was 500. The relatively large step limit was because of the allowance of back tracking, where the maximum amount of damping was varied between 2^{-5}, 2^{-8} by powers of two. A choice that we did not elect to use but very well could have is to use each matrix inversion more than once. This could be done by computing the inverse, and then iteratively using it to update until the cost function no longer decreases. We believe that any numerical operation that maintains the monotonic decrease of the cost function is fair game.

It is actually recommended to not use descent methods for small dimension problems; Newton converges too quickly to not use and with backtracking the region of convergence can increase substantially.

Another option would be to simply decrease the allowed damping, thus causing more failures, but run more searches in parallel.

Searching through the library of collected invariant 2-tori led to a number of candidates for fundamental tiles. This was a natural result of picking out the most frequent patterns that occur spatiotemporally. This section focuses on the numerical process of finding tiles; it is almost self explanatory. The claim is that the tiles are invariant 2-tori which shadow larger invariant 2-tori. Therefore we should be able to find these tiles by numerically clipping them out of larger invariant 2-tori and then passing them to the same numerical routine used to converge the larger invariant 2-torus. If the original invariant 2-torus has dimensions $x \in [0, L_0]$ and $t \in [0, T_0]$ and is defined on a lattice $[x_m, t_n]$ then the process is as follows. Find the approximate domain on which the shadowing occurs $x \in [0, x_i - x_j]$, $t \in [0, t_p - t_j]$; translational invariance allows us to start from the origin. The tile is then defined on the corresponding lattice of size $M', N' = M\frac{x_i - x_j}{L}, N * \frac{t_i - x_j}{T}$. M', N' are always taken to be even numbers for reasons specific to our computational codes. This leaves us with a field defined on this subset of the original lattice; this will never be doubly periodic. The discontinuities which result from the clipping are handled by simple truncation of the higher frequency spatiotemporal Fourier coefficients.

If possible, clippings were made such that the result minimized the discontinuities at the boundary. This is both numerically beneficial but also

motivated by the notion of tiles representing shadowing of small invariant 2-tori.

This process suffices to find tiles such that any other methods that improve the initial conditions are ignored.

The only step left is to converge these initial conditions numerically just like how was done with the larger invariant 2-tori. This process continues until we believe that we have captured all fundamental solutions depicting in our library of invariant 2-tori. This appeals to our intuition which begs the question: is there a quantitative manner to know whether our tile collection is complete? The answer to this question arises naturally as a consequence of the next component of this numerical method, namely, the gluing of invariant 2-tori and tiles.

It is one thing to claim that certain spatiotemporal invariant 2-tori are building blocks; it is another thing all together to be able to actually use them in this manner. We would like to remind the audience that the ability to construct and find solutions in this manner has not been witnessed in the literature. With this in mind our choices should be treated as preliminary ones; it is entirely possible and likely that many improvements could be made. This description covers both the implementation that worked for us for the spatiotemporal Kuramoto-Sivashinsky equation, as well as some alternatives.

Much like the clipping process used to find tiles combining solutions in space-time, the overarching idea of gluing is straightforward and intuitive. We lean towards simplicity such that the process of gluing and converging invariant 2-tori is only slightly more complex than the original method of trawling for invariant 2-tori. With this in mind, what do we mean exactly when we say that we are gluing invariant 2-tori? As invariant 2-tori are infinite space-time solutions the notion of gluing them doesn't actually make sense; the actual entities being glued are the compact support of these solutions. This is a familiar notion which has many different names: Brillouin zone, fundamental domain, unit cell of a lattice, etc. To distinguish between the infinite space-time invariant 2-tori and their finite representatives which we shall refer to as tiles.

The first step is to choose which invariant 2-tori to glue and how to arrange them. The general case is that we have a general $s_n \times s_m$ sized mosaic of tiles with no particular attention given to whether or not the tiles fit well together. The minimum requirement so that gluing is well defined operation is that tiles must have equal number of grid points along boundaries being glued. This creates a problem, however, as different tiles will have different spatiotemporal dimensions T, L because they are fundamentally different solutions. Therefore, the domains of each lattice are different but the number of grid points is the same, hence, the grid spacings are necessarily different. This problem actually helps provide a precise meaning to the term "gluing". Gluing is a method of creat-

ing initial conditions via the combination of spatiotemporal tiles which approximates the corresponding non-uniform rectangular lattice as uniform. The regularization of the lattice is a global transformation but it introduces error in the form of local tangent space distortions which, of course, depend on the local change in mesh size. In Fourier space, differentiation is equivalent to multiplication of the Fourier coefficients by the corresponding frequencies. Using this fact, we can create a crude bound on the error introduced to give us an idea as to how detrimental the approximation is. In a discrete setting, for a dimension of length d, the greatest frequencies that are accounted for by an N point discrete Fourier transform are $\frac{2\pi N}{d}$. Therefore, the error between an order n tangent of the tile and its gluing approximation scales like

$$\partial_d^n u - \partial_d^n u' \sim (2\pi N)^n (\frac{1}{d^n} - \frac{1}{d'^n})\hat{u}. \tag{18.12}$$

By substituting $d' = d + \delta d$ and assuming δd is small

$$
\begin{aligned}
\Delta \partial_d^n \hat{u} \quad &\sim \quad n\frac{\delta d}{d}\big(\frac{2\pi N}{d}\big)^n \hat{u} \\
&\equiv \quad \frac{\partial[\partial_d^n u]}{\partial d}\delta d\,.
\end{aligned}
\tag{18.13}
$$

This result, while quite obvious in hindsight, would be different if we had been using finite differences to compute the tangents. Therefore the total error of the approximation can be found by the summation of the error of each tile individually

$$\Delta F = \sum_z (\delta L)_z \frac{\partial F}{\partial L}\Big|_{u=u_z} + (\delta T)_z \frac{\partial F}{\partial T}\Big|_{u=u_z}\,. \tag{18.14}$$

We derived how the error depends on local changes to mesh size; we did not however describe how to *choose* the final mesh size. The choice of the parameters depends on how the gluing is performed. We describe two methods which differ in complexity there are a number of intermediate states but these two examples get the point across. The simplest method merely rediscretizes and concatenates the tiles, setting the new dimensions to be the average of the tile dimensions. Note that this averaging should only occur with respect to the dimension transverse to the gluing. For example, if gluing two tiles together in time, the period would be $T = T_1 + T_2$ but the spatial period would be $L = \frac{L_1+L_2}{2}$. In this case, the number of spatial grid points and the temporal grid spacing need to be the same. This same idea can be extended to arbitrary sized gluings;

generalizing to a summation over the tiles

$$
\begin{aligned}
T &= \frac{1}{s_x} \sum_{i,j=1,1}^{s_x,s_t} T_{ij} \\
L &= \frac{1}{s_t} \sum_{i,j=1,1}^{s_x,s_t} L_{ij} \,.
\end{aligned}
\tag{18.15}
$$

The more complicated alternative is to glue tiles in a pairwise fashion, building block by block. The problem with this method is that it is not agnostic to the order in which tiles are being glued as each iteration requires lattice regularization. For example, gluing four tiles together spatially would be completed in three pairwise steps; this results in the final approximation having period

$$
T = \sum_{i=1}^{s_x-1} \frac{T_i}{2^{s_x-i}}
\tag{18.16}
$$

where the index i represents the sequential gluing of tiles. Going even further, we can alternate between gluing and converging; this allows for much more complicated strategies for gluing such as gluing tiles together in ascending order of spatiotemporal domain size. The motivation for doing so is that even though there are no dynamical instabilities, the difficulty of finding invariant 2-tori still scales with their spatiotemporal domain size. Note that this process does not need to be done from scratch for each gluing; once converged, the result can be saved for later usage. As can be seen the options seem to only limited by our creativity, we opt for simple solutions as we have not developed any best practices as of yet. Before any more improvements can be discussed we first need to deciminate the results of the methods proposed thus far.

2020-1-27 Matt

Discounting the time it took to produce the codes used for the computations, it did not take much effort to complete the collection of invariant 2-tori. This search was performed over intermediately sized domains and all symmetry types.

The first test of the ideas was to converge coarse discretizations of known solutions. When converged using shooting type methods, the number of discrete time steps numbers in the thousands. When converged using other variational techniques such as the Newton descent method, [20] mentions using upwards of 512 to 1024 discrete time points. Meanwhile, the method proposed here can converge solutions on very coarse discretizations orders of magnitude smaller than these other methods. This is slightly disingenuous as the shooting type method does not require all of the points to be maintained in memory; this is merely an argument that

the memory requirements for spatiotemporal methods do not need to be nearly as large as one might imagine. This reduces even further if imposing discrete symmetries; a common occurrence in flows such as pipe and plane Couette flows [14]. The familiarity with finite difference methods leads to another foreseeable counter argument; coarse discretization which do not resolve the appropriate physical scales lead to nonsensical solutions, regardless of whether or not they converge. This is exactly the case; if the problem were to be composed of finite differences in physical space. The coarse discretization in Fourier space is sufficient to resolve all physically relevant modes a quick visual inspection is typically sufficient; this can be done by interpolating a finer grid via zero padding. If skepticism remains an alternative would be to alternative between zero padding and converging. This works but it will change the spatiotemporal dimensions if they remain free parameters and so the lattice dimension is best increased in small increments. It is possible to perform this type of extension to a very large dimension but it is very hard to decrease the error; we recommend using this as an error density such that the absolute tolerance becomes $NM \cdot 10^{-15}$ instead of 10^{-15}. This remains a qualitative value but there is evidence that the tolerance need not be machine precision for the calculations at least in the spatiotemporal setting which lacks dynamical instability. As a test of practicality of this bound a numerical experiment was ran which attempted to converge a known solution using a discretization which dwarfed the original. After a finite number of gradient descent steps a spatial strip was taken from the approximate solution and integrated in time to test whether or not this would reproduce the solution. A successful test increased a spatiotemporal discretization of size $[64, 32]$ to $[4096, 512]$. Not many tests were run so this could be an indication of sampling bias, but it was informative at least in regards to whether or not this formulation could work for higher dimensional equations.

Once this preliminary testing was completed, we started trawling the solution space for invariant 2-tori. The parameter ranges employed for the search varied, but the typical ranges were $L \in [22, 66]$, $T \in [20, 180]$. The typical lattice dimensions over these ranges were $N \times M \in [32, 128] \times [32, 64]$.

The typical pattern for finding a solution was as follows. An initial field with very large magnitude of the cost function, upwards of $\approx 10^{10}$, is annealed by the descent algorithm. This uses the method described in

typically ending at the maximum step limit instead of the numerical tolerance. The annealed approximation is then passed to the least-squares backtracking algorithm. The damping typically starts high until the the approximation nears a invariant 2-toruswith the last few steps typically being undamped. "Rough patches" are also common during the least-squares backtracking routine; this term represents local regions where the damping increases presumeably due to increased curvature of the

cost function.

The computation times to find solutions ranged from seconds to tens of minutes, depending heavily on the dimensionality of the discretization. The solutions which converged the fastest always resulted from smaller solutions which did not take much time at all to complete the descent algorithm; essentially they would be immediately passed to the least-squares algorithm.

After examination of our library of solutions we determined that there are only a small number of fundamental patterns. We have tentatively named these patterns after the basic physical processes they represent. The first tile is actually defined with $T = 0$

They can be described by the following physical processes.

Upon convergence of the guesses for these tiles, this number reduced even further upon realization that some of the guesses belong to the same continuous family.

Despite our best efforts to determine the opposite, no continuous symmetry was found that explains these continuous families of tiles.

The interpretation of these families is that instead of having a unique, finite set of tiles we instead

The most frequent patterns, that is, those which are presumably the best tile candidates are relatively simple to describe in terms of physical processes. This description is best carried out in the context of spatial waves present in each solution. The natural length scale of the equations

The most unstable wavelength, however, seems to mediate the interaction between these waves. The "most" fundamental of the tiles is what we have denoted as the streak tile.

Our naming convention appeals to similar shapes witnessed in fluid simulations. It has been argued that the natural length scale of the problem is the wavelength corresponding to the most unstable mode. Visual inspection of arbitrary solutions shows a slightly more detailed story best described as a tug-of-war between two different length scales. The most unstable wavelength results from the linearized spectrum; while informative it does not encapsulate the full story. Luckily the tiles The number of pronounced (amplitude above a threshold) wavelengths varies over time, seemingly oscillating between these two different scales.

The transition to the most unstable wavelength seems to be a transient phenomenon that accounts for the destruction of wavelengths via collision. This is not simply linear superposition of waves but the linear affects can be The equilibria

It should be noted that previously we claimed that there are only three tiles. This is actually disingenuous because when we use tiles in gluing access to their group orbit is used; that is, any symmetry copy or member
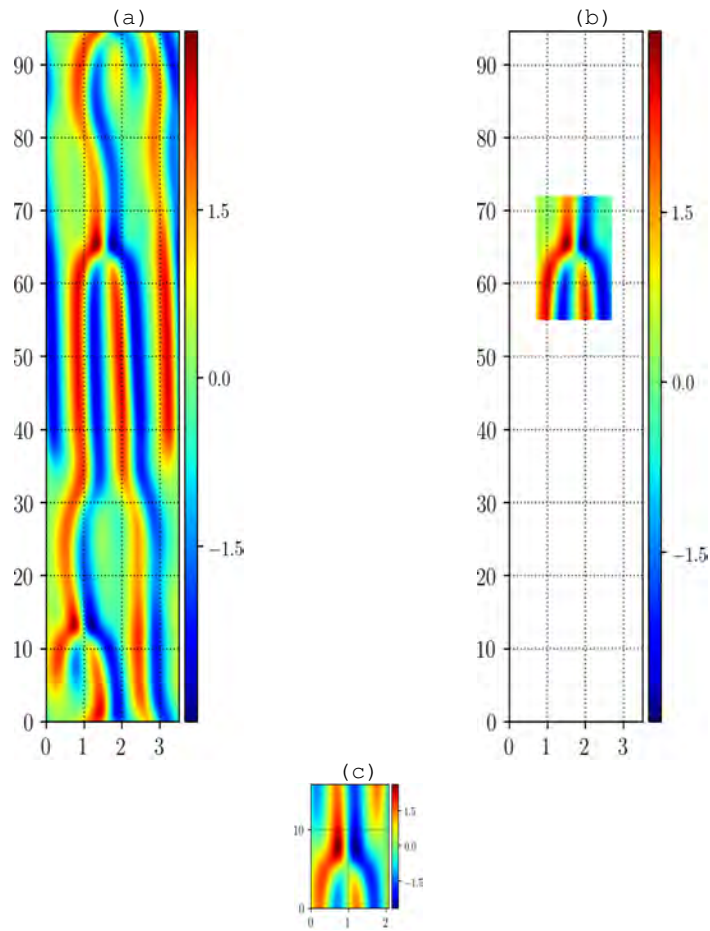
Figure 18.1: (a) $[L_a, T_a] = [3.50\cdots, 94.59\cdots]$ fundamental domain of an already computed invariant 2-torus with spatial translation symmetry. (b) The clipped-out $[L_b, T_b] = [2, 17]$ subdomain used the initial guess for the fundamental domain of a shift-reflect symmetric tile. (c) The converged $[L_c, 2T_c] = [2.07\cdots, 18.46\cdots]$ invariant 2-torus with spatial translation symmetry.
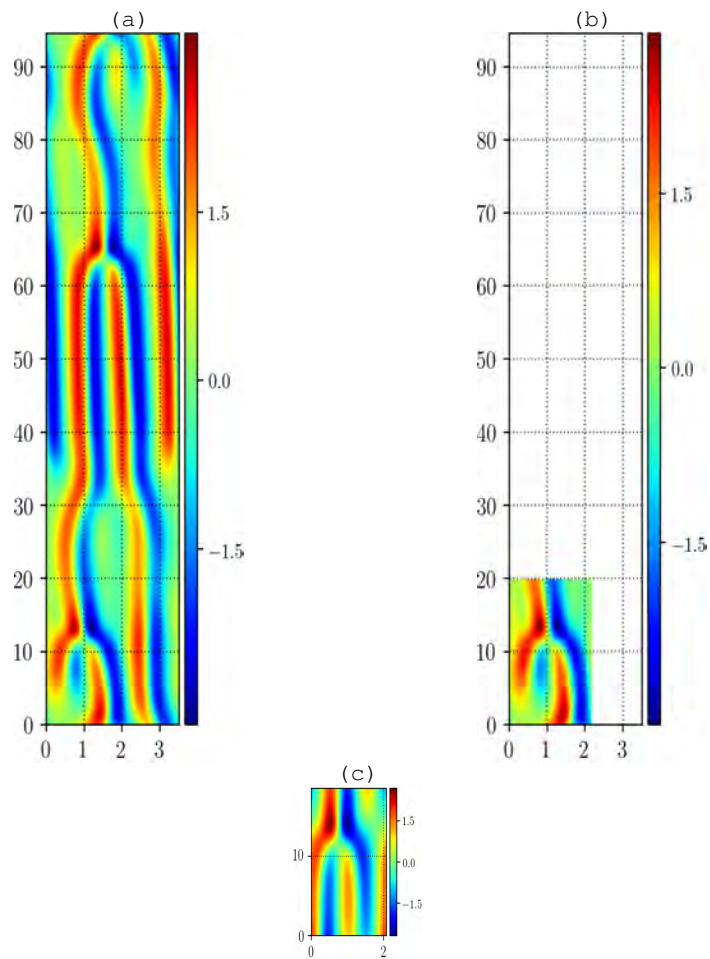
Figure 18.2: (a) $[L_a, T_a] = [3.50\cdots, 94.59\cdots]$ fundamental domain of an already computed invariant 2-torus with spatial translation symmetry. (b) The clipped-out $[L_b, T_b] = [2.2, 20]$ subdomain used the initial guess for the fundamental domain of a shift-reflect symmetric tile. (c) The converged $[L_c, 2T_c] = [2.07\cdots, 15.46\cdots]$ invariant 2-torus with spatial translation symmetry.
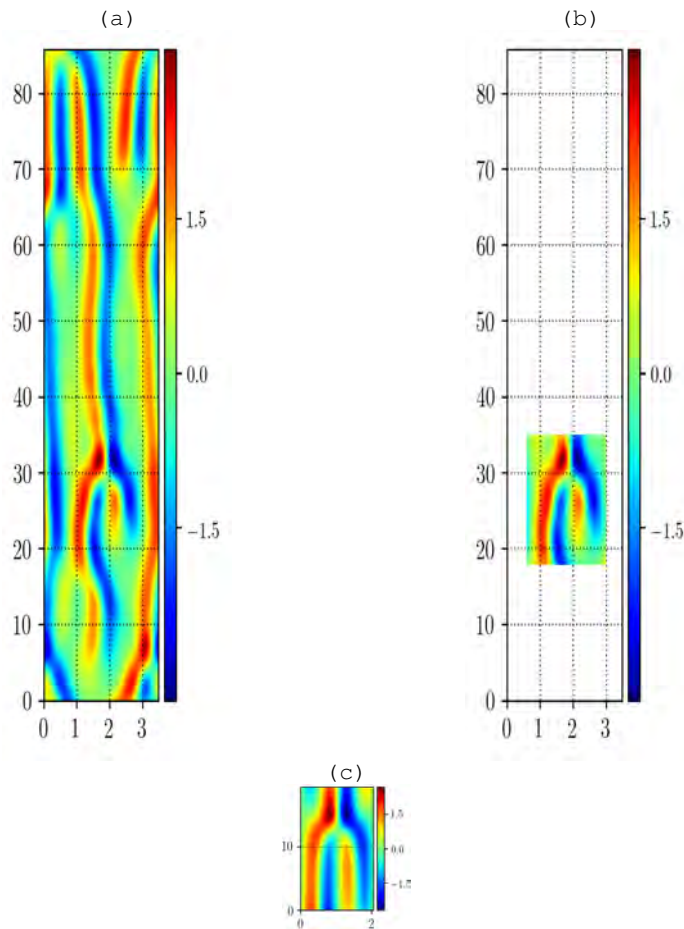
Figure 18.3: (a) $[L_a, T_a] = [3.50\cdots, 85.73\cdots]$ fundamental domain of an already computed invariant 2-torus with spatiotemporal shift-reflection symmetry. (b) The clipped-out $[L_b, T_b] = [2.6, 17]$ subdomain used the initial guess for the fundamental domain of a shift-reflect symmetric tile. (c) The converged $[L_c, T_c] = [2.06\cdots, 19.92\cdots]$ invariant 2-torus with spatial translation symmetry.
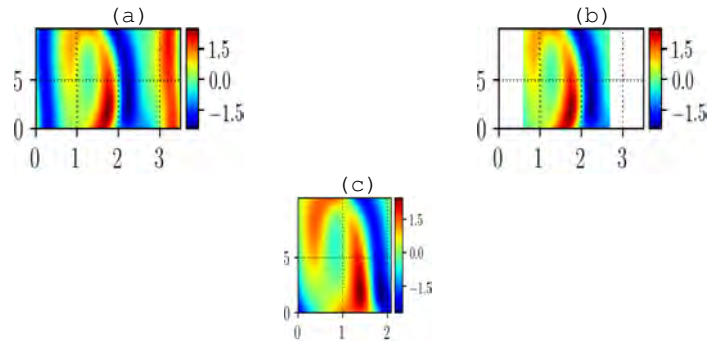
Figure 18.4: (a) $[L_a, T_a] = [3.50 \cdots, 10.25 \cdots]$ fundamental domain of an already computed invariant 2-torus with spatiotemporal shift-reflection symmetry. (b) The clipped-out $[L_b, T_b] = [2.1, 10.5]$ subdomain used the initial guess for the fundamental domain of a shift-reflect symmetric tile. (c) The converged $[L_c, T_c] = [2.08 \cdots, 9.22 \cdots]$ invariant 2-torus with spatial translation symmetry.

of their continuous family can be used. It is the tile's neighbors which determines which family member is used in the gluing process. There are many uses for the process of gluing; the most important being the eventually explanation of infinite space-time by virtue of spatiotemporal symbolic dynamics

By looking at the set of converged gluings it lacks the pattern corresponding to a gap being adjacent to a merger, spatially. Indeed, in almost every

Here are some examples,

This process depends on the neighbors of the tiles as well; it seems to be primarily influenced by spatial neighbors. For instance, in

Another common occurrence is the stretching of solutions in time where large swathes shadow equilibria. The numerical description of this effect is that during the variational search the time dimension being stretched, as evidenced by the large difference in time period. This reduces the magnitude of the temporal tangents which brings it close to equilibria In other words, stretching of the variational "rubber band" kills any tangential variation. This process is evidenced by numerical continuation of various solutions. For instance, the merger tile has a maximum spatial domain size at which point the torus essentially contracts into a relative equilibrium. This process is (numerically) irreversible; reducing the domain size of the newly found relative equilibrium does not bring the original merger tile back.

For our purposes a collection on the order of a thousand invariant 2-tori was collected but this was likely overkill; as seemingly indicated by the number of fundamental tiles.
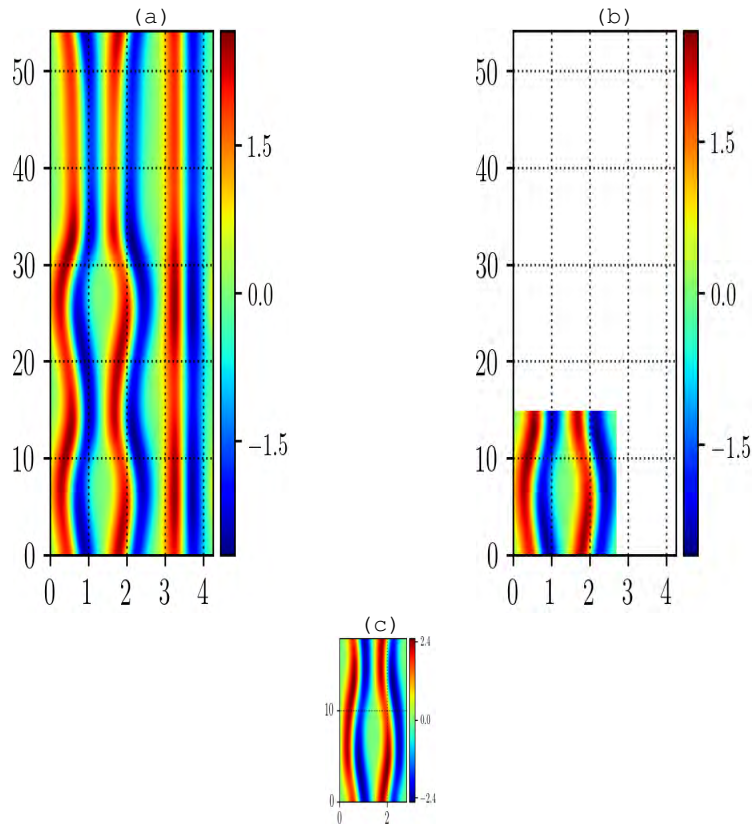
Figure 18.5: (a) $[L_a, T_a] = [4.25 \cdots, 54.13 \cdots]$ fundamental domain of an already computed invariant 2-torus with spatiotemporal shift-reflection symmetry. (b) The clipped-out $[L_b, T_b] = [2.7, 15]$ subdomain used the initial guess for the fundamental domain of a shift-reflect symmetric tile. (c) The converged $[L_c, T_c] = [2.90 \cdots, 17.95 \cdots]$ full reflection symmetric invariant 2-torus.
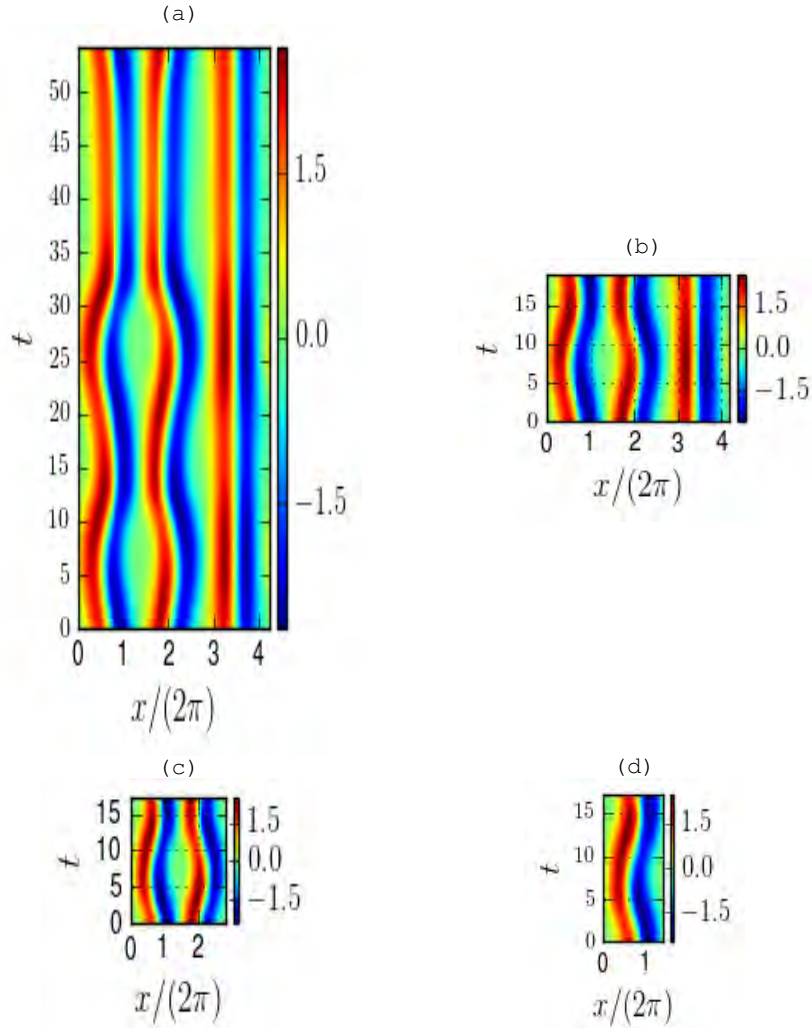
Figure 18.6: Sequential subdomain extraction to find tiles. (a) A periodic orbit from the collection of new solutions $[L_a, T_a] = [4.25 \cdots, 54.12 \cdots]$. By taking progressively smaller subdomains (b)-(d) and numerically converging them to invariant 2-tori at each step, we are able to find the smallest subdomain of (a) which can be converges to a invariant 2-torus, namely (d). (b)$[L_b, T_b] = [4.16 \cdots, 18.93 \cdots]$ (c)$[L_c, T_c] = [2.79 \cdots, 17.14 \cdots]$ (d)$[L_d, T_d] = [1.39 \cdots, 17.14 \cdots]$
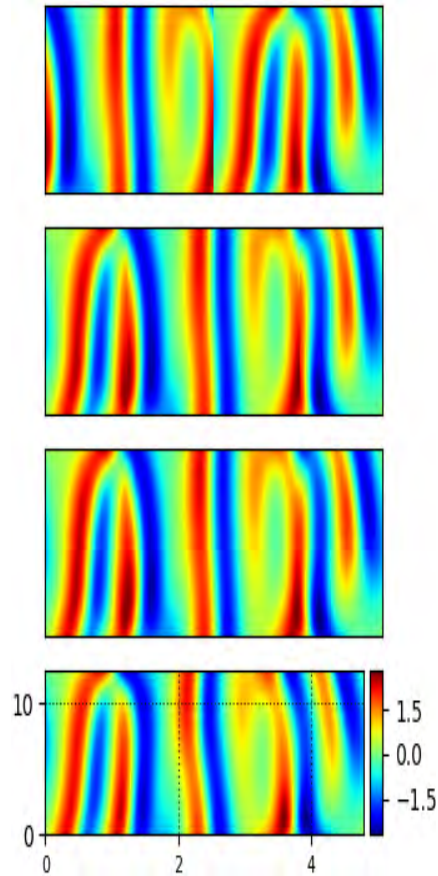
Figure 18.7: Spatial gluing of the two shortest shift-reflection invariant 2-tori. The sizes of the fundamental domains of these invariant 2-tori are $[L_1, T_1] = [3.5\cdots, 20.50\cdots]$ and $[L_2, T_2] = [3.5\cdots, 28.66\cdots]$ respectively. The result is a shift-reflection invariant 2-torus with $[L_{1,2}, T_{1,2}] = [6.79\cdots, 24.82\cdots]$ fundamental domain.
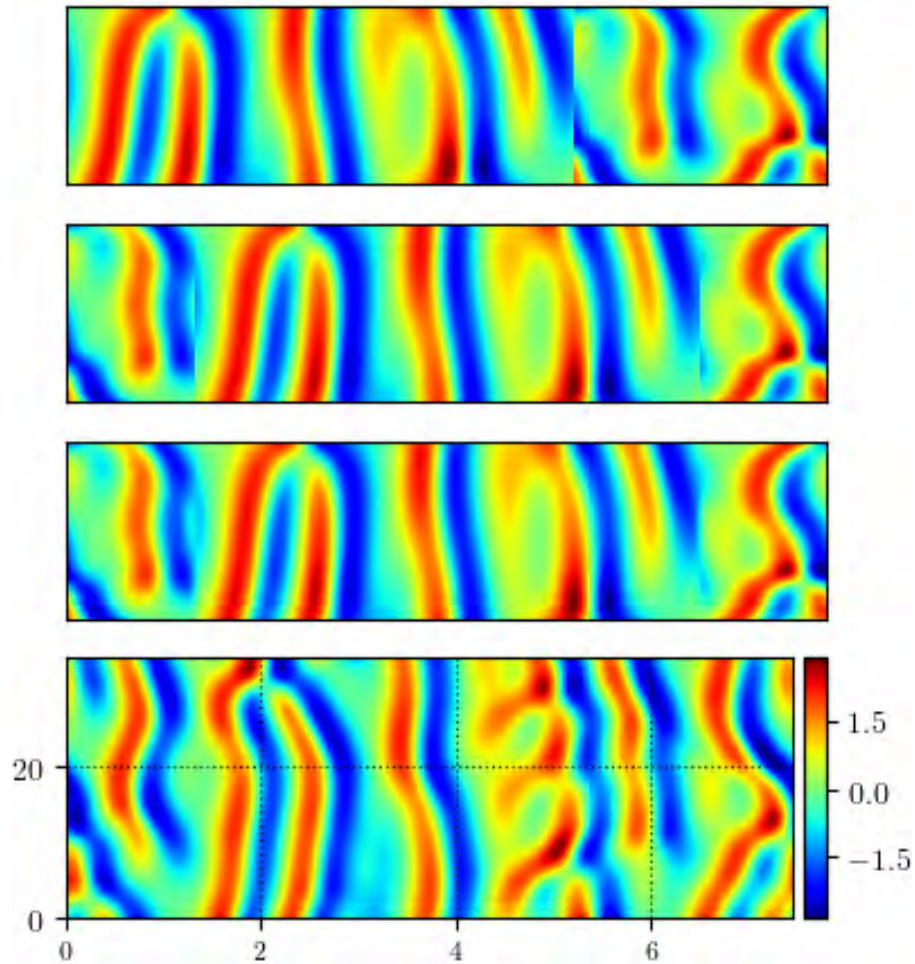
Figure 18.8: Gluing procedure which spatially combines the third shortest (period) shift-reflection invariant $[L_3, T_3] = [3.5\cdots, 64.70\cdots]$ invariant 2-torus with the resultant shift-reflection invariant invariant 2-torus from reffigfig:ppo12spaceglue with $[L_{1,2}, T_{1,2}] = [6.79\cdots, 24.82\cdots]$ fundamental domain. This results in another shift-reflection invariant 2-torus with the $[L_{1,2,3}, T_{1,2,3}] = [10.53\cdots, 68.84\cdots]$ fundamental domain. The dramatic change between the last two panels is presumably an effect of the discrepancy between the temporal period of the constituent solutions.
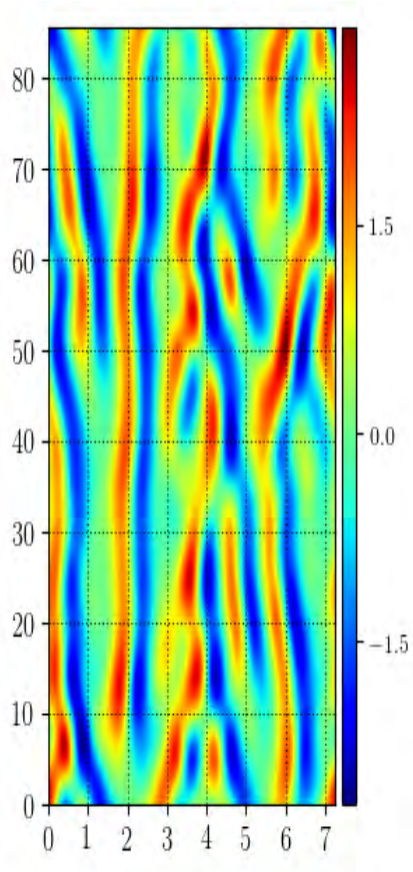
Figure 18.9: Spatial gluing of the two shortest shift-reflection invariant 2-tori. The sizes of the fundamental domains of these invariant 2-tori are $[L_1, T_1] = [3.5\cdots, 20.50\cdots]$ and $[L_2, T_2] = [3.5\cdots, 28.66\cdots]$ respectively. The result is a shift-reflection invariant 2-torus with $[L_{1,2}, T_{1,2}] = [6.79\cdots, 24.82\cdots]$ fundamental domain.
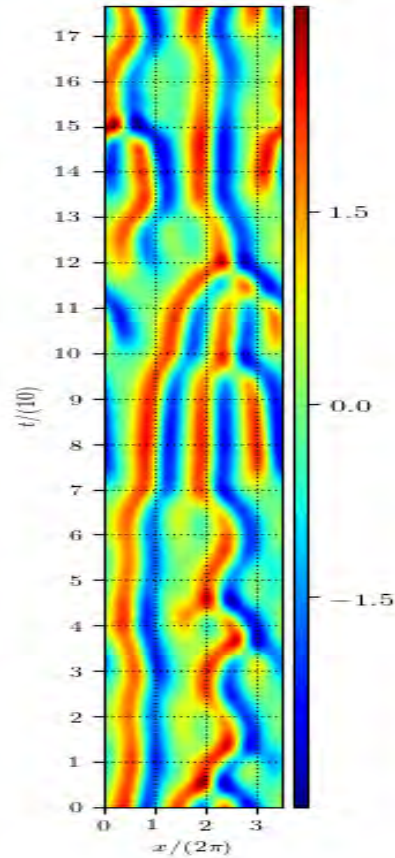
Figure 18.10: Spatial gluing of the two shortest shift-reflection invariant 2-tori. The sizes of the fundamental domains of these invariant 2-tori are $[L_1, T_1] = [3.5\cdots, 20.50\cdots]$ and $[L_2, T_2] = [3.5\cdots, 28.66\cdots]$ respectively. The result is a shift-reflection invariant 2-torus with $[L_{1,2}, T_{1,2}] = [6.79\cdots, 24.82\cdots]$ fundamental domain.
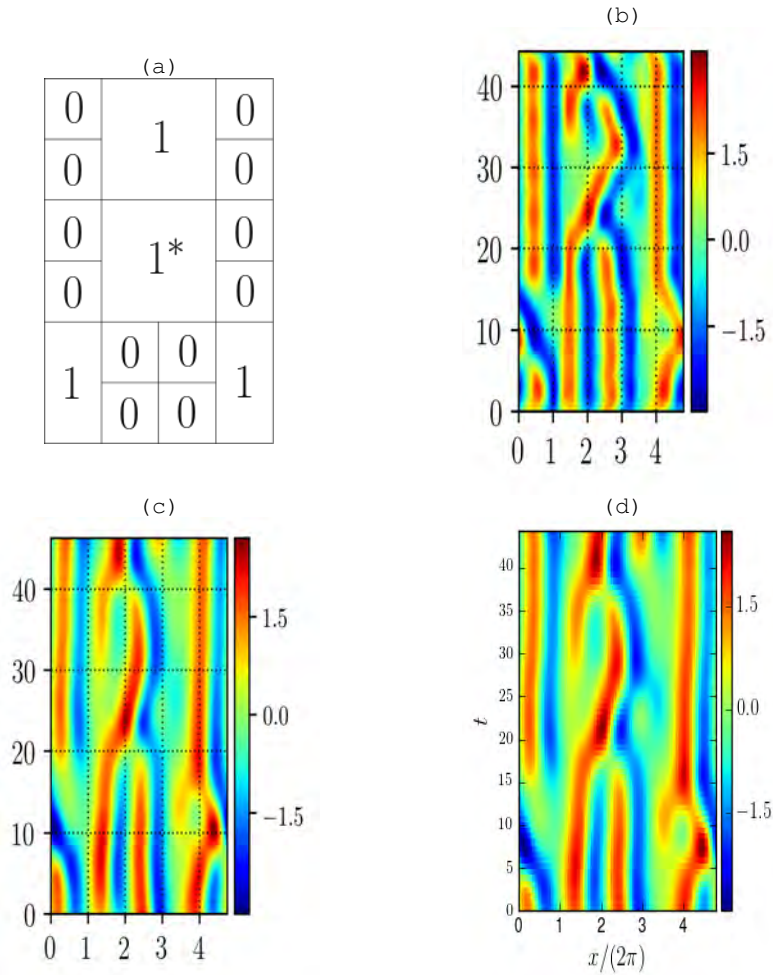
Figure 18.11: (a) Spatiotemporal symbolic block representation created using group orbits of three tile families, (b) initial condition produced by combining tiles according to (a); dimensions initialized at $[L_b, T_b] = [4.79 \cdots, 88.62 \cdots]$, (c) converged invariant 2-torus when using (b) as an initial condition, (d) targeted invariant 2-torus which (c) was trying to match.
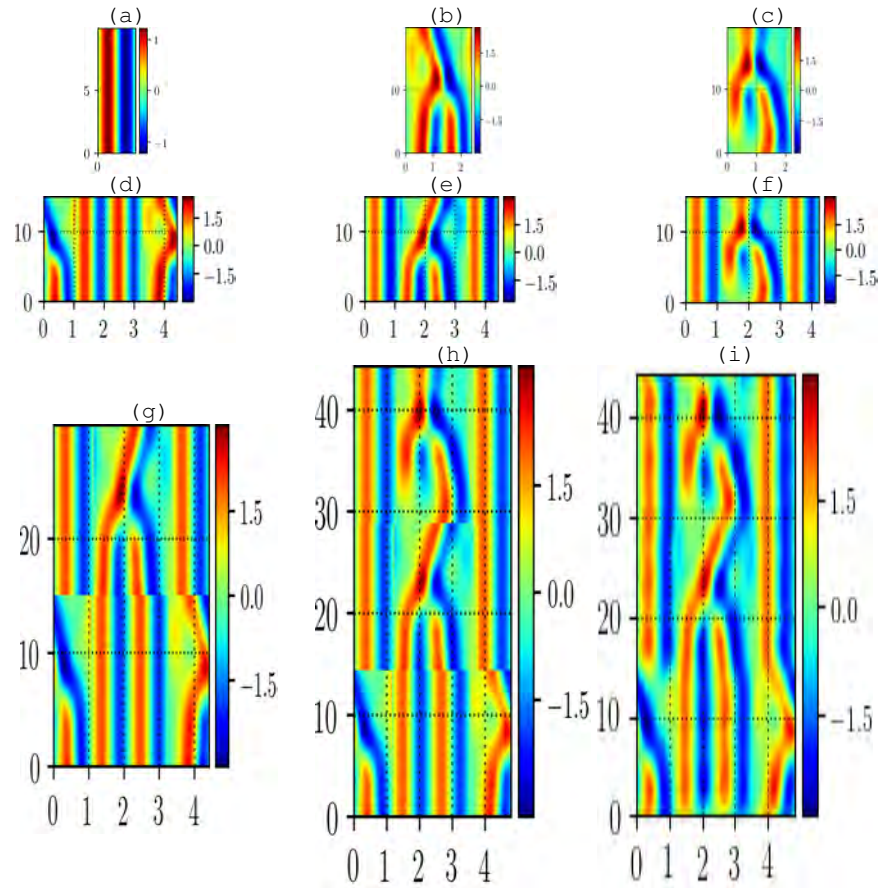
Figure 18.12: Demonstration of how to construct an initial condition corresponding to a specific spatiotemporal symbolic block. (a),(b) and (c) together are the set of tiles used for all other plots in this figure. (d) is a subdomain comprised of two copies of (a) and one copy of (b). (e) is a subdomain comprised of two copies of (a) and one copy of the reflection of (b). (f) is a subdomain comprised of two copies of (a) and a single copy of (c). The last row of figures demonstrate how to combine (d),(e), and (f). (g) is the combination of (d) and (e). (h) is the combination of (d),(e) and (f) (equivalently, (g) and (f)). Lastly (i) is the smoothed version of (h) which will serve as the initial condition.

Figure 18.13: (a) Initial spatiotemporal field for the one-by-two symbolic block given by (1.83) (b) Invariant 2-torus resultant from numerically converging (a), $[L_b, T_b] = [3.13 \cdots, 20.84 \cdots]$
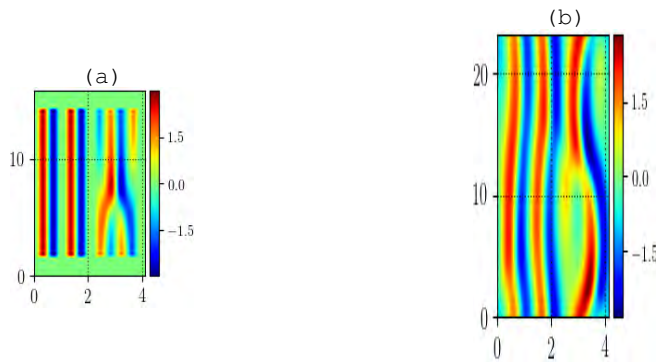
Figure 18.14: (a) Initial spatiotemporal field for the one-by-three symbolic block given by (1.84) (b) Invariant 2-torus resultant from numerically converging (a), $[L_b, T_b] = [4.12 \cdots, 23.15 \cdots]$.
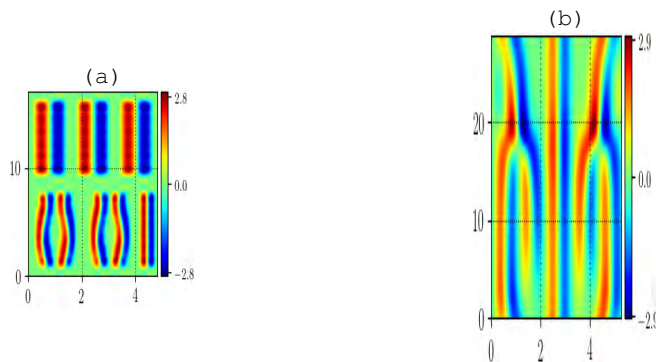
Figure 18.15: (a) Initial spatiotemporal field for the one-by-three symbolic block given by (1.84) (b) Invariant 2-torus resultant from numerically converging (a), $[L_b, T_b] = [4.12 \cdots, 23.15 \cdots]$.
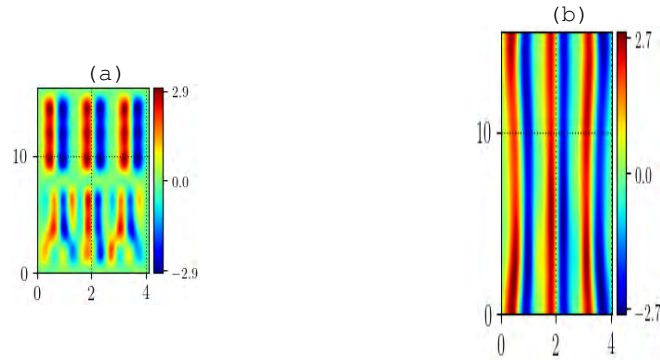
Figure 18.16: (a) Initial spatiotemporal field for the one-by-three symbolic block given by (1.84) (b) Invariant 2-torus resultant from numerically converging (a), $[L_b, T_b] = [4.12\cdots, 23.15\cdots]$.
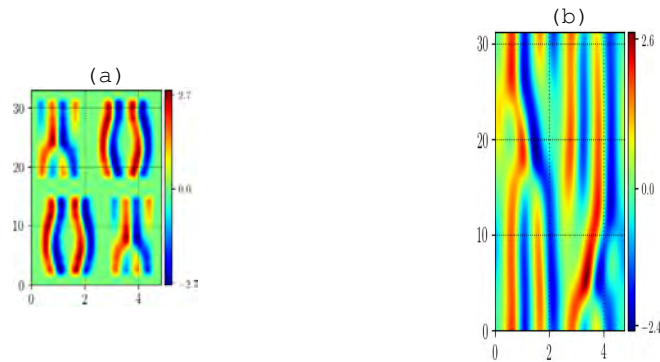
Figure 18.17: (a) Initial spatiotemporal field for the one-by-three symbolic block given by (1.84) (b) Invariant 2-torus resultant from numerically converging (a), $[L_b, T_b] = [4.12\cdots, 23.15\cdots]$.

It is of course desirable to match tiles based on their boundaries as to reduce the severity of numerical discontinuities. A more subtle reason to access the entire family is to match the spatiotemporal domain size of the neighbors. Solving the optimization problem is equivalent to enforcing the tangent space to behave according to the governing equations. The magnitudes of the each tangent; spatiotemporal derivatives, are affected by the magnitude of the temporal and spatial domain sizes.

This paper mainly sets the stage and shows the feasibility for a spatiotemporal theory. There is still much more work required to advance the theory.

Some of the main detractions and foreseeable criticism

Not only do we lack the symbolic dynamics to describe infinite spacetime, we also describe a smart system for enumerating all invariant 2-tori. We currently lack a systematic approach for the enumeration of all

Criticisms of these methods Solving the linear system directly by computing the (pseudo) inverse of the matrix is only available for problems of dimension smaller than those that occur in Navier-Stokes computations. In fact, this method wouldn't be feasible in the larger case at all and would have to be replaced with an alternative; a common choice is to use iterative methods such as GMRES [28]. Another aspect that has room for improvement is the choice of norm used in the cost function. There have been cases where the approximate invariant 2-torus hardly changes (visually) even though the cost function is decreasing from 10^{-4} to 10^{-14}. The tolerance is strict because we want the best approximations possible; especially in regards to the fundamental tiles whose acquisition is detailed next.

Did not include considerations of local non-zero galilean velocity.

A common criticism and source of skepticism as to these methods is the requirement to maintain the entire spatiotemporal discretization in memory. While this is proper cause for concern, comparisons with other studies shows a dramatic increase in performance. For example, in [21], the tolerance was much less strict, the discretization was larger, and the numerical methods required the inversion of large matrices.

In our case, coarse spatiotemporal discretizations remain viable and because the convergence is occurring in spectral space it is not only easier to interpolate points (via zero padding of the spectrum) but also produces more accurate results than with finite differencing.

2020-2-21 Matt Refs. [6, 7, 29] introduce and parallelize a method known as "spectral deferred corrections". Ref. [7] applies it to a square $L, T = 100$ domain of the Kuramoto-Sivashinsky equation. In the applications it does not assume periodic boundary conditions in time but it does treat the problem spatiotemporally. The distinction that is made is that time
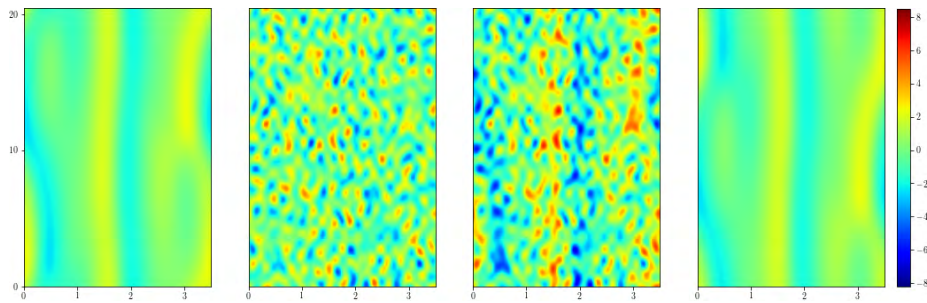
Figure 18.18: (a) Original, converged invariant 2-torus $[L = 21.99..., T = 20.50...]$, (b) aperiodic noise taken from standard normal distribution, multiplied by the L_∞ norm of (a), (c) is the sum of (a) and (b), (d) is the invariant 2-torus that (c) converges to, $[L = 22.18..., T = 20.58...]$.

integration of the discretized ODE's is not the same as solving the underlying PDE.

> *In all cases, the errors reported are computed by comparing to a temporally resolved run on the fine grid (i.e., the solution of the discretized ODE and not the solution to the underlying PDE).*

They use a coarse grid to represent the solution and then corrections are made by solving multi-shooting on a sequence of fine grids created via polynomial interpolation. Because they interpolate, they evaluate the equations of motion at the grid points and then use "spectral integration" to evaluate the integral. Ref. [6] do not use $x_{n+1} - f_n$ as their cost function for their "multishooting". For some reason their cost functions always starts from the beginning of the fine grid and then define the cost function to be $x_{n+1} - (x_0 + f^{t_{n+1}}(x_0))$. In, [7], the entire domain is not solved for at the same time, rather this process sweeps or scans through time (see figure 11). The parallelization component comes in from solving the optimization problem on each fine grid in parallel. The main application seems to be improving the temporal error introduced by time integration schema; specifically, it provides good corrections even though the order of the methods being applied in parallel are of lower order than the original method.

2020-03-03 Matt For a sense of how much noise is added, the maximum and minimum values of the fields in figure 18.18 are (a) $\approx \pm 2.47$ and (c) $\approx \pm 8$. All four fields are included in a single figure to make it easier to have them share the color legend.

2020-03-03 Matt

2020-03-03 Matt Added the skeletons for the body and future work sections of the paper.
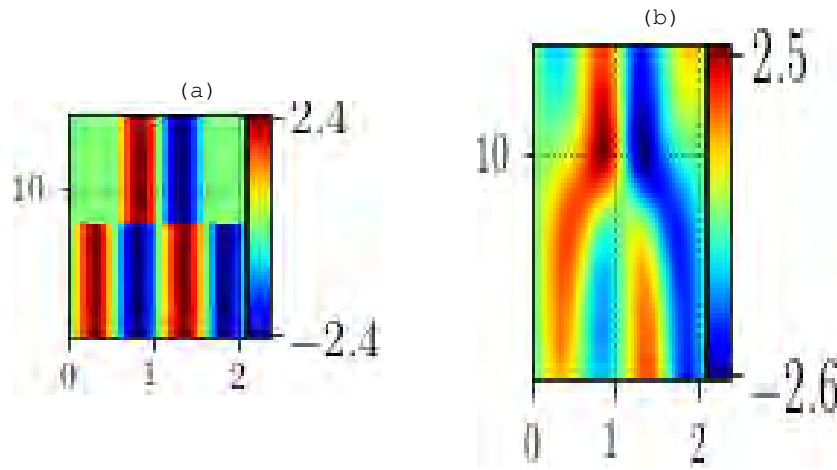
Figure 18.19: (a) Initial condition composed of three streaks and an region of zeros, imbued on a spatiotemporal domain approximating the known tile's domain size. (b) The tile that (a) converges to.

2020-03-05 Matt Condensed version of summary. want to check the length and wording at today's meeting.

2020-03-19 Matt physicists average over everything and get some number. Repetoire of admissible patterns, this is not the usual thing. Full description not an average number obtained. I say such and such patterns can exist, if this is the law that describe.

working on a problem that has been around since 1822, a century of wrong predictions (Eulerian flows). No one has a theory of turbulence that everyone agrees is *the* theory of turbulence. Work on this problem at a time when the computational methods available to me are able to describe the solutions compatible given the equations.

Critique based on the setting, Kuramoto-Sivashinsky equation, it is not a fluid it is a one-dimensional model but this puts me in common with many people. There is a large population that have followed this path as a means of exploring new ideas. Most recent nobody pays attention to it.

Approaching a problem that people understand is a problem. I am following one line of attack which is not the historical one. Starting with the laws and then deriving the consequences. Tackling a difficult problem which most people use to develop techniques (KSE) (GHC N-S, C-CHristianze-Pukradtze KSe). Not in the Kolmogorov spirit, derive some number Lots of instabilities in space and time, not able to extend results to larger domains because the methods we've been using are very unstable. Spatiotemporal has access to methods that cannot be done otherwise be done. Globally they are right and locally the Decent solutions with-
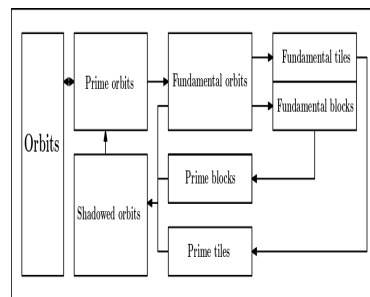
Figure 18.20: This flow chart represents the order that is required to make spatiotemporal constructions. The flow from orbits to prime orbits to fundamental orbits represents the process of searching for solutions and then clipping out the fundamental tiles. Once the fundamental tiles are converged, the fundamental tiles are well defined (the space-time on which the fundamental orbit sits) as well as the fundamental blocks (the names that we assign to the unique pattern found in the fundamental orbit). In order to glue, there are three requirements, the prime configuration of blocks, the prime tile that they are defined on, and the approximate state that exists on the prime tile. Only after the prime tile and prime block are in place can the fundamental orbits be laid out on the prime tile. With this, an approximate solution that is shadowed by a prime orbit is made. By converging this shadowed orbit we arrive at the prime orbit it is shadowed by. Symmetry operations and space-time periodicity then produce the entire (global) orbit.

out insisting on a very high accuracy. Able to describe general solution. This is exploratory and difficult problem. It is harder than our situation because we are using $1 - D$. Write it in such a way that they do not have to stare at the equations too much as opposed to previous formulations.

More credible setting than cat map setting. Use the fundamental patterns to describe larger and larger solutions.

The way that deciding on the fundamental patterns is done via the stability. It is derived. Every solution has a weight that is roughly inversely proportional to unstable directions. "There is a theory of temporal systems that says every such solution such as the one I am finding, its importance is given by 1 over stability. The big ones are unstable and take larger neighborhoods. When I say I have a fundamental tile, it has a very large neighborhood. In Lorenz we say we are close to this fixed point or that fixed point. Haven't done explicit derivation so I can only argue from analogy. The other way is the frequency. Historically they take very narrow spatial strips and look at temporal recurrences, more recurrences means more importances. This affects our intuition of importance. Now we say that we are extending this idea, close recurrence in time (something that everyone is comfortable with), and now just extending it to spacetime. Haven't succeeded mathematically, but have succeeded in finding these solutions.

Spatiotemporal defect. Spatiotemporal chaos literature supports this name. Number of rolls, at sometime the name changes. What it really is in my case is the skip by $\pi/2$ in the phase; more abstract wiggle. wiggle, skip, swerve, curve, bend, streaks wavy solutions at time, peaked at square root of two. Do not have wavy structure in time.

Fixed points in time much more robust. Much more characteristic shapes that are building up spatiotemporal solutions. GO down to smallest possible one and call them fundamental. Use the fundamental ones to build back up the others. Shown consistency, everything shown to the reader is a numerically exact solution to the law (equations). On a democratic footing. Believe solution is important because it shadows generic spatiotemporal solution by being seen frequently.

Many open problems that are not covered in this first paper. Reflects what is observed in this kind of system.

2020-03-22 Matt Task: Library results section Indication of completion: when there is sufficient information such that a reader in our field could walk away having a good idea of what kind of solutions have been and could be found?

To this end, need to describe the types of solutions and their importance.

Clipping and gluing periodic orbits have sections dedicated to them so this section considers everything excluding results of those types. I am also including continuation of in those sections because chronologically

clipping precedes finding fundamental periodic orbits. The types of solutions remaining then amount to the following brainstorming of examples:

- "homoclinic" orbit that occurs frequently in antisymmetric subspace.
- relative periodic
- preperiodic
- antisymmetric
- eqva? reqva?
- Solutions that would be antisymmetric upon imposition of reflection axis. (original "po")
- solutions seen in other papers?
- initial conditions?
- small
- (relatively) large orbits
- different members of the same group orbit.
- "homoclinic" orbit with different symmetries
- highly tilted rpos, nearing relative equilibria `rpo_L24p06_T69p30`
- "stretched" solutions that occur near transition of unstable mode to new frequency.
- underresolved?
- examples of very frequent fundamental periodic orbits shadowing

Stratifying these into categories to compile the narrative.

- example initial conditions.
- Examples of every symmetry type, size, repeats.
- Outliers, "homoclinic", "isolated" (typically antisymmetric), rpo tilt
- "bad" results, numerical under resolution
- orbits which demonstrate frequent repetition of a single pattern.

Added macros for the titles of fundamental periodic orbits and referral to the spatiotemporal domain size (lattice size? spatiotemporal area?) as well as subdomains

2020-03-31 Matt Other spatiotemporal methods such as the Newton descent method developed in [22] gave an indication as to the typical spatiotemporal discretization size required to resolve periodic orbits with $L = 22$ but not in the context of (1.26). Regardless of the discretization size, these known solutions would never be solutions to (1.26), due to the intrinsic error induced by numerical integration. Ref. [7] summarizes this nicely by saying "solving a discretized system of ODEs is different than solving the underlying PDE".

continuation of shift-reflect orbit as relative periodic? maybe the shift reflect is the bisection of the "real" fundamental periodic orbit. Look for invariants.

2020-04-13 Matt Looking forward, the main computational benefit of spatiotemporal methods is that spatiotemporal method can be computed in parallel; therefore, the method scales with the number of computing cores as opposed to computing speed. The idea is to subdivide a large spatiotemporal domain into small subdomains, solve the equations locally and then let these subdomains communicate with each other. This construction merges seamlessly with our spatiotemporal theory in the context of fundamental periodic orbits. These fundamental periodic orbits present topologically motivated computational subdomains as opposed to arbitrary ones. The downside, however, is that subdivision breaks the periodic boundary conditions and hence removes the ability to use a Fourier basis. Our intuition tells us that the best schematic moving forward goes something like this: for dimensions of small extent, assume periodic boundary conditions (if possible) and use a Fourier basis. For dimensions of large extent, when it is necessary to subdivide, use a Chebyshev polynomial basis on the subdomains. Likewise, for non-periodic boundary conditions we also recommend Chebyshev spectral methods. These choices incorporate our bias against finite element methods, but as long as the treatment is spatiotemporal and the inherent instability is not included, finite element methods might have merit. This is confusing but the concept is hard to explain and likely harder to understand.

To quell any confusion we offer the following example: it is intuitive to imagine a $3 - D$ spatial domain subdivided into cubes (for sake of simplicity). The extension of this to $4 - D$ space-time is to simply extend this subdivision so that each subdomain is now a $4 - D$ hypercubes. This is a method to find periodic orbits. Therefore the temporal dimension is always periodic. If the temporal period is small enough that subdivision is not required, then by following our own guidelines the computational domains would be discretized by Chebyshev collocation points in the three spatial dimensions but Fourier modes in the time dimension. Therefore, in this example, the subdomains are not $4 - D$ hypercubes but rather domains with three finite dimensions (space) and one infinite dimension (time). This is, of course, hard to visualize; at any given time the snapshot looks like a cube, string these (periodic) snapshots together and you get a periodic orbit. In $(2+1)$ dimensional space time the picture that comes to mind is a toroidal solenoid with square cross section. The usage of $4 - d$ hypercubes is assuming the "worst case" scenario when the computational domain is so large that each dimension *has to be* subdivided. It may be sufficient, however, to simply increase the number of Fourier modes (and in fact, this is what we will likely implement first). The main reason why we include this description is to incorporate non-periodic boundary conditions which occur in fluid dynamics calculations. Histor-

ically, these have been handled in fluid dynamics research by the afore-mentioned Chebyshev basis. This type of creative problem solving will be crucial for solving higher dimensional equations spatiotemporally. All of this speculation considers higher dimensional equations, but there is still much work to be done on the theory for the Kuramoto-Sivashinsky equation.

The suspected way forward is to use Hill's formula. Without going into too much detail, this relates the (infinite) determinant of the Hessian of the action functional to the characteristic polynomial of the monodromy matrix of a periodic orbit. Simply speaking, this would allow us to relate our variational formulation to stability, even in the absence of dynamics.

2020-04-16 Matt Ideas for names to replace "symbolic dynamics"

In our previous meeting we discussed the origin of symbolic dynamics which was to utilize discrete "time" to quantify chaotic dynamical systems (period moving through a 1-D time itinerary). Obviously we want to keep the word "symbolic" but we need a replacement for "dynamics".

The new name should be able to describe a *system* with which tori are described. In other words I believe it should account for the overarching hypothesis that we use: infinite space-time is a collection of space-time shadowing events. So it should be a concise way of saying "System of symbolic representation and shadowing?" which does not

I think that if we can find a word that fits the phrase "*d*-dimensional symbolic ******" then we will be straight.

Candidates that I've thought of to replace "symbolic dynamics" We likely still want to use the "linguistics" themed terminology like alphabet and grammar so perhaps we should stick

- *d*-dimensional symbolic syntax
- *d*-dimensional symbolic structuring
- *d*-dimensional symbolic system
- *d*-dimensional symbolic rendition
- *d*-dimensional symbolic characterization
- *d*-dimensional symbolic classification
- *d*-dimensional symbolic representation
- *d*-dimensional symbolic discretization
- *d*-dimensional symbolic presentation
- *d*-dimensional symbolic method
- *d*-dimensional symbolic fragmentation
- *d*-dimensional symbolic decoration
- *d*-dimensional symbolic marking

- d-dimensional symbolic tessellation
- d-dimensional symbolic amalgamation
- d-dimensional symbolic demarcation

We want to say that the solutions are $D + 1$ tori but the notation we decided on uses

How do we distinguish between our D+1 invariant tori and the 1-dimensional periodic orbits? We decided on using periodic orbits and fundamental periodic orbits but I feel like this makes it seem like we're not doing anything new.

2020-04-17 Matt The first key difference is that the governing equation dictates the spatiotemporal domain size in an unsupervised fashion. The results here are not The only reason why L was treated as fixed is due to the inherent instability it includes when treated as a varying quantity. This small detail, allowing the domain size L to vary, is not as trivial as it seems. This difficulty is especially evident in the Kuramoto-Sivashinsky equation, whose spatial derivative terms are of higher order than the first order time derivative, but also there is a spatial derivative present in the nonlinear component.

2020-04-30 Matt cut from tilebody.tex For example, in [20] the spatiotemporal dimensions used to define periodic orbits was stated to be $M = 32$ points in space (in their case the spatial period is fixed at $L = 22$) and either $N = 512$ or $N = 1024$ in time, depending on the time period. For our methods we found that for similar periods the spatial dimension remained the same but the temporal dimension could be reduced to either $N = 32$ or $N - 64$. This is an improvement by a factor of 16; we emphasize this improvement as perhaps the most common criticism of spatiotemporal methods is regarding the computational memory requirements.

The most notable is that we no longer have to grapple with exponential instabilities. One consequence of this is that we can now find periodic orbits starting only with randomly initialized Fourier coefficients defined on arbitrary fundamental tiles. This specifically eliminates the time-consuming processes of time integration and searching for close recurrences.

Sometimes, possible improvements hint towards the grammar of the symbolic dynamics. For instance, it seems unwise to glue the spatiotemporal streak and spatiotemporal defect temporally, as this does not conserve the number of wavelengths; additionally, there is a large discrepancy between the spatial periods. This implies that a single spatiotemporal streak should not be glued in time with a spatiotemporal defect. This configuration (spatiotemporal defect followed by two spatiotemporal streak in time) is inconsistent in a symbolic manner. Likewise, false positives occur when a guess for a block converges to the "wrong" periodic orbit. To

alleviate this problem we need topological invariants which can be used to both identify continuous families but also the fundamental periodic orbits they are being shadowed by.

2020-05-03 Matt comments on determining grammar in unsupervised manner. As a consequence of partaking in a extensive data science / machine learning training course I'm learning how to implement different types of neural networks.

This is likely the best manner with which to pursue automated, unsupervised identification of fundamental periodic orbits in periodic orbits going forward. Specifically, convolutional neural networks work very well on image recognition and there are specific techniques to "crowd count". Also with the addition of details such as max pooling, the process can be robust to translations and rotations (i.e. it has the potential to be able to pick up different members of each fundamental periodic orbit family. It would be worth testing but I'm guessing it will not be so easy as crowd counting techniques only count the number of people; they do not distinguish between people. There is also the possibility that fundamental periodic orbits are too similar looking to be distinguished by these methods.

2020-05-03 Matt Adding footnotes and highlights of most recent edits; the entire paper is essentially new in the past week, however.

clipping from tilebody In hindsight we learned that it is possible to impose shift reflection symmetry as opposed to spatial translation symmetry, using the original clipping as the fundamental domain. Because we know that every solution has a reflection partner due to the symmetries of the Kuramoto-Sivashinsky equation, every relative periodic orbits exists as a pair related by reflection having equal and opposite spatial shifts. Gluing these two solutions temporally creates and initial guess for a shift-reflect invariant periodic orbit. While not tested, it might be better to not assume relative periodicity is that the initial guess for the spatial shift parameter is sensitive to how the initial guess is clipped.

2020-05-14 Matt excerpt from "what" section.

The nonlinear term is computed in a *pseudospectral* fashion as elementwise product in physical space as opposed to a double-convolution in Fourier space. The definitions of each term is as follows: $\mathcal{F}$ and $\mathcal{F}^{-1}$ represent the forward and backwards spatiotemporal Fourier transform operators. Likewise, $\omega = [\frac{2\pi}{T}, \frac{4\pi}{T}, ..., \frac{2\pi N}{T}]$ and $\mathbf{k} = [\frac{2\pi}{L}, \frac{4\pi}{L}, ..., \frac{2\pi M}{L}]$ are the temporal and spatial frequencies corresponding to a set of Fourier modes. Their multiplication with the spatiotemporal Fourier coefficients produces the corresponding partial derivatives through spectral differentiation [1]. Technically speaking both ω and $\mathbf{k}$ actually represent a number of repeats of their frequencies; our usage of a vectorized notation avoids

indices but it should be understood that each contains $N \cdot M$ values, corresponding to the entire set of Fourier coefficients.

excerpt from gluing-what section; probably fits better in summary or results.

We already have the two edges of this symbol plane - the $L = 22$ minimal cell [3, 22] is sufficiently small that we can think of it as a low-dimensional ("few-body" in Gutkin and Klaus Richter [8–11] condensed matter parlance) dynamical system, the left-most column in the Gutkin and Osipov [16] $2D$ symbolic dynamics spatiotemporal table (not a 1-dimensional symbol sequence block), a column whose temporal symbolic dynamics we will know, sooner or later. Michelson [27] has described the other edge of the symbol plane, the $T = 0$ line whose analogy would be "many-body" steady state solutions. There are converged periodic orbits which resulted from these constructions but we have yet to determine or parse any grammar rules from said combinations.

2020-05-14 Matt Changes to tileintro: entire 'what' section reworded, symbolic dynamics exposition and numerical explanation of Fourier mode equation pruned. (in above blog post).

'new capabilities' in 'why' section pruned.

Initial guesses rearranged, instead of Fourier modes, then periods and discretization it is the other way around, which is the only logical way of actually doing it (to initialize the modes you need to know how many there are, of course).

old gluing section The exact numerical choices which define the method should be treated as preliminary ones; we believe that many improvements can (and should) be made. The only absolute requirement with this method that at the "gluing boundaries" between periodic orbits or fundamental periodic orbits there must be an identical number of points. It is of course recommended that the differences in periods be small but this is technically not required. As this is the direction we are heading anyway, we shall go into futher detail of the gluing technique in the context of spatiotemporal configurations of fundamental periodic orbits; a technique designed to determine the admissibility of blocks of the proposed 2-dimensional symbolic represention. The general case is that we have a $s_j \times s_k$ sized block. Each of these symbols represents a specific fundamental periodic orbit such that the state of each block can be represented as the configuration of $u_j \times u_k$ fundamental periodic orbit states. The mission is to combine these states in a numerically coherent manner. Before we detail the choices we made, first we discuss their motivations. There are two main sources of error resultant from gluing: discontinuities created at the gluing boundaries and the error introduced into the tangent space by the new approximations of $((\Delta t)_j, (\Delta x)_j)$. When combining fundamental periodic orbits, then, it makes sense that we make choices which attempt to reduce these factors. In the first version of

the fundamental periodic orbit gluing method, both of these are handled with zero-padding; albeit one occurs in Fourier space and the other occurs in physical space. The zero-padding in Fourier space is a method of interpolating points to increase the fidelity of the velocity field state. Each fundamental periodic orbit state is defined on a fundamental tile with (N_j, M_j) points and periods (T_j, L_j). The first step taken was to zero-pad the Fourier coefficients of each fundamental periodic orbit, increasing the resolution of each fundamental periodic orbit's state. This was done in a manner such that for each new fundamental tile discretization, $(\tilde{N}_j, \tilde{M}_j)$, the grid spacing are approximately constant between all fundamental periodic orbits

$$(\frac{T_j}{\tilde{N}_j}, \frac{L_j}{\tilde{M}_j}) = ((\Delta t)_j, (\Delta x)_j) \approx (\Delta t, \Delta x). \tag{18.17}$$

Technically these high resolution copies are no longer exact solutions, but because this is simply a method with which to create initial guesses we deemed this as acceptable. As previously mentioned, gluing is only well defined if the lattices being combined have the same number of grid points along the gluing boundary.

The physical space zero-padding is just as it sounds, a 'buffer region' of zeroes is appended to each fundamental periodic orbit state. Because it is done to each fundamental periodic orbit there will no longer be any discontinuities; the error therefrom is instead exchanged for error in the tangent space. Dynamically, we know that regions of zero valued velocity fields do not happen due to linear instability; the variational formulation is able to 'fill in' these regions with the correct values such that the final state is a solution.

Therefore (18.17) will be betrayed in one manner or another; the choice we made again utilizes padding, but this time we zero-pad in physical space. This introduces a 'buffer region' of zeros around each fundamental periodic orbits' original state. We elected for the simplest method for approximating the new periods which is to simply add or average, depending on the gluing direction. As an example, when gluing a pair of periodic orbits together in time the new temporal period for the approximation is set to be $T = T_1 + T_2$ while the spatial period is set to be $L = \frac{L_1 + L_2}{2}$ (if the gluing was in space, the average and summation operations would be permuted). In this case the number of spatial grid *points* and temporal grid *spacing* are made to be the same. These choices become less obvious when gluing is extended to arbitrary spatiotemporal combinations. The difficulty arises from maintaining as uniform of a grid spacing as possible while also satisfying the requirement for the equal number of points along each boundary. The current implementation combines the gluing methods for space and time by building up spatiotemporal combinations via spatial or temporal strips. This worked

sufficiently well such that "full" gluing process defined by gluing all constituents in a single step was left for future work.

2020-05-15 Matt intro, why, excerpts The variational formulation does not completely remove all challenges, however, such as finding periodic orbits on large spatiotemporal domains. However for our purposes we have no need to confront this challenge directly. The current goal is to find only the most important fundamental periodic orbits; believed to exist only on small spatiotemporal domains.

intro, what, excerpts There is no guarantee that the final periods will be near the original values, but the idea is that these initial guesses start closer, and hence converge, to periodic orbits of similar size.

That is to say, the corresponding region of discretized configuration space and the overlying state are extracted; providing an initial guess for an fundamental periodic orbit (or periodic orbit, depending upon what is clipped) which is passed to our optimization methods.

In regards to the Kuramoto-Sivashinsky equation, the clipping is currently a single step procedure; however, we shall demonstrate an iterative usage as other systems may not have this luxury. The process of finding fundamental periodic orbits via clipping is the process of distilling large periodic orbits into small periodic orbits. This smoothed initial guess is then used to search for a periodic orbit. Arbitrary fundamental periodic orbit combinations are not guaranteed to represent periodic orbits; this property is encapsulated by the symbolic representation that we are developing. In other words, gluing constitutes an empirical method used to probe and uncover a 2-dimensional spatiotemporal symbolic representation. Specifically the gluing process as it has just been described is the method that converts blocks into initial guesses for the corresponding periodic orbits.

As a reminder, our collection of periodic orbits need not range over all sizes; which we believe manifest as periodic orbits with small periods. Therefore, the search for periodic orbits was limited to what we consider as intermediate domain sizes. Periods were chosen from the ranges $T \in [20, 180]$ and $L \in [22, 88]$.

but were typically chosen to be powers of two; in order to leverage fast Fourier transforms. Typically, we used a rule of thumb which set the number of points in the spatial dimension as $M = 2^{\lfloor \log_2(L) \rfloor + 1}$ and the number of points in the temporal dimension as $N = 2^{\lfloor \log_2(T) \rfloor}$.

intro, how, excerpts As previously mentioned, we do not use approximate recurrences nor time integration to generate initial guesses. Instead, initial guesses can be generated by initializing arbitrarily sized domains with random noise. More specifically, random values are drawn from the standard normal distribution and assigned as the values of the corresponding Fourier modes. These modes may then rescaled in a manner that befits a doubly periodic solution of the Kuramoto-Sivashinsky

equation, manipulating the Fourier spectrum to match the relevant scales of the Kuramoto-Sivashinsky equation. In our experience, however, the initial guesses which are 'worse' with respect to the cost function actually converge more often; or, equivalently by our standards, they seem to get trapped by local minima less often. It is therefore hard to provide a recommendation for a single or 'best' manner with which to provide initial guesses. The numerical methods we employ do not seem to be interested in our desire to produce a physically motivated construction method drawn from our experience and intuition.

The termination of the descent is determined by either error threshold or step limit; though there are arguably better termination conditions such as the Wolfe or Goldstein conditions.

Euler's method is used because it is the simplest and fastest integration scheme. The integration need only be as accurate as necessary to decrease the cost function; we only care as to whether we are approaching a periodic orbit or not.

The first is to solve (**??**) in a least-squares manner [4], the second is to include constraints which make the system square, the third is to solve the system of *normal equations* which result from multiplication of both sides of (**??**) by $\nabla \mathbf{F}^\top$. We are not focused on finding unique or specific solutions (a specific member of a group orbit, uniquely determined by a square, invertible linear system). In fact, it is to our advantage to do exactly the opposite: increase the frequency of convergence by allowing for any member of a group orbit. The price of this is the acceptance that calculations may be redundant; however, the number of periodic orbits being infinite this seemed unlikely to be exceptionally dangerous. Hereafter it shall always be implied that any discussion pertaining to solving (**??**) shall be in a least-squares sense.

This is done in an inexact manner instead of finding the optimal step length, as would be the case in a line search. Specifically, we simply halve the step length until one of the criteria is met.

For the numerical methods, a handful of parameters are required such as the step limit and tolerance. Our typical choices, noting that they are likely suboptimal, are as follows: the tolerance of the cost function for the gradient descent was $J = 10^{-4}$ and the step limit was set to a multiple of the dimension, either $16NM$ or $32NM$. This means that if either (**??**) $J < 10^{-4}$ or the step limit is reached, then the descent method terminates, and the guess is passed to the least-squares implementation. The "heavy lifting" was delegated to the least-squares method with backtracking. The threshold for termination was originally set to double floating point precision but over time this was relaxed to incorporate the *cdof*, i.e. the current tolerance is on the order of $(NM) * 10^{-15}$; and the step limit, 500. For those familiar with Newton methods, this number of steps appears like overkill at first, but the allowance of backtracking negatively

impacts the rate of convergence.

The clipping process by definition returns initial guesses which are not doubly-periodic. To mitigate the error introduced by this we always increased the resolution prior to clipping and decrease it afterwards by means of zero-padding and Galerkin truncation of the Fourier coefficients, respectively.

This was especially true in the cases where the suspected fundamental periodic orbits were relative periodic orbits.

Clipping can be described quantitatively as follows. Let the dimensions of the original periodic orbit be $x \in [0, L_0]$, $t \in [0, T_0]$ defined on a spatiotemporal lattice with $N \times M$ sites. To create an initial guess via clipping, choose a rectangular subregion of the original periodic orbit's discretization, $n \leq N, m \leq M$. The periods are then given by the appropriate fractions of the original, $T_c = \frac{Tn}{N}$ and $L_c = \frac{Lm}{M}$. Because translation is free, the domain is relocated to the origin, such that the result is an initial guess $u_c(x, t)$ with $0 \leq t \leq T_c$, $0 \leq x \leq L_c$, where $u_c(x, t)$

he clipping process creates an initial guess with periods , where n and m represent the number of points in time and space which define the clipping's discretization. . Because translation is a free action, we say that the clipping is now

The main challenge of gluing is reconciling the differing discretizations and periods of the fundamental periodic orbits. Discretization by itself is a non-issue; one simply pads or truncates the Fourier spectrum such that along every shared boundary, each fundamental periodic orbit has the same number of points. The fundamental periodic orbits have different periods, however, so if they have an equal number of points that implies that they have an unequal grid spacing (Δt or Δx). This discrepancy affects the magnitudes of tangents and hence the quality of the gluing. In purely practical terms, the gluing of large arrangements of fundamental periodic orbits in a single step is more complex simply due to the number of boundaries. To deal with this complexity, a methodology is required; our prototype is an extension of pair-wise gluing, which shall be described now.

For notational purposes, let us call refer to the pair of orbits as orbit A and orbit B. As a preprocessing step these orbits are rediscretized so that they all have equal grid spacings. This seems to contradict our previous statements, but the initial uniformity allows for a tidier description. For sake of argument we'll be using space as the 'gluing direction'; the solutions are concatenated spatially. To retrieve the temporal gluing method, simply permute all mentions of space and time. Let orbit A be defined with periods $[T_a, L_a]$, on a discretization with $[N_a, M_a]$ points in time and space, respectively. Likewise for orbit B. When gluing in space, we set the temporal period of the gluing to be the average of the original periods, $T_{ab} = \frac{T_a + T_b}{2}$. This, in combination with the fact that the number of points

in the *time* dimension must be the same, leads us to rediscretize each orbit such that the new number of points in time is also the average of the originals $N_{ab} = \frac{N_a + N_b}{2}$. For space, no rediscretization is required, because the preprocessing step made the spatial grid spacings equal. Similarly, the new spatial period is simply set to be the sum of the originals $L_{ab} = L_a + L_b$. This choice may seem poor at first; the spatial period of the periodic orbit being shadowed by two constituents would be guaranteed to be larger than this sum (imagine a figure eight being shadowed by two circles). More precisely, $L_{ab} > L_a + L_b$ would be satisfied However, because we allow *both* time and space periods to change, it is possible to find a member of the shadowed orbit's family which does not satisfy this inequality. Now that we have the periods and discretization of the gluing, we can give it a precise definition. This particular gluing results in a field defined on a fundamental tile of dimensions $[T_{ab}, L_{ab}]$ and $N_{ab} \times M_{ab}$ points. The field is now piecewise defined such that

$$
u_{ab}(x,t) = \begin{cases} u_a(x,t) & 0 \leq x \leq L_a \,, \ 0 \leq t \leq T_{ab} \\ u_b(x,t) & L_a \leq x \leq L_b \,, \ 0 \leq t \leq T_{ab} \end{cases}
\tag{18.18}
$$

with boundary conditions $u_{ab}(0,0) = u_{ab}(L_{ab},0) = u_{ab}(0,T_{ab}) = u_{ab}(L_{ab}, T_{ab})$

This concludes the pairwise gluing method, in summary, in the gluing direction the number of points and periods are additive and in the transverse dimension these quantities are averaged.

There was no clear manner with how to proceed with gluing large arrangements of fundamental periodic orbits; our prototype is an extension of the pairwise gluing method. Let us represent the arrangement of fundamental periodic orbits as an array, where the rows correspond to time and the columns, space. For space-time gluing, we elect to first glue the fundamental periodic orbits into spatial strips, and then glue them in time. For example, let us have a $3x3$ array of fundamental periodic orbits. First, we glue each row together (spatial gluing), creating a $3x1$ array; the time period of each row come from averaging and the spatial period comes from summation. Then we glue these strips in time; such that now the time periods ares summed and the spatial periods, added. This produces the final gluing result: the final periods end up being the total sum, divided by the number of rows and columns in the array of fundamental periodic orbits; in this example, the resultant periods are $T = \frac{1}{3} \sum T_{ij}$ and $L = \frac{1}{3} \sum L_{ij}$ We propose some alternative methods for this in sect. 10.8 but currently, they are not fully developed.

The main challenge of gluing is reconciling the differing discretizations and periods of the fundamental periodic orbits. Discretization by itself is a non-issue; one simply pads or truncates the Fourier spectrum such that along every shared boundary, each fundamental periodic orbit has the same number of points. The fundamental periodic orbits have different periods, however, so if they have an equal number of points that implies

that they have an unequal grid spacing (Δt or Δx). This discrepancy affects the magnitudes of tangents and hence the quality of the gluing. In purely practical terms, the gluing of large arrangements of fundamental periodic orbits in a single step is more complex simply due to the number of boundaries. To deal with this complexity, a methodology is required; our prototype is an extension of pair-wise gluing, which shall be described now.

summary excerpts The difficulties are described here in the context of periodic orbit theory specifically cycle expansions. Cycle expansions are quantitative descriptions of chaotic attractors via summation over an infinite collection of prime orbits. This collection has a well defined hierarchy of importance as determined by periodic orbit's temporal periods and stability. This ranking is critical as it dictates how to truncate the infinite sum resulting from cycle expansion. In our case, however, we do not know what constitutes "primeness" with respect to continuous families. In addition, we currently do not have a manner with which to compute spatiotemporal topological invariants. In other words, we do not know how to rank and sum over periodic orbits in our description. Our intuition tells us that the analogous quantity to temporal periods should be the spatiotemporal area but this has not yet been confirmed explored.

2020-08-13 Matt Finally finished with data science / machine learning / deep learning / neural network certification program.

Roadmap for the next three months:

1. Finish Thesis
2. Finish Thesis presentation
3. Finish orbithunter (my python package) documentation, included in thesis
4. Discuss randomly connected RNN with Schatz, Grigoriev group.
5. (external to Physics) find a job, work on CNN symbolic dynamics
6. Future projects TBD.

2020-10-08 Matt I've looked and asked around but I cannot find an answer to a very simple question; I've attached it as an image.

For context: the projections I will actually be describing are projections onto symmetry invariant subspaces, the image is just a toy example of what I mean. I understand that the functions (in the image) are formally equivalent to one another but I am trying to explain that they are different numerically because the latter reduces the number of computational degrees of freedom. The example uses functions, but technically I am trying to explain the distinction in the context of matrix representations.

Is there a word for this distinction, or does one have to explicitly include it in the definition?

2020-10-09 Predrag mhm... In birdtracks.eu eq. (3.60) I think of each sub-block as a matrix of lower dimension. I would never write $\phi(\mathbf{v}) = [x, y, 0]^\top$, only $\phi(\mathbf{v}^{(\alpha)}) = [x, y]^\top$, in the α irrep.

2020-10-10 Predrag I'll talk in Moscow Monday morning about our spatiotemporal ideas, so I'm having a look at recent papers on variational methods:

Kerswell Exact Coherent States: Variational Methods lectures look good.

Daniel Lecoanet *et al.* Daedalus deserves a look.

Brunton *et al.* Machine Learning for Fluid Mechanics - have not checked it yet.

2020-10-22 Erik Aurell .

Title: Spatiotemporal tiling of the Kuramoto-Sivashinsky equation
Speaker: Matthew Gudorf (Georgia Tech)
Time & place: Thursday October 22 at 13.00 on zoom

Abstract: Motivated by space-time translational invariance, 'spatiotemporally chaotic' or 'turbulent' flows are recast as a (D+1)-dimensional spatiotemporal theory which treats space and time equally. In this formulation time evolution is replaced by a repertoire of spatiotemporal patterns taking the form of (D+1) dimensional invariant tori. Infinite space-time is then explained by the shadowing of these tori. This is formalized by the development of a (D+1)-dimensional symbolic dynamics whose alphabet is comprised of space-time tori of minimal size. Enumerating these spatiotemporal building blocks enables the construction of all admissible spatiotemporal patterns. These ideas are investigated in the context of the Kuramoto-Sivashinsky equation using new, open source spatiotemporal computational computing package 'orbithunter'. These codes are designed to offer easy access to new spatiotemporal techniques, persistent homology, convolutional neural networks and more.

The talk was not recorded. For seminars in the CS & BP series, see here.

2020-10-22 Matt Karoshi which can be translated literally as "overwork death" is a Japanese term relating to occupational sudden mortality. The most common medical causes of karoshi deaths are heart attacks or strokes due to stress and a starvation diet. Mental stress from the workplace can also cause karoshi through workers taking their own lives. People who commit suicide due to overwork are called karojisatsu. The phenomenon of death by overwork is also widespread in other parts of Asia.

I have worked out enough that I believe in my cardio but random palpitations and arrhythmia have me shook; probably psychosomatic. One last sprint to the finish....

2020-10-25 Predrag No karoshi, please, we already have fascists and COVID-19 to stress us out.

Just play it cool, boy, Real cool!.
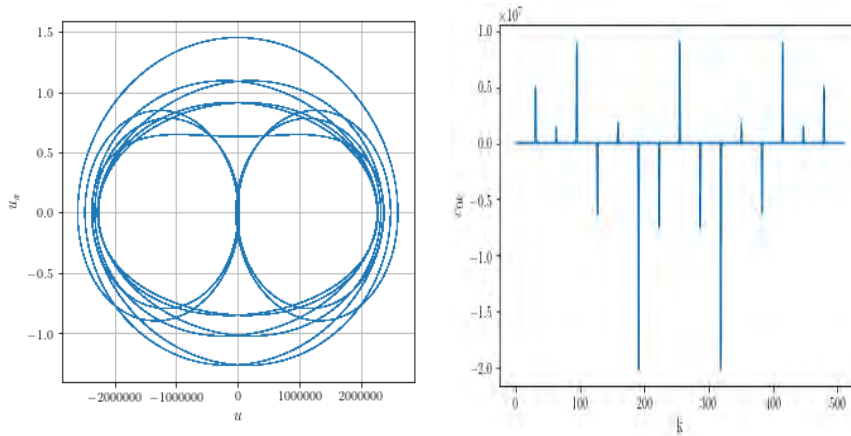
Figure 18.21: (left) Parametric plot of $u_x(x)$ vs. $u(x)$ for $L \approx 3974779240$ equilibrium. As the stable "cells" of Frisch, She and Thual [13], this equilibrium belongs to the asymmetric subspace, but as it has a number of winds it is (presumably) unstable. (right) Fourier coefficients $-i\, c_{0k}$. See the thesis [15] for definitions, spatially antisymmetric zeroth time kth spatial modes.
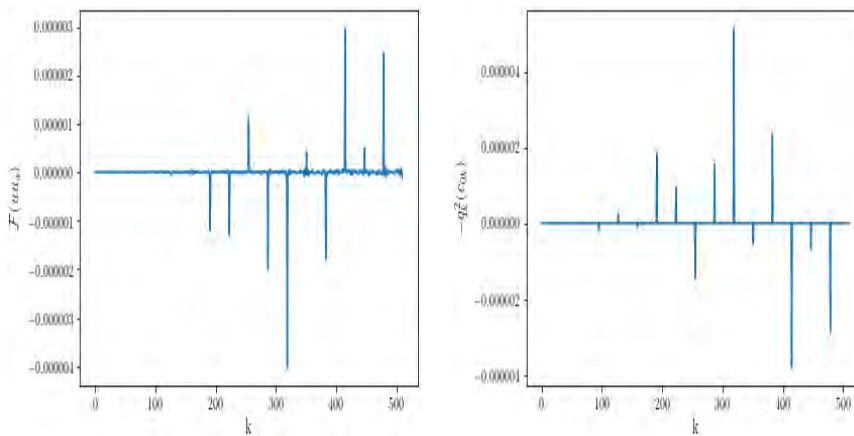
Figure 18.22: (left) Modes of uu_x for $L \approx 3974779240$ equilibrium. They are approximately the negative of (right) u_{xx} modes, in agreement with the wrong sign diffusion term "Burgers" eq. (18.19) for an equilibrium; the difference is the vanishingly small u_{xxxx} that can be neglected for such long wavelength solutions.

2020-10-22 Matt I found some big boys...like really big.... like a $L = 4 \cdot 10^9$ big equilibrium. The modes with all of the energy are multiples of $32n$ for a reason unknown to me other than simply saying 'aliasing'. I obviously do not have enough modes to resolve all scales but hey its kinda cool.

I can't tell if this is an interesting result, or if it's already known solutions from Michelson [27] or similar? The fourth derivative gets killed, so that the equations, for practical purposes, reduce to

$$u_t + u\, u_x = -u_{xx}\,. \tag{18.19}$$

I double checked it and I stand by the values, however I don't know if its worth anything. Some of the figures do not fit on the page so look for them in */figs/*.

2020-10-25 Predrag I suspect your $32n$ are the stable "cells" of Frisch, She and Thual [13] *Viscoelastic behaviour of cellular solutions to the Kuramoto-Sivashinsky model* (1986). Have to convert the units as in ChaosBook sect. 30.1.1 *Symmetries of Kuramoto-Sivashinsky equation* to compare.

"The fourth derivative getting killed" would make them into solutions of the wrong sign Burger's equation (18.19).

I looked into */figs/*, but there is nothing there other than figure 18.21 and 18.22. *EquilibriumOrbitKS_L3974779240p595_field_fdomain.png* color plot is not informative, for equilibria one plots $u(x)$ on $[0, L/2]$.

2020-10-25 Predrag Aren't you plotting twice as many wave-numbers in figure 18.21 (right) (right) as needed for an antisymmetric subspace solution? But then I do not understand the k-axis in figure 18.22, these do not mach up - should you get the same non-vanishing modes in all three figures?

2020-10-25 Predrag The single, universal, correct spatial mode-indexing convention [5] for all Kuramoto-Sivashinsky documents that we produce:

The horizontal, eigenmode / wavenumber axis should always be $j/\tilde{L} = 2\pi j/L$, and, due to the O(2) having 2-dimensional irreducible representations (sines & cosines, rather than $\exp(i2\pi j/L)$'s) one should always group Floquet exponents (and, I believe, Fourier modes as well) into $j, j+1$ pairs, plot them as a single, two-valued j.

I think you also want to use logarithmic scale on the y-axis, as everything is expected to fall off exponentially or faster for modes beyond the entangled, "physical", inertial-manifold modes. To trust your calculation, you always want to capture the beginning of the transient, "unphysical" modes in your spectrum.

What one chooses to pair for low j might be ambiguous, as the nonlinear interactions mix up the O(2) 2-dimensional linearly irreducible representations.
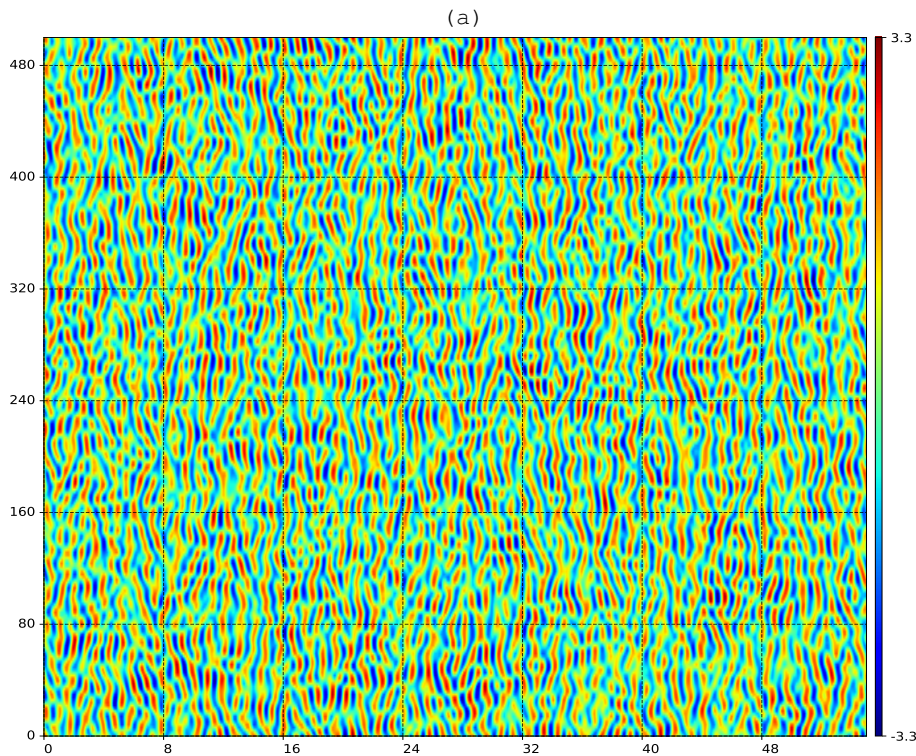
Figure 18.23: (a) Initial guess for orbit hunting. Periods $(L, T) \approx (500, 488)$.

This way wave-number plots for any L have the same x axis.

Should you know of any reason that we should not be joined in holy notational convention, speak now or forever hold your peace.

If you agree, follow our convention in ALL plots, it's our misfortune that none living has as much experience with Kuramoto-Sivashinsky as we do.

2021-04-12 Matt Getting really close to being able to find very very large periodic orbits. In figure 18.23 (a) the resolution is due to computational degrees of freedom; small amount of interpolation but too much would distort the field and make it look non-physical. For figure 18.24 (b) the residual is $\mathcal{O}(10^{-2})$; for a solution this large I find this to be quite the achievement. Requires lots of supervision however, to create an initial guess.

Getting very close to finding arbitrarily large periodic orbits for Kuramoto-Sivashinsky equation, however, when trying to develop a guide by implementing the Lorenz equations, the code fails quite miserably, when σ, b, ρ are fixed. In other words, discrete dimensions provide yet another

Figure 18.24: (b) Final result after about 6 hours (on my laptop) of application of conjugate gradient method. Dimensions $(L, T) \approx (555, 783)$. Discretization included 512 in space, 128 points in time, hence low resolution figure.
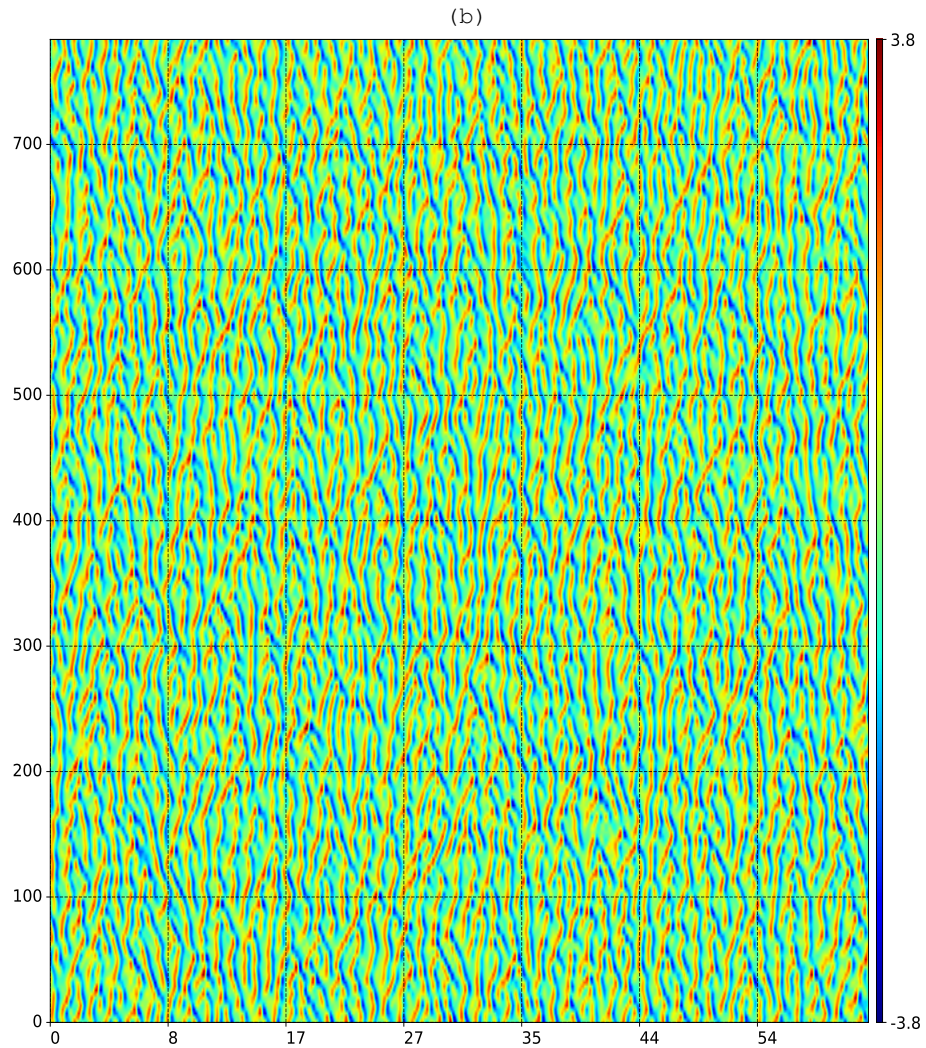
challenge. Unsure if unpalatable but my gut is telling me the quasi 2-d nature of the Lorenz attractor is causing this, meaning that for "extra flexibility", unconstrained parameters are needed, as I do not believe that the attractor would remain in the same plane, just my two cents.

2021-04-16 Predrag Interesting.

You started with u guess in range $u \in [-3.3, 3.3]$ and - even though the resulting solution is stretched out by 50% in time, the u range is barely bigger, $u \in [-3.8, 3.8]$. So somehow if you start with atypical guess pattern (no random walk in the local mean u), you end with atypical solution.

Contrast with $u \in [-5, 5]$ of figure 16.7 (and many large spacetime figures currently commented out, but fine otherwise). As I explain above (see **2019-05-13 Predrag** post), we expect the range of the color bar in such figures to grow proportionally to $\sqrt{L}$.

2022-03-05 Matt This is one of those things that, if true, is embarassing for me in hindsight. We have noticed that for solutions to the Kuramoto-Sivashinsky equation on large domains, it is painfully obvious that there are large swathes of space time that have non-zero Galilean velocity locally, even though the mean flow is beholden to the usual constraint $\int u dx = 0, \ \forall t$.

We have yet to explain this phenomenon, but I believe I might have some clues for where to start.

To set the stage, here's how all of this came about.

When performing the first tiling computations, there were large regions of space-time that went "uncovered" by the current set of fundamental orbits; that is, shadowing of the current set of fundamental periodic orbits was not detected. These regions had two distinct properties; not only was the local Galilean velocity non-zero, they also had locally non-zero spatial translation velocity, as indicated visually by the appearance of slanted fundamental periodic orbits. Indeed, when the current "defect" or "merger" fundamental periodic orbit was mapped onto a parallelipiped domain, i.e. giving it a fictitious numerical slant, then the regions became almost completely covered when using the "mean flow corrected L2 norm density" as a metric. This metric is simply computed by subtracting the mean flow in the shadowing window, taking the L2 difference with the fundamental periodic orbit and lastly dividing by the number of points in the spatiotemporal discretization,

$$D(u, u') = \frac{1}{NM} ||(u - \bar{u}) - u'||^2 \tag{18.20}$$

This idea behind this is exactly to only compare the shapes/patterns removing any local Galilean velocity, and also making the metric invariant, or at the very least, robust with respect to discretization sizes.

Being able to cover these previously uncovered regions begged the question; what is the relation between local Galilean velocity and local spatial translation speed? I'm still unsure if it is coincidence or confirmation bias, but every time a pair of non-zero Galilean velocity regions emerged (the mean flow is still conserved, so clearly if one subregion has non-negative local Galilean velocity, another region must have non-positive to cancel it out), it is very common for it to be preceded by a region which shadows the antisymmetric subspace (i.e. the "wiggle" and "streak" tiles). My bold claim is that the regions of non-zero Galilean velocity are resultant from the local reflection symmetry being broken. Considering the relation between the spatial reflection symmetry and spatial translation, this had some merit in my mind.

The crude test I thought of was this: if in some region we pick up a non-zero spatial translation velocity i.e. $u(x, t) \approx u(x - ct, t)$, and this coincides with picking up a non-zero Galilean velocity; then why don't we just compare $v + u(x + 2vt, t)$ and $u(x - ct, t)$? Here is what I did as a crude test.

Generate a large patch of space-time; find a candidate region that looks red-shifted or blue shifted (i.e. how local Galilean velocity manifests using our typical heat map coloring scheme for the spatiotemporal velocity field plot). Clip said region out. Compute the mean flow v on the region, compute the SO(2) rotation angle and corresponding spatial shift s between the field at $t' = 0$ and $t' = T'$. Compute the drift speed $c = s/T'$, and lastly compare v with $c/2$. treating the aperiodic spatial boundaries of the clipping as if they were periodic (a very crude approximation).

I'm currently in the process of generating a statistically significant way of verifying the claim, but initial attempts yielded both "good" results 0.157 vs. 0.159, and bad results seemingly off by a factor of two, -0.178 vs. -0.331.

At the very least it might be an avenue of research for someone interested in the study of symmetries of PDEs. Unfortunately I don't know anything about spontaneous symmetry breaking to make any rigorous claims; I am hoping a statistical approach will be convincing enough.

2020-03-05 Matt It seems I have provided another example for why statistics exists; the coincidental agreement previously provided was just that, coincidence; the computation of the spatial shift is simply too polluted by the Gibbs phenomenon resulting from clipping; a better way of computing local drift speed is needed; something utilizing the spatiotemporal derivatives most likely.

2020-03-26 Matt I bought a new rig and wanted to benchmark it with some numerical computations, so I decided to expand upon the ϕ^4 Euler–Lagrange equation results from yesterday. What took 27 seconds on my work laptop only took 2 on my new PC, which further reduced to 0.4 seconds when adding in a number of changes.

Changed the cost function to $0.5 * ||F||^2$ and adding the corresponding analytical gradient $J^\top F$ By adding in the analytical derivative the compute time decreased even further from 2 to 0.5 seconds. To test it further, I compute all cycles from length 2 to 10, inclusive. It only took 10 seconds; running it without the jacobian would take 240 seconds, just to give an idea as to how much an analytical expression for the (cost functions) jacobian helps.

We can do better, though. This still technically called the numerical optimization algorithm once for each initial condition (they were ran in parallel though). Instead, we can tensorize the N-cycle equations such that they are solved simultaneously. In other words, imagine stacking all cycle vectors as rows like layers in a cake. This creates a tensor with dimensions $3^N \times N$ (I'm avoiding usage of "matrix" because of the operations it implies; there is no matrix multiplication happening). This tensor is then converted into a vector of dimension $N * 3^N$.

By tensor-izing the equations in this way, I was able to get all cycles from length 2 to 10 down from 10 to 4.7 seconds or so. all cycles up to 11 takes about 20 seconds.

Additionally because I was having fun, I tensorized the Jacobian matrices as well; the Jacobians are computed by manipulating a $3 * *N \times N \times N$ tensor's elements; which can be easily iterated over and eigenvalues and eigenvectors computed for each $N \times N$ matrix.

With all of this tensorization it can produce (locally) all 7-cycles, jacobians, eigenvalues and eigenvectors in 0.1 seconds or so. Final benchmarks

all 7-cycles, their jacobians and respective eigenvalues and eigenvectors : 0.1 seconds all cycles up to and including length 12: 60 seconds

link for easy viewing

click here. [2]

2022-03-26 Predrag Wow! Wow! Can you check `blogCats.tex`, post **2020-03-18, 2020-03-23 Molei Tao** and see whether any of his suggestions are useful?

2022-03-26 Matt I did indeed choose the `l-bfgs-b` algorithm, but changing the algorithm is as easy as changing the string of characters from `l-bfgs-b` to any of the methods listed here.

Regarding Tao's papers; I found them useful as a resource for other things I am trying to accomplish, but I thought we were strictly in the deterministic setting, and so the fundamental idea of finding solutions to the

---

[2]Matt 2022-03-26: See the corresponding requirements text file in the GitHub repo to install the environment I used.

Euler-Lagrange equations stands, but I don't think any of the actual details regarding finding minimizers of the action in the presence of noise apply right now.

Regarding numerical methods and preconditioning; until we run into a wall, pretty sure the current l-bfgs-b setup is fine; by including the analytical Jacobian matrix I don't think preconditioning is really needed either, *unless* there is a desire to see what happens to the cycles in the $\mu \to 0$ or $\mu \to \infty$ limits. In those cases, I would probably try to find a non-trivial way of rescaling the matrix-vector product with the Jacobian matrix by a factor of μ^{-2}. In my experience preconditioning has the largest effect when there is a wide range in orders of magnitude. I.e. if the elements of your gradient range from 10^{-6} to 10^6, you should try to find some mapping to make them all order 1. This typically means finding a cheap way of approximating the inverse of the Jacobian matrix. For the Kuramoto-Sivashinsky equation I approximated the inverse of the linear terms, because that is where the largest discrepancy of magnitudes were resulting from.

2022-04-24 Matt April 22nd arXiv:2204.10066, (click for the pdf) follows Lasagna [23, 25] least squares shadowing methodology applied to Kuramoto-Sivashinsky. Check also refs. [17, 18, 24] and page 114, page 120 and page 657.

Similar to what we discussed on Friday, the practitioners of the least squares shadowing, refer to the partial derivatives which constitute the orbit Jacobian matrix as being the 'sensitivity" of spatiotemporal functionals which define observables.

It's all a matter of perspective and objective. We are interested in the underlying states themselves, as we want to derive them for cycle expansions and shadowing computations. The aerodynamic perspective is centered around the effect of their inputs on the observables of the system (how does a perturbation to my airfoil geometry affect drag?) and the optimal control aspect of the problem (i.e. along which eigenvector do I apply force to drive me towards a local minima of drag?).

In terms of mathematical construction, the main difference is that our cost functional is based explicitly around the satisfaction of the equations, $|F|^2 = 0$, which is directly solved via a minimization approach, or via a root solving methodology $F = 0$. Meanwhile, their cost functional is centered around the physical observables directly and is comprised of two terms: 1. the square of the first order variation of the fluid states u in terms of a set of "control parameters" s. 2. a Tikhonov regularization term (L_2 penalty) which penalizes deviation from the governing equations. In this sense, the second term is similar to how Lagrange multipliers are used in Lagrangian mechanics, but not exactly.

By defining the cost functionals themselves in terms of observables, i.e. the spatiotemporal average of the square of the state u^2 corresponds to an energy functional which they use as their starting point; we compute the energy as a follow up computation after finding the periodic orbits.

I'm not a fan of expanding the orbit Jacobian matrix in terms of Fourier modes, i.e. defining its elements are defined in terms of convolutions as I think it's much easier to view the orbit Jacobian matrix by decomposing into products of linear operators (i.e. discrete Fourier transform matrices, SO(2) derivatives, etc.). The reason why it is easier is quite literally because it demystifies the nature of the matrix-vector product, which is the key to resolve the computational memory issues that are often stated when describing the challenges of solving the least squares system of equations.

I'm also not a fan of interpretation of the eigenvectors of the orbit Jacobian matrix as optimal forcing directions. Why? Because engineering has not transcended spacetime and they don't ever apply spatiotemporal forcing; they apply a sequence of kicks in time.

Figure 1. also seems dubious to me. They use spatial boundary conditions $u(0,t) = u(L,t) = 0$ and $u_x(0,t) = u_x(L,t) = 0$, and they get spatiotemporal averages which are highly oscillatory near the boundaries.

To me, this seems much more likely to be a consequence of improper numerical implementation than it does to be something meaningful; i.e. a manifestation of the Runge phenomenon or Gibbs phenomenon.

They also mention that those averages are generated with respect to 1000 "random initial conditions". I'm hoping they mean that this is averaged over 1000 solutions which they found starting with 1000 random initial conditions, but they conveniently leave out how these are defined.

How does this affect us? I see this paper as being half committed to the notion of space-time; it's seen as a means to compute solutions but they still analyze the results in terms of temporal averages and scaling behavior as $T \to \infty$ without any mention of space.

2022-04-27 Predrag I think you should toot your horn, get in tauch with the authors, tell them about your PhD thesis and your unpublished work. An economical way is to give them the link to
ChaosBook.org/overheads/spatiotemporal/
It includes your thesis, and you can point out the talks and slides th——

—————————————————————————————————————
—————————————————————————————————————
—————————————————————————————————————
—————————————————————————————————————
—————————————————————————————————————
—————————————————————————————————————
—————————————————————————————————————
—————————————————————————————————————
—————————————————————————————————————
—————————————————————————————————————
—————————————————————————————————————
—————————————————————————————————————
—————————————————————————————————————
—————————————————————————————————————
—————————————————————————————————————
—————————————————————————————————————
—————————————————————————————————————
—————————————————————————————————————
—————————————————————————————————————
—————————————————————————————————————
—————————————————————————————————————
—————————————————————————————————————
—————————————————————————————————————
—————————————————————————————————————
—————————————————————————————————————
—————————————————————————————————————
—————————————————————————————————————
—————————————————————————————————————
—————————————————————————————————————
—————————————————————————————————————
—————————————————————————————————————
———————————————————————————————at might be relevant to this discussion, as well as make them aware of Orbithunter.

I am sorry I did not record Lan's presentation. You can ask him to do it again one of coming Friday 9am's, you two invite whoever you think should be there, and I'll record it this time.

2022-05-13 Matt Updated felines github repo; fixed a small notebook specific mistake in the phi k equation notebook, and finished a version of prime cycle counting for k-ary symbolic dynamics. It is a copy of Ibrahim's idea so gracias to him; I need to work on its computational efficiency, however.

2022-05-20 Matt I added everyone as collaborators but honestly it will be easier to just create an org via github; everyone will get yet another invite.

2022-05-22 Matt Created an organization via github: "chaotic-systems". Deployed phi-k codes as new python package `cyclehunter` which is now

installable via pip. Added a notebook `phik.ipynb` to the github repository to explain the library; it is very basic there is a discrepancy between Ibrahim's prime cycle counting and mine; need to confirm with counting equation to see who is right. For now, because I tried to make mine more efficient, I've only added mine, but have kept Ibrahim's code in his separate notebook

2022-07-23 Matt Ramblings of a mad man regarding using deep learning for symbolic dynamics and prediction/description of chaotic systems. First step: create a catchy name to capture the audience's attention, e.g. "The Language of Chaos" if trying to make analogies between symbolic grammars and natural language processing. I believe the goal would be to incorporate/account for the following properties in a new type of hybrid deep learning model.

1. Spatiotemporal symmetries; continuous and discrete

2. Admissibility of configurations of symbols

3. Satisfaction of the equations of motion

4. Unnatural representation of continuous families/group orbits of periodic orbits as uniformly spaced rectangular lattices

My original idea is as follows: build a CNN which incorporates the equations of motion, symmetries, continuous deformations (rubbery tiles) into a binary classification algorithm which determines "admissible" or "inadmissible". I think these could be incorporated into the cost functional, nonlinear activation layers, and deformable CNN layers (learns the "shape" of the convolutional grids, not just rectangular grids). If we do not capture the rubbery nature of tiles however, I think this is bound to fail. For continuous families of (discretized) periodic orbits it is analogous to being able to represent words with different letters, although even more pathological because the notion of "continuous deformation of a letter" doesn't exist.

The general idea behind CNN layers is that they learn the important geometries/shapes (whose dimension is dependent on the dimension of the convolution) through convolution. These shapes are then passed to fully connected layers which learn the combinations of those shapes that are important. Almost always these shapes are not invariant under symmetries; CNNs learn separately what a "left ear" and "right ear" look like when considering facial recognition, as far as I am aware. There are two approaches here I think; one is just include a huge sampling of group orbits and train on all of them; which, while brute force, is probably the better option as more training data is typically always beneficial. The second is to incorporate these symmetries into nonlinear activation layers which somehow encode or quotient them.

The grammar and admissibility is more concerned with the relative positions of symbols; it might be better to frame the problem in terms of finding the relative differences between neighboring regions of space time.

Once we have some notion of symbolic grammar, we pass the admissible configurations to an NLP predictive model which either tries to perform inference on future states (i.e. predicting time evolution) or inference on masked symbols (you mask some symbols in your configuration, it predicts the missing symbols).

If we were able to incorporate the BERT language model into the analysis I can almost guarantee this would take off like a rocket; it's an incredibly relevant, widespread, trusted model created by Google. The "T" in "BERT" stands for "transformers". To give an indication how popular this is, the seminal paper, Attention is All You Need was published in 2017 and already nearly has 50,000 citations; worth a skim for numerical practitioners and data scientists for sure.

Here is a motivation to use transformers for this task. 1. It already has built in the notion of encoding-decoding process of encoding symbolic representations as continuous representations, then decoding the symbolic representations, time dependence, as well as continuous translation symmetries.

> Most competitive neural sequence transduction models have an encoder-decoder structure. Here, the encoder maps an input sequence of symbol representations $(x_1, ..., x_n)$ to a sequence of continuous representations $z = (z_1, ..., z_n)$. Given z, the decoder then generates an output sequence $(y_1, ..., y_m)$ of symbols one element at a time. At each step the model is auto-regressive consuming the previously generated symbols as additional input when generating the next.

The issue with using typical NLP models is that they are sensitive to positional nature of sentence structure. Transformers, however, capture this with "positional encoding"; using $\sin$ and $\cos$ to encode phase; shocking!

> To this end, we add "positional encodings" to the input embeddings at the bottoms of the encoder and decoder stacks. The positional encodings have the same dimension dmodel as the embeddings, so that the two can be summed. There are many choices of positional encodings, learned and fixed. In this work, we use sine and cosine functions of different frequencies:

$$
\begin{aligned}
P_E(\text{pos}, 2i) &= \sin(\text{pos}/10000^{2i/dmodel}) \\
P_E(\text{pos}, 2i+1) &= \cos(\text{pos}/10000^{2i/dmodel})
\end{aligned}
$$

where pos is the position and i is the dimension. That is, each dimension of the positional encoding corresponds to a sinusoid. The wavelengths form a geometric progression from 2π to $10000 \cdot 2\pi$. We chose this function because we hypothesized it would allow the model to easily learn to attend by relative positions, since for any fixed offset k, $P_E(\text{pos} + k)$ can be represented as a linear function of $P_E(\text{pos})$.

References

[1] C. Canuto, M. Y. Hussaini, A. Quateroni, and T. A. Zhang, *Spectral Methods in Fluid Dynamics* (Springer, New York, 1988).

[2] M. C. Cross and P. C. Hohenberg, "Pattern formation outside of equilibrium", Rev. Mod. Phys. **65**, 851–1112 (1993).

[3] P. Cvitanović, R. L. Davidchack, and E. Siminos, "On the state space geometry of the Kuramoto-Sivashinsky flow in a periodic domain", SIAM J. Appl. Dyn. Syst. **9**, 1–33 (2010).

[4] J. E. Dennis and R. B. Schnabel, *Numerical Methods for Unconstrained Optimization and Nonlinear Equations* (SIAM, Philadelphia, 1996).

[5] X. Ding, H. Chaté, P. Cvitanović, E. Siminos, and K. A. Takeuchi, "Estimating the dimension of the inertial manifold from unstable periodic orbits", Phys. Rev. Lett. **117**, 024101 (2016).

[6] A. Dutt, L. Greengard, and V. Rokhlin, "Spectral deferred correction methods for ordinary differentail equations", BIT Num. Math. **40**, 241–266 (1997).

[7] M. Emmett and M. Minion, "Toward an efficient parallel in time method for partial differential equations", Commun. Appl. Math. Comput. Sci. **7**, 105–132 (2012).

[8] T. Engl, J. Dujardin, A. Argüelles, P. Schlagheck, K. Richter, and J. D. Urbina, "Coherent backscattering in Fock space: A signature of quantum many-body interference in interacting bosonic systems", Phys. Rev. Lett. **112**, 140403 (2014).

[9] T. Engl, P. Plöss, J. D. Urbina, and K. Richter, "The semiclassical propagator in fermionic Fock space", Theor. Chem. Acc. **133**, 1563 (2014).

[10] T. Engl, J. D. Urbina, Q. Hummel, and K. Richter, "Complex scattering as canonical transformation: A semiclassical approach in Fock space", Ann. Phys. **527**, 737–747 (2015).

[11] T. Engl, J. D. Urbina, and K. Richter, "The semiclassical propagator in Fock space: dynamical echo and many-body interference", Philos. Trans. Royal Soc. A **374**, 20150159 (2016).

[12] M. Farazmand, "An adjoint-based approach for finding invariant solutions of Navier-Stokes equations", J. Fluid M. **795**, 278–312 (2016).

[13] U. Frisch, Z. S. She, and O. Thual, "Viscoelastic behavior of cellular solutions to the Kuramoto-Sivashinsky model", J. Fluid Mech. **168**, 221–240 (1986).

[14] J. F. Gibson, J. Halcrow, and P. Cvitanović, "Visualizing the geometry of state-space in plane Couette flow", J. Fluid Mech. **611**, 107–130 (2008).

[15] M. N. Gudorf, Spatiotemporal Tiling of the Kuramoto-Sivashinsky Equation, PhD thesis (School of Physics, Georgia Inst. of Technology, Atlanta, 2020).

[16] B. Gutkin and V. Osipov, "Classical foundations of many-particle quantum chaos", Nonlinearity **29**, 325–356 (2016).

[17] D. Huang, S. Chernyshenko, P. Goulart, D. Lasagna, O. Tutty, and F. Fuentes, "Sum-of-squares of polynomials approach to nonlinear stability of fluid flows: an example of application", Proc. Roy. Soc. Ser A **471**, 20150622 (2015).

[18] D. Huang, B. Jin, D. Lasagna, S. Chernyshenko, and O. Tutty, "Expensive control of long-time averages using sum of squares and its application to a laminar wake flow", IEEE Trans. Control Systems Tech. **25**, 2073–2086 (2017).

[19] J. M. Hyman, B. Nicolaenko, and S. Zaleski, "Order and complexity in the Kuramoto-Sivashinsky model of weakly turbulent interfaces", Physica D **23**, 265–292 (1986).

[20] Y. Lan, Dynamical Systems Approach to $1 - d$ Spatiotemporal Chaos – A Cyclist's View, PhD thesis (School of Physics, Georgia Inst. of Technology, Atlanta, 2004).

[21] Y. Lan, C. Chandre, and P. Cvitanović, "Variational method for locating invariant tori", Phys. Rev. E **74**, 046206 (2006).

[22] Y. Lan and P. Cvitanović, "Unstable recurrent patterns in Kuramoto-Sivashinsky dynamics", Phys. Rev. E **78**, 026208 (2008).

[23] D. Lasagna, "Sensitivity analysis of systems using unstable periodic orbits", SIAM J. Appl. Dyn. Syst. **17**, 547–580 (2018).

[24] D. Lasagna, D. Huang, O. R. Tutty, and S. Chernyshenko, "Sum-of-squares approach to feedback control of laminar wake flows", J. Fluid Mech. **809**, 628–663 (2016).

[25] D. Lasagna, A. Sharma, and J. Meyers, Periodic shadowing sensitivity analysis of chaotic systems, 2018.

[26] P. Manneville, *Dissipative structures and weak turbulence* (Academic, New York, 1990).

[27] D. Michelson, "Steady solutions of the Kuramoto-Sivashinsky equation", Physica D **19**, 89–111 (1986).

[28] Y. Saad and M. H. Schultz, "GMRES: A generalized minimal residual algorithm for solving nonsymmetric linear systems", SIAM J. Sci. Stat. Comput. **7**, 856–869 (1986).

[29]   R. Speck, "Parallelizing spectral deferred corrections across the method",
       Comp. Vis. Sci. **19**, 75–83 (2018).

Chapter 19

Space-time, blogged

<div style="text-align: center">

I'm a space and time continuum
— Red Wanting Blue

</div>

<div style="text-align: right">

The latest entry at the bottom for this blog

</div>

2016-10-27 Predrag **The revolution** (in strongly nonlinear field theory) **will not** **be televised.** But it will be on YouTube.

2011-05-15 Predrag A. Hramov and A. Koronovskii [32], *Detecting unstable periodic spatio-temporal states of spatial extended chaotic systems*, arXiv:0708.4349.

2016-01-12 PC also of possible interest:

Llibre [46] *The averaging theory for computing periodic orbits*.

Also, Gutkin and Osipov [30] write "In general, calculating periodic orbits of a non-integrable system is a non-trivial task. To this end a number of methods have been developed," and then, for some reason, they refer to ref. [4].

2016-03-02 Predrag Also Pazó *et al.* [51] *Structure of characteristic Lyapunov vectors in spatiotemporal chaos*. Actually (I hesitated to bring it up) this line of inquiry goes smoothly into Xiong Ding's inertial manifold dimension project.

Not sure Li *et al.* [45] *Lyapunov spectra of coupled chaotic maps* is of any interest, but we'll know only if we read it.

Takeuchi and Sano [58] Role of unstable periodic orbits in phase transitions of coupled map lattices.

2016-08-15 Predrag : Before I start sounding critical: Rana, Adrien, Matt and Li are all good students / postdoc, and the work and what people learned this summer is very good. Now, to my first impressions.

<div style="text-align: center">778</div>

Matt's report is most in my taste. We still do not know whether there is something seriously wrong with the spatiotemporal proposal for Kuramoto-Sivashinsky, the core part of this whole research project, or is there a coding problem, but that's research. We'll sort it out eventually.

2016-09-28 Predrag Learned much more from Rafael de la Llave that I can possibly remember.

I explained that we turn a dissipative PDE with commuting continuous symmetries (time, space translations) into a set of 1st order PDEs in both time and space directions. Then we integrate spatiotemporally periodic solutions along the space directions just like we used to integrate the along the time direction. I explained that as a discretized version of that, we studdy 1D chain of diffusively spatiotemporal cats.

Rafael was very happy to hear that, because he has hardly ever done anything else in his life. Except piss off the Smale cult by publicly refusing to prove generic results. "Would you give your fiance a diamond, or a generic pebble of the street?"

2016-10-03 Predrag Various people focus on proving "local rigidity of partially hyperbolic algebraic actions." Katok's papers on this are absolutely unreadable.

Reinhardt and Mireles James paper deals with constructing unstable manifolds of steady states in parabolic PDE's and gets very close to establishing homoclinic intersections.

The concrete example they use is the Fisher equation, but it seems that the Kuramoto-Sivashinsky could work. The recoding is not trivial and that there are many things that will go wrong.

We had done some work on extending these techniques to periodic orbits. Of course, one needs to have the periodic orbits and, I know full well that this is not trivial (I have spent some time doing something and realized that I am not tough enough to do it). On the other hand, may be some infusion of strength and new ideas could be enough.

2016-10-24 Predrag A note on a conversation between Stephen Shenker and Paul Wiegmann. Shenker presented his work on a quantum black hole in a box, i.e., in a thermal equilibrium, and mentioned that this field theory has a leading positive Lyapunov exponent. Paul argued afterwards that a system in equilibrium cannot have positive Lyapunov exponents - they are a property of externally driven, out of equilibrium systems (let's say, Navier-Stokes turbulence). I believe here Stephen is right, will try to explain that first for finite-dimensional dynamical systems, and then for infinite-dimensional field theories.

What is 'chaos'? (ChaosBook.org, ver. 15.7, Sect. 1.3.1) In a 'chaotic' dynamical system, any two trajectories that start out very close to each other separate exponentially with time, and in a finite (and in practice, short) time their separation $\delta\mathbf{x}(t)$ attains the magnitude of L, the characteristic linear extent of the whole system. This property of *sensitivity to initial conditions* can be quantified as

$$|\delta\mathbf{x}(t)| \approx e^{\lambda t}|\delta\mathbf{x}(0)|$$

where λ, the mean rate of separation of trajectories of the system, is the *Lyapunov exponent*.

A positive Lyapunov exponent does not in itself lead to chaos. One could try to play 1- or 2-disk pinball game, but it would not be much of a game; trajectories would only separate, never to meet again. What is also needed is *mixing*, the coming together again and again of trajectories. While locally the nearby trajectories separate, the interesting dynamics is confined to a globally finite region of the state space and thus the separated trajectories are necessarily folded back and can re-approach each other arbitrarily closely, infinitely many times. The number of trajectories that return by time t can be quantified as

$$N(n) \approx e^{ht}$$

where h, the growth rate of the number of topologically distinct trajectories, is called the *"topological entropy"*. The word 'chaos' has in this context taken on a narrow technical meaning. If a deterministic system is locally unstable (positive Lyapunov exponent) and globally mixing (positive entropy) it is said to be *chaotic*.

While mathematically correct, the definition of chaos as 'positive Lyapunov + positive entropy' is useless in practice, as a measurement of these quantities is intrinsically asymptotic and beyond reach for systems observed in nature or simulated on computers. More powerful is Poincaré's vision of chaos as the interplay of local instability (unstable periodic orbits) and global mixing (intertwining of their stable and unstable manifolds).

Escape rates   (ChaosBook.org, ver. 15.7, Sect. 22.4) The above paragraph describes the essence of "chaos" for finite-dimensional dynamical systems, but not how to compute its consequences. That is accomplished by the periodic orbit theory. Consider the simplest possible chaotic system, with the state space partitioned into two intervals, with equal expanding multipliers, $|\Lambda_0| = |\Lambda_1| = e^\lambda$ (Bernoulli map, tent map).

[A side remark to Paul: Hamiltonian versions with uniform stretching, such as Arnold cat map, baker's map, Selberg zeta function, etc., work the same way, in equilibrium or away from it, modulo inessential details, such as pairing of eigenvalues, due to the symplectic invariance].

In the above $\lambda = \ln|\Lambda|/T$ is the cycle Lyapunov exponent. For an open system, the real part of the eigenvalue s_α gives the decay rate γ of αth eigenstate. If there was only one periodic orbit (zero entropy), the decay rate would equal the cycle Lyapunov exponent.

Our task is to determine the leading zero $z = e^{-\gamma}$ of the dynamical zeta function. The exponentially growing number of cycles with growing period balances the escape rate from individual cycles, and conspires to shift the zeros of the zeta function, and for this particular uniform stretching map correct formula is

$$0 = 1 - e^{\gamma - \lambda + h}, \qquad h = \ln 2. \tag{19.1}$$

This particular formula for the escape rate γ is a special case of a general relation between escape rates, Lyapunov exponents and entropies.

Physically this means that the escape induced by the repulsion by each unstable fixed point is diminished by the rate of backscatter from other repelling regions; the difference of the two is the actual escape rate.

What about nonlinear field theory and turbulence?

2016-10-27 Predrag A prologue. By 1972 I had completed, together with Kinoshita, what at the time was the largest and most expensive QFT calculation ever [38] (it broke CERN theory division computing budget). Once I emerged from the trenches, wiser for the experience, tthe main thing I had learned is that perturbative QED is stupid (colored text is live hypelinks), and doing QCD by Feynman diagrams is plain wrong.

If you are an atomic or nuclear physicist you think that quantum mechanics is a Hamiltonian and the energy spectrum. From that perspective, the Wigner surmise is the first thing to do if you see a complicated spectrum. It tells you what "random" means for distributions constrained by unitarity, time-reversal invariance, etc.. It's a diagnostic, not a theory. Not then, and not now.

If you are a field theorist, you think that quantum mechanics is path integrals, Lagrangians, their extrema (WKB/semiclassics), and $\hbar$ expansions

around these classical solutions. And you strive (i) write down equations, (2) solve them, and (3) predict, with no statistical assumptions or mindless averaging. One thing that "chaos" is not are Gaussians.

Since 1976 I knew that nonlinear equations can have infinitely many distinct unstable solutions, and, in order to organize them for the period-doubling and circle-maps [25] into the fundamental terms, and systematic series of exponentially small corrections, I invented cycle expansions [10], in an esoteric setting - not time evolution flow of a conventional dynamical system, but fictitious "time" of renormalization flows. Working backwards, I was able to relate them to zeta functions of Gutzwiller and Ruelle.

I derived the equation for the period doubling fixed point function (not a big step - it is the limit of his functional recursion sequence), which has since played a key role in the theory of transitions to turbulence. Since then we have generalized the universal equations to period n-tuplings; constructed universal scaling functions for all winding numbers in circle maps, and established universality of the Hausdorff dimension of the critical staircase.

This all reads like a Physics Today obituary for a buddy of Lenny Susskind. But it brings us to today, when for the next 6 weeks me and my plumber friends will work on how to fashion a theory of turbulence from myard ...

2016-11-06 Predrag Early references on the spatiotemporal invariants and invariant measures:

Ruelle [53] *Large volume limit of the distribution of characteristic exponents in turbulence* writes: " For spatially extended conservative or dissipative physical systems, it appears natural that a density of characteristic exponents per unit volume should exist when the volume tends to infinity. In the case of a turbulent viscous fluid, however, this simple idea is complicated by the phenomenon of intermittency.

In the case of a Hamiltonian system, and taking for ρ an ergodic component of the Liouville measure, one finds that the spectrum is invariant under change of sign.

For certain classes of physical systems *a large volume limit* exists (for equilibrium statistical mechanics this is the *thermodynamic limit*). We want to investigate the possibility of defining a large volume limit for certain dynamical systems. The idea is that, if several systems with independent dynamics occupy disjoint regions, the spectrum of the joint system is simply the union of the spectra of the subsystems (repeated characteristic exponents appear with added multiplicity). If an interaction between the subsystems is introduced, one may hope that this does not alter the spectrum much and that, in the large volume limit, a number of characteristic exponents per unit volume may be defined. "

He refers to the leading Lyapunov exponent as "characteristic exponent." Then the things get pretty technical, and I skimmed through the rest.

" The 'barber pole' turbulence which fascinated Feynman (Feynman et al. [5, II, Sect. 41-6]) appears in the flow between two concentric rotating cylinders and consists of an helical turbulent band alternating with a 'laminar' region. "

2017-01-24 Predrag Celebrating Finkelstein's *Reckless Ideas in Physics* by a night of thinking. Dunno whether the above papers are any good, but they have pushed us over the edge, and the log germinating process is over.

Dynamics is dead - the theory of turbulence is now again a branch of physics, on par with Ising models and quantum field theories, but this time around based on fundamental equations, with no statistical assumptions.

In turbulence, there is no more time, there is only spacetime, and DNS will have to follow - integrating forward in time from specified initial conditions is over. From now one has to parallelize and solve the equations in spacetime, globally and variationally, not step them incrementally in any given 1D spacetime direction - that problem is ill posed. And the game is to enumerate admissible patterns - symbolic dynamics will be more crucial than ever before.

2017-02-03 Björn Birnir A nice book to learn basic facts about PDEs is *Partial Differential Equations* by Fritz John [34].

Also, study the work of Christian Kuehn

2017-02-15 Predrag The *2017-01-24* declaration above that the dynamics is dead is not just another piece of Predrag bombast. In the Santa Barbara secret seminar (i.e., the one talk that was not recorded) it met some resonance with fluid dynamicists. In the Dresden MPIPKS talk it barely raised anyone's pulse (a quantum optics crowd - makes sense, what do they care about chaos). Only Denis Ullmo responded, and that is because he's been thinking about "mean field games," a new field of social sciences which uses constraint optimization methods. But I digress.

For me, this is a time of intellectual turmoil: dynamics is dead. I make fun of rocket scientists [60] discovering now, in 2013, that "the initial value problem of a chaotic dynamical system is *ill-conditioned*," but they are right. Since high school, I have been thinking incorrectly, like a physicist (formulating chaotic dynamics locally in time, as an initial value problem, to be integrated forward in time) while all along working correctly, as an engineer (solving for chaotic orbits globally, by variational methods). So DasBuch has to be rewritten, entirely, from chapter 4 on, with the ideas of Chapter 38 *Relaxation for cyclists* to be moved to the beginning of the exposition. All bits and pieces are already available, but the puzzle has to be fully reconfigured.

I credit the moronic citizenry for this insight - since November 9, the National Day of Shame, I have read no news, all my life is now local. Sit, think, talk to friends and family. It is amazing how peaceful and liberating is this quiet period, in-between the shameful deed and the major disasters that are about to befall us.

The real credit goes to Boris Gutkin and trying to decode how thinks: Spatiotemporal cat is a gift that goes on giving. For a single cat, things seem business as usual - dynamics is just a product of matrices, and if the eigenvalues are hyperbolic, at any finite discrete time the usual partition of state space issues, into exponentially shrinking regions of given finite symbolic dynamics. But the moment one goes to 2-dimensional spatiotemporal cat business as usual is impossible - advancing a spatial configuration one discrete step forward in time is impossible, as it is infinitely unstable.

This message is really nailed in by going to continuous spacetime.

2017-03-26 Predrag This might merit a quick read: and M. Balajewicz [49] *Lagrangian basis method for dimensionality reduction of convection dominated nonlinear flows*

2017-03-26 Predrag This might merit a quick read: A. Gouasmi, E. Parish and K. Duraisamy [28] *Characterizing memory effects in coarse-grained nonlinear systems using the Mori-Zwanzig formalism* looks interesting: " Reduced representations of complex, non-linear dynamical systems often require closure, that is finding a good representation of the contribution of the

discarded physics to the retained physics. In this work, we pursue the construction of closure models within the context of the Mori-Zwanzig (M-Z) formalism of irreversible statistical mechanics. In this setting, the effect of the unresolved states on the resolved states can be exactly represented as a time-history dependent integral, commonly referred to as memory, and a noise term. Evaluating the memory kernel requires the solution to the so-called orthogonal dynamics equation. An understanding of the structure and mechanics of the orthogonal dynamics is critical to the development of M-Z-based reduced models. The orthogonal dynamics equation, however, is a high-dimensional partial differential equation in free-space that is intractable in general. We propose an alternative method to compute the memory kernel that builds on the approximation that the orthogonal dynamics locally retains the structure of a Liouville equation. The method is demonstrated on Fourier-Galerkin simulations of the Kuramoto-Sivanshinsky (K-S) equation.

The proposed procedure provides accurate reconstruction of the memory integral and valuable insight into the structure and scaling of the memory kernel. "

2017-06-20 Predrag Elder *et al.* [23] *Spatiotemporal chaos in the damped Kuramoto-Sivashinsky equation*: " A discretized version of the damped Kuramoto-Sivashinsky (DKS) equation is constructed to provide a simple computational model of spatiotemporal chaos in one dimension. The discrete map is used to study the transition from periodic solutions to disordered solutions (i.e., spatiotemporal chaos). The numerical evidence indicates a jump discontinuity at this transition.

2017-06-13 Predrag Mike Schatz told us in February to look at Xu and Paul [61] *Covariant Lyapunov vectors of chaotic Rayleigh-Bénard convection*. We really should.

2017-06-20 Predrag I have asked Mark Paul about their calculation. He said that they computed ridiculously many covariant vectors - lake a thousand - and never saw and indication of the physical (invariant manifold) dimension. It is certainly above 100. They compute a large "fractal dimension;" according to a ChaosBook remark, any fractal dimension above 5 or so is not credible. Considering how much care estimating physical dimension took in Xiong's work, one would need to critically read through the paper before taking their results at the face value.

Bala(chandra) Suri feels that his 2D Kolmogorov flow would be the best experimental flow to try to find the physical dimension. I worry about that example - it has a rather complicated approximate discrete symmetry –I remember something like D_8 from Mohammad's elton blog– and a broken translation symmetry, that must produce tons of nearly degenerate covariant vectors.

My best candidates are still the small domain plane Couette flow and pipe flow.

2017-09-20 Predrag ruminations on spatiotemporal stability. Let's first recall how the measure ("inverse" of the "stability") of a pattern is computed for the spatiotemporal cat [29]. The $d = 2$ spatiotemporal cat "equations of motion" in the Lagrangian form are given by

$$(-\Box + s - 4)\, x_{nt} = s_{nt}\,, \qquad s_z \in \mathcal{A}\,, \tag{19.2}$$

with $\Box$ being the discrete spacetime Laplacian on $\mathbb{Z}^2$,

$$\Box\, x_{nt} := x_{n,t-1} + x_{n-1,t} - 4\, x_{nt} + x_{n,t+1} + x_{n+1,t}\,.$$

The symbols s_{nt} from the set $\mathcal{A} = \{\underline{3}, \underline{2}, \cdots, s-2, s-1\}$ on the right hand side of (19.2) are necessary to keep x_{nt} within the interval $[0, 1)$ The symbol $\lfloor x_{nt} \rfloor$ here denotes x_{nt} with the negative sign, i.e., '$\underline{3}$' stands for symbol '-3'. The block $\mathsf{M} = \{s_{nt} \in \mathcal{A}, \ (n, t) \in \mathbb{Z}^2\}$ can be used as a 2-dimensional symbolic representation of the lattice system state. Any solution X of (19.2) can be uniquely recovered from its symbolic representation M. By inverting (19.2) we obtain

$$x_z = \sum_{z' \in \mathbb{Z}^2} g_{zz'} s_{z'}, \qquad g_{zz'} = \left(\frac{1}{-\Box + s - 4}\right)_{zz'}, \tag{19.3}$$

where $g_{zz'}$ is the Green's function for the 2-dimensional discretized heat equation. A spatiotemporal cat lattice state M is admissible if and only if all x_z given by (19.3) fall into the interval $[0, 1)$.

Moving onto Kuramoto-Sivashinsky: first on solves the nonlinear fixed point equation, something like

$$v(x^*) = 0$$

where the state vector x is a finite discretization of the set of fields (1.34) over a compact $L \times T$ spatiotemporal invariant 2-torus, and v is constructed from a linear operator $\mathcal{L}(x)$, a matrix of first order space and time derivatives acting on x, plus a nonlinear term $\mathcal{N}(x)$. The equilibrium solution x^* is now taken as a background field (hopefully something related to the right side of (19.2)), and one looks at small deformations $y = \delta x = x - x^*$,

$$(\mathcal{L} - 1)\, y(x, t) = x^*(x, t)\,. \tag{19.4}$$

Inverting $(\mathcal{L} - 1)$ yields a $\det(\mathcal{L} - 1)^{-1} \times$ (co-matrices), so for large unstable eigenvalues, the inverse is exponentially small, just like for temporal dynamics ζ functions. This does not make sense as yet, but you get my drift... The $\det()^{-1}$ term should yield the likelihood of a given pattern, nothing to do with the "fictitious time" used in paranoid Newton to find the equilibrium pattern x^*.

2017-09-27 Predrag Knobloch suggests that we study:

> Klaus Kirchgässner [39], *Wave-solutions of reversible systems and applications* has 296 Google Scholar citations.

> Björn Sandstede and Arnd Scheel. This one (not sure ?): *On the structure of spectra of modulated travelling waves* [55]

2017-11-03 Predrag This flew by below the radar, sorry - in chapter 18 above, blog entry **2017-03-23** Matt wrote: " Also a note on symmetry, the way that J. F. Gibson Channelflow handles the spatial and temporal translation symmetry is to constrain the Newton steps to only progress in directions transverse to the spatial and temporal equivariance tangent directions. "

This is not a symmetry reduction. Separating the flow *locally* into group dynamics and a transverse, 'horizontal' flow, [1, 57] by the 'method of connections', [52], does not reduce the dynamics to a lower-dimensional reduced state space $\mathcal{M}/G$. In contrast to the method of co-moving frames, where one defines a mean phase velocity of a relative periodic orbit, the method of connections is inherently local. The two methods coincide for relative equilibria.

This is explained many places: **2013-09-19** entry in `siminos/blog/`, **2013-10-28** entry in `pipes/blog/` (there is actually a whole chapter there, currently commented, on getting Kreilos and Eckhardt to understand that, and correct their Kreilos, Zammert and Eckhardt [40] *Comoving frames and symmetry-related motions in parallel shear flows* prior to publication), sect. VI. *Bridges to nowhere* in ref. [11], sect. 3.1. *Method of connections* in Budanur *et al.* [6] *Relative periodic orbits form the backbone of turbulent pipe flow*, and towards the end of the very scholarly Remark 13.1 *A brief history of relativity, or, 'Desymmetrization and its discontents'*.

If that is what Channelflow still does, please alert John that this is wrong; give him a pdf printout of this blog, so he can reread the references himself. And please do tell me whether you had any luck communicating with him about this; it is important to us, because fluid dynamics community has by now learned a bit about periodic orbits, but almost nothing about the necessity of symmetry reduction for analysis of turbulent flows.

2017-11-03 Predrag I find it very hard to understand mathematical physics when it it is only described in words, without formulas. As an example of the way I would blog an article that I am reading it, I am starting here a discussion of López articles. In this case writing formulas is easy, as one can download her source files from arXiv:1502.03862. In this way one can discuss the particular step in her calculations by referring to the formula she is using.

2017-11-03 Predrag Matt mentioned that he is rereading Vanessa López paper [48], because she found relative periodic orbits of complex Ginzburg-Landau using spatiotemporal methods (He had already discussed the paper in blog entries **2017-03-14** and **2017-03-23** in chapter 18, though not in any detail.). My bad - I simply paid no attention to their numerical method.

López has since written a more detailed paper [47] on her PhD work. We usually cite López, Boyland, Heath and Moser [48] *Relative periodic solutions of the complex Ginzburg-Landau equation* for being the first to determine relative periodic orbits in a spatiotemporal PDE, though we had never used her method of finding relative periodic orbits. (I do object to her using a nonsensical formula from literature to average over relative periodic orbits, but that is unrelated to the problem of finding them.)

Indeed, in both papers she discretizes using Fourier series expansions in both space and time, in order to derive an underdetermined system of nonlinear algebraic equations from which invariant solutions of the complex Ginzburg-Landau equation are sought. That is described in sect. 3 *Numerical Method* of ref. [47].

She first defines the symmetries of the problem:

The complex Ginzburg-Landau have a three-parameter group [3] [1]

$$G = \mathbb{T}^2 \times \mathbb{R} \tag{19.5}$$

of continuous symmetries generated by spacetime translations $x \to x+\sigma$, $t \to t+\tau$ and a rotation $A \to e^{i\theta}A$ of the complex field $A(x,t)$, in addition to being invariant under the action of the discrete group of transformations $A(x,t) \to A(-x,t)$ of spatial reflections. If $A(x,t)$ is a solution, so are

$$e^{i\theta}A(x,t), \tag{19.6}$$
$$A(x+\sigma,t), \tag{19.7}$$
$$A(x,t+\tau), \tag{19.8}$$
$$A(-x,t), \tag{19.9}$$

for any $g(\theta,\sigma,\tau) \in G$. For a given solution $A(x,t)$ of the complex Ginzburg-Landau equation, consider the isotropy subgroup G_A of G at A [2],

$$G_A = \{(\varphi,S,T) \in G \mid A(x,t) = e^{i\varphi}A(x+S,t+T)\}, \tag{19.10}$$

which consists of elements of the symmetry group $G = \mathbb{T}^2 \times \mathbb{R}$ leaving the complex Ginzburg-Landau equation invariant.

---

[1]Predrag 2018-03-20: She thinks of a "group" not as a collection of group elements, but as its parameter space. In (19.5) $\mathbb{R}$ refers to time $t \in (-\infty,\infty)$, and $\mathbb{T}^2$ refers to the complex phase $\theta \in (0,2\pi)$, and the configuration space restricted to a periodic domain of length $x \in (0,L_x)$. Remember, for us also $x \in (-\infty,\infty)$.

[2]Predrag 2018-03-20: Looks like she is defining a triply-periodic relative periodic orbit $A(x,t)$?

López seeks solutions $A(x,t)$ of the complex Ginzburg-Landau equation satisfying

$$A(x,t) = e^{i\varphi} A(x+S, t+T), \qquad (19.11)$$

for $(\varphi, S, T) \in G$ also unknown and to be determined.

She represents $A(x,t)$ as a spatial Fourier series

$$A(x,t) = \sum_{m \in \mathbb{Z}} a_m(t) e^{iq_k x}, \qquad (19.12)$$

where $q_k = 2\pi m/L_x$ denotes the m-th wavenumber in the expansion. From the group-invariance condition (19.11) it then follows that the complex-valued Fourier coefficient functions $a_m(t)$ in (19.12) satisfy

$$a_m(t) = e^{i\varphi} e^{iq_k S} a_m(t+T) \qquad (19.13)$$

for all $m \in \mathbb{Z}$. Because of the presence of spatial translational symmetry the solutions sought can be restricted to those with elements $g(\varphi, S, T) \in G$ having $S \in [0, L_x)$.

O(2) **symmetry.** Since the complex Ginzburg-Landau equation is invariant under the action of the group $\mathbb{Z}_2$ of spatial reflections $A(x,t) \to A(-x,t)$, to any solution $A(x,t)$ of the complex Ginzburg-Landau equation having $(0, L_x, 0)$ and (φ, S, T) as generators of subgroups of the isotropy subgroup G_A there corresponds a solution $\tilde{A}(x,t) := A(-x,t)$ having $(0, L_x, 0)$ and $(\varphi, L_x - S, T)$ as generators of subgroups of the isotropy subgroup $G_{\tilde{A}}$. [... some details of incorporating the reflection symmetry we should also study ...] She calls the invariant solutions $(A; \varphi, L_x/2 \pm \delta, T)$ and $(\tilde{A}; \varphi, L_x/2 \mp \delta, T)$, as well as their corresponding orbits $G \cdot A$ and $G \cdot \tilde{A}$, *conjugate* to each other under the (involutive) action of the group $\mathbb{Z}_2$ of spatial reflection symmetry of the complex Ginzburg-Landau equation.

She writes: "The complex Ginzburg-Landau equation may admit solutions having symmetries other than (or in addition to) that defined by (19.11) and several of the solutions resulting from our study do have additional symmetries. For instance, there may exist solutions of the complex Ginzburg-Landau equation satisfying"

$$
\begin{array}{llll}
A(x,t) & = & e^{i2\pi/l} A(x + L_x/l, t), & \text{for some } l \in \mathbb{N}, l > 1, & (19.14) \\
A(x,t) & = & A(-x + 2c_1, t) & \text{for some } c_1 \in \mathbb{R}, & (19.15) \\
A(x,t) & = & -A(-x + 2c_2, t) & \text{for some } c_2 \in \mathbb{R}. & (19.16)
\end{array}
$$

The first one is standard: (19.14) describes solutions fixed by a composition of the actions (19.7) and (19.6), and gives $(2\pi/l, L_x/l, 0)$ as one generator of a subgroup of G_A. Symmetries (19.15) and (19.16) might be our pre-periodic orbits, they are, respectively, even about $x = c_1$ or odd about

$x = c_2$ for some real numbers c_1, c_2. Presumably awkwardly placed symmetry points in a conjugacy class, should all really be conjugated to the standard origin $x = 0$.

A solution having both symmetries (19.14) and (19.15) also satisfies

$$A(-x + 2(c_1 + L_x/(2l)), t) = \mathrm{e}^{\mathrm{i}2\pi/l} A(x, t) . \tag{19.17}$$

In particular, note that a solution satisfying (19.14) for $l = 2$ and which is even about $x = c_1$ is also odd about $x = c_2 = c_1 + L_x/4$.

Since the boundary conditions are periodic in x, she usea the spatial Fourier series (19.12) and substitutes into the complex Ginzburg-Landau equation to obtain an infinite system of ordinary differential equations (ODEs),

$$\frac{\mathrm{d}a_m}{\mathrm{d}t} = Ra_m - q_k^2(1 + \mathrm{i}\nu)a_m - (1 + \mathrm{i}\mu) \sum_{m_1 + m_2 - m_3 = m} a_{m_1} a_{m_2} a_{m_3}^*, \tag{19.18}$$

for the complex-valued functions $a_m(t)$. Under this transformation the symmetries (19.6–19.9) of complex Ginzburg-Landau equation become symmetries of (19.18). Thus, if $\boldsymbol{a}(t) = (a_m(t))$ is a solution of the system of ODEs (19.18), then so are

$$(\mathrm{e}^{\mathrm{i}\theta} a_m(t)), \tag{19.19}$$

$$(\mathrm{e}^{\mathrm{i}m\sigma} a_m(t)), \tag{19.20}$$

$$(a_m(t + \tau)), \tag{19.21}$$

$$(a_{-m}(t)), \tag{19.22}$$

for any $(\theta, \sigma, \tau) \in \mathbb{T}^2 \times \mathbb{R}$. In particular, (19.19) and (19.20) say that the ODEs (19.18) are invariant under the $\mathbb{T}^2$-action

$$(\theta, \sigma) \cdot (a_m(t)) = (\mathrm{e}^{\mathrm{i}\theta} \mathrm{e}^{\mathrm{i}m\sigma} a_m(t)).$$

She employs a spectral-Galerkin projection obtained by fixing an even number N_x and truncating the expansion (19.12) to include only the terms with indices m satisfying $-N_x/2 + 1 \leq m \leq N_x/2 - 1$. Both theory and computation [16, 36] shows that for sufficiently large N_x the behavior of this truncation captures the essential features of the complex Ginzburg-Landau dynamics.

From the condition (19.11) defining an invariant solution of the complex Ginzburg-Landau equation, it follows that the corresponding solution $\boldsymbol{a}(t)$ of the system of ODEs (19.18) satisfies

$$a_k(t) = \mathrm{e}^{\mathrm{i}\varphi} \mathrm{e}^{\mathrm{i}q_k S} a_m(t + T) \tag{19.23}$$

for all m and t (and where φ, S, T are to be determined).

As Matt pointed out in a conversation, a solution of the system of functional equations (19.23) can be expressed in the spacetime Fourier-Fourier basis for (19.18) as

$$a_k(t) = \mathrm{e}^{-\mathrm{i}\frac{\varphi}{T}t}\mathrm{e}^{-\mathrm{i}q_k\frac{S}{T}t}\sum_{j\in\mathbb{Z}}\hat{a}_{kj}\mathrm{e}^{\mathrm{i}\omega_j t}\,, \tag{19.24}$$

where $\omega_j = 2\pi n/T$ denotes the n-th frequency in the expansion. It might be most economical to do for Kuramoto-Sivashinsky precisely what López did for complex Ginzburg-Landau. It should be easier, as there is one less continuous symmetry.
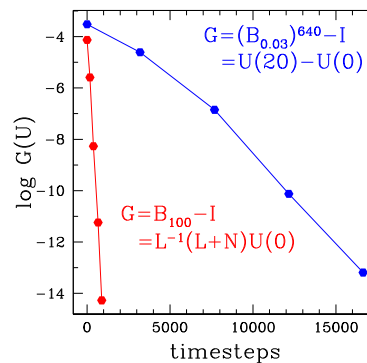
Figure 19.1: A Chanellflow equilibrium solution comparison between Laurette's Stokes method (in red) and the standard method (in blue).

2017-11-13 Predrag As fate would have it, I talked to Laurette Tuckerman, and she reminded me of her method of determining equilibria and relative equilibria that is some 20 times faster than the usual Newton, and it reminds me very much of Matt's approach. The references are BifAnal-TimeStep.pdf, mamun.pdf, timesteppers.pdf, and invpow_CICP.pdf.

Figure 19.1 is an example of (to me very impressive) convergence acceleration.

2018-02-06 Predrag I went to 5 (five!) seminars, colloquia and public lectures yesterday, plus spent couple of hours working with students one-on-one. Twitter is aflame with a debate whether professors really pull 60-hour weeks. Not sure that counts as 'work' (or, what in the notes that follow we call 'action'), especially the two math seminars that made impenetrable the topics I currently work on but - that might be counted as 'relaxation', but it sure was many hours. The second seminar of the day, while I still had some neurons lighting up, was *Discrete stochastic Hamilton-Jacobi equation* by Renato Iturriaga, CIMAT. He is a collaborator Georgia Tech's A. Fathi. This should be a flip side of Marsden's discrete Lagrangian methods, to be blogged here at some point. Here it goes:

$$\begin{aligned}\text{Lagrangian } L &: \quad TT^d \to \mathbb{R} \tag{19.25}\\ \text{Hamiltonian } H &: \quad T^*T^d \to \mathbb{R}\,. \tag{19.26}\end{aligned}$$

The dynamics is on the tangent bundle. T^* means symplectic structure. Minimizing L gives Euler-Lagrange equation (ODE). Minimizing H gives Hamilton-Jacobi equation (PDE). Can discretize Hamilton-Jacobi in two ways (1) add viscosity, (2) add discount factor (for 'discount factors' see, for example, here):

$$H(x, d_x U) = \Delta U + \epsilon. \qquad (19.27)$$

A Lax-Oleinik transformation gives a unique solution of (19.27). (And so on, but I give up - have another 17 things awaiting me.)

2018-02-06 Predrag I ran into an interesting discussion by Miles Stoudenmire: *Periodic vs Open or Infinite Boundary Conditions for DMRG, Which Should You Choose?* Stoudenmire says that when open BC achieves a given accuracy when keeping m states, then to reach the same accuracy with periodic BC one must keep m^2 states. I find it interesting, because I have a strong prejudice for periodic BC, but it really should not matter - if you are doing a large scale turbulence simulation free BC might make sense, if that decreases the cost of the computation.

2018-02-26 Predrag A snippet from internet:

Topological quantum computing (TQC) is a newer type of quantum computing that uses "braids" of particle tracks, rather than actual particles such as ions and electrons, as the qubits to implement computations. Using braids has one important advantage: it makes TQCs practically immune to the small perturbations in the environment that cause decoherence in particle-based qubits and often lead to high error rates.

2018-03-09 Predrag I uploaded my APS March Meeting 2018 slides.

2018-03-12 Predrag We are not alone. It is an obvious idea.

Kevin O'Keeffe, Hyunsuk Hong and Steven Strogatz of Cornell University, developed a 'swarmalator' model, consisting of oscillators whose phase dynamics and spatial dynamics are coupled, leading to simultaneous spatially-coordinated and synchronous behavior [50]. They say that 'synchronization' is self-organization in time, such as activation in heart cells, and that 'aggregations' is self-organization in space, like alignment of electron spins in magnetic material. In the synchronized state, the individual cells coordinate the timing of their oscillations, but they do not move through space. In swarming individuals move through space, but without conspicuously altering their internal states.

Now, what they actually do is very much in the style of the Winfree, Kuramoto, Strogatz' life work (fireflies in synch, etc.) and it might have too much detail of that kind for us to truly enjoy the work. They claim that "insights from biological synchronization have shed light on neutrino oscillations, phase locking in Josephson junction arrays (that one with Kurt as coauthor), ...," but I doubt that.

Say what you want, but they sure get the prize for the ugliest new terminology: "A rich phenomenology is expected for mobile oscillators whose phases affect their motion. We call these hypothetical systems 'swarmalators' because they generalize swarms and oscillators."

As they work with N 'particles' in continuous time and space, the simplest model is $2N$ all-to-all coupled ODEs (like Kuramoto models), a bit complicated at get go. Emphasis on "space" and "time" is fraudulent: what they really mean is that space dynamics of N interacting "particles" is coupled to the internal dynamics of these N "particles." It will provide employment for folks who have run out of ideas in their work on Kuramoto systems. In other words, this is just an ordinary, time evolving dynamical $2N$-dimensional system, where the physical interpretation of the first N dimensions differs from the second N dimensions. It is not even Hamiltonian, or anything. They do not use symmetries, even permutation ones. For us, a downer.

2018-02-06 Alex Haro You can compute Lyapunov exponents of the tangent dynamics to the torus. If you want something more explicit, as eigenvalues and "eigenvectors" (technically invariant bundles), you can discretize what is known as transfer operator. Angel Jorba has a paper on this brute force method. Rafael de la Llave, I. G. Kevrekidis and R. A. Adomaitis[3] used this method many years ago. In my papers with Rafael (see also chapter 3 of our book [31] *The parametrization method for invariant manifolds*) we use several efficient methods.

You could ask Rafael, or some PhD student from Barcelona, as Joan Gimeno.

2018-03-20 Predrag We can track the references through their recent numerical paper, Canadell and Haro [7] *Computation of quasi-periodic normally hyperbolic invariant tori: Algorithms, numerical explorations and mechanisms of breakdown*. From the abstract: " We present several algorithms for computing normally hyperbolic invariant tori [...]. The algorithms use different hyperbolicity and reducibility properties and compute also the invariant bundles and Floquet transformations. "

2018-04-12 Predrag Stephen Wolfram writes:

Cool. I like your idea (if I understood it) of making symbolic dynamics out of spacetime lumps of PDEs. (somewhat reminiscent of my space-time patches.

Simpler than Kuramoto-Sivashinsky, but seemingly just as "turbulent" is my PDE. I've been asking PDE people about this equation for years ...

---

[3]Predrag 2018-03-20: I was not able to pinpoint the particular references. Perhaps Adomaitis, Kevrekidis and de la Llave [2] *A computer-assisted study of global dynamic transitions for a noninvertible system* or *Predicting the complexity of disconnected basins of attraction for a noninvertible system*, a technical report from 1991.

nobody has ever told me anything interesting about it, beyond what's already in my notes.

P.S. Common response from kids: "What a strange coincidence that your name is the same as the name in Wolfram | Alpha. Oh, and that your computer has that same logo on it." :)

2018-05-02 Predrag In 2012 Wilczek hyothesized existence of 'Time crystals', see ...observed time crystals... and "Time Crystals Multiply": " Time crystals are different from other time-periodic systems (like pendula and beating hearts) in that they don't move to the rhythm set by their driving mechanism. Instead, they oscillate with a period that is an integer multiple of the driving period. In addition, according to most models, the periodic driving would overheat the crystal, and a discrete time crystal could only exist if the system is stabilized against heating by a disorder-induced phenomenon called many-body localization. "

I do not think we will run into them, because one needs higher time derivatives, see (19.28), but I am not sure. The credit for looking at things spatiotemporal globally perhaps goes back to Lagrange (the action is the cost function for mechanical systems). Any time you have a stable limit cycle you have a time crystal (they call that "spontaneous time-symmetry breaking", but chaotic dynamics selects an infinite set of periods (periods of unstable periodic orbits, generically not rationally related). But I keep looking at these papers, such as Sacha and Zakrzewski [54] *Time crystals: a review*. Who knows, we might learn something. They write:

Time crystals are time-periodic self-organized structures postulated by Frank Wilczek in 2012. Discrete (or Floquet) time crystals are structures that appear in the time domain due to spontaneous breaking of discrete time translation symmetry. The struggle to observe discrete time crystals is reviewed here together with propositions that generalize this concept introducing condensed matter-like physics in the time domain. We review strategies aimed at spontaneous breaking of continuous time translation symmetry.

Switching from space to time crystals exchanges the role of space and time. In the space crystal case we expect periodic behaviour in space at a fixed instant of time (i.e. at the moment when we perform a measurement of a system) while in the time crystal case we fix the position in space and ask whether a detector clicks periodically in time.

Assume the energy of a particle of the form

$$E = \frac{\dot{x}^4}{4} - \frac{\dot{x}^2}{2} \, . \tag{19.28}$$

The lowest energy corresponds to particle motion with velocity $\dot{x} = \pm 1$. Note that the energy (19.28) cannot be converted to the Hamiltonian smoothly: the Hamiltonian is a multi-valued function of the momentum with

cusps corresponding precisely to energy minima at $\dot{x} = \pm 1$ where the Hamilton equations are not defined (Shapere and Wilczek [56]).

The quantum version is based on taking a time-periodic (Floquet) Hamiltonian $H(t + T) = H(t)$ and then working with the complete set of Floquet eigenstates $|u_n(t + T)\rangle = |u_n(t)\rangle$, quasi-energies E_n,

$$|\psi(t)\rangle = \sum c_n e^{-iE_n t}|u_n(t)\rangle \,.$$

Quasi-energy spectrum is not bounded from below. It is periodic with a period $2\pi/T$ and it is sufficient to consider only a single Floquet zone in order to fully describe a system, in analogy to a Brillouin zone in condensed matter physics.

The general motivation is the same as our cat map discussion - they consider a rotor motivated by a Rydberg electron perturbed by a microwave field. Then they relate the quantum version to a tight-binding model.

2018-07-10 Predrag Of possible interest to Matt, as we will have to continue our invariant 2-tori: Engelnkemper *et al.* [24], arXiv:1808.02321, *Continuation for thin film hydrodynamics and related scalar problems*. They write " [...] how to apply continuation techniques [...] applied to a number of common examples of variational equations, namely, Allen-Cahn- and Cahn–Hilliard-type equations including certain thin-film equations for partially wetting liquids on homogeneous and heterogeneous substrates as well as Swift–Hohenberg and Phase-Field-Crystal equations. Second we consider nonvariational examples as the Kuramoto–Sivashinsky equation [...]. Through the different examples we illustrate how to employ the numerical tools provided by the packages auto07p and pde2path to determine steady, stationary and time-periodic solutions in one and two dimensions and the resulting bifurcation diagrams. "

2018-08-19 Predrag I have the periodic orbit theory formula for an equilibrium point (for the last 20-30 years!) in the boyscout version of ChaosBook (current sect. 22.3 *Equilibrium points*), but do not know what to do with it.

Very frustrating.

Now it is pressing - in the spatiotemporal formulation of turbulence the zeta functions (Fredholm determinants) are presumably 2-d or (1+3)-d Laplace/Fourier transforms of trace formulas, one dimension for each continuous symmetry: one Laplace transform for time, and one Fourier transform for each infinite spatial direction.

We have not written either the trace or the determinant formulas yet. The spatiotemporal cat periodic points (invariant 2-tori) counting suggests a way, so far unexplored.

Or, a deeper insight: in the spatiotemporal formulation of turbulence there are no periodic orbits, as there is no evolution, neither in space nor in time. All solutions are fixed points, and the important measure is not

the natural (Ruelle-Bowen-Sinai) infinite time measure, but the measure concept is more like the stat mech understanding of the Ising model - what is the likelihood of occurrence of a given spacetime configuration (admissible by the defining equations of the system)?

2018-08-21 Predrag Dong [17] *Organization of the periodic orbits in the Rössler flow* writes: "Numerical implementation of the variational method [...] a finite difference scheme is used to obtain accurate discrete loop derivatives. We use the five-point approximation. [that is of interest to us] We invert the matrix using the banded LU decomposition on the embedded band diagonal matrix, and treat the cyclic and border terms with the Woodbury formula."

Have to read these as well (Matt has had a look at Dong [19], did not see how to apply it to his own project):

Dong, Wang, Du, Uzer and Lan [22] *The ionized electron return phenomenon of Rydberg atom in crossed-fields*

Dong [19] *Topological classification of periodic orbits in the Kuramoto-Sivashinsky equation*

Dong [18] *Topological classification of periodic orbits in Lorenz system*

Dong [20] *Topological classification of periodic orbits in the Yang-Chen system*

2018-09-02 Predrag Ziessler, Dellnitz and R. Gerlach [64] *The numerical computation of unstable manifolds for infinite dimensional dynamical systems by embedding techniques*, arXiv:1808.08787: " we extend the novel framework developed by Dellnitz, Hessel-von Molo and Ziessler [15], arXiv:1508.07182, to the computation of finite dimensional unstable manifolds of infinite dimensional dynamical systems. To this end, we adapt a set-oriented continuation technique for the computation of such objects of finite dimensional systems. We show how to implement this approach for the analysis of partial differential equations and illustrate its feasibility by computing unstable manifolds of the one-dimensional Kuramoto-Sivashinsky equation as well as for the Mackey-Glass delay differential equation. "

2018-10-06 Predrag A summary of Wang, Wang and Lan [59] *Accelerated variational approach for searching cycles*.

Lan and Cvitanović [43] variational approach eliminates most Poincaré sections by discretizing continuous time evolution into small time steps. The approach requires storage of an entire trajectory in the computer memory, so the computational load is proportional to the number of discretization points. In order to extend the method to determination of connecting (homo/hetero-clinic) orbits, Dong and Y. Lan [21] designed an automatic mesh allocation algorithm which makes the guess points evenly distributed in arc length instead of in time, and thus avoids their accumulation near the ends of the connection, where the flow is exponentially approaching zero. In this paper they introduce several new schemes to allocate mesh points in different situations.

In their calculations of periodic orbits, they approximate the loop derivatives by a five-point banded matrices, with the periodic boundary condition.

Following Zhou, Ren and E [63], they reparametrize the loop parameter by a desired density of points (their eq. (6)), for example uniform in time, or uniform in arc length, and derive an effective equation to automatically allocate lattice points which capture local fine orbit structures, while keeping the exponential convergence of the variational approach.

The time-translational invariance of a periodic orbit leads to neutral direction in the update of the coordinates [43], which is eliminated by a gauge-fixing condition [21, 37, 63]. They use the usual Poincaré section plane condition (below their eq. (6)). A conservation law may supply another neutral direction for the variation. They use a two-dimensional Hamiltonian energy conservation neutral direction as an example of a way to remove such neutral direction by adding a Lagrange multiplier (their eq. (16)), while keeping the dynamics on the desired energy surface.

Utilizing the special structure of the matrix involved in the homotopy evolution, the lower-upper (LU) decomposition is implemented with greater efficiency and less memory. Their number of unknown elements in L and U is proportional to Nd instead of $(Nd)^2$ as in the usual LU decomposition, which greatly speeds up the computation.

Three examples are used to demonstrate the validity of the accelerated algorithm.

Left for the future:

1. The computation of the Jacobian in high-dimensional systems is time and resource consuming. How to overcome this difficulty remains a major challenge.
2. The computation of the weight function is quite cumbersome. There may exist an equivalent way for redistributing the lattice point but with much lighter computation load.

If you want to discuss this with Lan, we can get him online any time. Unfortunately Georga Tech prevents him from coming here February 2019, or perhaps as long as we live in Trumplandia.

2019-02-03 John Gibson I met Datseris at the last JuliaCon and attended his talk. His

DynamicalSystems.jl:
A Julia software library for chaos and nonlinear dynamics [14]

and

DynamicalBilliards.jl:
An easy-to-use, modular and extendable Julia package for dynamical billiard systems in two dimensions [13]

are really spectacular packages. You should assign a student to use them in a project.

Any volunteers? I have a dynamite (but difficult) turbulence project for you :)

His JuliaCon talk is here ▶ (click!). John is in the second row to the left, light blue shirt.

2019-02-21 John Gibson Saw this on Julia Discourse this morning: an interactive tool for exploring dynamical system

discourse.julialang.org/t/announcing-interactivechaos/21046

juliadynamics.github.io/DynamicalSystems.jl/dev/#interactivechaos

2019-02-25 Predrag As fate would have it, the new theoretical condensed matter physics assistant professor here, Glen Evenbly <glen.evenbly@gmail.com> does all his tensor networks computations in Julia. Han Liang visited him, explained the spatiotemporal cat, and they were both happy.

2019-03-24 John Gibson on defining the Kuramoto-Sivashinsky time scale:

$$u_t = -u_{xx} - u_{xxxx} - uu_x$$

Linear stability around $u = 0$ gives a maximally unstable mode [4] $\exp(i\alpha t)$ with $\alpha = 1/\sqrt{2}$ and wavelength $L = 2\pi/\alpha = 2\pi\sqrt{2}$.

We get a wavespeed $c \approx 3$ from the nonlinear wave term $-uu_x$, and the fact that u saturates at about $|u| = 3$. That gives a nonlinear time scale of about $t = 3$ from $t = L/c = 2\sqrt{2}\pi/3 \approx 3$.

Seems to be about right from viewing simulations. I don't have a good argument why u saturates at $|u| = 3$.

2019-02-26 Predrag Objection! We know that as L grows, the flame front $u(x,t)$ is a random walk in u with mean $\langle u \rangle(t) = 0$ (we used Galilean invariance to enforce that) and the variance $\langle u^2 \rangle(t)$ (the "kinetic energy") growing linearly with L (have a look at the color bar units in Matt's invariant 2-tori), so $|u|$ certainly does not saturate at 3. This global argument has to be turned into some local rate of growth of $|u|$, perhaps $|u_x|$. The steepness of kinks in the flame front might be bounded by the hyperviscosity...

2019-02-27 Predrag Machine learning workshop:
I moved my notes to *pipes/blog/dailyBlog.tex*

2019-02-27 Predrag Ispolatov [33] *Chaos in high-dimensional dissipative dynamical systems* cites a huge amount of literature that studies high dimensions and might have to be cited in our work.

---

[4]Predrag 2019-03-25: I think he means $\exp(\alpha t)$.

They solve numerically coupled systems of equations which contain second- and third-order nonlinear terms, with coefficients drawn from Gaussian distributions with zero mean and unit variance.

They find that the probability of chaos increases with the dimension of the phase space and that, essentially all trajectories become chaotic for $d > 50$, while for intermediate dimensions $d \succeq 15$, the majority of chaotic trajectories essentially fill out the available phase space.

[...] We assume that for sufficiently high d, all Jacobian eigenvalues are statistically independent. This assumption [...] is a rather strong approximation without which it seems impossible to derive analytical estimates, and which seems to result in reasonable results.

2019-05-19 Predrag SIAM DS19 talk by Joanna Slawinska, Abbas Ourmazd, Dimitrios Giannakis, and Joerg Schumacher *Vector-Valued Spectral Analysis of Complex Flows* have been doing this for a while, and a bunch of old literature comes with it...

Vector-Valued Spectral Analysis (VSA) is a recently developed framework [27] for spatiotemporal pattern extraction, based on the eigendecomposition of a kernel integral operator acting on vector-valued observables (spatially extended fields) of the dynamical system generating the data, constructed by combining elements of the theory of operator-valued kernels for multitask machine learning with delay-coordinate maps of dynamical systems. The method utilizes a kernel measure of similarity that takes into account both temporal and spatial degrees of freedom (whereas classical techniques such as EOF analysis are based on aggregate measures of similarity between "snapshots"). As a result, VSA extracts physically meaningful patterns with intermittency in both space and time, while factoring out any symmetries present in the data.

2019-06-01 Predrag Giannakis *et al.* [27] *Spatiotemporal pattern extraction by spectral analysis of vector-valued observables*:

"Vector-valued spectral analysis (VSA) is based on an eigendecomposition of a kernel integral operator acting on a Hilbert space of vector-valued observables of the system. [...] conventional eigendecomposition techniques decompose the input data into pairs of temporal and spatial modes with a separable, tensor product structure. The patterns recovered by VSA can be manifestly non-separable, requiring only a modest number of modes to represent signals with intermittency in both space and time. The kernel construction naturally quotients out dynamical symmetries in the data and exhibits an asymptotic commutativity property with the Koopman evolution operator of the system, enabling decomposition of multiscale signals into dynamically intrinsic patterns. Application of VSA to the Kuramoto-Sivashinsky model demonstrates significant performance gains in efficient and meaningful decomposition over eigendecomposition techniques utilizing scalar-valued kernels. [...] the

techniques described above recover from the data a set of temporal patterns and a corresponding set of spatial patterns, sometimes referred to as "chronos" and "topos" modes, respectively. [...] "

This looks like something it will take time to digest, but digest we must...

2020-01-22 Predrag Well, if we are going to have a revolution, nothing will remain untouched. In particular, we have to give up on the forward-in-time evolution operators, replace them by enforcing infinitesimal continuity equation at any spacetime instant.

Scary, as the solutions are supposed to be invariant spacetime measures, and those are horrible nowhere differential beasts. But invariant 2-toruss should save the day.

2020-08-04 Predrag When it comes to proofs that solutions like our Kuramoto-Sivashinsky exist, Akitoshi Takayasu want us to refer to 3 of his papers: "A method of verified computations for solutions to semilinear parabolic equations using semigroup theory," SIAM J. Numer. Anal., Vol. 55, pp. 980-1001,(2017)

Numerical verification for existence of a global-in-time solution to semilinear parabolic equations, J. Comput. Appl. Math., Vol. 315, pp. 1-16, (2017)

"Accurate method of verified computing for solutions of semilinear heat equations," Reliable Computing, Vol. 25, pp. 74-99, (2017).

I have not read them. Other work of this rigorous kind is by Piotr Zgliczynski *et al.*.

2020-10-20 Erik Aurell Thanks for the presentation, it was very enjoyable, and impressive. Thanks also for making it interactive, which is much more enjoyable than a zoom talk with slides. To follow up on the remark I made, the paper I was thinking about was Frisch, She and Thual [26]

2020-10-25 Predrag to Erik (& Lan, Roberto),

you are right, and thanks for reminding me: Frisch, She and Thual [26] *Viscoelastic behaviour of cellular solutions to the Kuramoto-Sivashinsky model* (1986) is an amazing paper (nobody writes papers like that one any more), we always cite it, but I had forgotten the "viscoelastic" in the title.

As you had noticed immediately, there are very long correlated patterns in the large scale simulations (not because of transients not having died out - the long-range correlations are always there), and - as Frisch et al write, they are a consequence of Galilean symmetry, in the following way:

'Visco': While on small finite domains we always work by fixing $\langle u \rangle = 0$, on large and infinity domains, u can attain any value, ie, the flame front velocity "diffuses" or executes a "random walk" - that's how I interpret a part of their paper. We actually routinely compute the

covariance $\langle u^2 \rangle / 2$ of this random walk, as that goes into our power-in/dissipation-out plots, ChaosBook Sect. 30.3 *Energy budget*, Figure 30.3.

'-elastic': I know precisely what spatiotemporal stability of a relative doubly-periodic solution is, but I do not understand how to identify the 'elastic' eigen-exponents when we study stability of our rubbery tiles.

For me the paper is very hard to digest (my fault, not theirs), but you have worked on this, you'll figure it out.

Basically, while they discuss long wavelengths compared to the typical wiggle-spacing, our problem is a single nearly marginal eigenvalue / eigendirection in deforming a small rubbery tile while infinitesimally changing both spatial and temporal period in determining the continuous family of what we would like to identify uniquely by a single spatiotemporal array of symbols.

Wow, that was a long sentence. My hunch is that we should pick the unique value where this eigenvalue is zero (the "least-strained" tile shape) to describe the whole continuous family of relative doubly-periodic solutions corresponding to a given ruberry shape. It should die at both ends through some abrupt, precise, shape-changing bifurcation. All other eigen-exponents are strictly away from zero, so the family should be isolated. It should not be possible to continuously transform distinct rubber tiles into one another for spatiotemporal discrete symbolic dynamics to make sense.

Matt has explored the bifurcations at the ends of the continuous families of rubber-tile deformations, but not sufficiently precisely to establish that.

2019-02-16 Predrag to Matt Eventually the study of the deformation of our "rubber alphabet tiles" should go to a chapter of its own. Currently the text above, around **2018-07-23 Matt continuous families** is what we have, and the main conceptual problem remains what point on the 1D continuous family of a rubber tile to take as the representative tile.

Here is a simple proposal - pick the point at which an "alphabet" tile is reflection symmetric; than the continuum of other solutions belongs to relative periodic tiles, with continuum of non-zero phase shifts.

Is this good enough?

2019-05-14 Predrag We might chose Galilean invariant elementary tiles (spatial derivatives of u), instead of Galilean equivariant u_j tiles.

2019-12-06 Matt & Predrag excerpt from a draft *spatiotemp/chapter/tiles.tex*:

$[\cdots]$ we have not investigated how the local Galilean velocities of the tiles affect the tiling procedure. We $[\cdots$ use] the Galilean invariance (12.31) to

set the mean velocity of the overall front to zero. For an arbitrary subregion of width $L_1 < L$, the mean velocity is generically $\langle u \rangle(t) \neq 0$. Actually, we know that as function of L the velocity front executes a random walk, [5] and hence the range of the color bar in a figure such as figure 1.1 has to grow proportionally to $\sqrt{L}$. The variance grows only in the spatial direction, in the time direction $E(t) \rightarrow E$. That implies that in gluing letters u_j of alphabet figure 1.10 into larger patterns, one also has to vary $\langle u_j \rangle(t)$ averaged over the tile of width L_j, in order to glue optimally. In other words, we have to use the Galilean symmetry group orbit of the letter u_j, and slice that group orbit at $\langle u_j \rangle(t_0) = 0$ for purposes of plotting its representative in figure 1.10. The tiles of figure 1.10 were all converged with under the zero mean velocity condition; locally, subdomains of the tiling have non-vanishing local Galilean velocities.

2020-10-23 Predrag We refer to Frisch *et al.* after (1.22), in figure 18.21, and in posts **2018-05-09 PC** and **2013-12-29 PC**. In

Cvitanović, Davidchack and Siminos [12] write: "For large system size, it is hard to imagine a scenario under which attractive periodic states (as shown in ref. [26], they do exist) would have significantly large immediate basins of attraction."

2021-03-20 Predrag I'm worried about 'rubbery tiles' in Matt's Kuramoto-Sivashinsky project, specifically about Frisch *et al.* "viscoelasticity" paper [26] that seems to describe long range correlations.

Graham know what they are, see **2017-01-26 Matt**, **M. Graham Talk** above.

See **2020-10-22 Matt** eq. (18.19), **2020-10-25 Predrag** above.

For some viscoelasticity papers to possibly ponder (have not tried to read them), search for **2021-03-20 Predrag** in svn repo *pipes*, *blog/blog.tex*.

2020-10-25 Predrag notes on Frisch, She and Thual [26] *Viscoelastic behaviour of cellular solutions to the Kuramoto-Sivashinsky model*:

"A multiple-scale analysis of the Kuramoto-Sivashinsky one-dimensional model of a flame front with 2π-periodic boundary conditions is presented. For arbitrary large values of the number M of linearly unstable modes there exist stable steady solutions of period $2\pi/N$ where N = O(M). These 'cellular solutions' exhibit elastic behaviour under perturbations of wavelength much larger than $2\pi/N$. The results are illustrated by numerical experiments. Elasticity has its origin in the translation and Galilean invariances. Similar invariance properties are likely to be at the root of the viscoelastic behaviour of turbulent flows conjectured by many authors."

They show that the stability of cellular solutions is related to their viscoelastic behaviour under large-scale weak perturbations. Actually this

---

[5]Predrag 2019-12-06: make sure that this is explained in the text elsewhere, then link here to the variance equation "with variance $E(t) = \frac{1}{2}\langle u^2 \rangle(t) \propto L$ by the extensivity of Kuramoto-Sivashinsky,"

stability is at best marginal: the KS equation is invariant under translations and Galilean transformations ; thus there are perturbations which cannot relax, namely weak uniform translations and addition of weak uniform velocities. When such perturbations are taken to be slightly non-uniform, slow but non-trivial dynamical behaviour sets in. This is a particular case of what is known as 'phase dynamics' (Kuramoto [41, 42],1984a,b; Pomeau & Manneville 1979; Coullet & Fauve 1984, 1985; Fauve 1985).

Technically, weak large-scale perturbations of the cellular solutions are governed by a linear p.d.e. with (spatially) rapidly varying coefficients. This may be asymptotically analysed by the same multiscale homogenization methods that are used in deriving the bulk properties of periodically inhomogeneous materials or flows (Bensoussan, Lions and Papanicolaou 1978 ; Papanicolaou & Pironneau 1981). Most problems studied so far by these techniques have only translation invariance. The presence in our case of the additional Galilean invariance gives rise to second-order rather than first-order dynamics in time.

2020-11-13 Predrag Johnson, Noble, Rodrigues and Zumbrun [35] *Behavior of periodic solutions of viscous conservation laws under localized and nonlocalized perturbations*: " when there exist conserved quantities, whether deriving from Hamiltonian structure/symmetries of the equations, or, as in the case of parabolic conservation laws considered here, simply from divergence form of the equations/conservation of mass, then there exist additional critical modes, and the formal WKB prediction becomes that of a more complicated hyperbolic-parabolic system of conservation laws rather than the scalar convected Burgers equation of the reaction-diffusion case.

Perhaps the best-known example of such a model is the Kuramoto-Sivashinsky equation, for which the formal asymptotic description of behavior via a hyperbolic-parabolic system of conservation laws was pointed out already in Frisch, She and Thual [26] under the alternative form of a damped scalar wave equation (the "viscoelastic behavior" of the title). "

but, on the whole, I doubt this paper will help us.

2020-11-15 Predrag Matt writes: "In this symbolic representation the columns code admissible time itineraries, and rows encode the admissible spatial profiles." I like the phrasing.

2020-11-23 Predrag Could it be that continuous $[L \times T]$ families somehow correspond to Floquet of 'Brillouin' bands?

2021-04-12 Predrag Matt started working as "Data Scientist" for a AI logistics startup Verusen.com.

Burak and Matt have committed to writing up the first draft of the Matt thesis paper.

2021-04-12 Predrag From Sep 2019 to present Matt has designed, developed, documented, deployed and dockerized Python package as Jupyter Notebook,

> Orbithunter guide
> GitHub Orbithunter
> docker.com login: orbithunter beThebest!
> orbithunter port is: -p 8887:8887

which serves as a framework for the study of nonlinear dynamics and chaos. Designed to maximize user friendliness and modularity to enable collaboration between scientists and comparison of their results. Acts as a high-level user interface of the SciPy and NumPy numerical Python packages and partial differential equations.

2021-06-28 Predrag Potentially of interest.

Salihah Alwadani, Kelowna, B. C., Heinz H. Bauschke, Julian P. Revalski and Xianfu Wang, *The difference vectors for convex sets and a resolution of the geometry conjecture*, arXiv:2012.04784, write:

Let X be a real Hilbert space, and $C_1, \ldots, C_m$ are nonempty closed convex subsets of X, with projectors $P_{C_1}, \ldots, P_{C_m}$ which we also write more simply as $P_1, \ldots, P_m$, and with $m \in \{2, 3, \ldots, \}$. We define the fixed point sets of the cyclic compositions by

$$
\begin{aligned}
F_m &:= \text{Fix}(P_m \cdots P_1), \\
F_{m-1} &:= \text{Fix}(P_{m-1} \cdots P_1 P_m), \ldots, \\
F_1 &:= \text{Fix}(P_1 P_m \cdots P_2).
\end{aligned}
\tag{19.29}
$$

Compositions of projectors are often employed in projection methods. This is a vast area which we will not summarize here; however, we refer the reader to ref. [8], arXiv:1802.07529 as a starting point, as well as the ref. [9], arXiv:2008.02260.

2021-08-27 Predrag Potentially of interest.

Zeng and Graham [62] *Symmetry reduction for deep reinforcement learning active control of chaotic spatiotemporal dynamics* (2021): "Deep reinforcement learning (RL) is a data-driven, model-free method capable of discovering complex control strategies [...] systems of flow control interest possess symmetries [...] Kuramoto-Sivashinsky equation (KSE), equally spaced actuators, and a goal of minimizing dissipation and power cost, we move the deep RL problem to a symmetry-reduced space [...] symmetry-reduced deep RL yields improved data efficiency [...] the symmetry aware control agent drives the system toward an equilibrium state of the forced KSE [...] despite having been given no explicit information regarding its existence."

Deep learning approaches that respect symmetries automatically rather than learn to approximate them from data are likely to have superior performance, [...] incorporating symmetries of the learning domain into the deep neural-network (NN) models. For example, the state-of-the-art [44] AlexNet NN image classifier spontaneously learns redundant internal representations that are equivariant to flips, scalings, and rotations.

Many flow geometries of interest possess symmetries to incorporate into the deep RL model.

Read also:

Lenc and Vedaldi [44] *Understanding image representations by measuring their equivariance and equivalence*, (2018).

Bucci, Semeraro, Allauzen, Wisniewski, Cordier and Mathelin [5] *Control of chaotic systems by deep reinforcement learning*, (2019).

2022-06-13 Chris Crowley Why is a time average distance from turbulence to an RPO in Taylor-Couette dependent on τ (time along the orbit), but not on θ (azimuthal orientation)? Both are symmetries of the system and I am having a difficulty wrapping my head around why those symmetries don't imply invariance to translations along both directions.

2022-08-03 Josh Pughe-Sanford Have yall every heard of GitHub.com/mxgmn/WaveFunctionCollapse *The Wavefunction Collapse Algorithm* explained very clearly by Robert Heaton?

Apparently creates large images that have the same "feel" as small seed tiles. I am so curious what it would do with yalls Kuramoto-Sivashinsky tiles. Would it produce qualitatively accurate dynamics?

2022-08-04 Matt I think "wavefunction collapse" is just a catchy name for Monte Carlo sampling from a probability distribution; specifically a distribution corresponding to an undirected probabilistic graphical model. You create a lattice, choose a site, sample from the PMF defined by the weights, then the remaining sites are conditioned on the sample you just made. Inadmissibility simply indicates a state whose conditional probability is zero. I am guessing their rules of admissibility are based only on neighboring states, such that the joint density can be factorized into pairwise potentials. I believe choosing the state based on entropy is simply a way of trying to sample/seed in a way to reduce correlation. Or that is at least what it seems like to me after a couple minute skim :)

In regards to Kuramoto-Sivashinsky. A means of tiling currently exists, it maps a configuration of symbols into a large spatiotemporal state, but no work has been done on the grammar. In other words I have a set of representative shapes but no informed decision on a probability distribution has been made (i.e. uniform and independent currently). Clearly you could calculate frequencies of states appearing in the large space-time limit and use that to inform the distribution, but only minimal work has been done towards that end.

So if we could determine the grammar and weights of each of the tile orbits (of which there are only a few continuous families) then we could probably use their codes. The one tricky detail is that it sounds like they require the tiles to be $[N \times N]$ in shape, but not all orbits are identical in their periods, so this would naturally induce error due to differences in the grid spacings.

2022-08-04 Predrag Wish they would stick to wedding planning and not misuse words like "wavefunction collapse" which already mean something quite different. Anyway:

This gets at the heart of the matter of *admissibility* in gluing. Once one has extracted from a large Kuramoto-Sivashinsky spatiotemporal pattern a small set of fundamental tiles (FTs) and assigned an alphabet to them, almost any large (for us doubly periodic, with the relative periodic orbit shift) random spatiotemporal tilling will be inadmissible.

Matt's approach has been to start with every such pattern as a rough spatiotemporal guess, and let his optimization algorithms descend to an admissible solution (perhaps adjusted to a nearby admissible pattern, with a nearby symbol block) or get stuck and thrown away.

My suggestion has been motivated by the way we enumerate temporally admissible itineraries: start with gluing all possible smallest spatiotemporal tile arrays, glue to them FTs from the edges to grow the next smallest tiles, list the inadmissible patterns as *pruning rules*, and from then on prune each inadmissible glue-on before checking for the existence of the corresponding (relative) periodic orbit. The probability of the periodic orbit is the inverse of its Hill determinant, so we could preferentially glue low Shannon entropy tilings first to obtain new pruning rules.

The whole thing is a minefield, so we would test it first on our space-time discretized spatiotemporal cat, ϕ^3 (Hénon) and ϕ^4 deterministic Euclidean field theories, where we can construct examples with exact trivial and nontrivial symbolic codings, and see how these "wedding collapse" algorithms do. Then move to Kuramoto-Sivashinsky and TC duct flows. Decades of person-years of research, I fear.

2022-10-28 Predrag A major conceptual breakthrough - the day 'rubbery tiles' died!

For the Kuramoto-Sivashinsky system at hand, we impose the constant mean dissipation rate (computed as along-time average over any ergodic trajectory) to be satisfied by every compact solution, resulting in a single (or no) solution contribution for each continuous family, see sect. 1.9.4.

Please either agree, or shoot me down. Important step in our program.

References

[1] R. Abraham and J. E. Marsden, *Foundations of Mechanics* (Benjamin-Cummings, Reading, MA, 1978).

[2] R. A. Adomaitis, I. G. Kevrekidis, and R. de la Llave, "A computer-assisted study of global dynamic transitions for a noninvertible system", Int. J. Bifur. Chaos **17**, 1305–1321 (2007).

[3] I. S. Aranson and L. Kramer, "The world of complex Ginzburg-Landau equation", Rev. Mod. Phys. **74**, 99–143 (2002).

[4] M. Baranger, K. T. R. Davies, and J. H. Mahoney, "The calculation of periodic trajectories", Ann. Phys. **186**, 95–110 (1988).

[5] M. A. Bucci, O. Semeraro, A. Allauzen, G. Wisniewski, L. Cordier, and L. Mathelin, "Control of chaotic systems by deep reinforcement learning", Proc. Roy. Soc. Ser A **475**, 20190351 (2019).

[6] N. B. Budanur, K. Y. Short, M. Farazmand, A. P. Willis, and P. Cvitanović, "Relative periodic orbits form the backbone of turbulent pipe flow", J. Fluid Mech. **833**, 274–301 (2017).

[7] M. Canadell and À. Haro, "Computation of quasi-periodic normally hyperbolic invariant tori: Algorithms, numerical explorations and mechanisms of breakdown", J. Nonlin. Sci. **27**, 1829–1868 (2017).

[8] Y. Censor and M. Zaknoon, "Algorithms and convergence results of projection methods for inconsistent feasibility problems: A review", Pure Appl. Funct. Anal. **3**, 565–586 (2018).

[9] P. L. Combettes and J.-C. Pesquet, "Fixed point strategies in data science", IEEE Trans. Signal Proc., 1–1 (2021).

[10] P. Cvitanović, "Invariant measurement of strange sets in terms of cycles", Phys. Rev. Lett. **61**, 2729–2732 (1988).

[11] P. Cvitanović, D. Borrero-Echeverry, K. Carroll, B. Robbins, and E. Siminos, "Cartography of high-dimensional flows: A visual guide to sections and slices", Chaos **22**, 047506 (2012).

[12] P. Cvitanović, R. L. Davidchack, and E. Siminos, "On the state space geometry of the Kuramoto-Sivashinsky flow in a periodic domain", SIAM J. Appl. Dyn. Syst. **9**, 1–33 (2010).

[13] G. Datseris, "DynamicalBilliards.jl: An easy-to-use, modular and extendable Julia package for dynamical billiard systems in two dimensions", J. Open Source Soft. **2**, 458 (2017).

[14] G. Datseris, "DynamicalSystems.jl: A Julia software library for chaos and nonlinear dynamics", J. Open Source Soft. **3**, 598 (2018).

[15] M. Dellnitz, M. Hessel-von Molo, and A. Ziessler, "On the computation of attractors for delay differential equations", J. Comp. Dynamics **3**, 93–112 (2016).

[16] A. Doelman, "Slow time-periodic solutions of the Ginzburg-Landau equation", Physica D **40**, 156–172 (1989).

[17] C. Dong, "Organization of the periodic orbits in the Rössler flow", Int. J. Mod. Phys. B **22**, 1850227 (2018).

[18] C. Dong, "Topological classification of periodic orbits in Lorenz system", Chin. Phys. B **27**, 080501 (2018).

[19] C. Dong, "Topological classification of periodic orbits in the Kuramoto-Sivashinsky equation", Mod. Phys. Lett. B **32**, 1850155 (2018).

[20] C. Dong, "Topological classification of periodic orbits in the Yang-Chen system", Europhys. Lett. **123**, 20005 (2018).

[21] C. Dong and Y. Lan, "A variational approach to connecting orbits in nonlinear dynamical systems", Phys. Lett. A **378**, 705–712 (2014).

[22] C. Dong, P. Wang, M. Du, T. Uzer, and Y. Lan, "The ionized electron return phenomenon of Rydberg atom in crossed-fields", Mod. Phys. Lett. B **30**, 1650183 (2016).

[23] K. R. Elder, H. Xi, M. Deans, and J. D. Gunton, "Spatiotemporal chaos in the damped Kuramoto-Sivashinsky equation", AIP Conf. Proc. **342**, 702–708 (1995).

[24] S. Engelnkemper, S. V. Gurevich, H. Uecker, D. Wetzel, and U. Thiele, "Continuation for thin film hydrodynamics and related scalar problems", in *Computational Modelling of Bifurcations and Instabilities in Fluid Dynamics*, edited by A. Gelfgat (Springer, Berlin, 2019), pp. 459–501.

[25] M. J. Feigenbaum, L. P. Kadanoff, and S. J. Shenker, "Quasiperiodicity in dissipative systems: A renormalization group analysis", Physica D **5**, 370–386 (1982).

[26] U. Frisch, Z. S. She, and O. Thual, "Viscoelastic behavior of cellular solutions to the Kuramoto-Sivashinsky model", J. Fluid Mech. **168**, 221–240 (1986).

[27] D. Giannakis, A. Ourmazd, J. Slawinska, and Z. Zhao, "Spatiotemporal pattern extraction by spectral analysis of vector-valued observables", J. Nonlin. Sci., 1–61 (2019).

[28] A. Gouasmi, E. Parish, and K. Duraisamy, Characterizing memory effects in coarse-grained nonlinear systems using the Mori-Zwanzig formalism, 2016.

[29] B. Gutkin, L. Han, R. Jafari, A. K. Saremi, and P. Cvitanović, "Linear encoding of the spatiotemporal cat map", Nonlinearity **34**, 2800–2836 (2021).

[30] B. Gutkin and V. Osipov, "Classical foundations of many-particle quantum chaos", Nonlinearity **29**, 325–356 (2016).

[31] Á. Haro, M. Canadell, A. Luque, J. M. Mondelo, and J.-L. Figueras, *The Parameterization Method for Invariant Manifolds* (Springer, New York, 2016).

[32] A. E. Hramov and A. A. Koronovskii, "Detecting unstable periodic spatio-temporal states of spatial extended chaotic systems", Europhys. Lett. **80**, 10001 (2007).

[33] I. Ispolatov, V. Madhok, S. Allende, and M. Doebeli, "Chaos in high-dimensional dissipative dynamical systems", Sci. Rep. **5** (2015) 10 . 1038/srep12506.

[34] F. John, *Partial Differential Equations* (Springer, New York, 1978).

[35] M. A. Johnson, P. Noble, L. M. Rodrigues, and K. Zumbrun, "Behavior of periodic solutions of viscous conservation laws under localized and nonlocalized perturbations", Invent. math. **197**, 115–213 (2013).

[36] M. S. Jolly, R. Témam, and C. Xiong, "Convergence of a chaotic attractor with increased spatial resolution of the Ginzburg-Landau equation", Chaos Solit. Fract. **5**, 1833–1845 (1995).

[37] G. Kawahara and S. Kida, "Periodic motion embedded in plane Couette turbulence: Regeneration cycle and burst", J. Fluid Mech. **449**, 291 (2001).

[38] T. Kinoshita and P. Cvitanović, "Sixth-order radiative corrections to the electron magnetic moment", Phys. Rev. Lett. **29**, 1534–1537 (1972).

[39] K. Kirchgässner, "Wave-solutions of reversible systems and applications", J. Diff. Equ. **45**, 113–127 (1982).

[40] T. Kreilos, S. Zammert, and B. Eckhardt, "Comoving frames and symmetry-related motions in parallel shear flows", J. Fluid Mech. **751**, 685–697 (2014).

[41] Y. Kuramoto, "Diffusion-induced chaos in reaction systems", Suppl. Progr. Theor. Phys. **64**, 346–367 (1978).

[42] Y. Kuramoto, *Chemical oscillations, waves and turbulence* (Springer, New York, 1984).

[43] Y. Lan and P. Cvitanović, "Variational method for finding periodic orbits in a general flow", Phys. Rev. E **69**, 016217 (2004).

[44] K. Lenc and A. Vedaldi, "Understanding image representations by measuring their equivariance and equivalence", Int. J. Comput. Vision **127**, 456–476 (2018).

[45] X. Li, Y. Xue, P. Shi, and G. Hu, "Lyapunov spectra of coupled chaotic maps", Int. J. Bifur. Chaos **18**, 3759–3770 (2008).

[46] J. Llibre, "The averaging theory for computing periodic orbits", in *Central Configurations, Periodic Orbits, and Hamiltonian Systems*, Advanced Courses in Mathematics - CRM Barcelona (Springer, Basel, 2015), pp. 1–104.

[47] V. López, Numerical continuation of invariant solutions of the complex Ginzburg–Landau equation, 2015.

[48] V. López, P. Boyland, M. T. Heath, and R. D. Moser, "Relative periodic solutions of the complex Ginzburg-Landau equation", SIAM J. Appl. Dyn. Syst. **4**, 1042–1075 (2006).

[49] R. Mojgani and M. Balajewicz, Lagrangian basis method for dimensionality reduction of convection dominated nonlinear flows, 2015.

[50] K. P. O'Keeffe, H. Hong, and S. H. Strogatz, "Oscillators that sync and swarm", Nat. Commun. **8**, 1504 (2017).

[51] D. Pazó, I. G. Szendro, J. M. López, and M. A. Rodríguez, "Structure of characteristic Lyapunov vectors in spatiotemporal chaos", Phys. Rev. E **78**, 016209 (2008).

[52] C. W. Rowley, I. G. Kevrekidis, J. E. Marsden, and K. Lust, "Reduction and reconstruction for self-similar dynamical systems", Nonlinearity **16**, 1257–1275 (2003).

[53] D. Ruelle, "Large volume limit of the distribution of characteristic exponents in turbulence", Commun. Math. Phys. **87**, 287–302 (1982).

[54] K. Sacha and J. Zakrzewski, "Time crystals: a review", Rep. Prog. Phys. **81**, 016401 (2017).

[55] B. Sandstede and A. Scheel, "On the structure of spectra of modulated travelling waves", Math. Nachr. **232**, 39–93 (2001).

[56] A. Shapere and F. Wilczek, "Classical time crystals", Phys. Rev. Lett. **109**, 160402 (2012).

[57] S. Smale, "Topology and mechanics, I." Inv. Math. **10**, 305–331 (1970).

[58] K. Takeuchi and M. Sano, "Role of unstable periodic orbits in phase transitions of coupled map lattices", Phys. Rev. E **75**, 036201 (2007).

[59] D. Wang, P. Wang, and Y. Lan, "Accelerated variational approach for searching cycles", Phys. Rev. E **98**, 042204 (2018).

[60] Q. Wang, S. A. Gomez, P. J. Blonigan, A. L. Gregory, and E. Y. Qian, "Towards scalable parallel-in-time turbulent flow simulations", Phys. Fluids **25**, 110818 (2013).

[61] M. Xu and M. R. Paul, "Covariant Lyapunov vectors of chaotic Rayleigh-Bénard convection", Phys. Rev. E **93**, 062208 (2016).

[62] K. Zeng and M. D. Graham, "Symmetry reduction for deep reinforcement learning active control of chaotic spatiotemporal dynamics", Phys. Rev. E **104**, 014210 (2021).

[63] X. Zhou, W. Ren, and E, W., "Adaptive minimum action method for the study of rare events", J. Chem. Phys. **128**, 104111 (2008).

[64] A. Ziessler, M. Dellnitz, and R. Gerlach, The numerical computation of unstable manifolds for infinite dimensional dynamical systems by embedding techniques, 2018.

Chapter 20

Spatiotemporal stability

20.1 Temporal lattice

Assume that a periodic orbit $x(T_p + t) = x(t)$ of a continuous time flow $\dot{x} = v(x)$ is known 'numerically exactly', that is to say, to arbitrary (but not infinite) precision. One way to present the solution is to give a single point $x(0)$ in the orbit, and let the reader reconstruct the orbit p by integrating forward in time, $x(t) = f^t(x(0))$, $t \in [0, T_p]$.

However, for a linearly unstable periodic orbit a single point does not suffice to present the orbit, because there is always a finite 'Lyapunov time' t_{Lyap} beyond which $f^t(x(0))$ has lost all memory of the periodic orbit p. This problem is particularly severe in searches for 'exact coherent structures' embedded in turbulence, where even the shortest period solutions have to be computed to the (for everyday fluid dynamics excessive) machine precision [19, 20, 31] in order to complete the first return to the initial state.

Instead of relaying on forward-in-time numerical integration, *global methods* for finding periodic orbits [5] view them as equations for the vector fields $\dot{x}$ on spaces of closed curves. In numerical implementations one discretizes the periodic orbit p into sufficiently many short segments [5, 11, 12, 14, 21], and lists a point for each segment

$$p = (x_1, x_2, \cdots, x_{|p|}) \,. \tag{20.1}$$

For a d-dimensional discrete time map f obtained by cutting the flow by a set of Poincaré sections, with the periodic orbit p of discrete period $|p|$, every segment can be reconstructed by a short time integration, and satisfies

$$x_{k+1} = f(x_k) \,, \tag{20.2}$$

to high accuracy, as for sufficiently short times the exponential instabilities are numerically controllable.

So, how accurate is such an orbit, i.e., how fast do errors grow for such globally specified orbit? In numerical work we know the cycle points only to a

finite precision

$$\hat{p} = (\hat{x}_1, \hat{x}_2, \cdots, \hat{x}_{|p|}), \quad \hat{x}_k = x_k + \Delta x_k, \tag{20.3}$$

where x_k are the exact periodic orbit points. Define the error field by $F(\hat{p}) = f(\hat{p}) - \sigma\hat{p}$, an operator which compares the forward map of every point in $\hat{p}$ with the next point $\sigma\hat{p}$, a $(|p|\times d)$-dimensional vector field obtained by stacking $|p|$ state space points $\hat{x}_k$

$$F(\hat{x}) = F \begin{pmatrix} \hat{x}_1 \\ \hat{x}_2 \\ \cdots \\ \hat{x}_{|p|} \end{pmatrix} = \begin{pmatrix} \hat{x}_1 - \hat{f}_{|p|} \\ \hat{x}_2 - \hat{f}_1 \\ \cdots \\ \hat{x}_{|p|} - \hat{f}_{|p|-1} \end{pmatrix}, \qquad \hat{f}_k = f(\hat{x}_k), \tag{20.4}$$

which measures the misalignment of every finite forward-in-time segment $f(\hat{x})_k$ with the next listed point $\hat{x}_{k+1}$ on the periodic orbit.

By (20.2), the exact discretized cycle (20.1) is a zero of this vector field, $F(x) = 0$. Assuming that the d-dimensional vectors Δx_k are small in magnitude, and Taylor expanding the one discrete time-step map f to linear order around the exact solution,

$$f(x_t + \Delta x_t) = x_{t+1} + \mathbb{J}_t \Delta x + (\cdots),$$

where

$$[\mathbb{J}_t]_{ij} = \frac{\partial f_i(x_t)}{\partial x_j}, \quad t = (1, 2, \cdots, |p|), \quad i, j = (1, 2, \cdots, d) \tag{20.5}$$

one finds that the neighborhood of entire cycle p is linearly deformed by the $[|p|d \times |p|d]$ orbit Jacobian matrix

$$\Delta x' = \mathcal{J}(x)\,\Delta x, \qquad \mathcal{J}_{ij}(x) = \frac{\partial F(x)_i}{\partial x_j}, \tag{20.6}$$

with

$$\mathcal{J} = 1 - \sigma\mathbb{J},$$

the one discrete time-step temporal $[d\times d]$ diagonal Jacobian matrix $\mathbb{J}$ evaluated on the entire cycle p, and σ the shift matrix

$$\sigma = \begin{pmatrix} 0 & & & & & \mathbf{1} \\ \mathbf{1} & 0 & & & & \\ & \mathbf{1} & 0 & & & \\ & & \mathbf{1} & & & \\ & & & \ddots & 0 & \\ & & & & \mathbf{1} & 0 \end{pmatrix}, \quad \mathbb{J} = \begin{pmatrix} \mathbb{J}_1 & & & & & \\ & \mathbb{J}_2 & & & & \\ & & \mathbb{J}_3 & & & \\ & & & \ddots & & \\ & & & & \mathbb{J}_{|p|-1} & \\ & & & & & \mathbb{J}_{|p|} \end{pmatrix}, \tag{20.7}$$

with $\mathbf{1}$ in the upper right corner assuring periodicity, $\sigma^{|p|} = \mathbf{1}$. [1]

Next, we address two questions: (i) how is the high-dimensional orbit Jacobian matrix $\mathcal{J}$ related to the temporal $[d\times d]$ Jacobian matrix $\mathbb{J}$? and (ii) how does one evaluate the orbit Jacobian matrix $\mathcal{J}$?

---

[1]Predrag 2019-10-10: this is σ^{-1} shift operator as defined in ChaosBook.

20.1.1 Second-order difference equation

2CB

A second-order difference equation with constant coefficients has the form

$$x_{t+2} + p_1 x_{t+2} + p_2 x_t = 0 \tag{20.8}$$

Let $x_{0,t} = x_t$, $x_{1,t} = x_{t+1}$, and rewrite this as a pair of coupled first-order difference equations

$$
\begin{aligned}
\mathsf{X}_{t+1} &= A\,\mathsf{X}_t\,, \qquad \mathsf{X}_t = (x_{0,t}, x_{1,t})^\top \\
A &= \begin{pmatrix} 0 & 1 \\ -p_2 & -p_1 \end{pmatrix}.
\end{aligned}
\tag{20.9}
$$

The characteristic equation

$$\lambda^2 + p_1 \lambda + p_2 = 0 \tag{20.10}$$

can be obtained by substitution $x_t = \lambda^n$ into the two-term recursion (20.8).

If $\lambda_1 \neq \lambda_2$, λ_j real, then the solution of (20.8) is

$$x_t = c_1 \lambda_1^t + c_2 \lambda_2^t\,. \tag{20.11}$$

If $\lambda_1 = \lambda_2 = \lambda$, then the solution is

$$x_t = c_1 \lambda^t + c_2 t \lambda^t\,. \tag{20.12}$$

If $\lambda_1 = \alpha + i\beta$, $\lambda_2 = \alpha - i\beta$, then the solution is

$$x_t = |\lambda|^t (c_1 \cos t\omega + c_2 \sin t\omega)\,, \tag{20.13}$$

where $\omega = \arctan(\beta/\alpha)$. To solve such second-order difference equation, one has to specify initial conditions, for example $x_0 = 1, x_1 = 0$.

(Based on Elaydi [17])

20.1.2 Third-order difference equation

One can always reformulate an k-term recursion relation (**??**) as a set of k coupled first-order difference equations (delay equations). For example, one can rewrite the three-term recursion relation (third-order difference equation)

$$x_{t+3} + p_1 x_{t+2} + p_2 x_{t+1} + p_3 x_t = 0 \tag{20.14}$$

as three coupled first-order difference equations

$$
\begin{aligned}
x_{0,t+1} &= x_{1,t}, \\
x_{1,t+1} &= x_{2,t}, \\
x_{2,t+1} &= -p_3 x_{0,t} - p_2 x_{1,t} - p_1 x_{2,t}\,.
\end{aligned}
\tag{20.15}
$$

---

[2]Predrag 2020-12-15: Transfer to ChaosBook.org. Once incorporated, remove from here)

where $x_{0,t} = x_t$, $x_{1,t} = x_{t+1}$, $x_{2,t} = x_{t+2}$. Compactly

$$
\begin{aligned}
\mathsf{X}_{t+1} &= A\,\mathsf{X}_t\,, \qquad \mathsf{X}_t = (x_{0,t}, x_{1,t}, x_{2,t})^\top \\
A &= \begin{pmatrix} 0 & 1 & 0 \\ 0 & 0 & 1 \\ -p_3 & -p_2 & -p_1 \end{pmatrix}.
\end{aligned} \tag{20.16}
$$

The eigenvalues of A are the characteristic roots of (20.14), see (**??**) and (**??**).

The discrete time derivative of a lattice state X evaluated at the lattice site t is given by the *difference operator*

$$
\dot{\mathsf{X}}_t = \left[\frac{\partial \mathsf{X}}{\partial t}\right]_t = \frac{x_t - x_{t-1}}{\Delta t} \tag{20.17}
$$

Eq. (20.16) can be viewed as a time-discretized, first-order ODE dynamical system

$$
\dot{\mathsf{X}} = v(\mathsf{X})\,, \tag{20.18}
$$

with the time increment set to $\Delta t = 1$

(Based on Elaydi [16])

20.2 Repeats of a prime Bravais cell

2021-06-11 Han

A lattice state X_p is *prime* if it is not a repeat of a smaller lattice state. The orbit Jacobian matrix of a period-$(r\|)$ lattice state X which is a r-th repeat of a period-$\|$ prime lattice state X_p has a tri-diagonal block circulant matrix form

$$
\mathcal{J} = \begin{bmatrix}
\mathbf{s}_p & -\mathbf{d} & & & -\mathbf{d}^\top \\
-\mathbf{d}^\top & \mathbf{s}_p & -\mathbf{d} & & \\
& \ddots & \ddots & \ddots & \\
& & -\mathbf{d}^\top & \mathbf{s}_p & -\mathbf{d} \\
-\mathbf{d} & & & -\mathbf{d}^\top & \mathbf{s}_p
\end{bmatrix}, \tag{20.19}
$$

where $\mathbf{s}_p$, $\mathbf{d}$ and $\mathbf{d}^\top$ are $[\|\times\|]$ block matrices

$$
\begin{aligned}
\mathbf{s}_p &= \begin{bmatrix}
s_0 & -1 & & & 0 \\
-1 & s_1 & -1 & & \\
& \ddots & \ddots & \ddots & \\
& & -1 & s_{\|-2} & -1 \\
0 & & & -1 & s_{\|-1}
\end{bmatrix}, \\[6pt]
\mathbf{d} &= \begin{bmatrix}
0 & \cdots & 0 \\
& \ddots & \vdots \\
1 & & 0
\end{bmatrix}, \quad
\mathbf{d}^\top = \begin{bmatrix}
0 & & 1 \\
\vdots & \ddots & \\
0 & \cdots & 0
\end{bmatrix}, \quad (20.20)
\end{aligned}
$$

and $\mathbf{d}$ and its transpose enforce the periodic bc's.

As $\mathcal{J}$ is a block circulant matrix, it brought into a block diagonal form by a unitary transformation, with a repeating block along the diagonal.

Note that matrices $\mathbf{s}_p$, $\mathbf{d}$ and $\mathbf{d}^\top$ are not circulant, the matrix $\mathcal{J}$ is *not* a block circulant with circulant blocks [3, 4, 32].

20.2.1 Bravais cell repeats symmetrized

2021-06-11 Han

The tri-diagonal block matrix can be projected into the symmetric subspace of the shorter lattice state. As an example, take the shorter lattice state of period $n = 4$, and the long lattice state given by the shorter lattice state repeated 4 times. Then the reflection operator can also be written into the 16-dimensional space of the long lattice state:

$$
\mathbf{d} \;=\; \left[\begin{array}{cccc|cccc|cccc|cccc}
0 & 0 & 0 & 1 & 0 & 0 & 0 & 0 & 0 & 0 & 0 & 0 & 0 & 0 & 0 & 0 \\
0 & 0 & 1 & 0 & 0 & 0 & 0 & 0 & 0 & 0 & 0 & 0 & 0 & 0 & 0 & 0 \\
0 & 1 & 0 & 0 & 0 & 0 & 0 & 0 & 0 & 0 & 0 & 0 & 0 & 0 & 0 & 0 \\
1 & 0 & 0 & 0 & 0 & 0 & 0 & 0 & 0 & 0 & 0 & 0 & 0 & 0 & 0 & 0 \\
\hline
0 & 0 & 0 & 0 & 0 & 0 & 0 & 1 & 0 & 0 & 0 & 0 & 0 & 0 & 0 & 0 \\
0 & 0 & 0 & 0 & 0 & 0 & 1 & 0 & 0 & 0 & 0 & 0 & 0 & 0 & 0 & 0 \\
0 & 0 & 0 & 0 & 0 & 1 & 0 & 0 & 0 & 0 & 0 & 0 & 0 & 0 & 0 & 0 \\
0 & 0 & 0 & 0 & 1 & 0 & 0 & 0 & 0 & 0 & 0 & 0 & 0 & 0 & 0 & 0 \\
\hline
0 & 0 & 0 & 0 & 0 & 0 & 0 & 0 & 0 & 0 & 0 & 1 & 0 & 0 & 0 & 0 \\
0 & 0 & 0 & 0 & 0 & 0 & 0 & 0 & 0 & 0 & 1 & 0 & 0 & 0 & 0 & 0 \\
0 & 0 & 0 & 0 & 0 & 0 & 0 & 0 & 0 & 1 & 0 & 0 & 0 & 0 & 0 & 0 \\
0 & 0 & 0 & 0 & 0 & 0 & 0 & 0 & 1 & 0 & 0 & 0 & 0 & 0 & 0 & 0 \\
\hline
0 & 0 & 0 & 0 & 0 & 0 & 0 & 0 & 0 & 0 & 0 & 0 & 0 & 0 & 0 & 1 \\
0 & 0 & 0 & 0 & 0 & 0 & 0 & 0 & 0 & 0 & 0 & 0 & 0 & 0 & 1 & 0 \\
0 & 0 & 0 & 0 & 0 & 0 & 0 & 0 & 0 & 0 & 0 & 0 & 0 & 1 & 0 & 0 \\
0 & 0 & 0 & 0 & 0 & 0 & 0 & 0 & 0 & 0 & 0 & 0 & 1 & 0 & 0 & 0
\end{array}\right]
$$

$$
=\; \left[\begin{array}{c|c|c|c}
\hat{R} & 0 & 0 & 0 \\
\hline
0 & \hat{R} & 0 & 0 \\
\hline
0 & 0 & \hat{R} & 0 \\
\hline
0 & 0 & 0 & \hat{R}
\end{array}\right] , \tag{20.21}
$$

where $\hat{R}$ is the reflection operator in the 4-dimensional space of the shorter

lattice state. Using the projection operator of this reflection matrix R:

$$P_{R^+} = \frac{1}{2} \left[\begin{array}{cccc|cccc|cccc|cccc} 1 & 0 & 0 & 1 & 0 & 0 & 0 & 0 & 0 & 0 & 0 & 0 & 0 & 0 & 0 & 0 \\ 0 & 1 & 1 & 0 & 0 & 0 & 0 & 0 & 0 & 0 & 0 & 0 & 0 & 0 & 0 & 0 \\ 0 & 1 & 1 & 0 & 0 & 0 & 0 & 0 & 0 & 0 & 0 & 0 & 0 & 0 & 0 & 0 \\ 1 & 0 & 0 & 1 & 0 & 0 & 0 & 0 & 0 & 0 & 0 & 0 & 0 & 0 & 0 & 0 \\ \hline 0 & 0 & 0 & 0 & 1 & 0 & 0 & 1 & 0 & 0 & 0 & 0 & 0 & 0 & 0 & 0 \\ 0 & 0 & 0 & 0 & 0 & 1 & 1 & 0 & 0 & 0 & 0 & 0 & 0 & 0 & 0 & 0 \\ 0 & 0 & 0 & 0 & 0 & 1 & 1 & 0 & 0 & 0 & 0 & 0 & 0 & 0 & 0 & 0 \\ 0 & 0 & 0 & 0 & 1 & 0 & 0 & 1 & 0 & 0 & 0 & 0 & 0 & 0 & 0 & 0 \\ \hline 0 & 0 & 0 & 0 & 0 & 0 & 0 & 0 & 1 & 0 & 0 & 1 & 0 & 0 & 0 & 0 \\ 0 & 0 & 0 & 0 & 0 & 0 & 0 & 0 & 0 & 1 & 1 & 0 & 0 & 0 & 0 & 0 \\ 0 & 0 & 0 & 0 & 0 & 0 & 0 & 0 & 0 & 1 & 1 & 0 & 0 & 0 & 0 & 0 \\ 0 & 0 & 0 & 0 & 0 & 0 & 0 & 0 & 1 & 0 & 0 & 1 & 0 & 0 & 0 & 0 \\ \hline 0 & 0 & 0 & 0 & 0 & 0 & 0 & 0 & 0 & 0 & 0 & 0 & 1 & 0 & 0 & 1 \\ 0 & 0 & 0 & 0 & 0 & 0 & 0 & 0 & 0 & 0 & 0 & 0 & 0 & 1 & 1 & 0 \\ 0 & 0 & 0 & 0 & 0 & 0 & 0 & 0 & 0 & 0 & 0 & 0 & 0 & 1 & 1 & 0 \\ 0 & 0 & 0 & 0 & 0 & 0 & 0 & 0 & 0 & 0 & 0 & 0 & 1 & 0 & 0 & 1 \end{array} \right]$$

$$= \left[\begin{array}{c|c|c|c} P_{\hat{R}^+} & 0 & 0 & 0 \\ \hline 0 & P_{\hat{R}^+} & 0 & 0 \\ \hline 0 & 0 & P_{\hat{R}^+} & 0 \\ \hline 0 & 0 & 0 & P_{\hat{R}^+} \end{array} \right] \tag{20.22}$$

the orbit Jacobian matrix is projected into the symmetric subspace and it still has the tri-diagonal form:

$$\mathcal{J} P_{R^+} = \left[\begin{array}{c|c|c|c} \mathbf{s}_p P_{\hat{R}^+} & -\mathbf{d} P_{\hat{R}^+} & 0 & -\mathbf{d}^\top P_{\hat{R}^+} \\ \hline -\mathbf{d}^\top P_{\hat{R}^+} & \mathbf{s}_p P_{\hat{R}^+} & -\mathbf{d} P_{\hat{R}^+} & 0 \\ \hline 0 & -\mathbf{d}^\top P_{\hat{R}^+} & \mathbf{s}_p P_{\hat{R}^+} & -\mathbf{d} P_{\hat{R}^+} \\ \hline -\mathbf{d} P_{\hat{R}^+} & 0 & -\mathbf{d}^\top P_{\hat{R}^+} & \mathbf{s}_p P_{\hat{R}^+} \end{array} \right] . \tag{20.23}$$

20.2.2 Repeats blog

2016-09-28 Predrag Amritkar *et al.* [1, 18] have investigated the stability of spatiotemporally periodic orbits in one- and two-dimensional coupled map lattices, i.e., $1+1$ and $1+2$ spatiotemporal dimensions. They derive conditions for the stability of periodic solutions in terms of the criteria for smaller orbits.

2020-06-01 Predrag Gade and Amritkar [18] *Spatially periodic orbits in coupled-map lattices* (a preliminary version of a part of this work was published as Amritkar, Gade, Gangal and Nandkumaran [1] *Stability of periodic orbits of coupled-map lattices*):

They are interested in stability, rather than our focus on instability.

They take CMLs with periodic orbits over $[L \times T]_0$ and study the stability of their periodic orbit 'replicas' $[kL \times T]_0$ obtained by repeating $[L \times T]_0$ k

times in the spatial direction, and show that orbit Jacobian matrix eigen-values of the replica follow from the small periodic orbit. Not obvious, as the replica periodic orbit has more directions to be stable/unstable in. The trick is observing that the replica orbit Jacobian matrix is a block circulant with circulant blocks. The stability matrices for such lattice states are block circulant and hence can be brought onto a block diagonal form through a unitary transformation, their eq. (19).

The textbook they use is Davis [10] *Circulant Matrices*.

They write:

We call $X_{||,r}$ the r replica solution of $X_{||,1}$. We address the problem of what can be stated about the stability properties of such spatially and temporally periodic solutions $X_{||,r}$, from the analysis of the stability matrices for $X_{||,1}$ of the building blocks [1]. In other words the question is, What is the effect of enlargement of phase space and the couplings on the stability of the replica solutions?

(Their eq. (16) is our (**??**). Note their block-circulant matrix eq. (18))

The trick is observing that the replica orbit Jacobian matrix is a block circulant with circulant blocks. The stability matrices for such lattice states are block circulant and hence can be brought onto a block diagonal form through a unitary transformation, their eq. (19). The unitary matrix which affects the block diagonalization is a direct product of Fourier matrices of sizes $[r \times r]$ and $[|| \times ||]$.

(2022-01-12 Predrag: but block matrix $\mathbf{s}_p$ in (**??**) is not circulant?)

The effects on the stability due to the enlargement of the state space and couplings manifest themselves through the eigenvalues of the additional blocks.

Our analysis leads to the following important conclusion about unstable periodic orbits. The matrix $\mathbf{s}_p$ appears as a block of the matrix $\mathcal{J}$. Hence, a solution built out of the replicas of unstable periodic orbits will also be unstable. Enlargement of state space and the effect of couplings cannot stabilize an unstable replica solution. The unstable periodic orbits are dense on the chaotic attractor. They are supposed to form the backbone of the dynamics on the attractor.

Our formalism will be useful if one tries to use unstable periodic orbits to analyze the spatially extended systems. It is clear that the replica solutions can be used to construct a hierarchy of unstable periodic orbits based on the orbits for building blocks. This may help in the organization of spatio-temporal chaos on the lines of arguments in ref. [6].

We have also discussed the two-dimensional extension of our formalism. From the convenient form in which the equations can be set, it is obvious that the generalization to higher dimensions is also possible. If one tries to analyze the problems similar to the ones analyzed here, in oscillator arrays this procedure can be easily used to simplify the computation.

Cited Gade and Amritkar [18] in LC21 as an early investigation of a lattice orbit Jacobian matrix. They did not know about 'Hill's formula.

2016-11-11 Predrag Bountis and Helleman [2] On the stability of periodic orbits of two-dimensional mappings: " We apply our criterion and derive a sufficient stability condition for a large class of periodic orbits of the widely studied "standard mapping" describing a periodically 'kicked' free rotator. "

I find this paper quite interesting, because the computation of Floquet multipliers, i.e., linearization of periodically 'kicked' free rotor, is full of matrices that look like Laplacians + a diagonal term which varies along the periodic orbit. For cat maps this term is constant, essentially the stretching factor s. This might help with interpreting coupled 'kicked' rotor lattices.

This is presumably related to the block circulant stability matrices [1, 18] for spatially and temporally periodic orbits in coupled map lattices.

2016-09-28 Predrag Zhilin*et al.* [33] *Spatiotemporally periodic patterns in symmetrically coupled map lattices* write: " The stability of the deduced orbits is investigated and we can reduce the problem to analyze much smaller matrices corresponding to the building block of their spatial periodicity or to the building block of the spatial periodicity of the original orbits from which we construct the new orbits. In the two-dimensional case the problem is considerably simplified. "

2019-02-04 Predrag A relative periodic block $\hat{p}$ is always preperiodic to a periodic block whose period $T_p = rT_{\hat{p}}$, so you can always Fourier-transform this larger torus. But the right way of doing is acting relative periodic block $\hat{p}$ with the translation d^r that makes it periodic, and then Fourier-transforming the minimal d-torus.

In this case we are still solving (**??**) except the rank $2d$ tensor is no longer a circulant tensor.

2019-02-04 Predrag The orbit Jacobian matrix times the translation d^r is circulant, I believe. That is how we compute the Jacobian matrices of relative periodic orbits in ChaosBook. But we can still solve for the eigenvectors. I have shown how to compute the eigenvectors and eigenvalues in (**??**–**??**) and verified this is correct for small blocks. In (**??**–**??**) I proved this is correct in any dimension. Using these eigenvectors we can diagonalize the orbit Jacobian matrix and get the inverse (Green's function). The only problem is even though the counting formula is very compact, it seems to me that now it is hard to simplify the topological zeta function.

2019-02-04 Predrag I doubt it. In ChaosBook we show that after symmetry reduction, counting relative periodic orbits is not any harder than counting periodic orbits.

2021-05-04 Predrag Can one write the orbit Jacobian matrix of a repeat of a p-cycle as a product of p-cycle orbit Jacobian matrices?

(**2021-06-14 Predrag** This is now accomplished by the block matrix formulation (20.23).)

$$
\mathcal{J}_p^{(2)} \mathcal{J}_p^{(1)} \;=\;
\begin{bmatrix}
1 & 0 & 0 & 0 & 0 & 0 \\
0 & 1 & 0 & 0 & 0 & 0 \\
0 & 0 & 1 & 0 & 0 & 0 \\
0 & 0 & 0 & \phi_0 & 1 & 1 \\
0 & 0 & 0 & 1 & \phi_1 & 1 \\
0 & 0 & 0 & 1 & 1 & \phi_2
\end{bmatrix}
\begin{bmatrix}
\phi_0 & 1 & 1 & 0 & 0 & 0 \\
1 & \phi_1 & 1 & 0 & 0 & 0 \\
1 & 1 & \phi_2 & 0 & 0 & 0 \\
0 & 0 & 0 & 1 & 0 & 0 \\
0 & 0 & 0 & 0 & 1 & 0 \\
0 & 0 & 0 & 0 & 0 & 1
\end{bmatrix}
$$

$$
\neq\;
\begin{bmatrix}
\phi_0 & 1 & 0 & 0 & 0 & 1 \\
1 & \phi_1 & 1 & 0 & 0 & 0 \\
0 & 1 & \phi_2 & 1 & 0 & 0 \\
0 & 0 & 1 & \phi_0 & 1 & 0 \\
0 & 0 & 0 & 1 & \phi_1 & 1 \\
1 & 0 & 0 & 0 & 1 & \phi_2
\end{bmatrix},
\tag{20.24}
$$

Another try:

$$
\mathcal{J}_p^{(2)} \mathcal{J}_p^{(1)} \;=\;
\begin{bmatrix}
1 & 0 & 0 & 0 & 0 & 1 \\
0 & 1 & 0 & 0 & 0 & 0 \\
0 & 0 & 1 & 1 & 0 & 0 \\
0 & 0 & 1 & \phi_0 & 1 & 0 \\
0 & 0 & 0 & 1 & \phi_1 & 1 \\
1 & 0 & 0 & 0 & 1 & \phi_2
\end{bmatrix}
\begin{bmatrix}
\phi_0 & 1 & 0 & 0 & 0 & 1 \\
1 & \phi_1 & 1 & 0 & 0 & 0 \\
0 & 1 & \phi_2 & 1 & 0 & 0 \\
0 & 0 & 1 & 1 & 0 & 0 \\
0 & 0 & 0 & 0 & 1 & 0 \\
1 & 0 & 0 & 0 & 0 & 1
\end{bmatrix}
$$

$$
\neq\;
\begin{bmatrix}
\phi_0 + 1 & 1 & 0 & 0 & 0 & 2 \\
1 & \phi_1 & 1 & 0 & 0 & 0 \\
0 & 1 & \phi_2 + 1 & 2 & 0 & 0 \\
0 & 0 & 1 & \phi_0 + 1 & 1 & 0 \\
0 & 0 & 0 & 1 & \phi_1 & 1 \\
\phi_0 + \phi_2 & 0 & 0 & 0 & 1 & \phi_2 + 1
\end{bmatrix},
\tag{20.25}
$$

(partly wrong, but does not matter), so orbit Jacobian matrices do not multiply.

But they do not add up, either, cannot reconcile the small block periodic bc's with the repeated block bc's. Defeated again.

2021-08-22 Predrag I believe was wrong in asking that we look at the stability of repeats of a shorter period block, eq. (**??**) above. That does not arise in the new formulation of periodic orbit theory; the Hill determinant is computed on any lattice state X in the orbit $\mathcal{M}_c$ of a lattice state X_c. There are only orbits, nothing is computed on repeats. There should be no repeats summation in the derivation of zeta functions.

2022-01-22 Predrag believes today that he was very wrong on **2021-08-22** :)

Example 20.1. ***Temporal lattice stability of a 3-cycle.*** *For for a 1-dimensional map* f*, orbit Jacobian matrix is an [$|p| \times |p|$] matrix:*

$$
\mathcal{J}(x) \;=\; \begin{pmatrix}
1 & & & & & -f'_{|p|} \\
-f'_1 & 1 & & & & \\
& \cdots & 1 & & & \\
& & \cdots & & 1 & \\
& & & & 1 & \\
& & & & -f'_{|p|-1} & 1
\end{pmatrix}. \tag{20.26}
$$

Let us invert a 3-cycle orbit Jacobian matrix $\mathcal{J}(x)$ *for such 1-dimensional map by hand, step by step. According to (20.6), the initial small* Δx *deviations from the periodic orbit (20.3) are mapped into deviations* $\Delta x'$ *a time step later by*

$$
\begin{pmatrix} \Delta x'_1 \\ \Delta x'_2 \\ \Delta x'_3 \end{pmatrix} = \begin{pmatrix} 1 & 0 & -f'_3 \\ -f'_1 & 1 & 0 \\ 0 & -f'_2 & 1 \end{pmatrix} \begin{pmatrix} \Delta x_1 \\ \Delta x_2 \\ \Delta x_3 \end{pmatrix},
$$

where the d*-dimensional vectyor* $\Delta x_i = \hat{x}_i - x_i$ *is the error at* i*th periodic point. In terms of the shift matrix* σ*, the one-time step cycle Jacobian matrix (20.26) can be written as*

$$
\mathcal{J} = \mathbf{1} - \sigma f', \quad \sigma = \begin{pmatrix} 0 & 0 & 1 \\ 1 & 0 & 0 \\ 0 & 1 & 0 \end{pmatrix}, \quad f' = \begin{pmatrix} f'_1 & 0 & 0 \\ 0 & f'_2 & 0 \\ 0 & 0 & f'_3 \end{pmatrix}. \tag{20.27}
$$

Suppose all $|f'_k| > 1$*, so forward in time the errors are growing. We can make errors contract by going backwards in time, i.e., evaluating the inverse matrix* $\mathcal{J}$*, and noting that every 3rd power* $(\sigma f')^3 = J_p \mathbf{1}$ *is diagonal,*

$$
\frac{1}{\mathbf{1} - \sigma f'} \;=\; \sum_{j=0}^{\infty} (\sigma f')^j = \sum_{k=0}^{\infty} J_p^k \sum_{\ell=0}^{2} (\sigma f')^\ell = \frac{1}{1 - J_p} \left[\mathbf{1} + \sigma f' + (\sigma f')^2 \right] \tag{20.28}
$$

$$
\;=\; \frac{1}{1-J} \left[\mathbf{1} + \sigma \begin{pmatrix} f'_1 & 0 & 0 \\ 0 & f'_2 & 0 \\ 0 & 0 & f'_3 \end{pmatrix} + \sigma^2 \begin{pmatrix} f'_2 f'_1 & 0 & 0 \\ 0 & f'_3 f'_2 & 0 \\ 0 & 0 & f'_1 f'_3 \end{pmatrix} \right],
$$

where $J_p = f'_3 f'_2 f'_1$ *is the forward-in-time stability of the cycle* p*, so*

$$
\begin{pmatrix} \Delta x_1 \\ \Delta x_2 \\ \Delta x_3 \end{pmatrix} = \frac{1}{1 - J_p} \begin{pmatrix} \Delta x'_1 + f'_3 \Delta x'_3 + f'_3 f'_2 \Delta x'_2 \\ \Delta x'_2 + f'_1 \Delta x'_1 + f'_1 f'_3 \Delta x'_3 \\ \Delta x'_3 + f'_2 \Delta x'_2 + f'_2 f'_1 \Delta x'_1 \end{pmatrix}.
$$

For an unstable cycle, the error gets contracted by overall factor $1/(1 - J)$*, with the earlier errors amplified by the orbit instability; for example,* Δx_3 *receives a contribution from two time steps in the past of form* $f'_2 f'_1 \Delta x'_1$*.*

By explicit evaluation, for 1-dimensional maps [3] $\mathcal{J}(x)^3 = (1 - J_p)\mathbf{1} + (...)$ *and*

$$
\mathrm{Det}\, \mathcal{J}_p = \det(1 - J_p) \tag{20.29}
$$

for the d*-dimensional case.* $\mathcal{J}(x)$ *is a cycle rotation by one time step; for a 3-cycle we are back, times a constant, uniform factor multiplying all errors by the rotation invariant scalar quantity* $\det(1 - J_p)$*, whose inverse happens to be the cycle-expansions' size of the neighborhood of cycle* p*.*
[4]

---

[3] Predrag 2019-10-10: Still have to derive this formula, probably by $\ln \det = \mathrm{tr}\, \ln$ relation
[4] Predrag 2019-09-28: I have inverted this Newton Jacobian matrix often, see for example

Example 20.2. ***Temporal lattice stability of a 3-cycle.***

Consider an period-|| lattice state X_p, with d fields $\{x_{t,1}, x_{t,2}, \ldots, x_{t,d}\}$ on each lattice site t satisfying the condition

$$x_t - f(x_{t-1}) = 0, \quad t = 1, 2, \cdots, ||, \tag{20.30}$$

where d-dimensional time evolution function. A deviation $\Delta\mathsf{X}$ from X_p must satisfy the linearized condition

$$\Delta x_t - \mathbb{J}_{t-1}\, \Delta x_{t-1} = 0, \qquad (\mathbb{J}_t)_{ij} = \left.\frac{\partial f(x)_i}{\partial x_j}\right|_{x_i = x_{t,i}}, \tag{20.31}$$

where $\mathbb{J}_t$ is the 1-time step $[d \times d]$ time-evolution Jacobian matrix. Let $\mathbb{1}_d$ be a d-dimensional identity matrix. For an period-|| lattice state X_p, the orbit Jacobian matrix $\mathcal{J}_p\,\Delta\mathsf{X} = 0$ is an $[||d \times ||d]$ matrix

$$\mathcal{J}_p \;=\; \mathbb{1} - d^{-1}\mathbb{J} = \begin{pmatrix} \mathbb{1}_d & & & & -\mathbb{J}_{||} \\ -\mathbb{J}_1 & \mathbb{1}_d & & & \\ & -\mathbb{J}_2 & \ddots & & \\ & & & \mathbb{1}_d & \\ & & & -\mathbb{J}_{||-1} & \mathbb{1}_d \end{pmatrix}, \tag{20.32}$$

where the $[||d \times ||d]$ matrix

$$d = \begin{pmatrix} 0 & \mathbb{1}_d & & & \\ & 0 & \mathbb{1}_d & & \\ & & & \ddots & \\ & & & 0 & \mathbb{1}_d \\ \mathbb{1}_d & & & & 0 \end{pmatrix}, \tag{20.33}$$

implements the shift operation, a cyclic permutation that translates forward in time the lattice state X_p by one site, $(d\mathsf{X})^\top = (x_2, x_3, \cdots, x_{||}, x_1)$.

To evaluate the Hill determinant (??), note that $d^{||} = \mathbb{1}$, that $\mathrm{Tr}\,(d^{-1}\mathbb{J})^k = ||\delta_{k,r||}\mathrm{tr}\,\mathbb{J}_p^r$ is non-vanishing only if k is a multiple of $||$, and expand

$$\begin{aligned} \ln\mathrm{Det}\,(\mathcal{J}_p) &= \mathrm{Tr}\,\ln(\mathbb{1} - d^{-1}\mathbb{J}) = -\sum_{k=1}^{\infty}\frac{1}{k}\,\mathrm{Tr}\,((d^{-1}\mathbb{J})^k) \\ &= -\mathrm{tr}\sum_{r=1}^{\infty}\frac{1}{r}\mathbb{J}_p^r = \ln\det(\mathbb{1}_d - \mathbb{J}_p). \end{aligned} \tag{20.34}$$

So, the Hill determinant for any hyperbolic 2-term difference equation on a temporal lattice is

$$\mathrm{Det}\,(\mathcal{J}_p) = \det(\mathbb{1}_d - \mathbb{J}_p).$$

---

eq. (16) and onward in Cvitanović, Dettmann, Mainieri and Vattay [7], click here. I have also introduced the notation for finite-time (shorter than the period) Jacobian matrices, see for example eq. (69) in Cvitanović and Lippolis [9], click here. But I have never done it the way I should have, by a discrete Fourier transform, into sum of irreps of C_n (AKA Fourier modes) and using characters for discrete Fourier transforms.

In the temporal Bernoulli case, the field x_t is a scalar, and the 1-time step $[d \times d]$ time-evolution Jacobian matrix (20.31) at any time is simply $\mathbb{J}_t = s$, so

$$N_{||} = |\text{Det } \mathcal{J}| = s^{||} - 1 \,, \tag{20.35}$$

in agreement with the time-evolution count.

In terms of the shift matrix d, the one-time step cycle Jacobian matrix (20.26) can be written as

$$\mathcal{J}_p = \mathbf{1} - d^{-1}\mathbb{J} \,, \quad d = \begin{pmatrix} 0 & 0 & \mathbf{1}_d \\ \mathbf{1}_d & 0 & 0 \\ 0 & \mathbf{1}_d & 0 \end{pmatrix}, \quad \mathbb{J} = \begin{pmatrix} \mathbb{J}_1 & 0 & 0 \\ 0 & \mathbb{J}_2 & 0 \\ 0 & 0 & \mathbb{J}_3 \end{pmatrix}. \tag{20.36}$$

Suppose all $\mathbb{J}_p \neq 1$. Note that every $||$th power $(d\mathbb{J})^3 = \mathbb{J}_p\mathbb{J}$ is diagonal,

$$\frac{1}{\mathbf{1} - d\mathbb{J}} = \sum_{j=0}^{\infty}(d\mathbb{J})^j = \sum_{k=0}^{\infty}\mathbb{J}_p^k \sum_{\ell=0}^{2}(d\mathbb{J})^\ell = \frac{1}{1 - \mathbb{J}_p}\left[\mathbb{J} + d\mathbb{J} + (d\mathbb{J})^2\right] \tag{20.37}$$

$$= \frac{\mathbf{1}}{\mathbf{1} - \mathbb{J}}\left[\mathbb{J} + d\begin{pmatrix} \mathbb{J}_1 & 0 & 0 \\ 0 & \mathbb{J}_2 & 0 \\ 0 & 0 & \mathbb{J}_3 \end{pmatrix} + d^2\begin{pmatrix} \mathbb{J}_2\mathbb{J}_1 & 0 & 0 \\ 0 & \mathbb{J}_3\mathbb{J}_2 & 0 \\ 0 & 0 & \mathbb{J}_1\mathbb{J}_3 \end{pmatrix}\right],$$

where $\mathbb{J}_p = \mathbb{J}_3\mathbb{J}_2\mathbb{J}_1$ is the forward-in-time stability of the cycle p.

To summarize, a discretized, temporal lattice periodic orbit linear stability can be computed in two ways - either by computing the $[|p|d \times |p|d]$ Jacobian matrix $\mathcal{J}(x)$, or by computing $\mathbb{J}_p$

$$|\text{Det}\, \mathcal{J}_p| = |\det\,(1 - \mathbb{J}_p)|\,, \tag{20.38}$$

where $\mathbb{J}_p$ is the $|p|$ time-steps $[d \times d]$ forward-time Jacobian matrix. In the limit of discretization $|p| \to \infty$ the left hand side is a *functional* determinant of an ∞-dimensional *operator*. Nevertheless, thanks to the discrete Fourier diagonalization of $\mathcal{J}(x)$, appendix **??**, the determinant $\text{Det}\, \mathcal{J}_p$ is easier to compute than the ill-posed $\mathbb{J}_p$. [5] [6]

The projection operator on the kth Fourier mode is

$$P_k = \prod_{j \neq k} \frac{d - \omega_j\, \mathbb{1}}{\omega_k - \omega_j}\,. \tag{20.39}$$

The set of the projection operators is complete,

$$\sum_k P_k = \mathbb{1}, \tag{20.40}$$

and orthonormal

$$P_k P_j = \delta_{kj} P_k \qquad (\text{no sum on } k)\,. \tag{20.41}$$

[TO BE CONTINUED]

20.3 Spatiotemporal lattice

In spatiotemporal settings, $\mathbb{J}_p$ can be defined only for finite numbers of spatial sites, and it gets funkier and funkier as the spatial direction increases (that is why we are able to work only with very small spatial domain Kuramoto-Sivashinsky discretizations). But, as shown for the spatiotemporal cat in ref. [8], $\text{Det}\, \mathcal{J}_p$ works just fine on any spatiotemporal torus. In particular, for any invariant 2-torus Kuramoto-Sivashinsky discretization.

20.4 Noether's theorem

2018-05-04 Predrag Moved this section to spacetime continuous systems `spatiotemp/blog.tex`

---

[5]Predrag 2019-10-10: $\mathcal{J}(x)$ is block-diagonalized by the discrete Fourier transform on a periodic lattice of three sites. Write up next the discrete Fourier evaluation of $\text{Det}\, \mathcal{J}_p$.

[6]Predrag 2019-10-10: Rewrite the derivation of the Hill-Poincaré-Van Vleck stability matrix (**??**) for symplectic / Lagrangian Hessians (orbit Jacobian matrix) using the shift matrix (20.27).

20.5 Stability blog

2019-10-10 Predrag Reread Lindstedt-Poincaré [28] Fourier method papers by Viswanath [29, 30]; his most accurate resolution of fractal structure of the Lorenz attractor. It is a very thin fractal, stable manifold thickness is of the order 10^{-4}. He has computed all 111011 periodic orbits corresponding to symbol sequences of length 20 or less, all with 14 digits accuracy.

2019-10-13 Predrag Viswanath [28] writes: " The Lindstedt-Poincaré technique uses a nearby periodic orbit of the unperturbed differential equation as the first approximation to a perturbed differential equation. One of the examples presents what is possibly the most accurate computation of Hill's orbit of lunation since its justly celebrated discovery in 1878.

The eigenvalues excluding 1 are called characteristic multipliers.

AUTO [13, 14] collocation method, Guckenheimer and Meloon [21], Choe and Guckenheimer [5] all set up their periodic orbits as in (20.4). Since the linear systems that they form are sparse, the cost of solution is only linear in the number of mesh points.

There are other variants of this forward multiple shooting algorithm: one is a symmetric multiple shooting algorithm and another is based on Hermite interpolation.

He dismisses harmonic balance methods for computing periodic orbits (Lau, Cheung and Wu [?15], and Ling and Wu [?16]) as being too expensive, of order $O(n^3)$, where the Fourier series are of width n, whereas his method is of order $O(n \ln n)$.

Wisvanath algorithm for computing periodic orbits is a "polyphony of three themes:" the Lindstedt-Poincaré technique from perturbation theory, Newton's method for solving nonlinear systems, and Fourier interpolation.

To compute n Fourier coefficients of $x(t)$, the fast Fourier transform (FFT) is applied to the function evaluated at n equispaced points in $[0, 2\pi)$. The width n of the Fourier series must be sufficiently large to pick up all the coefficients above a desired accuracy threshold.

If $(x_1, x_2, \cdots, x_m)$ are 2π periodic, so is $f(x_1, x_2, \cdots, x_m)$. To obtain its Fourier series from those of the x_i, interpolate x_i at equispaced points, evaluate f at those points, and apply the FFT. The inverse FFT can be used to interpolate a Fourier series at equispaced points [27]. In d state space dimensions, one needs d Fourier series, one for each coordinate in $\mathbb{R}^d$.

His 4 coupled Josephson junctions (10-dimensionalstate space) uses 64 Fourier modes.
"

The implementation of the algorithm must pay attention to the possibility of aliasing.

2019-10-13 Predrag Viswanath [29] writes: " The representation of periodic orbits by Fourier series is both accurate and efficient because, when a periodic orbit is analytic, the Fourier coefficients decrease exponentially fast, making its Fourier representation compact.
"

2019-10-13 Predrag Guckenheimer and Meloon [21] set up their periodic orbits as in (20.4), and have the same d-dimensional orbit Jacobian matrix variant of (20.26), but with extra, time-direction fixing diagonals, as they are looking at continuous time flows. Instead of the cyclic group, they use LU factorization. They get $1 - J_p$ matrix.

2019-10-14 Predrag Notes on Choe and Guckenheimer [5], a clear and enjoyable read:

Instead of relaying on forward-in-time numerical integration, *global methods* for finding periodic orbits view the vector field as an equation on a function space of closed curves. Here f is a Lipschitz continuous vector field on a smooth manifold $\mathcal{M}$, and $p : S^1 \to \mathcal{M}$ is a C^1 closed curve in $\mathcal{M}$.

Computer implementation of global methods for computing periodic orbits requires discretization of closed curves and approximation of the periodic orbit equations. One defines finite-dimensional submanifolds of the space of closed curves and approximates the periodic orbit equations as a map defined on this space.

They keep the number of discretization points fixed and increase the accuracy by *automatic differentiation*, constructing the Taylor series of trajectories at discretization points. They also compute stability matrix derivatives of the Taylor series coefficients with respect to the state space variables for use in the Newton iteration. As the degree of the computed Taylor series increases, their curves converge since the trajectories are analytic.

The Taylor series is obtained by repeated differentiation of the differential equation $\dot{x} = v(x)$ and recursive substitution of the values of derivatives $x^{(k)}(t)$ of increasing degree. To make the approximate curve smooth and continuous, they use a somewhat funky interpolation function they call $\beta(t)$.

[Predrag's aside: hopefully our strategy of using Fourier transforms has much faster convergence than Taylor series. Even if one wants polynomials, I suspect Chebyshev or Hermite or some other orthogonal sets would be better.]

Indeed, the Hermite splines, interpolating functions that arc polynomials of degree $2d + 1$, gave the best results in their computations.

They eliminate the time translation marginal eigenvalue by using sets of Poincaré section hyperplanes transverse to the vector field, and solving

for points that lie on the intersection of Poincaré section with the periodic orbit. They use the orthogonal complements to the vector field $v(x_i)$ at the mesh points x_i. The normal subspace to the vector field at x_i, is determined by computing the QR factorization of the $[d \times (d + 1)]$ matrix. There is a whole PhD thesis worth of detail here.

The structure of the Jacobian matrices that are used in the root finding has a simple sparsity pattern that can be exploited in its inversion. Explicit inversion of this block matrix in terms of the inverses of the individual blocks yields a relationship between the regularity of the root finding problem and the hyperbolicity of the periodic orbit. They relate the regularity of orbit Jacobian matrix $\mathcal{J}$ to the periodic orbit's monodromy matrix, their sect. 3. *Analysis*, using LU factorization. They show that $\mathcal{J}$ is invertible (needed for Newton schemes) if and only if the monodromy matrix M of the Poincaré section does not have 1 as an eigenvalue.

Since their methods produce smooth approximations to periodic orbits, they can evaluate the distance between the tangent vectors to a computed curve and the vector field along that curve. These error estimates enable them to develop strategies for mesh refinement that balance the error in different mesh intervals. Since the approximating solution in a mesh interval is determined entirely by its endpoints, mesh refinement is a simple process and does not change the structure of the discretized periodic orbit equations.

They define the error field (20.4) as operator $F(p) = f(p) - \sigma p$, with periodic orbits solutions satisfying $F = 0$. p are analytic curves, but Choe-Guckenheimer approximations are not analytic.

The starting data is an N-point *discrete closed curve* (20.3), a cyclically ordered collection of N points. Given a map S, on seeks seek systems of $(|p| \times d)$-dimensional vector field equations $F_S = 0$ whose solutions yield good approximations to periodic orbits of f. The convergence is takes place on a fixed mesh, but with increasing degree d of map S_d. They compute the orbit Jacobian matrix $\mathcal{J}$ and invert it to use in the Newton routine, but do not mention or discus computing $\det \mathcal{J}$.

They test their algorithm with the Hodgkin-Huxley equations, a moderately stiff 4-dimensional vector field with strongly stable directions. They do not boast, but their residual errors are of order 10^{-11}.

2022-05-06 Predrag Check out Wolfram Demonstrations Project *Learning Newton's Method*.

2022-05-06 Predrag Check out Kevin Zeng, Alec J. Linot and Michael D. Graham *Data-driven control of spatiotemporal chaos with reduced-order neural ODE-based models and reinforcement learning* arXiv:2205.00579: We combine data-driven nonlinear manifold dynamics with deep RL to control spatiotemporal chaos in the Kuramoto-Sivashinsky equation. The approach discovers and stabilizes a low-dissipation steady state!

Linot and Graham [25] *Data-driven reduced-order modeling of spatiotemporal chaos with neural ordinary differential equations*, (2022)

Also: M. A. Bucci, O. Semeraro, A. Allauzen, G. Wisniewski, L. Cordier, and L. Mathelin. *Control of chaotic systems by deep reinforcement learning*, Proceedings of the Royal Society A, 475(2231):20190351, 2019 DOI.

2022-07-11 Predrag Study these 2 papers which compute and discuss Hessian spectra:

Le Cun, Kanter and Solla [23] *Second order properties of error surfaces: Learning time and generalization* (1990), (click here).

Le Cun, Kanter and Solla [24] *Eigenvalues of covariance matrices: Application to neural-network learning* (1991).

The dynamical behavior of learning algorithms based on the minimization of the learning error function $E(W)$ through gradient descent is controlled by the second-order properties of $E(W)$, as represented by its Hessian matrix H. The cost function is quadratic in W, and can be rewritten in terms of a symmetric non-negative covariance matrix (or Hessian) of the inputs.

The diagonalization of R provides a diagonal matrix A formed by its eigenvalues and a matrix Q formed by its e—igenvectors.

20.6 Generating function literature

For the latest entry, go to the bottom of this section

2016-11-11 Predrag I still cannot get over how elegant the Gutkin-Osipov [22] spatiotemporal cat is. It is *linear*! (mod 1, that is - the map is continuous for integer s). A 1-dimensional cat map has a Hamiltonian (**??**), and they have written down the 2-dimensional Lagrangian, their Eq. (3.1) (or the "generating function", as this is a mapping). Their spatiotemporal cat generating function is defined on a spatiotemporal cylinder, infinite in time direction,

$$
\begin{aligned}
S(q_t, q_{t+1}) &= -\sum_{n=1}^{N} q_{nt} q_{1+n,t} - \sum_{n=1}^{N} q_{nt}(q_{n,t+1} + m_{n,t+1}^q) + \frac{a}{2}\sum_{n=1}^{N} q_{nt}^2 \\
&\quad + \frac{b}{2}\sum_{n=1}^{N}(q_{n,t+1} + m_{n,t+1}^q)^2 - m_{n,t+1}^p q_{n,t+1}\,, \qquad (20.42)
\end{aligned}
$$

where $q_t = \{q_{nt}\}_{n=1}^{N}$ is a spatially periodic state at time t, with q_{nt} being the coordinate of nth "particle" $n = 1 \ldots N$ at the moment of time $t \in \mathbb{Z}$, and $m_{n,t+1}^q, m_{n,t+1}^p$ are integer numbers which stand for winding numbers along the q and p directions of the 2N-torus. Note that $x_{1+n,t} = x_{1+(n\bmod N),t}$. The coefficients a, b, $s = a + b$ are integers which they specify. Gutkin and Osipov refer to the map generated by the action (20.42) as non-perturbed *coupled cat map*, and to an invariant 2-torus p as a "many-particle periodic orbit" (MPO) if q_{nt} is doubly-periodic, or "closed," i.e.,

$$
q_{nt} = q_{n+L,t+T}\,, \quad n = 1,2,\cdots,L\,, \quad t = 1,2,\cdots,T\,.
$$

2D symbolic representation Encode each invariant 2-torus (many-particle periodic orbit) p by a two dimensional (periodic) lattice of symbols a_{nt}, $(nt) \in \mathbb{Z}^2$, where symbols a_{nt} belong to some alphabet $\mathcal{A}$ of a small size. Each invariant 2-torus p is represented by $L \times T$ toroidal array of symbols:

$$
\bar{\mathcal{A}}_p = \{a_{nt} | (nt) \in \mathbb{Z}_{LT}^2\}\,.
$$

The Hamiltonian equations of motion can be generated using (**??**) but who needs them? Remember, a field theorist would formulate a space-time symmetric field theory in a Lagrangian way, with the invariant action.

2016-11-11 Predrag Percival and Vivaldi [26] state the Lagrangian variational principle in Sect. 6. *Codes, variational principle and the static model:* [7]

---

[7]Predrag 2016-11-12: eventually move to remark **??**

The Lagrangian variational principle for the sawtooth map on the real line states that the action sum (**??**) is stationary with respect to variations of any finite set of configurations x_t. Their discussion of how "elasticity" works against the "potential" is worth reading. For large values of stretching parameter s, the potential wins out, and the state x_t falls into the m_tth well: "the code may be considered as a labelling of the local minima of the Lagrangian variational principle."

Dullin and Meiss [15] *Stability of minimal periodic orbits* does the calculations in great detail.

2016-11-11 Predrag "mean action" = the action divided by the period

2018-12-07 Predrag as shown in (copied here from ChaosBook) example **??**, example **??**, and example **??** Hamiltonian spectral determinant and dynamical zeta function have a special form. Recheck against our cat map $1/\zeta_{\mathrm{AM}}$.

2019-10-14 Predrag The Jacobi operator acts on a discrete periodic lattice as

$$L\,u(t) = a(t+1)u(t+1) + b(t)u(t) + a(t-1)u(t-1)\,,$$

where a(t) and b(t) are real valued for each $t \in \mathbb{Z}$, and M-periodic in t. Jacobi operators are the discrete analogue of Sturm–Liouville operators, with many similarities to Sturm–Liouville theory.

2022-02-13 Josh & Sam Questions about how to best (and practically) evaluate cycle averaging formulas:

1. The numbers of terms in the expansion grows so quickly with respect to the minimal symbol length orbit excluded that we are not quite sure how and where to truncate the sum, even moderately sized collections of orbits.

2. Has anyone attempted to compute periodic orbits averages by numerically computing the zero and derivative of $F = \prod_p (1 - t_p)$ directly?

2022-02-11 Predrag .

1. Nobody so far has had enough understanding of Navier-Stokes periodic orbits to evaluate truncation errors. For low-dimensional systems:

   (a) If grammar is known, exponentially decreasing errors kick in only after 'fundamental' cycles are accounted for, read the end of ChaosBook sect. 18.3 *Determinant of a graph*

   (b) If symbolic dynamics is not understood, ChaosBook sect. 23.7 *Stability ordering of cycle expansions*

2. None has attempted it - an idea worth exploring.

(a) Watch out for ChaosBook sect. 22.4 *False zeros*: the unexpanded product $\prod_p (1 - t_p)$ is only a shorthand, just like for the original Riemann zeta function.

(b) If you expand the terms as a (pseudo)cycle expansion, numerically "computing the zero and derivative" seems to be what we already do?

3. But your question does lead to something that Matt Gudorf never explored in his thesis: Perhaps the most important insight of the spatiotemporal reformulation of 'chaos' is that the weight of periodic orbits (N-torus, if theory has N continuous symmetries) is given by its Hill determinant, see LC21 sect 8.2 *Periodic orbit theory for the retarded*.

(a) Can you think of new/better ways to evaluate $\mathrm{Det}\,\mathcal{J}$? Orbit Jacobian matrix $\mathcal{J}$ is big, but very sparse, and $\mathrm{Det}\,\mathcal{J}$ has a nice geometrical interpretation as a LC21 fundamental parallelepiped? The edges of the parallelepiped are the columns of the orbit Jacobian matrix, which are sparse, so maybe it is computable?

(b) In the continuum limit (more appropriate to Navier-Stokes?), maybe the best was is to follow LC21 Hill and Poincaré, and truncate Fourier series?

(c) For viscous flows, like Navier-Stokes, the infinity of transient, strongly dissipative modes immediately damp put, so the Hill determinant should only have the dimension of the *inertial manifold*. Does it?

2022-02-19 Predrag JAX is said to make evaluation of Jacobians trivial.

References

[1] R. E. Amritkar, P. M. Gade, A. D. Gangal, and V. M. Nandkumaran, "Stability of periodic orbits of coupled-map lattices", Phys. Rev. A **44**, R3407–R3410 (1991).

[2] T. Bountis and R. H. G. Helleman, "On the stability of periodic orbits of two-dimensional mappings", J. Math. Phys **22**, 1867–1877 (1981).

[3] B. L. Buzbee, G. H. Golub, and C. W. Nielson, "On direct methods for solving Poisson's equations", SIAM J. Numer. Anal. **7**, 627–656 (1970).

[4] M. Chen, "On the solution of circulant linear systems", SIAM J. Numer. Anal. **24**, 668–683 (1987).

[5] W. G. Choe and J. Guckenheimer, "Computing periodic orbits with high accuracy", Computer Meth. Appl. Mech. and Engin. **170**, 331–341 (1999).

[6] P. Cvitanović, R. Artuso, R. Mainieri, G. Tanner, and G. Vattay, *Chaos: Classical and Quantum* (Niels Bohr Inst., Copenhagen, 2022).

[7] P. Cvitanović, C. P. Dettmann, R. Mainieri, and G. Vattay, "Trace formulas for stochastic evolution operators: Weak noise perturbation theory", J. Stat. Phys. **93**, 981–999 (1998).

[8] P. Cvitanović and H. Liang, Spatiotemporal cat: A chaotic field theory, In preparation, 2022.

[9] P. Cvitanović and D. Lippolis, Knowing when to stop: How noise frees us from determinism, in Let's Face Chaos through Nonlinear Dynamics, edited by M. Robnik and V. G. Romanovski (2012), pp. 82–126.

[10] P. J. Davis, *Circulant Matrices*, 2nd ed. (Amer. Math. Soc., Providence RI, 1979).

[11] X. Ding, H. Chaté, P. Cvitanović, E. Siminos, and K. A. Takeuchi, "Estimating the dimension of the inertial manifold from unstable periodic orbits", Phys. Rev. Lett. **117**, 024101 (2016).

[12] X. Ding and P. Cvitanović, "Periodic eigendecomposition and its application in Kuramoto-Sivashinsky system", SIAM J. Appl. Dyn. Syst. **15**, 1434–1454 (2016).

[13] E. J. Doedel, "Nonlinear numerics", J. Franklin Inst. **334**, 1049–1073 (1997).

[14] E. J. Doedel, A. R. Champneys, T. F. Fairgrieve, Y. A. Kuznetsov, B. Sandstede, and X. Wang, *AUTO: Continuation and Bifurcation Software for Ordinary Differential Equations* (2007).

[15] H. R. Dullin and J. D. Meiss, "Stability of minimal periodic orbits", Phys. Lett. A **247**, 227–234 (1998).

[16] S. Elaydi, *An Introduction to Difference Equations*, 3rd ed. (Springer, Berlin, 2005).

[17] S. N. Elaydi, *Discrete Chaos* (Chapman and Hall/CRC, 2007).

[18] P. M. Gade and R. E. Amritkar, "Spatially periodic orbits in coupled-map lattices", Phys. Rev. E **47**, 143–154 (1993).

[19] J. F. Gibson, Channelflow: A spectral Navier-Stokes simulator in C++, tech. rep., `Channelflow.org` (U. New Hampshire, 2019).

[20] J. F. Gibson, J. Halcrow, and P. Cvitanović, "Visualizing the geometry of state-space in plane Couette flow", J. Fluid Mech. **611**, 107–130 (2008).

[21] J. Guckenheimer and B. Meloon, "Computing periodic orbits and their bifurcations with automatic differentiation", SIAM J. Sci. Comput. **22**, 951–985 (2000).

[22] B. Gutkin and V. Osipov, "Classical foundations of many-particle quantum chaos", Nonlinearity **29**, 325–356 (2016).

[23] Y. Le Cun, I. Kanter, and S. A. Solla, Second order properties of error surfaces: Learning time and generalization, in Adv. neural information processing systems, Vol. 3, edited by R. P. Lippmann, J. Moody, and D. Touretzky (1990).

[24] Y. Le Cun, I. Kanter, and S. A. Solla, "Eigenvalues of covariance matrices: Application to neural-network learning", Phys. Rev. Lett. **66**, 2396–2399 (1991).

[25] A. J. Linot and M. D. Graham, "Data-driven reduced-order modeling of spatiotemporal chaos with neural ordinary differential equations", Chaos **32**, 073110 (2022).

[26] I. Percival and F. Vivaldi, "A linear code for the sawtooth and cat maps", Physica D **27**, 373–386 (1987).

[27] L. N. Trefethen, *Spectral Methods in MATLAB* (SIAM, Philadelphia, 2000).

[28] D. Viswanath, "The Lindstedt-Poincaré technique as an algorithm for finding periodic orbits", SIAM Rev. **43**, 478–496 (2001).

[29] D. Viswanath, "Symbolic dynamics and periodic orbits of the Lorenz attractor", Nonlinearity **16**, 1035–1056 (2003).

[30] D. Viswanath, "The fractal property of the Lorenz attractor", Physica D **190**, 115–128 (2004).

[31] A. P. Willis, Openpipeflow: Pipe flow code for incompressible flow, tech. rep., `Openpipeflow.org` (U. Sheffield, 2014).

[32] W. L. Wood, "Periodicity effects on the iterative solution of elliptic difference equations", SIAM J. Numer. Anal. **8**, 439–464 (1971).

[33] Q. Zhilin, A. Gangal, M. Benkun, and T. Gang, "Spatiotemporally periodic patterns in symmetrically coupled map lattices", Phys. Rev. E **50**, 163–170 (1994).